



## European Fuel Cell

Conference & Exhibition

# EUROPEAN FUEL CELL PROCEEDINGS OF THE 7<sup>TH</sup> EUROPEAN FUEL CELL PIERO LUNGI CONFERENCE

12-15 december 2017 / **NAPLES**







# EUROPEAN FUEL CELL PROCEEDINGS OF THE 7<sup>TH</sup> EUROPEAN FUEL CELL PIERO LUNGHI CONFERENCE

To Piero Lunghi. We miss you a lot.

To you our gratitude for ever.

This book is dedicated to the memory of Piero Lunghi, creator of the European Fuel Cell Technology and Applications Conference, dear friend and colleague, who prematurely passed away in a car accident on damned November 9, 2007.

Piero made significant contributions in the field of fuel cells in the course of his too short career. He was the leading figure in the formation of the fuel cell research group at the University of Perugia and several activities and research projects initiated by him are still ongoing. This means that, thanks to Piero, many young people are working in this exciting research field and are coming to Naples to present their results. Therefore, Piero's memory is in the conference name but Piero's contribution is still in the contents of this book.

The memory of our friend Piero, his great personal generosity and energy, survives in our hearts, his contribution and his tenacity survive in the work of young people who carry on his vision throughout the world.

This year three best paper awards have been established in memory of Piero Lunghi, following his ideas and his actions "Plan as if you should live forever and work as if you should die tomorrow". The prize that has been made possible by his parents and his sister, Paola, aims to be a message to young researchers everywhere: your ideas, your projects can change the world.

Give them your passion, your strength, and make all necessary effort to realize them. There is no greater satisfaction than seeing one's ideas become reality and become part of the future of our world. Piero strongly desired this, and constantly followed this through with conviction, passion and dedication.

For a better future, we need young researchers of this kind.



# European Fuel Cell

Conference & Exhibition

---

**12-15 december 2017 / NAPLES**

EDITED BY

**Viviana Cigolotti**

CO-EDITED BY

**Chiara Barchiesi and Michela Chianella**

2017

**ENEA**

ITALIAN NATIONAL AGENCY FOR NEW TECHNOLOGIES, ENERGY  
AND SUSTAINABLE ECONOMIC DEVELOPMENT

Lungotevere Thaon di Revel, 76  
00196 ROME

**ISBN 978-88-8286-324-1**

## Supporting Institutions

---



**Regione Umbria**





# LOCAL COMMITTEE

## CHAIRMAN

Angelo **MORENO**

ENEA (Italian National Agency for New Technologies, Energy and Sustainable Economic Development) - Italy

## TECHNICAL PROGRAM MANAGER AND AUTHOR INFORMATION

Viviana **CIGOLOTTI**

ENEA (Italian National Agency for New Technologies, Energy and Sustainable Economic Development) - Italy

Stephen **McPHAIL**

ENEA (Italian National Agency for New Technologies, Energy and Sustainable Economic Development) - Italy

Elio **JANNELLI**

Dept. of Engineering - University of Naples "Parthenope" - ATENA Scarl Italy

Adele **PIANESE**

Dept. of Engineering - University of Naples "Parthenope" - ATENA Scarl Italy

Ludovica **COSENTINO**

ATENA Scarl, Italy

# ORGANIZING COMMITTEE

## CHINA

**Hongmei Yu**, Dalian Institute of Chemical Physics

## FINLAND

**Jari Kiviaho**, VTT Technical Research Center of Finland

## FRANCE

**Laurent Antoni**, CEA and President of the New European Research Grouping on fuel cells and Hydrogend

## GERMANY

**Detlef Stolten**, Forschungszentrum Jülich (FZJ)

**Christian Sattler**, DLR - German Aerospace Center, Vice-President of N.ERGHY

**Olaf Jedicke**, Karlsruhe Institut of Technology (KIT)

## ITALY

**Alberto Ravagni**, SOFCPower Spa

**Gianni Bidini**, Università degli Studi di Perugia

**Stefano Ubertini**, Università degli Studi della Toscana

**Marcello Baricco**, Università degli Studi di Torino

**Luigi Crema**, Fondazione Bruno Kessler

**Salvatore Freni**, Director of CNR ITAE

## JAPAN

**Takao Watanabe**, Central Research Institute of Electric Power Industry (CRIEPI)

**Kenchiro Ota**, Yokohama National University

## NETHERLANDS

**Marc Steen**, Head of Unit Cleaner Energy, Institute for Energy, Joint Research Centre, European Commission

## ROMANIA

**Eden Mamut**, University of Costanza

## SPAIN

**Fernando Palacin**, Director at the Foundation for Hydrogen in Aragon

**Iñaki Azkarate**, Tecnalia Corporación Tecnológica

## SOUTH KOREA

**Tae-Hoon Lim**, Korea Institute of Science & Technology (KIST)

## SWEDEN

**Bengt Ridell**, Sweco Energuide AB

## USA

**Subhash Singhal**, Pacific Northwest National Laboratory (PNNL)

# SCIENTIFIC COMMITTEE

## BULGARIA

**Daria Vladikova**, IEES

## CROATIA

**Frano Barbir**, FESB - University of Split

## DENMARK

**John Bögild Hansen**, Haldor Topsøe

## FINLAND

**Tiina Koljonen**, Technical Research Center of Finland (VTI)

## FRANCE

**Michel Cassir**, Chimie Paris Tech (ENSCP)

**Deborah Jones**, Université Montpellier

## GERMANY

**Alexander Michaelis**, Fraunhofer-Institut für Keramische Technologien und Systeme - IKTS Dresden

**Thomas Pfeifer**, Fraunhofer-Institut für Keramische Technologien und Systeme - IKTS Dresden

**Ludwig Jörissen**, Centrum für Sonnenenergie- und Wasserstoff-Forschung Baden-Württemberg - ZSW

## GREECE

**Tsiakaras Panagiotis**, University of Thessaly

**Thanos Stubos**, National Center for Scientific Research

«Demokritos»

## ITALY

**Mauro Scagliotti**, R.S.E. Spa - Ricerca sul Sistema Energetico

**Aristide Massardo**, Università degli Studi di Genova

**Maria Giovanna Minutillo**, Università degli Studi di Napoli "Parthenope"

**Alessandra Perna**, Università degli Studi di Cassino

**Umberto Desideri**, Università degli Studi di Pisa

**Angelo Basile**, ITM-CNR - Istituto per la Tecnologia delle Membrane del Consiglio Nazionale delle Ricerche

**Sergio Ulgiati**, Università degli Studi di Napoli "Parthenope"

**Vincenzo Palma**, Università degli Studi di Salerno

**Cesare Pianese**, Università degli Studi di Salerno

**Barbara Bosio**, Università degli Studi di Genova

**Rodolfo Taccani**, Università degli Studi di Trieste

Pierluigi Leone, Politecnico di Torino

**Nicola Massarotti**, Università degli Studi di Napoli "Parthenope"

**Luca Andreassi**, Università degli Studi di Roma "Tor Vergata"

**Andrea Casalegno**, Politecnico di Milano

**Massimo Santarelli**, Politecnico di Torino

**Vito Di Noto**, Università degli Studi di Padova

**Domenico Borello**, Università di Roma "La Sapienza"

**Pierangela Cristiani**, RSE - Ricerca sul Sistema Energetico S.P.A.

**Linda Barelli**, Università degli Studi di Perugia

**Marcello Romagnoli**, Università degli Studi di Modena e

Reggio Emilia

**Antonino Aricò**, CNR ITAE

**Gaetano Squarito**, CNR ITAE

**Stefano Campanari**, Politecnico di Milano

## JAPAN

**Koichi Eguchi**, Kyoto University

## NETHERLANDS

**Kas Hemmes**, Delft University of Technology - TU Delft

**P.V. Aravind**, Delft University of Technology - TU Delft

## PORTUGAL

**Carmen Rangel**, LNEG - National Laboratory of Energy and Geology

## ROMANIA

**Vasile Stanciu**, The National R-D Institute for Cryogenics and Isotopes Technologies - ICIT

**Iordache Ioan**, Institutul Național de Cercetare-Dezvoltare pentru Tehnologii Criogenice și Izotopice - ICSI Rm. Vâlcea

## SLOVENIA

**Stanko Hocevar**, National Institute of Chemistry of Slovenia

## SOUTH KOREA

**Suk Woo Nam**, Korea Institute of Science & Technology (KIST)

**Jonghee Han**, Korea Institute of Science & Technology (KIST)

**Sung Pil Yoon**, Korea Institute of Science & Technology (KIST)

**Jaeyoung Lee**, GIST

## SPAIN

**Javier Brey Sanchez**, H2B2

**Garcia Luis Alberto**, Tecnalia Corporación Tecnológica

**David Sanchez**, University of Sevilla

**Antonio García-Conde**, Spanish Hydrogen Association - IEA HIA

## SWEDEN

**Bin Zhu**, Royal Institute of Technology

**Carina Lagergren**, KTH

## SWITZERLAND

**Olivier Bucheli**, Solid Power

## TURKEY

**Cigdem Karadag**, TUBITAK Marmara Research Center

**Atila Ersoz**, TUBITAK Marmara Research Center

**Isil Isik Gulsac**, TUBITAK Marmara Research Center

**Fehmi Akgun**, TUBITAK Marmara Research Center

## UK

**Vladimir Molkow**, University of Ulster

**Robert Steinberger-Wilckens**, University of Birmingham

**Ioannis A. Ieropoulos**, University of the West of England, Bristol

## USA

**Abdelkader Hilmi**, Fuel Cell Energy

**Whitney Colella**, Gaia Energy Research Institute

**J. Robert Selman**, Illinois Institute of Technology

# TRACK MANAGER

Martin Andersson

Steven Beale

Manuel Bianco

Domenico Borello

Giovanni Cinti

Remi Costa

Pierangela Cristiani

Nicola Di Giulio

Andrea Facci

Kas Hemmes

Ioannis Ieropoulos

Carina Lagergren

Pierluigi Leone

Loredana Magistri

Nicola Massarotti

Stephen McPhail

Mariagiovanna Minutillo

Alessandra Perna

David Sánchez

Massimo Santarelli

Rodolfo Taccani

Francesco Trasino

Alberto Traverso

# EXHIBITOR



Located in the Science Park of the Swiss federal institute of technology (EPFL) in Lausanne, Fiaxell is manufacturing components for SOFC and SOEC research such as the Open Flanges test Set-Up™, short stack, gold, crofer 22H and nickel M\_Grid™, Cell-Connex™ for current collection and gas diffusion. We are also retailer for H2 generator, potentiostat/galvanostat/EIS analyzer and mass flow controller.

# SPONSOR



The Institute for Advanced Energy Technologies "Nicola Giordano" (hereinafter ITAE) is an Italian research centre founded in 1980 and belonging to the National Research Council (CNR) that is distributed all over Italy through a network of institutes aiming at promoting a wide diffusion of its competences throughout the national territory and at facilitating contacts and cooperation with local firms and organizations.

ITAIE is one of European leading research centre in the fuel cells and renewable energy fields and a full member of the Fuel Cells and Hydrogen Joint Technology Initiative of the European Community.

The research activity is organized in 4 sectors:

- 1 – Direct production of electric energy technologies
- 2 – Hydrogen and clean fuels production
- 3 – Energy transformation and storage technologies
- 4 – Integration of new energy technologies and renewable

Beside these four lines of research, there are three support activities that cut across all research lines and are: socio-economic impact analysis of cutting-edge energy technologies; study about the regulations governing the application and use of energy technologies; technology transfer and exploitation of R&D results.

The institute is provided with 19 equipped laboratories for preparative and characterization of materials and components, energy systems and for the construction and testing of devices and prototypes.

These laboratories are located in a building which is on three levels with a total area of 4800 square meters, and includes laboratories, offices, a conference room, a library, a guest quarters and the canteen.

Moreover, the ITAE has, in an area close to its headquarters, a "Center for new energetic technology testing, innovation and industrial promotion", that is a testing center supplying technical and scientific support to companies operating in the production of innovative energy systems



The Bioelectrochemical Society (BES) is an international scientific association founded by Giulio Milazzo in 1979 to promote understanding and cooperation among scientists interested in the application of electrochemical concepts and techniques to the fundamental or applied study of living systems.

BES is a non-profit making organization. The Society is composed of individuals and corporate members in the following categories: regular, honorary.

BES pursues its objective using various means, including:

- organising scientific meetings;
- publishing scientific works in periodicals or other forms;
- editing specialized periodicals;
- contributing to the development of a common language among scientists of the different disciplines involved in the (scientific, technical and applied) development of bioelectrochemistry, especially among the diverse groups interested in such aspects as energetics, pharmacology, medicine, etc.;
- stimulating the establishment, among its members, of co-operative programs on particular subjects, especially interdisciplinary, and, if the need arises, assuring the management of international programmes of study or research.
- attributing awards in the field of the Bioelectrochemistry.

BES is administered by a Council elected during BES biannual symposium for a term of four years by the General Assembly, Members of the BES Council may be chosen from all the categories of membership in the Assembly. There shall be a new Council every two years formed by the replacement of half of the members.



## FUNDING FUEL CELLS AND HYDROGEN TECHNOLOGY DEVELOPMENTS ACROSS EUROPE

The Fuel Cells and Hydrogen Joint Undertaking (FCH JU) finances Research & Development (R&D) and Demonstration projects on fuel cells and hydrogen. It is a unique public-private partnership between the European Commission, Europe's fuel cell and hydrogen industry and research organisations. A public-private partnership model works as an effective way for European intervention to coordinate R&D activities by pooling financial resources together.

The European Union is committed to changing its transport and energy systems in pursuing a future low carbon economy. Fuel Cells and Hydrogen (FCH) technologies hold great promise for energy and transport applications from the perspective of meeting Europe's energy, environmental and economic challenges.

Hydrogen can be produced using renewable energy sources, offering a clean fuel for road transportation. Moreover, hydrogen offers the ability to store electricity, addressing the intermittent character of renewable energy. When coupled with highly efficient, silent and clean fuel cells as energy convertors, hydrogen opens up new horizons for decreasing Europe's dependency on imported fossil fuels.

**The aim of the FCH JU is to accelerate the market introduction of these technologies, realising their potential as an instrument in achieving a carbon-lean energy system.**

Established in 2008, the FCH JU has supported 169 projects to date. Its second phase was approved by the Council of the European Union in May 2014 under the Horizon 2020 EU funding programme, with a total budget of €1.33 billion as FCH 2 JU. This marks Europe's continued confidence and support for fuel cells and hydrogen as key technologies for decarbonising our energy system, and creating a secure sustainable energy supply capable of generating new jobs.

The FCH JU programme is structured around two research and innovation pillars dedicated to **Transportation and Energy Systems**, complemented by a set of **Cross-Cutting** research activities.

### ENERGY

- Fuel cells for power and combined heat & power generation
- Hydrogen production and distribution
- Hydrogen for renewable energy storage (incl. blending in natural gas grid)

### CROSS-CUTTING ISSUES

(e.g. standards, consumer awareness, manufacturing methods, studies)

### TRANSPORT

- Road vehicles
- Non-road mobile vehicles and machinery
- Refuelling infrastructure
- Maritime, rail and aviation applications



# EFC17 EUROPEAN HYDROGEN TOUR

## from Brussels to Naples

The EFC17 European Hydrogen tour has two main goals. We intend to let European citizens, but above all Italian citizens, know that the electric Hydrogen and fuel cell vehicles are ready to enter the market. These vehicles together with battery electric ones and with all other electric vehicles based on the combination of battery and hydrogen fed fuel cells are the future of zero emissions transport. They are the answer to pollution problems and to improve the quality of our life. Another goal, which is more peculiar for Italy, is to highlight how late Italy is in the deployment of hydrogen infrastructures and in the promotion, in general, of the research and development of hydrogen and fuel cells technologies. We would like to make Italian politician aware of the importance of these technologies for our economy, for creation of new employments, for enhancing our competitiveness.



During the first part of the trip two hydrogen cars, supplied by FCH-JU, a Hyundai IX35 and a Toyota Mirai, will cross Belgium, Germany and Austria to reach Bolzano (Italy). In this case we won't have any problem because we will be able to fill the cars with Hydrogen in public HRS we will find along the trip just using the application H2.Live in our Smartphone. We are going to face many problems in the second part of the tour, i.e. from Bolzano to Naples. There are no public HRS we will be obliged to refill hydrogen in facilities where Hydrogen is produce and/or stored.



# MEDIA PARTNERS



**Fuel Cell & Hydrogen Energy Association (FCHEA)** is the trade association for the fuel cell and hydrogen energy industry, dedicated to the commercialization of fuel cells and hydrogen energy technologies. FCHEA members represent the full global supply chain, including fuel cell materials, components and systems manufacturers, hydrogen producers and fuel distributors, government laboratories and agencies, trade associations, utilities, and other end users.



**Fuel Cells Bulletin** is the leading monthly newsletter dedicated to reporting and analysing business and technology developments in the global fuel cell sector. The newsletter – published as a Digital Edition – contains a mix of news on automotive and mobile, small and large stationary, portable and micro, hydrogen fuelling and energy storage, commercialisation and research activities and demonstrations. Each issue has a feature article on a specific company, project, technology or topic of interest, as well as an extensive summary of new US patents, and a comprehensive events calendar.



**Renewable Energy Focus magazine** and its website provide a forum for debate and dialogue between research, industry, financial organisations and government bodies worldwide. With in-depth coverage and incisive editorial on all areas of renewable energy, Renewable Energy Focus takes an objective look at bioenergy, energy efficiency, energy infrastructure, energy storage (including fuel cells), geothermal, green buildings, hydro power, photovoltaic (PV), solar heating and cooling, solar thermal, wave and tidal energy, and wind power.



**Shmuel De-Leon Energy, Ltd.** is a leading company in the field of power sources knowledge. The company provides comprehensive collection of power sources knowledge tools and services:

- Consulting services
- Market research reports
- Batteries, Fuel cells and EV seminars and conferences
- Batteries, FC & EV Weekly newsletter
- Energy Sources On-Line web DataBase (batteries, fuel cells, capacitors and more...)
- Power sources solutions
- Representing Energy Storage testing and research equipment companies in Israel

# MEDIA PARTNERS



The mission of **The Electrochemical Society** is to advance theory and practice at the forefront of electrochemical and solid state science and technology, and allied subjects. To encourage research, discussion, critical assessment, and dissemination of knowledge in these fields, the Society holds meetings, publishes scientific papers, fosters training and education of scientists and engineers, and cooperates with other organizations to promote science and technology in the public interest. The vision of ECS is to be recognized as the steward of electrochemical & solid state science and technology. By creating uninhibited availability of the science through open access, ECS can Free the Science, and accelerate scientific discovery and innovation, leading the community as the advocate, guardian, and facilitator of our technical domain.



American Elements is the world leader in the industrial application of materials science. It has also been a key source for academic and corporate research, advancement and new product development in SOFC and PEM fuel cell materials and has been a decade long participant in the materials development component of the U.S. Dept. of Energy's SECA program. Our fundamental expertise in the properties, applications and cost-effective manufacturing of advanced and engineered materials, including ultra high purity refining (99.9999%) and nanotechnology (Mono Atomic Elements) scales allows us to meet the needs of thousands of global manufacturers (including over 30% of the Fortune 50), all U.S. and many foreign national laboratories, universities throughout the world, and our customers in a wide variety of industry groups, including energy, electronics, aerospace, defense, automotive, optics/photovoltaics, green technologies and pharma/cosmetics. The company provides both technical guidance and manufactured products in its 10,850 page online catalogue which includes over 3,000 elemental metal, metallic compound, ceramic and crystalline stock items. American Elements also produces numerous customer proprietary formulations from our network of production facilities strategically placed throughout the world.



Fast a not for profit private organization founded in 1897, represents 32 Italian scientific and technical associations covering the most important and priority European industrial sectors. Thanks to the competencies and expertise of the associations belonging to FAST network, the Federation is able to address significant stakeholders at regional and national level and to guarantee a permanent liaison with the most relevant EU industrial and research networks. FAST has a long standing relationship with different regional and local authorities providing them support in shaping and programming their policies with regards to innovation, research (FAST is a member of the Enterprise Europe Network, manages the Hyer secretariat -HyER - in Brussels), education and training and technical assistance to SMES.



H2IT is an independent and non-profit organization, launched in 2004 to formalize the activities of the working groups of the Italian Hydrogen Taskforce and promote the creation of an infrastructure for the use of hydrogen. The goal is to stimulate and develop the market for the use of hydrogen, to create a strong industry voice of companies and institutes involved in the sector, and to secure a leading role for Italy in the world market.



# PROCEEDINGS OF THE 7<sup>TH</sup> EUROPEAN FUEL CELL PIERO LUNGHI CONFERENCE ABSTRACTS



**European Fuel Cell**  
Conference & Exhibition

---

**12-15** december 2017 / **NAPLES**



## TEMPERATURE INFLUENCE ON TWO LAYERS YTTRIA STABILIZED ZIRCONIA MATRIX IMPREGNATED BY LITHIUM/POTASSIUM ELECTROLYTE FOR MOLTEN CARBONATE FUEL CELLS

J. Milewski\*, T. Wejrzanowski\*\*, K-Z Fung\*\*\*,  
Ł. Szablowski\*, R. Baron\*\*, J-Y. Tang\*\*\*, A. Szczęśniak\*,  
and C-T. Ni\*\*\*

\*Faculty of Power and Aeronautical Engineering, Warsaw University of Technology, Institute of Heat Engineering, 21/25 Nowowiejska Street, 00-665 Warsaw, (Poland)

\*\*Faculty of Material Science Engineering, Warsaw University of Technology, 141 Wołoska Street, 02-507 Warsaw, (Poland)

\*\*\*Department of Materials Science and Engineering, National Cheng Kung University, Tainan, (Taiwan)

**Abstract** - In this paper, the testing results of a composite electrolyte layer based on Yttria Stabilized Zirconia and Lithium/Potassium carbonates for its electrochemical performance as a matrix for MCFC are presented. The voltage-current density curves were collected in a range of temperatures: 500–800°C.

The idea is to use a dual conductive composite electrolyte as a matrix for Molten Carbonate Fuel Cells. This results in an improvement in the performance of the MCFC, by, in particular, increasing ionic conductivity through additional  $O^{2-}$  conduction.

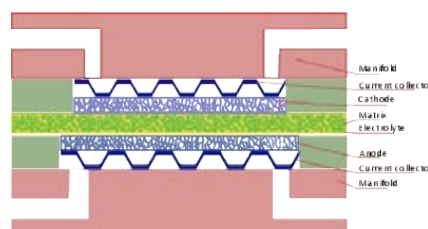
**Index Terms** – MCFC, composite electrolyte, dual conducting, YSZ.

### I. INTRODUCTION

Fuel price inflation and a long-term increase in electricity consumption have provided added impetus to the search for ultra-effective power generation systems based on biofuels or hydrogen as a primary fuel as an alternative to the fossil fuels. In contrast to classic power sources, fuel cells generate power in electrochemical reactions with potentially ultra-high efficiency. High temperature fuel cells (mainly Solid Oxide Fuel Cell and Molten Carbonate Fuel Cell) are considered as future electricity sources. Additionally, electrochemical power sources offer a great deal flexibility in the design of energy systems. Presently, state-of-the-art hybrid systems including SOFC and MCFC are being built in the power range of 250 kW up to several dozen MW. Research and development in this field is

predicted to result in an increase in the power of those kinds of systems in the future.

Molten Carbonate Fuel Cells (MCFCs) have developed rapidly in recent years due to their large scale capabilities, high efficiency with little pollution, and variety of fuel utilization. In contrast to low temperature fuel cells (e.g. Polymer Exchange Membrane Fuel Cell—PEMFC), the elevated temperature of MCFCs means nickel based catalysts can be used, which are cheaper than platinum.

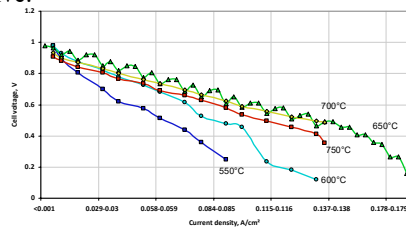


**Fig. 1. Schematic diagram of Molten Carbonate Fuel Cell layout**

The MCFC layout is presented in Fig. 1. The powder-based matrix retains the molten electrolyte by capillary forces. The matrix material needs to fulfill several requirements to be a good support for molten carbonates, the most important being: chemical stability in lithium, potassium, and sodium carbonates and no electric conductivity. The material which fulfills those



requirements is lithium alumina ( $\text{LiAlO}_2$ ), which is still the favored matrix material for MCFC, but there are some problems which are difficult to solve for this material such as: poor mechanical strength of ceramic materials, the problem of cracking in the  $\text{LiAlO}_2$  matrix for MCFC appears when the cells are stacked and operated at high temperatures. This necessitates the application of quite a thick matrix of around 0.9 mm. A thick matrix results in a need for the same thickness of electrolyte, which increases the ionic resistance of the electrolyte layer and lowers fuel cell performance. Additionally, as there is a limited number of manufacturers of  $\text{LiAlO}_2$ , it is quite expensive.



**Fig. 2. The temperature influence on two layers Yttria Stabilized Zirconia matrix impregnated by Lithium/Potassium carbonates**

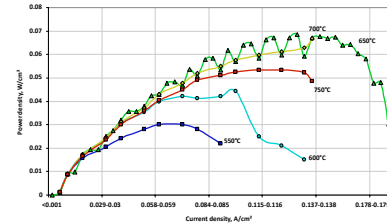
## II. MATRIX FABRICATION

The matrix for MCFC was fabricated by tape casting the ceramic/polymer slurry. Solsperser 20000 (Lubrizol) was used as dispersant, polyvinyl butyral – Mowital B 60 H (Kuraray) was used as binder, dibutyl phthalate – DBP (Chempur) as plasticizer, Agitan DF 311 M (Munzing Chemie) as defoamer. Ethyl alcohol (96%, Chempur) was used as solvent in all of the slurries. Ceramic powder used was 10YSZ (yttria-stabilized zirconia, 10% mol  $\text{Y}_2\text{O}_3$ , Tosoh).

Solid content in the slurries was kept at constant powder volume ratio to total volume of the slurry, based on densities of ceramic powders, in order to obtain the same thickness of green tapes. This assumption allows collating cell current (power density) measurements, as the membrane (matrix/electrolyte) thickness influences the overall cell performance. Slurries were prepared by high-energy milling selected ceramic powder in the solvent containing the dispersant for 18 h in Retsch RM400 planetary ball mill using sintered zirconia containers with 5 mm zirconia balls. Milling was conducted in order to obtain fine particle size for all three powders thus leading to smaller pore size of the matrix, necessary for proper operation of the cell (e.g. gas leak prevention) After first ball-milling, binder and remaining additives were added for another 3 hours of mixing and vacuum de-aired (0.1 bar, 30 seconds) in order to obtain homogeneous slurry for tape casting. Subsequently, green tapes of 8 cm width were casted on a polyethylene surface using a moving-blade tape caster device with doctor blade height set to 0.55 mm.

The influence of temperature on YSZ-based matrix MCFC

performance is shown in Fig. 2. The temperature varied in the range 550–750°C. There is a visible fuel cell performance improvement from 550 to 700°C, but then the performances of the fuel cells decrease themselves but still 750°C has higher voltage than 600°C. At the lowest applied temperature (550°C) the voltage is three times lower than for the most optimal temperature. In fact, usually fuel cell operation below 0.4 V is restricted due to fast fuel cell degradation at such a low voltage; thus the curve data collected at this temperature should not be taken into consideration for further discussion.



**Fig. 2. Temperature impact on power density for 2 layers SDC matrix as MCFC electrolyte**

It could be seen that the increase in temperature of the electrolyte brought about decreases in OCV and increases in power density. The increase in temperature from 550 to 700°C significantly increased the maximum power density (up to almost 0.07 W/cm<sup>2</sup> for manifolds made of 310 stainless steel)—see Fig. 2, probably due to the increase in ionic conductivity. Furthermore, the increase in temperature decreases Open Circuit Voltages and this could also have an impact on the operation of the fuel cell. The lower OCVs result from the Nernst equation as well as the rise in electric conductivity of the electrolyte layer together with ionic conductivity.

## III. CONCLUSION

The paper presents alternative matrix material for  $\text{LiAlO}_2$  which is a very effective support for molten carbonates. However, since there is a limited number of manufacturers, it is very expensive. Excellent performance was obtained for the YSZ-carbonate composite and nanocomposite electrolytes prepared using eutectic carbonates with a mixture of  $\text{Li}_2\text{CO}_3/\text{K}_2\text{CO}_3$ .

In contrast to the theory, the increase in temperature does not improve fuel cell efficiency. Temperature above 700°C results in the higher performances as for 750°C, an issue which merits further investigation.

## ACKNOWLEDGMENT

The project is co-financed by Polish National Center for Research and Development of Polish-Taiwanese/Taiwanese-Polish Joint Research Call granted by decision number DZP/PL-TWIII/16/2016.



## KINETIC INVESTIGATION OF THE OXYGEN REDUCTION REACTION ON LSCF-GDC COMPOSITE CATHODES FOR USE IN IT-SOFCs

M. Rahmanipour\*, G. Cordaro\*\*, A. Baricci\*, M. Zago\*, A. Donazzi\*

\*Dipartimento di Energia, Politecnico di Milano, via Lambruschini 4, 20156, Milano

\*\*Dipartimento di Chimica, Materiali e Ingegneria Chimica, Politecnico di Milano, Piazza Leonardo da Vinci 32, 20133, Milano

**Abstract** – A kinetic investigation of the Oxygen Reduction Reaction (ORR) was performed on LSCF-GDC composite cathodes spanning a wide range of operating conditions. EIS tests were carried out on symmetric cells between 700°C and 550°C under OCV conditions, with O<sub>2</sub>/N<sub>2</sub> mixtures at varying the O<sub>2</sub> molar fraction (5-100%). A dynamic, one-dimensional and physically-based model of the LSCF-GDC cathode was applied to rationalize the experimental results. The model simulates the spectra by solving mass and charge conservation equations, including terms for gas diffusion inside the electrode pores and solid state transport of oxygen vacancies inside the bulk of LSCF and GDC. A detailed kinetic scheme was chosen to describe the ORR mechanism, which took into account steps for adsorption and desorption, first and second electronation at the gas/electrode interface, interfacial and lattice ion transfer. An advanced numerical approach allowed to cut the computational times. Novel insights supporting the 2PB reaction pathway were provided by means of a sensitivity analysis on the kinetic parameters.

**Index Terms** – LSCF, IT-SOFC, ORR, modeling

### I. INTRODUCTION

LSCF-GDC composites are state-of-the-art cathodes for applications based on Intermediate Temperature – Solid Oxide Fuel Cells (IT-SOFC). LSCF (La<sub>0.4</sub>Sr<sub>0.6</sub>Co<sub>0.2</sub>Fe<sub>0.8</sub>O<sub>3-δ</sub>) is a perovskite oxide with mixed ionic and electronic conductive (MIEC) properties, which confer this material the capability of supplying electrons to the adsorbed oxygen atoms and transfer the oxygen ions within the lattice structure. This multifunctional character allows to break the paradigm of an ORR mechanism exclusively based on the Three Phase Boundary (TPB) concept, and opens up an additional transport route wherein oxygen is activated and transferred in the cathodic phase, asking only for two active interfaces (2PB) [1]. Although LSCF can be used as a pure material, composite architectures in combination with GDC (Ce<sub>0.8</sub>Ga<sub>0.2</sub>O<sub>2</sub>) are preferential in applications, in order to provide increased electrolyte/electrode contact area and limit thermal expansion mismatch. The co-presence of the two phases also prompts a beneficial overlap between the TPB and the 2PB routes. Given the wide application, a quantitative understanding of the oxygen reduction mechanism is a requisite for further optimization of the material, both under a design viewpoint (choice of LSCF/GDC ratio, layer thickness, particle size) and

an operational viewpoint (investigation and minimization of the degradation processes, material optimization). In this work, a physically-based electrode model with a multistep kinetic scheme is applied to rationalize impedance spectroscopy experiments performed on LSCF-GDC cathodes, covering a wide range of operating conditions in terms of temperature and composition. A kinetic insight in the 2PB mechanism is provided, with reference to the standard operating conditions.

### II. MATERIALS AND METHODS

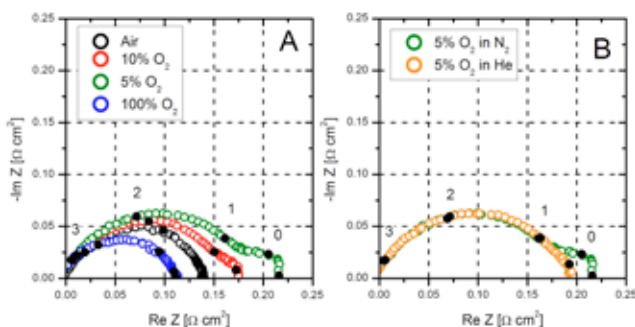
Symmetric LSCF-GDC/GDC/LSCF-GDC cells were tested. GDC electrolyte pellets (1 cm Ø, ~1 mm thick) were prepared by die-pressing. A LSCF-GDC ink (Fuel Cell Materials) with 50% weight fraction of LSCF was used to form the cathode. Granulometry analyses of the ink revealed that the particle size distribution was nearly unimodal, centered at 1 μm. The ink was mixed with graphite (0.2:0.8 graphite/ink ratio) and applied with blade coating on the two sides of the electrolyte. The layers were calcined in air (1000°C for 2 h) to reach adhesion: porous 20 μm thick LSCF-GDC cathodes were obtained. Ag meshes and paste were applied for the current collector. The EIS experiments (0.1 Hz – 100 kHz, 2 mV amplitude) were carried at OCV between 700°C and 550°C with O<sub>2</sub>/N<sub>2</sub> mixtures. At each temperature, the amount of O<sub>2</sub> was varied between 100% and 5% mol/mol. The tests were also repeated with O<sub>2</sub>/He mixtures to verify the impact of diffusive limitations. SEM micrographs allowed to access the morphologic characteristics of the cells.

The EIS experiments were analyzed with a one-dimensional, dynamic and heterogeneous model of the cathode. The model simulates impedance spectra and Bode plots by solving conservation equations of mass and charge in the electrode volume. The gas diffusion in the pores is described via the dusty gas approach, and a multistep kinetic scheme is adopted for the ORR. This scheme accounts for steps for O<sub>2</sub> adsorption and desorption, first and second electronation of O adsorbed atoms, formation and transport of the oxygen vacancies within the bulk of the LSCF and GDC phases. When available, the kinetic parameters (pre-exponential factors and activation energies) and

the transport parameters (vacancies diffusion coefficients and ion conductivity) were assumed from literature correlations and reliable measurements. Only seven unknown parameters, among the kinetic coefficients and the capacitances (surface and bulk), were calculated by fitting the simulated curves on the measured spectra. The fitting was performed by minimization of the squared residuals on the imaginary part and the real part of the Nyquist plots. The adequacy of the parameters was verified with a  $\chi^2$  analysis on the Bode plots [2]. The computational times were cut by linearization of the equations and solution in the frequency domain [3].

### III. RESULTS AND DISCUSSION

The cells were first tested at 700°C at varying the amount of O<sub>2</sub> (Fig. 1a). The round and flat shape of the arcs suggested the presence of more than one overlapped process, possibly related to ion transport and surface charging. A limited impact of mass diffusion was revealed only at 5% O<sub>2</sub> by comparing the curves in N<sub>2</sub> and He (Fig. 1b). An additional proof of the occurrence of mass diffusive limitations at 5% O<sub>2</sub> was provided by the Bode plots, wherein the peak at low frequencies disappeared when switching from O<sub>2</sub>/N<sub>2</sub> to O<sub>2</sub>/He mixtures. These results allowed for the unambiguous association of the small arc observed at low frequencies.

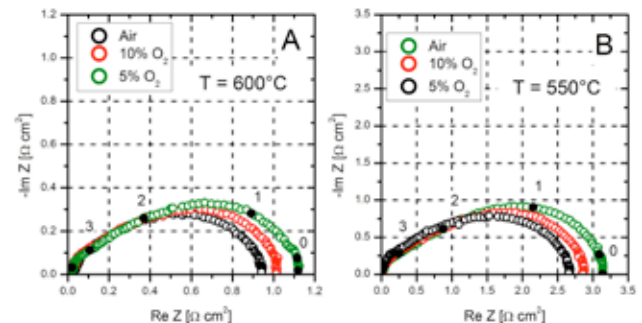


**Figure 1** – EIS tests at T = 700°C, P<sub>O2</sub> = 5 – 100%. A) O<sub>2</sub>/N<sub>2</sub> mixtures. B) dilution effect.

At decreasing the temperature, a different situation emerged, with a progressive transition from round arcs toward Gerischer-type arcs, which were visible at 600°C and 550°C (Fig. 2). At these temperatures, no impact of mass diffusion was revealed, even at the lowest O<sub>2</sub> partial pressures. The characteristic high-frequency linear slope was observed, although slightly depressed (33° instead of 45°), suggesting that inhomogeneity of the particles size and non-ideality of the reactive surface contributed to the final shape of the spectra.

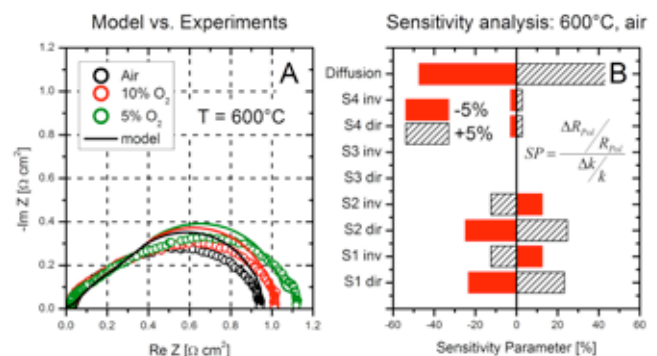
The numerical analysis of the spectra was carried out to individuate the rate determining step (RDS) of the ORR at each temperature. The morphologic parameters and the effectiveness factors were derived based on the percolation theory and on the results of the characterization (SEM, granulometry). The LSCF

vacancy diffusion coefficient, and the ionic and electronic conductivities were taken from relevant literature works.



**Figure 2** – EIS tests at P<sub>O2</sub> = 5 – 21%. A) 600°C. B) 550°C.

A good agreement was found in all the examined conditions, and the kinetic scheme was validated. The model results (an example is provided in Fig. 3a) showed that a close description of the real part of the spectra was achieved, accompanied by a moderate overestimation of the imaginary part, due to the non-ideality of the electrode microstructure. The sensitivity analysis allowed to highlight the RDS (Fig. 3b): at higher temperatures, the ORR was governed by the first electronation of the oxygen adatom, while at lower temperatures the vacancy diffusion in the LSCF structure prevailed. Once the determining steps were individuated, a reduced model analysis was performed to provide practical global rate equations for the main regimes.



**Figure 3** – A) Simulations at 600°C. B) Sensitivity analysis.

### IV. CONCLUSION

A physically-based detailed model was applied to rationalize the impedance spectra of LSCF-GDC composite cathodes. A robust, multistep kinetic scheme was validated spanning a wide range of conditions. The controlling kinetic steps of the ORR process were individuated at each temperature.

### REFERENCES

- [1] S. Haile, *Annu. Rev. Chem. Biomol. Eng.*, 3 (2012) 313
- [2] T. Yang et al., *ECS Transactions*, 68 (2015) 2397-2411
- [3] A.A. Kulikovskiy, *J. Electroanalytical Chem.*, 669 (2012) 28–34

## EFFECT OF ACID LOSS ON HT-PEM FUEL CELL DEGRADATION

N. Pilinski\*, P. Wagner\* and A. Dyck\*

\* DLR Institute of Networked Energy Systems, Carl-von-Ossietzky-Str. 15, 26129 Oldenburg (Germany)

**Abstract** – This investigation will present the impact of phosphoric acid loss on fuel cell degradation. Therefore, degradation rates and acid loss rates in product water and MEAs will be shown. Four MEAs from different suppliers are compared. To obtain results in a short time period fuel cell operation at high current densities of 0.6 A/cm<sup>2</sup> and 1 A/cm<sup>2</sup> over 500 hours will be used. That causes high water production resulting in higher acid loss rates. By investigating the different MEAs after operation it can be shown that the degradation rates depend on the begin of life acid doping levels which vary between the suppliers.

*Accelerated Stress Testing, Degradation, HT-PEMFC, Phosphoric acid.*

### I. INTRODUCTION

Polybenzimidazole (PBI) based high temperature proton exchange membrane fuel cells (HT-PEMFC) exhibit significant advantages in comparison to fuel cell systems operating at lower temperature. The main advantages are improved tolerance to impurities, enhanced electrode kinetics as well as easier heat and water management. Nevertheless, associated with higher operating temperatures there are also several degradation effects of HT-PEMFCs that are still under investigation [1]. Major durability challenges are the physical degradation of the PBI membrane, leaching of phosphoric acid from the membrane as well as catalyst degradation effects and carbon support corrosion [2, 3].

In this work, the influence of phosphoric acid (PA) loss on fuel cell degradation and performance will be shown. Therefore, accelerated stress tests (AST) with PBI based membrane-electrolyte-assemblies (MEA) from different suppliers were performed. High load conditions at 0.6 A/cm<sup>2</sup> and 1.0 A/cm<sup>2</sup> during the experiments provoked increased removal of acid from the MEA causing high degradation in a shorter time period [4]. Within single cell fuel cell test bench operation, supported by electrochemical characterization (polarization curve, electrochemical impedance spectroscopy, cyclic and linear sweep voltammetry) degradation rates have

been determined. Water traps closely placed at fuel cell gas exhaust allowed an allocation of acid loss during fuel cell operation. The water samples were collected in defined time periods and analysed by analytical methods like ion chromatography (IC) and inductive coupled plasma mass spectroscopy (ICP-MS) to achieve an overall nearly closed balancing of the phosphoric acid content of the examined MEAs. In addition, remaining acid loadings of the MEAs after operation were determined by titration. The results of this investigation permitted the correlation of acid loss and degradation rate with different types of MEAs.

### II. EXPERIMENTAL

#### A. Membrane Electrode Assembly (MEA)

The experiments were carried out with four MEAs from different suppliers. The nominal active surface area of the MEAs was ~25 cm<sup>2</sup>. The membrane polymer electrolyte consisted of phosphoric acid doped meta-PBI and para-PBI; the acid content varied between 11 and 23 mg/cm<sup>2</sup>. Table I gives an overview of the used MEAs.

TABLE I  
MEMBRANE MATERIAL AND PA LOADING FOR THE DIFFERENT SUPPLIERS.

No	Supplier	Component	MEA loading [mg <sub>H3PO4</sub> cm <sup>-2</sup> ]
1	Supplier A	p-PBI membrane	22.2 ± 4.5
2	Supplier B	p-PBI membrane	22.9 ± 1.5
3	Supplier C	m-PBI membrane	11.0 ± 0.6
4	Supplier D	PBI membrane	15.4 ± 1.0

#### B. Fuel Cell Test Stations and Fuel Cell Test Procedure

During the experiments a commercially available cell compression unit (CCU) from balticFuelCells (Germany) with 5-fold serpentine flow field (SFF) geometry bipolar plates (BBP) and a constant contact compression of 0.75 MPa was used.

The CCU was operated with the fuel cell test stations Evaluator C50-LT and C1000-LT from FuelCon AG

Copyright © 2017

(Germany) and inhouse engineering (Germany) test benches.

During operation, performed over ~500 h, load cycling between current density of 1 A/cm<sup>2</sup> for 16 minutes followed then by 4 minutes at 0.6 A/cm<sup>2</sup> were done.

### C. Determination of acid loss

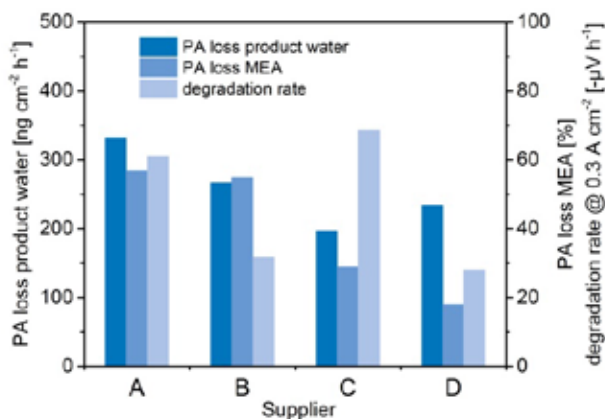
For investigation of acid loss in product water, water samples collected in defined time steps during fuel cell operation, were analysed by ion chromatography (850 Professional IC, Metrohm).

To determine the acid loss of the MEA after operation, titration method was used. Therefore, the samples were stirred in a solution of acetone/water over 30 minutes and titrated with sodium hydroxide.

The combination of electrochemical evaluation and determination of retained phosphoric acid within the MEA allowed the direct correlation between acid and performance loss.

## III. RESULTS

In figure 1 the acid losses in product water and MEA as well as degradation rates after operation at high current densities are shown.

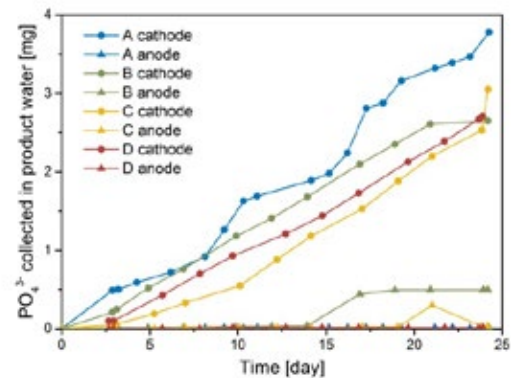


**Fig. 1. Acid losses (product water and MEA) and degradation rates after high current densities (0.6-1 A/cm<sup>2</sup>) of four MEAs from different suppliers.**

It can be seen that the results of the MEAs from supplier A and B, using the same type of membrane and similar PA loading, are different. The MEA from supplier B indicates an approx. 50% lower degradation rate after operation of 500 hours in comparison to supplier A. This is only partially supported by the acid losses through product water and from the MEA with supplier B. In general, the MEA of supplier C reveals the lowest acid loss in product water after operation but shows a higher degradation rate. Due to the lower PA doping levels at begin of life the acid release during operation will be less. In contrast, supplier D represents the lowest degradation rate with around -30 μV/h. The acid loss in product water is in

the same range like supplier B and C; the MEA also shows the lowest overall acid loss with 18 %.

Regarding the loss of phosphate in product water during operation time it can be seen that there is a linear trend over time with large losses on the cathode side as expected (figure 2). Here, supplier A shows the highest acid loss overall which can be attributed to the high doping level at begin of life.



**Fig. 2. Phosphate collected in cathode and anode product water during operation with supplier A, B, C and D.**

## IV. CONCLUSION

The degradation rates and acid losses differ from different types of MEAs (four suppliers) regarding membrane and acid doping levels. The lowest acid loss in MEA and degradation rate has been determined with MEA from supplier D. But to better understand the correlation between acid loss and degradation, it is necessary to perform more detailed investigations in the future.

## ACKNOWLEDGMENT

The authors would like to thank Vietja Tullius and Julian Büsselmann for the support at the test stations.

## REFERENCES

- [1] S. S. Araya, F. Zhou, V. Liso, S. L. Sahlin, J. R. Vang, S. Thomas, X. Gao, C. Jeppesen and S. K. Kaer, A comprehensive review of PBI-based high temperature PEM fuel cells, *International Journal of Hydrogen Energy*, Vol. 41, No. 46, 12 (2016), pp. 21310-21344.
- [2] M. A. Haque, A. B. Sulong, K. S. Loh, E. H. Majlan, T. Husaini and R. E. Rosili, Acid doped polybenzimidazole based membrane electrode assembly for high temperature proton exchange membrane fuel cell: A review, *International Journal of Hydrogen Energy* (2016), <http://dx.doi.org/10.1016/j.ijhydene.2016.03.086>.
- [3] G. Liu, H. Zhang, J. Hu, Y. Zhai, D. Xu and Z. Shao, Studies of performance degradation of a high temperature PEMFC based on H3PO4-doped PBI, *Journal of Power Sources*, 162 (2006), pp. 547-552.
- [4] S. Yu, L. Xiao and B. C. Benicewicz, Durability studies of PBI-based High Temperature PEMFCs, *Fuel Cells* (Weinheim, Germany), 8 (2008), pp. 165-174.



## A 90L PLUG-FLOW MULTI-ELECTRODE BIOELECTROCHEMICAL REACTOR FOR TREATMENT OF EFFLUENT FROM BREWERY BASED ON CONTINUOUS PROCESS.

O.A Okpu<sup>1\*</sup>, J. Andresen<sup>2\*\*</sup>, and A. Harper<sup>3\*\*</sup>

Institute of Mechanical, Process and Energy Engineering, Sustainable Engineering Group, Heriot Watt University, Edinburgh, EH14 4AS (oao54@hw.ac.uk)

**Abstract** – This work focused on a pilot scale-up MFC system for actual wastewater treatment, using a 90L plug-flow multi electrode bio-electrochemical reactor that has two independent sub-reactors consisting of eight anodes and eight cathodes facing each other in both sub-units. This reactor is operated under continuous mode for 120 days based on energy self-sufficiency. Effluent from a brewery distillery was used as substrate with a biomass granular as catalyst. The two identical sub-reactors were operated separately in order to strengthen performance of the electrodes. Average COD and TSS efficiency across both sub-reactor were 93% and 95%, respectively and a CE of 45.67%, over the 120 days showing that MFCs can be run on continuously.

**Index Terms** – Effluent, Influent, MFCs, Multi-Electrode Bio electrochemical, Plug-flow

### I. NOMENCLATURE

MFC<sub>1-2, 3-4</sub> – Microbial Fuel Cell (1-2, 3-4); COD – Chemical Oxygen Demand; TSS – Total Suspended Solid

### II. INTRODUCTION

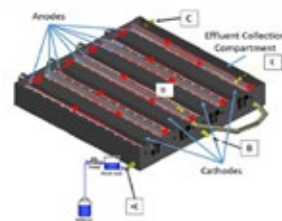
Considering the decrease in cost and increase in performance, microbial fuel cells (MFCs) have been generally accepted by most researchers as a sustainable technique for wastewater treatment [1]. Microbial Fuel Cell technology give a particular leverage over other bioelectrochemical treatment methods, which include direct electricity generation, low carbon footprint, low sludge yield, and ease of operation [2]. So far, a great variety of MFC-centred hybrid systems have been proved to be capable of changing the position of various wastewater from “waste” to “fuel” for electricity generation, such as brewery wastewater, domestic wastewater, landfill leachate, dye wastewater etc. [3]. However, scaling-up and energy utilization still constitute a major issue in the application of MFCs. Engaging the use of comparatively-sized MFCs that has an independently anode design with a plug-flow multi electrodes bioelectrochemical reactor is examined as most practicable or inevitable way of MFCs scaling-up. Therefore developing this kind of system remains a key challenge for construction of pilot scaling-up [4]. Therefore developing this kind of system remains a key challenge for construction of pilot scaling-up. Recent invention of construction of MFCs system is encountering difficulties related to its configuration and electrode systems. In this work, a pilot 90L plug-flow multi electrode bio- electrochemical reactor that has two independent sub-reactors consisting of four anodes and four cathodes facing each other in both sub-units for actual energy self-reliance and wastewater treatment was designed and constructed. Wastewater from a brewery situated somewhere South of Scotland was used as feed on a continuous mode through the entire sub-units. The aim of this study was to investigate the operations of the reactor: (a) determine viability of wastewater treatment; (b) formulate an energy balance which will estimate the ability of MFCs reactor to be able in pumping its effluent ;(c) investigate the use of this system on the practicability of pilot-scale MFCs fabrication in the area of up-scaling, stabilization of operations under real conditions, and

maintenance at ease. For this reason, a practicable demonstration of pilot-scale MFCs for both wastewater treatment process and energy utilization is suggested based on the investigations.

### III. METHODOLOGY

#### A. MFC configuration and operating conditions

Figure 1 shows the reactor that was divided into two subunits consisting of two anode and two cathodes with dual anode compartments surrounding a single cathode compartment with dual electrodes. The anodic compartments of each subunit were hydraulically connected in series, so that the effluent of the first chamber became the influent of the second. They were operated in continuous mode using anaerobic digestion liquid, with TCOD  $1102 \pm 515$  mg COD/L, TSS  $451.89 \pm 301.47$  mg/L, pH  $7.77 \pm 0.27$  in constant feeding at 1.008L/h, corresponding to a hydraulic retention time of 4 days. In order to allow continuous feed two dual channel peristaltic pumps (Masterflex L/S Easyload II, USA) were used, along with Masterflex C-Flex silicon tubes with internal diameter ranging from 3.1 to 9.7mm. The units were operated at ambient temperature  $22.60 \pm 1.71$  °C. Worth mentioning, that the units were not subjected at any artificial temperature fluctuations which could possibly affect their performance as the main purpose of this work was to observe their performance under real conditions.



**Figure 1:** Drawing Drawing of the Multi-electrode MFC unit showing the anode, cathode and effluent collection compartments. A) Influent input point for MFC<sub>(1-2)</sub>, B). Influent input point for MFC<sub>(3-4)</sub>, C). Effluent output point, D). Sampling port for MFC<sub>(1-2)</sub>, E). Sampling for MFC<sub>(3-4)</sub>.

#### B. Measurement, analyses and calculations

Samples of the influent and the effluent of the subunits were taken daily except from the days when polarization tests were taken place, as due to the different external resistance applied the samples would not be representative of the performance of the MFCs. Total Chemical Oxygen Demand (TCOD), Total Suspended Solids (TSS), pH in wastewater influent and effluent were measured according to standard methods [5].

### C. Electrochemical Measurement

All the individual cells were continuously monitored and the voltage were recorded in volts against time using a 20 channel multifunction data acquisition system (midi LOGGER GL820, GRAPHTEC) with one hour sample rate. All voltage measurements were also manually monitored and verified daily using a digital multimeter. Constant resistance discharge method was used to determine the polarization curves of each individual reactor (MFC-1, MFC-2, MFC-3, MFC-4) as described by [6]. In order to obtain the polarization and the power density curves, initially, each individual

	Influent	MFC <sub>1-2</sub>	MFC <sub>3-4</sub>
Conductivity ( $\mu\text{S/cm}$ )	$1418.30 \pm 184.74$	$1460.05 \pm 186.80$	$1756.74 \pm 213.34$
pHs	$7.78 \pm 0.28$	$7.91 \pm 0.24$	$7.83 \pm 0.21$
CEs	45.67%		

cell was kept in an open circuit mode without connecting any external resistance. Coulombic efficiency (CE) is used to express the amount of substrate that is converted into electricity and is estimated from the ratio of the output charge by a microbial fuel cell or other battery to the input of charge and is obtained in percentage according to [6-8]. The energy stored in the capacitor during a charging and discharging cycle was calculated using [9], while the electrical energy consumption of the pump was estimated using [10].

## IV. RESULT AND DISCUSSION

### A. Treatment of wastewater from a distillery

COD of effluent from a distillery was monitored for 120 days during this experiment. The behavior of the reactors were examined for wastewater treatment. At MFC<sub>1-2</sub>, the sub-reactor achieved a COD removal efficiency of 93% at an approximate removal rate of  $0.28\text{kg}/(\text{m}^3\cdot\text{d})$ , with effluent having COD of  $76.23 \pm 18.92\text{ mg/L}$ . For MFC<sub>3-4</sub>, the reactor achieved a COD removal efficiency of 91.75% at an approximate removal rate of  $0.28\text{kg}/(\text{m}^3\cdot\text{d})$ , with its effluent having COD of  $85.76 \pm 26.44\text{ mg/L}$ . This is represented on Figure 2. The total suspended solid (TSS) constitute a vital parameter in biological wastewater treatment. During operation at MFC<sub>1-2</sub>, the reactor had an effluent content of  $10.94 \pm 4.78\text{ mg/L}$  of TSS, which gives 97.38% of TSS removal at a removal rate of  $0.752\text{kg}/\text{m}^3\cdot\text{d}$ . For the corresponding TSS and removal value of MFC<sub>3-4</sub>, it was observed that the sub-unit had a TSS removal value of  $30.66 \pm 14\text{ mg/L}$  that represents 92.21% of the TSS removed at same removal rate. The overall average TSS value of the reactor is  $20.8 \pm 9.39\text{ mg/L}$  which is approximately 95% of the TSS removal from the sub-reactor as shows in Figure 2. This results shows the representation of various influent concentration at different days.

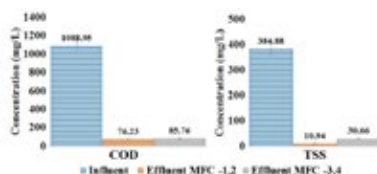


Figure 2: Water waste treatment for MFC<sub>(1-2)</sub> and MFC<sub>(3-4)</sub>.

Furthermore, the TSS removal in this pilot design of MFCs can be said to have occur due to the two major different sectors that

includes the particulate to soluble substrate, interference by the anode materials, and settling of suspended solids in the sub-units.

Also, a further study was conducted in investigating the pH and conductivity of the wastewater. This is considered as vital parameter for stability of waste water treatment using MFCs. There was seemingly changes in the pH over the influent and effluent for the both MFC1-2 and MFC4-5. The various average pH values are  $7.78 \pm 0.27$ ,  $7.91 \pm 0.25$ , and  $7.8 \pm 0.21$  respectively. For the conductivities, the average value for the influent, and the effluent for both MFC1-2 and MCF3-4 are represented as follows,  $1418.30 \pm 184.74\mu\text{S/cm}$ ,  $1460.05 \pm 186.80\mu\text{S/cm}$ , and  $1756.74 \pm 213.34\mu\text{S/cm}$  **Table 1**.

To evaluate the viability of energy generation, the power output was studied throughout the whole demonstration duration. A relative potential of each sub-unit was investigated, with an average maximum power density of  $180.90 \pm 120.41\text{ mW/m}^3$  before external capacitors were introduced to the reactors for self-sufficient operation. At day 15-60 of operations, the average maximum power density was  $38.53 \pm 28.96\text{ mW/m}^3$  with a corresponding current density of  $56.68 \pm 30.63\text{ mA/m}^3$ . At the end of day 61-120, an approximate increase of 8% of the average maximum power density ( $291.06 \pm 73.26\text{ mW/m}^3$ ) was experienced. This has a corresponding average maximum current density of  $666.84 \pm 252.88\text{ mA/m}^3$  as represented in **Fig. 3**.

Table 1: Changes in conductivities, pHs and CEs.

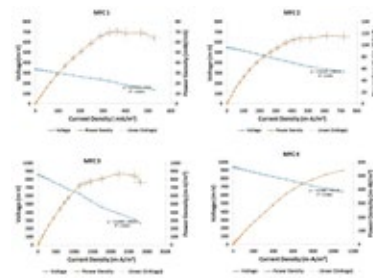


Figure 3: Polarization curve and Power Density for four sub-MFCs over 120 days of operation.

The energy generated and consumed were represented as kilo watt hour per cubic meter of the wastewater influent ( $\text{kWh/m}^3$ ). In this study, energy consumption was resolved to be the pumping process of feed into the reactor. The capacitor oriented system produces a maximum voltage of  $0.92 \pm 0.015\text{ V}$  at both the influent concentration. The average energy generated by the overall system is  $0.64 \pm 0.13\text{ kWh/m}^3$ , the energy generated consumed by the pump is  $0.0036\text{ kWh/m}^3$ , and the positive energy balance is  $0.6367 \pm 0.13\text{ kWh/m}^3$ .

## V. CONCLUSION

A 90L plug-flow multi-electrode biochemical dual MFCs was designed for the treatment of brewery spend wash in continuous operation mode that is energy self-sufficient at ambient temperature. The COD and TSS removal efficiency were 93% and approximately 95% respectively when fed with untreated wastewater. The overall maximum power and current density shows a reduction during operation on day 15-60, and rapid increase in day 61-120 after a partial maintenance operation was conducted. On this pilot scale-up study, treatment of wastewater and utilization of energy was looked into within respect to our discoveries. In all, this study considered appropriate parts that are promising for energy self-sufficiency in the operation of wastewater treatment.

## MICROBIAL FUEL CELLS TREATING URINE AS A SOURCE OF DISINFECTANT: A PATHOGENS' KILLING EFFICACY STUDY.

Oluwatosin Obata<sup>a\*</sup>, Irene Merino Jimenez<sup>a</sup>, John Greenman<sup>a,b</sup>, Ioannis Ieropoulos<sup>a\*\*</sup>,

<sup>a</sup> Bristol BioEnergy Centre, Bristol Robotics Laboratory, University of the West of England, BS16 1QY, UK

<sup>b</sup> Biological, Biomedical and Analytical Sciences, University of the West of England, BS16 1QY, UK

\*Tosin.Obata@uwe.ac.uk, \*\*ioannis.ieropoulos@brl.ac.uk

**Abstract** - Direct utilization of untreated urine for electricity generation has been reported in microbial fuel cells, where electricity generated can be used to power electronic devices. In addition, the catholyte accumulated at the cathode in the MFCs, could be exploited for its antimicrobial properties. In this study, the bactericidal properties of the catholyte generated from ceramic based MFCs cascade treating urine were tested against five bioluminescent pathogenic bacteria. Luminometer assay was conducted on the target pathogenic bacteria using a single-tube FB12 luminometer to quantify bioluminescence which correlates with culture viability in relative light units (RLU) using phosphate buffer saline as the control. Results of bacteria kill curve analysis indicate that all the pathogens tested were susceptible to the antimicrobial properties of the catholyte. This work suggests that the catholyte, generated as a byproduct of the power generation process of urine fed MFCs could be exploited as disinfectants in urinals.

**Keywords:** catholyte, MFCs, pathogen killing, urine

### I. INTRODUCTION

Microbial fuel cell (MFC) systems are an innovative technology for the direct conversion of organic matter into electricity generation. MFCs exploit the unique abilities of certain bacteria to donate electrons to an anode electrode, as a result of their normal metabolic reactions. Electricity is generated as a result of the biomass degradation as the anode becomes the terminal electron acceptor (Santoro et al. 2013; Walter et al. 2016). Interest in MFCs has grown significantly over the past decade as a result of increased interest and range of applications (Santoro et al. 2017). Direct utilization of untreated urine for electricity generation has been reported in microbial fuel cells, where electricity generated from the MFCs can be effectively used to power electronic devices. Nutrient recovery, such as ammonium, nitrogen or phosphate, has also been achieved from microbial fuel cells treating urine. Therefore, the utilization of untreated urine in microbial fuel cells could be used for both energy generation and product recovery. In addition, there is currently another potential application of the MFCs technology, where the catholyte accumulated at the cathode in the MFCs, could be exploited for its antimicrobial properties. The catholyte production in

ceramic MFCs is attributed to a combination of; i) water or hydrogen peroxide formation from the oxygen reduction reaction in the cathode, ii) water diffusion and iii) electroosmotic drag through the ion exchange membrane (Merino, et al., 2016). In the current study, catholyte synthesized within the cathodic chamber of the MFCs cascade were collected and tested against known pathogenic bacteria.

### II. MATERIALS AND METHODS

MFCs were assembled using terracotta cylinders sealed at one end (Orwell Aquatics, UK) with the following dimensions: length 10 cm, outside diameter 2.9 cm, inside diameter 2.1 cm, wall thickness 4 mm. The anode electrode was made of carbon veil (carbon loading 60 mg/cm<sup>2</sup>) with a macro surface area of 500 cm<sup>2</sup>, which was folded and wrapped around the terracotta tube with the use of nickel chromium (Ni-Cr) wire for current collection. The cathode was made of activated carbon (30% wet proofed with PTFE) as previously described (Gadja et al., 2016). The 30 cm<sup>2</sup> activated carbon-coated cathode was inserted into the cylinder and connected via stainless steel crocodile clip. The whole reactor was placed in the plastic container (60ml working volume) where the outer anode surface was fully immersed into the anolyte. Ni-Cr wire was used to connect both electrodes to the multi-channel Agilent 34972A (Farnell, UK) logging device and the electrical load. The bactericidal properties of the catholyte collected from urine-fed 3-MFCs cascade were tested against five bioluminescent pathogenic bacteria namely: *Escherichia coli* Nissle 1917, *Pseudomonas aeruginosa* PAO1, *Salmonella enterica* Typhimurium DT104, *Salmonella enterica* Enteritidis PT4, *Staphylococcus aureus* RN4220. Luminometer assay was conducted on the target pathogenic bacteria using a single-tube FB12 luminometer to quantify bioluminescence which correlates with culture viability in relative light units (RLU). Phosphate buffer saline (PBS pH 10.2) was used as the control to evaluate the biocidal efficacy. The pH of PBS was raised to 10.2 using conc. sodium hydroxide to match the pH of the catholyte.

### III. RESULTS AND DISCUSSION

The results of current generation indicated that all three MFCs produced more than 3mA with an average of up to 3.52mA after 12 days. In the same vein, power output from each of the MFCs was greater than 1mW, with an average power generation of 1.24mW after 12days of operation (Fig. 1).

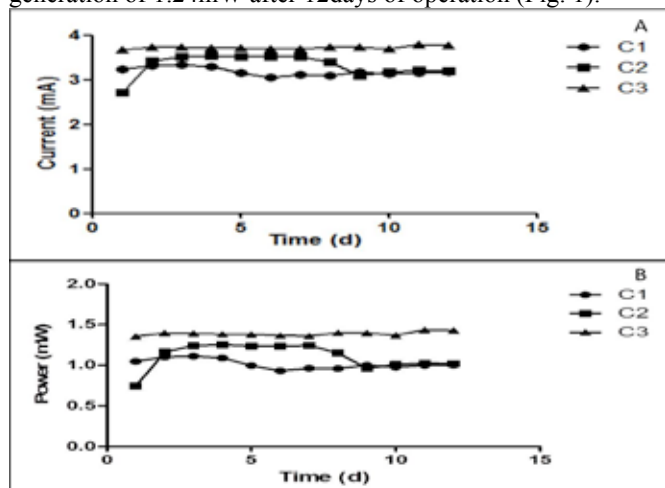


Figure 1. Result of (A) current and (B) power output of the cascade over a 12 day period. Catholyte from the 3 MFCs were collected and mixed before analyses and use.

Previous research has shown that power output is a determinant of the quality of the synthesized catholyte (Merino et al, 2016). Higher power output in MFCs is expected to enhance the catholyte potency as a biocidal agent.

Results of pathogen analysis showed that all pathogens increased with the addition of PBS even at an increased pH of 10.2. However, significant reduction in number was recorded in all pathogens tested against neat catholyte of similar pH. This result suggests that pH was not the main or only parameter responsible for the biocidal properties of the catholyte (Fig. 2).

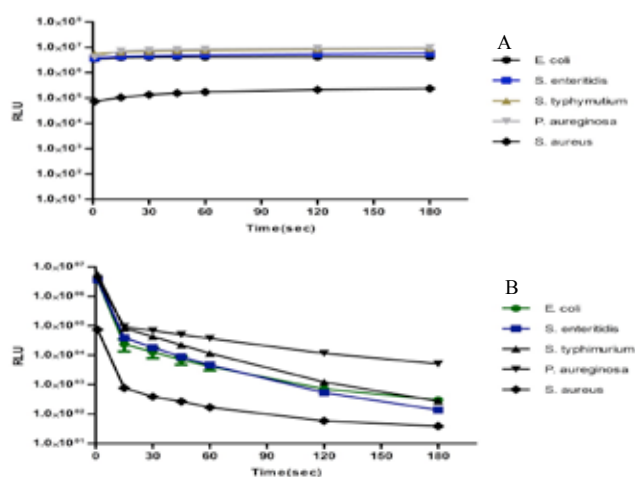


Figure 2. Bioluminescence measurement of pathogens exposed to neat (A) PBS (control- pH 10.2) and (B) catholyte (pH 10.2) over 180 minutes. RLU: Relative light unit

Results of bacteria kill curve analysis indicate that all the pathogens tested were susceptible to the antimicrobial properties of the catholyte with at least 3-fold order of magnitude reduction recorded. *E. coli*, *S. Typhimurium* DT104, *S. Enteritidis* PT4 were the most susceptible pathogens, with over 4-log reduction in pathogen numbers in 180 sec (Fig. 2). Overall, results showed that the unique composition of the catholyte brought about pathogen killing recorded in this study.

### IV. CONCLUSION

This work has shown catholyte synthesized as a byproduct of the power generation process in urine fed MFCs as a possible bactericidal agent (due to its unique composition). Thus, the catholyte generated could be exploited as disinfectants in urinals thereby reducing the need for synthetic disinfectants. Although catholyte has a uniquely high pH, this has been shown not to be the main bactericidal property of the catholyte. More work is currently being conducted to analyze the composition of the catholyte produced from different ceramic-based MFCs.

### ACKNOWLEDGMENT

This work is funded by the Bill and Melinda Gates Foundation.

### REFERENCES

1. Santoro C, Ieropoulos I, Greenman J, Cristiani P, Vadas T, Mackay A, et al. Power generation and contaminant removal in single chamber microbial fuel cells (SCMFCs) treating human urine. *Int J Hydrogen Energy*. 2013;38(26):11543–51.
2. Walter XA, Stinchcombe A, Greenman J, Ieropoulos I. Urine transduction to usable energy: A modular MFC approach for smartphone and remote system charging. *Appl Energy* [Internet]. 2016;4–10. Available from: <http://dx.doi.org/10.1016/j.apenergy.2016.06.006>
3. Santoro C, Arbizzani C, Erable B, Ieropoulos I. Microbial fuel cells: From fundamentals to applications. A review. *J Power Sources* [Internet]. 2017;356:225–44. Available from: <http://dx.doi.org/10.1016/j.jpowsour.2017.03.109>
4. Merino I, Greenman J, Ieropoulos I. Electricity and catholyte production from ceramic MFCs treating urine. *Int J Hydrogen Energy* [Internet]. 2016;42(3):1–9. Available from: <http://dx.doi.org/10.1016/j.ijhydene.2016.09.163>
5. Gajda, Iwona, John Greenman, Chris Melhuish, and Ioannis Ieropoulos. 2015. "Simultaneous Electricity Generation and Microbially-Assisted Electrosynthesis in Ceramic MFCs." *Bioelectrochemistry* 104:58–64. Retrieved (<http://dx.doi.org/10.1016/j.bioelechem.2015.03.001>).



## ADVANCED TESTING AND ANALYSIS OF SOFC DEGRADATION

D. Vladikova\*, Z. Stoyanov\*, B. Burdin\*, J. Laurentin\*\*, D. Montinaro\*\*\*, and M. Hubert\*\*

\*Institute of Electrochemistry and Energy Systems - BAS, 10 Acad. G. Bonchev St., 1113 Sofia, (Bulgaria)

\*\*Univ. Grenoble Alpes – CEA/LITEN, 17 rue des Martyrs, 38054 Grenoble, (France)

\*\*\*SOLIDpower S.p.A, Viale Trento 117, 38017 Mezzolombardo, (Italy)

**Abstract** - Solid Oxide Fuel Cells (SOFC) are regarded as a promising technology for economic power generation due to their high efficiency and large fuel flexibility. Durability is a severe hurdle towards their deployment. The near future targets in respect to Degradation Rate are about 0.1%/1000h, which needs improved monitoring and diagnostics. This work aims at introducing a new approach with increased sensitivity and information capability, named Differential Resistance Analysis (DRA). It applies differential analysis of the volt-ampere characteristics and thus operates with the Differential Resistance and its evolution during long term testing. Since derivatives are more sensitive to small deviations, the method has very high sensitivity, which is demonstrated on SOFC button cells tested up to 9000 hours. The results show that DRA is about 10 times more sensitive in respect to the classical Degradation Rate evaluation based on registration of the voltage decrease at constant current.

**Index Terms** - Degradation rate, differential resistance analysis, durability, volt ampere characteristics.

### I. INTRODUCTION

Solid Oxide Fuel Cells (SOFCs) appear as an attractive technology for economic power generation, presenting high efficiency and large fuel flexibility. One of the most severe hurdles towards their deployment is durability. Since the near future durability targets for stationary applications should reach 80 000 h, sustained innovation activities are needed in both diagnostics and manufacturing methods. An important focus area is the correct introduction of accelerated testing algorithms and sophisticated performance/degradation models to quantify the accelerating impact. Those approaches need improved monitoring with increased sensitivity to evaluate the state of health of a working FC, to detect and identify first signals of

critical operation, to introduce mitigation strategies for reversible degradation and to determine lifetime.

The current requirements for operational stability of fuel cells define the parameter “degradation rate” (DR). The near future target for SOFC is about 0.1% for 1000 hours. Usually for its definition the decrease of the voltage  $U$  at constant current  $I$  is used. During long term durability tests volt ampere characteristics (VAC) are taken combined with impedance measurements at definite working points. They form a big experimentally linked data set which is not still effectively exploited.

This presentation aims at introducing a new approach for complementary analysis of the accumulated data, named Differential Resistance Analysis (DRA). It applies differential analysis of the volt-ampere characteristics and thus operates with the differential resistance and its evolution during long term testing. The method ensures increased sensitivity and information capability in respect to degradation monitoring and diagnostics.

### II. RESULTS AND DISCUSSION

VACs are sensitive to operating parameters and degradation which reflects in the change of their shape. At constant operating conditions those changes are caused by degradation. Thus VAC shape analysis can become performance indicator.

The most commonly applied characteristic indicators extracted from the VAC are: open circuit voltage  $U_0$ , maximal power density  $P_{\max}$ , internal resistance  $R_i$  at  $P_{\max}$  and its corresponding area specific resistance  $ASR_{P_{\max}}$ . However, for another working point,  $R_i$  will have different value. For the calculation of the internal resistance in a given VAC point, two

approaches may be used - secant or tangential [1].

The developed method for analysis of VAC curves and their comparative assessment is performed through the tangential approach, calculating the parameter Differential Resistance  $R_d$ , i.e. the derivative of the voltage  $U$  in respect to the corresponding current  $I$  for every VAC point:

$$R_d = dU/dI \quad (1)$$

The new moment is the Differential Resistance Analysis, which gives the change of  $R_d$  as a function of the current (Fig. 1a) and reflects the VAC shape. Three characteristic regions can be separated: Region I which is connected with activation losses, Region 2, which concerns the transport losses and Region 3 where the gas diffusion limitations are dominating.

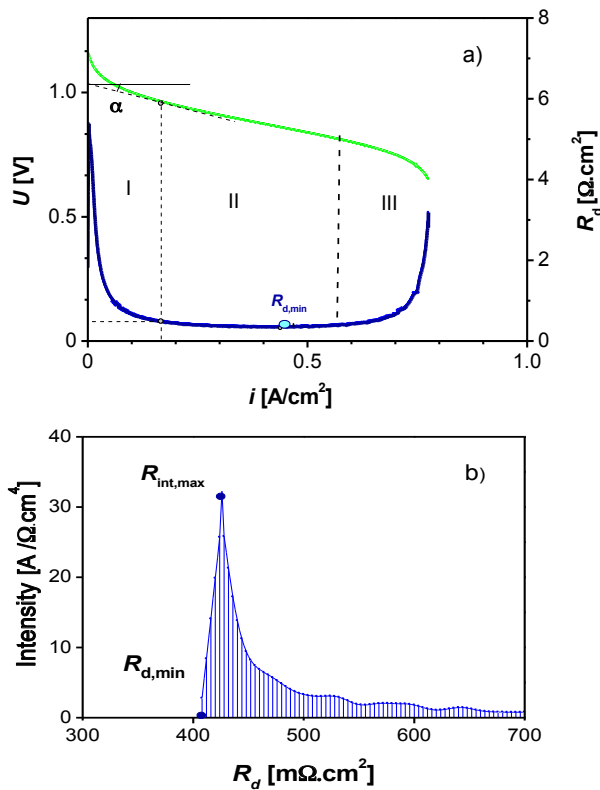


Fig. 1. Differential Resistance Analysis: (a) VAC (green) and  $R_d/I$  dependence (blue); (b) Spectral transform of the  $R_d/I$  dependence

The minimum of the differential resistance  $R_{d,min}$  is an important characteristic point for the cell performance. It reflects the state of health of the cell/stack at constant operating conditions, since it is determined by the intrinsic properties of the system and not by the external conditions (for instance the load current).

The application of the DRA tool makes the changes in the VACs during operation comparable and informative. Since derivatives are more sensitive to small deviations, the method has very high sensitivity. The operation with derivatives, however, increases the influence of the noise. The noise immunity of the DRA is improved by the spectral transform of the Differential Resistance (Fig. 1b). The spectral peak describes Segment II in Fig. 1a, while segments I and III are introduced in the spectral tail. The spectrum has 2 characteristic points:  $R_{d,min}$  and  $R_{d,max}$ , the second one giving the most stable value of the differential resistance, i.e. the value which is observed in a wider current range. The intensity  $S_j$  of the spectral pick

$$S_j = di/dR_d \quad (2)$$

is proportional to the current range with similar values of the Differential Resistance. The sharper the spectral line, the smaller the distribution of this parameter.

The DRA needs higher quality of the measurements and not a big number of data. For one volt-ampere characteristic, about 30-40 points are sufficient, but they should be measured after stabilization of the operating conditions. More details about the measurement conditions are given in the DRA protocol [2].

### III. CONCLUSION

The sensitivity of the DRA is illustrated on VACs of SOFC button cells tested between 1000 and 9000 hours. The results show that the analysis is about 10 times more sensitive than the classical evaluation of the voltage decrease at constant current.

The DRA based on the measured VACs is a useful tool with increased sensibility towards changes in the fuel cell during operation caused to degradation, which can ensure collection of reliable data from shorter tests.

### ACKNOWLEDGMENT

The research has received funding from FP7/2007-2013 Fuel Cells and Hydrogen Joint Undertaking (FCU-JU-2013-1) under grant agreement No 621207 and the Bulgarian National Science Fund under grant agreement E02/3/12.12.2014.

### REFERENCES

- [1] Hjelm, J., Degradation testing – quantification & interpretation, 2nd International Workshop on Degradation Issues of Fuel Cells, Thessaloniki, Greece, 21-23 September, 2011; Handbook of Test Procedures and Protocols, Chapter 2: Testing Procedures from the Literature, <http://www.durablepower.eu/index.php/handbook>
- [2] Stoyanov, Z., Vladikova, D., Burdin B., Recommendation for Measurements of Volt-Ampere Characteristics of Fuel Cells for Diagnostic Purposes, Handbook of Test Procedures and Protocols, Chapter 3: ENDURANCE Procedures and Protocols, <http://www.durablepower.eu/index.php/handbook>

## FUEL CELL BASED-ON POWERTRAIN TO HYBRIDIZE SMALL UNMANNED AERIAL VEHICLES

T. Donato, A. Ficarella and L. Spedicato  
University of Salento, 73100 Lecce (Italy)

**Abstract** - The proposed investigation aims at increasing the endurance of a small unmanned aerial vehicle (UAV) where the power request for propulsion can be satisfied by means of a battery and a fuel cell. The hybrid configuration allows the required power to be obtained at take-off and the fuel cell to support the battery in order to maintain the state of charge (SOC) in the other phases of flight. This operating mode avoids deep discharging, when the battery SOC falls down a suitable threshold, and overcharging, which exposes to risk of explosion in case of lithium batteries. The cost of adding different capacity batteries was evaluated in terms of the increase of mass and consequently decrease of endurance. The power split was conveniently defined at take-off to prevent from excessive hydrogen consumption and to maximize the endurance with respect to the non-hybrid configuration in which the only fuel cell is used.

**Index Terms** – gaseous hydrogen cells, lithium batteries, hybrid unmanned aircraft, indirect environmental impact.

### I. INTRODUCTION

Fuel cells can be used to extend the range of small unmanned aircraft because electric power systems only based on batteries are characterized by low energy density and offer endurance that varies within the interval from about 60 to 90 minutes [1]. Polymer electrolyte membrane (PEM) fuel cells are appropriate to generate electrical power on board because of their low operating temperature and high energy density [2]. Lithium batteries are generally preferred because they have greater power-to-weight ratio among the available storage system technologies [3]. Some literature works concern with the comparison between battery and fuel cell technologies for electric aircraft and they mainly consist of correctly estimating the endurance [4-6]. The indirect environmental impact for hydrogen production from methane reforming reaction can be evaluated by [5]. The aim of the proposed investigation was to design a hybrid electric power system for a UAV, with mass of 10 kg, including airframe, motor, propeller and control board

but excluding the source of power. The wingspan is 5.2 m and the lift over drag ratio is 17. The UAV can be equipped with a PEM fuel cell, with a mass of 6 kg, including the tank, the fuel, the regulator and the cooling system. The fuel cell is characterized by 36 cells, operating at 55 °C, and it has a maximum operating power of 600W. The hydrogen is gaseous and compressed at 5000 psi in a tank with a capacity of 22 liters. In hybrid configuration, a lithium polymer (Lipo) battery is added and its mass is summed to the base mass of 16 kg. The considered battery has a nominal operating voltage of 22.2V, a maximum continuous discharge current of 25A and it can supply a maximum power of 630W. The curve of required power was defined by considering the flight profile of a similar fuel cell powered UAV [2] excluding high winds and scaling the power because of the changed vehicle mass according to [7]. The fuel cell slowly responds to sudden load and the battery can buffer the fuel cell from transient current demands. But this event does not occur for the considered mission data. The flight speed was about 33 m/s at cruise. The power to be delivered by battery and fuel cell was obtained by resorting to the backward approach for complex aircraft [8].

### II. DESIGN AND MODELING

Different Lipo batteries were considered for the hybrid configuration with rated capacity from 8Ah to 16Ah. Their mass specifications are reported in Table I. If the UAV is equipped with the only fuel cell, it needs 560W at take-off and 300W at cruise [2]. When equipping with both fuel cell and battery, the take-off and cruise power increase with respect to the non-hybrid configuration because of the increased UAV mass as shown in Table I. At take-off both the battery and the fuel cell have to give power because the fuel cell alone is not able to satisfy the request. The take-off power to be delivered from the battery in splitting mode is  $P_{batt} = \alpha \cdot P_{prop}$ , where  $\alpha$  is the splitting factor and  $P_{prop}$  is the required propulsive power.

TABLE I

MASS AND POWER SPECIFICATIONS

Rated capacity (Ah)	Battery mass (kg)	UAV mass (kg)	Take-off power (W)	Cruise power (W)
8	1.58	17.58	616	330
10	1.98	17.98	630	337
12	2.37	18.37	644	344
14	2.80	18.80	659	352
16	3.27	19.27	675	361

The remaining power is given by the fuel cell. This mode was imposed for the first 100 minutes in order to cover up the take-off. In this phase of flight, the battery is discharged up to 60% of the SOC to safeguard the battery life. The fuel cell allows the battery to be recharged after that the fixed time of 100 minutes is elapsed so as to restore the initial capacity. While providing for recharging, the fuel cell satisfies the goal of propulsion. When the SOC reaches 100%, that is the full charge, the working mode switches from fuel cell to battery. In this way, the battery becomes the unique source of power as long as its SOC is over 60%. The fuel cell becomes again operative for recharge and propulsion when the SOC approaches 60%. Therefore, the charge-discharge cycle goes on and the fuel cell is able to recharge if the hydrogen is available. When the UAV runs out of fuel, the fuel cell cannot continue to recharge and so the battery is discharged at the SOC of 20%. The endurance is set as the flight time at which this SOC value is obtained. The SOC and the fuel consumption were estimated as in [5]. The curves of SOC and available hydrogen for the 8Ah Lipo battery, with recharge current of 0.7C and  $\alpha = 0.15$  are shown in Fig. 1.

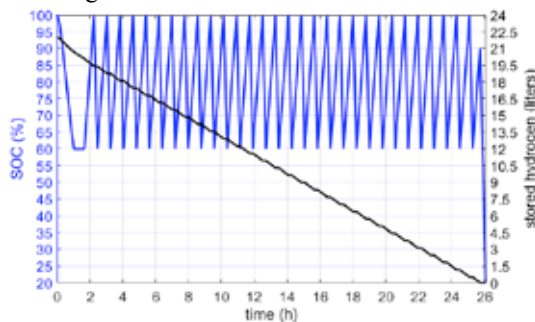


Fig. 1. Battery SOC and stored fuel

### III. SIMULATION RESULTS

A design of experiments was performed to evaluate the endurance when changing the capacity of the battery, the recharge current and the splitting factor between fuel cell and battery. The results are shown in Table II. The configuration of Fig. 1 with the best setting shows an endurance of 26.1 h, greater 8% than the value obtained in case of non-hybrid configuration, which turns out to be of 24.2 h. A sensitivity analysis revealed that  $\alpha$  has to be suitably chosen because a greater or smaller value than the bounds given in Table II entails an unfeasible configuration.

TABLE II  
ENDURANCE VALUES (IN HOURS)

	$\alpha$	0.1C	0.2C	0.3C	0.4C	0.5C	0.6C	0.7C	0.8C	0.9C	1C
8Ah	0.1	23.9	24.2	24.4	24.7	25.0	25.2	25.3	22.7	20.6	16.6
	0.15	24.6	24.9	25.2	25.4	25.7	26.0	26.1	23.3	20.9	17.0
10Ah	0.1	22.1	22.5	22.8	23.1	23.3	21.7	18.9	14.0	4.6	
	0.15	24.3	24.7	25.0	25.3	25.6	23.8	20.5	15.1	5.0	
	0.2	24.5	24.9	25.3	25.6	25.9	24.0	20.7	15.2	5.3	
12Ah	0.15	23.9	24.3	24.7	25.0	22.3	18.4	2.2			
	0.2	24.3	24.8	25.2	25.5	22.7	18.7	2.2			
14Ah	0.15	23.0	23.5	23.9	21.7	17.3	6.3				
	0.2	24.1	24.6	25.0	22.6	18.0	2.7				
	0.25	24.3	24.8	25.2	22.9	18.1	2.4				
16Ah	0.2	23.7	24.2	24.2	19.0	6.7					
	0.25	24.0	24.5	24.6	19.2	6.8					
	0.3	24.1	24.7	24.7	19.3	6.8					

### IV. CONCLUSIONS

A hybrid electric power system was designed for a UAV and the endurance values were compared for different Lipo batteries. The best endurance was obtained for low capacity battery and the recharge current had to be reduced at increasing the capacity. The use of fuel cell is crucial because a fast battery discharge occurs at take-off and the UAV is not able to complete this phase if equipped with the only battery.

### REFERENCES

- [1] Kim, T., Kwon, S., Design and development of a fuel cell-powered small unmanned aircraft, International Journal of Hydrogen Energy, Volume 37, 2012, pp. 615-622.
- [2] Swider-Lyons, K., Stroman, R., Gould, B., Rodgers, J., MacKrell, J., Schuette, M., Page, G., Hydrogen Fuel Cells for Small Unmanned Air Vehicles, ECS Transactions, Volume 64, 2014, pp. 963-972.
- [3] Khaligh, A., Zhihao, L., Battery, ultracapacitor, fuel cell, and hybrid energy storage systems for electric, hybrid electric, fuel cell, and plug-in hybrid electric vehicles: state of the art, IEEE Transaction on Vehicular Technology, Volume 59, 2010, pp. 2806-2814.
- [4] Verstraete, D., Lehmkuehler, K., Gong, A., Harvey, J.R., Brian, G., Palmer, J.L., Characterization of a hybrid, fuel-cell-based propulsion system for small unmanned aircraft, Journal of Power Sources, Volume 250, 2014, pp. 204-211.
- [5] Donato, T., Ficarella, A., Spedicato, L., Arista, A., Ferraro, M., A new approach to calculating endurance in electric flight and comparing fuel cells and batteries, Applied Energy, Volume 187, 2017, pp. 807-819.
- [6] Donato, T., Ficarella, A., Spedicato, L., A method to analyze and optimize hybrid electric architectures applied to unmanned aerial vehicles, accepted for publication in Aircraft Engineering and Aerospace Technology.
- [7] Ralph, D., Lorenz, Flight Power Scaling of Airplanes, Airships, and Helicopters: Application to Planetary Exploration, Journal of Aircraft, Volume 38, 2001, pp. 208-214.
- [8] Donato, T., Ficarella, A., Spedicato, L., Development and validation of a software tool for complex aircraft powertrains, Advances in Engineering Software, Volume 96, 2016, pp. 1-13.

## EFFECT OF THE GAS DIFFUSION LAYER DEFORMATION ON THE TRANSPORT PROCESSES AND PERFORMANCE OF A PEM FUEL CELL WITH INTERDIGITATED FLOW CHANNELS

Shian Li and Bengt Sundén

Department of Energy Sciences,  
Lund University. P.O. Box 118, SE-22100, Lund, (Sweden)

**Abstract** – When the assembly force is applied, the gas diffusion layer (GDL) deformation is observed and the geometry and transport parameters are also changed. Accordingly, the transport processes and cell performance are affected due to the deformation effect. In the present study, a three-dimensional, non-isothermal, two-phase flow model was developed and applied to investigate the effect of GDL deformation on transport phenomena in Proton exchange membrane (PEM) fuel cells with interdigitated flow channels. The current densities, liquid water saturation distributions, and oxygen concentration distributions for PEM fuel cells with homogeneous and inhomogeneous compression are presented and compared.

**Index Terms** – *inhomogeneous compression, interdigitated flow field, numerical simulation, PEM fuel cells.*

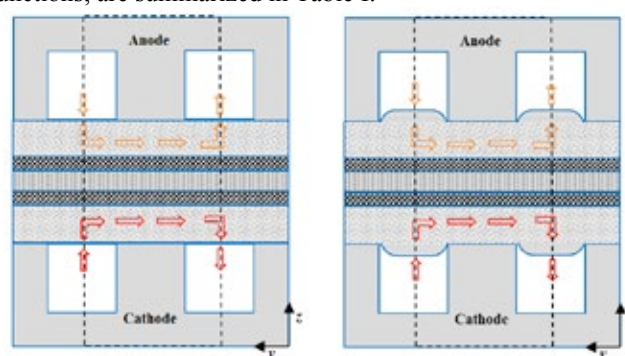
### I. INTRODUCTION

Proton exchange membrane (PEM) fuel cells are considered as the most promising alternative energy conversion devices with a wide range of applications due to their attractive advantages [1]. The gas flow channels fabricated on the current collector provide and guide reactant gases to the reaction sites at the catalyst sites. Many configurations of channels have been investigated in PEM fuel cells, e.g., parallel channel, serpentine channel, interdigitated channel and pin-type flow field [2]. The interdigitated channel forces the reactants to flow from one channel to neighbouring channel through the gas diffusion layer (GDL) under the rib. The GDL is one of the fuel cell components, which provides pathways for reactants/products, conducts electrical current, and provides mechanical support. In order to avoid gas leakage and minimize the contact resistance between different layers, a compression force is applied on the fuel cell stacks. With compression, the GDL deformation is observed and the geometry and transport parameters are changed. The effect of GDL deformation on transport

characteristics and cell performance in a PEM fuel cell with parallel channels was already widely and extensively investigated in the past decade [3-4]. However, the information of PEM fuel cells with interdigitated flow fields accounting for the deformation effect is still limited in the literature and therefore additional research is needed.

### II. MODEL DESCRIPTION

The computational domains of PEM fuel cells with homogeneous and inhomogeneous compression are shown in Fig. 1. The shape of GDLs under 1.0 MPa assembly force reported by Zhou et al. [4] is employed in the present study. In the mathematical model, the fluid flow is laminar; ideal gas law is applied for reactant gases; the catalyst layer is isotropic and homogeneous. The governing equations implemented in the commercial software Fluent by using the user defined functions, are summarized in Table I.



**Fig. 1. Schematic illustrations of the computational domains of PEM fuel cells: (a) homogeneous compression, (b) inhomogeneous compression.**

The properties of GDL are varied due to the deformation



resulting from the assembly force. The GDL porosity is determined by the following expression:

$$\varepsilon = 1 - (1 - \varepsilon_0) \frac{\delta_0}{\delta} \quad (9)$$

where  $\varepsilon_0$  is the initial porosity,  $\delta_0$  the initial thickness,  $\delta$  the thickness after compression,  $\varepsilon$  the porosity after compression.

The GDL permeability is calculated as:

$$K = \frac{d_f^2 \varepsilon^3}{16 k_{CK} (1 - \varepsilon)^2} \quad (10)$$

where  $d_f$  is the fiber diameter,  $k_{CK}$  the Carman-Kozeny constant. The value of  $\varepsilon$  is constant for the homogeneous case, while it is a function of y-coordinate for the inhomogeneous case. The transport parameters (permeability, mass diffusivity, thermal conductivity, and electrical conductivity) are affected by the variation of  $\varepsilon$ . The operating conditions: 353K, 1 atm, 100% relative humidity for both sides.

TABLE I  
GOVERNING EQUATIONS

Equation	General Form	
Mass	$\nabla \cdot (\rho \vec{u}) = S$	(1)
Momentum	$\nabla \cdot (\rho \vec{u} \vec{u}) = \nabla \cdot (\mu \nabla \vec{u}) - \nabla P + S_m$	(2)
Species	$\nabla \cdot (\rho \vec{u} Y_i) = \nabla \cdot (\rho D_{eff,i} \nabla Y_i) + S_s$	(3)
Energy	$\nabla \cdot (\rho C_p \vec{u} T) = \nabla \cdot (k_{eff} \nabla T) + S_T$	(4)
Electric Potential	$\nabla \cdot (\sigma_{eff,s} \nabla \phi_s) + S_{ep} = 0$	(5)
Proton Potential	$\nabla \cdot (\sigma_{eff,m} \nabla \phi_m) + S_{pp} = 0$	(6)
Liquid Water	$\nabla \cdot (\rho_l f(s) \vec{u}) = \nabla \cdot (\rho_l D_s \nabla s) + S_{hw}$	(7)
Dissolved Water	$-\nabla \cdot \left( \frac{n_d}{F} \sigma_m \nabla \phi_m \right) = \nabla \cdot \left( \frac{\rho_m}{M_m} D_\lambda \nabla \lambda \right) + S_{dw}$	(8)

### III. RESULTS AND DISCUSSION

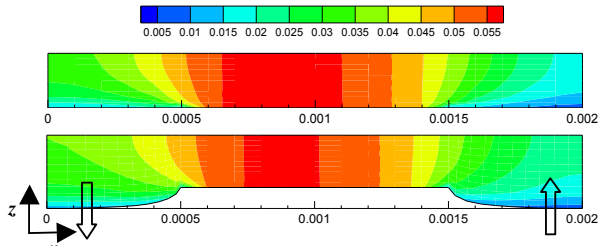


Fig. 2. Liquid water saturation distributions in the middle plane of GDLs: (a) homogeneous compression, (b) inhomogeneous compression.

The current densities of PEM fuel cells with homogeneous and inhomogeneous compression at 0.6 V are 0.4685 A/cm<sup>2</sup>, 0.4682 A/cm<sup>2</sup>, respectively. The liquid water saturation distributions in the middle plane of GDLs along the flow direction are shown in Fig. 2. It can be seen that the maximum water saturation appears at the regions under the rib for both cases, and the water saturation of the inhomogeneous case is lower than that of the homogeneous case. This is because the

porosity and permeability of GDL at the regions under the channel for the inhomogeneous case are higher than those of the homogeneous case, and then liquid water can be easily removed from the GDL.

The oxygen concentration distributions in the middle plane of GDLs along the flow direction are presented in Fig. 3. It is observed that the oxygen concentration gradually decreases from the inlet region to the outlet region for both cases. However, the oxygen concentration at the inlet region of the inhomogeneous case is higher than that of the homogeneous case. This is also attributed to the high porosity at this region.

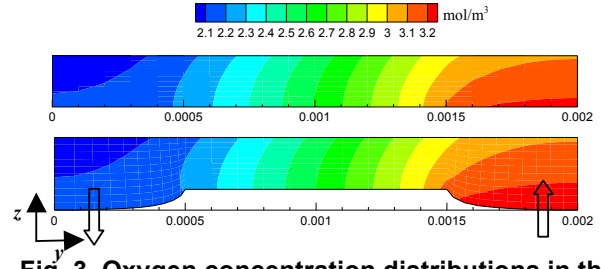


Fig. 3. Oxygen concentration distributions in the middle plane of GDLs: (a) homogeneous compression, (b) inhomogeneous compression.

### IV. CONCLUSIONS

The current densities of PEM fuel cells with homogeneous and inhomogeneous compression are identical. It is concluded that the cell performance is not affected by the inhomogeneous compression effect. However, the local transport processes are different due to the non-uniform distribution of porosity.

### ACKNOWLEDGMENTS

The work was carried out at the Department of Energy Sciences, Lund University. The first author gratefully acknowledges the financial support from China Scholarship Council (CSC).

### REFERENCES

- [1] Wang, Y., Chen, K.S., Mishler, J., Cho, S.C., Adroher, X.C., A review of polymer electrolyte membrane fuel cells: technology, applications, and needs on fundamental research, *Applied Energy*, Volume 88, 2011, Pages 981-1007.
- [2] Manso, A.P., Marzo, F.F., Barranco, J., Garikano, X., Garmendia, M., Influence of geometric parameters of the flow fields on the performance of a PEM fuel cell, *International Journal of Hydrogen Energy*, Volume 37, 2012, Pages 15256-15287.
- [3] Nitta, I., Karvonen, S., Himanen, O., Mikkola, M., Modelling the effect of inhomogeneous compression of GDL on local transport phenomena in a PEM fuel cell, *Fuel Cells*, Volume 8, 2008, Pages 410-421.
- [4] Zhou, Y.Z., Jiao, K., Du, Q., Yin, Y., Li, X.G., Gas diffusion layer deformation and its effect on the transport characteristics and performance of proton exchange membrane fuel cell, *International Journal of Hydrogen Energy*, Volume 38, 2013, Pages 12891-12903.

## REVEALING THE IMPACT THAT BIOFILM MORPHOLOGIES ON 3D PRINTED ELECTRODES HAVE ON MICROBIAL FUEL CELLS PERFORMANCE

S. Rengaraj\*, Z. Rymanasib\*\*, P. Iravani \*\*, J. L. Scott\*\*\*, M. Di Lorenzo\*

\*Department of Chemical Engineering, University of Bath, Claverton Down, Bath BA2 7AY, (UK)

\*\* Department of Mechanical Engineering, University of Bath, Claverton Down, Bath BA2 7AY, (UK)

\*\*\* Department of Chemistry, University of Bath, Claverton Down, Bath, BA2 7AY, (UK)

**Abstract** - Microbial Fuel Cell (MFC) technology shows a remarkable potential as a carbon-neutral and renewable energy technology. The aim of our research is to improve the system performance by focusing on: device design, electrode morphology and low-cost materials. With the aim of investigating the impact that the anode morphology has on the structure and electron transfer capability of the electroactive anodic biofilm, in this study we have developed and tested innovative 3D printed, micro-structured electrodes as the anode material.

**Index Terms** – Electrogenesis, microbial fuel cells, 3D printing

### I. INTRODUCTION

According to the International Energy Agency, in the next 20 years, global economic growth will lead to an approximately 47% increase in energy demand. If alternative technologies are not considered, this would lead to unacceptable greenhouse gas emissions with consequent severe changes to the climate and the Earth's system. Bioenergy can offer attractive carbon-neutral alternatives to fossil fuels. In this context, microbial fuel cells (MFCs) hold great promise as the basis for sustainable and clean bioenergy-conversion technologies [1]. These devices are capable of harvesting energy from carbohydrates, fatty acids and amino acids, contained in wastewaters and biomass from municipal, industrial and agricultural sources, through the mediation of bacteria [2]. Besides energy generation, MFCs have shown exciting potential in applications such as biosensors for water quality monitoring [3], water desalination [4], biohydrogen production [5] and robotics [6].

Despite recent advances, practical applications of MFCs are, however, still limited by poor power densities. Two major causes for such poor performance are: low electrogenesis efficiencies, due to fuel consumption through non-electrogenic reactions; and loss of electrons at the anode, due to poor electrical contacts between anodes and biofilms. High current efficiencies in MFCs imply that the degradation of the organic matter in the anodic chamber is directly associated with the generation of electrons and their efficient transfer to the anode [7]. As such, this study seeks to identify strategies to enhance the performance of the electroactive biofilm in MFCs, by investigating the influence that the morphology of 3D anodic structures, has on electrogenesis.

### II. MATERIALS AND METHODS

#### A. 3D printing of electrodes

Electrodes were 3D printed from conductive carbon containing inks prepared with cellulose binder dissolved in a solvent/ionic liquid mixture. Two electrode geometries, consisting of 0.7 x 0.7 x 0.1 cm<sup>3</sup> meshes, with a mesh size of 0.05 cm (Mesh1), and of 0.1 cm (Mesh2) were fabricated. The electrodes were printed by using a custom printing rig equipped with an auger-driven gel extruder. A gauge blunt-tip Luer Lock needle was employed for printing. The ink formulation is reported in Table 1.

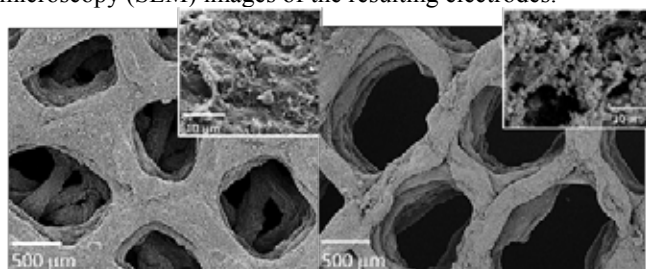
TABLE I  
INK FORMULATION

Component	Loading / wt%	Mass / g
Dimethyl sulfoxide (DMSO)	48.3	24.15

Copyright © 2017

1-Ethyl-3-methylimidazolium acetate (EmimOAc)	45.1	22.46
$\alpha$ -Cellulose	6	3
Carbon nanofibers (CNF)	0.6	0.3

The ink was preheated to *ca* 30 °C prior to loading into a syringe and installation onto the printing rig. The temperature of the print nozzle was set to 20 °C to prevent clogging and allow for the extruded ink to fuse with preceding layers to form a single cohesive object. The printed electrodes were phase inverted by immersion in deionised water; rinsed several times to extract all solvent/ionic liquid; immersed in 6 wt% aqueous glyoxal solution for 3 h; and heated at 90 °C for 1 h to allow cross-linking. Carbonisation was carried out in a tube furnace in flowing argon. The system was heated at a rate of 5 °C min<sup>-1</sup> to 900 °C and held at this temperature for 2 h before cooling to ambient temperature. Fig. 1 shows the scanning electron microscopy (SEM) images of the resulting electrodes.



**Fig. 1.** SEM images of the two 3D printed electrodes, Mesh1(left) and Mesh2 (right). The inserts show the biofilm coverage obtained.

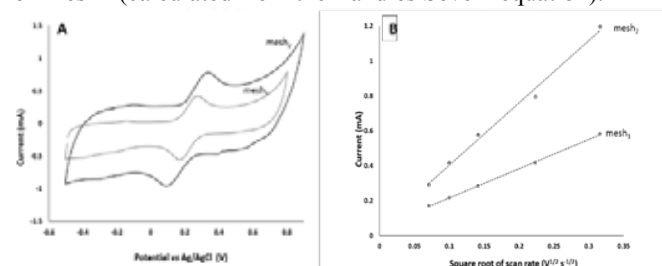
### B. Microbial Fuel Cell design and operation

The MFCs consisted of H-shaped devices, with two chambers (25 mL each) holding the anode and cathode and separated by a 0.1 x 0.1 cm<sup>2</sup> rectangular piece of Nafion117. The 3D printed conductive meshes (Mesh1 and Mesh2) were used as the anodes, leading respectively to MFC<sub>1</sub> and MFC<sub>2</sub>. In both cases, the cathode consisted of a rectangular piece of carbon cloth, 1.5 x 2 cm<sup>2</sup>. The anode chamber was filled with 20 mL of artificial wastewater (AW) [3], while the cathode chamber contained 20 mL of 50 mM potassium ferricyanide. The MFCs were operated in fed-batch mode, with anolyte changed on alternate days and catholyte renewed weekly. The electrodes were connected to an external resistor of 500  $\Omega$ , and the output voltage was monitored with a data logger (Pico Technology, UK). The anodic biofilm was enriched with 10% v/v anaerobic sludge provided by Wessex Water, UK, (COD: 2730 mg L<sup>-1</sup>). All electrochemical measurements were performed using a Metrohm Autolab potentiostat. To visualize the anodic biofilm morphology by SEM, the cells were fixed as previously described [3].

### III. RESULTS

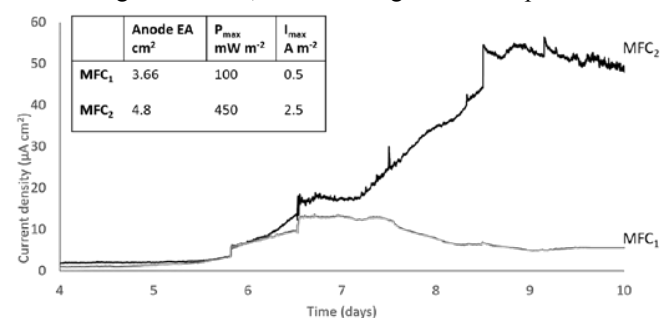
The electrochemical performance of the two meshes was characterized by cyclic voltammetry (CV) scans in the presence of the redox probe K<sub>3</sub>[Fe(CN)<sub>6</sub>]. Higher Faradaic and capacitive current was observed for Mesh2 compared to Mesh1 (Fig. 2A).

In particular, the scan rate dependent study (Fig 2B) revealed an electroactive surface area for Mesh2 1.3 times higher than that for Mesh1 (calculated from the Randles Sevcik equation).



**Fig. 2.** Electrochemical characterization in 5 mM potassium ferricyanide of the two meshes. A) CVs at the scan rate of 5 mV s<sup>-1</sup>. B) scan rate dependent study. The CVs were performed with the mesh as the working electrode, Ag/AgCl as the reference electrode and titanium mesh as counter electrode.

Nonetheless, when the conductive meshes were tested as anodes of MFCs, the steady-state output current obtained with MFC<sub>2</sub> was more than five times higher than MFC<sub>1</sub> (Fig. 3) and peak power and current densities obtained were also consequently higher for MFC<sub>2</sub>. The improved performance of MFC<sub>2</sub> must therefore be correlated to the biofilm morphology. As shown in Fig1, the smaller mesh size in Mesh1, leads to a full coverage of biofilm, thus reducing the total exposed area.



**Fig. 3.** Growth of electroactive biofilm onto the anode surface of the MFCs. Current densities refer to the total geometric surface area of the electrodes. External resistance: 500  $\Omega$ .

### IV. CONCLUSION

Through the use of two 3D printed conductive meshes, characterized by different mesh size, this study reveals the importance that anode structures have on biofilm morphology and therefore on electrogenesis.

### REFERENCES

- [1] Oliveira, V. B., *et al. Biochem. Eng. J.* 73, 2013, 55-64
- [2] Rabaey, K., Verstraete, W. *Trends Biotechnol.* 23, 2005, 291-298
- [3] Chouler, J. *et al. Electrochim. Acta* 231, 2017, 319-326.
- [4] Cao, X., *et al. Environ. Sci. Technol.* 43, 2009, 7148-7152.
- [5] Wang, A., *et al. Bioresource Technology* 102, 2011, 4137-4143.
- [6] Ieropoulos, I. A., *et al. ChemSusChem* 5, 2012, 1020-1026
- [7] Santoro, c. *et al. Journal of Power Sources*, 356, 2017, 225-244



## HIERARCHICAL STRUCTURED FOAMS OF POROUS NITROGEN-DOPED CARBON FOR PEM FUEL CELLS

R. Hempelmann\*, I. Radev\*\*, and H. Natter\*

\*Transfercentre Sustainable Electrochemistry,  
Saarland University and KIST Europe, Saarbrücken (Germany)

\*\*ZBT Duisburg Fuel Cell Research Center, Duisburg (Germany)

**Abstract** - A new strategy for designing the morphology and the chemical/physical properties of carbon structures in PEMFC has been developed by functionalization of porous carbon templates. In a thermal decomposition process self-prepared multilayer graphene foams (GF) or commercial carbon nanotubes (CNT) are coated with a nitrogen-containing carbon layer (NCL) which has a porous structure. The use of a nitrogen-rich ionic liquid as precursor generates a NCL with a very high nitrogen level of up to 35 wt%. Structural studies on the NCL confirm  $C_3N$  and  $C_3N_4$  species. Compared to uncoated GF it could be demonstrated that the functionalized porous carbon template (N-GF) has an increased electronic conductivity and electrochemical stability. Electrochemical characterizations of polymer electrolyte membrane fuel cells (PEMFC) prepared with Pt catalysts supported on N-GF show an increased performance which is attributed to improved mass transport properties and higher electronic conductivity of the porous composite material.

**Index Terms:** Graphene, N-doping, PEMFC catalyst carrier

### I. INTRODUCTION

Carbon is a very versatile and attractive material for many electrochemical devices. It exists in the allotropes diamond, graphite, carbon black (partly amorphous), carbon nanotubes and graphene, and it can be doped with Nitrogen, Phosphorous Sulphur or Boron. It exhibits chemical and physical stability as well as electronic and heat conductivity. Moreover, the sustainable nature and the possibility of rational control of its nanostructure are remarkable [1]. We are dealing with graphene [2] as catalyst carrier in PEMFC. In previous work [3] we have shown that graphene mixed with carbon nanotubes in the catalyst layer can improve the mass transport and thus increase the performance of PEMFC. In the present contribution we report about the improvement of the graphene catalyst carrier by

nitrogen doping. There are different nitrogen species in graphene: pyridinic N, pyrrolic N, pyridine-N-oxide and quaternary N [4]. Under the keyword “nitrogen doped graphene” the ISI web of knowledge indicates an exponential increase of the number of publications with more 6.500 publications essentially in the last 15 years, including our work [5, 6], what demonstrates the actuality of this topic.

### II. MATERIALS AND EXPERIMENT

We have prepared our carbonaceous catalyst carrier in a two-step thermal-process: i) Thermal decomposition of sodium acetate at  $800^\circ$  under inert gas for 1 min resulting in a graphene foam; washing and drying of the resulting graphene foam. ii) impregnation of this foam with the N-containing ionic liquid 1-ethyl-3-methylimidazolium dicyanamide and thermal treatment at  $600^\circ\text{C}$  for 1 min under inert gas. Figure 1 shows the result.

The decoration with Pt nanoparticles has been done electrochemically according to a procedure describe previously [7], resulting in a platinum loading of only  $0.4 \text{ mgPt cm}^{-2}$ .

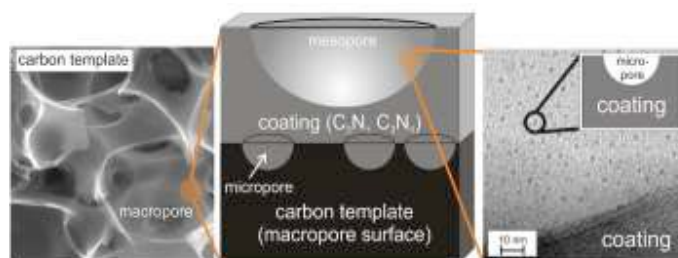


Fig. 1: Electron micrographs of the carbon template, the micropores and the coating of N-doped graphene

Copyright © 2017

A scheme of the hierarchical porosity is displayed in Figure 2.

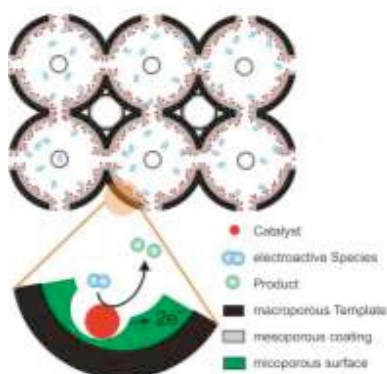


Fig. 2: Scheme of the hierarchical porosity of the N-doped graphene foam

#### IV. RESULTS

The specific surface area of N-doped graphene and N-doped CNT is significantly larger than that of the uncoated carbon substrates, in accordance with a decrease of the micro pore diameters. This is due to the formation of tiny gas bubbles during the short thermal treatment. Raman spectroscopy was applied to characterize the carbon structure. The shape of the 2D band in combination with its shifted peak position confirms a few layer graphitic structure and also the successful coating of the substrate walls. X-ray photoelectron spectra (XPS) show three distinct bands, evidence for carbon, oxygen and nitrogen species. The latter signal can be attributed to the aromatic C=N-C bonds of the  $C_3N_4$  structure, to pyridinic N, to N-(C)3 and amino groups (C-N-H). In electrochemical impedance measurements on complete MEAs with our self-made gas diffusion electrode as anode and a commercial cathode we observe the tendency: higher electrode surface areas are related to lower ohmic and charge transfer resistances.

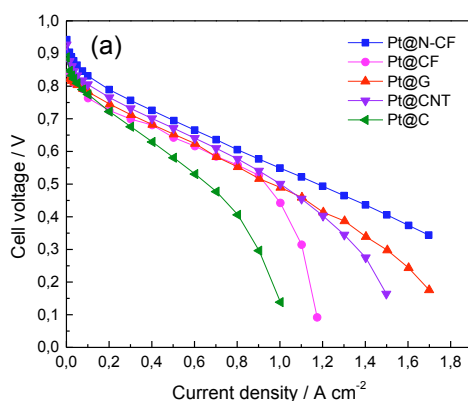


Fig. 3: Fuel cell performance of Pt on different catalyst support materials

The current-voltage curves of the corresponding MEAs are presented in Fig. 3. For comparison reasons we use the current density measured at 0.65 V. Pt@G shows the lowest  $i_{@0.65V}$  value and poor mass transport properties resulting from the roof tile morphologies of graphene flakes. Pt@CNT has an improved mass transport with a slightly increased  $i_{@0.65V}$ . This can be explained by the porous CNT-based morphology of the microporous catalyst layer (MPC). To improve the mass transport of the purely graphene-based MPC, CNT spacers (Pt@G/CNT) were introduced. This more porous morphology leads to an  $i_{@0.65V}$  of  $0.66 \text{ A cm}^{-2}$ . The influence of coated catalyst supports were measured on mixtures of Pt@N-G/CNT and Pt@G/N-CNT. The microstructure of these two samples should be the same and for this reason the difference in sample performance can be attributed to the conductivity of the catalyst supports.

#### V. CONCLUSION

We have developed a low-cost, scalable, synthetic method for preparing a hierarchical structured porous carbon foam consisting of GF coated with a N-containing carbon layer. The coating process can be applied to various carbon materials.

#### ACKNOWLEDGEMENT

Financial support by the AiF, project No 18128 N is gratefully acknowledged.

#### REFERENCES

- [1] S. A. Salvatore Arico, P. Bruce, B. Scrosati, J.-M. Tarasconi & W. van Schalkwijk, Nanostructured materials for advanced energy conversion and storage devices, *Nature Materials* Vol.4, 2005, 366
- [2] H. Chang & H. Wu, Graphene-based nanocomposites: preparation, functionalization, and energy and environmental applications, *Energy & Environmental Science* Volume 6, 2013, 3483
- [3] A. Marinkas, R. Hempelmann, A. Heinzl, V. Peinecke, I. Radev & H. Natter, Enhanced stability of multilayer graphene-supported catalysts for polymer electrolyte fuel cell cathodes, *Journal of Power Sources*, Volume 295, 2015, 79–91
- [4] Y. Deng, Y. Xie, K. Zou, X. Ji, Review on recent advances in nitrogen-doped carbons: preparations and applications in supercapacitors, *J. Mater. Chem. A*, Volume 4, 2016, 1144
- [5] E.-J. Oh, R. Hempelmann, V. Nica, I. Radev & H. Natter, New catalyst supports by surface modification of graphene and carbon nanotube structures with nitrogen containing carbon coating, *Journal of Power Sources*, Volume 341, 2017, 240–249
- [6] E.-J. Oh, R. Hempelmann, V. Nica, I. Radev & H. Natter, Coating procedure for chemical and morphological functionalization of multilayer-graphene foams, *Carbon*, Volume 121, 2017, 170–180
- [7] J. Mitzel, F. Arena, H. Natter, T. Walter, M. Batzer, M. Stefener & R. Hempelmann, Electrodeposition of PEM Fuel Cell Catalysts by the Use of a Hydrogen Depolarized Anode, *International Journal of Hydrogen Energy* 37, 2012, 6261–6267

## CHALLENGES OF NPGM OXIDE CATHODE WITH METAL OXIDE SUPPORT FOR ADVANCED PEFCs

K. Ota\*, T. Nagai\*, Y. Kuroda\*, K. Matsuzawa\*, S. Mitsushima\*\*\*, A. Ishihara\*\*

Yokohama National University,

\*Green Hydrogen Research Center, \*\*the Institute of Advanced Sciences

79-5 Tokiwadai, Hodogaya-ku, Yokohama, 240-8501 (JAPAN)

**Abstract** - The precious-metal-free and carbon-free cathodes based on oxides (titanium-niobium oxides mixed with  $\text{Ti}_4\text{O}_7$  ( $\text{Ti}_x\text{Nb}_y\text{O}_z + \text{Ti}_4\text{O}_7$ )) showed the superior durability. The ORR activity of the  $\text{Ti}_x\text{Nb}_y\text{O}_z + \text{Ti}_4\text{O}_7$  is higher than that of the  $\text{Ti}_4\text{O}_7$ . No degradation of the ORR performance of  $\text{Ti}_x\text{Nb}_y\text{O}_z + \text{Ti}_4\text{O}_7$  was observed during both start-stop and load cycle tests. In order to qualify the role of Nb oxide for ORR, we used  $\text{TiO}_2\text{-Nb}$  (Nb; 0.5, 1 and 5 atm%) rods as working electrodes. In reducing atmosphere treatment,  $\text{TiO}_2\text{-Nb}$  (0.5 atm%) rod had best ORR activity that was heat-treated at 800 °C. However  $\text{TiO}_2\text{-Nb}$ (5%) showed the best result in air treatment at 800°C. The heat-treatment temperature and the atmosphere are important to get high ORR activity.

**Index Terms** –cathode catalyst, non PGM catalyst, polymer electrolyte fuel cell, titanium oxide

### I. INTRODUCTION

Polymer electrolyte fuel cells are expected for the residential and transportable applications, due to their high power density and low operating temperature. Many ENEFARMS (micro CHP) are operating and fuel cell vehicles are also commercially available in Japan. However, the estimated amount of Pt reserve is limited and its cost is high. The dissolution of Pt cathode might be the final problem to be solved related to the stability in the present PEFC system. Additionally, the instability of carbon support is also a big problem especially for fuel cell vehicles. Carbon including graphite is thermochemically unstable at room temperature in air or oxygen containing atmosphere. A stable non-precious metal oxide cathode with stable metal oxide support would be the final goal for the cathode system of PEFC for fuel cell vehicles. In the future energy system fuel cells should be operated at higher efficiency such as 60 % (HHV) since their theoretical

efficiency is very high. To get this high efficiency, fuel cells should be operated at 0.9 V or higher. To get this high operation voltage, their operation temperature should be higher than 120 °C for PEFCs. At these high potential and temperature Pt and carbon are no more stable. We need new materials, such as metal oxides that are stable in acid and oxygen atmosphere.

We have reported that partially oxidized group 4 and 5 metal carbonitrides and organometallic complexes are stable in an acid solution and have definite catalytic activity for the oxygen reduction reaction (ORR) [1-7]. In this paper we will report our recent results of the group 4 and 5 metal oxide catalyst with metal oxide support without carbon.

### II. EXPERIMENTAL

Two types of  $\text{TiO}_2$  poly-crystalline rods with Nb addition were prepared. One is the reduced  $\text{TiO}_2$  poly-crystalline with Nb addition which were made by hot press at 1350 °C under reducing atmosphere. The other is the titanium oxide thin layer made by the arc plasma deposition (APD). All electrochemical measurements were performed in 0.1 mol  $\text{dm}^{-3}$   $\text{H}_2\text{SO}_4$  at 30 or 80 °C with a 3-electrode cell. Chronoamperometry (CA) was performed from 0.2 to 1.2 V vs. RHE under  $\text{O}_2$  atmosphere to obtain ORR current. The ORR current density was normalized by the electric charge of the double layer capacitance under  $\text{N}_2$  atmosphere.

### III. RESULTS AND DISCUSSION

The precious-metal-free and carbon-free cathodes based on oxides (titanium-niobium oxides mixed with  $\text{Ti}_4\text{O}_7$  ( $\text{Ti}_x\text{Nb}_y\text{O}_z + \text{Ti}_4\text{O}_7$ )) showed the superior durability [5]. The ORR

activity of the  $\text{Ti}_x\text{Nb}_y\text{O}_z + \text{Ti}_4\text{O}_7$  is higher than that of the  $\text{Ti}_4\text{O}_7$ , indicating that the  $\text{Ti}_x\text{Nb}_y\text{O}_z$  might have active sites for the ORR. Figure 1 shows the current-potential curves of some oxides. The highest onset potential of the  $\text{Ti}_x\text{Nb}_y\text{O}_z + \text{Ti}_4\text{O}_7$  was over 1.1 V with respect to reversible hydrogen electrode. No degradation of the ORR performance of  $\text{Ti}_x\text{Nb}_y\text{O}_z + \text{Ti}_4\text{O}_7$  was observed during both start-stop and load cycle tests. Therefore, we successfully demonstrated that the precious-metal and carbon-free oxide-based cathodes had superior durability under the cathode conditions of PEFCs.

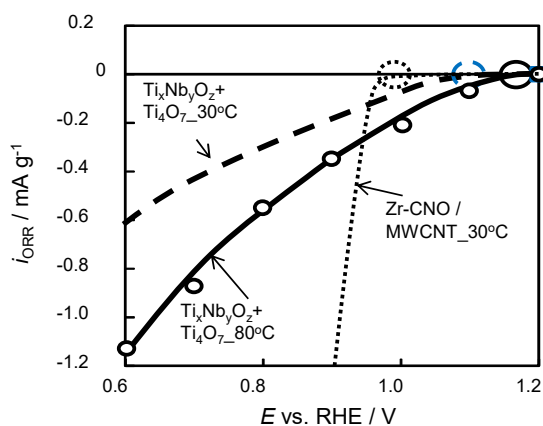


Fig.1 Potential-ORR current curves of  $\text{Ti}_x\text{Nb}_y\text{O}_z + \text{Ti}_4\text{O}_7$  and Zr-CNO/MWCNT.

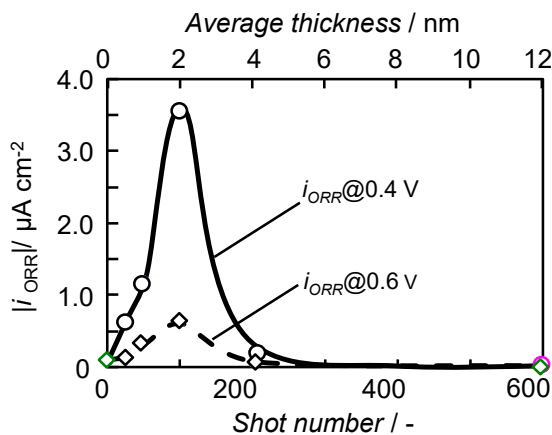


Fig.2 Dependence of ORR current on Titanium oxide thickness by APD.

In order to qualify the role of Nb oxide for ORR, we used  $\text{TiO}_2\text{-Nb}$  (Nb; 0.5, 1 and 5atm%) rods as working electrodes. In reducing atmosphere treatment,  $\text{TiO}_2\text{-Nb}$  (0.5atm%) rod had best ORR activity that was heat-treated at 800 °C. However  $\text{TiO}_2\text{-Nb}$ (5%) showed the best result in air treatment at 800°C.

The heat-treatment temperature and the atmosphere are important to get high ORR activity.

In order to apply metal oxide to the support of ORR catalyst they should have good electrical conduction. Most of metal oxides have poor electrical conductivity. However some of them, such as  $\text{Ti}_4\text{O}_7$  and the solid solution of titanium oxide and niobium oxide, have good electrical conduction even at room temperature. Figure 2 shows the ORR current on thin layer of titanium oxides made by the APD method. The currents increased up to the thickness of 2 nm and then decreased rapidly. This might owe to the electron conduction caused by the tunneling effect. If we could apply this effect to the ORR catalyst network, we might have a good ORR catalyst system for PEFCs even at the room temperature.

The activity might be affected by many factors. We are looking for the important factor for ORR.

#### IV. CONCLUSION

In the future energy system fuel cells should be operated at higher efficiencies such as 60 % (HHV) since their theoretical efficiency is more than 80% even at room temperature. To obtain this high efficiency, fuel cells should be operated at 0.9 V or higher. To get this high operation voltage, their operation temperature might be higher than 120 °C for PEFCs. We need new materials for the ORR catalyst system, ORR catalysts and their supports. Group 4 and Group 5 metal oxides might be good candidates for the future ORR system of PEFCs.

#### ACKNOWLEDGMENT

The authors wish to thank to the New Energy and Industrial Technology Development Organization (NEDO) for their financial support.

#### REFERENCES

- [1] A. Ishihara, Y. Shibata, S. Mitsushima, K. Ota, Journal of The Electrochemical Society, 155, B400-B406 (2008).
- [2] A. Ishihara, M. Tamura, Y. Ohgi, M. Matsumoto, K. Matsuzawa, S. Mitsushima, H. Imai, K. Ota,
- [3] Journal of Physical Chemistry, ser. C, 117, 18837-18844 (2013).
- [4] A. Ishihara, M. Chisaka, Y. Ohgi, K. Matsuzawa, S. Mitsushima, K. Ota, Physical Chemistry Chemical Physics, 17, 7643-7647 (2015).
- [5] N Uehara, A. Ishihara, M Matsumoto, H. Imai, Y. Kohno, K. Matsuzawa, S. Mitsushima, K. Ota, Electrochimica Acta, 182, 789-794 (2015).
- [6] A. Ishihara, M. Hamazaki, M. Arao, M. Matsumoto, H. Imai, Y. Kohno, K. Matsuzawa, S. Mitsushima, and K. Ota, Journal of The Electrochemical Society, 163 (7) F603-F609 (2016)
- [7] K. Ota, Y. Tamura, T. Nagai, K. Matsuzawa, S. Mitsushima, A. Ishihara, ECS Transactions, 75(14), 875-883 (2016)
- [8] M. Chisaka, A. Ishihara, H. Morioka, T. Nagai, S. Yin, Y. Ohgi, K. Matsuzawa, S. Mitsushima, K. Ota, ACS Omega, 2, 678-684 (2017)

## HYDROGEN CROSSOVER PHENOMENA IN POLYMER ELECTROLYTE MEMBRANE WATER ELECTROLYZERS

Aeri Jung\*, Akiko Inada\*, Ryo Saito\*\*, and Kohei Ito\*

\*Faculty of Engineering, Department of Mechanical Engineering,  
Kyushu University,

Motooka 744, Nishi-ku, Fukuoka 819-0395 (JAPAN)

\*\*Graduate School of Engineering, Kyushu University,  
Motooka 744, Nishi-ku, Fukuoka 819-0395 (JAPAN)

**Abstract** – In this study, quantitative analysis on the hydrogen crossover in a polymer electrolyte membrane water electrolyzer (PEMWE) system was conducted. To perform this research, both theoretical and experimental analysis were performed with single PEMWE equipped experimental setup. Through the theoretical analysis, related parameters for crossover phenomenon in PEMWE, such as the amount for reacting with oxygen and existing as hydrogen, was defined. Based on this, the entire hydrogen crossover rate was divided to each part for precise measurement from the experiment. As a result, the total hydrogen crossover rate was measured through the experiments, moreover, the proportion between the combusted (as water) and remained hydrogen was also found among the permeated hydrogen.

**Index Terms** – Crossover phenomenon, Hydrogen peroxide formation reaction (HPFR), Polymer electrolyte membrane water electrolyzer (PEMWE), Water formation reaction (WFR)

### I. NOMENCLATURE

#### Nomenclature

J	crossover rate [ cc/min ]
i	current density [ A/cm <sup>2</sup> ]
F	Faraday constant [ C/mol ]
K	permeability [ mol/cm <sup>2</sup> s ]
l	membrane thickness [ μm ]
P	pressure [ Pa ]
T	temperature [ K ]
A	active area [ cm <sup>2</sup> ]

#### Subscript

MEA	membrane
AN	anode

CA	cathode
EXP	(ideally) expected
EXH	exhausted (by water formation reaction)
H <sub>2</sub>	hydrogen
O <sub>2</sub>	oxygen

### II. INTRODUCTION

As eco-friendly and efficient energy resources have been highlighted for the new energy systems, hydrogen has an attractive according to the achievement in technologies of various fuel cell systems. With this trends, the water electrolyzer has been suggested for the effective hydrogen production system [1]. However, the durability and safety of this system should be improved more for successful commercialization in industrial markets [2].

Among many reasons for deterioration of the materials in a polymer electrolyte membrane water electrolyzer (PEMWE) system, especially hydrogen crossover is one of the important phenomena that strongly related to the performance, durability and safety of the systems [3]. With this reason, more precise understanding on hydrogen crossover phenomenon is strongly needed. Therefore, quantitative analysis on the hydrogen crossover in a PEMWE system was conducted through this research. Experimental analysis based on theoretical approach was performed, the total hydrogen crossover rate and the proportion between combusted (as water) and remained hydrogen was found as a result.

### III. THEORETICAL APPROACH

Firstly, each term in crossover phenomenon in a PEMWE should be explained. Permeated hydrogen can be existed in opposite side as three different materials: remained as itself,



combusted as water (by water formation reaction, WFR), formed as hydrogen peroxide formation reaction, HPFR). Based on this, all parameters related to the crossover phenomena in PEMWE case can be listed as shown in Fig. 1. Equations are built by considering the mass balance equation for anode and cathode side and each parameters are obtained by measuring from the experiment and solving equations.

$$\text{Eqn. 1: } J_{MEA}^{O_2} = J_{EXP}^{O_2} - J_{EXH,AN}^{O_2} - J_{EXH,CA}^{O_2} - J_{H_2O_2} - J_{REM}^{O_2}$$

$$\text{Eqn. 2: } J_{MEA}^{H_2} = J_{EXP}^{H_2} - J_{EXH,AN}^{H_2} - J_{EXH,CA}^{H_2} - J_{H_2O_2} - J_{REM}^{H_2}$$

$$\text{Eqn. 3: } J_{EXH,AN}^{H_2} = 2 \times J_{EXH,AN}^{O_2}, \text{ Eqn. 4: } J_{EXH,CA}^{H_2} = 2 \times J_{EXH,CA}^{O_2}$$

$$\text{Eqn. 5: } I_{2F} = J_{EXP}^{H_2} + J_{H_2O_2}, \text{ Eqn. 6: } I_{4F} = J_{EXP}^{O_2}$$

$$\text{Eqn. 7: } J_{PER}^{H_2} = A K_{H_2} \frac{P_{CA}^{H_2} - P_{AN}^{H_2}}{L} = J_{EXH,AN}^{H_2} + J_{REM}^{H_2}$$

$$\text{Eqn. 8: } J_{PER}^{O_2} = A K_{O_2} \frac{P_{AN}^{O_2} - P_{CA}^{O_2}}{L} = J_{EXH,CA}^{O_2} + J_{REM}^{O_2} + J_{H_2O_2}$$

Fig.1. Mass balance equations on crossover phenomenon in PEMWE system

#### IV. RESULT AND DISCUSSION

##### A. Hydrogen crossover rate under different current densities

Total hydrogen crossover rate can be divided into two parameters which are exhausted by WFR and remained hydrogen. Among these, remained hydrogen can be measured from the experiment and exhausted hydrogen by WFR can be calculated with measured data. Obtained hydrogen crossover rate and proportion of this compared to produced hydrogen at different currents (1, 3 A) are shown in Fig. 2. As shown in Fig. 2, hydrogen crossover rate is increased for higher current case and this tendency coincides well with other research [3].

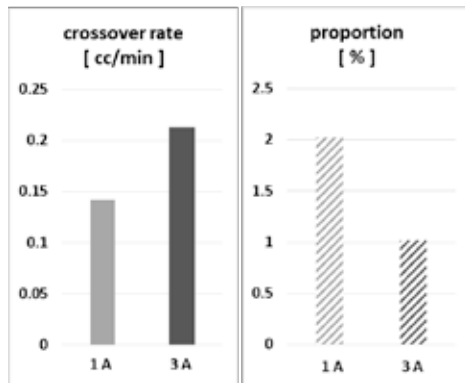


Fig.2. Hydrogen crossover rate and its ratio under different currents

##### B. Quantitative analysis on crossover rates

Based on both theoretical approach and experimental result, all parameters in Fig. 1 are obtained and ratio of these parameters compared to the ideally produced hydrogen are

represented in Fig. 3. As shown in Fig. 3, around 1.02% of the expected hydrogen production rate are crossed-over to opposite side. It is found that 98.19% of the permeated hydrogen is combusted as water (by WFR) and the rest is remained as itself with oxygen at the outlet.

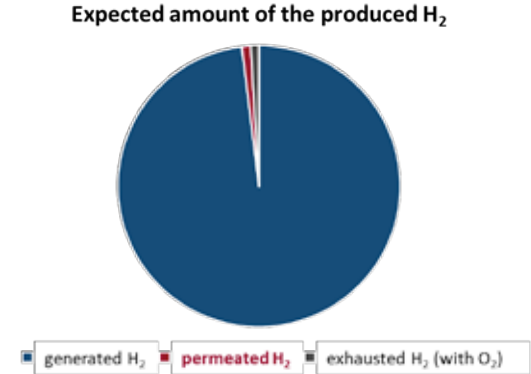


Fig.3. Quantitative proportion in hydrogen crossover rate at 3 A

#### V. CONCLUSION

Hydrogen crossover rate in PEMWE system is quantitatively analyzed through this study. Based on the theoretical approach, the proportion of the combusted and remained hydrogen is suggested as a result. This result is expected to contribute to predict each effect of the hydrogen crossover on performance, durability and safety of PEMWE system.

#### ACKNOWLEDGMENT

This research was supported by JSPS KAKENHI Grant Number 16H02316.

#### REFERENCES

- [1] A.H. A. Rahim, A. S. Tijani, S.K. Kamarudin, S. Hanapi, An overview of polymer electrolyte membrane electrolyzer for hydrogen production: Modeling and mass transport, Journal of Power Sources, Volume 309, 2016, pp. 56-65.
- [2] S.A. Grigoriev, P. Millet, S.V. Korobstev, V.I. Porembskiy, M. Pepic, C. Etievant, C. Puyenchet, V.N. Fateev, Hydrogen safety aspects related to high-pressure polymer electrolyte membrane water electrolysis, International Journal of Hydrogen Energy, Volume 34, 2009, pp. 5986-5991.
- [3] Hiroshi I., Naoki M., Masayoshi I., Akihiro N., Cross-permeation and consumption of hydrogen during proton exchange membrane electrolysis, International Journal of Hydrogen Energy, Volume 41, 2016, pp. 20439-20446.



## DETAILED PHYSICAL MODELLING OF INTERMEDIATE TEMPERATURE SOLID OXIDE FUEL CELLS

B.Conti<sup>a,b</sup>, E. Arato<sup>a</sup>, S.J. McPhail<sup>b</sup>, Francesca Santoni<sup>b,c</sup>,  
Davide Pumiglia<sup>b</sup> and B.Bosio<sup>a</sup>

<sup>a</sup>DICCA-University of Genoa, Via Opera Pia 15, (Italy)

<sup>b</sup>C.R. ENEA Casaccia, Via Anguillarese 301, (Italy)

**Abstract** – In order to optimise the performance and the operating conditions of Intermediate Temperature Solid Oxide Fuel Cells (IT-SOFCs), an effective synergy between experimentation and simulation is fundamental. For this purpose, starting from the SIMFC (Simulation of Fuel Cells) code set up and successfully validated by PERT (Process Engineering Research Team) for Molten Carbonate Fuel Cells, a new code has been developed for planar IT-SOFCs. The new release of SIMFC allows the calculation for planar IT-SOFCs fed in co-flow of the maps of the main electrical, chemical and physical parameters on the cell plane: flow-rate, current density, polarisations, thermodynamic ideal voltage, etc. The model has been validated on IT-SOFC single cells in ENEA laboratories of C.R. Casaccia (Rome.) Thanks to an innovative multi-sampling apparatus which permits simultaneous local measurement of temperature and gas compositions on the cell plane, it has been possible to validate also the local maps obtained by means of SIMFC.

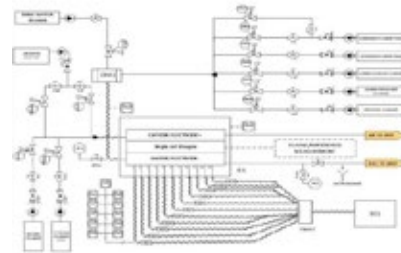
**Index Terms** – Electrode kinetics, single cell experimentation, detailed modelling, Intermediate Temperature Solid Oxide Fuel Cells.

### I. INTRODUCTION

From 1969s different kinds of fuel cells are under development [1]. Nowadays one of the more interesting type of fuel cells under study are Intermediate Temperature SOFCs (IT-SOFCs), because of their high efficiency [2]. The synergy between experimentation and simulation is proposed as the better approach to evaluate performance and correct behaviour of a chemical process. For this purpose, starting from SIMFC (Simulation of Fuel Cells) code set-up by PERT-UNIGE (Process Engineering Research Team) for Molten Carbonate Fuel Cells [3], a new code is set-up for IT-SOFCs based on local mass, energy, charge and momentum balances. This code takes into account the reactions occurring in the IT-SOFC as well as their kinetics thanks to experiments carried out on single cells in ENEA laboratories of C.R. Casaccia (Rome).

### II. EQUIPMENTS AND METHODS

The experimental setup, shown in Figure 1, presents the innovative feature to be able to measure locally, by means of eleven detection points, temperatures and gas compositions over the anode surface of cell.



**Fig. 1 IT-SOFC single cell facility**

In order to define an electrokinetic model for IT-SOFCs, in this work a semiempirical relationship is adopted that allows the prediction of the performances by quantifying the dissipations as a function of the operating conditions and physico-chemical parameters. In particular, the cell voltage  $\Delta V$  is calculated as follows:

$$\Delta V = \Delta E - \eta_{Ohm} - \eta_{anode} - \eta_{cathode} \quad (1)$$

The ideal voltage  $\Delta E$  is evaluated by means of the Nernst equation:

$$\Delta E = E_{an} - E_{cat} = E_0 + \frac{RT}{zF} \ln \frac{\prod_i p_i^{\alpha_i}}{\prod_j p_j^{\alpha_j}} \quad (2)$$

where  $E_0$  is the standard potential in reversible condition whose expression is obtained as a function of temperature by [4],  $T$  is the temperature,  $z$  is the number of charge transferred with reaction,  $F$  is the Faraday constant,  $\alpha_i$  and  $\alpha_j$  are the stoichiometric coefficient and partial pressure of the  $i$ -th reagent or  $j$ -th product respectively.

$\eta_{Ohm}$  is the voltage loss due to the purely Ohmic internal resistance,  $\eta_{anode}$  and  $\eta_{cathode}$  are the polarizations at the electrode

scale due to activation and reactant diffusion phenomena. Preliminary, also taking account of the reference operative conditions, a linear dependence of voltage losses versus the current density has been assumed. So, a local resistance  $R$  is defined as:

$$\Delta V = \Delta E - R * J, \quad \text{where } R = R_{\eta Ohm} + R_{\eta anodo} + R_{\eta catodo} \quad (3)$$

On the basis of the literature, it is possible to write:

$$R_{\eta Ohm} = P_1 * T * \exp(P_2/T) \quad (4)$$

while the linearization of the Butler-Volmer equation leads to write the electrode polarisations as follows:

$$R_{\eta anodo} = \frac{P_3 e^{P_4/T}}{P_5 p_{H_2}} \quad \text{and} \quad R_{\eta cathode} = \frac{P_6 e^{P_7/T}}{P_8 p_{O_2}} \quad (5)$$

where  $P_1, P_2, P_3, P_4, P_5, P_6, P_7$  and  $P_8$  are parameters identified by fitting experimental data or by literature values referred to similar cells.

### III. RESULTS AND DISCUSSION

IT-SOFCs used for the experimental campaign consist of LSC cathode, Ni-YSZ anode, YSZ electrolyte with 121 cm<sup>2</sup> of active area and provided by Elcogen AS (Estonia). For each test, carried out at low utilization factor to avoid diffusion problems, temperature or gas composition are changed maintaining the other variables constant (with N<sub>2</sub> balancing). For each test impedance spectra and characteristic curves are collected ensuring that the cell reaches the steady state condition.

From the fitting on polarization curves and impedance spectra and assuming  $R_{\eta cathode}$  almost constant in the studied conditions, the following parameters are identified:

$P_1 = 2 \cdot 10^{-9}$  (Ohm\*cm<sup>2</sup>)/K,  $P_2 = 10896$  K,  $P_3 = 7.7347$  Ohm\*cm<sup>2</sup>\*Pa<sup>0.5</sup>,  $P_4 = 0.5$ ,  $P_5 = 13230$  K,  $R_{\eta cathode} = 0.34$  Ohm\*cm<sup>2</sup>.

In Figure 2, as an example, a comparison between experimental and simulated data referring to a reference characteristic curve is shown.

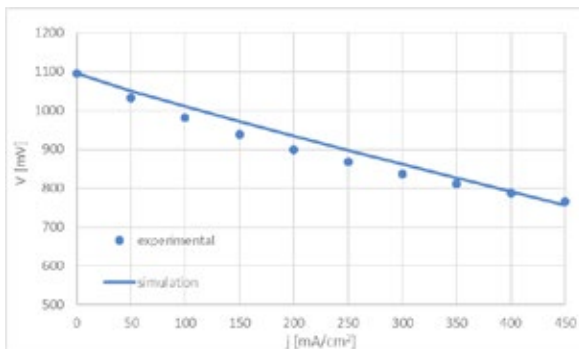


Fig. 2 - Characteristic and simulated curves with anodic molar composition: 80% H<sub>2</sub>, 16% N<sub>2</sub>, 4% H<sub>2</sub>O and cathodic molar composition: 79% N<sub>2</sub> and 21% O<sub>2</sub>.

Thanks to the innovative experimental setup developed in ENEA laboratories and using the code based on finite element method, it is possible to map the anodic composition and compare experimental and simulated results. In Figure 3 data at two electric loads are reported (130 mA/cm<sup>2</sup> and 250 mA/cm<sup>2</sup>).

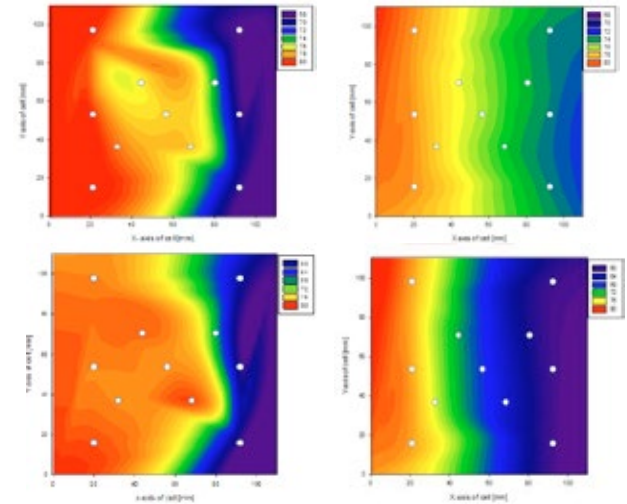


Fig. 3 - Top: On the left the experimental map of the molar fraction of H<sub>2</sub> at 130 mA/cm<sup>2</sup>, on the right the simulated one. Bottom: on the left the experimental map of the molar fraction of H<sub>2</sub> at 250 mA/cm<sup>2</sup>, on the right the simulated one.

The agreement between experimental and simulated data is acceptable and the next aim is to improve the predictive capability of the model in a wider range of operating conditions.

### IV. CONCLUSION

The SIMFC code developed for the MCFC technology, with appropriate modifications, is adapt for SOFC technology simulation and its optimization can provide an interesting tool useful for diagnostic, predictive and design issues.

### REFERENCES

- [1] Bockris, J., O'M. & Srinivasan S., Fuel Cell: Their electrochemistry. New York: McGraw-Hill, 1969.
- [2] E., Barsoukov, J. R., Macdonald, Impedance Spectroscopy Theory, Experiment, and Applications Second Edition, A John Wiley & Sons, Inc., Publication., 2005.
- [3] B., Bosio, N., Di Giulio, S.W., Nam, A., Moreno, An effective semi-empiric model for MCFC kinetics: Theoretical development and experimental parameters identification, International Journal of Hydrogen Energy, Vol. 39, 2014, Pages 12273-12284.
- [4] C.B., Munoz, P., Davide, S. J., McPhail, S., Giulio, D., Montinari, G., Comodi, M., Carlini, F., Polonara, More accurate macro-models of solid oxide fuel cells through electrochemical and microstructural parameter estimation - Part II: Parameter estimation, Journal of Power Sources, Volume 286, 2015, Pages 321-329.

## OPTIMIZED ELECTROLYZER OPERATION: EMPLOYING FORECASTS OF WIND ENERGY AVAILABILITY, HYDROGEN DEMAND, AND ELECTRICITY PRICES

F. Gröger<sup>1</sup>, O. Hoch<sup>1</sup>, J. Hartmann<sup>1</sup>, M. Robinius<sup>2</sup> and D. Stolten<sup>2,3</sup>

<sup>1</sup> Reiner Lemoine Institut gGmbH, Rudower Chaussee 12, 12489 Berlin, (Germany)

<sup>2</sup> Institute of Electrochemical Process Engineering (IEK-3), Forschungszentrum Jülich GmbH, Wilhelm-Johnen-Str., 52428, (Germany)

<sup>3</sup> Chair for Fuel Cells, RWTH Aachen University, c/o Institute of Electrochemical Process Engineering (IEK-3), Forschungszentrum Jülich GmbH, Wilhelm-Johnen-Str., 52428, (Germany)

**Abstract** - One of the main advantages of fuel cell based mobility over other sustainable mobility concepts is the flexible production of hydrogen via electrolysis. To date, it is unclear how electrolysis at hydrogen refueling stations should be operated in order to achieve the lowest possible costs despite the constraints of hydrogen demand. This study proposes and evaluates an intelligent operating strategy for electrolysis capable of exploiting times of low electricity prices while participating in the spot market and maximizing wind energy utilization when combined with a wind farm. This strategy is based on a simulation model considering imperfect forecasts (e.g. of wind availability or energy prices) and non-linear electrolyzer behavior. Results show that this approach reduces hydrogen production costs by up to 9.2 % and increases wind energy utilization by up to 19 %, respectively.

**Index Terms** – Electrolysis, Forecast, Operation, Optimization

### I. INTRODUCTION

Hydrogen-based mobility shows lower overall efficiency compared to battery electric vehicles (BEV) [1]. On the other hand, BEV's energy demand is rather inflexible and requires coupled energy provision, while hydrogen can be produced via electrolysis at hydrogen refueling stations (HRS) whenever electric energy from renewables is available or the energy price is low. Hydrogen can then be stored in gas vessels at a significantly lower cost than the cost of storing electric energy. The electrolyzer's operator, however, intends not only to optimize operation in terms of low average energy prices and high renewable utilization, but also needs to meet hydrogen demand at any time. Thus, flexibility is not unlimited. To date, an applicable, practice-oriented strategy for electrolyzer operation at an HRS is missing.

Therefore, this study proposes and evaluates an intelligent

operating strategy for electrolysis. It is incorporated within an optimization and simulation framework. Section II describes the underlying methodology, which is applied to two scenarios in section III. Results are discussed in section IV, followed by conclusions in section V.

### II. METHODOLOGY

The proposed operating strategy provides quarter-hourly indications regarding ideal electrolyzer load and operating points of all other components, e.g. compressor or hydrogen storage. In order to determine the optimum, it is required to not only simulate the system's current but also future behavior based on forecasts of energy prices, wind energy availability, and hydrogen demand.

#### A. Basic Framework and Component Models

The presented approach extends a basic, existing framework and uses non-linear models of relevant HRS components: electrolyzer, compressor, storage, and dispenser. Furthermore, modelling of the electricity intraday spot market as well as hydrogen demand from passenger cars is also included. Additionally, a wind turbine is integrated into the HRS model. The basic framework comprises the aforementioned component models and is based on section-wise linearization and adapted linear equation system optimization [2]. For each simulated time step, the framework determines the ideal operating decision for all components. However, it is incapable of considering forecasts or future component behavior, and instead uses rules and heuristics. Thus the determined operating decision is based on the respective time step only. Therefore, it can be considered myopic. This framework and these component models have been developed within a project on an

existing HRS in Berlin, Germany. A basic description of this project and its models is available in the final project report [3].

#### B. Advanced Framework for Intelligent Operation

The presented framework extends the myopic approach in order to take forecasts into account. All time steps are simulated consecutively as in the myopic approach (in the following referred to as main steps). For each main step, however, all possible decisions of the respective main step (instead of just the ideal one) are calculated and evaluated in terms of previously defined optimization targets, e.g. low costs. Then, a hypothetical future of the current main step is also simulated. In this process, forecasts of electricity price, wind energy availability, and hydrogen demand are incorporated. Finally, the most promising option of the current main step is chosen, based on the main step (as in the myopic approach) as well as the projected future steps. The simulation is then continued with the next main step and so on.

Instead of using perfect foresight, this approach can process realistic and imperfect forecasts and limited forecast horizons in order to only consider information that would be available when applying this strategy to a real-world HRS.

### III. APPLICATION TO REAL-WORLD SCENARIOS

This approach is applied to two scenarios of an HRS. The first scenario comprises models of electrolyzer (450 kW rated power, 630 kW overload power), low pressure storage (45 bar, 380 kg capacity), compressor (33.6 kg/h), and dispenser including hydrogen cooling. This setup reflects the situation at the aforementioned HRS in Berlin [3]. Furthermore, quarter-hourly hydrogen demand according to HRS class “small” [4] (168 kg per day) is provided as well as German intraday spot market participation with data from 2015 [5].

The second scenario is identical except for an additional wind turbine (1.6 MW rated power) that also supplies an electrolyzer with higher rated power (545 kW) and adjusted storage capacity (770 kg). The rated powers of wind turbine and electrolyzer as well as the storage capacity have been determined through topology optimization using the myopic approach. Produced electricity which cannot be used by the electrolyzer is fed into the electrical grid and compensated.

Intraday electricity price forecasts are determined based on day-ahead pricing, taking place at 12 o'clock of the previous day. Real wind energy forecasts are used and hydrogen demand is forecast based on a specially developed algorithm, accounting for the chosen HRS class “small”. Forecast horizon is 24 hours.

Simulation is conducted for one year in quarter-hourly steps. For better comparison, scenarios are additionally evaluated with the basic, myopic approach. The HRS is assumed to be sited in Germany, and respective taxes and surcharges are therefore taken into account. Capital and operational expenditures are considered via annuity calculation.

### IV. RESULTS

Results show that intelligent operation reduces hydrogen costs by 1.1 % to 13.28 €/kg in scenario one and by 9.2 % to 11.52 €/kg in scenario two. Accordingly, combining an HRS with a wind turbine leads to 13 % lower hydrogen costs compared to spot market participation only. The intelligent operating strategy effectively maximizes wind energy utilization (74 % renewable hydrogen vs. 62 % with myopic operation). Without taxes and surcharges, costs are reduced by 59 % to 5.41 €/kg in scenario one and by 28 % to 8.32 €/kg in scenario two. Currently, hydrogen is sold at 7.98 €/kg + VAT.

### V. CONCLUSION

Electrolysis at an HRS provides flexibility potential in terms of load profile. But until now it has been unclear how it should be operated in order to harness low energy prices and maximize renewable energy utilization when constrained by hydrogen demand. The presented approach provides an intelligent operating strategy, considering forecasts of electricity price, wind energy availability, and hydrogen demand. It is applicable to a real-world HRS with onsite electrolysis.

Hydrogen production costs are reduced by 9.2 % to 11.52 €/kg in scenario two, and wind energy utilization is increased significantly compared to a simple, conventional operating mode.

### ACKNOWLEDGMENT

The authors gratefully acknowledge the funding of this work by research projects H2BER and ImplaN. H2BER (grant-agreement 03BV242) is part of the "National Innovation Program Hydrogen and Fuel Cell Technology" funded by the German Federal Ministry of Transport and Digital Infrastructure. ImplaN (grant-agreement 03ZZ0727) is funded by the German Federal Ministry of Education and Research.

### REFERENCES

- [1] C. Bauer, et. al., „The environmental performance of current and future passenger vehicles: Life Cycle Assessment based on a novel scenario analysis framework“, *Applied Energy*, p. 13, 2015.
- [2] F. Grueger, et. al., „An approach for the simulation and control of microgrids under of various energy forms and mass flows“, 9th International Renewable Energy Storage Conference, March 2015
- [3] Reiner Lemoine Institut gGmbH, „H2BER: Entwicklung, Erprobung und Bewertung intelligenter Betriebsstrategien für die verschiedenen Komponenten und die Gesamtsteuerung der Wasserstoff-Tankstelle am Flughafen (BER)“, Leibniz-Informationszentrum Technik und Naturwissenschaften
- [4] H2 Mobility, „70 MPa Hydrogen Refuelling Station Standardization“, 2010.
- [5] „EPEX Spot SE“, [Online]. Available: <https://www.epexspot.com/de/marktdaten/intradaycontinuous>.



## IMPROVEMENT OF HIGH ELECTRICAL EFFICIENT SOFC GENERATOR WITH A MULTI-STAGE SOFC SYSTEM AND FUEL REGENERATION PROCESS

○T. Dohkoh\*, K. Nakamura\*, T. Nakajima\*, M. Shirai\*,  
S. Taku\*, K. Isshiki\*, T. Ide\*, K. Ogasawara\* and K. Fujita\*  
\* Tokyo Gas Co., LTD., Suehiro-Cho 1-7-7, Tsurumi-Ku,  
Yokohama, Kanagawa, 230-0045 (Japan)

### Abstract -

Increasing the fuel utilization ratio (Uf) is effective to improve electrical efficiency of an SOFC system. To increase Uf, we focused on fuel regeneration process. In this process, the reaction products of the first cell-stack, such as steam (H<sub>2</sub>O) and carbon dioxide (CO<sub>2</sub>), are removed from the anode off-gas. Then, the regenerated anode off-gas is used as a fuel of the second cell-stack. In this study, we evaluated the properties of a membrane module for the fuel regeneration process at a two-stage stack SOFC system. The membrane module demonstrated high permeation of H<sub>2</sub>O and CO<sub>2</sub> with low permeation of hydrogen.

*Index Terms – Solid Oxide Fuel Cell, fuel utilization ratio, CO<sub>2</sub> separation, Separation membrane*

### I. INTRODUCTION

Fuel cell is well known as a high electrical efficient generator. It has commercialized for business and residential use. Compared to residential use, the demand of power in business use is larger than that of heat. Therefore, we aim to develop a high efficient power generate system with the solid oxide fuel cell (SOFC).

Some factors affect the electrical efficiency. In this research, we focused on the fuel utilization ratio (Uf). Generally, the Uf of SOFC is limited to around 70% to protect anode from oxidation caused by decrease of fuel concentration. However, we realized a Uf value of 92.0% by a multi-stage SOFC system and fuel regeneration process.[1] In this system, there are two SOFC stacks connected in series and a fuel regenerator which removes steam (H<sub>2</sub>O) and carbon dioxide (CO<sub>2</sub>) from the anode off-gas of first SOFC stack and provides the regenerated gas to second SOFC stack as fuel.

Until today, we have developed four types of SOFC hotboxes by combining stacks, a reformer, a combustor, a vaporizer, regenerators, and heat exchangers. The 1<sup>st</sup> generation hotbox demonstrated the high Uf value of 92.0% using CO<sub>2</sub>

absorber and water condenser as fuel regenerators with the assistance of electrical heaters.[2-3] The 4<sup>th</sup> generation hotbox demonstrated a high electrical efficiency under the thermal self-sustainable condition without the electric heater. In particular, DC-power output was 4.13 kW at total Uf of 90.2% and DC-electrical efficiency was 73.0%LHV under the condition. This 4<sup>th</sup> hotbox adopted only water condenser as a fuel regenerator because the anode off-gas contains more volume of H<sub>2</sub>O than that of CO<sub>2</sub>. Therefore, it is possible to improve the electrical efficiency of hotbox by removing CO<sub>2</sub>. For commercialization of the fuel regeneration process, both CO<sub>2</sub> absorber and water condenser have problems. CO<sub>2</sub> absorber makes the SOFC system complicated because it needs the cycle of absorption and desorption and so the SOFC system needs to have several absorbers. Water condenser increases the heat loss of the SOFC system because the gas is cooled by it. Therefore, the fuel regenerators with simple configuration and low heat loss process are required.

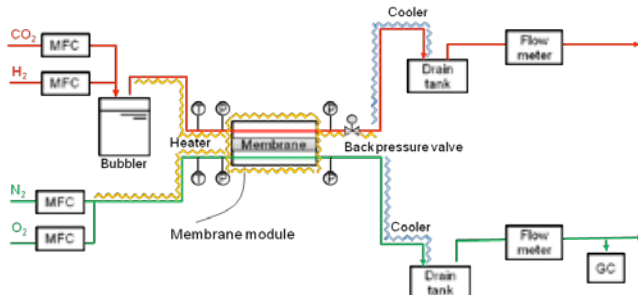
In this study, we focused on a separation membrane for the fuel regenerator because it can separate gas continually without cooling. We evaluated its permeation of CO<sub>2</sub>, H<sub>2</sub>O and hydrogen (H<sub>2</sub>).

### II. EXPERIMENTS

#### A. Flow diagram of evaluation device

Figure 1 shows the flow diagram of the evaluation device for membrane module. Separation membrane module was covered and heated by heating jacket. Dew point-controlled H<sub>2</sub> and CO<sub>2</sub> were used as the feed gas. Dry N<sub>2</sub> and O<sub>2</sub> were used as the sweep gas. The temperatures of these feed and sweep gases were controlled constant using line heater and heating jacket. The pressure of feed gas at the inlet of the membrane module was also controlled using back pressure valve. The outlet of

sweep gas was opened to the atmosphere. The contents of sweep gas discharged from membrane module were measured using gas chromatograph. The permeate flow rate of  $H_2$  and  $CO_2$  were calculated from these contents and the flow rate converted into a reference flow. The permeate flow rate of  $H_2O$  was calculated from the weight of water condensed in feed gas line per unit time and the flow rate per unit time of water introduced to inlet of feed gas.



**Fig. 1. Flow diagram of the evaluation device for membrane module.**

#### B. Evaluation of permeation ratio on different temperatures

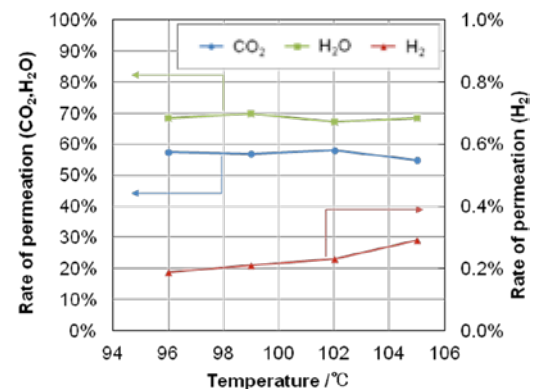
The feed gas was simulated as anode off-gas from first SOFC stack at a two-stage stack SOFC system whose generation amount is approximately 0.63 kW. The dew point was 91°C and the pressure was 125 kPa (abs). The flow rate of  $H_2$  and  $CO_2$  were 2.6 NL/min and 1.3 NL/min, respectively. In the fact, the anode off-gas includes CO. In this study, CO was replaced with the same amount of  $H_2$ . The flow rate of dry  $N_2$  for sweep gas was 10 NL/min. To investigate the relation between temperature and permeation, the permeation of  $H_2$ ,  $CO_2$  and  $H_2O$  were evaluated from 96°C to 105°C by controlling the temperature of gases and membrane module.

#### C. Durability test

The temperature, dew point and pressure of the feed gas were adjusted to 96°C, 91°C and 125 kPa (abs), respectively. The flow rate of  $H_2$  and  $CO_2$  were 2.6 NL/min and 1.3 NL/min respectively. Dry  $N_2$  and  $O_2$  were used as sweep gas to simulate Air and its flow rate was 30 NL/min. The durability of permeation ratio was evaluated under the condition.

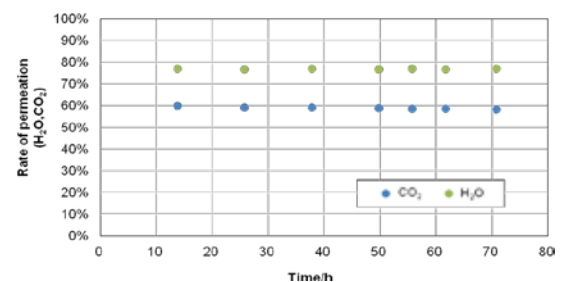
### III. RESULTS

The dependence of permeation on temperature is shown in Fig. 2. The rate of  $H_2O$  permeation was constant around 70% in the range from 96°C to 105°C. The rate of  $CO_2$  permeation was constant at around 58% in the range from 96°C to 102°C and decreased to 55% at 105°C. The rate of  $H_2$  permeation was less than 0.3% and quite lower than those of  $CO_2$  and  $H_2O$ .



**Fig. 2. Dependence of permeation ratio on temperature.**

The result of durability test was shown in Fig. 3. The rates of  $H_2O$  and  $CO_2$  permeation were constant around 80% and 60% over 70 h, respectively.



**Fig. 3. Change of permeation ratio with time.**

### IV. CONCLUSION

We evaluate properties of a membrane module for the fuel regeneration process. As a result, we confirmed that the membrane module has a potential to remove  $H_2O$  and  $CO_2$  selectively from anode off-gas including  $H_2$ . Moreover, the separation properties were stable over 70 h. These results indicate the membrane module is a promising process as the fuel regenerator of the two-stage SOFC stack system.

### REFERENCES

- [1] S. Elangovan, et al., J. Electrochem. Soc., Volume 144, 1997, Pages 3337-3342.
- [2] T. Somekawa, et al., Applied Thermal Eng., Volume 114, 2017, Pages 1387-1392.
- [3] S. Taku, et al., Proceeding of 2015 Fuel Cell Seminar & Energy Exposition, Los Angeles, 2015, R&D33-1.



## OPERATING EXPERIENCES WITH A 50 KW SOEC UNIT INTEGRATED WITH A CATALYTIC METHANATION UNIT FOR BIOGAS UPGRADING.

John Bøgild Hansen\*, B. Christian Dannesboe\*\*

\*Haldor Topsøe A/S, Kgs. Lyngby, Denmark

\*\*Aarhus University, Aarhus, Denmark

**Abstract** - Haldor Topsøe A/S has designed, constructed and operated a plant for upgrading 10 Nm<sup>3</sup>/h of raw biogas to pipeline quality RNG at the biogas research centre of Aarhus University in Foulum, Denmark. The hydrogen for the methanation of the CO<sub>2</sub> in the biogas is produced by 8 Solid Oxide Electrolyzer Cell stacks. The biogas is desulfurised to below 5 ppb S before being metanated in a boiling water reactor loaded with high temperature resistant methanation catalyst. Operating experiences from extended test runs (> 3 months) will be described and discussed. The role of the concept in energy scenarios with a high penetration of intermittent, renewable power production is quantified using Denmark as an example

**Index Terms** – Biogas Upgrading, Desulfurisation, Methanation, SOEC.

### I. NOMENCLATURE

SOEC = Solid Oxide Electrolyzer Cell.

### II. INTRODUCTION

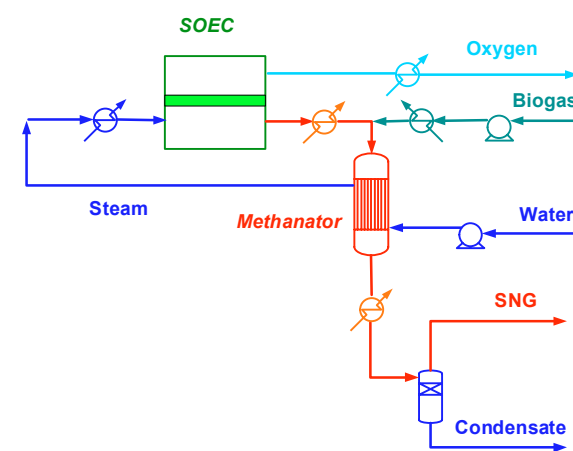
The share of electricity production from wind and solar reached 52 % of net generation in Denmark from January to September, 2017 and the goal is to achieve 100 % in 2035. There exists also a large potential for biogas production. The present project aims at utilizing renewable electricity to generate hydrogen by means of SOEC and hydrogenate the CO<sub>2</sub> in the biogas catalytically to methane.

### III. PROCESS DESCRIPTION

Biogas is compressed to around 20 bar g and desulfurized by using activated carbon followed by removal of refractory sulfur compounds using specially adopted Haldor Topsøe catalysts.

The desulfurized biogas is then mixed with hydrogen from the SOEC unit. See Fig. 1. The CO<sub>2</sub> in the biogas is then

converted to methane using high temperature resistant methanation catalyst in a two bed boiling water reactor with water separation between the beds. The steam generated in the boiling water reactors are used as feedstock together with some hydrogen recycle in the SOEC unit.



\_Fig. 1. Overall process layout.

### IV. THE PROJECT

The above process has been demonstrated in a pilot plant located at Aarhus University's premises in Foulum, Denmark and uses gas from the large experimental biogas reactor on site. The SOEC based pilot plant can produce 10 Nm<sup>3</sup>/h of upgraded biogas. This capacity ensures correct linear velocities and heat transfer in the boiling water reactor so the results can easily be scaled up. The SOEC unit consists of 8 stacks which in total consumes 50 kW electricity and produces approx. 16

Nm<sup>3</sup>/h of hydrogen. A picture of the unit is shown as Fig. 2.



Fig. 2. The biogas upgrading pilot plant in Foulum

## V. RESULTS.

Despite a number of problems related to power supplies, biogas and hydrogen compressors etc. which have caused a number of unintended shut downs and full thermal cycles the SOEC stacks have been operated at design production rate for more than 2200 hours.

The operating strategy has been to keep the production rate steady and compensate for stack degradation by increasing the inlet temperature keeping the voltage constant at the thermoneutral value. The data are shown on Fig. 3.

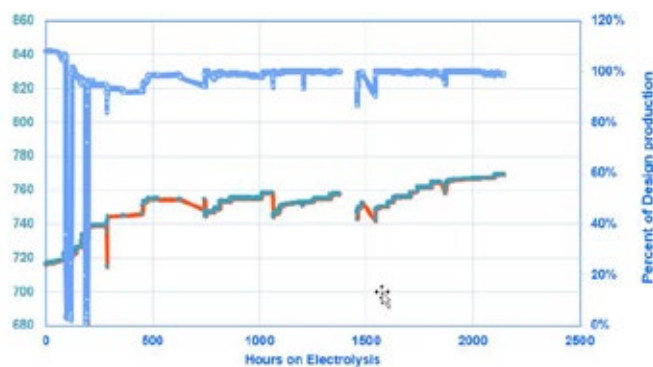


Fig. 3. Production rate and operating temperature vs time on stream

After the initial rather fast degradation observed in the first 450 operating hours the stack performance stabilized and showed only minor degradation subsequently.

The very high energy efficiency close to 100 % when generating hydrogen from steam with SOEC has been confirmed. The time required for startup of the SOEC unit from ambient conditions is around 10 hours, but the load can be varied from 3-4 % to 100 % within seconds, which is of course important when using intermittent power generation from renewables.

The unit has been remotely controlled most of the time.

The methanator performance has been excellent with most of the reaction occurring in the top part of the reactor as revealed by the temperature profiles shown on Fig. 4. The desulfurisation section has also been functioning flawlessly as evidenced by the methanator temperature profile, which has not changed throughout the experimental runs.

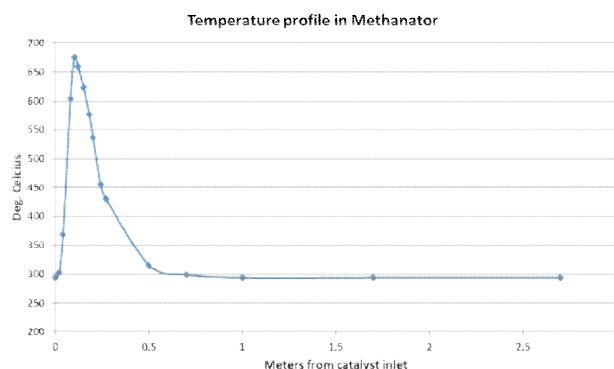


Fig. 4. Temperature profile in the methanator.

It has been possible to surpass the requirements to pipeline quality gas (basically more than 95 % CH<sub>4</sub> and less than 2 % H<sub>2</sub>) as shown on Fig. 5.

Position	CH <sub>4</sub>	CO <sub>2</sub>	N <sub>2</sub>	H <sub>2</sub>
Inlet	56	43	1	0
Exit 1 <sup>st</sup> stage	94.58	0.27	0.91	4.23
Product gas	97.69	0.00	0.95	1.36

Fig. 5. Gas Analyses. The reactor consists of two stages with water condensation in between stages.

## VI. CONCLUSION

It has been demonstrated that biogas can be upgraded using SOEC and methanation with very high efficiency for more than 2200 hours. If the total biogas potential in Denmark was utilized and upgraded by means of electrolysis ten percent of the final energy consumption could be covered and one ton of CO<sub>2</sub> saved per capita and year.

## ACKNOWLEDGMENT

The authors gratefully acknowledge the financial support from the Danish Energy Ministry's EUDP programme.

## MANUFACTURING LOW-COST AND BIODEGRADABLE PAPER MICROBIAL FUEL CELLS

J. Chouler\*, S. Rengaraj\*, R. Grubb\*, J. L. Scott\*\*, C. C. Bof Bufon\*\*\*, M. Di Lorenzo\*

\*Department of Chemical Engineering, Claverton Down, BA2 7AY, (UK)

\*\* Department of Chemistry, Claverton Down, BA2 7AY, (UK)

\*\*\* Brazilian Nanotechnology Laboratory, 13083-970, Campinas, Sao Paulo (BR)

**Abstract** - The limited fraction of water available for personal use is seriously compromised by a plethora of pollutants generated on a daily basis by domestic, agricultural and industrial activities. As such, there is an increasing impetus to develop tools capable of assessing water quality in real time, for which microbial fuel cell (MFC) technology has enormous potential. Herein we describe the fabrication of a MFC device that is amenable to mass production, using a scalable and cheap method that will allow cost effective production from a renewable raw material that is biodegradable at end-of-life, such as paper.

**Index Terms** – microbial fuel cells, paper, screen-printed electrodes.

### I. INTRODUCTION

Access to safe water is a human right. Nonetheless, it is still a luxury in many less developed areas of the world, where basic infrastructure and effective quality controls are often missing. In this context, it is extremely important to establish methods for water quality analysis that do not require expensive laboratory equipment and/or skilled personnel, yet provide rapid response and have onsite functionality.

In recent years, microbial fuel cell (MFC) technology has demonstrated promising potential as a tool for water quality monitoring [1]. Despite their promise, practical implementation of MFCs as sensors is still restricted by the use of expensive manufacturing materials and device designs that are not suitable for portable applications, due to the need for pumps during operation. All these aspects reflect in an increase in both capital and operating costs. There is therefore a great need for innovative and cost-effective MFC designs.

Here we propose the use of paper for the development of innovative, light and recyclable MFCs, which are also cost-effective, easy-to-operate and safe-to-dispose of. Paper has been already explored for the fabrication of MFCs [2-5]. In this study, however, we report the first *single*-component paper MFC (pMFC), obtained by patterning carbon-based electrodes onto a single sheet of paper. The device is membrane-less, as the paper substrate itself acts as the separator between the two electrodes. Moreover, there is no need for sample pumping, since capillary forces in the paper create autonomous microfluidics that can be manipulated by changing the paper structure, thus tuning the performance of the device. The resulting pMFC device has an extremely simple and easy-to-fabricate design, and is prepared from fully biodegradable, non-polluting components.

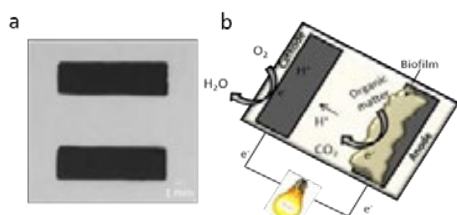
### II. MATERIALS AND METHODS

#### A. Device fabrication

The MFCs consisted of two carbon-based electrodes (10 x 30 mm<sup>2</sup>) patterned onto filter paper (Whatman grade 1), with a spacing of 15 cm (Fig. 1). The graphite ink was prepared by combining 2.85 g of a 1:1 mixture of cyclohexanone and acetone with 0.150 g of cellulose acetate and stirring for 2 h, before addition of 1 g of graphite and mixing for 2 min. The electrodes were patterned by using adhesive layers to delineate the target area, and spreading the graphite ink over the surface with a squeegee. The so-patterned paper was pre-dried under a fume hood for 1 hr, the adhesive layers carefully removed and

Copyright © 2017

the device was dried in an oven at 60 °C for 15 min. The conductivity of the resulting electrodes, determined by the four-terminal probe method using an Ivium Compactstat 104 (B08084, Ivium Technologies, NL), was  $108 (\pm 28) \Omega \text{ sq}^{-1}$ .



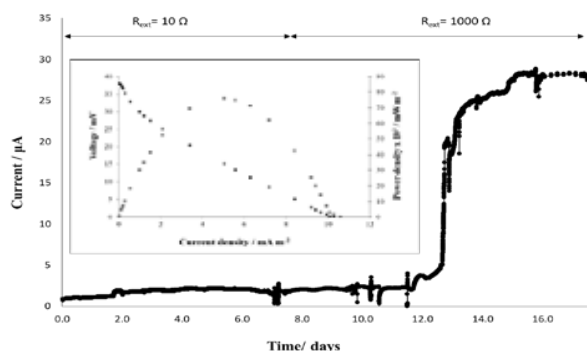
**Fig. 1.** a) Actual photograph of the pMFC; b) working principles

### B. Operation of the paper MFCs

Artificial wastewater (AW), containing 10 mM potassium acetate ( $\text{COD} = 950 \pm 32 \text{ mg L}^{-1}$ ), was prepared as previously described [6]. The medium was autoclaved and purged with nitrogen before being fed to the pMFCs. Titanium wire, glued with conductive paste onto the patterned electrodes, was used to connect the MFC anode and cathode to a voltmeter (ADC-24 Pico data logger, Pico technology, UK) and voltage,  $V$ , was continuously monitored under closed circuit conditions by applying an external load,  $R_{\text{ext}}$ , to polarise the cell. To achieve enrichment of electrochemically active bacteria at the anode, the anodes of the pMFCs were submerged in a sealed 100 mL vessel containing 10% v/v anaerobic sludge provided by Wessex Water, UK. The pH of the solution was  $7.5 \pm 0.1$  and the conductivity  $7.14 \pm 0.15 \text{ mS cm}^{-1}$ . Ten percent of the solution was replaced daily with freshly prepared AW. Electrochemical analysis was performed using an Autolab PGSTAT128N (Metrohm, UK). Polarisation curves were recorded in two-electrode mode at a scan rate of  $5 \text{ mV s}^{-1}$ .

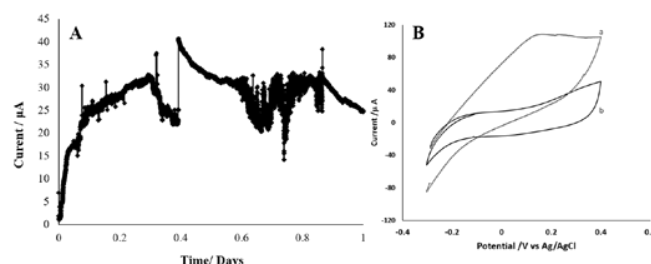
## III. RESULTS

The anodes of the pMFCs were enriched for 18 days. During the first week, the electrodes were connected to a low  $R_{\text{ext}}$  to promote the selection of electroactive bacteria at the anode. Subsequently a high  $R_{\text{ext}}$  was used.



**Fig. 2.** Enrichment of the pMFC. Inset: power and polarization curves obtained after 17 days of operation. Data is the average of two replicates with 10% maximal variation.

A rapid increase in the current output was observed after 12 days of incubation and a stable current was obtained after 15 days (Fig. 2). The OCV was 40 mV and the peak power density, at 15 mV, was  $76 \times 10^{-3} \text{ mW m}^{-2}$ . The OCV is much lower than other MFCs reported [7], probably due to oxygen diffusion to the anode. This drawback is counteracted by the extremely simplified manufacturing and consequent cost reduction of the proposed device, which facilitate mass production. The pMFCs were operated for up to 30 days, after which a decay in the current output was observed, due to the device degradation (data not shown). After approximately two months in AW, the pMFC was almost fully degraded. To speed up the enrichment stage, a poised anode potential strategy was tested. In this way, a steady current was reached after only one day (Fig. 3A).



**Fig. 3.** A) Anode enrichment of the pMFC at a poised potential of 0.2 V. B) cyclic voltammetry scans (at a rate of  $5 \text{ mV s}^{-1}$ ) in artificial wastewater of the fuel cell with an enriched anodic biofilm (curve a) and of a fuel cell that has not been inoculated with bacteria (curve b).

The electrochemical performance of the anodic biofilm so obtained was compared with an unenriched fuel cell. In the absence of bacteria, no oxidation peak was observed (Fig. 3B).

## IV. CONCLUSION

This study reports the first paper MFC fabricated by patterning carbon electrodes onto a single piece of paper. Its electrochemical performance is analyzed and a method to speed-up the enrichment stage is reported. This pMFC can lead to light, easy-to-use and biodegradable single-use MFC-sensors for water quality monitoring, which are affordable to all.

## ACKNOWLEDGMENT

The authors wish to thank the Engineering and Physical Sciences Research Council (EPSRC) and the Centre for Doctoral Training in Sustainable Chemical Technologies (EP/P510907/1; EP/G03768X/1).

## REFERENCES

- [1] Chouler, J. & Di Lorenzo, M. *Biosensors* 5, 2015, 450–470.
- [2] Winfield, J. *et al. J. Mater. Chem. A* 3, 2015, 7058–7065.
- [3] Hashemi, N. *et al. Technology* 4, 2016, 98–103.
- [4] Lee, S. H., *et al. Sci. Rep.* 6, 2016, 28588.
- [5] Fraiwan, A. & Choi, S. A. *Biosens. Bioelectron.* 83, 2016, 27–32.
- [6] Chouler, J. *et al. Electrochim. Acta* 231, 2017, 319–326.
- [7] Ieropoulos, I., *et al. Bioelectrochemistry* 78, 2010, 44–50.

## LASER-ABLATED SPENT BATTERY GRAPHITE ROD AS ELECTRODE FOR MICROBIAL FUEL CELL APPLICATION

A.R. Montes-Ochoa\*, C. Frausto-Reyes\*\*, M. Ortiz-Morales\*\*,  
Sofia E. Acosta-Ortiz\*\*\*, F. Caballero Briones\*\*\*\*, Manuel  
Sanchez Cardenas\*, S-K. Kamaraj\*

\* Universidad Politécnica de Aguascalientes, Ingeniería en Energía Calle  
Paseo San Gerardo No. 207. Fracc. San Gerardo. Aguascalientes, Ags.  
México, 20342, (Mexico) y-Present Address

Unidad Especializada en Energías Renovables – Tecnológico Nacional de  
México, Blvd. San Pedro 500, Parque Industrial Ferropuerto Mieleras,  
Torreón, Coahuila de Zaragoza, México, C.P. 27400.

\*\*Centro de Investigaciones en Óptica, A.C. Prol. Constitución 607, Fracc.  
Reserva Loma Bonita Aguascalientes, 20200, México.

\*\*\* Lasertech, S.A. de C.V. Blvd. Olivares Santana 113, Fracc. El Dorado,  
Aguascalientes, 20235, México

\*\*\*\* Centro de Investigación en Ciencia Aplicada y Tecnología Avanzada  
del IPN, Unidad Legaria, 11500 (Mexico)

### Abstract

Reuse of materials is attractive for their potential economic and environmental benefits. At this perspective, we have extracted the graphite rod (GR) from the spent battery and used as electrode materials in the dual chamber microbial fuel cell (MFC), to treat the wastewater at the anodic chamber. The maximum volumetric power production of  $140.48 \text{ mW/m}^3$ , the volumetric current density of  $341.16 \text{ mA/m}^3$  at the  $0.410 \text{ V}$  was observed in spent battery graphite rod as electrode materials (anode and cathode) in MFCs. Further, the surface of that graphite rod was fractured/irradiated by laser ablation, in order to increase the superficial contact area of the electrodes. Systematically evaluated the fractured graphite rod (F-GR) as electrode materials in MFCs as follows: a) F-GR as an anodic current collector and GR as a cathodic current collector, b) F-GR as a cathodic current collector and GR as an anodic current collector, c) F-GR applied both the anode and cathodic current collector. From the conclusion, use of both side F-GR as electrode materials improved 15 times higher volumetric power production ( $2210.55 \text{ mW/m}^3$ ). This configuration MFCs in series has used to power the LED.

**Index Terms** – microbial fuel cells, graphite rod, laser, wastewater.

### I. INTRODUCTION

Sustainable reuse of materials is attractive from the economic and environmental point of view. Further usage of these materials as an electrode for the application of Microbial fuel cells (MFCs) are quite attractive. Generally, carbon-based

materials are widely used as electrode materials in many forms such as carbon cloth, carbon paper, carbon felt, graphite fiber brush and graphite rod. Each of one has their own merits and demerits related to cumbersome synthesis methods to the application. Many reports showed that the surface modification of electrodes with Nano-based carbon materials and/or chemical functionalization methods on the base of above-mentioned electrodes [1]. Even though graphite rods are widely used materials in MFCs because of the good electrical conductivity, chemical stability, and relatively cost-effective price, although it is difficult to increase the surface area. Herein, we proposed the green benign method to alteration of graphite rod surface with the aid of Laser, used as electrode materials and systematically evaluated in MFCs.

### II. MATERIALS AND METHODS

#### A. Construction of clay cup based MFC, characterization, and operation

The commercial clay cup (3 mm thickness) was procured from the local market of Aguascalientes, México [2]. Graphite rod used as an anodic and cathodic current collector was placed inside and outside of the clay cup (GR-MFCs). The wastewater collected from the Universidad Politécnica de Aguascalientes (UPA) served as inocula and medium to be treated. The



graphite rods are treated with laser, further, it was evaluated systematically as electrode materials for anode alone (An-F-GR-MFCs), cathode alone (Ca-F-GR-MFCs) and Both Electrode (F-GR-MFCs). At regular time intervals, with the aid of a Fluke digital multimeter potential was registered. Polarization and power curve was obtained by linear sweep voltammetry at a scan rate of 1 mV/s with two electrode configuration. The Power density (PD,  $\text{mW/m}^2$ ,  $\text{mW/m}^3$ ) and current density (CD,  $\text{mA/m}^2$ ,  $\text{mA/m}^3$ ) were calculated on the basis of exposed surface area and volume. Finally, four of the F-GR-MFCs in series connection was used for providing power for the LED and Two digital clocks.

#### B. Laser system and Physical characterization of graphite rod

Laser irradiation was applied to the graphite rod samples using Ytterbium pulsed fiber laser (IPG Photonics i-series marker model YLP-1-100-30-30-HC) with an average power output of about 30W and a wavelength of 1064. Raman spectroscopy of the samples was obtained by the Renishaw 1000B; excitation wavelength of the laser is 830 nm.

### III. RESULTS AND DISCUSSION

The collected spend battery graphite rods are separated and the chemical treatment to eliminate the impurities, which is exposed to laser irradiation (laser wavelength 1064 nm) with an average laser power of 11.5 W and frequency 80 kHz at two different scan rate (500 mm/s and 100 mm/s). The battery graphite rod exhibits the high degree of disorder peak (D) that breaks the translational symmetry i.e. edges, finite size effects, impurities, etc. This could be observed at  $1350\text{ cm}^{-1}$ . Also, it shows the graphitic peak (G) at  $1580\text{ cm}^{-1}$  in a less prominent. The intensity ratio of the D and G bands i.e. ( $I_D/I_G$  ratio) helps to estimate the defects of carbon-based samples, where a higher ratio ( $I_D/I_G = 1.65$ ) ensures more defects on battery graphite rod. In the low scan rate (100 mm/s) laser-irradiated sample at the center exhibit, the  $I_D/I_G = 0.52$ , which was lesser than the high scan rate (500 mm/s) laser irradiated at center ( $I_D/I_G = 1.42$ ). This might be due to the insufficient time for tuning the graphitic plane since the high scan rate shows the higher disorder at the center. Interestingly, higher scan rate produces the less disorder at the edges of the samples ( $I_D/I_G = 0.40$ ). However, low scan rate exhibits the very narrow range disorder ration between the center and edges (0.49 to 0.52) of the graphite rod. Later well-defined laser irradiated GR exploited as electrode materials in MFCs systematically. Table I provides the MFC polarization and power curve parameters. When the use of irradiated graphite rod as electrode materials, the performance of MFCs gradually increases and attained the maximum higher power performance in both side (anode and cathode) use of electrodes in F-GR-MFCs. The possible reason behind the improvement associated with the increment of contact surface area and further this could improve the charge

transfer reaction in anodic and cathodic reactions. Finally connected the four of the F-GR-MFCs in Series able to power the LED and two digital clocks (Fig.1.). The laser treatment performed under ambient condition and does not require any cumbersome pre and post chemical treatment. Hence the cost of this treatment is effective with the performance improvement, compared to the standard carbon-based electrodes.

TABLE I  
POLARIZATION AND POWER CURVE PARAMETERS OF MFCs

Parameters	An-F-GR-MFCs	Ca-F-GR-MFCs	F-GR-MFCs	GR-MFCs
$PD_a(\text{mW/m}^2)$	8.26	17	69.07	4.39
$PD_v(\text{mW/m}^3)$	264.22	544	2210.55	140.48
P (mW)	0.013	0.027	0.11	0.007
CD ( $\text{mA/m}^2$ )	24.04	42.32	156.94	10.66
CD ( $\text{mA/m}^3$ )	769.14	1354.37	5022.28	341.16
I (mA)	0.038	0.067	0.251	0.017
E (V)	0.340	0.401	0.440	0.410



Fig. 1. F-GR-MFCs prototype to power LED and digital clocks

### IV. CONCLUSION

An environmental benign method of graphite electrodes for microbial fuel cells application has been carried out by Laser irradiation. For optimum improvement was observed in use of both side irradiated graphite rod electrodes (F-GR-MFCs). Our method also justifies the economic and environmentally benign.

### ACKNOWLEDGMENT

KSK would like to acknowledge the funding agency of CONACYT and SEP México.

### REFERENCES

- [1] Wei, J., P. Liang, and X. Huang, Recent progress in electrodes for microbial fuel cells. *Bioresource Technology*, Volume 102(20), 2011, Pages 9335-9344.
- [2] Sathish-Kumar, K., Alejandro, E.R., Selvasankar, M., Jaime G-M., Claudio F-R., José T-R., European Fuel Cell Technology & Applications Conference, 2015, Proceeding of the 6th European fuel cell Piero Lunghi Conference, ELECTRICITY GENERATION FROM NOPAL BIOGAS WASTE BIOMASS USING CLAY CUP (CANTARITO) MODIFIED MICROBIAL FUEL CELL, (EFC15153), Pages 183-184, ISBN 978-88-8286-324-1.



## **SURFACE MODIFIED CLAY BASED AIR CATHODE MICROBIAL FUEL CELLS FOR WASTEWATER TREATMENT**

G.J. Bárcenas Durón<sup>\*</sup>, K.Gunaseelan<sup>\*\*</sup>, S. Gajalakshmi<sup>\*\*</sup>, F. Caballero Briones<sup>\*\*\*</sup>, K. Sathish-Kumar<sup>\*y</sup> and F. Aguirre Sámano<sup>\*</sup>

<sup>\*</sup>Universidad Politécnica de Aguascalientes, Ingeniería en Energía, Aguascalientes, Ags. C.P. 20342.México.y-Present Address  
Unidad Especializada en Energías Renovables – Tecnológico Nacional de México, Blvd. San Pedro 500, Parque Industrial Ferropuerto Mieleras, Torreón, Coahuila de Zaragoza, México,C.P. 27400.  
<sup>\*\*</sup>Centre for Pollution Control & Environmental Engineering, Pondicherry University, Kalapet, Puducherry 605014, India.  
<sup>\*\*\*</sup>Instituto Politécnico Nacional, Laboratorio de Materiales Fotovoltaicos, CICATA Altamira. México.

**Abstract** - The present work focuses on the surface modification of cantarito (clay cup) based air cathodic microbial fuel cell system for the treatment of wastewater. This configuration achieves maximum volumetric power production of 504.11 mW/m<sup>3</sup>. However, it was maintained only for a short period; after which there was fall in the power generation and associated to water losses. To overcome this, acrylic based varnish and Arabic gum were applied on both the sides of the clay cup to improve the stability and avoid loss. Interestingly, acrylic based varnish and Arabic gum painted clay cup produced the maximum volumetric power production of 942.82mW/m<sup>3</sup> and power production of 629.56 mW/m<sup>3</sup> was maintained for long period of operation of up to 350 hrs and drastically reduced the water losses. Finally, energy harvested from the wastewater was powered by the low power electronics.

**Index Terms** – microbial fuel cells, clay cup, wastewater treatment, acrylic varnish.

### **I. INTRODUCTION**

Microbial fuel cells (MFCs) have emerged as a niche technology for conversion of organic substrate into direct electricity with the aid of biocatalyst placed on the fuel cell systems. The separators act as one of the remarkable factors, which separate the two compartments of the cells as anode and cathode, which further influence the power generation. Different kinds of separators had been evaluated in MFCs, such as Nafion, Ultrex, bipolar membranes, polystyrene, glass wool, nanoporous filters and microfiltration membrane. Due to the deprived performance stability and cost of the above

commercial membranes, interest was re-directed to exploit the natural composite materials like ceramics. There have been many reports (different compositions and thickness effect) stating the successful implementation of ceramic materials in MFCs [1]. However, there is a lack of surface modification of clay separator in the air cathodic MFCs systems. In this way, the research reported here focuses on the study made on the surface modification of clay with acrylic varnish and Arabic gum to address the major problem of water evaporation in the air cathodic MFCs. Moreover, the improved MFCs configuration was able to power the digital clock.

### **II. MATERIALS AND METHODS**

#### **A. Construction of clay cup based MFC, characterization, and operation**

Clay cup (3 mm thickness) was procured from the local market of Aguascalientes, México. Graphite felt used as an anodic current collector, was placed inside the clay cup. The wastewater collected from the Universidad Politécnica de Aguascalientes (UPA) served as inocula and medium to be treated. The outside of clay cup wrapped with stainless steel mesh (304) coated with spent battery catalyst act as cathode. This was designated as C-MFCs. Further, the clay cup was painted by acrylic varnish and Arabic gum on the surface, AV-C-MFCs, and AG-C-MFCs respectively. At regular time intervals, with the aid of a Fluke digital multimeter open circuit potential (OCP) was registered. Polarization and power curve

Copyright © 2017

was obtained by linear sweep voltammetry at a scan rate of 1 mV/s with two electrode configuration, where employed cathode was working electrode and anode as a counter as well as a reference electrode. The Power density (PD,  $\text{mW/m}^2$ ,  $\text{mW/m}^3$ ) and current density (CD,  $\text{mA/m}^2$ ,  $\text{mA/m}^3$ ) were calculated on the basis of exposed surface area and volume. Finally, two of the AV-C-MFCs in series connection was used for providing power for the digital clock operated for 350 hrs.

### III. RESULTS AND DISCUSSION

The first batch operation of intermittent electrochemical characterization was carried out for 350 hrs. Whereas the open circuit potential (OCP) was periodically registered, the electrochemical characterization was performed when the potential of fuel cells stabilized. C-MFCs gradually increased the OCP and attained 0.707 V at 250 hrs, delivering the maximum volumetric power density of  $504.15 \text{ mW/m}^3$  (Table 1.) obtained from Linear Sweep Voltammetry (LSV) with the 70% removal of COD. But the stability of the maximum potential was maintained for a very short period of time. Further substantial amount of water losses across the clay separator was recorded. Generally, water loss in the clay based MFCs are quite common in the passive air cathodic systems. In order to avoid the water loss and improve the stability of the Clay based MFCs, the commercial acrylic varnish and Arabic gum were applied on the surface of the clay. The negative functional group of acrylic ( $\text{H}_2\text{C}=\text{CH}-\text{C}(=\text{O})-$ ) is of interest. Previous studies of the authors reported improved power generation in clay based two chamber MFCs [2]. The natural composite materials of Arabic gum consist of a mixture of polysaccharide and glycoproteins which have been exploited as an additive in ceramic glazes. These properties drove to use Arabic gum for surface modification of clay. The acrylic varnish modified (AG)-C-MFCs attained the maximum OCP of 0.727 V at 216 hrs and exposed maximum volumetric power density of  $942.82 \text{ mW/m}^3$  from LSV (Table 1.) and 88 % removal of COD. Interestingly it showed that 72 hrs of potential stability and prevention of water evaporation upto 94 %. The maximum open potential reached at 0.610 V at 234 hrs and showed  $629.69 \text{ mW/m}^3$  from LSV (Table 1.) with COD removal of 82% in Arabic gum modified C-MFCs. This exposed the potential stability of 84 hrs and avoidance of 92 % of water evaporation.

The second batch operation was carried out by the closed circuit operation, where  $100 \Omega$  of resistance was applied for 350 hrs. During the closed circuit operation, the average volumetric power density was as follows: AV-C-MFCs ( $106.32 \text{ mW/m}^3$ ) > AG-C-MFCs ( $52 \text{ mW/m}^3$ ) > C-MFCs ( $1.08 \text{ mW/m}^3$ ).

Notably, better performance was encountered in the surface modified C-MFCs, which could associate with the prevention of water loss at the anodic chamber; further it prevented the cathodic reaction by transport of excess water molecule on the

cathodic surface. In the case of acrylic varnish painted MFCs, acryloyl group could favor the cationic movement responsible for the high power production with higher stability performance [2]. Moreover, clay based separator performance is limited by the thickness, composition, and porosity. At the final stage, when two AV-C-MFCs were connected in series, it was able to power the digital clock for 350 hrs.

TABLE I  
POLARIZATION AND POWER CURVE PARAMETERS OF C-MFCs

Parameters	C-MFCs	AG-C-MFCs	AV-C-MFCs
$\text{PD}_a(\text{mW/m}^2)$	2.11	5.30	5.41
$\text{PD}_v(\text{mW/m}^3)$	504.15	629.69	942.82
P (mW)	0.00484	0.00143	37.95
CD ( $\text{mA/m}^2$ )	8.750	25.49	16.39
CD ( $\text{mA/m}^3$ )	2244.4	2640	2858.67
I (mA)	0.0022	0.0084	0.115
E (V)	0.22	0.260	0.33

a – exposed surface area; b- volume



Fig. 1. AV-C-MFCs powered digital clock

### IV. CONCLUSION

The surface modification with Arabic gum and acrylic varnish did not only improve the stability of performance but also avoided the water loss in the clay based MFCs. Hence the experiments create an opportunity for further studies which need to focus on the surface modification of natural ceramic materials to avoid the major problem of water loss in the passive air cathode.

### REFERENCES

- [1] Winfield, J., Iwona, G., John, G., Ioannis, I, A Review of the Use of Ceramics in Microbial Fuel Cells, Bioresource Technology, 215, 2016, 296-303.
- [2] Sathish-Kumar, K., Alejandro Esqueda, R., Selvasankar, M., Jaime G-M., Claudio F-R., José T-R, Electricity Generation from Nopal Biogas Waste Biomass Using Clay Cup (Cantarito) Modified Microbial fuel cells, European Fuel Cell Technology & Applications Conference, 2015, Proceeding of the 6th European fuel cell Piero Lunghi Conference, 183-184, ISBN 978-88-8286-324-1.

## NUMERICAL MODELING OF AN AUTOMOTIVE DERIVATIVE PEM FUEL CELL CHP SYSTEM WITH SELECTIVE MEMBRANES

Andrea L. Facci\*, Gabriele Loreti\*, Thijs Peters\*\*, and  
Stefano Ubertini\*

\*Department of Economy, Engineering, Society, and Business.  
University of Tuscia, (Italia)

\*\*SINTEF Materials and Chemistry, P.O. Box 124 Blindern, N-  
0314, Oslo, (Norway)

**Abstract** - We present possible alternative configurations of a CHP plant based on an automotive derivative PEM fuel cell. Starting from a baseline CHP plant using the pressure swing adsorption (PSA) technology to separate hydrogen, we evaluate an alternative configuration by substituting the PSA with selective membranes.

**Index Terms** – CHP, Fuel Cell, Hydrogen, Membrane reactor.

### I. INTRODUCTION

In the last two decades, fuel cells are entering the market of distributed CHP systems [1,2]. Specifically, PEM are the most mature and promising for commercialization [3]. Large initial costs are the major obstacle to a massive production of PEM-based CHP plants [1,2]. At the same time the EU sets the ambitious milestone of 42% global efficiency for PEM-based CHP systems.

Fuel processing, and in particular syngas purification, significantly affects both the plant cost and efficiency.

In this paper, we assess the utilization of H<sub>2</sub>-selective membrane technology for syngas purification in comparison to traditional pressure swing adsorption (PSA).

### II. DESCRIPTION OF SELECTIVE MEMBRANES

An emerging separation technology that can be an alternative to PSA-based H<sub>2</sub> purification, is the use of H<sub>2</sub>-selective dense metal membranes. These membranes, based on palladium and its alloys, have frequently been proposed over the past decade to separate H<sub>2</sub> from a shifted syngas and simultaneously facilitate the capture of CO<sub>2</sub> [4]. Due to their optimum operating temperature of 300 – 500 °C, Pd-based membranes show a perfect match with the operating conditions of the WGS reaction. The H<sub>2</sub> flux through the membrane is driven by the difference of hydrogen partial pressure across the membrane as described by Eq. (1) [5].

$$J_{H_2} = K_{H_2} (p_{H_2,ret}^n - p_{H_2,perm}^n) \quad (1)$$

where  $K_{H_2}$  is the membrane permeance to hydrogen,  $p_{H_2,ret}^n$  and  $p_{H_2,perm}^n$  are the H<sub>2</sub> partial pressures on the retentate and permeate side of the membrane, and  $n$  is the driving force exponent.

### III. POWER PLANT DESCRIPTION AND MODELING

We numerically analyze the performance of a CHP plant based on a low temperature PEM-FC. Such a plant includes a fuel processor that convert pipeline natural gas into high purity H<sub>2</sub>, and an automotive derivative FC that produces electrical and thermal power. The baseline plant is described in details in [6]. Here, we assess the effect of substituting the PSA-based H<sub>2</sub> purification with selective membranes to separate H<sub>2</sub> from the syngas. We consider two different configurations: (i) substituting the PSA with selective membranes; (ii) integrating the membranes with the water gas shift (WGS) reactor, replacing both the WGS reactor and the PSA process. Both configurations are schematically represented in Fig. 1. The relevant processes (i.e. reforming, WGS, PSA separation membrane separation) occur at 12 bar pressure in all the configurations.

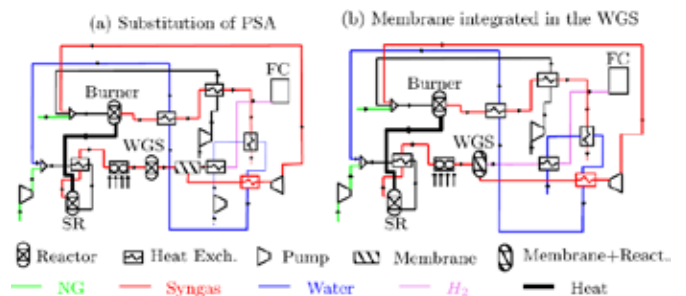


Fig. 1. Schematic representation of the considered power plants.

The steady state modelling of the power plant is performed through a thermodynamic lumped parameter approach, except for the PSA and the FC that are simulated through black-box

phenomenological models. Simulations are carried out in Aspen Plus [7] combined with proprietary Fortran models. The numerical model for the baseline plant is described in details in [6]. Following the approach in [5], the membrane reactor is modeled as a sequence of equilibrium reactors and finite area membrane separators, as represented in Fig. (2). For this, Eq. (1) is numerically integrated along the membrane surface to determine to hydrogen mass flow and concentration in the retentate and permeate gas streams.

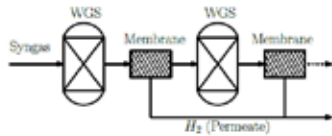


Fig. 2 Discretization of the WGS-membrane reactor.

#### IV. RESULTS AND DISCUSSION

We assess the effectiveness of the selective membrane integration by comparing the plant configuration presented in section II to the baseline plant described in [6] in terms of net electrical efficiency ( $\eta_{glob}$ ) and total efficiency ( $\eta_{total}$ ).

##### A. Substitution of PSA with selective membranes

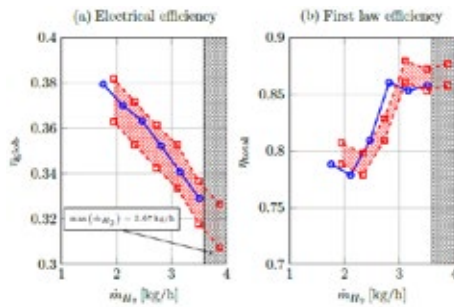


Fig. 3 Performance of the CHP plant with membrane separator after the WGS. The blue line represents the baseline plant performance. The red band between the two lines identifies the performances for atmospheric PEMFC and pressurized PEMFC (8 bar).

If  $H_2$  is required at high pressure (i.e. 8 bar),  $\eta_{glob}$  is reduced (Fig. 3(a)). Such a reduction is in the range [4.4%; 5.5%]. However, if  $H_2$  can be delivered to the FC at relatively low pressure (i.e. 1.2 bar) the membrane separator is slightly more efficient compared to the PSA. The total efficiency is not significantly varied by substituting the PSA with selective membranes.

##### B. Integration of selective membranes with the WGS reactor

We note from Figure 4(a) that the electrical efficiency of the modified plant is generally larger compared to the baseline configuration, except when  $H_2$  is compressed to 8 bar. In the latter case, the power plant efficiency is only marginally reduced with respect to the baseline configuration, while for lower  $H_2$  pressures the efficiency increment can be significant. The total efficiency is not significantly varied by substituting the PSA with the selective membranes.

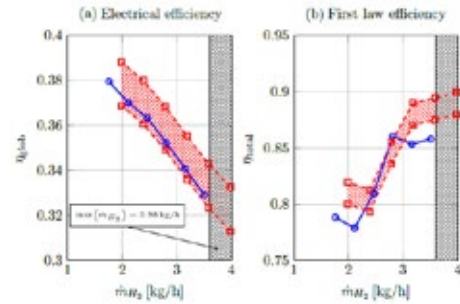


Fig. 4 Performance of the CHP plant with membrane separator integrated in the WGS. Refer to Fig. 3 for colors and symbols.

#### V. CONCLUSION

$H_2$ -selective membrane technology might improve the plant efficiency and reduce its complexity if directly integrated in the WGS. The efficiency is maximized if  $H_2$  can be utilized at low pressure. If  $H_2$  must be compressed the integration of selective membranes in the WGS still has a merit in terms of plant simplification. In fact, cooling and dehydration of the syngas before purification are not required.

#### ACKNOWLEDGMENT

This project has received funding from the Fuel Cells and Hydrogen Joint Undertaking under grant agreement No 671396. This Joint Undertaking receives support from the European Union's Horizon 2020 research and innovation program and United Kingdom, Germany, Greece, Croatia, Italy, Switzerland, Norway. Swiss partners are funded by the State Secretariat for Education, Research and Innovation of the Swiss Confederation.

#### REFERENCES

- [1] International Energy Agency, IEA advanced fuel cells implementing agreement and annual report, 2010.
- [2] Guzy, C. PEM fuel cells for distributed generation, in Washington Fuel Cell Summit, 2012.
- [3] F. Cappa, A. L. Facci, and S. Ubertini, Proton exchange membrane fuel cell for cooperating households: A convenient combined heat and power solution for residential applications, *Energy*, Volume 90, 2015, Pages 1229-1238.
- [4] R. Bredesen, K. Jordal, O. Bolland, High-temperature membranes in power generation with  $CO_2$  capture, *Chemical Engineering and Processing: Process Intensification*, Volume 43, 2004, Pages 1129-1158.
- [5] L. Roses, G. Manzolini, S. Campanari, E. De Wit, and M. Walter. Techno-economic assessment of membrane reactor technologies for pure hydrogen production for fuel cell vehicle fleets. *Energy & Fuels*, Volume 27, 2013, pages 4423-4431.
- [6] A. L. Facci, G. Loreti, S. Ubertini, F. Barbir, T. Chalkidis, R. P. Ebling, T. Peters, E. Skoufa, R. Bove, Numerical Assessment of an Automotive Derivative CHP Fuel Cell System, *Energy Procedia*, Volume 105, 2017, Pages 1564-1569.
- [7] Aspen Tech, Aspen Plus Unit Operation Models Reference Manual.



## ANALYSIS OF THE PERFORMANCES OF A FUEL CELL CHP SYSTEM UNDER DIFFERENT ENERGY DEMAND AND CLIMATE SCENARIOS

Andrea Luigi Facci\* and Gabriele Loreti\*

\*Department of Economy, Engineering, Society, and Business.  
University of Tuscia, (Italia)

**Abstract** – In this paper we assess the effective performance of a cogeneration plant based on low temperature PEM fuel cells in different energy scenarios. We vary the energy demand (office apartment district, clinic, hotel, and supermarket) and the climatic condition (Hot, Cooling Based, Moderate, Heating based, and Cold). We also consider two control strategies: one that minimizes the energy cost, and one that minimizes the primary energy consumption. The plant performance is analyzed comparing the energy cost and the primary energy consumption to the business as usual scenario. The payback time is also evaluated to assess the economic feasibility to the plant.

**Index Terms** – CHP, Fuel Cells, Climate conditions, Energy demand.

### I. INTRODUCTION

The International Energy Agency (IEA) estimates that CHP systems together with district heating and cooling could save 950 Mton/year of carbon dioxide emissions by 2030 [1]. Fuel cells, and specifically PEM-FCs, are one of the most promising prime movers for distributed energy generation [2-4] due to their flexibility, high efficiency, reduced noise, and low pollutant emissions.

In this paper we estimate the economic feasibility, and the effective reduction of primary energy consumption of a PEM-FC based CHP plant for different building scenarios.

The effectiveness of a power plant is largely determined by its control strategy [5-9]. Therefore, a management policy must be hypothesized to estimate economic feasibility, profitability and energy impact of the plant. Here, we consider two optimized control strategies: one that minimizes the energy cost, and one that minimizes the primary energy consumption.

### II. METHODOLOGY

We study the CHP plant schematically represented in Fig. 1. The performance of the plant components is retrieved from literature [10,11] and varies as a function of the set-point.

We utilize the methodology introduced in [6,8,9] to determine the plant control strategy. Such a methodology minimizes a prescribed objective function through a graph based algorithm.

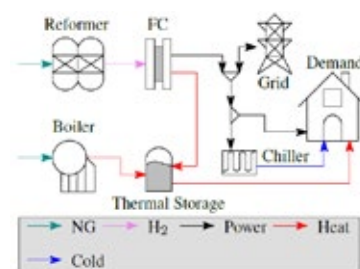


Fig 1. Schematic of the CHP plant in study.

We consider two different objective functions, minimum cost and minimum primary energy consumption (PEC), and we apply the methodology to 25 different energy management scenarios obtained combining 5 buildings (office apartment district, clinic, hotel, and supermarket) and 5 climatic conditions (Hot, Cooling Based, Moderate, Heating based, and Cold).

The energy demands for all the buildings and climates are retrieved from the “Reference buildings database” of the DOE [12].

For the economic analysis we assumed that the capital cost of the CHP plant is 2000 €/kW, the cost of electricity is 11.02 c€/kWh and the cost of natural gas is 6.54 €/GJ.

### III. RESULTS AND DISCUSSION

PEC reduction, cash flow and pay back time are systematically represented for all the considered cases in Fig 1 (economic optimization) and in Fig 2 (PEC minimization). Cogeneration consistently reduces the energy cost and the primary energy consumption for all the considered cases irrespective to the hypothesized control strategy.

According to economic optimization, PBP is below 10 years for all the considered cases, and is between 4 and 5 years for all the building typologies, except for the hotel and the office in moderate climate. The PBP is only marginally influenced by the climatic conditions. However, colder climates have generally lower PBP, larger cost reduction and lower primary energy consumption. In fact, a colder climate facilitates the heat

recovery from the prime mover throughout the year, improving the total system efficiency.

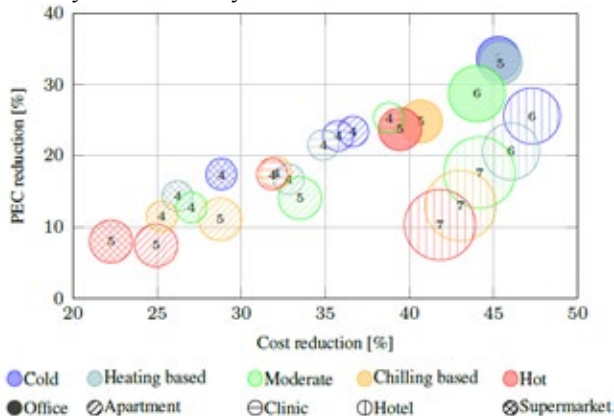


Fig 2. Comparison between the different scenarios for the minimum cost strategy: the area of the circles is proportional to the PBP.

Also PEC minimization allows a significant reduction of energy costs, as evidenced in Fig. 3. Moreover, switching from economic optimization to PEC minimization boosts the impact of CHP on the energy system. In fact, the PEC is reduced up to 70% with respect to cost minimization. The improvement of the energy efficiency is more relevant in hot climates, where exploiting CHP is more complicate. Such an improvement of the energy performance requires an increment of the expenses. However, the cost increment is relatively limited being in the range [2.5%, 20%]. Similarly, the PBP is incremented by only 1 year and the economic feasibility of the proposed plant is not compromised switching from economic optimization to PEC minimization.

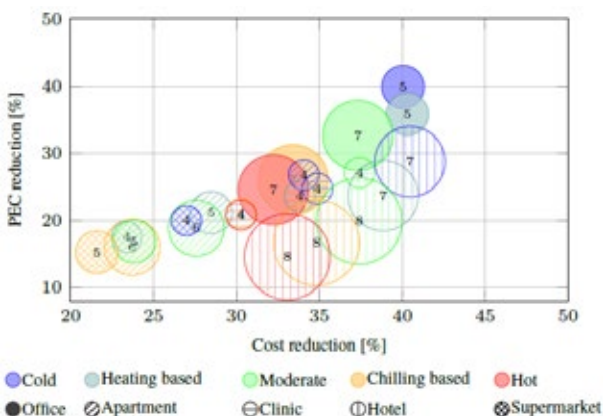


Fig 3. Comparison between the different scenarios for the minimum PEC strategy: the area of the circles is proportional to the PBP.

#### IV. CONCLUSIONS

In this paper we systematically demonstrated the effectiveness of an innovative CHP plant based on low temperature PEM fuel cells. Moreover, we assessed the effects of the management policy on the plan economic profitability and efficiency. The presented analyses clearly demonstrate the role of the control

strategy, and suggest to PEC minimization should be favored with respect to economic optimization. In fact, PEC minimization yields significant improvements of the system efficiency with only moderate economic penalties.

#### ACKNOWLEDGMENT

This project has received funding from the Fuel Cells and Hydrogen Joint Undertaking under grant agreement No 671396. This Joint Undertaking receives support from the European Union's Horizon 2020 research and innovation program and United Kingdom, Germany, Greece, Croatia, Italy, Switzerland, Norway. Swiss partners are funded by the State Secretariat for Education, Research and Innovation of the Swiss Confederation.

#### REFERENCES

- [1] International Energy Agency. Combined heat and power evaluating the benefits of greater global investment; 2008
- [2] A. L. Facci, V. Cigolotti, E. Jannelli, S. Ubertini, Technical and economic assessment of a SOFC-based energy system for combined cooling, heating and power, In *Applied Energy*, Volume 192, 2017, Pages 563-574, ISSN 0306-2619.
- [3] F. Cappa, A. L. Facci, S. Ubertini, Proton exchange membrane fuel cell for cooperating households: A convenient combined heat and power solution for residential applications, In *Energy*, Volume 90, Part 2, 2015, Pages 1229-1238, ISSN 0360-5442.
- [4] Brown JE, Hendry CN, Harborne P. An emerging market in fuel cells? Residential combined heat and power in four countries. *Energy Policy* 2007;35:2173e86.
- [5] D. Chiappini, A. Facci, L. Tribioli, S. Ubertini SOFC Management in Distributed Energy Systems. *ASME. J. Fuel Cell Sci. Technol.* 2011;8(3):031015-031015-12.
- [6] A. Facci, L. Andreassi, F. Martini, S. Ubertini Comparing Energy and Cost Optimization in Distributed Energy Systems Management. *ASME. J. Energy Resour. Technol.* 2014;136(3):032001-032001-9.
- [7] A. Facci, L. Andreassi, F. Martini, S. Ubertini Optimization of CHCP Operation Strategy: Cost vs Primary Energy Consumption Minimization. *ASME. ASME International Mechanical Engineering Congress and Exposition*, Volume 6A: Energy
- [8] A. L. Facci, L. Andreassi, S. Ubertini, Optimization of CHCP (combined heat power and cooling) systems operation strategy using dynamic programming, In *Energy*, Volume 66, 2014, Pages 387-400, ISSN 0360-5442
- [9] A. L. Facci, L. Andreassi, S. Ubertini, E. Sciubba, Analysis of the Influence of Thermal Energy Storage on the Optimal Management of a Trigeneration Plant, In *Energy Procedia*, Volume 45, 2014, Pages 1295-1304, ISSN 1876-6102
- [10] A. L. Facci, G. Loreti, S. Ubertini, F. Barbir, T. Chalkidis, R. P. Ebling, T. Peters, E. Skoufa, R. Bove, Numerical Assessment of an Automotive Derivative CHP Fuel Cell System, *Energy Procedia*, Volume 105, 2017, Pages 1564-1569.
- [11] E. Fabrizio, M. Filippi, J. Virgone, An hourly modelling framework for the assessment of energy sources exploitation and energy converters selection and sizing in buildings, *Energy and Buildings* 41 (10) (2009) 1037–1050.
- [12] US Department of Energy. Buildings energy data book; 2012. <http://buildingsdatabook.eren.doe.gov/ChapterIntro2.aspx>.





### III. RESULTS AND DISCUSSION

The performance of the CHCP plant are reported in Fig. 3. The efficiency of the FC is maximized at part load. Thereafter, such a prime mover is particularly suited to effectively follow the variable energy demand in DG systems. Moreover, the maximum efficiency (38%) is larger compared to alternative technologies of this power (i.e. internal combustion engines).

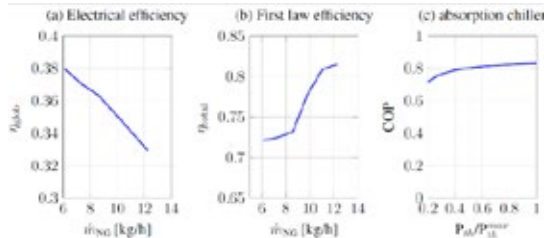


Fig. 3. Performance of the CHCP plant as a function of set-point.

The COP of the absorption chiller, reported in Fig. 3(c) is relatively low, due to the low grade of the input thermal energy. However, it is designed to utilize energy that would otherwise be wasted, contributing to improve to performance.

To assess the plant behavior in a realistic energy management scenario we assume that it serves a building composed of 4 residential units, whose energy demand is retrieved from [12]. The costs of electricity and natural gas are 22 c€/kWh and 15 €/GJ respectively.

	Cost [k€/year]	PEC [TJ/year]	PBP [Year]
Reference	230	9.02	NA
Baseline CHP	100	6.21	3
Modified CHP	90	5.22	4

Tab. 1 Relevant performance of the considered CHP plants.

Tab. 1 show that both the baseline and the modified plant significantly reduces energy cost and primary energy consumption. For the Pay back Period we assumed that the costs of the FC and of the absorption chiller are 3000 €/kW and 1200 €/kW respectively. The introduction of absorption chillers boost the plant performance, reduces the energy cost by 60% with respect to the separate production and by 10% with respect to the baseline CHP. Similarly it reduces the PEC by 42% with respect to separate production and by 16% compared to the baseline CHP.

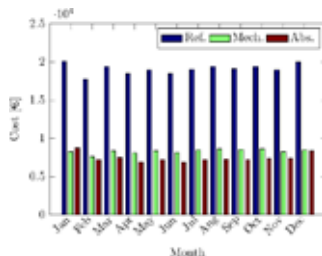


Fig. 4: Seasonal variation of the energy cost.

The absorption chiller is particularly effective in reducing the energy cost during summer and transitional seasons (see Fig. 4) for the larger chilling demand.

### IV. CONCLUSION

The results of this study evidence that small scale PEM - CHCP plants can effectively contribute to improve the energy performance in the residential sector. Moreover, the development of small absorption chillers could significantly contribute to enhance the effectiveness of such plants, in terms of economic sustainability and energy efficiency.

### ACKNOWLEDGMENT

This project has received funding from the Fuel Cells and Hydrogen Joint Undertaking under grant agreement No 671396. This Joint Undertaking receives support from the European Union's Horizon 2020 research and innovation program and United Kingdom, Germany, Greece, Croatia, Italy, Switzerland, Norway. Swiss partners are funded by the State Secretariat for Education, Research and Innovation of the Swiss Confederation.

### REFERENCES

- [1] International Energy Agency. Combined heat and power evaluating the benefits of greater global investment; 2008
- [2] F. Cappa, A. L. Facci, S. Ubertini, Proton exchange membrane fuel cell for cooperating households: A convenient combined heat and power solution for residential applications, In Energy, Volume 90, Part 2, 2015, Pages 1229-1238, ISSN 0360-5442.
- [3] Brown JE, Hendry CN, Harborne P. An emerging market in fuel cells? Residential combined heat and power in four countries. Energy Policy 2007;35:2173e86.
- [4] A. L. Facci, G. Loreti, S. Ubertini, F. Barbir, T. Chalkidis, R. P. Ebling, T. Peters, E. Skoufa, R. Bove, Numerical Assessment of an Automotive Derivative CHP Fuel Cell System, Energy Procedia, Volume 105, 2017, Pages 1564-1569.
- [5] Aspen Tech, Aspen Plus Unit Operation Models Reference Manual
- [6] A. Facci, L. Andreassi, F. Martini, S. Ubertini Comparing Energy and Cost Optimization in Distributed Energy Systems Management. ASME. J. Energy Resour. Technol. 2014;136(3):032001-032001-9.
- [7] A. Facci, L. Andreassi, F. Martini, S. Ubertini Optimization of CHCP Operation Strategy: Cost vs Primary Energy Consumption Minimization. ASME. ASME International Mechanical Engineering Congress and Exposition, Volume 6A: Energy
- [8] A. L. Facci, L. Andreassi, S. Ubertini, Optimization of CHCP (combined heat power and cooling) systems operation strategy using dynamic programming, In Energy, Volume 66, 2014, Pages 387-400, ISSN 0360-5442
- [9] A. L. Facci, L. Andreassi, S. Ubertini, E. Sciubba, Analysis of the Influence of Thermal Energy Storage on the Optimal Management of a Trigeneration Plant, In Energy Procedia, Volume 45, 2014, Pages 1295-1304, ISSN 1876-6102
- [10] US Department of Energy. Buildings energy data book; 2012. <http://buildingsdatabook.eren.doe.gov/ChapterIntro2.aspx>.

## STRUCTURED CATALYSTS FOR THE CO WATER GAS SHIFT REACTION

V. Palma, M. Martino

Univ. of Salerno, Dep. of Industrial Engineering, via G. Paolo II 132,  
84084, Fisciano, Italy.

Tel: +39089969275, e-mail: mamartino@unisa.it.

**Abstract** – This paper describes our results on the use of highly conductive carriers for the preparation of structured catalysts for the process intensification of the Water Gas Shift reaction. A procedure for the preparation of the structured catalysts is presented, and the results of the characterization and of the activity tests are expounded. The effectiveness of the washcoating process is highlighted from the low losses at the ultrasound adherence test, the rightness of the choice of the catalytic formulation is validated from the good performance of the structured catalyst, the significant effect of the carrier is demonstrated from the comparison with the performance of a powder catalyst with the same catalytic formulation.

**Index Terms** - Water Gas Shift, structured catalyst; thermal conductivity.

### I. NOMENCLATURE

GHSV: gas hourly space velocity  
HTS: high-temperature water-gas shift  
LTS: low-temperature water-gas shift

### II. INTRODUCTION

The WGS is an exothermic reversible reaction, thermodynamically favored at low temperature, operating downstream of reforming processes. It allows to reduce the CO percentage, in the syngas stream, to less than 0,3%. The actually process provides two stages, HTS and LTS, under adiabatic conditions, with an intercooling. The heat of the reaction induces a thermal gradient on the catalytic bed, with a much higher temperature at the outlet of the bed, with respect the inlet, limiting the CO conversion. The strategy to overcome these limitations, is the two-stages process, the HTS allows the most of the conversion in a short time, while the LTS allows to reach high conversion.

This kind of configuration combines a fast reaction in HTS

and high CO conversion in LTS, however, it presents significant disadvantages, such as high energy consumption, high operating and plant costs and moreover the difficulty to operate in small-scale applications.

A valid alternative is the use of structured catalysts based on highly conductive carriers. These catalysts, due to their conductivity, can flatten the thermal profile over the catalytic bed, by retro-diffusion of the heat of the reaction, by increasing the temperature at the inlet and decreasing the temperature at the outlet of the bed, resulting in a net increase of the CO conversion [1]. Through the use of this catalysts is theoretically possible to realize a single-stage WGS process.

In this work we present our results on the use of aluminum-based structured catalysts for the WGS reaction [2].

### III. EXPERIMENTAL

The structured catalysts were prepared by washcoating an aluminum monolith carrier with an Alumina-based slurry. The washcoat slurry was prepared by suspending high surface area  $\gamma$ -alumina (Puralox SCCa 150/200) in a colloidal solution of pseudoboehemite (Pural SB) and methylcellulose acidified to  $\text{pH} \approx 4$  with nitric acid. The carrier was dipped in the washcoat for 20 minutes, then the excess of slurry was removed by centrifuge, and the resulting artifact was dried at 120°C for 2 hours and calcined at 450°C for 3 hours. This procedure was repeated until reaching the desired loading. The resulting derivate was firstly impregnated with a ceria nitrate solution, subsequently with a tetramine platinum nitrate solution, dried at 120°C and calcined at 450°C, to obtain the structured catalyst with the desired chemical composition. For reference an aliquot of the washcoat slurry was dried, calcined and impregnated with the appropriate salts precursors, to obtain a powder with the same chemical composition of the structured

catalysts. The resistance of the washcoat to the mechanical stress was tested by the ultrasound adherence tests; after a 30 minutes of solicitation, the loss was less than 3 wt% with respect the washcoat.

The catalysts were fully characterized by XRD, Raman, B.E.T. method and H<sub>2</sub>-TPR experiments, while the WGS experiments were performed at atmospheric pressure, in the temperature range of 423-673 K, with a reacting mixture of 8% CO, 30% H<sub>2</sub>O and N<sub>2</sub> balance, in a stainless steel tubular reactor with an internal diameter of 30 mm and a length of 40 cm, at a GHSV of 10000 h<sup>-1</sup>. The composition of the reaction products were monitored on dry basis, the water in the outlet gas stream was condensed through a refrigerator Julabo F12, the gas was sent to an ABB system equipped with the non-dispersive infrared analyzer Uras 14 for CO, CO<sub>2</sub> and CH<sub>4</sub> and the thermal conductivity detector Caldos 17 modules for H<sub>2</sub>.

#### IV. RESULTS AND DISCUSSION

The trend, obtained with the structured catalyst PtCeAlWM, of the CO conversion in function of the temperature, was reported in figure 1. The conversion approached the equilibrium for temperatures over 260°C, however a conversion of 50% was still obtained at 220°C.

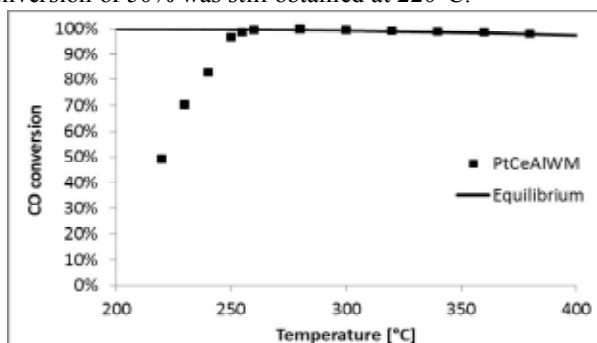


Figure 1. CO conversion for 1Pt/20CeO<sub>2</sub>/8Al<sub>2</sub>O<sub>3</sub>/M catalyst.

The hydrogen selectivity was almost 99% until 350°C, for higher temperature the occurrence of the methanation reaction gave rise to a reduced selectivity, however the volumetric percentage of methane did not exceed the 0,1% in the outlet gas stream in all cases studied.

With the aim to highlight the effect of the carrier, some experiments were made in adiabatic condition, comparing the CO conversion obtained with the structured catalyst with that obtained with a powder with the same chemical composition, diluted with quartz glass to obtain the same catalytic volume. These experiments were carried out at GHSV of 33800 h<sup>-1</sup>, without dilution (21% CO, 79% H<sub>2</sub>O), at a fixed inlet reaction temperature of 260°C. The temperature of the catalytic was monitored both at the inlet and at the outlet of the bed, to highlight the effect of the conductivity of the carrier. The

experiments were performed a multiphase process. The catalysts were heated at a fixed temperature of 260°C (bypass temperature), with a mixture of water and nitrogen; at the thermal equilibrium of the system the nitrogen was replaced with the same volumetric amount of CO, to start the reaction. The reaction proceed until a new thermal equilibrium wasn't reached; the corresponding inlet and outlet temperatures of the beds and the conversions, were compared.

In the case of the structured catalyst the temperatures at the inlet and the outlet of bed exceeded 310°C, with a difference between them of few degrees, while the CO conversion was 90%. In the case of the powder catalyst a huge difference of temperature there happened between the inlet and the outlet of the bed. The temperature at the inlet was few degrees over the bypass temperature, while the outlet temperature was over 350°C, with a lower conversion.

These results confirmed the benefit in using highly thermal conductive structured carriers for processes in which exothermic reactions are involved.

#### V. CONCLUSION

In this paper we showed our results on the use of structured carriers for the process intensification of the WGS reaction; the basic idea, however, is applicable to all the exothermic reactions in adiabatic processes. The heat of the reaction of this systems disadvantages both in the kinetics and in the thermodynamic, the thermal gradient, on the catalytic bed, is a serious limitation the efficiency of the system. We propose to overcome this limitation by flattening the thermal profile over the catalytic bed, obtaining a corresponding increase in the conversion. With the results that we showed in this paper we demonstrate the concrete possibility to realize a strong process intensification of these systems.

#### REFERENCES

- [1] Palma, V., Pisano, D., Martino, M., Ciambelli, P. Structured catalysts with high thermoconductive properties for the intensification of Water Gas Shift process. *Chemical Engineering Journal*, Volume 304, 2016, pp. 544-551. DOI: 10.1016/j.cej.2016.06.117.
- [2] van Dijk, H.A.J., Boon, J., Nyqvist, R.N., van den Brink, R.W. Development of a single stage heat integrated water-gas shift reactor for fuel processing. *Chemical Engineering Journal*, Volume 159, 2010, pp. 182-189. DOI: 10.1016/j.cej.2010.02.046.

## ANODES OF MICROBIAL FUEL CELL: WHAT ACTUALLY HAPPENS INSIDE PORES?

P. Chong\*, B. Erable\*, and A. Bergel\*

\*Laboratoire de Génie Chimique, Université de Toulouse, CNRS,  
INP, UPS (France)

**Abstract** – Three-dimensional porous anodes should enhance the performance of microbial fuel cells provided that they make the largest possible surface area accessible for microbial colonization. Many studies have tested various kinds of porous electrodes (foams, sponges, cloths, felts...) but it remains difficult to correlate the efficiency of a 3-dimensional electrode with the size of its porous structure. The purpose of the present work was to characterize how the electrochemical performance and microbial colonization of an anode confined in a channel was impacted by the channel height.

**Index Terms** – Microbial anode, bioanode, pore size, porous electrode, microbial electrochemical technology.

### I. INTRODUCTION

Three-dimensional (3D) porous anodes are being increasingly used to boost the power density of microbial fuel cells [1] since they are assumed to offer a large surface area for the development of the microbial electrocatalyst. However, when compared in identical conditions, some 3D porous anodes have been shown not to perform better than two-dimensional electrodes because microbial biofilms do not significantly penetrate into the porous structure of the electrode [2]. The purpose of this work was to characterize the impact of the porosity size on the mechanism of microbial colonization inside a porous structure. This was a pioneering work with the objective of establishing basic rules for optimizing 3D microbial electrodes.

### II. EXPERIMENTAL APPROACH

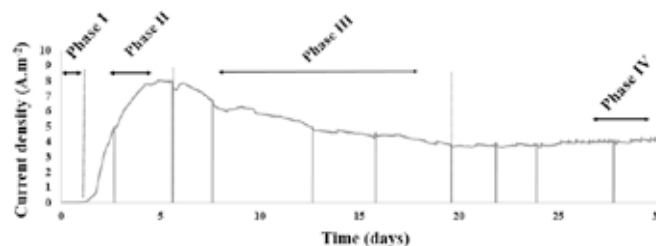
An original experimental set up was designed to work at the scale of a single pore i.e. a channel. All the channels were 10 cm long and had a rectangular cross section of 1 cm width. The impact of the channel height was studied by using two values: 1 mm or 5 mm. The channels were machined by pressing a Teflon part onto a flat carbon cloth electrode. Each channel was used

as the working electrode of a 3-electrode set-up. Reactors were filled with synthetic medium (50 mM bicarbonate buffer, 10 mL.L<sup>-1</sup> macronutrients, 1 mL.L<sup>-1</sup> micronutrients, 1 mL.L<sup>-1</sup> vitamins, 4.5 g.L<sup>-1</sup> KCl and 2.4 g.L<sup>-1</sup> NaH<sub>2</sub>PO<sub>4</sub>.H<sub>2</sub>O) and inoculated with a pre-existing microbial anode prepared from garden compost. The carbon cloth anode in the pore was polarized at -0.20 V/SCE and the concentration of acetate, used as the substrate, was maintained at 20 mM. At the end of the experiments, after 5, 10 or 30 days, the pores were disassembled and bacterial colonization inside the pore was observed by epifluorescence microscopy and analysed by statistical analysis of biofilm volume coverage ratios [2]. Each experiment was performed in quadruplicate.

### III. RESULTS

#### A. Effect of the channel height on electrochemical performance

Regardless of the channel height, all the current-time curves had similar features, with four distinct phases: I) a lag period, II) fast increase to a maximum value  $J_{max}$ , III) slow decrease, and IV) stabilization of the current density at a value lower than  $J_{max}$  (Fig 1).



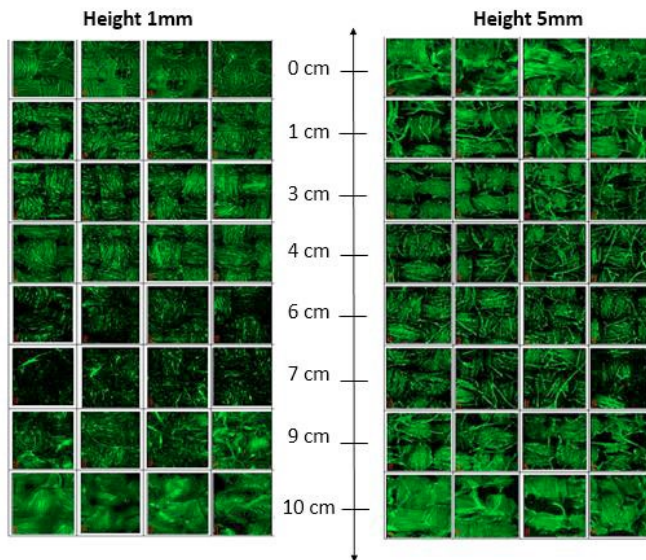
**Fig. 1.** Chronoamperometry during polarization at -0.20 V/SCE with a channel 5 mm high (straight lines correspond to acetate addition to keep the concentration at 20 mM).



The channel height impacted the start-up time (duration of phase I). Channels with heights of 1 mm and 5 mm started to generate electricity after 1.8 and 1.2 days, respectively. Moreover, the larger channel height (5 mm) led to a stabilized current (phase IV) 60% higher than those produced by the 1-mm channels. It may be concluded that channels with larger cross-sectional area led to earlier current production and higher long-term current density because they offered easier access to the electrode interior for both bacteria and substrate. Surprisingly, the duration of phase II did not depend on the channel height. When the current started to increase,  $J_{\max}$  was always reached very fast, in around 2 days, whatever the channel height.

#### B. Bacterial profile inside the channel

The bacterial profile along the channels (length 10 cm) was observed via epifluorescence microscopy by taking images at 8 locations from one end to the other (Fig 2).



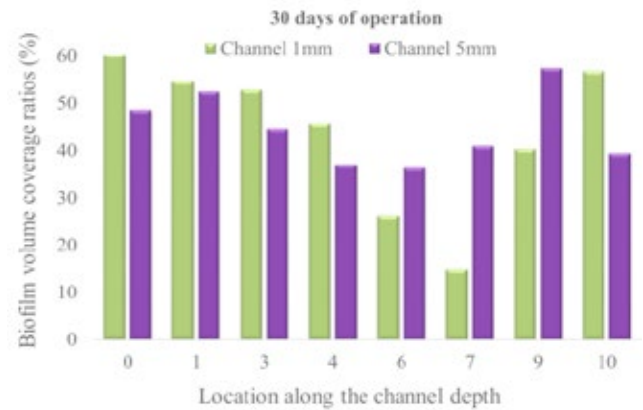
**Fig. 2.** Bacteria profile inside channels of 1 and 5 mm height obtained by epifluorescence microscopy after 30 days (4 images were taken and averaged for each of the 8 locations).

The microbial biofilm was always more compact and thicker at the extremities of the channel than inside. The internal colonization was different for the two channel heights: microbial colonization was homogeneous and complete inside the 5 mm channels, while the 1 mm channels presented areas of lower microbial density at than in the rest of the channel. These results confirmed that, even after 30 days of polarization, limiting phenomena that were detrimental to the internal development of the microbial biofilm occurred in the 1 mm high channels.

#### C. Biofilm volume coverage ratios

Statistical analysis of biofilm volume coverage ratios was carried out after 5, 10 and 30 days of polarization. After 10

days, the entire depth of the 5 mm channels was colonized, with an average biofilm volume coverage ratio of 50%, while the coverage ratio never exceeded 25% at central part of the 1 mm channels, even after 30 days of polarization (Fig 3).



**Fig. 3.** Biofilm volume coverage ratios inside 1 and 5 mm high channels after 30 days of polarization.

## IV. CONCLUSION

When the aim is to design efficient 3D porous microbial electrodes, the characteristic porosity size is inevitably a key parameter. The systematic study performed here by designing well-defined channels showed a clear limiting effect of the 1 mm height compared to 5 mm. The initial lag time was slightly longer (1.8 vs. 1.2 days) and the long-term current density was 60% lower. Analysis of the microbial colonization inside the channels showed that the innermost parts of the 1 mm channels presented lower bacteria density. A porosity size of 1 mm significantly limited the colonization of the channels but, surprisingly, it did not impact the time required to reach the maximum value of the current density. In addition to producing basic knowledge required to design optimal microbial anodes, the method and set-up implemented here also provide a new tool to progress in deciphering the complex world of electroactive biofilms.

## ACKNOWLEDGMENT

This work was carried out within the framework of the Bioelec project (ANR-13-BIME-006).

## REFERENCES

- [1] Ketep, S., Bergel, A., Calmet, A., Erable, B, Stainless steel foam increases the current produced by microbial bioanodes in bioelectrochemical systems, *Energy & Environmental Science*, Volume 7, 2014, pp. 1633-1637.
- [2] Blanchet, E., Erable, B., Delia, M., Bergel, A, Two-dimensional carbon cloth and three-dimensional carbon felt perform similarly to form bioanode fed with food waste, *Electrochemistry Communications*, Volume 66, 2016, pp. 38-41.

## FEASIBILITY OF DOPED METAL OXIDES AND GRAPHITIZED CARBON AS A STABLE CATHODE CATALYST SUPPORT FOR LOW TEMPERATURE POLYMER ELECTROLYTE MEMBRANE FUEL CELL

Paritosh Kumar Mohanta<sup>1\*</sup>, F.Regnet<sup>2\*</sup> & Ludwig Jörissen<sup>3\*</sup>

<sup>\*</sup>Zentrum für Sonnenenergie-und Wasserstoff-Forschung Baden-Württemberg, Helmholtzstr. 8, D-89081 Ulm (Germany)

**Abstract** – We investigated cathode catalyst supports different from the traditional carbon black (CB) for PEMFC. A graphitized carbon (GC) and a doped metal oxide were investigated in this work. An antimony doped  $\text{SnO}_2$  (ATO) of reasonable electronic conductivity and surface area was developed successfully. The supported Pt electrocatalysts were prepared by modifying the well-known polyol process. After annealing, the electrochemical characterizations of the supported catalysts were done to measure the ECSAs, ORR activities, corrosions and finally the catalysts were processed to MEAs for single cell performance measurements. Both ATO and GC supported catalysts showed high ECSA survival rate under potential cycling in 0.5M  $\text{H}_2\text{SO}_4$  compared to CB supported catalyst. However, we observed catalyst support interactions in ATO lowering the performance in single electrode and MEA studies comparison to CB. Among all of the investigated supported catalysts, the GC supported catalyst showed the highest stability and performance.

**Index Terms** – PEMFC, ATO, Graphitized Carbon, Catalysts

### I. INTRODUCTION

Although CB is widely used as support for noble metals, the sensitivity of carbon based support materials towards oxidation under the cathode operating conditions is one of the major causes of PEMFCs performance degradation. A stable support could increase the fuel cell life time to the desired level. However, potential supports need to provide high surface areas, high electronic conductivities and stabilities towards the acid environment at the potentials encountered at the fuel cell cathode under steady state and transient conditions. Highly stable carbon based and non-carbon based cathode catalyst support materials were proposed in references [1]. In this work a doped metal oxide (ATO) and a GC have been chosen for deeper investigation.

### II. EXPERIMENTAL

#### A. Synthesis/preparation of supports and supported catalysts

An ATO (5at%Sb in Sn) was synthesized using a co-

precipitation process as described elsewhere [2]. A GC (Timcal-167) was oxidized at 600°C in air for 90 minutes in order to increase its wettability and surface areas. A CB (Cabot, Vulcan XC72) was also taken for comparison. The supported Pt electrocatalysts were prepared by using an already developed modified polyol process [2] and then annealed at 250°C for 1h. Annealing of CB and GC supported catalysts were performed under reducing atmosphere (95%Ar - 5%  $\text{H}_2$ ) whereas the ATO supported catalyst was treated under oxidizing condition (in air) in order to keep Sb (V) states of the ATO.

#### B. Characterization of the supports and the supported catalysts

A Sorptomatic 1990 instrument was used to measure the BET surface areas of the supports. The electrical conductivities were determined using a homemade four point measuring device. The average Pt particle size of the synthesized catalysts were measured via XRD (Siemens D5000) using a TOPAS software. The contents of Pt on the supported catalysts were measured via ICP-OES analysis (Acros FHS12). Both of the supports corrosion and the Pt- corrosion tests were performed in 0.5M  $\text{H}_2\text{SO}_4$  at 25°C in a three electrode configuration using a Zahner IM6 potentiostat. A rotating disk electrode (RDE) setup was used to measure the ORR activities of the catalysts in 0.1M  $\text{HClO}_4$  at 50mV/s scan rate at room temperature. MEAs were prepared via catalyst coated membrane techniques in a Nafion®NR212 (50.8µm) membrane while using 0.3mg/cm<sup>2</sup> Pt loading on both electrodes. Cathodes of the MEAs were prepared with the supported catalysts to be investigated while keeping the anodes with a commercial Tanaka catalyst (18.5wt%Pt on CB) constant for all MEAs. A standard FC technology single cell with triple serpentine flow fields and 25cm<sup>2</sup> active surface areas was used to conduct MEA performance tests.

### III. RESULTS

The BET surface areas of the investigated CB, GC and ATO

supports were measured as 192, 60 and 50 m<sup>2</sup>/g respectively. The electrical conductivities of the materials were calculated as 2.6, 2.1 and 0.7 S/cm respectively. The Pt particle sizes of CB, GC and ATO supported non-annealed catalysts were measured as 3.0, 2.9 and 3.5 nm respectively whereas annealed catalysts were 5.5, 5.8 and 4 nm respectively. The increases of Pt particle size due to annealing were varying depending on the types of supports and annealing atmospheres. The Pt content of the supported annealed catalysts were measured as 18.8 (Pt/CB), 19.7 (Pt/GC) and 19.1 (Pt/ATO) respectively.

#### A. Supports corrosion

Fig. 1 shows the Electrochemical Surface Area Survival Rate (ECSA-SR) of both GC and ATO supported catalysts are higher than the traditional CB supported catalyst under accelerated support corrosion test (1.0 & 1.5 V vs RHE @ 500 mV/s) [2]. After 60,000 cycles, the ECSA-SR of GC, ATO and CB supported catalysts were measured as 92%, 85% and 54% respectively.

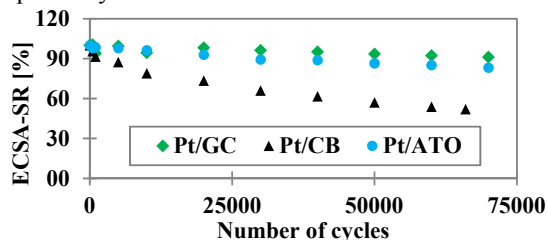


Fig. 1: Comparison of supports corrosion

#### B. Pt - corrosion

Fig. 2 displays the Pt corrosion is lower in both GC and ATO supports than in CB support after 40,000 potential cycles between 0.6 & 1 V vs RHE at 50 mV/s voltage scan rate. Thus smaller Pt particle corrode more is not universal; Pt corrosion is also closely related to the metal support interaction.

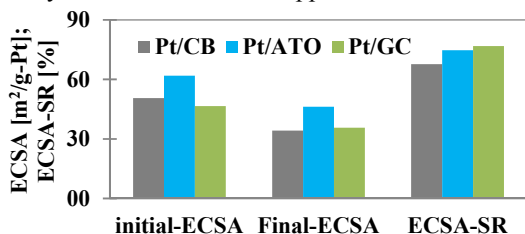


Fig. 2: Comparison of Pt corrosion of the catalysts

#### C. ORR activity

Due to unfavorable metal support interactions and low electronic conductivity, lower mass activity of Pt/ATO (320 A/g-Pt) than Pt/CB (651 A/g-Pt) catalyst was observed. The determination of the ORR activity of Pt/GC is in progress.

#### D. MEA test

It was found necessary to optimize the ionomer content in the catalyst layers for all supported catalysts in order to reduce the oxygen transport resistance which thought to be hindering

the MEA performances [3]. The MEA with Pt/GC catalyst (29 wt% ionomer, the optimum) shows the highest performance at high current densities followed by the Tanaka catalysts (37.5 wt% ionomer the optimum) and Pt/CB (40 wt% ionomer, the optimum) as shown in the upper part of the Fig. 3. On the other hand, the MEA performance of Pt/ATO (10 wt% ionomer, the optimum) is the lowest partly due to the lower electrical conductivity of the ATO compared to carbon based supports. Furthermore, an unfavorable metal support interaction could be also possible.

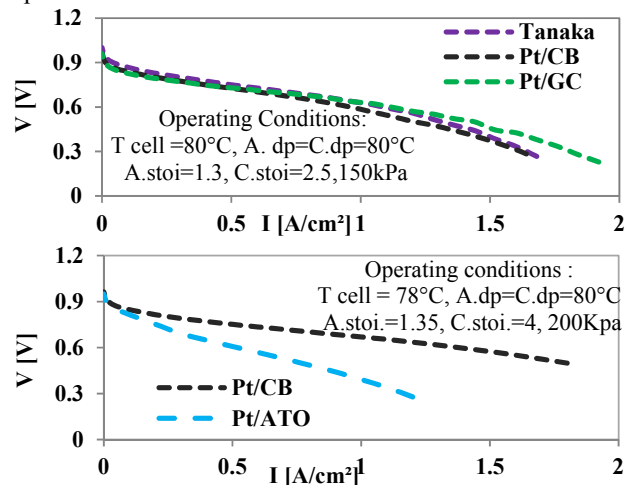


Fig. 3: I-V curves of the catalysts

#### IV. CONCLUSION

Both GC and ATO supported Pt catalysts showed superior stability over CB supported Pt catalyst in acid electrolyte under potential conditions. We found that the Pt corrosion not only depends on the Pt particle size but also on type of support. Single cell MEA performance of GC supported catalyst is comparable with CB supported catalyst. A correlation of MEA performance with ionomer content and the BET surface area of the catalysts were also established. Despite metal-support interactions, ATO was identified as promising candidates for long term stable fuel cell operation, whereas GC was identified as promising candidates in terms of both of the stability and the performance.

#### ACKNOWLEDGMENT

Funding of the project GECKO by the Federal Ministry of Education and Research (BMBF) is gratefully acknowledged.

#### REFERENCES

- [1] Yan-Jie Wang, David P. Wilkinson & Jiujun Zhang, Chem. Rev., 2011, 111 (12), pp 7625–7651
- [2] Paritosh Kumar Mohanta, C. Glöckler, A. O. Arenas and Ludwig Jörissen, International Journal of Hydrogen Energy Volume 42, Issue 46, 16 November 2017, Pages 27950-27961
- [3] A. Kongkanand, M.F. Mathias, J. Phys. Chem. Lett., 2016, 7 (7), pp 1127–1137

EFC17033

## VERSATILE CATALYST MATERIALS FABRICATION BY LOW-PRESSURE PLASMA TREATMENTS

Y. Busby\*, M. da Silva Pires\*, E. Haye\*, V. Stergiopulos\*\*, N. Job\*\*, J.-J. Pireaux\* and L. Houssiau\*

\* Laboratoire Interdisciplinaire de Spectroscopie Electronique (LISE-PMR), University of Namur, 61 Rue de Bruxelles, 5000 Namur, (Belgium)

\*\* University of Liège, Department of Chemical Engineering – Nanomaterials, Catalysis, Electrochemistry (NCE), Sart-Tilman, B-4000 Liège, (Belgium)

**Abstract,** An alternative solvent-free method is explored for the processing of Pt/C, Ni/C and Pt-Ni catalysts based on a low-pressure radio-frequency plasma treatment of solid (powder) precursors. A porous carbon xerogel is used as catalyst support, mixed with an organometallic precursor and treated in a plasma discharge at different power and in different plasma chemical environments. The nucleation of metal nanoparticles, their morphology evolution and chemical state are characterized by combining in-situ optical emission spectroscopy, transmission electron microscopy, X-ray diffraction and X-ray photoelectron spectroscopy. Results show that the plasma processing offers a high flexibility in tuning the size and oxidation state of Ni and Pt nanoparticles and also allows for a controlled functionalization of the carbon support; these properties demonstrate the high potential of plasma processing route for the fabrication of green and efficient catalysts nanomaterials.

*PEMFC catalyst, RF Plasma, Carbon functionalization, nanocomposites*

### I. INTRODUCTION

The catalyst materials participate to about one third of the final cost of proton-exchange membrane fuel cells (PEMFC); this is mostly due to the rarity of commonly-used noble-metal such as platinum nanoparticles (Pt NPs) and because of the production costs. The conventional wet chemical routes which are used for catalysts synthesis usually involve multiple steps and are associated with an extensive use of solvents. Solvents strongly contribute to the energetic and environmental impact of the catalyst and may lead to the well-known poisoning effects on Pt NPs.[1] To develop new catalyst processing routes and to reduce the noble metal content become a more and more urgent issues. In this context, Nickel-based catalysts and Pt-Ni/C bimetallic catalysts have attracted attention for their enhanced catalytic properties versus the oxygen reduction reaction and higher stability respect to Pt/C catalysts.[2] Recently, low-pressure oxygen plasmas treatments have been applied to prepare Pt/C catalysts for PEM applications by

treating a mixture of solid precursors (Pt acetylacetonate and carbon black) under stirring conditions.[3] In this work, we have varied the plasma chemistry by varying the injected gas mixture (comprising Ar, N<sub>2</sub>, NH<sub>3</sub> or O<sub>2</sub>) in the plasma discharge and investigated the nucleation, growth and chemical state of Pt and/or Ni nanoparticles on high surface area carbon xerogel. X-ray diffraction (XRD), transmission electron microscopy (TEM) and X-ray photoelectron spectroscopy (XPS) have been applied to fully characterize the nanocomposite materials. Moreover, chemical analysis on the composite materials has demonstrated that the plasma chemistry allows for the functionalization of the carbon materials with oxygen (C-O, C=O, etc.) or nitrogen (C-N) containing functional groups which can be relevant for developing more durable catalyst materials.[4]

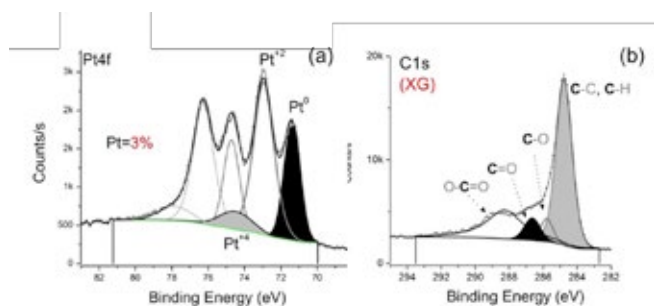
### II. RESULTS

#### A. Pt/C catalysts

Pt/C catalysts have been prepared by treating Pt acetylacetonate and a high surface area carbon xerogel [4] under different plasma conditions and chemistries following the procedure described in [3]. The plasma treatment conditions (RF power and treatment time) have been optimized to ensure reaching the full decomposition of the crystalline organometallic precursor, and the generation of Pt NPs was checked by XPS (see the example in Fig. 1) which was applied to XRD through which we derived the average NPs size through the Debye-Scherrer formula. In particular, this process optimization led us to develop of a two-steps plasma process where the first step is a prolonged (60-120 min) O<sub>2</sub>:Ar plasma (4:2 sccm) treatment at low-energy (at RF power  $P_{RF} < 100$  W) to nucleate metal NPs followed by a short (10-30 min) high-energy plasma treatment (at RF power  $120 < P_{RF} < 150$  W) during which the particles growth occurs. The fine tuning of the treatment conditions allows to end up with a Pt/C catalysts with

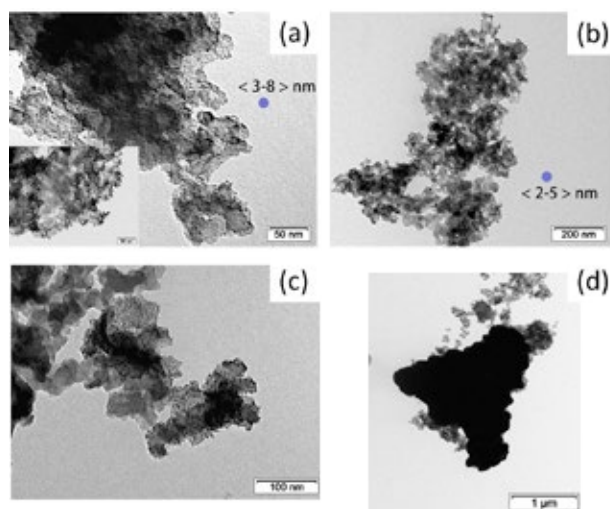


the desired morphology, i.e. isolated Pt NPs of about 2-5 nm, while avoiding particles agglomeration as shown in STEM images in Fig. 2a and 2b.



**Fig. 1.** HR-XPS spectra from an optimized Pt/C catalyst treated in an oxygen plasma. (b) Carbon xerogel functionalization with carbonyl and carboxyl groups.

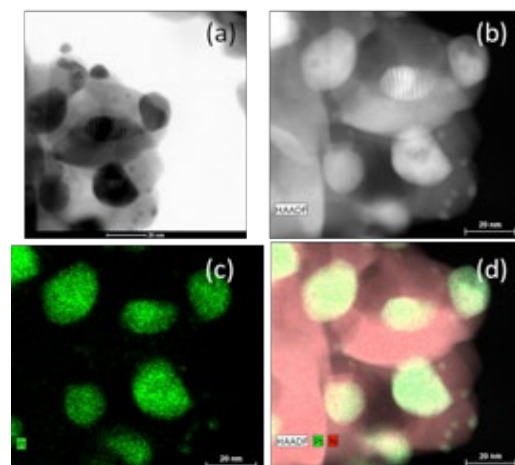
Nickel based catalysts have been prepared following a similar methodology from Nickel acetylacetonate precursor; we have varied the plasma conditions in a large window of RF power (between 90 and 200 W) and in Ar:N<sub>2</sub>, Ar:O<sub>2</sub> and ArNH<sub>3</sub> plasma chemistries. The best Ni/C catalysts morphology is obtained for 150 W Ar:NH<sub>3</sub> plasma treatments in which the Nickel NPs, diameter is between 5 and 8 nm, however some Ni agglomeration was evident from TEM (Fig. 2c and 2d).



**Fig. 2.** STEM analysis on (a, b) Pt/C catalysts made by a one-step (a) and a two-step plasma process and (c, d) Ni/C catalysts made by two-step Ar:NH<sub>3</sub> plasma treatment.

#### B. Bimetallic Pt-Ni Catalysts

The optimization of the treatment conditions for the Pt and Ni organometallic precursors has allowed to deposit Pt-Ni bimetallic catalysts (Fig.3); however, while Pt tends to form well-defined NPs, with Nickel we could not avoid the formation of a continuous film due to the different NPs formation kinetics.



**Fig. 2.** STEM (a, b) and EDX imaging of (c) Pt and (d) Ni plus Pt obtained on a bimetallic Pt-Ni/C plasma catalyst.

### III. CONCLUSION

Plasma processing appears as a flexible tool to deposit extremely flexible catalysts nanomaterials for PEMFCs. It allows to tune the NP size, its chemical state and to modify the carbon surface properties and chemical stability through the controlled addition of oxygen or nitrogen-containing groups.

### ACKNOWLEDGMENT

We acknowledge the SIAM technological platform at University of Namur and SERMA Technologies (Grenoble).

### REFERENCES

- [1] Bartholomew, C.H., Mechanisms of catalyst deactivation. Applied Catalysis A: General, Volume 212, 2001, Pages 17–60.
- [2] Escaño, M.C., Gyenge, E., Nakanishi, H., Kasai, H., Pt/Cr and Pt/Ni Catalysts for Oxygen Reduction Reaction: To Alloy or Not to Alloy? Journal of Nanoscience and Nanotechnology, Volume 11, 2011, Pages 2944–2951.
- [3] Laurent-Brocq, M., Job, N., Eskenazi, D., Pireaux, J.-J., Pt/C catalyst for PEM fuel cells: Control of Pt nanoparticles characteristics through a novel plasma deposition method. Applied Catalysis B: Environmental, Volume 147, 2014, Pages 453–463.
- [4] Salinas-Torres, D., Léonard, A.F., Stergiopoulos, V., Busby, Y., Pireaux, J.-J., Job, N., Effect of nitrogen doping on the pore texture of carbon xerogels based on resorcinol-melamine-formaldehyde precursors. Microporous and Mesoporous Materials, Volume 256, 2018.
- [5] Piedboeuf, M.L.C., Leonard, A.F., Deschamps, F.L., Job, N., -Carbon xerogels as model materials: toward a relationship between pore texture and electrochemical behavior as anodes for lithium-ion batteries. Journal of Materials Science, Volume 51, 2016, Pages 4358–4370.



## HYLAW – A PROJECT DESIGNED TO REDUCE VULNERABILITIES OF THE HYDROGEN ECONOMY IN EUROPE

Ioan Iordache<sup>1,3</sup>, Nicolas Kraus<sup>2</sup>, Dorin Scitea<sup>1,3</sup>, Sabine  
Skiker<sup>2</sup>, Ioan Stefanescu<sup>1</sup>, Nicolas Brahy<sup>2</sup>

1. National Research and Development Institute for  
Cryogenics and Isotopic Technologies - ICSI Rm. Valcea, (Romania)
2. Hydrogen Europe, Brussels, (Belgium)
3. Romanian Association for Hydrogen Energy, Rm. Valcea,  
(Romania)

**Abstract** - The project, entitled HyLAW, aims to provide a comprehensive review of the legal and administrative barriers faced in fuel cell and hydrogen technology deployment and use across Europe.

The HyLAW project consortium brings together 23 partners from 18 European countries and is led by Hydrogen Europe.

The partners will identify legal framework and administrative processes (LAP) issues and impacts faced at the diverse levels across Europe. Industry stakeholders with hands-on experience in deployment and of requirements for compliance in different countries are associated to the project. It will thereby enable a step-change in awareness of LAP barriers to key audiences, ranged from national policymakers to individual planning officers, along with those looking to deploy and operate fuel cell and hydrogen (FCH) technologies with a view to boost the FCH market and advocate for better regulation to support the uptake of FCH technologies.

**Index Terms** - HyLAW, legal framework and administrative processes (LAP), national associations

### I. INTRODUCTION

The Hydrogen economy is to become a reality in the next years, but it has a weak point, it is considered as a synergy of competitive technologies in a mature and non-constrained market. As any other technology these must, first, exceed the border of the theory, research, development and demonstration and, second, face a number of non-technical barriers.

The HyLAW stands for Hydrogen Law and removal of legal barriers to the deployment of fuel cells and hydrogen applications. It is a flagship project aimed at boosting the market uptake of hydrogen and fuel cell technologies providing

market developers with a clear view of the applicable regulations whilst calling the attention of policy makers on legal barriers to be removed. The project brings together 23 partners from Austria, Belgium, Bulgaria, Denmark, Finland, France, Germany, Hungary, Italy, Latvia, Norway, Poland, Romania, Spain, Sweden, Portugal, the Netherlands and United Kingdom and is coordinated by Hydrogen Europe.

The HyLAW partners will first identify the legislation and regulations relevant to fuel cell and hydrogen applications and legal barriers to their commercialisation. They will then provide public authorities with country specific benchmarks and recommendations on how to remove these barriers.

The consortium brings together 23 partners from 18 countries across Europe and is led by Hydrogen Europe.

The group will have the unique capability of identifying legal framework and administrative processes (LAP) issues and impacts faced at regional and national level across Europe. Industry stakeholders with hands-on experience in deployment and of requirements for compliance in different regions and countries are associated to the project. It will thereby enable a step-change in awareness of LAP barriers to key audiences, ranged from national policymakers to individual planning officers, along with those looking to deploy and operate fuel cell and hydrogen (FCH) technologies with a view to boost the FCH market and advocate for better regulation to support the uptake of FCH technologies.

HyLAW started in January 2017 and will run until December 2018. The database will be maintained by Hydrogen Europe for minimum three years after completion of the project.

By addressing legal barriers, the project will be key to

unlocking the potential of widespread uptake of FCH technologies. Through a publicly available online database, it will create a highly accessible and sustained awareness of regulatory and legal-administrative barriers, based on experience from existing deployments.

## II. RESULTS AND DISCUSSIONS

The key project targets for HyLAW will be delivered through the next:

- Formation of a network of national hydrogen and fuel cell associations in order to create a long term collaboration beyond the duration of the project, ultimately further consolidate and strengthen the sector under one umbrella.
- Establishing the framework and administrative processes (LAP) database covering 18 partner countries and effectively disseminating these findings through the consortium as well as existing Hydrogen Europe's and partners networks.
- Integrating the regulatory experience of FCH JU and other demonstration programmes.
- Ensuring that the LAP database will provide a comparative information source between the different countries covering all FCH technologies.
- Updating the LAP database for three years beyond project completion and maintaining database access and supporting documents for five years beyond project completion. Identifying and quantifying LAP impacts in time and/or resource terms.
- Preparation of national policy papers for the 18 partner countries and of a pan European policy paper with identification of best practices and recommendations towards policy makers to remove legal barriers
- Dissemination activities based on workshops in each of the 18 partner countries and a pan-European event in Brussels

Overall, HyLAW will be instrumental in addressing and unlocking the potential of FCH technologies. It will create a user-friendly and practical awareness of existing regulatory and legal-administrative barriers via the web portal as well as foster the sector via the creation of a network of supporting national associations. The project will provide exchange and dialogue between those looking to deploy, those looking to use, and those looking to manage the operation of FCH technologies. The collection of regulatory information from 18 countries will allow the partners to benchmark countries legal and administrative processes, identify best practices and draw recommendations to the policy makers on this basis. The project will remove uncertainties, build enthusiasm for supporting FCH technology deployment and boost the FCH market– therefore securing early benefits during the project and lasting impacts for the wider FCH industry and stakeholders beyond the end of project activities.



**Fig. 1. HyLAW Partners**

## ACKNOWLEDGMENT

The HyLAW project has received funding from the Fuel Cells and Hydrogen 2 Joint Undertaking under grant agreement No 737977. This Joint Undertaking receives support from the European Union's Horizon 2020 research and innovation programme.

## ELECTRIC TRANSPORT PROCESS FOR THE BULK OF A PEM FUEL CELL

Jiatang Wang\*, Jinliang Yuan\*\*, and Bengt Sundén\*

\*Department of Energy Sciences, Lund University, P.O. Box 118,  
Lund SE-221 00, (Sweden)

\*\*Faculty of Maritime and Transportation, Ningbo University,  
Fenghua Road 818, Ningbo 315211, (China)

**Abstract** - Performance of a proton exchange membrane (PEM) fuel cell is very sensitive to its electric resistance appearing in its functional components. In this paper, the electric resistance as well as related parameters of a cell is evaluated by a recently developed numerical method in the through-plane direction of the electrodes. The results show that the channel/rib structure leads to non-homogeneous electric field and current flow, especially within the region around the corner of bi-polar plates (BPP) close to the channel. In addition, the current below the channel flows across with a longer distance from the middle of the gas diffusion layer (GDL) to the BPP's shoulders. Finally, the electric resistance is predicted with  $99.4 \text{ m}\Omega \text{ cm}^2$  of the bulk of an entire cell for the studied case condition.

**Index Terms** –electric resistance, electrode, numerical method, PEM fuel cell.

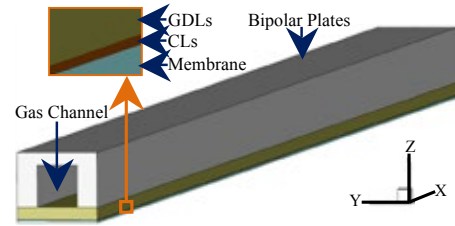
### I. INTRODUCTION

Electric resistance plays an important role for the performance of a proton exchange membrane (PEM) fuel cell [1]. It is known that a smaller ohmic loss resulting from a small electric resistance favors a better cell performance. The effort on decreasing the electric resistance is of interest to optimize the cell performance.

Previous research works have been concentrated on investigating ohmic resistances caused by electron transfer through electrodes (in through-plane direction) [2]. A comparison of the electric resistance under the shoulders and channels has shown that the total electric resistance under the channels is much higher than that under the shoulders caused by the channel/rib structures in a PEM fuel cell [3]. In the present study, the evaluation of the electric resistance and electric transport process are conducted by a newly developed electron transfer model implemented in an open source library of OpenFOAM. The distribution of the electric field and current density are presented and analyzed.

### II. NUMERICAL DESCRIPTION

A half-cell, i.e., the anodic side is selected as the representative domain for the electric resistance modeling, as shown in Fig. 1.



**Fig. 1. Schematic illustrations of the electric resistance model.**

The governing equation for the electron transfer through the entire domain can be evaluated by a Laplacian equation [4],

$$\nabla \cdot (\sigma \nabla \varphi) = 0 \quad (1)$$

where  $\varphi$  is electric potential and  $\sigma$  is electric/protonic conductivity. Then the electric field, local current density and electric resistance of the domain can be obtained by the following equations [5], respectively,

$$E_e = -\nabla \varphi \quad (2)$$

$$j = -\sigma \nabla \varphi \quad (3)$$

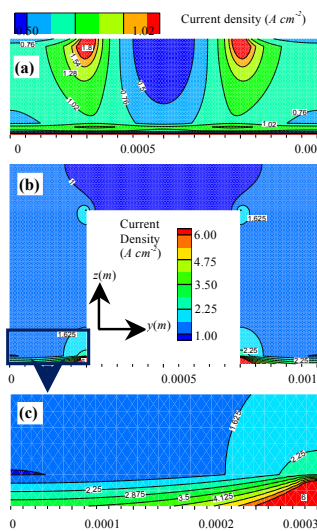
$$R_\Omega = \frac{|\varphi_{\max} - \varphi_{\min}|}{\bar{j}} \quad (4)$$

where  $\bar{j}$  is the average current density,  $\varphi_{\max}$  and  $\varphi_{\min}$  are the maximum and minimum electric potential occurring in the domain, respectively. A constant current density  $i = 0.7 \text{ A cm}^{-2}$  was applied at the membrane as the current source for the

Laplacian equation. The missing parameters of this model can be found in [6].

### III. RESULTS AND DISCUSSIONS

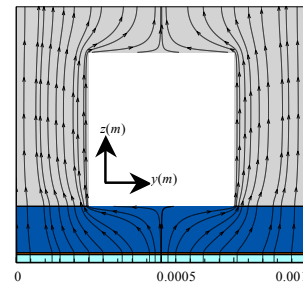
The local current density is predicted and presented in Fig. 2 for the domain at the cell middle ( $x=0.025\text{ m}$ ). It is clear that the highest current density occurs in the gas diffusion layer (GDL) below the corner of the bi-polar plates (BPP) close to the channel. This highest value can be clearly observed in Fig. 2c, which is a magnification of the bottom shoulders of the BPP (blue rectangular areas) in Fig. 2b. It is found that the maximum current density appears in a larger distribution area at the bottom of the BPP close to the channel. This is so because the electric current flows upward more easily from the GDL to the BPP's shoulder around the corner.



**Fig. 2. Current density distribution at the cell middle in (a) anodic GDL and catalyst layer (CL), (b) anodic BPP and (c) magnification of blue rectangular area shown in (b).**

The streamlines of the electric field are presented in Fig. 3 at the cell middle ( $x=0.025\text{ m}$ ). The lines and arrows illustrate the current flow direction which starts from the current source (generated at the membrane interface) to the lower potential zone appearing at the top surface of BPP. Only a portion of the BPP makes contact and the other portion is open for access of reactant gases and removal of products, while the GDL bridges the channels and redistributes the electric current. As shown, the current below the channel flows across with a longer distance from the middle of the GDL to the BPP's shoulders. In other words, the electric field is redistributed and becomes more uniform from the shoulders to the top of BPP. It is noted that the electric field at the BPP's corner close to the channel is significantly concentrated. In addition, the electric resistance of an entire cell was predicted as  $99.4\text{ m}\Omega\text{ cm}^2$  based on this

model.



**Fig. 3. Streamlines of electric field transfer through membrane and anodic cell at the cell middle.**

### IV. CONCLUSION

In the present study, an electric transport process model was developed in OpenFOAM to predict the through-plane electric properties of a PEM fuel cell. The predicted results show that the BPP's corner close to the channel becomes a concentrated area for the electric field and current, because of the channel/rib structure. Furthermore, the current below the channel flows a longer distance to the shoulders compared with the one below the shoulders. Finally, the electric resistance is predicted as  $99.4\text{ m}\Omega\text{ cm}^2$  of the bulk of an entire cell based on this model.

### ACKNOWLEDGMENT

The research work was carried out at the Department of Energy Sciences, Lund University, Sweden. The first author gratefully acknowledges the financial support from China Scholarship Council (CSC).

### REFERENCES

- [1] Barbir, F., PEM Fuel Cells: Theory and Practice, Cambridge, Academic Press, 2013.
- [2] Higier, A., Liu, H., Effects of the difference in electrical resistance under the land and channel in a PEM fuel cell, International Journal of Hydrogen Energy, Volume 36, 2011, Pages 1664-1670.
- [3] Higier, A., Liu, H., Direct measurement of current density under the land and channel in a PEM fuel cell with serpentine flow fields, Journal of Power Sources, Volume 193, 2009, Pages 639-648.
- [4] Yang, W.J., Kang, S.J., Kim, Y.B., Numerical investigation on the performance of proton exchange membrane fuel cells with channel position variation, International Journal of Energy Research, Volume 36, 2012, Pages 1051-1064.
- [5] Berning, T., Lu, D., Djilali, N., Three-dimensional computational analysis of transport phenomena in a PEM fuel cell, Journal of Power Sources, Volume 106, 2002, Pages 284-294.
- [6] Wang, J., GDL Deformation and its Effects on Electric resistance and Transport Phenomena in a PEM Fuel Cell [Doctoral Dissertation], Sweden: Lund University, 2017.

## EXPERIMENTAL STUDY OF THE CARBON DEPOSITION ON THE ANODE OF AS-SOFC UNDER VARIED FUEL VELOCITY

K. Motylinski\*, M. Skrzypkiewicz\*, Y. Naumovich\*,  
M. Wierzbicki\*, and J. Kupecki\*

\*Department of High Temperature Electrochemical Processes  
(HiTEP), Institute of Power Engineering, Augustowka 36, 02-981  
Warsaw, (Poland)

**Abstract** - The elevated operating temperature of the solid oxide fuel cells (SOFC) enables favorable kinetics of oxidation of gas mixtures including carbon-containing components such as CO. The presence of carbon-based components in the fuel might result in the deposition of soot on the anode of the fuel cell. This process depends on the thermodynamic, kinetic and electrochemical conditions. In the current study, it was claimed that in addition to above-listed parameters, the anodic gas velocity has also an influence on the carbon deposition phenomenon.

The effect of the gas velocity on formation of the carbon deposits was experimentally investigated using 5cm x 5cm anode supported solid oxide fuel cells (AS-SOFC) under 750°C and anodic gas velocities 0.1 ÷ 0.7 m/s. Experiments were performed for open circuit and constant current load 3 A.

**Index Terms** – SOFC, carbon deposition, soot formation, EIS

### I. INTRODUCTION

Solid oxide fuel cells are electrochemical energy conversion ceramic devices which operate at elevated temperature, typically in range from 600°C to 900°C. The elevated temperature allows to use carbon-containing species as fuels such as a reformat gas containing carbon monoxide. The presence of carbon-based components in the fuel might result in deposition of solid carbon particles on the fuel cell anode. This might lead to several undesirable effects such as the partial or complete loss of the electrochemical activity, distortion of mass-flow distribution or even mechanical destruction of the cell. The process of carbon formation and deposition in the anodic compartment of SOFC depends on the thermodynamic and kinetic conditions, including the steam-to-carbon ratio (S/C), temperature, catalytic properties of the material of the anode, and the current generated by the cell.

In the current study, it is claimed that another parameter

affecting the rate of the carbon deposition process is the anodic gas velocity. The flow parameters influence the kinetics of the multiphase electrochemical reaction, especially on the porous surfaces.

In the performed experiments, carbon deposition process was observed for various anode gas velocities, while maintaining constant all other operation parameters: gas composition, operating temperature and electric current drawn from the cell.

### II. EXPERIMENTAL METHODOLOGY

The test was performed on a single, planar 5cm x 5cm anode supported solid oxide fuel cell (AS-SOFC) based on Ni-YSZ anode with the effective area of the cathode of approximately 16 cm<sup>2</sup>. The material parameters of the cell are shown in Fig. 1.

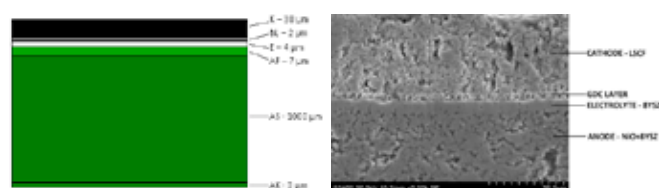


Fig. 1. Thickness of the interlayers of the analysed AS-SOFC (left) and its microstructure (right) [1]

The cell was placed inside a ceramic housing between two gold current collectors. The operating temperature for the each experiment was kept at 750±1°C. In the current study, specific anode gas composition was chosen and maintained in order to simulate a situation where reformat gas is delivered directly to the fuel cell. The proposed composition was a dry mixture of 12.5% H<sub>2</sub>, 37.5% CO and 50% N<sub>2</sub>. Based on the known






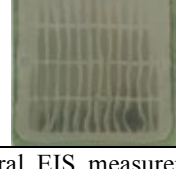


dimensions of the gas channels in the cell housing, it was possible to calculate the anode gas velocities for different fuel flows. The determined velocities range was from 0.1 to 0.7 m/s for fuel flows from 120 Nml/min to 640 Nml/min, respectively. Six separate experiments were performed under two operation conditions: open circuit (three test-runs) and constant current load 3A (another three test-runs). Under constant load, fuel flows from 120 to 640 Nml/min correspond to from 38% to 7% of reactant utilization, respectively. The electrochemical impedance spectroscopy technique (EIS) was used to monitor the fuel cell degradation in the three latter experiments. The duration of every test was seven hours excluding heat-up, cell reduction and cool-down stages. In order to compare the influence of carbon deposition on fuel cell operation and short time degradation, the EIS measurements were performed at the beginning and at the end of the experiments under 3 A load.

### III. RESULTS AND DISCUSSION

The results of the six performed experiments are shown in Table 1. The *post-mortem* analysis of the samples shown that carbon deposition process is directly correlated with the gas velocity. The formation of carbon occurs faster under OCV operation, during which no consumption of CO and H<sub>2</sub> occurs, resulting in high concentration of carbon-containing CO and low concentration of H<sub>2</sub>O, that, if present, would cause further CO reduction according to WGS reaction  $\text{H}_2\text{O} + \text{CO} \rightarrow \text{H}_2 + \text{CO}_2$ .

TABLE I  
CARBON DEPOSITION FOR VARIOUS ANODE GAS VELOCITIES

Anode gas velocity	OCV	3A
0.1 m/s		Test not performed
0.3 m/s		
0.5 m/s		
0.7 m/s	Test not performed	

For the fuel cell under 3 A load, several EIS measurements

were performed. The frequency range was set from 10 kHz to 77 mHz, with 10 mV amplitude. One of the EIS comparisons, before/after carbon deposition under 3 A and 0.5 m/s, is shown in Fig. 2.

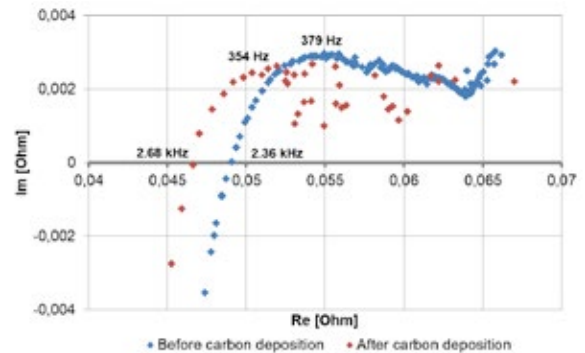


Fig. 2. EIS measurements for experiment with 0.5 m/s anode gas velocity and under current 3A

The performed measurements show that carbon formation results in a minor decrease of the contact resistance between the electrode and the current collector in the analyzed short-term operation (shift of the EIS spectrum to the left). At the same time, the carbon deposition has a major effect on the electrochemical fuel cell stability, resulting in observable oscillations of the voltage as well as causes the irreversible cell degradation leading to a permanent damage (post-mortem observations).

### IV. CONCLUSION

The realized experiments showed that in both open circuit and under galvanostatic load (3 A) conditions, anode gas velocity demonstrated a visible impact on the carbon deposition process in solid oxide fuel cells. The higher the velocity, the fastest and more aggressive carbon formation on the cell anode occurs. Future works need to be focused on determining the carbon deposition boundaries for different gas compositions and velocities.

### ACKNOWLEDGMENT

This work was financially supported by the National Science Centre, Poland, Grant No. 2015/19/N/ST8/01876.

### REFERENCES

- [1] Kluczowski R., Krauz M., Kawalec M., Ouweltjes J.P., Near net shape manufacturing of planar anode supported solid oxide fuel cells by using ceramic injection molding and screen printing, *Journal of Power Sources*, Volume 268, 2014, pp. 752-757.

## FUEL CELLS IN THE AERONAUTICAL SECTOR

Maria del Pilar Argumosa

INTA, Propulsion Dept., Ctra. Ajalvir km 4. 28850 Torrejón de  
Ardoz, Madrid, (Spain)

**Abstract** - Fuel Cells, as power source, are a promising and versatile technology. The transport sector has demonstrated its use in the last 15 years, and now Fuel cell cars are commercially available.

Fuel cells on aerospace application have also been developed in several space missions; but what about the aeronautical sector?. Have already been proved this technology in this market or there are some handicaps to success in it?

This is the matter of this article. It covers a fast view of the state of the art of the use of fuel cell in the aeronautical, following by a more detail outlook on specific applications as UAVs, small aircrafts and commercial aircrafts.

The main target will be to show which are the advantages but also the bottlenecks and challenges of using current developed fuel cells in real aeronautical scenarios.

This article is based on the INTA's participation in three different projects:

- STO/NATO/SET 173\_Fuel cells and other emerging Manportable Power Technologies for the NATO Warfighter
- EU/FP7/FCH-JU/GA325342/HYCARUS\_Airborne FCs.
- Comunidad de Madrid\_S2013/MAE-2975/PILCONAER

**Index Terms** – fuel cell systems, hydrogen, aeronautic, aerial vehicles

### I. NOMENCLATURE

UAV\_ Unmanned aerial vehicles

FC\_ Fuel cell

### II. INTRODUCTION

The main requirements demanded to a power system for any aeronautical application include: “Low Weight”, “High Reliability” and “Performance Stability” at different environmental conditions. But depending on the specific application other factors can promote or handicap the use of this technology.

### III. AERONAUTICAL VEHICLES

#### A. Unmanned Aerial Vehicles

UAVs have been widely used in the military world but now

they are sparking interest in civil applications, fuel cells could provide the power to propel these vehicles but also power their on board electronic devices. Fuel cells compete with internal combustion engine and with batteries, but we will see that depending on some features of the UAV, some advantages can be reached thanks to fuel cells systems [1]. A detailed analysis of some UAVs configuration, based on actual fuel cell systems, shows which points can help to success in this kind of vehicles. Missions and environmental requirements are key factors. Mini UAVs, ranged from 200 to 500 W of power, can take advantage of this technology providing higher energy density (400 Wh/kg) than Li-on batteries (145 Wh/kg). Although for bigger UAVS (regular size with 10 – 50 kW power requirement) ICE propulsions has still better performance. New developments on FC stacks are needed to reach good performance to fit in the demanding aeronautical sector, taking into account the hard environmental requirements. This is the target of the PILCONAER research project financed by Madrid Regional Government.

**FUEL CELLS in the Aeronautical Sector**

**Small UAVs**

UAV	W (kg)	Wingspan (m)	Autonomy (h)	FC type	Power (W)	Fuel Storage	FC Manufacturer
Spider Lion	2.54	2.2	3.3	PEM	100	CGH <sub>2</sub>	Protonex Tech. Corp.
Georgia Tech UAV	16.4	6.6	0.75	PEM	500	CGH <sub>2</sub>	
Hyfish	6	1	0.25	PEM	1000	CGH <sub>2</sub>	Horizon FC Technology
Puma	9.7	2.6	9	PEM		Chemical hydride	Protonex Tech. Corp.
Pterosaur	5	5.5	15.5	PEM	650	CGH <sub>2</sub>	Horizon FC Technology
HuEndurance	10	3.3	10	PEM	1000	CGH <sub>2</sub>	EnergyOR
Ion Tiger	NA	NA	26	PEM	500	CGH <sub>2</sub>	Protonex Tech. Corp.

**Fig. 1. Fuel cells in Small UAVs**

#### B. Light Aircrafts

Several LIGHT AIRCRAFTS have demonstrated the viability of being propelled by electrical engines powered by Fuel cell systems. The lower fuel cell system specific fuel consumption (90 gr/kwh of H<sub>2</sub> vs 500 gr/kwh of petrol) than

the ICE, gives an initial advantage to this technology, but some others factors have to be taken into account to assure a successful flight if you try to power this kind of planes with an electrical fuel cell system.

Optimization of aerodynamic designs (allowing gliding), improvements on main and auxiliary equipment performance to comply with the strict aeronautical environmental requirements.

But the airworthiness certification of this FC aircraft is still a great handicap to enter in the market.

#### FUEL CELLS in the Aeronautical Sector

##### CIVIL AVIATION



Fig. 2. Examples of FC powered airplanes

##### C. Commercial Aircraft

COMMERCIAL AIRPLANES are also considering the use of fuel cell as a promising technology to supply part of the electricity demanded by the future More Electric Aircrafts.

Commercial aviation is looking for more environmental friendly Aircrafts, fuel cells system is a clean technology that can help to reduce fuel consumption and greenhouse gas emissions.

Airbus, DLR and Parker Aerospace are together studying the use of multifunctional fuel cell concept (MFFC) as a future replacement for today's gas turbine based APUs, but some other operation in the aircraft are also candidates for fuel cell power units.[2]

TABLE I  
OPERATION WHERE FC TECHNOLOGIES CAN BE INTRODUCED

Emergency Power	Inerting systems	Ground Electricity Power
	Auxiliary power units	Water production
		Fire extinction

The EU commission is funding some projects as the HYCARUS, where aeronautical partners and fuel cell partners are working together to demonstrate that this technology can be used onboard to power auxiliary equipment, reaching a TRL 6 level and being safe to fly.

To prove compliance with airborne requirements (pass successfully all the tests requested by the airworthiness standards as RTCA DO-160) requires a big effort in this kind of

developments.



Fig. 3. : Airworthiness standards compliance

#### IV. CONCLUSION

Fuel cell technology may be a good way to improve the UAVs performance, but it depends on the mission. Environmental factors are also important.

It is necessary to calculate in each mission scenario, whether fuel cells have better performance than batteries or internal combustion engines. In general, fuel cells will be favored above batteries by longer missions and lower average power demands.

Suitable components with aeronautical performances must be developed helping the use of this technology on bigger aircraft as auxiliary power units

Aerial Vehicles powered by FC are only competitive when low power and high endurance are the main requirements. (UAVs)

In Small Aircraft, mainly gliders, they are also viable, but the performance are lower than using an ICE.

In big aircraft, FC are viable only for APUs, RATs or Ground power. However, big barriers have still to be overcome: Airborne requirements and intended aircraft cabin integration induce a specific set of design constraints that are not considered when defining performance targets in the automotive area: Off-the-shelf aeronautical components are not optimized to this technology; Design and structural requirement to get Aeronautical certification makes these components heavier, further optimization is required. The challenges to get the airworthiness certification in this kind of systems are showing as that there is still a hard work to success on these technologies.

#### REFERENCES

- [1] STO/NATO/SET 173\_Fuel cells and other emerging Manportable Power Technologies for the NATO Warfighter.
- [2] <https://www.asdreports.com/news-3198/multifunctional-fuel-cells-will-replace-traditional-apus-global-aerospace-military-apu-market>

## OXIDATIVE STEAM REFORMING OF ETHANOL IN A FLUIDIZED BED OVER CeO<sub>2</sub>-SiO<sub>2</sub> SUPPORTED CATALYSTS

V. Palma, C. Ruocco, and A. Ricca

Department of Industrial Engineering, University of Salerno, Via  
Giovanni Paolo II 132, 84084 Fisciano, SA, Italy

**Abstract** - A Pt-Ni/CeO<sub>2</sub>-SiO<sub>2</sub> catalyst was developed for the oxidative steam reforming ( $H_2O/C_2H_5OH=4$ ,  $O_2/C_2H_5OH=0.5$ ,  $T=500^\circ C$ ) of ethanol and its performances in packed (PBR) and fluidized bed reactors (FBR) were compared. Fluidized bed operation reduced carbon formation rate of almost 4 times with respect to the fixed bed reactor and improved hydrogen yields were also observed. In the FBR, the test was performed for 400 h and the system reached a plateau condition where ethanol conversion and hydrogen yield were almost 80% of the equilibrium value. This behavior was studied by measuring coke selectivity at regular intervals and it was possible to link the steady performance to the achievement of a zero net rate of carbon formation.

**Index Terms** – Coke, reforming, fluidized bed, hydrogen.

### I. INTRODUCTION

Hydrocarbons reforming is a mature technology and the employment of alternative H<sub>2</sub> sources (i.e. bioethanol) for this process is a very promising route in the search for sustainable energy solutions. At that end, steam reforming of ethanol under oxidative conditions (OESR) is preferred [1]: O<sub>2</sub> co-feeding and partial ethanol oxidation allows providing the required reaction heat directly within the catalytic bed; moreover, O<sub>2</sub> strongly helps to reduce coke deposition, a serious concern for catalyst lifetime. This process is commonly studied in fixed bed reactors (PBR); however, in a process intensification view, fluidized bed reactors (FBR) attract increasing interest, due to the improved heat and mass transfer rates, limited cold spot risk as well as reactor plugging due to coke formation [2].

This study is focused on OESR over a bimetallic Pt-Ni catalyst supported on CeO<sub>2</sub>-SiO<sub>2</sub>. The research is devoted to highlight the role of reactor configuration (fixed and fluidized bed) on catalyst activity and stability. The evolution of coke during the reaction in FBR was also studied to describe the plateau condition reached during the stability test.

### II. EXPERIMENTAL

Pt-Ni/CeO<sub>2</sub>-SiO<sub>2</sub> catalysts were prepared using a wet impregnation method. First, an aqueous solution of Ce(NO<sub>3</sub>)<sub>3</sub>·6H<sub>2</sub>O (Strem Chemicals) was prepared with a total metal concentration of 1.5 M, in order to reach a support composition of 30wt% in ceria. The calcined support (mesoporous silica gel, 90-115 μm, Sigma-Aldrich), was added to the solution and impregnation was carried out for 2 h at 80°C. The resulting solid was dried overnight and calcined at 600°C for 3h. For Ni and Pt impregnation, performed sequentially, a known amount of nickel nitrate hexahydrate and platinum chloride (Strem Chemicals) was dissolved in deionized water. After impregnation, the same procedure reported above was followed. Ni and Pt content was fixed to 10wt% and 3wt%, respectively, on the basis of ceria mass. The catalyst performances for OESR were evaluated at 500°C, atmospheric pressure and ethanol partial pressure of 0.1 ( $H_2O/C_2H_5OH$  of 4 and  $O_2/C_2H_5OH$  of 0.5). Prior to the reaction, the catalyst (7 g.) diluted with the bare CeO<sub>2</sub>-SiO<sub>2</sub> (22.6 g), was reduced at 600°C for 1 h using 5 %H<sub>2</sub>/N<sub>2</sub> mixture; afterwards, the reacting mixture was fed to the reactor with a total flow-rate of 770 Ncm<sup>3</sup>·min<sup>-1</sup> (corresponding to a weighty hour space velocity WHSV of 4.1 h<sup>-1</sup>). Further tests were performed at WHSV of 12.3 h<sup>-1</sup> and catalytic mass as well as total flow rates were changed accordingly. The reactor exit was monitored with an FT-IR Spectrophotometer (Thermo-Scientific) and two analyzer modules (ABB), capable of detecting H<sub>2</sub> and O<sub>2</sub> concentrations.

### III. RESULTS AND DISCUSSION

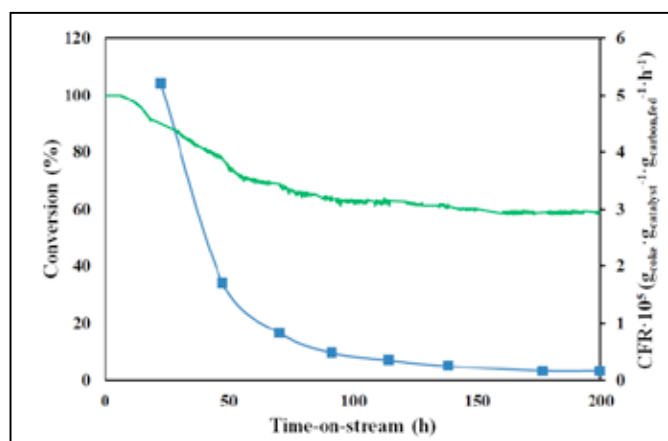
A comparative study on the effect of fluidized bed and fixed bed reactor in OESR was preliminary carried out at WHSV=4.1 h<sup>-1</sup>. In both the operative modes, a stable behavior was initially

Copyright © 2017



observed: ethanol was completely converted for almost 130 h of TOS and hydrogen yield fairly agreed with the value predicted by thermodynamics. However, hydrogen profile in the fluidized bed reactor was always higher than that of the fixed bed and a faster deactivation was recorded in the PBR. This clearly indicates that fluidization favors methane steam reforming reaction. In fact, methane concentration slightly decreased in comparison to the PBR, thus resulting in a higher hydrogen production. In addition, the synthesis gas ratio ( $\text{molH}_2/\text{molCO}$ ) increased of almost 40% in the FBR. Moreover, thermo-gravimetric analysis (TGA) performed on the spent catalysts proves that FBR allows coke selectivity reduction of almost 4 times: due to the constant catalyst recirculation, particles were continuously exposed to steam and oxygen. As a result, carbon formed would be readily removed via gasification reactions. The stability test over the Pt-Ni/CeO<sub>2</sub>-SiO<sub>2</sub> catalyst in the FBR was carried out for almost 400 h and only a partial deactivation was observed, which resulted in ethanol conversion as well as hydrogen yield lowering from 100% to 80% and 43.5 to 36%, respectively. In fact, after almost 300 h of TOS, the system reached a stationary condition with no more activity decay. The test was performed for further 100 h and the system was found to hold the plateau condition. These results suggest that carbon formation does not follow a constant trend during the test; conversely, it is supposed that coke deposited during test progressively deactivate the most reactive catalytic sites, involved in both reforming and by-products formation pathways. As a result, catalyst activity remained unchanged with no further increase in catalyst deactivation. In order to investigate the above hypothesis, a further test in FBR was performed over the Pt-Ni/CeO<sub>2</sub>-SiO<sub>2</sub> catalyst: at regular intervals, the test was stopped and a sample was withdrawn and characterized by TGA to study the variation of carbon formation rate (CFR, defined as the ratio between coke mass and the product of catalytic mass, the total mass of carbon fed as ethanol during the test and the time-on-stream) with TOS (time-on-stream). However, in order to accelerate the achievement of the stationary condition, WHSV was triplicate: the results of stability test are shown in Figure 1. At 12.3 h<sup>-1</sup>, the system reached a stationary condition after almost 150 h; CFR was quite high at the beginning of the test and displayed a decreasing trend with TOS. In particular, the carbon formation rates after 175 and 200 h were almost the same, proving that the net rate of carbon formation (i.e. the difference between carbon formation and carbon gasification rate) was equal to zero. Also other authors studied reforming reaction in FBR over Ni-based catalysts [3]. However, a different behavior was found: almost steady performances were followed by a severe drop in ethanol conversion and finally a slow decrease in ethanol conversion until total deactivation of the catalyst. Conversely, at the conditions of Figure 1, after almost 50 h of TOS, coke deposition was drastically attenuated

and a satisfactory activity was still observed after 200 h of test.



**Fig. 1. Trend of C<sub>2</sub>H<sub>5</sub>OH conversion and CFR during OSR over Pt-Ni/CeO<sub>2</sub>-SiO<sub>2</sub> in FBR, 500°C, H<sub>2</sub>O/C<sub>2</sub>H<sub>5</sub>OH=4, O<sub>2</sub>/C<sub>2</sub>H<sub>5</sub>OH=0.5, WHSV=12.3 h<sup>-1</sup>.**

#### IV. CONCLUSION

In this work, OESR was studied over a Pt-Ni/CeO<sub>2</sub>-SiO<sub>2</sub> catalyst in fixed and fluidized bed reactors at 500°C. In FBR, superior performance was observed with a coke selectivity reduction of almost 4 times. The catalyst in FBR reached a plateau condition after 300 h of test at 4.1 h<sup>-1</sup>, where ethanol conversion and hydrogen yield were equal to 80% of the equilibrium values. This behavior was linked to the coke formation rate lowering during the test, which was attested to 0.00000162 g<sub>coke</sub> · g<sub>catalyst</sub><sup>-1</sup> · g<sub>carbon,fed</sub><sup>-1</sup> · h<sup>-1</sup> after 175 h at 12.3 h<sup>-1</sup>.

#### ACKNOWLEDGMENTS

The research leading to these results has received funding from the European Union's Seventh Framework Programme (FP7/2007-2013) for the Fuel Cells and Hydrogen Joint Technology Initiative under grant agreement no. 621196. The present publication reflects only the author's views and the FCH JU and the Union are not liable for any use that may be made of the information contained therein.

#### REFERENCES

- [1] Han, X., Wang, Y., Zhang, Y., Yu, Y., He, H., Hydrogen production from oxidative steam reforming of ethanol over Ir catalysts supported on Ce-La solid solution, *International Journal of Hydrogen Energy*, Volume 42, 2017, Pages 11177-11186
- [2] Shi, Y., Du, X., Yang, L., Sun, Y., Yang, Y., Experiments on hydrogen production from methanol steam reforming in fluidized bed reactor, *International Journal of Hydrogen Energy*, Volume 38, 2013, Pages 13974-13981.
- [3] Montero, C., Ochoa, A., Castaño, P., Bilbao, J., Gayubo, A., Monitoring Ni<sup>0</sup> and coke evolution during the deactivation of a Ni/La<sub>2</sub>O<sub>3</sub>-αAl<sub>2</sub>O<sub>3</sub> catalyst in ethanol steam reforming in a fluidized bed, *Journal of Catalysis*, Volume 331, 2015, Pages 181-192.



## MODELING ANALYSIS OF FLOW FIELD GEOMETRICAL FEATURES IN POLYMER ELECTROLYTE FUEL CELLS POROUS MEDIA

M. Messaggi\*, A. Baricci\*, R. Mereu\*, M. Zago\*, F. Inzoli\*, A. Casalegno\*

\* Politecnico di Milano, Department of Energy, via Lambruschini 4, 20156 Milan, (Italy)

**Abstract** - The present work gets insights into the mass transport phenomena taking place in hydrogen PEMFC with a modelling analysis based on computational fluid dynamics to interpret experimental data. Experimental polarization curves and electrochemical impedance spectroscopy (EIS) have been performed on membrane electrode assembly in H<sub>2</sub>/O<sub>2</sub> and H<sub>2</sub>/Air configurations. PEMFC models (2D and 3D) have been considered and ad hoc simulations have been carried out to investigate the effects of geometrical features present in real flow fields: oxygen depletion under current collector, flow mixing in channel bends, flow bypass between adjacent channels. In addition to polarization curves, impedance spectra are simulated: local spectra are simulated along a 3D channel showing a low frequency feature that appears progressively moving along the channel in consequence of oxygen depletion on active sites. This feature is adopted to assess the effect of mass transport in PEMFC and discuss the effect of channel bends and rib/channel.

**Index Terms** – CFD, EIS, Model, PEMFC.

### I. INTRODUCTION

Polymer electrolyte membrane fuel cells (PEMFC) are electrochemical devices that are investigated as an alternative to internal combustion engines in automotive applications, thanks to their intrinsic characteristics of high power density, virtually zero emission of pollutants and fast start-up. Power density of PEMFC at the current stage of research is impacted by limitation in oxygen transport at the cathode side, because of the effect of flow field, molecular/Knudsen diffusion in porous media and transport into primary catalyst pores flooded by the electrolyte. The scope of this work is to get insights into the mass transport phenomena taking place in hydrogen PEMFC with a modelling analysis based on computational fluid dynamics (CFD) to interpret experimental data.

### II. MODEL DEVELOPMENT

Isothermal and single-phase 3D model (in ANSYS® Fluent) and 2D model (in COMSOL Multiphysics®) with two configurations, along the channel and transverse to the channel, have been developed coupling both fluid dynamics and electrochemistry. The investigated geometries are a straight

channel, a channel with a bend and an interdigitated distributor. Only results for the straight channel and for the channel with bend are reported and discussed here for the sake of brevity.

#### A. Mass Balance

Conservation of mass (Eq. 1) is assured in channels and porous media of the domain [1]:

$$\varepsilon \frac{\partial \rho}{\partial t} + \nabla \cdot (\rho \mathbf{u}) = S_m \quad (1)$$

#### B. Momentum Balance

The momentum conservation equation (Eq. 2) is solved in distributor channels and porous media [1]:

$$\frac{1}{\varepsilon} \frac{\partial (\rho \mathbf{u})}{\partial t} + \frac{1}{\varepsilon^2} \nabla \cdot (\rho \mathbf{u} \mathbf{u}) = -\nabla p + \nabla \cdot \boldsymbol{\tau} + S_u \quad (2)$$

#### C. Species Balance

Also conservation of chemical species is granted, according to Eq. 3 [1]:

$$\varepsilon \frac{\partial (\rho Y_k)}{\partial t} + \nabla \cdot (\rho \mathbf{u} Y_k) = \nabla \cdot \mathbf{J}_k + S_k \quad (3)$$

#### D. Charge Balance

Charge conservation in the solid and electrolyte is described by Eq. 4 and 5. The effect of the double layer current is taken into account [1]:

$$-C_{dl} \frac{\partial \eta}{\partial t} + \nabla \cdot (\sigma_s \nabla \phi_s) + S_s = 0 \quad (4)$$

$$C_{dl} \frac{\partial \eta}{\partial t} + \nabla \cdot (\sigma_l \nabla \phi_l) + S_l = 0 \quad (5)$$

#### E. Kinetic model

Butler-Volmer (Eq. 6) and Tafel (Eq. 7) laws are used to describe reaction rates for ORR (Oxygen Reduction Reaction) ( $i_c$ ) and HOR (Hydrogen Oxidation Reaction) ( $i_a$ ), including the Flooded Agglomerated Model (FAM) at the cathode [1]:

$$i_a = i_{0,a} \left( \frac{c_{H_2}}{c_{ref}} \right)^\gamma \left[ \exp \left( \frac{\alpha_a F \eta_a}{RT} \right) - \exp \left( - \frac{(1-\alpha_a) F \eta_a}{RT} \right) \right] \quad (6)$$

$$i_c = E_{FAM} i_{0,c} \left( \frac{c_{O_2}}{c_{ref}} \right)^\gamma \exp \left( - \frac{\alpha_c F \eta_c}{RT} \right) \quad (7)$$

### III. RESULTS

The effect of oxygen depletion along the channel is analysed with the 2D model: the simulation of the EIS (Fig. 1), performed according to the procedure described in [1], reveals an increase in the amplitude of the low frequency element of the local impedance spectra moving from the inlet to the outlet of the channel, due to the reducing availability of the oxygen, consumed by the electrochemical reactions.

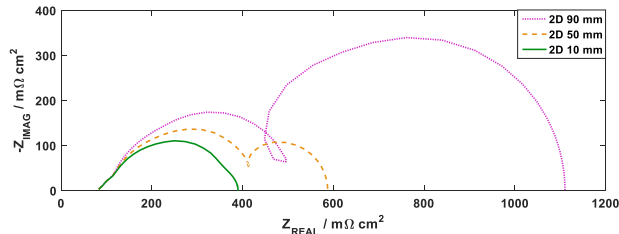


Figure 1. Results of 2D simulations of oxygen depletion along the channel at  $0.2 \text{ A cm}^{-2}$ : comparison of local spectra recorded at different positions along the channel from channel inlet.[1]

Then a complete mixing of the flow of reactants is imposed at half of the length of the channel in the 2D model, in order to simulate a possible effect of a bend in the flow field. The overall performances are not affected, while the simulated spectra, presented in Fig. 2a, show a reduction of the low frequency element of the global spectrum due to the imposed mixing. Moreover, comparing the local spectra obtained immediately before and after the mixing point (Fig. 2b) it is possible to observe a complete suppression of the low frequency feature, because the oscillation of oxygen in the channel is not transferred through the mixing. Then these results are compared with the local spectra before and after the bend simulated with the complete 3D geometry (Fig. 2c), which shows an increasing amplitude of the low frequency element through the bend, thus revealing the absence of complete mixing in the bend in the investigated conditions.

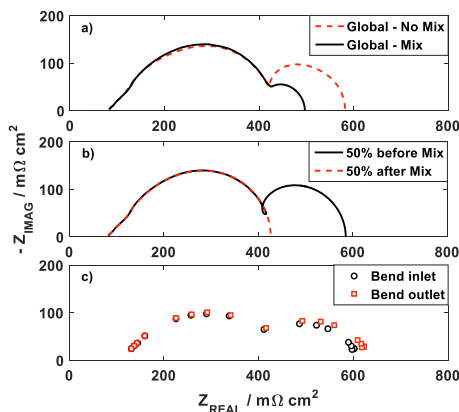


Figure 2. Impedance spectra simulated at  $0.2 \text{ A cm}^{-2}$  under low stoichiometry in the 2D configuration to evaluate the effect of complete flow mixing: a) comparison of average impedance spectra simulated with mixing and without mixing; b) comparison of local impedance spectra simulated before and after the bend in presence of flow mixing; c) local EIS recorded before and after the bend in the 3D model with serpentine flow field.[1]

The analysis of the effect of the rib of the current collector is performed with the 2D model on a plane transverse to the channel, comparing two configurations, with and without the rib (1D), at high stoichiometry. From Fig. 3a it is possible to notice the effect on the polarization curve of the depletion of the oxygen under the rib, with a reduced performance especially at high current densities. The EIS simulated in the configuration with the rib (Fig. 3b) shows a greater high frequency resistance if compared with the 1D configuration, because of the larger path made by the current to reach the collectors, and a distortion of the low frequency part of the spectrum, due to the sluggish diffusion of the oxygen in the porous media under the rib.

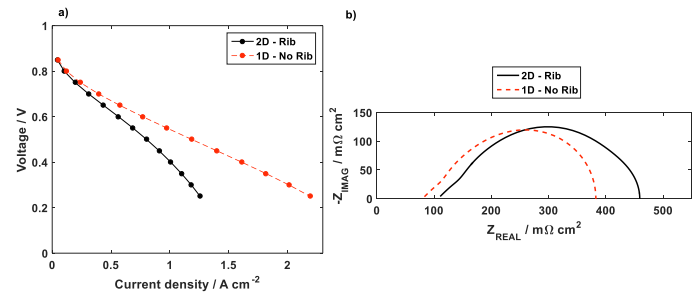


Figure 3. Results of the 2D simulations that analyse the effect of the rib: (a) polarization curve of the 2D rib/channel configuration compared 1D configuration; (b) impedance spectra simulated at  $0.2 \text{ A cm}^{-2}$  in 2D and 1D configurations.[1]

### IV. CONCLUSION

A model of PEMFC is developed, simulating polarization curves and impedance spectra, which allow a better distinction of the physical phenomena.

The effect of the depletion of the oxygen along the channel causes the appearance of a low frequency element in the spectrum, with increasing amplitude moving along the channel, while the depletion of oxygen under the rib causes a distortion of the spectrum at low frequency. Moreover a greater high frequency resistance is noticed in presence of the rib.

Introducing a complete mixing of the flow, a suppression of the low frequency element is noticed, because the oxygen oscillation cannot be transferred through the mixing point.

Considering a complete 3D geometry with a bend, an additional bypass flow of reactants arises under the rib between two adjacent channels, because of pressure and concentration gradients, causing a reduction of the low frequency element of the spectrum, while the mixing of the flow in the bend is not observed in the investigated conditions. For the interdigitated geometry, the bypass flow is maximized, since all the reactants are forced to pass under the rib to reach the outlet.

### REFERENCES

- [1] A. Baricci, R. Mereu, M. Messaggi, M. Zago, F. Inzoli, A. Casalegno, Application of computational fluid dynamics to the analysis of geometrical features in PEM Fuel Cells flow fields with the aid of impedance spectroscopy, Applied Energy, volume 205, pages 670-682.

## FLOATING MFC FOR BOD MONITORING IN REAL TIME: FIELD TEST IN A WASTEWATER TREATMENT PLANT

M. Tucci\*, A. Goglio\*, A. Schievano\*, S.P. Trasatti\*\*, M. Papacchini\*\*\* and P. Cristiani\*\*\*\*

\*Department of Agricultural and Environmental Science (DISAA), University of Milan

Via Celoria 2, 20133 Milan (Italy)

\*\*Department of Chemistry University of Milan, Via Celoria 2, 20133 Milan (Italy)

\*\*\*INAIL Settore Ricerca, Certificazione e Verifica, Dipartimento di Innovazione Tecnologica (DIT) Laboratorio di Biotecnologie, Rome, Italy

\*\*\*\*RSE – Ricerca sul Sistema Energetico S.p.A., Sustainable Development and Energy Sources Department, v. Rubattino 54, 20134 Milan (Italy)

### Abstract

A simple and low-cost MFC-based BOD sensor is presented. The structure of the sensor consisted in a floating frame in polystyrene, holding identical carbon cloth plane electrodes separated by a clay layer and an insulating felt in polypropylene. The submerged anode and the air cathode were connected to a circuit with 100 $\Omega$  of external load. Calibration tests were performed in laboratory: a set of cells constructed with this configuration were placed in a tank using acetate as the carbon source and raw wastewater as both inoculum and electrolyte. The Total Organic Carbon (TOC) and Total Inorganic Carbon (TIC) were continuously monitored with a portable TOC Analyzer. The current production showed a linear relationship up to 34 ppm TOC. These cells were then placed in the denitrification tank of the wastewater treatment plant of Carimate (CO) and the current production was measured and correlated to the load of organic carbon.

**Index Terms** – Bioelectrochemical sensors, BOD analysis, Microbial Fuel Cells, Wastewater

### I. INTRODUCTION

The Biological Oxygen Demand (BOD) measurement is a key factor for the wastewater treatment process. Currently the BOD<sub>5</sub> test is the most widely used. However, this method has some analytical and operational limitations, such as questionable accuracy and irreproducibility, labour intensity and time consumption. Therefore, this method is not effective for process control and real-time monitoring where rapid feedback is needed [1].

Since the current or the charge generated from a Microbial Fuel Cell (MFC) are proportional to the concentration of fuel used

under non saturated conditions [2], Microbial Fuel Cells (MFCs) are attracting increasing attention as a tool for on-line BOD monitoring. Over the years, very different set-up and configurations have been developed for this purpose [3–6]. However, very few of them seem to focus on a real wastewater treatment application.

### II. MATERIALS AND METHOD

#### A. Cell construction

The structure of the sensor consisted in a polystyrene floating frame, holding identical plane electrodes made of carbon cloth (SAATI P10) separated by a clay layer and an insulating polypropylene felt. The submerged anode (13x10 cm) and the air cathode (16x16 cm) were connected to a circuit with 100 $\Omega$  of external load. This simple and low-cost construction allows an easy applicability in a real plant in multiple copies, with an estimated overall price of 1.70€ for one cell.

#### B. Calibration in laboratory

Two cells constructed as previously described were placed in a stirred tank and fed with acetate as the carbon source. Raw wastewater was the both inoculum and the electrolyte. Calibrations were performed by subsequent addition of acetate. Samples of the wastewater in the tank were collected for the analysis.

#### C. Wastewater treatment plant

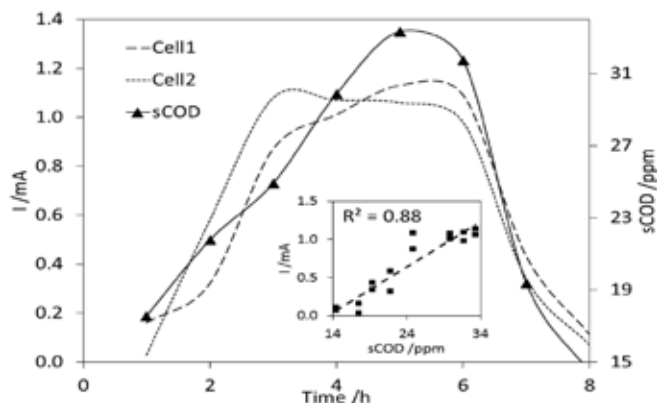
Six identical cells constructed as previously described were placed directly in the denitrification tank of the wastewater treatment plant of Carimate (CO). Samples of the wastewater were collected nearby the cells for the analysis.

#### D. Measurements

The TOC and the TIC were continuously monitored with Sievers 820 Portable Total Organic Carbon Analyzer. The potential difference across the resistance (R) of every MFC was acquired every 6 min via a multichannel Data Logger (Graphtechmidi Logger GL820). The generated current (I) was calculated by the equation  $I = V/R$ , where I is the current flowing through the external resistance. The soluble Chemical Oxygen Demand (sCOD) of the wastewater samples was measured by a spectrophotometric method. Each sample was filtered with syringe filters (Sartorius, 0,45 $\mu$ m porosity), and then added to HT-COD cuvette test (Hach Lange GmbH), and digested at 175 °C for 15 min (Lange HT 200 S). After cooling, the COD value was read by an UV- spectrophotometer (Lange DR 3900).

### III. RESULTS AND DISCUSSION

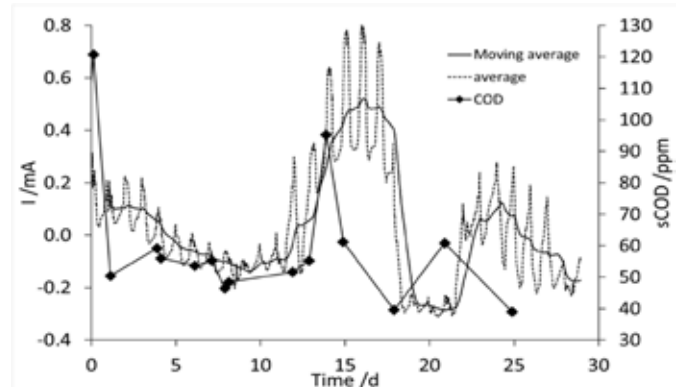
Fig. 1 shows the current trend of two cells and sCOD when subsequent additions of acetate were performed. The increase and decrease of sCOD are followed by the current with a very short response time. The graphic in the frame of Fig 1 depicts a linear correlation between the current signal and the concentration of sCOD in a range between 13 and 34 ppm with a  $R^2$  of 0.88. For higher concentration of sCOD the linear relationship is lost, until the system is completely saturated and the current reaches a plateau around 100 ppm (data not shown).



**Fig. 1. Trends of current of two MFCs and sCOD during subsequent addition of acetate. Linear correlation between current and sCOD in the frame.**

Fig. 2 depicts the average current trend of the six MFCs placed in the denitrification tank of the plant (dotted line). This trend is characterized by daily peaks, which seem strongly related to the periods of illumination of the cathodic surface. In order to exclude this interference, the moving average of the current was calculated (period 100, solid line), and the trend follows the increase and decrease of the soluble COD (diamonds). However, a delay between the peaks can be noticed, which is probably due to the presence of recalcitrant organic compounds in the wastewater. Indeed, the degradation of these compounds

operated by the anodic biofilm is normally much slower than the sole acetate.



**Fig. 2. Trends of average current of six cells and sCOD in the denitrification tank over 30 days.**

### IV. CONCLUSION

A new prototype of floating MFC BOD sensor has been successfully tested in a real wastewater treatment plant. Further investigations should address the decrease of the impact of environmental factors as well as the response time on the current signal, and the enhancement of the sensibility of the sensor.

### ACKNOWLEDGMENTS

The authors acknowledge Sud Seveso Servizi S.p.a. for the chance to operate in the wastewater treatment plant of Carimate (CO), and Paolo Bonelli and Fausto Otero, for the support in the construction of the voltage acquisition system.

### REFERENCES

- [1] Di Lorenzo, M., Curtis, T. P., Head, I. M., and Scott, K., 2009, "A Single-Chamber Microbial Fuel Cell as a Biosensor for Wastewaters," *Water Res.*, 43(13), pp. 3145–3154.
- [2] Grattieri, M., Minteer, S. D., and Hasan, K., 2013, "Bio-Electrochemical Systems as A Multipurpose Biosensing Tool: Present Perspective and Future Outlook."
- [3] Franzetti, A., Daghighi, M., Parenti, P., Truppi, T., Bestetti, G., Trasatti, S. P., and Cristiani, P., 2017, "Monod Kinetics Degradation of Low Concentration Residual Organics in Membraneless Microbial Fuel Cells," *J. Electrochem. Soc.*, 164(3), pp. H3091–H3096.
- [4] Kumlanghan, A., Liu, J., Thavarungkul, P., Kanatharana, P., and Mattiasson, B., 2007, "Microbial Fuel Cell-Based Biosensor for Fast Analysis of Biodegradable Organic Matter," *Biosens. Bioelectron.*, 22(12), pp. 2939–2944.
- [5] Pasternak, G., Greenman, J., and Ieropoulos, I., 2017, "Self-Powered, Autonomous Biological Oxygen Demand Biosensor for Online Water Quality Monitoring," *Sensors Actuators B Chem.*, 244(January), pp. 815–822.
- [6] Jang, J. K., Pham, T. H., Chang, I. S., Kang, K. H., Moon, H., Cho, K. S., and Kim, B. H., 2004, "Construction and Operation of a Novel Mediator- and Membrane-Less Microbial Fuel Cell," *Process Biochem.*, 39(8), pp. 1007–1012.

## HARMONIC SIGNAL ESTIMATION IN THE TIME DOMAIN FOR ON-LINE ELECTROCHEMICAL IMPEDANCE SPECTROSCOPY

D. Ritzberger\*, and S. Jakubek\*

\*Technische Universität Wien, Getreidemarkt 9/E325, (Austria)

**Abstract** – On-line monitoring of the electrochemical impedance typically involves the buffering of streaming data and subsequent use of the fast Fourier transform. This leads to an inherent trade-off between time and frequency resolution and biased amplitude estimates due to frequency leakage. In this work, time-domain estimation techniques, namely recursive least squares and Kalman filtering, are utilized for the estimation of amplitude and phase of harmonic output responses and its advantages are discussed. Furthermore, it is shown how the Kalman filter can be parameterized to filter out disturbances, present in any industrial application, which would otherwise lead to distorted estimates when applying the fast Fourier transform.

**Index Terms** – electrochemical impedance spectroscopy, on-line harmonic signal estimation, recursive least squares, Kalman filter

### I. INTRODUCTION

The electrochemical impedance spectroscopy (EIS) is a potent tool in fuel cell diagnostics. Complete impedance spectra are typically obtained by single sinusoidal excitations with increasing frequency and subsequent off-line estimation of amplitude and phase of the harmonic output response. When real-time impedance information during dynamic operating conditions are desired, it is advantageous to continuously monitor the impedance at fixed frequencies of interest [1-2]. Thereby, streaming current and voltage data is buffered into windowed segments for which the fast Fourier transformation (FFT) is applied. The inherent trade-off, when using the sliding window FFT, between time and frequency resolution is well known, as an increase of the frequency resolution is only obtained by increasing the window length, which also increases the time it takes to fill the data buffer. Additionally, when the frequency of a sampled harmonic signal is not coinciding with a point on the frequency resolution grid of the FFT, spectral leakage is present leading to distorted estimations. Although, by applying windowing functions or using overlapping data segments the influence of the aforementioned problems can be reduced, the question if there are alternatives better suited for the

on-line estimation of harmonic signal parameters (and subsequently the electrochemical impedance) is of importance. In this work, time-domain techniques such as recursive least squares (RLS) and the Kalman filter [3] are investigated for the harmonic signal estimation.

### II. METHODOLOGY

#### A. Harmonic Signal in Discrete Time Domain

A multi-harmonic signal with known angular frequencies  $\omega_1 \dots \omega_N$  is described as

$$y(k) = \sum_{n=1}^N A_n \cos(\omega_n k \Delta t) + \sum_{n=1}^N B_n \sin(\omega_n k \Delta t). \quad (1)$$

Thereby  $\Delta t$  denotes the sampling time and  $k$  the discrete time index. The amplitude and phase of the  $n$ -th harmonic signal content are given by

$$\begin{aligned} V_n &= \sqrt{A_n^2 + B_n^2}, \\ \varphi_n &= \tan^{-1} \left( \frac{B_n}{A_n} \right). \end{aligned} \quad (2)$$

#### B. Recursive Least Squares

Note that the Eq. (1) is linear in its parameters  $A_n$  and  $B_n$ , which facilitates the use of computationally inexpensive linear parameter estimation techniques. After obtaining  $k$  samples and rearranging Eq. (1) in matrix form,

$$\begin{aligned} Y(k) &= X(k)\theta(k), \\ Y(k) &= \begin{bmatrix} y(1) \\ \vdots \\ y(k) \end{bmatrix}, \theta(k) = \begin{bmatrix} A_1 \\ B_1 \\ \vdots \\ A_N \\ B_N \end{bmatrix} \\ X(k) &= \begin{bmatrix} \cos(\omega_1 1 \Delta t) & \sin(\omega_1 1 \Delta t) & \cdots \\ \vdots & \vdots & \\ \cos(\omega_1 k \Delta t) & \sin(\omega_1 k \Delta t) & \cdots \end{bmatrix} \end{aligned} \quad (3)$$



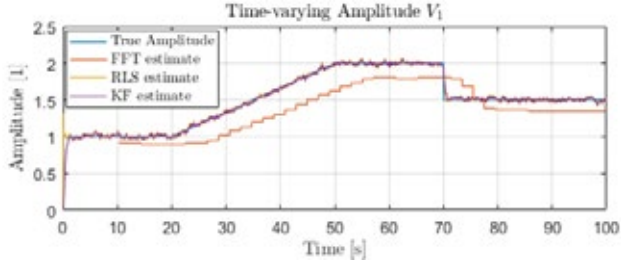


Fig. 1: Comparison of time-varying amplitude  $V_1$  with estimates

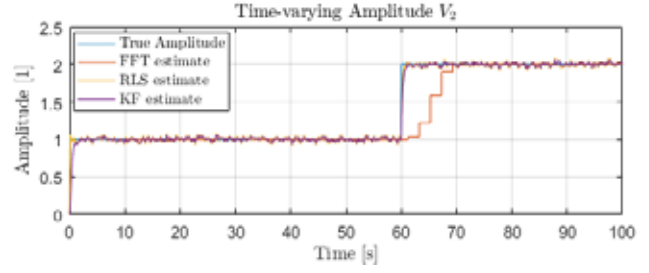


Fig. 2: Comparison of time-varying amplitude  $V_2$  with estimates

the harmonic signal parameters can be estimated using least squares:

$$\theta(k) = (X(k)^T X(k))^{-1} X(k)^T Y(k). \quad (5)$$

To avoid the inefficient re-estimation of the parameters at the next sampling instance using the complete dataset, the recursive least squares algorithm is used:

$$\theta(k+1) = \theta(k) + K_R(k, \lambda) (y(k+1) - x(k+1)^T \theta(k)). \quad (6)$$

Thereby,  $y(k+1)$  and  $x(k+1)^T$  is the measured signal and regressor line at the next time step,  $K_R(k, \lambda)$  is the time dependent RLS filter gain, and  $\lambda$  is a weighting parameter on historic data, e.g. tuning parameter for the responsiveness and variance of the RLS algorithm.

### C. Kalman Filter

As an alternative to the aforementioned RLS algorithm, the Kalman filter can be used. By defining Eq. (1) as the output equation, and by assuming a random walk model for the parameter evolution in the Kalman filter prediction step

$$\hat{\theta}(k+1) = \hat{\theta}(k) + w(k), \quad (7)$$

where  $w(k)$  is a Gaussian process noise with zero mean and  $\text{cov}(w) = Q$ , the parameter update equation has in general the same form as the RLS filter:

$$\theta(k+1) = \theta(k) + K_K(k, Q) (y(k+1) - x(k+1)^T \theta(k)). \quad (8)$$

The process noise covariance matrix is thereby used as the tuning parameter in deriving the Kalman filter gain  $K_K(k, Q)$ .

By assuming

$$Q = qI, \quad (9)$$

where  $I$  denotes the identity matrix, the performance of the Kalman filter is identical to the RLS algorithm.

The advantage of the Kalman filter approach lies in the fact, that by including a constant offset term in Eq. (1) and using the additional degrees of freedom in weighting, the Kalman filter can be parameterized to filter out additional disturbances present in the signal.

### III. RESULTS

A bi-tonal signal sampled with  $\Delta t = 0.01[s]$ ,  $\omega_1 = 2\pi 10 [rad/s]$  and  $\omega_2 = 2\pi 25 [rad/s]$  is used to evaluate the performance of the RLS and Kalman filter as opposed to the FFT. The time varying amplitudes and its estimates can be observed in Fig.1 and 2.

The sliding window FFT utilized 1024 data points per windowed segment, 80% overlap and a Hann windowing function. In Fig. 1, a biased FFT estimate due to spectral leakage is observed, as the excitation frequency in  $\omega_1$  does not coincide with a discrete frequency on the FFT grid. Amplitudes estimated by the time-domain filter approaches are unbiased. Even in the unlikely event that the excitation frequency happens to exactly coincide with a point on the FFT grid (Fig. 2) it can be observed, that the convergence of the time-domain filters is significantly faster.

### IV. CONCLUSION

In this work, time-domain filters are proposed to be used when on-line estimating the electrochemical impedance from multi-harmonic output signals as opposed to the sliding-window FFT. As the excitation frequencies in the time-domain approach can be chosen freely, the issue of biased estimates due to spectral leakage is resolved. Additionally, faster convergence to time-varying amplitudes is achieved, making this approach more suitable in dynamic operating conditions of the fuel cell

### ACKNOWLEDGMENT

This work has been supported by AVL List GmbH.

### REFERENCES

- [1] Katayama, N., Sumio K. "Real-time electrochemical impedance diagnosis for fuel cells using a DC-DC converter." IEEE Transactions on Energy Conversion 30.2 (2015): 707-713.
- [2] Cooper, K. R., and M. Smith. "Electrical test methods for on-line fuel cell ohmic resistance measurement." Journal of Power Sources 160.2 (2006): 1088-1095
- [3] Ljung, Lennart, and Torsten Söderström. Theory and practice of recursive identification. Vol. 5. Cambridge, MA: MIT press, 1983.

## THIN-FILM MAGNETRON SPUTTERED CATALYSTS SUPPORTED ON HIGH-SURFACE SUBLAYERS FOR PEM WATER ELECTROLYSIS

P. Kúš, A. Ostroverkh, Y. Yakovlev, R. Fiala, I. Khalakhan,  
M. Dubau, V. Matolin

Department of Surface and Plasma Science, Faculty of  
Mathematics and Physics, Charles University,  
V Holešovičkách 2, 180 00 Prague 8 (Czech Republic)

**Abstract** – Major drawback of proton exchange membrane water electrolyzers is their dependence on noble metals. The amount of Ir and Pt, the state-of-the-art catalysts for individual half reactions, has to be decreased significantly should the technology enter mass production. This work addresses above mentioned problem by conducting complex characterization of supported low-loading catalysts for anode as well as cathode side of the cell. Membrane electrode assemblies were prepared in unconventional way, using magnetron sputtering for thin-film catalyst deposition onto high-surface porous structures. 50 nm of Ir ( $113 \text{ ug.cm}^{-2}$ ) were sputtered on TiC based support sublayer, printed on anode side of the membrane and 3nm of Pt ( $6.5 \text{ ug.cm}^{-2}$ ) were deposited on nanostructured etched nitrogenated carbon ( $\text{CN}_x$ ), carried on gas diffusion layer on cathode. High efficiencies and specific currents were obtained, considering the low content of noble metals.

**Index Terms** – proton exchange membrane water electrolyzer, high-surface support sublayer, low-loading catalyst

### I. INTRODUCTION

Proton exchange membrane water electrolyzers (PEMWE) are the backbone of near-future hydrogen economy. By fast-response electricity to hydrogen conversion, the PEMWEs will not only stabilize the electrical grid based on renewable sources of energy but also provide high-purity hydrogen for variety of fuel cell powered devices, ranging from consumer electronics to vehicles. Wider commercialization of PEMWE technology is however hindered by high prices of noble metals which are necessary for catalyzing the redox reactions within the cell. Namely, platinum for hydrogen evolution reaction, running on cathode, and iridium for oxygen evolution reaction on anode. Possible way of how to lower the loading of Pt and Ir is by using conductive high-surface nanostructures as catalyst supports in conjunction with thin-film catalyst deposition.

In the following text, we present unique preparation technique of membrane electron assembly (MEA). Noble metal catalysts are magnetron sputtered in very low loadings onto the surface of porous sublayers (located on gas diffusion layer or

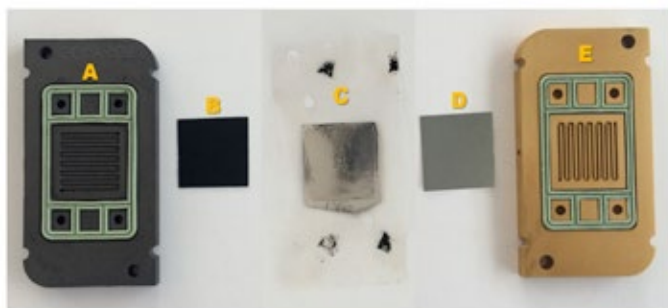
directly on membrane), forming so to say localized three-phase boundary. Corrosion resistant TiC-based sublayer is used as a support material on anode, whereas nanostructured etched nitrogenated carbon ( $\text{CN}_x$ ) serves the same role on cathode. By using this configuration, we were able to significantly decrease the amount of noble metals (to thickness of just tens of nanometers), while keeping the performance reasonably high.

### II. EXPERIMENTAL

Ink for anode high-surface sublayer consisted of TiC nanoparticles, Nafion<sup>®</sup> solution (5 wt%), isopropanol and deionized water ( $1 \text{ ml.g}^{-1}$  and  $0.1 \text{ ml.g}^{-1}$  in respect to TiC). It was ultrasonically stirred for 1 h and afterwards spread on PTFE transient foil and let dry. Subsequently, the support material was hot-pressed ( $120 \text{ }^\circ\text{C}$ ,  $150 \text{ kg.cm}^{-2}$ , 150 s) from transient foil onto anode side of Nafion<sup>®</sup> NE1035 membrane. The loading of TiC-based support sublayer was  $0.2 \text{ mg.cm}^{-2}$ . Afterwards, 50 nm of Ir catalyst were magnetron sputtered in Ar atmosphere directly on top of the membrane with TiC-based sublayer. More info on anode catalyst preparation process can be found in [1]. Sintered powder porous Ti sheet, coated with Pt was used as a current collector.

A modified Sigracet<sup>®</sup> GDL 29BC served as a catalyst carrier on the cathode side of the cell. In order to create the high-surface etched structure on top of it, first 200 nm of nitrogenated carbon were sputtered (from C target reactively in  $\text{N}_2$  atmosphere), after that additional 10 nm of  $\text{CeO}_2$  were sputtered (from ceramic  $\text{CeO}_2$  target reactively in  $\text{Ar}:\text{O}_2$ , 400:1). The  $\text{CeO}_2$  sputtering causes simultaneous etching of  $\text{CN}_x$  layer and deposition of  $\text{CeO}_2$ , leading to creation of highly porous noodle-like structures. This process is thoroughly described in [2,3]. Finally, on top of this complex system, 3 nm of Pt in Ar atmosphere were sputtered.

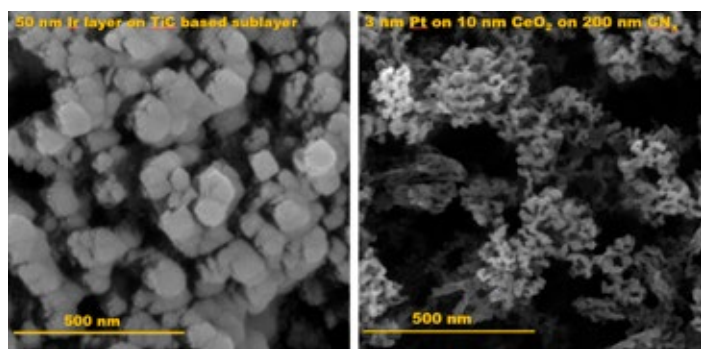
The active area of cell was  $4.62 \text{ cm}^2$  (Fig. 1).



**Fig. 1** Testing cell: graphite end plate (A), cathode catalyst on Sigracet® GDL 29BC (B), anode catalyst on Nafion® NE1035 membrane (C), Ti anode current collector (D), TiN coated Ti anode end plate (E)

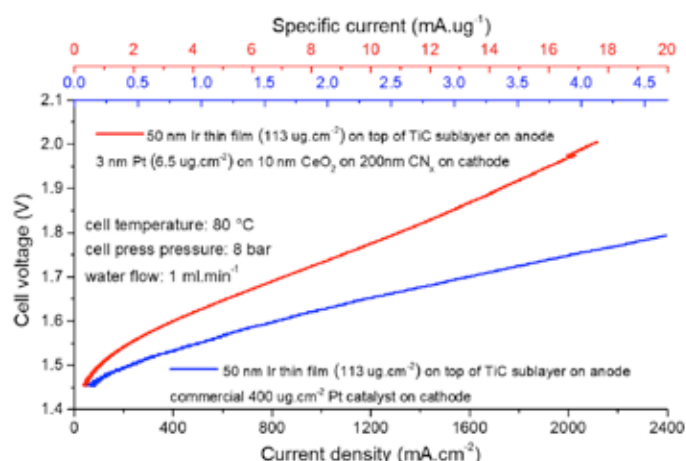
### III. RESULTS

Scanning electron microscope (SEM) micrographs of anode and cathode catalysts can be seen in Fig. 2.



**Fig. 2** SEM micrographs of anode (left) and cathode catalysts (right)

After assembling the cell, 24 h break-in procedure followed, consisting of repetitive switching of constant voltage from 1.6 V to 1.7 V. The **IV curve** obtained after break-in can be seen in Fig.3. compared to **reference curve** (with commercial cathode).



**Fig. 3** Performance of catalyst in PEMWE cell

Note that upper horizontal axis displays the current per loading of catalyst. Considering bulk density of Pt and Ir, the combined loading of noble metals (50 nm Ir + 3 nm Pt) is just under 120 ug.cm<sup>-2</sup> (113 ug.cm<sup>-2</sup> of Ir + 6.5 ug.cm<sup>-2</sup> of Pt) Specific current of tested PEMWE cell (mA.ug<sup>-1</sup>) is therefore 2-3 times higher than in high-loading commercial counterparts [4].

Regarding durability, The PEMWE cell was furthermore tested for 5 consecutive days (in dynamic as well as in static operation) with no notable performance deterioration.

### IV. CONCLUSION

Magnetron sputtering proves to be suitable method for thin-film deposition of anode as well as cathode catalysts for PEMWE. It enables precise control of noble metal loading and distribution.

TiC nanoparticles are suitable substitution for high-surface carbon black on the anode side of the cell, capable of withstanding aggressive corrosive environment of low pH and high potentials.

Nanostructured etched nitrogenated carbon is a unique alternative for conventional carbon black, particularly when using thin-film low-loading catalyst.

Tested set-up of thin-film supported anode and cathode catalysts with combined loading of just 120 ug.cm<sup>-2</sup> yields remarkable values of specific current.

Herein described approach of thin-film low-loading catalyst deposition might be relevant when noble metal reduction is the topmost priority.

### ACKNOWLEDGMENT

This project was supported by Charles University Grant Agency (GAUK No. 1016217) and by CERIC consortium.

### REFERENCES

- [1] Kúš, P., Ostroverkh A., Ševčíková, K., Khalakhan, I., Fiala, R., Skála, T., Tsud, N., Matolin, V., Magnetron sputtered Ir thin film on TiC-based support sublayer as low-loading anode catalyst for proton exchange membrane water electrolysis, International Journal of Hydrogen Energy, Volume 41, Issue 34, 2016, Pages 15124-15132
  - [2] Dubau, M., Lavková, J., Khalakhan, I., Haviar, S., Potin, V., Matolin, V., Matolinová, I., Preparation of Magnetron Sputtered Thin Cerium Oxide Films with a Large Surface on Silicon Substrates Using Carbonaceous Interlayers, ACS Applied Materials and Interfaces, Volume 6, Issue 2, 2014, Pages 1213-1218
  - [3] Haviar, S., Dubau, M., Lavková, J., Khalakhan, I., Potin, V., Matolin, V., Matolinová, I., Investigation of Growth Mechanism of Thin Sputtered Cerium Oxide Films on Carbon Substrates, Science of Advanced Materials, Volume 6, Issue 6, 2014, Pages 1278-1285
- Carmo, M., Fritz, D. L., Merge, J., Stolten, D., A comprehensive review on PEM water electrolysis, International Journal of Hydrogen Energy, Volume 38, 2013, Pages 4901-4934

## HIGH PERFORMANCE PEM ELECTROLYSER FOR COST-EFFECTIVE GRID BALANCING APPLICATIONS - HPEM2GAS

A.S. Aricò\*, S. Siracusano\*, V. Baglio\*, N. Van Dijk\*\* and L. Merlo\*\*\*

\* CNR-ITAE, Via Salita S. Lucia sopra Contesse 5 – 98126 Messina, (Italy)

\*\* ITM Power (Research) Ltd, Europa Link, S9 1XU - Sheffield, UK, (UK)

\*\*\* Solvay Specialty Polymers Italy SpA, viale Lombardia, 20 20021 – Bollate, (Italy)

**Abstract** - The HPEM2GAS project is addressing research and development in the field of PEM water electrolysis. Membrane-electrode assemblies (MEAs) designed for polymer electrolyte membrane (PEM) water electrolysis, based on Aquivion®, perfluorosulfonic acid (PFSA) membrane, with various cathode and anode noble metal loadings, were investigated in terms of both performance and durability. Utilizing a nanosized Ir-Ru oxide solid solution anode catalyst and a supported Pt/C cathode catalyst, in combination with the Aquivion® membrane, gave excellent electrolysis performances exceeding  $3 \text{ A} \cdot \text{cm}^{-2}$  at 1.8 V terminal cell voltage (~80 % efficiency) at 80 °C in the presence of a noble metal loading of  $1.4 \text{ mg} \cdot \text{cm}^{-2}$ . A very small loss of efficiency, corresponding to 30 mV voltage increase, was recorded at  $3 \text{ A} \cdot \text{cm}^{-2}$  using a total noble metal catalyst loading of less than  $0.5 \text{ mg} \cdot \text{cm}^{-2}$ . Steady-state durability tests, carried out for >1000 h at  $3 \text{ A} \cdot \text{cm}^{-2}$ , showed excellent stability for the MEA with low noble metal catalyst loading (cell voltage increase ~5-10  $\mu\text{V/h}$ ). Therefore, operation at very high current densities is possible in the presence of low catalyst loading and a reduction of capital costs may be achieved without compromising significantly the stack durability.

**Index Terms** – Electro-catalysts, Hydrogen, Low noble metal loading, Polymer Electrolyte Membrane Water Electrolysis.

### I. INTRODUCTION

A significant problem that a future energy system must address is the excess of renewable energy that cannot be transferred to the grid when demand is low and thus must be curtailed by the grid operators. The increasing production of renewable energy can contribute to reduce the carbon footprint of the electricity grid. However, the intermittent nature of renewable power sources can cause relevant energy management issues as the proportion of energy generation by renewables increases. A proper solution is to convert the intermittent surplus of electrical energy into hydrogen and storing the energy chemically. Electrolysis of water using renewable energy sources is one of the most promising

chemical processes to produce “green” hydrogen economically with the high purity needed for fuel cell based electric vehicles [1].

Three main technologies are currently used in the electrolysis sector, namely: alkaline electrolyzers, solid oxide electrolyzers and polymer electrolyte membrane (PEM) electrolyzers.

The main features of PEM electrolysis are the high operating current densities, high efficiency at low temperature, excellent dynamic behaviour, rapid start-up/response and high stability during duty cycles [1]. These characteristics make polymer exchange membrane water electrolysis (PEMWE) ideal for either grid stabilization or direct coupling with renewable energy sources.

In the present work, we demonstrate that electrolysis operation at very high current densities is possible in the presence of low catalyst loading [1-3]. Thus, a reduction of capital costs may be achieved without compromising significantly the stack durability [1].

### II. EXPERIMENTAL

Electrolysis cells were manufactured using an Ir-Ru oxide oxygen evolution catalyst and a Pt/C hydrogen evolution catalyst [1,3]. A chemical stabilised Aquivion® SSC ionomer with 90  $\mu\text{m}$  thickness and an equivalent weight (EW) of 1000 g/eq supplied by Solvay Specialty Polymers [1] was used as membrane. A catalyst-coated membrane methodology was adopted to prepare the membrane-electrodes assembly (MEA).

The PEM electrolyser performance was evaluated at different temperatures (30-90 °C) and under ambient pressure. 18.2 M $\Omega$ ·cm deionized water (Milli-Q Integral, Millipore) was supplied to the anode compartment. The recirculating water was maintained at the same temperature of the cell. Electrochemical measurements, including polarization curves, electrochemical impedance spectroscopy (EIS), galvanostatic durability tests, were made using an Autolab PGSTAT 302

Copyright © 2017



Potentiostat/Galvanostat equipped with a current booster (Metrohm) and FRA (frequency response analyser). These were complemented by an ex-situ physicochemical analysis.

The main MEA characteristics are listed in Table I.

TABLE I  
CATALYST LOADING AND COMPOSITION IN THE INVESTIGATED MEAS

Membrane	Anode (IrRuOx) mg·cm <sup>-2</sup>	Cathode Pt mg·cm <sup>-2</sup>	Total noble metal loading mg·cm <sup>-2</sup>	MEA type
Aquivion® SSC	1.27	0.5	1.77	High loading
Aquivion® SSC	1.27	0.1	1.37	Intermediate loading
Aquivion® SSC	0.34	0.1	0.44	Low loading

### III. RESULTS AND DISCUSSION

By using advanced electro-catalysts and MEA fabrication procedures, it was possible to operate the electrolysis cell at a current density of 3 A·cm<sup>-2</sup> whereas the total noble metal loading was decreased from 1.77 to 0.44 mg·cm<sup>-2</sup> MEA. A very high conversion efficiency (>80%) was achieved at 3 A·cm<sup>-2</sup> with low catalyst loading [3]. This was made possible in our context by the use of improved electro-catalysts and short-side chain perfluorosulfonic ionomer enhancing the reaction rate at the electrode-electrolyte interface [1-3].

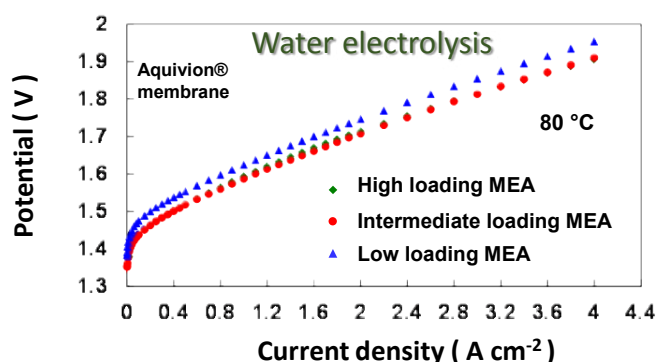


Fig. 1. Water electrolysis polarization behaviour for different catalyst loading-based MEAs at 80 °C

Good stability of these systems for operation at 3 A·cm<sup>-2</sup> is recorded using durability tests of 1000 h [3] whereas most literature reports deal with endurance tests up to 1 A·cm<sup>-2</sup>.

Assessment of stability characteristics at high current densities is of fundamental interest to evaluate the reliability of such systems for real-life operation [1,3].

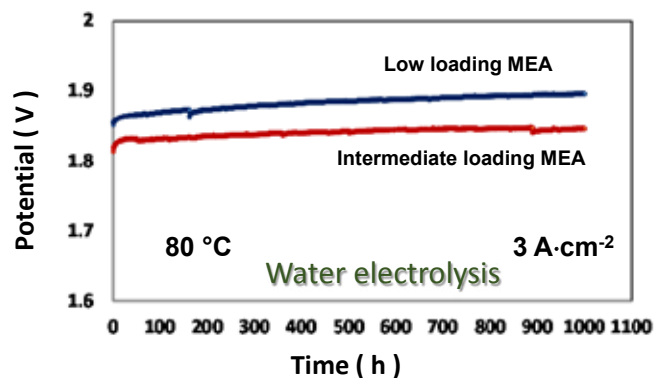


Fig. 2 Durability tests at 3 A cm<sup>-2</sup> and 80 °C for two different catalyst loading-based MEAs in the water electrolysis cell

To allow for a proper comparison of the results achieved with different systems, a new approach to express the stability factor for assessing the durability of the electrolysis cell was identified, as reported in the following [1]:

Stability Factor (SF) = 1 / (Voltage increase rate · Initial cell overvoltage) = h·V<sup>-2</sup>

### IV. CONCLUSION

The degradation mechanism for PEM electrolysis MEAs has been investigated using both ex-situ characterizations and in-situ methods. We have identified that a relevant factor influencing the degradation rate in the PEM water electrolysis is associated to a change of the Lewis acidity characteristics for the Ir and Ru cations.

### ACKNOWLEDGMENT

The research leading to these results has received funding from the European Community's H2020 Programme. Work performed was supported by the Fuel Cells and Hydrogen Joint Undertaking in the context of project HPEM2GAS G.A. 700008.

### REFERENCES

- [1] Siracusano, S., Baglio, V., Van Dijk, N., Merlo, L., Aricò, A.S. Enhanced performance and durability of low catalyst loading PEM water electrolyser based on a short-side chain perfluorosulfonic ionomer, Applied Energy, Volume 192, 2017 Pages 477-489.
- [2] Siracusano S., Baglio V., Grigoriev S.A., Merlo L., Fateev V.N., Aricò A.S. The influence of iridium chemical oxidation state on the performance and durability of oxygen evolution catalysts in PEM electrolysis, Journal of Power Sources Volume 366, 2017 pp. 105-114.
- [3] Siracusano S., Hodnik N., Jovanovic P., Ruiz-Zepeda F., Šala M., Baglio V., Aricò A. S. New insights into the stability of a high performance nanostructured catalyst for sustainable water electrolysis Nano Energy, doi.org/10.1016/j.nanoen.2017.09.014.



## OPTIMIZING HYDROGEN PRODUCTION IN A MICROBIAL ELECTROLYSER USING A WEAK ACID SOLUTION AS CATHOLYTE

E. Roubaud\*, R. Lacroix\*\*, S. Da Silva\*\*, A. Bergel\*, R.  
Basséguy\* and B. Erable\*

\*Laboratoire de Génie Chimique, Université de Toulouse, CNRS,  
INPT, UPS, Toulouse, (France)

\*\*6T-MIC Ingénieries, 9 rue du développement – ZI de Vic,  
31320 Castanet-Tolosan, (France)

**Abstract** – This paper focuses on optimizing hydrogen production in microbial electrolysis cells (MEC) through the use of electrocatalytic weak acid solutions. Current-potential curves were obtained with three different weak acids: phosphate, formate and carbonate solutions. Carbonate was selected for additional tests since it is one of the best catalysts in terms of performance and the most eco-friendly. Varying the concentration of the carbonate solution showed that working with a 0.2 M solution would reduce the hydrogen production overpotential by 420 mV at a current density of 10 A/m<sup>2</sup>, in comparison to raw domestic wastewater. These results enable a reduction of the energy consumption of hydrogen-producing MECs by 30% (based on an applied voltage of 1.5 V).

**Index Terms** – Hydrogen, microbial electrolysis cell, wastewater treatment, weak acid solutions as electrolyte

### I. INTRODUCTION

Microbial electrolysis applied to wastewater treatment is a process allowing hydrogen to be produced at low cost [1]. Typically, a microbial electrolysis cell (MEC) generates hydrogen in the voltage range of 0.5 V to 1.5 V while a conventional alkaline electrolyser needs an operating voltage of 2.0 to 3.0 V. The electrolysis voltage required to generate hydrogen in an MEC is lowered through the use of an electroactive microbial biofilm capable of oxidizing the organic matter of wastewater on the anode (instead of water oxidation). Several areas of technological improvements are currently being explored in order to (i) reduce the internal resistance of MECs, (ii) improve the kinetics of hydrogen production and its purity on low cost electrode materials, and (iii) maximize the rate of oxidation of the polluting load of the wastewater.

In this exciting field, the work presented here focused on optimizing hydrogen production through the use of electrocatalytic solutions as catholytes in order to boost the kinetics of hydrogen evolution on stainless steel electrodes. It was demonstrated in 2010 that aqueous

electrolytes containing weak acids, such as phosphate solution for example, catalysed the reduction of water on stainless steel cathodes highly efficiently [2]. We tried to optimize the nature of the weak acid and its concentration so as to obtain the best possible cathode kinetics for wastewater treatment applications.

### II. MATERIAL AND METHOD

Current-potential curves were obtained from linear voltammetries performed between -0.5 V/SCE and -1.5 V/SCE on stainless steel electrodes immersed in various weak acids and potassium chloride (KCl) solutions. Experiments were carried in a 150 mL three-electrode electrochemical cell using a potentiostat (VSP, Biologic) controlled by the EC-Lab software. The working electrode was a 1.5x2 cm<sup>2</sup> AISI 316L plate ground with abrasive discs (P800, P1200, P2400), the reference electrode was a saturated calomel electrode (SCE) and the counter-electrode was a 1.5x2 cm<sup>2</sup> DSA plate. In some cases, the pH was adjusted to 8.0 to be compatible with the pH of the wastewater.

### III. RESULTS AND DISCUSSION

Experiments showed that the current-potential curves obtained with the weak acid solutions were at less negative potentials than the curve obtained with a KCl solution of similar conductivity. These results confirmed the catalytic effect of weak acids on the water reduction kinetics. When comparing the three weak acids: formate, carbonate and phosphate solutions, results showed significantly better performances in terms of water reduction kinetics with carbonate and phosphate electrolytes than with formate (Fig. 1).

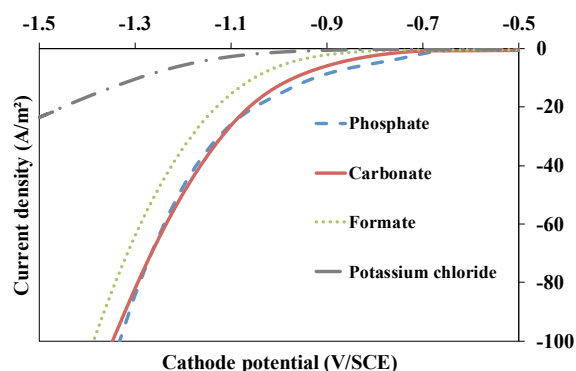


Fig. 1. Current-potential curves obtained in 150 mM weak acid solutions + 100 mM KCl solutions, scan rate 10 mV/s, pH=8.0

To complete the optimization of the cathodic reaction, carbonate was selected for technical and environmental reasons since phosphate is responsible for dystrophication and eutrophication phenomena and because working with a carbonate solution could be a way of storing CO<sub>2</sub> in dissolved form. Additional tests were then performed with carbonate electrolyte at increasing concentrations to estimate the overpotential gain it could offer compared to a classical reduction occurring in real domestic wastewater (Fig. 2).

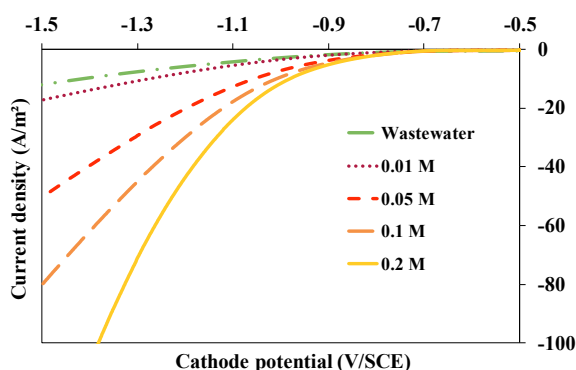


Fig. 2. Current-potential curves obtained in carbonate solutions at increasing concentrations and raw domestic wastewater, scan rate 10 mV/s, pH=8.0

Fig.2 shows that, at a given potential, the current density increases with the carbonate concentration. To our knowledge, the best performances found in the literature in terms of current density obtained with MECs working with real wastewater are around 10 A/m<sup>2</sup> [3]. Working with a carbonate solution concentrated at 0.2 M as the catholyte would reduce the stainless steel cathode overpotential by 420 mV at a current density of 10 A/m<sup>2</sup>, in comparison with the use of wastewater as the catholyte.

Current-potential curves were obtained with 1M carbonate solution, the pH of which was adjusted to various values between 7.0 and 12 (Fig. 3).

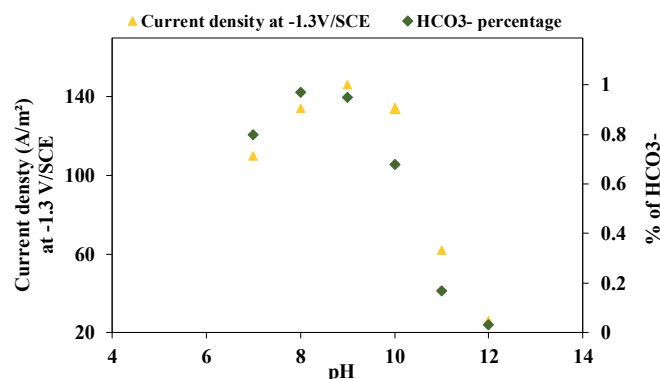


Fig. 3. Relation between the percentage of HCO<sub>3</sub><sup>-</sup> species and the current density obtained at -1.3 V/SCE depending on the pH of a 1M carbonate solution.

Comparing the cathodic current density obtained at -1.3V/SCE and the proportion of HCO<sub>3</sub><sup>-</sup> species at each pH unit showed a direct correlation between H<sub>2</sub> production performances and the quantity of HCO<sub>3</sub><sup>-</sup> (Figure 3). This means that the HCO<sub>3</sub><sup>-</sup> ions are responsible for the catalytic effect of carbonate.

Experiments are now being conducted with various grades of stainless steel containing different nickel proportions, nickel alloys and graphite in order to select the most efficient material for the cathode.

#### IV. CONCLUSION

Working with a carbonate solution as the catholyte in an MEC allows the cathode overpotential, and consequently the global cell voltage, to be significantly reduced. Our future work will develop and experimentally evaluate a membrane-integrated MEC design, separating wastewater anolyte and carbonate catholyte. Modelling work with the Comsol® software will allow the reactor geometry to be optimized to reduce the internal resistance of the MEC as far as possible.

#### ACKNOWLEDGEMENT

This work was funded by the French ANR within the framework of the WE-MET project (ERANETMED 2015 European call).

#### REFERENCES

- [1] H. Liu, S. Grot, and B. E. Logan, "Electrochemically assisted microbial production of hydrogen from acetate," *Environ. Sci. Technol.*, vol. 39, no. 11, pp. 4317–4320, 2005.
- [2] L. De Silva Muñoz, A. Bergel, D. Féron, and R. Basséguy, "Hydrogen production by electrolysis of a phosphate solution on a stainless steel cathode," *Int. J. Hydrogen Energy*, vol. 35, pp. 8561–8568, 2010.
- [3] J. Yu, Y. Park, B. Kim, and T. Lee, "Power densities and microbial communities of brewery wastewater-fed microbial fuel cells according to the initial substrates," *Bioprocess Biosyst. Eng.*, 2015.

# METAL FOAM COOLING CHANNELS IN POLYMER-ELECTROLYTE FUEL CELL SYSTEMS

Anthony D. Santamaria\*, Jingru Zhang

Department of Mechanical Engineering  
 Western New England University  
 Springfield, MA 01119

**Abstract** - Low temperature polymer-electrolyte fuel cells are receiving increased attention due to new vehicle models being released by major automotive OEMs such as Toyota, Honda, and Hyundai. Boasting increased power density, reduced system volume, extended vehicle range, and reduced cost these next generation FCVs will further this technology's market penetration. There remains, however, many areas where advanced materials may be explored to improve PEFC performance. Metal foams which are known for high surface area and low density have been explored for PEFC usage, however, their adoption remains to be realized. This work analyzes the use of metal foam filled cooling channels inside a cell stack. The study explores the use of an air based cooling fluid since the high surface area of the foam compensates for the low heat capacity of air. The high foam porosity and low density & viscosity of air reduces the parasitic pressure drop which means higher flow rates can be achieved.

## I. INTRODUCTION

Maintaining consistent temperature profiles in PEFCs (polymer-electrolyte fuel cell) is critical to system performance, efficiency, and lifetimes. Traditional designs implement coolant channels embedded between bipolar plates to remove excess heat [1]. These channels may circulate fluid or in some cases implement air cooled methods. As designers seek to increase PEFC power density, microchannel heat sinks have been investigated for their minimal size, however; may suffer increased parasitic pumping losses [2, 3]. In order to increase the thermal performance of microscale PEFC cooling channels this work examines the impact of embedding metal foam into the channels. Metal foams with low density and high surface area may

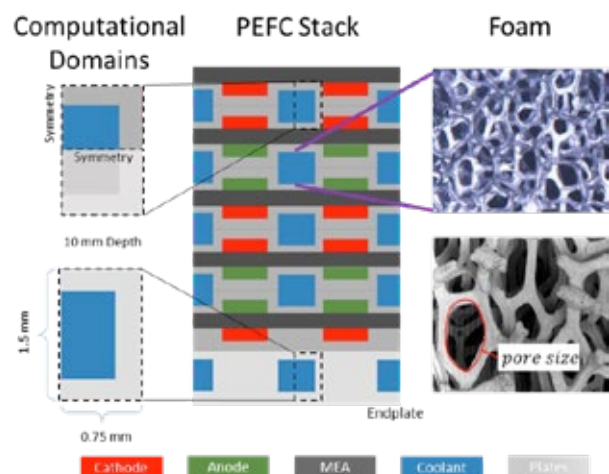


Fig. 1. Overview of PEFC design & computational domain including coolant channel locations. SEM images highlight foam placement and structure.

increase effective thermal conductivity and reduce flow rates. Combining experimental and numerical methods, an analysis of foam embedded micro cooling channels was undertaken to test their feasibility.

## II. METHODS

### A. Experimental

A test setup was designed using a 1.5x1.5 mm channel (5.5 cm long) filled with nickel metal foam from Sumitomo Electric Industries, Table 1 outlines the samples studied. While this results in a hydraulic diameter slightly larger than "microscale" it is a good starting place for model validation. Pressure drop data was collected for a range of flow rates and the

\*Corresponding author e-mail: anthony.santamaria@wne.edu

properties of the metal foam such as porosity, permeability, contact area, inertial coefficient.

**Table 1.** Characteristic of the metal foam samples

Sample Grade	PPI	$d_p$ (mm)	Surface area per volume	Porosity ( $\epsilon$ )
G3	17~23	0.65	850	0.961
G4	27~33	0.45	1250	0.945
G5	37~43	0.35	1850	0.941

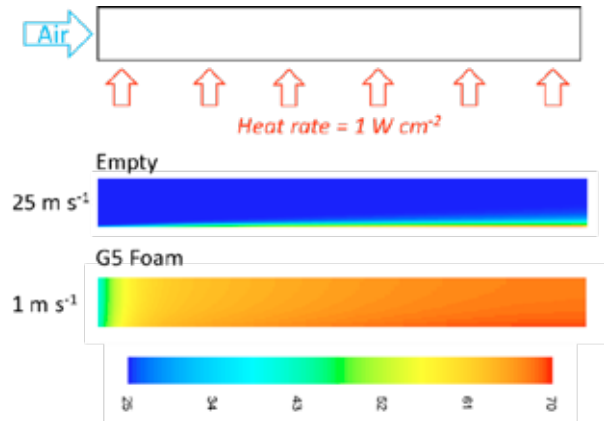
### B. Numerical

ANSYS was used to solve incompressible and steady state fluid conservation equations including mass, energy, and momentum. The momentum equation was modified using Darcy and Brinkman equations [5]. Effective thermal conductivity as a function of temperature for the foam was calculated using an analytical equation [6]. Dry air with an inlet temp of 25 °C was utilized as the coolant. The model was used to calculate the air velocity required to maintain a maximum temperature of 70 °C for a 1 W cm<sup>-2</sup> heat flux which is typical for PEFC operation. Modeling results were validated using experimental results from previous work [7].

### III. RESULTS

Results showed that metal foam enhanced the empty channels heat transfer effectiveness and required lower superficial velocities to do so. Numerically obtained temperature distributions show that the foam conducts heat and evenly transfers it to the air where as empty channels result in large temperature gradients along their cross section. Overall the G5 foam filled channel required approximately 1/25 the air flow rate of the empty channel to maintain a maximum temperature of 70 °C at the given heat flux. Additionally, the higher effective thermal conductivity due to the foam better distributes temperature throughout the channel compared to the empty. This may prevent cold spots along PEFC reaction channels especially at positions farthest from the heat producing reaction sites such as channel corners where liquid condensation can occur and cause flooding. The pressure drop of the 1 m s<sup>-1</sup> G5 case was lower than that measured of the 25 m s<sup>-1</sup> empty channel which means parasitic pumping power may also be conserved.

\*Corresponding author e-mail: anthony.santamaria@wne.edu



**Fig. 2.** Numerical results showing temperature gradient differences between empty and foam embedded cooling channels maintaining a max temp of 70 °C. The G5 foam required 1/25 the air flow rate.

### IV. CONCLUSIONS

Early results from this work show that metal foam embedded in micro coolant channels may greatly improve thermal performance. PEFC systems may benefit significantly from designs that implement similar foams. Further work will expand on these results to full scale in-situ studies.

### REFERENCES

- [1] Brambilla, M., Mazzucchelli, G., "Fuel cell with cooling system based on direct injection of liquid water", US Patent 6,835,477, assigned to Nuvera Fuel Cells Europe S.r.l., 2004.
- [2] Zhang, J., Lin, P. T., Jaluria, Y., "Design and Optimization of Multiple Microchannel Heat Transfer Systems", Journal of Thermal Science and Engineering Applications. 2013; 6(1): 011004-011004-10. doi: 10.1115/1.4024706.
- [3] Ramos-Alvarado, B., Li, P., Liu, H., Hernandez-Guerrero, A., "CFD study of liquid-cooled heat sinks with microchannel flow field configurations for electronics, fuel cells, and concentrated solar cells", Applied Thermal Engineering 31, 2494-2507, 2011
- [5] DuPlessis, P., Montillet, A., Comiti, J., and Legrand, J., "Pressure Drop Prediction for Flow Through High Porosity Metallic Foams," Chem. Eng. Sci., 49, 1994, pp. 3545–3553.
- [6] Bhattacharya, A., Calmidi, V.V., Mahajan, R.L., "Thermophysical properties of high porosity metal foams," Int. J. Heat Mass Transfer, 2002, vol. 45, pp. 1017-1031.
- [7] Calmidi, V. V., and Mahajan, R. L., "Forced Convection in High Porosity Metal Foams", J. Heat Transfer 122(3), 557-565, 2000, doi:10.1115/1.1287793

# NUMERICAL ANALYSIS OF HT STEAM ELECTROLYSIS WITH AN SOEC TO SEPARATE GAS CONVERSION IMPEDANCE FROM OVERALL IMPEDANCE FOR PROPER ESTIMATION OF GENUINE CELL PERFORMANCE

Y. Tanaka\*, M.P. Hoerlein\*\*, and G. Schiller\*\*

\*National Institute of Advanced Industrial Science and Technology (AIST),  
Tsukuba Central 2, Umezono 1-1-1, Tsukuba, Ibaraki 305-8568, (Japan)

\*\*German Aerospace Center (DLR), Institute of Engineering  
Thermodynamics, Pfaffenwaldring 38-40, 70569 Stuttgart, (Germany)

**Abstract** - It is important to understand a genuine cell performance or overvoltages for cell-and-stack development for high temperature steam electrolysis with solid oxide cells (SOEC) to produce hydrogen. A quasi-1D simulation model was developed to estimate total area-specific resistance corresponding to overvoltages ( $R_{tot}$ ) by separating gas conversion impedance (GCI), which originates from gas composition change in gas channels during electrochemical impedance measurement. GCI and  $R_{tot}$  for a square cell were estimated as  $0.012\text{--}0.011 \Omega \text{ cm}^2$  and  $0.209\text{--}0.216 \Omega \text{ cm}^2$ , respectively, at  $0.0\text{--}1.0 \text{ A cm}^{-2}$ ,  $800^\circ\text{C}$ , and relatively high flow rates. Even though GCI is small compared to  $R_{tot}$ , ignoring the GCI will result in higher simulation errors at current densities  $\geq 0.5 \text{ A cm}^{-2}$ . Simulation results attained  $\pm 0.3 \%$  precision against measured cell voltages using a  $16\text{-cm}^2$  square cell at  $750\text{--}850^\circ\text{C}$ . Therefore, the developed simulation method was found to be accurate and useful for estimating GCI and  $R_{tot}$  for SOEC development.

**Index Terms** - electrochemical impedance interpretation, Gas conversion impedance estimation, SOEC, steam electrolysis for  $\text{H}_2$  production

## I. INTRODUCTION

The more renewable power is employed, the more excess intermittent power produced from photovoltaic and wind power plants destabilizes power grids [1]. The excess power can be converted to chemical energy such as hydrogen with water or steam electrolysis. In particular, steam electrolysis with a solid oxide cell (SOEC) at  $700\text{--}900^\circ\text{C}$  will give high energy efficiency above 90% in higher heating value base.

Electrochemical impedance spectroscopy is used as a powerful tool to estimate overvoltages (ohmic, activation, and concentration). Considering analogy from solid oxide fuel cells (SOFC) at practical size, however, the spectra will contain gas

conversion impedance (GCI) at practical electrolysis conditions, or reduced-flow-rate to electrolyze most of steam (e.g. 80-90 %). Takano et al. reported that GCI in SOFC arise from gas composition change in impedance measurement where ac current is superimposed [2]. GCI changed with fuel utilizations.

Therefore, we presumed that GCI will also appear in steam electrolysis that is reverse operation of SOFC. We estimated GCI and total overvoltage ( $R_{tot}$ ) using a quasi-1D simulation model for an experimentally used  $4 \text{ cm} \times 4 \text{ cm}$  cell. We will discuss GCI consideration to estimate  $R_{tot}$  from impedance spectra by comparing simulation results and experimental ones.

## II. SIMULATION METHOD

As already published in detail elsewhere [3], a  $4 \text{ cm} \times 4 \text{ cm}$  cell was modeled where  $\text{H}_2\text{O-H}_2$  and  $\text{O}_2\text{-N}_2$  are supplied to cathode (fuel-electrode) and anode (air-electrode) in co-flow configuration assuming isotherm in the whole cell. These gases flow to x-direction which was divided to 100 segments. Equivalent circuit is considered at each segment that consists of a R-RC-RC-E circuit, as in Fig. 1, where each resistance accounts for ohmic, activation, and concentration voltages. Total resistance is defined as  $R_{tot}$  ( $= R_{ohm} + R_{act} + R_{dif}$ ) corresponding to total overvoltages representing cell performance.

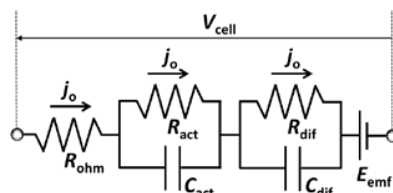


Fig. 1. Equivalent circuit used for simulation

Copyright © 2017



Cell voltage,  $V_{\text{cell}}$  is assumed to be common at every segment since metallic current collectors were used in experiment. Therefore, we obtain the following equation;

$$j_o = \frac{V_{\text{cell}} - E_{\text{emf}}}{R_{\text{ohm}} + R_{\text{act}} + R_{\text{dif}}} = \frac{V_{\text{cell}} - E_{\text{emf}}}{R_{\text{tot}}}$$

where  $j_o$  is local current density,  $E_{\text{emf}}$  is electromotive force calculated from partial pressure of steam, hydrogen, and oxygen. Gas pressure is presumed to be 101.325 kPa and pressure drop in the cell is ignored. Advection-convection equations were solved for steam, hydrogen, and oxygen.

Overall real-part impedance (ORI) should consist of  $R_{\text{tot}}$  and GCI as in SOFC and ORI is equal to differential slope of a voltage-current-density curve ( $\partial V / \partial J$ ). Therefore, GCI could be obtained by  $V$ - $J$  curve simulation and  $\text{GCI} = \partial V / \partial J - R_{\text{tot}}$  where  $R_{\text{tot}}$  is presumed from measured impedance spectra. Selection of  $R_{\text{tot}}$  gave only small deviation of GCI only by 0.0010  $\Omega \text{ cm}^2$  at 800°C and  $R_{\text{tot}} = 0.200$ -0.300  $\Omega \text{ cm}^2$ . Then,  $R_{\text{tot}}$  was determined by ORI – GCI.

### III. RESULTS AND DISCUSSION

#### A. GCI estimation and its validation

Gas conversion impedances (GCI) were calculated from  $V$ - $J$  curve simulations assuming total area-specific resistance  $R_{\text{tot}} = 0.200 \Omega \text{ cm}^2$  at 800°C. As summarized in Table I, GCI was estimated as 0.0122-0.0109  $\Omega \text{ cm}^2$  at  $J = 0.00$ -1.00  $\text{A cm}^{-2}$ . It was also found that these GCI accounts for a quarter of the lower frequency arch in an impedance spectrum obtained experimentally. The rest 3/4 can be attributed to concentration overvoltage in the 1 mm-thick Ni-8YSZ cathode, considering the used ac frequency range down to 0.5 mHz.

Then, the total area-specific resistance  $R_{\text{tot}}$  was determined and cell voltages were simulated at 0-1.0  $\text{A cm}^{-2}$ . As exhibited in Table I,  $R_{\text{tot}} = 0.209$ -0.216  $\Omega \text{ cm}^2$  was obtained. Simulated cell voltage agreed by  $\pm 0.21 \%$  with experimentally measured ones. Another simulation also elucidated that ignoring even such small GCI results in large errors in cell voltage simulation; e.g. 0.6% or higher at  $J \geq 0.5 \text{ A cm}^{-2}$ . Therefore, the developed method is valid to evaluate GCI and  $R_{\text{tot}}$ .

TABLE I

ESTIMATION OF GCI, TOTAL AREA-SPECIFIC RESISTANCE  $R_{\text{TOT}}$ , CELL VOLTAGE

$J (\text{A/cm}^2)$	GCI ( $\Omega \text{ cm}^2$ )	$R_{\text{tot}}$ ( $\Omega \text{ cm}^2$ )	Simulated cell voltage (V)	Experimental cell voltage (V)
0.00	0.0122	0.2094	0.8716	0.872
0.06	0.0121	0.2135	0.8855	0.885
0.12	0.0120	0.2072	0.8983	0.899
0.25	0.0118	0.2090	0.9261	0.927
0.50	0.0115	0.2141	0.9838	0.984
1.00	0.0109	0.2163	1.0983	1.096

#### B. $V$ - $J$ curve simulation versus measured curve

Using the developed method,  $V$ - $J$  curves were simulated at 750, 800, and 850°C using fixed  $R_{\text{tot}} = 0.364$ , 0.215, and 0.159

$\Omega \text{ cm}^2$ , respectively. The fixation of  $R_{\text{tot}}$  leads to easier cell voltage simulation. As shown in Fig. 2, simulated cell voltages accorded well with experimentally measured ones. Statistical analyses clarified that simulation errors to the measured ones were  $\pm 0.42 \%$  at 750°C,  $\pm 0.26 \%$  at 800°C, and  $\pm 0.22 \%$  at 850°C at 95 % level of confidence, giving high precision. The measured cell voltages at 750°C deviated more than the rest, so that the simulation error seems larger at the temperature.

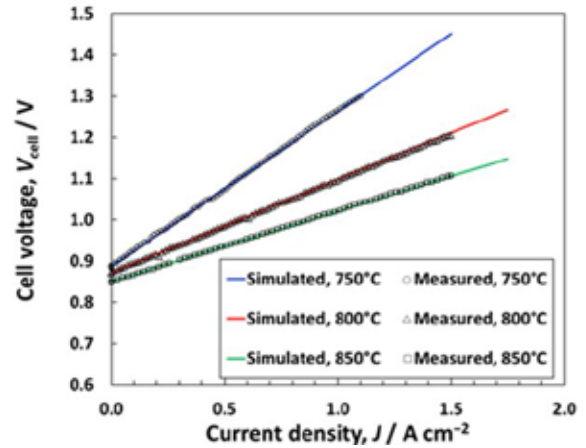


Fig. 2.  $V$ - $J$  curve simulation with measured one.

### IV. CONCLUSION

Gas conversion impedances (GCI) in high temperature steam electrolysis were successfully estimated by the developed simulation method. This leads to proper understanding of total overvoltages, or genuine cell performance in research and development of cell and stacks. Considering GCI, cell voltages were numerically simulated with  $\pm 0.3 \%$  precision against experimentally measured ones. In conference, case study results will be presented at more practical electrolysis conditions, or reduced flow rates.

### ACKNOWLEDGMENT

The first author is grateful to Dr. G. Schiller and German Aerospace Center (DLR) for his implementing this research at DLR Stuttgart.

### REFERENCES

- [1] Singh, A., Frei, T., Chokani, N., Abhari, R.S., Impact of unplanned power flows in interconnected transmission systems – Case study of Central Eastern European region, Energy Policy, Volume 91, 2016, pp. 287-303
- [2] Takano, K., Nagata, S., Nozaki, K., Monma, A., Kato, T., Kaga, Y., Negishi, A., Kato, K., Inagaki, T., Yoshida, H., Hosoi, K., Hoshino, K., Akbay, T., Akikusa, J., Numerical simulation of a disk-type SOFC for impedance analysis under power generation, Journal of Power Sources, Volume 132, 2004, pp. 42-51.
- [3] Tanaka, Y., Hoerlein, M.P., Schiller, G., Numerical simulation of steam electrolysis with a solid oxide cell for proper evaluation of cell performances, International Journal of Hydrogen Energy, Volume 41( 2), 2016, pp. 752-763.

## INTENSIFYING n-DODECANE STEAM REFORMING UNIT WITH MONOLITH CATALYST

A. Vita, C. Italiano, L. Pino, M. Laganà, V. Recupero  
CNR, Institute of Advanced Technologies for Energy “Nicola Giordano”,  
Via S. Lucia 5, 98126 Messina, (Italy)

**Abstract** - In the framework of National Research Project “High Efficiency Technologies for Onboard Environmental and Sustainable Energy Use” (TESEO), the CNR-ITAE has developed and tested a syngas generator (DSR I) based on Steam Reforming (SR) of n-dodecane ( $n\text{-C}_{12}\text{H}_{26}$ ) as surrogate of diesel, with maximum hydrogen production of  $1.5 \text{ Nm}^3/\text{h}$  for Solid Oxide Fuel Cells (SOFCs), as on-board Auxiliary Power Unit. A Packet bed annular reactor ( $200 \text{ cm}^3$ ) containing a commercial 2wt%Rh-based catalyst (220g) has been used in the SR unit. In this work, with the aim to reduce noble metal usage and intensify the SR process, 1wt%Me/CeO<sub>2</sub> (Me = Rh, Pt) cordierite monolithic catalysts (diameter = 2cm, length = 15cm, 400psi,  $47 \text{ cm}^3$ ), have been prepared, with a novel coating technique based on Solution Combustion Synthesis (SCS).

**Index Terms** – liquid hydrocarbons reforming, structured catalysts, syngas, fuel processor, intensification process, APU.

### I. INTRODUCTION

#### Background

The request for cleaner energy production to minimise environmental impact due to the population growth and the economic development is becoming increasingly urgent. In Europe, air quality has been a major issue since the early 1970s and during the years the EU adopted a series of ambitious actions to further decrease pollutant emissions throughout the continent [1], especially for the transportation sector. In this regard, the use of Auxiliary Power Units (APU), based on various fuel cell types, can play an important role in the transition towards a sustainable and environmentally-friendly energy system. A fuel cell APU has the potential of providing electrical energy with higher efficiencies and low environmental impact, than conventional power generation units. Actually, liquid hydrocarbons (gasoline, diesel and jet fuels) are prospective candidates to feed a fuel cell APU, since they are easily transportable and their distribution infrastructures are readily available. Appropriate fuel cells for APU systems are Proton Exchange Membrane Fuel Cells (PEMFCs) and Solid Oxide Fuel Cells (SOFCs). For PEMFCs case, the direct utilisation of H<sub>2</sub> in some transport-related applications is

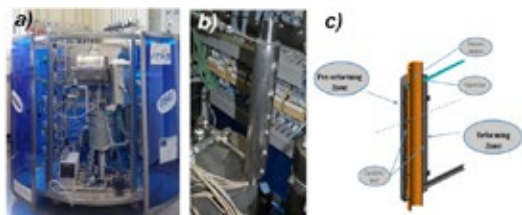
hindered by storage issues, thus a useful approach is a reforming unit located up-stream to the SOFC cell. This configuration combines the high reactivity of a hydrogen-rich stream with the high energy density of an organic liquid fuel. In recent years a lot of research was focused on the design of durable diesel reforming catalysts, with the aim to overcome the principal degradation phenomena mainly due to the deposition of deleterious carbon species. In addition, the development of efficient and compact fuel processors represent another key factor. Noble metals (Pt, Ru, and Rh) catalysts are more active and stable than Ni catalysts in reforming reactions due to a different coking mechanism that results in major resistance to carbon deposition but at the same time more expensive. One way to reduce the total amount of noble metals in the catalysts, maintaining at the same time high performances, is to deposit active catalytic layers on structured supports (ceramic or metallic monoliths or foam). The utilisation of structured catalysts, for process intensification, not only contribute to saving the material cost, but help to overcome some typical issues of packet bed reactors related to heat and mass transfer limitations, especially at high gas flow rates, allowing the design of small and compact reactors [2].

### II. EXPERIMENTAL

#### Steam Reforming unit (DSRI)

The syngas generator (DSR I) is based on SR of n-dodecane ( $n\text{-C}_{12}\text{H}_{26}$ ) as a surrogate of diesel, with a maximum hydrogen production of  $1.5 \text{ Nm}^3/\text{h}$ . The developed fuel reformer (fig. 1) consisted of a fuel injection part (including tanks for steam and fuel) in conjunction with a fuel/steam vaporising/mixing part and a catalytic converting part based on packet bed annular reactor ( $200 \text{ cm}^3$ ) containing a commercial 2wt%Rh-based catalyst (220 g) operating at two different temperatures ( $500^\circ\text{C}$  in the pre-reforming zone and  $800^\circ\text{C}$  in the reforming zone, fig.1c). In addition, low-cost subunits that incorporate mainly standard components (recycle reservoirs, manual /automatic valves, pressure regulators/transducers, flow meters, and

ancillaries) have been designed in order to get the requirements of small size and high modularity. Moreover, the reformer includes a completely automated acquisition data and control system [3].



**Fig. 1.** a) View of 1.5 kW Fuel Processor (net size [mm] = 800 diameter × 1000 height, b) Integrated packet bed reactor c) reactor 3D rendering

#### Structured catalyst preparation and preliminary scale up

Previously, 1.5wt%Me/CeO<sub>2</sub> (Me = Rh, Pt) cordierite monolithic catalysts (diameter = 1cm, length = 1.5cm, 400cpsi, vol.=1,7cm<sup>3</sup>), have been prepared, with a coating technique based on Solution Combustion Synthesis (SCS) [2]. The deposition process was repeated several times until reaching the desired amount (catalyst loading = 0.180mg, 6.7mg/cm<sup>2</sup>) of catalytic layer overall the supports. In this work, a first scale up of the coating method was carried out on a bigger cordierite support (diameter = 2cm, length = 15cm, 500cpsi, vol.=47cm<sup>3</sup>, fig. 2a). Several samples have been prepared (1wt%Pt/CeO<sub>2</sub>: catalyst loading = 12-24g, 10-20mg/cm<sup>2</sup>, 1wt%Rh/CeO<sub>2</sub>: catalyst loading = 12-16g, 10-13mg/cm<sup>2</sup>) for investigation activities at macro-scale level in the DSR I unit in order to fix the optimal catalyst loading and optimize the scale-up procedure.

### III. RESULTS AND DISCUSSION

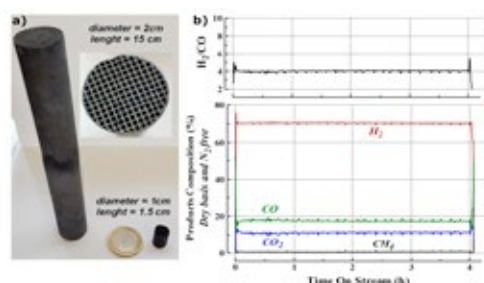
#### Structured catalysts characterization

The prepared catalysts were characterised by XRD, SEM, and TEM analysis, the porosity (via helium pycnometer) and the mechanical stability (via sonication treatment) were also determined and compared. The prepared structured catalysts have shown interesting results in terms of uniform thin coating (thickness between 9–25μm, depending on the coating amount), high mechanical strength (elevate adherence value between 98.6-98.9%), high porosity (≈79%) associated with little noble metal particles (≈5nm) well distributed on ceria support.

#### Performance of the DSR I with structured catalysts

All the prepared structured catalysts have been tested in the DSR I unit with the double catalyst bed configuration (pre-reforming and reforming zone). Five thermocouples have been positioned along the structured catalysts to register the axial temperature behaviour during the preliminary tests. The tests have been carried out at fixed S/C=2.5 and T<sup>set</sup> = 800°C,

varying the GHSV between 7600 – 15000h<sup>-1</sup> (WSV=14858–44313Nml·g<sub>cat</sub><sup>-1</sup>·h<sup>-1</sup>). The Composition of reagents and products was analyzed by an Agilent GC system equipped with a 7890A GC with FID and TCD detectors; ABB Continuous Processes Gas Analyzer (AO 2020) was used for continuous measurements. Among the monoliths tested, the 1wt%Rh/CeO<sub>2</sub> based one (total catalyst loading = 16mg, 13mg/cm<sup>2</sup>) has shown the best performances (fig. 2b) in terms of full n-dodecane conversion and high hydrogen production (>70% dry basis and N<sub>2</sub> free), moreover, the CH<sub>4</sub> concentration at the outlet was below 1% and the others by-products (C<sub>2</sub>H<sub>4</sub>, C<sub>2</sub>H<sub>6</sub>, C<sub>3</sub>H<sub>6</sub>, C<sub>3</sub>H<sub>8</sub>, C<sub>4</sub>H<sub>10</sub>) principally derived from the cracking phenomena are absent or present in traces (<10<sup>-4</sup>%). The absence of carbon deposition has been also revealed. The Pt based catalysts showed insufficient activity especially regarding the high amount of by-products formation.



**Fig. 2.** a) Structured 1wt%Rh/CeO<sub>2</sub> catalysts. b) Test results of DSRI unit with structured Rh-based catalyst (13mg/cm<sup>2</sup>) at T=800°C, S/C=2.5 and GHSV=15000h<sup>-1</sup>.

### IV. CONCLUSION

Compared with packed bed reactor [3], the structured reactor, based on 1wt%Rh/CeO<sub>2</sub> catalyst, demonstrated comparable activity and selectivity to hydrogen associated with total n-dodecane conversion and absence of carbon deposition with catalyst amount and reactor volume significantly reduced. In addition, the SCS coating method can be seen as a suitable procedure to deposit the catalyst on a ceramic monolith. This method requires relatively cheap reactants, simple equipment, and low-cost facilities, letting to reduce production costs. Moreover, the method is potentially easily scalable to any kind size, and type of application.

### REFERENCES

- [1] I., Bagayev, J., Lochard, EU air pollution regulation: A breath of fresh air for Eastern European polluting industries, Journal of Environmental Economics and Management volume 83, 2017, pp 145–163.
- [2] A., Vita, G., Cristiano, C., Italiano, L., Pino, S., Specchia, Syngas production by methane oxy-steam reforming on Me/CeO<sub>2</sub> (Me = Rh, Pt, Ni) catalyst lined on cordierite monoliths, Applied Catalysis B: Environmental, 162, 2015, 551–563.
- [3] C., Fabiano, C., Italiano, A., Vita, L., Pino, V., Recupero “Performance of 1.5 Nm<sup>3</sup>/h hydrogen generator by steam reforming of n-dodecane for naval applications” International Journal of Hydrogen Energy, 41, 2016, 19475-19483.

## H<sub>2</sub>S ADSORPTION FROM BIOGAS MIXTURES USING A KOH-KI ACTIVATED CARBON: EVALUATION OF DESULFURIZATION MECHANISM THROUGH SPENT SAMPLES POST-ANALYSIS

L. Barelli<sup>a</sup>, G. Bidini<sup>a</sup>, M. Casciola<sup>b</sup>, N. de Arespacochaga<sup>d</sup>, A. Donnadio<sup>c</sup>, L. Pérez<sup>d</sup>, E. Sisani<sup>a\*</sup>, C. Miranda<sup>e</sup>

<sup>a</sup> Department of Engineering, University of Perugia, Via G. Duranti 93, 06125 Perugia (Italy)

<sup>b</sup> Department of Chemistry, Biology and Biotechnology, University of Perugia, Via Elce di Sotto 8, 06123 Perugia (Italy)

<sup>c</sup> Department of Pharmaceutical Science, University of Perugia, Via del Liceo 1, 06123 Perugia (Italy)

<sup>d</sup> Water Technology Center CETaqua, Carretera d'Esplugues 75, 08940 Cornellà de Llobregat, Barcelona (Spain)

<sup>e</sup> GRADED Spa, Via Gen. Girolamo Calà Ulloa, 38 - 80141 Naples, (Italy), <http://graded.it>

**Abstract** - Activated carbons treated with KOH-KI are suitable sorbents for H<sub>2</sub>S removal from biogas matrices finalized to high temperature fuel cell applications, especially in the case of high moisture content in the inlet mixture. A commercial KOH-KI activated carbon was employed to adsorb H<sub>2</sub>S in dynamic adsorption tests performed both at lab scale and in a pilot plant fed by biogas from wastewater treatment processes. On the basis of breakthrough tests results and spent samples post-analysis (XRD, FTIR, SEM-EDX, TG-DTA, N<sub>2</sub>/H<sub>2</sub>O adsorption-desorption and pH measurements), a physical-chemical adsorption mechanism aimed at process optimization was developed. Main outcomes revealed the presence of different sulfur species in the spent samples (e.g. elemental sulfur, K<sub>2</sub>SO<sub>4</sub>). Spent samples post-analysis explain the positive role of humidity and oxygen in the inlet mixture and also their synergetic effect, confirming the results of the adsorption runs previously performed.

**Index Terms** – activated carbons, biogas, H<sub>2</sub>S adsorption, spent samples post-analysis.

### I. NOMENCLATURE

AC activated carbons, XRD X-ray diffraction, FTIR Fourier-transform infrared spectroscopy, SEM scanning electron microscopy, EDX energy dispersive X-ray spectroscopy, TG-DTA thermogravimetric-differential thermal analysis.

### II. INTRODUCTION

High temperature fuel cells are attractive power systems due to their high efficiency and reduced environmental emissions, especially when a renewable source, as biogas from biomass anaerobic digestion, is used. Since these systems are very sensitive to the presence of impurities in the fuels, the concentration of hydrogen sulfide in biogas mixtures has to be strongly reduced down to sub-ppm levels, to assure a correct system operation and to preserve fuel cell lifetime [1]. Among the sorbents employed for low temperature H<sub>2</sub>S removal, activated carbons treated with KOH showed high potential for biogas desulfurization, thus they are very effective in presence

of high humidity content in the inlet gas mixture. Moreover, the addition of KI reduces the risk of sulfuric acid formation [2].

In this work, a commercial KOH-KI activated carbon was used in dynamic H<sub>2</sub>S adsorption runs for biogas purification both at lab scale and in a pilot plant located in Barcelona. The spent samples were then analyzed with different methods, in order to understand the reaction mechanism, finalized also to evaluate possible regeneration strategies.

### III. EXPERIMENTAL

A commercial KOH-KI activated carbon (Desotec Airpel Ultra DS) was used to carry out different adsorption tests both at lab scale and in a pilot plant for H<sub>2</sub>S removal from biogas matrices. The latter operated after a biotrickling filter; the inlet biogas came from a wastewater treatment plant and its composition was characterized by CH<sub>4</sub>/CO<sub>2</sub> ratio average value 1.75, H<sub>2</sub>S in the range 100-1800 ppm<sub>v</sub>, O<sub>2</sub> about 2 %mol and relative humidity (R.H.) 90%. In the lab tests, starting from the pilot plant composition, breakthrough runs were performed on a fixed bed reactor under different operating conditions: CH<sub>4</sub>/CO<sub>2</sub>=1, H<sub>2</sub>S 100 ppm<sub>v</sub>, R.H. 0-90% and oxygen 0-2 %mol.

Several spent samples were analyzed after adsorption runs and the results were compared to the virgin carbon. The spent samples were characterized through N<sub>2</sub> and H<sub>2</sub>O adsorption-desorption isotherms, SEM-EDX, TG-DTA, FTIR, XRD analyses and pH measurements.

### IV. RESULTS

The outcomes of lab tests in terms of adsorption capacity relative to 1 ppm<sub>v</sub> as outlet H<sub>2</sub>S concentration are reported in Table I. It can be observed that filter performance increased in presence of high percentage of humidity and small amounts of oxygen.



**Table I** Operating conditions used in the lab tests and obtained H<sub>2</sub>S adsorption capacities calculated from breakthrough curves

Test n°	Lab tests operating conditions	C <sub>ads</sub> H <sub>2</sub> S (mg/g)
B12	CH <sub>4</sub> /CO <sub>2</sub> (1:1) - R.H. 0% - O <sub>2</sub> 0%	24.46 ± 0.50
B16	CH <sub>4</sub> /CO <sub>2</sub> (1:1) - R.H. 0% - O <sub>2</sub> 2%	23.61 ± 0.54
B20	CH <sub>4</sub> /CO <sub>2</sub> (1:1) - R.H. 90% - O <sub>2</sub> 0%	33.90 ± 0.72
B24	CH <sub>4</sub> /CO <sub>2</sub> (1:1) - R.H. 90% - O <sub>2</sub> 2%	39.57 ± 0.95

B.E.T. analysis on virgin carbon identified a mainly microporous sorbent (isotherm profile type I), containing a wide microporous distribution, with a quite amount of mesopores, resulting from the hysteresis cycle at relative pressure (P/P<sub>0</sub>) above 0.5. The spent samples presented lower values of specific surface area and micropore volume, coherently with the adsorbed sulfur on the basis of breakthrough results. On the contrary, the B.E.T. analysis conducted on pilot plant spent samples until saturation, revealed a specific surface area lower than 5 m<sup>2</sup>/g and a negligible residual micropore volume (Table II).

**Table II** B.E.T. analysis results on virgin and spent AC Ultra DS samples after H<sub>2</sub>S adsorption tests

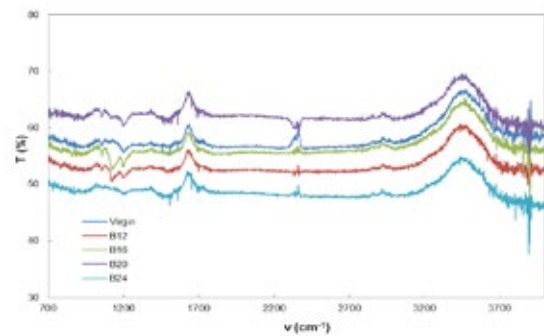
Sample	Surface area (m <sup>2</sup> /g)	Micropore volume (cm <sup>3</sup> /g)
Virgin AC	1100	0.44
Spent lab tests (B24)	855	0.34
Spent pilot plant	< 5	0

Adsorption-desorption H<sub>2</sub>O isotherms at 25°C carried out on virgin sorbent highlighted a certain hydrophilic character of the carbon, due to the presence of impregnate that acts as nucleation center for water molecules. Moreover, the hysteresis cycle does not close at relative pressure below 0.5, which means that there are strong interaction centers between adsorbate and adsorbent (associated with the impregnate) in mesopores that strongly retain water even at low relative pressures.

The presence of sulfur in the spent samples was confirmed by SEM-EDX analysis, resulting in an average value of 1.4 %wt for the lab tests and 47.5 and 27.3 %wt for the pilot plant T (top-saturated, near gas injection) and B (bottom-saturated) samples respectively. Moreover, pH measurements revealed a slight difference between virgin (pH 10.1) and spent (pH 9.6) samples, due to the increase of acidity caused by H<sub>2</sub>S.

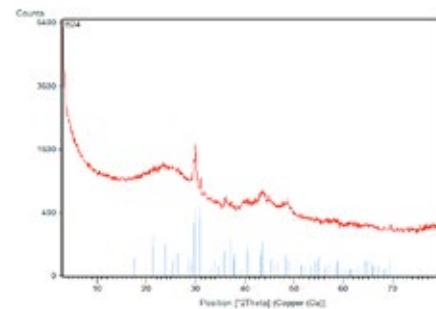
From TG-DTA analysis, four weight losses appeared, associated to surface water vaporization (100°C), water vaporization inside the pores (100-440°C), sulfur loss (440-650°C) and sulfate degradation (> 650°C).

Regarding FTIR analysis (Figure 1), bonds at 1650 and around 3500 cm<sup>-1</sup> are typical of -OH vibration. A H-S stretching (2500 – 2600 cm<sup>-1</sup>) is not observed, therefore H<sub>2</sub>S physical adsorption can be discarded, while signals at 1150 cm<sup>-1</sup> can be associated to sulfates. XRD analysis revealed the presence of oxidized species on all the samples after H<sub>2</sub>S adsorption: oxidation of H<sub>2</sub>S occurred even if the gaseous oxygen was not present in the gas matrix, due to the oxygen-containing surface functionalities of the carbon fibers [3].



**Figure 1** FTIR analysis results

In Figure 2, it is possible to recognize the presence of K<sub>2</sub>SO<sub>4</sub> on spent sample B24, formed by the reaction between sulfates and potassium hydroxide. In the pilot plant, elemental sulfur (S) and (K<sub>2</sub>SO<sub>4</sub>) were found for top-saturated and bottom-saturated samples respectively, revealing different oxidation steps along the filter.



**Figure 2** XRD analysis results on B24 spent sample (K<sub>2</sub>SO<sub>4</sub>)

## V. CONCLUSIONS

On the basis of the obtained results, the expected reaction mechanism can be divided into different oxidation steps: a first H<sub>2</sub>S oxidation, catalyzed by the activated carbon, to form solid sulfur (S, S<sub>8</sub>), adsorbed on carbon pores, and water; further oxidation of elemental sulfur to sulfur dioxide and sulfates; sulfates reaction with KOH, impregnated on carbon surface, to form K<sub>2</sub>SO<sub>4</sub>. The presence of water allows H<sub>2</sub>S dissolution and oxygen radicals formation, which facilitates sulfur oxidation, increasing H<sub>2</sub>S adsorption capacity.

## ACKNOWLEDGMENT

This work was carried out with the financial support of H2FC project (FP7, Grant Agreement N° 284522). Some activities were supported by the Italian Government, with the PON project “Smart Generation - Sustainable Systems and Technologies for the energy generation – PON03PE\_00157”

## References

- [1] A. Lanzini, H. Madi, V. Chiodo, D. Papurello, S. Maisano, M. Santarelli, J. Van herle, Prog. Energy Combust. Sci. 61 (2017) 150.
- [2] W. Feng, S. Kwon, E. Borguet, R. Vidic, Environ. Sci. Technol. 39 (2005) 9744.
- [3] A. Bouzaza, A. Laplanche, S. Marsteau, Chemosphere 54 (2004) 481.



## ARTIFICIAL INTELLIGENCE TECHNIQUES FOR PERFORMANCE SIMULATION: SOLID OXIDE FUEL CELLS V-J CURVE PREDICTION VIA ARTIFICIAL NEURAL NETWORKS

A. Baldinelli\*, L. Barelli\*, G. Bidini\*, F. Bonucci\*\* and F.C. Iskenderoğlu\*\*\*

\* Dipartimento di Ingegneria, Università degli Studi di Perugia, Via Duranti 93 Perugia (Italy)

\*\*VGA S.r.l, Via dell'Innovazione Deruta, (Italy)

\*\*\*Atılım University University, Ankara (Turkey)

**Abstract** – For their high flexibility of operation, Solid oxide fuel cells (SOFCs) are promising candidates to coach the transition towards cleaner and efficient energy generation. Yet, SOFC performance might be markedly affected by fuel composition variability and operative parameters. For that, a reliable simulation tool is necessary for SOFC performance, to optimize its working point and to provide a suitable control. Given the high variability ascribed to the fuel and the electrochemical system high non-linearity, the implementation of artificial intelligence techniques, like Artificial Neural Networks (ANNs), is worth considering. In ANNs, the correlation between system inputs and outputs is handled by virtual *neurons*, establishing in-out correlations without entering in knotty kinetics and material properties issues.

For what above, a suitably sized experimental campaign is to be designed to provide a large data-set. This to guarantee high ANN performance in the voltage estimation and, at the same time, a wide application domain of the neural simulator.

**Index Terms** – Artificial Neural Networks, Low-carbon fuels, Simulation, Solid Oxide Fuel Cells, Control algorithms

### I. INTRODUCTION

Solid Oxide Fuel Cells (SOFCs) show high flexibility with regard to the fuel, yet their performances might be sensitive to the variation of the fuel composition and the operative conditions. For instance, a change in temperature not only has an impact on the electrolyte conductivity, but also affects chemical kinetics of internal reforming, shift, etc. Similarly, as the anode feeding total flow rate decreases, the gas residence time at the active sites of the cells increases, allowing equilibrium-driven internal process to proceed. For that, a reliable simulation tool is necessary to forecast SOFC performance in a given plant scheme and to further optimize its working point. Beside detailed modelling approaches, taking into account gas diffusivity and reactions kinetics – with a high degree of non-linearity – the implementation of artificial intelligence techniques [1], [2], namely Artificial Neural Networks (ANNs), deserves attention. ANNs are non-linear informational processing devices, which

simulate the behaviour of a biological neural network. They work on the basis of interconnected elementary calculations (called *neurons* likewise biologic cells – Fig.1), calling for no detailed information about the investigated system. Through a development process called *training*, ANNs can learn the relationship between input and output based on the training data-sets. Being wide and consistent the training data-sets, ANNs run without having deep insight of the phenomenon under investigation, yielding with a very short computational time an implicit representation of complex and generally non-linear phenomena. This technique is flexible and can be used both in simple simulation and system control applications.

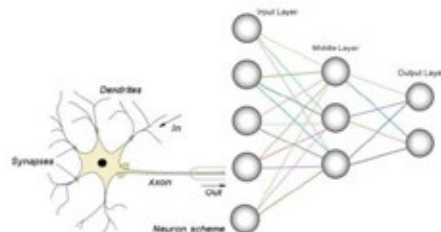


Fig. 1. Artificial neurons logic

### II. EXPERIMENTAL ACTIVITY

#### A. Materials

Commercial anode-supported NiYSZ/8YSZ/LSCF SOFC button cells are used (thickness anode/electrolyte/cathode: 240/8/50  $\mu\text{m}$ , outer diameter: 30 mm, active area: 3.14  $\text{cm}^2$ ). The sealing used is Aremco Ceramabond 552. The test rig and related equipment are fully described in [3].

#### B. Methods

The button cell is started up with a standard procedure. Hence, it undergoes reduction and it is firstly validated with a polarization test under hydrogen. All the data for the ANN are

Copyright © 2017

retrieved performing polarization tests, when starting operative load is 0 A (OCV) and it is increased by 0.157 A current steps (corresponding to 50 mA/cm<sup>2</sup>). Measurements are collected with a sampling frequency of 1 Hz and averaged on a 120-samples basis.

### C. Test Campaign

The experimental data set is based on 45 tests, resulting from all the possible combinations of the process decision variables: temperature, flowrate and gas composition. In detail, to define a wide application domain, temperature was varied according to three levels: 700, 750 and 800°C. The anode feeding was changed simulating five syngas mixtures resulting from different synthesis processes (synA – wood air gasification, synB – sludge air gasification, synC – wood oxygen gasification, synD – steam methane reforming and syn E – organic matter anaerobic digestion), whose specific composition is reported in Fig. 2. Since syngas are heterogeneous gas mixtures made of H<sub>2</sub>, CO<sub>2</sub>, CH<sub>4</sub>, CO and N<sub>2</sub>, the total flow rate was related to equivalent hydrogen (definition given at [4]): for this parameter, three levels are assumed: 10.8, 14.7, 23.2 ml/min/cm<sup>2</sup>. In such a manner, keeping constant current load, fuel utilization is varied.

All of the tests are performed on the same specimen in order to eliminate discrepancies due to the initial setup. In each test condition, a polarization curve is obtained. Dead-time between one test and the following is reduced to the minimum duration (average 2 hours), to lower the likelihood of cumulative damage and to sort comparable results.

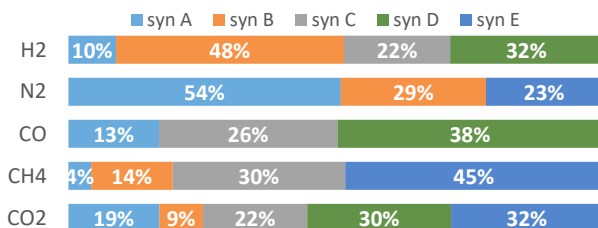


Fig. 2. Syngas components volume fractions

### D. Results

After the first validation of the cell under hydrogen feeding, the polarization curves introduced hereinabove were successfully acquired. Time-average results are summarized in a 1260-row matrix which is functional to the ANN training. Hence, from each test, on the input section, the test matrix includes: current load, temperature, H<sub>2</sub>, CO<sub>2</sub>, CH<sub>4</sub>, CO and N<sub>2</sub> volume flowrates. As output section, the matrix shows voltage outputs related to each combination of the previous parameters. Here, an example of experimental data retrieved is presented: the V-j curves plotted in Fig. 3 are related to 9 tests, featuring the systematic variation of operative temperature and fuel utilization.

## III. ARTIFICIAL NEURAL NETWORK ASSET

The aim of the ANN approach here proposed is to predict the polarization behaviour of a SOFC. Upon the

knowledge of a few input parameters, the ANN is shaped and trained to predict voltage losses. Specifically, multi-layer feed forward neural network architectures with two hidden layers are chosen and a Back Propagation learning algorithm based on gradient descent with momentum is considered. This technique allows a network to respond not only to the local gradient, but also to recent trends in the error surface. Acting like a low pass filter, momentum allows the network to ignore small features in the error surface. The model is realized in MATLAB, with a random initial distribution of weights. The number of neurons in the input and output layers is equal to the number of input and output parameters respectively. Different network architectures, characterized by different neurons number in the hidden layers, are considered. For each architecture a training-test campaign is scheduled subdividing the samples number between training and testing phases according to the ratio 5:1.

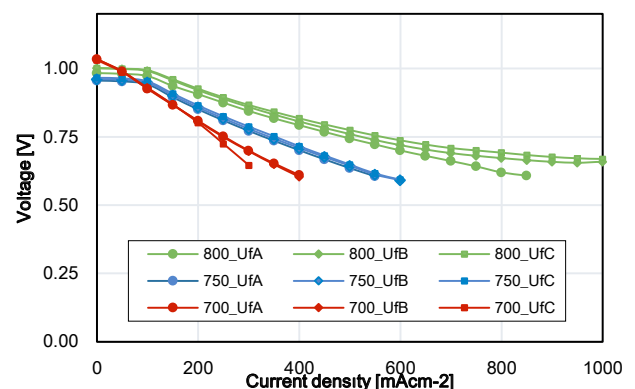


Fig. 2. Syn B polarization curves

## IV. CONCLUSION

The method here presented is applied to collect a wide experimental data set, which is functional to the development of an artificial intelligence tool based on ANN providing out voltage in function of main operating conditions (temperature, total flow rate, gas components volume fractions). First, the criterion to design a suitable test campaign is described to gather a large data-set and define a wide application domain, then the approach to train the neural network is presented.

## REFERENCES

- [1] W. R. W. Daud, R. E. Rosli, E. H. Majlan, S. A. A. Hamid, R. Mohamed, and T. Husaini, "PEM fuel cell system control: A review," *Renew. Energy*, vol. 113, pp. 620–638, 2017.
- [2] P. E. M. Almeida and M. G. Simões, "Neural optimal control of PEM fuel cells with parametric CMAC networks," *IEEE Trans. Ind. Appl.*, vol. 41, no. 1, pp. 237–245, 2005.
- [3] A. Baldinelli, L. Barelli, G. Bidini, A. Di Michele, and R. Vivani, "SOFC direct fuelling with high-methane gases: Optimal strategies for fuel dilution and upgrade to avoid quick degradation," *Energy Convers. Manag.*, vol. 124, pp. 492–503, 2016.
- [4] A. Baldinelli, L. Barelli, and G. Bidini, "Performance characterization and modelling of syngas-fed SOFCs (solid oxide fuel cells) varying fuel composition," *Energy*, vol. 90, pp. 2070–2084, 2015.

## SYNTHESIS AND CHARACTERIZATION OF HIGH-PERFORMANCE SOLID ACID FUEL CELL ELECTRODES WITH MINIMIZED CATALYST LOADING

F. P. Lohmann\*, P. S. C. Schulze\*\*, M. Wagner\*, O. Naumov\*, B. Abel\*, and Á. Varga\*

\* Leibniz Institute of Surface Engineering, Permoserstraße 15, 04318 Leipzig, (Germany)

\*\*now at Fraunhofer Institute for Solar Energy Systems, Heidenhofstrasse 2, 79110 Freiburg, (Germany)

**Abstract** – Low electrode impedance paired with low catalyst loading in intermediate and low temperature fuel cells is extremely difficult to achieve, posing a major obstacle to commercialization. The relatively new solid acid fuel cell (SAFC) technology comes with a unique combination of advantages such as a solid electrolyte, mild operating temperature, fuel flexibility and high resistance to poisoning. Here we demonstrate a scalable and facile route to obtain nanostructured composite SAFC electrodes consisting of Pt-decorated carbon nanotubes (Pt/CNT) and  $\text{CsH}_2\text{PO}_4$  electrolyte microparticles. The electrochemically active surface area (ECSA) is a key parameter in fuel cell research. We establish surface oxide reduction as method to measure the ECSA in SAFCs to enable further research.

**Index Terms** – fuel cell, platinum oxide, solid acid, electrochemically active surface area

### I. INTRODUCTION

SAFCs are a quite new class of fuel cells. They use  $\text{CsH}_2\text{PO}_4$  as solid electrolyte and operate at an intermediate temperature of around 240 °C. SAFC electrodes are resistant to CO poisoning and can also use alcohols as fuel.[1] The state-of-the-art membrane electrode assemblies (MEA) consist of a powder mixture of Pt nanoparticles, Pt/C, and  $\text{CsH}_2\text{PO}_4$  with a Pt loading of 7.7 mg/cm<sup>2</sup>. [2] As in other fuel cell types, decreasing the Pt loading is essential for broad commercial application.

One way to do so is to anchor the Pt nanoparticles on CNTs. This prevents agglomeration and improves the electric connectivity of the particles. Thoi *et al.* showed that Pt/CNTs can substantially lower the Pt mass-normalized electrode resistance in SAFCs.[3] Unfortunately, the employed fabrication route is not easily scalable and no fuel cell measurements were reported. We therefore developed a facile

and scalable synthesis route for obtaining Pt nanoparticles on CNTs and employ them as catalyst in SAFC electrodes.

In addition, an *in-situ* measurement of the ECSA is of great utility for further electrode development. It allows comparison of different catalyst materials and electrode architectures and enables deeper understanding of electrode degradation processes. Several methods for ECSA determination are known for liquid electrolyte systems at low temperatures.[4] However, because of the solid electrolyte and the elevated temperature the only viable method for SAFCs is surface oxide reduction. We validate this approach for *in-situ* measurements of the ECSA in SAFCs using a thin-film Pt electrode. Additionally, we demonstrate the applicability to powder electrodes and point out several interesting aspects that can now be investigated with the new method.

### II. EXPERIMENTAL

#### A. Pt/CNT Synthesis and Characterization

Pt/CNT were prepared by heating a mixture of  $\text{Pt}(\text{acac})_2$  and OH-functionalized CNTs to 200 °C under reduced pressure. The electrode powder was obtained by mixing the Pt/CNT with  $\text{CsH}_2\text{PO}_4$  in a weight ratio of 1:10. Symmetric MEAs were fabricated by uniaxial pressing carbon paper, electrode powder and electrolyte powder. These MEAs are denominated ‘Pt/CNT’ and have, with 0.41 mg/cm<sup>2</sup>, a 95% lower Pt loading than the reference MEAs.[5] These were fabricated using a state-of-the-art electrode mixture of Pt black, Pt/C, naphthalene and  $\text{CsH}_2\text{PO}_4$  [2] and are denominated ‘Pt/C’.

The MEAs’ electrode impedance was measured under humidified  $\text{H}_2$  at 240 °C. IV-curves were recorded at the same

temperature with humidified  $H_2$  and  $O_2$  at the anode and cathode respectively.

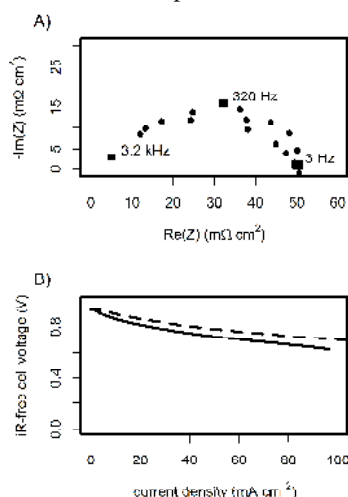
### B. Active Surface Area Determination

Two types of MEAs were fabricated: One with a Pt foil working electrode on a  $CsH_2PO_4$  pellet and a powder counter electrode, and a standard powder electrode MEA as the previously mentioned. Pt surface oxide was formed and reduced by applying cyclic voltammetry with a lower vertex potential of 0.1 V and a successively increasing upper vertex potential. The Pt/C MEA was additionally subjected to accelerated degradation tests.

## III. RESULTS

### A. Pt/CNT-MEA

Pt nanoparticles of ca. 3 nm are obtained. The electrode impedance of the Pt/CNT MEA is slightly better than the state of the art ( $60 \text{ m}\Omega \text{ cm}^2$ )[6], although the Pt loading is 95% lower. The IV-curves show comparable current output.[5]



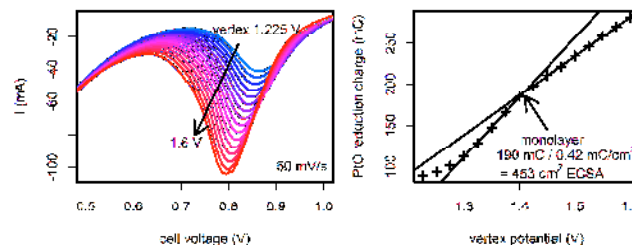
**Fig. 1. A) Electrode impedance of the Pt/CNT MEA and B) IV-curves of the Pt/CNT and the Pt/C MEA (dashed).**

### B. Active Surface Area Determination

The integrated PtO reduction charge plotted against the vertex potential shows a slope change indicating the point of oxygen monolayer formation as known from literature. The corresponding charge is divided by the area-normalized charge for PtO reduction to yield the ECSA. The obtained value for the Pt foil electrode agrees well with the surface area determined by hydrogen desorption measurements in  $H_2SO_4$ . The method is thus validated with the independent measurements.

The ECSA of the powder electrode is obtained in the same fashion. The potential improvements of SAFC electrodes become clear as the ECSA is only 12% of the full employed Pt powder surface area of the electrode. Interestingly, in contrast

to PEMFCs, the harsh ADT does not lead to a significant decrease in ECSA. This suggests qualitative differences in the degradation mechanisms of the electrodes, e.g. no Pt dissolution due to the absence of liquid water.



**Fig. 2. The powder electrode PtO reduction peaks increase with increasing vertex potential.**

## IV. CONCLUSION

We present a simple and scalable route to obtain SAFC electrodes with state-of-the-art performance but 95% reduced Pt loading. Additionally, we establish surface oxide reduction for the *in-situ* determination of the ECSA in SAFCs. This will enable improvements of SAFC electrode architecture and further insights into the electrode degradation.

## ACKNOWLEDGMENT

We are indebted to A. Prager, A. Sobottka, I. Reinhardt, P. Hertel, and C. Laube for analytic measurements. The authors acknowledge funding by the German Federal Environmental Foundation, the Stiftung Industrieforschung, the European Social Fund, and the Volkswagen Stiftung.

## REFERENCES

- [1] Chisholm, C. R., *et al.*, From Laboratory Breakthrough to Technological Realization: The Development Path for Solid Acid Fuel Cells, *Electrochem. Soc. Interface*, Vol. 18, 2009, p. 53.
- [2] Uda, T., Haile, S. M., Thin-Membrane Solid-Acid Fuel Cell, *Electrochem. Solid-State Lett.*, Vol. 8, 2005, pp. A245-A246.
- [3] Thoi, V. S., Usiskin, R. E., Haile, S. M., Platinum-decorated carbon nanotubes for hydrogen oxidation and proton reduction in solid acid electrochemical cells, *Chem. Sci.*, Vol. 6, 2015, pp. 1570-1577.
- [4] Łukaszewski, M., Soszko, M., Czerwiński, A., Electrochemical Methods of Real Surface Area Determination of Noble Metal Electrodes – an Overview, *Int. J. Electrochem. Sci.*, Vol., 2016, pp. 4442-4469.
- [5] Lohmann, F. P., *et al.*, The next generation solid acid fuel cell electrodes: stable, high performance with minimized catalyst loading, *J. Mater. Chem. A*, Vol. 5, 2017, pp. 15021-15025.
- [6] Haile, S. M., *et al.*, Solid acid proton conductors: from laboratory curiosities to fuel cell electrolytes, *Faraday Discuss.*, Vol. 134, 2007, pp. 17-39.

## SCHIBZ – LARGE FUEL CELL HYBRID SYSTEMS

K. Leites

thyssenkrupp Marine Systems GmbH, Hermann-Blohm-Straße 3,  
20457 Hamburg (Germany)

**Abstract** - Under the project name SchIBZ thyssenkrupp Marine Systems and 6 partners from industry and science developed a unique fuel cell system for seagoing vessels and containerized applications. The outstanding feature of this system is the use of low Sulphur diesel oil as fuel.

The system is based on solid oxide fuel cells coupled with a unique reforming unit for diesel fuel. The components are modular so power outputs roughly between 50 and 500kW per system can be realized.

The advantages of the system are a high electrical efficiency of about 50%, very low gaseous emissions without exhaust treatment and the possibility for heat recovery for further energy efficiency.

The consortium has built up a demonstration plant for trials of up to 2 years. Further development activities will comprise adaption to other fuels, improvements at the electrical side and scaling.

**Index Terms** – decentralized, low Sulphur diesel oil, ships, SOFC

### I. INTRODUCTION

The global shipping is faced with ever more stringent emission regulations. While short sea shipping is evaluating battery electric solutions, ocean going vessels have further to use hydrocarbon based fuels, to be able to store the necessary energy amount in an acceptable volume.

Still a favorite fuel is diesel oil, since the handling is very well known and the intrinsic safety is high. To reduce emissions internal combustion engines have to be equipped with a number of auxiliary systems. An elegant alternative solution would be a fuel cell system, if able to use diesel oil. Therefore, thyssenkrupp Marine Systems initiated a project to investigate the possibilities and develop a system according to the findings.

After rating the features of several configurations, the combination of low-Sulphur diesel oil and high temperature fuel cells promised to be the best solution, although one with considerable development needs. To execute this development thyssenkrupp Marine Systems sought for partners with the

respective know how. The project is part of a so-called lighthouse initiative, named e4ships.

### II. DESIGN OF THE FUEL PROCESS

Since fuel cells cannot convert liquid fuels directly, these must be converted into the fuel gas, by means of a reforming unit. The so-called reformat gas from hydrocarbon fuels contains not only  $H_2$  but also  $CH_4$ ,  $CO/CO_2$  and  $H_2O$ . The energy for the evaporation of the liquid fuel and the conversion should be taken from the exhaust gas energy of the fuel cell for best efficiency.

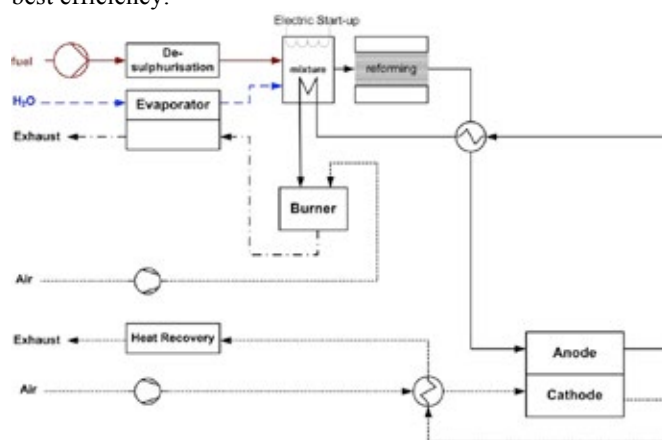


Fig. 1. SOFC fueled by road diesel [1]

A straight forward system can be achieved by using solid oxide fuel cells, see Fig. 1. There is enough excess heat to promote the reforming process with a high level of hydrogen production. To enhance performance and lifetime desulphurisation should be applied. This is achieved with a catalyst material which serves as Sulphur trap [2].

To make best use of the energy in the anode off-gas it is oxidized in a catalytic burner for pre-heating purposes in the process. This concept provides values of more than 50%



electrical system efficiency.

The fuel cell power system consists of one reforming unit connected to several fuel cell modules. The reforming unit contains all BoP components. The power electronics and the automation are separated from the actual fuel cell.

### III. DESIGN OF THE ELECTRICAL PROCESS

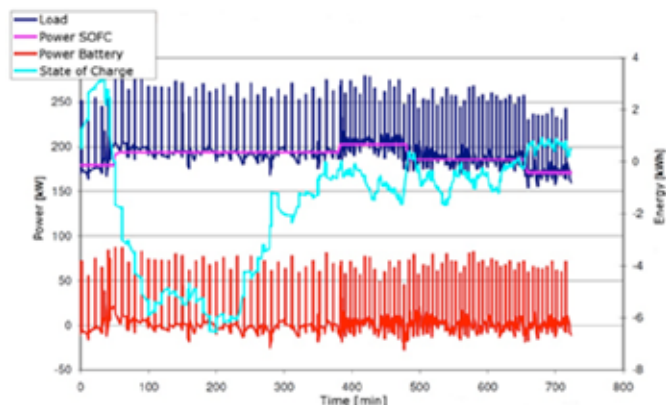


Fig. 2. Excerpt from the load graph of the test vessel

Since SOFC are not capable of rapid load changes, energy buffers are needed to cope with the transient load requirements in small, isolated networks. A calculation method was developed to size energy buffers such that they suit the actual network load profile. The idea behind this concept is that the fuel cell provides an average current over some time and the energy buffer takes care of higher or lower power demands, as shown in Fig.2.

Fuel cells as well as the most energy buffers are DC sources. It is useful to connect them via a DC rail and then convert the total current to AC for the board network. For this concept, every power source is coupled with a DC/DC converter to provide a fixed voltage level at the DC rail.

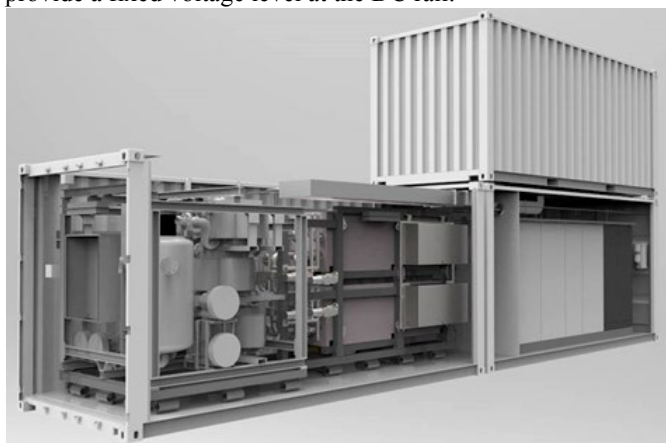


Fig. 3. ULSD-SOFC demonstration system incl. energy storage and auxiliary systems

### IV. THE DEMONSTRATION PLANT

To verify the seaworthiness of the power supply system a 50 kWe demonstrator was designed and commissioned this summer, see Fig. 3. A failure mode and effect analysis (FMEA) was performed to ensure that it fulfils the class requirements of DNV GL for main power supplies on merchant ships.

The control and monitoring system is designed for a fully automatic operation of the plant with restricted user interface for the crew inside the machinery control room.

### V. ACTUAL RESULTS

During the commissioning of the test installation a number of operation parameters were gathered. It is expected that the lifetime of the cells will be in the range of 20.000 h as demonstrated in smaller assemblies.

The system showed the expected efficiency around 50% and the cleanliness of the exhaust, Fig.4. The effect of the energy storage system could not be validated up to now, since the connection to the shore based power network inhibits the usage of them.

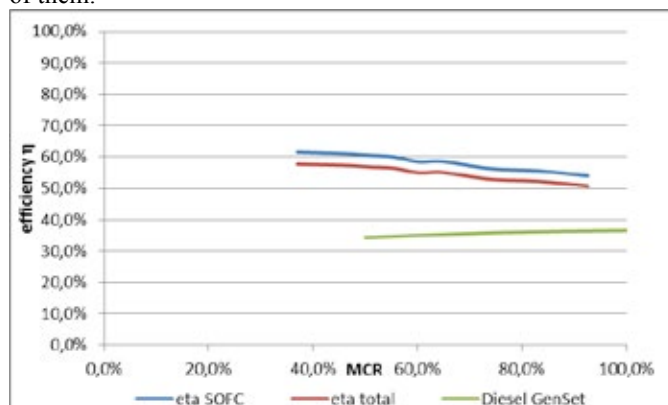


Fig. 4. Efficiency curve of the FC plant vs. a diesel genset

### ACKNOWLEDGMENT

The consortium of the project SchIBZ would like to thank the Federal Ministry of Transport and Digital Infrastructure (BMVI) and the National Organisation for Hydrogen and Fuel Cell Technology (NOW) for the continuing support under the National Innovation Program for Hydrogen and Fuel Cells (NIP).

### REFERENCES

- [1] LEITES, K.; KRUMMRICH, S.; NEHTER, P.; BAUSCHULTE, A.; KLEINOHLE, N.; KÜHNAU, W.; CLAUSSEN, S. (2013), SchIBZ – Application of solid oxide fuel cells for oceangoing ships, 5th Int. Conf. Fundamentals and Developments of Fuel Cells
- [2] NEHTER, P.; KLEINOHLE, N.; BAUSCHULTE, A.; LEITES, K. (2014), Diesel based SOFC APU for marine applications, 11th European SOFC and SOE Forum

## EXPLORING PT CATALYST THIN-FILMS ON STABILIZED NANO POROUS ELECTROLYTE

M. Wagner\*, B. Abel\*, and Á. Varga\*

\* Leibniz Institute of Surface Modification, Permoserstraße 15,  
04318 Leipzig, (Germany)

**Abstract** – As in other low and intermediate temperature fuel cells, the performance of solid acid fuel cells is limited by the electrodes. Creating composite nanostructured electrodes of  $\text{CsH}_2\text{PO}_4$  solid acid nanoparticles and Pt nanoparticles is an effective strategy to alleviate this performance limitation. Spray drying was used to fabricate electrolyte nanostructures, with the layer size systematically varied between 0 and 16  $\mu\text{m}$ . DC magnetron sputtering was used to deposit a 30 nm Pt thin-film. AC impedance spectroscopy was employed to analyze the electrode impedances in a humidified hydrogen environment. The optimal electrolyte layer size was determined to be  $\sim 5 \mu\text{m}$  with an extremely low Pt loading of  $0.06 \text{ mg/cm}^2$  and electrode impedance of  $\sim 0.8 \Omega\text{cm}^2$ , resulting in a Pt mass normalized activity of  $20 \text{ S/mgPt}$ .

**Index Terms** – fuel cell, porous electrode, solid acid

### I. INTRODUCTION

Electrochemical energy conversion devices are receiving increasing attention due to their size-independent and high conversion efficiencies compared to combustion engines.[1] Especially fuel cells are considered to play an important role in a sustainable energy future. A relatively new type of fuel cell, namely solid acid fuel cell (SAFC), based on the proton conducting electrolyte material  $\text{CsH}_2\text{PO}_4$ , combines several fundamental advantages.[2] Its solid state, low cost and non-toxic electrolyte with an intermediate operating temperature of ca.  $240^\circ\text{C}$ , allows simple cell design with low cost interconnect materials.[3]

Being an all solid-state system, SAFC electrode performance is dependent on the specific activity of the catalyst and the microstructure of the electrode. For a given electrocatalyst material, the goal is to increase the electrocatalytically active three-phase boundaries. The state-of-the-art cell reported by Uda *et al.* consists of composite electrodes of Pt black, Pt on carbon nanoparticles, and electrolyte microparticles and a  $25 \mu\text{m}$  thin electrolyte membrane.[4] A platinum loading of

$7.7 \text{ mg/cm}^2$  gives a mass-normalized activity – defined as the inverse area specific resistance, divided by the Pt loading – of  $2.2 \text{ S/mgPt}$ .

Efforts to increase the mass-normalized activity include using nanometer sized  $\text{CsH}_2\text{PO}_4$  particles, in order to maximize the density of the electrocatalytically active triple phase boundaries, between Pt catalyst, the electrolyte and the gas phase. For  $\text{CsH}_2\text{PO}_4$  nanoparticle synthesis, both electrospray deposition and spray drying have been employed successfully.[5,6]

In the present study, we use spray drying to synthesize  $\text{CsH}_2\text{PO}_4$  nanoparticles and determine the optimal nanostructure layer thickness by systematically varying the amount of the deposited  $\text{CsH}_2\text{PO}_4$ .

### II. EXPERIMENTAL

#### A. Electrode fabrication

To synthesize porous nanostructured electrodes, the spray-drying method (Büchi B90) was used. In this process, a precursor solution consisting of  $\text{CsH}_2\text{PO}_4$ , methanol (Alfa Aesar, 99.9%), DI-water and polyvinylpyrrolidone (PVP, Alfa Aesar,  $1,300,000 \text{ g/mol}$ ) with previously optimized concentration and composition [6], is vaporized by a piezoelectric spray head. The aerosol is transported by a hot inert gas stream ( $\text{N}_2 + \text{CO}_2$ ) towards the area, where the particles are deposited electrophoretically. During transport, the solvent evaporates and the solid acid electrolyte material precipitates, forming dry, solid nanoparticles. A custom-made pellet holder allows the deposition of nanoparticles on both sides of the electrolyte without modifying the other side. DC magnetron sputtering (Edwards Auto 306) was used to deposit a 30 nm Pt thin film on the electrolyte nanostructures

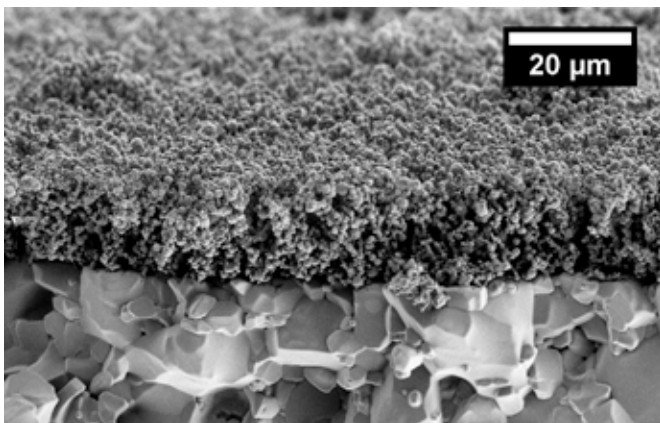
### B. Electrochemical characterization

Electrochemical impedance measurements were conducted with an impedance analyzer (Biologic VSP 300) with 10 mV perturbation amplitude over a frequency range of 1 MHz to 100 mHz. To retain the porous nanostructure of the electrodes, a carbon paper spacer ring (Toray Inc. TGP-H-120, ID = 16 mm, OD = 20 mm) was placed on each side of the symmetric electrochemical cell. The measurements were performed under humidified  $H_2$  at 240°C. The IVC curves were recorded with 10 mV  $s^{-1}$  scan rate with the above-mentioned instrument. The voltage was later corrected for ohmic resistance as determined with impedance spectroscopy. The thickness of the porous layers was in a range of 5 to 6  $\mu m$ . All samples had the same platinum content of 0.064 mg/cm<sup>2</sup> for each electrode.

## III. RESULTS

### A. Electrode fabrication

After spray drying with a precursor solution containing 10 g/l  $CsH_2PO_4$  for 90 min a porous electrolyte structure with a thickness of about 15  $\mu m$  was generated. The particle size varied between 50 nm and 1  $\mu m$ .

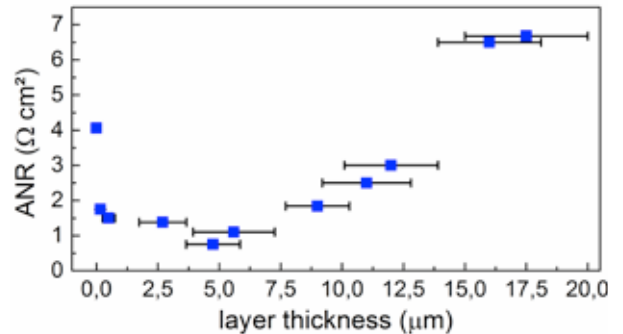


**Fig. 1. Porous electrolyte structure applied onto a dense electrolyte pellet**

### B. Electrochemical characterization

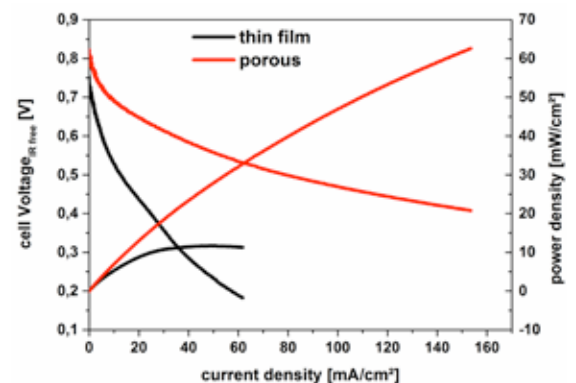
The measured electrode resistance plotted against the layer size of the porous electrode shows a fast decrease in the beginning followed by a slow increase for layer sizes exceeding 5  $\mu m$ . SEM images show that during the sputtering process platinum penetrated about 5  $\mu m$  into the structure. A further increase of the porous electrode thickness is therefore not affecting the active area. The increase of the electrode resistance can be explained by the use of the polymer PVP, which is necessary in order to stabilize the structure [6]. During the spray drying process, PVP forms a very thin shell around the particle and acts as a proton transport barrier. The protons

generated in the upper part of the porous electrode have to pass through a number of barriers which increases the electrode resistance.



**Fig. 2. Electrode resistance depending on the layer thickness of the porous electrode.**

For fuel cells in general the oxygen reduction reaction is the rate limiting step. The cell with the porous electrodes yielded a significantly higher power output compared to the cells with a thin film electrode. Hence it can be concluded, that the conducted architectural changes in the electrode structure affect the anodic hydrogen oxidation and cathodic oxygen reduction in a similar way. Therefore symmetric impedance measurements are a sufficient way to analyze the improvements in the electrode architecture done by spray drying.



**Fig. 3. IR free polarization plots for a Pt thin film cell and a cell with structured electrodes.**

## IV. CONCLUSION

We present a fast and scalable technique to fabricate porous SAFC electrodes. Structuring the electrode greatly decreases the resistance but a stabilizing agent is needed in order to prevent fast agglomeration of the structure. Due to PVP there is a negative impact of the layer thickness in contrast to a positive impact by the area increase. For our conditions an optimal layer size of 5  $\mu m$  was found, exhibiting a corresponding mass normalized activity of 20 S/mg<sub>Pt</sub> which is a huge improvement of the platinum utilization compared to the 2.2 S/mg<sub>Pt</sub> reported

## MODELLING ANALYSIS OF DEGRADATION IN LOW PLATINUM POLYMER ELECTROLYTE MEMBRANE FUEL CELLS

A. Baricci\*, H. Yu\*\*, L. Guetaz\*\*\*, A. Casalegno\*,  
R. Marchesi\*, and R. Maric\*\*

\* Politecnico di Milano, Dipartimento di Energia  
via Lambruschini 4, Milano (Italy)

\*\* University of Connecticut,  
44 Weaver Road Unit, Storrs (United States of America)

\*\*\* Commissariat à l'énergie atomique et aux énergies alternatives,  
17 Avenue des Martyrs, Grenoble, (France)

**Abstract** - Durability is a key issue of polymer electrolyte membrane fuel cells (PEMFC) with low Platinum loading, mainly because of the instability of Platinum catalyst nanoparticles in the cathode catalyst layer (CL). Degradation of catalyst is critical in consequence of several mechanisms, among which Platinum dissolution. As proposed in the literature, a possible strategy to mitigate Platinum dissolution consists in the development of CLs with gradient properties. In the present work, a theoretical analysis of Platinum dissolution is applied to the interpretation of degradation data recorded under accelerated stress tests (AST) on catalyst-coated membranes (CCMs) with 25 cm<sup>2</sup> active area and low Pt loading. A transient model referenced to the literature has been calibrated and validated on a set of experimental data to get insight into the catalyst degradation. The model predicts the formation of a catalyst depleted zone near the interface with polymer membrane, in agreement with TEM observations and the effect of a gradient catalyst structure in the catalyst layer is analyzed.

**Index Terms** - degradation modelling, impedance spectroscopy, PEMFC, Platinum dissolution.

### I. INTRODUCTION

Lowering Platinum loading is a strategic target to meet the cost of PEMFC systems for automotive application, but fundamental research is still needed to understand two major problems that are observed when catalyst active surface (ECSA) is reduced below a critical value. The first problem is the onset of unknown transport losses that impact the power density. It has been proposed in the literature that this transport loss could result from sluggish oxygen diffusion in the 2-10 nm film of ionomer that covers the catalyst [1], but the resulting transport

resistance far exceeds what is measured in bulk membranes. The second problem is durability [2]: an important degradation mechanism in PEMFC is the loss of catalyst active surface at cathode, which dramatically affects performance of low Pt CLs. This loss of ECSA is attributed mainly to ripening or to the precipitation of catalyst inside the polymer membrane (to form the Platinum band) in consequence of hydrogen crossover.

In this work, dissolution and PEMFC models are applied to AST data to capture the main effects of degradation in low Pt loading samples. Degradation of uniform samples is compared to the degradation of samples produced with gradient structures.

### II. EXPERIMENTAL

Details about the experimental part are available in [3-4]. CCMs have been produced by Reactive Spray Deposition Technique (RSDT) with a Platinum loading of 0.1 and 0.05 mg cm<sup>-2</sup> for cathode and anode. Samples that have been studied in this work are summarized in Table 1: uniform samples with average particle size of 2nm and 5nm have been studied for comparison, while two gradient samples have been fabricated: *GRADIENT1* shows nanoparticles with 5nm size next to the membrane and 2nm nanoparticles in the region next to the GDL; *GRADIENT2* shows higher Platinum loading next to the membrane.

Catalyst layers have been tested in PEMFC configuration to evaluate performance and durability with the AST for electrocatalyst (U.S. Department of Energy), consisting in 30k potential cycles with triangular wave between 0.6 V and 1.0 V at 50 mV s<sup>-1</sup> under inert atmosphere (N<sub>2</sub> 50 ml min<sup>-1</sup>).

Copyright © 2017



TABLE I  
SAMPLES DISCUSSED IN THE ANALYSIS

Code	Characteristic	Pt loading
KB2nm	Average particle size 2nm; Pt/C 0.4. Uniform.	C: 0.1 mg cm <sup>-2</sup> ; A: 0.05 mg cm <sup>-2</sup> .
KB5nm	Average particle size 5nm; Pt/C 0.4. Uniform.	C: 0.1 mg cm <sup>-2</sup> ; A: 0.05 mg cm <sup>-2</sup> .
GRADIENT1	Pt/C 0.4. Next to membrane: particle size 5nm; next to GDL: particle size 2nm.	C: 0.1 mg cm <sup>-2</sup> ; A: 0.05 mg cm <sup>-2</sup> .
GRADIENT2	Particle size 2nm. Next to membrane: Pt/C 0.6. Next to GDL: Pt/C 0.4.	C: 0.1 mg cm <sup>-2</sup> ; A: 0.05 mg cm <sup>-2</sup> .

### III. MODELLING

Degradation under AST is modelled according to [5]. Platinum mass conservation is solved in 1D across the catalyst layer (Eq. 1), where  $C_{Pt}$  is dissolved Pt concentration in the ionomer phase:

$$\frac{\partial C_{Pt}}{\partial t} = D \frac{\partial^2 C_{Pt}}{\partial x^2} + \sum_k^N n_k 4\pi r_k^2 B [C_s(r_k) - c] \quad (1)$$

The source/sink term in Eq. 1, accounts for Pt dissolution and re-deposition which depends on the saturated concentration of dissolved Pt in the ionomer phase ( $C_s$ ) which can capture the dependence of the dissolution rate on particle size, as proposed in [5].  $B$  is a fitting parameter that indicates the average dissolution rate constant in the adopted AST cycle.

1D PEMFC model that can simulate both polarization curve and impedance spectra [6] is applied to the experimental data.

### IV. RESULTS AND DISCUSSION

Detailed discussion of the experimental results regarding durability of gradient samples is reported in [3-4]. In Fig. 1, the evolution of ECSA during AST is reported; good consistency is found for simulated and measured data. Particle size distribution before AST is obtained from TEM data. The model can predict the improvement in durability introduced by gradient samples, even though not quantitatively identical to the experiment. Sensitivity is performed on model parameters.

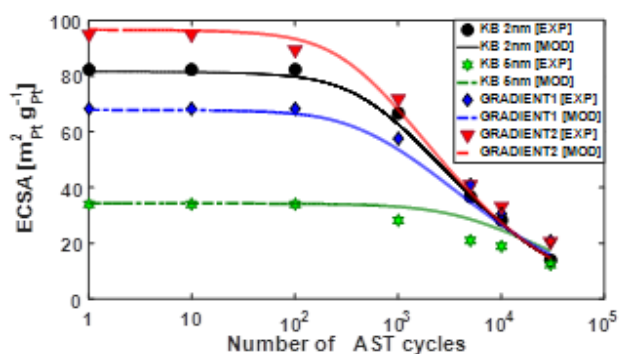


FIGURE I. Evolution of ECSA during durability test.

Simulated distribution of local ECSA in CL is reported in Fig. 2. The model can predict that gradient samples can mitigate depletion of Platinum in the CL next to the membrane, where a higher ECSA is observed after AST. This result is confirmed by TEM observation performed on aged samples [3-4].

Simulation of EIS data (*not shown*) shows that Pt depletion in the CL is responsible for an additional Ohmic loss inside the CL because of increased path length for ion transport. This effect appears in the impedance spectrum as an elongation of the 45° linear branch.

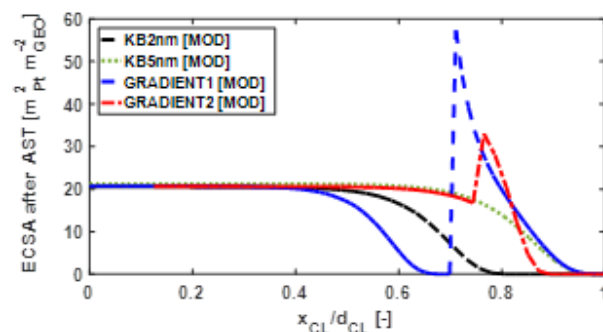


FIGURE II. Distribution of ECSA across the catalyst layer.

### V. CONCLUSION

Durability of low Platinum loading samples has been studied in this work by combining experimental and theoretical works. Depletion of Pt in the catalyst layer region next to the membrane has been predicted for uniform samples. Gradient structures can mitigate this degradation mechanism by retaining Pt inside the CL and reducing Pt lost in the band.

### REFERENCES

- [1] Weber AZ, Kusoglu A. Unexplained Transport Resistances for Low-Loaded Fuel-Cell Catalyst Layers. *J Mater Chem A* 2014;2. doi:10.1039/C4TA02952F.
- [2] Zhang S, Yuan X, Hin JNC, Wang H, Friedrich KA, Schulze M. A review of platinum-based catalyst layer degradation in proton exchange membrane fuel cells. *J Power Sources* 2009; 194:588–600. doi:10.1016/j.jpowsour.2009.06.073.
- [3] Yu H, Baricci A, Bisello A, Casalegno A, Guetaz L, Bonville L, et al. Strategies to mitigate Pt dissolution in low Pt loading proton exchange membrane fuel cell: I. A gradient Pt particle size design. *Electrochim Acta* 2017. doi:10.1016/j.electacta.2017.07.093.
- [4] Yu H, Baricci A, Casalegno A, Guetaz L, Bonville L, Maric R. Strategies to mitigate Pt dissolution in low Pt loading proton exchange membrane fuel cell: II. A gradient Pt loading design. *Electrochim Acta* 2017. doi:10.1016/j.electacta.2017.06.145.
- [5] Takeshita T, Murata H, Hatanaka T, Morimoto Y. Analysis of Pt Catalyst Degradation of a PEFC Cathode by TEM Observation and Macro Model Simulation. *ECS Trans* 2008; 16:367. doi:10.1149/1.2981871.
- [6] Baricci A, Casalegno A. A simple analytical approach to simulate the electrochemical impedance response of flooded agglomerates in polymer fuel cells. *Electrochim Acta* 2015; 157:324–32. doi:10.1016/j.electacta.2015.01.044.



## DEMONSTRATION OF FUEL CELL ELECTRIC BUS OPERATION IN HAWAII VOLCANOES NATIONAL PARK

Scott R. Higgins, James “Mitch” Ewan, Richard Rocheleau  
Hawaii Natural Energy Institute, University of Hawaii, Honolulu, HI

**Abstract** - A novel device called the Environmental Sensor System is designed to provide real time environmental air contaminant analysis to allow the fuel cell system to protect the integrity of the fuel cell from environmental contaminants. This is accomplished through continuous sampling of the ambient air used to fuel the fuel cell. The integration of this supplementation device will allow fuel cell systems to safely and reliably operate in extreme environmental conditions which previously would have resulted in stack poisoning from air contaminants.

### I. NOMENCLATURE

Fuel Cell Electric Bus = FCEB

Environmental Sensor System = ESS

Hawai'i Volcanoes National Park = HAVO

### II. INTRODUCTION

Proton Exchange Membrane (PEM) fuel cells produce electricity by combining oxygen and hydrogen in the presence of a platinum catalyst[1] and have been demonstrated as a reliable power source for stationary[2] and mobile applications[3]. To fuel PEM fuel cells, hydrogen is typically sourced from a high pressure, on board vessel and oxygen is sourced from the surrounding air. Air contaminants contained within the air sourced as fuel could be poisonous to the fuel cell and cause the fuel cell performance to drop[4]. Air quality varies based on location and can be highly contaminated depending on the area of operation[5]. Air contamination is comprised of both atmospheric particulates and poisonous gases which can be due to natural [6] or industrial sources[7]. For example, PEM fuel cells used to power automobiles could be exposed to internal combustion engine exhaust[8] from other vehicles on the roadway and PEM fuel cells used in stationary industrial applications could be exposed to industrial exhaust gases such as flue gas exhaust[7]. Air contamination has the potential to cause temporary or permanent performance loss when the contaminant gas molecule forms a chemical or physical bond with the platinum catalyst on the surface of the electrode and hinders the active catalyst site, rendering it unusable[4]. The PEM fuel cell industry has approached this problem by applying increasingly complex air filtration technologies to the cathode air inlet over the past 25 years,

starting with large particulate filtration and then incorporating both chemical and particulate filtration[9].

In this publication, the authors present the next advancement in fuel cell air filtration technology. A novel sensor device called the Environmental Sensor System (ESS) was designed and fabricated which detects air contamination entering the cathode fuel inlet and transmits that data to the fuel cell control system in real time. This information will allow fuel cell control systems to be preprogrammed to respond to changing air contaminant conditions by adjusting operation of the fuel cell in response to air contamination conditions. In addition, the cumulative exposure of contaminants to the air filter can be calculated to allow the air filter to be exchanged at the appropriate time. The ESS also detects contaminants which break through the air filter to allow an emergency shut down of the fuel cell to protect it from contaminant exposure in real time, extending its lifetime and significantly reducing O&M costs. The ESS is capable of sensing multiple air contaminants using a customizable array of air contaminant sensors. The ESS has beneficial application in multiple types of fuel cell systems. As a demonstration of the technology, the ESS is currently being installed on two retrofitted fuel cell powered buses which will be operated in Hawai'i Volcanoes National Park (HAVO). In support of the demonstration, an air filtration test bed has been fabricated at the Hawai'i Sustainable Energy Research Facility (HiSERF) where laboratory experiments have been completed to allow estimates of adsorption capacity of contaminants on commercial air filters to be used on the fuel cell electric bus.

The Environmental Sensor System (ESS) is designed to be incorporated into any fuel cell system to allow real time, continuous air contaminant monitoring to allow the fuel cell operator or control software to protect the fuel cell from air contaminants from changing environmental contaminants. To allow for use in a variety of environmental conditions, the sensor array is designed for customizability. The ESS has the potential to house four standard electrochemical sensors (3 electrode sensors) in addition to a photoionization detector. As the process flow shows in Figure 1, the air sample is drawn through ESS to provide air contaminant data.

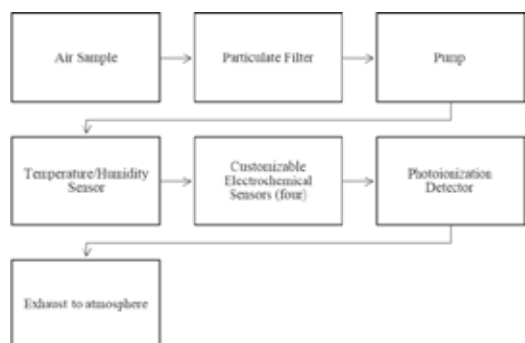


Figure 1: Environmental Sensor Array process flow diagram. Pressure sensor not shown.

As a demonstration, the Environmental Sensor System (ESS) will be installed and utilized on two fuel cell buses. Both buses are in the process of being retrofitted to be powered by a battery which is charged by a 33KW fuel cell (Hydrogenics Hy PM HD 30), therefore we describe the buses as fuel cell electric buses (FCEB). The buses have been converted to FCEB by US Hybrid Inc. and will be operated in the Hawaii Volcanoes National Park (HAVO). HAVO experiences intermittent volcanic eruptions containing sulfur dioxide ( $\text{SO}_2$ ), hydrogen sulfide ( $\text{H}_2\text{S}$ ) and other air contaminants. The result of the eruptions is intermittent air contamination up to 5 ppm in areas where the FCEB will operate. This is an excellent environment to demonstrate the ESS technology. A fuel cell operating in this environment without an ESS would quickly succumb to  $\text{SO}_2$  and  $\text{H}_2\text{S}$  poisoning. The ESS will be equipped with  $\text{SO}_2$  and  $\text{H}_2\text{S}$  electrochemical sensors to detect contaminants from volcanic eruptions. The ESS is also equipped with nitric oxide (NO), nitrogen dioxide ( $\text{NO}_2$ ) and volatile organic compound (VOC) sensors to detect emissions from other traditional internal combustion engine (ICE) vehicles in HAVO.

### III. CONCLUSION

The Environmental Sensor System (ESS) was developed to sense air contaminants commonly known to damage fuel cells (sulfur dioxide, hydrogen sulfide, nitric oxide, nitrogen dioxide and volatile organic compounds) in the environment from which fuel cells source air for cathode fuel. The ESS was integrated into a fuel cell electric bus to allow constant real time air contaminant data to be collected. An air filtration test stand was fabricated to test the contaminant adsorption capacity of the commercial air filtration used on the buses to allow an estimate of filter lifetime based on cumulative air contaminant exposure detected by the ESS and to develop a relationship between flowrate and adsorption capacity. The ESS was successfully tested for communication with the CAN bus control software. The bus control software was preprogrammed to protect the fuel cell from air contaminant exposure using the ESS as a signaling device to turn off the fuel cell in the case of air contaminant levels which would overwhelm the air filter or in the case that the air contamination had broken through the air filter. Once the two fuel cell electric buses are completed with integrated

ESS, preliminary testing will be completed in Honolulu before the technology is demonstrated in Hawai'i Volcanoes National Park.

### ACKNOWLEDGMENT

The authors would like to thank the Office of Naval Research for support under Asia Pacific Research Initiative for Sustainable Energy Systems 2012 (N00014-13-1-0463) and 2013 (N00014-14-1-0054).

### REFERENCES

- [1] C. Berger, Handbook of fuel cell technology, Prentice-Hall, Englewood Cliffs, N.J., 1968.
- [2] A.J.L. Verhage, J.F. Coolegem, M.J.J. Mulder, M.H. Yildirim, F.A. de Bruijn, 30,000 h operation of a 70 kW stationary PEM fuel cell system using hydrogen from a chlorine factory, International Journal of Hydrogen Energy 38(11) (2013) 4714-4724.
- [3] T. Fletcher, R. Thring, M. Watkinson, An Energy Management Strategy to concurrently optimise fuel consumption & PEM fuel cell lifetime in a hybrid vehicle, International Journal of Hydrogen Energy 41(46) (2016) 21503-21515.
- [4] J. St-Pierre, Proton exchange membrane fuel cell contamination model: Competitive adsorption followed by a surface segregated electrochemical reaction leading to an irreversibly adsorbed product, Journal of Power Sources 195(19) (2010) 6379-6388.
- [5] M. Masiol, S. Squizzato, G. Formenton, R.M. Harrison, C. Agostinelli, Air quality across a European hotspot: Spatial gradients, seasonality, diurnal cycles and trends in the Veneto region, NE Italy, Science of The Total Environment 576 (2017) 210-224.
- [6] P.A. Nadeau, C.A. Werner, G.P. Waite, S.A. Carn, I.D. Brewer, T. Elias, A.J. Sutton, C. Kern, Using  $\text{SO}_2$  camera imagery and seismicity to examine degassing and gas accumulation at Kilauea Volcano, May 2010, Journal of Volcanology and Geothermal Research 300 (2015) 70-80.
- [7] K. AlRafea, A. Elkamel, S.A. Abdul-Wahab, Cost-analysis of health impacts associated with emissions from combined cycle power plant, Journal of Cleaner Production 139 (2016) 1408-1424.
- [8] J. Gallus, U. Kirchner, R. Vogt, T. Benter, Impact of driving style and road grade on gaseous exhaust emissions of passenger vehicles measured by a Portable Emission Measurement System (PEMS), Transportation Research Part D: Transport and Environment 52, Part A (2017) 215-226.
- [9] D.M. Kennedy, D.R. Cahela, W.H. Zhu, K.C. Westrom, R.M. Nelms, B.J. Tatarchuk, Fuel cell cathode air filters: Methodologies for design and optimization, Journal of Power Sources 168(2) (2007) 391-399.

## VISUALIZATION OF WATER IN GAS DIFFUSION LAYERS WITH NEUTRON DARK-FIELD IMAGING

M. Siegwart\*\*\*, R. P. Harti\*\*, M. V. Manzi-Orezzoli\*, J. Vallsecchi\*\*, C. Grünzweig\*\*, T. J. Schmidt\*\*\*\* and P. Boillat\*\*\*

\* Electrochemistry Laboratory (LEC), Paul Scherrer Institute (PSI), (Switzerland)

\*\*Laboratory for Neutron Scattering and Imaging (LNS), Paul Scherrer Institute (PSI), (Switzerland)

\*\*\*Laboratory of Physical Chemistry, Department of Chemistry & Applied Biosciences, ETH Zürich, (Switzerland)

**Abstract** – Gas diffusion layers (GDLs) were studied with neutron dark-field and transmission imaging in the dry state and filled with heavy water, which was injected through a channel. For transmission imaging the strong attenuation of channel water prohibits the analysis of the water distribution in the GDL behind the channel. In contrast, the channel water does not disturb the dark-field imaging signal, as this technique is selectively sensitive to structures in a given size range. Therefore, the method can be applied for the selective visualization (and quantification) of water in the GDL. In addition, we show that dark-field imaging can also be used to visualize damages of the GDL.

**Index Terms** – Gas diffusion layer, Water visualization, Gas diffusion layer damage, Dark-field imaging

### I. INTRODUCTION

Optimization of water management of polymer electrolyte fuel cells (PEFCs) is an important lever to improve performance. To understand the impact of liquid water in gas diffusion layers (GDLs) on performance, a method that allows for visualization and quantification of water in the GDL is of great interest. Conventional neutron transmission imaging is a powerful tool for visualizing the water distribution behind typically used flow field materials such as aluminum or steel during *in situ* experiments. In order to quantify water in the different layers over the cross section, imaging of the cell can be performed with the cell membrane parallel to the beam [1]. To avoid saturation of the signal due to large water thicknesses, the width of the cell is limited to 20-30 mm in this configuration. Neutron dark-field imaging offers new possibilities to visualize water in the GDL, as this technique is selectively sensitive for structures in the size range of the pores of GDLs. Using a neutron grating interferometer [2] which produces interference fringes, the dark-field image (DFI) is obtained simultaneously to the transmission image (TI).

Microstructures in the size range from one to several tens of micrometers and with a scattering length density different from their surroundings cause neutron scattering to ultra-small angles, which results in a loss of interference fringe amplitude. The DF-signal is a measure for this amplitude loss and is therefore related to the amount of scattering to ultra-small angles caused by the sample. As large homogenous structures do not cause coherent neutron scattering at these angles, mm-sized water aggregates, which can be present e.g. in the flow fields of fuel cells, do not significantly contribute to the DFI. Therefore, dark-field imaging can be used to selectively analyze water distributed in the microstructure of GDLs. Additionally, local changes in microstructure of the GDL, such as GDL damages, can be visualized with dark-field imaging.

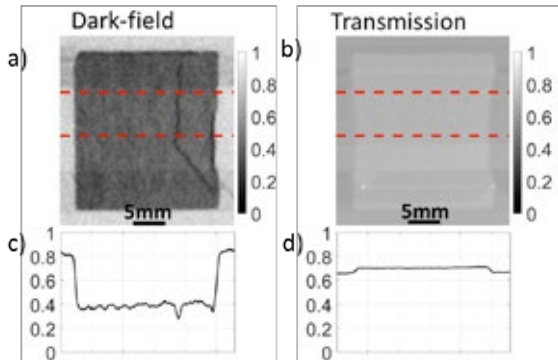
### II. EXPERIMENTAL

An in-house constructed aluminum device was used to fill the GDLs with water. In this setup pressurized water flows through a 1 mm deep channel which is covered with the GDLs. The tested GDLs were of type TGP-H-060 plain (Toray, Japan) and H2315 (Freudenberg, Germany) with an in-house applied fluorinated ethylene propylene coating (30 wt%) and had an area of 20 x 22 mm<sup>2</sup>. In the test device the GDLs were compressed to 150  $\mu$ m, which is about 75 % of their original thickness. The experiments were performed at the ICON beamline [3] at the Swiss Spallation Neutron Source (SINQ) with a neutron grating interferometer which consists of three gratings [2].

### III. RESULTS

When comparing a DFI (Fig 1a) and TI (Fig 1b) of a dry GDL (Toray, TGP-H-060 plain) the higher contrast in the DFI between the rubber gasket and the area covered by the GDL is

clearly apparent. The signal intensity of 0.7 in Fig 1b is attributable solely to the attenuation of the aluminum test device. The damage of the GDL is invisible in the TI (Fig 1b and d) whereas a crack is visible in the DFI (Fig 1a and c). For clarity the averaged signal intensity between the dashed red lines is also plotted (Fig 1c and d). Here again, we see that the DFI captures, in contrast to the TI, microstructure variations of the GDL.



**Fig. 1. Signal intensity of a GDL with a crack:**  
a) Dark-field, b) Transmission

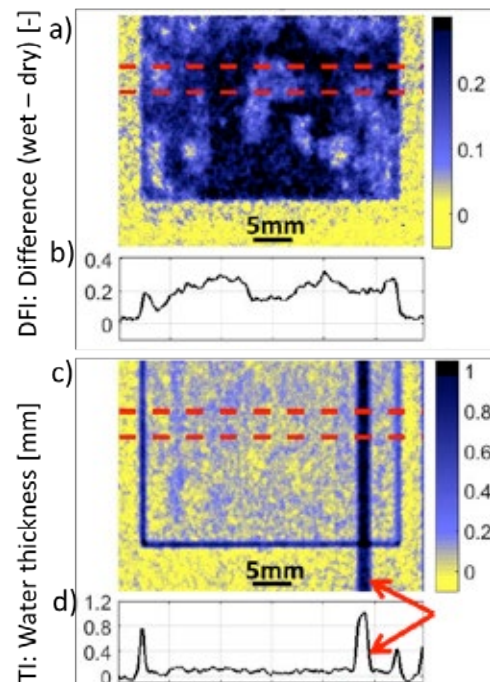
Figure 2 contains color coded dark-field (Fig 2a) and transmission (Fig 2c) images of the water signal obtained from a heavy water filled Freudenberg H2315 GDL. The water signal of the DFI (Fig 2a) was obtained by subtracting the intensity of the dry from the water filled GDL. For the TI (Fig 2c) the water thickness is calculated using Lambert-Beer-law and represented with a color code as well. The high contrast between wet and dry in the DFI is due to the significant difference in scattering length density between D<sub>2</sub>O and air. In analogy to Fig 1 the averaged signal intensity between the dashed red lines is also plotted (Fig 2b and d).

The most important difference between DFI (Fig 2a and b) and TI (Fig 2c and d) is that the 1 mm deep channel used for filling the GDL with water (highlighted with red arrows) results in a strong signal in the TI, whereas it does not appear in the DFI. Therefore, the DFI allows for an analysis of the water distributed in the microstructure over the whole surface area of the GDL without an overlapping (and disturbing) signal from the channel. In future studies, we aim to establish a quantitative relationship between the water thickness and microstructure in the GDL and the DF-signal during fuel cell operando experiments. This will allow for analyzing GDL water without the important perturbation by channel water inherent to transmission imaging.

## I. CONCLUSION

A high contrast between heavy water and air in the DFI allows for visualizing the water distribution in the GDL. The DF-signal is not disturbed by the water present in a 1 mm deep injection channel because the DF-signal is selectively sensitive to structures in a given size range, which scatter neutrons to

ultra-small angles. In addition, dark-field imaging can be used to visualize GDL damages. This is of potential interest for studies on the impact of freeze/thaw cycles.



**Fig. 2. Water distribution in a GDL: a) Difference of DFI between D<sub>2</sub>O- filled and dry GDL b) D<sub>2</sub>O thickness calculated from TI**

## ACKNOWLEDGMENT

The authors gratefully acknowledge Dirk Scheuble for building the experimental setup and for his support during experiments.

This study is financially supported by the PSI CROSS initiative.

## REFERENCES

- [1] Boillat, P., et al., *In situ* observation of the water distribution across a PEFC using high resolution neutron radiography. *Electrochemistry Communications*, 2008. 10(4): p. 546-550.
- [2] Grünzweig, C., et al., Design, fabrication, and characterization of diffraction gratings for neutron phase contrast imaging. *Review of Scientific Instruments*, 2008. 79(5): p. 053703.
- [3] Kaestner, A.P., et al., The ICON beamline - A facility for cold neutron imaging at SINQ. *Nuclear Instruments & Methods in Physics Research Section a-Accelerators Spectrometers Detectors and Associated Equipment*, 2011. 659(1): p. 387-393.



## LOCAL OPTIMIZATION OF PEMFC AND DMFC CATALYST LAYERS COMPONENTS FOR IMPROVED DURABILITY

C. Rabissi\*, M. Zago\*, M. Agostinelli\*, M. Odgaard\*\*, L. Grahl-Madsen\*\*, R. Marchesi\* and A. Casalegno\*

\*Politecnico di Milano, Dip. Di Energia, Via Lambruschini 4a, Milano (Italy)

\*\*EWII Fuel Cells A/S, Emil Neckelmannsvej 15, Odense (Denmark)

**Abstract** – Both *proton exchange membrane* (PEMFC) and *direct methanol fuel cells* (DMFC) technologies are limited in durability by a severe performance degradation determining a strongly localized heterogeneous components fading. Avoiding such localized early aging in critical areas could lead to improved durability for the overall device.

A custom macro-Segmented fuel cell hardware, provided with local reference electrodes, has been developed to perform a detailed local investigation of performance and durability. The analysis revealed uneven current distribution during operation, most likely due to uneven reactants and products distribution, particularly related to components localized flooding or dehydration. Inhomogeneous performance distribution showed a strong impact on MEA heterogeneous fading, revealing analogies between the two technologies. Local optimization of catalyst layers formulation and operating protocol have been developed, assisted by modeling simulations, aiming to an homogeneous operation. Important improvements have been obtained on durability, demonstrated by local degradation testing and by post-mortem analysis of samples, confirming the validity of the methodology and the large scope for improvements still available.

**Index Terms** - PEMFC, DMFC, local optimization, durability

### I. INTRODUCTION

*Polymer electrolyte membrane fuel cell* (PEMFC) is considered a promising technology, especially for power generation and vehicular applications, thanks to its favorable features: absence of liquid electrolyte, low temperature operation, fast startup, and high power density. The high-density liquid fueled *direct methanol fuel cell* (DMFC) technology represents a further development, particularly interesting for portable electronics and small vehicular applications. However, some detrimental factors still prevent large-scale diffusion of both technologies, mainly related to high cost of the materials and their durability [2]; particularly, locally resolved measurements and local post-mortem analysis [3,4] revealed the development of strongly heterogeneous degradation in aged cells. A prolonged local inhomogeneity in operating conditions might play a key role in early localized aging of cell components; thus, it has to be understood and properly mitigated to improve overall device's lifetime.

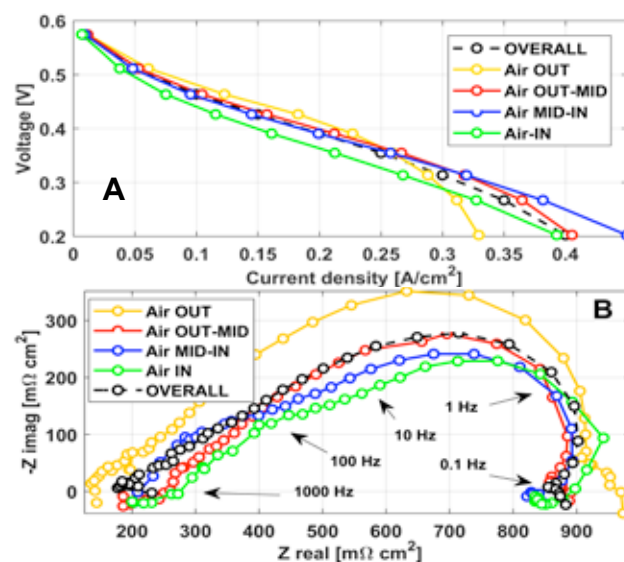
This work aims to elucidate the main mechanisms

originating such uneven distribution of current density over the cell active area, developing improvements in order to optimize cell operation in local stability and durability.

### II. EXPERIMENTAL METHODOLOGY

In order to perform a detailed investigation of localized performance and degradation over the cell surface and its originating mechanisms, a novel setup has been developed. The macro-Segmented Fuel Cell (mSFC) [1] permits an actively full control on each macro-segment of the cell, enabling complete electrochemical characterization of four macro-areas with limited reciprocal interference, without requiring any MEA segmentation. The prototype mSFC has four segments at both cathode and anode with four reference electrodes on a triple channel serpentine flow field and is suitable for square 25 cm<sup>2</sup> MEAs. Reference testing condition and protocols are thoroughly discussed in [3].

### III. EXPERIMENTAL INVESTIGATION



**Fig. 1. DMFC I-IV curves (A) and I-EIS (B) analysis**  
Regarding DMFC investigation, diagnostics based on *local polarization curves* (I-IV, Fig. 1A), and the respective *local*

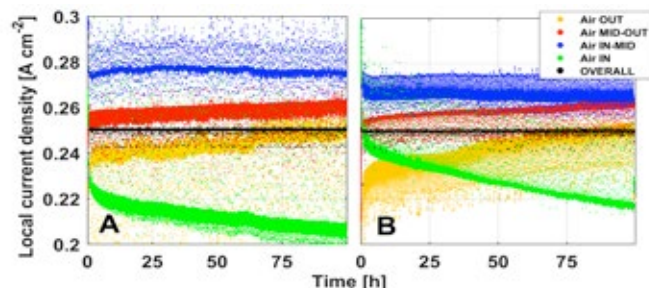


electrochemical impedance spectroscopy (I-EIS, Fig. 1B) performed at nominal current density ( $0.25 \text{ A cm}^{-2}$ ), permitted to confirm the strong local heterogeneity of current density distribution ( $\Delta i_{\text{MAX}}/i=32\%$ ) in reference operating condition at  $0.25 \text{ A cm}^{-2}$  and to elucidate the main determining mechanisms.

From an experimental local performance parametric characterization, the uneven distribution seemed mainly influenced by water-related limitations at cathode side:

- air-inlet area of the cell (green curves) appears as limited by dehydration, showing a noticeably higher slope of I-IV curves (Fig. 1A) and the highest value of *high frequency resistance* (HFR) together with the most prolonged linear branch among all I-EIS spectra (Fig. 1B). This has been related to the dehydrating effect of air feeding that, due to the high liquid content present at anode side, in DMFC is typically fed 15% RH or lower. Local polymer dehydration, both contained in the *catalyst layer* (CL) and constituting the electrolyte membrane, increase proton transport resistance of the components and determines a localized increase in ohmic and kinetic losses at cathode inlet area;
- air outlet area (yellow curves) shows flooding related mass transport limitations, showing a low limiting current density in the I-IV curves (Fig 1A), together with I-EIS disturbances at low frequency and the lowest HFR between all I-EIS spectra ( $150 \text{ m}\Omega \text{ cm}^{-2}$ , Fig 1B). This determines an incipient flooding condition that limits the proper diffusion of oxygen (already low in partial pressure) towards the active sites, determining noticeable concentration losses.

These steady-state limitations show up to increase in magnitude during actual cell operation, as in Figure 2A, where the current density distribution trend during a 100 h galvanostatic degradation test is reported.



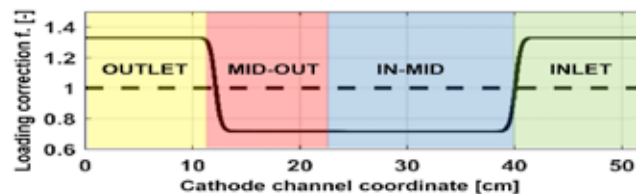
**Fig. 2. DMFC current density distribution during 100h degradation test before (A) and after (B) optimization**

PEMFC case, here not reported for sake of shortness, shows very strong analogies with DMFC case just analyzed, emphasizing strong similarities between the technologies.

#### IV. OPTIMIZATION

A deep analysis of the scientific literature [4] and the employment of a previously developed numerical model [5], properly improved, showed that good results might be obtained through proper MEA components local properties modification for both PEMFC and DMFC. Aiming to a uniform current distribution during operation, a novel MEA has been simulated, developed and realized by optimizing local catalyst and ionomer loading (increasing loading at inlet and outlet and

decreasing at cell center, as in Fig. 3), together with improvements of the operating protocol (based on cathode stoichiometry and RH optimization).



**Fig. 3. Improved catalyst loading profile**

The testing of the improved samples reveals stronger uniformity and stability in current density distribution, particularly due to cathode inlet area where performance is increased, enabling a sensible self-hydration mechanism. The performance homogeneity gain is noticeable also during actual operation (Fig. 3B), where the more uniform performance distribution showed to have an important beneficial effect on cell durability (degradation rate 50% to 70% lower on a 500-h basis) confirmed also by post-mortem analysis of aged samples, promisingly revealing a large scope for improvements.

#### V. CONCLUSION

This work, based on experimental local degradation investigation, post-mortem analysis and modeling simulation aimed to elucidate the mechanisms originating uneven fading of DMFC and PEMFC MEAs.

- Water distribution influences local current heterogeneity;
- Uneven operating condition promote fading of MEA critical areas;
- Modifying local CL formulation affects current distribution;
- Homogeneous current distribution during operation sensibly improves MEAs durability.

#### ACKNOWLEDGMENT

This work was supported by the FCH-JU FP7 project Second ACT (EC GA 621216).

#### REFERENCES

- [1] C. Rabissi, J.L. Bonde, et al., Novel macro-segmented fuel cell approach to investigation of localized degradation in PEMFCs, Proceedings of 6<sup>th</sup> European Fuel Cell EFC 2015
- [2] A. Mehmood, M.A. Scibioh, et al., A review on durability issues and restoration techniques in long-term operations of direct methanol fuel cells, J. Power Sources 297 (2015), 224-241
- [3] F. Bresciani, C. Rabissi et al., A combined in-situ and post-mortem investigation on local permanent degradation in a direct methanol fuel cell, J. of Power Sources 306 (2016), 49-61
- [4] Y. Zhang, A. Smirnova et al., Design of a proton exchange membrane (PEM) fuel cell with variable catalyst loading., J. of Power Sources 291 (2015), 46-57
- [5] M. Zago, A. Casalegno, et al., Water transport and flooding in DMFC: Experimental and modeling analyses. Journal of Power Sources 217 (2012), 381-391

## ECONOMIC AND ENERGY SAVINGS ANALYSIS OF PEM FUEL CELL BASED MICRO-COGENERATION SYSTEMS IN RESIDENTIAL APPLICATIONS

G. Di Marcoberardino\*, L. Chiarabaglio\*, G. Manzolini\*, S. Campanari\*

\*Politecnico di Milano, Dipartimento di Energia, Via Lambruschini 4, 20156, Milano, Italy

**Abstract** - This work, developed within the Italian project MICROGEN 30, aims at investigating the benefits of 10 kW<sub>el</sub> PEMFC based system with an innovative membrane reformer when applied to a residential application. Results are compared to solutions where a steam reformer is coupled with low temperature or high temperature PEM fuel cell stacks. The three CHP systems are integrated in a distributed generation scenario, working as suppliers of electricity and heat to two or more residential users. Micro-CHP energy and economic balance is evaluated using an in-house software, based on an heuristic algorithm that explores and defines the optimal CHP system operating strategy versus defined load and tariff profiles. The innovative configuration achieves the highest micro-CHP economic yearly. The economic analysis also sets the maximum cost of the innovative CHP system being economically competitive with respect to centralized power generation and conventional boilers. Results indicate the possibility of a successful commercial deployment when the system cost will fall in the range 2500-3500 €/kW.

**Index Terms** - Micro-CHP system; PEM fuel cell; Target cost; Annual energy balance

### I. NOMENCLATURE

CHP	Combined heat and power
HT/LT	High/Low temperature
MR	Membrane reactor
PEMFC	Polymer electrolyte membrane fuel cell type
RMF	Reverse metering factor
SR	Steam reformer

### II. INTRODUCTION

Over the last years, micro-CHP PEM fuel cell based systems overtook becomes a leading technology, also thanks to the high volumes deployed in Japan [1]. The growing market and development of PEMFC in small scale power production systems relies on their high net electric efficiency, very low pollutant emissions, fast start-up and modularity making them a promising option when applied to distributed cogeneration in the urban areas. As shown in Fig. 1, conventional fuel processor for hydrogen production consists of 4 stages: SR or ATR, two WGS and a PrOx. Fuel processor simplification is one of the main opportunities for reducing micro-CHP cost. So this work, developed within Italian project MICROGEN 30

(‘Industry 2015’ program), investigates the adoption of: (i) a membrane reformer reactor (MR) with the integration of hydrogen perm-selective membranes, thanks to their unique feature of separating pure hydrogen; (ii) HT-PEM fuel cell stack, allowing the use of lower purity reformed hydrogen (from HT-WGS) as fuel.

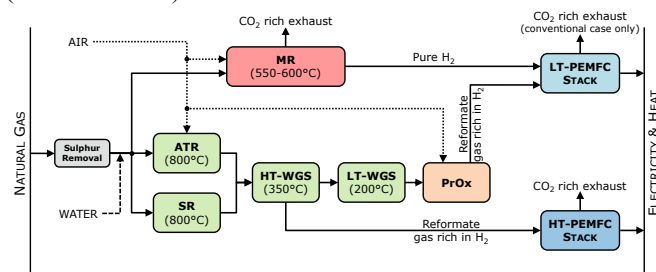


Fig. 1 Schematic diagram of conventional and innovative configurations for micro-cogeneration systems based on PEM fuel cell.

The benefits of applying a 10 kW<sub>el</sub> PEMFC based system with an innovative membrane reformer to residential users are compared to conventional or alternative solutions where a steam reformer is coupled with low temperature or high temperature PEM fuel cell stack. An annual micro-CHP simulation analysis of each solutions investigates (i) the advantages of a distributed small power production with respect to centralized power generation and conventional boilers in terms of economic saving and fuel consumption and (ii) the bearable capital cost of system based on PEM fuel cell.

### III. MICRO-CHP SYSTEMS PERFORMANCE

All the CHP systems models, designed for a net power output of 10 kW<sub>el</sub>, are developed in Aspen Plus<sup>®</sup>. Performance of the three systems were carried out both at rated and partial load highlighting that MR-LTPM has the best electric efficiency (42.7%), SR-HTPEM has the highest thermal efficiency (60.9%) while the total efficiency are quite similar (87-90%). No significant difference can be outlined at partial load, in Fig. 2, where electric efficiency increase for all the CHP up to 70-80% of the load. From a thermal point of view, the trend is similar in all cases: the thermal efficiency gets lower in off-design conditions.

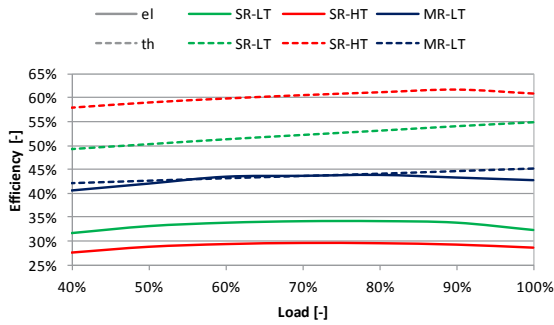


Fig. 2 Micro-CHP systems performance at partial load

#### IV. ANNUAL ENERGY AND ECONOMIC ANALYSIS

An economic analysis is appropriate for understanding the market potentialities of the three configurations when facing a combined heat and power application. A typical scenario of the electric and thermal network is shown in Fig. 3.

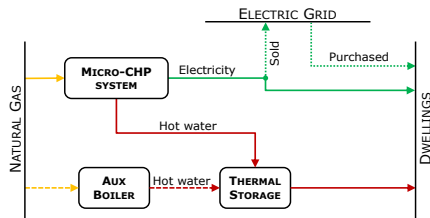


Fig. 3 Scenario scheme optimized with the model

The study is carried out with an in-house heuristic model developed by Group of Energy Conversion Systems (GECOS) at Politecnico di Milano [2] for combined heat, power and cooling plant (CCHP). The optimization model provides hourly detailed information about the operating conditions of the micro-CHP system together with the electric and thermal balance to the grid/user. The investigation of cases with 2, 4, 8, 12 and 24 dwellings, installing the unit in Germany or in Italy, is interesting to find the best option that maximize the yearly savings (and so the best size of the micro-CHP system). Fig. 4 shows a general increase of the savings when going from few to many dwellings. Increasing the number of dwellings yields different positive effects: (i) the electric and thermal demand is high enough to result in a continuous operation of the micro-CHP system, thus cutting down the start-up costs and working at high (close to nominal) efficiency; (ii) possible heat dissipations in time periods featuring an electrical-load driven regulation become smaller thanks to the larger average heat demand; (ii) for the SR-LTPeM and MR-LTPeM solutions, the cost of electricity produced by the micro-CHP is always cheaper than the electric grid electricity, even without any thermal demand. A target investment cost is finally calculated, defined as a 'maximum bearable cost' with the hypothesis of allowing the system to achieve an investment net present value (NPV) equal to 0 at the end of the CHP life. Maximum bearable investment costs of 2500-3500 €/kW are found for at least 12 dwellings and  $RMF > 0$  in the Italian case or for any  $RMF$  in

German case.

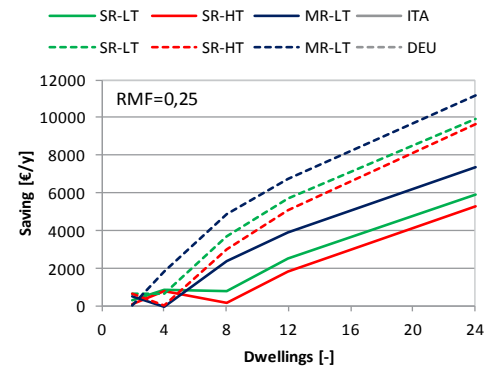


Fig. 4 Annual operating saving with a RMF equal to 0.25

#### V. CONCLUSION

This work summarized the potentiality of three micro-CHP PEMFC solutions to supply two or more residential users in a distributed generation scenario replacing the common electricity and thermal production technology. Thermodynamic analysis indicated that MR-LTPeM solution has the best electric efficiency (42.7%), SR-HTPeM has the highest thermal efficiency (60.9%) while the total efficiency are quite similar (87-90%). An annual simulation of the micro-CHP system was developed, revealing that economic saving increases with the number of dwellings and with RMF. Maximum bearable investment costs of 2500-3500 €/kW are found for at least 12 dwellings and  $RMF > 0$  in the Italian case or for any  $RMF$  in German case; although this is not yet the current cost of this type of CHP units, it can be achieved with a full industrialization and with mass production. In scenarios where the electricity sold to the grid has no economic value, combined with a too small dwellings number, the maximum bearable cost falls below 1000 €/kW indicating that there are limited chances that the system will be economically competitive even in the future, unless specific subsidies for energy savings are adopted by governments.

#### ACKNOWLEDGMENT

This work was partially funded within the Microgen30 project (EE01\_00013) funded by Italian Ministry of Economic Development with the program Industria 2015.

#### REFERENCES

- [1] D. Hart et al., The Fuel Cell Industry Review 2015, 2015.
- [2] A. Bischi et al., Cogeneration systems optimization: Comparison of multi-step and mixed integer linear programming approaches, Int. J. Green Energy. 13 (2016). doi:10.1080/15435075.2016.1161635.

## ECONOMICAL OPTIMIZATION OF A HYBRID SYSTEM GAS TURBINE SIZE WITH SOFC STACK DEGRADATION

A. Cuneo\*, V. Zaccaria\*\*, D. Tucker \*\*\* and A. Sorce\*

\*Thermochemical Power Group, Università di Genova, Via  
Montallegro 1, 16145, Genova, (Italy)

\*\* Mälardalen University, Högscoleplan 1, 72320 Västerås  
(Sweden)

\*\*\* U.S. DOE National Energy Technology Laboratory, 3610  
Collins Ferry Rd., 26507 Morgantown, WV (USA)

**Abstract** - The coupling of a pressurized solid oxide fuel cell (SOFC) and a gas turbine has been proven to result in extremely high efficiency and reduced emissions. The presence of the gas turbine can improve system durability compared to a standalone SOFC, because the turbomachinery can supply additional power as the fuel cell degrades to meet the power request. Since performance degradation is an obstacles to SOFC systems commercialization, the optimization of the hybrid system to mitigate SOFC degradation effects is of great interest. In this work, an optimization approach was used to innovatively study the effect of gas turbine size on system durability for a 400 kW fuel cell stack. A larger turbine allowed a bigger reduction in SOFC power before replacing the stack, but increased the initial capital investment and decreased the initial turbine efficiency. Thus, the power ratio between SOFC and gas turbine significantly influenced system economic results.

**Index Terms** – design optimization, economic analysis, hybrid systems, SOFC degradation

### I. NOMENCLATURE

C	Cost [\$]
$\eta$	Efficiency [%]
P	Power [kW]
EOL	End of life
GT	Gas turbine
IRR	Internal rate of return
mGT	micro gas turbine
SOFC	Solid Oxide Fuel Cell

### II. INTRODUCTION

Due to the growing global energy consumption, decreasing fossil fuel resources and increasing global environmental

concerns, finding an appropriate way for efficient power generation with low emissions has become a matter of issue. SOFC-gas turbine integration has attracted significant attention because of its high efficiency potential [1]. In pilot-scale plants, normally the SOFC generates most of the power, working with fairly high fuel utilization and high stack efficiency **Error! Reference source not found.** However, system performance optimization has been normally considered in design conditions, without considering stack performance degradation over time. The Authors previously analyzed the effect of fuel cell degradation on the hybrid systems performance, suggesting that a design in which fuel cell stack and gas turbine are about the same size could be beneficial from an economic point of view [3]. However, no optimization analysis was performed to understand the optimal power share between SOFC and gas turbine. In this respect, this study will fill the gap optimizing the mGT size with respect to the Internal Rate of Return (IRR).

### III. MODEL DESCRIPTION

The model used in this analysis is a 1D model that simulates a co-flow, planar, anode-supported SOFC. An overview of the hybrid system model is presented in Figure 1. The full description of the model is reported in [3]. The model includes a relationship to evaluate the SOFC degradation over time. The recuperated gas turbine cycle is modeled as a black box, based on a map of the recuperated cycle efficiency as function of generated power. A correlation between nominal mGT efficiency and mGT size was extrapolated from literature data as shown in Eq. 1 [4].

$$\eta = 22.237 \cdot P^{0.0606} \quad (1)$$



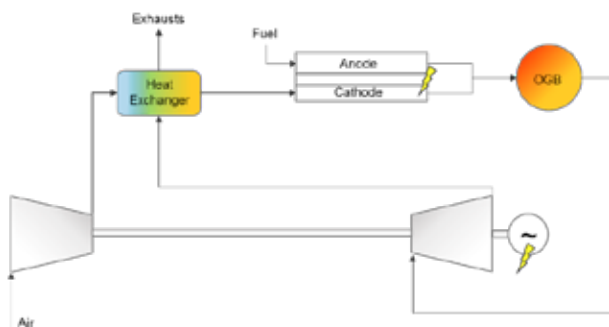


Fig. 1. Schematic layout of the hybrid system

An operating strategy in which fuel cell voltage and total system power are maintained constant was selected based on [3]. An economic analysis was implemented to evaluate the IRR. The system end of life (EOL) was evaluated as the turbine power reached the considered design condition, since total system power cannot be maintained constant after that point. The optimization problem was set to find the best mGT size to maximize the IRR considering both capital cost and variable costs. The economic assumptions were based on a previous work [3] referring to the USA market. A cost function for the mGT cost was extrapolated from industrial data and employed in the economic optimization [4]:

$$C = -159.7 \cdot \ln P + 2089.2 \quad (2)$$

#### IV. RESULTS

The optimization problem was solved using a genetic algorithm. The objective function to maximize was the IRR and the decision variable the mGT size, which was varied between 100kW and 500kW. Table 1 shows the main results for different mGT size; clearly, small mGT sizes allow a low capital cost but the fuel cell life is very short and the plant is not economically convenient. On the other hand, a large mGT allows a longer FC life but with an important capital investment.

TABLE 1  
MAIN PARAMETERS FOR DIFFERENT MGT SIZE (THE OPTIMUM POINT IS HIGHLIGHTED IN BOLD)

mGT size [kW]	190	250	300	350	400	<b>403</b>	450
mGT design efficiency [%]	0.306	0.311	0.314	0.317	0.320	<b>0.321</b>	0.322
Capital cost [k€]	557,7	621,9	673,5	723,8	772,9	<b>775,9</b>	821,1
FC life [Years]	1	2	3	7	20	<b>21</b>	40
IRR [%]	-0.799	-0.520	-0.175	0.068	0.126	<b>0.128</b>	0.101

Figure 2 shows both the power share between SOFC and mGT for four different mGT size and the efficiency profiles. The mGT works in a strong off-design condition at the beginning of the life, with a lower efficiency as the turbine size increases. The benefit of a larger turbine was, on the other hand, a longer system lifetime.

The optimization algorithm found the optimum point for an mGT size equal to 403 kW (in bold in Table1). Hence, the best economic condition to work with this kind of systems is to share the power between SOFC and mGT with a percentage of nearly 50%. In this way, the capital cost of the mGT is quite high but,

since the plant operates for a longer period, the capital cost is covered by the revenues from the electrical energy sold to the grid.

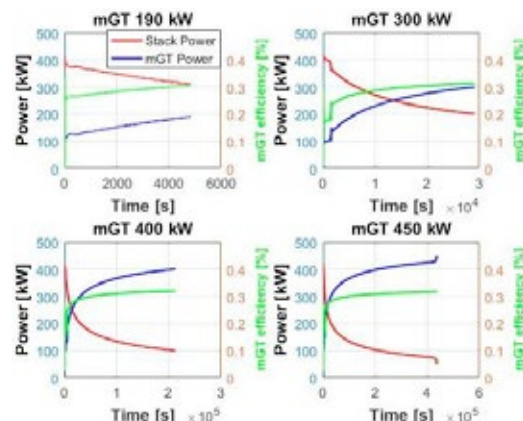


Fig. 2. Power share and mGT efficiency for different mGT size

#### V. CONCLUSION

An optimization study to understand the effect of the gas turbine size on system durability of SOFC/GT systems was performed. After evaluate the optimum gas turbine size, a detailed analysis of the fuel cell performance was analyzed. Although in current pilot-scale plants, normally the SOFC generates most of the power, if the SOFC degradation is considered in the design process, the best economic condition to work with this kind of systems is to share the power between SOFC and mGT with a percentage of 50%. Hence, in designing this kind of systems, the effect of SOFC degradation cannot be neglected

#### REFERENCES

- [1] Buonomano, A., Francesco, C., Dentice d'Accadia, M., Palombo, A., Vicidomini, M., Hybrid solid oxide fuel cells–gas turbine systems for combined heat and power: a review, Applied Energy, Volume 156, 2015, pp. 32-85
- [2] Kitagawa, Y., Tomida, K., Nishiura, M., Hiwatashi, K., Kishizawa, H., Oozawa, H., Kobayashi, Y., Takeuchi, Y., Mihara, M., Development of high efficiency sofc power generation at mhps, Fuel cell seminar and energy exposition, 2015
- [3] Zaccaria, V., Tucker, D., Traverso, T., A distributed real-time model of degradation in a solid oxide fuel cell, part I: Model characterization, Journal of Power Sources, Volume 311, 2016, pp.175-1816
- [4] Rosa do Nascimento, M.A., de Oliveira, L., dos Santos, E.C., Gomes, E.E.B., Fagner, Dias, L.S., Velásques E.I.G., Alexis, R., Carrillo, M., Micro Gas Turbine Engine: A Review, Progress in Gas Turbine Performance, 2013, Dr. Ernesto Benini (Ed.), InTech
- [5] Capstone, Product Specification Models C600, C800, and C1000 Capstone MicroTurbine, 460051 Rev. D (July 2009)



# POLYACRYLONITRILE DERIVED CARBON BASED NANOFIBER MATS AS CATHODES IN AIR-CATHODE MICROBIAL FUEL CELLS

Giulia Massaglia <sup>a,b,\*</sup>, Valentina Margaria <sup>a</sup>, Adriano Sacco <sup>a</sup>, Micaela Castellino <sup>a</sup>, , Marzia Quaglio<sup>a</sup>,

<sup>a</sup> Center For Space Human Robotics, Istituto Italiano di Tecnologia@POLITO, C.so Trento 21, 10129 Torino, Italy

<sup>b</sup> DISAT, Politecnico di Torino, Corso Duca Degli Abruzzi 24, 10129, Torino, Italy

**Abstract** –This work aims to optimize the performances of Air Cathode Single Chamber Microbial Fuel Cells (SCMFCs). To reach this goal, the attention is focused on the development of N-doped carbon nanofibers (N-CNFs) as catalyst layer at the cathode, leading thus to provide the direct oxygen reduction reaction (ORR). Therefore, the catalyst layer in SCMFCs must ensure a number of electrons as close as possible to the ideal value of 4. N-CNFs, thanks to their content of nitrogen defects together with their high surface area, are among the most promising catalyst layer at the cathode. N-CNFs are prepared by using electrospinning technique, starting from a polymeric solution containing polyacrylonitrile. The spun nanofibers were stabilized at 280 °C in air and thermally treated at 900 °C under inert atmosphere for 1 hour. The good electrochemical behavior and typical properties of the nanostructures permitted to apply N-CNFs as catalyst layer in SCMFCs.

**Index Terms** – N-doped Carbon Nanofibers, Electrospinning, Single Chamber Microbial Fuel Cells, polyacrylonitrile.

## I. NOMENCLATURE

Polyacrylonitrile (PAN); N-doped Carbon nanofibers (N-CNFs); Platinum/carbon (Pt/C); Single Chamber Microbial Fuel Cells (SCMFCs); N-N dimethylformamide (DMF); commercial carbon paper (CP); X-ray photoelectron spectroscopy (XPS); Rotating Ring Disk Electrode (RRDE);

## II. INTRODUCTION

Nowadays the presence in water of various compounds, deriving from synthetic and natural traces, can induce

effects on its quality and on human health [1]. The development of strategies to clean water is one of the main humanitarian targets of the future. The SCMFCs can represent a new method able to monitor the water quality, obtaining real time in situ measurements and with good operational stability [2]. SCMFC is a bio-electrochemical system able to directly transduce the chemical energy into electrical energy by the action of microorganisms (exoelectrogens), which are able to oxidize the organic matter (so called fuel). In this configuration, the oxygen is the terminal electron acceptor. The catalyst layer must ensure a number of electrons as close as possible to the ideal value of 4, leading thus to ensure the direct oxygen reduction reaction (ORR) and avoid the intermediate reduction reaction, which releases H<sub>2</sub>O<sub>2</sub> that is toxic for microorganisms. Platinum is currently the best performing catalyst, however it is expensive and not-abundant, then its application must be limited. In order to develop a nanostructured material with a high surface area, able to increase the number of catalytic sites exposed to oxygen, carbon nanofiber mat is investigated [3]. Indeed, N-CNFs, thanks to their content of graphitic, pyrrolic and pyridinic nitrogen defects together with their high surface area, are among the most promising catalyst layer at the cathode [3]. N-CNFs are prepared by using electrospinning technique, starting from a polymeric solution containing PAN, chosen thanks to its high yield of carbonization together with its high content of nitrogen. As spun these nanofibers were stabilized at 280 °C in air and thermally treated until 900°C under inert atmosphere for 1h to obtain N-CNFs. XPS confirmed a high content of graphitic nitrogen and a proper amount of pyridinic one in CNFs, leading thus to improve

ORR performances. Good electrochemical properties of the samples were established by Rotating Ring Disk Electrode (RRDE). The calculated electron transfer number is equal to 3.9 for N-CNFs, which is quite similar to the ideal value of 4, obtained with Pt/C catalyst used as reference materials. The good electrochemical behavior and typical properties of the nanostructures permitted to apply N-CNFs as catalyst layer in SCMFCs. In order to evaluate the performances of the nanostructured material in SCMFCs, N-CNFs or Pt/C catalysts were deposited on carbon paper (CP).

### III. EXPERIMENTAL SECTIONS

#### A. Material and Methods

PAN (average molecular weight Mw=150,000kDa) and DMF (assay 99.8%) were purchased from Sigma Aldrich. Samples were prepared by electrospinning technique, starting from polymeric solutions containing 12wt% PAN in DMF. As spun these nanofibers were stabilized at 280 °C in air and thermally treated at 900°C under inert atmosphere for 1h to obtain conductive N-doped carbon nanofibers. XPS is performed in order to establish the nitrogen defects content and its position related to the nearby carbon atoms in the main chains of N-CNFs. N-CNFs are characterized by a high content of graphitic nitrogen and by an enough amount of pyridinic and pyrrolic nitrogen, as shown in Fig.1a).

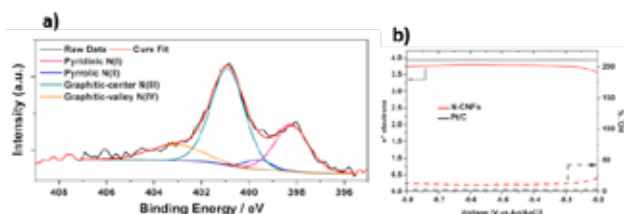


Fig. 1. a) High-resolution N1s spectra for N-CNFs; b) Comparison of electron transfer number (left axis) and peroxide hydrogen (right axis) evaluated from RRDE measurements of N-CNFs (purple line and dash line) compared with the commercial catalyst based on Pt/C (black line and dash line)

Moreover, this sample is characterized by a high electrical conductivity, close to 0.5 S/cm. All these properties of N-CNFs, such as high conductivity, high content of graphitic nitrogen and an enough amount of pyridinic and pyrrolic nitrogen, enhance their electrocatalytic behaviour for ORR, as also confirmed by several work in the literature [3]. The RRDE technique allows validating the catalytic pathways of the proposed materials by using 4-electrodes measurements. RRDE measurements were performed by cathodically scanning the disk electrode in the range  $-0.3 \div -0.8$  V vs Ag/AgCl with fixed scan rate (5 mV/s) and rotating speed (2500 RPM); the ring electrode was maintained at 0.2 V. In particular, the currents of disk and ring are measured; the disk current is related to the four-electron ORR of the analysed materials, while the current of the ring electrode is associated to the two electron ORR peroxide species [4]. The percentage of  $\text{H}_2\text{O}_2\%$  and the electron transfer number were calculated with the following equation (1):

$$\text{HO}_2^- \% = 200 \times \frac{I_{\text{R}}/N}{I_{\text{D}} + I_{\text{R}}/N} \quad n = 4 \times \frac{I_{\text{D}}}{I_{\text{D}} + I_{\text{R}}/N} \quad (1)$$

The Fig.1b). shows the results for N\_CNFs, compared with the Pt/C, which ensures a number of electron equal to 3.96. It is possible to notice that N-CNFs provides a number of electron transfer close to 3.9, indicating that this catalyst proceeds the direct ORR through an efficient 4-electron pathways similar to that of Pt/C electrode.

Thanks to their good electrochemical properties and their morphological characteristics, N-CNFs, developed as catalyst layer on the cathode, optimize the SCMFCs overall performances. Indeed, the maximum power density reached with N-CNFs (close to 150 mW/m<sup>2</sup>) is two order of magnitude higher than the one obtained with Pt catalyst layer (equal to 4 mW/m<sup>2</sup>), as sketched in Fig.2.

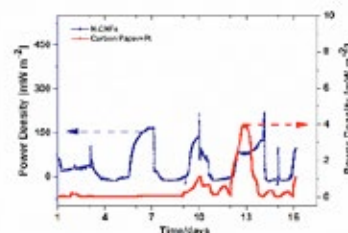


Fig.2. Comparison of power density trend of SCMFCs with N-CNFs as catalyst layer (left axis) and power density trend reached by SCMFCs with Pt/C catalyst layer, defined as reference cathode electrode (right axis)

### IV. CONCLUSION

In this work, we demonstrate the optimization of SCMFCs obtained by designing N-CNFs as catalyst layer on the cathode electrode. Indeed, N-CNFs showed good electrical conductivity and exhibited noticeable features for their application as an ORR catalyst, thanks to its high amount of graphitic-N together with the content of pyridinic-N, as confirmed by XPS. Their good electrochemical properties, added to all intrinsic properties of the nanostructures, permitted to develop this sample as catalyst layer on cathode electrode in SCMFCs. We designed the cathode electrode by applying N-CNFs on commercial carbon based electrode (CP), compared with Pt/C deposited on CP, used as reference material. The obtained results confirm the improvement of overall device performance with N-CNFs as catalyst, leading to reach a maximum power density two order of magnitude higher than the one obtained with Pt/C layer.

### REFERENCES

- [1] Schwarzenbach R et al. The challenge of micropollutants in aquatic systems. *Science* 2006; 313: 1072-1077
- [2] Di Lorenzo et al., A small-scale air-cathode microbial fuel cell for on-line monitoring of water quality. *Biosensors and Bioelectronics* 2014; 62:182-188
- [3] Yang D.S et al. Preparation of Nitrogen-Doped Porous Carbon Nanofibers and the Effect of Porosity, Electrical Conductivity, and Nitrogen content on their Oxygen Reduction Reaction Performance. *ChemcatChem*. 2014, 6: 1236-1244
- [4] Orazem M., Tribollet B. *Electrochemical impedance spectroscopy*. Hoboken, New Jersey: Wiley, 2008

## DEMCOPEM-2MW COGENERATIVE PEM FUEL CELL UNIT FOR HYDROGEN RECOVERY FROM CHLOR-ALKALI INDUSTRY IN CHINA: FIRST MONTHS OF OPERATION AND PRELIMINARY DATA ANALYSIS

G. Guandalini\*, S. Foresti\*, S. Campanari\*, J. Coolegem<sup>o</sup>, J. ten Have<sup>^</sup>

\*Politecnico di Milano, Energy department, Milano (Italy)

<sup>o</sup> Nedstack fuel cell technology B.V., Arnhem (The Netherlands)

<sup>^</sup> MTSA Technopower B.V., Arnhem (The Netherlands)

As part of demonstrative DEMCOPEM-2MW FP7 EU Project, the 2-MW world largest PEM fuel cell unit was built and set in operation in September 2016. The plant recovers byproduct hydrogen from a chlor-alkali chemical plant in China, supporting the stability of electricity supply to the chemical plant. First months of operation data are now available, evidencing an actual performance coherent with the expected net electric efficiency (about 50%). The plant will be operated for several months, gaining experience on PEM fuel cell management and performances in real industrial environment. The influence of boundary conditions on decay is also object of the investigation.

**Index Terms** - chlor-alkali plant, DEMCOPEM-2MW, hydrogen recovery, PEM fuel cell

### I. NOMENCLATURE

BOL	Beginning of Life
PEM FC	Polymeric Electrolyte Membrane Fuel Cell

### II. INTRODUCTION

The 2-MW world largest PEM fuel cell unit of the DEMCOPEM-2MW project was installed in the chlor-alkali plant in China and started the production in September 2016. After an initial period of partial load operation, 2-MW full power has been reached at the beginning of the year. The plant layout includes blowers, humidifiers and heat recovery sections, as depicted in Fig. 1.

The modular plant recovers the byproduct hydrogen of the chemical process, valuing it as electricity for the electrolysis units of the plant. The unit supports the economics, reducing at the same time the risk of grid electricity shortage. The plant is also designed for low-temperature (about 60 °C) heat recovery from stacks cooling system (HX 2); in case of no thermal load, the corresponding heat is dissipated (HX 3). It should be noticed that this heat is currently not exploited by the chemical

plant and therefore thermal efficiency is only an estimate based on measurements.

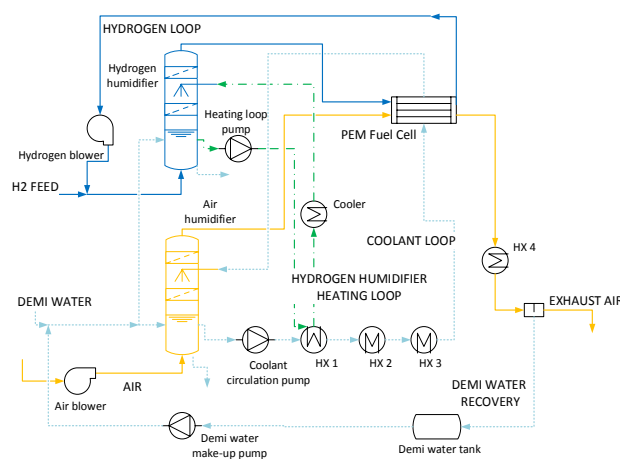


Fig. 1 - Simplified DEMCOPEM plant layout

Demi water is condensed from the exhaust air flow (HX 4) and recovered in the plant.

Modeling of the large PEM FC systems has been performed, considering the appropriate detail level [1] and previous experience [2]; lumped approach for cells modeling is considered as far as for other main components (blowers, humidification). All the interactions between components and the influence of operating conditions (load, temperature, reactants excess) are taken into account. A constant decay is also assumed for FC voltage that allows to investigate the trend of plant performance during lifetime. Comparison with on-field measurements yields errors of few percentage points, validating the approach and the modelling of components. The model is able to accurately simulate the operating point of the stacks at different load conditions and excess air flow. The resulting performances of the plant are in line with the expected values,

confirming the validity of the technological solutions adopted. Simulated operating conditions slightly differ from the measurements from the plant, supporting the investigation of unexpected phenomena and the operation strategy definition.

### III. PLANT OPERATION

The plant has been operated for several months without relevant issues, resulting in high availability. Nevertheless, operation hours are slightly lower than expected, but they were strongly influenced by the availability of high-quality hydrogen from the upstream industrial plant. Actually, the coupled chemical plant management strategy reduces hydrogen production, limiting the average capacity factor of the PEM plant to about 62%, with the plant working often at partial load (some groups in hot stand-by).

During the first ten months of operation, more than 5.8 GWh<sub>el</sub> have been produced and the heat available for recovery has been about 3.0 GWh<sub>th</sub>, as shown in Fig. 2. Because of some discontinuous data acquisition, about 20% of the data are estimated considering average production in the period. More than 350 tons of byproduct hydrogen has been recovered. The avoided CO<sub>2</sub> emissions are calculated considering the reduction of electric consumption of the chlor-alkali plant. This substituted electricity would have been produced by Chinese power system, for which an average emission factor of 1100 kg<sub>CO2,eq</sub>/MWh<sub>el</sub> has been assumed.

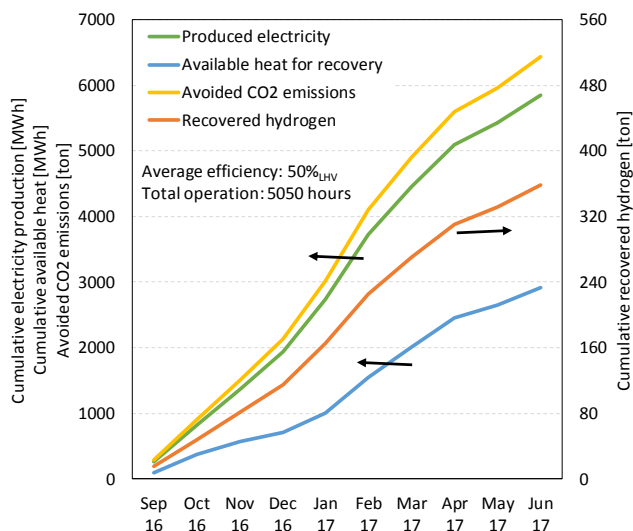


Fig. 2 – Cumulative electricity and heat production during first months of operation, and corresponding recovered hydrogen and avoided emissions (20% of the data are estimated because of lack of measurements).

Globally, the plant electrical efficiency remains around 56-57% (gross electrical efficiency) and around 50% (net electrical efficiency). The measured BOL electric efficiency was 55% (beyond the estimated project objectives), while the heat available for recovery is about 21% of the input, resulting in a theoretical combined heat and power efficiency of 76 % (to be compared with the expected value of 85%). Anyway, the harsh

climate strongly influences the performances of the plant; a reduction of thermal efficiency to 12-17% was measured during winter months, when air temperatures dropped below 0°C.

The simulated energy balance of the plant is presented in Fig. 3, at BOL and after 1000 hours of operation, evidencing the contribution of the different components.

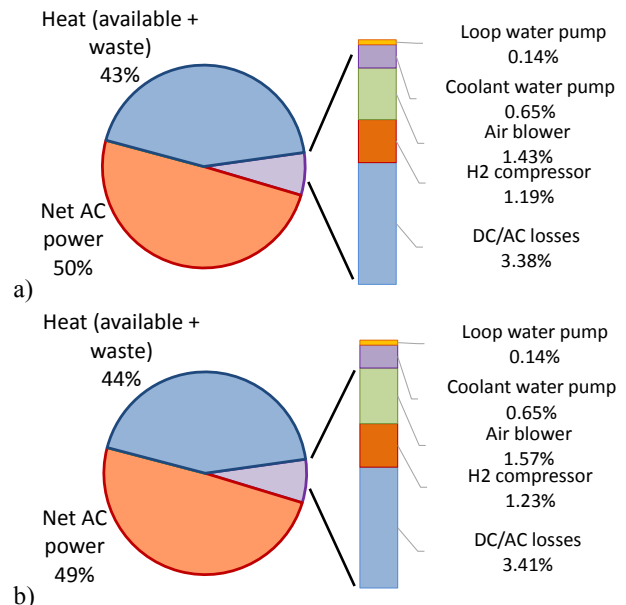


Fig. 3 – Plant energy balances at a) BOL and b) after 1000 hours of operation

### IV. CONCLUSION

In conclusion, the use of a cogenerative PEM FC system is a suitable solution for hydrogen recovery in chlor-alkali plants, where energy consumptions are high and high purity hydrogen is available as byproduct. The actual performance is coherent with the expected net electric efficiency (about 50%). From long-term operation estimations, based on plant simulation, the electric efficiency loss during lifetime (about 6%) is partially recovered as additional heat. Most of the thermal energy is anyway lost because of the low flexibility of the heat circuit of the industrial plant, leaving room for a better integration between the chemical plant and PEM FC systems.

### ACKNOWLEDGEMENTS

This work was carried out in the framework of the FP7-FCH-JU project “DEMCOPM-2MW”, cofunded by the FCH JU under grant agreement n° 621256.

### REFERENCES

- [1] Guandalini G., Foresti S., Campanari S., Coolegem J., Ten Have J., “Simulation of a 2 MW PEM Fuel Cell Plant for Hydrogen Recovery from Chlor-Alkali Industry”, Energy Procedia, 105, pp. 1839-1846, 2017.
- [2] Verhage A., Coolegem J. *et al.*, “30,000 h operation of a 70 kW stationary PEM fuel cell system using hydrogen from a chlorine factory”, Int J of Hydrogen Energy, 38(11), 2013



## ***SOLAR-ASSISTED REVERSIBLE SOLID OXIDE CELL (RSOC) INTEGRATED WITH HEAT-PIPES FOR ELECTRIC ENERGY STORAGE AND H<sub>2</sub> PRODUCTION: TECHNICAL ASSESSMENT***

G. Guandalini\*, L. Mastropasqua\*, D. Straniero\*, S. Campanari\*, D. Ferrero\*\*, A. Lanzini\*\*, M. Santarelli\*\*

\*Department of Energy, Politecnico di Milano, Via Lambruschini 4, 20156 Milan (Italy)

\*\* Department of Energy (DENERG), Politecnico di Torino, Corso Duca degli Abruzzi 24, Torino 10129 (Italy)

*This work explores reversible high-temperature solid oxide cells (rSOC) and the possibility of integrating the thermal need of the electrolyser with concentrated solar power (CSP). The system can act both as fuel cell (SOFC) and electrolyser (SOEC) with a single Balance of Plant (BoP), exploiting the same heat recovery heat exchangers network and feed systems. The produced hydrogen and oxygen-enriched air streams are stored in pressurised tanks and consumed during reverse operation. The stack thermal management is addressed through layers of heat pipes integrated in the stack and connected to an external high temperature molten salt heat storage. The cell is operated below the thermoneutral voltage in SOEC operation, in order to exploit the stored heat. The overall system is modelled considering the case of a 20 kW modular unit. Single-step hydrogen production electric efficiency is around 80%, and the resulting ideal system round trip efficiency (RTE) is approximately 60%.*

**Index Terms** – reversible SOC, electric energy storage, hydrogen, heat pipes

### **I. INTRODUCTION**

The reliable integration of large shares of renewable sources of electricity is one of the most disputed factors in sustainable electricity supply, due the low dispatchability of wind and solar photovoltaic (PV) power generation. In this scenario, energy storage systems (ESS) could act as regulators that manage fluctuations, improving system flexibility and aiding the transition to newer and cleaner generation technology [1].

Within this background, electrochemical systems are receiving increasing attention due to their potential to act as a high-efficiency and zero-emission long-term energy storage, able to perform energy management services including energy seasonal shifting and peak shaving. They store energy in hydrogen or other syngas fuels when low-priced electrical energy is available on the market (e.g. due to a surplus of renewables) and produce electrical power back during peak loads. With respect to conventional electrochemical storage,

based on different charge/discharge technologies (e.g., alkaline electrolyzers and PEM fuel cells), a reversible system has the potential to reduce investment costs and complexity, performing the task through a single electrochemical device.

In this work, an innovative configuration of electrochemical energy storage, reversible Solid Oxide Cells (rSOC) is proposed and analysed. The main goal of the study is to envisage a system to be coupled with a 30 MW wind farm [2] and balance the prediction error on the produced power output which can be sold on the energy market (improve dispatchability).

### **II. PLANT MODELLING**

A zero-dimensional cell model is built, able to represent electrochemical and thermal phenomena in both electrolysis and fuel cell modes. A state-of-the-art Ni/YSZ-supported planar SOC is fed with pure hydrogen only. Polarization curves are obtained at different temperatures, 750°C and 850°C and validated against experimental data from literature [3].

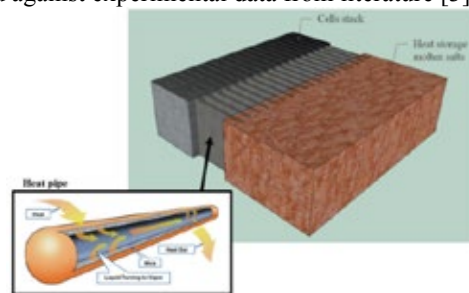


Figure 1 – Schematic representation of the integration between the rSOC stack and the thermal storage via heat-pipes

The resulting electro-chemical cell model is integrated in the overall plant simulation that computes the thermodynamic properties of each state of the process and solves material and energy balances (AspenPlus process simulator). The system is



designed to exploit the same BoP for both SOEC and SOFC modes, reducing the system complexity and costs and ensuring an easier plant management. SOEC and SOFC operation is respectively set at 750 and 850 °C as inlet stream temperatures. The SOFC works always in exothermic regime while SOEC is characterised, in our design, by an endothermic behaviour (sub-thermoneutral voltage operation). In a well-balanced system, the heat requirement of the latter is satisfied by the waste heat surplus from the former. The thermal management is performed by means of a thermal storage (molten salts from solar applications – KCl-MgCl<sub>2</sub> [4]), whose integration with the cells stack is carried out via reversible heat pipes (see Figure 1). They exploit a phase-changing working fluid (sodium – Na) that continuously circulates internally from the cooler to the hotter section, moved by diffusion in a wick.

Finally, SOEC operation requires high temperature water vapor feed. The required thermal power to the evaporation section is provided by a direct steam Fresnel collector, supported by the thermal storage at low irradiance, as depicted in Figure 2.

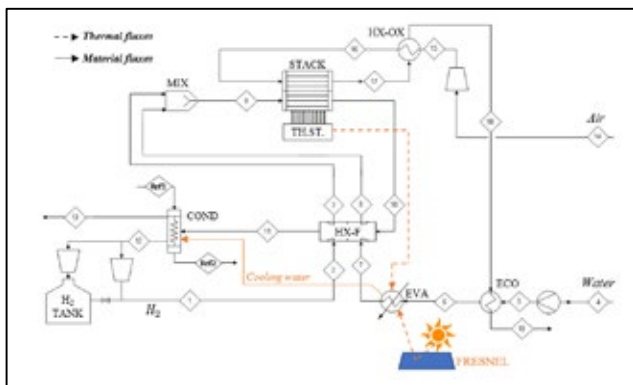


Figure 2 – System layout and integration with a Fresnel collector

### III. RESULTS AND DISCUSSION

The working strategies are envisaged to operate the system as a pure energy storage one, so hydrogen should be consumed by the system itself at the end of the considered time period.

The system is simulated with two diverse energy input profiles: a) ideal case with sinusoidal energy input/demand; b) real profiles of a 30 MW wind farm.

Case “a” is useful to highlight which are the self-sustaining operating conditions in the considered time period and which are characterised by an incompatibility (either due to hydrogen or heat shortage in the system balance) with the provided profiles. It can be shown that operation may determine a continuative heat defect in the system; a possible solution, considered in this work, is the integration of thermal resistances into the molten salts heat storage to provide the required heat at the expense of an increase of power demand. Nevertheless, this procedure negatively affects the RTE, that drops from theoretical system efficiency of 63% (case with no losses) to values around 57%, but ensures a satisfying number of equivalent hours (Capacity Factor CF approx. 65% on a month basis).

When taking into account the effects of thermal losses and also stack thermal ramp limitations (100°C/h), the RTE can approach 50% if the system is operated with the aid of the following strategies:

- Limitation of SOFC nominal power output
- Increase of the SOEC vs. SOFC nominal power ratio
- Improved thermal insulation and sizing of heat storage for loss minimisation
- Electrical reheat of molten salts heat storage
- Correct phasing between the daily energy input profile with the solar irradiation one

The coupling with the real energy profile (case “b”) is performed sizing the rSOC system to an input capacity of 2 MW. The results show an RTE on annual basis of about 40% in the best case and above 5600 equivalent operating hours. The fraction of energy input dissipated due to heat losses is ~34%, evidencing that further optimisation of heat management is required to reach competitive performances. However, the system successfully operates with a seasonal shifting, working as a net producer during summer periods and storing energy in winter months.

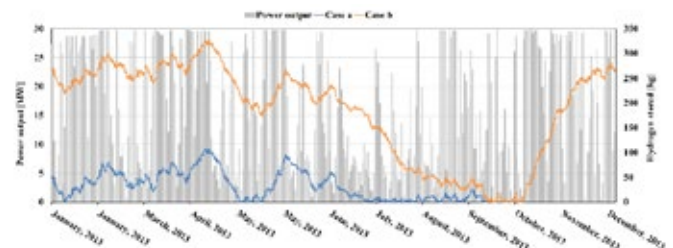


Figure 3 – Wind plant power output and stored hydrogen profile with (a)  $H_{2,in}=50$  kg (b)  $H_{2,in}=269$  kg

### IV. CONCLUSIONS

This work shows how a rSOC plant with integrated heat storage has the potential of performing a flexible correction of the energy production forecast for an intermittent RES, carrying out seasonal energy shifting in the year time-frame. Future developments and improvements of the system design and operation will focus on the improvement of RTE, optimisation of thermal management and of the choice of nominal conditions in relation to the specific coupling with the renewable energy profile. The economics of the proposed reversible energy storage system will be evaluated considering also the possibility of selling services on the electricity market and the production of synthetic fuels.

### REFERENCES

- [1] IEA (International Energy Agency), Harnessing variable renewables: A guide to the balancing challenge, OECD/IEA, Paris, France, 2011.
- [2] G. Guandalini, S. Campanari, Wind power plant and power-to-gas system coupled with natural gas grid infrastructure, in: Proc. ASME Turbo Expo 2015, Montreal, Canada, 2015.
- [3] P. Kazempoor, R.J. Braun, Model validation and performance analysis of regenerative solid oxide cells for energy storage applications, Int. J. Hydrogen Energy. 39

## EXPERIMENTAL INVESTIGATION OF AN ELECTRIC MINIBUS WITH A FUEL CELL RANGE EXTENDER

M. Villarini\*, G. Malandrino\*\*, and E. Bocci\*\*\*

\*Tuscia University, via S. Camillo De Lellis, snc - 01100 Viterbo, Italy

\*\*Enertecna s.r.l., via della Polveriera, 14 - 00184 Rome, Italy

\*\*\*Marconi University, v. Via Plinio 44 - 00193 Rome, Italy

**Abstract** - Promotion of public transportation can become an effective way to address land transport problems if its development is accompanied by reduction of energy consumption and pollutants emission. An experimental analysis of a 4285 kg electric driven minibus powered by fuel cells has been accomplished in order to set out the detailed energy consumption and assess the potential of technology evolution. A 12 kW fuel cell stack powers a plug-in electric powertrain composed of a 24.8 kW electric traction motor, capable of recovering brake energy, and a 72V/125Ah battery representing the electric energy storage. The fuel cell supplies power, by a 38-58V/72V DC/DC converter, and can feed the traction battery or, through a DC Bus and a chopper, the electric motor. The battery feeds the electric motor by the DC Bus as well. Energy consumption of auxiliary components are fed by a dedicated battery. Purpose is to evaluate system's performances.

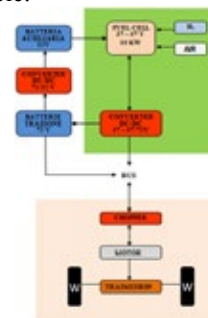
### I. INTRODUCTION

Continuous variations in the running of an urban vehicle in urban area increase traction consumption and then pollution. Electric vehicle has more advantages (both technical and economical) than endothermic motor vehicle[1]: high performance in paths with frequent stops; energy recovery in braking phase; high energy efficiency. Coupling battery supply and fuel cell (FC) is a new scenario of research [2] and is an economic alternative compared to traditional vehicles. An obstacle is short life span of the devices used [3]. Literature shows examples of hybrid vehicles suitable to public transport but does not treat a realistic stress test in term of load and so the main purpose of this paper is to analyze the complete potential of an electric minibus. Powertrain, data interface and monitoring system of vehicle have been described. Methodology encompassed both 3 different loads (225 kg, 700 kg and 1120 kg) tests and endurance tests of minibus consumption.

### II. MINIBUS

The fuel cell delivers current to a voltage that varies in the range 38÷58 V(peak current 350 A); a DC/DC converter raises and stabilizes the voltage at 72 V(for the BUS operating), also recharges 72 V battery.

The 125 Ah traction batteries, also rechargeable by plug-in, power the bus. All the power generated feed the chopper; chopper performs the function of regulating the voltage level and supply electric motor; it also provides a power return to the traction batteries during braking phase. Electric motor, through a reducer, divides the power to the front wheels (Figure 1). In Table 1 are summarized most important parameters of the vehicle.



TecnoBus Gulliver U520ESP			
DIMENSION[m]		MASSE[kg]	
Length	5.30	Tare	4285
Length	2.07	Axis ant.	2050
Height	2.75	Axis post.	2235
Height from ground	0.16	Total mass	6045
Motor PME TA18			
Position	front		
Supply	72 V CC		
Eccitation	series		
Cooling	Forced air		
Max Power	24.8 kW		
Max Torque	235 Nm		
Supply current	Max 600 A		

**Figure 1 Block scheme of system (left), Minibus and motor parameters (right)**

### III. EXPERIMENTAL SETUP AND MODEL

For calculation of theoretical power required for the vehicle to complete the various load cycles, considered forces that come into play during the motion of vehicle: force of inertia; force of gravity; resistance to motion (tire friction and aerodynamic resistance). Result of forces is:  $F_m = F_{in} + F_g + F_r$

1.  $F_{in} = m \cdot a$ , it's force applied to mass  $m$  and  $a$  it's acceleration produced;

2.  $F_g = m \cdot g \cdot \sin(\alpha)$ , it is the gravity force component along the vehicle direction;
3.  $F_{rp} = m \cdot g \cdot f_0 + m \cdot g \cdot K \cdot V^2 + 0.5 \cdot \rho \cdot S \cdot C_x \cdot V^2$ , it is the resistive force, depending from tire friction ( $m \cdot g \cdot f_0 + m \cdot g \cdot K \cdot V^2$ ) and aerodynamic resistance ( $0.5 \cdot \rho \cdot S \cdot C_x \cdot V^2$ ).

Overall power needed by vehicle motion is:

$$P = (m \cdot a + m \cdot g \cdot \sin(\alpha) + m \cdot g \cdot f_0 + m \cdot g \cdot K \cdot V^2 + 0.5 \cdot \rho \cdot S \cdot C_x \cdot V^2) \cdot V$$

Measurements were realized by means of the bus control and Labview.

#### A. Bus Control

Bus Control is a software for dialogue with digital dashboard of vehicle. This software through a serial cable has allowed to communicate with the graphical interface of the on-board display, to monitor certain operational magnitudes, to set specific parameters and to save real time data during load cycles. Chosen the acquisition rate (2Hz), data were transferred to the excel platform to be processed: bus speed; itineraries covered; hours of bus operation; voltage of traction batteries; current supplied by traction batteries and residual energy; auxiliary battery voltage; temperature of motor and of traction batteries.

#### B. Labview Acquisition

Field point modules, controlled through LabVIEW (National Instruments), permitted voltage and current measurements (1 to 10Hz acquisition frequency). Field point is supplied with lead/acid battery (12V from 56Ah). Data has been sent to a pc where is installed Labview.

### IV. RESULTS

Three experiments were carried out by covering, by the minibus, an asphalt distance of 1671 m in the first test and 1635 m in the second and third. Weight load of the minibus affects vehicle performances that are better at lowering of weight loads with the only exception of recovered energy which assumes higher values for a load increase. Increase of weight, raises energy required to brake vehicle and, therefore, energy that can be recovered. Furthermore, tests of vehicle autonomy have been made, lap taken by the vehicle is represented by a ring of about 104 meters, with 3 people and equipment on board. 9985 m were traveled in 2702 s, on road mainly composed of ground ( $f_0 = 0.020$ ). Data are contained in Table 1:

	Test 3 persons	Test 10 persons	Test 15 persons	Autonomy test 3 persons
Mass [kg]	4520	4995	5415	4520
Meters covered[m]	1671	1635	1635	189150
Time [s]	303	386	398	51185
Speed (*) [km/h]	33.20 19.90 11.60	30.00 15.40 10.10	30.10 14.80 10.90	21.70 13.30 4.60
Acceleration (**) [m/s <sup>2</sup> ]	-2.00 2.00	-1.78 2.17	-1.50 1.61	-1.39 1.39

Voltage (***) [V]	61.80 82.40 71.40	60.90 82.30 74.70	65.80 85.10 78.20	52.30 73.90 64.00
Current (***) [A]	-41.30 431.50 113.50	-35.00 570.20 108.80	-49.10 477.30 111.20	-34.00 335.00 115.00
Theoretical Power (***) [kW]	-24.80 24.40 4.10	-17.20 26.40 4.30	-22.10 26.30 4.50	-11.98 17.25 3.61
Real Power (***) [kW]	-3.30 26.60 7.70	-2.80 34.80 7.80	-4.10 34.60 8.30	-2.20 20.70 7.00
Theoretical Energy [J]	2219627	2727595	3072385	332564561
Real Energy [J]	2395836	3050602	3322066	359979179
Recovered Energy [J]	45059	38057	60055	4303395

Table 1

- (\*) On order: max value, middle value and standard deviation;  
 (\*\*) On order: min value and max value;  
 (\*\*\*) On order: min value, max value and medium value.

### V. CONCLUSION

The vehicle described in this paper has proven to be reliable and has shown performance to justify its use. The minibus has shown that, with at 75% of maximum admissible load (i.e. a 15 people test), its performance, in terms of maximum speed and acceleration, has been reduced (compared with a 3-person test) respectively of 10% and 38%, ensuring a maximum speed of 30 Km/h and acceleration of 1.6 m/s<sup>2</sup>. The autonomy on the basis for minimum weight load can reach till 189 km by means of FC. A good adaptability to loads has been demonstrated and a 73% yield of the chopper traction unit has been determined, remaining fairly constant at varying load conditions. To make a realistic simulation of minibus performances and consumptions, a model of the system in SIMULINK/MATLAB has been developed. A share of the energy is represented by consumption of auxiliary equipment whose charges are difficult to evaluate individually because some of them operate at constant power, while others depend on operating conditions. The full paper results will show the trend of traction power, FC power and energy stored of the analyzed powertrain.

### REFERENCES

- [1] Xu L, Li J, Hua J, Li X, Ouyang M. Optimal vehicle control strategy of a fuel cell/battery hybrid city bus. *Int J Hydrogen Energy* 2009;34:7323–33. doi:10.1016/j.ijhydene.2009.06.021.
- [2] Cai Y, Ouyang MG, Yang F. Impact of power split configurations on fuel consumption and battery degradation in plug-in hybrid electric city buses. *Appl Energy* 2017;188:257–69. doi:10.1016/j.apenergy.2016.11.126.
- [3] Hu X, Johannesson L, Murgovski N, Egardt B. Longevity-conscious dimensioning and power management of the hybrid energy storage system in a fuel cell hybrid electric bus. *Appl Energy* 2015;137:913–24. doi:10.1016/j.apenergy.2014.05.013.

# Modelling electrode and membrane processes in an anion-exchange membrane fuel cell

H. Grimler\*, A. Carlson\*, H. Ekström\*,\*\*, C. Lagergren\*,  
R. Wreland Lindström\*, and Göran Lindbergh\*

\* Applied Electrochemistry, School of Chemical Science and Engineering,  
KTH Royal Institute of Technology, SE-100 44 Stockholm, (Sweden)

\*\* COMSOL AB, Tegnérgatan 23, 111 40 Stockholm, (Sweden)

**Abstract** - To better understand which processes that limits the performance in an anion-exchange membrane fuel cell (AEMFC), a physical performance model has been developed. The model considers a tertiary current distribution and is validated against experimental results. The results show that both the anode and the cathode contributes to significant polarisation in the system

**Index Terms** – Physical based model, anion-exchange membrane fuel cell (AEMFC), tertiary current distribution

## I. INTRODUCTION

To mitigate problems related to emissions, the use of traditional fuels has to decrease and be replaced by renewable fuels or electric drivelines. Fuel cells are a promising technology for the automotive industry that can decrease the emissions.

Among the polymer electrolyte fuel cells, much attention has been paid to the proton-exchange membrane fuel cell (PEMFC) that is efficient and has a great potential for the transport sector. Currently, one major shortcoming with the PEMFC is the high cost related to the membranes and the platinum containing electrodes. An anion-exchange membrane fuel cell (AEMFC) uses more environmentally friendly membranes and can potentially be less expensive than the PEMFC [1]. However, a problem, could be the water management in the cell. Since water is produced at the anode and consumed at the cathode, there is a risk that the anode side becomes flooded and that the cathode side dries out.

To deal with the water management problem, it is important to better understand how water is transported through the cell. Therefore, a full cell model that considers concentration dependent kinetics as well as water transport through the cell has been developed.

## II. EXPERIMENTAL AND MODEL

Experiments using a Tokuyama membrane and ionomer, and Pt/C catalysts were carried out to get polarisation data and to investigate the water transport through the cell membrane. Parameters varied were reactant partial pressures, inlet humidity and catalyst loadings. The inlet humidity were controlled using humidifiers from Fuel Cell Technologies, Inc. Humidity and gas temperature sensors were also installed at the inlet and outlet pipes of the cell using four sensors of type HYT939 from B+B Sensors.

The base case of the experiments used  $0.4 \text{ mg}_{\text{Pt}} \text{ cm}^{-2}$  on both anode and cathode, 95% relative humidity at both electrodes and pure  $\text{O}_2$  and pure  $\text{H}_2$ . All experiments were run at a cell temperature of  $50^\circ\text{C}$ , with dry gas flow rates of  $7.4 \text{ l}_\text{n}\text{h}^{-1}$  at both electrodes.

A model has been developed in Comsol Multiphysics that considers the current distribution as well as the mass transport. The electrodes are treated as consisting of a gas diffusion layer (GDL) and a catalyst layer (CL) that are separated by a membrane of constant thickness.

The current distribution is based on concentration dependent Butler-Volmer kinetics, and the conductivity of the polymer phase in the electrodes assumed to be a fraction of the membrane conductivity. Mass transport in the gas phase of each electrode was modelled using the Maxwell-Stefan set of equations, using binary diffusion coefficients to define the interactions between all gas phase species.

A parasitic cross-over current density was assumed to occur due to hydrogen diffusing over the membrane and reacting readily at the cathode side. It was modelled as proportional to the hydrogen partial pressure at the anode-membrane interface.



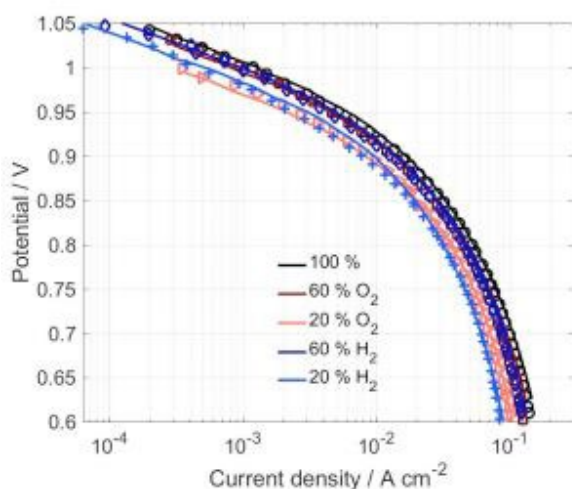


Figure 1. Model fit to experimental data with different partial pressures of  $O_2$  and  $H_2$ . The marks are experimental data and the lines the model fit to the data. The experimental data was obtained at 95 % relative humidity and at a cell temperature of 50 °C. The curves are not IR-corrected.

In one of the experiments done, the water content in the cell inlets was varied asymmetrically. From this, the water flux as a function of difference in vapour pressure over the membrane was determined.

A number of physical parameters such as exchange current densities, electrode polymer phase conductivity, charge transfer coefficients and hydrogen cross-over current were obtained by optimising the model against experimental data with varying partial pressures.

### III. RESULTS

Figure 1 shows an example fit of the model to experimental data. The partial pressures of the reactant gases have been varied and parameters fitted. The figure shows that the model correlates well with the experimental data when optimised for the five data sets simultaneously. So far, mass transport limitations at higher current densities have not been incorporated into the model as the potential region down to 0.7 V is where a fuel cell primarily operates in real applications. To fully describe the system, mass transport phenomena will be considered as a second step.

Figure 2 shows the contribution to cell potential from the anode, cathode and membrane. Most of the overpotential arises due to the cathode kinetics, but the anode contribution becomes more important as the current density increases. The losses due to the membrane resistance are very small compared to the losses of the electrodes.

Initial investigations of mass transport have shown that the effect is still small at 0.7 V, the overpotentials seen in Figure 2 is therefore mainly due to kinetic effects.

### IV. CONCLUSIONS

The model fits well to experimental data and shows that both the anode and cathode contributes to the losses in the fuel cell system.

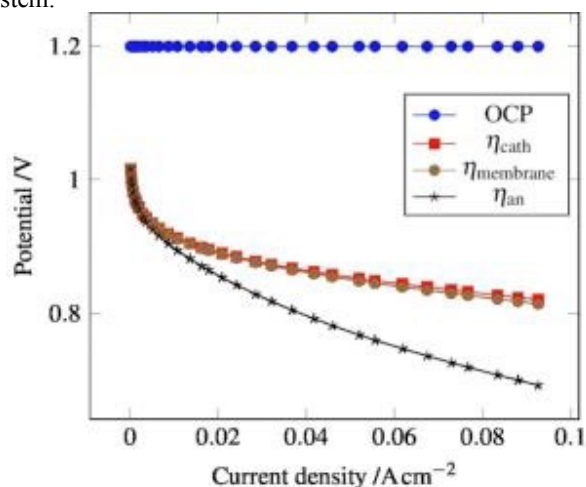


Figure 2. Polarisation curve, indicating the contribution from the different components of the cell. As can be seen, the membrane's resistance is negligible compared to the resistance in the electrodes. The cathode also contributes more to the losses than the anode.

### Acknowledgement

Thanks to Swedish Energy Agency and StandUp for Energy for funding this research.

### REFERENCES

- [1] Sen Huo, Jae Wan Park, Pu He, Dawei Wang, and Kui Jiao. Analytical modeling of liquid saturation jump effect for hydrogen alkaline anion exchange membrane fuel cell. *International Journal of Heat and Mass Transfer*, 112(Supplement C):891–902, 2017. ISSN 0017-9310. doi: [doi.org/10.1016/j.ijheatmasstransfer.2017.04.137](https://doi.org/10.1016/j.ijheatmasstransfer.2017.04.137).



## PHOTOACOUSTIC SPECTROSCOPY – A TOOL FOR GAS MEASUREMENTS IN PEM FUEL CELLS

H. Bettermann\*, V. Chmiel\*, and I. Radev\*\*

\*Institute of Physical Chemistry, Heinrich-Heine-University  
Düsseldorf, Universitätsstr.1, Düsseldorf, (Germany)

\*\*Fuel Cell Research Center, Carl-Benz-Str. 201, Duisburg,  
(Germany)

**Abstract** - This contribution presents a specific photoacoustic setup as an alternative tool for diagnosing gas compositions in fuel cells. The usefulness of this setup was proven by pursuing the electrochemically induced oxidation of carbon denoted as carbon corrosion. Carbon corrosion was investigated by changing electrochemical potentials between 0.1 and 1.6 V and measuring the resulting evolution of CO<sub>2</sub>. For this purpose, the cathode flow field was loaded with N<sub>2</sub> while the anode flow field was charged with H<sub>2</sub>. The potential-dependent changes of CO<sub>2</sub> evolution were correlated to partial reactions of a recently presented model of carbon corrosion.

**Index Terms** – Photoacoustic spectroscopy, carbon corrosion

### I. INTRODUCTION

Beside in-situ electrochemical methods which provide thorough characterizations of processes inside PEM fuel cells, gas compositions have been investigated by various methods like gas chromatography, mass spectrometry, differential electrochemical mass spectroscopy or Raman spectroscopy.

This contribution presents a specific photoacoustic setup for inspecting fuel cell processes. The underlying photoacoustic effect converts energy absorbed by molecules into sound. After absorption of pulsed light by sample molecules, the absorbed energy is dissipated into heat pulses which are transferred adiabatically into sound. Basic components of photoacoustic setups are a pulse light source, a sample cell, a sensitive microphone and a unit for signal processing.

The usefulness of this setup was proven by measuring CO<sub>2</sub> that was set free during the electrochemically induced oxidation of carbon support of catalyst particles. Carbon becomes unstable in the presence of water and potentials above 0.207 V. It reacts to CO<sub>2</sub> due to  $C + 2H_2O \rightarrow CO_2 + 4H^+ + 4e^-$ . The photoacoustic setup was used to detect the CO<sub>2</sub> emission at

electrochemical potentials between 100 mV and 1.6 V. To prevent reactions not directly associated with carbon corrosion the cathode flow field of the fuel cell was loaded with nitrogen while the anode flow field was charged with hydrogen. CO<sub>2</sub> evolutions were correlated to a model of carbon corrosion which comprehensively describes the chemical overall conversion by a series of partial reactions [1].

### II. EXPERIMENTAL

#### A. Photoacoustic Setup

CO<sub>2</sub> was excited by a DFB-diode laser (7mW at 2723 nm; Toptica Photonics). An optical chopper modulated the light. The cylindrical sample cell (bore diameter: 5 mm, length: 228 mm) was operated as an acoustic resonator (resonance frequency: 1174 Hz at 80° C in air). The microphone was set in the center of the cell. Gas inlet and gas outlet were positioned next to both ends of the channel, respectively. Sound was recorded by a MEMS microphone (omnidirectional directivity, sensitivity 125 mV/Pa, Knowles). The microphone signals were amplified and processed by an audio mixing console (X1222; Behringer) and then directed to a computer.

#### B. Selection of the excitation wavelength

In view of small changes of CO<sub>2</sub> concentrations, efficient absorption was achieved by exciting an overtone mode (centered at 2.69 μm) in the NIR-region. Since this transition is spectrally congruent with the totally symmetric OH stretching mode of water, the excitation of a single rotational-vibrational transition at 2723 nm (3672.4 cm<sup>-1</sup>), which was well isolated from next-neighbored transitions of water, warranted unambiguous detection of CO<sub>2</sub>.

Copyright © 2017

### C. Flow Field, MEA Preparation and Pre-Aging

The cathode flow field of the fuel cell (single cell, electrode area 50cm<sup>2</sup>) was made from a polymer carbon composite.

A commercial GDL with a MPL (H23C8, Freudenberg FCCT) included was coated with a catalyst dispersion by an ultrasound vaporizer. Anode and cathode catalyst loadings were set to 180 and 360 µgcm<sup>-2</sup>, respectively. Both electrodes were hot pressed on both sides onto the Nafion 117 (Du Pont) membrane.

Pre-aging of the MEAs was carried out by operating the cell (cathode air, anode H<sub>2</sub>) at 0.4 V with stoichiometric coefficient of 1.5 (anode) and 2.5 (cathode) for 80°C and 90% RH for 1h. Subsequently, U/j-cycles were recorded (e.g., 0.3 - OCV, 1 mVs<sup>-1</sup>) with the same stoichiometric coefficients related to 0.7 Acm<sup>-2</sup>.

### D. Operational Conditions of Measurements

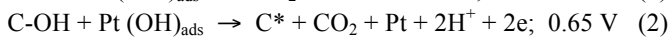
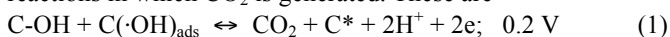
Microphone signals were referred to sample concentrations by measuring various mixtures of N<sub>2</sub> and ambient air (set to 400 ppm CO<sub>2</sub>) under the operational conditions (80°C, 90% RH) of corrosion measurements.

The cathode exhaust was by-passed and one pipe was directed to a heated vessel which prevented flooding of the sample cell with liquid water. The sample cell itself was kept at 80°C. The corrosion experiment was performed by setting gas flows to 50 L/h H<sub>2</sub> (anode) and 100 L/h N<sub>2</sub> (cathode) at 80 °C and 90 % RH. The H<sub>2</sub>/N<sub>2</sub> experiment was carried out in a two electrode arrangement. For voltages larger 100 mV, current densities were below 10 mA/cm<sup>2</sup> and the anode (50 L/h H<sub>2</sub>) was set as reference electrode to which the potentials were related.

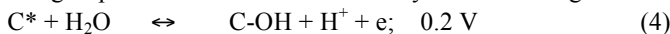
## III. RESULTS

Fig. 1 depicts the CO<sub>2</sub> evolution of the MEA as a function of chosen electrochemical potentials. Potentials were tuned between 100 mV and 1.6 V in steps of 20 mV and held for 3 min.

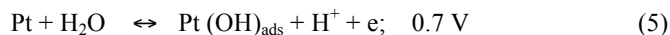
The CO<sub>2</sub> evolution does not rise steadily with increasing potentials but exhibits maxima at specific potentials. Key peaks are found at about 200, 670 and about 1000 mV. According to the carbon corrosion model [1], the potentials, at which the peaks were recorded, correspond to three proposed partial reactions in which CO<sub>2</sub> is generated. These are



Reactions are initiated by the presence of surface hydroxy groups C-OH and OH radicals adsorbed on the carbon surface. The formation of CO<sub>2</sub> requires a sufficient concentration of C-OH groups which are made available by the initializing reaction



Eq. 2 is supported by a reaction (eq. 5), which becomes active at nearly the same potential which belongs to reaction (2).



Since the CO<sub>2</sub> productions from eq. 1-3 are accompanied by the formation of defect sites C\* of the carbon surface, the processes in which CO<sub>2</sub> generation is involved seem to be self-sustaining.

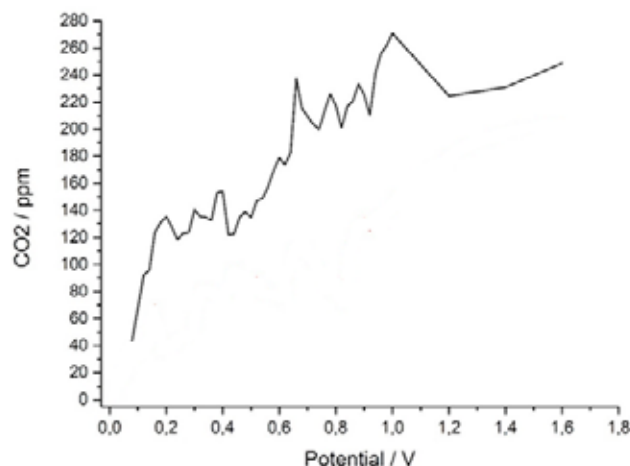


Fig. 1: Potential-dependent CO<sub>2</sub> evolution of a MEA (Johnson Matthey, 46.2 wt. % Pt/Vulcan XC-72R (36wt.% ionomer, Nafion 117); potential changes in steps of 20 mV; potentials held for 3 min; operating conditions: 80°C, 90% RH

Beside the peaks at 0.2, 0.67 and about 1.0 V it is still open to which partial reactions, in which CO<sub>2</sub> is generated, the remaining peaks belong.

## IV. CONCLUSION

Under conditions of high relative humidity and partial presence of liquid water the photoacoustic measurements enabled a detailed insight into the CO<sub>2</sub> evolution during carbon corrosion when changing electrochemical potentials. The measurements allow to conclude that carbon corrosion seems to be even more complex as it is proposed by the already complex model of corrosion and it is suggested that some more still hidden reactions contribute to the overall reaction.

## ACKNOWLEDGMENT

The authors gratefully acknowledge financial funding by the project IGF 17851N (AiF, German Federal Ministry for Economic Affairs and Energy)

## REFERENCES

- [1] A. Pandey, Z. Yang, M. Gummalla, V.V. Atrazhev, N. Y. Kuzminykh, V.I. Sultanov, S. Burlatsky, A Carbon Corrosion Model to evaluate the effect of steady state and transient operation of a polymer electrolyte membrane fuel cell, J. Electrochem Soc., Vol. 160, 2013, 160, pp. F972-F979

## PEM FUEL CELLS AND VANADIUM REDOX FLOW BATTERIES: TWO TECHNOLOGIES FOR STORING ELECTRICITY THROUGH A FLOW PROCESS

M. Minutillo \*, S. Kim \*\*, A. Perna \*, D.K. Kim\*\*\*

\* Department of Engineering, University of Naples Parthenope, Centro Direzionale Isola C4, Naples, Italy

\*\* KIST Europe, Campus E 71, 66123 Saarbrücken, Germany

\*\*\* School of Mechanical Engineering, Chung-Ang University, 06974 Seoul, South Korea

**Abstract** - Current energy policies and strategies are mainly addressed to sustain the diffusion of renewable energy source technologies; however, their intermittency represents an obstacle to their extensive penetration into the grid. In order to enhance the utilization of the renewable energy sources for the power generation, electric energy storage solutions are indispensable.

Existing storage technologies are characterized by different storage capacity, storage efficiency and discharge time and thus, the choice of the best technology depends on its application.

Fuel cells/electrolyzers and flow batteries represent a potential solution for the electrical energy storage in the future. These systems that are based on electrochemical flow processes can be considered as a good alternative to the conventional batteries based on classic electrochemical batch processes, because they allow high energy storage thanks to their reaction products that can be stored independently from the stack design.

This study aims to analyze similarities and differences between reversible fuel cells, working at low temperature, and vanadium redox flow batteries. The comparison is carried out taking into account the process type, the BoP needs, the ionic transport in the membranes, the operating conditions and the storage capacity (pressure and volume). In this study the analysis is based on experimental and numerical evaluations.

**Index Terms** - energy storage, reversible fuel cell, vanadium redox flow battery, performance comparison.

### I. INTRODUCTION

The most widely used method to categorize EES technologies is based on the form of energy stored in the system: mechanical, electrochemical, electrical, thermochemical, chemical and thermal energy storage [1].

Chemical energy storage is the only concept, which allows storage of large amounts of energy, up to the TWh range, and for greater periods of time-even as seasonal storage.

Among chemical storage technologies, those operating at low temperature like reversible PEM fuel cell and vanadium

redox flow batteries (VRFB) have recently drawn much attention.

A Reversible PEM (RePEM) is a single unit that can function either in electrolyzer mode (charging mode) or fuel cell mode (or discharging mode). In the forward direction of reversible reaction water disassociates into hydrogen and oxygen, and in the reverse reaction recombination of constituent elements to forms water.

The VRFB stores and releases energy by utilizing the redox chemistry in an acid media between vanadium (V) ions in different oxidation states.

In this paper the main characteristic and performance of an electric energy storage system based on both mentioned technologies are compared.

### II. REVERSIBLE PEM DESCRIPTION

The main features of this technology, that make PEM fuel cell ideal for realizing electric energy storage systems from renewable energy sources are: high current densities, high efficiency, good dynamic response, and rapid start-up and shut-down. Moreover, these systems can provide the high degree of hydrogen gas purity with extremely low traces of detrimental contaminants [2]. Fig.1 shows the polarization curve of the cell used in the present study [3].

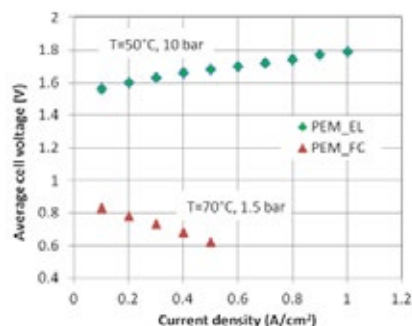


Fig. 1. Polarization curves in both operating mode [3].

### III. VANADIUM REDOX FLOW BATTERY DESCRIPTION

The configuration of VFB is similar to the fuel cell structure. The charge-discharge reactions are shown schematically in Fig. 2. During discharging process, oxidation reaction occurs at anode and reduction reaction occurs at cathode.

While these oxidation reduction reactions, hydrogen ions are diffused across the membrane and electrons are transported from anode to cathode through the connected circuit.

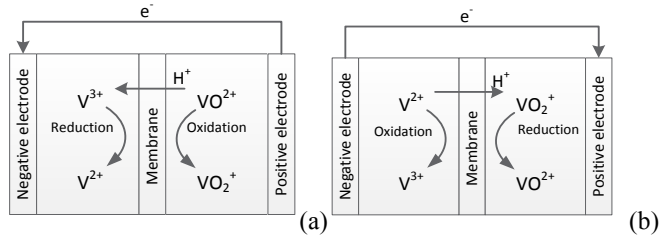


Fig. 2. Vanadium redox flow battery reactions: (a) charge reaction (b) discharge reaction.

The VFB cell voltage curve and average cell voltage, measured in our test station, during the charging and discharging phases, are shown in Fig. 3. Cut-off voltages of charge and discharge were set as 1.7 V and 1.0 V respectively [4,5].

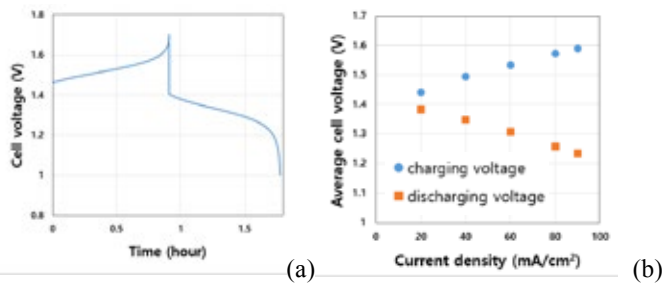


Fig. 3. VRFB unit cell performance: (a) charge-discharge curve at current density = 60 mA/cm², (b) average voltages depending on current densities.

### IV. EES SYSTEM COMPARISON

A comparison between a Reversible PEM fuel cell and a Vanadium flow battery (VRFB) is illustrated in table 1.

TABLE I  
COMPARISON BETWEEN RPEM AND VRFB TECHNOLOGIES

System	RePEM	Flow battery
Process	Two phase flow (gas and liquid)	One phase flow (liquid)
Ionic transport in membrane	H <sup>+</sup>	H <sup>+</sup> or HSO <sub>4</sub> <sup>-1</sup> , SO <sub>4</sub> <sup>-2</sup>
Electrodes	Carbon cloth	Carbon felt
Electrolyte	Polymer	Vanadium solution
Catalysts	Yes (i.e. Pt)	no
Reaction progress	Utilization factor	State of Charge
Storage volumes	H <sub>2</sub> /H <sub>2</sub> O	Vanadium electrolyte (1.6M Vanadium ions in 2.0M sulfuric acid)
Operating Pressure	1- 30 bar	Ambient
Operating Temperature	< 100 °C	< 40°C

Reactants Crossover	Yes	Yes
OCV	0.9-1.0 V	1.0 – 1.15 V
Current density	100-1000 (mA/cm <sup>2</sup> )	60-80 (mA/cm <sup>2</sup> )

In order to compare EES systems based on the above mentioned technologies, it has been assumed that the storage system has to be sized in order to store about 10 kW of renewable electric power for 8 hours per day. The calculated data are summarized in table 2.

TABLE II  
COMPARISON BETWEEN REPEM AND VRFB IN A10 kW SIZE EES SYSTEM

System	RePEM-based EES system	VRFB-based EES system
Power (kW) (charging/discharging mode)	9.9/1.76	11.1/7.2
N. of cells x stack	22	40
Number of stacks	2	3
Active area (cm <sup>2</sup> )	250	1000
Nominal voltage (V) (charging/discharging mode)	1.8/0.64	1.55/1.25
Nominal current (A/cm <sup>2</sup> ) (charging/discharging mode)	1/0.5	0.06
Power consumption (kW) (compression)	0.428	-
Storage volumes (liters)	78 (H <sub>2</sub> at 250 bar) 23 (H <sub>2</sub> O)	3000
Voltage* and Energy** efficiency (%)	36/18	81/65

\*V<sub>DISCHARGING</sub>/V<sub>CHARGING</sub>, \*\*E<sub>DISCHARGING</sub>/E<sub>CHARGING</sub>

### V. CONCLUSION

The comparison between the studied EES systems has highlighted that a VRFB system is an interesting solution on a long term but only if the energy density can be clearly increased (high storage volume), while it has better performance in terms of voltage and energy efficiency.

### REFERENCES

- [1] Perna A, Minutillo M, Jannelli E, Hydrogen from Intermittent Renewable Energy Sources as Gasification Medium in Integrated Waste Gasification Combined Cycle Power Plants: A Performance Comparison, Energy 94 (2016) 457-465.
- [2] Siracusano S, Baglio V, Van Dijk N, Merlo L, Aricò AS Enhanced performance and durability of low catalyst loading PEM water electrolyser based on a short-side chain perfluorosulfonic ionomer, Applied Energy 192 (2017) 477-489
- [3] Ito H, Miyazaki N, Ishida M, Nakano A, Efficiency of unitized reversible fuel cell systems, International Journal of Hydrogen Energy 41 (2016) 5803-15
- [4] Ye, R., Henkensmeier, D., Yoon., S., Huang, Z., Kim., D.K., Chang, Z., Kim, S., Chen, R., Redox Flow Batteries for Energy Storage: A Technology Review, J. Electrochem. En. Conv. Stor.. 2017; JEECS-17-1050, accepted.
- [5] Chen, R., Kim, S., Chang, Z., Redox Flow Batteries: Fundamentals and Application, Redox: Principles and Advance Applications, Chapter: 5, Publisher: InTech, pp.103-118.

## TITANIUM-MOLYBDENUM BASED MATERIALS AS ANODE FOR DIRECT BIO GAS SOLID OXIDE FUEL CELLS

A.Garbujo<sup>1</sup>, G.Carollo<sup>1</sup>, A.Bedon<sup>1</sup>, M.M.Natile<sup>2</sup>, C.Niccolet<sup>3</sup>, S.Fourcade<sup>4</sup>, F.Mauvy<sup>4</sup>, A.Glisenti<sup>1</sup>

<sup>1</sup>University of Padova, Dept. Chemical Sciences, Padova, 35131, (Italy)

<sup>2</sup>CNR-ICMATE, Dept. Chemical Sciences, Padova, 35131 (Italy)

<sup>3</sup>Dept. of Materials Science and Engineering, Cambridge, Massachusetts, 02139 (United States)

<sup>4</sup>Institut de Chimie de la Matière Condensée de Bordeaux ICMCB- CNRS, Université de Bordeaux, Pessac, 33600 (France)

**Abstract** -  $\text{SrTi}_{1-x}\text{Mo}_x\text{O}_3$   $x=0.1, 0.4$  perovskites were studied as anodes for SOFC directly fed with bio-gas. The materials were prepared by citrate route and tested versus sustainable reactions (methane oxidation and dry reforming) and characterized by electrochemical impedance spectroscopy. Both samples are active in methane oxidation but only  $\text{SrTi}_{0.9}\text{Mo}_{0.1}\text{O}_3$  shown a good activity in methane dry reforming reaching around 60% of  $\text{CH}_4$  conversion at 800°C. The electrodes printed on YSZ pellets with GDC as barrier layer revealed high ASR at 800°C. A significantly resistance decreasing was obtained by the infiltration of 30%wt of Ni achieving  $0.85 \Omega \cdot \text{cm}^2$  at 830°C under hydrogen on  $\text{Ni-SrTi}_{0.6}\text{Mo}_{0.4}\text{O}_3$ . The results encouraged further studies on Ti-based perovskites aimed at optimizing the device operating with infiltration and on electrodes morphology.

**Index Terms** - Bio-gas, Critical Raw Materials free, methane dry reforming, SOFC.

### I. INTRODUCTION

The increasing energy demand and air pollution are two of main challenges that researchers nowadays are trying to solve. The Solid Oxide Fuel Cells (SOFCs) are electrochemical devices that can be an answer to both the problems. SOFCs are characterized by some peculiarities related to the solid electrolyte and to the operative temperature, such as high efficiency, higher resistance to poisoning and fuel flexibility. The use of sustainable fuels that can be processed directly into the cell could greatly increase the performance and simplify the fuel cell. Ni Yttria stabilized zirconia (Ni-YSZ) cermet is the state of art anode for SOFC but suffers of carbon deposition, Ni coarsening and it is limited by three boundaries phases. [1] Due to the versatility of perovskites, it was possible to design a titanium-molybdenum based anode that should be able to fulfil all requirements. [2]

### II. EXPERIMENTAL

#### A. Synthesis

The titanium based perovskites  $\text{SrTi}_{1-x}\text{Mo}_x\text{O}_3$  ( $x=0.1$  and  $0.4$ ) were obtained through citrate method starting from  $\text{SrCO}_3$

(Sigma Aldrich  $\geq 98\%$ ), Titanium(IV) isopropoxide (Sigma Aldrich 97%) and Ammonium molybdate tetrahydrate (Sigma  $\geq 99\%$ ). The citric acid was dissolved in a water solution and consequently the Ti liquid precursor was added to the solution through a syringe.  $\text{HNO}_3$  concentrated solution was added to the citric solution ( $\text{HNO}_3$ :water = 1:1) kept stirred, to dissolve the titanium precipitate. The other precursors were dissolved in water separately. The strontium carbonate was dissolved in water after adding a few mL of  $\text{HNO}_3$ . The solutions were mixed and neutralized to pH 7-8 by adding  $\text{NH}_3\text{OH}$ . The gel obtained, after evaporation, was finally burn in a self-combustion ignited by the heater. The ashes were grinded and calcined under wet hydrogen at 1200°C for 6h. The symmetric half-cell was prepared starting from the commercial powder of electrolyte dry pressed into a pellet. Through screen printing the barrier layer and the electrodes layers were deposited and then calcined at 1300°C. On the symmetric cell, nickel infiltration was carried out by using 1M solution prepared from nitrate precursor. Few drops of Ni solution were dripped on the electrodes; after this step a thermal treatment at 450°C for 30 minutes under air was carried out. The final cell was calcined at 800°C for 1h under hydrogen.

#### B. Characterization

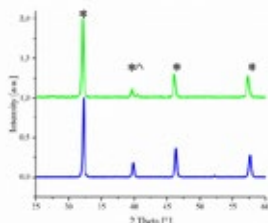
The structural characterization was performed with a Bruker D8 Advance diffractometer using a  $\text{Cu K}_\alpha$  radiation (40kV, 40mV,  $\lambda = 0.154 \text{ nm}$ ) with Bragg-Brentano geometry. The temperature programmed reduction (TPR) was carried out with an Autochem II 2920 Micromeritics using a TCD detector. The catalytic tests were performed on a quartz reactor with an internal diameter of 4 mm. The thermocouple was placed up to catalyst bed. The GHSV was  $\sim 100,000 \text{ h}^{-1}$  flowing 2%  $\text{CO}_2$  and 2%  $\text{CH}_4$  for dry-reforming reactivity tests and 2%  $\text{CH}_4$  and 3%  $\text{O}_2$  for methane oxidation. The gases were detected through GC (Agilent 7890A) equipped with a TCD.



### III. RESULTS

#### A. X-Ray Diffraction

The x-ray diffraction patterns, figure 1, have shown the formation of desired phase and the peaks shift to lower angle as a function of molybdenum loading demonstrating the penetration of Mo into the perovskitic cell. No secondary phases were observed on  $\text{SrTi}_{0.9}\text{Mo}_{0.1}\text{O}_3$  while a small segregation of Mo is observed on  $\text{SrTi}_{0.6}\text{Mo}_{0.4}\text{O}_3$  sample.

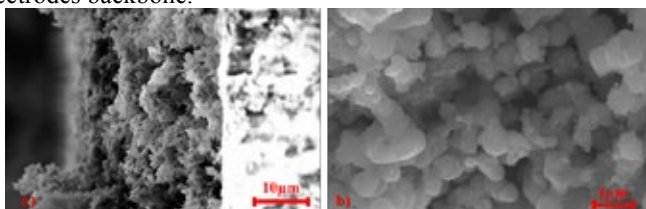


**Fig. 1.** XRD patterns of  $\text{SrTi}_{0.9}\text{Mo}_{0.1}\text{O}_3$  (blue) and  $\text{SrTi}_{0.6}\text{Mo}_{0.4}\text{O}_3$  (Green). [\*] perovskite, [^] Mo.

The samples' stability versus electrolytes Yttria stabilized Zirconia (YSZ) and Gadolinium doped ceria (GDC) was checked by mixing carefully the powders and heating at 1300°C under hydrogen for 6h. The titanates revealed chemical compatibility with GDC but they reacted with YSZ inducing the formation of  $\text{SrZrO}_3$  and  $\text{SrMoO}_4$  insulating phases.

#### B. SEM

The cross-section of symmetric cell  $\text{SrTi}_{0.9}\text{Mo}_{0.1}\text{O}_3/\text{GDC}/\text{YSZ}$  can be seen in SEM image, figure 2a. The electrode thickness was 25  $\mu\text{m}$  while the GDC layer had a thickness of 2-3  $\mu\text{m}$ . The high porosity of  $\text{SrTi}_{0.9}\text{Mo}_{0.1}\text{O}_3$  if compared with the electrolyte is also visible. The successful infiltration process was observed in figure 2b displaying the homogenous Ni particles dispersion (diameter  $\sim 20\text{nm}$ ) into the electrodes backbone.



**Fig. 2.** SEM images of the interface  $\text{SrTi}_{0.9}\text{Mo}_{0.1}\text{O}_3/\text{electrolyte}$  a) and a detail of  $\text{Ni-SrTi}_{0.6}\text{Mo}_{0.4}\text{O}_3$  b).

#### C. TPR

The TPR performed on  $\text{SrTi}_{1-x}\text{Mo}_x\text{O}_3$   $x=0.1, 0.4$  did not show any signal confirming the stability under reductive environment. TPR carried out on  $\text{SrTi}_{0.9}\text{Mo}_{0.1}\text{O}_3$  loaded with 30% wt of Ni through wet deposition shown a large peak related to the reduction of  $\text{NiO}$  to  $\text{Ni}$  between 400°C and 600°C compatible with the Ni amount deposited.

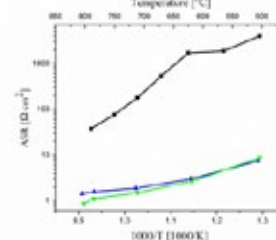
#### D. Catalytic tests

The catalytic performances on methane oxidation and methane dry reforming were tested on powders samples. Both

$\text{SrTi}_{0.9}\text{Mo}_{0.1}\text{O}_3$  and  $\text{SrTi}_{0.6}\text{Mo}_{0.4}\text{O}_3$  show activity in methane oxidation (40% and 46%  $\text{CH}_4$  conversion at 850°C, respectively) figure 3. In contrast, the methane dry reforming was observed only in  $\text{SrTi}_{0.9}\text{Mo}_{0.1}\text{O}_3$  (58%  $\text{CH}_4$  and 53 %  $\text{CO}_2$  conversion at 800°C).

#### E. Electrocatalytic tests

The Arrhenius plot of area specific resistance (ASR) with and without Ni infiltration, are compared in figure 4. In absence of Ni, the maximum ASR obtained was 27.2  $\Omega\cdot\text{cm}^2$  for  $\text{SrTi}_{0.9}\text{Mo}_{0.1}\text{O}_3$  at 830°C. The infiltration of 30%wt of Ni decreased the ASR to 0.85  $\Omega\cdot\text{cm}^2$  and 1.42  $\Omega\cdot\text{cm}^2$  for  $\text{Ni-SrTi}_{0.6}\text{Mo}_{0.4}\text{O}_3$  and  $\text{Ni-SrTi}_{0.9}\text{Mo}_{0.1}\text{O}_3$  respectively at 830°C.



**Fig. 4.**  $\text{SrTi}_{0.9}\text{Mo}_{0.1}\text{O}_3$ ,  $\text{Ni-SrTi}_{0.9}\text{Mo}_{0.1}\text{O}_3$  (blue) and  $\text{Ni-SrTi}_{0.6}\text{Mo}_{0.4}\text{O}_3$  (Green).

### IV. CONCLUSION

In this contribution we studied  $\text{SrTi}_{1-x}\text{Mo}_x\text{O}_3$   $x=0.1, 0.4$  as anodes for SOFCs active towards sustainable reactions. XRD analysis had shown the chemical compatibility between the samples and GDC electrolyte. Good activities towards methane oxidation (46%  $\text{CH}_4$  conversion for  $\text{SrTi}_{0.6}\text{Mo}_{0.4}\text{O}_3$  at 850°C) and methane dry reforming (58%  $\text{CH}_4$  conversion for  $\text{SrTi}_{0.9}\text{Mo}_{0.1}\text{O}_3$ ).

The symmetric half-cell (electrode/GDC/YSZ) shown a large ASR (27.2  $\Omega\cdot\text{cm}^2$ ) which greatly decreased when 30%wt Ni was infiltrated reaching the best performance of 0.85  $\Omega\cdot\text{cm}^2$  at 830°C on  $\text{Ni-SrTi}_{0.6}\text{Mo}_{0.4}\text{O}_3$ . The significant improvement observed by means of infiltration allow to consider these economically and environmentally sustainable anodes as very promising anodes in direct biogas SOFCs in spite of the low performance (when compared with the state of art materials) paving the way to further improvement by chemical and morphological engineering of the device. The anode backbone activity shown with respect to methane also suggests the possibility to explore different metal (or alloys) infiltrations (Cu, Fe) as an example for enhancement of electrical conductivity and electrocatalytic activity. [3] [4]

### REFERENCES

- [1] S. Mc Intosh, R. J. Gorte, *Cells Chem. Rev.* 104, 2004, 4845-4866.
- [2] M. A. Peña and J. L. G. Fierro, *Chem. Rev.* 2001, 101, 1981-2017.
- [3] G. Carollo, A. Garbujo, D. Ferri, M.M. Natile, A. Glisenti, *Proceedings of SEEP* 2017.
- [4] S. Zha, et al. *Electrochem. Soc.*, 2004 151 (8) A1128-A1133.

## HI-SEA (HYDROGEN INITIATIVE FOR SUSTAINABLE ENERGY APPLICATION): DEVELOPMENT OF A JOINT LABORATORY FOR PEM AND H<sub>2</sub> MARINE APPLICATIONS

G. Borgogna\*, E. Speranza\*, A. Dellacasa\*, T. Lamberti\*\*, M. De Campo\*\*, A. N. Traverso\*\*, L. Magistri\*\*, A.F. Massardo\*\*

\* Fincantieri S.p.a.

\*\* DIME-TPG Polytechnic School, University of Genoa, Italy

**Abstract** - The present paper presents an assessment of the installation of a real plant's scale Proton Exchange Membrane (PEM) fuel cell laboratory. The facility developed in the frame of a long time signed agreement between Fincantieri S.p.A. and the University of Genoa named "HI-SEA (Hydrogen Initiative for Sustainable Energy Application)", it integrates a Hybrid PEM power generator system with the research laboratory of the Thermochemical Power Group (TPG) of the University of Genova [1] – Savona Campus. The HI-SEA laboratory is composed by 8 PEM fuel cell stacks for a total power of 260 kW. Two series of 4 stacks each are connected through a DC/DC converter each in parallel to an electric bus where a 60 kW AC/DC converter is connected, to enable the simulation of battery or supercapacitors hybrid systems. The laboratory presents also the possibility to study in more details single subsystem including cogeneration and trigeneration systems as well as hydrogen storage subsystems coupling.

**Index Terms** – Laboratory, PEM fuel cell, Cogeneration, Marine.

### I. NOMENCLATURE

BOP – Balance Of Plant  
E-Hub – Energy Hub  
FC – Fuel Cell  
MH – Metal Hydride  
PEMFC – Proton Exchange Membrane Fuel Cell  
SOFC – Solid Oxide Fuel Cell

### II. INTRODUCTION

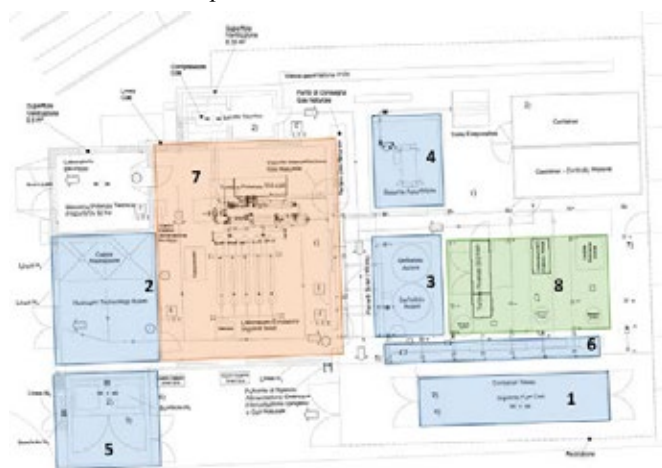
The HI-SEA Joint Laboratory represents the first large scale PEMFC test rig especially dedicated to the study of FC application onboard ships and for marine application in general. The goal of the laboratory is to define the best design for a modular FC system for ship application able to guarantee

the maximum life span of FC stacks without omit performance.

### III. EXTENDED ABSTRACT PREPARATION

The laboratory presents a number of facilities that enable the study of various configurations of FC systems, hybrid systems with cogenerations or trigeneration as showed. The design and development of the laboratory already gives the possibility to mature experiences as described in the following. Finally, the next year research plan is presented.

#### A. Facilities description

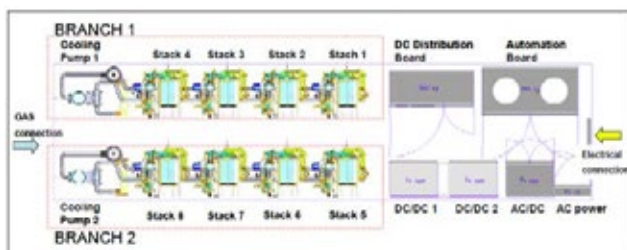


**Fig. 1. HI-SEA planimetry**

The HI-SEA laboratory (light blue spaces and number from 1 to 6 in Figure 1) presents a unique presence of facilities that make it suitable for the study of ships power generator systems:

1. PEMFC power systems, with 260 kW; 2. Dedicated space for test and analysis of 30 kW stacks and MH hydrogen storage tanks; 3. Large heat storage systems; 4. Absorber chiller of 100 kWth; 5. Hydrogen storage; 6. Water cooling system; 7. UTC laboratory of Rolls-Royce; 8. Lab scale E-Hub connected to a real smart grid.

The Rolls-Royce UTC laboratory gives the opportunity to merge studies on PEMFC with SOFC hybrid systems. The E-Hub composed by 100 kW<sub>e</sub> TG, 20 kW<sub>e</sub> ICE, 1.1 kW<sub>e</sub> PV solar panels and 10 kW<sub>p</sub> thermal solar panels [1], gives the opportunity to study the behavior of the PEMFC systems in a grid with different sources of electrical and thermal power, enabling the development of design tools for smart grid controls. The presence of water storage systems with temperatures and flows measurement will enable to assess the potentiality of the PEMFC system for cogeneration. Moreover, the absorber chiller comply with the thermal output of the PEMFC and will permit to test at a real system size the coupling of the systems, an important achievement for the reduction of onboard energy consumption. Finally, the equipped space will permit tests and analysis of single FC stacks and of MH tanks, with the possibility to develop an optimum thermal integration between them.



**Fig. 2. PEMFC system scheme**

The first and main goal of the laboratory is the definition of the best design and size of a modular FC system for ship application. The PEMFC facility enables to connect 3 or 4 stacks in series for each of the two branch, with or without DC/DC to control the output tension. Moreover, the 60 kW AC/DC rectifier together with the controllable electric load will permit the simulation of any kind of battery packs, enabling the assessment of the optimum balance between FC and battery dimension as a function of the Operational Profile and the best integration of PEMFC in a DC grid. Different operational profile will be tested to investigate the possibility to use PEMFC system to power only auxiliaries or propulsion too.

#### *B. Matured Experience*

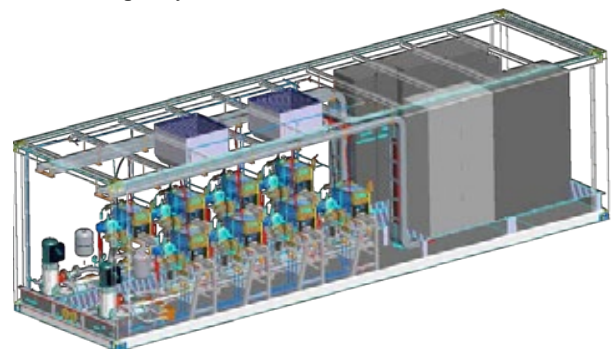
During the design phase of the HI-SEA laboratory, as well as during the previous project related to it, the team has been able to develop important knowhow and experience, among all, the design and operating principle of all the BOP components that represents the real issue for the marinization of the PEMFC systems.

#### *C. Research Plan*

A research plan for the first year of studies has been developed. The first objective is the evaluation of the PEMFC system various power configurations. The system will be operated with single and double FC branch, testing the functioning of the branch in parallel with and without DC/DC control. Later a battery hybrid configuration will be assessed taking advantage of the AC/DC rectifier and the electric controllable load to simulate the presence of batteries with the advantage of speeding-up their natural discharge and recharge behavior. Moreover, various configuration of single and double FC branch, with or without DC/DC control will be tested to evaluate the behavior of PEMFC electrically connected in parallel to the battery. The last configuration that will be explored will simulate the behavior of PEMFC to recharge batteries. The experimental results will be collected and exploited to develop diagnostic simulation models and dynamic simulation models, in order to develop tools to help the design process of future PEMFC systems.

#### IV. CONCLUSION

The HI-SEA Joint Laboratory represents the first and largest effort to solve key challenges in the energy sector and to generate solutions for the low-emission ships and enhance the innovation capacity of a new business sector.



**Fig. 3. PEMFC complete system**

#### ACKNOWLEDGMENT

The PEMFC system was built in 2015 as result of the project named “TESEO, Tecnologie ad alta Efficienza per la Sostenibilità Energetica ed ambientale On-board” [2], in collaboration with CNR-ITAE of Messina. The HI-SEA Joint Laboratory is funded by Fincantieri spa.

#### REFERENCES

- [1] TPG Laboratory: <http://www.tpg.unige.it/TPG/ies-laboratory/>
- [2] Project “TESEO, Tecnologie ad alta Efficienza per la Sostenibilità Energetica ed ambientale On-board”, MIUR cofounded projet PON02\_00153\_2939517, OR 2 in collaboration with Fincantieri, Isotta Fraschini Motori, CNR ITAE

## EXPERIMENTAL STUDY OF FUEL RECIRCULATION IN SOLID OXIDE FUEL CELL INTEGRATED WITH WATER REMOVAL UNIT

J. Kupecki\*, L. Szablowski\*\*, K. Motylinski\*, A. Zurawska\*,  
Y. Naumovich\*, A. Szczesniak\*\*, and J. Milewski\*\*

\*Department of High Temperature Electrochemical Processes  
(HiTEP), Institute of Power Engineering, Augustowka 36, 02-981  
Warsaw, (Poland)

\*\*Institute of Heat Engineering, Warsaw University of Technology,  
Nowowiejska 21/25, 00-665 Warsaw, (Poland)

**Abstract** – The solid oxide fuel cell (SOFC) can exhibit outstanding performance in stationary applications. The operation of fuel cells and the achievable efficiency is limited by several factors including the fuel utilization (FU). Typical values of the parameter lay in range 0.65-0.80 in single pass of fuel. Higher utilization of fuel can be achieved through fuel recirculation.

The 50 x 50 mm anode supported solid oxide fuel cell (AS-SOFC) was analysed using dedicated test bench. The experimental setup was equipped with couple of heat exchangers integrated with a chiller which allowed the reduction of the anode off-gas temperature to 0°C.

In the study, the effect of different levels of recirculation was analysed for a steady-state operation at given current density of the cell. This allowed quantifying the overall gain due to recycling of the anode off-gas. In selected operating conditions the increase of voltage was in range 18–31%.

**Index Terms** – SOFC, experimental characterization, fuel recirculation

### I. INTRODUCTION

The inherent advantage of SOFC can be explored by elevating fuel utilization by the recovery of remaining fuel in the anodic off-gases. Several methods were under consideration, including high- and low-temperature recirculation, an ejector or advanced connections including the in-series and multi-stage SOFC stacks. Utilization of the concept of chiller-based water removal is now proposed and evaluated.

### II. METHODOLOGY

The methodology was focused on analyzing the voltage of SOFC with and without recirculation process. The 50 x 50 mm

anode supported solid oxide fuel cell (AS-SOFC) shown in Fig. 1 produced in the Ceramic Department CEREL of The Institute of Power Engineering was analysed using the test bench in the Institute of Heat Engineering, Warsaw University of Technology. The metallic housing was adopted for characterization of the solid oxide fuel cell, and a dedicated sealing was prepared to eliminate leakages of both the fuel and the oxidant (see Fig. 2). The experimental setup was equipped with couple of heat exchangers integrated with a chiller (see Figs. 3 and 4) which allowed the reduction of the anode off-gas temperature to 0°C thus completely eliminating the water content from the lean fuel. The SOFC was fed with 4 NI/h of pure hydrogen and 30 NI/h of air. The peristaltic pump 120U/DV from Watson Marlow was used for recirculation of the exhaust of the anode. The rotational speed was adjusted to recycle between 0 and 9.55 NI/h. It should be noted that the earlier value represents no recirculation, and later describes the volumetric flow which does not include the water content. The application of the chiller in the test bench allowed complete removal of water from the recycled stream.

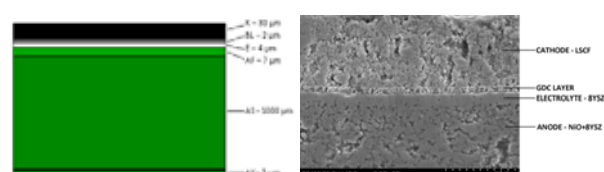


Fig. 1. Thickness of the interlayers of the analysed AS-SOFC (left) and its microstructure (right)



The parameters of the layers are given in Table 1. In the next step the cell was laser-cut in order to fit into the metallic housing for electrochemical characterization (Fig. 2).

TABLE I  
PARAMETERS OF THE INTERLAYERS OF THE AS-SOFC

Layer	Material	Thickness	Porosity
Cathode layer (K)	$\text{La}_{0.6}\text{Sr}_{0.4}\text{Fe}_{0.8}\text{Co}_{0.2}\text{O}_{3-\delta}$	30 $\mu\text{m}$	25 vol. %
Barrier layer (BL)	$\text{Gd}_{0.1}\text{Ce}_{0.9}\text{O}_2$	1.5 $\mu\text{m}$	-
Electrolyte (E)	8YSZ	4 $\mu\text{m}$	-
Anode functional layer (AF)	NiO/8YSZ 50/50 wt. %	7 $\mu\text{m}$	-
Anode support (AS)	NiO/8YSZ 66/34 wt. %	1.0 mm	25 vol. %
Anode contact layer (AK)	NiO	3 $\mu\text{m}$	-

In the next step the cell was laser-cut in order to fit into the metallic housing for electrochemical

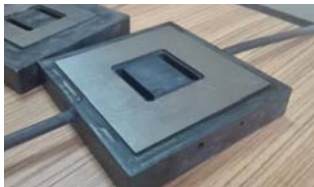


Fig. 2. Metallic housing used in the study

The housing was sealed using composite sealing and closed inside the high temperature vessel. The test rig was modified in order to allow engagement of the recirculation module. The cooler, heat exchanger and new piping were added. The schematic drawing of the setup for the experimental characterization of the cell under recirculation conditions can be seen in Fig. 4.



Fig. 3 The high temperature vessel used in the study

The current scope of the work was focused on elimination of the water content from the exhaust gases through cooling from the operating temperature (above 700°C) to 0°C. The methodology was oriented at observation of the effect of fuel recirculation on the electrochemical performance of the cell. In order to analyze the effect, several reference points were selected including. The level of recirculation was adjusted by

the manipulation of the rotational speed of the peristaltic pump.

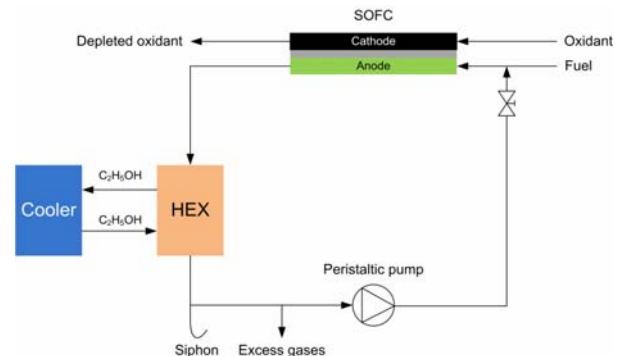


Fig. 4 Schematic drawing of the setup for fuel recirculation

The voltage gain for different levels of recirculation can be seen in Fig. 5. It should be noted that closing of the recirculation valve allows for slight (less than 300 Pa) pressure build up in the anodic compartments which results in marginal increase of the voltage of SOFC.

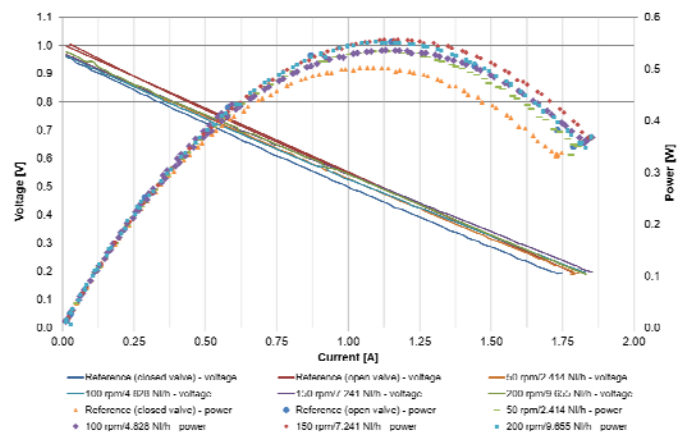


Fig. 5 comparison of the electrochemical performance (current-voltage and power) of cell under different working conditions

### III. CONCLUSION

The recirculation based on chilling of the anodic off-gas enables removal of entire volume of water once the gas is cooled to 0°C. The preliminary characterization of the cell based on the analysis of current-voltage and the power density curves allowed to compute the overall gain in the performance of the cell. It was observed that the value depends on the level of recirculation, but can be as high as 30%.

Auxiliary power consumption of the recirculation system is related to the parasitic power of the peristaltic pump and operation of the chiller unit. Combination of the concept in stationary SOFC-based system can however offer several advantages which will be explored in the second phase of the study.



## THE NUMERICAL MODEL FOR PREDICTIVE SIMULATION OF THE AS-SOFC STACK OPERATED IN DIR-SOFC MODE WITH PRESENCE OF HYDROGEN SULPHIDE IN THE FEEDING GAS

J. Kupecki\*, K. Motylinski\*, M. Blesznowski\*, D. Papurello\*\*, A. Lanzini\*\*, and M. Santarelli\*\*

\* Department of High Temperature Electrochemical Processes,  
Institute of Power Engineering, Augustowka 36, 02-981 Warsaw,  
(Poland)

\*\*Department of Energy (DENEG), Politecnico di Torino, Corso  
Duca degli Abruzzi 24, Torino 10129, (Italy).

**Abstract** – Experimental analysis of planar 100 mm x 100 mm SOFC cell was performed in direct internal reforming (DIR) mode of operation. The cell was examined as DIR-SOFC with and without the presence of H<sub>2</sub>S in the feeding gas. The results were analysed in order to find the correlation between the presence of the poisoning agent and the electrochemical performance. The lumped volume model was applied for the determination of the cell voltage. Using the experimental data it was possible to compute the relative change of the model parameters which describe the ionic and electronic conductivity of the SOFC cell. Model was adopted for predictive modeling of the solid oxide fuel cell operated with the presence of hydrogen sulphide.

**Index Terms** – SOFC, numerical modeling, experimental characterization, DIR-SOFC

### I. INTRODUCTION

The catalytic properties of anode materials of solid oxide fuel cells and their high operating temperature enable internal reforming of hydrocarbonaceous fuels. This feature allows to eliminate the external fuel processor and reduce the complexity of SOFC-based power units. Fuels such as natural gas and biogas contain however several impurities and other trace compounds which cause the deactivation and passivation of the catalytic materials of SOFCs and lead to rapid performance degradation. The accepted levels of compounds such as the hydrogen sulphide and hydrochloric acid were experimentally determined for different solid oxide fuel cells. It was proven that certain concentrations of these gases can be tolerated and will not cause a substantial drop of the cell voltage. This can be

well predicted for long-term operation of fuel cells.

### II. METHODOLOGY

Current study was oriented at evaluating anode supported solid oxide fuel cell (AS-SOFC) during operation in direct internal reforming mode (DIR-SOFC) with and without the presence of hydrogen sulphide. The motivation of the study was to define the correlation between the cells performance and the presence of H<sub>2</sub>S during operation with partial and complete direct internal reforming. The lumped volume model (LVM) was developed for the determination of the voltage of a cell, which was operated in a DIR mode. In the next step, the fuel cell was fueled by gas containing hydrogen sulphide. As a results, the model can be applied for simulation of planar cell which uses the anodic compartments for the steam reforming of incoming fuel and observe the effect when the direct internal reforming of a fuel containing H<sub>2</sub>S takes place. The model is based on experimental data which were measured for a planar 100 mm x 100 mm AS-SOFC.

In the second step, the numerical tool was used for sensitivity analysis of the degraded SOFC in order to define possible changes of the operational parameters. The focus of the study was to apply the equivalent electric circuit model which correlated several parameters with the voltage of the SOFC. In such a manner, it was possible to investigate the relative change of the ionic and electronic conductivity of the cell exposed to different working conditions, including DIR and feeding of hydrogen sulphide.

[illegible]

The SOFC cell was characterized inside a ceramic housing with golden current-voltage collectors. The mica sealing was adjusted to reduce the leakages of the fuel and the oxidant. Characterization of the cell was done with gradual step-wise increase of the ratio of direct internal reforming in consecutive steps: 0, 10, 25, 50, 75, 100 and then returning to 0. The flow streams of incoming fuel components for different cases are summarized in Table 1. The purpose of the variation was to maintain constant hydrogen equivalent for all cases.

DIR	CH <sub>4</sub> [Nml/min]	CO [Nml/min]	H <sub>2</sub> [Nml/min]	Total flow including all components [Nl/min]
0	7.33	251.25	623.08	2437.36
10	37.83	209.33	540.19	2369.75
25	76.41	156.64	384.26	2220.24
50	126.03	88.90	245.86	2096.39
75	164.07	39.23	141.94	2011.57
100	192.92	0.80	55.56	1930.78

Figure 10 is a line graph showing the variation of output voltage (mV) on the y-axis (ranging from 0 to 1200) against current (A) on the x-axis (ranging from 0 to 25). The graph displays data for ten different series, all showing a linear decrease in voltage as current increases. The series are: DIR0 (red line with circles), DIR25 (yellow line with circles), DIR75 (black line with circles), DIR100 (orange line with circles), DIR0 H2S (green line with circles), DIR10 H2S (blue line with circles), DIR25 H2S (cyan line with circles), DIR50 H2S (purple line with circles), DIR75 H2S (dark green line with circles), and DIR100 H2S BIS (dark blue line with circles). The DIR0 and DIR100 BIS series show the highest voltage, while the DIR100 H2S series shows the lowest voltage at higher currents.

Copyright © 2017

$$E_{SOFC} = \frac{E_{max} - \eta_f i_{max} r_1}{\frac{r_1}{r_2}(1 - \eta_f) + 1} \quad (1)$$

Figure 1 consists of two scatter plots. The left plot shows the relationship between the ratio of direct internal reforming (x-axis, 0 to 100) and the relative increase of the ionic resistance (y-axis, 0% to 40%) for the 1000°C series. The right plot shows the same relationship for the 1200°C series, with the y-axis ranging from 0% to 60%. Both plots include a linear regression line and a horizontal reference line at 40%.

Ratio of direct internal reforming	Relative increase of the ionic resistance (%) - 1000°C	Relative increase of the ionic resistance (%) - 1200°C
0	~2%	~0%
10	~8%	~5%
20	~15%	~10%
40	~19%	~15%
60	~18%	~25%
80	~18%	~35%
100	~34%	~58%

### III. CONCLUSION

## REFERENCES

## NEW INSIGHTS INTO MICROBIAL FUEL CELL-BASED SENSORS: THE ROLE OF FLUID DYNAMIC AND MATERIAL SELECTION

M. Quaglio\*, G. Massaglia\*\*\*, M. Gerosa\*\*\*, V. Margaria\*,  
A. Chiodoni\*, G.P. Salvador\*, N. Vasile\*, S.L.  
Marasso\*\*\*\*, M. Cocuzza\*\*\*\*, C.F. Pirri\*\*\*, and G.  
Saracco\*

\* Center For Sustainable Future Technologies @POLITO, Istituto  
Italiano di Tecnologia, Corso Trento 21, 10129 Torino, (Italy)

\*\* Applied Science and Technology Department, Politecnico di  
Torino, Corso Duca Degli Abruzzi 24, 10129, Torino, (Italy)

\*\*\*CNR-IMEM, Parco Area delle Scienze 37a, Parma, (Italy)

**Abstract** - This work proposes a novel approach to optimize and enhance the performances of single chamber microbial fuel cells (SCMFCs) based sensors implementing fluid dynamic simulations. When different flow rates are applied (i.e., 25 mL/h and 100 mL/h) the electrolyte flows differently into the cell, changing its speed and the drift-area in which the fluid/electrolyte is directly pumped by the drift process. Simulations show that the drift-area is optimized when using asymmetric squared SCMFCs (a-SCMFCs). In line with the fluid dynamic results, a-SCMFCs were fabricated by 3D-printing and then tested as potential sensors, exposing them to different sodium acetate concentrations. With the aim to enhance the role of fluid dynamics on the response of the devices, we tested commercial carbon-based materials with different morphologies as anodes. We show that further optimization is possible by careful identification and selection of the experimental parameters influencing fluid motion.

**Index Terms** –fluid dynamic modeling; microbial fuel cell; MFC-based sensor.

### I. INTRODUCTION

Microbial fuel cells (MFC) directly convert the chemical energy entrapped in organic matter into electrical energy, without the need of additional transduction. Interestingly if the device is maintained under non-saturated fuel, keeping constant the other parameters, variations in the feed concentration are directly proportional to the current generated by exoelectrogenic bacteria during oxidation. This is the principle governing the application of MFCs as an intriguing class of biosensor, for real-time, in-situ monitoring of water quality. [1] It has already been demonstrated that cell architecture and operative parameters as the flow rate have a preeminent role to

determine the final response of MFC-based biosensors.[2,3] With this respect fluid dynamic modelling [3] has demonstrated to be a potent tool to investigate MFCs, gaining a new point of view of the processes occurring inside the device. Indeed, even if it is obvious that a chemical-to-electrical energy conversion is the key process for the MFC operation, it is less obvious how much that conversion process can be influenced by the way the fluid (i.e., the electrolyte) can move inside the reactor.

This work proposes a novel approach to optimize and enhance the performances of single chamber microbial fuel cells (SCMFCs) investigated as sodium acetate sensors.

### II. EXPERIMENTAL

Fluid dynamic simulations were carried out by COMSOL Multiphysics®. Asymmetric squared SMCFC were fabricated by 3D printing (OBJET 30, Stratasys Ltd.). The electrodes area was 6.25 cm<sup>2</sup>, and the inner free volume was 12.5 mL. Two commercial carbon materials were used as anodes: carbon felt (CF, Sigratherm) and carbon paper (CP, Fuel Cell Earth LLC). Morphology of the materials was analyzed by field effect scanning electron microscopy (FESEM, ZEISS Merlin). Cathodes were fabricated applying polytetrafluoroethylene based diffusion layers (Fuel Cell Earth LLC) to the external side, and Pt based catalyst (by Sigma Aldrich) on the inner surface.[3] Titanium wires (Goodfellow) were used as electron collectors. A river sediment (Valle d'Aosta) was used as the inoculum source. The reference electrolyte was constituted by 12 mM of sodium acetate and 5.8 mM of ammonium chloride dissolved in phosphate buffer solution. All experiments were conducted in duplicate. After acclimation sodium acetate concentration was varied from 0.7 to 9 mM for the sensing

experiments. The SMFCs were run in fed batch mode, pumping fresh electrolyte by peristaltic pumps with different acetate concentrations into the reactors for 1 h with a minimum waiting time of 24 h before new replenishment. Two flow rates were tested: 25 mL/h and 100 mL/h.

### III. RESULTS AND DISCUSSION

When the electrolyte is forced to move by the pumping system, a drift process occurs into the reactor, that involves only a part of the inner volume. As a result, we can define a new parameter, the drift-area, which describes the percentage of the area in which the fluid is directly replaced during pumping. We have already demonstrated [3] that a misalignment of the inlet and outlet ports with respect to the symmetry axis of the reactor induces an asymmetric distribution of fluid trajectories inside the cell. The key result is that the drift-area is higher for the a-SCMFC (i.e., 65%, and 55% for the SCMFC, at 25 mL/h). The difference between the two reactors becomes more marked for higher flow rates: 56% for the a-SCMFC and 40% for the SCMFC, at 100 mL/h [3]. The simulated fluid distributions into the a-SCMFC for two flow rates are shown in Fig. 1a).

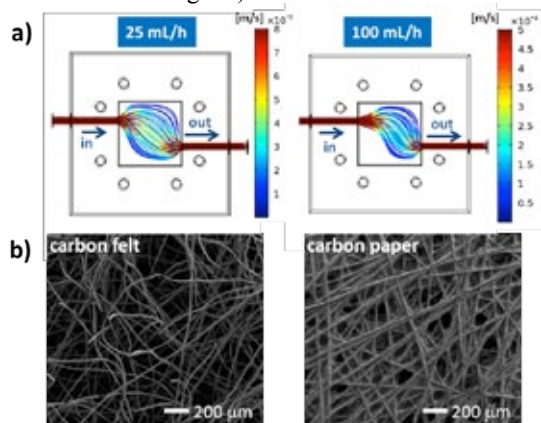


Fig. 1. a) Simulation of electrolyte distribution during the drift process at two different flow rates; b) morphology of CF and CP analyzed by FESEM.

To investigate more deeply the role of the drift process on the performance of MFC-based sensors, we fabricated by 3D-printing the simulated a-SCMFC, and tested the effect of the morphology of the anodic material. We selected and compared commercial CF and CP as anodes. Their morphology is shown by FESEM in Fig. 1b). Both materials are made of standard carbon fibers with an average diameter close to 10 µm, the difference is due to their 3D arrangements. In CF, fibers are only mechanically connected by entanglements, resulting in a highly porous material that can be colonized in depth by microorganisms, and in which the electrolyte can easily penetrate favoring diffusion of nutrients. On the contrary, in CP, fibers are connected by a carbon-based binder, resulting in a thin (i.e., 200 µm thick) membrane-like material with a good surface roughness to favor the anchoring of microorganisms on its top. Based on their morphology, we expect CP-based anodes to be more adequate to emphasize the rapid flow of the

electrolyte caused by high flow rates. Both the a-SCMFCs with the CP-based and the CF-based anodes were tested as potential sensors of sodium acetate variation. The response of the devices is reported in Fig. 2. For both materials a linear behavior has been obtained for both the flow-rates. Nonetheless, as expected, the device with the flat CP-based anode behaved significantly better, with a significantly higher sensitivity.

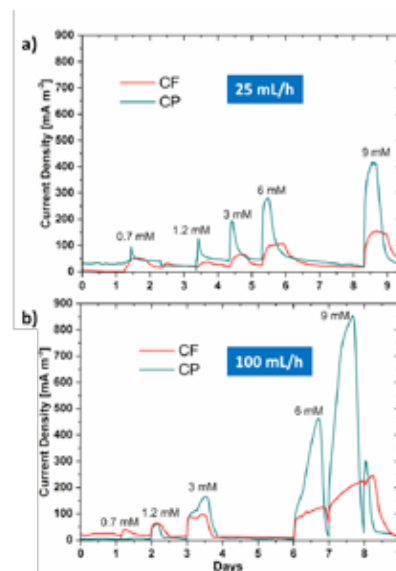


Fig. 2. Analysis of the behavior of a-SCMFC based sensors using CF or CP based anodes at two different flow rates: 25 mL/h in a) and 100 mL/h in b).

The improvement is particularly marked for the highest flow rate: when the electrolyte is pumped at 100 mL/h a sensitivity of 95.8 mA·m<sup>-2</sup>/mM is obtained for CP-based anodes, which is seven times higher than the one for CF-based anodes.

### IV. CONCLUSIONS

This work demonstrates that SCMFC based sensors can be optimized by a fluid dynamic approach. Optimization is strictly related to the ability of the reactor to favor the drift process inside it to speed up the response of the device. Nonetheless, further improvement requires combining the cell architecture to proper material selection.

### REFERENCES

- [1] Chouler, J., Di Lorenzo, M., Water Quality Monitoring in Developing Countries; Can Microbial Fuel Cells be the Answer?, Biosensors, Volume 5, 2015, Pages 450–470
- [2] Di Lorenzo, M., Thomson, A. R., Schneider, K., Cameron, P. J., Ieropoulos, I., A small-scale air-cathode microbial fuel cell for on-line monitoring of water quality, Biosensors and Bioelectronics, Volume 62, 2014, Pages 182-188.
- [3] Massaglia, G., Gerosa, M., Agostino, V., Cingolani, A., Sacco, A., Saracco, G., Margaria, V., Quaglio, M., Fluid Dynamic Modeling for Microbial Fuel Cell Based Biosensor Optimization, Fuel Cells, 2017, doi:10.1002/fuce.201700026

## IMPROVING THE HIGH TEMPERATURE PERFORMANCES OF NAFION-BASED MEMBRANES WITH SILICA-BASED MESOSTRUCTURED FILLERS FOR H<sub>2</sub>/O<sub>2</sub> PEM FUEL CELLS

B. Ozogul, M. C. Karaeyvaz, B. Ficicilar and F. Geyikci

Ondokuz Mayıs University, Faculty of Engineering,  
Chemical Engineering Department, 55139 Kurupelit, Samsun, (Turkey)

**Abstract** - In this paper, Nafion/SCMS-3 composite membrane was prepared using solvent-casting method. Properties of the composite membrane were investigated by Thermogravimetric Analysis (TGA), Fourier Transform Infrared Spectroscopy (FTIR), water uptake and compared with neat Nafion membrane. Analysis results showed that adding of SCMS into Nafion has improved water uptake capability of membrane.

**Index Terms** – Composite membrane, Nafion, PEM fuel cell, SCMS silica.

### I. INTRODUCTION

Nafion is the most widely used membrane as the electrolyte in PEM fuel cells due to their high proton conductivity (100 mS.cm<sup>-1</sup>) at temperatures below 100°C, mechanical strength, chemical stability and longevity (>60.000 hours) [1,2]. Ionic conductivity of Nafion reduces because of dehydration of water at the high temperature, above 100°C.

Mixing inorganic nanoparticles such as silica into Nafion is considered as an effective method to achieve the desired properties such as high ionic conductivity, effective water and thermal management, low water-dependency in a polymer membrane [3]. In this regard, mesoporous silica having a spherical geometry is used in this study. Usage of spherical silica as fillers increase water uptake capacity and enable ion transfer since water molecules can hold on the pores in the shell of silica. Water uptake for Nafion can be maintained with high surface area and tortuous pore structure with the use of Solid Core Mesoporous Shell (SCMS) silica.

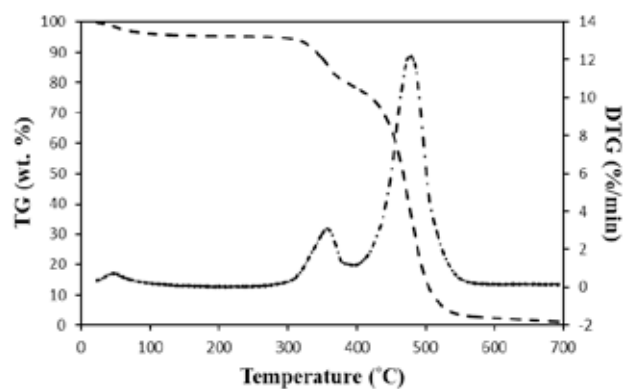
In this study, SCMS silica was synthesized and Nafion/SCMS-3 composite membrane was manufactured using solvent casting procedure. The composite membrane and neat Nafion membrane were characterized by using TGA, FTIR and water uptake measurements.

### II. EXPERIMENTAL

15 wt. % Nafion solution was dried at 80°C in an oven. 10 wt. % of Nafion solution in DMAc (N-N dimethylacetamide) was prepared. The polymer mixture was stirred for 2 hours in a magnetic stirrer. The required amount of SCMS silica was added to polymer. The mixture was stirred in an ultrasonic bath for 1 hour and cast onto glass surface. It was allowed to dry at 100°C overnight. Particle size and the content of SCMS in composite membranes were 400 nm and 3 wt.%, respectively.

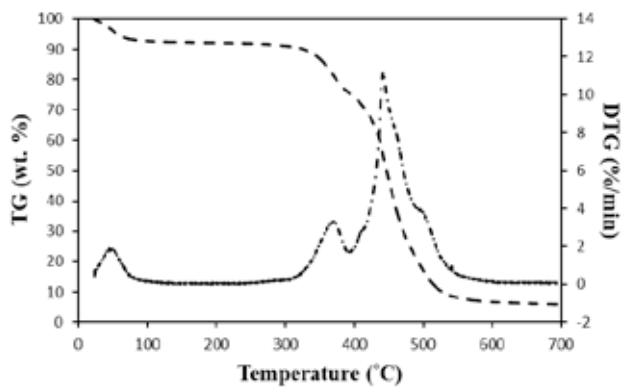
### III. RESULTS

#### A. Thermal Analysis



(a)





(b)  
Fig. 1. TG and DTG curves for a) Nafion and  
b) Nafion/SCMS-3 membranes.

Fig. 1 shows that TG and DTG curves of Nafion and Nafion/SCMS-3 membranes between 25 and 700 °C. The first peak (25-100 °C) which can be seen for both membranes is occurred due to evaporation of water. The other peak between temperatures 300 °C and 400 °C represents decomposition of the  $\text{-SO}_3\text{H}$  groups. The last peak (400-550 °C) is caused by the degradation of Nafion polymer chain [4]. At the end of the thermal process, about 1.1 and 5.9 wt. % of total mass remained as solid residue for Nafion and Nafion/SCMS-3 membranes, respectively.

#### B. Water Uptake

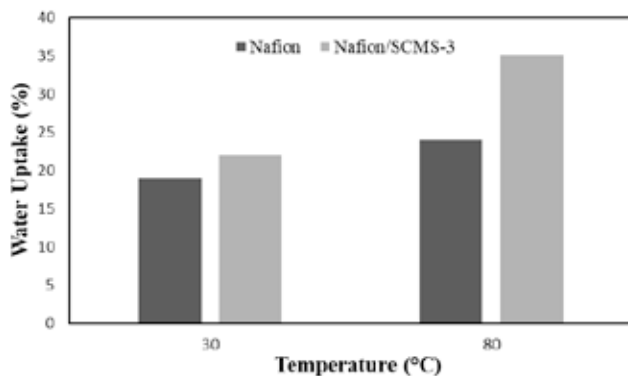


Fig. 2. Water uptake of Nafion and Nafion/SCMS-3 membranes.

Fig. 2 shows the water uptake results for the Nafion and Nafion/SCMS-3 nanocomposite membranes at 30 and 80 °C. According to the results of the analysis, the water uptake for both membranes increased with temperature and due to the hygroscopic nature of the SCMS, the water uptake capacities of the membranes increased with the addition of silica compared to neat Nafion.

#### C. Fourier Transform Infrared Spectroscopy (FT-IR)

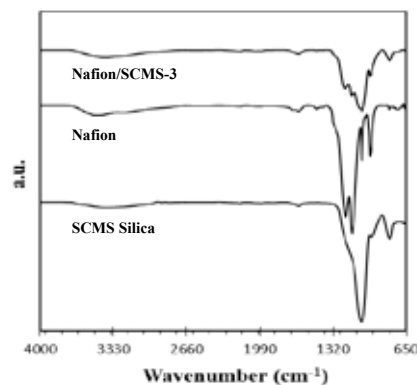


Fig. 3. FT-IR spectra of SCMS silica, Nafion and Nafion/SCMS-3 membranes.

FT-IR spectra of SCMS silica, Nafion and Nafion/SCMS-3 are given in Fig. 3. Symmetric and asymmetric C-F stretching bands are seen around 1156  $\text{cm}^{-1}$  and 1231  $\text{cm}^{-1}$ , respectively. The peak around 980  $\text{cm}^{-1}$  is related to  $\text{CF}_2\text{-CF(R)-CF}_3$  groups. S-O stretching band is seen at 1056  $\text{cm}^{-1}$ . The peak around 800  $\text{cm}^{-1}$  is related to  $\text{SiO}_2$  for the synthesized composite membrane.

#### IV. CONCLUSION

In this study, thermal properties, water uptake and FT-IR spectra of Nafion/SCMS-3 and neat Nafion membranes were investigated. Water uptake capability of Nafion membrane was increased with the use of SCMS silica.

#### REFERENCES

- [1] Alvarez, A., Guzmán, C., Carbone, A., Saccà, A., Gatto, I., Pedicini, R., ... & Arriaga, L. G. Composite membranes based on micro and mesostructured silica: A comparison of physicochemical and transport properties. *Journal of Power Sources*, Volume 196, 2011, Pages 5394-5401.
- [2] Yang, C. W., Chen, C. C., Chen, K. H., & Cheng, S. Effect of pore-directing agents in SBA-15 nanoparticles on the performance of Nafion®/SBA-15n composite membranes for DMFC. *Journal of Membrane Science*, Volume 526, 2017, Pages 106-117.
- [3] Rodgers, M. P., Shi, Z., & Holdcroft, S. Transport properties of composite membranes containing silicon dioxide and Nafion®. *Journal of Membrane Science*, Volume 325, 2008, Pages 346-356.
- [4] Devrim, Y., Erkan, S., Baç, N., & Eroglu, I. Improvement of PEMFC performance with Nafion/inorganic nanocomposite membrane electrode assembly prepared by ultrasonic coating technique. *International Journal of Hydrogen Energy*, Volume 37, 2012, Pages 16748-16758.

## NOVEL HIGH PERFORMANCE SPES/SCMS AND SPEEK/SCMS COMPOSITE MEMBRANES FOR HIGH TEMPERATURE H<sub>2</sub>/O<sub>2</sub> PEM FUEL CELLS

M. C. Karaeyvaz, B. Ozogul, B. Ficicilar and F. Geyikci  
Ondokuz Mayıs University, Faculty of Engineering, Chemical  
Engineering Department, 55139 Kurupelit, Samsun (Turkey)

### Abstract

The aim of this work is improving the ionic conductivity mechanical and thermal stability of sPEEK and sPES membranes at high temperatures herein preparing composite membranes using SCMS (solid core mesoporous shell) silica additive. Composite membranes which contains 3 % (w/w) SCMS silica are prepared by solvent casting method using DMAc as solvent. The N<sub>2</sub> adsorption results for SCMS silica showed it has mesoporous structure, 386.8 m<sup>2</sup>/g surface area and 0.41 cc/g pore volume. Spherical geometry with 400 nm particle diameter observed from SEM images. Obtained composite Nafion/SCMS-3 has a thickness of 60 µm.

**Index Terms** – Composite membrane, SCMS silica, sPEEK, sPES.

### I. INTRODUCTION

There is a trend pertinent with hydrocarbon based polymer membrane alternate to nafion since nafion membrane has some disadvantages because of it's high cost, high fuel permeability and low proton conductivity at elevated temperature and low humidity levels [1,2]. Among the nonfluorine containing polymers, PEEK and PES membranes has good mechanic and thermal properties but their low ionic conductivity restricts their use as a membrane for PEM fuel cells [3]. Hybrid organic-inorganic composite membranes are seen as an alternate to obtain a membrane which has both high ionic conductivity and good mechanical strength [1,4]. Conserving humidity, decreasing electro osmotic drag and fuel permeability and development of mechanic and thermal properties without decreasing proton conductivity are targeted by the use of hydrophilic inorganic-organic composite membranes [4]. Hydrophilic membranes can adsorb more water and it provides proton transfer. Hydrophilic inorganic additive materials such

as SiO<sub>2</sub> [5, 6] is used for the synthesis of composite membranes in the literature. Mesoporous silica materials have porous structure and high surface area and enable water adsorption and studies related with composite membranes remarks that spherical geometry facilitates ion transfer and water molecules can adsorb on pores [7, 8]. Synthesis of membranes which have good mechanical properties and high proton conductivity at elevated temperature due to water retention was intended by use of SCMS silica additive for sPEEK and sPES hydrocarbon polymers.

### II. EXPERIMENTAL

#### A. Synthesis of SCMS Silica Additives

The synthesis of SCMS silica was achieved as prepared elsewhere [9]. 3,14 ml ml of ammonia solution was added 74 ml of ethanol and 10 ml deionized water containing solution. 6 ml of TEOS was added to prepared solution and stirred 1 h at 40°C. At the end of 1 h 5 ml TEOS and 2 ml C18TMS solution was added slowly to the mixture and stirred 1h. The colloids were washed with deionized water until neutral pH and dried at 80°C for 12 h. After that, materials were calcined at 600°C under dry air flow.

#### B. Preparation of Composite Membranes

PEEK was dried at 100°C overnight before sulfonation. 5 wt. % PEEK-H<sub>2</sub>SO<sub>4</sub> solution was obtained by adding PEEK into the H<sub>2</sub>SO<sub>4</sub> step by step and stirred for 5 h at 50°C. After this period, resulting solution was added into the ice cooled water slowly to end sulfonation reaction and stirred 1 h and left overnight. Obtained polymer precipitate was washed with deionized water until neutral pH and dried at 100°C for 10 h. Sulfonated PEEK (sPEEK) was dissolved in DMAc (10 wt. % sPEEK solution). 3 wt % SCMS additives were added to

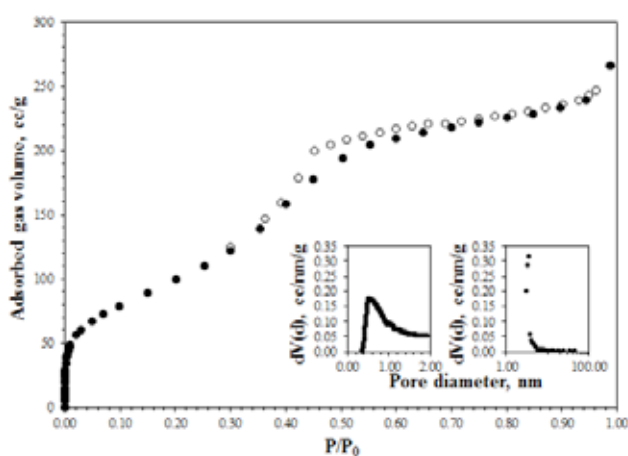
Copyright © 2017

polymer solution and ultrasonicated for 1 h. The resulting mixture was cast onto petri dishes and solvent was evaporated slowly. Evaporation was achieved for 1 day at room temperature, 1 day at 50°C and 1 day at 100°C respectively. Prepared membranes was removed from petri dish by wetting with deionized water. All the obtained membranes was stored at deionized water before testing.

### III. RESULTS AND DISCUSSION

SCMS silica was characterized by N<sub>2</sub> adsorption-desorption and scanning electron microscope (SEM). Obtained isotherm and pore size distribution graphs was given at figure 1. Isotherm shape corresponds to mesoporous materials and sample also contains micropores (adsorbed volume smaller than 0.02 relative pressure). Surface area values are given at table 1. BJH surface area and volume are nearly 70% of BET surface area and total pore volume. Average meso and micro pore sizes are 3.50 nm and 0.53 nm respectively. Particle size of the SCMS is obtained from SEM images (figure 2) and it is 400 nm and all the particles has nearly the same size.

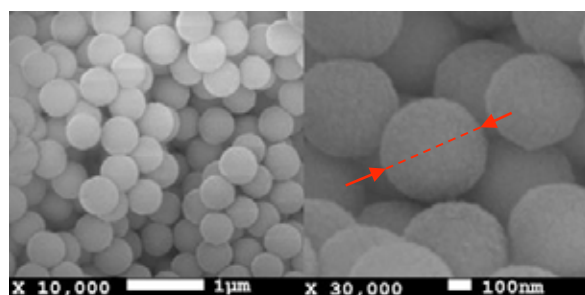
The average thickness of the synthesized membrane which contains 3 wt% SCMS silica is 60 µm. Characterization studies related with membrane properties such as proton conductivity, water uptake, gas/fuel (H<sub>2</sub>/O<sub>2</sub>/air) permeability, thermal stability and performance tests in H<sub>2</sub>/O<sub>2</sub> PEM fuel cell are under progress and going to be presented at congress.



**Fig. 1.** N<sub>2</sub> adsorption/desorption isotherm and pore size distributions (HK and BJH methods).

**TABLE 1.** PHYSICAL PROPERTIES OF SCMS SILICA.

BET Surface area, m <sup>2</sup> /g	386.78
BJH Surface area, m <sup>2</sup> /g	277.65
Pore volume, cc/g	0.41
BJH pore volume, cc/g	0.28
Average mesopore diameter, nm	3.50
Average micropore diameter, nm	0.53
Particle size, nm	400



**Figure 2.** SEM images of SCMS silica.

### IV. CONCLUSION

Synthesized SCMS silica has desired mesoporous structure and spherical geometry as seen from N<sub>2</sub> adsorption and SEM images. Measured thickness of 3 wt % SCMS silica containing membrane is almost same at different sides and it resembles homogeneous dispersion of silica particles.

### REFERENCES

- [1] Kim, D. J., Jo, M. J., Nam, S. Y., A review of polymer-nanocomposite electrolyte membranes for fuel cell application. *Journal of Industrial and Engineering Chemistry*, 21, 2015, 36-52.
- [2] Rikukawa, M.; Sanui, K. Proton-conducting polymer electrolyte membranes based on hydrocarbon polymers. *Progress in Polymer Science*, 25.10, 2000, 1463-1502.
- [3] Hasani-Sadrabadi, Mohammad M., et al. Novel high-performance nanocomposite proton exchange membranes based on poly (ether sulfone). *Renewable Energy*, 35.1, 2010, 226-231.
- [4] Li, Q., et al. Approaches and recent development of polymer electrolyte membranes for fuel cells operating above 100 °C. *Chemistry of materials*, 15.26, 2003, 4896-4915.
- [5] Rodgers, M. P., Shi, Z., Holdcroft, S., Transport properties of composite membranes containing silicon dioxide and Nafion®. *Journal of Membrane Science*, 325.1, 2008, 346-356.
- [6] Zhang, J., et al. High temperature PEM fuel cells. *Journal of power Sources*, 160.2, 2006, 872-891.
- [7] Lou, L., Pu, H., Preparation and properties of proton exchange membranes based-on Nafion® and phosphonic acid-functionalized hollow silica spheres. *International journal of hydrogen energy*, 36.4, 2011, 3123-3130.
- [8] Yu, Q., et al. Single-ion Polyelectrolyte/Mesoporous Hollow-Silica Spheres, Composite Electrolyte Membranes for Lithium-ion Batteries. *Electrochimica Acta*, 182, 2015, 297-304.
- [9] Kim, J. H., et al. Hollow core/mesoporous shell carbon capsule as an unique cathode catalyst support in direct methanol fuel cell. *Applied Catalysis B: Environmental*, 88.3, 2009, 368-375.

## STABILITY, REGENERABILITY AND SULFUR POISONING OF LOW LOADING Rh-BASED CATALYST FOR STEAM REFORMING OF N-DODECANE

C. Italiano, A. Vita, M. Laganà, L. Pino, V. Recupero  
CNR-ITAE "Nicola Giordano", Via S. Lucia sopra Contesse 5, 98126 Messina, Italy

**Abstract** – 0.6wt.% Rh/CeO<sub>2</sub> catalyst was synthesized by the Solution Combustion Synthesis (SCS) method, producing a low-cost noble metal-based system due to the simultaneous high dispersion and low metal phase content. The catalyst was characterized by the XRD, N<sub>2</sub>-physisorption, CO-chemisorption, TPR, TPO and TEM measurements. Deactivation by carbon deposition was investigated in Steam Reforming (SR) of n-dodecane, used as surrogate for diesel fuel, in order to explore the appropriate coke-free reaction conditions. The catalyst regenerability was also investigated. Then, the effect of sulfur poisoning was studied in SR of n-dodecane doped with thiophene, used as model compound for the organic sulfur in diesel fuel. Stability tests were performed at various steam-to-carbon ratio (S/C = 1–2.5), space velocity (GHSV = 16,000–40,000 h<sup>-1</sup>) and sulfur content (0–100 ppm S).

**Index Terms** – Hydrogen, Dodecane Steam Reforming, Rh catalyst, Carbon deposition, Sulfur poisoning.

### I. INTRODUCTION

Diesel, with its existing logistic infrastructure, considerable well-to-wheel efficiency, safe handling feature, adequate world-wide fuel storage and high energy density, is an attractive source of H<sub>2</sub> production via SR. However, coke and carbon deposition still remain a major challenge in the processing of sulfur-containing heavy hydrocarbons.

In this study, the performance of Rh/CeO<sub>2</sub> catalyst was studied towards SR of sulfur-free n-dodecane, used as surrogate for diesel fuel. Stability tests were carried out over 100 h of time-on-stream at GHSV = 16,000 h<sup>-1</sup>, varying the steam-to-carbon (S/C) molar ratio from 2.5 to 1.0. Moreover, the regeneration ability of the system was studied at S/C = 1 and GHSV = 40,000 h<sup>-1</sup> through deactivation/regeneration cycles. Then, the sulfur tolerance (30, 60 and 100 ppm of sulfur) was investigated under SR of n-dodecane doped with thiophene, used as model compound for the organic sulfur in diesel fuel. The catalytic tests were carried out using the experimental set-up previously described [1]; the temperature-controlled bed

configuration (500–800°C) was used in order to avoid carbon/coke deposition due to cracking of n-dodecane.

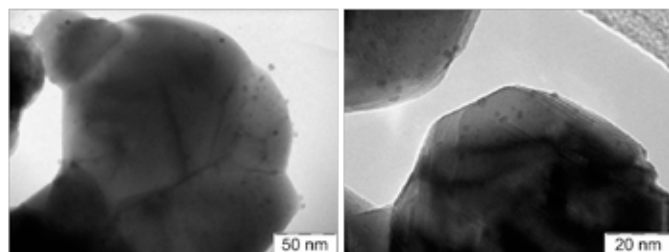
### II. RESULTS AND DISCUSSION

#### A. Characterization of fresh Rh/CeO<sub>2</sub> catalyst

Nanosize crystalline metal oxides were produced by solution combustion method. Table I shows the main properties of the synthesized Rh/CeO<sub>2</sub> sample. The characterization results of the Rh/CeO<sub>2</sub> catalyst suggested that CeO<sub>2</sub> crystallite sizes of ca. 20 nm were obtained. At the same time, highly dispersed system was synthesized, with Rh sizes of ca. 2–5 nm, as evidenced by CO-chemisorption and TEM analysis (Figure I). Moreover, XRD patterns highlighted the formation of the Ce-Rh-O solid solution coupled with a SMSI as revealed from TPR results.

**TABLE I**  
TEXTURAL AND STRUCTURAL PROPERTIES OF SYNTHESIZED Rh/CeO<sub>2</sub> SAMPLE.

S <sub>A</sub> <sub>BET</sub> (m <sup>2</sup> /g)	XRD		CO-chemisorption		TEM
	CeO <sub>2</sub> lattice parameter (nm)	CeO <sub>2</sub> particle size (nm)	Rh particle size (nm)	Rh dispersion (%)	Rh particle size (nm)
31.0	0.5386	21.9	5.8	18.9	2–4



**FIGURE I**  
TEM IMAGES OF THE AS PREPARED Rh/CeO<sub>2</sub> CATALYST.

### B. SR of sulfur-free *n*-dodecane

Rh-based catalyst showed stable catalytic activity at S/C of 2.5 with H<sub>2</sub> concentration of ca. 50% (N<sub>2</sub>-free basis) and absence of by-products (Figure II). Decreasing the S/C to 1.5, the activity remained stable, while significant deactivation was observed at S/C of 1 after 50 h of time-on-stream [2].

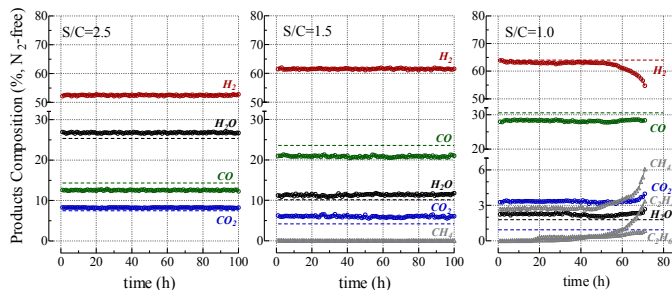


FIGURE II

SR STABILITY TESTS OF SULFUR-FREE N-DODECANE AT DIFFERENT S/C RATIO.

Three types of carbon deposits were identified in steam reforming of *n*-dodecane at S/C = 1, namely amorphous, filamentous and pyrolytic carbon (Figure III). However, the regeneration step, carried out under air flow, allowed to restore the initial activity, due to the removal of carbon deposits. Indeed, deactivation/regeneration cycles were repeated, indicating that full catalyst regeneration was possible.

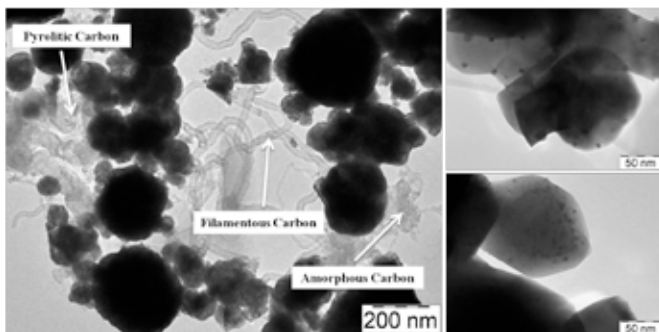


FIGURE III

TEM IMAGES OF THE USED Rh/CeO<sub>2</sub> CATALYST AT S/C = 1.

### C. SR of sulfur-containing *n*-dodecane

Reforming experiments were performed at three different sulfur concentrations, namely 30, 60 and 100 ppm S. A slight decrease in catalytic performance, in term of H<sub>2</sub> concentration, was observed, becoming more pronounced by increasing the sulfur concentration in the feed. Moreover, a significant improvement in the sulfur tolerance was observed increasing the steam-to-carbon (S/C) ratio from 1.5 to 2.5 (Figure IV).

Coking seems to be the main deactivation mechanism in the SR of sulfur-containing *n*-dodecane and it was promoted by increasing the sulfur concentration. The formation of Rh sulfide could explain the loss of activity observed, allowing for thermal

cracking reactions of the hydrocarbon adsorbed on the sulfur-poisoned active phase and migrated to the support surface.

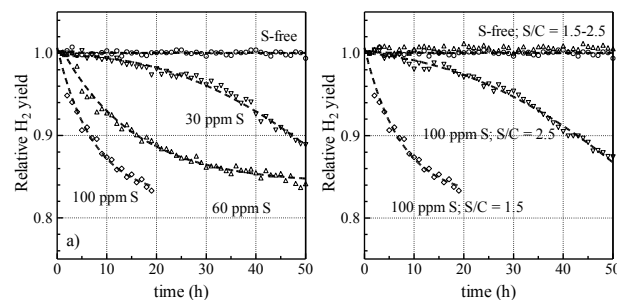


FIGURE IV

SR STABILITY TESTS AT DIFFERENT SULFUR CONTENT.

Huge amounts of pyrolytic carbon were found on the support, as evidenced in TEM and TPO analysis, justifying the thermal cracking mechanism. However, partial deactivation due to oxysulfides formation on the CeO<sub>2</sub> support could not be excluded, especially at high sulfur content (100 ppm S) that favoured Ce<sub>2</sub>O<sub>2</sub>S formation. The presence of oxysulfides increased the surface acidity and suppressed, in turn, the carbon gasification, inhibiting the interactions between carbon deposits and surface oxygen species. The beneficial effect of steam in combination with H<sub>2</sub> allowed removing the sulfide specie and favoring the gasification of coke, leading to improved sulfur tolerance of the Rh/CeO<sub>2</sub> catalyst.

### III. CONCLUSION

The solution combustion synthesized 0.6wt.% Rh/CeO<sub>2</sub> catalyst showed an outstanding catalytic activity for the steam reforming of sulfur-free *n*-dodecane, due to high metal dispersion and strong metal-support interaction. The presence of sulfur enhanced the carbon deposition rate, which was the main cause of catalyst deactivation. Higher steam content improved the gasification of carbon and the sulfur resistance of the Rh/CeO<sub>2</sub> catalyst for the steam reforming of *n*-dodecane. due to the regeneration capacity of steam and H<sub>2</sub>.

### REFERENCES

- [1] Vita, A., Italiano, C., Fabiano, C., Pino, L., Laganà, M., Recupero, V., Hydrogen-rich gas production by steam reforming of *n*-dodecane. Part I: Catalytic activity of Pt/CeO<sub>2</sub> catalysts in optimized bed configuration, Applied Catalysis B: Environmental, Volume 199, 2016, Pages 350-360.
- [2] Vita, A., Italiano, C., Pino, L., Laganà, M., Recupero, V., Hydrogen-rich gas production by steam reforming of *n*-dodecane. Part II: Stability, regenerability and sulfur poisoning of low loading Rh-based catalyst, Applied Catalysis B: Environmental, Volume 218, 2017, Pages 317-326.



## PROCESS SIMULATION MODEL OF HT-PEM FUEL CELL BASED MICRO-CHP SYSTEMS INCLUDING PERFORMANCE DEGRADATION ISSUES

R. Taccani<sup>1\*</sup>, T. Chinese<sup>1,2</sup>, N. Zuliani<sup>1</sup>, F. Ustolin<sup>1</sup>, B. Marmiroli<sup>3</sup>, H. Amenitsch<sup>3</sup>

<sup>1</sup> University of Trieste, via Valerio 10, 34127 Trieste (Italy)

<sup>2</sup> Cenergy srl, c/o AREA Science Park - Basovizza, 34100 (Italy)

<sup>3</sup> Institute of Inorganic Chemistry, Graz University of Technology, Stremayrgasse 9/IV, Graz 8042, Austria

**Abstract** - This work focuses on the experimental analysis of degradation of HTPEM MEAs and the degradation modeling for long term performance analysis of HTPEM based CHP system. In the presented research, experimental data on MEAs degradation due to different operation conditions have been collected and compared. Degradation data have been used to develop a degradation model that has been implemented in a micro-CHP energy simulation model. The micro-CHP performance has been assessed over long period of time taking into account the stack degradation.

**Index Terms** - Degradation, Fuel Cells, HTPEM, micro-CHP, Modeling.

### I. INTRODUCTION

Fuel cells based Combined Heat and Power (CHP) systems have the great advantage to maintain good electrical efficiencies for small size plants and during part load operation.

A promising technology is represented by High Temperature Polymer Electrolyte Membrane (HTPEM) fuel cells. However, a major problem for this type of fuel cells is the degradation rate that is higher than Low Temperature Fuel Cells (LTPEM FC). Losses in MEA performance associated with fuel cell operation typically occur via processes related to degradation of the catalyst layer [1,2]. To better understand the degradation phenomena involved in PEM fuel cells, several diagnostic tools have been used in this research, in particular: Polarization Curve (PC), Electrochemical Impedance Spectroscopy (EIS) and Cyclic Voltammetry (CV). Among nano-morphological analysis techniques, Small Angle X-ray Scattering (SAXS) has been used to support the study of catalyst degradation. SAXS is a method to characterize the MEA of a fuel cell and its degradation since it is able to give information about size, shape and distribution of catalyst nano-particles over large portion of the active area and, in principle, in-situ [3]. When analyzing CHP systems, performance over long period is an important factor and, therefore, degradation should be considered. In this work, the energy simulation model developed by the authors in

[4], has been improved taking into account the degradation of the fuel cell stack in order to assess the performance of the system over long period of operation. System parameters, such as electrical and thermal energy production, import/export of electricity and primary energy savings have been calculated and compared for different system configurations.

### II. METHODOLOGY

The MEAs used in the test are Celtec-P 1000, commercial H<sub>3</sub>PO<sub>4</sub>/PBI MEAs for high temperature PEM fuel cells produced by BASF Fuel Cell. All tests have been performed following the methodology already used by the authors in previous works [1,3]. The system modeled is composed of a 1 kW<sub>el</sub> fuel cell system, which encompasses a fuel processor and a HTPEM fuel cell stack, and a 3 kWh lithium battery pack. An auxiliary boiler is used when heat from the fuel cell system is not sufficient for providing the heating demand. Fuel cell system, battery pack and grid are electrically connected by means of a power conditioning system. Additional information on the system were presented by the authors in [5]. In order to take into account for fuel cell performance degradation, a reference polarization curve for a new CHP system (zero hour of operation) has been considered and a degradation rate has been taken into account that allows modeling the polarization curve considering stack performance variation over time. The voltage degradation over time is modeled according to the following equation:

$$V_{cell}(j,t) = V_{0,cell}(j) - DR_{cell}(j) \times t$$

Where  $j$  is the current density (mA/cm<sup>2</sup>),  $DR$  is the single cell degradation rate (μV/h),  $t$  is the operational time (h). The obtained time-dependent polarization curves have been implemented in the previous described process model and the fuel cell system efficiency over time has been calculated.

Copyright © 2017

### III. MAIN RESULTS

Table 1 shows the degradation rates for MEAs tested with different load profiles and the Pt particle size variation caused by ageing test.

TABLE 1 Pt PARTICLE SIZES AND DEGRADATION RATES FOR ALL MEAs

MEA label	Load profile	$r_{\text{mean}}$ (nm)	Deg.rate ( $\mu\text{V/h}$ )
MEA 263 [1]	Untouched	2.61	-
MEA 264 [1]	Triangular [0.01 – 0.5]V	4.54	34
MEA 265 [1]	Triangular [0 – 0.5]V -2s OCV	5.28	45
MEA 266 [1]	Start & Stop cycles	5.02	55
MEA 271 [3]	Triangular [0 – 0.5]V -2s OCV	5.51	44
MEA 272 [3]	Constant load 0.22 A/cm <sup>2</sup>	4.65	30
MEA 273 [3]	Constant load 0.22 A/cm <sup>2</sup>	4.41	29
MEA 274	Constant OCV	3.82	444
MEA 275	Untouched	2.38	-
MEA 276	Start & stop cycles	-	81
MEA 277	Constant OCV	-	124

Data show that load cycling is more stressing than constant load operation and that OCV is the most detrimental operational condition. SAXS analysis, together with other electrochemical techniques, is expected to support the quantification of degradation attributable to the different operating conditions. Experimental polarization curves measured in different aging tests have been used to implement an overall degradation rate as shown in Figure 1, where polarization curves degradation is shown over time.

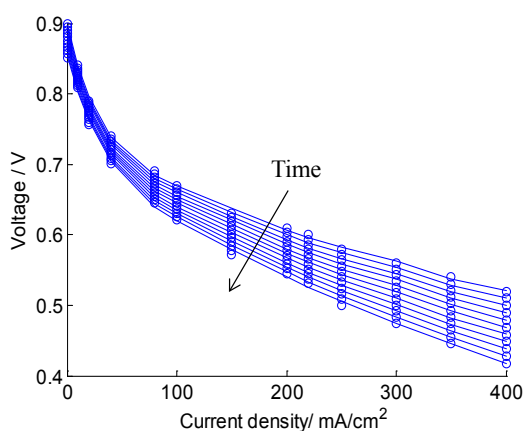


FIGURE 1 CELL POLARIZATION CURVES OVER ONE YEAR OF OPERATION. EACH CURVE REPRESENTS FUEL CELL PERFORMANCE AFTER 796 H OF OPERATION [6].

As shown in Figure 2, fuel cell degradation on 1kWe CHP and battery system causes a 10% annual electrical production reduction, and an increase of the thermal energy production of 4%. Degradation causes also a Primary Energy Saving (PES) variation from 22% to 20% over one year of operation. Neglecting cost issues, in order to recover the annual electrical energy loss due to the fuel cell performance degradation over time, a larger fuel cell stack can be chosen. If, for the same power demand profile, a 1.2kWe CHP system is chosen, the electrical production reduction due to degradation is about 8%

while the increasing of thermal production is about 6%, and PES would be again 22%.

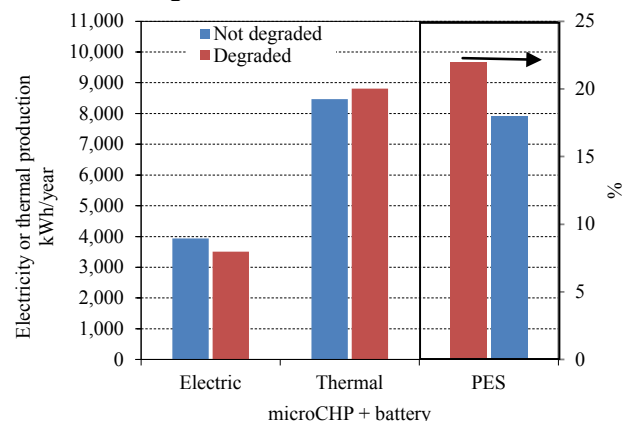


FIGURE 2 MICRO-CHP SYSTEM ENERGY BALANCE

### CONCLUSIONS

Degradation data on HTPEM MEAs have been collected for different operational conditions and experimental data have then been used to infer a possible degradation rate used to develop a simulation model to assess the long term performance of residential micro CHP system. The loss of electrical efficiency can be compensated by the higher thermal production. The detrimental effect can be mitigated choosing to increase the size of the stack, even if this condition affects system cost. In particular, the model allows assessing the impact of battery storage on system energy production, primary energy saving and on the import and export of energy from the electrical grid. In the future, the degradation model could be improved taking into account for the degradation attributable to the different operating conditions.

### REFERENCES

- [1] Valle F, Zuliani N, Marmioli B, Amenitsch H, Taccani R. SAXS Analysis of Catalyst Degradation in High Temperature PEM Fuel Cells Subjected to Accelerated Ageing Tests. *Fuel Cells* 2014;14:938–44.
- [2] Moçotéguy P, Ludwig B, Scholta J, Barrera R, Ginocchio S. Long term testing in continuous mode of HT-PEMFC based H3PO 4/PBI celtec-PMEAs for  $\mu$ -CHP applications. *Fuel Cells* 2009;9:325–48.
- [3] Taccani R, Chinese T, Boaro M. Effect of accelerated ageing tests on PBI HTPEM fuel cells performance degradation. *Int J Hydrogen Energy* 2017;1–9.
- [4] Zuliani N. Energy simulation model and parametric analysis of a micro cogeneration system based on a HTPEM fuel cell and battery storage. *Spec Issue ICAE 2013* 2013;1–10.
- [5] Zuliani N, Taccani R. Simulation Model of a High Temperature PEM Fuel Cell Based Cogeneration System. *23th Int. Conf. Effic. Cost, Optim. Simul. Environ. Impact Energy Syst.*, 2010.
- [6] Taccani R, Chinese T, Zuliani N. Performance analysis of a micro CHP system based on high temperature PEM fuel cells subjected to degradation. *Energy Procedia* 2017;126:421–8.

## THE ROLE OF HYDROGEN MOBILITY IN FULFILLING EU 2050 TARGETS ON GHG EMISSIONS REDUCTION

P. Colbertaldo\*, G. Guandalini\*, and S. Campanari\*

\*Department of Energy, Politecnico di Milano, Via Lambruschini 4A, 20156 Milano (Italy)

**Abstract** - In this work, the role of alternative mobility in road transport is studied, focusing on the introduction of hydrogen fuel cell electric vehicles (FCEVs) and plug-in electric vehicles (PEVs) in the long-term evolution of the Italian energy system. The contribute of hydrogen vehicles in achieving target GHG emissions reduction is studied; a comparison between PEV-only or FCEV-only scenarios shows that an integration of the two technologies leads to better results than the deployment of a single solution.

**Index Terms** – emissions reduction, energy system integration, hydrogen, mobility.

### I. INTRODUCTION

In the effort to tackle climate change, the European Union (EU) set an ambitious target of 80% reduction in greenhouse gases (GHG) emissions below 1990 level by 2050 [1], with contributions from all energy sectors. Being the second largest emitter after power generation, road transport plays a key role. The ‘Strategic Plan for Alternative Fuels’ presented by Italy in November 2016 includes, among others, hydrogen and electricity as clean energy vectors for mobility. While the growing presence of Plug-in Electric Vehicles (PEVs) affects the electrical load, the addition of Fuel Cell Electric Vehicles (FCEVs) creates a demand for clean hydrogen that could be satisfied by electrolysis-based solutions fed with renewable electricity. Thus, the power and transport sector tend to interweave, increasing overall networks complexity while potentially improving the exploitation of intermittent resources.

Taking into account the transformation of the power sector in terms of RES installation, electrical load evolution, and energy exchange with the transport sector, this work investigates the effects of the evolution of vehicles fleet and hydrogen consumption on the overall RES shares and GHG emissions. The synergy between power and mobility sectors is analysed, mainly assured by Power-to-Gas (P2G) plants for the generation of clean hydrogen for FCEVs as well as by the direct consumption of electricity by PEVs. Although introducing an efficiency-affected energy conversion step, the P2G technology

exploits the surplus electricity generated by wind and solar plants, allowing long-term energy storage in the form of fuel [2]. The potential for emission reduction from a large deployment of hydrogen in Italy is evaluated, considering a long-term very-high-RES scenario.

### II. METHODOLOGY AND DATA

Aiming to a comprehensive analysis, a dedicated lumped nodal model has been developed that simulates the hourly behaviour of the power grid, i.e. the balance of generation and demand (grid + PEVs) in each market zone, taking into account inter-zonal connection limits and assuming a priority dispatch for RES-generated electricity. Intra-zonal electric-to-electric storage is included in the form of existing pumped-hydro plants and newly installed battery systems, whose capacity is calculated as a technical optimum based on reaching a minimum number of annual equivalent working cycles. Generation and demand profiles are rescaled from historical ones, while electricity for PEVs charging is profiled with two daily peaks [3]. At each time step, if any surplus electricity is available, it is exploited by P2G devices to produce hydrogen that then feeds FCEVs. The installed electrolyzers capacity in each zone is determined to guarantee a minimum amount of equivalent operating hours (1500 h/y). The average energy efficiency of electrolyzers and balance-of-plants is set at 65%, equal to the best solutions available today [4]. No intra-zonal constraints are imposed on hydrogen consumption, as the cost of mere fuel transport is estimated similar to the one of diesel (8.3 c€ per 100 km transport per 100 km travelled by the final vehicle, against 7.9).

#### A. Electric power sector scenario

The installed capacity of wind and solar plants is assumed equal to the technical maximum, i.e. the max possible installation constrained by available resources, space, and environmental protection, disregarding an analysis of

economical profitability [5,6]. The electric grid load is assumed to grow by 0.3% yearly [7].

TABLE I  
POWER SECTOR SCENARIO: RES INSTALLED CAPACITY AND LOAD

	2015	2050
Wind capacity	18.9 GW	49.1 GW
Solar PV capacity	9.1 GW	110.2 GW
Grid load	300 TWh/y	340 TWh/y

### B. Transport sector scenario

The model focuses on light-duty vehicles. Characterization of their energy demand requires information about fleet composition, total number of vehicles, travelled distances and average consumptions. For the 2050 scenario, the shares of vehicles by technology is based on [8], while the operational parameters are equal to today's best available technology. The 'new' vehicles are assumed to substitute equally gasoline and diesel cars in terms of yearly travelled distance. A 10% presence of biofuels in fossil fuels is considered.

TABLE II  
TRANSPORT SECTOR SCENARIO: LIGHT-DUTY VEHICLES FLEET EVOLUTION

	Gasoline	Diesel	NG / LPG	Hybrid	Plug-in hybrid	Pure electric	Fuel cell	# vehicles
2015	49.7 %	41.9 %	8.1 %	0.2 %	<0.1 %	<0.1 %	0.0 %	37.3 mln
2050	9.6 %	6.7 %	3.0 %	16.2 %	19.3 %	14.8 %	30.4 %	36.0 mln

## III. RESULTS AND DISCUSSION

The simulation offers a complete overview on energy flows among zones, electricity generation by RES technology, P2G feeding and operation, and need for additional non-renewable production. Among them, the two most significant quantities for this analysis are the coverage of electrical load by each technology and the satisfaction of hydrogen demand for transport by P2G. Moreover, these values are used to compute the GHG emissions in the future scenario, to be compared with 1990 data to assess the compliance with EU target.

### A. RES shares

Table III shows that, even with the high increase of installed RES considered in the study, the power sector does not reach a 100%-RES load coverage. On the other side, road transport shift towards clean energy vectors is remarkable: 81% of the hydrogen demand and 63% of the electricity request are zero-emission. Thus, almost 40% of the primary energy consumption by light-duty vehicles comes from clean sources.

TABLE III  
LOAD COVERAGE AND HYDROGEN CLEAN GENERATION

RES share on electrical load	63.0 %
Surplus electricity available for P2G	46.0 TWh/y
Installed P2G capacity (total Italy)	26.2 GW
Hydrogen generated by P2G	735.5 kton/y
Coverage of H <sub>2</sub> mobility demand	81.4 %
RES share on primary energy for mobility	38.4 %

### B. GHG objectives

The EU target for GHG emissions reduction specifies sectorial goals: 93-99% for power and 54-60% for transport [1]. Based on model results<sup>1</sup>, even with the high increase in RES installation, the power sector does not reach the ambitious objective. On the contrary, the strong introduction of alternative vehicles lets the light-duty transport sector attain the goal. Here, the 81% emission-free hydrogen fed to FCEVs is a key player.

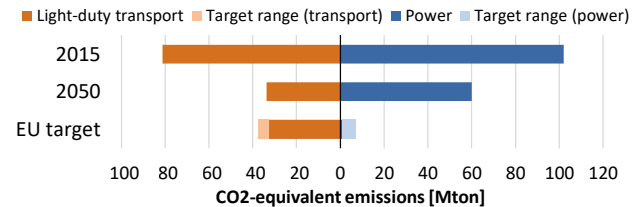


Fig. 1. GHG emissions from simulations, compared with EU target.

Alternative scenarios that consider the fraction of 'new' vehicles (45.2% of the fleet) as consisting of only PEVs or only FCEVs show worst results: both options present lower RES share and higher GHG emissions than the case with a mix of technologies.

## IV. CONCLUSIONS

A model of the interweaved power and transport networks allows assessment of their evolution in future scenarios. A high-RES, high-H<sub>2</sub> evolution of the Italian energy system has been studied. Results show that the integration of P2G solutions for long-term storage of clean energy plays a remarkable role, allowing to approach the ambitious EU targets for GHG emissions reduction.

## REFERENCES

- [1] European Commission, A roadmap for moving to a competitive low carbon economy in 2050, 2011.
- [2] M. Lehner, R. Tichler, H. Steinmueller, M. Koppe, Power-to-Gas: Technology and Business Models, Springer, 2014.
- [3] DEFINE, DEFINE Synthesis Report, 2015.
- [4] Fuel Cells and Hydrogen Joint Undertaking, Development of Water Electrolysis in the European Union, 2014.
- [5] R. Hoefnagels, M. Junginger, G. Resch, C. Panzer, A. Held, RE-Shaping Project - Long Term Potentials and Costs of RES - Part I, 2011.
- [6] P.R. Defaix, W.G.J.H.M. van Sark, E. Worrell, E. de Visser, Technical potential for photovoltaics on buildings in the EU-27, Solar Energy. 86 (2012) 2644–2653.
- [7] ENTSO-E, Ten-Year Network Development Plan 2016. Scenario Development Report, 2015.
- [8] IEA, Technology Roadmap - Hydrogen and Fuel Cells, 2015.

<sup>1</sup> Emission reduction is calculated as difference between 2015 and 2050 simulated cases, then compared to the goal 2015-2050, obtained from the 1990-2050 target by taking into account the variations occurred from 1990 to 2015 (-26.5% and +14.1% for power and light-duty road transport respectively).

## DYNAMIC MODEL AND EXPERIMENTAL TESTS OF A SYSTEM COUPLING PROTON EXCHANGE MEMBRANE FUEL CELL AND METAL HYDRIDES HYDROGEN STORAGE

M. De Campo\*, T. Lamberti\*, A. Sorce\*, L. Magistri\*.

\* DIME-TPG Polytechnic School, University of Genoa (Italy)

**Abstract** - The present paper presents a study for the integration of a Proton Exchange Membrane (PEM) fuel cell and a Metal Hydride (MH) hydrogen storage system. The result of the study is a dynamic model able to simulate the behavior of a complete system to help the design of marine application power generators. In order to develop a feasible and realistic design tool, the model has been validated against experimental data.

**Index Terms** – Fuel Cell, Metal Hydrides, Marine, Models.

### I. INTRODUCTION

The Thermochemica Power Group TPG [1] is investing its knowhow and experience in the development of design tools to spread the hydrogen technology into the maritime sector. The TPG gave birth to the UNIGE spin-off named H2Boat S.c.a.r.l. [2] that collaborate along with Fincantieri S.p.a. also into the new HI-SEA Joint Laboratory [3]. The goal of these studies is to evaluate power generation technologies and energy storage technologies experimentally with small scale prototypes in order to permit the validation of simulation models. The former will be used as tools to support the design of larger systems as well as to support test operations conducted into the HI-SEA laboratory. At the state of the art, the only known power train that use a FC and MH coupled system is the one installed onboard the U212 Submarine of the Italian/German Navy. Only few other small prototypes have been built. About the system simulation, a reference paper for thermally coupled system is represented by [4].

### II. FC AND MH MODELS AND TEST FACILITY

The studies have been conducted on two systems: PEM fuel cell and MH hydrogen storage system. For both, a Simulink dynamic model has been constructed using empirical equations to reproduce the characteristic curves, based on the experimental data collected into the laboratory. The BOP

(Balance of Plant) has been modeled taking into account energy and mass balance equations, equilibrium properties and reaction kinetics.

#### A. PEMFC model

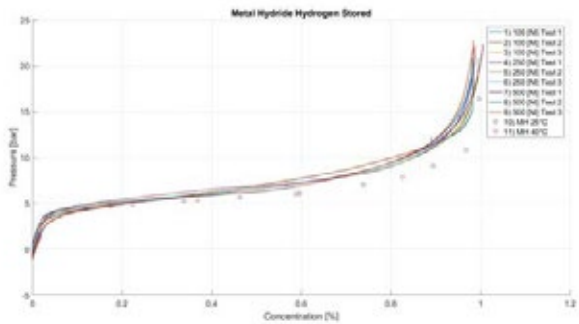
The characteristic curve of a Fuel Cell (FC) is represented by the Current-Tension (I-V) curve of a single cell. The phenomena that rule the shape of the curve are well known and deeply studied [5][6]. Many studies try to find correlations between cell physical properties and the I-V curve also with good correlations [7]. However, at a system level, many detailed FC data are unnecessary and more important, difficult to found. For these reason an empirical approach has been considered, to define the characteristic curve from experimental data. The FC has been simulated with a 0-D semi-empirical model, able to reproduce different kind of PEM starting from experimental data regression to design the I-V curve including the influence of partial pressures and temperature, as explained in [8]. Thanks to this approach the model is able to reproduce virtually any kind of FC system, requiring only few experimental points to define the characteristic curve.

#### B. MH model

The MH model is based on the F. Gonzatti and F. Farret work [9], it simulates the dynamic process of hydrogen absorption and discharge from a  $\text{LaNi}_5$  metal hydride. The Pressure-Composition-Temperature (PCT) curve is characteristic of MH composition, but MH systems performance are strongly dependent on the canister and thermal management design. Generally MH system producers provide the PCT curve obtained from static experiment of small samples. The goal is to develop an empirical approach based on this curves, in order to setup the model adaptable to any kind of MH system. Experimental data show that a hysteresis process between static and dynamic condition is present (Figure 1) that



require deeper analysis.

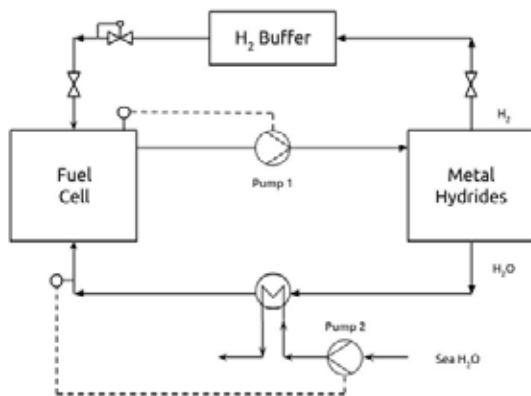


**Fig. 1. Dynamic and static point hysteresis**

The present model has been corrected considering experimental data, the study is going on.

### C. Coupled model

The coupled system has been created connecting the water cooling system of the PEMFC to the water MH heating system. A secondary sea water cooling system has been simulated to control the PEMFC temperature. All the components have been simulated considering the energy balance. The circuits losses have been designed on the base of a preliminary system design. Figure 2 presents the coupled system concept.



**Fig. 2. System P&ID**

The control strategy optimize the heat transfer from the FC to the MH by Pump 1.  $T_{FC}$  is computed inside the FC module while  $\dot{m}_1$  is the parameter controlled by Pump 1. Inside the MH model  $T_{MH}$  is calculated while the temperature of the FC cooling inlet passing through the heat exchanger is controlled by Pump 2 on the base of the required FC temperature, considering a constant temperature of sea water equal to  $15^\circ\text{C}$ .

### D. Experiment data

The models have been set up and validated against experimental data collected by the prototype developed by H2Boat. The former consist of a 300 W [10] water cooled low temperature PEMFC directly connected to a hydrogen storage

system composed by three canister of 500 NL [11] AB5 low temperature MH.

## III. CONCLUSION

The present work represents the first step towards the assessment of hydrogen technology for ships and boats that will be conducted in parallel with the HI-SEA laboratory. It has been demonstrated that a direct thermal coupling PEMFC and MH is feasible. A simulation model has been validated, that will be used for future studies on the system control and sizing to increase the total system efficiency.

## ACKNOWLEDGMENT

The experimental data have been collected into the (TPG) Laboratories with prototypes equipped by H2boat S.c.a.r.l..

## REFERENCES

- [1] <http://www.tpg.unige.it/TPG/>
- [2] <http://h2boat.it/>
- [3] G. Borgogna et al., HI-SEA (Hydrogen Initiative For Sustainable Energy Application): development of a joint laboratory for PEM and H2 applications, European Fuel Cell Conference 2017, Extended Abstract, EFC17077.
- [4] Z. Jiang, R. Dougal, S.Liu et al. , Simulation of a thermally coupled metal-hydride hydrogen storage and fuel cell system, Journal of Power Source 142 (2005) 92-102.
- [5] Ronald F. Mann, John C. Amphlett, Michael A.I. Hooper, Heidi M. Jensen, Brant A. Peppley, Pierre R. Roberge, Development and application of a generalised steady-state electrochemical model for a PEM fuel cell, In Journal of Power Sources, Volume 86, Issues 1–2, 2000, Pages 173-180, ISSN 0378-7753.
- [6] J. T. Pukrushpan, A. G. Stefanopoulou and Huei Peng, "Modeling and control for PEM fuel cell stack system," Proceedings of the 2002 American Control Conference (IEEE Cat. No.CH37301), Anchorage, AK, USA, 2002, pp. 3117-3122 vol.4.
- [7] J. C. Amphlett, R. M. Baumert, R. F. Mann, B. A. Peppley, P. R. Roberge, and T. J. Harris, Performance Modeling of the Ballard Mark IV Solid Polymer Electrolyte Fuel Cell: II . Empirical Model DevelopmentJ. Electrochem. Soc. 1995 142(1): 9-15; doi:10.1149/1.2043959
- [8] Alejandro J. del Real, Alicia Arce, Carlos Bordons, Development and experimental validation of a PEM fuel cell dynamic model, In Journal of Power Sources, Volume 173, Issue 1, 2007, Pages 310-324, ISSN 0378-7753.
- [9] F. Gonzatti and F.A. Farret (2016). Mathematical and experimental basis to model energy storage systems composed of electrolyzer, metal hydrides and fuel cells. Energy Conversion and Management, 132, 241-250.
- [10] G300 PEM Fuel Cell, 300 Wp, Genport.
- [11] H2Bond Metal Hydride Canister, 500 NL hydrogen storage, Labtech Ltd.

## SHORT STACK KIT FOR THE OPEN FLANGE™ SET-UP USING SOFT MICA SEALS

P. Coquoz\*, A. Pappas\*, N. Coton\*, F. Cottier\*, H.  
Middleton\*\*, R. Ihringer\*

\* Fiaxell Sàrl, EPFL Innovation Park, PSE A, 1015 Lausanne,  
(Switzerland)

\*\* Faculty of Engineering Science, University of Agder, 4879  
Grimstad, (Norway)

**Abstract - Results from Fiaxell's SOFC/SOEC short stack kit designed for the Open Flanges Set-Up, using ASC (2R-Cell) cells with Crofer 22H interconnects are presented. The stack incorporates compressible mica seals that demonstrated high fuel utilization (up to 82%).**

The tests performed for this study used two cells with a square flow-field pattern. Current-voltage characteristics were measured as well as fuel utilization and electrical efficiency.

**Index Terms** – short stack, soft mica seals, open flange set-up

### I. INTRODUCTION

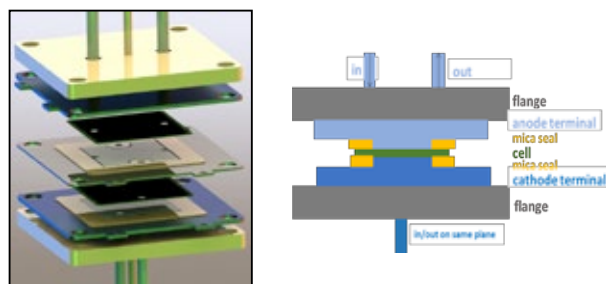
Fiaxell is the manufacturer of the Open Flange™ Set-Up that was developed in order to test SOFC and SOEC cells. The Set-Up allows researchers to do various experiments, such as current-voltage characteristics, polarization, impedance spectroscopy measurements, electrolysis, co-electrolysis and in situ gas processing (POX, SR) thanks to its integrated steam generator [1].

Fiaxell is now offering a complete short stack kit that can be directly mounted onto the Open Flange™ Set-Up platform. This kit allows researchers to perform a range of experiments and to study stack parameters such as flow distribution, electrical contact resistance, gas inlet and outlet temperatures, and to investigate protective coatings to avoid chromium evaporation, in situ fuel processing and sealing gas tightness. Each parameter can be independently characterized and optimized by combining ideal and real stack conditions on both sides of the cell, for instance Crofer® steel on the anode and gold mesh on the cathode.

In this work we examine the application of Crofer 22H interconnects with flow pattern designs for 52 X 52 mm cells. Alternatively, custom designs can be chemically grooved and laser cut by Fiaxell. The short stack kit is used with soft mica seals that ensure sufficient gas tightness. These seals have been designed to be easily removed and replaced, contrary to the use of glass based sealants that require mechanical grinding to be removed.

Mechanical simulations and calculations have been made to ensure that the design of the end Flange™ is adequate to compress the entire stack without any distortion or stress concentration points, especially on the thin interconnect plates.

### II. DESCRIPTION OF THE SHORT STACK KIT



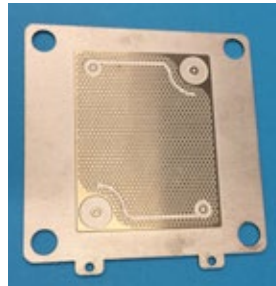
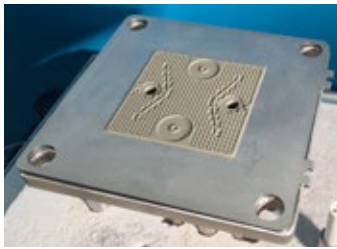
**Fig. 1. Left: 3D rendering of a multi cell mounting. Right: Cross-section drawing of the short stack with single cell. The terminals are identical but mounted perpendicular to one another.**

The short stack kit (Figure 1) consists of two terminal plates with inlet and outlet tubes welded on each plate. The interconnect flow-field patterns were made using a chemical etching technique on Crofer plates; the design presented in this article has an internal manifold (the gases pass through holes in the cells). The depth of the etching can be controlled, so the height can be adapted for instance to the required gas pressure drop.

The terminal and double-sided interconnects on both air and fuel have been chosen identical for simplification. The cell dimensions have to be slightly larger than the flow field pattern. This ensures the tightness of the assembly by the pressure of the cell edges on the soft mica seal. The same mica sealant is used for tightness around the cell holes (See Figure 3, right). Potential reading for each cell is performed with wires welded

on protruding tabs (see Figure 2, right and Figure 3, right). Homogenous pressure is obtained thanks to thick and stiff Inconel 600 flanges of 6 mm. The force on the stack is controlled by 4 external calibrated springs.

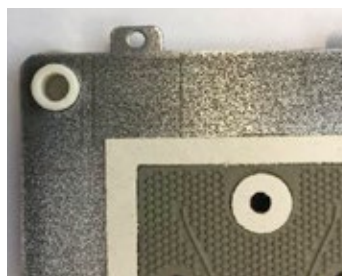
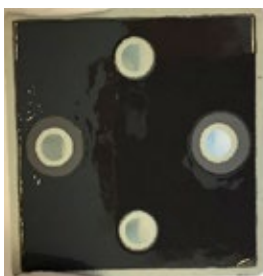
Different designs can be manufactured for the short stack kit. In this paper the results for a square design with deflector (Figure 2, left) are presented. Other designs for 80x60 mm cells (as shown in Figure 2, right) have been manufactured and tested.



**Fig. 2. Left: Interconnect (for 52x52mm cells) with square design with NiO paste painted on it. Right: Interconnect for rectangle shapes cells (76x60 mm).**

### III. EXPERIMENTAL RESULTS

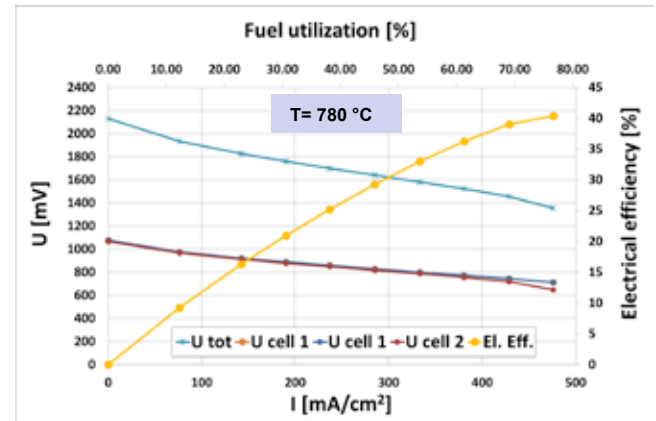
The short stack kit was then tested with a two-cell short stack, 2R-Cells (redox resistant) of 52x52mm. The cathode is a LSCF-GDC composite cathode with a size of 46x46 mm. The active area (printed area minus holes and seals) was calculated to be about 14 cm<sup>2</sup>. In order to prevent chromium poisoning and lower the electrical resistance, the air sides of the interconnects are coated with CuMn<sub>2</sub>O<sub>4</sub> and heat treated at T>800°C for a few hours. On fuel sides a nickel oxide paste is painted (as seen on Figure 3, right). Finally, undried pastes are applied on both sides of the cells before stack mounting. Nickel oxide is applied on anode side and LSC on the cathode (Figure 3, left picture), to ensure lower contact resistance.



**Fig. 3. Left: Fresh LSC ink is screen printed on cathode to improve the electrical contact. Right : The SOFT mica sealing is rolled at the same level than the interconnect plane.**

Figure 4 presents the electrical performances of the two-cell short stack. The measurements were performed at 780°C with dry H<sub>2</sub> (200 ml/min) and air (1000 ml/min). An electrical

efficiency of 40,4 % was reached with a power density of 322 mW/cm<sup>2</sup>. The cells showed similar behavior up to 76 % fuel utilization.



**Fig. 4. Electrical performances of the two cells short stack (H<sub>2</sub>: 200 ml/min, air: 1000 ml/min, T=780°C). The short stack reaches an efficiency of 40.4% with a power density of 322 W/cm<sup>2</sup>.**

After the experiment the stack was dismantled and the different parts were examined. The mica seals showed no failures. The cells showed no oxidation in the active area indicating that the tightness was sufficient. The imprint of the flow pattern was visible on the cells electrodes showing that satisfactory electrical contact was made across the area of the cells.

### IV. CONCLUSION

The short stack kit has demonstrated its ability to perform experiments with multiple cells. The soft mica seal and the flow patterns are appropriate to achieve high fuel utilization. The two-cell short stack reached 78% FU while exhibiting similar behavior for both cells. The electrical efficiency reached higher than 40% and the power density higher than 300 mW/cm<sup>2</sup>. Post-mortem examination showed no failure on the mica seals or on the cells.

Further work on multi cell stack will be performed, as well as the testing of different flow-field patterns.

### REFERENCES

- [1] G. Rinaldi, S. Diethelm, J. Van herle, ECS Transactions, 68 (1) 3395-3406 (2015)

## PERFORMANCE RECOVERY FROM NO<sub>2</sub> EXPOSURE IN PEM FUEL CELL

Y. Acevedo Gomez, G. Lindbergh, and C. Lagergren

Applied Electrochemistry, School of Chemical Science and  
Engineering, KTH Royal Institute of Technology, SE-100 44  
Stockholm, (Sweden)

**Abstract** – The hydrogen fuel cell vehicle market is projected to increase in the coming years, and fuel cell vehicles will operate in an environment where they coexist with combustion engine vehicles. In this context, the PEM fuel cell will be exposed to significant amounts of contaminants on the roads that will decrease its performance and durability. In the present study the PEM fuel cell is exposed to 100 ppm of nitrogen dioxide in the airflow. Different methods for recovery of performance were tested; recovery during constant current load and by subjecting the cell to successive polarization curves. The results showed that the successive polarization curves are the best choice for recovery. However, recovery at low current density and high potential is also a good alternative.

**Index Terms** – Contaminant, Nitrogen dioxide, PEM fuel cell, Recovery of performance.

### I. INTRODUCTION

The proton exchange membrane (PEM) fuel cell has been considered a promising technology due to its low operating temperature, high power densities, low emissions, and quiet operation [1], and it is a good alternative as a clean power source that can replace the internal combustion (IC) engine in vehicles [2]. The coexistence of these two types of vehicles will lead to a dramatical decrease in performance of the fuel cell, as it is well known that some contaminants from fuel combustion drastically affect the catalyst layer and the proton conductivity of the membrane in the PEM fuel cell.

Nitrogen dioxide is mainly present as a pollutant due to roads traffic, in which nitric oxide is emitted by fossil fuel combustion processes, and combined with oxygen from the air produce nitrogen dioxide. Nitric oxide may also enter in the fuel cell and with the excess of oxygen be converted into nitrogen dioxide inside the fuel cell. The presence of NO<sub>2</sub> in the oxidant stream affects

severely the fuel cell performance by degradation of the cathode catalyst.

Our study is aimed to contribute to the improvement of the durability of the fuel cell, by testing different methods in order to find an adequate recovery strategy, one that may be used online in real situation. In this investigation, nitrogen dioxide was introduced together with air in the cathode side during 3 hours. Then, different recovery methods were carried out, such as successive polarization curves, and recovery at different constant current densities.

### II. EXPERIMENTAL SET-UP

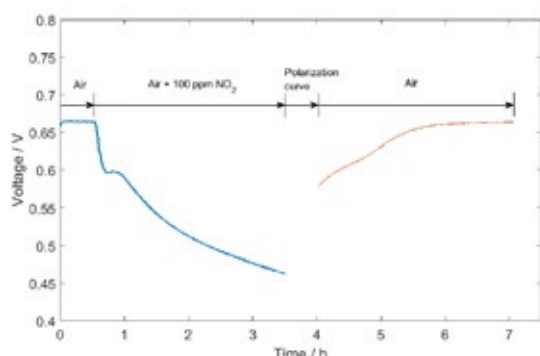
The electrochemical measurements were carried out in a cell from Fuel Cell Technologies Inc. with graphite plates using a spiral gas channel over a circular area of 3 cm<sup>2</sup>. Swagelok fittings were used to couple the cell to the humidifiers. The cell temperature was 80 °C and the gases were humidified to 90 % with an external control before they entered the fuel cell. The gas flow rates for hydrogen, nitrogen and air were controlled by flowmeters (Brooks Instruments B. V.), and for nitrogen dioxide a mass flow controller (Alicat Scientific) was used. The cell was connected to a Solartron Interface SI1287 potentiostat, controlled by CorrWare software. A Gore MEA of thickness 25 µm was used. The catalyst loading was 0.45 mg/cm<sup>2</sup> Pt-Ru alloy on the anode and 0.4 mg/cm<sup>2</sup> Pt on the cathode. Carbel<sup>TM</sup> was utilized as gas diffusion media.

### III. RESULTS AND DISCUSSION

The performance degradation after introducing 100 ppm of NO<sub>2</sub> together with air, and its subsequent recovery is shown in Figure 1. The measurement was done at a constant current density of 0.5 A cm<sup>-2</sup>. The figure shows the dramatic performance degradation, a



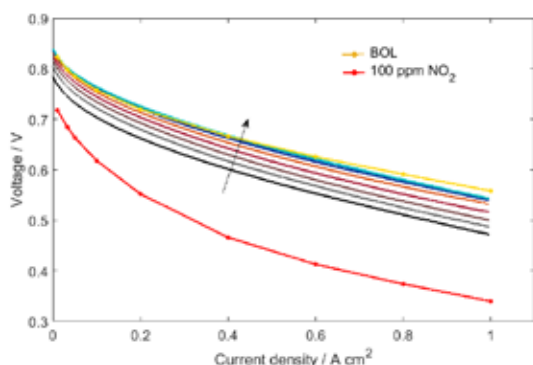
decrease by 203 mV after 3 hours of contamination. However, the fuel cell performance was completely recovered after introducing clean air for 3 hours.



**Fig. 1. Fuel cell performance during addition of 100 ppm NO<sub>2</sub> and the following recovery at 0.5 A cm<sup>-2</sup>.**

In order to decrease the recovery time two different methods for recovery were tested: Successive polarization curves, and galvanostatic hold at different current densities. In order to compare the performance recovery methods, the same contamination procedure, as shown in Figure 1, was done in all experiments.

Figure 2 shows the successive polarization curves done as a performance recovery method. In total, eight polarization curves were recorded in 55 minutes until almost no difference was seen between them. As seen in the figure, a complete recovery was reached for current densities below 0.6 A cm<sup>-2</sup>, while at high current densities 13 mV still needs to be recovered.



**Fig. 2. Successive polarization curves for recovery.**

It can be seen that the performance recovery was almost complete in a shorter period of time than running the recovery with pure air. This recovery may be attributed to the rapid removal of NO<sub>2</sub> from the Pt catalyst when being swept over different potentials where oxidation of NO<sub>2</sub> may occur [3,4].

For the second performance recovery method, different constant current densities were applied for the

recovery in pure air. The recovery procedure was tested for four different current densities.

A trend in the results is that at higher current densities the recovery time is shorter (~ 100 min at 1 A cm<sup>-2</sup>), which is in line with the results with ammonia contamination obtained by Lopes et al. [5]. However, the performance recovery recorded at 0.2 A cm<sup>-2</sup> shows the opposite, an even lower recovery time (~ 90 min). This feature may be due to the oxidation of NO<sub>2</sub> at 0.75 V as showed by Jing et al. [3] and Chen et al. [4] where it was also indicated that NO<sub>2</sub> is not strong absorbed on Pt surface.

#### IV. CONCLUSION

This study shows that it is possible to find an adequate performance recovery method that can work in a fuel cell car in a real traffic situation with large amounts of NO<sub>2</sub>. By replacing the NO<sub>2</sub>-contaminated air by clean air, a complete recovery of the performance is reached in 3 h. However, by using other recovery methods a faster recovery time can be reached. Of the two tested in this study the method with successive polarization curves is the best option.

#### ACKNOWLEDGMENT

This work was supported by the European project Biogas2PEM-FC (FP7) and the Swedish governmental initiative StandUp for Energy.

#### REFERENCES

- [1] Moore, J.M., Adcock, P.L., Lakeman, J.B., Mepsted, G.O., The effect of battlefield contaminants on PEMFC performance, *Journal of Power Sources*, Volume 85, 2000, Pages 254 – 260.
- [2] Moore R.B., Raman V., Hydrogen infrastructure for fuel cell transportation. *Int. Journal Hydrogen energy*, Volume 23, No 7, 1998, Pages 617 – 620.
- [3] Jing F., Hou M., Shi W., Fu J., Yu H., Ming P., Yi B., The effect of ambient contamination on PEMFC performance, *Journal of power sources*, Volume 166, 2007, Pages 172 – 176.
- [4] Chen M, Du C, Zhang J., Wang P., Zhu T., Effect, mechanism and recovery of nitrogen oxides poisoning on oxygen reduction reaction at Pt/C catalysts, *Journal of power sources*, Volume 196, 2011, Pages 620 – 626.
- [5] Lopes T., Sansiñena J.-N., Mukundan R., Hussey D.S., Jacobson D.L., Garzon F.H., Diagnosing the effects of ammonia exposure on PEFC cathodes, *Journal of the electrochemical society*, Volume 161, 2014, Pages F703 – F709.



## A preliminary study of coupling between turbine speed and fuel cell gradients in a hybrid system

Paolo Pezzini, Kenneth “Mark” Bryden  
U.S. Department of Energy  
Ames Laboratory  
1620 Howe Hall, Ames, Iowa, 50011

**Abstract**—Based on experience with combined cycle gas turbine power systems variable speed gas turbines are often proposed for fuel cell gas turbine hybrid systems as a means to improve efficiency during load following operations. However, because of the coupled nature of the fuel cell and gas turbine variable speed gas turbine controls may reduce the life of the fuel cell and increase the risk of fuel damage. Using the Hyper facility at the National Energy Technology Laboratory (NETL) this paper reports preliminary research results of three experimental control scenarios focusing on the impact of turbine controls on fuel cell cathode temperature and pressure gradients. The results indicate that fixed speed turbine operation may provide the best overall plant performance relative to fuel cell life and risk of damage.

### Introduction

In stand-alone gas turbine electrical power generation systems, constant turbine speed matches the generator speed and frequency of the AC distribution. However, when the turbine operates at a part-load condition there is a substantial decrease in efficiency. Because of this variable gas turbine speed engines are generally used to improve efficiency during part-load operations. Similarly, in fuel cell gas turbine hybrid systems variable gas turbine speed engines are often proposed [1, 2]. However, studies presented at the 2016 Low Emission Advanced Power (LEAP) Workshop found that cathode temperature and pressure gradients should stay below 3°C/min, 10°C/cm, and 0.05 bar/min to avoid any fuel cell damage on the ceramic material [3]. However, strong coupling between the turbine speed, cathode airflow, temperature and cathode pressure suggests that constant turbine speed operation is needed to avoid excessive cathode temperature and pressure gradients that could damage to the fuel cell material and reduce the life of the fuel cell.

In this paper, the Hyper facility was used to examine the impact of a small (4 kW) turbine load perturbation on a fuel cell. The NETL Hyper project is 400 kW hybrid power test facility combining a recuperated gas turbine cycle and a solid oxide fuel cell stack (Fig. 1) in which a cyber-physical model is used to simulate a solid oxide fuel cell. Three experimental studies were conducted

- Case 1—Hyper was operated in open-loop configuration in which there were no controls implemented to maintain a constant turbine speed or a constant cathode airflow. This was to characterize the impact of a 4 kW turbine load perturbation on cathode airflow, pressure, temperature and turbine speed.
- Case 2—The same 4 kW turbine load perturbation used in Case 1 was performed with a single-input single-output controller to keep the cathode airflow and hence the temperature in the fuel cell constant. No control action was implemented to maintain turbine speed constant. During this experiment, the hot-air bypass was automated.
- Case 3—A multi-agent control approach in which the simultaneous cooperation of two agents was used to control the turbine speed through the simultaneous operation of the bleed-air and auxiliary fuel valve during a 4 kW turbine load perturbation. The cathode airflow was not controlled.

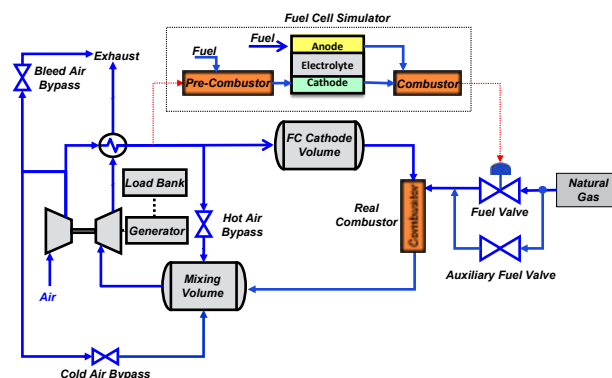


Figure 1: Fuel cell gas turbine hybrid layout at NETL

Hyper’s cyber-physical fuel cell system is very sensitive to fuel cell and/or turbine load perturbations. For instance, small changes to the turbine load affects the turbine speed operation, which in turn affects the cathode airflow that drives the fuel cell model, and hence the waste heat that drives the gas turbine combustor. This is of particular concern during the open-loop configuration when turbine speed and cathode airflow were not controlled and a large power perturbation could result in an excessive deviation and damage to the Hyper facility. Because

of this a 4 kW turbine load perturbation representing ~1% of the total hybrid power generation was used all the three cases.

## Results and Discussion

In Case 1 a 4 kW step in turbine load resulted in 1000 rpm of turbine speed change (2.4%) and 6% deviation in the cathode airflow. The temperature gradient of the fuel cell solid temperature on the average was 6°C/min, and the pressure gradient was 0.04 bar/min. Because a 4 kW change is a relative small step the pressure gradient does not violate the limit of 0.05 bar/min, however, based on these results it is likely during load following operations in large scale plants this limit would be easily violated.

In Case 2 (Fig. 2) a single-input single-output controller implemented on the hot-air bypass valve kept the cathode airflow constant (3% deviation), but the cathode pressure was still affected due to the changing turbine speed. As shown the turbine speed still varied by 1000 rpm resulting in a pressure gradient still 0.04 bar/min. However keeping the cathode airflow constant improved the fuel cell temperature gradients by 23-25% to 4.6°C/min on average.

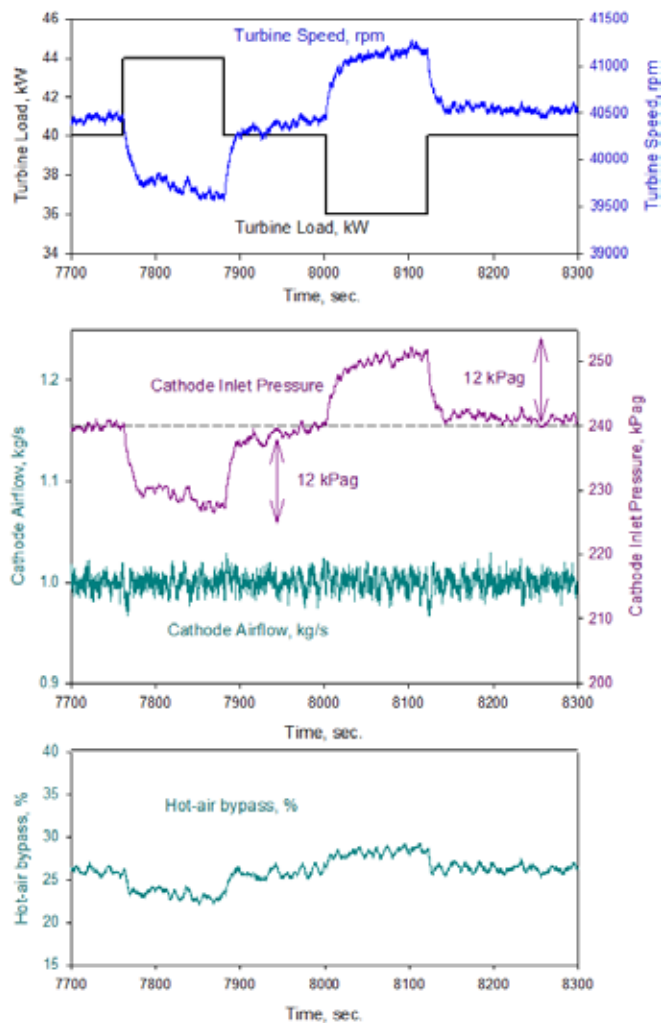


Figure 2: Case 2 cathode airflow control during turbine load changes

In Case 3, a turbine speed controller was used to maintain turbine speed during the perturbation. Controlling the turbine speed at nominal condition to optimize load following in a fuel cell gas turbine hybrid power system is a significant challenge. At nominal conditions the maximum efficiency of the hybrid system is only ensured when the waste heat generated by the fuel cell entirely drives the gas turbine. To achieve this the auxiliary fuel valve that is traditionally used to start up the turbine and warmup the fuel cell is set at the lower limit because any supplemental fuel would decrease system efficiency. During transient operations, an increase of auxiliary fuel flow can control the turbine when the waste heat from the fuel cell decreases or turbine load increases. On the other hand, when the turbine load decreases or the waste heat from the fuel cell increases, a turbine over speed occurs and can potentially damage the turbine and/or the fuel cell. Since the auxiliary fuel valve is set at a lower limit to maximize the system efficiency, an additional actuator is required to mitigate this effect such as the compressor bleed-air valve. This actuator is generally not designed to control the turbine speed, but it is a standard actuator designed in any gas turbine system to discharge cold compressor air into the atmosphere. However, it has a strong effect on the turbine shaft speed, but similar to the auxiliary combustor, it cannot be maintained open at nominal conditions without sacrificing efficiency.

In Case 3 preliminary experiments found that the cooperation of two agents, the auxiliary fuel valve and bleed-air valve, yielded a feasible control approach that can keep the turbine speed constant under load following transients. During 4 kW turbine load perturbations, this control strategy kept the turbine speed deviation below 500 rpm (1.2%) even without optimization of the control parameters. Also, controlling the turbine speed kept the cathode airflow relatively constant by (4% deviation). This result is consistent with previous work [4]. The maximum cathode pressure gradient was 0.03 bar/min, a 25% decrease over Case 1 and Case 2. As airflow through the cathode was uncontrolled the temperature gradient of the fuel is similar to Case 1.

## Conclusions and future work

This paper presented a preliminary study of the impact of turbine and fuel cell controls on fuel cell temperature and pressure gradients in a fuel cell gas turbine hybrid cycle during load following operations. These results suggest that constant speed turbine control should be considered for gas turbine fuel systems. A more detailed study on the fuel cell parameters during turbine speed control is planned.

## References

- [1] Traverso, L. Magistri, A. F. Massardo, "Turbomachinery for the air management and energy recovery in fuel cell gas turbine hybrid system," *Energy*, Vol 35, Issue 2, pp. 764 – 777, 2010;
- [2] R. Roberts, J. Brower, Jabbari, Ghezal-Ayagh, "Control design of an atmospheric solid oxide fuel cell/gas turbine hybrid system: variable versus fixed speed gas turbine operation," *Journal of Power Sources*, Vol. 161, Issue 1, pp 484 – 491, 2006;
- [3] D. Tucker, "Technical Notes," LEAP 2016;
- [4] P. Pezzini, K. M. Bryden, D. Tucker, L.E. Banta, "Multi-Coordination of Actuators in Advanced Power Systems," proceedings to ASME Turbo Expo 2015, GT2015-42993;

EFC17093

## INSIGHTS INTO PRESSURIZED VS ATMOSPHERIC SOLID OXIDE FUEL CELL OPERATION

David Tucker\*, Nor Farida Harun\*, Dan Oryshchyn\*\*, and Lawrence Shadle\*

\*National Energy Technology Laboratory (NETL), 3610 Collins Ferry Rd, Morgantown, WV 26507-0880 (USA)

\*\* NETL, 1450 SW Queen Ave., Albany, OR 97321 (USA)

**Abstract** – Solid oxide fuel cells (SOFC) reject waste heat at temperatures high enough for effective integration with mechanical power generation technologies. The hybridization of SOFC and gas turbine technologies provides an increase in system efficiency and an opportunity for increased system flexibility. The integration of fuel cell and gas turbine technologies represents significant challenges for the perceived benefits, such as efficiency, flexibility, and reduced cost.

To quantify the benefits of hybridization and pressurization of an SOFC system, a real-time distributed model of a SOFC was used to simulate performance of a pressurized hybrid in comparison to a stand-alone fuel cell configuration. Gatecycle was used to simulate the balance of plant components, compressor, turbine, heat exchangers, and steam cycles. The stand-alone fuel cell made use of a blower for airflow and thermal management with a steam cycle for waste heat recovery. In all cases, total system power and total fuel cell current density were kept constant so that the number of cells and efficiencies could be compared at varying fuel utilizations. The system size and efficiency for each hybrid case was then compared to the atmospheric system for quantitative evaluation of performance metrics.

**Index Terms** – efficiency, hybrid power cycle, solid oxide fuel cell, turbomachinery, pressurized vs atmospheric.

### I. INTRODUCTION

Although system studies conducted by numerous researchers have established SOFC gas turbine hybrids as the most efficient conversion of fossil fuels to electric power, complications arising from fuel cell pressurization to dynamic system control have inhibited the commercialization of these systems [1]. Regardless of gains in efficiency and emissions reductions, economic viability is paramount to successful commercialization of any technology. In this regard, much of the research in the U.S. has been focused on reducing fuel cell cost and improving performance to support atmospheric SOFC operation [2]. Pressurization of SOFCs, and ultimately hybridization with heat engines, can only occur if the potential benefits outweigh the risks associated with such complex system integration.

Considering the current prices of fossil fuels, efficiency alone is insufficient to warrant the costs associated with coupling an SOFC to a gas turbine. Even standalone fuel cell systems are driven to higher current densities, sacrificing efficiency for reduced costs. However, recent hybrid system

studies suggest that hybrid power systems can achieve unprecedented flexibility, an essential element to achieve responsible penetration of renewable energy resources into today's power grid [3].

For a closer look at both efficiency and flexibility, a system comparison was completed with both standalone and hybrid power cycles so that potential benefits of hybridization could be more easily quantified. Flexibility was evaluated through variation of fuel cell fuel utilization. A design basis comparison was used where the size of the fuel cell and associated bottoming cycle were optimized for a fixed power output of 550 MW while the fuel utilization was varied.

### II. PROCESS ANALYSIS

A direct fired, recuperated cycle (Figure 1) was chosen for this study to represent the most challenging, yet most efficient hybrid system. In this case, the compressor (pressure ratio of 4) and turbine were on a single shaft, and the compressor airflow was routed directly through the fuel cell cathode. Although there is sufficient energy in the exhaust for a bottoming cycle, none was used for simplicity. An anode recycle was also considered for the cycle. The hot-air bypass shown was used to limit turbine inlet temperature, and hence the fuel cell cathode inlet temperature, at lower SOFC fuel utilizations. A syngas composition was used in both cases.

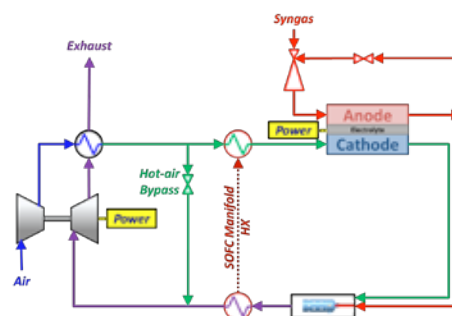


Fig. 1. Direct fired, recuperated SOFC- gas turbine hybrid system.

For standalone fuel cell cycle at atmospheric pressure, a steam bottoming cycle was used to recover any waste heat from the system (Figure 2).

In both cases, the balance of plant was simulated using GateCycle as described in previous studies [4]. The SOFC was

Copyright © 2017

simulated using a distributed fuel cell model for higher fidelity of heat transfer to the bottoming cycles and a more accurate temperature and current density distribution in the SOFC. The number of 20 x 20 cm cells and fuel flow were varied to achieve target power output and fuel utilization. In the hybrid case, the cathode airflow was adjusted to achieve target average SOFC temperature and inlet to outlet  $\Delta T$ . For the hybrid, the compressor airflow was greater than the cathode airflow due to the need for additional cooling flow to limit the turbine exhaust gas temperature.

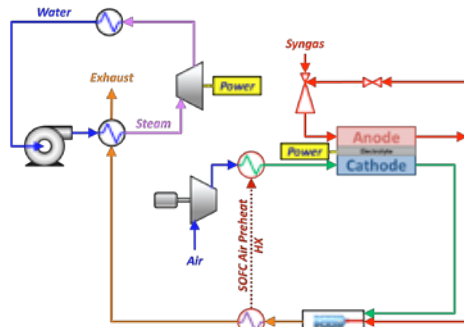


Fig. 2. Standalone atmospheric SOFC system with steam bottoming.

### III. RESULTS AND DISCUSSION

As shown in Figure 3, in both cases, the power share of the fuel cell in the system increases almost linearly with fuel utilization ( $U_f$ ). At 90%  $U_f$ , almost all the power is derived from the fuel cell in the atmospheric case, where in the hybrid case, only 74% of the power is derived from the SOFC.

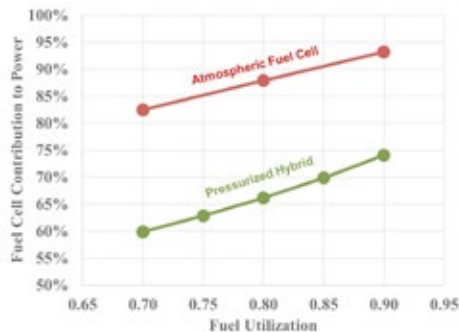


Fig. 3. Power distribution as a function of fuel utilization.

The efficiency is shown in Figure 4. Between 70% and 90% fuel utilization, the efficiency for the standalone SOFC consistently increases with  $U_f$ , as expected. However, the hybrid shows far more insensitivity to variation in fuel utilization, indicating greater flexibility. In both cases, anode recycle resulted in significant reduction in efficiency.

The change in efficiency is shown as a fraction of power produced by the fuel cell in Figure 5. In this case, the hybrid case is taken down to a power split of 53/47 fuel cell to turbine. A straight line was fitted to the curves. The slope of the hybrid case is fairly shallow, while the atmospheric fuel cell efficiency depends on high  $U_f$  and fuel cell power share.

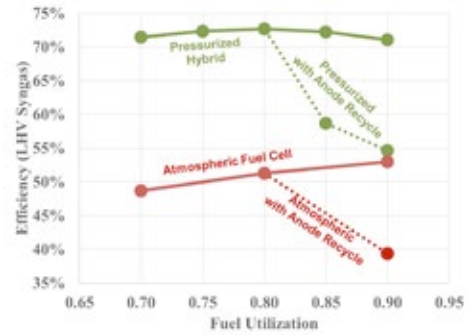


Fig. 4. System efficiency as a function of fuel utilization

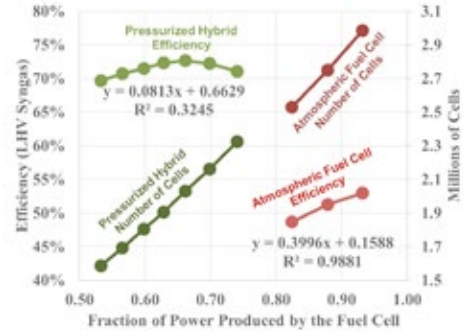


Fig. 5. System efficiency and SOFC size as a function of SOFC power share

Another consequence of hybridization shown in Figure 5 is the total size of the fuel cell required, indicated by the total number of cells needed for the constant power output. Pressurization and reduced power split offer the opportunity to substantially reduce the size of the fuel cell in the system. Assuming the cost of the fuel cell was significantly higher than the other components, the total system cost could be reduced.

### IV. CONCLUSION

When comparing an atmospheric SOFC system to a pressurized hybrid on a design basis, fuel cell size could be reduced while maintaining high efficiency due to the insensitivity of the hybrid to fuel utilization. For a 550 MW system, the design space fuel cell size varied by a factor of two. In neither case could anode recycle be justified for the syngas composition used in the study.

### REFERENCES

- [1] Thomas A. Adams, II, Jake Nease, David Tucker, Paul I. Barton, "Energy Conversion with Solid Oxide Fuel Cell Systems: A Review of Concepts and Outlooks for the Short- and Long-Term," *Ind. Eng. Chem. Res.*, 2013, 52 (9), pp 3089–3111
- [2] Vora, S. D. "SECA Program Overview and Status," *ECS Trans.* 2013, 57(1), pp 11-19
- [3] Tucker, D.; Haynes, C.; Geoghegan, P. "Needs and Approaches for Novel Characterization of Direct Hybrid Fuel Cell/Gas Turbines," *Proceedings of the ASME 2015 Power and Energy Conversion Conference*, June 28-July 2, 2015, San Diego, California, U.S.A., Paper number PowerEnergy2015-49232.
- [4] Nor Farida Harun, David A. Tucker, Lawrence J. Shadle, Danylo B. Oryshchyn (2017) Design Performance Analysis of the Fuel Utilization Effects on Solid Oxide Fuel Cells in Gas Turbine Hybrid Systems, *Proceedings of ASME Turbo Expo 2017: Power for Land, Sea and Air GT2017-64055*.



DURABILITY ISSUES IN PRECIOUS-GROUP-METAL FREE PEMFC CATHODES

*Andrea Bisello\**, *Andrea Baricci\**, *Andrea Casalegno\**, *Madeleine Odgaard\*\**, *Alexey Serov\*\*\**,  
*Plamen Atanassov\*\*\**

\* Department of Energy, Politecnico di Milano, Via Lambruschini 4, 20156 Milan (Italy)

\*\* EWII Fuel Cells A/S, Emil Neckelmanns Vej 15 A&B, 5220 Odense SØ (Denmark)

\*\*\* Department of Chemical and Biological Engineering, Center Micro-Engineered Materials,  
University of New Mexico, Albuquerque, NM 87106, (USA)

**Abstract** – Replacement of noble metal catalysts used in oxygen reduction reaction (ORR) is a research goal in the proton membrane fuel cells. In this work, mass transport limiting phenomena in Fe-N-C catalyst layers are studied. A specific methodology, that combines in-situ characterization of performance and modelling activity, is adopted to elucidate the contribution of electronic/ionic transport losses in catalyst layer with controlled properties. CCL impedance spectra, which take into account ORR activation and electron, proton, and oxygen transport losses are simulated. Analysis shows that a regime of mixed ion and electron transport limitations describes correctly the main features of impedance spectra. Degradation is negligible under nitrogen at 0.6V, supporting catalysts materials oxidation or water formation as main reasons for performance loss.

**Index Terms** – Electrochemical impedance spectroscopy, Mass transport limitations, Non platinum group metal catalysts, PEMFC model

## I. INTRODUCTION

Polymer electrolyte fuel cells (PEMFCs) are regarded as a promising technology to replace the internal combustion engine in future vehicles. Recently, Toyota and Hyundai both launched fuel cell electric vehicles on the market, and in the meantime, many other car manufacturers plan to do the same by 2020. However, in order to achieve wide commercial viability, certain key strategic objectives must be achieved: the reduction of cost related to precious catalyst commonly utilized in electrodes and the improvement of durability. Two are the common approaches adopted: limit the amount of platinum loading or develop highly active and durable catalyst free of Platinum group metals (PGM). A promising route consists in the development of catalyst based on metal-nitrogen-carbon (M-N-C) for the oxygen reduction reaction occurring at cathode<sup>1,2</sup>. Even though enormous efforts have been made to develop non-noble metal catalysts in the last several decades, the current state of the art non-PGM electrocatalyst has yet to achieve the catalytic activity of platinum. Because of mass-transport limitations related to electrode thickness, cathodes catalyst

layer must attain the same kinetic current density as Pt-based cathodes<sup>1</sup>. Furthermore, the effect of degradation on performance is still debated and the proposed mechanisms are not understood in depth, as well as their dependence on operating conditions. This work aims at increasing the understanding of mass transport limiting phenomena during operation of a well-known Fe-N-C catalyst and the evolution during degradation.

## II. EXPERIMENTAL

The catalysts studied in the present work were synthesized by modified SSM<sup>3</sup>. The specific reagents formulation is proprietary technology developed by University of New Mexico and Pajarito Powder LLC. Catalyst Coated Membrane (CCM) were produced by EWII Fuel Cells A/S on Nafion XL membrane. The MEA was assembled using a Sigracet 29BC gas diffusion layers (GDLs). The MEAs were loaded into the cell testing hardware (Fuel Cell Technologies) using triple serpentine pattern graphite flow plates (25 cm<sup>2</sup>). Specific CCL samples with controlled properties of catalyst loading (1 - 2 - 4 mg cm<sup>-2</sup>) and ionomer content (35 - 45 wt%) were studied. Every samples were pre-heated to 80 °C feeding H<sub>2</sub>/N<sub>2</sub> at 100% RH. Polarization curves and in-operando EIS were performed at 80 °C feeding 0.5/1.0 sccm at 100% RH and outlet pressure of 1 bar<sub>(g)</sub>. The first stage was a systematic investigation of performance evolution on 1 – 4 mg cm<sup>-2</sup> / 35 - 45 wt% samples. For the hold test, the load was applied potentiostatically to 0.60 V at steady state for 150 hours. Polarization curves and in-operando EIS were recorded at Beginning of Test (BoT), after 20 h, at End of Test (EoT). Gathered experimental data of different samples were analyzed by 1D PEMFC model. Simulation of polarization curves and impedance spectra were performed solving system of equations for the steady state (DC part) and afterwards system of equations for the transient behavior (AC part). For a description of equations see reference<sup>4</sup>.



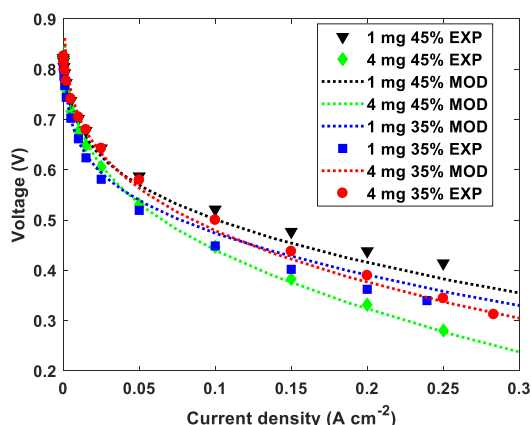


Figure 2 - Comparison between experimental polarization curves and model results at BoT for samples at different catalyst loading and ionomer content

### III. RESULTS AND DISCUSSION

The comparison between experimental data and simulated polarization curves is reported in Figure 1. Calibration parameters are fitted on 1 mg cm<sup>-2</sup> 45 wt% samples. To take into account the different CL morphology, the exchange current density ( $i_0$ ) and the proton conductivity ( $\sigma_{i,CL}$ ) were corrected for the others samples (only for 35 – 45 wt%). As a result, model can simulate with good consistency experimental data. As shown in Figure 1, respect to performance of 1 mg cm<sup>-2</sup> 35 wt% sample an increase in catalyst loading or ionomer content translates into an increase of performance. By contrast, the sample (4 mg cm<sup>-2</sup> 45 wt%) with higher loading and ionomer content shows the worst performance. This fact is simply explained as an increase of mass transport limitations due to thicker electrodes. To decouple measured mass transport phenomena, it's useful take a look at impedance spectra. Without the effect of transport and kinetics phenomena, the high frequency resistance could be represents as a short-circuit composed by system resistance (membrane and contact resistance) and electronic resistance ( $R_{e,CL}$ ) of CCL<sup>5</sup>. According to experimental data,  $R_{e,CL}$  follows a linear correlation with the CCL thickness. During the holding test, an evolution of HFR is visible, and the variation is more pronounced for samples with thicker electrodes (+40% for 4 mg cm<sup>-2</sup> 45 wt% sample), meanwhile the HFR for 1 mg cm<sup>-2</sup> 35 wt% sample remains almost constant. This could be explained by a decreasing of electron conductivity during operation. Parametric studies on 2 mg cm<sup>-2</sup> has shown a dramatically increase of HFR value during operation in O<sub>2</sub> atmosphere, while holding at 0.60 V<sub>RHE</sub> in H<sub>2</sub>/N<sub>2</sub> has shown a negligible effect. This suggest an oxidative degradation of catalyst material. Although it is not possible to impute performance evolution to worsening of electronic conductivity, this phenomenon must be taken into account as a proxy of catalyst layer structure degradation. Sensitivity analysis on simulated data revealed how performance depends

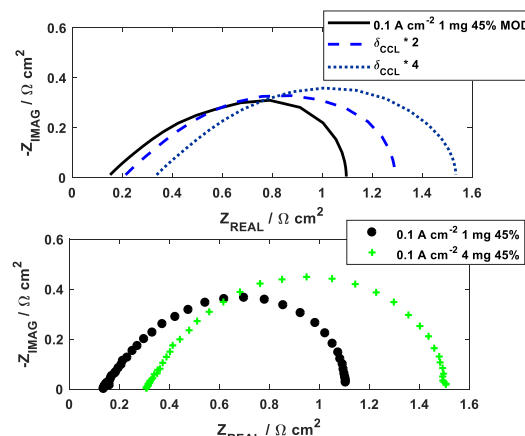


Figure 1 - a) Sensitivity analysis on CL thickness for 1 mg cm<sup>-2</sup> 45 wt% sample. b) Comparison between experimental spectra of 1-4 mg cm<sup>-2</sup> 45 wt%

on mixed ion and electron transport limitations. A decrease of electron conductivity parameter results in a shift of the active domain into the CL towards the GDL, and an increase of HFR value of impedance spectra. Furthermore, a worsening of ion conductivity results in an increase of 45° linear branch and this leads to an increase of charge transfer resistance. These effects of mixed ion and electron transport limitations are clearly visible on Figure 2 where sensitivity analysis on simulated data and experimental impedance spectra for 1 – 4 mg cm<sup>-2</sup> 45 wt% are reported.

### IV. CONCLUSION

The parametric investigation of cathode catalyst layer morphology parameters during real operating conditions is performed. A regime of mixed ion and electron transport limitations describes correctly the main features of impedance spectra. In particular, high frequency resistance is related to poor electronic conductivity and it dramatically increases during operation in oxygen meanwhile holding in inert atmosphere seems to be ineffective. This suggests a key role of catalyst layer structure degradation on performance evolution.

### REFERENCES

1. Lefèvre, M. *et al. Science (80-. )*. **324**, 71–74 (2009).
2. Serov, A. *et al. J. Power Sources* **327**, 557–564 (2016).
3. Serov, A. *et al. Adv. Energy Mater.* **4**, 1301735 (2014).
4. Baricci, A. *et al. Fuel Cells* **14**, 926–937 (2014).
5. Leonard, N. D. *et al. J. Electrochem. Soc.* **162**, 1253–1261 (2015).

## FUEL UTILIZATION IMPACTS ON SYSTEM EFFICIENCY IN GAS-TURBINE/SOLID-OXIDE-FUEL-CELL HYBRID SYSTEMS

D. Oryshchyn\*, N. F. Harun\*\*, D. Tucker\*\*, and L. Shadle\*\*

\*USDoE, NETL, 1450 Queen Av. NW, Albany, OR 97321, (U.S.A)

\*\*USDoE, NETL, 3610 Collins Ferry Rd, Morgantown, WV 26505, (U.S.A)

**Abstract** – A design study was conducted to characterize the performance of a hybrid power generator comprising a solid-oxide fuel-cell (SOFC) and gas turbine (GT). Thermal management within the hybrid system and GT performance was compared with and without anode recycle (AR), operating at 90% total stack fuel utilization ( $U_f$ ). A reference case at 65%  $U_f$  was included to evaluate performance without anode recycle. The cases without AR had dramatically higher efficiencies, ~71%. The reference case was only 0.4% lower than the case with 90%  $U_f$ , but it dropped to only 55.5% with AR. The turbine efficiency increased slightly for AR, but there was a significant loss in fuel cell efficiency as a result of decreased Nernst potential. Heat exchange within the SOFC manifold, from the SOFC system's post-combustor to cathode-inlet air, needed to be nearly zero for low- $U_f$  cases, but about 48% for higher  $U_f$  cases.

**Index Terms** - anode recycle, fuel utilization, hybrid efficiency, solid oxide fuel cell gas turbine hybrid.

### I. NOMENCLATURE

Anode-recycle (AR), SOFC post-combustor (CMB), Hot-air (HA), Heat exchanger (HX), Single pass (SP), Turbine (TRB)

### II. INTRODUCTION

A design-point study was conducted to investigate the impact of  $U_f$  on a solid-oxide fuel-cell (SOFC) and gas turbine (GT) hybrid system, comparing systems producing equivalent power, but with a range of fuel utilization ( $U_f$ ). Previous studies have been conducted, but have employed lumped models of the fuel-cell stack for the SOFC [1]. Conventional wisdom is to achieve the highest  $U_f$  in the fuel cell; however, there is potential to reduce SOFC degradation and size of fuel cell stack by reducing  $U_f$  [2, 3].

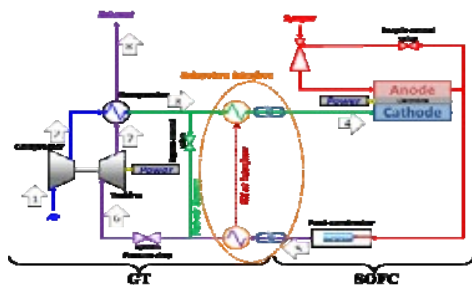
The performance of the SOFC stack was investigated in detail as a function of  $U_f$  [2]. In that work, even though the SOFC stack was maintained at identical thermal conditions across the cell, operating at lower  $U_f$  reduced both localized

current density and electrochemical losses. This eventually reduced the initial degradation rates.

In this study, effects of  $U_f$  and AR were analyzed for the same cases presented by Harun et al. [2], focusing instead on the performance in the bottoming gas turbine cycle and heat exchangers. Cases included 65% and 90%  $U_f$ , single-pass (SP); 90% stack  $U_f$  using anode recycle on 65%  $U_f$  cells. Experimental work has attained 90% SP  $U_f$  [3]. With design advances in cell-temperature control, we assume this will also be possible with syngas.

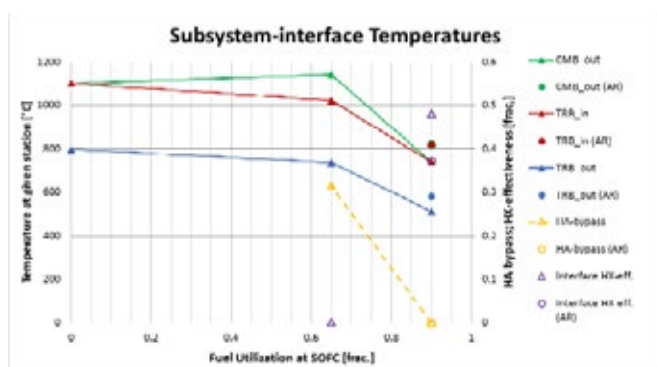
### III. METHODS

The direct fired SOFC-GT hybrid system depicted in Fig. 1 was simulated as described by Harun et al. [2] in two parts: SOFC and GT. The SOFC part, including the fuel-cell stack and post-combustor, was simulated via a one-dimensional model built in MATLAB [3]; the GT part, including the recuperated turbine engine, subsystem-interface heat exchange, and the total-system pressure-drop, was simulated using GateCycle®.  $\Delta P$  was a function of the amount of air routed through the hot-air bypass. This is represented in the loop as the dashed purple valve in Fig. 1. The blue chain links drawn in this figure within the dashed orange oval and labeled “subsystem interface” indicate data exchange between the two models. The turbomachinery performance was simulated based upon isentropic efficiencies for the 5MW Mercury 50 system – a commercial recuperated turbine.

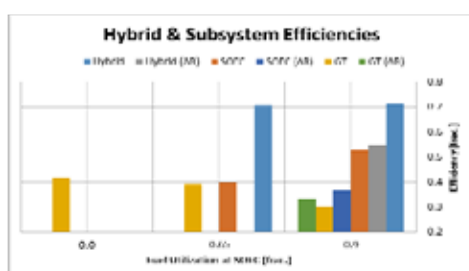


## IV. RESULTS AND DISCUSSION

The model of the GT alone shows the combustor output at the desired turbine inlet temperature (1100 °C). Temperature drop across the turbine is similar between the 0% and 65% cases. This temperature drop is slightly smaller when  $U_f$  is 90% (both in SP and AR cases).

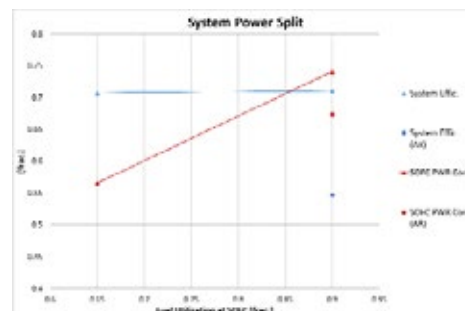


**Fig. 2. Temperature history from SOFC through bottoming turbine**



**Figure 3: Subsystem energy efficiencies**

The overall hybrid efficiency is nearly the same between single-pass design-cases at 65% and 90%  $U_f$ . The efficiency of the SOFC subsystem is higher at the higher  $U_f$ , while the GT subsystem efficiency is lower. The efficiency impact resulting from AR is greater in the SOFC than in the GT, driving the hybrid's efficiency. The GT efficiency alone is shown for comparison (at 0%  $U_f$ ).



**Fig. 3. Share of power produced at the fuel cell.**

Though the hybrid's efficiency remains nearly flat between the 65% and 90% SP cases, the share of power produced at the SOFC increases. The 90% case still requires significant power share from the GT. Thus, the lower efficiency of the GT at this  $U_f$  degrades the hybrid performance

## V. CONCLUSIONS

AR significantly reduced the efficiency of this direct fired SOFC-GT hybrid system. On the other hand, reducing  $U_f$  had very little effect on overall efficiency even when employing very conservative turbomachinery. The result was substantial reductions in the designed size of SOFC stack, recuperator, and manifold heat exchanger for the reference case. Thus, shifting the power split in favor of the gas turbine holds real promise for improving the economics for this technology.

## ACKNOWLEDGMENT

This work was funded by the U.S Department of Energy Crosscutting Research program, implemented through the Technology Development & Integration Center, Coal, in The Office of Fossil Energy.

## REFERENCES

- [1] Tarroja, B., Mueller, F., Maclay, J., and Brouwer, J., Parametric thermodynamic analysis of a solid oxide fuel cell gas turbine system design space, *Journal of Engineering for Gas Turbines and Power*, Volume 132, 2010, Pages 072301-1 to 072301-11.
- [2] Harun, N., Shadle, L., Oryshchyn, D., Tucker, D., Fuel Utilization Effects on System Efficiency and Solid Oxide Fuel Cell Performance in Gas Turbine Hybrid Systems, *Proceedings: ASME Turbo Expo 2017*, Charlotte, NC, June 26-30, 2017
- [3] Fang, Q., et al., SOFC stack performance under high fuel utilization, *International Journal of Hydrogen Energy*, Volume 40, 2015, Pages 1128-1136
- [4] Zaccaria, V., Tucker, D., Traverso, A., Operating strategies to minimize degradation in fuel cell gas turbine hybrids, *Applied Energy*, Volume 192, 2017, Pages 437-445.

## NANO-HYBRIDS; THE EFFECT OF TURBINE EFFICIENCY ON FUEL CELL- TURBINE HYBRID PERFORMANCE

Lawrence Shadle\*, Dave Tucker\*, Dan Oryshchyn<sup>+</sup>, Nor  
Farida Harun\*, and Michael Shelton<sup>†</sup>

\*National Energy Technology Laboratory (NETL), 3610 Collins  
Ferry Rd, Morgantown, WV 26507-0880 (USA)

<sup>+</sup> NETL, 1450 SW Queen Ave., Albany, OR 97321 (USA)

<sup>†</sup>A.K. Supply, Inc., 8000 King St., Anchorage, AK 99518 (USA)

**Abstract** –A systems analysis was conducted to evaluate the effects of hybrid scale on overall performance. The benchmark was the highly efficient turbine in a 550 MW hybrid power system. This was compared to a nano-hybrid system of 20 kW with reduced isentropic efficiencies for the smaller scale turbomachinery. Electrical efficiency was remarkably high even with the small inefficient turbomachinery. The SOFC share of the power was a low 68% for a fixed SOFC fuel utilization ( $U_f$ ) of 0.7.

**Index Terms** – efficiency, hybrid power cycle, solid oxide fuel cell, turbomachinery.

### I. INTRODUCTION

Research is being conducted at NETL to improve the potential for early deployment of highly efficient power cycles. Solid oxide fuel cell (SOFC) - gas turbine hybrids are arguably the most efficient power cycle conceived. This cycle is a suitable candidate for many relatively small-scale applications because of its operating flexibility, large turndown, and low emissions [1,2]. In a design study of a 550 MW fuel cell - turbine hybrid the best efficiencies and costs were achieved with approximately equal power split between fuel cell and turbine when operating on a methane free syngas [3,4]. The natural progression of development of these systems, however, will require deployment at much smaller scales.

A detailed parametric analysis was conducted by Tarrajo et al. [5] on direct-fired hybrid evaluating the effects of  $U_f$ , oxygen utilization, current density, and pressure ratio. While the sizes of the turbine and compressor were permitted to vary, the efficiency of this equipment was fixed at a level consistent with micro-turbomachinery. In this analysis, the fuel composition was employed as used in the large-scale design studies [3,4], but the turbomachinery performance was downgraded to reflect the inability to achieve the same efficiency in smaller equipment. In this way, we assessed the potential impact of operating at a scale suitable to early technology deployment on its performance.

### II. PROCESS ANALYSIS

The hybrid power cycle studied was comprised of a

compressor and turbine on a common shaft, the compressed air was preheated by the turbine exhaust via a recuperator before being sent to the cathode of the SOFC (Figure 1).

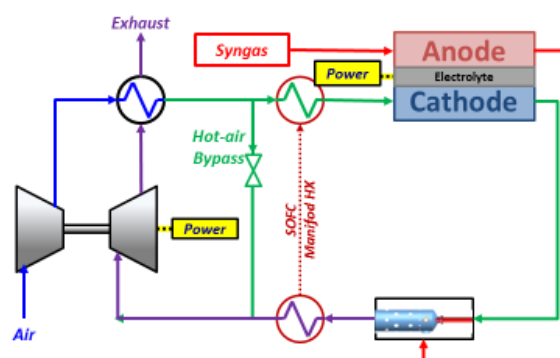


Fig. 1. Direct fired SOFC- gas turbine hybrid system.

Syngas was fed to the SOFC anode. The unconverted fuel and air were burned in a post combustor. The vitiated air was expanded through the turbine.

Thermal management of the fuel cell was achieved by one or more of several options. Excess heat and airflow was diverted around the SOFC using the hot air bypass valve (HA). When additional heat was required in the SOFC it was extracted from the products of the post combustor within the SOFC manifold, albeit with low effectiveness (<0.5). Additional heat could be provided by injecting fuel into the air flow prior to cathode inlet in a pre-combustor (not shown); however, this was found to be unnecessary.

A systems analysis was conducted to evaluate the effects of hybrid scale on overall performance. The compressor, turbine, and heat exchangers were simulated using GateCycle® as described by Harun et al. [4]. The Fuel Cell was simulated using NETL's 1-dimensional fuel cell model. The number of 20 x 20 cm cells and fuel flow were varied to achieve target power output and  $U_f$ . The cathode airflow was adjusted to achieve a target average solids temperature of 835°C. Post combustion was simulated by adiabatically reacting the unconverted fuel from the anode with the vitiated air from the

cathode. Heat management was conducted in Gatecycle®, varying the manifold heat exchange effectiveness, HA bypass to achieve the required cathode airflow and temperature.

A simple sensitivity analysis was conducted. The isentropic efficiency of the compressor ( $\eta_c$ ) and turbine ( $\eta_t$ ) were varied. For the 550 MW and 20kW-1 cases the flows and equipment sizes were varied, including the number of fuel cell, recuperator surface area, and pipe diameters, to achieve target operating conditions. The turbomachinery was the same for both cases:  $\eta_c=0.836$  and  $\eta_t=0.87$ . In case 20kW-1c  $\eta_c$  was dropped to 0.73. In case 20kW-1t  $\eta_t$  was dropped from 0.87 to 0.77. In case designated 20kW-2 both  $\eta_c$  and  $\eta_t$  were reduced to 0.73 and 0.77, respectively.

### III. RESULTS AND DISCUSSION

Oryshchyn et al. reported that hybrid power system performance was near optimum when  $U_f=0.7$  [3]. Using this  $U_f$  the operating conditions and performance of a nano-hybrid system with nominal size of 20 kW hybrid are compared to the 550 MW plant in Table 1. Because the size of individual planar cells in an SOFC is constant 20 by 20 cm, the effect of changing the number of cells had much larger relative impact on the 20kW case. The SOFC stack size was approximately 32 cells for 20kW case, but was 1,805,000 cells for the 550 MW case. Thus, it was not possible to achieve a fixed 20 KW hybrid output. For this reason, the SOFC stack was not adjusted to achieve the same power output during the sensitivity study.

TABLE 1. NANO HYBRID PERFORMANCE COMPARED TO A UTILITY SCALE SYSTEM FOR  $U_f=0.7$

Case	550 MW [3,4]	20kW- 1	20kW- 1c	20kW- 1t	20kW- 2
$\eta_t$ [%]	87	87	87	77	77
$\eta_c$ [%]	83.6	83.6	73	83.6	73
Power [kW]	550,000	18.3	17.5	17.2	16.2
Power split: FC/total	0.60	0.60	0.63	0.64	0.68
$T_{IT}$ [C]	1018	1018	1016	981	980
$T_{RO}$ [C]	287	287	305	279	298
HA Bypass [%]	20	21	21	31	31
System $\eta_t$ %	72	68	65	64	60

The overall system efficiency was reduced for the nano-hybrid (case 20kW-1) even assuming the same turbomachinery performance due to differences in thermal management. The overall electric efficiency,  $\eta$ , dropped from the 550 MW case to 25kW-1, but it remained high at 68%. In both cases the power split was 60:40 between the SOFC and the gas turbine.

When  $\eta_c$  and  $\eta_t$  were downgraded individually in cases 20kW-1c and 20kW-1t, the power split increased slightly in favor of the SOFC, while the  $\eta$  dropped by 3 and 4 percentage points, respectively. The HA bypass was unaffected by reducing the compressor performance; however, it increased from 21 to 31% for the downgraded turbine. On the other hand,

a higher loss of energy through the recuperator was seen with downgraded compressor performance than that found with the downgraded turbine. The recuperator out temperature,  $T_{RO}$ , increased with downgraded compressor, but the reverse was found for the downgraded turbine.

When both  $\eta_c$  and  $\eta_t$  were downgraded together, the result was an overall drop of 8% points in  $\eta$ . Ironically the power split increased by 8% points in favor of the more efficient SOFC cycle. For the same size SOFC stack, ~24 m<sup>2</sup> surface in both the cathode and anode, the SOFC electric power output remained constant producing 11 kW, but the reduction in turbomachinery performance resulted in a loss of overall hybrid power output amounting to 11.5% less than the more efficient turbomachinery producing 18.3 kW electricity. The combination of the higher flow demand by the turbine, the lower  $T_{IT}$ , and higher compressor power demand resulted in the lower combined performance. However, the amazing fact was that  $\eta$  remained high at levels above 60% even for the very conservative reduction in isentropic efficiencies in both the compressor and turbine.

### IV. CONCLUSION

The simulated performance of a nano-hybrid power system of nominal 20 kW size exhibited high  $\eta$  despite utilizing inefficient turbomachinery with isentropic  $\eta$  reduced by 10 percentage points. The resulting power split was lower than those traditionally considered for hybrid cycles at 68:32 SOFC: gas turbine. Reducing the power split in favor of the GT results in a lower capital cost because the SOFC is the costlier equipment. Current cost estimates for RGT and SOFC are \$400 and \$5000/kW, respectively [3]. This analysis demonstrates that hybrid power systems can maintain high system efficiency even at very small scale even though the turbomachinery is less efficient than utility scale equipment. We believe that this is a direct consequence of the fact that inefficiencies in rotating equipment can be recovered by the recuperator where waste heat can be very efficiently returned to the SOFC.

### REFERENCES

- [1] Costamagna, P.; Magistri, L.; Massardo, A. (2001) *Journal of Power Sources*, vol. 96, pp. 352-368.
- [2] Reyhani, H. A.; Meratizaman, M.; Ebrahimi, A.; Pourali, O.; Amidpour, M. (2016) *Energy* 107, 141-164.
- [3] Oryshchyn, D.; Harun, N.F.; Tucker, D.; Zaccaria, V.; Shadle, L.J. (2018) submitted to *Journal of Applied Energy*, Nov. 30, 2017.
- [4] Harun, N.F.; Tucker, D.A.; Shadle, L.J., Oryshchyn, D.B. (2017) *Proceedings of ASME Turbo Expo 2017: Power for Land, Sea and Air*, GT2017-64055.
- [5] Tarroja, B.; Mueller, F.; Maclay, J.; Brouwer, J. (2010) *Journal of Engineering for Gas Turbines and Power*, vol. 132, July, pp. 072301:1-11.



EFC17098

# Shut-down cycles as accelerated degradation tests of metallic bipolar plates in proton exchange membrane fuel cells

Björn Eriksson\*, Annika Carlson\*, Anna Jansson\*\*, Rakel Wreland Lindström\*, Göran Lindbergh\*,  
Carina Lagergren\*

\* Applied Electrochemistry, School of Chemical Science and Engineering,

KTH Royal Institute of Technology, SE-100 44 Stockholm, (Sweden)

\*\* Sandvik Materials Technology, SE-811 81 Sandviken, (Sweden)

**Abstract** – The lifetime of coated stainless steel bipolar plates (BPPs) is investigated using shutdown strategies as an accelerated degradation test (ADT). The effect of 1550 shutdowns is evaluated from contact resistance measurements and from cyclic voltammetry. The results show that the bipolar plate is not affected by the ADT, however, the membrane electrode assembly (MEA) is adversely affected. The cathode catalyst layer is severely reduced during the cycling, causing performance loss. The results show that air purge shutdown cycling for 1550 cycles is not an effective ADT for BPP.

**Index Terms** - Degradation, BPP, ADT, proton exchange membrane fuel cell (PEMFC)

## I. INTRODUCTION

Bipolar plates (BPPs) are crucial components when constructing proton exchange membrane fuel cell (PEMFC) stacks. They function as gas separators and current collectors, and enable water and thermal transport throughout the stack. Furthermore, the BPPs need to be stable in both reducing and oxidizing environments, since the BPPs face both the cathode and anode of the PEMFC. The BPP accounts for roughly 80 % of stack weight and 45 % of the cost [1]. As such, development of cost efficient BPPs is one of the main challenges for PEMFC research. Metallic BPPs allow for good mechanical properties, such as good machinability and gas impermeability [2]. However, pure stainless steel is readily corroded in fuel cell environment. This can be mitigated by coating the steel plate, which increases the corrosion resistance and lowers the contact resistance [3]. Coated metallic BPPs have shown to be relatively stable during steady state measurements [4]. Therefore, accelerated degradation tests (ADTs) are required to enable more effective evaluation of the lifetime and main degradation causes. Shut-down cycles have previously shown to affect the carbon corrosion of electrodes in PEMFC. The bipolar plates utilized in this study have a carbon coating, as such it is theorized that similar corrosion can also occur on the

BPPs. Once the coating is degraded the stainless steel would be susceptible for further corrosion, which would cause a high increase in internal contact resistance (ICR).

## II. EXPERIMENTAL

### A. PEMFC assembling and measurements

In-situ measurements were carried out in an in-house fuel cell [5] using a commercial MEA (GORE PRIMEA 0.1/0.4 mg<sub>Pt</sub>cm<sup>-2</sup> loading), and a Sigracet 25 BC gas diffusion layer (GDL). The bipolar plate used in this study is a coated stainless steel (Sandvik). Prior to mounting in the cell the bipolar plate was cleaned for 15 min in ethanol and water in an ultrasonic bath. To be able to measure the contact resistance a two-probe setup was used. The first probe is placed on the GDL, while the second is in contact with the bipolar plate.

### B. Shutdown cycling

The shutdown procedure utilized in this study is the “Air purge” [6]. A schematic version is shown in **Fig.1**. The procedure starts with 10 s open circuit potential (OCP), during which reactant gases are added to the system, afterwards a current density load of 0.5 Acm<sup>-2</sup> is applied for 40 s, this is followed by 10 s additional OCP. The last step includes shutting off the hydrogen inlet and instead flowing dry air in the anode compartment.

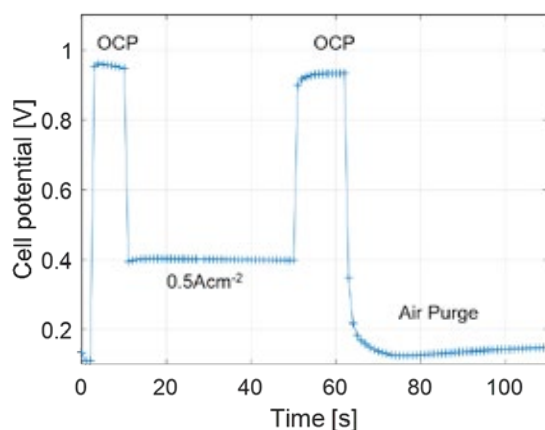


Fig 1- Cell potential during the 2<sup>nd</sup> cycle of the shutdown cycle using air purge. Cell temperature: 80 °C, anode gas: 2.5 bar hydrogen with relative humidity of 50 %, cathode gas: 2.5 bar pressure air with relative humidity of 30 %.

### III. RESULTS

The effect of the shutdown cycling on the internal contact resistance, ICR, is shown in **Fig.2**. As can be seen the ICR does not change significantly during the cycling. The bumps in the ICR at cycle 600 and 1450 are due to readjusting the clamping pressure to 8 bar.

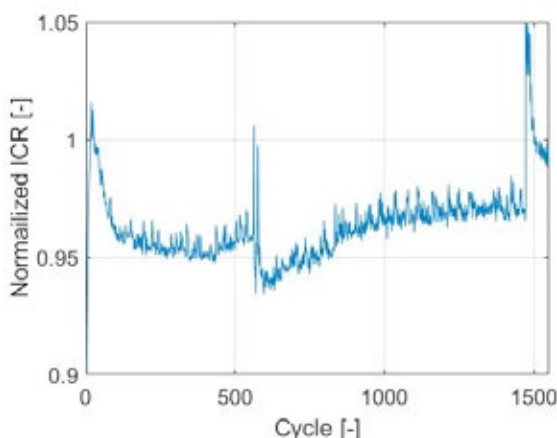


Fig 2- Normalized ICR of the bipolar plate during shutdown cycling

While the BPP is unaffected by shutdown cycling, the MEA is affected. These effects are clearly seen in the cyclic voltammogram, **Fig.3**. As shown the electrochemical surface area, ECSA, of the cathode is severely diminished during these tests, showing approximately a 70 % loss. However, no additional resistances or increase in crossover could be detected. This suggests that the main effect of the cycling is carbon corrosion in the electrodes, which is in line with previous results [4].

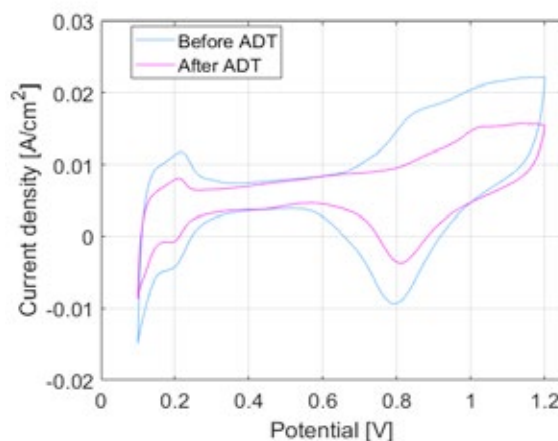


Fig 3- Cyclic voltammetry before and after ADT for sample without bipolar plate with a sweep rate of 100 mVs<sup>-1</sup>. Cell temperature: 80 °C, anode gas: 2.5 bar hydrogen with 95 % RH, cathode gas: 2.5 bar nitrogen with 95 % RH.

### IV. CONCLUSION

Shutdown cycling of PEMFC cells with BPP was conducted. The results show that the ICR remains constant which indicates that the BPP is unaffected by these procedures. However, the MEA, especially the cathode catalyst layer, is affected. As such this type of shutdown strategy can be questioned as an ADT for BPP ageing. Further surface analyses and testing of BPPs are required to find suitable ADT for ageing of the BPP.

### ACKNOWLEDGMENT

We acknowledge funding from Strategic Vehicle Research and Innovation (FFI), and from STandUp for Energy, Sweden.

### REFERENCES

- [1] H. Tsuchiya and O. Kobayashi, 2004, 'Mass production cost of PEM fuel cell by learning curve', *Int. J. Hydrogen Energy*, vol 29, pp. 985-990
- [2] Karimi A, Et al, 2012, 'A Review of Metallic Bipolar Plates for Proton Exchange Membrane Fuel Cells: Materials and Fabrication Methods' *Advances in Materials Science and Engineering*, vol 2012,
- [3] Oyarace A Et al. , 2013, 'Operating conditions affecting the contact resistance of bi-polar plates in proton exchange membrane fuel cells', *Journal of Power Sources*, vol. 231, pp. 246-2255
- [4] Lee S.J, Et al. 2005, "Stainless steel bipolar plates", *Journal of Power Sources*, vol. 145, pp 363-368
- [5] Gode. P, Et al. 'Membrane Durability in a PEM Fuel Cell Studied using PVDF Based Radiation Grafted Membranes, *Fuel Cells*, Volume 3, 2003, Pages 21-27
- [6] Oyarace A, Et al. , 2014, 'Comparing shut-down strategies for proton exchange membrane fuel cells', *Journal of Power Sources*, vol. 254, pp. 232-240

## APPLICATION OF PLATINUM COATED ALUMINUM SEPARATOR TO PASSIVE TYPE PROTON EXCHANGE MEMBRANE FUEL CELL

Dong Kyu Kim\*, Kwon Pil Park\*\*, Ilchae La\*\*\*, Junghun Lee\*\*\* and Sangwon Kim\*\*\*\*

\* School of Mechanical Engineering, Chung-Ang University, Seoul, 06974, South Korea

\*\* Department of Chemical Engineering, Sunchon National University, Suncheon, Jeollanam-do, 57922, South Korea

\*\*\* CNL Energy Co, 1149-15 Jaegi-Dong, Dongdaemun-gu, Seoul, 02465, South Korea

\*\*\*\*KIST Europe, Campus E 71, 66123 Saarbrücken, Germany

**Abstract** – Weight reduction is important for the portable fuel cell stack such as unmanned airplane or drone. We suggest aluminum alloy as a separator because the weight of the stack depends mainly on the weight of the separator plate. Aluminum alloy is corroded under PEM fuel cell operation condition. To prevent corrosion of aluminum separator, nickel plating and platinum plating were applied on aluminum alloy separator and corrosion improvement was compared.

The temperature control in passive stack is very important since the passive stack is cooled by forced convection by fan, which is also connected to the air supply to the cathode. The best performance is obtained at a temperature of 40 °C in the passive PEM fuel cell stack.

**Index Terms** – passive type PEM fuel cell, aluminum separator, corrosion resistance, temperature control

### I. INTRODUCTION

Proton exchange membrane (PEM) fuel cell is widely used as energy converting devices in diverse transportation vehicles such as automobiles, buses, submarines and airplanes. Weight reduction is the most important issue for air transport application such as unmanned airplane or drone. Passive type PEM fuel cell is considered for the drone application since the stack weight could be reduced significantly by removing air supplying Balance of Plant (BoP) in cathode side. However, the disadvantage of the passive type PEM fuel cell is that the output power can be reduced because the air is supplied by natural convection or forced convection using blower instead of air compressor or air pump. Therefore, it is important to reduce the weight and maintain the output power in passive type PEM fuel cell development.

### II. PASSIVE FUEL CELL STACK STRUCTURE

The passive fuel cell stack was designed and manufactured by CNL Energy, which is shown in Figure 1. One side of the separator is the reaction surface of the anode, and the other side is the cathode and air cooling surface. Unlike the active stack, the anode, cathode, and cooling channels are formed on one separator, so the weight and volume can be reduced by half comparing to active stack. The stack is composed of 40 cells and weighs 1.01 kg. The stack dimension is 170 mm (L) \* 70 mm (W) \* 145 mm (H) with active area of 20cm<sup>2</sup>.

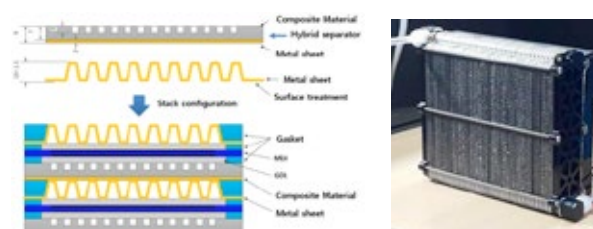


Fig.1. Passive PEM fuel cell stack configuration

### III. RESULTS AND DISCUSSION

#### A. Separator modification

We proposed an aluminum alloy separator to reduce weight instead of a conventional carbon composite material separator. Aluminum has high electrical and thermal conductivity, low density and sufficient mechanical strength, but is corroded under PEM fuel cell operating conditions.

Copyright © 2017

We tested the corrosion resistance of aluminum (Al 1050) by varying the platinum plating thickness. The corrosion process is accelerated by immersing the plated aluminum alloy at 80 °C for 4 hours in Fenton solution (30% H<sub>2</sub>O<sub>2</sub> + 4 ppm FeSO<sub>4</sub> 6H<sub>2</sub>O) and 0.1M H<sub>2</sub>SO<sub>4</sub> solution. The resistance was measured after 1 cm<sup>2</sup> specimen was inserted between gold-coated plates and pressed at 150 N / cm<sup>2</sup>.

As shown in Table 1, the electrical resistance is reduced by platinum plating, and the resistance decreases as the thickness of the platinum plating increases, resulting in a resistance of 1.0 mΩ·cm<sup>2</sup> or less at a thickness of 0.5 μm. Especially, the resistance values of 1.0 μm thickness platinum plating aluminum alloy before and after corrosion are 0.31 mΩ·cm<sup>2</sup> and 0.32 mΩ·cm<sup>2</sup>, which shows very small change in electrical resistance even after corrosion, confirming excellent corrosion resistance.

TABLE I

ELECTRICAL RESISTANCE CHANGE BEFORE AND AFTER CORROSION

Platinum plating thickness (μm)	0	0.05	0.1	0.5	1.0	
Electrical resistance (mΩ·cm <sup>2</sup> )	Before corrosion	118	5.2	1.32	0.64	0.31
	After corrosion	173	111	83.3	7.74	0.32

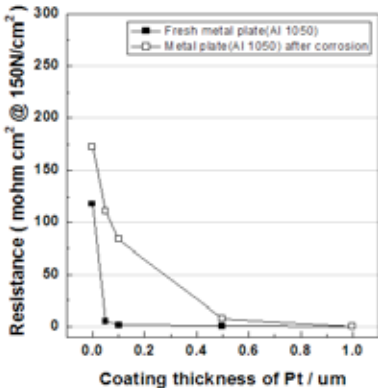


Fig. 2. Electrical resistance change depending on platinum plating thickness

B. Temperature control

Active stack is supplied with non-humidified hydrogen and air humidified using water generated by fuel cell reaction. The passive stack is supplied with hydrogen and air in non-humidified condition. Fan functions air supply and stack cooling. If the fan power is increased, the amount of supplied air is increased and cooling effect is improved, but the electrolyte membrane dehumidification can be accelerated. If the fan power is lowered, the cooling effect is reduced and the electrolyte membrane can be dried due to the temperature rise of the stack. The electrolyte membrane dryness is related to the stack performance degradation. Figure 3 shows that as the stack output power increases, the heat generated at stack increases

and the stack temperature increases. When the stack temperature exceeds 40 °C, the performance degradation due to the electrolyte membrane drying becomes remarkable. Figure 4 shows the performance of 40cell passive stack is 375 W at a stack voltage of 24 V (cell voltage 0.6 V).

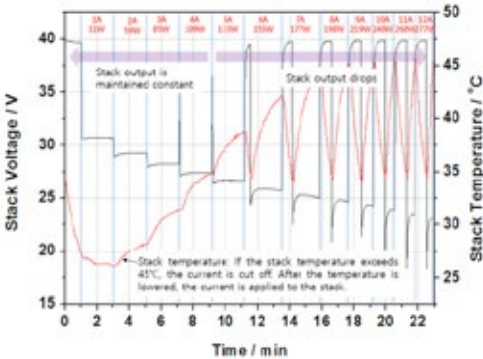


Fig. 3. Stack performance test with temperature

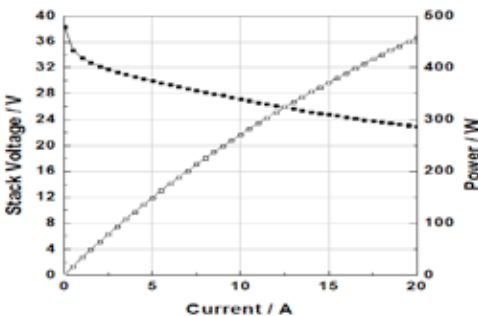


Fig. 4. Passive stack performance (40 cells)

IV. CONCLUSIONS

Platinum plated aluminum alloy is suggested as separator material of passive PEM fuel cell stack. When platinum is plated on aluminum alloy with 1 μm thickness, the electrical resistance is reduced to 0.31 mΩ·cm<sup>2</sup> and the corrosion resistance is improved dramatically. The best performance of the stack was obtained at 40 °C of stack operation temperature.

ACKNOWLEDGEMENT

This work was funded by project no. 20133030030690 from Korean Energy Technology Evaluation and Planning (KETEP). The authors acknowledge the assistance from project partners, Ace Industrial Co. and Korea Automotive Technology Institute (KATECH).

REFERENCES

[1] Jung, H., Oh, S., Jeong, J., Na, I., Chu, C., Park, K., Characteristics of Al Alloy as a Material for Hydrolysis Reactor of NaBH<sub>4</sub>, Korean Chem. Eng. Res., 53(6), 2015, pp. 677-681.  
 [2] Choi, H., Jang, H., Kim, D., Aluminum bipolar plates for fuel cell, KR20150067695A.

## Redox flow battery instead of rSOC for resilient energy systems in off-grid remote areas or in non- or low interconnected islands: why not?

L. Barelli\*, G. Bidini\*, M. Casciola\*\*, G. Discepoli\*, A. Donnadio\*\*, F. Gallorini\*\*\*, E. Troni\*\*

\* Department of Engineering, Università degli Studi di Perugia, via Duranti 93, 06125 Perugia, (Italy)

\*\* Department of Chemistry, Università degli Studi di Perugia, Via Elce di Sotto, 8 06123 Perugia, (Italy)

\*\*\* VGA srl, Via dell'innovazione SNC, 06053 Deruta (Italy)

**Abstract** - Penetration of renewable energy plants is strongly slowed by the characteristic intermittency and fluctuating production trend, which significantly mismatches with typical users' load profiles, with negative impacts on grid stability and safety. The widespread of energy storage could mitigate these issues; rSOC and VRFB application is compared for off-grid remote areas or in non- or low interconnected ones.

**Index Terms** – rSOC, VRFB, micro-grid, energy storage.

### I. INTRODUCTION

In off-grid remote areas or in non- or low interconnected ones, where storage applications are characterized by large capacity with respect to the installed power, reversible Solid Oxide Cells (rSOC) currently deserve particular attention since hydrogen-based power-to-power systems can avoid the installation of large-size conventional batteries whose power and energy ratings are inevitably coupled.

Vanadium redox flow battery (VRFB) fulfills the same function since stored energy and power can be independently sized. Moreover, the higher efficiency (> 85%), operation flexibility, durability and lower safety issues (e.g. related to the tank) represent significant advantages, as resulting in the present paper where both technologies are investigated and compared when applied to a particular case-study.

### II. EXPERIMENTAL

The flow battery test bench is composed by three subsystems: the hydraulic, the electrical and the sensors one.

The hydraulic system manages the electrolyte (1.0 M VOSO<sub>4</sub> in 5 M H<sub>2</sub>SO<sub>4</sub>) transport from the anodic/cathodic tanks to the battery and back to the tanks and nitrogen bubbling to avoid external air recall.

The electrical system defines the function mode (e.g. charge or discharge) and the BioLogic SP-240 equipment leads the test executed in the present paper. The sensors system includes thermocouples and voltage sensors, the latter connected with the BioLogic instrument.

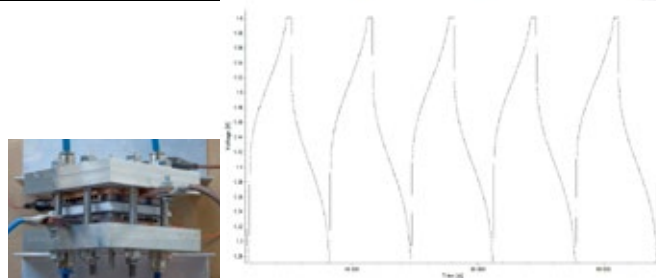
The tested flow battery is a sandwich of different components (Fig. 1); from the outside: aluminium plate (it compresses the inner components by a 8 screws system), Mica sheet (electric insulator), Copper plate (current collector), graphite plate, viton seal, teflon gasket, carbon felt (SGL carbon Sigracell), Nafion

115 membrane (treated with H<sub>2</sub>SO<sub>4</sub> in order to favor the hydration and increase the permeability).

In Table 1, main parameters of cyclic charge and discharge test are listed. Fig. 1 shows voltage trend in cyclic charge and discharge tests.

**Table 1 main parameters of cyclic charge and discharge test**

Parameter	Value	Unit
Cell Area	6	Cm2
Current Density	50	mA/cm2
Charge/Discharge Current	600	mA
Charge Voltage Limit	1.6	V
Charge Current Limit	100	mA
Charge Voltage Limit	1.6	V
Charge Current Limit	100	mA
Discharge Voltage Limit	0.5	V



**Figure 1 VRFB cell assembly and cycling**

### III. MODELLING

Two different codes were developed for the evaluation, over 1 year, of micro-grid (MG) energy performance in case of adoption of rSOC and VRFB respectively. In both cases the MGs are constituted by residential users (load: 1.9 kW mean and 29 kW peak) and the installation of a 5kW PV plant (yearly production was determined by applying the PVGIS [1] for a positioning in central Italy).

Specific strategies are implemented in the codes to manage the energy exchanges among the users, the RES plant, the storage system and the grid with 1-minute step; in particular:

- "Priority of load satisfaction" for the VRFB. The storage power profile is continuously modulated to fill the positive or negative gap between load and PV production.



- “Priority of storage charge/discharge” for the rSOE due to its technological features. It performs 1 charge/discharge cycle in a day, under charge/discharge constant power. For each month, on the basis of the related daily mean PV production profile, the constant charge power and (known rSOE round trip efficiency) the discharge one were determined.

The codes have in input the yearly PV profile, the load, the storage power profile (only for rSOE case), storage technical features (maximum power, capacity, round trip efficiency).

#### IV. RESULTS

As first step, the VRFB capacity was determined, fixed an installed power of 5kW and an efficiency of 88% as resulting from the test over 70 cycles, to achieve a sufficient independence level of the MG from the grid. The sensitivity analysis from 5 to 160 kWh (rows 1-7 of Table 2) revealed that for capacity greater than 40kWh the self-consumption increment rate remains at 1%. A 40kWh VRFB allows an increase in self-consumption of about 69% with respect to the case of No Storage (NS) devices. The energy sent to the grid is reduced from 5944kWh (NS case) to 375kWh over one year improving the independence of the MG. 40 kWh corresponds also to the maximum daily PV production in the year.

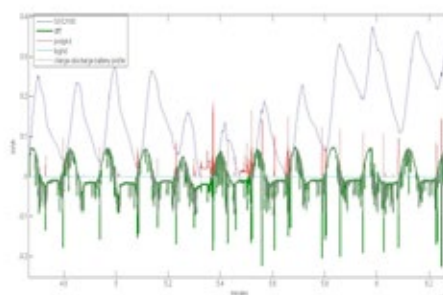
**Table 2 MG energy performance (kWh)**

Capacity	To Storage	From Storage	From Grid	To Grid	Self-cons.
5 (VRFB)	2185	1923	8851	3138	7631
10 (VRFB)	3554	3127	7791	1938	8686
20 (VRFB)	5057	4450	6627	620	9846
30 (VRFB)	5275	4642	6459	439	10004
<b>40 (VRFB)</b>	<b>5358</b>	<b>4715</b>	<b>6394</b>	<b>375</b>	<b>10059</b>
80 (VRFB)	5508	4847	6278	284	10134
160 (VRFB)	5694	5011	6134	199	10199
<b>40 (rSOE)</b>	<b>10997</b>	<b>4405</b>	<b>13941</b>	<b>1488</b>	<b>6874</b>

Fig. 2 gives an example of the main energy profiles (from/to grid, red/light blue lines) and the SOC one (grey, in terms of the stored energy divided by 100) for some days in function of the difference (green) between load and PV production. The VRFB power profile is completely overlapped to this one.

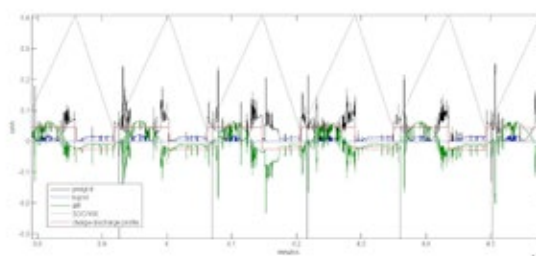
Considering 1.35V and 1.5V as mean and maximum cell voltage, as results from the test, the stack is composed by 35 cells (square, 0.46m side) in series working under a current density of 50 mA cm<sup>-2</sup>. It corresponds to a maximum current of 105.8 A at 48V.

The rSOC was compared at same installed power and capacity, (5 kW, 40 kWh) considering a round trip efficiency of 40% as indicated in [3] for an ambient pressure stack, considering also the pressurized hydrogen storage at 800 bar.



**Figure 2 Results of MG simulation - VRFB**

According to the “priority of storage charge/discharge” management strategy (see the constant rSOE power profile – red line – in Fig. 3 and the related SOC trend), the MG simulation over a year provides the results summarized in the last row of Table 2.



**Figure 3 Results of MG simulation - VRFB**

#### CONCLUSIONS

Greater energy performance were found in case of VRFB adoption due to higher efficiency and flexibility in operation. Specifically, with respect to the rSOE application, energy purchased from the grid is halved and energy sent to the grid reduced of 1 order of magnitude, with an increase in self-consumptions of about 46%. The energy density instead is strongly increased (about 2 orders of magnitude) in case of rSOC, but safety and technological issues are enhanced in the VRFB case since electrolyte is stored at ambient conditions. What above, together with their long life operation, makes VRFBs attractive for stationary applications where large capacity with respect to the installed power is required.

#### ACKNOWLEDGEMENTS

Authors thank Prof. R. Marassi for useful technical discussion and scientific contribution

#### REFERENCES

1. Huld, T. et al. *Solar Energy*. **2012**, 86, 1803-1815.
2. Xi, J. et al. *J. Memb. Sci.* **2017**, 522, 45–55, doi:10.1016/j.memsci.2016.09.012.
3. Milewsky, J. et al. *Int J. of Hydrogen Energy*. **2017**, 42/5, 3498-3509, doi: 10.1016/j.ijhydene.2016.08.067.

## PERFORMANCE ANALYSIS OF FUEL CELLS UTILIZATION IN MARINE APPLICATIONS

R. Taccani, N. Zuliani

University of Trieste, Via A. Valerio 10, 34127 Trieste – Italy

**Abstract** - In this study, a process simulation model of an electric power generation system based on fuel cell and battery storage has been implemented considering an on-board installation. Typical ship operating profiles have been considered and an energy and emission analysis has been carried out for different plants size and lay-outs. In particular, Liquid Natural Gas (LNG) and hydrogen, as fuels, have been taken into account. Results shows that fuel cells and batteries have the potential to reduce fuel consumption, emissions, and offer advantages in the management of boil off gas if LNG is used with conventional dual fuel diesel engines.

**Index Terms** –fuel cells, marine propulsion, LNG, ship efficiency.

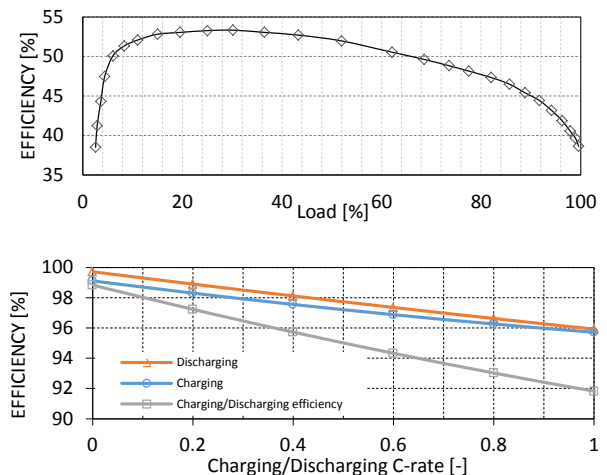
### I. INTRODUCTION

In the last years, growing efforts have been made by the International Maritime Organization (IMO) to reduce emission emitted by sea going vessels [1], [2]. For this reasons ship owners need to adopt solutions to bring exhaust emissions within these and other future limits. The use of different fuels such as Liquefied Natural Gas (LNG), is an interesting alternative to expensive and bulky exhaust gases after-treatment equipment or fuel with low sulphur content [3],[4]. However, in order to seek for a more efficient and sustainable solution, different energy systems should be employed. In particular, fuel cells have some advantages over diesel engines and, in literature, several studies have been carried out to demonstrate fuel cells on board application [5], [6]. In this work, a process simulation model of an electric power generation system based on a fuel cells and a battery is used to carry out a preliminary energy balance in order to evaluate system efficiency, emission reduction and tank size variation respect to conventional marine propulsion systems.

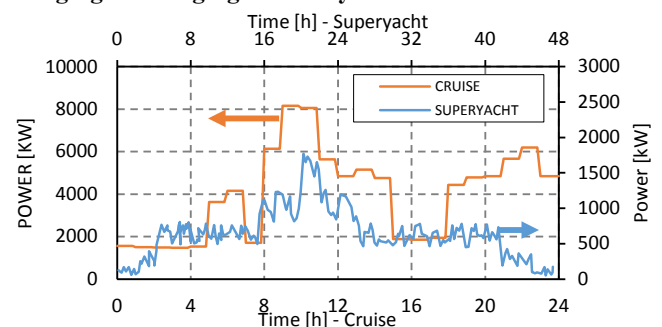
### II. METHODOLOGY

A traditional diesel engine based generation plant is compared with a fuel cell based generation system. The fuel cell generation system is composed of a Polymer Electrolyte Membrane (PEM) fuel cell stack, and a battery pack. Battery is

used for peak sheaving thus reducing fuel cells size and improving efficiency during load transients. When LNG is used, a steam reforming



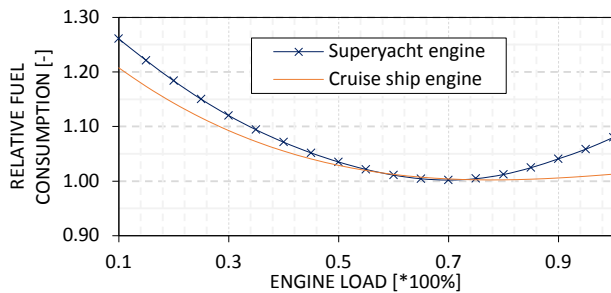
**Figure 1. Top: FC system efficiency variation with load. Bottom: Battery charging, discharging and charging/discharging efficiency**



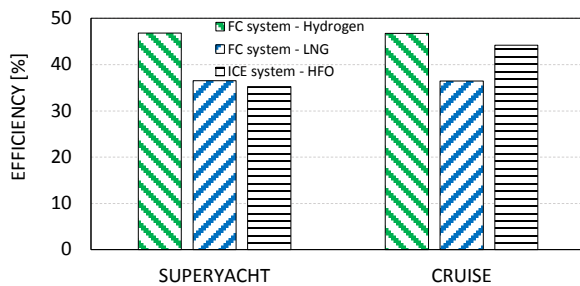
**Figure 2. Cruise ship and superyacht operating profile**

based fuel processor, for converting LNG in hydrogen is also taken into account. The whole system provides the total propulsion and auxiliary energy power demand. The PEM fuel

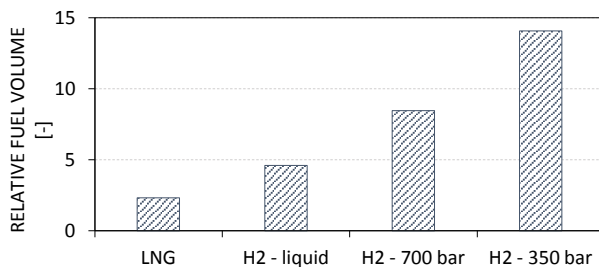
cell efficiency variation with load considered is shown in Figure 1 Top. The process model take into account for battery charging and discharging efficiency change as presented in Figure 1 Bottom.



**Figure 3. Relative fuel consumption variation with load for the considered diesel engines [7]**



**Figure 4. System average conversion efficiency for the two considered ships fueled with hydrogen, LNG or HFO**



**Figure 5. Fuel volume increase respect to HFO**

Two different ships with the corresponding operating profiles have been investigated (Figure 2): a superyacht and a cruise ship. Cruise ship installed power is 34,4 MW while superyacht installed power is 3.3 MW. These ships are chosen as they sail most of the time in Emission Control Areas (ECA). Two different fuels have been also considered: hydrogen and LNG. System average conversion efficiency, fuel volume required and emission are calculated.

### III. RESULTS

Figure 3 shows relative fuel consumption rate variation with load for the diesel engines considered in this study. Figure 4 shows system average conversion efficiency of the two considered ships fueled with hydrogen, LNG or Heavy Fuel Oil (HFO). When fueled with hydrogen, the efficiency is the

highest in both cases. When considering a superyacht, as the main propulsion engines can be used for long period at low loads to satisfy hotel load (in the case of equal load sharing among engines) fuel cells can be an interesting solution to increase efficiency. Figure 3 shows the alternative fuels volume requirements referenced to HFO. Liquid hydrogen volume requires approximately more than 4 times the space needed by HFO, while LNG needs approximately 2 times the space needed by HFO.

### IV. CONCLUSIONS

The use of fuel cells and batteries on ships have the potential to reduce fuel consumption and emissions especially for ships where the engine operates often in transient conditions and at part loads. However, a significantly reduction of the useful cargo volume has to be taken into account, especially when hydrogen is considered. The use of LNG, instead, is less space demanding but, in this case, the operating profile and ship engine characteristics significantly influence system efficiency. Overall, when PEM fuel cells and LNG are considered, it is necessary to carefully design the system in order to achieve an efficiency improvement, as the fuel processing is responsible for significant losses. Nevertheless, in terms of emissions, fuel cells offer always a benefit. The research will continue considering other types of fuel cells, such as Solid Oxide Fuel Cells, that allows to reach higher efficiency. When considering cruise ships, an interesting solution could be the use of LNG in conventional dual fuel engines together with fuel cells to manage the boil off gas produced in the tanks.

### REFERENCES

- [1] Prevention of Air Pollution from Ships, IMO website, visited on 31/08/201: <http://www.imo.org/en/OurWork/environment/pollutionprevention/airpollution/pages/air-pollution.aspx>
- [2] Brynolf, S., Magnusson, M., Fridell, E., & Andersson, K. (2014). Compliance possibilities for the future ECA regulations through the use of abatement technologies or change of fuels. *Transportation Research Part D: Transport and Environment*, 28(X), 6–18. <https://doi.org/10.1016/j.trd.2013.12.001>.
- [3] IMO. Air pollution and energy efficiency studies. “Studies on the feasibility and use of lng as a fuel for shipping”. (2016). IMO Albert Embankment, London Se1 7Sr, [www.imo.org](http://www.imo.org).
- [4] F. Burel, R. Taccani, N. Zuliani, Improving sustainability of maritime transport through utilization of liquefied natural gas (LNG) for propulsion, *Energy* 57 (2013) 412–420.
- [5] De-Troya, J. J., Álvarez, C., Fernández-Garrido, C., & Carral, L. (2016). Analysing the possibilities of using fuel cells in ships. *International Journal of Hydrogen Energy*, 41(4), 2853–2866. Van Biert, L., Godjevac, M., Visser, K., & Aravind, P. V. (2016). A review of fuel cell systems for maritime applications. *Journal of Power Sources*, 327(X), 345–364. <https://doi.org/10.1016/j.jpowsour.2016.07.007>

Jalkanen, J. P., Johansson, L., Kukkonen, J., Brink, A., Kalli, J., & Stipa, T. (2012). Extension of an assessment model of ship traffic exhaust emissions for particulate matter and carbon monoxide. *Atmospheric Chemistry and Physics*, 12(5), 2641–2659. <https://doi.org/10.5194/acp-12-2641-2012>

(EFC17104)

## TRACE COMPOUNDS IMPACT ON SOFC PERFORMANCE: EXPERIMENTAL AND MODELLING APPROACH

Davide Papurello\*, Massimo Santarelli, Andrea Lanzini  
Department of Energy (DENERG), Politecnico di Torino, Corso  
Duca degli Abruzzi, 24, 10129, Turin, Italy.

**Abstract** - The present work investigates the performance of anode supported solid oxide fuel cells in case of co-feeding of different trace compounds. Electrochemical impedance spectroscopy is the investigation technique used to analyze the impedance spectra. Typical biogas from Organic Fraction Municipal Solid Waste trace contaminants that follow an initial failure in the cleaning system, such as sulphur, aromatic compounds and siloxanes, have been simultaneously tested. Tests showed that the most deleterious impact for the SOFC was due to the H<sub>2</sub>S action. This influences mostly the electrochemical losses respect to diffusion losses, even if this last are not null and can be accounted as a secondary effect. On the contrary, the co-presence of D4 and H<sub>2</sub>S mitigates in the short-term the effect that the only D4 produces when fed with biogas. The most relevant consequence produced by C<sub>7</sub>H<sub>8</sub> was recorded in the low frequency of Nyquist plot, affecting mainly the mass transport phenomena.

**Index Terms** - SOFC, biogas, trace compounds

### I. INTRODUCTION

A SOFC system can be fed with natural gas, biogas from anaerobic digestion process, landfill gas, etc. [1–3]. Moreover, fuel mixtures can contain several trace compounds that can decrease the SOFC performance and act as contaminants for the SOFC anode electrode. These compounds can deactivate nickel active sites at the three-phase boundary, they can promote the carbon deposition and obstruct the anode pores. The nature and pollutant concentrations are strictly related to the adopted process and to the treated substrates [4]. Previous studies have been focused on the consequences of a single trace contaminant, highlighting that sulphur, chlorine, silicon and aromatic compounds can degrade irreversibly cell performances above fixed values [5,6]. This paper wants to fill the gap between modeling results and experimental tests on the SOFC versatile fuel feeding with renewable fuels.

### II. MATERIAL AND METHODS

A Solidpower planar ASC cell was used for the experimental tests. The experimental set-up used was described elsewhere [7]. The concentration of poisons were established taking into account the minimum flow rate that the mass flow controller. H<sub>2</sub>S concentration was fixed to 0.46 ppm(v) for 10 days. The tested siloxane (D4) concentration was 0.15 ppm(v) for 72 h. In the last step of experiment, a third pollutant was introduced, toluene (45.7 ppm(v)) for six days.

### III. RESULTS

Ultra-low concentrations of H<sub>2</sub>S poisoning were analysed. The cell was tested at an operating temperature of 750 °C with 50% pre-reformed biogas at a steam-to-carbon ratio equal to 1. An initial voltage drop followed by a steady state cell voltage was observed. Even if the voltage assumes values from 0.85 V to 0.74 V in the 240 h of test (0.46 V/1000 h), the fastest degradation came about in the first 80 h of operation (1.125 V/1000 h). Second phase of pollutants testing is represented by the contemporary presence of H<sub>2</sub>S and D4 as model compound for siloxanes. After 1 h of exposure of the second pollutant, the polarization loss assumed a value similar to that detected in the last test with the H<sub>2</sub>S only. The situation appeared to be slightly different after 72 h, when the increase in the total loss was about 0.09 Ω·[cm]<sup>2</sup> compared to the H<sub>2</sub>S case. The losses were due to a 65% to activation and to a 34% to transportation. It was determined an increase of 0.06 Ω·[cm]<sup>2</sup> and 0.05 Ω·[cm]<sup>2</sup> in the high and low frequency arches, respectively. The total losses increased to 0.35 Ω·[cm]<sup>2</sup> compared to the clean biogas, but 0.25 Ω·[cm]<sup>2</sup> were recorded when only H<sub>2</sub>S acts. In the last phase of experiment a third pollutant was introduced. The losses increase of 0.15 Ω·[cm]<sup>2</sup> and they mostly affect the low frequency arch of Nyquist plot. This last aspect is verifiable observing that the high frequencies account only for 20% of the total. Considering all the pollutants introduced, the C<sub>7</sub>H<sub>8</sub> had the highest consequences on diffusivity of fresh fuel at the anode. Being the second arch related to the mass transport mechanisms, process linked to the promotion of carbon deposition can be mentioned. This hypothesis is also confirmed by previous studies [5].

Copyright © 2017



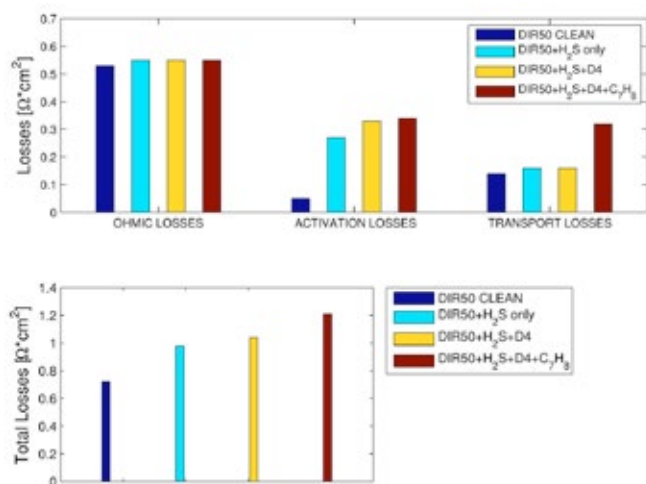


Fig. 1. Summary of losses in the most degrading conditions.

The resulting simulation curve is depicted in Fig. 2 where the comparison with the experimental test is reported. The overlap between the two curves is satisfactory respected for current densities not excessively high. On the contrary, the high current densities determine a major distance between simulation and experimental points.

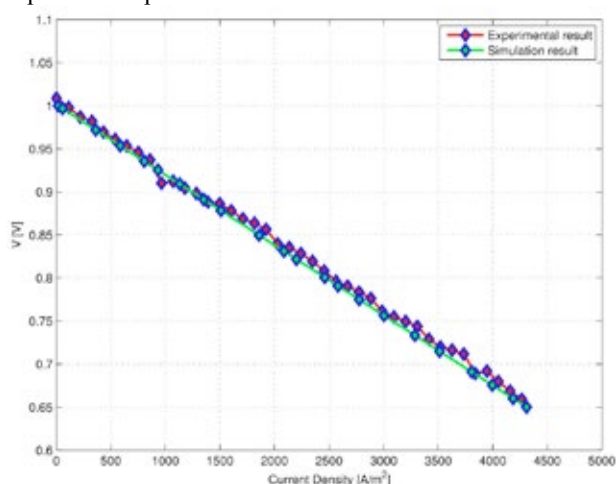


Fig. 2: Polarization curves: experimental and simulated in presence of H<sub>2</sub>S

#### IV. CONCLUSION

From results emerges that the most deleterious impact on short-term for the SOFC was due to the H<sub>2</sub>S action. This influences mostly the electrochemical losses compared to diffusion losses, even if this last are not null and can be accounted as a secondary effect. On the contrary, D4 effects must be divided in short-term and long-term effects. Regarding the short-term, the co-presence of D4 and H<sub>2</sub>S there is an increasing on the total losses compared to the previous condition with only H<sub>2</sub>S. D4 deposits everywhere from the distribution channel to the electrolyte-anode interface. D4 contamination determines a slow degradation in time. This means that a stable condition is not reached during the experimental tests. A forecast of long-term performance shows that D4 has the most deleterious

effects as consequence of a not stable working condition. At the end, toluene takes into account the presence of aromatic compounds the biogas produced from anaerobic digestion. The most relevant consequence produced by this compound was recorded in the low frequency of Nyquist plot, affecting mainly the mass transport phenomena. In fact, molecules' cracking occurs because reforming reactions of tars are obstructed in presence of a biogas mixture and this induces to carbon deposition related problems.

#### REFERENCES

- [1] D. Papurello, A. Lanzini, L. Tognana, S. Silvestri, M. Santarelli, Waste to energy: Exploitation of biogas from organic waste in a 500 W solid oxide fuel cell (SOFC) stack, *Energy*. 85 (2015) 145–158. doi:10.1016/j.energy.2015.03.093.
- [2] D. Papurello, E. Schuhfried, A. Lanzini, A. Romano, L. Cappellin, T.D. Märk, S. Silvestri, M. Santarelli, F. Biasioli, Proton transfer reaction-mass spectrometry as a rapid inline tool for filter efficiency of activated charcoal in support of the development of Solid Oxide Fuel Cells fueled with biogas, *Fuel Process. Technol.* 130 (2015) 78–86. doi:10.1016/j.fuproc.2014.09.042.
- [3] D. Papurello, S. Silvestri, L. Tomasi, I. Belcari, F. Biasioli, M. Santarelli, Biowaste for SOFCs, *Energy Procedia*. 101 (2016) 424–431. doi:10.1016/j.egypro.2016.11.054.
- [4] D. Papurello, C. Soukoulis, E. Schuhfried, L. Cappellin, F. Gasperi, S. Silvestri, M. Santarelli, F. Biasioli, Monitoring of volatile compound emissions during dry anaerobic digestion of the Organic Fraction of Municipal Solid Waste by Proton Transfer Reaction Time-of-Flight Mass Spectrometry, *Bioresour. Technol.* 126 (2012) 254–265. doi:10.1016/j.biortech.2012.09.033.
- [5] D. Papurello, A. Lanzini, D. Drago, P. Leone, M. Santarelli, Limiting factors for planar solid oxide fuel cells under different trace compound concentrations, *Energy*. 95 (2016) 67–78. doi:10.1016/j.energy.2015.11.070.
- [6] D. Papurello, R. Borchellini, P. Bareschino, V. Chiodo, S. Freni, A. Lanzini, F. Pepe, G.A. Ortigoza, M. Santarelli, Performance of a Solid Oxide Fuel Cell short-stack with biogas feeding, *Appl. Energy*. 125 (2014) 254–263.
- [7] D. Papurello, A. Lanzini, P. Leone, M. Santarelli, The effect of heavy tars (toluene and naphthalene) on the electrochemical performance of an anode-supported SOFC running on bio-syngas, *Renew. Energy*. 99 (2016) 747–753. doi:10.1016/j.renene.2016.07.029.



**PRELIMINARY DESIGN OF A MW-CLASS DEMO SYSTEM FOR CO<sub>2</sub> CAPTURE WITH  
MCFC IN A UNIVERSITY CAMPUS COGENERATION PLANT**

L. Mastropasqua\*, M. Spinelli\*, S. Campanari\*

\*Department of Energy, Politecnico di Milano, Via Lambruschini 4,  
20156 Milan (Italy)

**Abstract** - In the present work, the preliminary design of a 1 MW<sub>el</sub> MCFC demo plant downstream a Combined Heat and Power (CHP) Internal Combustion Engine (ICE) installed at the Politecnico di Milano campus is investigated. The study envisages two purification strategies for the CO<sub>2</sub>-rich stream at the MCFC anode outlet: i) CO<sub>2</sub> separation and compression in a cryogenic unit; ii) the anode exhausts are burned in a catalytic oxy-combustor. An economic analysis is performed to assess the feasibility of such an installation within the campus cogeneration grid. The use of MCFCs to capture CO<sub>2</sub> at a distributed generation scale allows reaching interesting energy and environmental performances, highlighted by promising values of the Specific Primary Energy Consumption for CO<sub>2</sub> Avoided (SPECCA=0.9-1.9 MJ/kgCO<sub>2</sub>) and Carbon Capture Ratios (CCR=68-84%). The economic analyses reveal acceptable values for the cost of electricity and the cost of CO<sub>2</sub> avoided, respectively close to 130 €/MWh<sub>el</sub> and 100 €/tCO<sub>2</sub>.

**Index Terms** – MCFC, Carbon Capture and Storage, Combined Heat and Power, Distributed generation

I. INTRODUCTION

Electrochemical devices come of aid to the down-sizing of Carbon Capture and Storage (CCS) applications to distributed generation systems [1]. In particular, exploiting the inherent operating nature of high temperature fuel cells and their intrinsic modularity allows producing enriched streams of CO<sub>2</sub> which are then easily purified for long-term storage.

The application to distributed Combined Heat and Power (CHP) systems is particularly interesting. In this work, the thermodynamic and economic performance of a Molten Carbonate Fuel Cell (MCFC)-based system is assessed as a post-combustion CCS system used to retrofit the existing Jenbacher J612 2 MW natural gas-fed Internal Combustion Engine (ICE) installed at the Politecnico di Milano “Leonardo da Vinci” campus. This work aims at:

- Propose a retrofit configuration to implement post-combustion CCS to the CHP Internal Combustion Engine (ICE) unit, exploiting the information available from a commercial-scale MCFC unit

- Introduce the preliminary thermodynamic analysis and compare it with a commercial scale system without CCS
- Assess the feasibility of the new installation in terms of economic attractiveness

II. PLANT MODELLING

The thermodynamic system analyses presented in this work are carried out using an in-house developed software call “GS”. The plant layout is built by assembling in a coherent network the different components selected in a library containing over 20 basic modules. Each component is modelled using a 0D approach. As far as the MCFC model is concerned, it performs mass and energy balances on the component using the inlet thermochemical variables supplied by the system analysis. The electrochemical model computes the most important losses contributions and it is compared against the experimental data reported in *Spinelli et al., 2015* [2], in which a CCS operation is explored using a commercial stack supplied with natural gas.

Two configurations are explored concerning the CO<sub>2</sub> purification section: i) the CO<sub>2</sub>-rich stream from the MCFC anode outlet is purified and compressed in a cryogenic unit; ii) the anode outlet is burned in a catalytic oxy-combustor supplied with an external source of oxygen. For both configurations, an AspenPlus model is employed to simulate both the CO<sub>2</sub> cryogenic purification section and the compression system.

As a reference MCFC plant without CCS is considered the commercial module rated at 1400 kW<sub>el</sub> (AC) proposed by FuelCell Energy. The operating conditions are selected according to the manufacturer’s suggestions in terms of fuel conversion, maximum CO<sub>2</sub> utilisation factor (i.e., 90%) and minimum operating voltage (i.e., 0.60-0.7 V).

In CCS mode, the MCFC cathode would be supplied with the exhaust gases from the ICE subsequently to an appropriate cooling and dehydration step. Also, note that all the water needs required to ensure an adequate S/C ratio at the anode inlet are obtained from the condensation of the steam content in the ICE exhaust gases; this ensures a favourable water balance of the system. The two proposed systems are depicted in Figure

1, respectively the MCFC post-combustion system with cryogenic CO<sub>2</sub> purification in Figure 1a and the oxy-fuel system and CO<sub>2</sub> compression in Figure 1b.

Note that the first system (case A) is characterised by a burner on the cathode line, exploiting the off-gas stream, rich in H<sub>2</sub> and CO, to further concentrate the CO<sub>2</sub> content at the cathode inlet. Subsequently to the electrochemical separation, the CO<sub>2</sub> molar fraction in the exhaust stream at the stack is approximately ≈1.55%. The anode outlet is cooled down and dehydrated prior being sent to the cryogenic section.

The second system (case B), on the other hand, exploit an oxy-combustor on the anode line to concentrate the CO<sub>2</sub> content even further. This allows employing a simpler CO<sub>2</sub> compression train to reach the required conditions for liquefaction and storage. Note that, due to the limited size of the considered application, the oxygen supplied to the burner is envisaged to be delivered to the plant by an external supplier and stored locally.

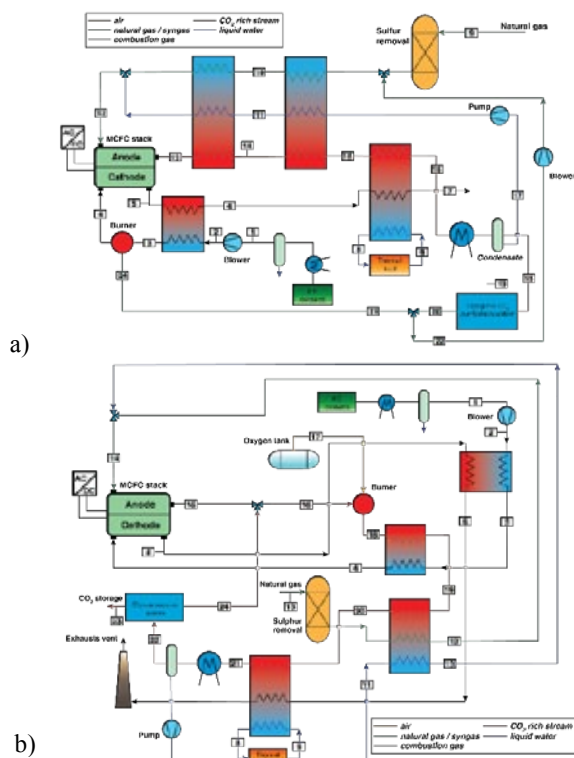


Figure 1 – MCFC post-combustion system: Case a) with cryogenic CO<sub>2</sub> purification section; Case b) with oxy-fuel combustion and CO<sub>2</sub> compression section

### III. RESULTS AND DISCUSSION

Table I presents the operating conditions and overall performance of the overall plant including the ICE, whilst Table II summarises the results of the preliminary economic analysis which compares the two systems with CCS. The main outcomes confirm that the MCFC modules constitute the biggest cost of the total investment (i.e., 62-63%), based on an

assumed ‘mid-term perspective’ specific cost of 1620 €/kW. It is also interesting to note that the obtained CCA is close to the target value of 100 €/ton<sub>CO<sub>2</sub></sub> typical of conventional CCS technologies (i.e., solvents-based CCS [3]).

TABLE I  
SUMMARY OF THE MAIN THERMODYNAMIC AND GREENHOUSE GAS EMISSION PERFORMANCE OF THE NEW PROPOSED MCFC-BASED CCS SYSTEMS

Parameter	Units	Case A	Case B
$\dot{Q}_{NG}$ (LHV)	kW	5329.0	5638.0
$\dot{W}_{el}$ (ICE+MCFC), net	kW	2282.0	2358.0
$\dot{Q}_{CHP}$	kW	2090.0	2283.0
$\eta_{el}$	%	42.82	41.83
CCR	%	73.76	80.11
SPECCA	MJ kg <sub>CO<sub>2</sub></sub> <sup>-1</sup>	0.909	1.395

TABLE II  
ECONOMIC ANALYSIS OF THE PROPOSED MCFC-BASED CCS SYSTEMS

Parameter	Units	Case A	Case B
MCFC	k€	1002.0	1002.0
BoP	k€	375.0	450.0
CO <sub>2</sub> compression	k€	216.0	159.0
Total investment	k€	1593.0	1611.0
O&M	€ MWh <sub>el</sub> <sup>-1</sup>	15.0	16.0
Fuel	€ MWh <sub>el</sub> <sup>-1</sup>	62.0	64.0
COE	€ MWh <sub>el</sub> <sup>-1</sup>	130.0	132.0
CCA	€ ton <sub>CO<sub>2</sub></sub> <sup>-1</sup>	107.0	104.0
CCC	€ ton <sub>CO<sub>2</sub></sub> <sup>-1</sup>	105.0	102.0

### IV. CONCLUSION

This study proposes a techno-economic feasibility study for the installation of a MCFC-based demonstration plant, which could retrofit the exhaust line of a 2 MW CHP ICE currently installed at Politecnico di Milano. Two CCS configurations are proposed, which differ on the CO<sub>2</sub> purification technology.

It is concluded that the system keeps a high electrical efficiency (41.8-42.8% for the two cases in CCS mode vs. the original 44.4% of the stand-alone ICE) while adding 280-350kW net power. Moreover, the CCS system allows achieving a CCR between 73% and 80% with respect to the system without CCS. Finally, the cost of the post-combustion system is dominated by the cost of the stack, which accounts for approximately 63% of the total investment cost.

### REFERENCES

- [1] L. Mastropasqua, S. Campanari, J. Brouwer, Electrochemical carbon separation in a SOFC-MCFC poly-generation plant with near-zero emissions, J. Eng. Gas Turbines Power. (2017). doi:10.1115/1.4037639.
- [2] M. Spinelli, S. Campanari, M.C. Romano, S. Consonni, T.G. Kreutz, H. Ghezel-ayagh, et al., Molten Carbonate Fuel Cells as Means for Post-Combustion CO<sub>2</sub> Capture: Retrofitting Coal-Fired Steam Plants and Natural Gas-Fired Combined Cycles, (2015) 1–13.
- [3] United States Department of Energy, Cost and

## DEVELOPMENT OF REDOX STABLE, MULTIFUNCTIONAL SUBSTRATES FOR ANODE SUPPORTED SOFCS

B. R. Sudireddy, S. P. Foghmoes, T. Ramos, and P. Holtappels  
Department of Energy Conversion and Storage, Technical University  
of Denmark, Frederiksborgvej 399, DK-4000 Roskilde (Denmark)

**Abstract** - Redox stable solid oxide fuel cells are beneficial in many aspects such as tolerance against system failures e.g fuel cut off and emergency shut down, but also allow for higher fuel utilization, which increases efficiency. State-of-the-art Ni-cermet based anodes suffer from microstructural changes upon redox cycling, while other properties such as catalytic activity for methane reforming and/or water gas shift, thermal conductivity in addition to electronic conductivity for current pickup are highly wanted for SOFC applications.

In order to combine the advantages of a redox stable anode with a multifunctional anode support, the development of a two layer fuel electrode based on a redox stable strontium titanate layer for the electrochemically active layer and a redox stable Ni-YSZ support was pursued. Half-cells with well adhering strontium titanate anode layers on state-of-the-art Ni-YSZ cermet supports have been achieved. Redox tolerance of the half-cell depends could be increased by optimizing the redox stability of the cermet support.

**Index Terms** – SOFC, anode supports, redox stability, ceramic anode.

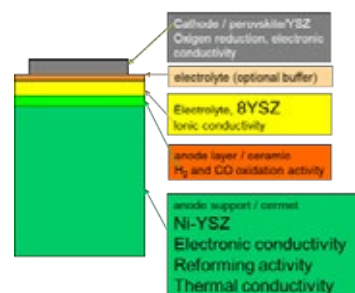
### I. INTRODUCTION

Redox stable solid oxide fuel cells are beneficial in many aspects such as tolerance against system failures e.g fuel cut off and emergency shut down, but also allow for higher fuel utilization increasing efficiency. Related to redox tolerance, is also overload tolerance.

State-of-the-art Ni-YSZ cermet electrodes can be tailored in microstructure so they possess a certain redox stability, however, usually through a coarse grained microstructure on the expense of electrochemical activity.

A redox stable anode can be prepared by mixed or electronically conducting ceramics, and promising results have been published for strontium titanate based

electrodes infiltrated with electrocatalytically active metal particles [1,2]. However, these ceramic materials suffer from low mechanical strength, low electrical and thermal conductivity and insufficient catalytic activity for internal reforming or water-gas shift reaction. All these properties are known to be important for efficient operation of SOFC cells, and are usually provided by a Ni-cermet based anode support ( see Fig. 1).



**Fig. 1.** Concept of a redox stable anode supported SOFC

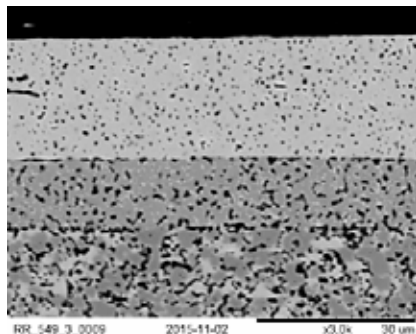
In order to combine the advantages of a redox stable anode with a multifunctional anode support, the development of a two layer fuel electrode based on a redox stable ceramic anode layer for the electrochemically active layer and a redox stable Ni-YSZ support was pursued.

### II. RESULTS

The concept of the redox stable, multifunctional anode anode support is shown in Fig. 1, indicating the different layers and functionalities. Cells with strontium titanate based anode layers ( $\text{Sr}_{0.94}\text{Ti}_{0.9}\text{Nb}_{0.1}\text{O}_{3-\delta}$ ) (STN) and Ni-

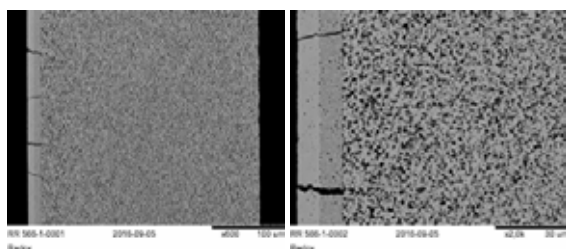
YSZ ( $\text{Zr}_{0.84}\text{Y}_{0.16}\text{O}_{1.92}$  (8YSZ)) anode supports have been prepared by tape casting the individual layers and subsequent lamination and sintering

Fig. 2 shows an STN anode (middle layer) integrated onto a NiO-8YSZ support (bottom) with a Sc-modified zirconia electrolyte layer (top layer). Well adhering layers can be achieved for various types of Ni-YSZ supports and both yttria and scandia modified zirconia as electrolyte layer. The cells could be successfully reduced in 9%  $\text{H}_2$  at 850 C without any visible damage to the microstructure.



**Fig. 2.** Microstructure of a STN anode layer integrated between a Sc-stabilized zirconia electrolyte (top) and a NiO-YSZ cermet (bottom) layer

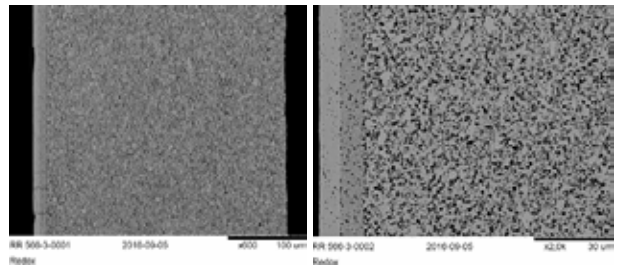
The cells were further tested as regards their redox tolerance by two redox cycles between 9%  $\text{H}_2$  in Ar humidified with 3% water and air at 850C. Fig 3 shows the microstructure of cells with a “standard” Ni-YSZ anode support with an STN anode and 8YSZ electrolyte layer. While the anode support has survived the redox cycles, cracks have been developed through the electrolyte and anode layer, most probably resulting from dimensional changes in the anode support during re-oxidation.



**Fig. 3.** Microstructure of a “standard” Ni-YSZ anode supported cell with STN anode after redox cycling

The redox tolerance of anode supports can to a large extent be tailored by the Ni/YSZ particle size distribution and the Ni-volume fraction in the Ni-cermet [3,4].

Fig 4 shows the microstructure of an STN layer integrated onto a redox optimized Ni-YSZ support after redox cycling. Significantly reduced number cracks through the anode and electrolyte layer are observed, indicating an increased redox stability of the anode supported half-cell.



**Fig. 4.** Microstructure of a redox optimized Ni-YSZ anode supported cell with STN anode after redox cycling

### III. CONCLUSION

Ni-YSZ cermet based anodes and supports are state-of-the-art and have been developed up to industrial fabrication. Redox stable ceramic anode layers can be integrated into standard Ni-cermet anode supports, which allows for the development of a full redox stable anode supported cell, without the need for completely new substrate developments. This has been proven on a rather fine-grained Ni-YSZ support, and even better redox stability is expected by using more coarse, low Ni-containing anode supports.

### ACKNOWLEDGMENT

Parts of the research leading to these results has received funding from the Fuel Cells and Hydrogen Joint Undertaking under grant agreement n° 256730 and from the Danish ForskEL project “SOFC4Ret”.

### REFERENCES

- [1] P. Holtappels, J. T. S. Irvine, B. Iwanschitz, L. T. Kuhn, L. Y. Lu, Q. Ma, J. Malzbender, A. Mai, T. Ramos, J. Rass-Hansen, B. R. Sudireddy, F. Tietz, V. Vasechko, S. Veltze, M. C. Verbräeken, Full Ceramic Fuel Cells Based On Strontium Titanate Anodes, An Approach Towards More Robust SOFCs, ECS Transact. 57(1) (2013) 1175-1184
- [2] M. C. Verbräeken, B. Iwanschitz, E. Stefan, M. Cassidy, U. Weissen, A. Mai, J. T. S. Irvine, Short Stack and Full System Test Using a Ceramic A-Site Deficient Strontium Titanate Anode, Fuel Cells, 15(5) (2015), 682–688
- [3] Final Report EU Integrated project Real-SOFC
- [4] T. Ramos et al. Unpublished results DTU Energy (former Risø National Laboratory), DK.



## Dynamic modeling of a reversible solid oxide cell

Sanggyu Kang\*\*\* and Kook-Young Ahn\*\*\*

\*Korea Institute of Machinery and Materials, 156 Gajeongbukro Yuseonggu Daejeon, (Republic of Korea)

\*\*University of Science and Technology, 217 Gajeongro Yuseonggu Daejeon, (Republic of Korea)

**Abstract** - The objective of the study is to develop the quasi three dimensional dynamic modeling of a R-SOC and find out the optimal operating conditions for minimizing the heat supply for the steam electrolysis. In order to resolve the mass conservation in the R-SOC, the cell is discretized into five control volumes in the flow perpendicular direction. The cell is also discretized into seven control volumes in the flow perpendicular direction to resolve the energy conservation. In order to capture the characteristics distribution of the R-SOC, the cell is also discretized into one hundred control volumes in the flow parallel direction. The model has been validated by comparison with the published data of the current-voltage polarization curve. The model has been simulated at the steady-state by varying the steam/hydrogen composition, temperature, pressure, and current density. The model is helpful to find out the optimal operating schemes for the R-SOC stack.

**Index Terms** – High temperature steam electrolysis, Reversible solid oxide cell (R-SOC), Dynamic modeling, Optimal operating schemes

### I. Introduction

High temperature steam electrolysis has been regarded as a strong candidate for the energy storage system due to its high efficiency and capability for extension to a large scale system. The reversible solid oxide cell (R-SOC) requires higher amount of thermal energy compared to the low temperature steam electrolysis and high temperature steam. The temperature gradient between stack inlet and outlet should be maintained within some ranges for the stack stability and durability. There have been many researches on the solid oxide electrolysis cell (SOEC). Wendel et al. conducted a numerical analysis on a SOEC system [1]. They find the optimal operating voltage with the numerical study. Giorgio et al. developed a lumped R-SOC stack model and studied on a usage of a thermal energy storage for the SOEC model [2]. The objective of the work is to develop the quasi three-dimensional dynamic modeling of a R-SOC. The unit cell is discretized into five and seven control volumes to resolve the mass balance and energy conservation, respectively. To resolve the characteristics distribution of the R-SOC, which is also discretized into nine

control volumes along the flow parallel direction. The unit cell is validated by comparing the simulation data with the experimental data from both of the SOFC and SOEC mode. The model has been simulated at the steady-state by varying the temperature and pressure, and current density. The model is helpful to find out the optimal operating schemes for the R-SOC stack.

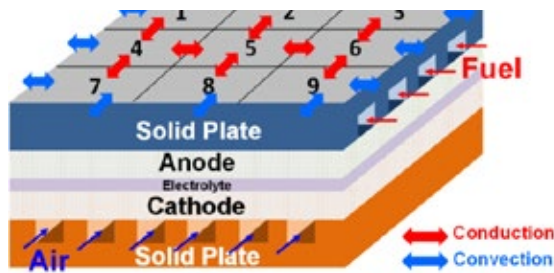
### II. Modeling Description

A quasi three-dimensional dynamic model of R-SOC stack has been developed to capture the R-SOC performance. Table 1 presents the specifications for the R-SOC stack. The R-SOC is discretized into five control volumes and seven control volumes along the cross-sectional direction to resolve the mass and energy conservation, respectively. Diffusion fluxes of the oxygen ion to the anode electrode control volume is determined for the boundary between the electrolyte and the electrode control volume. The heat generated at TPB is transferred to the electrode, the gas channel, and the solid plate by conduction or convection. The R-SOC model is discretized into nine control volumes in the stream-wise direction to resolve the heat transfer between each local section, shown in Figure 1. The natural convection at the outside of solid plate and the conduction between each local solid plate and are considered.

Table 1. R-SOC specifications

Parameter	Unit	SOFC	SOEC
Current Density	mA/cm <sup>2</sup>	275	310
Voltage	V	0.64	1.22
Active Area	mmXmm	210X48	
Cell number	-	1,500	
Fuel utility	-	0.71	-
Steam-H <sub>2</sub> conversion ratio	-	-	0.5



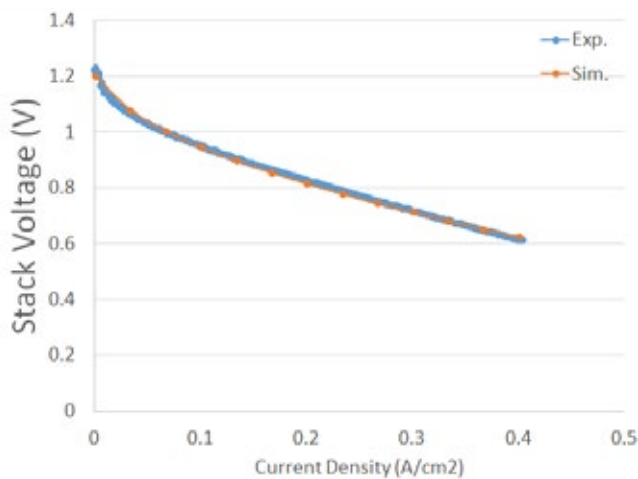


**Fig. 1. Schematic diagram of the SOEC discretization**

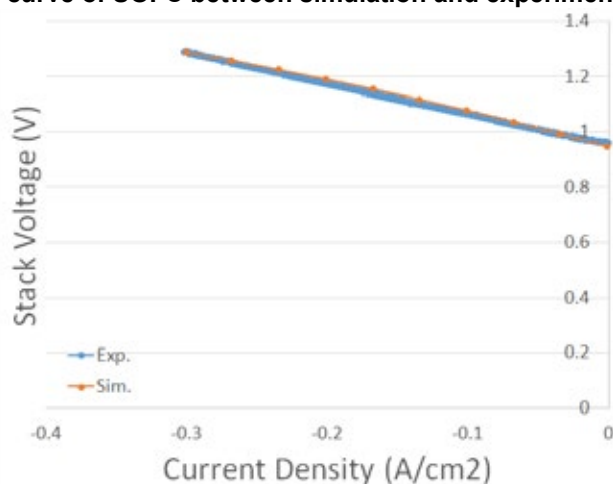
### III. Results and Discussions

#### A. R-SOC Model Verification

In order to validate the reversible SOFC/SOEC model, the current-voltage polarization curves from the model in both of the SOFC and SOEC mode has been compared the experimental data. The simulation results are in good agreement with the experimental data within slight error.



**Fig. 2. Comparison of current-voltage polarization curve of SOFC between simulation and experiment**



**Fig. 2. Comparison of current-voltage polarization curve of SOEC between simulation and experiment**

The present mode is simulated to obtain the SOFC and SOEC performance by varying the operating parameters of temperature and pressure. The SOFC net voltage of the SOFC and SOEC required voltage are obtained by subtracting the overvoltages from the Nernst voltage and by adding the overvoltages to the Nernst voltage, respectively. Thus, the SOFC net voltage is appeared at higher operating pressure. In SOEC mode, the required voltage at higher operating pressure is higher at low current density and becomes to be lower at higher current density. That is, increased pressure could cause the required energy for the SOEC at high operating current density. The Nernst voltage and activation overvoltage are increased and decreased with the temperature increase. Thus the SOFC net voltage and SOEC required voltage are increased and decreased with the temperature increase.

### IV. Conclusions

In this study, quasi three-dimensional dynamic model of R-SOC has been developed in Matlab-Simulink®. The present model is validated by comparison with the experimental data. The model has been simulated at the steady-state by varying the temperature and pressure, and current density. The model is helpful to find out the optimal operating schemes for the R-SOC stack.

### References

- [1] Giorgio PD, Desideri U. Potential of reversible solid oxide cells as electricity storage system. *Energies* 2016;9(662):1-14.
- [2] Wendel CH, Braun RJ. Design and techno-economic analysis of high efficiency reversible solid oxide cell systems for distributed energy storage. *Applied Energy* 2016;172:118-131.
- [3] O'Hayre R, Cha SW, Colella W, Prinz FB. *Fuel cell fundamentals*. 2nd ed. John Wiley & Sons; 2009.

### Acknowledgement

This work was supported by the Korea Institute of Energy Technology Evaluation and Planning(KETEP) and the Ministry of Trade, Industry & Energy(MOTIE) of the Republic of Korea (No. 20163010140530).

# Operation strategies for cold start of PEMFC systems

G. Montaner Ríos\*, J. Schirmer\*\*, and J. Kallo\*\*

\* Deutsches Zentrum für Luft- und Raumfahrt (DLR) Institut für Technische Thermodynamik, Hein-Saß-Weg 22, 21129, Hamburg, (Germany)

\*\* Deutsches Zentrum für Luft- und Raumfahrt (DLR) Institut für Technische Thermodynamik, Pfaffenwaldring 38-40, 70569, Stuttgart, (Germany)

**Abstract** - This work presents an extensive review on cold start of PEMFC systems, studying the different cold strategies as well as the relevant operating parameters that influence the cold start. Based on the prior study, an operation strategy for the shutdown and cold startup of a PEMFC system is tested with a 4 kW commercial PEMFC developed for a commercial aircraft application. The aim of the experimental work is to test the ability to self-start from -20°C, to study the effect of startup temperature and to determinate the startup time. The obtained experimental results are to be presented at the conference.

**Index Terms** – PEMFC, cold start, strategy, freezing point.

## I. INTRODUCTION

The startup ability of a proton exchange membrane fuel cell (PEMFC) system from subzero temperatures (also named cold start) is essential, especially for mobile applications. Extensive research has been carried out about this topic and several operation strategies have been developed for the cold start of a fuel cell automobile. However, this study is proved in a PEMFC system for aircraft applications.

## II. EXTENDED ABSTRACT

### A. Cold Start Analysis and Strategies

The key to a successful cold start is the balance between the heat generated and the ice formation, so that the cell temperature rises above freezing point before all pores are plugged with ice.

Several design parameters and operating conditions have an influence on this balance. Strategies to improve a cold start can be classified into those which assist water removal (e.g. purge gas) and decrease ice formation and into those which are based on a heating solution to increase temperature quickly. Purging during shutdown can be carried out through dried or humidified purge gas, purge with compressor air, and vacuum dried purge. To avoid freezing can be utilized a microporous layer, antifreeze, or thermal insulation of the stack. Additionally warmup strategies during startup can be categorized into external or internal. Among the first group the most common method is using a heater to warm the coolant. Moreover a catalytic burner can be used as well to produce heated gas. However, it is preferable to use the heat generated within the stack; for example by potentiostatic startup, reactants starvation, decreasing the thermal mass (coolant loop), etc. [1].

Numerous studies have shown that a quick cold start should be conducted in potentiostatic mode under conditions near short circuit and with very low water content in the membrane. Since a potentiostatic start increases the current density that leads to more heat generated [2-4]. Water removal using a dry purge gas upon shut down improves cold start properties by easing the water transport to the membrane during startup. It has been proved that the cold start length increases with the purge duration until its optimal purge time [5, 6].

Copyright © 2017

## B. Experimental

The experimental study was conducted with a PEMFC system for aircraft applications. The cold start experiments were carried out with a 4 kW stack and the cathode was feed with pure oxygen instead of air. A small coolant loop with lower thermal mass was developed to improve cold start. The procedure followed to carry out each test consisted of four main steps: conditioning, purging upon shutdown, freezing to start test temperature, and cold start. The cold startup was run by a potentiostatic mode and the purge method used was: dry gases ( $N_2$  in the cathode and  $H_2$  in the anode), at  $40^\circ\text{C}$  and during 3 minutes.

## C. Results and Discussion

The startup temperature strongly affects cold start, the startup time increases if the temperature is lower [7, 8]. The experimental results of cold start at  $-5^\circ\text{C}$ ,  $-10^\circ\text{C}$  and  $-20^\circ\text{C}$  by a constant value of 0,55 V are shown in Fig. 1.

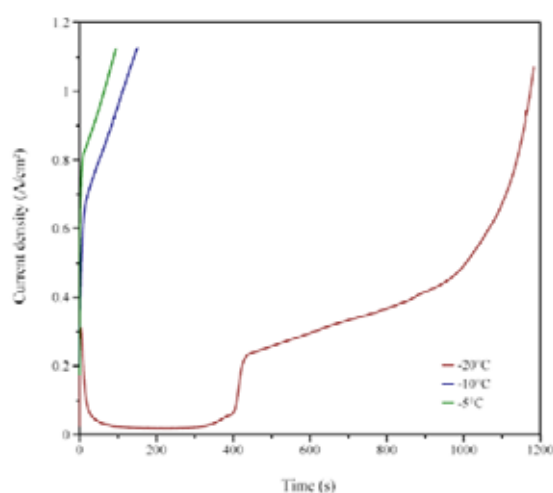


Fig. 1. Current density for the cold start operation at  $-5^\circ\text{C}$ ,  $-10^\circ\text{C}$ ,  $-20^\circ\text{C}$

Test results proved that the stack is able to self-start at low temperature ( $-20^\circ\text{C}$ ); however it takes 15 min to reach more than 50% of its nominal power. Figure 1 shows the cold start performance at  $-20^\circ\text{C}$ , which can be classified into some phases. First, water produced by ORR in the catalyst layer is transported into the membrane till a peak power. In the second phase, ice formation reduces the electrochemical effective surface area and thus the stack performance decreases. Thirdly, the performance remains near zero till the melting point is reached. Next, the performance increases all at once as catalyst layer and gas diffusion are free again and the stack can operate normally. Finally, after the sudden rise, performance increases exponentially due to cells are flooded with the thawed water. However a cold start just needs 3 s to reach 50% of  $P_{\max}$  at  $-10^\circ\text{C}$  and 1 s at  $-5^\circ\text{C}$ .

## III. CONCLUSION

Several strategies to improve the PEMFC cold start were presented. Additionally an experimental study with a PEMFC system for aircraft applications was performed with the proposed procedure in order to prove its ability to self-start at  $-20^\circ\text{C}$ . Moreover the effect of the startup temperature on the cold start performance was shown and discussed. The remaining results of this study will be presented during the conferences, as well as the necessary next steps in this research to achieve an immediate startup at  $-20^\circ\text{C}$  too.

## ACKNOWLEDGMENT

This work is part of the research project n° 03BV241D supported by the Federal Ministry of Transport and Digital Infrastructure of Germany. The authors would also like to thank their colleagues F. Becker, S. Corners, I. Sokolov and C. Werner for their support during this project.

## REFERENCES

- [1] A. Amamou, S. Kelouwani, L. Boulon, K. Agbossou, Comprehensive Review of Solutions and Strategies for Cold Start of Automotive Proton Exchange Membrane Fuel Cells, IEEE Access, Volume 4, 2016, Pages 4989-5002.
- [2] K. Jiao, I. E. Alaefour, G. Karimi, X. Li, Cold start characteristics of proton exchange membrane fuel cells, International Journal of Hydrogen Energy, Volume 36, Issue 18, 2011, Pages 11832-11845.
- [3] F. Jiang, C.-Y. Wang, Potentiostatic Start-Up of PEMFCs from Subzero Temperatures, Journal of the Electrochemical Society, Volume 155 (7), 2008, Pages B743-B751.
- [4] R. K. Ahluwalia, X. Wang, R. Kumar, Fuel Cell Systems Analysis, DOE Hydrogen Program Review, Annual Merit Review Proceedings, 2006.
- [5] Y. Wang, P. P. Mukherjee, J. Mishler, R. Mukundan, R. L. Borup, Cold start of polymer electrolyte fuel cells: Three-stage startup characterization, Electrochimica Acta, Volume 55, 2010, Pages 2636-2644.
- [6] S. Ge, C.-Y. Wang, Characteristics of subzero startup and water/ice formation on the catalyst layer in a polymer electrolyte fuel cell, Electrochimica Acta, Volume 52, 2007, Pages 4825-4835.
- [7] R. Ichikawa, Y. Tabe, T. Chikahisa, Ice Formation and Current Distribution in the Catalyst Layer of PEM Fuel Cell at Cold Start, ECS Transactions, 41 (1), 2011, Pages 733-740.
- [8] Y. Tabe, M. Saito, K. Fukui, T. Chikahisa, Cold start characteristics and freeing mechanism dependence on start-up temperature in a polymer electrolyte membrane fuel cell, Journal of Power Sources, Volume 208, 2012, Pages 366-373.

## Dynamic modeling of a solid oxide electrolyser cell system for distributed energy storage

Sanggyu Kang\*\*\*, Youngsang Kim\*, Sangho Lee\*, Youngduk Lee\*\*\*, and Kook-Young Ahn\*\*\*

\*Korea Institute of Machinery and Materials, 156 Gajeongbukro Yuseonggu Daejeon, (Republic of Korea)

\*\*University of Science and Technology, 217 Gajeongro Yuseonggu Daejeon, (Republic of Korea)

**Abstract - Abstract - The objective of the study is to develop the dynamic modeling of a high temperature steam electrolysis system by Matlab-Simulink® and performed the system analysis to achieve the system optimization. The whole system is composed of a reversible solid oxide cell (R-SOC), fuel/steam supply system, air supply system, hydrogen storage system, and etc. The fuel/steam supply system is composed of the fuel valve, pump and evaporator. Air supply system consists of a heat exchanger and air blower. The surplus electricity and the steam of 750 °C are supplied to the R-SOC system to generate the hydrogen. In order to improve the system efficiency, certain portion of the off-gas from the hydrogen electrode from the R-SOC stack is recirculated by regenerative blower or ejector. The system analysis has been conducted to determine the system performance. In order to achieve the system optimization, the system net efficiency with various operating conditions have been compared.**

**Index Terms – Renewable energy, Solid oxide electrolysis cell, Reversible solid oxide cell (R-SOC), System dynamic modeling, System analysis**

### I. Introduction

Renewable energy has been regarded as a final destination for the power generation for human society. Power generation from the renewable energy stand-alone system could not fully satisfy the load power variation. Thus, renewable power system should be developed by combining with the energy storage system (ESS) to make up for the discrepancy between load power and power generation. Among several types of the ESS, the hydrogen electrolysis is most suitable for long period storage and large scale energy storage. There have been many researches on the solid oxide electrolysis cell (SOEC) system. The objective of the work is to develop the dynamic modeling of a high temperature steam electrolysis system. The renewable energy hybrid system consists of the reversible solid oxide cell (SOC) stack, steam boiler using the solid refused fuel (SRF), and metal hydride for storing the hydrogen. In order to achieve the system optimization, the system model is composed of the quasi three-dimensional dynamic model of R-SOC, two-dimensional dynamic model of heat exchanger, lumped dynamic model of blower and pump. In order to optimize the proposed system, the mass and energy balance have been resolved with the system model and investigated the system performance by

varying the operating parameters of temperature and pressure. The present study can provide the basic insight for optimal design of the advanced renewable energy hybrid system.

### I. Modeling Description

#### A. SOEC system

R-SOC system is composed of the R-SOC stack, heat exchangers, pump, and blower. In case of electrolysis cell mode, high temperature steam generated from the SRF boiler, which is higher than 700 °C, is flowing into the R-SOC stack to produce the hydrogen. In the fuel cell mode, the stored hydrogen is entering the R-SOC stack to generate the electricity. The schematics of the solid oxide fuel cell (SOFC) system and solid oxide electrolysis cell (SOEC) system have been presented in Fig. 1 and Fig. 2, respectively. Table 1 and Table 2 show the respective target value for the SOFC system and SOEC system.

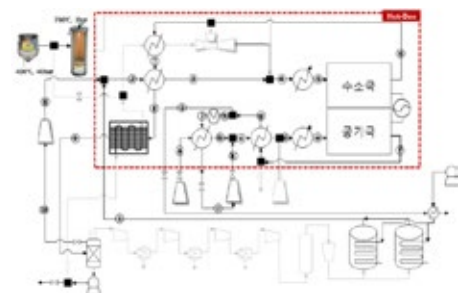


Fig. 1. The schematics of the SOFC system

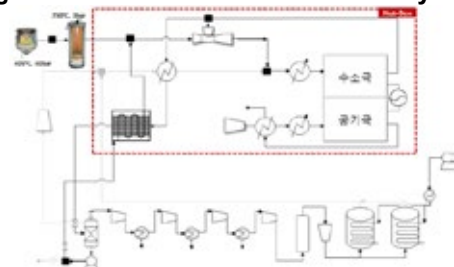


Fig. 2. The schematics of the SOEC system

#### B. R-SOC stack



has been developed to capture the R-SOC performance. Table 1 presents the specifications for the R-SOC stack. The R-SOC is discretized into five control volumes and seven control volumes along the cross-sectional direction to resolve the mass and energy conservation, respectively. Diffusion fluxes of the oxygen ion to the anode electrode control volume is determined for the boundary between the electrolyte and the electrode control volume. The heat generated at TPB is transferred to the electrode, the gas channel, and the solid plate by conduction or convection. The R-SOC model is discretized into nine control volumes in the stream-wise direction to resolve the heat transfer between each local section, shown in Figure 1. The natural convection at the outside of solid plate and the conduction between each local solid plate and are considered.

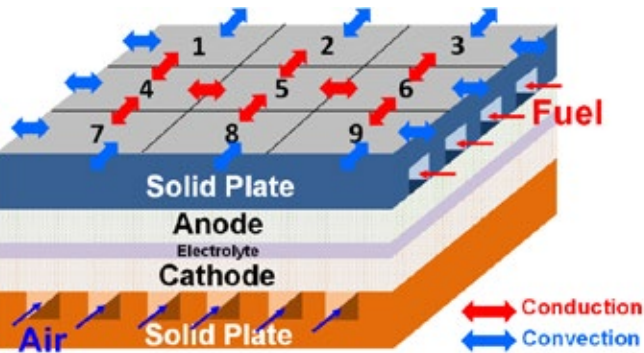
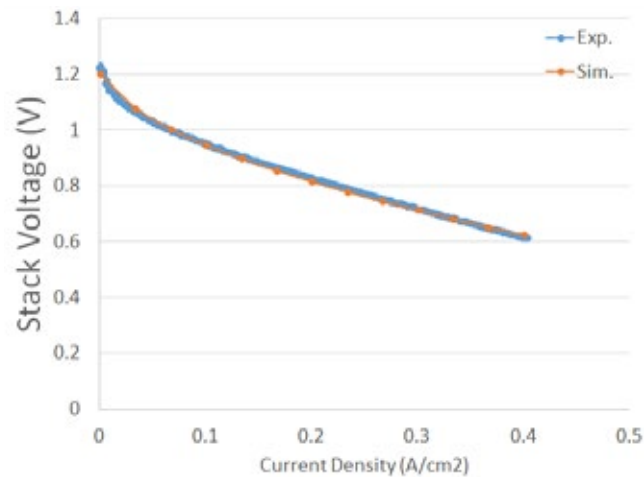


Fig. 1. Schematic diagram of the SOEC discretization

## II. Results and Discussions

### A. R-SOC Model Verification

In order to validate the reversible SOFC/SOEC model, the current-voltage polarization curves from the model in both of the SOFC and SOEC mode has been compared the experimental data. The simulation results are in good agreement with the experimental data within slight error.



curve of SOFC between simulation and experiment

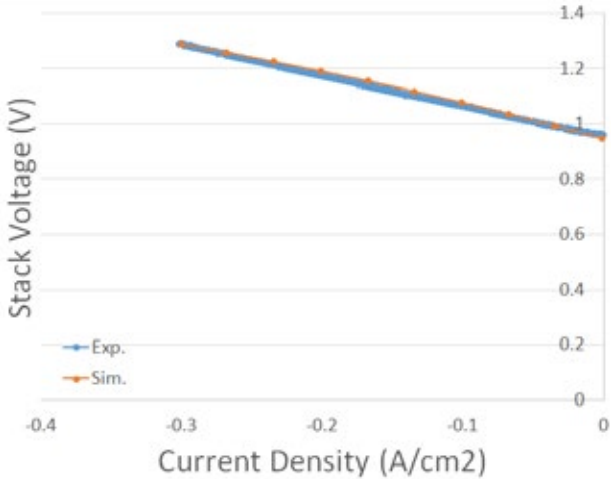


Fig. 4. Comparison of current-voltage polarization curve of SOEC between simulation and experiment

## III. Conclusions

In this study, dynamic model of SOEC system has been developed in Matlab-Simulink®. The R-SOC stack model is validated by comparison with the experimental data. Several R-SOC system have been developed and their system efficiency have been compared with various operating conditions and strategy.

## References

[1] Dincer I, Zamfirescu C. Sustainable hydrogen production options and the role of IAHE. *Int J Hydrogen Energy* 2012;37(21):16266e86.

[2] Bockris J. The origin of ideas on a hydrogen economy and its solution to the decay of the environment. *Int J Hydrogen Energy* 2002;27:731e40.

## Acknowledgement

This work was supported by the Korea Institute of Energy Technology Evaluation and Planning(KETEP) and the Ministry of Trade, Industry & Energy(MOTIE) of the Republic of Korea (No. 20163010140530).



## GIANT CANE AS LOW-COST MATERIAL FOR MICROBIAL FUEL CELLS ARCHITECTURES

S. Marzorati\*, A. Goglio\*, D. Mombelli\*\*, C. Mapelli\*\*, S.P. Trasatti\*\*\*, P. Cristiani\*\*\*\*, A. Schievano\*

\*e-Bio Center, via Celoria 2 - 20133 Milano (Italy)

\*\* Sezione Materiale per Applicazioni Meccaniche, Dipartimento di Meccanica - Politecnico di Milano, via La Masa 1 - 20156 Milano, (Italy)

\*\*\*Department of Environmental Science and Policy, via Celoria 2 - 20133 Milano (Italy)

\*\*\*\* RSE – Ricerca sul Sistema Energetico S.p.A., via Rubattino, 54, 20100 Milano, (Italy)

**Abstract** - Novel solutions for cylindrical Microbial Fuel Cells (MFCs) design are hereby proposed, starting from a ligno-cellulosic material: Giant Cane. Giant Cane is cylindrical, porous and can be used (as it is) as separator or (pyrolyzed) as cathode in low-cost MFCs architectures.

First, Giant Cane was used as tubular separator for MFC modules. This system yielded  $30\text{--}40\text{ mWm}^{-2}$ , relatively low compared to state-of-the-art. However, the generated electric field was enough to sustain electro-osmotic drag. Over 70 days of operation, deposition phenomena of valuable elements (Ca, Mg, Mn, K and others) were observed.

Secondly, pyrolyzed Giant Cane was set as the cathode. The as-obtained MFC, equipped with the pyrolyzed cathode, underwent remarkable deposition phenomena of micro and macronutrients.

By these solutions, the MFC modules are almost completely built by biogenic/low-cost materials. At the end of MFCs life cycle, MFCs impregnated by micro and macronutrients, can be reused as bio-fertilizers in agriculture.

**Index Terms** – Bio-fertilizers, ligno-cellulosic biomass, microbial fuel cells, nutrients recovery.

### I. NOMENCLATURE

GC: Giant Cane

MFC: Microbial Fuel Cell

MPL: Microporous Layer

OCP: Open Circuit Potential

ORR: Oxygen Reduction Reaction

### II. INTRODUCTION

Research in the field of MFCs has been tremendously expanding over the last decades, due to their appealing ability to treat different kind of wastewater, producing electricity through bioelectrochemical reactions [1]. However, materials costs of electrodes, architecture and membranes have been severely affecting the full-scale applications of this

biotechnology. Costs and architecture should be strongly optimized. In order to eliminate expensive commercial membranes, some researchers recently introduced cylindrical separators made of ‘terracotta’ [2]. Others developed similar systems by means of natural rubber [3] or earthen pot [4]. These low cost MFCs showed performance comparable to many sophisticated systems employing expensive membranes.

On the side of the electrodes’ costs, the hindered kinetics for ORR is a well-known and discussed topic in the fuel cells and MFCs field. Efforts towards the possibility of reducing costs of catalysts for ORR represent an evergreen scientific focus [5].

A ligno-cellulosic biomass, Giant Cane (*Arundo Donax L.*), was selected in this work as the porous matrix to be used as a separator or (if pyrolyzed) as a cathode in MFCs architectures. The aim of this work is to investigate Giant Cane (as it is) as separator and (pyrolyzed) as the cathode in cylindrical MFCs. To date, this concept has never been presented in literature.

An explorative experiment to test the properties and performance of cylindrical air-cathode MFCs based on this ligno-cellulosic material is here presented.

### III. MATERIALS AND METHODS

#### A. MFCs equipped with Giant Cane-based separator and a standard cathode.

Fig. 1 (GC-A) shows a schematic of the first experimental setup, GC-A. A carbon cloth anode was fixed around the external face of the Giant Cane cylinder, set as the separator. A carbon cloth cathode (added with an activated carbon MPL) was positioned in the inner part of the cane.

#### B. MFCs without separator and equipped with pyrolysed Giant Cane as cathode

Fig. 1 (GC-B) shows a schematic of the second experimental

setup, GC-B. A carbon cloth anode was fixed around the external face of the Giant Cane cylinder. A 900°C pyrolyzed Giant Cane was set as the cathode, wrapped by some felt to avoid the short circuit.

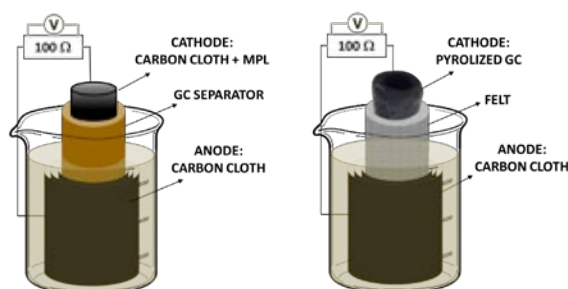


Fig. 1. Schematic of GC-A and GC-B experimental setup.

#### C. MFCs operation

GC-A and GC-B were positioned in glass jars, immersed in swine manure, run in batch mode at  $(25 \pm 1)^\circ\text{C}$  and cyclically fed with sodium acetate. Cell potential difference was recorded across external loads of  $100\ \Omega$  by a data logger.

### IV. RESULTS AND DISCUSSION

#### A. Power production and deposition phenomena

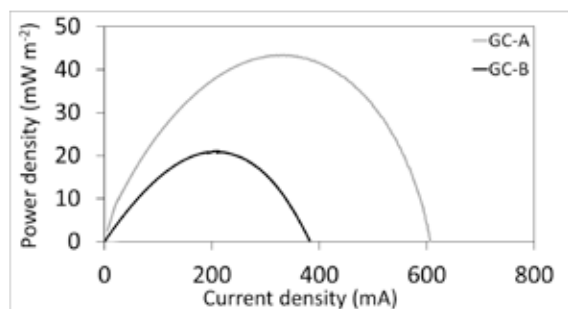


Fig. 2. Power density curves.

Under  $3\ \text{g l}^{-1}$  sodium acetate feeding and  $100\ \Omega$  external load, GC-A and GC-B yielded  $40$  and  $20\ \text{mW m}^{-2}$ , respectively, relatively low if compared to state-of-the-art MFCs, oriented to electricity harvesting [6]. However, the generated electric field was enough to sustain electro-osmotic ions mobility and to establish high pH conditions (pH 11-12) at the cathode. The generated potential difference induces ion movement within the reactor. Cations in the anolyte are attracted to the cathode. Once they approach the vicinity of the cathode, increased pH, due to ORR occurring, is known to favor the precipitation of a variety of salts. For instance, the solubility of many carbonates (like  $\text{MgCO}_3$  and  $\text{CaCO}_3$ ) decreases as the pH increases.

Over 70 days of operation, electro-migration and deposition phenomena of valuable elements (Na, Ca, Mg, Mn, K, etc.) were observed, both inside the separator (in the case of GC-A) and on the cathode (both in GC-A and GC-B).

Simultaneously, partial biodegradation of the ligno-cellulosic biomass, drove partial release of organic carbon, nitrogen, phosphorous and other elements in the anodic chamber of GC-A. The biodegradation phenomenon deserves to be carefully considered, when the aim of MFCs is wastewater treatment together with nutrients recovery.

### V. CONCLUSION

By the proposed solutions, the MFC modules are almost completely built by biogenic/low-cost materials. Both the configurations demonstrated good conductivity, allowing the MFCs to operate with a relative low internal resistance. These results address towards the possibility of using cylindrical-shaped biomass as separators and/or cathode to fabricate low-tech MFC modules. At the end of their life, resulting enriched by valuable macro and micronutrients, such MFCs could be completely re-used as bio-fertilizers to agricultural production.

### ACKNOWLEDGMENT

This work was financed by the SIR 2014 Grant (PROJECT RBSI14JKU3, BiofuelcellAPP), Italian Ministry of University and Research (MIUR) and by the Research Fund for the Italian Electrical System in compliance with the Decree of March, 19<sup>th</sup> 2009.

### REFERENCES

- [1] Puig, S., Serra, M., Coma, M., Cabré, M., Balaguer, M.D., Colprim, J., Effect of pH on nutrient dynamics and electricity production using microbial fuel cells, *Bioresource Technology*, Volume 101, 2010, pp. 9594-9599.
- [2] Pasternak, G., Greenman, J., Ieropoulos, I., Comprehensive Study on Ceramic Membranes for Low-Cost Microbial Fuel Cells, *ChemSusChem*, Volume 9, 2015, pp. 201588-96.
- [3] Winfield, J., Ieropoulos, I., Rossiter, J., Greenman, J., Patton, D., Biodegradation and proton exchange using natural rubber in microbial fuel cells, *Biodegradation*, Volume 24, 2013, 733-739.
- [4] Behera, M., Jana, P.S., Ghangrekar, M.M., Performance evaluation of low cost microbial fuel cell fabricated using earthen pot with biotic and abiotic cathode, *Bioresource Technology*, Volume 101, 2010, pp. 1183-1189.
- [5] Lefèvre M., Proietti E., Jaouen F., Dodelet J.-P., Iron-based catalysts with improved oxygen reduction activity in Polymer Electrolyte Fuel Cells, *Science*, Volume 324, 2009, pp. 71-74.
- [6] Santoro C., Arbizzani C., Erable B., Ieropoulos I., Microbial fuel cells: From fundamentals to applications. A review, *Journal of Power Sources*, Volume 356, 2017, pp. 225-244.

## NEW TERRACOTTA-BASED MICROBIAL FUEL CELLS TREAT WASTEWATER WHILE PROVIDING NUTRIENTS FOR MICROALGAE CULTIVATION

A. Colombo\*, G. Rusconi Clerici\*, A. Idà\*\*, M. Rebecchi\*, and A. Schievano\*

\*e-Bio Center, Department of Science and Policy, Università degli Studi di Milano, Via  
Celoria 2, 20133 Milano, (Italy)

\*\*Algaria srl, Piazzale Aquileia 6, 20144 Milano, (Italy)

**Abstract** – Photosynthetic organisms (PM) like *Spirulina* are normally cultivated at full-scale in raceway-like ponds, requiring optimized culture media prepared by chemicals. The integration of bioelectrochemical systems like Microbial Fuel Cells (MFCs) in algal ponds, would allow simultaneous removal of nutrients from wastewater and their recovery for PM growth. In the present work the investigation of electro-migration, diffusion and uptake of nutrients by PM was achieved by operating tubular terracotta MFCs with *Spirulina* culture in the cathodic compartment. Analysis of anodic and cathodic solutions allowed evaluating the fate of anions and cations upon MFC operation. The way the ion transport was affected by nutrients uptake in microalgae biomass were investigated with control MFC without *Spirulina*. The transport of nutrients across terracotta separator was evaluated also with respect to open-circuit reactors, set as additional control.

**Index Terms** – microalgae, nutrients recovery, photo-microbial fuel cells, *Spirulina*.

### I. NOMENCLATURE

PM: Photosynthetic Microorganisms

MFC: Microbial Fuel Cell

P-MFC: Photo-Microbial Fuel Cell

W-MFC: Microbial Fuel Cell without microalgae

OC: open circuit control reactors

### II. INTRODUCTION

PM (like microalgae and cyanobacteria) have been addressed as oxygen suppliers for the cathodic oxygen reduction reaction in MFCs [1]. In these systems, named P-MFCs, the double-chambered configuration seems to be the most promising, because of the presence of a membrane or a porous separator that would allow effective separation between PM in cathodic compartment and anaerobic bacteria in anodic one [2].

This approach lays the basis for an innovative application of

MFC as a way to assist the cultivation of PM, while treating organic-rich wastewater. Depending on the type, wastewaters are rich in essential elements (mainly K, N, and P and trace elements) for the growth of PM. In double-chambered P-MFCs, nutrients removed by wastewater upon MFC operation migrate to the cathodic compartment and be recovered through uptake by PM.

In a previous work [3], *Spirulina* was successfully cultivated in the cathodic compartment of P-MFCs while treating swine-farming wastewater in anodic compartment. Results showed that photosynthetic oxygen was sufficient to sustain MFC operation [4], ensuring COD removal and power densities ( $0.8-1 \text{ W m}^{-2}$ ) approaching those of air-cathode MFCs run as control. Moreover, most nutrients were recovered into the cathodic compartment, while only negligible COD leaked through the porous separator.

Moving from those findings, the fate of nutrients and ions was evaluated by operating tubular terracotta P-MFCs with the aim of possibly elucidate electro-migration, diffusion and uptake of nutrients by microalgae. The transport of nutrients across terracotta separator was evaluated with respect to open-circuit reactors, set as control. A control W-MFC was also considered to assess the effects of algae growth onto MFC operation.

### III. MATERIALS AND METHODS

#### A. Experimental set-up and acclimation

Terracotta cylinders (10 cm height, 5 cm internal diameter, 4 mm thickness) were used as both structural element of the MFC and as porous separator between anodic and cathodic compartment. MFCs were set up with carbon-based electrodes in glassy reactors. Anode was allocated into the cylinder, while

the GDL-modified cathode was wrapped around the terracotta.

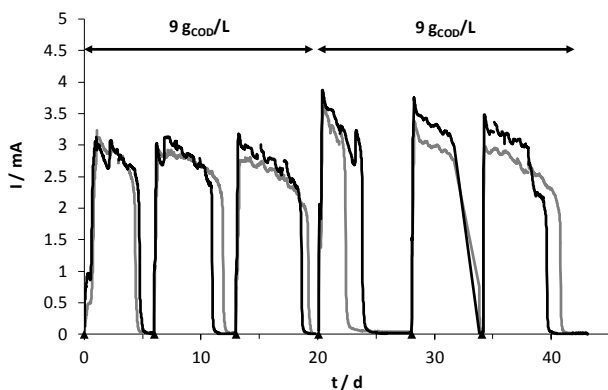
Anodic compartment were inoculated with diluted swine manure diluted (1:10). Cathodic compartment were inoculated with *Spirulina*. Synthetic wastewater was used as culture medium in both compartments. A 40-days acclimation period was run, till a reproducible and stable current generation trend was achieved. Control reactors were set as follows: i) control culture of *Spirulina*, ii) OC; iii) W-MFC. Experiments were run in duplicate.

#### B. Operation and analytics

All reactors were identically run in batch mode at  $(35 \pm 1)$  °C under day-night illumination regime. Solution in cathodic chambers was continuously aerated to keep the solution mixed and to fix dissolved oxygen concentration. Anodic chambers were periodically fed with sodium acetate as COD source ( $9 \text{ g}_{\text{COD}}/\text{L}$ ), in order to mimic an organic-rich wastewater. Cell potential difference (V) of MFCs was recorded across a  $50 \Omega$  external load. Anodic and cathodic solutions were characterized in terms of variation of COD, pH, conductivity and chemical composition over about 60 days of operation. Algal biomass growth was also monitored. Electrochemical performances were determined by power curves in term of maximum power density  $P_{\text{max}}$  and internal resistance  $R_{\text{int}}$ .

#### IV. RESULTS AND DISCUSSION

Lab P-MFCs with *Spirulina* cultures and  $9 \text{ g}_{\text{COD}}/\text{L}$  wastewater were able to effectively remove COD in anodic chamber (up to 95%), with negligible COD losses to PM culture in cathodic chamber. Similar performances were observed for P-MFCs and control W-MFCs both in terms of current generation (Figure 1) and COD removal (>93%).



**Figure 1** – Current generation of P-MFC and W-MFC.

Merits parameters of investigated systems are listed in Table 1. As expected, MFC systems ensured higher COD removal capabilities when compared with OC systems.

Within a batch cycle, pH and conductivity in the cathodic

chamber of MFC continuously increased

In each batch cycle, a consistent amount of main nutrients (Mg, K, Mn, P) were removed from anodic chamber and partly recovered into cathodic chamber, where *Spirulina* growth almost linearly ( $40 \text{ mgTSS L}^{-1}\text{d}^{-1}$ ) with a trend typical of algal culture in illuminated environment under day-night illumination.

High pH in cathodic chamber would ensure alkaline environments suitable for *Spirulina* growth.

TABLE I  
MERITS PARAMETERS OF INVESTIGATED REACTORS

Reactor type	Anodic sCOD removal (%)	CE (%)	R <sub>int</sub>
S-MFC	95	34	53
S-OC	82	-	-
W-MFC	93	29	46
W-OC	84	-	-

#### V. CONCLUSION

Terracotta acts well as separator between anodic and cathodic microbiological population, even if the effective prevention of contamination will be the focus of a further study.

The use of terracotta is promising in plant-scale hybrid system coupling MFC and microalgae cultivation, due to its dual role as structural element and porous separator.

#### ACKNOWLEDGMENT

This work has been entirely financed by the Italian Ministry of University and Research (MIUR), within the SIR2014 Grant (project RBSI14JKU3, BiofuelcellAPP).

#### REFERENCES

- [1] Gajda I, Greenman J, Melhuish C, Ieropoulos I. Photosynthetic cathodes for Microbial Fuel Cells. *Int J Hydrogen Energy* 2013;38:11559–64.
- [2] Elmekawy A, Hegab HM, Vanbroekhoven K, Pant D. Techno-productive potential of photosynthetic microbial fuel cells through different configurations. *Renew Sustain Energy Rev* 2014;39:617–27.
- [3] Colombo A, Marzorati S, Lucchini G, Cristiani P, Pant D, Schievano A. Assisting cultivation of photosynthetic microorganisms by microbial fuel cells to enhance nutrients recovery from wastewater. *Bioresour Technol* 2017;237:240–8.
- [4] Rago L, Cristiani P, Villa F, Zecchin S, Colombo A, Cavalca L, et al. Influences of dissolved oxygen concentration on biocathodic microbial communities in microbial fuel cells. *Bioelectrochemistry* 2017;116:39–51.

# The challenge of nutrients recovery by terracotta Microbial Fuel Cells

A. Goglio\*, S. Marzorati\*, S. Quarto\*\*, E. Falletta\*\*, P. Cristiani\*\*\*, A. Schievano\*

\* e-BioCenter, via Celoria 2 - 20133 Milan (Italy)

\*\* Department of Chemistry, University of Milan, Via Balzaretti 9, 20133 Milan (Italy)

\*\*\* RSE – Ricerca sul Sistema Energetico S.p.A., via Rubattino 54, 20100 Milan (Italy)

**Abstract** - Terracotta has been studied as a low-cost material to fabricate porous air-water separators, in air-cathode microbial fuel cells (MFCs). Maximizing the air-water interface with such structures could facilitate the scaling up of MFCs for treating wastewater, while recovering nutrients. The tests were repeated with two different wastewaters: swine manure and synthetic wastewater. Over 180 MFCs operation days, consistent amounts of the main macro and micronutrients (C, N, P, K, Fe, Mn, Ca and Mg) were removed from the wastewaters. The electro-osmotic forces generated by the MFCs and the high cathodic pH values (9-11) were the predominant factors leading to salts precipitation on both cathodes and terracotta membrane. Water evaporation from the air-water interface also contributed to elements precipitation, but to a lesser extent. This study aims at the terracotta MFCs in view of recovering nutrients from wastewaters towards a future use in agriculture as bio-fertilizers or soil conditioner enriched of macro and micro nutrients.

**Index Terms** - Microbial fuel cells, nutrients recovery, organic-rich wastewater treatment, circular economy

## I. NOMENCLATURE

MFC: Microbial Fuel Cell  
OCP: Open Circuit Potential  
MPL: Micro porous Layer  
SM: Swine Manure  
SW: Synthetic Wastewater

## II. INTRODUCTION

It is widely recognized that wastewater derived from food production chains should be treated in a sustainable way, to minimize environmental contamination, while maximizing the recovery of valuable resources (carbon and nutrients) [1]. Nutrient removal from water solution and recovery as renewed

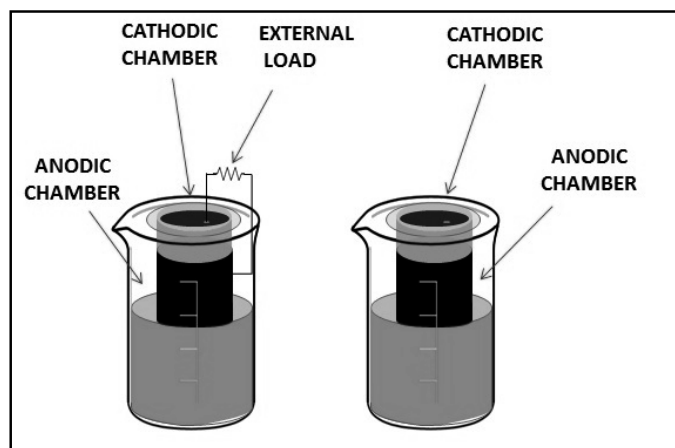
fertilizers is of particular interest, because of the potential threat of natural water bodies over-fertilization, the limited mining resource and high cost associated with nutrient production [2]. Currently, micro porous layers (MPL) are used in MFCs to separate the liquid in the anodic chamber from the air-exposed cathodic surface, while increasing cathodic surface area [3] and guaranteeing low ionic resistance [4]. Over long-term operations (more than 60 days), clogging and biofouling, due to organic materials as well as inorganic salts deposition on electrodes surfaces, strongly invalidate cell performances [5]. Terracotta was introduced in recent studies as low-cost and biocompatible air-water separator [6]. The aims of this work are the possibility of recovering macro and micro nutrients (N, P, K, Fe, Mn, Ca and Mg) and suspended organic matter can be recovered by biofouling while treat organic rich wastewater. Moreover, these materials can be directly recycled as base for organic-mineral fertilizers and soil conditioners, in agricultural applications.

## III. MATERIALS AND METHODS

### A. MFCs configuration

Figure 1 shows two different set-up (4 MFC and 4 OCP) were studied over a relatively long period (180 days) fed with two different types of wastewater: Swine manure and synthetic wastewater. The cylindrical terracotta MFC are characterized by 20 cm height, 5 cm internal diameter and 4 mm thickness. Anodes and cathodes were both composed of carbon cloth with projected area of 1500 cm<sup>2</sup> and 360 cm<sup>2</sup>, respectively. The MFCs systems are connected across 150  $\Omega$  external load.





**Figure 1 - MFCs configuration**

#### IV. RESULTS AND DISCUSSION

##### A. Electrochemical characterization of the MFCs

Throughout the duration of the experiment, several electrochemical measurements were carried out: current density trends, open circuit potential and power curves. Moreover, the systems are characterized by a power density of  $30\text{--}40\text{ mW m}^{-2}$ .

##### B. Salt removal from wastewater and deposition phenomena on terracotta membrane

Over 180 MFCs operation days, consistent amounts of the main macro and micronutrients (C, N, P, K, Fe, Mn, Ca and Mg) were removed from the wastewaters. This could in principle be due to: a) deposition of organic and inorganic fractions on the air-water interface separators (terracotta and/or MPL); b) precipitation or settling at the bottom of the anodic chamber. Nitrogen was removed by both  $\text{N-NH}_3$  stripping at water-air interface and nitrification-denitrification phenomena.

Ammonium removal could be related to microbial nitrification or to chemical-physical processes. Nitrification could have occurred with two main mechanisms: a) at the anode, by electroactive anode-respiring bacteria, or at the air-water interface, by microaerophilic communities. Other processes could have concurred to ammonium removal: a) adsorption on the electrodes (both anode and cathode) and on the terracotta membrane; b) ammonia stripping from the air-water interface. Depending on the buffer, capacity of the liquid medium, slight increases in pH is typical in anaerobic environments, as result of volatile fatty acids consumption. Regardless to the type of wastewater, the pH never exceeded pH 8.5. The electro-osmotic forces generated by the MFCs and the high cathodic pH values (9–11) were the predominant factors leading to salts precipitation on both cathodes and terracotta membranes. Water evaporation from the air-water interface also contributed to elements precipitation, but to a lesser extent. This is a key point to favor inorganic salt depositions within the internal porosity of the terracotta membranes. This encourages the use of MFCs,

made of low-cost air-water porous membrane, to improve nutrients recovery as precipitated salts at the cathode.

#### V. CONCLUSION

After that, the terracotta membrane gets saturated with organic and inorganic forms of various nutrients, it could be ready to be re-utilized as soil conditioner. It is useful to have a look at the content in exchangeable nutrients. Soil conditioners and amendments have the characteristic of improving physical and chemical characteristics of soil, such as its structure, making slight fertilization, facilitate water retention, cation exchange capacity and plant roots growth. Terracotta has the composition of clay, which is known to have high cation exchange capacity and be a good soil conditioner. The enrichment in nutrients after the experiment in MFCs happens thanks to particularly high pH conditions and ionic concentrations during the process. Once distributed as soil amendment, these nutrients would return in soluble forms, available for plant roots uptake. Surely, more detailed chemical characterization and study could help in elucidate the forms and the availability of the nutrients, measured here as total content.

#### ACKNOWLEDGMENT

This work was financed by the SIR 2014 Grant (PROJECT RBSI14JKU3, BiofuelcellAPP), Italian Ministry of University and Research (MIUR) and by the Research Fund for the Italian Electrical System in compliance with the Decree of March 19th 2009.

#### REFERENCES

- [1] Verstraete, W., Van de Caveye, P., Diamantis, V., 2009. Maximum use of resources present in domestic “used water.” *Bioresource Technology*, 100 (23), 5537–5545.
- [2] Rittmann, B. E., Mayer, B., Westerhoff, P., Edwards, M., 2011. Capturing the lost phosphorus. *Chemosphere*, 84(6), 846–853.
- [3] Ghadge A.N., Jadhav D.A., Pradhan H., Ghangrekar M.M., 2015. Enhancing waste activated sludge digestion and power production using hypochlorite as catholyte in clayware microbial fuel cell., *Bioresour. Technol.* 182, 225–31.
- [4] Cristiani P., Carvalho M.L., Guerrini E., Daghighio M., Santoro C., Li B., 2013. Cathodic and anodic biofilms in Single Chamber Microbial Fuel Cells, *Bioelectrochemistry*. 92, 6–13.
- [5] Santini, M., Marzorati, S., Fest-Santini, S., Trasatti, S., Cristiani, P., 2017. Carbonate scale deactivating the biocathode in a microbial fuel cell. *J. Power Sources* 356, 400–407.
- [6] Pasternak, G., Greenman, J., Ieropoulos, I., 2015. Comprehensive Study on Ceramic Membranes for Low-Cost Microbial Fuel Cells, *ChemSusChem*. (2015) 88–96.

# Numerical Simulation of MFC Performance: a Lattice Boltzmann Study

Vesselin K. Krastev<sup>1</sup> and Giacomo Falcucci<sup>2,3</sup>

<sup>1</sup>DEIM - School of Engineering - University of Tuscia, Largo dell'Università, 01100 Viterbo, Italy

<sup>2</sup>Dept. of Enterprise Engineering "Mario Lucertini" - University of Rome "Tor Vergata", Via del Politecnico 1, 00133 Rome, Italy

<sup>3</sup>John A. Paulson School of Engineering and Applied Sciences - Harvard University, 29 Oxford St., 02138 Cambridge (MA), USA

## ABSTRACT

In this work, a novel numerical approach is proposed for the simulation of electrochemical and power performance of Microbial Fuel Cells (MFC). Our model is based on the Lattice Boltzmann Method, a numerical approach based on an optimized formulation of Boltzmann's Kinetic Equation, which has been successfully applied to phenomena of technical and engineering interest in recent years. Employing a multi-component LBM solver, an accurate prediction of species transport and electrochemical reactions is achieved inside the reactor chamber. The direct conversion of organic substrate into  $e^-$  and  $H^+$  as by-products of microbes metabolism has been modeled according to previous experimental activity. The physical and electrochemical characteristics of anode and cathode electrodes have been accounted for and their effects on internal species transport and charge transfer is accurately simulated. The good agreement between our results and the experiments in literature highlight the reliability and versatility of LBM to predict the performance of MFCs and to shed light on the complex phenomena occurring inside the reactors.

## I. INTRODUCTION

Microbial Fuel Cells (MFCs) have been the object of remarkable research efforts all over the world, as they have proven capable of bringing a sustainable and effective solution to the wide-spread problem of waste management, [1, 2, 3]. However, due to the complex and heterogeneous phenomena that take place inside MFC reactors, due to the presence of bacteria strains, such a technology is not yet ready for a massive industrial exploitation.

In this paper, we propose a novel numerical methodology, able to predict the performance of MFCs in terms of polarization and power trends, based on the Lattice Boltzmann Method (LBM), [4, 5]. In recent years, LBM has been successfully employed in a wide range of complex scientific and technical problems, including multi-phase, multi-component and reacting flows within complex geometries, [6, 7, 8].

The results of this novel numerical approach have been validated by means of comparison to previous experimental tests, performed at the Energy Lab of the University of Naples "Parthenope" and

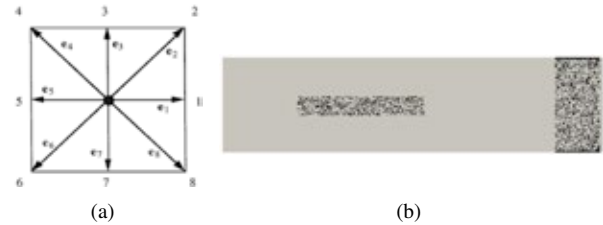


Figure 1: (a): sketch of the D2Q9 lattice used in this work, [9]; (b) sketch of the computational domain: the anode electrode is represented by the porous region on the left, while the cathode is the porous region at the right end.

already published in the literature, [2], highlighting the reliability and versatility of the proposed methodology. According to these results, our LBM approach can provide a useful tool for the design of future-generation MFC reactors.

## II. NUMERICAL METHOD

The description of the transport phenomena taking place inside the MFC reactor is performed through a multi-component implementation of the Lattice Boltzmann Method, [9]:

$$f_i^\alpha(\mathbf{x} + \mathbf{c}_i, t + 1) - f_i^\alpha(\mathbf{x}, t) = \omega(\alpha) [f_i^{eq, \alpha}(\mathbf{x}, t) - f_i^\alpha(\mathbf{x}, t)], \quad (1)$$

in which  $f_i^\alpha(\mathbf{x}, t)$  is the probability density function of finding a particle of species  $\alpha$  at time  $t$  and at site  $\mathbf{x}$ , moving along the  $i$ -th lattice direction defined by the discrete speeds  $\mathbf{c}_i$ , with  $i = 0, \dots, b$  (see Fig. 1). The lattice time step  $\Delta t$  has been taken as the unit of time for simplicity. The left hand-side of Eq. 1 represents the free-streaming of molecules, whereas the right-hand side accounts for the collisional relaxation towards the local equilibrium  $f_i^\alpha(\mathbf{x}, t)$ , which is expressed as a low-Mach, second-order expansion of a local Maxwellian, namely:

$$f_i^{eq, \alpha}(\mathbf{x}, t) = w_i \rho^\alpha(\mathbf{x}, t) \left[ 1 + \frac{\mathbf{c}_i \cdot \mathbf{u}(\mathbf{x}, t)}{c_s^2} + \frac{(\mathbf{c}_i \cdot \mathbf{u}(\mathbf{x}, t))^2}{2 c_s^4} - \frac{|\mathbf{u}(\mathbf{x}, t)|^2}{2 c_s^2} \right]. \quad (2)$$

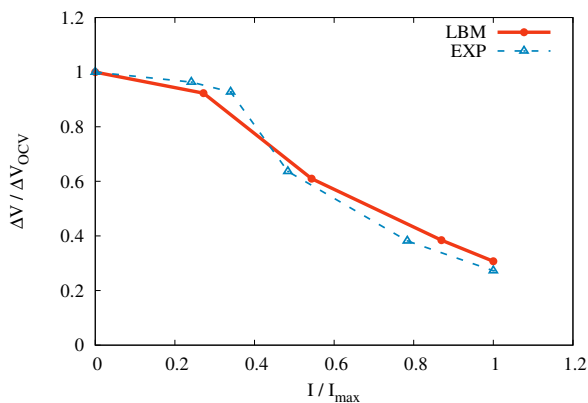


Figure 2: Polarization curve obtained by means of the proposed LB model, compared to the experimental data presented in [2]. The Figure highlights the remarkable agreement between the results of our numerical simulations and the experimental measurements in the literature.

The relaxation to local equilibrium takes place on a time-scale  $\tau(\alpha) = 1/\omega(\alpha)$ : with this approach, each species  $\alpha$  in our system can relax to its own local equilibrium.

The macroscopic hydrodynamic quantities, namely species concentration,  $C^\alpha(\mathbf{x}, t)$ , and velocities,  $\mathbf{u}^\alpha(\mathbf{x}, t)$ , are retrieved according to the following:

$$C^\alpha(\mathbf{x}, t) = \sum_{i=0}^b f_i^\alpha(\mathbf{x}, t), \quad C^\alpha(\mathbf{x}, t) \mathbf{u}^\alpha(\mathbf{x}, t) = \sum_{i=0}^b c_i f_i^\alpha(\mathbf{x}, t). \quad (3)$$

As a result of Eq. 1, it is possible to follow the evolution of a *carrier* species (water, in our case), in which two other species are transported: the solid organic waste and protons  $H^+$ , respectively, [6, 9].

In this work, in fact, without loss of generality we focus on a simplified mechanism for MFC operation, according to which the bacteria at the anode digest organic waste producing electrons  $e^-$  and protons  $H^+$  as the output of their own metabolism: the present model is fully flexible and can account for an arbitrary number of species  $\alpha$  and chemical reactions, but we devote these studies to future works.

**CHARGE MOTION WITHIN THE REACTOR** The motion of ions inside the reactor is due to the presence of diffusion, repulsion between positive ions and potential difference between the electrodes. The diffusion process is automatically accounted for in the LBM scheme reported in Eq. 1, [9]; repulsion and the effect of electrode potentials act only on  $H^+$  species.

The repulsive force between positive ions is modeled via a pseudo-potential approach, which has been successfully employed in the LBM framework for multi-phase and multi-component investigations, [10, 8], accounting their concentration. The force is given by  $F = -G c_s^2 \frac{\nabla \cdot \psi^2}{2}$ , in which  $\psi$  is the pseudo-potential that accounts for the local density of the  $H^+$  species,  $\psi = 1 - e^{-[H^+]}$  and  $G$  represents the strength of the repulsive interaction, which is given by  $G = q/c_s^2$ , with  $q$  the electrical charge of  $H^+$  ions. The potential difference between the two electrodes is fixed as the input parameter for the operation of our MFCs.

### III. RESULTS & DISCUSSION

Figure 2 shows the comparison between the polarization and power curves obtained by means of our numerical method and the experimental data presented in [2]. The quantities in Fig. 2 are normalized

according to the maximum values obtained in the simulation and in the experimental campaign, respectively. The Figure highlights the remarkable agreement in polarization and power trends computed by means of our computational approach, compared to the experimental measurements taken in the Energy Lab of the University of Naples “Parthenope” and reported in [2].

### IV. CONCLUSIONS

In this paper, we have proposed a novel numerical approach based on the Lattice Boltzmann Method (LBM) for the evaluation of the electrochemical performance of Microbial Fuel Cells (MFC). The results of the numerical method have shown a remarkable agreement with experimental measurements taken from the literature, proving the reliability and versatility of the proposed approach.

### ACKNOWLEDGEMENTS

The numerical simulations were performed on *Zeus* HPC facility, at the University of Naples “Parthenope”; *Zeus* HPC has been realized through the Italian Government Grant PAC01\_00119 *MITO - Informazioni Multimediali per Oggetti Territoriali*, with Prof. Elio Jannelli as the Scientific Responsible. Fruitful and inspiring discussions with Prof. Sauro Succi (for the Lattice Boltzmann Modeling) and Prof. Bruce E. Logan (for the MFC performance and internal processes) are kindly acknowledged.

### REFERENCES

- [1] Nastro, R.A., Falcucci, G., Minutillo, M. and Jannelli, E., 2017. Microbial Fuel Cells in solid waste valorization: trends and applications. In *Modelling Trends in Solid and Hazardous Waste Management* (pp. 159-171). Springer Singapore.
- [2] Jannelli, N., Nastro, R.A., Cigolotti, V., Minutillo, M. and Falcucci, G., 2017. Low pH, high salinity: Too much for microbial fuel cells?. *Applied Energy*, 192, pp. 543-550.
- [3] R.A. Nastro, N. Jannelli, M. Minutillo, M. Guida, M. Trifuoggi, L. Andreassi, A.L. Facci, V.K. Krastev, G. Falcucci, 2017. Performance Evaluation of Microbial Fuel Cells Fed by Solid Organic Waste: Parametric Comparison between Three Generations. *Energy Procedia*, 105, pp. 1102-1108.
- [4] Montessori, A., Falcucci, G., La Rocca, M., Ansumali, S. and Succi, S., 2015. Three-dimensional lattice pseudo-potentials for multiphase flow simulations at high density ratios. *Journal of Statistical Physics*, 161(6), pp.1404-1419.
- [5] Krastev, V.K., Falcucci, G., Jannelli, E., Minutillo, M. and Cozzolino, R., 2014. 3D CFD modeling and experimental characterization of HT PEM fuel cells at different anode gas compositions. *International Journal of Hydrogen Energy*, 39(36), pp.21663-21672.
- [6] Krastev, V.K., Amati, G., Jannelli, E., and Falcucci, G., "Direct Numerical Simulation of SCR Reactors through Kinetic Approach," SAE Technical Paper 2016-01-0963, 2016, <https://doi.org/10.4271/2016-01-0963>.
- [7] Falcucci, G., Ubertini, S., Bella, G., De Maio, A. and Palpacelli, S., 2010. Lattice Boltzmann modeling of diesel spray formation and break-up. *SAE International Journal of Fuels and Lubricants*, 3(2010-01-1130), pp.582-593.
- [8] Falcucci, G., Amati, G., Krastev, V.K., Montessori, A., Yablonsky, G.S. and Succi, S., 2017. Heterogeneous catalysis in pulsed-flow reactors with nanoporous gold hollow spheres. *Chemical Engineering Science*, 166, pp.274-282.
- [9] Falcucci, G., Succi, S., Montessori, A., Melchionna, S., Prestinzi, P., Barroo, C., Bell, D.C., Biener, M.M., Biener, J., Zugic, B. and Kaxiras, E., 2016. Mapping reactive flow patterns in monolithic nanoporous catalysts. *Microfluidics and Nanofluidics*, 20(7), pp.1-13.
- [10] Falcucci, G., Bella, G., Shiatti, G., Chibbaro, S., Sbragaglia, M. and Succi, S., 2007. Lattice Boltzmann models with mid-range interactions. *Communications in computational physics*, 2, pp.1071-1084.

## H<sub>2</sub> PURIFICATION VIA POLYMERIC MEMBRANES SEPARATION

A. Iulianelli\*, A. Figoli\*, C. Algieri\*, L. Donato\*, A. Garofalo\*, F. Galiano\*, F. Russo\*, F. Dalena\*\*, A. Basile\*  
\* ITM-CNR, via P. Bucci Cubo 17/C - University of Calabria  
– Rende (CS), 87036 (Italy)  
\*\* Chemistry Dpt., via P. Bucci Cubo 17/C - University of Calabria – Rende (CS), 87036 – Italy

**Abstract** - New polymeric membranes are used for purifying H<sub>2</sub>-rich gas mixtures, in particular thermally treated (at 120 °C) poly-ether-ether-ketone with Cardo group (PEEK-WC) and poly-lactic-acid (PLA). In this work, dense PLA membranes showed great results overcoming the Robeson's upper-bound (2008) with an ideal selectivity H<sub>2</sub>/CO<sub>2</sub> around 25 and H<sub>2</sub> permeability of 25 barrer. PLA membranes have been tested at ambient conditions, constituting a cost-effective solution for recovering hydrogen from gaseous mixtures coming from a reforming stage, meanwhile concentrating in CO<sub>2</sub> the retentate stream. PEEK-WC membranes have been experimentally characterized for low/medium temperature operation (80 °C), showing interesting results in terms of H<sub>2</sub>/CH<sub>4</sub> separation, with an ideal selectivity value higher than 40. For PEEK-WC thermally treated membranes, the H<sub>2</sub> permeating flux increased with transmembrane pressure from 25 to 80 °C, reaching 20 barrer of H<sub>2</sub> permeability at 80 °C.

**Index Terms** - H<sub>2</sub> separation, PEEK-WC, PLA, membranes

### I. INTRODUCTION

Although a large number of polymeric materials has been studied and applied to hydrogen separation, the number of polymers useful realistically in commercial systems is still limited. The individuation of the most adequate polymeric material for membrane preparation, showing high hydrogen permeating flux combined to good hydrogen perm-selectivity and high mechanical resistance as well, represents a big challenge. In this work, we propose two polymers, PEEK-WC (an amorphous modified poly(ether ether ketone) with Cardo-group) and PLA (polylactic acid, a versatile aliphatic polyester), particularly for applications in hydrogen separation. The purpose of this work is to analyze the effect of a thermal

treatment on PEEK-WC membrane samples and to compare their H<sub>2</sub> permeation performance with other existent experimental data on PEEK-WC membranes (without any thermal treatment). Furthermore, PLA membranes were pioneeristically applied for separating hydrogen from other gases of interest at ambient temperature. The ideal transport properties of the prepared PEEK-WC and PLA membranes were measured by using pure gases (CH<sub>4</sub>, CO<sub>2</sub>, H<sub>2</sub>, O<sub>2</sub> and N<sub>2</sub>), with the scope of evaluating the permeance and the H<sub>2</sub>/other gas ideal selectivity and for screening also their correlation with the parameters related to the NIPS (non-induced phase separation) membrane preparation.

### II. EXPERIMENTAL

PEEK-WC polymer (in powder form) used in this work (Figure 1) has been supplied by Changchun Institute of Applied Chemistry (Academia Sinica, China).

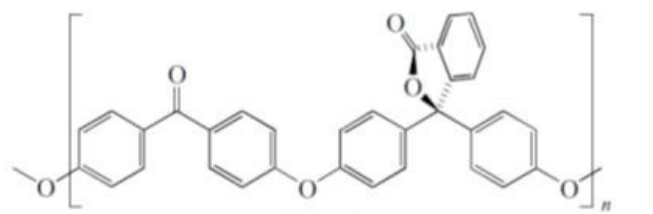


Figure 1. Structure of the poly(oxa-p-phenylene-3,3'-phthalido-p-phenylene-oxa-p-phenylene-oxy-p-phenylene).

PLA polymer is supplied by Cargill-Dow Inc. (USA) with the trade name of Nature Green® 100D, and its structure is



represented in Figure 2.

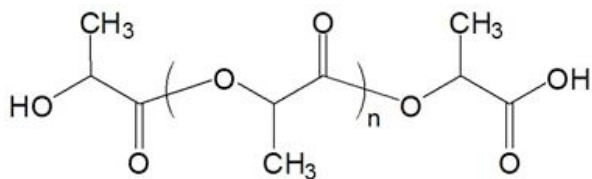


Figure 2. Structure of the poly(2-hydroxypropanoic acid).

Both PEEK-WC and PLA membranes were prepared by phase inversion technique. The different solutions were stirred for 24 h at room temperature until complete dissolution of the polymers. For PLA, after 2 h of degassing, the dope solution was cast over a glass plate by means of a casting knife (Elcometer ® 3570) with a thickness of ~ 150 µm. Afterwards, the solvent was left to evaporate at 25 °C for 12 h and, hence, in an oven at 40 °C for other 12 h. The solution of PEEK-WC was casted onto a glass support using a casting knife Braive Instruments, with a thickness of ~ 250 µm.

### III. DISCUSSION

PEEK-WC membranes have been already studied in the past for gas separation applications [1]; nevertheless, in this work at 80 °C PEEK-WC membrane, thermally treated up to 120 °C, gained interesting results in terms of perm-selectivity, particularly for H<sub>2</sub>/CO<sub>2</sub> and H<sub>2</sub>/CH<sub>4</sub> separation, reaching the values of 20 and 44, respectively.

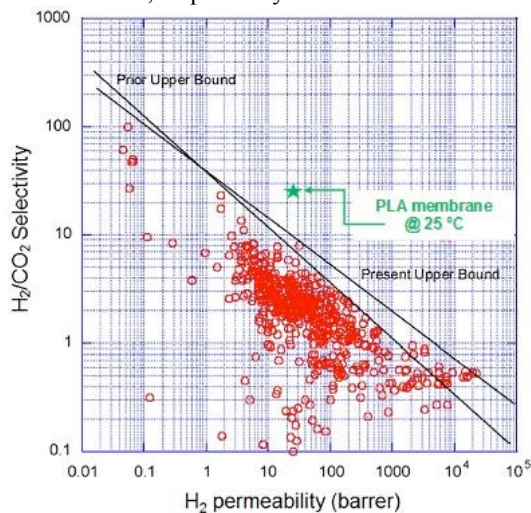


Figure 3. Permeation characteristics of PLA membrane over Robeson H<sub>2</sub>/CO<sub>2</sub> selectivity-H<sub>2</sub> permeability upper-bound. Adapted from Robeson [2].

The permeation of H<sub>2</sub> through PEEK-WC membrane can be mostly assigned to the diffusivity contribution, whilst CO<sub>2</sub> one

is mainly solubility-dependent. Moreover, H<sub>2</sub> is a smaller species among the ones considered in this work, therefore the faster.

The higher temperature leads to an enhanced diffusivity and a reduced solubility. As a consequence, the increase in H<sub>2</sub> permeability over temperature is much more pronounced than the other gas species and this is traduced in a higher selectivity. The utilization of PLA in H<sub>2</sub> separation at 25 °C can be considered as a pioneeristic solution, because it points out the potentiality of this polymeric material in this field with further economic benefits due to the low temperature operation. Figure 3 shows the Robeson's plot in terms of H<sub>2</sub>/CO<sub>2</sub> selectivity against H<sub>2</sub> permeability, confirming that PLA membrane overcomes the Robeson's upper-bound (2008).

### CONCLUSION

In this work, a thermally treated PEEK-WC polymer at 120 °C showed the best performance at 80 °C, achieving an ideal selectivity H<sub>2</sub>/CH<sub>4</sub> of 44, representing an interesting results if compared to other PEEK-WC data in literature. Furthermore, we observed that the thermal treatment determined a reduction of the void sizes and a decrease of chain flexibility, responsible of gas permeability depletion of the species with larger kinetic diameters (CO<sub>2</sub> and CH<sub>4</sub>). The application of PLA membranes for H<sub>2</sub> purification allowed to reach a great H<sub>2</sub>/CO<sub>2</sub> separation, as confirmed by the overcome of the Robeson's upper-bound (H<sub>2</sub>/CO<sub>2</sub> ideal selectivity = 25 with an H<sub>2</sub> permeability = 25 barrer at ambient temperature), representing a pioneeristic finding in this study.

### REFERENCES

- [1] A. Iulianelli, A. Gugliuzza, G. Clarizia, D. Ebrasu, A. Bevilacqua, F. Trotta, A. Basile, Sulfonation of PEEK-WC polymer via chloro-sulfonic acid for potential PEM fuel cell applications, *Int. J. Hydrogen En.*, 35 (2010) 12688-12695.
- [2] L.M. Robeson, The upper bound revisited, *J. Membrane Sci.*, 320 (2008) 390.



EFC17117

# HYDROGEN PRODUCTION BY STEAM GASIFICATION OF BIOMASS: IMPROVING THE GAS CLEANING UNIT BY REPLACEMENT OF BIODIESEL SCRUBBING WITH A TEMPERATURE SWING ADSORPTION

Jürgen Loipersböck\*, Markus Luisser\*, Gerald Weber\*,  
David Knöbl\*\*, Reinhard Rauch\*\*\*, Hermann Hofbauer\*\*\*\*

\*BIOENERGY2020+, 7540 Güssing, Wienerstraße 49 (Austria)

\*\*FH Burgenland, 7423 Pinkafeld, Steinamangerstraße 21 (Austria)

\*\*\* Karlsruher Institut für Technologie, 76021 Karlsruhe (Germany)

\*\*\*\* TU Wien Institut of Chemical Engineering, 1060 Vienna  
Getreidemarkt 9/166 (Austria)

**Abstract** – Hydrogen production from dual fluidized bed gasification (DFB) of biomass has a potential as key technology to fulfil the aims of the UN and EU to reduce fossil fuel demand. A research plant producing 3 Nm<sup>3</sup> of hydrogen per hour was set up during the last years. First results showed the possibility to produce hydrogen with a purity of more than 99.99 % out of biomass. However techno economic analyze showed the need of a consumable reduction. Therefor a temperature swing adsorption (TSA) was set up to replace a biodiesel scrubber for gas cleaning. The first results show the possibility of using a temperature swing adsorption in the process chain. Nevertheless extensive experiments have to be done to get enough knowledge of the long term stability and possible cost reduction.

**Index Terms** –gas cleaning, gasification, hydrogen production, temperature swing adsorption

## I. NOMENCLATURE

AC	activated carbon
BTX	Benzene, toluene, xylene
CHP	Combined Heat and Power
HPLC	High pressure liquid chromatography
PAH	poly-aromatic hydrocarbons
PSA	Pressure Swing Adsorption
TSA	Temperature Swing Adsorption
WGS	water gas shift

## II. INTRODUCTION

Hydrogen usage is a key to a renewable future. Chemical industry and refineries have huge demand on hydrogen for hydration processes. The bulk amount of hydrogen in Europe is derived by fossil fuels, especially by natural gas steam reforming. If this hydrogen can be replaced by renewable hydrogen a major step towards a greener energy policy can be done.

Together with other renewable hydrogen production routes,

hydrogen produced from steam gasification of biomass is a promising way to reach these ambitious goals.

Fig. 1 shows a flow scheme of a hydrogen production plant which uses DFB gasification as key technology.

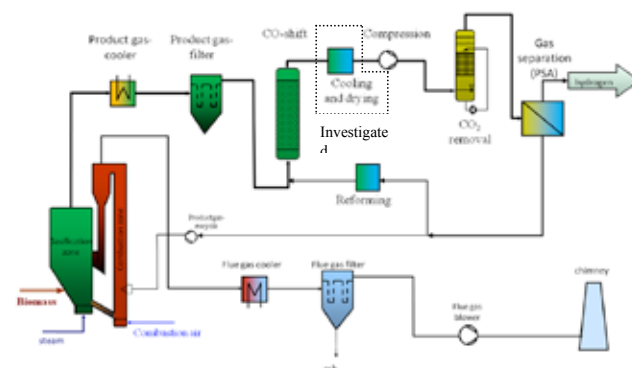


Fig. 1: Flow sheet of the hydrogen production plant.

Tar rich gas is extracted from the CHP after a dust removal. At the gas outtake a temperature of 180 °C is common. For the water gas shift stage a Fe/Cr based catalyst is used. After the shift stage a tar and water removal is done by biodiesel scrubbing. This gas gets compressed and CO<sub>2</sub> is removed. Hydrogen separation is done by pressure swing adsorption (PSA). The tail gas of the PSA can be reformed and recycled to the water gas shift stage, to boost the hydrogen yield.

To be combatable with other mature technologies further optimizations have to be done. Lower quality biomass has to be used, which results in an increased amount of impurities. These impurities can be hydrated over the water gas shift stage (WGS) or removed by gas cleaning as already investigated in [1].

Thus, higher amounts of impurities can be expected, more

economical way for gas cleaning must be investigated.

In this work, the possibility of replacing the biodiesel scrubber with a temperature swing adsorption, to reduce operation costs, is investigated. Therefor activated carbon is tested with several tar components and adsorption properties are investigated.

### III. MATERIAL AND METHOD

To investigate these behaviors the tar composition of the product gas of a DFB gasifier, after the dust filter, was analyzed and model components were identified according to ECN [2].

With these model tars a lab investigation was done by testing the properties of activated carbon (AC). Extensive chemical analyzes were done to measure the tar components.

An overview of the impurity composition is given in table I.

TABLE I  
IMPURITY CONTENT OF PRODUCT GAS AFTER DUST FILTER [3]

Impurity	Quantity	Unit
H <sub>2</sub> S	150-200	ppm
COS	5-9	ppm
Thiophene	20-25	ppm
Mercaptane	1-10	ppm
Tar	2-5	g/Nm <sup>3</sup>
BTX	15-20	g/Nm <sup>3</sup>

To estimate the tar concentration for the experiments, several tar analyzes were considered. A maximum tar concentration of 25 g/Nm<sup>3</sup> (including BTX) was chosen. To classify the tars and their condensation behavior the model of ECN was used. Tars were categorized in five classes. [2]

To summarize the tars present in real synthesis gas, this model was used to classify tars. Thiophene, toluene and naphthalene were chosen as model tars for the experiments.

For testing of activated carbon (AC) a test facility was set up. This facility consists of a gas flow controller and a HPLC pump to control the tar flow. These two streams are mixed in an evaporator and the tar containing gas is evaporated completely. After this the gas is sent to a temperature controlled AC test tube where the tars are adsorbed. Tar measurement after the AC test tube is done to measure the adsorption capacity of the AC.

A parameter variation, regarding tar composition and adsorption temperature was done.

### IV. RESULTS AND DISCUSSION

First results show a temperature variation as depicted in Fig. 2. It can be seen that the tar concentration at the outlet of is increasing with time and temperature. However 18 m-% can still be adsorbed at temperatures of 83 °C. As inlet concentration 25 g/m<sup>3</sup> of tars were used. After the adsorption process an outlet concentration of 0.03 g/m<sup>3</sup> could be measured. This shows a possible tar removal efficiency of 99.9 %.

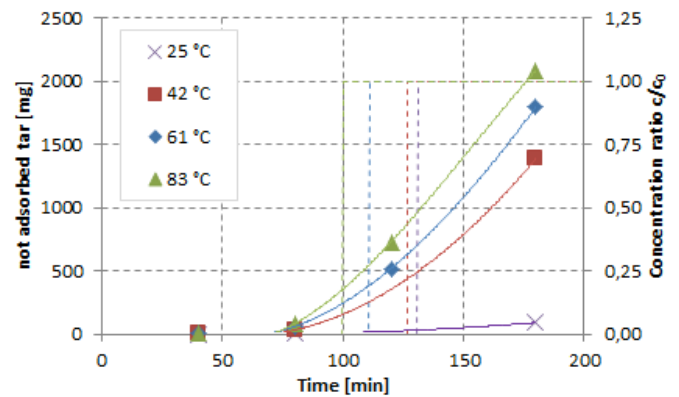


Fig. 2: Flow scheme of activated carbon test facility

These results show the possibility of using the AC at higher temperatures, if regeneration is done.

### V. CONCLUSION

First results showed the possibility of using activated carbon for gas cleaning in the existing hydrogen production plant. Still it is necessary to investigate the behavior of different tars during the adsorption process as well as the interaction of the tars with other substances. This investigation will be part of the full paper. Another investigation will be done in future regarding desorption properties of the used activated carbon und studying the possibility of using a TSA for gas cleaning.

### ACKNOWLEDGMENT

This work was carried out within the framework of Bioenergy2020+ GmbH. Bioenergy2020+ is funded by the states of Burgenland, Niederösterreich and Steiermark within the Austrian COMET program, managed by the research promotion agency Austria (FFG). This project has received funding from the European Union's Horizon 2020 research and innovation program under grant agreement No. 680395.

### REFERENCES

- [1] Loipersböck, J., Lenzi, M., Rauch, R., Hofbauer, H., Hydrogen production from biomass: The behavior of impurities over a CO shift unit and a biodiesel scrubber used as a gas treatment stage, Korean Journal of Chemical Engineering, 34, 2017, Pages 2198-2203
- [2] ECN-Biomass, Thersites the ECN tar dew point site, ECN-E&S, 2009
- [3] Chianese, S., Loipersböck, J., Malits, M., Rauch, R., Hofbauer, H., Molino, A., Musmarra, D., Experimental investigations of hydrogen production from CO catalytic conversion of tar rich syngas by biomass gasification, Fuel Processing Technology, 132, 2015, Pages 182-191

## STATE-OF-THE-ART CAPEX DATA FOR WATER ELECTROLYSERS, AND THEIR IMPACT ON RENEWABLE HYDROGEN PRICE SETTINGS

Joris Proost

Université catholique de Louvain (UCL), Division of Materials and  
Process Engineering, Place Sainte-Barbe 2, B-1348 Louvain-la-Neuve,  
(Belgium)

joris.proost@uclouvain.be

**Abstract** - Within the framework of the Hydrogen Implementing Agreement (HIA) of the International Energy Agency (IEA), a new Task 38 was started early 2016, entitled "Power-to-Hydrogen and Hydrogen-to-X : System Analysis of techno-economic, legal and regulatory conditions". Within this framework, a specific task force was set-up for the compilation of state-of-the-art technical and economical data on large-scale water electrolyser systems, both based on PEM and alkaline technology. The objectives set forward have been twofold. Firstly, to offer policy makers and industry with comprehensive trends and guidelines for further electrolyser cost reduction (CAPEX, in Euro/kW) into the MW-scale. Secondly, to provide objective technological & economic arguments for converging towards a realistic electrolytic (and hence renewable) H<sub>2</sub> market price (in Euro/kg). This should help water electrolysis to become competitive with SMR technology for (local) H<sub>2</sub> production, and hence to start making H<sub>2</sub> a competitive fuel.

**Index Terms** - electrolyser, CAPEX, H<sub>2</sub> price, alkaline, PEM

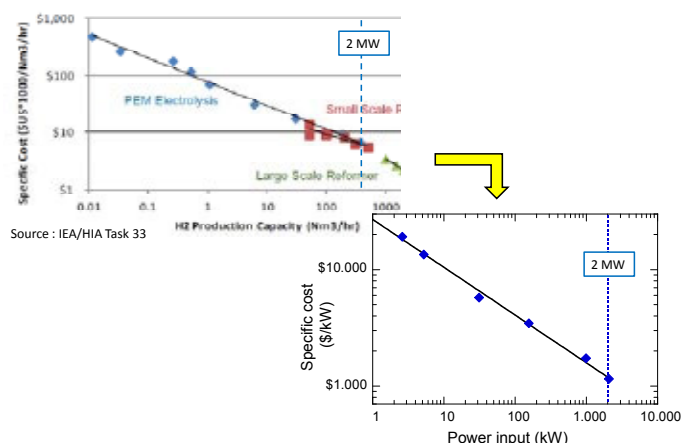


Fig. 1. CAPEX data for PEM electrolyzers, collected from Task 33, as a function of H<sub>2</sub> production capacity (top) and replotted as a function of equivalent power input (bottom).

### I. INTRODUCTION

As a starting point for setting up a specific task force on electrolyser data within IEA/HIA Task 38, published data from previous Task 33 have been (re-)considered, as shown in Figure 1. This plot shows on the one hand the actual CAPEX evolution of PEM electrolyser systems, both as a function of H<sub>2</sub> production capacity (top) and equivalent electrolyser power input (bottom). It also superimposes on the same graph data collected for both small and large scale steam methane reformer systems (SMR), the main H<sub>2</sub> production technology used today. Based on these data, it can be recognised that in order for water electrolysis to be a viable technological choice for H<sub>2</sub> production, a process intensification into the MW-range is absolutely mandatory. This is not only a necessary condition to become competitive, in terms of CAPEX, to SMR H<sub>2</sub> technology, but also a prerequisite to be able to couple to >MW-scale renewable electricity production capacities, as is typical for today's on-shore wind mills. The latter is an absolute boundary condition for any water electrolyser technology in order to produce fully renewable, green and clean H<sub>2</sub>.

### II. RESULTS & DISCUSSION

#### A. Comparing CAPEX for PEM and alkaline electrolyzers

In a first stage, an attempt was made to complement the previous compilation effort of Task 33 with CAPEX data for alkaline water electrolyser, as the latter are today still considered to be the most mature and durable technology, especially for large-scale and long-term renewable H<sub>2</sub> production. CAPEX data are shown in Figure 2 as a function of power input, on a full electrolysis system level including the following components :

- Transformer(s), rectifier(s), control panel with PLC ;

Copyright © 2017

- Water demineralizer/deionizer ;
- Electrolyser stack(s) ;
- Gas analysers, separators and separating vessels ;
- Scrubber or gas purifier system & recirculating pump ;
- Dry piston compressor @ 15 bar (note that PEM systems are typically self-pressurising upto 20/50 bar).

From this graph, it is easily seen that alkaline electrolyzers are (much) more susceptible to CAPEX reduction upon scaling than PEM, especially for single stack systems. In particular, for alkaline systems, a CAPEX of 750 Euro/kW, considered to be critical for storage purposes, is already realistic today for a single stack 2 MW system. For PEM, such a critical CAPEX value should become within reach for 5 MW systems, probably requiring multi-stack systems as will be shown further below.

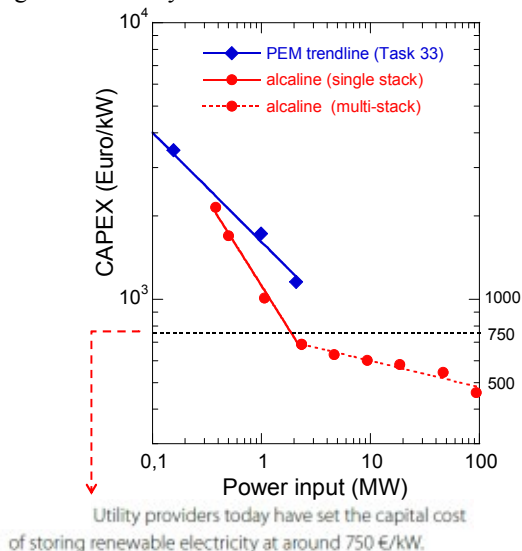


Fig. 2. CAPEX data for both PEM and alkaline electrolyzers, plotted as a function of power input. Data for alkaline systems are based on a single stack of 2.13 MW consisting of 230 cells, 2.6 m<sup>2</sup> in size. Note that the change in slope for alkaline electrolyzers corresponds to the use of multi-stack systems.

### B. Perspectives for further reduction in CAPEX (in Euro/kW)

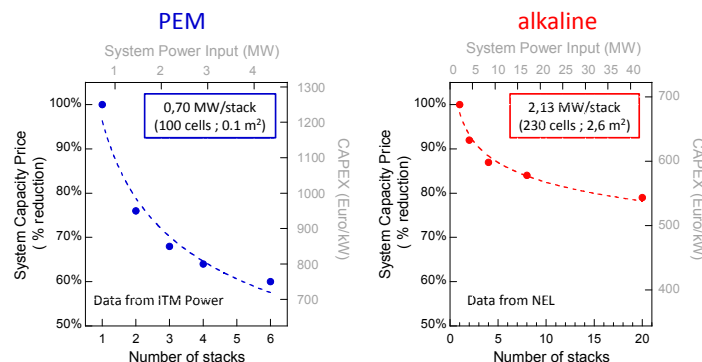


Fig. 3. Reduction in CAPEX upon use of multi-stack systems, both for PEM (left) and alkaline (right) electrolyzers.

Figure 3 gives some perspectives for further CAPEX reduction based on multi-stack systems, both for PEM (left) and alkaline (right). It is clearly observed that such a further reduction upon scaling is much more pronounced (on a relative % scale) for a multi-stack PEM design than for alkaline. However, in absolute terms, CAPEX values below 500 Euro/kW can be expected for alkaline systems when scaling up to 100 MW, based on an intelligent engineering design of a 40 stack system.

### C. Impact of CAPEX on electrolytic H<sub>2</sub> price (in Euro/kg)

Finally, based on the above CAPEX data, some projections can be made regarding price settings for electrolytic (i.e. renewable) H<sub>2</sub>. To this end, some simulations from the literature have been gathered in Table I. As can be expected, for setting a realistic H<sub>2</sub> price, other parameters beyond simply electrolyser CAPEX values intervene as well, including operating hours and (renewable) electricity cost. Nonetheless, it seems that an electrolytic H<sub>2</sub> price of less than 4 Euro/kg is very realistic by 2020, very much comparable to SMR H<sub>2</sub>.

TABLE I  
ELECTROLYTIC H<sub>2</sub> PRODUCTION COSTS ACCORDING TO VARIOUS SCENARIO'S

Scenario	1	2	3	4	5
CAPEX electrolyser (Euro/kW)	2000	800	800	800	800
Efficiency electrolyser	60%	80%	80%	80%	80%
Annual operating hours	7000	2000	1000	500	7000
Electricity cost (Euro/MWh)	70	70	140	0	60
Electrolytic H <sub>2</sub> price (Euro/kg)	7.0	6.1	12.2	10.5	3.7

source : AFHYPAC Fiche 3.2.1 (2015)

### III. CONCLUSIONS

At this stage of the IEA/HIA Task 38, the following major conclusions have been reached :

- For alkaline systems, a CAPEX of 750 Euro/kW, considered to be critical for storage purposes, is already realistic today for a single stack, 2 MW system ;
- For PEM, such CAPEX should become within reach for 5 MW systems, requiring multi-stack systems ;
- CAPEX values below 400 Euro/kW have been projected for alkaline systems, but this will require further upscaling upto 100 MW ;

Moreover, from the CAPEX data collected, it seems that a H<sub>2</sub> price of less than 4 Euro/kg is very realistic by 2020, very much comparable to SMR H<sub>2</sub>.

### ACKNOWLEDGMENTS

Participation of JP to the IEA/HIA Task 38 and the IEA/HIA ExCo is supported by the Public Service of Wallonia – Dept. of Energy and Sustainable Building.

Copyright © 2017

## MICROBIAL DESALINATION CELL CASCADE

I. Merino-Jimenez\*, Alexey Serov\*\*\*, C. Santoro\*\*\*, P. Atanassov\*\*\*, J. Greenman\*\*\* and I. Ieropoulos\*\*\*

\* Bristol BioEnergy Centre, Bristol Robotics Laboratory, University of the West of England, BS16 1QY (UK)

\*\* Biological, Biomedical and Analytical Sciences, University of the West of England, BS16 1QY (UK)

\*\*\* Department of Chemical & Biological Engineering, Center for Micro-Engineered Materials (CMEM), University of New Mexico, Albuquerque, NM 87131 (USA)

**Abstract** - Microbial desalination cell (MDC) offers a decentralized wastewater treatment solution as well as an energy-efficient saline water desalination system, which also produces electricity. However, several factors need to be optimised such as: i) the membrane materials properties; ii) overall power density output; and iii) increase of the desalination efficiency. This work focuses on the third part (iii). To enhance the desalination rate and improve the wastewater treatment, a system with 6 MDCs stacked in a cascade configuration has been tested. All three chambers had a volume of 33 mL with a cross-membrane area 25 cm<sup>2</sup>. The results showed that by cascading the MDCs the total desalination efficiency was substantially increased over 20% compared to that achieved from a single stage MDC, which is an excellent initial demonstration of the benefits of sequential treatment. As shown in this work, the MDCs cascade can be effectively optimised to achieve the desired desalination level whilst generating power. To the best of the Authors' knowledge, this is the first report in open literature that described the MDC cascade principles.

**Index Terms** – Microbial fuel cell, cascade effect, desalination, wastewater treatment.

### I. INTRODUCTION

MDC is a newly developed environmentally friendly technology, which integrates the microbial fuel cell (MFC) process and electrodialysis for wastewater treatment, water desalination and production of renewable energy [1]. It offers a great alternative to the energy demanding conventional methods, which only achieve 50 % recovery [2]. Higher amounts of electricity and improved wastewater treatment have been reported through MFC cascades [3], and so the objective in this study was to apply the cascade effect on desalination.

### II. MATERIALS AND METHODS

In order to increase the desalination rate of a saline solution of 30 g L<sup>-1</sup>, a total of 6 MDCs were assembled and set up in a cascade configuration, as that shown in Fig 1. Each MDC consisted of three chambers with an empty volume of 33 mL: anodic, middle (desalination) and cathodic chamber.

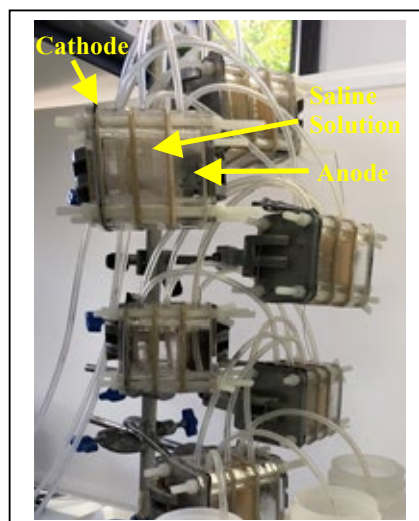


Fig. 1. Picture of the MDC cascade.

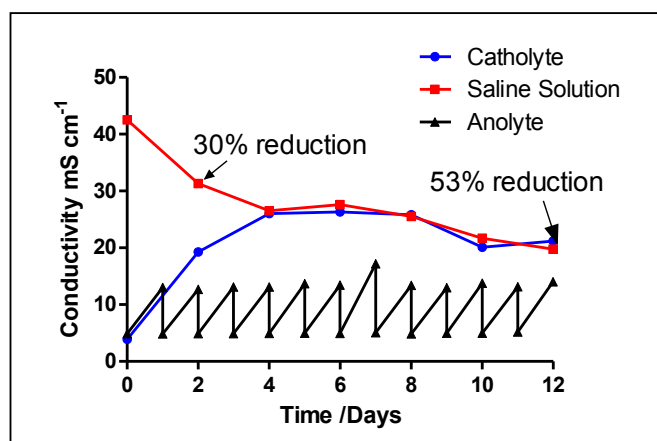
Anode and desalination chambers were separated by a cation exchange membrane (CEM, CMI-7000, Membrane International Inc, USA), whereas an anion exchange membrane (AEM, FumaTech FAA-3-50 50 µm, Germany) separated the



desalination and cathode chambers. The anode electrode consisted of carbon veil ( $20 \text{ g cm}^{-2}$ ) of  $270 \text{ cm}^2$  area folded. Fe-N-C catalyst was prepared using nicarbazin (NCB) as organic precursor by sacrificial support method (SSM) as previously reported [4]. The anodic chamber was fed 20 mM sodium acetate in wastewater, whereas the cathodic chamber contained sodium phosphate buffer (25 mM). The anolyte solution was replenished every day in order to maintain measurable amounts of power generation. The saline and catholyte solutions were replenished every second day for 12 days (6 cycles). The pH and conductivity of all the solutions were measured before and after each MDC. The power generated from the MDCs was calculated from the cell voltage, which was continuously monitored. All MDCs were running under 500 ohms load.

### III. RESULTS AND DISCUSSION

The changes in conductivity of the solutions used are shown in Fig. 2. A decrease in conductivity of  $11.2 \text{ mS cm}^{-1}$  was obtained after the first cycle. The desalination rate decreased to  $4.8 \text{ mS cm}^{-1}$  after the second cycle. The conductivity barely changed during the third cycle, probably due to the underperforming operation of that MDC. After that, the decrease in conductivity was constant  $2.61 \text{ mS cm}^{-1}$  per cycle, reaching  $19.9 \text{ mS cm}^{-1}$  at the end of the sixth cycle.



**Fig. 2. Conductivity of the three solutions in the MDCs changes along the cascade**

The conductivity of the catholyte solution increased from 3.91 to a maximum of  $26.3 \text{ mS cm}^{-1}$ . The anolyte solution also became more conductive, following the same pattern on a daily basis. The pH values of the saline solution and the catholyte increased from 6.7 and 8 to 8.1 and 9.1, respectively. On the contrary, the anolyte solution pH decreased by a factor of 0.5.

A total desalination of 53 % was achieved in this work. In theory and considering that the pattern followed after the third cycle would remain constant, the desalination could be complete by adding 8 MDCs to the cascade. However, that number could potentially be reduced by increasing the power output, decreasing the ohmic losses and improving the design.

Cao et al. reported 90% desalination in the first ever reported MDC [5] for a system in batch with anode, desalination and cathode chambers of 27, 3 and 27 mL capacity, respectively, part of a 100 mL recirculation system on either side, with the cathode consisting of ferricyanide. Although very high percentage of desalination was achieved with a salinity removal as high as  $30 \text{ g L}^{-1}$ , the volume of clean water obtained was very low (3 mL) and the absolute removal was approximately 0.09 g NaCl per batch. In the present study, the volume of all three chambers was equal (33 mL), achieving a total of  $20 \text{ g L}^{-1}$  salinity removal, with 0.65 g NaCl absolute removal. Despite desalinating a larger volume of water, the design of the MDCs must be further improved to achieve higher water volumes and higher desalination rates before it can be utilized at large scale.

### IV. CONCLUSION

For the first time, a cascade of MDCs has been tested showing promising results. The desalination achieved increased from 30 % to 53 % by cascading the MDCs. Moreover, the wastewater treatment was also increased whilst electricity was generated. The power generated per MDCs was approximately  $100 \mu\text{W}$  and that could be multiplied by electrically connecting the MDCs. The number of MDCs in cascade could be further increased to obtain an enhanced desalination.

### ACKNOWLEDGMENT

The authors would like to acknowledge the Bill and Melinda Gates Foundation for the financial support to this project under the grant no. OPP1094890 and OPP1139954.

### REFERENCES

- [1] Saeed, H.M., Hussein, G.A., Yousef, S., Sif, J., Al-Asheh, S., Fara, A.A., Azzam, S., Khawaga, R., Aidan, A., Microbial desalination cell technology: A review and a case study. *Desalination* 359, 2015, Pages 1-13.
- [2] MacHarg, J., Seacord, T. S., Sessions, B. Affordable Desalination Collaboration (ADC) baseline tests reveal trends in membrane performance. *Desalination Water Reuse* 18, 2008, Pages 2-10.
- [3] Ledezma, P.; Greenman, J.; Ieopoulou, I.; MFC-cascade stacks maximize COD reduction and avoid voltage reversal under adverse conditions. *Bioresour Technol* 134, 2013, Pages 158-165.
- [4] C. Santoro, A. Serov, S. Rojas Carbonell, L. Stariha, J. Gordon, K. Artyushkova, P. Atanassov. A family of Fe-N-C oxygen reduction electrocatalysts for microbial fuel cell (MFC) application: Relationships between surface chemistry and performances. *Appl. Catal., B.* 205, 2017, Pages 24-33.
- [5] Cao, X., Huang, X., Liang, P., Xiao, K., Zhou, Y., Zhang, X., Logan, B.R. A New Method for Water Desalination Using Microbial Desalination Cells. *Environ. Sci. Technol.* 2009, 43, 7148–7152.

**EFC17120**

# EFFECT OF LOAD CYCLE PROFILES ON DEGRADATION RATE OF A SOLID OXIDE ELECTROLYSER STACK

A. Olivier Thomann\*, B. Mikko Kotisaari\*, C. Dario  
Montinaro\*\* and D. Olli Himanen\*

\*VTT Technical Research Centre of Finland Ltd., Fuel Cells,  
Biologinkuja 5, FI-02150 Espoo, (Finland)

\*\*SOLIDPower SpA, Viale Trento 115/117, 38017  
Mezzolombardo, Trento, (Italy)

**Abstract** - Power-to-gas technology is expected to play an essential role in supporting the integration of large share of intermittent renewable electricity sources to the grid. For this purpose, power-to-gas technology needs to exhibit the capability of flexible operation to match weather-dependent production pattern. The present work focuses on the dynamic operation of a Solid Oxide Electrolyser (SOE) stack. Dynamic operation can cause thermal stress in the cells and stack components and thus reduce the lifetime of the electrolyser stack. However, there is a limited amount of published work on the load cycling of SOE stack and its effect on the degradation rate. Especially, there is little data available on the effect of the load cycle parameters such as the current ramp rate and the voltage setpoint. The present work evaluates the effect of different load cycle profiles on the degradation rate in steam electrolysis and co-electrolysis modes.

**Index Terms** - Durability, Hydrogen production, Load cycling, Solid Oxide Electrolysis Cell (SOEC).

## I. INTRODUCTION

The present work aims at answering the following questions: Can a SOEC stack withstand intermittent operation? How to quantify degradation related to the load cycling? Do cycling parameters (current ramp rate, plateau time) affect the degradation measurement?

## II. METHODS

The test object was a stack prototype manufactured by SOLIDpower. The stack had six planar hydrogen electrode supported cells and ferritic stainless steel interconnects coated with a  $\text{MnCo}_2\text{O}_4$  protective layer. A description of the stack and the test station and its instrumentation can be found in [1].

The test plan consisted of nine cycling conditions with different set of current ramp rate, plateau time, number of cycle and inlet gas composition as described in Table I. Before and after each load cycling conditions, the stack was kept 150 h in a stable condition. The inlet cathode gas composition in steam electrolysis (SE) consisted of 90%  $\text{H}_2\text{O}$  and 10%  $\text{H}_2$  and in co-electrolysis (C), of 65%  $\text{H}_2\text{O}$ , 25%  $\text{CO}_2$  and 10%  $\text{H}_2$ . All the experiment were conducted in a furnace kept at 750 °C.

TABLE I LOAD CYCLING (LC) TEST CONDITIONS

		Voltage condition	Current	N. of cycles	Plateau time	Duration	Current ramp
			A/cm <sup>2</sup>	#	min	h	A/min
LC1	SE	OCV-TNV	0-0.75	1500	0.5	40	1000
LC2	SE	OCV-TNV	0-0.75	150	10	150	3
LC3	SE	OCV-1.41	0-0.94	128	10	150	3
LC4	SE	OCV-TNV	0-0.75	447	10	150	1000
LC5	C	OCV-TNV	0-0.65	447	10	150	1000
LC6	C	OCV-TNV	0-0.65	164	10	150	3
LC7	C	OCV-TNV	0-0.65	8182	0.5	150	1000
LC8	SE	OCV-TNV	0-0.75	150	10	150	3
LC9	SE	OCV-TNV	0-0.75	21	700	514	3

## III. RESULTS AND DISCUSSION

The results are illustrated in Figure 1 where the voltage is plotted against test time. The degradation rates are listed in table II. *Degradation during steady-state* refers to the degradation prior to the load cycling condition.

The interpretation is made difficult because for an identical condition, the degradation rate of the stack is different depending on the cumulative test time. For example, in steady-state steam electrolysis, the degradation was recorded to be 50, 22, 6 or -2 mV/kh depending of the time during the test. This shows that the degradation is partly influenced by the testing history. The general trend of the stack voltage is a decrease of

Copyright © 2017

the degradation over time. This trend makes comparison of the degradation related to the load cycling difficult. Therefore, a correction of the degradation rate is proposed. The corrected degradation rate corresponds to the degradation rate during a load cycling condition minus the averaged degradation during the steady-state condition before and after the load cycling condition. The corrected values can be found in Table II. A few observations can be made:

- The degradation rates during load cycling are higher than in steady-state, however, the increase is limited. Over 11000 load cycles were performed, which caused a cumulated degradation of about 60 mV. That number of cycle would correspond to a stack that is load cycled every day for 30 years. This suggests that durability under load cycling is not a limiting factor to use such stack to an intermittent electricity source.
- Load cycling in co-electrolysis has similar corrected degradation rates compared to electrolysis of water only. This suggests that the stack tested is suitable for co-electrolysis operation in combination with intermittent renewable electricity source.
- High frequency of load cycling does not increase necessarily the degradation rate. When the stack was cycled over 8000 times in 150 h, the corrected degradation rate was about half compared to the value when it was cycled 450 times in 150 h (31 mV/kh (LC7) against 59 mV/kh (LC5)). This becomes obvious if the degradation is expressed in  $\mu\text{V}/\text{cycle}$ , with only 1  $\mu\text{V}/\text{cycle}$  when the stack was cycled 8000 times (LC7) against 20  $\mu\text{V}/\text{cycle}$  when cycled 450 times in the same amount of time. This shows that the load cycle profile chosen can have an effect on the degradation measured. In addition, the way degradation is expressed can affect significantly the results (mV/kh during load cycling or  $\mu\text{V}/\text{cycle}$ ).
- Very high ramp rate (1000 A/min) does not necessarily increase the degradation rate compared to slower ramp rate (3 A/min). The lower corrected degradation rates are found during the condition LC1 and LC7, which both uses the high ramp rate. However, if we compare the condition with longer plateau time (600s), using a faster ramp doubled the corrected degradation rate in steam electrolysis (see values for LC2 and 4). Conversely, in co-electrolysis the corrected degradation rate was not much affected by the change of ramp rate (59 mV/kh against 52 mV/kh). Therefore, a coherent relationship between the degradation rate and the current ramp rate cannot be establish with the data available.

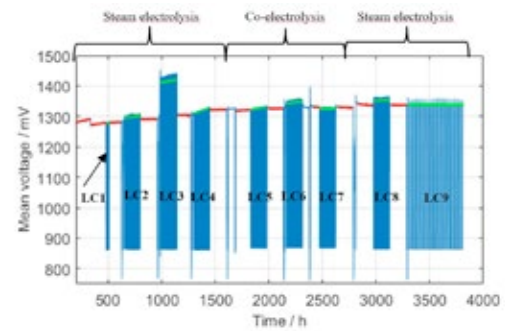


Fig 1 Average stack voltage against test time.

TABLE II DEGRADATION RATES

	Degradation during steady-state	Degradation during load cycling	Corrected degradation during load cycling	Corrected degradation per cycle
	mV/kh	mV/kh	mV/kh	$\mu\text{V}/\text{cycle}$
LC1	50	71	35	0.9
LC2	22	66	52	52.0
LC3	6	66	60	70.3
LC4	6	124	118	39.6
LC5	21	71	59	19.8
LC6	3	43	52	47.6
LC7	-21	15	31	0.6
LC8	-43	26	49	49.0
LC9	-2	-3	-1	-24.5

#### IV. CONCLUSIONS

A SOEC stack was extensively tested in load cycling conditions. It was found that load cycling increases to a limited extent the degradation, but the increase was acceptable considering the amount of load cycle performed (>11000 cycles). The effect of different load cycling profiles were also discussed. Successful co-electrolysis and load cycling experiments indicate that the tested type of stack is a suitable candidate for hydrogen and syngas production powered by intermittent electricity supply.

#### ACKNOWLEDGMENT

This research has received funding from the European Union's 7th Framework Programme (FP7/2007-2013) for the Fuel Cells and Hydrogen Joint Technology Initiative under grant agreement No 621173 and from the Horizon 2020 research and innovation programme under grant agreement No 731224.

#### REFERENCES

- [1] Kotisaari, M., et al. "Evaluation of a SOE Stack for Hydrogen and Syngas Production: a Performance and Durability Analysis." *Fuel Cells* (2016).

(EFC17121)

## DISTRIBUTED RELAXATION TIMES TECHNIQUE FOR THE DETERMINATION OF FUEL CELL LOSSES

Davide Papurello\*, Massimo Santarelli, Andrea Lanzini  
Department of Energy (DENERG), Politecnico di Torino, Corso  
Duca degli Abruzzi, 24, 10129, Turin, Italy.

**Abstract** - An equivalent circuit model was adopted to interpret the deconvoluted electrochemical impedance spectra of an NiYSZ/YSZ/GDC/LSCF solid oxide fuel cell obtained by varying the operating temperature and the oxygen partial pressure under a fixed load. This allowed to unfold the physicochemical processes occurring within the anode supported cell and to identify which elements are responsible for major polarisation losses. Furthermore, this model has proved to be effective even in the high frequency region, which is often beset by the onset of troublesome artifacts, as underlined by the comparison with the galvanic current interruption technique.

**Index Terms** - Complex non-linear least square (CNLS), Distributed relaxation times (DRT), Electrochemical impedance spectroscopy (EIS), Polarization resistances

### I. INTRODUCTION

In this work the adopted equivalent circuit is validated through experimental results under a wide range of temperature and oxygen partial pressures, as proposed in [1], and may be used to analyze in detail all the losses imputable to the electrodes and the electrolyte with the ultimate aim to improve the cell performance. However, differently from previous works approaching the same topic [2,3], this paper focuses on electrochemical impedance spectroscopy performed under load rather than at OCV. Thus attempting to provide valuable insight into specific mechanisms of solid oxide fuel cell in real applications, especially concerning the Oxygen Reduction Reactions at the Mixed Ionic Electronic Conductor. At the same time this paper wants to establish a comparison basis for future works based on SOFCs fed by syngas, for which the operating voltage plays an important role on kinetic reactions.

### II. MATERIAL AND METHODS

The SOFC analyzed in this work is an anode supported cell, made by Solidpower spa (Italy) with a circular shape with a surface area of 47 cm<sup>2</sup> composed of a cermet anode (Ni-YSZ 8% mol ) with a thickness of 240 μm, an MIEC cathode (La<sub>0.6</sub> Sr<sub>0.4</sub> Co<sub>0.2</sub> Fe<sub>0.8</sub> O<sub>(3-δ)</sub>) of 42 μm, a solid electrolyte (8% mol YSZ) of 8 μm and a buffer layer (Gd<sub>0.1</sub> Ce<sub>0.9</sub> O<sub>(2-x)</sub>) of about 4/5 μm. All the tests were carried out on the single planar cell and performed at the IN.TE.S.E laboratory (Innovation Technologies for Energy Sustainability)

of the Energy Department of Politecnico di Torino, as described also elsewhere [4–11].

### III. RESULTS

Cathode oxygen partial pressure and temperature dependencies

The evolution of the impedance spectra at the operating conditions listed in Table 1, shows the shift of the total ASR toward higher values with the reduction of the oxygen partial pressure as confirmed by the reduction of the cell voltage, at the operating point, in the Current-Voltage curves shown in Fig.1 and for all the tested oxygen partial pressure.

TABLE I  
OPERATING CONDITIONS FOR THE ASC UNDER ANALYSIS

Temperature	680/840 (ΔT=20)	°C
Cathode PO <sub>2</sub>	0.21/0.1/0.05/0.04	atm
Anode PH <sub>2</sub> O	0.15	atm
Load	255	mA cm <sup>-2</sup>

The impedance spectra are depicted in Fig.2. This obviously implies a reduction of cell performance as a consequence of the limited amount of oxygen available for the Oxygen Reduction Reaction. In fact, the widening of the arc, at low frequencies (right side of the figure), due to the corresponding reduction of the partial pressure suggests the occurrence of concentration polarizations phenomena in the cathodic porous electrode and since, with the temperature shift from 840 °C to 760 °C, the amplitude of the arc (on x and y-axis) increases slightly, the contribution of these losses, on the overall ASR, becomes increasingly lower. Contrariwise, the depressed arc, occurring at high frequencies, is not affected by this change in the gas mixture composition thus allowing to establish a relationship between this last and the anodic processes.

Copyright © 2017



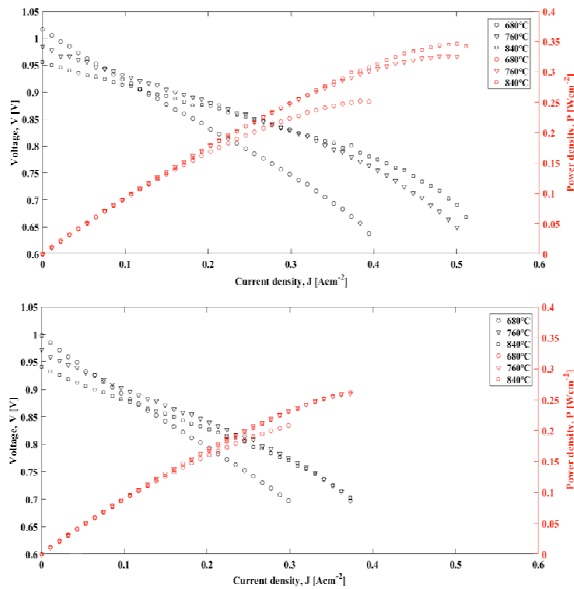


Fig. 1. Experimental C/V curve and power density determined for different temperatures and oxygen partial pressure of 0.21 – 0.04 atm.

Five main processes, reported in Table 2 (see Fig3), are distinguishable even if the interpretation of related changes are difficult to understand due to overlapping phenomena in the entire frequency range.

TABLE II

OPERATING CONDITIONS FOR THE ASC UNDER ANALYSIS

Process	Characteristic frequency	Electrode	Physical Meaning
P1A	>104 Hz	Anode	Oxygen ion transport
P2A	103-3×103 Hz	Anode	Charge transfer (TPB)
P1C	3×101-102 Hz	Cathode	Bulk diffusivity and oxygen exchange phenomena
P3A	4×10-1-6×10-1 Hz	Anode	Gas diffusion
P2C	4×10-2-7×10-2 Hz	Cathode	Gas diffusion only at low oxygen partial pressure

The reduction of the total ASR is clearly visible increasing the temperature as well as the ohmic resistances reduction and amplitude of the semi-depressed arc. The latter implies that the anode activation processes are thermally activated. An improvement of the cell performances with temperature is in fact also found in the experimental Current Voltage curves. However, for the arc in the low frequency region the anodic concentration contribution seems to remain almost unchanged. The processes previously identified by means of DRTs are present at all values of temperature. Increasing the temperature the relaxation frequencies of the processes are shift toward lower frequencies. This proves the energy activation of relaxation frequencies.

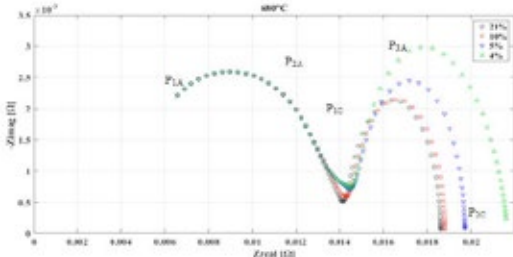


Fig. 2. EIS (0.1 Hz – 20 kHz) spectra obtained at different Temperature under different oxygen partial pressure in the frequency range 20 KHz-0.01 Hz.

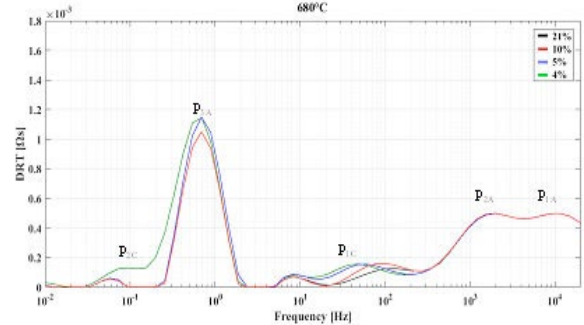


Fig. 3. DRT obtained at 680 °C corresponding to the EIS spectrum of Fig. 2.

#### IV. CONCLUSION

The electrochemical performance of an SOFC constituted by an LSCF electrode has been investigated at different cathode gas partial pressure and operating temperature not in OCV conditions. The five processes here identified have been unambiguously attributed to anode and cathode electrode phenomena and validated by comparing the trends of the relative resistances to the ones available from literature.

#### REFERENCES

- [1] E. Barsoukov, J.R. Macdonald, Impedance Spectroscopy: Theory, Experiment, and Applications, 2nd Edition, 2005.
- [2] Q. Huang, M. Liu, M. Liu, Impedance Spectroscopy Study of an SDC-based SOFC with High Open Circuit Voltage, Electrochim. Acta. 177 (2015) 227–236. doi:10.1016/j.electacta.2014.11.065.
- [3] A. Leonide, SOFC modelling and parameter identification by means of impedance spectroscopy, Karlsruhe, 2010.
- [4] D. Papurello, A. Lanzini, P. Leone, M. Santarelli, S. Silvestri, Biogas from the organic fraction of municipal solid waste: Dealing with contaminants for a solid oxide fuel cell energy generator, Waste Manag. 34 (2014) 2047–2056.
- [5] D. Papurello, A. Lanzini, D. Drago, P. Leone, M. Santarelli, Limiting factors for planar solid oxide fuel cells under different trace compound concentrations, Energy. 95 (2016) 67–78. doi:10.1016/j.energy.2015.11.070.
- [6] D. Papurello, A. Lanzini, S. Fiorilli, F. Smeacetto, R. Singh, M. Santarelli, Sulfur poisoning in Ni-anode solid oxide fuel cells (SOFCs): Deactivation in single cells and a stack, Chem. Eng. J. 283 (2016) 1224–1233. doi:10.1016/j.cej.2015.08.091.
- [7] D. Papurello, A. Lanzini, P. Leone, M. Santarelli, The effect of heavy tars (toluene and naphthalene) on the electrochemical performance of an anode-supported SOFC running on bio-syngas, Renew. Energy. 99 (2016) 747–753. doi:10.1016/j.renene.2016.07.029.
- [8] V. Chiodo, A. Galvagno, A. Lanzini, D. Papurello, F. Urbani, M. Santarelli, S. Freni, Biogas reforming process investigation for SOFC application, Energy Convers. Manag. 98 (2015) 252–258. doi:10.1016/j.enconman.2015.03.113.
- [9] D. Papurello, C. Iaffrè, A. Lanzini, M. Santarelli, Trace compounds impact on SOFC performance: Experimental and modelling approach, Appl. Energy. (2017) 0–1. doi:10.1016/j.apenergy.2017.09.090.
- [10] D. Papurello, E. Schuhfried, A. Lanzini, A. Romano, L. Cappellin, T.D. Märk, S. Silvestri, M. Santarelli, F. Biasioli, Proton transfer reaction-mass spectrometry as a rapid inline tool for filter efficiency of activated charcoal in support of the development of Solid Oxide Fuel Cells fueled with biogas, Fuel Process. Technol. 130 (2015) 78–86. doi:10.1016/j.fuproc.2014.09.042.
- [11] D. Papurello, L. Tognana, A. Lanzini, F. Smeacetto, M. Santarelli, I. Belcari, S. Silvestri, F. Biasioli, Proton transfer reaction mass spectrometry technique for the monitoring of volatile sulfur compounds in a fuel cell quality clean-up system, Fuel Process. Technol. 130 (2015) 136–146. doi:10.1016/j.fuproc.2014.09.041.



(EFC17122)

## WASTE TO ENERGY WITH AN SOFC GENERATOR SYSTEM - PILOT PLANT EXPERIMENTATION

Davide Papurello\*, Stefano Modena\*\*, Silvia Silvestri\*\*\*, Franco Biasioli\*\*\*, Daniela Bona\*\*\*, Luca Tomasi\*\*\*

\*Department of Energy (DENERG), Politecnico di Torino, Corso Duca degli Abruzzi, 24, 10129, Turin, Italy.

\*\*SolidPower Spa, V.le Trento 115/117, Mezzolombardo, TN 38017, Italy.

\*\*\*Fondazione Edmund Mach, Biomass and Renewable Energy Unit, Via E. Mach, 1, 38010 San Michele a/A, Italy.

**Abstract** - A dry anaerobic digester pilot plant was adopted to produce 0.5 - 1 Nm<sup>3</sup>/h of biogas from OFMSW. This biogas was processed, filtered and stored in bottled gas prior to feed the reformer and the SOFC stack generator. PTR-MS instrument was adopted as a Direct Injection Mass Spectrometry technique able to monitor rapidly and reliably the trace compounds contained in the biogas. Hydrogen sulfide and siloxane compounds were the most dangerous compounds for SOFC detected and monitored, with concentrations that range from 2 - 73 ppmv for H<sub>2</sub>S, and 100 - 400 ppbv for D4. A constant electrical power of 1900 W was achieved from the generator, with an electrical efficiency of 64% at nominal conditions.

**Index Terms** - SOFC, biogas, PTR-MS, Gas cleaning section

### I. INTRODUCTION

The conversion of biomass into energy can be attained through different technologies. Among them the anaerobic fermentation of organic matter has interesting aspects [1-3]. The most common anaerobic digestion (AD) biogas contaminants are sulfur compounds, terpene and carboxyl compounds [1]. These compounds affect strongly fuel cell performance [4-7]. A specific combination of impurity removal methods has to be used to ensure a fuel gas with the quality that meets the fuel cell tolerance defined by the manufacturer [3,8-11]. Two or at a maximum three steps are required: a primary clean-up step, in which a condenser and a first sorbent bed are inserted, followed by a fine guard bed before the biogas is delivered to the fuel cell system. The use of a condenser appears to be useful, essentially to remove water. The goal of the present work has been to build and to test an experimental pilot plant for energy production exploiting organic waste with SOFCs. Three main research sections on biogas exploitability are reported: (1) starting from biogas production from an OFMSW anaerobic dry digestion process through (2) a pilot gas cleaning section with commercial sorbents to feed (3) a 2500 Wel SOFC stack.

### II. MATERIAL AND METHODS

The anaerobic digester adopted for the biogas production was described elsewhere [1,3,10,12]. The biogas produced from organic waste was 0.5-1 Nm<sup>3</sup>/h. A gas cleaning section was built according to our previous work [12]. A Solidpower 2.5

kWe Engen was adopted and coupled to the experimental plant, see Fig. 1.

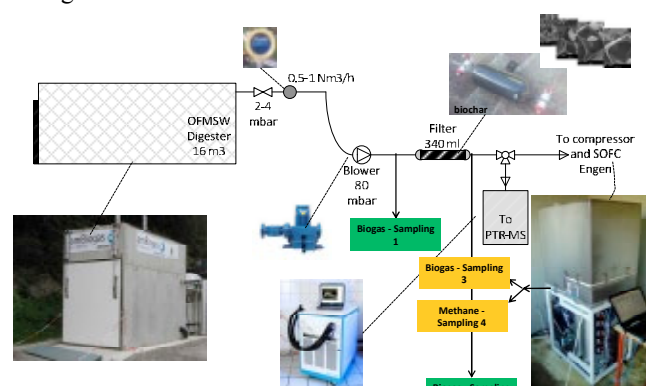


Fig. 1. Pilot plant – dry anaerobic digester of OFMSW, gas cleaning section, PTR-MS monitoring section, ENGEN SOFC stack.

### III. RESULTS

Trace compounds monitored along the biogas production process were analysed. Biogas produced has the following composition:

TABLE I  
BIOGAS COMPOSITION

Compound	Concentration range (ppmv)
Hydrogen sulfide	40-110
Butanethiol	10-80
2-butanone/butanal	0-800
2-Pentanone/Pentanal	0-30
p-Cymene	0-50
Monoterpenes	0-300
Toluene	0-900
D4	0.07-0.12

The main concentration is related to sulfur compounds, carbonyls, aromatic and terpenes. These concentrations are strongly reduced with the gas cleaning section. The sulfur concentration is about 100-500 ppbv, while carbonyls and carboxyls have a concentration around 0.75-3.5 ppmv. Terpenes and aromatic compounds have a concentration around 1 ppmv. Such biogas composition feed SOFC energy generator with a

Copyright © 2017

direct coupling. In the following figure is described the voltage produced; the steam to carbon ratio and fuel flow used. When the temperature is below 500 °C the fuel flow is switched from biogas to pure methane. The operating temperature was about 600 °C.

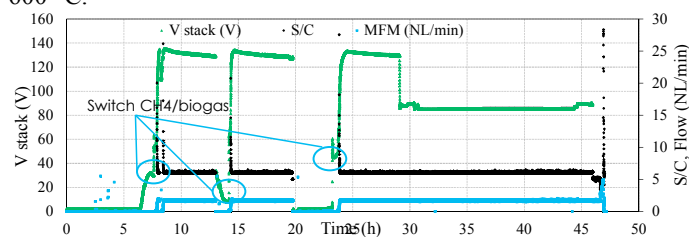


Fig. 2. Voltage, steam to carbon ratio and fuel flow of the ENGEN.

The voltage and power produced is quite stable along the process, except when the temperature of the stack decrease due to biogas composition and flow. The stable power produced was able to ensure an electrical efficiency around 64%.

#### IV. CONCLUSION

In this work the SOFC Engen (2.5 Kwe) was fed directly with the biogas produced treating organic waste. The electrical power produced was stable along the process for more than 50 h with an electrical efficiency of 64% and a temperature around 600 °C.

#### REFERENCES

- [1] D. Papurello, C. Soukoulis, E. Schuhfried, L. Cappellin, F. Gasperi, S. Silvestri, M. Santarelli, F. Biasioli, Monitoring of volatile compound emissions during dry anaerobic digestion of the Organic Fraction of Municipal Solid Waste by Proton Transfer Reaction Time-of-Flight Mass Spectrometry, *Bioresour. Technol.* 126 (2012) 254–265. doi:10.1016/j.biortech.2012.09.033.
- [2] D. Papurello, S. Silvestri, L. Tomasi, I. Belcari, F. Biasioli, M. Santarelli, Biowaste for SOFCs, *Energy Procedia*. 101 (2016) 424–431. doi:10.1016/j.egypro.2016.11.054.
- [3] D. Papurello, A. Lanzini, P. Leone, M. Santarelli, S. Silvestri, Biogas from the organic fraction of municipal solid waste: Dealing with contaminants for a solid oxide fuel cell energy generator, *Waste Manag.* 34 (2014) 2047–2056.
- [4] D. Papurello, A. Lanzini, P. Leone, M. Santarelli, The effect of heavy tars (toluene and naphthalene) on the electrochemical performance of an anode-supported SOFC running on bio-syngas, *Renew. Energy*. 99 (2016) 747–753. doi:10.1016/j.renene.2016.07.029.
- [5] D. Papurello, A. Lanzini, D. Drago, P. Leone, M. Santarelli, Limiting factors for planar solid oxide fuel cells under different trace compound concentrations, *Energy*. 95 (2016) 67–78. doi:10.1016/j.energy.2015.11.070.
- [6] H. Madi, A. Lanzini, D. Papurello, S. Diethelm, C. Ludwig, M. Santarelli, J. Van herle, Solid oxide fuel cell anode degradation by the effect of hydrogen chloride in stack and single cell environments, *J. Power Sources*. 326 (2016) 349–356. doi:10.1016/j.jpowsour.2016.07.003.
- [7] A. Lanzini, H. Madi, V. Chiodo, D. Papurello, S. Maisano, M. Santarelli, S.D.X. X, Dealing with fuel contaminants in biogas-fed solid oxide fuel cell (SOFC) and molten carbonate fuel cell (MCFC) plants: Degradation of catalytic and electro-catalytic active surfaces and related gas purification methods, *Prog. Energy Combust. Sci.* 61 (2017) 150–188. doi:10.1016/j.pecs.2017.04.002.
- [8] D. Papurello, L. Tomasi, S. Silvestri, M. Santarelli, Evaluation of the Wheeler-Jonas parameters for biogas trace compounds removal with activated carbons, *Fuel Process. Technol.* 152 (2016) 93–101. doi:10.1016/j.fuproc.2016.06.006.
- [9] D. Papurello, E. Schuhfried, A. Lanzini, A. Romano, L. Cappellin, T.D. Märk, S. Silvestri, M. Santarelli, F. Biasioli, Proton transfer reaction-mass spectrometry as a rapid inline tool for filter efficiency of activated charcoal in support of the development of Solid Oxide Fuel Cells fueled with biogas, *Fuel Process. Technol.* 130 (2015) 78–86. doi:10.1016/j.fuproc.2014.09.042.
- [10] D. Papurello, L. Tognana, A. Lanzini, F. Smeacetto, M. Santarelli, I. Belcari, S. Silvestri, F. Biasioli, Proton transfer reaction mass spectrometry technique for the monitoring of volatile sulfur compounds in a fuel cell quality clean-up system, *Fuel Process. Technol.* 130 (2015) 136–146. doi:10.1016/j.fuproc.2014.09.041.
- [11] D. Papurello, E. Schuhfried, A. Lanzini, A. Romano, L. Cappellin, T.D. Märk, S. Silvestri, F. Biasioli, Influence of co-vapors on biogas filtration for fuel cells monitored with PTR-MS (Proton Transfer Reaction-Mass Spectrometry), *Fuel Process. Technol.* 118 (2014) 133–140. doi:10.1016/j.fuproc.2013.08.011.
- [12] D. Papurello, A. Lanzini, L. Tognana, S. Silvestri, M. Santarelli, Waste to energy: Exploitation of biogas from organic waste in a 500 W solid oxide fuel cell (SOFC) stack, *Energy*. 85 (2015) 145–158. doi:10.1016/j.energy.2015.03.093.

## HIGHLY ACTIVE NITROGEN-DOPED MESOPOROUS CARBON FILM CATALYST FOR OXYGEN REDUCTION REACTION

Zhi-peng Yu<sup>a</sup>, Jin-hua Piao<sup>b\*</sup>, Panagiotis Tsiakaras<sup>c,d\*</sup>, Zhen-xing Liang<sup>a,\*</sup>

<sup>a</sup>Key Laboratory on Fuel Cell Technology of Guangdong Province, School of Chemistry and Chemical Engineering, South China University of Technology, Guangzhou 510641, P.R. China.

<sup>b</sup>School of Food Science and Engineering, South China University of Technology, Guangzhou 510641, P.R. China.

<sup>c</sup>Laboratory of Alternative Energy Conversion Systems, Department of Mechanical Engineering, School of Engineering, University of Thessaly, Pedion Areos, Volos 383 34, Greece.

<sup>d</sup>Laboratory of materials and devices for electrochemical power industry, Ural Federal University, 19 Mira Str., Yekaterinburg 620002, Russia.

Corresponding authors: E-mail: [zliang@scut.edu.cn](mailto:zliang@scut.edu.cn) (Z.X. Liang); E-mail: [tsiak@uth.gr](mailto:tsiak@uth.gr) (P. Tsiakaras).

**Abstract** - Nitrogen-doped mesoporous carbon (NMC) film is developed by using mesoporous silica film as hard template. The structure of silica template is finely tuned by systematically exploring the synthesis conditions. Salient findings are as follows: 1) graphene oxide (GO) is essential in deriving a thin silica film and 2) with hexadecyltrimethylammonium bromide (CTAB) as a co-template, mesopore are introduced through the plane of the silica film.

**Index Terms** - fuel cells; mesoporous silica film; nitrogen-doped mesoporous carbon nanosheets; oxygen reduction reaction.

### I. INTRODUCTION

In previous work, we have developed a co-operative assembly method with dual templates, *viz.* a non-ionic triblock copolymer (P123) and GO, to synthesize an ultrathin 2D semi-ordered mesoporous silica film [1-3]. It is found that hydrogen bonding in the tri-component system plays a key role in the co-operative assembly in generating the unique morphology. Now the question is how about the electrostatic force when using an ionic surfactant. Cetyltrimethylammonium bromide (CTAB); this is a cationic surfactant widely used as a template to direct the synthesis of ordered mesoporous silicas, like MCM-48 [4-5]. We supposed that the electrostatic interaction between cationic ammonium ions and the negatively charged GO will be effective in directing the ordered mesoporous structure. In line with this understanding, an ultrathin mesoporous silica film is synthesized with the aid of dual templates, (*viz.* GO and CTAB), which is then used as a template to synthesize NMC sheet. As an example of application, its electrocatalytic activity towards ORR is extensively investigated.

### II. RESULTS AND DISCUSSION

Figure 1 shows the small-angle X-ray diffraction (XRD) patterns. SiO<sub>2</sub>/GO-0 shows an excellent ordered pore structure of cubic crystallographic space group *Ia $\bar{3}d$* . The reflection peaks are gradually weakened and negatively shifted when increasing the GO concentration. The results indicate that the pore ordering degree gradually degrades and the pore size increases when adding the co-template GO, confirming the above analysis that GO plays a key role in co-operative assembly with silica and CTAB.

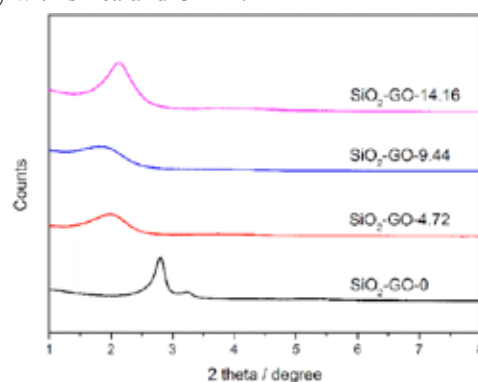


Figure 1. Small-angle XRD patterns of the synthesized SiO<sub>2</sub>/GO-*x* (*x*=0, 4.72, 9.44, 14.16 mg mL<sup>-1</sup>).

In one word, the above characterizations indicate that semi-ordered mesoporous silica film is successfully synthesized by using the dual templates.

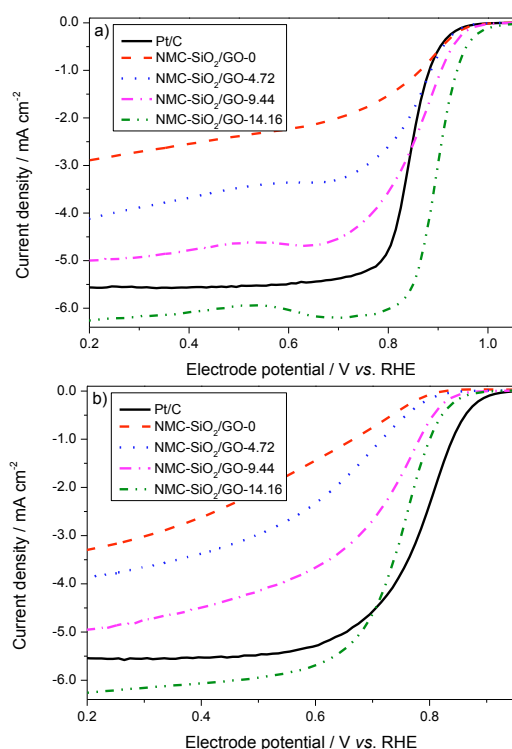
**Figure 2** shows the ORR polarization curves of the carbon catalysts. It is seen that in both media, the electrocatalytic activity is much better for carbon synthesized with the dual templates than the sole template. First, this result is due to the fact that the former ones have a much higher N dopant content and the  $C_{N-activated}$  content than the latter one. More importantly, the dual-template derived carbon features a 2D nanosheet morphology, which favors the exposure of the active sites and the mass transfer of the reactive species.

As a result, the active sites in 2D carbon nanosheet are more accessible and efficiently utilized in the electrode than in 3D carbon (*viz.* NMC-SiO<sub>2</sub>/GO-0).

For the three 2D carbon nanosheets, the electrocatalytic activity roughly follows the order of:

***NMC-SiO<sub>2</sub>/GO-4.72 < NMC-SiO<sub>2</sub>/GO-9.44 < NMC-SiO<sub>2</sub>/GO-14.16.***

Such a difference is rationalized as follows. First, the onset potential is found to be the same for all of the carbon catalysts, indicating that the chemical nature and the intrinsic activity of the active sites remain the same.



**Figure 2.** Oxygen reduction reaction polarization curves of the carbon materials: a) O<sub>2</sub>-saturated 0.10 M KOH solution; b) O<sub>2</sub>-saturated 0.10 M HClO<sub>4</sub> solution.

It is, thus, inferred that the difference in the polarization performance should solely be originated from both the content and its utilization efficiency of the active sites. It is noted that the order of the electrocatalytic activity agrees well with the change in the  $C_{N-activated}$  content and the specific surface area. As such, it is rationalized that the amount of active sites and

their accessibility synergistically result in the change of the overall electrochemical performance.

Finally, we noted that NMC-SiO<sub>2</sub>/GO-14.16 yields a much better activity than does the Pt/C catalyst by outperforming 60 mV in half-wave potential ( $E_{1/2}$ ) in alkaline media; while in acid media, its activity is comparable to Pt/C with 30 mV lower in  $E_{1/2}$ . The superior electrocatalytic activity makes this catalyst of practical interests for fuel cells.

### III. CONCLUSION

Nitrogen-doped mesoporous carbon (NMC) nanosheet is synthesized by a nanocasting method, in which semi-ordered mesoporous silica film is used as a template. Physical characterizations reveal that the NMC nanosheet features a high content of nitrogen dopant, an ultrathin thickness (1.5 nm) and high specific surface area (687 m<sup>2</sup> g<sup>-1</sup>), favoring both the catalysis and the mass transfer of the reactive species. Electrochemical tests confirm that the NMC nanosheet yields a superior oxygen reduction electrocatalytic activity, which is comparable or even better when compared with the commercial Pt/C catalyst.

### ACKNOWLEDGMENT

The work was jointly supported by the National Natural Science Foundation of China (Nos. 21676106, 21476087, 21576101), Science and Technology Program of Guangzhou (201704030065), National Key R&D Program of China (No. 2016YFB0101200 (2016YFB0101204)), and CAS Key Laboratory on Fuel Cells and Composite Electrochemical Power Sources.

Prof. Tsiakaras is also grateful to Ministry of Education and Science of the Russian Federation (Mega-Grant, contract no. 14.Z50.31.0001) for support.

### REFERENCES

1. Long GF., Wan K., Liu M.Y., Liang Z.X., Piao J.H., Tsiakaras P., Active Sites and Mechanism on Nitrogen-Doped Carbon Catalyst for Hydrogen Evolution Reaction, *Journal of Catalysis*, 348:151-159, 2017.
2. Wan K., Tan A.D., Yu Z.P., Liang Z.X., Piao J.H., Tsiakaras P., 2D Nitrogen-Doped Hierarchically Porous Carbon: Key Role of Low Dimensional Structure in Favoring Electrocatalysis and Mass Transfer for Oxygen Reduction Reaction, *Applied Catalysis B: Environmental*, 209:447-454, 2017.
3. Yu ZP, Piao JH, Liang ZX. Synthesis of 2D Nitrogen-Doped Mesoporous Carbon Catalyst for Oxygen Reduction Reaction, *Materials*, 10:197-203, 2017.
4. Wan K., Long GF., Liu M.Y., Liang Z.X., Tsiakaras P., Nitrogen-doped ordered mesoporous carbon: Synthesis and active sites for electrocatalysis of oxygen reduction reaction, *Applied Catalysis B: Environmental*, 165:566-571, 2015.
5. Alfredsson V, Anderson M. Structure of MCM-48 Revealed by Transmission Electron Microscopy, *Chem Mater.*, 8:1141-6, 1996

## LIFE CYCLE ASSESSMENT (LCA) OF A RESIDENTIAL SOFC SYSTEM FOR ENERGY PRODUCTION

A. Petrillo\*, F. De Felice\*\*, M. Minutillo\*, E. Jannelli\*, F. Zomparelli\*\*, Giuseppe Patanè\*\*\*

\*Department of Engineering, University of Naples Parthenope, Centro Direzionale, Naples, (Italy)

\*\*Department of Civil and Mechanical Engineering, University of Cassino and Southern Lazio, Cassino, (Italy)

\*\*\*Meridionale Impianti Spa, Via S. Simonetta 26/D - 20867 Caponago (MB) – (Italy), <http://www.merimp.com>

**Abstract** – Solid Oxide Fuel Cells (SOFCs) systems represent a new and alternative solution to conventional power generation systems. In this research LCA methodology has been applied to evaluate the environmental competitiveness of a specific type of SOFC with a conventional technology.

**Index Terms** – Comparative Analysis, LCA, SOFC, Residential use.

### I. INTRODUCTION



SOFCs offer many advantages over conventional methods of electrical generation, including higher efficiencies and lower emissions [1], [2], [3]. Nevertheless, there is still a need for research on SOFCs sustainability benefits. This research proposes the environmental impact associated with a SOFC m-CHP unit using a LCA method. LCA is a well-known tool which uses a systematic set of procedures for compiling and examining the inputs and outputs of materials and energy and the associated environmental impacts directly attributable to the functioning of a product or service system throughout its life cycle. ISO standards 14040 and 14044 have been used as framework and guidelines [4]. The novelty of the present work, in the framework of sustainability evaluations, is the comparative study of two specific systems that is ENGEN-2500 (SOFC) and DACHS G5.5 (ICE) in our regional context, located in Italy.

### II. LCA OF SOFC SYSTEM

#### A. Goal and scope definition

The goal of this LCA is to investigate the environmental performance of ENGEN-2500 system with a conventional technology or DACHS G5.5. The two analyzed systems are

shown in Figure 1. The functional unit has been chosen 1 kWh of electricity as produced by the SOFC system. System boundaries included: production, use and end of life phases.

	ENGEN-2500 (SOFC)	DACHS G5.5 (ICE)
		
$P_{EL, nom}$ [kWe]	2,5	5,5
$P_{TH, nom}$ [kWth]	2	14,7
$\eta_{EL}$ [%]	50	27
$\eta_{TH}$ [%]	40	72

**Fig. 1. Systems under study (ENGEN-2500 and DACHS G5.5)**

#### B. Inventory analysis

Data collection has been performed, including calculation and allocation procedures with SimaPro® v.8, using Ecoinvent® v.3 database. Whenever possible, primary data has been used; the rest of data have been provided as secondary data such as literature sources and expert's opinions [5], [6]. Figure 2 summarizes some inputs used for inventory analysis.

	ENGEN-2500 (SOFC)	DACHS G5.5 (ICE)
Natural gas from low pressure (<0,1 bar)	620 kg	1200 kg
Electricity low voltage (natural gas)	150 kWh	880 kWh

**Fig. 2. Example of Inventory Analysis**



Figure 3 shows a graphical representation of LCA model for ENGEN 2500 realized using Simap<sup>ro</sup>® V.8. Similarly, a graphical representation of LCA model for DACHS G5.5 has been realized.

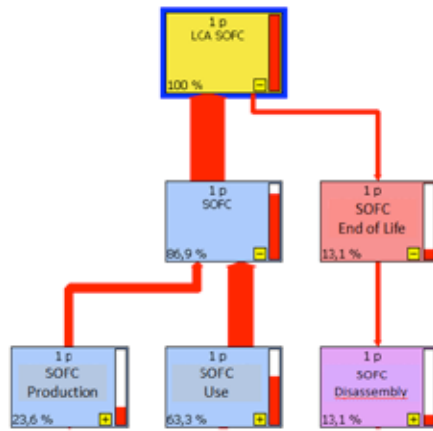


Fig. 3. LCA ENGEN-2500

### C. Impact assessment

Ecoindicator 99 method has been used for the assessment of environmental aspects [7]. It is an end-point approach which considers three damage categories: 1) human health (expressed as DALY - Disability Adjusted Life Years), 2) resources depletion and 3) ecosystem quality (expressed as the percentage of species that have disappeared in a certain area due to the environmental load). Figure 4 shows an example of LCA impacts assessment. Similarly, use and end of life phases have been evaluated.

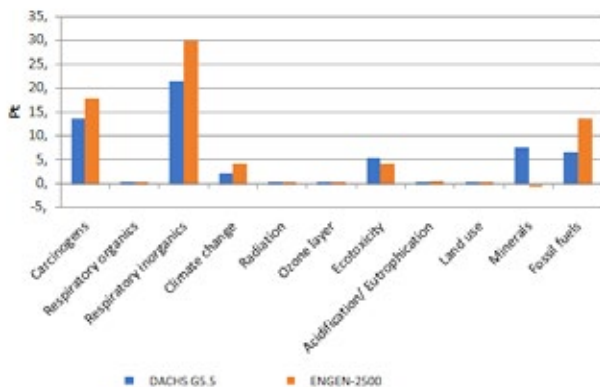


Fig. 4. LCA impacts assessment - production

### D. Results

Main results can be summarize as follows: 1) for SOFC system the critical phase is related to operation phase with 68% of the total impact, the second one is the production phase characterized by an impact of 23.6% and the third one is the end of life phase with a 13.1% of impact; 2) the life cycle analysis of the conventional system (ICE) shows that the most critical phase is operating with 67.8% versus 18.4% of the end

of life and 13.8% of production phase; 3) a comparison life cycles analysis has shown that the most critical environmental technology is the conventional system. This result is due to the use phase where conventional system impacts + 33% respect the SOFC system. However, it is worthy to note that for the SOFCs there are two critical issues. The first one concerns the use of large quantities of natural gas used during the operation phase. The second one is the use of chromium for stack production.

### III. CONCLUSION

The environmental impacts associated with an SOFC power generation system have been assessed quantitatively using the LCA method. The calculation results highlighted the need to identify technological solution to solve the environmental criticalities and to improve the environmental performance of SOFCs. Furthermore, future research will investigate a combination of Life Cycle Assessment (LCA) and Life Cycle Costing (LCC) in order to evaluate both potential environmental impacts and potential costs.

### ACKNOWLEDGEMENT

This research was funded by University of Naples Parthenope, "Bando di sostegno alla ricerca individuale per il triennio 2015-2017. Annualità 2015" and by the Italian Government, PON project "Fuel Cell Lab – Innovative systems and high efficient technologies for polygeneration – PON03PE\_00109.

### REFERENCES

- [1] Staffell, I., Ingram, A., Kendall, K., Energy and carbon payback times for solid oxide fuel cell based domestic CHP. *Int J Hydrog Energy* 2012;37:2509–23.
- [2] Strazza, C., Del Borghi, A., Costamagna, P., Traverso, A., Santin, M., Comparative LCA of methanol-fuelled SOFCs as auxiliary power systems on-board ships. *Appl Energy* 2010;87(5):1670–8.
- [3] Singhal, S.C., Solid oxide fuel cells: past, present and future. *Green Energy Technol* 2013;55:1–23.
- [4] ISO 14040:2006. Environmental management and life cycle assessment e principles and framework.
- [5] Borglum, B., Development of solid oxide fuel cells at versa power systems. In: *Proceedings of Fuel Cell Seminar*; 2009 November 17. Palm Springs, California, U.S.
- [6] Karakoussis, V., Brandon, N.P., Leach, M., van der Vorst R., The environmental impact of manufacturing planar and tubular solid oxide fuel cells. *Journal of Power Sources*, 101, 1:10–26.
- [7] PRé-Consultants, 2000. The Eco-indicator 99 Technical Report. Amersfoort, The Netherlands: PRé Consultants.

# A TECHNO-ECONOMIC AND ENVIRONMENTAL ANALYSIS OF AN INNOVATIVE IRON-LANTHANUM CHEMICAL CONVERSION COATING PROCESS FOR IT-SOFC STEEL INTERCONNECTS

Andi Mehmeti\*, Andrea Masi\*\*, Stefano Frangini\*\* and Stephen McPhail\*\*

\*Parthenope University of Naples, Centro Direzionale Isola C4, 80143, Naples, Italy

\*\* ENEA, Casaccia Research Center, Via Anguillarese 301, 00123 Rome, Italy

**Abstract** – This study conducts a streamlined environmental and economic analysis of a novel protective coating method for IT-SOFC steel interconnects. The quantification of life-cycle environmental indicators stresses that reduction of materials is of a crucial ecological relevance. The primary driver of the overall environmental footprint is lithium carbonate, accounting approximately for 40% of total impacts. The impacts due to energy are less significant. Regarding economic analysis, quantified results show that method is characterized by appealing costs, thus suggesting the economic validity and further development of the technique. Further life-cycle thinking analysis is needed to identifying areas of potential improvement to and compare with other methods in a cross-sectional analysis.

**Index Terms** - SOFC, perovskite coatings, interconnects, LCA

## I. Introduction

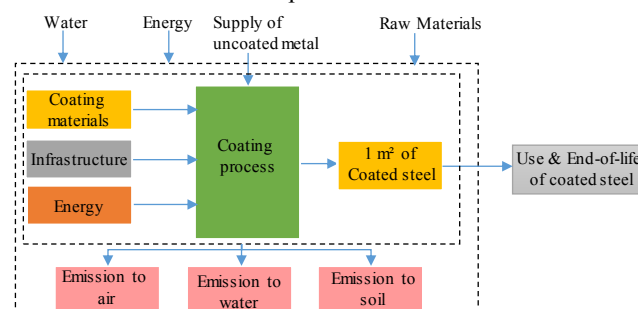
Development of functional coatings and barrier layer materials are necessary for improving the long-term functionality of Solid Oxide Fuel Cells metallic interconnects and thereby of the system electro-chemical performance [1]. Among various coating methods, chemical conversion techniques are widely used in industry as simple and cost-effective surface treatments, requiring minimal surface preparation or consolidation post treatments. Hence, they may represent a promising strategy to passivate stainless steel interconnects at low manufacturing costs. However, a life-cycle approach combining environmental and cost assessment should be taken into account to reveal the sustainability of a product or service without disregarding any burden shift [2]. Such accurate information based on life cycle impacts is needed to lead policymakers and consumer decisions. This paper address both the economic and environmental issues of a novel protective coating method for IT-SOFC steel interconnects. The technique allows to chemically transform the stainless steel surface into a La-Fe perovskite-based conversion coating through an alkaline molten carbonate dip treatment [3,4]. An attributional Life Cycle Assessment (LCA) was employed to primary environmental impacts and assess the overall footprint. The outcomes are addressed to researchers in the field of fuel cells to facilitate the exchange of technical information and have a

better understanding of the implications of novel coating techniques.

## II. MATERIALS AND METHODS

### A. Environmental analysis

This study investigates the environmental impacts of corrosion protection coatings, from the raw material production through coating formulation, production, and transport, as well as their application (Figure 1). The scope only includes the coating system and associated operations, thus, it does not include the manufacture of the downstream final products (steel substrate) or their use, since they are modeled by the downstream user of the steel products.



**Figure 1. System boundaries and life cycle stages of the study**

The defined functional unit (FU) is a coating of 1 m<sup>2</sup> area – 0.5 μm thickness coating surface of the coated metal substrate. The inputs (scaled to the defined FU) to the coating process are presented in Table 1.

TABLE I. Inventory data for coating deposition.

Input	Unit	Thin coating	Price (€/Kg)
Sodium carbonate (Na <sub>2</sub> CO <sub>3</sub> )	kg/m <sup>2</sup>	0.449	15
Lithium carbonate (Li <sub>2</sub> CO <sub>3</sub> )	kg/m <sup>2</sup>	0.337	45
Magnesium Oxide (MgO)	kg/m <sup>2</sup>	0.035	170
Lanthanum oxide (La <sub>2</sub> O <sub>3</sub> )	kg/m <sup>2</sup>	0.043	350
Electricity (Grid RER)	kWh/m <sup>2</sup>	0.648	0.15

The primary data were retrieved from experimental procedures,

while background data was modeled using LCA databases. The impact assessment was run on SimaPro tool using ReCiPe method (mid-point Hierarchist perspective).

### B. Economic analysis

The price of chemicals taken as reference for the estimate of the salt cost is presented in Table 1. Overall the final cost is analyzed in four distinct categories: the capital cost (CC) of manufacturing equipment, the direct cost of material, energy and labor, maintenance cost (5% of CC), and the final cost of interconnect finished.

## III. RESULTS AND DISCUSSION

Table 2 present the environmental profile for chemical conversion method. Primary impacts which can be directly attributed are global warming (GWP), toxicity, ionizing radiation and resource depletion (mainly fossil fuel). The GWP results of this study are dominated by raw materials (lithium carbonate and lanthanum oxide) and to a lesser extent electricity consumption (Figure 2).

Table II. Quantified mid-point environmental impact indicators for coating.

Impact category	Indicator
Climate change (kg CO <sub>2</sub> eq/m <sup>2</sup> )	2.89E+00
Ozone depletion (kg CFC-11eq/m <sup>2</sup> )	2.79E-07
Terrestrial acidification (kg SO <sub>2</sub> eq/m <sup>2</sup> )	1.32E-02
Eutrophication (kg Peq/m <sup>2</sup> )	5.48E-03
Toxicity (kg 1,4-DBeq/m <sup>2</sup> )	1.32E+00
Photochemical oxidant formation (kg NMVOC/m <sup>2</sup> )	7.79E-03
Particulate matter formation (kg PM10eq/m <sup>2</sup> )	4.88E-03
Ionising radiation (kBq U235eq/m <sup>2</sup> )	6.52E-01
Land Occupation (m <sup>2</sup> a/m <sup>2</sup> )	1.51E-01
Natural land transformation (m <sup>2</sup> a)	3.03E-04
Water depletion(m <sup>3</sup> /m <sup>2</sup> )	1.03E-01
Metal depletion(kg Feeq/m <sup>2</sup> )	2.06E-01
Fossil depletion(kg oil/m <sup>2</sup> )	7.17E-01

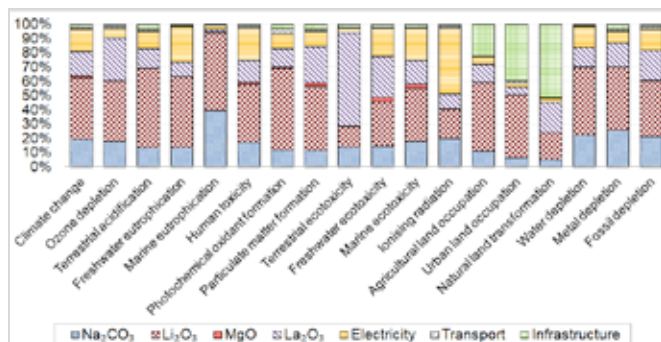


Fig. 2. Breakdown of resource impacts for each environmental category

The influence of transport is negligible with less than 2% share for all impact categories, while infrastructure accounts from 1 to 56.3 % (land occupation and transformation). The analysis of the environmental impact assessment is affected by different assumptions in the inventory data, especially for salt-life time (considered only for 200 treatments). For example, longer exploitation of the salt (e.g. by 25%) and use of cheaper

technical grade chemicals could reduce the GWP by more than 15% and the other environmental effects due to the lifetime prolongation and a higher number of treatments.

Table 3 present the economic evaluation of coating process. Capital cost is responsible for 67% of total cost. Among the different cost items in operation, a large part of the cost would be ascribable to the salt. The coating cost per interconnect [5] range from 1.65 € (aerosol) to 2.65 € (plasma), thus showing that the passivation method may be characterized by appealing costs.

Table III. Coating cost using chemical conversion method.

Category	Chemical conversion
Cost (€/m <sup>2</sup> )	129.1
Coating cost per interconnect (€/part)	1.93
Coating Cost per Kilowatt (€/kW)	7.71

## IV. CONCLUSION

This pilot study has quantified the principal environmental impacts of an innovative iron-lanthanum chemical conversion coating process for IT-SOFC steel interconnects. The quantification of life-cycle environmental indicators stress that reduction of materials is of a crucial ecological relevance. By far the most effective opportunity to further reduce the environmental footprint of chemical coatings lies in the reduction of materials, followed by optimization of energy usage. Empirical cost and performance data show that initial costs are comparable with other coating methods, thus proving the validity of the method. Hence, further environmental life-cycle thinking analysis are needed to identifying areas of potential improvement to and compare with other methods in a cross-sectional analysis.

## ACKNOWLEDGMENT

The study has been developed within the FCH-JU funded Project SCoReD2.0 (Steel Coatings for Reducing Degradation in SOFC).

## REFERENCES

- [1] Shaigan, N., Qu, W., Ivey, D. G., & Chen, W. (2010). A review of recent progress in coatings, surface modifications and alloy developments for solid oxide fuel cell ferritic stainless steel interconnects. *Journal of Power Sources*, 195(6), 1529-1542.
- [2] Finkbeiner, M., Schau, E. M., Lehmann, A., Traverso, M., Towards life cycle sustainability assessment. *Sustainability*, 2(10), 2010, pp 3309-3322.
- [3] S. Frangini, A. Masci, F. Zaza, Molten salt synthesis of perovskite conversion coatings: A novel approach for corrosion protection of stainless steels in molten carbonate fuel cells, *Corrosion Science*. 53 (2011) 2539–2548.
- [4] Masi, A., Frangini, S., Carlini, M., Masci, A., McPhail, S, Evaluation of a novel perovskite-based conversion coating for corrosion protection of 13Cr ferritic stainless sheets of steel under relevant SOFC oxidizing conditions, *ECS Transactions* 68, no. 1, 2015, pp 1625-1632.
- [5] Seabaugh, M., Beachy, M., Ibanez, S., Kimbrell, R., Day, M., Thrun, L., Swartz, S, Manufacturing analysis of SOFC interconnect coating processes." In 11 Th Annual SECA Workshop, Pittsburgh, PA. 2010.

## DEVELOPMENT OF HIGHLY DURABLE NI-YSZ BASED SOFC ANODE BY USING INFILTRATION TECHNIQUE

S.B. Lee<sup>\*,\*\*</sup>, M. S. Khan<sup>\*,\*\*</sup>, R.H. Song<sup>\*,\*\*</sup>, J.W. Lee<sup>\*,\*\*</sup>,  
T.H. Kim<sup>\*,\*\*</sup>, S.J. Park<sup>\*,\*\*</sup> and J.E. Hong<sup>\*,\*\*</sup>

\* Fuel Cell Research Center, Korea Institute of Energy Research,  
Republic of Korea

\*\* Department of Advanced Energy Technology, University of  
Science and Technology, Republic of Korea

*Ni grain growth in Solid Oxide Fuel Cell (SOFC) anodes is one of the major causes of performance degradation. to overcome Ni(OH)<sub>2</sub> formation, some transition metals (Fe, Cr and Co) are infiltrated into the anode. These metals have lower Gibbs Free Energy for the formation of their corresponding hydroxides as compared to Ni(OH)<sub>2</sub>. Therefore, it was hypothesized that these metals can act as sacrificial anodes for Ni by evaporating from the anode and hence retarding the Ni grain growth and its loss. Triple phase boundary (TPB) density was calculated by image analysis techniques before and after operation. A clear relation was found between ASR change rate determined from electrochemical measurements and TPB density change rate calculated from image analysis.*

### I. INTRODUCTION

Solid Oxide Fuel Cells (SOFCs) are the future energy devices for efficient conversion of chemical energy into electrical energy. These energy materials have been demonstrated to perform well on laboratory scale as well as small and portable devices over the past few years. However, high cost and degradation of their components are still the two main issues in their commercialization. Therefore, several studies are being carried out to reduce their cost and improve the life time for practical applications, which has been assigned to be 20,000h for mobile while 40,000h for stationary applications [1].

The objectives of this study were to develop some methods in order to inhibit the Ni grain growth during the long term operation of SOFCs. To retard the evaporation of Nickel in the form of Nickel hydroxide Ni(OH)<sub>2</sub>, transition metals such as Fe, Cr and Co were added into Ni-YSZ anodes. These metals can act as sacrificial anodes for Ni, because of lower Gibbs Free Energy values for the formation of their corresponding volatile hydroxides as compared to Ni(OH)<sub>2</sub>. The transition metals were

added to porous Ni-YSZ anode scaffold by infiltration method. Nano-sized particles were sporadically dispersed on the Ni-YSZ surface, confirmed by Scanning Electron Microscopy (SEM). X-Ray Diffraction (XRD) patterns show a very good chemical compatibility between the added metals and Ni-YSZ anodes. Symmetric cells were then prepared and the Area-Specific Resistance (ASR) was monitored at 1000 °C, with a fuel gas containing 25vol% H<sub>2</sub>, 75vol% N<sub>2</sub>, for more than 250h. To control accelerated evaporation condition of anode, relative humidity in anode gas was fixed at 12%. The difference in the amount of the added metal before and after long-term test was determined by EDS analysis. Change in the grain size distribution of Ni particles and TPB density, before and after long term test, were calculated by image analysis. Well-defined relations were obtained among ASR change rate determined from electrochemical measurements and grain size distribution and TPB density change rate calculated from image analysis.

### II. EXPERIMENTAL

A powder mixture containing 60 wt% NiO and 40 wt% YSZ (Fuel Cells Materials, USA) was ball milled with ethanol for 48 hrs. After drying and sieving, the powder was mixed with a solvent ( $\alpha$ -terpinol) and a binder (mixture of  $\alpha$ -terpinol and ethyl cellulose) to produce AFL paste (53% solid loading). This paste was then symmetrically screen printed on YSZ substrate (Fuel Cells Materials, USA) and subsequently pre-heated and sintered, respectively, at 350 °C for 3 h and 1350 °C for 5 h in air. The effective area of sintered AFL was 1 cm<sup>2</sup> and 15-25  $\mu$ m thick. After sintering, the AFL was subjected to infiltration using 0.5M solutions of precursor salts Cr(NO<sub>3</sub>)<sub>3</sub>.9H<sub>2</sub>O, Co(NO<sub>3</sub>)<sub>3</sub>.6H<sub>2</sub>O and Fe(NO<sub>3</sub>)<sub>3</sub>.9H<sub>2</sub>O. 0.3g of Triton X-100 was

Copyright © 2017



added in these solutions to reduce their surface tension and improve the wettability. A vacuum pressure of 0.1atm was applied to infiltrate the solution in between the pores of AFL. The samples were then heated at 110 °C to evaporate excess water. Five consecutive infiltration steps were carried out to get a fine distribution of particles throughout the microstructure. Decomposition of the nitrate salts was finally carried out at 350 °C for 2h. The heating and cooling rates used in all the experiments were 100 °C/min.

### III. RESULTS

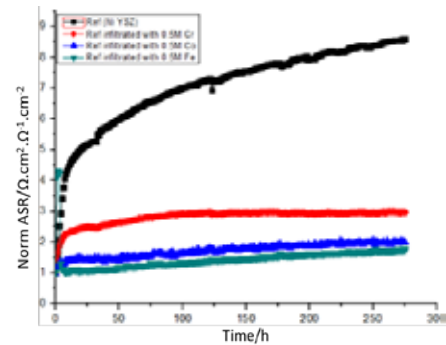
The cell studied in our case is symmetric anode material on electrolyte support. Therefore, the total ASR can be ascribed as the sum of various resistances such as internal resistance of AFL, contact resistance between electrode and current collector and internal wires resistance. In this study we are trying to determine the ASR change rate due to metal particles addition. Therefore, we defined a parameter “Normalized ASR” which is the ratio of instantaneous value of ASR to its initial value. This parameter sets the initial value to 1 and then determines the total corresponding change after the long term test.

The Normalized ASR graph for conventional as well as the infiltrated anodes is provided in Fig. 1. This graph clearly demonstrates the effect of metal addition as well as the effect of humidity on the long term performance of anode. The value of humidity was fixed at 12% during the long term exposure of samples. It has been observed that the metal infiltrated anodes exhibit much better long term performance as compared to conventional Ni-YSZ anode, by showing much lower values of ASR even after 250h. However, all of the anodes including the conventional Ni-YSZ anode demonstrate the same kind of behavior i.e. a much faster increase in ASR during the initial stages but a slow increase and relatively stable behavior at the longer times.

Total ASR change rate was calculated as the difference between the final and initial normalized ASR values divided by the total time of experiment. Table.1 compares these changes in ASR values for reference as well as infiltrated anodes. From the table also, it is evident that the anodes infiltrated with metal particles are showing relatively better performance as compared to reference Ni-YSZ anode. 0.5M  $\text{Fe}(\text{NO}_3)_3 \cdot 9\text{H}_2\text{O}$  infiltrated anode is showing an ASR increasing rate of 0.00633/h, at 1000 °C which is lowest among all the infiltrated anodes tested. Similarly, Ref (Ni-YSZ) is showing the highest value of ASR change rate of 0.03123/h, at the given operating conditions.

Image analysis shows that Grain size distribution has shifted towards the larger values, while the TPB density has decreased, after the long term test at 1000 °C for 275h. Introduction of humidity in the fuel has resulted in the formation of larger grains which ultimately result in lower TPB density. However, the introduction of metal particles has significantly improved the long term performance stability of Ni-YSZ anode. As formulated

in our hypothesis, they have formed their hydroxides and have evaporated from the anode, thus preventing  $\text{Ni}(\text{OH})_2$  formation. This evaporation behavior is quite clear from the EDS analysis results, which also show a significant reduction in the amount of metals concentration after the long term experiment. In this way, they have retarded the Ni grain growth, by evaporation-condensation mechanism, to a significant level and helped in maintaining higher TPB density during the long term operation. The higher value of TPB length or density provides more reaction sites which ultimately results in reduction in ASR magnitude.



**Fig. 1. Normalized ASR behavior for Ref. Ni-YSZ sample and infiltrated samples**

### IV. CONCLUSION

During the normal SOFC operating conditions, a much lower humidity is produced on the anode side. The added particles can sustain in the anode for a long time because of lesser reactions due to lesser amount of  $\text{H}_2\text{O}$ . Therefore, it can be concluded that infiltrated metal particles, can increase the cell life for a considerable amount of time, before they are completely vaporized from the anode.

### REFERENCES

- [1] Li. X, (2006), Principles of fuel Cells, New York: Taylor & Francis Group, NY 10016.
- [2] M.S. Khan, S.B. Lee, R.H. Song, J.W. Lee, T.H. Lim, S.J. Park, Effect of infiltrated transition metals on nickel morphology change and area-specific resistance of Ni-YSZ based SOFC anode during long-term operation, Journal of Electroceramics, Volume 35, 2015, pp. 81-89.



## ECONOMIC ANALYSIS OF A SUSTAINABLE ENERGY CHAIN BASED ON RENEWABLE HYDROGEN AND FUEL-CELL-POWERED BICYCLES.

A. Forcina\*, M. Minutillo\*, A. Lubrano Lavadera\* , N. Jannelli\*, A. Prigiobbo\*\*

\* Department of Engineering - University of Naples "Parthenope", Naples

\*\* COELMO Spa, Via delle Industrie, 278 Agglomerato Industriale ASI, Acerra - Naples, (Italy), <http://www.coelmo.it>

**Abstract** - The proposed study aims to analyze, from an economic point of view, a sustainable energy chain based on a solar-driven electrolysis system that produces renewable hydrogen used as fuel in fuel-cell-powered bicycles proposed for a bike sharing system. Starting from an energetic analysis previously performed, this study is devoted to demonstrate that the proposed sustainable energy chain is able to create value by providing a competitive service. The proposed economic analysis has been divided into two sections. The first section consists in the cost assessment of the facility in order to determinate hydrogen production cost, independently from its final usage, and the second one consists in analyzing the bike-sharing system cost. By matching the results of this economic analysis, the minimum bike rent price, necessary to balance out either the bike-sharing system and the overall system cost, has been assessed.

**Index Terms** – Bike sharing, economic analysis, fuel cell, hydrogen production, sustainable energy chain.

### I. INTRODUCTION

Hydrogen-mobility, through the use of bicycles, might contribute to reduce pollution in urban areas, and the development of a bike-sharing scheme might contribute to solve traffic congestions. Furthermore, if hydrogen is produced by renewable energy sources the proposed mobility is completely eco-friendly and sustainable. In this scenario, a novel more efficient electric bicycle, in which the battery is replaced by a fuel cell system that generates electric power by using hydrogen as primary energy, can be an attractive solution [1,2].

### II. ENERGY CHAIN DESCRIPTION

In this study, the attention has been focused on a solar-driven electrolysis system to produce renewable hydrogen to power electric bicycles involved in a bike-sharing project proposed in

a Southern Italy tourist place. The proposed sustainable energy chain is organized in the following sections:

**Hydrogen production:** The PV power plant is grid connected and the grid is used as a “storage” unit to control and stabilize the electric energy production due the solar fluctuations.

The annual amount of the electricity supplied from the grid is assumed equal to the electricity exported to the grid (surplus). Thus the hydrogen production can be considered as a “fully renewable production”.

**Storage facility:** The storage facility consists of: a) a rectifier; b) a control unit; c) an UPS (uninterruptible power supply); d) a demineralization unit e) a hydrogen compression unit; f) high pressure vessels (at 420 bar).

**Hydrogen transportation system:** The hydrogen production and storage facility make hydrogen available at high pressure (420 bar) in order to minimizing costs and dimensions.

The hydrogen is then used as fuel in two different vehicles: 1) the hydrogen van (Hy-van), for transporting the metal hydride cartridges, that are used as storage system in the Hy-bike, from the hydrogen production site to the docking stations, according to the bike sharing program; 2) the Hy-bike.

**Hydrogen bike and sharing program (BSP):** The bike sharing system provides a number of 75 bicycles. Penisola Sorrentina, in Italy, has been chosen for a feasibility study, since the natural topography of the territory.

Docking stations will be installed in five hotels, one for each of the five Municipalities involved in the project.

Figure 1 shows a schematic of the proposed energy chain.

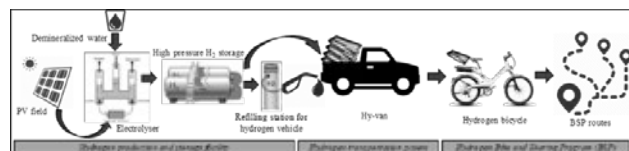


Fig. 1. Hydrogen renewable hydrogen chain graphic scheme

### III. ECONOMIC ANALYSIS

An economic analysis has been performed to evaluate the cost effectiveness of the proposed model, highlighting both critical cost components and areas to improve.

In the proposed analysis, as first step, the hydrogen production cost has been calculated independently from its final usage. The analysis is based on the following assumptions:

- The lifetime of the hydrogen production facility is 20 years;
- Money value discount rate (i) is 1%;
- Cost assessment includes capital, replacement, operating and maintenance and money costs.

The assumed costs are not taken from literature, but are based on real market offered prices (Italian market). Prices can strongly vary depending on each Country and, therefore, it is important to particularize the analysis based on the local area where the system is going to be implemented. Hydrogen cost consists of four principal components: i) capital cost, ii) O&M cost, iii) replacement cost, iv) electricity cost. Facility total cost during its lifetime is shown in table I.

TABLE I  
FACILITY TOTAL COST DURING ITS LIFETIME

Year	Total cost (CapEx + OpEx) (€)	Capitalization factor	Final cost (€)
1	328,050.00	1.00	328,050.00
2	336,051.00	1.01	339,251.00
3	344,051.00	1.02	350,484.00
4	352,052.00	1.03	361,750.00
5	360,052.00	1.04	373,048.00
6	368,053.00	1.05	384,379.00
7	376,053.00	1.06	395,743.00
8	384,054.00	1.07	407,141.00
9	392,054.00	1.08	418,573.00
10	400,055.00	1.09	430,039.00
11	408,055.00	1.10	480,500.00
12	416,056.00	1.11	492,425.00
13	424,056.00	1.12	504,390.00
14	432,057.00	1.13	516,394.00
15	440,057.00	1.14	528,439.00
16	448,058.00	1.15	540,523.00
17	456,058.00	1.16	552,649.00
18	464,059.00	1.17	564,816.00
19	472,059.00	1.18	577,024.00
20	480,060.00	1.19	589,257.00

By taking into account, the facility lifetime total cost and the amount of hydrogen production (36,347 kg per year), estimated by the energy analysis, previously carried out [3], the hydrogen production cost is 16.21 €/kg. Regarding electricity cost, it is important to underline how an electricity cost decreasing, can lead an hydrogen production cost reduction. When the electricity cost is equal to 0.12 KWh (USA market value) or 0.1764 KWh (EU average market value), the hydrogen production cost is respectively 12.54 and 14.31 €/kg

As second step the analysis has been conducted considering the the bike-sharing system cost too. The assumptions are:

- The rate of demand is known, and spread unevenly throughout the year;
- The lifetime of the bike-sharing system of 10 years;

- The assumed money value discount rate (i) is 1%;
- Cost assessment includes CapEx, OpEx and money costs;
- O&M cost calculated as a 5% of the capital cost (excluding high-pressure tanks cost).

To calculate the present value of a cash flow, a discount rate has been used to take in account interests on capital expenditures. Based on the previous assumptions, the bike-sharing break-even cost (BEC) is 1.74 € for each hour of usage of one Hy-bike (table II).

TABLE II  
BIKE-SHARING TOTAL COST (EXCLUDING FUEL AND TRANSPORT COST)

Year	Total cost (€)	Bikes operation period (h)	BEC (€)
1	491,750.00	56,775	8.66
2	546,910.00	113,550	4.82
3	602,114.00	170,325	3.54
4	657,363.00	227,100	2.89
5	712,656.00	283,875	2.51
6	767,995.00	340,650	2.25
7	823,380.00	397,425	2.07
8	878,812.00	454,300	1.93
9	934,290.00	510,975	1.83
10	989,815.00	567,750	1.74

By adding transport and fuel costs, an overall cost of 2.22 €/h results. To balance out all the proposed system cost, which includes not just the bike-sharing system, but also the production facility over its 20 years' lifetime, a 4.5 €/h rental price has to be assumed.

### IV. CONCLUSION

This study has allowed: i) to determinate the hydrogen production cost, ii) to evaluate the break-even cost of the overall proposed energy chain (the hourly rental price of each electric bicycle). It is underlined that the rental price is in line with the market, demonstrating the ability of the energy chain of generating profit.

### ACKNOWLEDGMENT

This research was supported by the University of Naples "Parthenope" for the project "Hy-bike reliability and safety allocation" (2015) and by the Italian Government, with the PON project "Fuel Cell Lab – Innovative systems and high efficient technologies for polygeneration – PON03PE\_00109

### REFERENCES

- [1] Jannelli E., Di Giorgio P., Lubrano Lavadera A., Desideri U., Modelling and prototyping of an active control system for fuel cell-battery power unit toward sustainable mobility. Hypothesis XII Procedia, 2017, pp 132-133.
- [2] Bartolozzi I., Rizzi F., Frey M., Comparison between hydrogen and electric vehicles by life cycle assessment: A case study in Tuscany, Italy, Applied Energy, 101 (2013) 103-111.
- [3] N. Jannelli, M. Minutillo, A. Lubrano Lavadera, A. Forcina, From renewable hydrogen production to its utilization in a fuel-cell-powered bicycle: a sustainable energy chain. Submitted to Energy.

## POWER TO BUTANOL PRODUCTION VIA HIGH TEMPERATURE CO-ELECTROLYSIS FOR SUSTAINABLE MOBILITY

A. Perna\*, M. Minutillo\*\*, E. Galloni\*, F. Scala\*, G. Liguori\*\*\*

\*Department of Civil and Mechanical Engineering, University of Cassino and Southern Lazio, Cassino (Italy)

\*\*Department of Engineering, University of Naples "Parthenope", Naples (Italy)

\*\*\*MECOSER SISTEMI Spa, Via Saggese 75, 80013 Casalnuovo, Naples - Italy, <http://www.mecosersistemi.it>

**Abstract** - This paper investigates the feasibility of butanol as alternative fuel for transportation, starting from its production, from renewable hydrogen, to its utilization in SI (Spark Ignition) engines. In particular, the production pathway is based on the HT (high temperature) co-electrolysis by using the solid oxide technology and on the GtL (gas to liquid) plant via the intermediate product methanol. In order to evaluate the PtB (Power to Butanol) system performance and behavior, thermochemical and electrochemical models have been developed and validated by means of experimental data. Then, the behavior of a small, turbocharged spark-ignition engine, firing with gasoline-butanol blends (up to 40% butanol mass percentage), has been investigated and analyzed by means of experimental tests carried out at different engine operating points. Results show that butanol is a viable alternative to fossil fuels in the transportation sector.

**Index Terms** – Renewable source, SOEC, butanol, SI engine

### I. INTRODUCTION

Transport in Europe is currently 94% dependent on oil and 84% of it is imported. This means high levels of pollutant emissions, strong oil dependence and high costs. At a European level, new directives have recently been adopted to find alternative fuels, like biofuels. The power-to-liquid (PtL) route, through hydrogen production together with CO<sub>2</sub> from industrial processes, is an attractive approach and a promising alternative to biofuels production. Currently, research efforts into renewable liquid fuels suitable for gasoline replacement are focused on butanol (BuOH) thanks to its interesting features such as low miscibility with water, high heating value and good compatibility with existing gasoline engines and fuel pipeline infrastructure. Furthermore, with respect to other alcohols, butanol is less volatile, less hygroscopic and less corrosive, thus the damage risks for the engines are lower.

In this paper the feasibility of BuOH as alternative fuel for transportation, starting from its production, from renewable hydrogen (solid oxide electrolysis technology), to its utilization in a small, turbocharged spark-ignition engine where it is added to gasoline is investigated.

### II. POWER TO BUTANOL PLANT

The mixed alcohol catalysts are classified into two main categories: a) modified Fischer–Tropsch synthesis, b) modified Methanol (MeOH) synthesis (K, Zn, Cr, Cu based) catalysts [1]. Figure 1 shows the modular configuration of the proposed PtB (power to BuOH) plant sized to produce about 100 kg per day of BuOH.

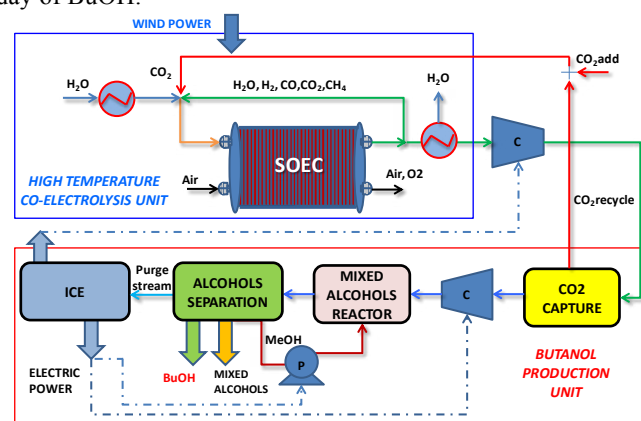


Fig. 1 PtB plant lay-out

It consists of: (i) high temperature co-electrolysis (HTCE) unit using solid oxide electrolytic cells (SOEC), (ii) CO<sub>2</sub> capture unit based on Selexol technology, (iii) mixed alcohols reactor (MAR) with modified MeOH catalyst, (iv) alcohols separation unit where the BuOH is separated from gaseous and liquid components, (v) additional power production unit (Internal Combustion Engine, thermal efficiency 0.4).

The plant performance analysis has been carried out by a thermo-electrochemical model developed by integrating the SOEC model [2] with chemical reactors according to configurations and data available in the technical literature [1]. Table I reports the main operating data and performances of the PtB plant. The captured CO<sub>2</sub> is recycled and mixed with the additional CO<sub>2</sub> from external source, equal to  $1.51 \cdot 10^{-2}$  kg/s.

Copyright © 2017

TABLE I  
PLANT PERFORMANCES IN TERMS OF MASS AND ENERGY BALANCES

<i>HT Co-Electrolysis unit</i>		
SOEC electric power	kW	203
N. of stacks/cells - Active area	cm <sup>2</sup>	10/61 - 550
Cell nominal conditions	A/cm <sup>2</sup> @V	0.4/1.45
Operating Temperature/pressure	°C/bar	750/1.013
Anode flow rate (H <sub>2</sub> O/CO <sub>2</sub> =0.467)	kg/s	2.45·10 <sup>-2</sup>
Anode off gas recycling ratio	%	19.8
Anode off gas composition	mol%	H <sub>2</sub> 46.3, H <sub>2</sub> O 5.5, CO 40.3, CO <sub>2</sub> 6.3, CH <sub>4</sub> 1.5
<i>Butanol Production unit</i>		
H <sub>2</sub> /CO		1.15
CO <sub>2</sub> capture removal	%	71
Operating pressure of CO <sub>2</sub> capture	bar	30
Operating pressure of MAR	bar	76
Operating temperature of MAR	°C	325-340
Inlet MAR stream composition	mol%	H <sub>2</sub> 51.5, CO 44.8, CO <sub>2</sub> 2.0, CH <sub>4</sub> 1.7
Purge stream flow rate	kg/s	10.5·10 <sup>-3</sup>
Purge stream LHV	MJ/kg	9.15
Mixed alcohols flow rate	kg/s	1.37·10 <sup>-3</sup>
Mixed alcohols LHV	MJ/kg	31.8
i-BuOH flow rate	kg/s	1.24·10 <sup>-3</sup>
<i>Overall plant performance</i>		
Electric power consumption	kW	11
Electric power production	kW	38.5
Net electric power	kW	27.5
i-BuOH chemical power	kW	42.6
Power to BuOH (PtB) efficiency *	%	20.9
Cogeneration* efficiency **	%	55.9

\*BuOH chemical power/ SOEC electric power

\*\* (BuOH chemical power+Mixed alcohols chemical power+ Net electric power)/ SOEC electric power

### III. EXPERIMENTAL TESTS ON SI ENGINE

Steady tests have been performed on a 4-cylinder, 16-valve, port fuel injected, turbocharged spark-ignition engine [3]. The engine total displacement is 1.4 liters and the compression ratio is 9.8. During the tests both the injection and the ignition timing have been tuned by an on-line programmable engine control unit. Two blend concentrations have been analyzed: B0 (straight regular grade gasoline: C-H-O 7.9-14.8-0, air-fuel ratio (A/F) equal to 14.6 LHV=43.5 MJ/kg) and B40 (40 wt% i-BuOH: C-H-O 6-12.4-0.5, A/F=13.2, LHV=40.5 MJ/kg). Tests have been carried varying both the engine speed and load. In each case the spark timing has been tuned in order to obtain the maximum brake torque (knock limited), while the injection duration has been tuned for obtaining stoichiometric mixtures. The torque output slightly decreases when the engine is fueled by B40 (Table II), due to the heat released per volume unit of stoichiometric A/F (air to fuel) mixtures that decreases with increasing butanol concentration [4]. At stoichiometric conditions, the specific fuel consumption increases of about 13% when the engine fires with B40, because of the lower energy density of BuOH with respect to pure gasoline.

TABLE II

MAIN VALUES MEASURED FOR STOICHIOMETRIC AIR-FUEL (A/F) OPERATION. ENGINE SPEED: 3000 RPM, MANIFOLD ABSOLUTE PRESSURE (MAP): 0.46 BAR. THE COMBUSTION DURATION IS GIVEN BY 0-90% BURNT FUEL MASS

		B0	B40
Specific Fuel Consumption	g/kWh	370	418
Torque	Nm	31.2	29.9
Thermal Efficiency	-	0.22	0.21
Exhaust Gas Temperature	°C	664	651
Combustion Duration	°	43.5	42.3
HC-NO <sub>x</sub> -CO <sub>2</sub>	g/kWh	1.0-19-45-1235	0.9-18-42-1229

Results show that the engine brake overall efficiency decreases as well as the exhaust gas temperature and the combustion duration when the engine burns B40 instead of B0, while the specific pollutants remain practically the same. Table III reports the main values measured at high loads. B40 allows to operate with spark timings more advanced than those characterizing the engine firing with B0.

TABLE III

MAIN VALUES MEASURED AT KNOCK LIMITED SPARK ANGLE. ENGINE SPEED: 1500 RPM, MAP: 1.11 BAR

		B0	B40
Knock Limited Spark Angle*	°	-6.0	-7.3
Specific Fuel Consumption	g/kWh	247	274
Torque	Nm	116	117
Thermal Efficiency	-	0.34	0.33
Exhaust Gas Temperature	°C	667	658
Combustion Duration	°	30.1	32.2
HC-NO <sub>x</sub> -CO <sub>2</sub>	g/kWh	1.6-12.9-790	2.1-11.6-786

\*Knock intensity is quantified by means of the in-cylinder pressure curves analysis [4]

### IV. CONCLUSION

Results have highlighted that: a) PtB efficiency is higher (21%) than the efficiency achieved by using biomass (16%) as renewable source [1]; b) SI operates with spark timings more advanced than those characterizing the engine firing with B0.

### ACKNOWLEDGMENT

Research supported by Naples "Parthenope" University, for the project "Power to gas for sustainable mobility: an advanced plant configuration for multi-fuels production" (2016) and by the Italian Government, PON project "Smart Generation - Sustainable Systems and Technologies for the energy generation - PON03PE\_00157"

### REFERENCES

- [1] Okoli CO, Adams II TA, Brigljevic B, Liu JJ, Design and economic analysis of a macroalgae-to-butanol process via a thermochemical route, Energy Convers Manag 123 (2016) 410–422
- [2] Perna A, Minutillo M, Lubrano Lavadera A, Jannelli E, Combining plasma gasification and solid oxide cell technologies in advanced power plants for waste to energy and electric energy storage applications, <https://doi.org/10.1016/j.wasman.2017.09.022>
- [3] Galloni E, Fontana G, Staccone S, Scala F. Performance analyses of a spark-ignition engine firing with gasoline–butanol blends at partial load operation. Energy Convers Manag 2016;110:319–26.
- [4] Galloni E. Knock-limited spark angle setting by means of statistical or dynamic pressure based methods. Energy Convers Manag 2016;116:11–7.

## PRELIMINARY STUDY OF A REVERSIBLE SOLID OXIDE CELL COUPLED TO A RENEWABLE POWER PLANT BASED ON LABORATORY CHARACTERIZATION

M. Graziadio<sup>1\*</sup>, G. Apuzzo<sup>2\*\*</sup>, R. Vellone<sup>3\*\*</sup>, S. J. McPhail<sup>4\*\*\*</sup>, M. Carlini<sup>5\*</sup>,

<sup>\*</sup>Engineering Faculty, University of Tuscia, DAFNE - Via S.M. in Gradi n.4, 01100 Viterbo, (Italy)

<sup>\*\*</sup>Department of mechanical engineering, University of Roma 3 – Via Vito Volterra, 62, 00146 Roma, (Italy)

<sup>\*\*\*</sup>Department of Energy Technologies, Via Anguillarese, 301, 00123 Rome, (Italy)

**Abstract** - Reversible Solid Oxide Cell (Re-SOC) technology is attracting great interest and is considered to be one of the most promising energy conversion and storage systems. The same Re-SOC cell can work as a power generator (SOFC) and as an electrolyser (SOEC) by simply switching the direction of the electric current. Working in both ways permits the Re-SOC to cover a great field of applications without compromising on the multiple benefits of solid oxide cell technology, as fuel flexibility, insignificant emissions, environmental sustainability and efficiency

This paper is focused on the dimensioning of an energy storage system based on Re-SOC stacks for the on-site power stabilization of a full-scale renewable-power plant, based on laboratory performance data obtained on a short stack supplied by a major European industry. After preliminary characterization tests to establish the good performance of the tested stacks, a simulated operation profile is applied to evaluate stack response to the cyclic buffering and stabilization of excess and shortage of power generated by the renewable power plant, producing H<sub>2</sub> when the production of electricity is higher than the demand and to providing electricity when the power generated from the renewable source is insufficient.

**Index Terms** – Reversible Solid Oxide Fuel Cell (Re-SOC), Electrical Energy Storage (EES), Electrolysis, Renewable power plant, durability, Operation under varying current

### I. INTRODUCTION

The use of renewable sources such as solar, wind, geothermal and hydroelectric power will become the most important substitute for the traditional generation of electricity from coal and nuclear power plants, leading to a sustainable energy future with lower greenhouse gas emissions. These technologies have developed rapidly thanks to continuous scientific innovations that have reduced wind and solar costs in small and medium scale applications, becoming mature. However, in large scale applications, it is necessary to further

develop long term energy storage with the aim of filling the gap between supply and demand and allowing renewable energy to serve as a continuous supply source on demand [1]. Electrical Energy Storage (EES) is one of the promising technologies since it has shown unique capabilities in coping with some critical characteristics of electricity, for example hourly variation in demand and price. Re-SOC technologies, thanks to the ability of switching the electric current direction, are able to work either as power generator (SOFC) or as an electrolyzer (SOEC), showing all the essential characteristics for being an EES system classified as Chemical Energy Storage system [2]. The present study evaluates the dimensioning of a Re-SOC stack coupled to a renewable power plant using a monthly wind profile as a reference case (Partinico Eolic Park –Palermo (Italy)). The purpose is to assess the feasibility and endurance of a Re-SOC working as Energy Electricity Storage system (EES).

### II. EXPERIMENTAL PART

After a procedure of start-up and reduction based on manufacturing recommendations, the Re-SOC stack has been characterized using polarization curves and Electrochemical Impedance Spectroscopy analysis in order to establish the initial performance of the tested system in both operation modes. With the aim of simulating a real on-site power generation of a full-scale renewable power plant, a realistic testing load profile in combined SOFC/SOEC mode was defined in order to evaluate the stack response to a daily cycling, consisting of buffering, stabilization of excess and shortage of the generated power, producing H<sub>2</sub> when the

Copyright © 2017



production of electricity is higher than the demand and providing electricity when the power generated from the renewable source is insufficient. In order to study the influence of electric and/or thermal effects on degradation, testing of the stack assembly unit was performed with different current densities, simulating the electricity demand. For the long-term test, the rate of degradation was reported as a voltage variation at a given time:

$$\frac{\Delta V_{stack}}{\Delta t} = \frac{V_{stack}(t_1) - V_{stack}(t_0)}{t_1 - t_0} \left( \frac{V}{s} \right) \quad (1)$$

At the end of the testing under current variations, the experimental results were employed for the dimensioning of a system consisting of reversible stacks coupled to a renewable power plant, taking in account all the other devices present into the system such as AC/DC converter, H<sub>2</sub> Reservoir Tanks, H<sub>2</sub> compressor, etc.

### III. RESULT AND DISCUSSION

After the characterization tests to evaluate the good performance of the system, the stack was tested under several repetitive cycles that work for 3h in SOFC mode and 20h in SOEC mode to verify system resistance and operational flexibility of working in combined mode. Figure 1 shows the voltage profile of the stack after eight daily cycles consisting of 23 hours of test (and 1 hour for switching between SOFC and SOEC modes). Successively, based on the electrical profile coming from a renewable wind power plant (Partinico Eolic Park –Palermo (Italy))., the stack was tested under varying current in both SOFC/SOEC modes depending on the daily electrical demand. As shown in Fig. 2, during night, when the electricity demand is lower than the supply from the power plant, the stack runs in electrolysis mode, producing H<sub>2</sub> which will be subsequently compressed and stored into the tanks. Instead, during day, the stack works in fuel cell mode producing electricity by switching polarization.

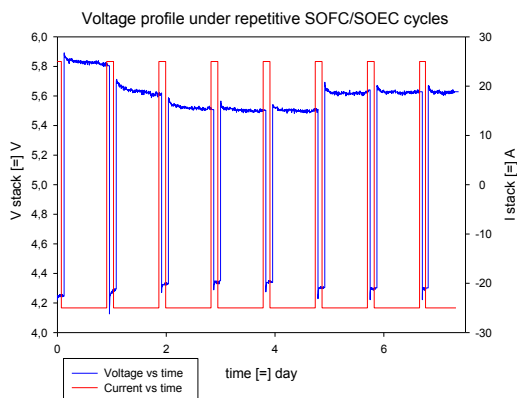


Fig. 1. Voltage (blue) and current (red) trends under eight repetitive cycles

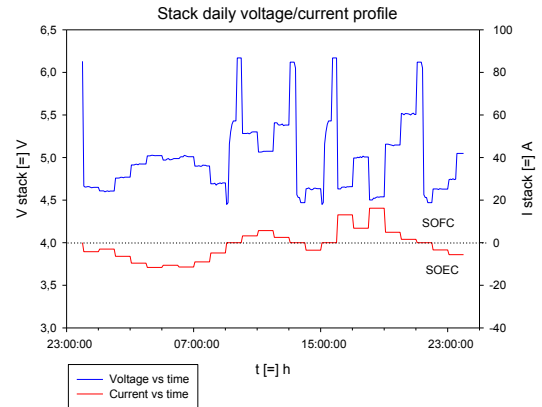


Fig. 2. Voltage (blue) and current (red) trends during a normal daily testing in SOFC/SOEC modes depending on TERNA's data.

### IV. CONCLUSION

Re-SOC devices have great potential as Electrical Energy Storage (EES) systems. The capability to produce hydrogen in "excess" of electricity via water electrolysis is an important concept since this universal energy carrier can be used in different sectors besides conversion in electricity if is it requested, such as transport, mobility, heating and the chemical industry. In addition, the continuous switching between power storage and power generation modes, following a typical daily wind and power demand profile, does not seem to create problems on the stability and performance of the stack, which exhibits a low degradation rate.

### ACKNOWLEDGMENT

The research has received funding from the European Union's Horizon 2020 research and innovation programme under grant agreement No 731224 (BALANCE). Call identifier: H2020: LCE-2016-2017: LCE-33-2016

### REFERENCES

- [1] Uwe Albrecht: *Hydrogen as storage option in the energy system of the future*, Presentation, Ludwig-Bölkow-System technik GmbH, 10th annual meeting of the network for fuel cells and hydrogen (NRW), 9 Dec 2010.
- [2] Bundesministerien BMWI und BMU Energiekonzept für eine umweltschonende, zuverlässige und bezahlbare Energieversorgung Bericht, Bundesministerium für Wirtschaft und Technologie (BMWi) und Bundesministerium für Umwelt (BMU), September 2010.

# HIGH PERFORMANCE OF SCALED-UP PtCu<sub>3</sub>/C OXYGEN REDUCTION ELECTROCATALYST: AN XPS AND MEA STUDY

N. Hodnik\*, M. Bele\*, S. Hočevar\*,\*\*, P. Jovanovič\*, M.  
Gatalo\*, A. Pavlišič\*, F. Ruiz-Zepeda\*, M. Gaberšček\*, I.  
Gatto\*\*\*, A. Saccà\*\*\*, A. Patti\*\*\*, A. S. Aricò\*\*\*

\*National Institute of Chemistry, Hajdrihova 19, 1000 Ljubljana (Slovenia)

\*\*Mebius d.o.o., Na Jami 3, 1000 Ljubljana, (Slovenia)

\*\*\*CNR-ITAE, Via Salita S. Lucia sopra Contesse 5 – 98126 Messina,  
(Italy)

## ABSTRACT

The oxygen reduction reaction (ORR) properties of a proprietary PtCu<sub>3</sub>/C alloy catalyst having a Pt-skin and characterized by homogeneously dispersed core-shell nanoparticles are evaluated in single cell tests using a standard protocol. The electrochemical study reveals that the BoL mass activity (at 0.9V<sub>IRfree</sub>) is 1.125 A/mg<sub>Pt</sub> at a Pt electrode loading of 0.2 mg/cm<sup>2</sup>. The analysis of polarization curves and EIS spectra with a physical model indicates that at high current density the oxygen transport is limited by the microporosity of catalyst carbon support.

**Index Terms** - PEM Fuel Cell, MEA, catalyst, Pt-alloy, XPS

## I. INTRODUCTION

Two main drivers for hydrogen-powered automotive fuel cell system cost lowering were recognized: fuel cell stack PGM loading and its power density. Both are connected with ORR catalysis. Thus, the R&D is focused on synthesis and production of durable Pt-containing electro-catalysts for ORR with mass activity higher than 1 A/mg<sub>Pt</sub>, which would enable PGM loading of 0.065 g<sub>PGM</sub>/kW<sub>gross</sub> [1]. In this study we present an evaluation of proprietary Pt-skin catalyst [2] characteristics obtained with *in-situ* single

cell tests.

## II. EXPERIMENTAL

A PtCu<sub>3</sub>/C alloy catalyst with intermetallic ordered shell on the top of a disordered core nanoparticles tightly embedded (anchored) into a carbon support was synthesized via a scaled-up procedure (50 g in one batch) based on modified sol-gel synthesis using a gelatin precursor [2]. At the surface of intermetallic ordered shell atomically thin Pt-skin was identified. Milling was performed in Ar-saturated n-hexane with 800 µm ZrO<sub>2</sub> balls at 3600 rpm for 5 minutes.

The structure of catalyst was characterized with XRD, SEM, HR-TEM and XPS. Its ORR activity was, in addition, also tested with standard *ex-situ* RDE and CV methods. The catalyst inks and MEAs were prepared according to the procedure described in ref. [3]. *In situ* electrochemical studies (polarization curves and EIS) were performed in a 5 cm<sup>2</sup> single cell, at temperatures of 80°C and 95°C, pressure of 3 bar<sub>abs</sub> and relative humidity (R.H.) of 100%. The flow rates were varied to have constant stoichiometry of either 2 and 1.5 or 4 and 3 for O<sub>2</sub> and H<sub>2</sub>, respectively.

### III. RESULTS AND DISCUSSION

#### A. Polarization curves

At 95 °C, a targeted operating temperature for automotive applications, the polarization curve in Fig. 1 has an OCV of 1.026 V, a current density of 0.442 A/cm<sup>2</sup> at 0.8 V and a peak power density of 791 mW/cm<sup>2</sup> at 1.5 A/cm<sup>2</sup> and 0.532 V. The ORR catalyst mass activity derived from IR-free polarization curve is 1.125 A/mg<sub>Pt</sub> at 0.9 V vs. RHE and 95 °C. These single cell data exceed the US DOE targets for 2020 at low current density. The drawback and the future challenge is high cell resistance at high current density.

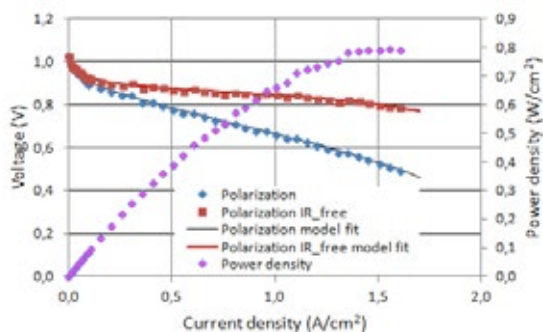


Fig. 1. Single cell test data for the unmilled PtCu<sub>3</sub>/C catalyst sample (P<sub>load</sub> anode/cathode = 0.2 mg/cm<sup>2</sup>; T<sub>cell</sub> = 95°C; RH = 100%; P<sub>cath</sub> = P<sub>an</sub> = 3 bar; H<sub>2,stoich</sub> = 3.0; O<sub>2,stoich</sub> = 4.0)

#### B. Impedance spectra

The impedance spectra scanned at 95°C and presented in Fig. 2 reveal that the unmilled catalyst sample has a lower polarization resistance than the milled one. This is confirmed by simulated impedance spectra in which the parameters were the same as those obtained from fitting the polarization curves with Kulikovsky's physical model [4]. The results indicate oxygen mass transport limitations by microporosity of catalyst carbon support at high current density.

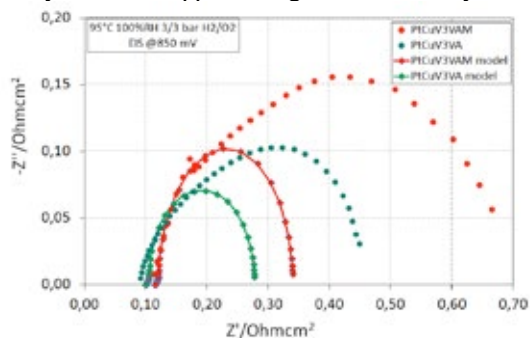


Fig. 2. Single cell impedance spectra with unmilled (green) and milled (red) PtCu<sub>3</sub>/C catalyst at 95°C and 850 mV. Circles: measured EIS spectra (units: Ohm); diamonds: EIS spectra simulated with parameters obtained from polarization curves fitted with model [4] (units: Ohmcm<sup>2</sup>).

The main contributor to the size of the impedance arc

is oxygen concentration at the interface and inside the gas diffusion layer. In the unmilled catalyst, this concentration has about twice higher value (on the order of 6.0·10<sup>-6</sup> mol cm<sup>-3</sup>) than in the milled sample. Further optimization of support pore size distribution is underway to address this issue.

#### C. XPS spectra analysis

XPS results show Pt surface enrichment and presence of different carbon hybridizations. Significant modification of the electronic properties of Pt in the proprietary catalyst vs. a conventional Pt/C catalyst is observed. These features are most likely responsible for the enhanced ORR activity and clearly show the electronic effect of Cu subsurface enrichment in the nanoparticle core over the Pt skin layer. Both, core-shell alloy structure and modified carbon support chemistry may play a role in producing enhanced fuel cell performance.

### IV. CONCLUSION

An analysis of proprietary Pt-skin ORR catalyst was performed by using structural and electrochemical methods. *In situ* single cell measurements and impedance spectroscopy data at an operating temperature of 95°C, which is the targeted for automotive applications, reveal that the begin-of-life (BoL) catalyst performances exceed the US DOE performance targets for 2020 at low current density, and enable the preparation of ultra-low Pt loading cathodes. At high current density, the oxygen mass transport in the microporous carbon support is, however, hindered. As a consequence, the cell voltage at rated power is about 130 mV lower than the targeted performance [1]. Further optimization of the catalyst synthesis parameters is underway.

#### ACKNOWLEDGMENT

Financial support from the Slovenian Research Agency (P2-0393, P2-0152 and Z2-8161) is acknowledged.

#### REFERENCES

- [1] James, B.D., et al., Fuel Cell Systems Analysis, Strategic Analysis Inc., 2017 DOE Hydrogen and Fuel Cells Program Review, 8 June 2017.
- [2] Bele, M., et al., Electrocatalytic Composite(s), Associated Composition(s) and Associated Process(es), US 9147885 (B2), 2015-09-29.
- [3] Zignani, S. C., et al., Towards Highly Performing and Stable PtNi Catalysts in Polymer Electrolyte Fuel Cells for Automotive Application, Materials 10 (2017) 317-334.
- [4] Kulikovsky, A.A., A Physically-Based Analytical Polarization Curve of a PEM Fuel Cell, Journal of The Electrochemical Society, 161 (3) (2014) F263-F270.

## HYDROGEN BASED HYBRID POWER UNIT FOR LIGHT VEHICLES: OPTIMIZATION OF FUEL CELL MANAGEMENT BY MEANS OF AN EVOLVED BATTERY STATE OF CHARGE EVALUATION

E. Jannelli\*, P. Di Giorgio\*, A. Lubrano Lavadera\*, M. Minutillo\*, M. Migliaccio\*, S. Cotecchia\*\*

\*University of Naples "Parthenope", Centro Direzionale Is.C4, Naples, (Italy)

\*\*Protom Group Spa Via Vic. S. Maria del Pianto, CPN – Ed. 6, 80143 - Naples, (Italy), <http://www.protom.com>

**Abstract** - Electrification of transport (electro-mobility) is considered an essential strategy to meet Europe's climate and energy challenges. The policy related to battery-powered vehicles is mainly focused on the technological optimization in order to reduce weight and volume and to increase durability and energy density. An interesting solution for improving battery-powered vehicles is to adopt hybrid configurations in which the electric motor uses both energy stored in a battery and energy produced in a fuel cell stack fed by hydrogen.

In this paper a hybrid power unit, developed to be installed on light vehicles (i.e. bike, scooter, etc.), is analyzed and its performance is evaluated taking into account the optimal control strategy that shares the produced power between the two energy sources (battery and fuel cell). Results in terms of overall system efficiency show that the proposed control strategy allows to manage the electric power demand maximizing the fuel economy without sacrificing the performances of the vehicle.

**Index Terms** – hybrid vehicles, hydrogen, fuel cell, control strategy

### I. INTRODUCTION

In the prospective of reduction of greenhouse gases emissions and fossil fuel consumption, electric mobility is gaining an increasing interest: Battery Electric Vehicles (BEVs) and Fuel Cell Electric Vehicles (FCEVs) appear to be the best options to replace internal combustion engines that characterize conventional mobility [1]. In fact, both of these solutions allow for exploiting the energy produced by renewable sources storing it as chemical energy or as hydrogen. Polymer electrolyte membrane (PEM) fuel cells are very interesting in automotive applications because of their low starting time and operating temperature. Fuel cells, in fact, offer energy power decoupling, since the autonomy is only related to the storage sizing, while the power to the stack size. Moreover, the fueling time is heavily reduced and the energy density of hydrogen is higher when compared with batteries. Fuel cells, on the other

hand, above all if hydrogen is produced from water electrolysis, have lower electric to electric efficiency and, generally, present problems due to water management with the sudden current increases [2], that characterizes a typical vehicle duty cycle and do not allow for kinetic energy recovery. The addition of an energy buffer such as a battery pack could allow to recover the kinetic energy during brakes and to power assist the fuel cell system when the power requested is higher than the rated one, above all during transient power demand. Moreover, the whole system could be redesigned allowing downsizing of the components and cost reduction. Therefore, hybrid configurations in which the electric motor uses both energy produced in a fuel cell stack fed by hydrogen and energy stored in a battery represent an interesting solution. The aim of this study is to define and test a flexible control system, developed for a hybrid power unit that is able to optimize the fuel cell operation and to avoid the battery overcharging.

### II. SYSTEM DESCRIPTION

#### A. Power unit

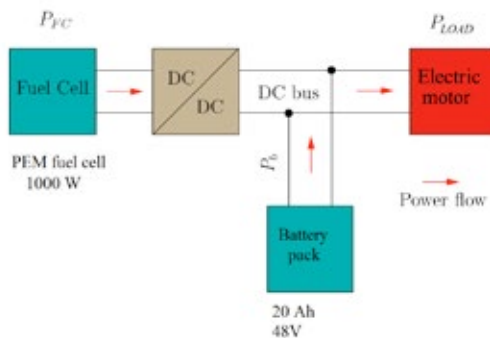
The power unit has to provide power for a 2kW brushless electric motor, and it is composed by a 1000 W PEM fuel cell stack, an externally controlled DC/DC and a 20 Ah LiFePO4 battery (see Table 1 and Figure 1), and a more accurate description of its dimensioning can be found in [3].

TABLE I - POWER UNIT COMPONENTS

Component	Description
Fuel Cell stack	Two 500W PEM fuel cells (12-24V operative range)
Li-ion battery	20Ah, 48V LiFePO4 battery
DC/DC	Mean Well SD-1000W-48V
Electronic Load	Chroma 2.6 kW

The power sharing is controlled varying the DC/DC output

voltage: if the voltage is higher than the battery OCV (open circuit voltage), the battery is charged, otherwise, current is drawn from the battery [3].



**Fig. 1. Hybrid power unit schematics**

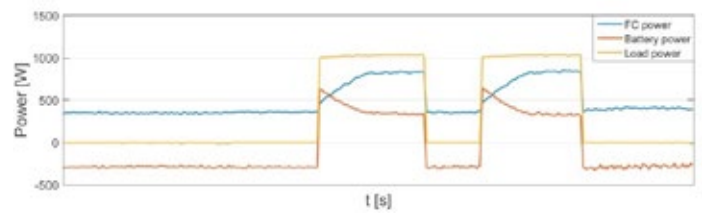
### B. Control strategy

The proposed control strategy aims to maximize the fuel economy without sacrificing the performances of the vehicle. If the battery state of charge is higher than a high threshold value, the fuel cell stack is off, and the battery provides all the energy needed by the motor. When the battery state of charge drops below the high SOC (state of charge) threshold value, the fuel cell turns on and operates in load balancing mode producing constant power with the maximum efficiency. If the battery state of charge becomes lower than the low SOC threshold, the fuel cell starts operating in load following mode, charging the battery when it is possible and producing all the power needed by the electric motor until its rated power is reached. The intermittent power draw in the last operation mode could cause a severe fuel cell life time reduction. To reduce fuel cell performance depletion, positive step current increases were avoided forcing the fuel cell to adapt to the new power demand following a linear ramp. In Figure 2 the power sharing caused by a load step increase is reported. The battery state of charge was estimated using an Unscented Kalman Filter.

### III. EXPERIMENTAL PROCEDURE

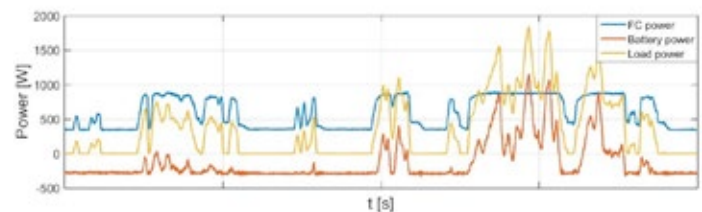
The control strategy was implemented using two different PI controllers: one for the load balancing operation and one for the load following operation. The whole control system (PI controllers and the Kalman filter) was implemented on an Arduino Mega 2560 board, implying very low computational cost. The data acquisition system was realized using the Arduino-LabView interface: another Arduino board that communicates with LabView also acquires the measurement signals that arrives to the control board.

The power unit and the implemented control system were tested in dynamic conditions, following the load profile of a WLTP class 1 cycle for light vehicles (the maximum velocity was scaled according to the rated velocity of the electric scooter). The power request was simulated using a programmable electronic load (2.6 kW maximum power).



**Fig. 2. Power sharing during step load increase**

The cycle was repeated until the hydrogen and battery complete depletion, in order to also evaluate the scooter driving range using this control strategy. In figure 3 is reported the power sharing between the fuel cell and the battery during a single WLTP cycle in low SOC condition.



**Fig. 3. Power sharing during a single WLTP cycle**

### IV. CONCLUSION

Good results were obtained during the tests carried out. The Kalman filter was able to estimate with sufficient precision the battery SOC, and the new control strategy was able to increase the vehicle fuel efficiency when compared to a simple load following strategy.

### ACKNOWLEDGMENT

This research was supported by the University of Naples "Parthenope", for the project "Sviluppo di sistemi di mobilità sostenibile con tecnologie smart capaci di utilizzare le risorse di Internet of Things (IoT)" (2016), and by the Italian Government, with the PON project "Fuel Cell Lab – Innovative systems and high efficient technologies for polygeneration – PON03PE\_00109

### REFERENCES

- [1] Wood, E., Wang, L., Gonder, J., and Ulsh, M., "Overcoming the Range Limitation of Medium-Duty Battery-Electric Vehicles through the use of Hydrogen Fuel-Cells," SAE Int. J. Commer. Veh. 6(2):2013.
- [2] R. Borup, J. Meyers, B. Pivovar, Y.S. Kim, R. Mukundan, N. Garland, et al., Scientific aspects of polymer electrolyte fuel cell durability and degradation, Chem. Rev. 107 (2007) 3904–3951.
- [3] E. Jannelli, P. Di Giorgio, A. Lubrano Lavadera, U. Desideri, Modelling and prototyping of an active control system for fuel cell-battery power unit toward sustainable mobility, HYPOTHESIS XII - June 28-30, 2017 - Syracuse, Italy

Copyright © 2017



## HYDROGEN RICH GAS PRODUCTION FROM WET ETHANOL REFORMER IN INERT POROUS MEDIA

Pil Hyong Lee\*, Hyun Jin Im\*\*, and Sang Soon Hwang\*

\*Department of Mechanical Engineering, Incheon National University, 119 Academy-ro, Yeonsu-gu, Incheon, (Korea)

\*\*ContiTech Fluid Korea, 100 Jiksan-ro, Seobuk-gu, Cheonan-si, Chung Nam, (Korea)

**Abstract** - In this paper, superadiabatic flame reforming process in the porous media reformer was investigated using a two dimensional approached with UDF and Williams mechanism. The Williams mechanism developed by combustion research group at UC San Diego is employed for ethanol combustion. To verify the existence of superadiabatic flame, the reforming process under the equivalence ratio of 3.0 and inlet velocity of 30cm/s was investigated. Its result shows that the flame with temperature spike can be stabilized in a porous media reformer. The temperature on this peak was roughly 502K higher than the adiabatic flame temperature of 1,160K for a thermodynamic equilibrium results at these same conditions. At ultra-rich equivalence ratio of 3.0, the conversion efficiency of hydrogen and carbon monoxide was estimated 34.16% at 30% of water fraction and 63.22% at without water.

**Keywords** : Superadiabatic flame, Wet Ethanol, Reforming, Hydrogen

### I. INTRODUCTION

Fossil fuel reforming describes the process of reforming commonly available fossil fuels into hydrogen rich gas. The hydrogen produced by fuel reforming can be used in fuel cells and internal combustion engines for cooling of gas turbines and generators, and in heavy petro-chemical processes. Hydrogen rich gas is primarily produced by the catalytic steam reforming of natural gas, a process that is very efficient and well-understood. Natural gas, however, is non-renewable and has a volatile property and when combusted, contributes to rising atmospheric carbon dioxide concentrations.[1] Ethanol is a renewable fuel, provided it is derived from feedstock, biomass and waste products, and has high enough hydrogen content in order to be a candidate for hydrogen rich gas generator through a reforming process. Many have suggested, however, that the energy required to produce ethanol is greater than the energy content of the final product. Water removal, which takes place in distillation and dehydration steps, is one of the most significant energy-consuming steps in the production process. A mixture with 15% ethanol requires no energy for distillation, while a mixture with 80% ethanol requires about 10% of the

chemical energy in the ethanol.[2]

In order to reduce production cost, one of promising solutions is considered as a direct thermal partial oxidation of ethanol or wet ethanol by superadiabatic flame under ultra-rich condition without Pt catalyst.[3]

In this paper, superadiabatic flame reforming process in the porous media reformer using a two dimensional approached with UDF and Williams mechanism was investigated. The Williams mechanism for ethanol combustion (288 reaction and 50 species) developed by combustion research group at UC San Diego is employed.[4]

### II. NUMERICAL MODELS

#### 1. Governing Equations

Mass conservation, momentum conservation, energy conservation and species conservation equations for reactive fluid flow are as follows

##### 1.1 Mass conservation equations

$$\frac{\delta(\rho_g \epsilon)}{\delta t} + \nabla \cdot (\rho_g \epsilon u) = 0 \quad (1)$$

##### 1.2 Momentum conservation equations

$$\frac{\delta(\rho_g \epsilon u u)}{\delta t} + \nabla \cdot (\rho_g \epsilon u u) = -\epsilon \nabla P + \nabla \cdot (\epsilon \tau) + R \quad (2)$$

##### 1.3 Energy conservation equations at fluid region

$$\begin{aligned} & \frac{\delta \epsilon \rho_g C_g T_g}{\delta t} + \nabla \cdot (\epsilon u (\rho_g C_g T_g + P)) \\ &= h_v (T_s - T_g) + \nabla \cdot [\epsilon (k_g + \sum_i \rho_{g_i} C_{g_i} D_{T_i}) \cdot \nabla T_g] \quad (3) \\ & - (\epsilon \sum_i \rho_{g_i} h_i Y_i (u_i - u)) + \epsilon (\tau u_0) + \epsilon \dot{Q} \end{aligned}$$

##### 1.4 Energy conservation equations at solid region

$$\frac{\delta[(1-\epsilon)\rho_s C_s T_s]}{\delta T} = \nabla \cdot (k_s \nabla T_s) + h_v (T_g - T_s) \quad (3)$$

### 1.5 Species conservation equations

$$\frac{\delta(\epsilon \rho_g Y_i)}{\delta T} + \nabla \cdot (\epsilon \rho_g u Y_i) = -\nabla \cdot (\epsilon \rho_g Y_i V_i) + \epsilon \dot{W}_i \quad (5)$$

In this paper, combustion process in the porous media reformer using a two dimensional approaches with Williams mechanism was investigated. The Williams mechanism contains 288 reactions and 50 species. The numerical simulation model is based on Semi-Implicit Method for Pressure Linked Equation Consistent algorithm using segregated solver of Ansys Fluent.

### 2. Numerical Simulation Models

Fig. 1 represents the configuration of porous media reformer. Commercial porous media reformer is 150mm long, 3mm heights is composed of a pure alumina foam. The computational mesh structure which is divided into 750×15 and boundary conditions are set to constant mass flow rate at the inlet and constant pressure condition at the outlet respectively.

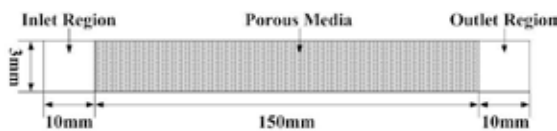


Fig. 1. Schematic diagram of porous media reformer

## III. RESULTS AND DISCUSSIONS

### 1. Superadiabatic flame under ultra-rich reforming condition

Fig. 2 presents the temperature curve for porous media reformer under equivalence ratio of 3.0 and inlet gas velocity of 30 cm/s was simulated. The temperature on this peak was roughly 502K higher than the adiabatic flame temperature of 1,160K for a thermodynamic equilibrium calculation results at these same conditions.

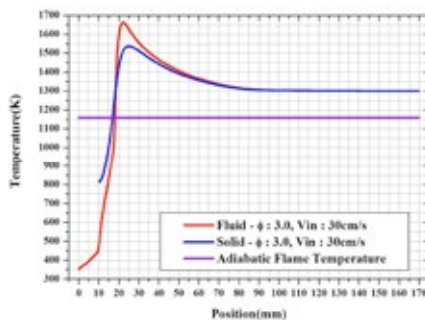


Fig.2. Comparison of gas and solid temperature

### 2. Conversion efficiency of hydrogen and carbon monoxide

The conversion efficiency of hydrogen and carbon monoxide for each condition was estimated by Equation (6) and (7) and the results are compared and shown in Fig. 3.[2]

$$\eta_{H_2} = 100 \times \frac{2 \times \dot{N}_{H_2}}{6 \times N_{C_2H_5OH}} \quad (6)$$

$$\eta_{CO} = 100 \times \frac{\dot{N}_{CO}}{6 \times N_{C_2H_5OH}} \quad (7)$$

At equivalence ratio of 3.0, increasing the water fraction leads to increase of hydrogen conversion efficiency and also decrease of carbon monoxide conversion efficiency. The conversion efficiency of hydrogen was calculated as 34.16% at water fraction 30% and the corresponding efficiency for carbon monoxide was calculated as 63.22% at water fraction 0%.

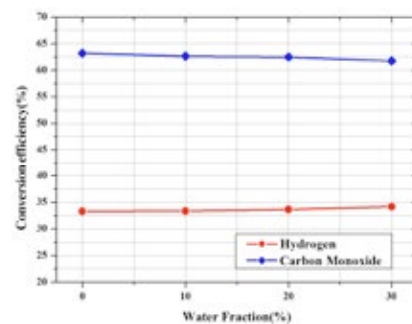


Fig. 3. Comparison of conversion efficiency at different water fraction

## IV. CONCLUSION

Numerical simulation results for reforming process by superadiabatic flame in porous media can be summarized as follows.

- 1) The peak temperature of superadiabatic flame was higher than the adiabatic flame temperature of 1,160K for a thermodynamic equilibrium calculation results at these same condition and the flame with temperature spike can be stabilized in a porous media.
- 2) At ultra-rich equivalence ratio of 3.0, the conversion efficiency of hydrogen and carbon monoxide was estimated as 34.16% at 30% of water fraction and 63.22% at without water.

## REFERENCES

- [1] O'Hayre R, Cha SW, Colella W, Prinz FB, 2006, Fuel cell fundamentals, New York, Wiley.
- [2] C. H. Smith, D. M. Leahey, L. E. Miller, J. L. Ellzey, Conversion of wet ethanol to syngas via filtration Combustion : An experimental and computational investigation, Proceedings of the Combustion Institute, Volume 33, 2011, pp. 3317–3324.
- [3] P. H. Lee, S. S. Hwang, Superadiabatic flame for production of hydrogen rich gas from methane, International Journal of Hydrogen Enrgy, Volume 41, 2016, pp.11801-11810.
- [4] P. Saxena, F.A. Williams, Numerical and experimental studies of ethanol flames, Proceedings of the combustion institute, Volume 31, pp. 1149-1156.

## LOW-FREQUENCY EIS INTERCEPT AS A DIAGNOSTIC TOOL FOR PEM FUEL CELLS DEGRADATION

I. Pivac\*, I. J. Halvorsen\*\*, D. Bezmalinović\*, F. Barbir\*, and F. Zenith\*\*

\*FESB University of Split, R. Boskovicca 32, 21000 Split, (Croatia)

\*\*SINTEF Digital, Strindveien 4, Trondheim, (Norway)

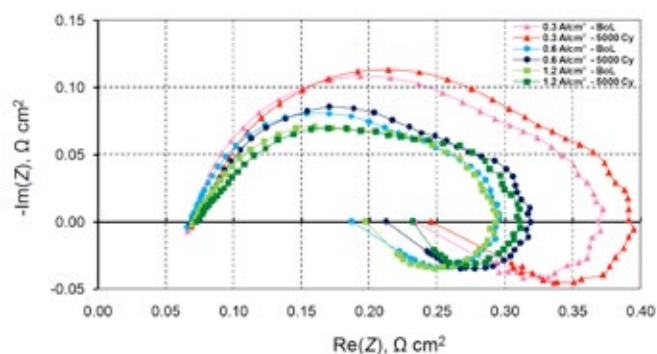
**Abstract** - Several diagnostic tests, such as polarization curves, electrochemical impedance spectroscopy (EIS), and cyclic voltammetry (CV), were conducted periodically to monitor performance degradation during an accelerated stress test (AST) for catalyst degradation on a single proton exchange membrane (PEM) fuel cell, which involves voltage cycling. From the results of the EIS measurements taken during the AST at three different current densities, catalyst degradation is clearly shown. The low-frequency intercept (Total R) increased most significantly. The simulation results with an 11-element impedance model show very good agreement with experimental data and consistency with the polarization change curves and CV. The obtained impedance at Total R is purely real, and it can be a useful and perhaps sufficient indicator for catalyst degradation and determination of the cell current state from just one parameter value, which is very promising for the future implementation in the PEM fuel cell control system.

**Index Terms** - catalyst degradation; accelerated stress test; electrochemical impedance spectroscopy; low-frequency intercept

### I. ACCELERATED DEGRADATION TESTS AND DIAGNOSTICS

In this paper, the applicability of the low-frequency intercept in the impedance spectrum was preliminary investigated during an accelerated stress test (AST) as a diagnostic tool for catalyst degradation performed on a water-cooled single proton exchange membrane (PEM) fuel cell hardware in a co-flow configuration from ElringKlinger with a 50 cm<sup>2</sup> active area MEA. Several diagnostic techniques, such as polarization curves, electrochemical impedance spectroscopy (EIS) and cyclic voltammetry (CV) were conducted periodically to monitor performance degradation during the AST. The cell has been subjected to the AST designed to target electrocatalyst degradation, which involves 40 s long potential cycling profile with rest times of 10 s at 0.6 V and 30 s at 0.9 V with 1 V s<sup>-1</sup> voltage ramps. The voltage was imposed on the cell at 65°C and 0.5 bar(g) via an external instrument (BioLogic SP-150) as the cell was in a non-operating mode, i.e. nitrogen was used on

the cathode and hydrogen on the anode side with constant flows of 0.4 SLPM and inlet relative humidities (RH) of 100% (dew point of 65°C). A Scribner Associates 890CL Teledyne Medusa fuel cell test station with an electronic load and a frequency response analyzer was used for the experiments, especially EIS measurements, which were conducted in galvanostatic mode in the frequency range from 3.981 kHz to 10 mHz with AC signal amplitude of 10% of the DC current. Each scan took around 30 minutes with additional 5 minutes of stabilization phase prior to each testing. Comparison of EIS measurements at 0.3, 0.6 and 1.2 A cm<sup>-2</sup> is shown in Fig. 1 at the beginning of life (BoL) and after 5000 cycles on a degrading hydrogen/air fuel cell operated at 65°C and 0.5 bar(g), with reactants inlet RH of 83.4% (dew point of 61°C) and constant stoichiometry of 4.0/2.0.



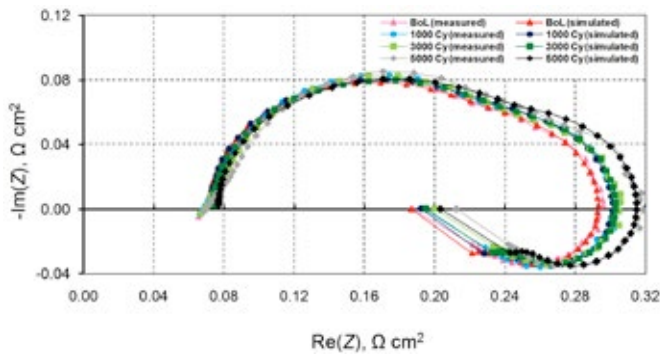
**Fig. 1. Nyquist plots at different current densities at the BoL and after 5000 cycles of AST**

From the results of the EIS measurements taken during the AST, catalyst degradation is clearly shown. The semicircles' high-frequency branches are more tilted/distorted with degradation, indicating an increase in the catalyst layer (CL) ionic resistance, while the low-frequency loops, representing mass transport losses, are getting bigger. As a result, the

rightmost real-axis intercept on the Nyquist diagram around 0.5 Hz or lower (maximum real impedance and the highest resistive losses), increased most significantly, while the membrane resistance (the leftmost real-axis intercept at high frequencies) increased only slightly. Obviously, there is a mixture of increase in activation losses (related to the loss of the cathode electrochemical active surface area, ECSA) and mass transport losses. This concurs also with the findings (at least qualitatively) of the polarization change curves analysis and CV measurements, which indicated a slight loss of the ECSA caused by platinum dissolution due to intentional frequent voltage cycling. The loss of the ECSA apparently resulted in slight structural changes within the CL, as the slight increase in mass transport suggests.

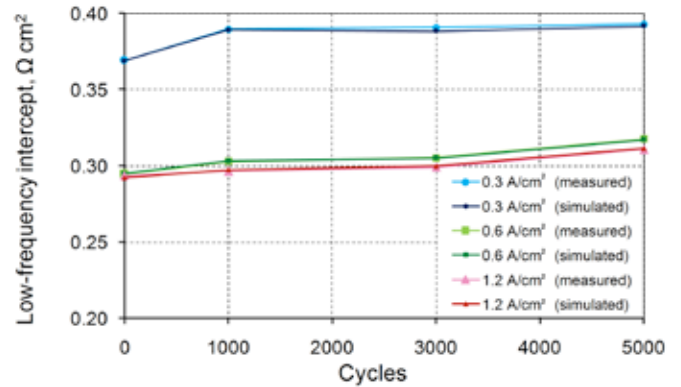
## II. APPLICATION OF MODEL TO FUEL CELL DEGRADATION STUDY

In the authors' recently published paper [1], an 11-element impedance model of PEM fuel cell was developed as a modified Randles equivalent circuit, capable of capturing the processes that cause the low-frequency inductive loop in the impedance spectra. It was validated by a series of experiments varying the operating conditions. Here, it has been applied on the periodical impedance measurements at the BoL, after 1000, 3000 and 5000 cycles to monitor performance degradation during the AST at three different current densities, and simulation results show very good agreement with the experiments. An example of model fitting results compared with experimental data at  $0.6 \text{ A cm}^{-2}$  during the AST is given in the Fig. 2.



**Fig. 2. Comparison of measured and simulated impedance spectra at  $0.6 \text{ A cm}^{-2}$  during the AST**

The low-frequency intercept is the sum of all model resistors [1] and it shows a rising trend during the AST at every measured current density (Fig. 3). Their overall values in the same point of AST are lower at higher current densities, and their rising trends are similar at all current densities.



**Fig. 3. Comparison of low-frequency intercepts at different current densities during the AST**

## III. CONCLUSION

The observed single PEM fuel cell moderately degraded during the AST after 5000 voltage cycles. The catalyst degradation was diagnosed with periodical EIS measurements taken during the AST at three different current densities. The low-frequency intercept increased most significant during the AST, with a rising and similar trend at every measured current density, whereas the membrane resistance increased only slightly. This concurs also with the findings of the polarization change curves analysis and CV measurements, which indicated a slight loss of the ECSA caused by platinum dissolution due to intentionally frequent voltage cycling. The loss of the ECSA apparently resulted in slight structural changes within the CL, as the slight increase in mass transport suggests.

As the obtained impedance at the low-frequency intercept is purely real and shows the most significant change with degradation, it can be a useful and perhaps sufficient indicator for catalyst degradation. Therefore, the new on-line algorithm for direct impedance estimation, based on relay excitation feedback, will find the appropriate frequency and calculate the impedance. The algorithm establishes a stable limit cycle oscillation with specified small amplitude and will converge quite fast to the frequency with the desired phase properties of the impedance. The algorithm can be implemented in ordinary fuel-cell control systems. Thus, catalyst degradation can be monitored without the need of measuring the whole impedance spectrum, and it will determine the current state of the fuel cell from just one parameter value, which is very promising for the future implementation in the fuel cell control system. The direct identification approach will be further explored.

## REFERENCES

- [1] Pivac, I., Šimić, B., Barbir, F., Experimental diagnostics and modeling of inductive phenomena at low frequencies in impedance spectra of proton exchange membrane fuel cells, *Journal of Power Sources*, Vol. 365, 2017, pp. 240-248.



# IN-SITU DIAGNOSIS OF PROTON EXCHANGE MEMBRANE FUEL CELL PERFORMANCE WITH Pt/TiO<sub>2</sub> CATHODE CATALYST

Abha Bharti\* and Gouri Cheruvally\*\*

\* Energy Systems Division, \*\* Polymers and Special Chemicals Group,  
Propellants, Polymers, Chemicals & Materials Entity, Vikram Sarabhai  
Space Centre, Thiruvananthapuram, (India)

**Abstract** - The performance characteristics and durability of Pt/TiO<sub>2</sub> cathode catalyst in proton exchange membrane (PEM) fuel cell under operation is investigated in this study. Accelerated durability test (ADT) in conjunction with *in-situ* cyclic voltammetry (CV), chrono-amperometry (CA), electrochemical impedance spectroscopy (EIS) and polarization study was employed to elucidate the performance. Results showed improved fuel cell performance after ADT revealing good durability characteristics of Pt/TiO<sub>2</sub> catalyst.

**Index Terms** – Accelerated durability test, Durability, PEM fuel cell, Pt/TiO<sub>2</sub> cathode catalyst

## I. INTRODUCTION

The wide scale commercialization of PEM fuel cell has been limited by the poor durability aspect of its catalyst for oxygen reduction reaction (ORR) at the cathode [1]. Pt catalysts supported on TiO<sub>2</sub> (Pt/TiO<sub>2</sub>) have gained significant attention and have been explored with promising results [2]. However, the durability investigations with Pt/TiO<sub>2</sub> catalysts have been largely limited to half cell evaluations which are not the real representations of actual performance characteristics in PEM fuel cell. In this article, an in-depth study carried out on the performance and durability characteristics of Pt/TiO<sub>2</sub> as an ORR catalyst in PEM fuel cell under operation is presented. ADT in conjunction with CV, CA, EIS and fuel cell polarization was employed to elucidate the durability aspects of Pt/TiO<sub>2</sub> catalyst.

## II. EXPERIMENTAL

### A. *In-situ* Electrochemical Evaluation

All the electrochemical experiments were carried out *in-situ* in a single cell PEM fuel cell at  $25 \pm 2^\circ\text{C}$  using Solatron SI1257 potentiostat and frequency response analyzer controlled using commercial software (Corrware and ZPLOT, respectively from M/S Scribner Associates Inc.). The performance and durability characteristics of Pt/TiO<sub>2</sub> catalyst (contains 20 wt% Pt, synthesized by acid catalyzed sol-gel route and microwave assisted modified chemical reduction route [2]) were evaluated before and after subjecting it to ADT by potential cycling of the cathode between 0.2 to 1.2 V vs. SHE for 6000 cycles at the scan rate of 50 mVs<sup>-1</sup>.

## III. RESULTS AND DISCUSSION

### A. *In-situ* electrochemical testing of Pt/TiO<sub>2</sub> catalyst

Fig. 1 shows the CV curves of Pt/TiO<sub>2</sub> catalyst before and after ADT. The peak in CV after ADT was similar to that before ADT which indicated 88% retention of ESA ( $51 \text{ m}^2\text{g}^{-1}$  vs.  $58 \text{ m}^2\text{g}^{-1}$ ). In spite of the slight decrease in ESA after ADT, positively shifted oxidation- reduction potential and higher reduction current was observed indicating good durability characteristics of Pt/TiO<sub>2</sub> catalyst along with improved ORR activity after cycling [3].

The changes in activity and stability of the Pt/TiO<sub>2</sub> catalyst were monitored through CA measurements at polarization potential of +0.7 V. It was observed that at the end of 10000 s, two times higher current density ( $0.10 \text{ Acm}^{-2}$  vs.



0.05 Acm<sup>-2</sup>) was obtained after ADT as compared to before ADT, demonstrating no loss in performance or degradation and a significant increase in activity of Pt/TiO<sub>2</sub> catalyst. This observation of enhanced activity after cycling was contrary to the expectation.

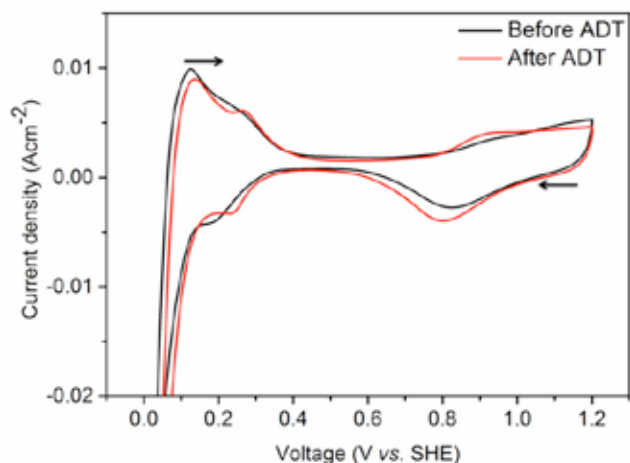


Fig. 1. CV curves of Pt/TiO<sub>2</sub> catalyst at scan rate of 20 mVs<sup>-1</sup>

The increased ORR kinetics after ADT is indicative of the availability of more triphase boundaries (TPBs) where actual catalysis occurs and hence, more number of effective Pt active sites for ORR [4]. The change in ionic conductivity of the membrane and its influence on effective Pt utilization/TPBs were studied from capacitance plots presented in Fig. 2. The high frequency slope of the curve with Pt/TiO<sub>2</sub> catalyst after ADT is markedly steeper as compared to before ADT, indicating enhanced proton conductivity [5]. Additionally, an increase in limiting capacitance was observed after ADT (ca. 0.23F vs. ca. 0.16 F). Higher limiting capacitance normally means that a larger fraction of the catalyst layer is being utilized indicating formation of more TPBs. This results in enhanced catalyst utilization and hence better fuel cell performance. This was also reflected by fuel cell polarization results. Higher cell voltage (0.805 V vs. 0.717 V at current density of 50 mAcm<sup>-2</sup>) and hence, better performance was exhibited by Pt/TiO<sub>2</sub> catalyst after ADT in line with the previous results.

#### IV. CONCLUSION

Pt/TiO<sub>2</sub> was explored as cathode catalyst in PEM fuel cell and evaluated through *in-situ* electrochemical techniques for performance and durability characteristics. The electrochemical investigations revealed an increase in cell performance after cycling tests which was attributed to improved ionic conductivity of MEA and Pt utilization achieved with the formation of more tri-phase boundaries. The study demonstrated the potential for applicability of Pt/TiO<sub>2</sub> as a high performing cathode catalyst for PEM fuel cell applications.

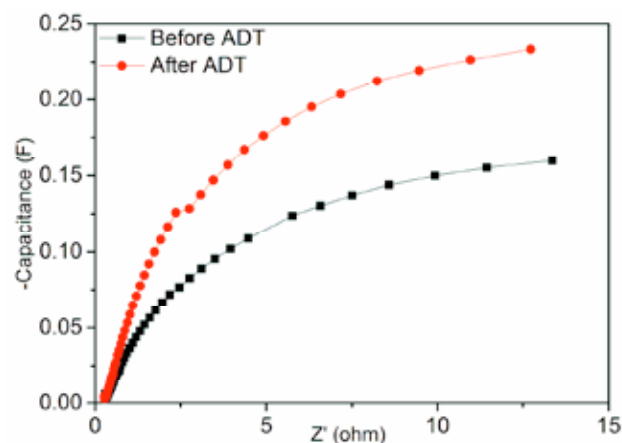


Fig. 2. Capacitance plots of Pt/TiO<sub>2</sub> catalyst

#### ACKNOWLEDGMENT

The authors thank the authorities of VSSC for granting permission to publish this work. One of the authors (Abha Bharti) is thankful to Indian Space Research Organization (ISRO) for the research fellowship. Analytical support received from the members of Analytical and Spectroscopy Division (ASD) and Materials Characterization Division (MCD), VSSC, and the valuable support received in conducting the experiments from members of Fuel Cell Section (FCS), Energy Systems Division (ESD), VSSC are gratefully acknowledged. The authors also acknowledge NIIST, Trivandrum and AIMS, Cochin for TEM and XPS analysis, respectively.

#### REFERENCES

- [1] R. Borup, J. Meyers, B. Pivovar, Y.S. Kim, R. Mukundan, N. Garland, D. Myers, M. Wilson, F. Garzon, D. Wood, Scientific aspects of polymer electrolyte fuel cell durability and degradation, *Chemical reviews*, 107 (2007) 3904-3951.
- [2] A. Bharti, G. Cheruvally, V-doped TiO<sub>2</sub> supported Pt as a promising oxygen reduction reaction catalyst: Synthesis, characterization and in-situ evaluation in proton exchange membrane fuel cell, *Journal of Power Sources*, 363 (2017) 413-421.
- [3] H. Wu, D. Wexler, H. Liu, Pt-Ni/C catalysts using different carbon supports for the cathode of the proton exchange membrane fuel cell (PEMFC), *Materials Chemistry and Physics*, 136 (2012) 845-849.
- [4] S. Park, Y. Shao, H. Wan, P.C. Rieke, V.V. Viswanathan, S.A. Towne, L.V. Saraf, J. Liu, Y. Lin, Y. Wang, Design of graphene sheets-supported Pt catalyst layer in PEM fuel cells, *Electrochemistry communications*, 13 (2011) 258-261.
- [5] M.C. Lefebvre, R.B. Martin, P.G. Pickup, Characterization of ionic conductivity profiles within proton exchange membrane fuel cell gas diffusion electrodes by impedance spectroscopy, *Electrochemical and solid-state letters*, 2 (1999) 259-261.

EFC17139

# A MULTI-SCALE APPROACH TO POLYMER ELECTROLYTE FUEL CELL CHARACTERISATION

J. Hack\*, Q. Meyer\*, F. Iacoviello\*, P. Cullen\*, N. Mansor\*,  
P. Shearing\*, N. Brandon\*\* and D. Brett\*

\* Electrochemical Innovation Lab, Department of Chemical Engineering,  
University College London, Torrington Place, London, WC1E 7JE, UK

\*\* Department of Earth Science & Engineering, Royal School of Mines,  
Imperial College London, Prince Consort Road, London, SW7 2BP, UK

**Abstract** – Due to the complex, hierarchical structure of the materials in polymer electrolyte fuel cells (PEFC), a multilength scale approach to their characterisation has been adopted. Electrochemical characterisation techniques have become relatively standard, but the use of X-ray computed tomography (X-ray CT) for 3-dimensional, non-destructive visualisation of PEFCs is an emerging field. The use of a suite of X-ray CT instruments has allowed for a full characterisation of the fuel cell components, from the stack level to the catalyst layer. The breadth of information that can be gained using X-ray imaging techniques will allow for further development of materials and fabrication techniques.

**Index Terms** – Multi length scale, polymer electrolyte fuel cells, X-ray computed tomography

## I. NOMENCLATURE

MEA – Membrane electrode assembly

PEFC – Polymer Electrolyte Fuel Cell

X-ray CT – X-ray computed tomography

## II. INTRODUCTION

Fuel cells are gaining attention for use as alternative energy sources in a range of applications from vehicles to stationary power [1]. Polymer electrolyte fuel cells (PEFCs) are of particular interest for transportation applications, due to their low operating temperatures (60 – 100 °C) and high electrical efficiency [2]. However, issues surrounding their durability remain a point of interest, especially pertaining to the degradation of materials in the membrane electrode assembly (MEA).

Whilst electrochemical characterisation techniques give vital information about fuel cell performance, imaging provides insight into the materials structures in

PEFCs.

X-ray computed tomography (X-ray CT) is a particularly useful technique for materials characterisation and is being increasingly used for 3-dimensional analysis of PEFCs [3, 4]. A distinct advantage of the technique is the ability to do non-destructive imaging of the internal components of PEFCs *in situ* and *in operando*.

However, because the materials constituting a PEFC span a large range of length scales, understanding the material structures across this range requires use of multiple instruments. This work addresses this challenge of imaging the PEFC across the length scales to present a complete picture of materials that make up a PEFC.

Table I shows the suite of X-ray CT instruments that were used in this work, along with some of the most important metrics when selecting the most suitable technique for the size of the feature of interest.

Table I Information about the suite of X-ray CT instruments used for 3D characterisation of the PEFCs. The achievable energy range of the instrument, the beam type and the achievable pixel dimension are given.

Instrument	Energy range/kV	Beam profile	Minimum pixel resolution
Nikon 225 eV	3 – 225	Polychromatic cone beam	1 µm
Zeiss Xradia Versa 520	30 – 160	Polychromatic cone beam	300 nm
Zeiss Xradia Ultra 810	5.4	Monochromatic quasi-parallel beam	64 nm (large field-of-view (LFOV)), 16 nm (HiRes)

Copyright © 2017

### III. RESULTS

#### A. Macroscale Characterisation

Primarily used for stack metrology, macroscale characterisation has been carried out using the Nikon 225 XT instrument. The large field-of-view (FOV) and the ability to use X-ray beam energies up to 225 kV make the technique particularly suitable for investigating flow-field design, or locating interior components, such as the thermocouple, in a commercial stack. Gathering metrics about stack features at the macroscale allows for a more in-depth understanding of the stack manufacture and assembly.



Figure 1 Volume rendering of a commercial UPP fuel cell (Intelligent Energy) - a device used for charging of portable electronics

#### B. Microscale Characterisation

The MEA is a layered structure comprising the two electrodes (anode and cathode), which sandwich the polymeric membrane. Correlating the electrochemical degradation to changes in the microstructure of the electrode has been possible using X-ray micro-CT (Figure 2).

Fibres in the gas diffusion layer (GDL) can be segmented from the catalyst layer (CL) and variation in the CL structure in the beginning-of-life (BOL) and end-of-life (EOL) samples has been observed (Figure 2).

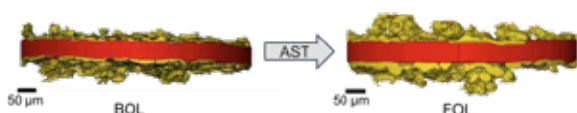


Figure 2 Volume rendering of an MEA (Fibres have been removed), with Nafion membrane (red) and catalyst layer (CL, yellow). Changes in the layer height are seen for the CL from the beginning-of-life sample (left) to the post-AST, end-of-life sample (right).

#### C. Nanoscale Characterisation

Because of the high flux of the 5.4 kV X-ray beam in the Zeiss XRadia Ultra 810, some materials can degrade upon exposure to the beam. An example of this is the polymeric membrane Nafion, which is used as the electrolyte in the PEFC. Studies found that the sample had moved vertically downwards during scanning, corresponding to 30 % of the FOV (Figure 3). Thus, an alternative approach to sample preparation has been taken involving embedding the sample in epoxy.

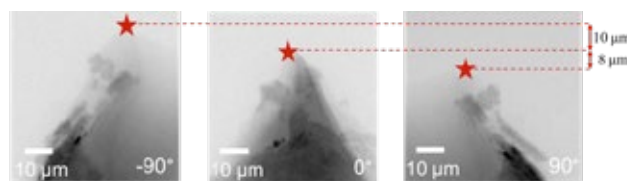


Figure 3 Radiographs of the prepared sample in the Ultra. From L-R, subsequent rotation of 90 deg shows vertical sample drift as the Nafion membrane degrades under the X-ray beam.

### IV. CONCLUSION

PEFCs are a promising alternative energy source and characterisation is essential for understanding their performance and degradation. Materials in the PEFC span a range of length scales, from centimetre, stack-level fixtures and fittings to nanometre catalyst nanoparticles. This makes 3D imaging a particular challenge; capturing information at the desired resolution requires selection of a suitable instrument. This work has addressed this challenge by adopting a multiscale approach to characterisation of PEFCs.

By considering the X-ray energy and the pixel resolution of a suite of X-ray CT instruments, the various components of the fuel cell and MEA have been visualised. Macroscale characterisation has been used for stack metrology. X-ray micro-CT has enabled visualisation of electrode layers and interfaces in the MEA, as well as imaging the effects of degradation. Finally, the challenge of sample preparation for X-ray nano-CT has been overcome by embedding and the technique has been used to gain insight into features of the CL. A deeper knowledge and understanding of internal structures in PEFCs materials across the length scales serves to further allow for material and fabrication development.

### ACKNOWLEDGMENTS

J. Hack acknowledges a studentship from the EPSRC CDT for the Advanced Characterisation of Materials (EP/L015277/1).

### REFERENCES

- [1] T. Wilberforce, A. Alaswad, A. Palumbo, M. Dassisti, A.G. Olabi, *Advances in stationary and portable fuel cell applications*, International Journal of Hydrogen Energy, Volume 41, 2016, Pages 16323-16576, pp. 16509-16522.
- [2] J. Park, H. Oh, T. Ha, Y.I. Lee, K. Min, A review of the gas diffusion layer in proton exchange membrane fuel cells: Durability and degradation, *Applied Energy*, Volume 155, 2015, Pages 1-950, pp. 866-880.
- [3] W.K. Epting, S. Litster, Microscale measurements of oxygen concentration across the thickness of diffusion media in operating polymer electrolyte fuel cells, *Journal of Power Sources*, Volume 306, 2016, Pages 1-832, pp. 674-684.
- [4] I.V. Zenyuk, D.Y. Parkinson, G.Hwang, A.Z. Weber, Probing water distribution in compressed fuel-cell gas-diffusion layers using X-ray computed tomography, *Electrochemistry Communications*, Volume 53, 2016, Pages 1-44, pp. 24-28.

EFC17140

# EFFECT OF DIFFERENT FLOW FIELD PATTERN ON PEMFC PERFORMANCE

Joy Marie R. Mora<sup>1</sup>, Felipe E. Mojica<sup>3</sup>, Joey D. Ocon<sup>1,2,\*</sup>, and  
Po-Ya Abel Chuang<sup>3,\*</sup>

<sup>1</sup>Energy Engineering Program, College of Engineering, University of the  
Philippines Diliman, Quezon City 1101, (Philippines)

<sup>2</sup>Department of Chemical Engineering, College of Engineering, University of  
the Philippines Diliman, Quezon City 1101 (Philippines)

<sup>3</sup>School of Engineering, University of California Merced, California 95340  
(United States)

Corresponding Authors: [abel.chuang@ucmerced.edu](mailto:abel.chuang@ucmerced.edu), [jdocon@up.edu.ph](mailto:jdocon@up.edu.ph)

**Abstract** – Performance of polymer electrolyte membrane fuel cell (PEMFC) using different flow field designs is evaluated under various sets of operating conditions. The degree of membrane electrolyte hydration is determined by measuring the high frequency resistance (HFR). The results showed that pressure drop along flow field channels has a positive effect on performance attributing to efficient water removal and improved convective mass transfer. The results also indicated that the effect of stoichiometry to performance is limited and dependent on other cell operating parameters.

**Index Terms** – PEM fuel cells, Flow field design, Pressure drop, Membrane hydration

## I. INTRODUCTION

One of the most important factors influencing the performance of proton exchange membrane fuel cells (PEMFCs) is water balance within the cell. In the operation of PEMFCs, sufficient level of membrane electrolyte hydration must be maintained to ensure optimal proton conductivity, while, at the same time, the excess water must be removed to prevent flooding and to admit fresh reactant gases to the catalyst layers. This can be achieved by using appropriately designed PEMFC components (Fig. 1). Among the PEMFC components, bipolar plates are considered crucial as they supply fuel and oxidant to the membrane-electrode assembly (MEA), remove product water, collect the produced current, and provide mechanical support [1], [2].

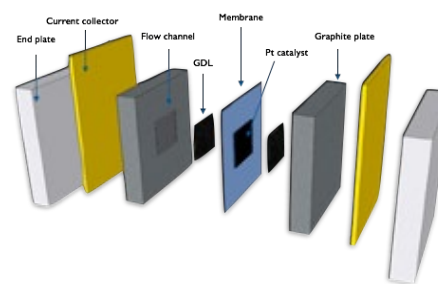


Fig. 1. Schematic of a polymer electrolyte fuel cell assembly

As evidenced by previous studies, PEMFC performance is not only influenced by flow field channel designs, but also by several operating parameters such as cell temperature, relative humidity (RH) of reactant gas streams, operating pressure, stoichiometry, and mass flow rates.

In this study, performance of PEMFC using three different flow field designs is evaluated under various sets of operating conditions. Similar to previous studies, degree of membrane electrolyte hydration is determined by measuring the high frequency resistance (HFR) [3]–[5].

## II. RESULTS AND DISCUSSION

The measured maximum cathode pressure drop values for the three flow fields are presented in the table below.

Copyright © 2017



TABLE 1  
MAXIMUM PRESSURE DROP (IN KPA) AT CATHODE SIDE UNDER DRY  
AND WET CONDITIONS

	SS: Single Serpentine	MS: Multiple Serpentine	SP: Straight Parallel
Dry polarization	1.70	0.62	0.79
Wet polarization	3.32	0.44	0.53

A single cell assembled with straight parallel flow field, which has low pressure drop, performed poorly under fully humidified condition (Fig. 2) and experienced frequent flooding as manifested by the fluctuations in current density readings during the experiment. The single serpentine, which has the highest pressure drop, performed well under most conditions, but experienced water accumulation at the end of the channel as is typical for this type of flow field. The accumulated water at the end of channel is also observed when the cell was taken apart after the experiment. The multiple serpentine, designed to address the pressure drop issue of the single serpentine, showed the highest performance in terms of current density especially at high humidity (100% RH).

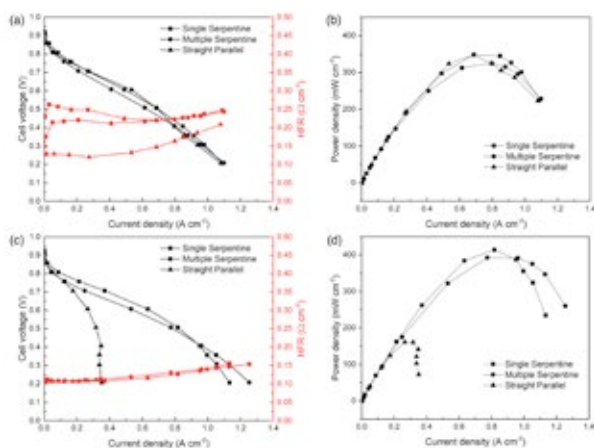


Fig. 2. Polarization and power density curves using different flow field designs (a), (b) under dry condition (80°C, 100 kPa<sub>abs</sub>, 50% RH, stoichiometric ratio 2/2), and (c), (d) under wet condition (80°C, 100 kPa<sub>abs</sub>, 100% RH, stoichiometric ratio 2/2).

HFR values for all flow field channels experienced an increase towards the high current density region. This is due to a slight decrease in membrane hydration caused by an increased rate of net water transport from anode to cathode via electro-osmotic drag. This net water transport from anode to cathode leads to a drier membrane at the anode side. Another possible cause of membrane dry-out is the slight increase in cell temperature experienced at high current densities ( $\Delta T$  for SS: 0.31°C (dry), 0.42°C (wet); MS: 0.27°C (dry), 0.46°C; SP: 0.34°C (dry), 0.07°C (wet)).

In order to investigate active removal of water from the cell, stoichiometric sensitivity analysis is performed. From the results, it is evident that relative humidity of reactant gases has a positive effect on cell performance across all test conditions. At low RH conditions, the membrane tends to dry-out at a faster rate as stoic is increased than at high RH conditions.

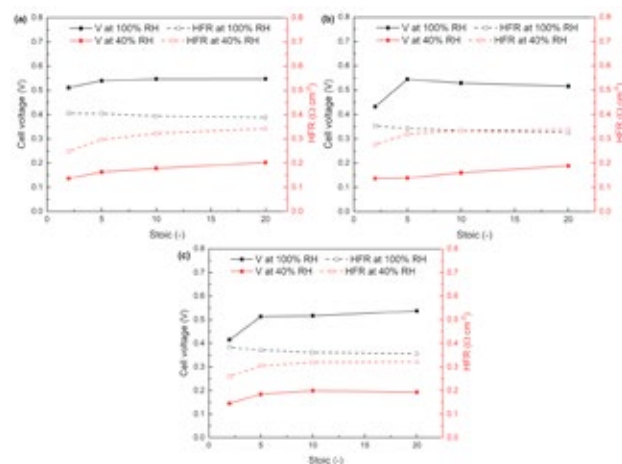


Fig. 3. Stoic sweep curves using (a) single serpentine, (b) multiple serpentine and (c) straight parallel flow fields.

### III. CONCLUSION

In summary, PEMFC performance using three different flow field designs were investigated under various test conditions. Results indicated that membrane hydration can be adjusted not only by the inherent flow field design, but also by modifying the operating conditions.

Ultimately, the results from this study allow for better understanding the effect of different operating conditions on membrane hydration and cell performance, which can consequently help in improving water management in PEMFC.

### ACKNOWLEDGMENT

This work was supported by the GREEN Power Program (IIID 2015-09) from the Commission on Higher Education – Philippine California Advanced Research Institutes (CHED-PCARI) of the Republic of the Philippines.

### REFERENCES

- [1] D. Spornjak, A. K. Prasad, and S. G. Advani, "In situ comparison of water content and dynamics in parallel, single-serpentine, and interdigitated flow fields of polymer electrolyte membrane fuel cells," *J. Power Sources*, vol. 195, no. 11, pp. 3553–3568, 2010.
- [2] P. Wawdee, S. Limtrakul, T. Vatanatham, and M. W. Fowler, "Water transport in a PEM fuel cell with slanted channel flow field plates," *Int. J. Hydrogen Energy*, vol. 40, no. 9, pp. 3739–3748, 2015.
- [3] C. Y. Lee, Y. M. Lee, and S. J. Lee, "Local area water removal analysis of a proton exchange membrane fuel cell under gas purge conditions," *Sensors*, vol. 12, no. 1, pp. 768–783, 2012.
- [4] D. Gerteisen, N. Zamel, C. Sadeler, F. Geiger, V. Ludwig, and C. Hebling, "Effect of operating conditions on current density distribution and high frequency resistance in a segmented PEM fuel cell," *Int. J. Hydrogen Energy*, vol. 37, no. 9, pp. 7736–7744, 2012.
- [5] I. S. Hussaini and C. Y. Wang, "Visualization and quantification of cathode channel flooding in PEM fuel cells," *J. Power Sources*, vol. 187, no. 2, pp. 444–451, 2009.



# ALKALINE OXYGEN EVOLUTION REACTION PERFORMANCE OF $\text{IrO}_2$ CATALYST USING KOH AND $\text{NaNO}_3$ AS ELECTROLYTES

Maricor Divinagracia<sup>1</sup>, Guangfu Li<sup>3</sup>, Joey D. Ocon<sup>1,2,\*</sup>, and  
Po-Ya Abel Chuang<sup>3,\*</sup>

<sup>1</sup>Energy Engineering Program, College of Engineering, University of the  
Philippines Diliman, Quezon City 1101 (Philippines)

<sup>2</sup>Department of Chemical Engineering, College of Engineering, University  
of the Philippines Diliman, Quezon City 1101 (Philippines)

<sup>3</sup>School of Engineering, University of California Merced, California 95340  
(United States)

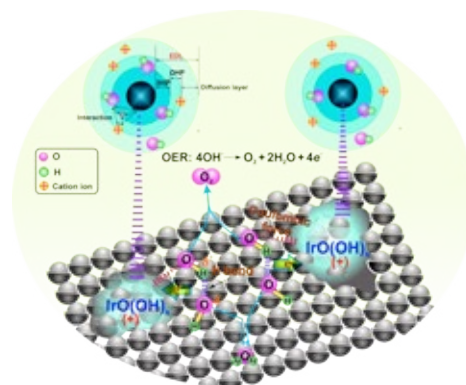
**Abstract** – Electrocatalysing oxygen evolution reaction (OER) is studied in various alkaline electrolyte solution. It is found that the catalyst activity increases with increasing KOH concentration, ascribing to the improved reaction kinetics, and  $\text{OH}^-$ , electron- and  $\text{O}_2^-$  transport in the electrical double layer. To study the ionic effect in the electrolyte, a supporting electrolyte  $\text{NaNO}_3$  is added to KOH. Our results show that  $\text{NaNO}_3$  improves ohmic conductivity, while suppresses  $\text{OH}^-$  adsorption in the reaction interface.

**Index Terms** – Alkaline electrolyte solution, Oxygen evolution reaction, Reaction interface, Water electrolysis

## I. INTRODUCTION

Research in oxygen evolution reaction (OER) has flourished for over several decades [1]. The advance of OER has been driving innovations related to energy conversation and storage technologies, such as water electrolyzers, due to its dominating effect in system efficiency, stability and cost. In alkaline media, noble metal catalysts can be replaced by less-expensive transition-metal materials, which is a significant advantage over such reaction occurred in acid media [2]. It is clear that the electrolyte types and concentration may determine the catalyst activity and stability, caused by different  $\text{OH}^-$ ,  $\text{O}_2$  and electron transports at the reaction interface between the catalyst layer surface and adjacent bulk liquid electrolyte.

During OER process, the reaction interface forms electrical double layer (EDL) due to  $\text{OH}^-$  adsorption and accumulation as a response of interfacial alternation [3]. The schematic illustrating the EDL structure is given in Fig. 1. In porous oxide catalysts, the EDL has structural and chemical flexibility. It is thus highly possible that different electrolyte solutions can result in alternations of the formed EDL, which in turn affects the rate of OER. Therefore, investigating and understanding of EDL with various electrolyte solutions can provide new insights for OER electrocatalysis.



**Fig. 1.** Schematic of the aqueous-based electrochemical interfaces for electrocatalytic OER. EDL: electrical double layer; IHP: inner Helmholtz plane; OHP: outer Helmholtz plane.

In this study, we used a typical three-electrode system to investigate the performance of the commercial  $\text{IrO}_2$  catalyst in different KOH concentrations. With emphasis of EDL function, the relationship between electrolyte solution and formed EDL is established to accurately capture catalyst performance, which can greatly benefit the design of high-efficiency OER catalysts.

## II. RESULTS AND DISCUSSION

Experimental measurements were performed in a typical thin-film rotating disk electrode system. The loaded catalyst layer contains  $0.24 \text{ mg cm}^{-2}$   $\text{IrO}_2$  and  $0.12 \text{ mg cm}^{-2}$  nafion polymer serving as a binder. The studied KOH concentration ranged from 0.1 - 4.0 M, which covers most published literature involving OER catalyst evaluation. The results shown in Fig. 2 confirm that the interfacial electrochemical behaviors are governed by the concentration of electrolyte solutions.

Compared with 0.1 M KOH, the linear sweep voltammetry

(LSV) shows that using 4.0 M KOH brings over 5-fold increased activity in the studied potential window, i.e. 1.4 - 1.65 V. This improvement of the reaction kinetics is quantified by the fitted Tafel slopes, which further validated the importance of OH<sup>-</sup> adsorption in OER. In general, the Tafel slopes obtained with different OH<sup>-</sup> concentrations are close to 60 mV dec<sup>-1</sup>, indicating that the rate-determining step in the reactions is a chemical step rather than an electron-transfer step, specifically OH<sup>-</sup> adsorption ( $\text{MOH} + \text{OH}^- \rightarrow \text{MO}^- + \text{H}_2\text{O}$ ) [4]. With this value of Tafel slope, the reaction order  $m_{\text{OH}^-} = 2$  is predicted, having two OH<sup>-</sup> equivalents to be involved in the overall reaction prior to and including the RDS [5]. It can be clearly observed that OH<sup>-</sup> adsorption significantly reduces the reaction efficiency at 10 mA cm<sup>-2</sup> at 0.1 M KOH concentration.

In-situ electrochemical impedance spectra at 1.55 V are carried out to evaluate the various interfacial resistance and electrochemical behaviors during OER. The raw data are simulated by the equivalent circuit  $L, R_\Omega, (R_{ct}Q_1)$ , and  $(R_1Q_2)$ , where  $L, R_\Omega, R_{ct}$  and  $Q$  symbolize inductor, ohmic resistance, charge transfer resistance, and capacitance, respectively. The capacitive components are represented by constant phase elements (CPE) to model semi-circles arising from inhomogeneous and porous surfaces. Generally CPE is defined by  $Z_{CPE} = 1/C_f(i\omega)^n$ , where  $C_f$  is the constant related to the electrode capacitance and  $n$  ( $0 \leq n \leq 1$ ) is an empirical constant. When  $n$  is 1, the electrode behaves like a pure capacitor. Thus, the  $n$  value close to unity signifies better electrocapacitive activity [6]. For both  $Q_1$  and  $Q_2$ , the obtained  $n$  approaches unity ( $\sim 0.9999$ ) particularly at higher OH<sup>-</sup> concentrations. The  $(R_1Q_2)$  circuit represents the diffusion/adsorption of reaction intermediates due to slow diffusion through reaction interface in a porous material [7]. The ohmic ( $R_\Omega$ ) and transport ( $R_{ct}+R_1$ ) resistances decrease with increasing KOH concentration. The resistance reduction attribute to the enhanced performance as the KOH concentration increases. Similar trend of performance improvement can be observed from increasing electrochemical surface area (ECSA) obtained from EIS due to the improved OH<sup>-</sup> transport and adsorption in EDL.

To further study the ion conductivity effect in the electrolyte, the supporting electrolyte solution of NaNO<sub>3</sub> was added into the KOH electrolyte solution. Adding NaNO<sub>3</sub> can reduce the ohmic resistance by increasing solution ionic conductivity. Surprisingly, the data indicate that adding NaNO<sub>3</sub> suppress OH<sup>-</sup> adsorption in EDL, which is an adverse effect in OER performance.

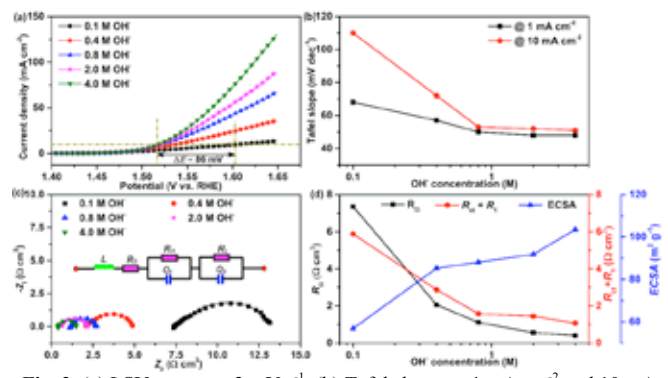


Fig. 2. (a) LSV curves at 2 mV s<sup>-1</sup>, (b) Tafel slopes at 1 mA cm<sup>-2</sup> and 10 mA cm<sup>-2</sup>, (c) EIS spectra at 1.55 V and (d) ECSA as a function of OH<sup>-</sup> concentration.

### III. CONCLUSION

In summary, catalyst performance in various alkaline electrolyte solutions can be characterized by EDL behaviors and effects. Our work indicates that the increased OER activity with increasing OH<sup>-</sup> concentration is resulted from the improvement of interfacial mass and charge transport as well as reaction kinetics. Further study of adding a supporting electrolyte, NaNO<sub>3</sub>, show reduced ohmic resistance, but extra resistance of OH<sup>-</sup> adsorption in EDL.

### ACKNOWLEDGMENT

This work was supported by GREENPower Program (IIID 2015-09) from Commission on Higher Education - Philippine California Advanced Research Institutes (CHED-PCARI) of the Republic of the Philippines.

### REFERENCES

- [1] Chakhalian, J., Millis, A.J., Rondinelli, J., Whither the oxide interface, *Nature Materials*, Volume 11, 2012, pp. 92-94.
- [2] Varcoe, J.R., Atanassov, P., Dekel, D.R., Herring, A.M., Hickner, M.A., Kohl, P.A., Kucernak, A.R., Mustain, W.E., Nijmeijer, K., Scott, K., Xu, T., Zhuang, L., Anion-exchange membranes in electrochemical energy systems, *Energy & Environmental Science*, Volume 7, 2014, pp. 3135-3191.
- [3] Bae, J.H., Han, J.-H., Chung, T.D., Electrochemistry at nanoporous interfaces: new opportunity for electrocatalysis, *Physical Chemistry Chemical Physics*, Volume 14, 2012, pp. 448-463.
- [4] Suen, N.-T., Hung, S.-F., Quan, Q., Zhang, N., Xu, Y.-J., Chen, H.M., Electrocatalysis for the oxygen evolution reaction: Recent development and future perspectives, *Chemical Society Reviews*, Volume 46, 2017, pp. 337-365.
- [5] Doyle, R., Lyons, M., *The Oxygen Evolution Reaction: Mechanistic Concepts and Catalyst Design*, 2010.
- [6] Khilari, S., Pandit, S., Varanasi, J. L., Das, D., Pradhan, D., Bifunctional Manganese Ferrite/Polyaniline Hybrid as Electrode Material for Enhanced Energy Recovery in Microbial Fuel Cell, *ACS Appl. Mater. Interfaces*, Volume 7, 2015, pp. 20657-20666.
- [7] Rastan, E., Hagen, G., Tunold, R., Electrocatalysis in water electrolysis with solid polymer electrolyte, *Electrochimica Acta*, Volume 48, 2003, pp. 3945-3952.

EFC17142

# A STOCHASTIC APPROACH FOR PEMFC MATERIAL IDENTIFICATION

Piergiorgio Alotto\*, Massimo Guarnieri\*

\*Department of Industrial Engineering – University of Padua,  
via Giovanni Gradenigo 6/a, 35131 Padova, (Italy)

**Abstract** – The characterization of fuel-cell materials is crucial for addressing the development of advanced functionalized materials and for fitting fuel-cell models, which are used in performance evaluation and device optimization. This identification still remains challenging when dealing with *in situ* measurements. The presentation regards a method for dealing with this problem that is based on stochastic optimization. Such techniques are usually applied to specific fuel-cell problems, mostly using semi-empirical models. We present an original formulation that makes use of an accurate zero-dimensional multi-physical model of a PEMFC and of two cooperating stochastic algorithms, particle swarm optimization (PSO) and differential evolution (DE), to extract multiple material parameters from a sufficiently large set of experimental data taken under controlled physical conditions. The method is suitable for application in other fields where fitting of multiphysics nonlinear models is involved.

**Index Terms** - *In situ* material characterization, Multiphysics modeling, Multiple identification, Stochastic methods.

## I. INTRODUCTION

The full characterization of Fuel Cells involves a number of physical parameters which are important for quantifying and comparing the performance of the materials and for trimming analytical and numerical models. Careful *ex situ* measurements of such parameters can be performed by means of a number of diagnostic techniques, whose results are however not completely consistent with fuel cell operation due to several side effects. Conversely, *in situ* measurements can provide meaningful operational values, but a very few techniques are available to determine a limited number of parameters.

An alternative strategy consists in multiple parameter identification from multiple fundamental measurements

performed in different conditions, e.g. at different current density, temperature, pressure, concentration, and humidification. If there is only one unknown parameter, the solution is easy, requiring just a statistical interpolating technique. In the case of multiple unknown parameters the problem becomes increasingly challenging with the number of parameters, as duplicity problem emerges, i.e., several groups of parameters may lead to the same performance (e.g. polarization curve). A number of numerical tools have been proposed to face this kind of problems. Stochastic mathematical models have been applied to the analysis of fuel cells for more than ten years, but typically to specific problems and by means of simple semi-empirical models, with an increased number of articles published in the last years. We present an original formulation that makes use of an accurate zero-dimensional multi-physical model of a polymer electrolyte membrane fuel cell and of two cooperating stochastic algorithms, particle swarm optimization (PSO) and differential evolution (DE), that proved to be successful in extracting multiple material parameters (exchange current density, mass transfer coefficient, diffusivity, conductivity, activation barriers ...) from the experimental data of multiple polarization curves under controlled temperature, gas back pressure and humidification.

## II. NUMERICAL METHODOLOGY

### A. PEMFC model

A multiphysical PEMFC model has been developed that uses the material parameters to be identified. The model takes into account the different domains forming a single PEM fuel cell, namely the polymeric membrane, the anodic and cathodic

catalyst layers, the anodic and cathodic diffusion layers, and the anodic and cathodic flow channels. The major electrochemical, fluid-dynamics, electrical, and thermal effects occurring in these domains have been considered in the model. At this aims, it includes the Nernst equation for computing the reversible cell voltage, accounting for entropic temperature and concentrations variations. The temperature and concentration dependent Butler-Volmer equation accounts for the irreversible losses related to electrochemical kinetics. An Arrhenius-like equation is used to express the exchange current density and its variations. Concentration gradients and related losses in the gas diffusion layers (GDLs) are computed by means of Fick's first law with Bruggemann-corrected diffusivities. In order to compute the ohmic losses, the Vogel-Tamman-Fulcher model has been used for the membrane conductivity, assuming linear hydration distribution. Both diffusive and osmotic-drag hydrogen cross-over have been modeled, as well as the thermal gradient due to internal losses and heat diffusion and dissipation.

### B. Stochastic identification

An *ad hoc* hybrid optimization scheme has been developed that combines two of the most successful stochastic optimizers, namely the Particle Swarm Optimization (PSO) and the Differential Evolution (DE), and works as shown in Fig. 1.

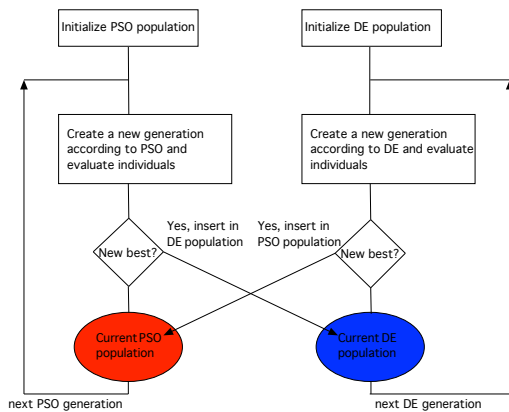


Fig. 1 - Hybrid scheme based on the combination of PSO and DE

These optimizers work on populations of sets of variables (in our case tentative values of the unknown material parameters), which evolve collectively with the aim of obtaining a specified performance, which is expressed as the minimum a fitness function (in our case the matching of the model  $V_{\text{mod}}$  and experimental  $V_{\text{exp}}$  cell voltages in every different working condition, stated by current density, temperature, gas pressure, and membrane hydration). In our procedure the fitness function was chosen as:

$$f(t) = 0.5 \max |x_i| + 0.5 \sqrt{\sum x_i^2}, \quad x_i = V_{\text{mod}} - V_{\text{exp}}$$

In order to overcome duplicity problems, namely several solutions able to fit the optimization problem, which typically arises when a large number of unknown are to be identified at the same time, a selective procedure was also implemented. It consists in subdividing the solution in sub-solutions, each related to no-load, low current density, intermediate current density, and high current density, so as to identify only a subset of unknowns in each of them (which are predominant in open circuit voltage, activation losses, ohmic losses and concentration losses).

## III. RESULTS

The method was tested on a set of experimental data taken on a specifically made single PEMFC operated in a test facility that allows controlled conditions. Some results are given in fig. 2 for an identification performed on a single polarization curve and in fig. 3 for one performed simultaneously on several polarization curves.

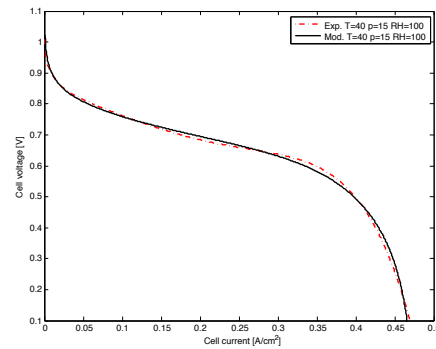


Fig. 2 – Results of the identification run on a single polarization curve. Dashed: experimental, continuous: optimized model

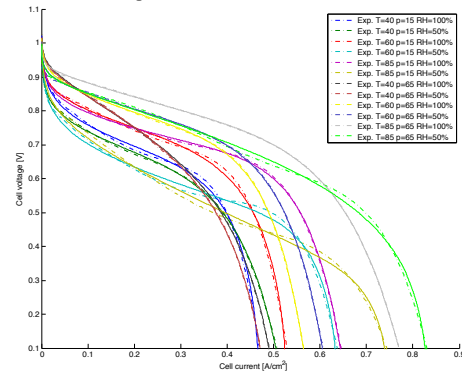


Fig. 3 – Results of the identification run simultaneously on several polarization curves. Dashed: experimental, continuous: optimized model

These and other results will be widely discussed in the presentation.

## REFERENCES

- [1] Guarnieri M., Negro E., Di Noto V., Alotto P., A Selective Hybrid Stochastic Strategy for Fuel-Cell Multi-Parameter Identification, Journal of Power Sources, volume 332,2016, pp. 249–264.

## Fuel Cell Electric buses in Europe: From demonstration to commercialization (Results of the HighVLOcity – 3Emotion projects)

*Valentine Willmann, Communication manager High V.LO-City –Hyer, Brussels (Belgium)*

*Liesbet Vanhoof, Communication manager 3Emotion, WaterstofNet, Turnhout (Belgium)*

**The High V.LO-City and the 3Emotion projects, co-funded by the Fuel Cells and Hydrogen Joint Undertaking, are helping to decarbonise the public transport sector in Europe by deploying zero emission fuel cell buses in 10 cities and regions in Europe.**

It is now widely acknowledged that the future of public transport buses will have to be zero emission.

Fuel Cell electric buses are one of the technologies that meet that requirement.

### ***I. Fuel Cell Electric Buses***

FCEBs are a type of electric buses, using fuel cells and batteries to power the electric motor. Instead of storing energy in large batteries, fuel cells use hydrogen **and** oxygen to generate electricity, producing only heat and water as a by-product.

Hence they produce no harmful emissions, less noise and vibrations, and they have a longer range (400 km) than battery electric buses. The buses can also be refuelled in less than 12 minutes and only need to be refuelled once a day.

At this moment about 70 buses are already in operation in Europe, with around 150 more buses to be deployed in the next few months. They drove more than 8 500 000 km, which means a total reduction of more than 9000 kg of CO<sub>2</sub> and 3 400 000 litres of Diesel.

The readiness of the technology has been proven and significant hurdles in the operation of the buses have been identified and overcome.

### ***II. High V.LO-City and 3Emotion: 43 FCEB's at 9 locations in Europe***

The High V.LO-City and 3Emotion project, are the 3th and 4th European demonstration projects, co-funded by the Fuel Cells and Hydrogen Joint Undertaking, deploying 43 FCEB's and their hydrogen refuelling infrastructure in 9 European cities, including two Italian cities.

The main objectives of the High V.LO-City project are to reduce the total cost of ownership of the buses and to increase the overall operational availability of the buses.

High V.LO-City has four demonstration sites in Europe:

- 4 buses are operating in Aberdeen, Scotland since March 2015
- 5 buses and a refuelling station are in operation in Antwerp, Belgium since December 2014
- 2 buses are operating in Groningen, the Netherlands since February 2017 with the refuelling station to start operations in December 2017
- 3 buses and a refuelling station will start operations in San Remo, Italy, in the next few weeks.

3Emotion has six demonstration sites in Europe:

- 6 buses in Rotterdam (NL). Two buses are in operation in the city center of Rotterdam since September 2017. 4 intercity buses are planned to be operational in Q3 2018. An existing refuelling station is expanded.



- 2 new buses and the further use of 8 buses in London (UK): the 8 buses are in operation since 2011, the 2 new buses be operational November 2017.
- 2 buses in Versailles (FR) and a new refuelling station (planned Q4 2018)
- 3 buses in Aalborg (DK) and a new refuelling station (planned Q1 2019)
- 5 buses in Rome (IT) and a update existing refuelling station (planning tbc)
- 3 articulated buses in Pau (FR) and a new refuelling station (planned Q3 2019)

Each deployment site has string local drivers to deploy hydrogen buses: some regions are producing a lot of excess renewable energy that can be transformed into hydrogen for instance. For other regions, the hydrogen sector represents a strong economic development opportunity. For all the sites, zero-emission buses are a suitable option to replace diesel buses.

Policy drivers are also very important, as there is a strong political and regulatory push for cities and regions to reduce their emissions from the transport sector. Decarbonising the public transports is often seen as the first step to decarbonise transport on the local level.

The hydrogen used by the buses in the projects is either produced by electrolysis with green electricity, or is an industrial by-product.

### **III. First conclusions**

With more than 26 buses already in operation, first conclusions can be drawn from these two projects which are preparing the ground for large scale deployment and market uptake of FCEBs in Europe in the next few years.

Good results have already been achieved since the beginning of the projects.

In High V.LO-City, the refuelling stations have reached an average availability of more than 97%, which means that they are highly reliable and they can be used in full commercial operation. The buses in operation are now reaching 80% of average availability, which brings the fuel cell technology closer to the conventional fuel technologies. The average refuelling time of the buses is between 10 and 12 minutes, which is very similar to the refuelling time of a diesel bus.

The projects have also demonstrated that the pollution savings are very important for Co2 but also for PM and for Nox emissions. We have also noticed that both the bus drivers and the passengers are highly enjoying fuel cell buses.

It is now important to share the lessons learned of the projects. The projects showed for instance that roles and responsibilities need to be clearly defined at the beginning of the project. The deployment of vehicles also needs to be aligned with the infrastructure construction. Training and communication are key points: drivers and technicians need to be well trained before and after the deployment of buses, and bus passengers need to be informed about the new technology.

The projects have shown that for an optimal operation of the buses, the new technology needs to be introduced smoothly in the larger fleet. An initial teething period is necessary so expectations need to be well managed.

The projects have also made big steps towards the deployment of larger fleets of fuel cell buses, by reducing the teething period and by working on the supply chain of spare parts for instance.

The projects have also collaborated to create a fuel cell buses knowledge base: the website [www.fuelcellbuses.eu](http://www.fuelcellbuses.eu). The objective of this website is to gather all useful information and experience about the operation of fuel cell buses in Europe. The information on this website is in particular aimed at buses operators and municipalities willing to deploy fuel cell buses in their bus fleets in the near future.

### **IV. Next steps**

After the High V.LO-City and the 3Emotion projects, the objective is now to move from small demonstration fleets to larger fleets of 10 to 20 buses per site. More cities in Europe have already announced that they will deploy fuel cell buses in the next few years, especially as part of the JIVE project, that will deploy 139 buses in 5 and associated refuelling infrastructure across the UK, Germany, Italy, Latvia and Denmark in the next 6 years.

The larger deployment of fuel cell buses will contribute to bring the capital costs of the buses down, and will bring the operation of the buses closer to the operation of conventional fuel buses.

EFC17144

# STACK-BASED TECHNOLOGIES FOR ENERGY STORAGE: A COMPARATIVE ASSESSMENT

Massimo Guarnieri\*

\*Department of Industrial Engineering – University of Padua,  
via Giovanni Gradenigo 6/a, 35131 Padova, (Italy)

**Abstract** – Mobile and stationary energy storage systems will grow worldwide in the next future due to the evolution toward carbon-free renewable energy sources. On one side energy storage is the most challenging hurdle to the success of electric mobility. On the other side, stationary storage is expected to face not only the intermittency of renewable sources, but also to offer advanced services in the framework of the smart-grid concept. Electrochemical storage systems are the solution of choice to face most of these services. Among them Fuel Cells and Redox Flow Batteries exhibit high potentials because of their power/energy independent sizing, that makes them extremely attractive when longer discharge times are needed. Both are made of several cells connected together to form stacks, which are fed with fuel delivered from external tanks. Nevertheless, they present major differences, which make the one or the other more suitable for specific services.

**Index Terms** – Electrochemical Energy Storage, Fuel Cells, Redox Flow Batteries.

## I. INTRODUCTION

Stationary and mobile energy storage systems will grow worldwide in the next future due to the evolution toward non-polluting carbon-free renewable energy sources. According to a 2011 report of the Boston Consulting Group, stationary energy storage market will increase to US\$10B/year in the next years, totaling US\$280B investments by 2030 at an installed power of 330 GW, i.e. 250÷300% of present 128 GW. In fact, stationary energy storage is expected to face not only the intermittency of renewable sources, but also to offer advanced services in the framework of the smart-grid concept, both at national and local

(mini-grid, micro-grid) levels. These services range from power quality, with sag compensation, power smoothing, grid stabilization and frequency regulation, to energy management, with load leveling, load following, power balancing, peak shaving, and time shifting (when hourly pricing is offered) up to investment deferral. Mobile energy is expected to exhibit an increase similar to stationary applications, due to the expansion of electric mobility, either road, waterborne, and airborne APU, which will add to the already vast market of portable electronics. Energy storage is regarded as the most challenging hurdle to the full success of electric mobility.

We can rely on and are developing a number of different technologies to face this energy storage demand. The most important are: Pumped Hydro Energy Storage (PHES), Compressed Air Energy Storage (CAES), Thermal Energy Storage (TES), Flywheel Energy Storage (FES), Superconducting Magnetic Energy Storage (SMES), Supercapacitor Energy Storage (SES), and ElectroChemical Energy Storage (ECES). PHES is a very consolidated technology that covers 99% of the installed storage power, but it cannot provide services with very fast dynamics and its plants undergo strict geographical requirement since it needs high-level and low-level reservoirs, which are easily available only in mountain areas. Moreover the creation of artificial reservoirs implies a not-negligible environmental impact. Other technologies present even tighter site and/or operational issues or are in an early phase of development. In this framework, ECES will play a pivotal role for both stationary and mobile uses, because of its advantages on other technologies.

Copyright © 2017

## II. FUEL CELLS AND REDOX FLOW BATTERIES

As a matter of fact, ECES systems are the solution of choice in many applications because of their localization flexibility, round-trip efficiency, scalability, and other appealing features. Among them Fuel Cells (FCs) and Redox Flow Batteries (RFBs) present the unique feature of using fluid fuel/electrolytes so that electrochemical reactions can last as long as fluids are pumped into the cells. Consequently, power (that depends on the cell size) and energy (that depends on the fuel/electrolytes volume) are independently rated. This feature makes them extremely versatile and competitive when long discharge times are needed. Both these conversion devices use (typically) planar cells, which develop a voltage in the order of one volt and are sized at the required current, and resort to a similar structure, which consists of several cells connected in series by means of bipolar plates to form stacks which produce voltages of some tens of volts. In both cases, fluids are delivered to the stacks from external tanks, sized at the energy rating. Nevertheless, they also present major differences, in terms of current density, energy density that can be stored in the fluids, fluid viscosity and conductivity, electrical efficiency. These differences make FCs and RFBs suitable for different services.

### A. Fuel Cells

Polymer electrolyte membrane FCs (PEMFCs or also PEFCs) exhibit high current density (around  $2 \text{ Acm}^{-2}$ ) that results in high surface power density ( $0.3\text{--}1.2 \text{ Wcm}^{-2}$ ), but their efficiency remains relatively low (55%–60%). Since hydrogen is very light, fuel energy density is quite high (33–39 kWh/kg). Low operating temperatures assure short start-up times and relatively fast dynamics, but also involve expensive catalyzers based on precious metals (even in the case of platinum-free system, which appear at hand). Even though durability (2,500 hours) and cost remain an issue, PEMFC are gaining an increasing consensus for electrical mobility in FC electric vehicles (FCEVs) due to their superior range with respect to battery electric vehicles (BEVs), particularly after the Toyota Mirai has been put on the market and with the next commercialization of other FCEVs by major car producers. High temperature FCs such as SOFCs and MCFCs (600–800°C), are fuel-tolerant, have similar efficiencies (60%) with good power densities ( $0.35 \text{ Wcm}^{-2}$ ) and get rid of precious metal catalyzers, but have slower dynamics which prevent their use for a number of services. The high temperatures of SOFCs and MFCs allow them to be profitably used in Combined Power and Heat (CPH) system, with very good overall efficiency. On the other hand FCs, although being theoretically reversible, are typically developed into unidirectional devices in order to achieve optimal performance. Thus, they must be complemented with PEM or alkaline electrolyzers (PEMEC, AEC) when used for grid energy storage. The round-trip efficiency (43%–48%) is quite less than a competitive figure.

### B. Redox Flow Batteries

As well as FCs, RFBs are the object of vast researches but lay at an earlier development stage. The presently commercialized type is the all vanadium version (VRFB). It exhibits response-time in the order of milliseconds, high overloading (400%) for short times, good round-trip efficiency (75% and over), room temperature operation, low self-discharge, and extremely long durability (20,000 cycles). Moreover, they are fully reversible, so that one device performs both charge and discharge. On the other hand, they have low current, power and energy densities (around  $0.2 \text{ Acm}^{-2}$ ,  $0.15 \text{ Wcm}^{-2}$ ,  $50 \text{ Wh/kg}$ ). These features make RFBs unsuitable for mobile applications, at least in the all vanadium chemistry, but they are a competitive alternative for stationary energy storage. In fact, their cost per managed energy (cost per discharged energy per number of cycles) is unsurpassed by other ECES system, as shown in Fig. 1, which presents the main data of five stationary ECES systems which have been recently commissioned for a multi-technology energy storage facility under construction in Venice.

TABLE 1 - THE MAIN DATA OF COMPETING ELECTROCHEMICAL STORAGE TECHNOLOGIES FOR STATIONARY SERVICES.

ECES TECHNOLOGY	ENERGY DENSITY [WPA/KG]	DISCHARGE TIME [h]	RESPONSE TIME	ROUND-TRIP EFFICIENCY	CYCLE LIFE [10 <sup>3</sup> ]	CAPEX [€/KWH]	CAPEX [€/KWH]	CAPEX [€/KWH/CYCLES]
Advanced Pb-acid	25–50	1–2	ms	75%	0.8	1.8	770	86.3
Na-S	150–120	2–6	ms	80%	4.5	3.6	450	10.0
Na-Ni-Cl	95–120	0.5–2	ms	90%	4.5	3.55	1638	36.4
Li-ion	100–200	1	ms	87%	4.0	0.71	1246	31.1
H <sub>2</sub> electrolyzers/FCs	800–1300	>10	10 <sup>3</sup> ms	24%	0.3	73	<1880	<626.7
VRFB	24	>10	ms	75%	20	2.65	<863	<4.8

Costs include ancillaries (discharge times are at rated power; cost figures based on 2015 commercial contracts; capex = capital expenditure).

Fig. 1 - Main data of competing electrochemical storage technologies for stationary services - costs include ancillaries (discharge times are at rated power; cost figures based on 2015 commercial contracts; capex = capital expenditure).

RFBs' potentials have been recognized by the Joint Center for Energy Storage Research, the U.S. program led by the Argonne National Laboratory, which considers them as the most promising "after lithium" energy storage technology.

## III. RESULTS

The comparison of FCs and RFBs for mobile and stationary storage will be widely discussed in the presentation.

## REFERENCES

- [1] C. Pieper, H. Rubel, "Revisiting energy storage. There is a business case," Boston Consulting Group Report, Feb. 2011
- [2] P. Alotto, M. Guarnieri, F. Moro, "Redox Flow Batteries for the storage of renewable energy: a review", *Renew. Sust. Energ. Rev.*, 29 (2014): 325-335
- [3] G. Spagnuolo, G. Petrone, P. Mattavelli, M. Guarnieri, "Vanadium Redox Flow Batteries: Potentials and Challenges of an Emerging Storage Technology", *IEEE Industrial Electronics Magazine*, 10 (4), (2016): 20-31
- [4] Crabtree G., Next Generation Energy Storage Beyond Lithium Ion, UIC Physics Club, Argonne National Laboratory, July 28, 2015., presented at the 228<sup>th</sup> ECS Meeting, Phoenix, AZ, Oct. 11-15, 2015.

## POWER-TO-HYDROGEN AND HYDROGEN-TO-X: LATEST RESULTS OF TASK 38 OF THE IEA HYDROGEN IMPLEMENTING AGREEMENT

P. Lucchese<sup>1</sup>, C. Mansilla<sup>1</sup>, F. Dolci<sup>2</sup>, R. R. Dickinson<sup>3</sup>, C. Funez<sup>4</sup>, L. Grand-Clément<sup>5</sup>, S. Hilliard<sup>6</sup>, J. Proost<sup>7</sup>, M. Robinius<sup>8</sup>, M. Salomon<sup>6</sup>, and S. Samsatli<sup>9</sup>

<sup>1</sup> CEA, Université Paris Saclay, Gif-sur-Yvette (France)

<sup>2</sup> European Commission, Petten (Netherlands)

<sup>3</sup> Hydricity Systems Australia and University of Adelaide, Centre for Energy Technology, Adelaide (Australia)

<sup>4</sup> Centro Nacional del Hidrógeno, Puertollano (Spain)

<sup>5</sup> PersEE, Paris (France)

<sup>6</sup> Clean Horizon Consulting, Paris (France)

<sup>7</sup> Université catholique de Louvain, Division of Materials and Process Engineering, Louvain-la-Neuve (Belgium)

<sup>8</sup> Institute of electrochemical process engineering (IEK-3), Forschungszentrum Jülich GmbH, Jülich (Germany)

<sup>9</sup> Department of Chemical Engineering, University of Bath, Bath (United Kingdom)

**Abstract** - Task 38 of the Hydrogen Implementing Agreement of the IEA is dedicated to the analysis of Power-to-Hydrogen and Hydrogen-to-X pathways, with a final objective of providing business developers and policy makers with recommendations to enable hydrogen as a key energy carrier for a sustainable integrated energy system. This paper offers an appraisal of the recent work, mostly dedicated to review and state-of-the-art analysis.

**Index Terms** – HIA, Power-to-Hydrogen, Power-to-X

### I. INTRODUCTION

Energy systems are changing around the world due to a variety of factors [1]-[2]:

- Increasing demand for energy in the world due to globalization and emerging countries;
- Increasing renewable share in the energy mix, especially in the electricity mix;
- Greenhouse gas constraints and CO<sub>2</sub> emission reduction targets in the energy sector;
- Local pollution constraints;
- Deregulation in the energy system, allowing new challengers to enter the market;
- Energy security constraints, system reliability objectives;
- Decentralisation of energy production systems.

The balancing of the electricity grid is increasingly challenging as the installed renewable energy capacity is increasing. Solutions such as transmission super grids, smart

grids, energy storage, demand management, and back-up capacity implementation can contribute; but new measures that go beyond increasing transmission capacity and flexible generation or consumption will have to be introduced to manage the grid as the level of renewable energy sources is increased. Power-to-hydrogen (PtH) system components are clearly part of the broader picture [3]. Hydrogen production via electrolysis makes it possible to quickly adjust the power consumption: electrolyzers can reach full load operation in a few seconds [4]. They can also decrease demand in sub-seconds for providing frequency control services. As a result, hydrogen production can be an economically and technically attractive way to contribute to power systems management.

The “Power-to-hydrogen” concept means that, especially once hydrogen is produced from low-carbon electricity, a potentially large portfolio of uses is possible. Applications across diverse sectors include transport, green chemistry, electrification (i.e. power storage), blending with natural gas, and also the general business of merchant hydrogen for energy or industry. Providing ancillary services or grid services for the electricity grid, transport or distribution grid may also be considered. Indeed, hydrogen can provide flexible energy storage and carrier options which could help in managing the energy system. With these benefits in mind, a task of the Hydrogen Implementing Agreement (HIA) of the International Energy Agency (IEA) was approved in October 2015 by the 72<sup>nd</sup> HIA Executive Committee as “Task 38”, to examine



hydrogen as a key energy carrier for a sustainable integrated energy system. It is entitled: “Power-to-Hydrogen and Hydrogen-to-X: System Analysis of the techno-economic, legal and regulatory conditions”. This paper presents the Task and its latest achievements.

## II. TASK DESCRIPTION

The general objectives of the Task are: i/ to provide a comprehensive understanding of the various technical and economic pathways for power-to-hydrogen applications in diverse situations, ii/ to provide a comprehensive assessment of existing legal frameworks, and iii/ to present business developers and policy makers with general guidelines and recommendations that enhance hydrogen system deployment in energy markets. A final objective will be to develop hydrogen visibility as a key energy carrier for a sustainable and smart energy system, within a 2 or 3 horizon time frame: 2030 and 2050, for example. The work is slated to take place over a four-year period, and is structured in two phases:

- 1/ a general state-of-the-art survey of existing studies on techno-economic and business cases, existing legal framework, including demo/deployment projects;

- 2/ detailed specific cases studies, based on detailed targets defined during the first phase, together with elaboration of legal and regulatory conditions, policy measures, and general guidelines for business developers as well as public and private financial mechanisms and actors.

Today, the task gathers over 50 experts of 37 organisations from 17 countries.



Fig. 1. Affiliations of the Task 38 members

## III. LATEST ACHIEVEMENTS

The first phase involved several actions. To start with, the main PtH pathways and interconnections were identified in a way that overcomes the ambiguities inherent in the term “Power-to-Gas”. In turn, this aims at providing solid and easier to understand foundations for building legal and regulatory frameworks for new business opportunities [5].

Another part was dedicated to the compilation of state-of-the-art technical and economic data on large-scale water electrolyser systems, both for PEM and alkaline technology, from the major electrolyser manufacturers worldwide [6]. A workshop on PtH demonstrations will also help identify the

next steps towards commercialization.

An extensive literature review of the current PtH literature was undertaken [7]. The aim was to capture diversity within the current literature and draw some major conclusions from it. Over 200 documents were reviewed with a methodology developed to analyze the variety of studies considered. This reviewing effort relied on the participation of the members of Task 38, both to co-construct a database of existing studies on PtH and to review the works. The first step is almost complete and will be followed by in-depth analysis of the most relevant studies. A similar approach is being applied for the review of the regulatory and legal context for PtH, in a number of countries. Business cases will be assessed, building on this thorough review step.

Modelling is not neglected either. A workshop was organized by the University of Bath on energy system modelling and the role of hydrogen. Lively and productive debates dealt with the key issues and future avenues for hydrogen systems research. Data is a key issue in this context, to be addressed in a more global IEA HIA approach.

## IV. CONCLUSION

Task 38 of the Hydrogen Implementing Agreement is dedicated to the analysis of PtH pathways, with a final objective of providing business developers and policy makers with recommendations to enable hydrogen as a key energy carrier for a sustainable integrated energy system. Recent work was mostly dedicated to review and state-of-the-art analysis. Building on this, next steps will also involve modelling to develop relevant recommendations.

## ACKNOWLEDGMENT

This work was conducted in the framework of the Task 38 of the IEA HIA. The Task is coordinated by the Institute for techno-economics of energy systems (I-tésé) of the CEA, with the support of the ADEME.

## REFERENCES

- [1] IEA, "Renewable Energy: Medium-Term Market Report 2016: Market Analysis and Forecasts to 2021," 2016.
- [2] New York State, "Reforming the Energy Vision: Whitepaper March 2016", New York, 2016.
- [3] SBC Energy Institute (2014), Leading the Energy Transition Factbook, Hydrogen-based energy conversion - More than storage: system flexibility.
- [4] A. Godula-Jopek, Hydrogen production by electrolysis, Wiley, 2015.
- [5] R. Dickinson et al., Power-to-Hydrogen and Hydrogen-to-X pathways: Opportunities for next energy generation systems, EEM15 conference, Dresden, Germany, June 6-9, 2017.
- [6] J. Proost, State-of-the-art CAPEX data for water electrolyzers, and their impact on renewable hydrogen price settings, EFC17 conference, Naples, Italy, December 12-15, 2017.
- [7] M. Robinius, et al., Power-to-Hydrogen and Hydrogen-to-X: Which markets? Which economic potential? Answers from the literature, EEM15 conference, Dresden, Germany, June 6-9, 2017.



## WATER TRANSPORT SIMULATION IN A GDL OF PEMFC USING LBM

D. H. Jeon\*

\*Department of Mechanical System Engineering, Dongguk  
University, Gyeongju, Republic of Korea

**Abstract** - The effect of rib on the dynamic behavior of liquid water transport in gas diffusion layer (GDL) is studied. The mechanism of water transport dynamics investigated using multiphase lattice Boltzmann method (LBM). Simulation with a simplified two-dimensional model is used to predict liquid water transport processes in local regions, instead of pursuing a three-dimensional numerical analysis for the entire domain. The observation of lattice Boltzmann (LB) simulation shows that the rib changes the water transport behavior and significantly affects the water transport in GDL.

**Index Terms** – PEMFC, LBM, GDL Water transport.

### I. NOMENCLATURE

A nomenclature list, if needed, should precede the Introduction.

### II. INTRODUCTION

Water management is one of the challenges in polymer electrolyte membrane fuel cells (PEMFCs) and regarded as a critical issue for achieving high performance PEMFC. While the membrane should have sufficient hydration to maintain good proton conductivity, excessive amount of water generated and accumulated in the membrane electrode assembly (MEA) can cause flooding in catalyst layer (CL).

In this study, the dynamic behavior of liquid water in the GDL is investigated numerically using a two-dimensional LBM approach. The two-phase intermolecular potential model proposed by Shan and Chen is used to examine the microscopic behavior occurring at the pore-scale in a complex porous structure. The effective permeability of GDL from two-dimensional simulation is verified by comparing the LB result with analytical solution and experimental results in the literature. The cross-sectional water distribution and water saturation profiles are presented to understand the wetting characteristic in the GDL. The effect of rib structure on the water transport behavior in the GDL is discussed.

### III. MODEL DEVELOPMENT

#### A. Lattice Boltzmann Method (LBM)

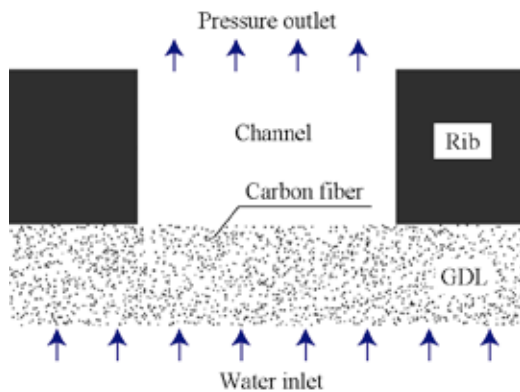
LBM simulates mass transport of multi-phase mixture by tracking movements of particle ensembles on a mesoscale-level. In this study, we developed the Shan-Chen pseudo-potential based two-phase LB model that allows the separation of two immiscible fluids if the interaction force between the fluids is larger than a threshold value. The time variation of distribution functions is calculated by performing a simple law of collision and streaming steps. The multiphase LB Model with a single relaxation time (SRT) for collision operator is applied in the lattice Bhatnagar-Gross-Krook (LBGK) equation. The time evolution of this model can be written as

$$f_i(\mathbf{x} + \mathbf{e}_i \Delta t, t + \Delta t) = f_i(\mathbf{x}, t) - \frac{\Delta t}{\tau} [f_i(\mathbf{x}, t) - f_i^{eq}(\mathbf{x}, t)] + S_i(\mathbf{x}, t) \quad (1)$$

More detailed description of the LB model can be found in Ref. [1].

#### B. Computational domain

The schematic domain of LB model for the simulation is shown in Fig. 1. The computational domain consists of channel, rib and the GDL. The dimension of calculation domain is  $2000 \times 1000 \text{ lu}^2$  (lu: lattice unit). The GDL height is set to 400 lu, a rib height to 600 lu, and a channel width to 1000 lu. The porous structure of the GDL is constructed as impermeable solid particles and pore area which has void space. The commercial carbon paper SGL<sup>®</sup> 10BA with 5% PTFE content is taken into consideration for the modeling of GDL, and thus the porosity and particle diameter are set to 0.88 and 10 lu, respectively [2]. The boundary conditions proposed by Zou and He [3], who implemented it on the inlet/outlet boundaries and the no-slip

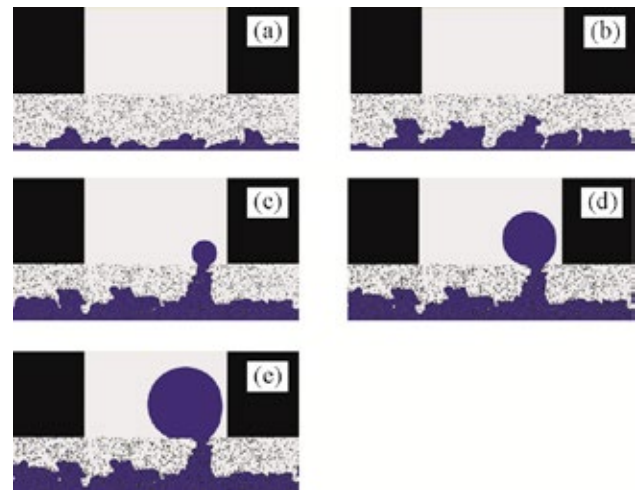


**Fig. 1.** Computational domain of two-dimensional LB model.

bounce back, are applied. The inlet condition is set to the bottom boundary with the inflowing velocity of  $1.0 \times 10^{-4}$  lu.

#### IV. RESULTS AND DISCUSSION

Fig. 2 shows the liquid water distribution in the GDL. Present model consists of two fluids, i.e., liquid water and gaseous air. In the picture, blue and light grey represent the liquid water and gaseous air, respectively. A constant velocity is given for liquid water at the inlet to push gaseous air toward the outlet. Fig. 2(a) presents liquid water distribution at  $1.0 \times 10^6$  lattice time, and the wettability distributions are presented after each  $0.5 \times 10^6$  lattice time as shown in Fig. 2(b) ~ 4(e). As shown, the invaded liquid water travels through the pores between the carbon fibers, presenting complex flow patterns due to the complicated structures of GDL. Consequently, the air moves driven by the mean flow motion of the water. In Fig. 2(a), liquid water is observed at the bottom, indicating that the GDL accumulates the water from the inlet. Liquid water forms several water clusters and the clustered water presents convex water fronts due to hydrophobic carbon fibers. In Fig. 2(b), liquid water selects some preferential paths to flow in the in-plane or through-plane direction which has lower resistance force. Liquid water selects relatively wide throats while the linked water clusters form a single flow path through a merging process. Once the dominant path has selected, the water flows into the main branch and stretches toward the channel. In Fig. 2(c), the water breakthrough occurred at the end of the dominant path. This figure indicates that the dominant path leads the water breakthrough. In Fig. 2(d) and (e), the water droplet becomes larger as lattice time increases. However the water distribution inside the GDL is little changed. This is attributed to the formation of the droplet in the channel which increases the water droplet size through the dominant path, while suppressing the water spread in the GDL. These figures indicate that the large pores are mainly used as a pathway for liquid water transport, and thus the small pores can be available for gaseous reactant transport. These figures indicate that the



**Fig. 2.** Simulated sequence of transient water transport in the GDL. (a)  $1.0 \times 10^6$  lattice time, (b)  $1.5 \times 10^6$  lattice time, (c)  $2.0 \times 10^6$  lattice time, (d)  $2.5 \times 10^7$  lattice time, and (e)  $3.0 \times 10^7$  lattice time

liquid water selectively stretches toward the wider pore area as well as the channel region.

#### ACKNOWLEDGMENT

This research was financially supported by the National Science Foundation of Korea (NRF) grant funded by the Korea government (NRF-2016R1D1A1A09916637).

#### REFERENCES

- [1] Jeon D.H, Kim H., Effect of compression on water transport in gas diffusion layer of polymer electrolyte membrane fuel cell using lattice Boltzmann method, J Power Sources 294, 2015, pp. 393-405.
- [2] Gostick J.T., Fowler M.W., Pritzker M.D., Ioannidis M.A., Behra L.M, In-plane and through-plane gas permeability of carbon fiber electrode backing layers, J Power Sources 162, 2006. pp. 228-238.
- [3] Zou Q., He X., On pressure and velocity boundary conditions for the lattice Boltzmann BGK model, Phys Fluids 9, 1997, pp. 1591-1598.

**Biochar-cathode-based Microbial Fuel Cells and carbon metal mesh performances in Solid-Phase-MFCs fed with the Organic Fraction of Municipal Solid Waste (OFMSW).**

Rosa Anna Nastro\*, Fabio Flagiello, Viviana Cigolotti\* and  
Elio Jannelli\*

\* Department of Engineering, University of Naples Parthenope,  
Centro Direzionale Isola C4, Naples - Italy

\*\* ENEA - Italian National Agency for New Technologies, Energy  
and Sustainable Development

**Abstract –**

In recent years, the research about cheap and effective materials to be used as components in Microbial Fuel Cells (MFCs) has done significant progresses, even in sight of a scaling-up and wide application of MFCs to waste and water remediation. Biochar material has been ascribed as a good candidate for the set-up of low environmentally impactant and cheap electrodes, with particular regards to anodes. In the present research, we explored the utilization of a biochar-based material produced in the steel industry as a potential cathode material for single chamber, air-cathode, cuboid MFCs fed with vegetable residues among the Organic Fraction of Municipal Solid Waste (OFMSW). A cathode made of a nickel mesh current collector, an activated carbon layer, and a porous PTFE (Polytetrafluoroethylene) diffusion layer was purchased from VITO (Mol, Belgium) and used as an already established cathode material for MFCs. Before being used in MFCs, both materials were preliminary tested by a Cyclic Voltammetry (CV) by using iron hexacyanoferrate (III) 0.02 M in a KCl solution (0.1 M). Then, cuboid MFC (30 ml in volume) with carbon fiber brush (Mill-Rose Ltd.) as anode were inoculated with an OFMSW suspension in PBS buffer (pH 7, 30% solid/liquid ratio) opportunely homogenized. MFCs (in double replicas) run at 25°C for three weeks. On the whole, three cycles of experiments were performed. Polarization curves were performed every 48 hours using loads within a 1000000-100 Ohm range. Cyclic Voltammetry (CV) was performed as well. The MFCs performances were evaluated in terms of Power Density (PD) and Current Density (CD). Our results showed for biochar a lower PD and CD performance during the first two weeks of operation in comparison to the nickel-mesh/activated carbon electrode, but recyclable and reusable even if in presence of a significant amount of acidogenic bacteria. After three cycles of utilization, biochar cathode performance significantly decreased. Nevertheless, the use of biochar-based material could contribute to the application of MFC technology to solid organic waste treatment and valorization.

**Index Terms** - Biochar, Organic Fraction of Municipal Solid Waste, Microbial Fuel Cells.

**I. INTRODUCTION**

Electrodes material and geometry play a role of fundamental importance in Microbial Fuel Cells (MFCs) performances, as well as in other Bioelectrochemical Systems (BESs) [1]. Recently, among other carbon-based materials, biochar (BC) have attracted the interest of many researchers. Biochars are complex heterogeneous materials consisting of mineral phases, amorphous carbon, graphitic carbon, and labile organic molecules, many of which can be either electron donors or acceptors. Such redox properties are at the basis of the interaction of biochar with plant roots, soil microorganisms, organic matter, nutrients to form organo-mineral-biochar, which increase soil fertility [2]. These features make biochar a competitive electrode material for MFCs at significantly lower cost than traditional materials (such as activated carbon), but also because of the possibility of using spent BC electrodes as an agricultural amendment, thus reducing the environmental burden of MFC operation [3]. In this study, we present the preliminary results of a survey aimed at assessing the potential utilization of *Pinus resinosa* wood biochar bars to build cathodes for MFCs (B-MFCs) fed with organic solid residues from the Organic Fraction of Municipal Solid Waste (OFMSW). B-MFC performance were compared to the ones obtained by MFC provided with a cathode made-up by a nickel-mesh collector, activated-carbon layer and a porous PTFE diffusion layer (N-MFC) purchased from VITO Ltd.

**II. MATERIALS AND METHODS**

Bars of 5 cm width, 6 cm height were obtained from a high temperature pyrolysis (850 °C) biochar produced from *Pinus resinosa* wood and compressed by an industrial press at 700 ton/cm<sup>2</sup>. The bars were further exposed to high temperatures (1000-1200 °C) during furnaces operation and, eventually, used, cut into slices of 0.4 cm thickness. Cuboid, membraneless MFCs (30 mL in volume) provided by a carbon fiber-brush (Mill-Rose Ltd) as an anode were provided with the biochar-based slices (previously washed with freshwater) as cathode (7.0 cm<sup>2</sup> projected area).

Before being used in MFCs, we tested the biochar material (1 cm<sup>2</sup> surface sample, 0.4 cm thickness) with a Cyclic Voltammetry (CV) at 5 mV/s. Iron hexacyanoferrate (III) (0.02 M) in a KCl solution (0.1 M)



was used as test solution to verify the redox properties. An Ag/AgCl electrode was used as reference in the voltammetry experiments. Then, cuboid MFC (30 ml in volume) with carbon fiber brush (Mill-Rose Ltd.) as anode were inoculated with an OFMSW suspension in PBS buffer (pH 7, 30% solid/liquid ratio) and run in duplicate at 25°C for three weeks. MFCs electrochemistry was investigated by CV by the use of an AUTOLAB Potenziostat, (Methrom) provided with a carbon glossy electrode. The data collection hardware was based on the Arduino board MEGA 2560, composed by a load array (for polarization curve acquisition) within a 1000000-100 Ohm range. The software for data acquisition was ad-hoc developed in our Lab with LabVIEW Interface For Arduino, (LIFA) package. After a starting Open Circuit Voltage (OCV) phase (24 hours), MFCs were serially connected to a 1000  $\Omega$  resistor for 24 hours. Polarization experiments were performed every 48 hours and the cells kept at maximum power.

### III. RESULTS

CV carried out with iron hexacyanoferrate (III) revealed for biochar material two reduction (at +170 mV and +387 mV) and an oxidation peaks at +570 mV.

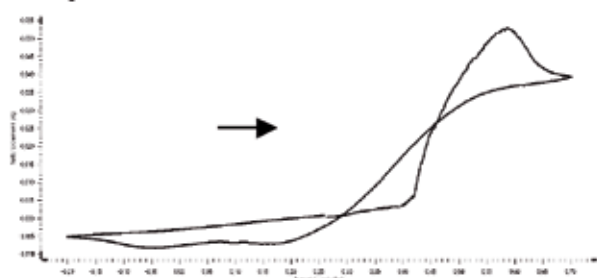


Figure 1: Biochar CV (mV/s) in iron hexacyanoferrate (III) 0.02M, 0.1 M KCl.

No net peaks were, instead, observed in CV (5 mV/s scan speed) performed in both MFCs fed with organic substrates. This result could be ascribed to a low electroactivity of the microflora present in the waste itself, as we did not use any inoculum. B-MFC achieved its optimal performance in terms of stability, PD and CD per  $\text{m}^2$  of cathode surface and  $\text{Kg}$  of solid substrates, after 10 days of operation (Fig.2)

Even if both cells showed cell design point at 3000  $\Omega$ , B-MFC had lower outputs values than N-MFC ( $0.27 \text{ W m}^{-2} \text{ Kg}^{-1}$  instead of  $0.72 \text{ W m}^{-2} \text{ Kg}^{-1}$  and a maximum of  $7.4 \text{ A m}^{-2} \text{ Kg}^{-1}$  instead of  $8.7 \text{ A m}^{-2} \text{ Kg}^{-1}$ ). But, unlike nickel-mesh-collector-activated-carbon-PTFE-layer material, biochar kept its properties even after being reused in other experiments. As to pH, a drop from 7.0 to 4.5 was measured in N-MFC after two days of operation, while in B-MFC pH values did not significantly deviate from  $6.6 \pm 0.3$  along with the experiment. After dropping to 4.5, pH in N-MFC was adequately corrected to  $7.0 \pm 0.2$  and kept around that value by using KOH 1M. Difference in pH values could be ascribed to the prevalence, in N-MFC, of fermentative bacteria: even though N-MFC had higher power outputs during the first two weeks, a progressive reduction of N-MFC performance were observed later on. At last, N-MFC underwent to a voltage reversal due to an electrode fouling. An analysis at Scanning Electron Microscope is going to be performed to evaluate the microbial growth and the effect of acidogenesis on cathodes materials.

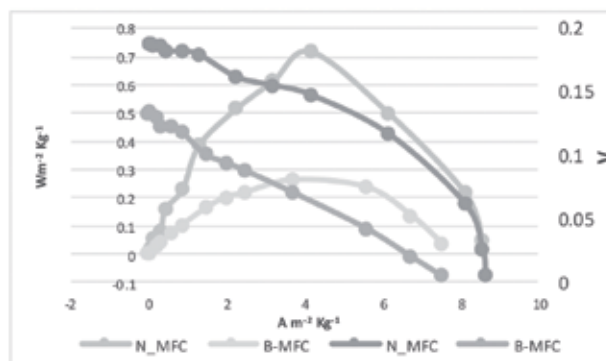


Figure 2: Power and polarization curves after 2 weeks of operation.

### IV. CONCLUSION

Biochar based material from steel industry showed different advantages in comparison to a nickel-mesh- collector, activated-carbon and PTFE-layer electrode: as a scrap material it is very cheap and, due to its properties, it was able to sustain MFC fed with organic residues and with an acidogenic microflora as main component. Given its properties, once exhausted, it could be crushed and used as soil amendment. Our study confirms biochar-based material potentialities in the application of MFCs to solid organic residues treatment and valorization.

### REFERENCES

- [1] Nastro, R.A., Jannelli, N., Minutillo, M., Guida, M., Trifuoggi, M., Andreassi, L., Facci, A.L., Krastev, V.K. and Falcucci, G., Performance evaluation of Microbial Fuel Cells fed by solid organic waste: parametric comparison between three generations. *Energy Procedia*, 2017, 105: 1102-1108.
- [2] Joseph S., Husson O., Graber E.R., van Zwielen L., Taherymoosavi S., Thomas T., Nielsen S., Ye J., Pan G., Chia C., Munroe P., Allen J., Lin Y., Fan X. and Donne S. The Electrochemical Properties of Biochars and How They Affect Soil Redox Properties and Processes. *Agronomy* 2015, 5: 322-340; doi:10.3390/agronomy5030322
- [3] Huggins T.M., Latorre A., Biffinger J.C. and Ren Z.J. Biochar Based Microbial Fuel Cell for Enhanced Wastewater Treatment and Nutrient Recovery. *Sustainability* 2016, 8(2), 169; doi:10.3390/su8020169.
- [4] Zhang F., Cheng S., Pant D., Van Bogaert G., Logan B.E. Power generation using an activated carbon and metal mesh cathode in a microbial fuel cell. *Electrochemistry Communications* 2009, 11: 2177-2179.

## DEMOSOFC PROJECT: RESULTS FROM AN INDUSTRIAL-SIZE BIOGAS-FED SOFC

M. Acri\*, U. Fausone\*, E. Fontell\*\*, M. Gandiglio\*\*\*, S. Giarola\*\*\*\*, T. Hakala\*\*, A. Hawkes\*\*\*\*, J. Kiviaho\*\*\*\*\*, A. Lanzini\*\*\*, E. Lorenzi\*, M. Rautanen\*\*\*\*\*, M. Santarelli\*\*\*

\* SMAT - Società Metropolitana Acque Torino S.p.A. - Corso XI Febbraio, 14 - 10152 Torino (IT)

\*\* Convion Ltd. - Tekniikantie 12 - FIN-02150 Espoo (FI)

\*\*\* Departmen of Energy, Politecnico di Torino - Corso Duca degli Abruzzi 24 - 10129 Torino (IT)

\*\*\*\* Chemical Engineering Department, Imperial College London - London, SW7 2AZ (UK)

\*\*\*\*\* VTT technical research centre of Finland LTD - P.O. Box 1000, FI-02044 VTT (FI)

**Abstract** – The EU-funded DEMOSOFC project aims to demonstrate the technical and economic feasibility of operating a 174 kWe SOFC in a wastewater treatment plant. The fuel for the three SOFC modules (3x58 kWe) is biogas, which is available on-site from the anaerobic digestion of sludge collected from the treated wastewater. A heat-recovery loop allows to recover useful thermal energy from the hot SOFC exhaust gases (90 kWth). The present work is related to the plant layout description and first on-field test of the entire plant.

**Index Terms** – SOFC, fuel cell, biogas, WWTP

### I. NOMENCLATURE

CHP	Combined Heat and Power
HEX	Heat Exchanger
ICE	Internal Combustion Engine
MCFC	Molten Carbonate Fuel Cell
P.E.	Person Equivalent
PM	Particulate Matter
SOFC	Solid Oxide Fuel Cell
VOC	Volatile Organic Compounds
WWTP	Waste Water Treatment Plant

### II. INTRODUCTION

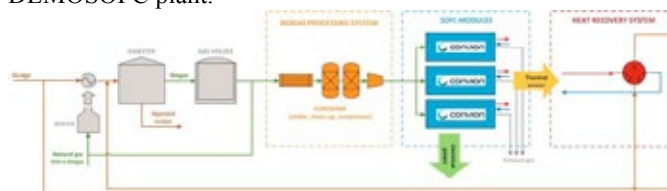
The DEMOSOFC plant [1] is the first European industrial size Solid Oxide Fuel Cell (SOFC) system. The plant aims at demonstrating the technical and economic feasibility of industrial size SOFC systems, with focus on bio-based fuels feedings (e.g. biogas). Industrial size fuel cell systems, usually Molten Carbonate Fuel Cells, MCFCs) are already available outside Europe, especially in USA [2-3], Japan and South Korea. Key advantages of fuel cell based industrial systems in

biogas plants have been deeply demonstration in the authors' previous works [4]–[7] and include:

- High efficiency increase respect to traditional biogas-fed Internal Combustion Engines (ICEs), especially for low-medium size systems. ICEs usually show electrical efficiency ranging from 35-38% to 43%, when the plant size increases from tens of kW to MW size. SOFC systems can indeed provide values higher than 55%.
- Zero emissions to atmosphere in terms of NO<sub>x</sub>, SO<sub>x</sub>, VOC and PM, which are traditionally a criticality in standard combustion engine.

### III. PLAN LAYOUT

The DEMOSOFC site WWTP is located in Collegno, in the Turin premises (IT). The Collegno plant is serving around 180'000 Person Equivalent (P.E.), both residential and industrial users, and currently, exploits biogas for heating-only in a boiler. The integrated biogas-SOFC plant includes three main units: 1) the biogas clean-up and compression section; 2) the three SOFC power modules, and 3) the heat recovery loop. activated carbons). Figure 1 shows a schematic layout of the DEMOSOFC plant.



**Fig. 1. Schematic DEMOSOFC plant layout.**

Copyright © 2017



### A. Biogas cleaning system

A special focus of the demonstration is the deep and reliable removal of harmful contaminants for the SOFC, present in the raw biogas. The biogas processing system includes a first stage of adsorption reactors filled with impregnated activated carbons removal (Figure 2) and a compressor up to 4 bar(g). The biogas cleaning system has been designed after a one-year monitoring of biogas composition in Collegno, where H<sub>2</sub>S (20 ppm max.) and siloxanes (average 1 ppm) have been detected as the main harmful components to be removed. In-line and real-time gas analysis are installed to monitor the removal efficiency of the biogas clean-up unit (Figure 2). The online gas sensor can detect continuously both H<sub>2</sub>S and siloxanes.



**Fig. 2. Activated carbons reactors and online biogas monitoring system.**

### B. SOFC Module

The core of the DEMOSOFC plant are the three C50 SOFC units supplied by Convion (1<sup>st</sup> module is shown in Figure 3).



**Fig. 3. First C50 SOFC Module.**

The modules can provide 55% electrical efficiency and 30% thermal efficiency, which is recovered through an internal HEX fed by exhaust gas and a water-glycol mixture. The three SOFC modules will produce 174 kW<sub>e</sub>, which will cover 25-30% of the WWTP electrical consumption.

### C. Heat Recovery Section

Heat recovered from the SOFC unit is completely transferred to the sludge entering the anaerobic digester.



**Fig. 4. Circulation pumps and secondary sludge-water HEX.**

Circulation pumps and three-way valves for regulation have been installed (Figure 4) and a new sludge-water heat-exchanger is supporting the existing one.

## IV. FIRST RESULTS

The entire system has been started in mid-October. The cleaning system has been tested from the early summer to verify the effectiveness of the contaminants removal and check measurements from the online gas analyzer. SOFC start-up procedure from cold state to full load lasts around 48 hours. First tests were devoted to verify the functionality of all internal equipment after the transport of the first C50 module to Italy.

## V. CONCLUSION

The DEMOSOFC plant is starting its operational phase with the first module start-up. Operation will provide essential results on the overall plant performance, integration with the existing WWTP, operational costs for biogas cleaning, stacks degradation and lifetime.

## ACKNOWLEDGMENT

The research leading to these results has received funding Q8 from the Fuel Cells and Hydrogen 2 Joint Undertaking under grant agreement No. 671470 “DEMOSOFC (Demonstration of large SOFC systems fed with biogas from WWTP).” This Joint Undertaking receives support from the European Union’s Horizon 2020 research and innovation program.

## REFERENCES

- [1] “DEMOSOFC project official website,” 2016. [Online]. Available: [www.demosofc.eu](http://www.demosofc.eu). [Accessed: 20-Dec-2015].
- [2] P. Margalef, T. Brown, J. Brouwer, and S. Samuelsen, “Conceptual design and configuration performance analyses of polygenerating high temperature fuel cells,” *Int. J. Hydrogen Energy*, vol. 36, no. 16, pp. 10044–10056, 2011.
- [3] Fuel Cell Energy, “Fuel Cell Power Plants: Biofuel Case Study – Tulare, CA (DOE-NREL Workshop),” 2012.
- [4] M. Gandiglio, D. Drago, and M. Santarelli, “Techno-economic Analysis of a Solid Oxide Fuel Cell Installation in a Biogas Plant Fed by Agricultural Residues and Comparison with Alternative Biogas Exploitation Paths,” *Energy Procedia*, vol. 101, no. September, pp. 1002–1009, 2016.
- [5] A. S. Mehr *et al.*, “Solar-assisted integrated biogas solid oxide fuel cell (SOFC) installation in wastewater treatment plant: energy and economic analysis,” *Appl. Energy*, vol. 191, pp. 620–638, 2017.
- [6] E. Rillo, M. Gandiglio, A. Lanzini, S. Bobba, M. Santarelli, and G. Blengini, “Life Cycle Assessment (LCA) of biogas-fed Solid Oxide Fuel Cell (SOFC) plant,” *Energy*, vol. 126, pp. 585–602, 2017.
- [7] M. Gandiglio, A. Lanzini, A. Soto, P. Leone, and M. Santarelli, “Enhancing the energy efficiency of wastewater treatment plants through co-digestion and fuel cell systems,” *Front. Environ. Sci.*, vol. 5, p. 70, 2017.

## APPLICATION OF THE DRT (DISTRIBUTION OF RELAXATION TIME) TO THE ELECTROCHEMICAL IMPEDANCE SPECTRA OF MOLTEN CARBONATE FUEL CELLS

E. Audasso\*, S.W. Nam\*\*, J.H. Han\*\*, E. Arato\* and B. Bosio\*

\* Department of Civil, Chemical and Environmental Engineering, University of Genova, (Italy)

\*\* Fuel Cell Research Center, KIST - Korea Institute of Science and Technology, (South Korea)

**Abstract** - The modelling of chemical processes is fundamental to support both the experimental and the industrial activities. In previous works the authors developed a kinetic model to describe the behavior of Molten Carbonate Fuel Cells (MCFCs) on the basis of collected I-V curves. Successively, the model was compared with an analysis of the Electrochemical Impedance Spectra (EIS) and, as a result, the same dependence on operating conditions were obtained verifying its capability. In recent years, interest toward the study of the distributed relaxation times (DRT) applied to impedance spectra has grown, despite a clear interpretation is still missing. In this work the authors analysed the DRT of MCFCs and compared the result to the model to verify the agreement between the model and the phenomena described by DRT.

**Index Terms** – DRT application to MCFCs, kinetics of MCFCs, MCFC modelling.

### I. NOMENCLATURE

$R_{TOT}$ : total cell resistance [ $\Omega \text{ cm}^2$ ]  
 $p$ : operating pressure [atm]  
 $p_i$ : partial pressure of the i-th component [atm]  
 $P_j$ : j-th semi-empirical coefficient [var., see eq. 1]  
 $T$ : operating temperature [K]  
 $y_i$ : molar fraction of the i-th component

### II. INTRODUCTION

Molten Carbonate Fuel Cells (MCFCs) are a well-known technology used for both energy production and as a mean for carbon capture. Study on MCFCs are mainly focused on new materials and on the realization of models that can help simulations in integrated plants, but study on the occurring phenomena are still important to assure good performance. Electrochemical Impedance Spectroscopy (EIS) is considered as a powerful tool to assess MCFC stability and performance. In fact, EIS analysis allows the identification of the kinetics

phenomena occurring in the cell and of the affecting operating parameters. However, this technique is still under continuous study, since its analysis results quite complex. In recent years, EIS has been coupled with the distributed relaxation times (DRT) method, in particular for the study of SOFCs [1] and PEMFs [2]. The DRT method allows converting impedance data into a distribution of the time constants involved in the considered system. For this reason, DRT is considered as a useful tool to analyse the stability of the cell without the need of knowing beforehand the electrochemical equivalent circuit.

In previous work the authors developed a kinetic model based on the polarization curves of MCFCs [3] and then verified its validity also through the analysis of EIS spectra [4]. Through this work the authors want to verify if the model respects the phenomena and the dependences that DRT can show.

Equation 1 [3] describes the total cell resistance as sum of the ohmic resistance and the resistances due to the reactant gas polarization (anode  $\text{H}_2$  and cathode  $\text{CO}_2$  and  $\text{O}_2$ ). For the values of the parameters  $P_j$  consult the references [3].

$$R_{TOT} = P_1 e^{\left(\frac{P_2}{T}\right)} + \frac{P_3 T e^{\left(\frac{P_4}{T}\right)}}{p \ln(1 - 1.5 y_{\text{CO}_2})} + P_5 T e^{\left(\frac{P_6}{T}\right)} p^{0.5} y_{\text{CO}_2} y_{\text{O}_2} + \frac{P_7 T e^{\left(\frac{P_8}{T}\right)}}{p \ln(1 + y_{\text{H}_2})} \quad (1)$$

### III. EQUIPMENTS AND METHODS

The cells used for the experimental campaign were made of a Lithiated-NiO cathode, a Ni+2% Al anode, a  $\text{Li}_2\text{CO}_3\text{-K}_2\text{CO}_3$  with a 62:38 ratio electrolyte, a  $\gamma\text{-LiAlO}_2$  matrix, all of which was contained between stainless steel frames. The total active area was of  $100 \text{ cm}^2$ . The tests were performed with a gas standard composition of  $\text{H}_2$ ,  $\text{CO}_2$  and  $\text{H}_2\text{O}$  in a molar ratio of 72:18:10 at the anode side (total flow rate:  $218 \text{ Nm}^3 \text{ h}^{-1}$ ) and of  $\text{N}_2$ ,  $\text{O}_2$  and  $\text{CO}_2$  in a 55:15:30 molar ratio at the cathode side (total flow rate:  $524 \text{ Nm}^3 \text{ h}^{-1}$ ) at an operating temperature of 923 K. For each test, temperature or gas composition were changed maintaining the other variables constant (the

composition through N<sub>2</sub> balancing) to study the effects of only one variable each time. Different cells were used while changing examined variable to ensure that stress would not affect the cell performance and stability. Impedance spectra were collected, when the cells were stable, using a Solartron S11287 1260B machine.

#### IV. RESULTS

The DRT spectra has been derived from the EIS spectra using a mathematical tool developed in Matlab by Wan et al. [5] and called "DRTtools".

In Figure 1 the DRT plots at different operating temperatures and compositions are shown.

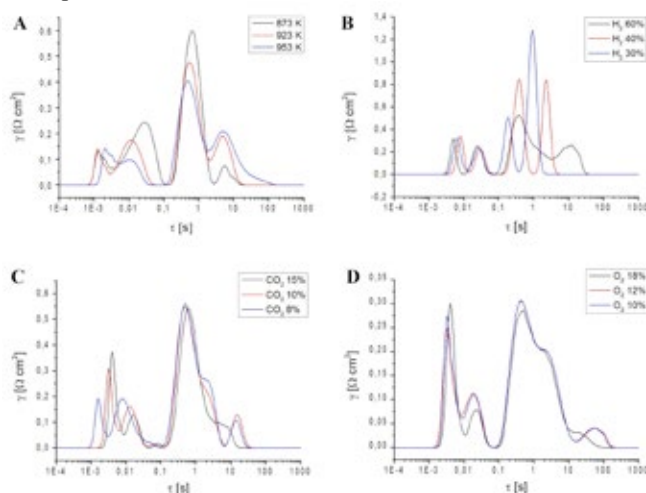
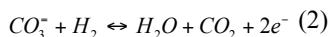


Figure 1: DRT at different operating temperature with a standard composition (A), and with different composition at 923 K (B: varying anode H<sub>2</sub>, C: varying cathode CO<sub>2</sub> and D: varying cathode O<sub>2</sub>).

It appears that the resistance of the overall process is determined by four main phenomena.

As it clearly appears from figure 1-A, temperature affects all the phenomena, and in particular, except for one, to an increasing temperature corresponds a decreasing resistance for the phenomenon.

The graph 1-B shows the effects that are due to the H<sub>2</sub> composition. It is clear that it affects the fourth peak starting from low frequencies with both a shifting to the right and an increasing intensity with decreasing H<sub>2</sub> content. The phenomenon identified by this this peak can be associated with the anode hydrogen oxidation reaction (2) and results in accordance with the developed model that sees a higher H<sub>2</sub> polarization resistance at lower H<sub>2</sub> concentrations (see Eq. 1).

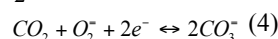
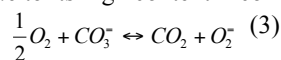


Another phenomenon represented by the third peak appears to be slightly influenced by the H<sub>2</sub> concentration. However, the shift of the peak happens only for the lowest analyzed composition (30%) and the increase in the intensity only for the medium one (40%). For these reasons these effects have been

considered not significant in this preliminary analysis.

The first peak and the second peak appear to be influenced mainly by temperature, with decreasing resistance for increasing temperature, and CO<sub>2</sub> composition. As for the first peak, a shift and a decrease of intensity, suggesting decreasing resistance with increasing CO<sub>2</sub> content, have been registered. This peak can be associated with the reaction between O<sub>2</sub> and CO<sub>3</sub><sup>-</sup> ions that produces CO<sub>2</sub> and peroxide ions (3), whose polarization decreases for increasing CO<sub>2</sub> content. As for the second peak, it is clear that it is influenced by only the concentration of CO<sub>2</sub> that, if increases, decreases the resistance. This peak can be associated with the reaction of CO<sub>2</sub> with the peroxide ions to form carbonate (4).

As expected, the studied variations of the O<sub>2</sub> composition do not appear to have any significant contribution to the resistance due to its high content if compared to the CO<sub>2</sub> one [3].



The phenomena and their trends that appear in the DRT spectra result in accordance with the resistance and trends predicted by the kinetic model.

#### V. CONCLUSION

In this work the authors showed that the phenomena that can be identify through the DRT spectra are in accordance with a previously developed kinetic model for MCFCs based on theoretical analyses and experimentally validated. Coupling DRT analysis and modelling can be a way to further improve the diagnostic approaches to ensure the cell performance and stability.

#### REFERENCES

- [1] Boigues Muñoz, C., Pumiglia, D., McPhail, S. J., Montinaro, D., Comodi, G., Santori, G., Carlini, M., Polonara, F., More accurate macro-models of solid oxide fuel cells through electrochemical and microstructural parameter estimation – Part I: Experimentation, *Journal of Power Sources*, Volume 294, 2015, Pages 658-668.
- [2] Weiß, A., Schindler, S., Galbiati, S., Danzer, M.A., Zeis, R., Distribution of Relaxation Times Analysis of High-Temperature PEM Fuel Cell Impedance Spectra, *Electrochimica Acta*, Volume 230, 2017, Pages 391-398.
- [3] Audasso, E., Bosio, B., Nam, S., Extension of an effective MCFC kinetic model to a wider range of operating conditions, In *International Journal of Hydrogen Energy*, Volume 41, 2016, Pages 5571-5581.
- [4] Arato, E., Audasso, E., Barelli, L., Bosio, B., Discepoli, G., Kinetic modelling of molten carbonate fuel cells: Effects of cathode water and electrode materials, In *Journal of Power Sources*, Volume 330, 2016, Pages 18-27.
- [5] Wan, T.H., Saccoccio, M., Chen, C., Ciucci, F., Influence of the Discretization Methods on the Distribution of Relaxation Times Deconvolution: Implementing Radial Basis Functions with DRTtools, *Electrochimica Acta*, Volume 184, 2015, Pages 483-499.

## TURBOCHARGED SOLID OXIDE FUEL CELL SYSTEM: DESIGN AND EMULATION

M. De Campo, M.L. Ferrari and L. Magistri

Thermochemical Power Group (TPG) - University of Genoa, Via Montallegro 1 (Italy)

**Abstract** - This paper presents a design model of a turbocharged solid oxide fuel cell system fueled by biogas. The aim of this plant layout is the development of a low-cost solution considering the coupling of the solid oxide fuel cell (SOFC) with a low-cost machine such as a turbocharger (instead of a microturbine). The whole system model calculates the operational conditions and realizes the coupling between the turbocharger, the recuperator and the solid oxide fuel cell system (comprising SOFC, air pre-heater, fuel compressor and pre-heater, reformer, off-gas burner and anodic ejector). This model also supports the design of an emulator test rig in which a burner, located inside a thermal insulated vessel, replaces the solid oxide fuel cell system. The emulator test rig will be useful to study the matching between the turbocharger and the fuel cell to validate simulation models, design innovative solutions and test the control system of the whole plant.

**Index Terms** - Solid oxide fuel cell, turbocharger, low-cost layout, emulator rig.

### I. NOMENCLATURE

OGB	Off-Gas Burner
REF	REformer
SOFC	Solid Oxide Fuel Cell

### II. INTRODUCTION

SOFC based systems are promising for high efficiency near-zero emission power generation [1]. However, they are not ready for a wide commercialization for cost issues and not completely solved technological problems [1]. For this reason, plant layouts based on standard commercial devices are interesting to decrease component costs. These options could be significant for the system future even in case of efficiency decrease in comparison with the high performance layouts [2]. So, in this work attention is focused on an SOFC stack pressurized with a commercial turbocharger. Even if this layout is not able to maximize the plant efficiency (the machine is not equipped with the generator), it is a low-cost solution for exploiting the SOFC pressurization benefit [2].

An initial analysis was carried out with a validated design

system model [3]. This was necessary to define the system design and the operative possible conditions for such innovative SOFC based plant. Moreover, it was an essential preliminary modelling activity for the sizing of an experimental rig able to emulate the system.

Finally, special attention is devoted to the design of the experimental rig for performing further analysis on this promising SOFC based system. It is an emulator test rig based on the coupling of a turbocharger with a vessel. This component will be essential to emulate the SOFC behaviour (the cathodic side) including a properly controlled combustor and ceramic material. Moreover, the plant layout includes bypass lines and a bleed duct for tests devoted to dynamic operations, control issues, surge prevention, etc. The emulation approach with rigs not including a real fuel cell was demonstrated [4,5] to produce significant experimental results for such complex innovative systems.

### III. PLANT LAYOUT

The SOFC system is based on the coupling of an SOFC with a turbocharger (Fig.1). The compressed air flow is pre-heated with a recuperator using the exhaust thermal content. Then, the air flow reaches the fuel cell cathodic side through the pre-heating system. On the anodic side the bio-gas fuel (50% CH<sub>4</sub>, 50% CO<sub>2</sub> - molar fractions) is compressed and used in the primary duct of an anodic ejector [3]. This device is necessary to generate an anodic recirculation to feed the reformer (upstream of the anodic side) with a significant steam amount. Finally, the SOFC exhaust flows are mixed in the Off-Gas Burner (OGB) located just upstream of the turbine.

### IV. DESIGN MODEL

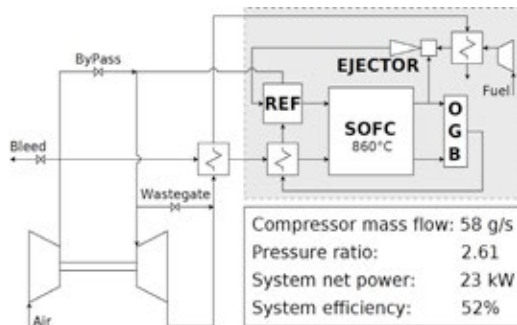
The system design model was developed in Matlab-Simulink using component tools previously validated in other SOFC system works [3] considering tests on existing experimental facilities [5] and on the turbocharger. The plant complete model



includes the following components: turbocharger (compressor, turbine and shaft), recuperator, reformer, SOFC stack, air pre-heater, off-gas burner, fuel compressor and pre-heating system and anodic ejector for flow recirculation. The system model is based on the following main aspects: performance map interpolation for the turbocharger, Number of Transfer Units for the recuperator, reforming and shifting equations for the reformer, the electrochemistry equations (including losses) for the stack, combustion process calculation for the OGB, and mass/momentum/energy equations for the ejector [3]. Although it is a design model, the performance maps are necessary because the turbocharger coupling is not obtained at its standard operative conditions.

## V. MODEL RESULTS

The model was used to evaluate the design main property values (Fig.1). The simulation was carried out considering the bypass valve opened at 1.8% (necessary margin for control reasons) and the SOFC fuel utilization at 0.8. Bleed and wastegate valves were fixed in the fully closed position.



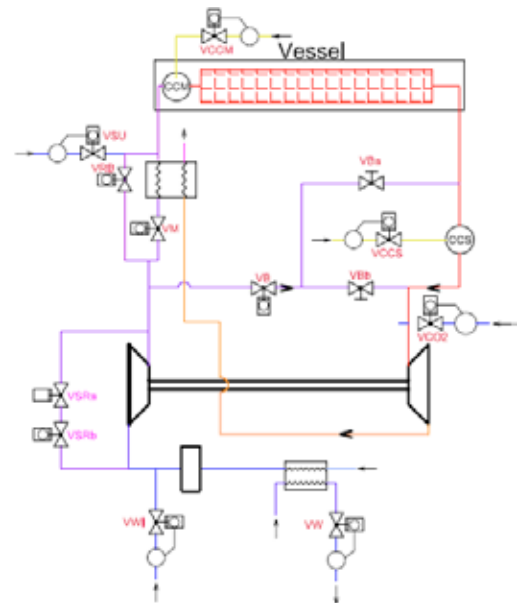
**Fig. 1. SOFC turbocharged system: plant layout and main design values.**

Since the fuel cell temperature was considered fixed at 860°C, the model calculated the matching with the turbocharger considering a 14.6 m<sup>2</sup> cell area (for the electrochemical reactions). For future research activities, this model can simulate the behavior of the whole system in the off-design and at different ambient conditions.

## VI. EMULATOR TEST RIG

On the basis of the system design data presented in the previous paragraph, an emulator test rig (Fig.2) was developed considering the coupling of a turbocharger with a cathodic vessel. The vessel is including a burner (CCM in Fig.2) followed by inert ceramic materials to emulate the SOFC thermal behavior. The rig is also equipped by a recuperator for air pre-heating, a start-up combustor (CCS in Fig.2), bypass lines for control reasons and to emulate different operative conditions (e.g. different SOFC inlet temperatures), a bleed line and an air/water heat exchanger for ambient temperature control. Moreover, the plant includes also three inlet lines for

the start-up air (managed by the VSU valve), compressor intake humidification (managed by the VWI valve) and a CO<sub>2</sub> injection (managed by VCO<sub>2</sub> valve).



**Fig. 2. Emulator rig layout.**

## VII. CONCLUSION

The model presented in this work allowed to define the design property values of the turbocharged SOFC system. These data (mainly the pressure ratio and the mass flow rate) were used to develop an emulator test rig. This will be an essential facility for tests on SOFC/turbocharger coupling, risk prevention, development of control system tools, model validation, and innovative solutions.

## REFERENCES

- [1] Zaccaria V., Tucker D., Traverso A., Transfer function development for SOFC/GT hybrid systems control using cold air bypass. *Applied Energy*, 165 (2016) 695-706.
- [2] Massardo A.F., Lubelli F., Internal Reforming Solid Oxide Fuel Cell - Gas Turbine Combined Cycles (IRSOFC-GT). Part A: Cell Model and Cycle Thermodynamic Analysis. *Journal of Engineering for Gas Turbines and Power*, 122 (2000) 27-35.
- [3] Magistri L., Bozzolo M., Tarnowski O., Agnew G, Massardo A.F., Design and off-design analysis of a MW hybrid system based on Rolls-Royce integrated planar solid oxide fuel cells. *Journal of Engineering for Gas Turbines and Power*, 129 (2007) 792-797.
- [4] Zhou N., Yang C., Tucker D., Evaluation of Cathode Air Flow Transients in a SOFC/GT Hybrid System Using Hardware in the Loop Simulation. *Journal of Fuel Cell Science and Technology*, 12 (2015) 011003\_1-7.
- [5] Ferrari M.L., Pascenti M., Magistri L., Massardo A.F., MGT/HTFC hybrid system emulator test rig: Experimental investigation on the anodic recirculation system. *Journal of Fuel Cell Science and Technology*, 8 (2011) 021012\_1-9.



## STEAM - STRESSOR FOR ACCELERATED TESTING OF Ni/YSZ CERMET ELECTRODES

Alexandra Ploner\*, Anke Hagen\*, Anne Hauch\*

\*Technical University of Denmark, Department of Energy  
Conversion and Storage, 4000 Roskilde, (Denmark)

**Abstract** – Solid Oxide fuel cell (SOFC) commercialization is challenged by the ability to predict their lifetime. The development of accelerated life time tests (ALT) is a possible solution to overcome this challenge. Based on former experimental studies, steam as stressor at the anode is investigated in context of ALT. Via durability testing of cells, the time-dependent responds with regard to steam could be identified. Additionally, microstructural evolution experiments allowed separating the two different time scales for the main degradation phenomena in Ni-YSZ electrodes. Such data provides the basis for establishing accelerated life-time tests and models.

**Index Terms** - accelerated testing, solid oxide fuel cell, impedance spectroscopy, SEM, degradation, durability

### I. INTRODUCTION

Commercialization of SOFCs is challenged by necessity to conduct long-term tests (months to years) to forecast their durability/lifetime. A valuable tool for reducing testing times is ALT. According to comprehensive experimental results primary stressors can be temperature, overpotential or current density for the cell/electrodes and steam/hydrogen ratio for the fuel electrode [1]. Vapor pressure of Chromium-species and  $p(\text{O}_2)$  are considered as stressors for the oxygen electrode [2]. This study focusses on steam as stressor affecting degradation of the Ni/YSZ cermet electrode.

### II. RESULTS AND DISCUSSION

#### A. Experimental

Single repeating unit (SRU) tests were carried out on planar, fuel electrode supported Ni/YSZ based SOFCs. Cell composition, start-up and reduction procedure can be found elsewhere [1].

TABLE 1 lists testing conditions for TEST A and TEST B. During long-term testing and between each testing period Impedance spectra (IS) were recorded. TEST A contained 6 test sequences. In cell TEST B testing sequence six of TEST A was

conducted right after the reduction and the initial characterization. The aim was to investigate fuel electrode degradation as a function of test settings with respect to the amount of steam directly at the electrode and test history.

TABLE 1 CONDITIONS FOR TEST A, TEST B

seq.	t / h	$j / \text{Acm}^{-2}$	$p(\text{H}_2\text{O})_{\text{in}}$	$p(\text{H}_2\text{O})_{\text{out}}$	FU / %	ox.
A (1)	1000	0.5	0.25	0.53	37	O <sub>2</sub>
A (2)	1000	0.5	0.25	0.36	15	O <sub>2</sub>
A (3)	300	0.5	0.25	0.53	37	O <sub>2</sub>
A (4)	350	0.5	0.25	0.81	74	O <sub>2</sub>
A (5)	300	0.5	0.4	0.85	74	O <sub>2</sub>
A (6)	300	0.5	0.72	0.93	74	O <sub>2</sub>
B	300	0.5	0.72	0.93	74	O <sub>2</sub>

Furthermore, microstructural evolution experiments in steam using a tube furnace for two differently processed Ni/YSZ half cells with different initial microstructural parameters (radius,  $r_0$  and porosity) were performed.

Post-mortem analysis of the electrochemical tested cells A, B and the half cells were carried out using a Zeiss Supra 35 microscope. A description of the imaging procedure can be found in [3].

#### B. Test A and Test B

Test A was started with an inlet fuel mixture of  $p(\text{H}_2\text{O})/p(\text{H}_2)$  of 0.25/0.75. After 1000 h, the  $p(\text{H}_2\text{O})/p(\text{H}_2)$  ratio and/or steam flow rate of the exhaust fuel were stepwise increased.

After sequence 1 of cell TEST A both electrodes exhibited an ASR increase. This increase was minor after seq. 2. Rising the outlet steam flow rate (seq. 2), increasing fuel utilization (seq. 3 + 4) and additionally increasing steam partial pressure of the inlet fuel (seq. 5 + 6) seemed to have rather small additional effects on the cell degradation. It is a very intriguing result that the cell can be operated at conditions of such high steam content without significant degradation over several thousands of hours. All degradation seems to lie within the first

1000 h of operation at much less severe operating conditions – as regard to the steam content.

For cell test B (seq. 6 of test A) degradation in a period of approx. 200 h was observed which levelled off in the final 100 h of testing. Obviously, a high inlet steam partial pressure ( $p_{in}=0.72$ ) and even higher outlet steam partial pressure ( $p_{out}=0.93$ ), have different effects when applied on a fresh (Test B) or pre-aged cell (Test A). FIGURE 1 compares the response.

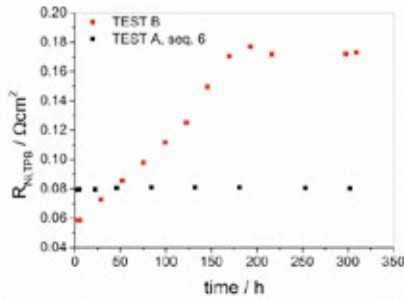


FIGURE 1 ASR INCREASE OVER TIME FOR TEST A (SEQ.6) AND TEST B

Additionally, microstructure and percolating network of cell A and cell B were investigated after testing. While test A shows similar 2D microstructural properties between inlet and outlet, this differs in the case of cell B. The outlet segment shows large areas of a damaged Ni-network, particularly at the active anode/electrolyte interface. Statistical analyses of different cell areas are summarized in TABLE 2.

TABLE 2 NI PERCOLATION OF CELL A AND B

sample	analyzed area / $\mu m^2$	Fraction of percolating Ni
Ref.	5806	0.33
A <sub>center+out</sub>	19925	0.259
B <sub>in</sub>	10269	0.256
B <sub>out</sub>	8590	0.192

### C. Furnace Testing

As the overall steam content directly at the SOFC anode was identified as critical parameter, ex-situ experiments were carried out on the SOFC half-cell to quantify the acceleration due to steam. The observed development of the Ni mean intercept length (MIL) could be described via a simple exponential correlation.

$$MIL(t) = r_0 + \Delta r [1 - \exp(-t/\tau_1)] \quad (1)$$

This behavior is in agreement with various previous studies of the phenomenon for other anode microstructures [1,4]. Additionally the trend in percolation was investigated. This second (long-term) degradation phenomenon could also be described via an exponential relation. However, with a characteristic time constant;  $\tau_2$ ; being roughly  $\tau_2/\tau_1 \sim 2$ .

### D. Discussion

The major degradation in the electrochemical tests happens between 0-1000 h. After this period, the Ni-YSZ electrode shows nearly no ASR increase. In the case of cell test A, the ‘stabilization’ is reached after approx.1000 h. For test B, this

effect is observed after ca. 200 h. However, the cell in Test B showed a significantly larger ASR ( $R_{Ni,TPB}$ ) increase over a shorter testing time (200 h) as the cell in Test A over a total of 3500 h. This result seems counterintuitive.

Microstructural investigations give a plausible explanation for the significant differences of cell degradation in test A and B. Degradation in both cells can be assigned to Ni-particle coarsening and Ni-Ni percolation loss when compared to the active anode layer of a reference cell. For cell test B the second phenomenon, particularly in the cell outlet area leads to large areas of non-percolated Ni particles. As this observation is particularly made in the outlet segment, it implies that mainly steam as parameter is the source for the seen degradation. Interestingly, while cell A tolerates the same externally applied operating conditions after 3000 h of operation, cell B is heavily affected when exposed to those conditions from the start.

The presence of steam certainly seems to enhance the mobility of the present phases, i.e. Ni, external or internal impurities [5]. Whereas cell A re-organizes and reaches a stable surface/interface energy under much less steam exposure, morphology changes of cell B are taking place in a more active environment which enhances shape changes of Ni-particles or build-up of impurities at the triple phase boundary regions (TPB) and so resulting in more inactive TPBs.

### III. CONCLUSION

In the context of ALT, a shift of steam threshold with time seems to happen. Furthermore, due to the degradation behavior of TEST A, it can be concluded that the accelerating impact of steam is restricted to early degradation, however might not be a sufficient stressor for long-term degradation effects. The ratio of the determined kinetic values of two early degradation phenomena, i.e. most likely particle growth and percolation loss in Ni-YSZ, can be used to establish a valuable semi-empirical model for ALT measurements.

### REFERENCES

- [1] Hauch, A., Mogensen, M., and Hagen, A. Ni/YSZ electrode degradation studied by impedance spectroscopy - Effect of  $p(H_2O)$ . Solid State Ionics, Volume 192(1), 2011, pp. 547-551
- [2] Schuler, J. A., Willemin, Z., Hessler-Wyser, A., Comminges, C., Steiner, N., and Van herle, J. Cr-poisoning in  $(La,Sr)(Co,Fe)O_3$  cathodes after 10,000 h SOFC stack testing. J. Power Sources, Volume 211, 2012, pp.177-183
- [3] Thyden, K. Microstructural degradation of Ni-YSZ anodes for solid oxide fuel cells. 2008
- [4] Faes, A., Hessler-Wyser, A., Presvytes, D., Vayenas, C. G., and Van herle, J. Nickel-Zirconia Anode Degradation and Triple Phase Boundary Quantification from Microstructural Analysis. Fuel Cells, Volume 9(6), 2009, pp.841-851
- [5] Hauch, A., Mogensen, M., and Hagen, A. Ni/YSZ anode - Effect of pre-treatment on cell degradation and microstructure. Solid State Ionics, Volume 196, 2011, pp. 8931-8941.

## LOW SINTERING TEMPERATURE OF BISMUTH-DOPED 8YSZ FOR IT-SOFC APPLICATIONS

E. Audasso\*, B. Bosio\*, L. Spiridigliozzi\*\*, G. Dell'Agli\*\*, S. P. Yoon\*\*\*, G. Accardo\*\*\*

\*Department of Civil, Chemical and Environmental Engineering, University of Genova (Italy)

\*\*Department of Civil and Mechanical Engineering, University of Cassino and Southern Lazio (Italy)

\*\*\*Fuel Cell Research Center, KIST - Korea Institute of Science and Technology (South Korea)

**Abstract** - In this work 4mol% of Bi-doped 8YSZ electrolytes were synthesized by a simple co-precipitation route and then sintered at very low temperatures (i.e. 900 - 1100°C). The as-synthesized powders were characterized from the structural, microstructural and thermal point of view. Electrochemical properties of the best pellets were evaluated by Electrochemical Impedance Spectroscopy (EIS). Very high values of relative densities (i.e. >95%) were achieved upon all sintered pellets, whose microstructure was highly homogeneous and characterized by micrometric grains. Definitively, Bi has proved to be an excellent sintering aid for YSZ, highly improving its densification at lower temperatures and even increasing its total ionic conductivity.

**Index Terms** - Co-precipitation, Fuel Cells, Sintering, YSZ

### I. INTRODUCTION

Cubic yttria stabilized zirconia (8YSZ) has been widely applied in a variety of fields, with specific interest as electrolyte in solid oxide fuel cells (SOFC) thanks to its adequate mechanical and electrochemical properties along with high thermal and chemical stability [1-2]. However, 8YSZ ionic conductivity at intermediate temperatures (~600°C) needs to be improved in order to increase its use in the intermediate temperature solid oxide fuel cells (IT-SOFC) [3-5]. Moreover, YSZ sintering temperature usually reaches as about 1600°C during its production, thus causing manufacturing difficulties. To both decrease sintering temperatures and improve YSZ ionic properties, the effect of several dopants has been studied [6]. Among them, Bi<sub>2</sub>O<sub>3</sub> has been extensively studied but with conflicting results reported in literature [7-8]. In this work 4% mol of Bi-doped 8YSZ (4BiYSZ in the following) electrolytes were prepared and sintered at 900°C and 1100°C in order to study their electrochemical properties.

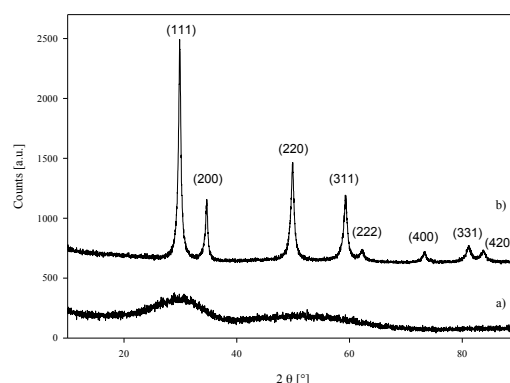
### II. MATERIALS AND METHODS

ZrO(NO<sub>3</sub>)<sub>2</sub>·nH<sub>2</sub>O and Bi<sub>2</sub>O<sub>3</sub>, used as starting materials, were dissolved in diluted nitric acid. Subsequently, an excess ammonia solution was added to the system to let the co-precipitation occurred. The co-precipitate was then filtered, repeatedly washed with deionized water and finally dried overnight at 70°C. The calcination was carried out in air at 500

°C for 1 h. The powders were characterized by DTA-TG and X-Ray Diffraction. The calcined powders were formed in cylindrical shape by uniaxial pressing and finally sintered in air at 900°C and 1100°C by using 5°C/min as heating rate and 3h as soaking time.

### III. RESULTS AND DISCUSSION

XRD measurements reveal that all co-precipitates were formed by an amorphous hydrous doped-zirconia xerogel (Figure 1a), according also with previous results for similar systems [9-10]



**Fig. 1.** XRD diffraction patterns of as-synthesized powders (a) and of calcined powder (b).

The DTA-TG thermograph (not reported here) of the co-precipitate shows a very sharp exothermic peak at about 520°C representing the crystallization of the amorphous phase into cubic fluorite phase, as confirmed also by the diffraction pattern, related to the sample calcined at 600°C for 1h (Figure 1b), which shows only the peaks of YSZ cubic fluorite phase. The calcined powders are nanostructured as confirmed by the crystallite size, calculated by Scherrer equation applied to (111) diffraction peak, equal to 19 nm.

The sintered samples are very well densified for both the sintering temperatures, since the relative densities, measured by hydrostatic balance, are 96.5 % and 98.6 % for samples fired at 900 and 1100°C respectively.

Their microstructure, revealed by SEM analysis, confirms the high level of densification. Both pellets present a homogeneous microstructure, characterized by regular and equiaxed grains, whose size is of about 1  $\mu\text{m}$ . Sample sintered at 900°C exhibits smaller grains and more residual porosity due to the lower sintering temperature, although adequate as SOFC electrolyte. Figure 2 shows two exemplary micrographs, related to sample fired at 1100°C, in which the very dense texture appears.

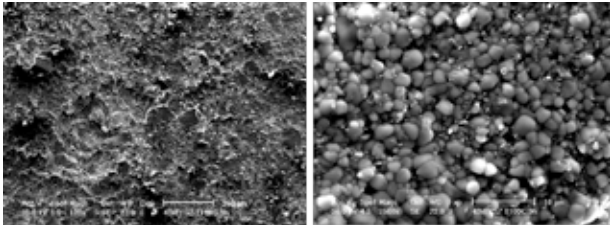


Fig. 2. SEM micrographs of sample sintered at 1100°C for 3h.

Finally, both sintered pellets were characterized by EIS in order to investigate their electrochemical properties. The Arrhenius plot in the temperature range of 650–900°C is reported in Figure 3. The electrochemical properties achieved for each 4BiYSZ sample are higher than traditional 8YSZ electrolytes sintered in the temperature range of 1300–1650°C [11]. The total ionic conductivity, recorded at 650°C, is  $6.06 \cdot 10^{-2}$  S/cm and  $4.44 \cdot 10^{-2}$  S/cm for 4BiYSZ sintered at 1100°C and 900°C respectively. The higher ionic properties depend on the microstructure due to the different sintering temperature. In fact, the performance of solid electrolytes is affected by many factors such as the microstructure and average grain size. The caused difference in the ionic properties is thought to be the different characteristics of the sintered pellets, which resulted from the different sintering temperature

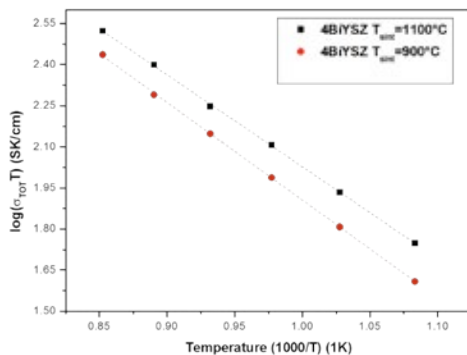


Fig. 3. Arrhenius plot for 4BiYSZ electrolytes

#### IV. CONCLUSION

By using a simple and cheap co-precipitation synthesis route, it has been possible to produce very well densified 4BiYSZ pellets. Bi has proved to have useful effects upon sintering behavior and total ionic conduction of 8YSZ, lowering the sintering temperature of YSZ well below their typical values. Although further investigations upon synthesis and sintering

parameters have to be done, 4BiYSZ can be used as high performance zirconia-based electrolytes in IT-SOFCs.

#### ACKNOWLEDGMENT

This work was supported by KRF – Korea Research Fellowship through the National Research Foundation of Korea and funded by the Ministry of Science, ICT and Future Planning of Republic of Korea (Grant Number 2016H1D3A1908428)

#### REFERENCES

- [1] Han, M., Tang, X., et al (2007). Fabrication, microstructure and properties of a YSZ electrolyte for SOFCs. *Journal of Power Sources*, 165(2), 757-763.
- [2] Nagao, M., Kobayashi, K., et al (2014). Low-temperature Sintering of Yttria-stabilized Zirconia Using Bismuth–Vanadium Oxide as a Sintering Aid at 800° C. *Chemistry Letters*, 43(12), 1887-1889.
- [3] Accardo, G., Ferone, C., et al (2016). Electrical and microstructural characterization of ceramic gadolinium-doped ceria electrolytes for ITSOFCs by sol-gel route. *Journal of applied biomaterials & functional materials*, 14(1): e35-e41
- [4] Accardo, G., Ferone, C., et al (2016). Influence of Lithium on the Sintering Behavior and Electrical Properties of Ce<sub>0.8</sub>Gd<sub>0.2</sub>O<sub>1.9</sub> for Intermediate Temperature Solid Oxide Fuel Cells Energy Technology 4,409-416.
- [5] Dell'Agli, G., Spiridigliozzi, L., et al (2016). Effect of the mineralizer solution in the hydrothermal synthesis of gadolinium-doped (10% mol Gd) ceria nanopowders. *Journal of applied biomaterials & functional materials*, 14(2), e189-e196.
- [6] Flegler, A. J., Burye, et al (2014). Cubic yttria stabilized zirconia sintering additive impacts: A comparative study. *Ceramics International*, 40(10), 16323-16335.
- [7] Liu, L., Zhou, Z., et al (2016). Effect of Bismuth Oxide on the Microstructure and Electrical Conductivity of Yttria Stabilized Zirconia. *Sensors*, 16(3), 369-379.
- [8] Hui, L. I., Alexander, K. O. N., et al (2016). Fast firing of bismuth doped yttria-stabilized zirconia for enhanced densification and ionic conductivity. *Journal of the Ceramic Society of Japan*, 124(4), 370-374.
- [9] Accardo, G., Dell'Agli, et al (2017). Electrical behaviour and Microstructural characterization of Magnesia Co-doped ScSZ Nanopowders Synthesized by Urea Co-precipitation. *Chemical Engineering Transaction*, vol.57.
- [10] G. Dell'Agli, G. Mascolo, et al (2006) Weakly-agglomerated nanocrystalline (ZrO<sub>2</sub>)<sub>0.9</sub>(Yb<sub>2</sub>O<sub>3</sub>)<sub>0.1</sub> powders hydrothermally synthesized at low temperature, *Solid State Sci* 8, 1046-1050
- [11] K. Prabhakaran, M.O. Beigh, et al. (2007) Characteristics of 8 mol% yttria stabilized zirconia powder prepared by spray drying process, *Journal of Materials Processing Technology* 189, 178–181.



## ORR ACTIVITY OF N-DOPED CARBON AEROGEL SUPPORTED COBALT CATALYST PREPARED BY SUPERCRITICAL DEPOSITION

Seçil Ünsal<sup>a</sup>, Selmi Erim Bozbağ<sup>a</sup>, Bahareh Deljoo<sup>b</sup>, Mark Aindow<sup>b</sup>, Can Erkey<sup>a,c</sup>

<sup>a</sup>Department of Chemical and Biological Engineering, Koç University, Sarıyer 34450, Istanbul, Turkey

<sup>b</sup>Department of Materials Science and Engineering, Institute of Material Science, University of Connecticut, Storrs, CT 06269-3136, USA

<sup>c</sup>Koç University Tüpraş Energy Center (KUTEM), Koç University, Sarıyer, 34450, Istanbul, Turkey  
e-mail: cerkey@ku.edu.tr

**Abstract** - In this study, a novel N-doped CA supported Co catalyst was prepared using SCD (Supercritical Deposition) with subsequent NH<sub>3</sub> treatment. An onset potential of 0.93 V vs RHE compared was obtained which is very close that of the Pt-Vulcan (0.95V vs RHE) toward the Oxygen Reduction Reaction (ORR). Effects of pyrolysis temperature, Co deposition and N doping on the ORR activity were investigated. The electrocatalyst pyrolyzed at 800 °C (N-Co-CA-800) had the highest ORR activity of 9.02 mA/mg<sub>cat</sub> (calculated at 0.8 V vs RHE) as compared to N-CA and Co-CA (5.21 and 3.63 mA/mg<sub>cat</sub>, respectively). Higher activity was associated with the Co-N<sub>x</sub> and graphitic N sites on the N-Co-CA-800 catalyst based on the XPS results.

**Index Terms** – Supercritical Deposition, Non-precious Metal Catalyst, Carbon Aerogel, Fuel Cells

### I. INTRODUCTION

The oxygen reduction reaction (ORR) which occurs at the cathode of a hydrogen fuel cell has sluggish kinetics and requires the usage of Pt at high loadings for satisfactory fuel cell performance. Although carbon supported Pt catalysts are considered among the best ORR catalysts, high cost of Pt severely hinders the widespread commercialization of fuel cells. To overcome this drawback, development of low-Pt, Pt-free and even metal free carbon based nanomaterials for ORR has been attracting increased attention[1]. Among these, transition metal containing (usually Co, Fe) N-doped carbon materials are one of the most promising candidates[2]. Here, we report a new technique to synthesize N-M-C catalyst (M=non-precious metal). We prepared highly active N-doped CA supported Co catalysts using Supercritical Deposition (SCD) combined with ammonia treatment and evaluated the effect of Co and N doping as well as the pyrolysis temperature on ORR activity.

### II. METHODOLOGY

#### A. Preparation of Cobalt Loaded Resorcinol (R) Formaldehyde (F) Aerogels(RFAs) by Supercritical Deposition

RFAs (resorcinol formaldehyde aerogels) were synthesized by the sol-gel route with the initial molar ratios of R/C, R/W and R/F was set as 0.5, 200 and 0.02 during the synthesis followed by supercritical fluid extraction. RFAs were impregnated with Co(acac)<sub>3</sub> in supercritical CO<sub>2</sub> at 80 °C and 20.7 MPa and kept at this condition until all the precursor inside the vessel adsorbed on the RFA. Subsequently, the system was depressurized slowly and the Co-RFA composite sample was removed from the vessel.

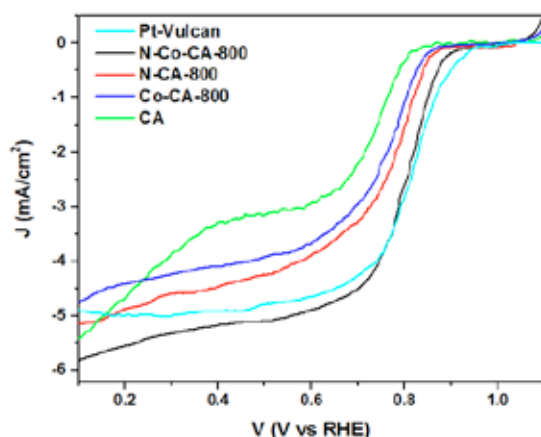
#### B. Preparation of N- doped Carbon Aerogel Supported Cobalt Catalyst

To obtain N-doped carbon aerogel supported cobalt catalyst, the prepared Co-RFA samples were subjected to pyrolysis under NH<sub>3</sub> flow (10% in He) at various temperatures in a tube furnace for 6 hours. The resulting materials are referred to as N-Co-CA-xxx, where xxx denotes the pyrolysis temperature in °C. Moreover, a Co-CA and an N doped CA sample were prepared by pyrolysis in flowing N<sub>2</sub> and NH<sub>3</sub> respectively.

### III. RESULTS AND DISCUSSIONS

The Co loaded samples were pyrolyzed in a stream of 10% NH<sub>3</sub> in He in the temperature range between 700°C - 1000°C and highest activity ( $E_{\text{onset}} = 0.93$  V vs RHE) was obtained for the one pyrolyzed at 800 °C i.e. N-Co-CA-800 which is very close to that of Pt/Vulcan ( $E_{\text{onset}} = 0.95$  V vs RHE). The TEM images of N-Co-CA-800 sample revealed the existence of Co nanoparticles covered by carbon shells. The surface area, average pore size and pore volume of the sample was 550 m<sup>2</sup>/g,

18 nm, 2 cm<sup>3</sup>/g by N<sub>2</sub> adsorption/desorption isotherms. Different types of C-N sites, as well as Co-N and metallic Co were detected by high resolution N1s and Co2p XPS spectra of the samples. Co-CA did not have any N1s peak in its XPS spectra. Figure 1 shows the RDE results of samples where the activity decreased in the following order: N-Co-CA-800 (9.02) < N-CA-800 (5.21) < Co-CA-800 (3.63) < CA (1.07), where the numbers in parenthesis represent activity in mA/mg<sub>cat</sub> determined at 0.8 V vs RHE.

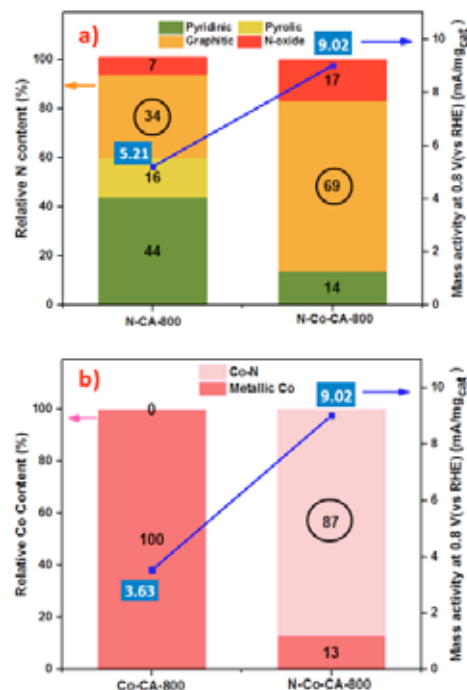


**FIG.1 RDE curves at 1600 rpm and 5 mV/sec in O<sub>2</sub> saturated 0.1 M KOH solution**

Figure 2 illustrates the relationship between the mass activity and the N or Co speciation (deconvoluted from N1s (a) and Co2p (b) spectra). A pyrrolic N site was observed for the N-CA-800 and was absent for the N-Co-CA-800 sample. Instead, percentage of graphitic N site was doubled in N-Co-CA-800 as compared to N-CA-800 which correlates with the increase in mass activity from 5.21 mA/mg<sub>cat</sub> to 9.02 mA/mg<sub>cat</sub>, as shown in Figure 2a. Figure 2b shows the comparison of the mass activity and the Co speciation in Co-CA and N-Co-CA. All of the cobalt in Co-CA appeared in metallic form. On the other hand, Co-N<sub>x</sub> sites with a XPS peak center at 780.3eV were observed for N-Co-CA and they dominate the Co speciation. This suggests that the Co-N<sub>x</sub> species may be the active sites for the ORR or may play an important role in the catalytic cycle. The high Co-N<sub>x</sub> and graphitic N content of N-Co-CA-800 seem to lead to high ORR activity.

#### IV. CONCLUSION

Highly active N-doped CA supported Co catalysts was synthesized using SCD combined with ammonia treatment. Co containing sample pyrolyzed at 800 °C (N-Co-CA-800) had the highest ORR activity which is 9.02 mA/mg<sub>catalyst</sub> as determined from the current density at 0.8 V vs RHE in 0.1 M KOH. The activity of N-Co-CA-800 for the ORR was higher than that the only N doped and only Co doped CA. N-Co-CA-800 had a



**FIG.2 Variation of Mass Activity with**  
**a) Content of different N species (%) of N-CA and N-Co-CA obtained from N1s spectra**  
**b) Content of different Co species (%) of Co-CA and N-Co-CA obtained from Co2p spectra.**

very close onset potential of 0.93 V vs RHE (where the cathodic current reaches 0.1 mA/cm<sup>2</sup>) compared to Pt-Vulcan (0.95 V vs RHE) in alkaline medium. This high activity correlated with the concentration of the Co-N<sub>x</sub> and graphitic N sites for the N-Co-CA-800 catalyst.

#### ACKNOWLEDGMENT

We are grateful for the financial support of TÜBİTAK with grant number 213M024. We also acknowledge the support of Koç University Surface Science Technologies Center (KUYTAM), Koç University Tüpraş Energy Center (KUTEM), collaborative support of TARLA project and UConn/FEI Center for Advanced Microscopy and Materials Analysis (CAMMA).

#### REFERENCES

- [1] Wua, G., Santandrea, N., Kellogga, W., Gupta, S., Ogoke, O., Zhang, H., Whang, H. L., Dai, L., Carbon Nanocomposite Catalysts for Oxygen Reduction and Evaluation Reactions: From Nitrogen Doping to Transition-Metal Addition, *Nanoenergy*, 2016, Volume 29, 83-110
- [2] Qian, Y., Liu, Z., Zhang, H., Wu, P., Cai, C., Active Site Structures in Nitrogen-Doped Carbon- Supported Cobalt Catalysts for Oxygen Reduction Reaction, *ACS Applied Materials & Interfaces*, Volume 8, 2016, 32875-32886

EFC17156

# NANOSTRUCTURED NICKEL HYDROXIDE AS ANODE CATALYST FOR DIRECT ETHANOL FUEL CELLS

Jun Jeffri B. Lidasan\* and Prof. Joey D. Ocon, Ph.D\*

\*Laboratory of Electrochemical Engineering (LEE), Department of  
Chemical Engineering, University of the Philippines Diliman,  
(Philippines)

**Abstract** - Direct ethanol fuel cells provide a cleaner alternative to the use of fossil fuels. However, further improvements to the performance of catalysts in ethanol oxidation have to be attained before the technology becomes viable for commercial applications. Nanostructured nickel hydroxide catalysts show promising properties for use in energy conversion and storage devices. Few studies have been done to test nickel hydroxide as an anode catalyst for DEFCs. The study explores the synthesis of nanostructured  $\alpha$ -Ni(OH)<sub>2</sub> hollow microspheres using a facile solvothermal method with different parameters, such as the variation of temperature and time of heating, and the effect of the addition of oleylamine as a surfactant, to produce variations in morphology. The catalyst's activity and stability is then tested for ethanol oxidation reaction. The catalyst was able to achieve a stable current density of 16 mA cm<sup>-2</sup>.

**Index Terms** - direct ethanol fuel cell, electrocatalyst, ethanol oxidation, nickel hydroxide

## I. INTRODUCTION

Direct ethanol fuel cells (DLFCs), a type of fuel cell that use ethanol as fuel instead of the more common hydrogen, may be able to solve the problem of the typical hydrogen fuel cells. Since the fuel is in liquid form, the problems in distribution and storage are solved. However, a major problem DEFCs face has low power output because of the slow kinetics of the ethanol oxidation reaction. [1] Numerous studies have explored electrocatalysts address this problem and have found alloys of noble metals to be ideal catalyst materials. [2, 3]

Few studies have reported that nickel-based materials show good catalytic activity towards ethanol oxidation. [4] Nickel is an abundant metal in the earth's crust which suggests that it may be a cheaper alternative to noble metal catalysts.

In this work, nanostructured nickel hydroxide is considered as an electrocatalyst for ethanol oxidation in alkaline media.

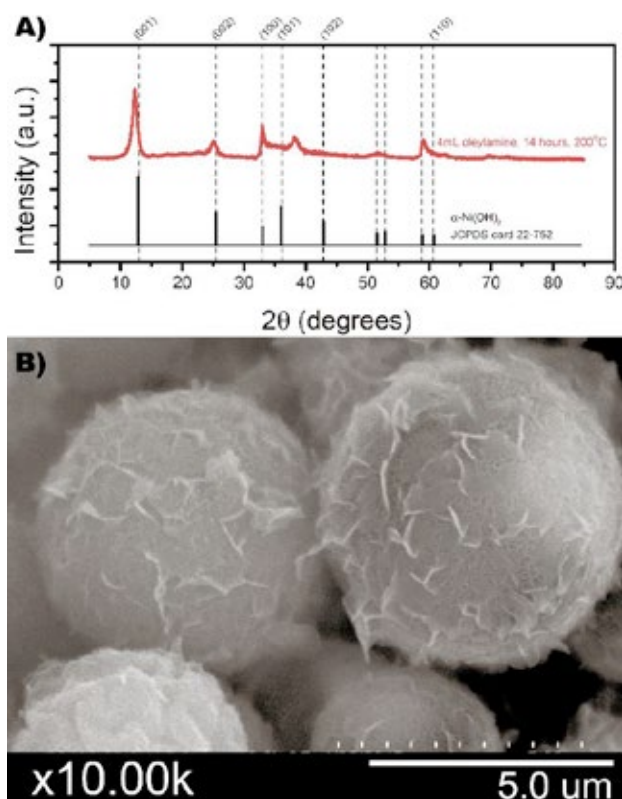


Figure 1.  $\alpha$ -Ni(OH)<sub>2</sub> hollow microspheres with nanosheets: a) XRD pattern with reference [6] and its b) SEM image

## II. EXPERIMENTAL

### A. Solvothermal Synthesis

Ni(OH)<sub>2</sub> was synthesized via a facile solvothermal method [5] using Ni(NO<sub>3</sub>)<sub>2</sub> · 6H<sub>2</sub>O, ethanol, and oleylamine as precursors. Temperature (160 to 200 °C), period of heating (4 to 24 hours), and amount of oleylamine (0 to 4 mL) were varied to control the morphology of the produced Ni(OH)<sub>2</sub> catalyst.

Copyright © 2017

## B. Physiochemical characterization

The XRD pattern in Figure 1a generally follows that of the  $\alpha$ -phase crystal structure of  $\text{Ni}(\text{OH})_2$  from the reference which is generally known to have better electrochemical properties compared to the other known occurring  $\beta$ -phase. [7] Other samples that were tested were also of the  $\alpha$ -phase albeit having slightly different peak widths and some peak shifts.

$\alpha$ - $\text{Ni}(\text{OH})_2$  hollow microspheres with nanosheets have been successfully synthesized as seen in Figure 1b. This is similar to the results of the synthesis procedure of work of Gao et. al (2015) [5]. Other nanostructures formed were nanoflakes and a more ordered assembly of nanosheets that are similar to those embedded in the hollow microsphere formed.

## C. Electrochemical testing

Cyclic voltammetry and chronoamperometry were performed to test the activity and stability of the catalyst. All electrochemical tests were done in 1M KOH electrolyte using Ag/AgCl as reference electrode, Pt wire as the counter electrode and GCE as working electrode where  $\text{Ni}(\text{OH})_2$  is deposited.

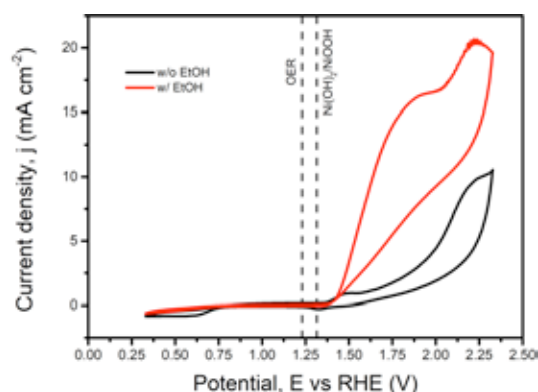


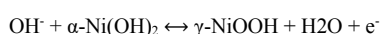
Figure 2. Cyclic voltammetry of  $\alpha$ - $\text{Ni}(\text{OH})_2$  hollow microspheres with nanosheets deposited on GC electrode in the presence (—) and absence (—) of ethanol

The cyclic voltammetry in Figure 2 showed that the ethanol oxidation on the  $\alpha$ - $\text{Ni}(\text{OH})_2$  hollow microspheres occurs at an onset potential of  $\sim 1.35$  V vs RHE. The difference in the rise of the activity suggests that the activity is due to ethanol oxidation, peaking at around  $\sim 16$  mA  $\text{cm}^{-2}$  before the next onset potential – which may be attributed to oxygen evolution, which occurs at higher overpotentials for this case.

Chronoamperometry was performed at 1.53 V vs RHE for 30 minutes.  $\alpha$ - $\text{Ni}(\text{OH})_2$  hollow microspheres with nanosheets showed a remarkably stable current density throughout the test – maintaining a current density of  $\sim 16$  mA  $\text{cm}^{-2}$  similar to the peak reached in the cyclic voltammetry though at a lower overpotential.

## III. PROPOSED MECHANISM OF ETHANOL OXIDATION

The CV curve without ethanol also shows a slight onset increase in activity at around the same onset potential of the ethanol oxidation. This may be attributed to  $\alpha$ - $\text{Ni}(\text{OH})_2$  oxidation which has a redox potential of 1.32 V vs RHE.  $\alpha$ - $\text{Ni}(\text{OH})_2$  has been known to easily oxidize to  $\gamma$ - $\text{NiOOH}$  at low anodic overpotentials in alkaline environment. [4] Previous works have suggested that the mechanism of ethanol oxidation on nickel-based electrodes may be dependent on the  $\alpha$ - $\text{Ni}(\text{OH})_2$ / $\gamma$ - $\text{NiOOH}$  redox pair [4, 8, 9] which may be expressed as:



Ethanol oxidation occurs in the catalyst/electrolyte interface: the outer layer of  $\text{NiOOH}$ . Ethanol adsorbs to the catalyst surface which results into an autocatalytic process where the  $\gamma$ - $\text{NiOOH}$

reacts with the ethanol and its intermediates until it is oxidized to acetic acid. Hence, ethanol is not oxidized before  $\gamma$ - $\text{NiOOH}$  is formed from the oxidation of  $\alpha$ - $\text{Ni}(\text{OH})_2$ . This indicates that the rate of ethanol oxidation is dependent on the rate by which  $\alpha$ - $\text{Ni}(\text{OH})_2$  oxidizes to  $\gamma$ - $\text{NiOOH}$ .

## IV. CONCLUSION

This work reports the synthesis of  $\alpha$ - $\text{Ni}(\text{OH})_2$  through a facile solvothermal synthesis. Morphology control was achieved through the variation of solvothermal parameters which produced varied nanostructures.  $\alpha$ - $\text{Ni}(\text{OH})_2$  hollow microspheres showed promising activity and was able to achieve a stable current density by applying a low overpotential with respect to the  $\alpha$ - $\text{Ni}(\text{OH})_2$ / $\gamma$ - $\text{NiOOH}$  redox pair

The proposed mechanism of ethanol oxidation is also presented in this work. Its understanding plays an important role in considering  $\text{Ni}(\text{OH})_2$  as an electrocatalyst for DEFCs since the activity occurs at a different potential region than that of ethanol's theoretical oxidation potential which may have consequences in the overall cell potential for DEFC application.

## ACKNOWLEDGMENT

The authors acknowledge the financial support of the Engineering Research & Development for Technology (ERDT) Program of DOST.

## REFERENCES

- [1] Kamarudin, M. Z. F., Kamarudin, S. K., Masdar, M. S., & Daud, W. R. W. (2013). Review: Direct ethanol fuel cells. *International Journal of Hydrogen Energy*, 38(22), 9438–9453.
- [2] Antolini, E. (2007). Catalysts for direct ethanol fuel cells. *Journal of Power Sources*, 170(1), 1–12.
- [3] Akhairi, M. A. F., & Kamarudin, S. K. (2016). Catalysts in direct ethanol fuel cell (DEFC): An overview. *International Journal of Hydrogen Energy*, 41(7), 4214–4228.
- [4] Barbosa, A. F. B., Oliveira, V. L., Van Drunen, J., & Tremiliosi-Filho, G. (2015). Ethanol electro-oxidation reaction using a polycrystalline nickel electrode in alkaline media: Temperature influence and reaction mechanism. *Journal of Electroanalytical Chemistry*, 746, 31–38.
- [5] Gao, M., Sheng, W., Zhuang, Z., Fang, Q., Gu, S., Jiang, J., & Yan, Y. (2014). Efficient water oxidation using nanostructured  $\alpha$ -nickel-hydroxide as an electrocatalyst. *Journal of the American Chemical Society*, 136(19), 7077–7084.
- [6] Xu, L., Ding, Y. S., Chen, C. H., Zhao, L., Rimkus, C., Joesten, R., & Suib, S. L. (2007). 3D flowerlike  $\alpha$ -nickel hydroxide with enhanced electrochemical activity synthesized by microwave-assisted hydrothermal method. *Chemistry of Materials*, 20(1), 308–316.
- [7] Oliva, P., Leonardi, J., Laurent, J. F., Delmas, C., Braconnier, J. J., Figlarz, M., ... Guibert, A. de. (1982). Review of the structure and the electrochemistry of nickel hydroxides and oxy-hydroxides. *Journal of Power Sources*, 8(2), 229–255.
- [8] Kim, J.-W., & Park, S.-M. (2005). Electrochemical Oxidation of Ethanol at Nickel Hydroxide Electrodes in Alkaline Media Studied by Electrochemical Impedance Spectroscopy. *Journal of the Korean Electrochemical Society*, 8(3), 117–124.
- [9] Miao, Y., Ouyang, L., Zhou, S., Xu, L., Yang, Z., Xiao, M., & Ouyang, R. (2014). Electrocatalysis and electroanalysis of nickel, its oxides, hydroxides and oxyhydroxides toward small molecules. *Biosensors and Bioelectronics*, 53, 428–439.



# NUMERICAL ANALYSIS OF A BIOGAS POWERED HYBRID MGT-SOFC POWER PLANT

T. Krummrein\*

\*German Aerospace Center (DLR), Institute of Combustion Technology, Pfaffenwaldring 38-40, 70569 Stuttgart (*Germany*)

**Abstract** – The hybrid power plant containing a solid oxide fuel cell (SOFC) and a micro gas turbine (MGT) is a promising technology. It provides a highly efficient power plant with low emissions and high fuel flexibility. This study investigates the use of biogas as fuel in a hybrid power plant demonstrator. Numerical simulations show a reduction of the operating range while the system efficiency decreases only slightly.

***Index Terms*** – biogas, hybrid power plant, operating range, numerical simulation

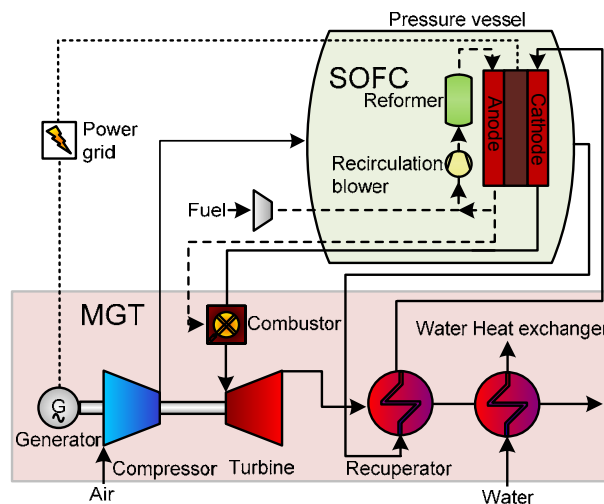
## I. INTRODUCTION

Biogas power plants stand out from other renewable energy plants as they can be placed almost everywhere and they are capable for baseload. As the amount of available biomass is limited such power plants should achieve a high efficiency. Furthermore, fluctuating biogas qualities must be handled in such a power plant.

Hybrid power plants (HyPP) can handle these challenges. They combine a solid oxide fuel cell (SOFC) with a micro gas turbine (MGT). This results in a power plant with a high electric efficiency even in part load and high fuel flexibility [1]. Therefore HyPP are very suitable for the use of biogas.

In the EU Horizon 2020 project “Bio-HyPP” such a biogas powered HyPP is investigated. At the DLR Institute of Combustion Technology a HyPP demonstrator is currently being built. It consists of a SOFC in planar design with about 30 kW electric power output and a MGT with about 3 kW electric power output.

Fig. 1 shows the layout of the demonstrator. For simplification only components and flows are shown which are necessary for steady state. The compressed air is first used to purge the remaining air volume of the SOFC pressure vessel. This achieves a pressure compensation of the SOFC, controls the temperature of the auxiliary units and prevents an ignitable mixture in case of leakages. In the recuperator the air is preheated by exhaust gases before it supplies the SOFC



**Fig. 1:** Layout of the hybrid power plant (simplified).

cathode. A fuel recirculation and a reformer guarantee a hydrogen rich and almost methane free fuel supply for the anode. In this concept one combustion system combines the functionality of a SOFC off gas burner for standard operating conditions and a gas turbine combustor for start-up and shut-down procedures. This combustor is developed at DLR for this project. A water heat exchanger at the outlet allows the use of the remaining exhaust gas energy for cogeneration.

## II. SIMULATION MODEL

The simulation model of the hybrid power plant is built with a steady state simulation tool. It is based on Matlab/Simulink and contains 0D models of all plant components. The simulation tool is a redesign of an existing in-house tool [2], exceeding it in calculation speed and flexibility of modelling complex cycles.

Turbomachinery is modelled by experimentally gained turbo maps. The SOFC stack model is developed at the DLR Institute

of Engineering Thermodynamics and is parameterized by measurements. Heat and pressure losses of the components are also included. These are represented by estimates as no measurement data is available yet.

The boundary conditions of the simulation are listed in Table I.

TABLE I  
SIMULATION BOUNDARY CONDITIONS

Turbine outlet temperature (TOT)	1060 K	Recuperator efficiency	90 %
Stack temperature ( $T_{\text{Stack}}$ )	1073 K - 1123 K	Shaft speed	120 rpm - 240 krpm
Recirculation rate	80 %	CH <sub>4</sub> content in fuel	40 vol-% - 100 vol-%

### III. INFLUENCE OF BIOGAS ON THE SYSTEM

To simulate a biogas driven HyPP a mixture of methane and carbon dioxide is used as fuel. Simulations with methane contents between 40 and 100 volume percent were performed. As expected, gas compositions and fuel mass flow depends strongly on the fuel methane content. But besides these, the impact of the system is relatively small: For example, the Nernst potential at SOFC outlet reduces less than 2 % for biogas with 70 % methane content compared with pure methane as fuel. For a fuel with 40 % methane content the change is still below 5 %. As Nernst potential is an indicator of SOFC performance, which in turn dominates system performance, the methane content is of small importance for the maximum HyPP efficiency. This small efficiency decrease is depicted in Fig. 2 for the lines of constant temperature (solid and dashed lines). Furthermore, it can be seen that electric efficiencies over 60 % can be achieved. Also the flat efficiency line over the electric power at a specific stack temperature shows that efficiency is very high even in part load.

### IV. INFLUENCE OF BIOGAS ON THE OPERATING RANGE

The operating range of the hybrid power plant is limited by several conditions Here the following are considered according to manufacturer specification and technical experience:

- Maximal shaft speed of the MGT (240 000 rpm)
- Maximal (850 °C) and minimal (800 °C) stack temperature
- Minimal cell voltage to avoid nickel oxidation (0.68 V)
- Maximal single pass fuel utilization (FU) of the SOFC to avoid cell degradation due to local fuel starvation. (70 %)

Fig. 2 shows the simulated operating range in dependence of electric power output and methane content of the fuel. Towards high electrical power it is limited by the maximal MGT shaft speed. The turbine outlet temperature is fixed to a maximal value due to material properties. Therefore the FU increases to small electric power and limits the operating range. The maximum and minimum system efficiency is determined

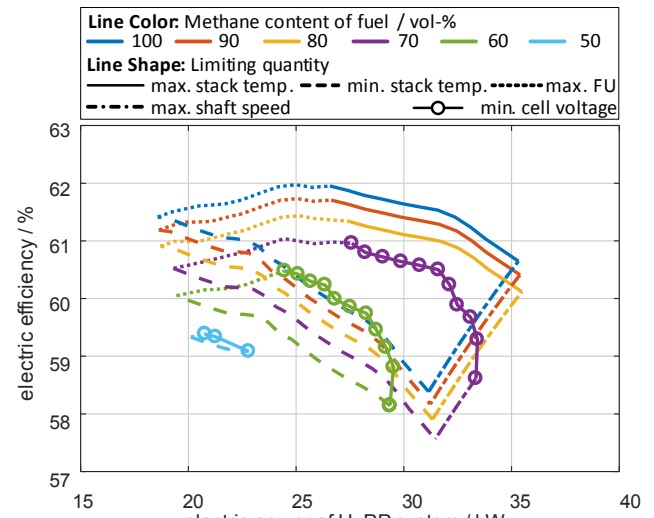


Fig. 2: Operating range of HyPP with biogas and a recirculation rate of 80 %.

by the maximum and minimum stack temperature, respectively. But with decreasing methane content of the fuel the cell voltage decreases. According to section III the relative decrease is quite small: For a biogas with 40 % methane content the cell voltage is reduced by less than 7 %. However, the absolute decrease is large enough to result in a cell voltage below the minimum value. Therefore, the operating range is significantly reduced and for fuel methane contents below 50 % no operation is possible within the boundary conditions.

### V. CONCLUSIONS

Numerical simulations of a hybrid power plant demonstrator shows, that the methane content in biogas fuel hardly influences the system quantities from a relative point of view. However, a reduction of the methane content diminishes the operating range and can even prevent operation as the absolute value of the cell voltage falls below its limit.

### ACKNOWLEDGMENT



This project has received funding from the European Union's Horizon 2020 research and innovation programme under grant agreement No 641073 ([www.bio-hypp.eu](http://www.bio-hypp.eu)).

### REFERENCES

- [1] M. Henke, N. Klemp, M. Hohloch, T. Monz and M. Aigner, "Validation of a T100 Micro Gas Turbine Steady-State Simulation Tool," in *Proceedings of ASME Turbo Expo 2015: Turbine Technical Conference and Exposition, GT2015-42090*, June 15-19, Montreal, Canada, 2015.
- [2] P. Costamagna, L. Magistri and A. Massardo, "Design and part-load performance of a hybrid system based on a solid oxide fuel cell reactor and a micro gas turbine," *Journal of Power Sources*, pp. 352-368, 2001.

# EFFECTS OF MATERIAL STRUCTURE EVOLUTIONS ON THE PERFORMANCE DEGRADATION OF SOFC

Jiang Zhu and Zijing Lin\*

Department of Physics, University of Science and Technology of China, Hefei 230026, China

\*E-mail address: [zjlin@ustc.edu.cn](mailto:zjlin@ustc.edu.cn)

**Abstract** - The power output of SOFC affected by the evolutions of the structures of cell components is examined by multi-physics simulations. Explicit considerations are given to the material set of SS430 interconnect, Ni-YSZ anode and YSZ electrolyte. The degradation mechanisms considered include the oxidation of SS430, the coarsening of Ni particles and the phase transformation of YSZ material. The oxidation is found to cause a rapid performance degradation, but its effect can be minimized by anti-oxidation coating. The degradation due to the Ni agglomeration is also significant, but can be eliminated by a microstructure design of the Ni-YSZ anode. The decrease of YSZ conductivity is found to affect the cell degradation only moderately. The simulation results show that an overall long-term degradation rate of less than 0.3% can be achieved by interconnect coating and anode microstructure design.

**Index Terms** - Interconnect oxidation, Multi-physics modeling, Ni agglomeration, YSZ electrolyte

## I. INTRODUCTION

SOFCs are fuel flexible and receive a broad attention. Long-term performance stability is essential for the commercialization of SOFC technology. Among the sources of degradation, the changes in the material properties of the cell components due to their structural evolutions are the most fundamental.

The long-term behaviors of key property parameters of YSZ electrolyte, Ni-YSZ anode, LSM-YSZ cathode and SS430 interconnect have been examined experimentally. However, it is difficult to quantify experimentally the effect of the property changes on the cell output due to the involvement of other degradation mechanisms such as mechanical stress damage.

In this work, multi-physics numerical simulations are used to

examine the influence of each cell component and the combined effect of the cell components on the long-term cell performance. In particular, the multi-physics simulations are used to examine the effects of anti-oxidation coating of interconnect and microstructure design of anode on the cell performance.

## II. COMPUTATIONAL METHOD

The multi-physics model of SOFC includes the geometric model, the governing equations for the physical processes, the material and operation parameters and boundary conditions. A detailed description of such a model can be found in Ref.[1].

## III. RESULTS AND DISCUSSIONS

Based on the experimental data of Ref.[2], the effect of LSM-YSZ cathode on the cell degradation is found to be very limited. Therefore, attention is given below to the degradations induced by the SS430 interconnect, Ni-YSZ anode and YSZ electrolyte.

### A. Degradation Due to Interconnect Oxidation

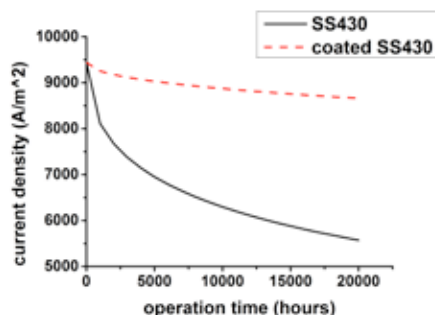


Fig. 1. Degradation due the increase of interconnect area specific resistance.

The electronic conductivity of interconnect decreases with the oxide scale growth. The rate of oxide scale growth can be much reduced by coating  $\text{NiCoFeO}_4$  on the SS430 surface. Based on Wagner's law of oxidation and the experiment of Ref.[3], the change of the interconnect area specific resistance with time can be determined. The corresponding cell outputs are shown in Fig.1. As seen in Fig.1, the oxidation of SS430 causes a rapid cell degradation. Fortunately, more than 80% of the degradation are eliminated by the protective coating.

#### B. Degradation Due to Ni particle coarsening

The agglomeration of Ni particles affects the TPB length and the electronic conductivity of the anode. Based on a model validated by the experimental data of Ni agglomeration [3], the changes of the TPB length and conductivity can be computed. The variations of the current output for two sets of initial Ni-YSZ particle sizes are shown in Fig.2. As seen in Fig.2, the cell output may decrease rapidly for one set of the particle sizes, or remain very stable for another set of the particle sizes.

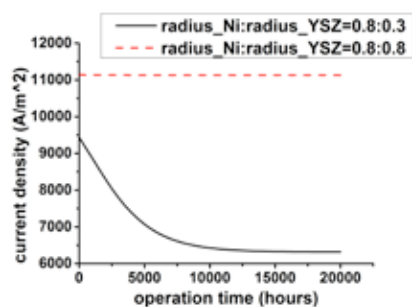


Fig. 2. Degradation due to the Ni particle agglomeration

#### C. Degradation Due to the YSZ phase transformation

YSZ transforms from cubic to tetragonal phase over time, resulting in a decrease of its ionic conductivity. By fitting the experimental data of Ref.[4], an analytical expression for the YSZ ionic conductivity is deduced. The degradation of cell performance thus determined is shown in Fig.3. It is seen that, though the resulting cell performance decreases very fast in the beginning, it remains stable later on.

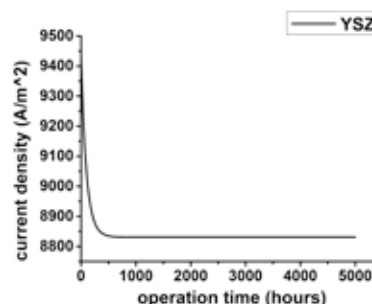


Fig. 3. Degradation due to the decrease of YSZ conductivity

#### D. Overall Degradation of the Cell

The overall cell degradation caused by the changes in the microstructures of interconnect, electrolyte and anode is shown in Fig.4. By an anti-oxidation coating of SS430 and a choice of the initial Ni-YSZ particle sizes, it is possible to see an overall long-term cell degradation rate of less than 0.4%/1000h, much better than the commercial requirement of 1-2%/1000h.

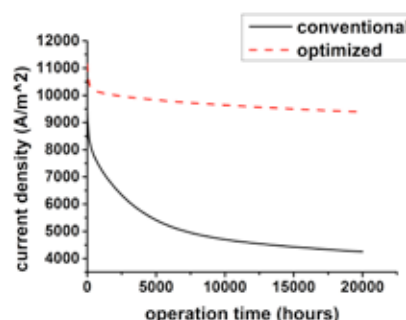


Fig. 4. Degradation of the overall cell performance.

## IV. CONCLUSIONS

The structural evolutions the cell materials may substantially affect the long-term performance of SOFC. Simulations show that both the oxidation of interconnect and the coarsening of Ni particles can cause a rapid cell degradation. The degradation associated with YSZ is fast initially, but is negligible after ~1000h. Through an interconnect coating and a design of the anode microstructure, a long-term cell stability much higher than the commercialization requirement can be achieved.

## ACKNOWLEDGMENTS

The National Natural Science Foundation of China (11374272, 11574284 & 11774324) and Collaborative Innovation Center of Suzhou Nano Science and Technology.

## REFERENCES

- [1] W. Kong, J. Li, S. Liu, Z. Lin, The influence of interconnect ribs on the performance of planar solid oxide fuel cell and formulae



# 3D MULTIPHYSICS MODELING BASED MECHANICAL STRESS ANALYSIS OF PLANAR SOFC STACKS

Xiurong Fang and Zijing Lin

Department of Physics, University of Science and Technology of China,  
Hefei 230026, China

**Abstract** - Damage by mechanical load and temperature gradient is a major factor limiting the long-term stability of SOFC stacks. Numerical simulations are performed to analyze the mechanical stress, mechanical failure probability and creep strain of a planar SOFC stack with different temperature ( $T$ ) profiles. For an isothermal stack, the maximum stress decreases with  $T$ , but the anode failure probability and creep strain rate increase with  $T$ . The dependence of the anode failure probability on the Ni content and its oxidation state is examined. For an operating stack, a multi-physics CFD model is used to determine the  $T$ -profile. The creep strain rate shows a complicated relation with the stress and  $T$ . The average creep rate of the operating stack is found to be over 50% higher than that of an isothermal stack with the same average  $T$ . A  $T$ -distribution deduced from a multi-physics fully coupled model is essential for a reliable prediction of the creep rate and the corresponding lifetime of an operating stack.

**Index Terms** - Creep strain, Failure probability, Stress

## I. INTRODUCTION

Solid oxide fuel cells (SOFCs) are attractive power production devices due to their high energy conversion efficiency and fuel flexibilities. The planar design of SOFC is widely studied for its high power density. However, the planar design is also prone to thermal stress induced mechanical failure. Here, numerical simulations are used to examine the thermal mechanical behaviors of planar SOFC stacks.

## II. COMPUTATIONAL METHOD

A standard structural mechanics model is used for the thermal mechanical analysis. The geometric model of planar SOFC stack is discretized by an FEM commercial software. A detailed description of the modeling approach including the boundary conditions and material properties can be found in Ref.[1]. The temperature distribution of an operating 5-cell

stack is determined by performing simulations with a 3D multi-physics fully-coupled CFD model [2]. The grid dependence of the thermal mechanical results is tested and a grid with the best balance of the accuracy and computational efficiency is used.

## III. RESULTS

### A. Stress distribution in an isothermal cell

Based on the finding of Ref.[3] that all stresses go to zero after reduction at 800°C, the stress distribution for  $T=700^\circ\text{C}$ , OT, is shown in Fig.1. The stress in the anode is mainly tensile while that in the electrolyte and cathode are compressive. The stress profiles are similar for different  $T$ , but differ in their magnitudes. At 700 °C , the maximum stress of anode, electrolyte and cathode are 6.49, 78.4 and 8.27 MPa, much smaller than the corresponding residual stress at the room temperature (RT) of 32.2, 532 and 30.3 MPa, respectively.

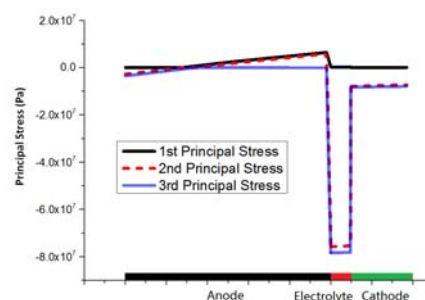


Fig. 1 Principal stress distributions at  $T=700^\circ\text{C}$ .

### B. Mechanical failure probability

Fig.2 shows the anode failure probability varying with its Ni content and oxidation state, with the effective mechanical

properties of the anode determined by the model described in Ref.[1]. The failure probability increases rapidly with the Ni content, consistent with the experimental findings. Overall, the mechanical failure probability is low and considered safe if Ni in the solid Ni-YSZ phase is below 50vol.%.

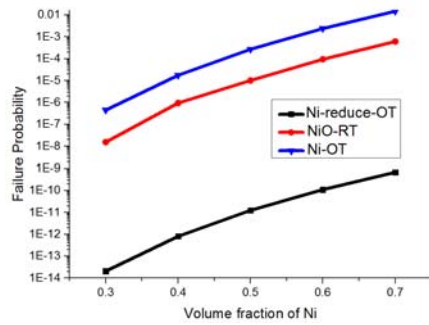


Fig. 2 Mechanical failure probability of Ni-YSZ anode.

### C. Creep Strain Rate

Creep is dependent on both stress and temperature. For a Ni volume content of 45%, the maximum stress and the corresponding creep strain rate of the anode are shown in Fig.3. The stress decrease with the increase of  $T$ , as the SOFC cell is stress free at 800°C. However, the creep strain rate increases monotonically with  $T$ , despite the decrease of the stress. The creep strain rates shown in Fig.3 is consistent with the recent experimental data of Ref.[4].

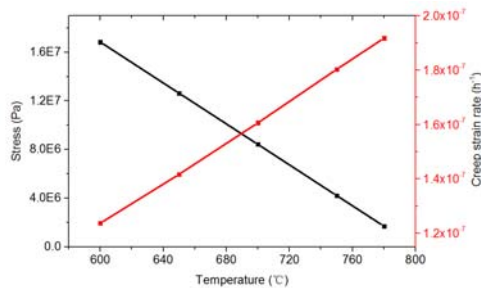


Fig. 3 Stress and creep strain rate of anode at different temperature.

### D. Temperature distribution of an operating stack

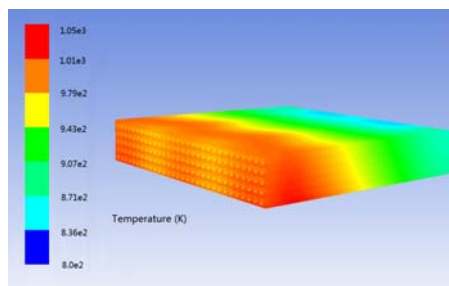


Fig. 4 Temperature distribution in a 5-cell stack

An example of the  $T$  distribution of an operating 5-cell stack determined by a multi-physics fully coupled CFD model is

shown in Fig.4. There is a large  $T$ -difference in the stack due to the competition of electrochemical reaction and heat transport. The  $T$ -distribution is also different for different cells in the stack, mainly caused by the uneven fuel and air streams supplied to the cells.

### E. Creep Rate and Stress Distributions of Operating Stack

The stress and creep strain rate for the  $T$ -profile of Fig.4 are displayed in Fig.5. The creep rate shows complicated relations with the stress and  $T$ . The maximal creep strain rate is found with a medium  $T = 660^\circ\text{C}$ . The average creep rate of the anode is  $2.3\text{e-}7/\text{h}$ , about 50% above the corresponding result of Fig.3. The results show that operations with uniform  $T$ -distributions are helpful for increasing the stack operating lifetime.

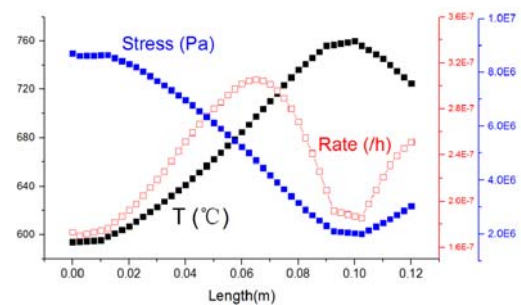


Fig. 5 Temperature, stress and creep rate distributions in an operating stack.

## IV. CONCLUSION

Thermal mechanical stress, failure probability and creep strain rate of SOFCs are analyzed.  $T$ -distributions are determined by a multi-physics CFD model and significantly affect the creep strain rate. A reliable lifetime prediction and operating condition optimization require the temperature profiles determined by accurate multi-physics stack modeling.

## REFERENCES

- [1] Li J, Kong W, Lin Z. Theoretical studies on the electrochemical and mechanical properties and microstructure optimization of micro-tubular solid oxide fuel cells. *Journal of Power Sources*. 2013;232:106-22.
- [2] Li A, Song C, Lin Z. A multiphysics fully coupled modeling tool for the design and operation analysis of planar solid oxide fuel cell stacks. *Applied Energy*. 2017;190:1234-44.
- [3] Frandsen HL, Makowska M, Greco F, Chatzichristodoulou C, Ni DW, Curran DJ, et al. Accelerated creep in solid oxide fuel cell anode supports during reduction. *Journal of Power Sources*. 2016;323:78-89.
- [4] Wei J, Malzbender J. Steady state creep of Ni-8YSZ substrates for application in solid oxide fuel and electrolysis cells. *Journal of Power Sources*, Volume, 360, 2017; Pages, 1-10.

## USING A SOCIAL ACCOUNTING MATRIX TO ESTIMATE MACRO ECONOMIC EFFECTS OF A REVOLUTION IN ROAD TRANSPORT IN ITALY

M. Rao\*, M. Gaeta\*\*, and U. Ciorba\*

\*ENEA, Rome, (Italy)

\*\*RSE, Milan, (Italy)

**Abstract** - We evaluate the macro-economic effects of a modal shift in road transport sector in Italy in order to take account of a changes in Italian car sector. We consider two distinct scenarios of alternative mobility based on a significant investments in BEVs (Battery Electric Vehicles), PHEVs (Plug-In Hybrid Electric Vehicles) and FCEVs (Fuel Cell Electric Vehicles). We use a 65-by-65 SAM table developed by University of Roma "Tor Vergata", to calculate the macroeconomic impacts. With these assumptions, two scenarios for policy simulation was designed according to alternative hypothesis of RES penetration in Italian electric generation mix. The result shows the effects of the alternative scenarios on the Value Added and FTE Labor Units using as a counterfactual scenario the abovementioned 1) respect to the alternative **Vehicle** based scenario.

**Index Terms** - TIMES Italia, SAM, Road Transport Shift, BEVs, PHEVs, FCEVs, macro-economic impact.

### I. INTRODUCTION

This work perform a first order assessment of the macroeconomic evaluation of a scenario characterized by a strong diffusion of alternative mobility systems based on BEVs, PHEVs and FCEVs.

### II. MATERIALS AND METHODS

The used tools was:

- a 65-by-65 Social Accounting Matrix developed by ENEA and University of Tor Vergata based on year 2010;
- a set of investment coming from a specific scenario produced by TIMES Italia model, in order to simulate a baseline for the evaluation regarding to the transport sector;
- a set of assumptions in order to simulate the modal shift object of this study

- the software for linkage between TIMES Italia model and SAM provided by the authors

#### A. Assumptions

We started from the investment costs for the transport sector group in the baseline scenario. These costs were re-proportioned by modifying the investments on the basis of a heterogeneous set of information on the difference between average costs of the standard vehicle fleet, and average costs of the alternative vehicle fleet.

It has been assumed that the costs of the finished product can reflect with a certain degree of approximation the investment costs of the products themselves.

The period of construction of the investments was set equal to the weighted arithmetic average of the periods of each single sub-group of the transport sector, following the classification consistent with the TIMES Italia model.

During the construction period, the exogenous sector is Capital Formation.

During the period of the regime, the Household sector was placed as an exogenous sector.

The time horizon considered is 15 years, from 2016 to 2030: we've use as a final an year significant for various international public policies of the energy and industrial sectors.

The basic hypothesis formulated for the fleet changes is a linear decrease of the number of traditional vehicle, progressively replaced by BEV, PHEV and FCEV vehicles with a cost assumptions based on a weighted indices composed using the values of the traditional and alternative vehicles.

For regime period, two distinct orders of effects were taken into account:

a progressive increase in Household expenses due to the reduction in fuel costs;

a reduction in revenues from the Government and Refinery sectors, proportional to the trend of decreasing in fuel

consumption.

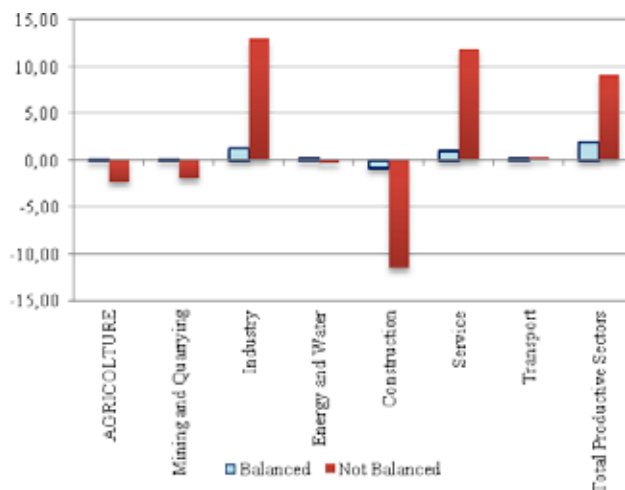


Fig. 1 Average annual net impact of REV Scenario versus Baseline Scenario (Value Added) - mld euros

Results shows that total net impact on productive sectors move from circa 2 mld euros per year (in a balanced scenario, in which the investment in new types of vehicles are compensated by decrease in Taxes for Government and Revenues of Refinery Sector).

The effects on FTE Labor Units follows the same trend of the Value Added: another significant information is the percentage variation of the impact between the two hypothesis of scenario (with and without compensation).

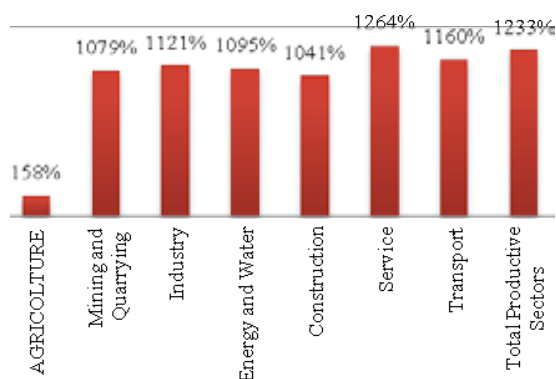


Fig. 2 Percentage variation between Vehicle Scenario Balanced versus not Balanced (Value Added) - mld of euros - %

The results are strongly dependent on the specific basic assumptions. In the hypothesis of compensation operated by Government and Refinery sectors (proportional decrease of Taxes and Revenues, respectively), the impact appears very low: without the formulated hypothesis the impact would be very overestimated.

### III. CONCLUSION

This first attempt to enter in a complex matter like the economics of the road transport sector revolution shows that a positive impacts on global system is possible. However, in the regime period, the hypothesis about some of the key sector (Government sector and Refinery sector, in this work) become crucial in order to determine the intensity of the policy impact.

### ACKNOWLEDGMENT

The authors wish to thanks Cataldo Ferrarese, Carmela Notaro and Prof. Pasquale Lucio Scandizzo from University of Rome "Tor Vergata" and Openeconomics.

### REFERENCES

- [1] Klaassen, M., Vos, D., Seebregts, A., Kram, T., Kruitwagen, S., Huiberts, R., et al. (1999) *Markal-IO : Linking an input-output model with MARKAL*. Bilthoven, The Netherlands: NOP Commission..
- [2] Rao, M., Ciorba, U., Tommasino, M. C., Gaeta, M - *A SOFTWARE APPLICATION FOR TIMES-SAM LINKAGE*, RT 2015/19/ENEA
- [3] Loulou, R., Goldstein, G., & Noble, K. (2004). *Documentation for the MARKAL Family of Models*. Paris: IEA
- [4] Loulou, R., Remne, U., Kanudia, A., Lehtila, A., & Goldstein, G. (2005). PART I. In R. Loulou, U. Remne, A. Kanudia, A. Lehtila, & G. Goldstein, *Documentation for the TIMES Model* (p. 1-78). Paris: IEA
- [5] Miller, R., & Blair, P. D. (2009). *Input-Output Analysis: Foundations and Extensions*. New York: Cambridge University Press.
- [6] Scandizzo, P., & Ferrarese, C. (2015). *Social accounting matrix: A new estimation methodology*. Journal of Policy Modeling, 14-34
- [7] Rao, M., & Tommasino, M. C. (2014). *Updating technical coefficients of an input-output matrix with RAS- the TRIOBal software*. Roma: ENEA
- [8] Mesnard, L. d. (2002). *Failure of the normalization of the RAS method : absorption and fabrication effects are still incorrect*. The Annals of Regional Science, 139-144
- [9] Gilchrist, D., & St. Louis, L. (1999). *Completing input-output tables using partial information with an application to Canadian data*. Economic System Research, 185-193
- [10] Rao, M., & Tommasino, M. (2015). *An analysis of the effects of internal constraints application on the accuracy measures in projecting a social accounting matrix with iterative methods. The case of Italian SAM for years 2005 and 2010*. Roma: ENEA



## ELECTRODEPOSITED NICKEL IRON TELLURIDE FILM ON NICKEL FOAM AS EFFICIENT ELECTROCATALYST FOR OXYGEN EVOLUTION REACTION

Joseph R. Ortenero<sup>\* \*\*</sup>, Joey D. Ocon<sup>\*</sup>, Qiang Huang<sup>\*\*</sup>

<sup>\*</sup>National Graduate School of Engineering,  
University of the Philippines, Diliman, Quezon City 1101, (Philippines)

<sup>\*\*</sup>Chemical and Biological Engineering,  
The University of Alabama, Tuscaloosa 35401, (USA)

**Abstract** - Efficient water splitting electrocatalyst is necessary to usher the revolution of sustainable and clean energy future. The main bottleneck in the splitting of water for hydrogen production lies in the sluggish kinetics of the oxygen evolution reaction (OER). Transition metal chalcogenides have become attractive anodic material for OER due to its abundance and low cost for alkaline water electrolyzer. Oxides, sulfides and selenides have been reported as promising electrocatalyst for OER; however, no study has yet been reported for tellurides. In this study, we explored the viability of nickel iron telluride for oxygen evolution reaction. The nickel iron telluride serves as precursor for the generation of a more reactive oxide during anodic oxidation. The telluride-derived electrocatalyst has overpotential of 265 mV at 10 mA/cm<sup>2</sup>. A short-term stability measurement showed constant potential for a period of 24 hours. This work elucidated the viability of transition metal telluride as anodic electrocatalyst for water splitting.

**Index Terms** - Nickel iron telluride, oxygen evolution reaction, transition metal chalcogenide, water splitting

### I. INTRODUCTION

Interest in transition metal chalcogenides has accelerated in recent years in search for abundant, low-cost and efficient catalyst for renewable energy storage. This is especially noticeable in the number of research on the first row transition metals such as Ni, Co and Fe combined with chalcogenides such as oxides, sulfides, selenides and other non-metals such as phosphides, carbides and nitrides<sup>[1]</sup>. However, more work is still needed to understand the mechanism at which these catalysts aid in water splitting. Major challenge exists in the design of an efficient OER catalyst due to sluggish kinetics of reaction compared to HER<sup>[2]</sup>. Hence, understanding the complex four-electron transfer in OER combined with efficient catalyst and effective electrode

design is a step towards renewables to alternative hydrogen energy storage.

### II. EXPERIMENTAL METHODS

#### A. Materials

The precursors and other chemicals in the experiment were used as received. Nickel (II) sulfate hexahydrate (NiSO<sub>4</sub>·6H<sub>2</sub>O, 98%), iron (II) sulfate heptahydrate (FeSO<sub>4</sub>·7H<sub>2</sub>O, 99%), selenium (IV) oxide (SeO<sub>2</sub>, 99.4%), tellurium (IV) oxide (TeO<sub>2</sub>, 99.99%) were purchased from Alfa Aesar. Potassium chloride (KCl) and trace metal grade 95-98% sulfuric acid were sourced from BDH® VWR Analytical. Water was purified using Thermoscientific Barnstead Nanopure water purification system with a resistivity of 18.2 Mohm-cm. Nitrogen (N<sub>2</sub>, 99.999%) was purchased from Airgas.

#### B. Electrode Preparation

NiSe, NiFeSe and NiFeTe were electrodeposited on a nickel foam substrate at constant current density of 10mA/cm<sup>2</sup> geometric area. The nickel foam (NF) strip has a dimension of 1cm by 1cm. Prior to the galvanostatic deposition, NF were soaked in a 0.1M H<sub>2</sub>SO<sub>4</sub> under sonication for 10 min, washed with deionized (DI) water, immersed in an ethanol solution under sonication for 10 min, and finally rinsed with DI water.

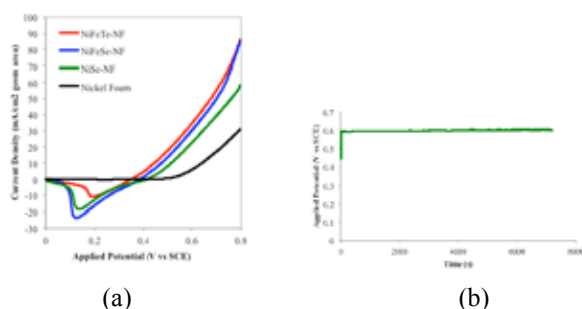
Saturated calomel electrode (SCE) was used as reference electrode and platinum wire as counter electrode. A three-compartment cell was designed to carry-out the electrodeposition, LSV, CV and EIS experiments. A porous glass frit separates the working electrode (WE) from the counter electrode (CE). N<sub>2</sub> gas was bubbled for 30min before the start of each experiment.

### III. RESULTS AND DISCUSSION

#### A. Linear Sweep Voltammetry and Chrono Potentiometry

The galvanostatic deposition was carried out for 30 minutes in an acid-sulfate bath. After air drying for 1-hour the NiFeTe-NF strip was analyzed for composition using X-ray fluorescence spectroscopy (XRF) and then immersed in a 1.0M KOH solution for activity and stability measurement.

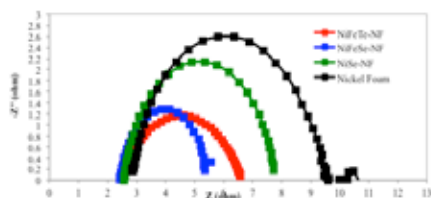
Linear sweep voltammogram shown in Fig. 1 shows that NiFeTe could catalyze OER with overpotential of 265 mV at 10mA/cm<sup>2</sup>. NiFeTe is slightly more active than NiFeSe, which has overpotential of 295 mV at the same current density. NiFeTe is also better than NiSe and nickel foam, which have overpotential of 333mV and 459mV, respectively. The onset potential for NiFeTe is 173 mV at 0.5mA/cm<sup>2</sup> current density. This is lower than that of NiFeSe, NiSe and nickel foam, which have onset overpotential of 208 mV, 242 mV and 320 mV at 0.5 mA/cm<sup>2</sup>, respectively. Earlier report showed that NiSe is a good catalyst for OER, in this study incorporating Fe has significantly improved OER activity. Fe-doped catalyst has been reported to improve catalytic activity in NiFe layered double hydroxide. It has been established that Ni is the catalytic center for nickel-based catalysts; addition of little amount of Fe improved that catalytic performance through some electronic interaction with Ni centers.



**Figure 1.** Catalytic activity of NiFeTe compared with other nickel-based catalysts. (a) LSV polarization curve of NiFeTe for OER (b) 2-hr stability test

#### B. Electrochemical Impedance Spectroscopy

EIS study showed a trend of decreasing charge transfer resistance,  $R_{ct}$ , NF>NiSe> NiFeTe>NiFeSe as shown in the Nyquist plot of Fig. 2.



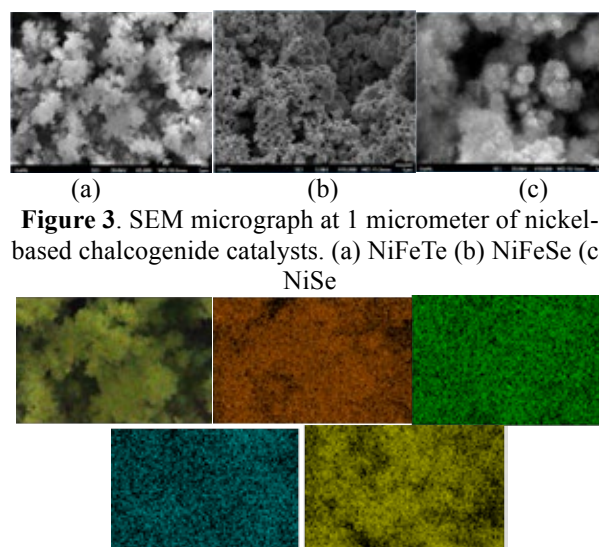
**Figure 2.** Nyquist plot of NiFeTe and other nickel-based chalcogenides.

This partially confirms the result of LSV, which showed NiFeTe as a more active catalyst for OER than

NiSe and nickel foam. However, charge transfer resistance of NiFeSe is slightly lower than that of NiFeTe, which contradicts earlier result of LSV. It can be explained by poor adhesion of NiFeTe particles on the NF substrate as it was observed that some particles of NiFeTe peel off from the support after anodic scan.

#### C. Material Characterization

SEM micrograph of NiFeTe in Fig. 3a shows coral-like structures formed by electrodeposition process. The nanostructures provides high surface area for catalyzing the evolution of oxygen. Fig. 4 shows the uniform distribution of Ni, Fe, Te and O over the catalyst surface.



**Figure 3.** SEM micrograph at 1 micrometer of nickel-based chalcogenide catalysts. (a) NiFeTe (b) NiFeSe (c) NiSe  
**Figure 4.** Elemental distribution of NiFeTe obtained from SEM-EDS. (a) EDS layered image (b) Te La1,2, (c) Ni Ka1, (d) Fe Ka1 and (e) O Ka1

### IV. CONCLUSION

NiFeTe shows better electrocatalytic activity towards OER in alkaline solution than nickel foam and NiSe. It also demonstrates slightly better performance than NiFeSe. Further experiment is required to verify NiFeTe/NiFeSe activity in alkaline solution.

#### ACKNOWLEDGMENT

The authors would like to acknowledge the Department of Science and Technology (DOST)--Philippines and Engineering Research and Development for Technology (ERDT) for the funding.

#### REFERENCES

- [1] Xu, X., Fang, S., Hu, X, A nickel iron diselenide-derived efficient oxygen evolution catalyst, Nature Communications 7:12324 doi: 10.1038/ncomms12324 (2016)
- [2] McCrory, C., Jung, S., Ferrer, I., Chatman, S., Peters, J., Jaramillo, T., Benchmarking hydrogen evolving reaction and oxygen evolving reaction electrocatalysts for solar water splitting devices, Journal of the American Chemical Society, Volume 137, 2015, pp. 4347-435

## DEVELOPMENT OF MICRO FUEL CELLS FOR HEARING AIDS

J. L. Bonde\*, O. Tynelius\*, K. Vestentoft\*, T. Lund-Olesen\*, T. Bader\*, C. M. Pedersen\*, H. E. M. Wisaeus\*, J. H. Hales\* and Leif H. Christensen\*

\* Nano Production and Micro Analysis , The Danish Technological Institute, Gregersensvej 1, DK 2630 Taastrup, (Denmark)

**Abstract** - The Danish Technological Institute is developing advanced energy systems powered by solar cells, batteries and fuel cells. Selected results from ongoing projects will be presented. Results from the FCpHi project will be presented in detail.

The target of this project is the development of a Direct Methanol Fuel Cell powered hearing aid that only needs refueling once a day with a maximum refueling time of 30 s.

A major task is to prove the lifetime and performance of the passive  $\mu$ DMFC system developed in house. The fuel cells have been tested with respect to the requirements of a hearing aid in an end user environment.

Different techniques are used for stress testing and analysis in the study. The stress tests are operation in various environmental conditions, exposure to potential contaminants and operation with different load profiles. During and after the stress tests the fuel cells are subjected to various in and ex situ analysis. In addition to electrochemical measurements, SEM-EDX and  $\mu$ CT scans are used.

**Index Terms** – DMFC, hearing aid, micro fuel cell, lifetime

### I. INTRODUCTION

The latest generations of hearing aids are getting more and more advanced, one of the recent advances is the introduction of wireless streaming to the hearing aids. This in turn has consequences for the power consumption which is expected to increase. Currently available hearing aids are generally powered with Zinc air batteries, a few hearing aid manufacturers are introducing rechargeable battery solutions. In the FCpHi project a passive micro DMFC system has been designed and integrated in a hearing aid. With respect to the battery solutions the major innovation is an easy instant recharge/refueling. In addition the expected increasing energy consumption can be met by increasing the methanol storage capacity.



**Fig. 1. DMFC powered hearing aid and refueling station.**

### II. METHODS

In house micro fuel cell production, test and development has been set up. This includes the ability make load tests on 400 fuel cells concurrently, environmental testing, impedance testing and post mortem analysis with SEM-EDX and  $\mu$ CT.

### III. RESULTS

A Direct Methanol Fuel Cell for hearing aids that only needs refueling once a day with a maximum refueling time of 30 s has been developed.

The micro DMFC is mechanically integrated with an internal reservoir and designed to fit inside a hearing aid. Performance and fuel consumption has been tailored to meet the hearing aid power consumption.

The micro DMFC unit can operate in a stable manner under the environmental conditions that hearing aids typically are exposed to.

Both accelerated stress tests and continuous load test have been performed and currently more than 2 million test hours have been logged. The cells with the longest lifetime have now been in operation for more than 5 years with an average degradation of 2  $\mu$ V/hour.

#### IV. CONCLUSION

A passive micro DMFC has been integrated into a hearing aid and tested under different operating conditions.

Currently more than 2 million test hours have been accumulated, this data is used to predict the potential lifetime and in the continues improvement of the fuel cell design and fuel cell components. The cells with the longest lifetime have currently been in operation for more than five years with an average degradation of 2  $\mu\text{V}/\text{hour}$ .

#### ACKNOWLEDGMENT

The FCpHi project is supported by the Danish Innovation Foundation.

Copyright © 2017



**TOWARDS MONOLITHICALLY PRINTED MFCs: A REPORT ON THE  
DEVELOPMENT OF A 3D-PRINTABLE MEMBRANE ELECTRODE ASSEMBLY  
(MEA)**

P. Theodosiou\*, J. Greenman\*\*, C. Melhuish\* and I.  
Ieropoulos\*

\* Bristol BioEnergy Centre, Bristol Robotics Laboratory, University  
of the West of England, BS16 1QY (UK)

\*\* Biological, Biomedical and Analytical Sciences, University of the  
West of England, BS16 1QY (UK)

**Abstract** – Additive manufacturing (3D-printing) and Microbial fuel cells (MFCs) are two rapidly growing technologies which have been previously combined to advance the development of the latter. In the same line of work this paper reports on the fabrication of novel membrane electrode assemblies (MEAs) using materials that can be 3D printed or extruded from the EvoBot platform. Materials such as air dry terracotta, air dry Fimo™ and standard terracotta were tested against conventional cation exchange membrane (CEM) material. The MEA was made by painting the materials with custom made graphite coating. The results showed that the MFCs with the printable materials performed better when compared to the ones using CEM. These findings suggest that monolithically printed MFCs may be feasible, as printable MEAs can lower the internal resistance of MFCs, and help realise mass manufacturing.

**Index Terms** – MFC, EvoBot, Membrane electrode assembly, MEA, 3D-printing

## I. INTRODUCTION

Renewable energy production from waste using microbial fuel cell (MFC) technology is attracting increasing attention. MFCs are bio-electrochemical devices that use microorganisms as biocatalysts to convert chemical energy (stored in organic matter) into electrical energy [1]. MFCs consist of a positive cathode and a negative anode, which are separated by a semi-permeable membrane. Microorganisms are inoculated in the anodic compartment and through substrate oxidation, release electrons to the anode electrode. The two electrodes are connected by an external circuit, which allows the flow of electrons from the anode to the cathode. One of the main contributors affecting both cost and performance in MFCs is the commercially available membrane, which tends to be expensive. To overcome this, alternative MFC architectures and materials need to be identified. One design is the membrane electrode assembly (MEA) that improves power output by reducing the internal resistance [2]. This study looks at 3D

printing MFCs using novel extrude-able materials that can be produced from the EvoBot platform (Fig. 1). The focus is on the development of cost-effective MEAs using extrude-able air-dry membranes coated with conductive paint.

## II. MATERIALS AND METHODS

### A. MFC architecture and feedstock

Twelve cubic analytical size MFCs were assembled with only one chamber, which formed the 25mL anode, so as to have an oxygen-diffusion cathode. All the cells were inoculated with activated sludge (Wessex Water, UK) and fed with neat human urine collected anonymously from healthy individuals.

### B. Membrane materials

Three types of potentially extrude-able membranes were tested against a conventional CEM (Membranes International, USA); these were two air-dry clays (Fimo™ and terracotta (Staedtler, German)) and standard non-air dry terracotta clay (Tiranti, UK) (Fig. 2A). The latter was kilned at a temperature of 1070 °C prior to use, to allow the structural bonding of the clay and ensure durability, whereas the other two were dried overnight at room temperature. The thickness of the tested membranes was consistent for all the custom made membranes (2.5mm). The control membrane required activation in 5% NaCl at 40° C prior to use. The membranes were directly glued to the anode chamber with inert aquatic sealant (Aquabits, UK).

### C. Membrane electrode assembly and polarization experiment

A conductive graphite coating was applied to each membrane and formed the cathode electrode (Fig. 2B). The coating was fabricated using polyurethane rubber coating (PlastiDip), white spirit and graphite powder. The membranes were coated with the conductive cathode mixture and the surface resistance was measured for each coating, until the

lowest possible value was achieved (100-200 Ohms). After the membrane electrode assembly had dried, a cable was attached to the cathode using conductive wire glue, to form the cathodic current collector (Fig. 2B). Fixed load (value) and polarisation experiments were conducted for the MFCs. In the latter case, resistance values ranging between 3.74 – 30  $\Omega$  were connected for 3 minutes to record the MFC polarisation behaviour based on the different membranes.

#### Figure 1: EVOBOT Robotic Platform

EVOBOT is a 3D-printer modified to work as a robot, which can operate MFC experiments and extrude soft materials through the syringes on board.



Figure 2: Membrane Materials and MEA setup

### III. RESULTS AND DISCUSSION

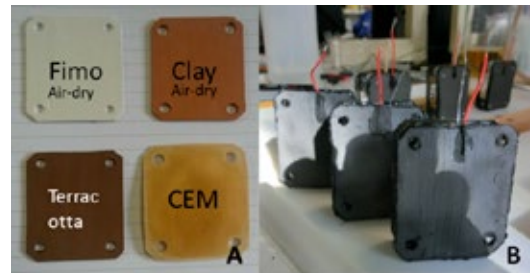
Initially, the air-dry terracotta (70  $\mu$ W) outperformed the other materials, whereas the commercially available CEM was the least performing (30  $\mu$ W) (Fig. 3). Air-dry Fimo™ and kilned terracotta were almost identical in terms of power output (50  $\mu$ W). The experiment started with a 2.7 k $\Omega$  load, and after fourteen days, both air-dry clay and Fimo™ were performing at identical levels. Following polarisation analysis, the optimal external resistance was identified (1 k $\Omega$ ). Once the MFCs were connected to this lower resistance value, the performance levels began to diverge and Fimo™ was producing the highest power output. The results from the polarisation experiment (data not shown) differed with the real-time data, suggesting that the air-dry clay was the best performing with 123  $\mu$ W, followed by Fimo™ with 79  $\mu$ W. However, in all cases, the soft materials were operating better than the conventional cation exchange membrane. The materials tested as alternative membranes come in the form of soft modelling clay, which makes these suitable for extrusion from the EVOBOT platform. As the uncured form of the electrode material is also fluid, it can be applied using EVOBOT by incorporating a brush/roller on the actuation layer

robot. This will apply the conductive coating onto the dried extruded membranes, and help produce a uniform layer on the surface.

#### Figure 3: Initial power output profile of the MFCs

### IV. CONCLUSION

The findings presented in this study demonstrate for the first time that soft materials cured in air can be used as membranes for MFCs, and in addition, even improve power output. This offers a great advantage over the conventional and expensive CEMs, and is a novelty in the MFC field. The EVOBOT



robotic platform is flexible and can be modified to extrude such membranes.

This is an exciting development and a step

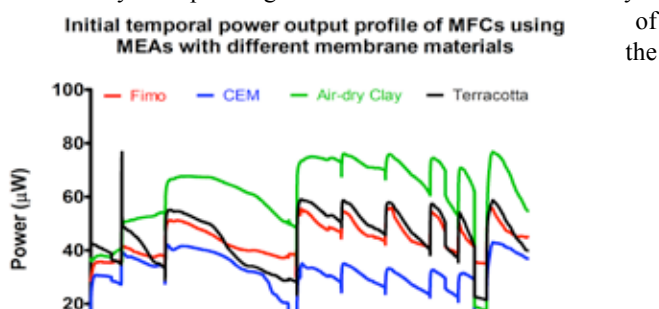
towards the overall goal of the EVOBLISS project, which is to monolithically 3D-print MFCs using EVOBOT.

### ACKNOWLEDGMENT

The authors would like to thank the European Commission for the financial support of this work through the FP7-ICT, grant agreement 611640 (EVOBLISS project).

### REFERENCES

- [1] Bennetto HP. Electricity generation by microorganisms. *Biotechnol Educ* 1990;1:163–8.
- [2] Nandy A, Kumar V, Mondal S, Dutta K, Salah M, Kundu PP. Performance evaluation of microbial fuel cells: Effect of varying electrode configuration and presence of a membrane electrode assembly. *N Biotechnol* 2015;32:272–81. doi:10.1016/j.nbt.2014.11.003.



## THE PERFORMANCE OF VARYING/DIFFERENT POLYTETRAFLUROETHYLENE (PTFE) COATED CARBON FABRIC CLOTH ON ELECTRICITY PRODUCTION IN MICROBIAL FUEL CELL (MFC) USING SYNTHETIC (CHEMICAL) WASTEWATER.

MB. Molala\*, and S. duPlessis\*\*

\*University of Johannesburg, Doornfontein Campus, (South Africa)

\*\*University of Johannesburg, Doornfontein Campus, (South Africa)

*Abstract - During the research, the following objectives were met; Determining the effect of temperature and pH on the efficiency of the MFC, scaling the feasibility of synthetic wastewater in electricity generation, determining the performance of the anode in power generation and to evaluate the performance of different PTFEs coated carbon on power generation. Firstly, The MFC was operated at 33-35 degrees Celsius and pH was kept at 7. Secondly, power and current densities were calculated from the voltage per resistance and the construction of power curves was determined using power and current densities. Lastly, COD tests were conducted and the anode electrode was made up of different PTFEs (0%, 30%, and 50%) carbon coated cloths. Principal results showed a 50% PTFE is more efficient in generating power; however, the performance of individual carbon cloths varies significantly with the percentage of coating added and this affects the performance of the MFC.*

**Index Terms** - COD, Power curves, PTFE, and Synthetic wastewater.

### I. INTRODUCTION

The research project will regulate the performance of different PTFE coated carbon fabric cloth on electricity production in MFC. Microbial fuel cells are configured to produce electricity through the transfer of electrons and protons to and from the anode and cathode through the breakdown of organic matter; this will be done using a CMI7000S proton exchange membrane. The following will be covered; Firstly, the justification of research. Secondly, the experimental methodology. Thirdly, the results and discussions and finally, the conclusion and other sources (acknowledgements and references).

### II. EXTENDED ABSTRACT

#### A. Methods and Materials

1. Assembling of Single chamber:

- Aim: Prepare a chamber with anode and cathode compartments for the synthetic wastewater
- Methods:
  1. Prepare a solution of distilled water.
  2. Cleaning of single chamber.
  3. Assembling of anode and cathode compartment.
- 2. Wastewater preparation:
  - Aim: To prepare a sample of synthetic wastewater for microbial fuel cell
  - Methods:
    4. Prepare chemical wastewater.
- 3. Taking readings (OCV, Voltage & Amps):
  - Aim: To get the overall voltage running through the circuit where both terminals are connected to an external load/resistor
  - Methods:
    5. Connect a multi-meter to the fuel cell.
    6. Connect an external load (resistor).
- 4. Taking COD levels:
  - Aim: To get the Chemical oxygen demand, this is to indirectly measure the amount of organic material in the water, also ensuring water quality
  - Methods:
    7. Take standard hatch samples to measure the COD levels.
- 5. Temperature and pH readings:
  - Aim: To maintain temperature and pH levels constant throughout the experiment
  - Methods:
    8. Set the temperature on the ecobath (35°C).
    9. pH readings (7).

#### B. Equipment's/Materials

- Multimeter-(DT9205A-Aaron): A DT9205A-Aaron multi-meter display device was used to

measure the voltage, current and external resistance

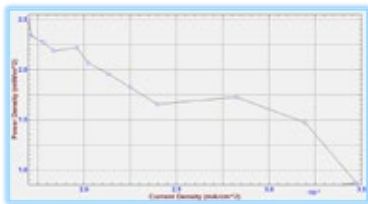
- DR 3900 Spectrometer (Hatch Loveland machine): DR 3900 spectrometer machine was used to measure the concentration and COD levels before and after each experiment
- pH meter: A pH which is an electronic device that was used to measure the pH (acidity or basicity)

### C. Results and Discussion

#### PTFE Coated (0%) Anode

Results of the uncoated (0%) PTFE.

An OCV of 0.263V and a cell voltage of 0.147V on the start at an external resistance of 2400 Ohms was achieved. The cell voltage decreased to 0.025V at an external resistance of 200 Ohms.



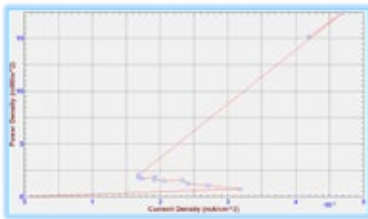
**Fig. 1.:** Power density vs Current density curves for (0%) uncoated carbon cloth.

Fig. 1. clearly shows that the maximum power density output of the 0% uncoated carbon cloth produced was  $2.5 \text{ mW.m}^{-2}$  at a current density of  $0.00171 \text{ mA.cm}^{-2}$  with fixed external resistance of 2400 Ohms. The graph shows a decrease of power density with an increase in current density.

#### PTFE Coated (50%) Anode

Results of the coated carbon cloth 50% PTFE.

An OCV of 0.362V and a cell voltage of 0.362V on the start at an external resistance of 2400 Ohms. From the given table above the cell voltage decreases as the applied external resistance decreases. The cell voltage decreased to 0.115V at an external resistance of 200 Ohms.



**Fig. 2.:** Power density vs Current density curves for 50% PTFE coated carbon cloth.

Fig. 2 shows that the maximum power density output of the 50% PTFE coated carbon cloth produced was  $17.472 \text{ mW.m}^{-2}$  at a current density of  $0.00469 \text{ mA.cm}^{-2}$  with fixed external

resistance of 2200 Ohms. The graph shows a decrease in power density and a decrease in current density.

### D. Discussion

Comparison between the different PTFE carbon coatings, the maximum power density output was produced from the 50% PTFE ( $17.472 \text{ mW.m}^{-2}$ ) than on the other coated PTFE carbon cloth. Hence, this indicates that the 50% carbon cloth performs much better than the other verify carbon coated PTFE.

The 50% coated carbon cloth produced the most power density showing an OCV of 0.362V and a cell voltage of 0.362V on the start at an external resistance of 2400 Ohms. The cell voltage decreases as the applied external resistance decreases. The cell voltage decreased to 0.115V at an external resistance of 200 Ohms.

Fig. 1 shows that the maximum power density output of the 50% PTFE coated carbon cloth produced was  $17.472 \text{ mW.m}^{-2}$  at a current density of  $0.00469 \text{ mA.cm}^{-2}$  with fixed external resistance of 2200 Ohms. The graph shows a decrease in power density and a decrease in current density.

The maximum voltage output of the 50% PTFE produced was 0.372V at a current density of  $0.0014697 \text{ mA.cm}^{-2}$  with fixed external resistance of 2200 Ohms.

### III. CONCLUSION

- The 50% PTFE coated anode generates the most power density output compared to the other carbon coatings which makes it more efficient in generating power
- An enactment of the individual coated carbon cloths varies significantly with the type of percentage coating which is applied on the cloth
- The performance of the carbon cloth directly affects the overall performance of the microbial fuel cell
- Currently there isn't enough literature with regards to the performance of bio-electrochemical properties between the different coated carbon cloths

### ACKNOWLEDGMENT

Dr. S duPlessis has been the ideal supervisor and mentor. His sage advice, insightful criticisms, and patient encouragement aided the writing of this report in innumerable ways and for his time and effort in grooming me into writing a good report and his guidance and motivation. I would also like to thank Dr. R. Huberts whose steadfast support of this project was greatly needed and deeply appreciated. List of relevant acknowledgements below:

- Dr S. duPlessis (Mentor & Supervisor)
- Dr R. Huberts (Co-supervisor)
- Prof P. Olubambi (Supporter)
- Mr A. Martinus (Lab supervisor)

## Pt/C Catalyst for Direct Methanol Fuel Cell Operating with SBA-3 into Nafion Electrolyte

Nihat Ozer Ucar\*, Gulce Cakman\*, Berker Ficicilar\*

\*Ondokuz Mayıs University, Department of Chemical Engineering, Kurupelit Campus, Atakum, 55139, Samsun

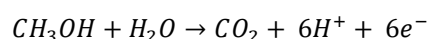
**Abstract** - The large surface area and large pore volume of porous structures increase the importance of these materials progressively. Direct Methanol Fuel Cell (DMFC) becomes prominent because it does not cause environmental pollution, it is silent and cheaper. Otherwise, The purpose of this project, constituted of Pt/C catalyst and enhance of nafion electrolyte with using SBA-3 porous material. The project made in two parts. In the first part, the synthesized SBA-3 porous material converted to carbon structure and then Pt/C catalyst integrated into the DMFC. The other part of the research is to examine the cell performance by adding 1% and 5% SBA-3 silica material into the Nafion, which is the electrolyte of the DMFC by using dropcasting method. At the end of the research, the performance of the fuel cell measured by using Maynuo M9714 DC electronic load and the cyclic voltammetry and impedance will be measured by using Iviumstat.h.

**Keywords:** Direct Methanol Fuel Cell, SBA-3, Mesoporous Carbon, Catalyst

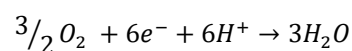
### I. INTRODUCTION

Methanol has a relatively high volumetric theoretical energy density compared to other systems such as conventional batteries. Thanks to this, it can be used in small portable applications. A direct methanol fuel cell (DMFC) consists of two electrodes that are separated by a proton exchange membrane via an external circuit[1].

The direct methanol fuel cell (DMFC) consists of an anode electrode at which methanol is electro-oxidised to CO<sub>2</sub> through the reaction:



and a cathode at which oxygen is reduced to water or steam[2]:



Dupont's Nafion is the polymer electrolyte membrane material most frequently used for this type of application. However the nafion membranes also have several disadvantages such as a decrease in the ionic conductivity and low humidity at high temperatures[3]. Hereby, porous material is good candidate for the polymer membranes because it helps to maintain a suitable hydration of the membrane under fuel cell operating conditions and the mechanical properties are improved.

In this work, Pt/C catalyst, which is synthesized SBA-3, integrated into the DMFC and also examine the cell performance by adding 1% and 5% SBA-3 silica material into the nafion.

### II. EXPERIMENTAL

#### A. Production of SBA-3

SBA-3 was prepared using cetyltrimethylammonium bromide(CTMABr) as a template and TEOS as a Silica source. An aqueous solution of HCl(37%) was added in order to control the pH of the system. 1g of CTMABr, 25mL of water and 10ml of HCl added in 250mL of beaker. Acidic solution was mixed with vigorous stirring at 30°C for 15 min. 2,5mL of TEOS was added dropping to the acidic solution. After 2 h, the white precipitate was aged at room temperature for 12h. The sample was filtered and dried overnight. After drying it, SBA-3 was



calcined at 550°C in air for 5h. The heating rate was 2°C/min.

### *B. Preparation of SBA-3/Nafion Nanocomposite*

A 5% (w/w) Nafion solution was selected to manufacture the film. The original solution was dried at 50°C until obtaining a dry residue, successively diluted in dimethylacetamide as a solvent (10%, w/w, solution). Two different amount of SBA-3 powder (1%, w/w and 5%, w/w) was added and dispersed in an ultrasonic bath. After the casting, the membrane was dried on a hot plate at 80°C, then thermally treated at 155°C. A chemical treatment in 7M HNO<sub>3</sub>, 5%(w/w) H<sub>2</sub>O<sub>2</sub>, 1M H<sub>2</sub>SO<sub>4</sub> was carried out to purify the membrane. A membrane with a thickness of 60µm was obtained.

### *C. Synthesis of SBA-3 type Carbon Structure*

One gram of SBA-3 was added to a solution composed of 1.25g of sucrose and 0.14 g of H<sub>2</sub>SO<sub>4</sub> in 5g of H<sub>2</sub>O. The mixture was placed in a drying oven for 100°C and subsequently the oven temperature was increased to 160°C and maintained for 6h. The sample turned dark brown or black during the treatment in the oven. The silica sample, containing partially polymerized and carbonized sucrose, was heat-treat again at 100°C and 160°C after the addition of 0.8 g of sucrose, 0.09g of H<sub>2</sub>SO<sub>4</sub> and 5g of H<sub>2</sub>O. The carbonization was completed by heating up to 900°C under N<sub>2</sub> gas. The carbon-silica composite obtained after pyrolysis was washed with 5 wt% HF at room temperature in order to remove the silica template. The template-free carbon product was filtrated, washed with ethanol and dried at 120°C

### *D. Preparation of Pt/C Catalyst using SBA-3 type Carbon as a template*

In a 100 mL beaker, 1 mL of an aqueous solution of 0.05 M H<sub>2</sub>PtCl<sub>6</sub>.6H<sub>2</sub>O was mixed with 50 mL of Ethylene glycol and 0.5 mL of 0.8M KOH was added dropwise. 0.04 g of SBA-3 type carbon were uniformly dispersed in the mixed solution by ultrasonication. The beaker was placed in the center of a microwave oven and heated for 60 s. The resulting suspension was filtrated and the residue was washed with acetone. The solid product was dried at 120°C overnight in a vacuum oven.

### *E. Membrane Electrode Assemblies*

For a DMFC anode, a carbon-paper diffusion layer was brushed with a catalyst paste consisting of Pt-Ru (Pt:Ru = 1:1) and 9 wt% of Nafion. The total metal loading on the anode was 9 mg/cm<sup>2</sup>. Similarly, the cathode was constructed by using a teflonized carbon paper as diffusion layer. The synthesized Pt/ SBA-3 type carbon catalyst was mixed with Nafion solution and spread on the diffusion layer by a spray gun giving 9 wt% of Nafion. The total metal loading on the cathode was 5 mg/cm<sup>2</sup>. Finally, the membrane/electrode assemblies were constructed by hot pressing at 135°C and 3 MPa for 10 min.[4].

## III. RESULTS

SBA-3 porous material and mesoporous carbon characterised physically by XRD, TGA, BET and SEM.

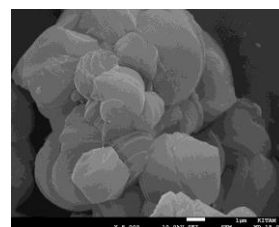


Fig. 1. SEM images of SBA-3

The performance of the fuel cell will be measured by using Maynuo M9714 DC electric load and the cyclic voltametry and impedance will be measured by using Iviumstat.h.

## REFERENCES

- [1] Kimberly M. McGrath, G. K. Surya Prakash, George. A. Olah, Direct Methanol Fuel Cells, J. Ind. Eng. Chem. , Vol 10, 2004, Pages 1063-1080
- [2] A. Hamnett, Mechanism and Electrocatalysis in the direct methanol fuel cell, Catalysis Today 38, 1997, Pages 445-457
- [3] Yilser Devrim, Ayhan Albostan , Enhancement of PEM fuel cell performance at higher temperatures and lower humidities by high performance membrane electrode assembly based on Nafion/zeolite membrane, International Journal of Hydrogen Energy 40, 2016, Pages 11328-15335
- [4] Jung-Hyun Nam, Yoon-Young Jang, Young-Uk Kwon, Jae-Do Nam, Direct methanol fuel cell Pt-carbon catalysts by using SBA-15 nanoporous templates, Electrochemistry Communications 6, 2004, Page 737-741

## IMPACT AND SOLUTIONS TO SOLVE THE LIMITATION OF OXYGEN TRANSPORT IN BIOCATHODES

W. Richard\*, B. Erable\*, and A. Bergel\*

\*Laboratoire de Génie Chimique, Université de Toulouse,  
CNRS, INP, UPS, Toulouse (France)

**Abstract** – The growth and electrocatalytic efficiency of aerobic cathodic biofilms are significantly affected by the bioavailability of oxygen in solution. Original electrode configurations are proposed to counterbalance (partially) the low solubility of oxygen in aqueous medium and its low diffusion rate. Current densities and colonization are significantly improved by working with cathodes positioned close to the air-electrolyte interface or with respiration cathodes.

**Index Terms** – Microbial fuel cell, Oxygen reduction reaction, Biocathode, Oxygen bioavailability and transport.

### I. INTRODUCTION

The maximum performance of oxygen microbial cathodes is not yet up to the level of the best abiotic cathodes, but they offer other unrivaled advantages in terms of stability and resilience of their electrocatalytic activity when exposed in complex and dirty aqueous media (wastewater, leachate...). The low availability of oxygen in aqueous media (0.24 mM pH 7, 20 °C), or the small amount of aerobic biofilm colonizing the cathodic materials are among the factors explaining the rather poor performance of oxygen microbial cathodes [1,2]. The level of oxygen in an aqueous medium containing microorganisms is not stable. It is depending of gas exchange with air and it is also subject to fluctuations caused by biological oxygen consumption processes (respiration). The atmospheric oxygen supply in aqueous medium is determined by the size of the exchange surface between air and water relative to the volume of water. The single phenomenon of exchange by simple diffusion is a slow phenomenon (Fig. 1). In practical application, this means that intensive water circulation, accompanied by good mixing of air and water, is required to maintain the oxygen level at 100% of the maximum solubility. To overcome the problems of energy cost of improving the oxygen transfer in solution, we were interested to explore two parallel innovative paths: (i) the development of floating

oxygen microbial cathodes, and (ii) the formation of aerobic biofilms on passive air-breathing carbon cathodes (without catalyst), to maximize oxygen availability in aqueous media.

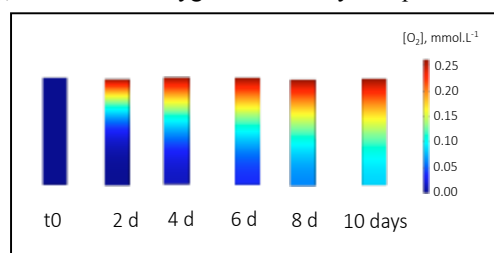


Fig. 1. Evolution of the oxygen concentration profile in a water column of 100 mm open to the air. Oxygen transfer calculation was based only on diffusion transport (Fick law),  $D_{O_2} = 2.10^{-5} \text{ cm}^2/\text{s}$ .

### II. EXPERIMENTAL APPROACH

We compare the development of oxygen reducing microbial cathodes in 700 mL bioelectrochemical reactor filled with compost leachate under different experimental cathode configurations: (A) on “classically” 10 cm deep immersed cathodes; (B) on floating cathodes; (C) on carbon-based air breathing cathodes. All the experiments of microbial biocathode formation were operated at a constant electrode potential of -0.2 V/SCE because this electrode potential is optimal for the formation of reproducible oxygen reducing biofilm regardless of the cathode configuration (Fig. 2). At lower cathodic potential such as -0.5 V/SCE, abiotic oxygen reduction occurring directly on the electrode surface prevents biofilm to form on the surface of the cathode.

When the cathodic biofilm catalyzing the reduction of oxygen was formed, the electrocatalytic performances for oxygen reduction of the oxygen reducing microbial biocathodes were then compared by cyclic voltammetry. The different biofilm structures and the bacterial coverage on electrodes were analyzed and compared by epifluorescence microscopy

Copyright © 2017

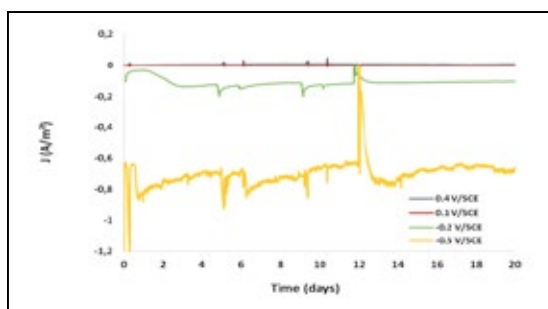


Fig. 2. Determination of the optimal cathode potential for the formation of reproducible microbial oxygen reducing biocathodes.

### III. RESULTS

#### A. “Classically” immersed biocathodes formation

Two types of materials (carbon and stainless steel) and two different carbon structures were compared in duplicate as an aerobic biofilm support. In soil leachate, on stainless steel and on carbon felt electrodes, the reduction current values did not change or very little, proving that a cathodic biofilm developed poorly on the electrode. On the carbon cloth, the current reached an average density of  $-0.7 \text{ A/m}^2$  after two weeks of polarization (Tab.1) and increased to  $-0.8 \text{ A/m}^2$  when the catholyte was changed by a clean mineral medium. The interpretation of the cyclic voltammeteries shows that the biocathode has two electrocatalytic oxygen reduction systems at 0.15 and  $-0.3 \text{ V/SCE}$ . These two distinct mechanisms have been already precisely described by Rimboud et al. in 2016 [3].

Tab. 1. Effect of the electrode material and design on the bioelectrochemical performances and the biofilm colonization of oxygen reducing biocathodes.

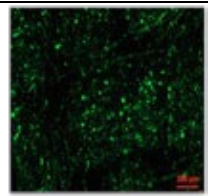
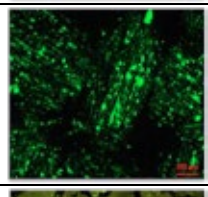
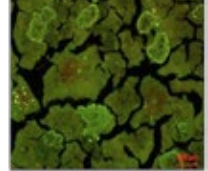
Electrodes	$J_{\max}$ ( $\text{A/m}^2$ )	Oxygen reduction catalysis	Biofilm colonization
Stainless steel (254 SMO)	-0.05	/	LOW
Carbon felt	-0.03	/	LOW
Carbon cloth	-0.70	++	HIGH

#### A. Methods to enhance oxygen transport

Optimizing the supply of oxygen to the bacterial cells of the biofilm is a necessity to maximize the current densities of microbial oxygen cathodes. The use of a floating electrode configuration is a way of optimizing the transport of oxygen in solution since the water layer between the biofilm and the air is minimal. Using an air-breathing cathode is also theoretically an effective means of providing a saturating concentration of oxygen at the interface biofilm-electrode in biological cathode. In the two configurations tested, the oxygen supply is directly provided by the ambient air, which eliminates the need to agitate (hydrodynamic) or to create a forced aeration of the catholyte. As expected, the floating electrode has a behavior comparable to that of an immersed electrode but with higher current densities ( $1.0$  vs.  $0.7 \text{ A/m}^2$ ). The floating electrode is therefore sufficiently exposed to water to allow the

development of a biofilm and the oxygen supply is certainly less limiting. The face exposed to the catholyte is also much colonized than a classically immersed electrode (Tab. 2). Biofilm thickness reached its maximum on the respiration cathode thus showing that the oxygen supply is maximized compared to a conventional biocathode. However, the maximum current density is lower, probably because the carbon paper of the respiration cathodes offers a specific surface area accessible to the biofilm that is lower than the carbon cloth.

Tab. 2. Effect of the cathode configuration on the bioelectrochemical performances and the biofilm colonization of oxygen reducing biocathodes.

Methods of biocathode formation	$J_{\max}$ ( $\text{A/m}^2$ )	Oxygen reduction catalysis	Biofilm observation
(A) “Classically” immersed Carbon Cloth	-0.7	++	
(B) “Floating” Carbon cloth	-1.0	+++	
(C) “Air-breathing”	-0.6	+	

### IV. CONCLUSIONS

By bringing the cathode closer to the air-catholyte interface the current densities of the biocathodes are improved by more than 40%. The use of respiration cathode allows the formation of a thicker and denser aerobic biofilm.

### ACKNOWLEDGMENT

This work was funded by the French ANR within the framework of the Bioelec project (ANR-13-BIME-006).

### REFERENCES

- [1] Erable, B., Feron, D., Bergel, A., Microbial catalysis of the oxygen reduction reaction for microbial fuel cells: a review. Chemsuschem, volume 5, 2012, pp. 975–987.
- [2] Huang, L., Regan, J.M., Quan, X., Electron transfer mechanisms, new applications, and performance of biocathode microbial fuel cells. Bioresource Technology, volume 102, 2011, pp. 316–323.
- [3] Rimboud, M., Bergel, A., Erable, B., Multiple electron transfer systems in oxygen reducing biocathodes revealed by different conditions of aeration/agitation. Bioelectrochemistry, volume 110, pp. 46-51.

## AN ELECTROCHEMICAL METHOD FOR THE DETERMINATION OF BOTH CONCENTRATION AND DIFFUSION COEFFICIENT OF AMMONIA IN NITROGEN

A. Kalyakin<sup>1</sup>, E. Gorbova<sup>1</sup>, A. Vylkov<sup>1,3</sup>, D. Medvedev<sup>1,3</sup>, A. Demin<sup>1,3</sup>, A. Volkov<sup>1</sup>  
and P. Tsiakaras<sup>1,2,3</sup>

<sup>1</sup>Laboratory of Electrochemical Devices Based on Proton Solid Oxide Electrolytes, Institute of High Temperature Electrochemistry, Ural Branch of RAS, 20, Akademicheskaya Str., Yekaterinburg 620990, Russia.

<sup>2</sup>Laboratory of Alternative Energy Conversion Systems, Department of Mechanical Engineering, School of Engineering, University of Thessaly, Pedion Areos, Volos 383 34, Greece.

<sup>3</sup>Laboratory of materials and devices for electrochemical power industry, Ural Federal University, 19 Mira Str., Yekaterinburg 620002, Russia.

**Abstract** - In the present investigation an electrochemical method for the determination of concentration and diffusion coefficient of ammonia in nitrogen, by using a solid-state amperometric sensor based on yttria-stabilized zirconia (YSZ) electrolyte, is proposed. The measured quantity of the studied sensor is the limiting current. The experiments are performed for the ammonia concentration levels of 0.1–5 vol.% in the temperature interval of 375–430 °C. It is shown that the limiting current level is reached at temperature values not higher than 400 °C and it is linearly proportional to the ammonia concentration. This allows obtaining a calibration curve (limiting current vs. ammonia concentration) for the ammonia determination in NH<sub>3</sub>/N<sub>2</sub> mixtures. Using the obtained results and diffusion channel parameters, coefficients of ammonia diffusion in nitrogen can be calculated. It is found that they are in a good agreement with table values. It is also found that under experimental conditions the ammonia electrochemical oxidation reaction leads to the formation of N<sub>2</sub> rather than N<sub>2</sub>O or NO. The results obtained demonstrate the possibility of using such amperometric sensor for the analysis of ammonia-gas mixtures where diluent gas is nitrogen or another inert gas.

**Index Terms** – amperometric sensor; oxygen-ionic electrolytes; YSZ; diffusion barrier; electrochemical cell; limiting current; ammonia

### I. INTRODUCTION

Solid electrolytes based on zirconium oxide are currently widely used in many branches of science and technology [1]. Oxygen and hydrogen amperometric sensors for the analysis of average and high concentrations of the analyzed component are widely used [2,3]. In recent years, solid electrolytes with proton conductivity are also considered as perspective materials in the fabrication of amperometric and

potentiometric solid-electrolyte sensors [4]. Currently there are no literature data on the use of amperometric sensors, based on oxygen-ionic or proton-conducting electrolytes, for the analysis of ammonia. In practical cases, measurement of the content of ammonia in mixture with nitrogen is of interest as it can be used in technology of production: ammonia, nitrogen fertilizers, explosives, polymers, nitric acid, soda (by an ammoniac method) and other products of chemical industry [5]. In the present work for the measurement of the ammonia in gaseous mixtures with nitrogen, an electrochemical sensor based on oxygen-ionic solid-state electrolyte was fabricated and tested. The sensor consisted of two electrochemical cells with a gas cavity between them and a capillary connecting the sensor cavity to the analyzed environment.

### II. EXPERIMENTAL

The electrochemical cells of the sensor shown in **Fig. 1** have dimensions 11 x 11 mm and 1 mm thick. The recess has a depth of 0.5 mm, while its area is 60 mm<sup>2</sup>. The platinum electrodes were deposited on the opposite sides of each electrolyte plate; platinum wires were attached to the electrodes, painted by a platinum paste in order to reach a good contact between wires and electrodes after a treatment at 1100 °C for 1 h.

The prepared plates consist the internal space of the electrochemical cell (chamber) after high-temperature gluing, using a high-temperature sealant. A thin-walled chromo-nickel steel capillary with an internal diameter of 160 µm and a length of 22 mm was glued between the plates, providing connection between internal and external gas spaces of the sensor.



### III. RESULTS AND DISCUSSION

A new amperometric sensor (Fig. 1) was designed, fabricated and tested in the present work. It consists of two plates of oxygen ion solid electrolyte YSZ and is equipped with a chromo-nickel steel capillary as a diffusion barrier.

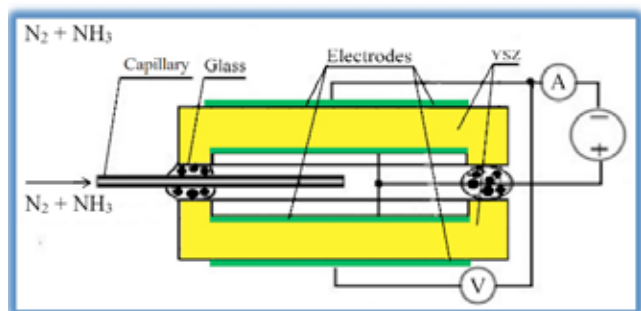


Fig. 1 Scheme of an amperometric sensor

It was found that the sensor limiting current in the mixture *nitrogen + ammonia* linearly depends on ammonia concentration up to 5 % (Fig. 2). The sensor demonstrated acceptable dynamic characteristics under changing ammonia concentration: transitional time did not exceed 200 s (Fig.3).

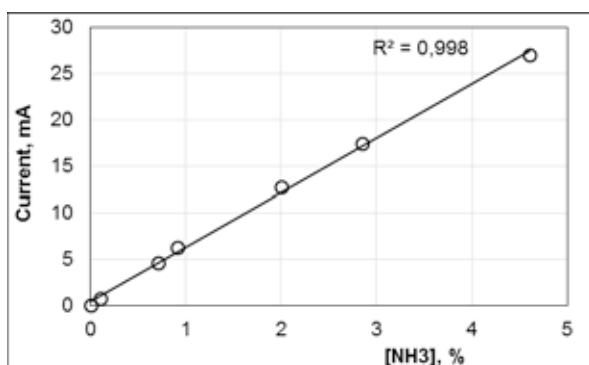


Fig. 2 Dependence of sensor's limiting current on ammonia concentration.

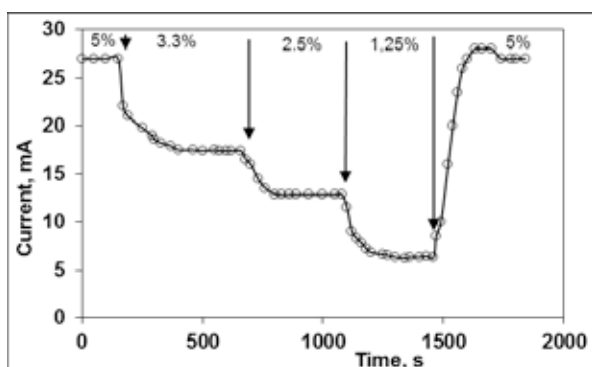


Fig. 3 Effect of NH<sub>3</sub> concentration change on sensor's current. Applied voltage 1,2 V, temperature 400 °C.

### IV. CONCLUSION

The current investigation concerns with the fabrication of an amperometric sensor based on oxygen ion solid electrolyte with a diffusion barrier from chromo-nickel steel for the measurement of ammonia content in its mixtures with nitrogen.

The sensor exhibits good working capacity for the determination of ammonia in the range between 0,1 to 5 vol.% at temperature values from 375 to 400 °C.

The as fabricated sensor is also successfully used for the determination of ammonia diffusion coefficient in nitrogen at elevated temperature. The experimental data obtained at temperatures 375-400 °C are in good agreement with the theoretically calculated ones.

The analysis of the experimental data allows one to conclude that electrochemical oxidation of ammonia on platinum electrodes at temperatures between 375 and 400 °C proceeds with the formation of molecular nitrogen.

It should be noted that the adopted capillary from chromo-nickel steel it is not applicable as a diffusive barrier for the analysis of the above mixture at temperatures higher than 400 °C because of catalyzing the reaction of ammonia decomposition. Very likely the utilization of diffusion channel materials that inhibit ammonia decomposition will allow obtaining experimental diffusion coefficient values at higher temperatures.

Finally, it can be stated that the proposed electrochemical device could be a very useful tool not only for the gas analysis but also for measuring the gas diffusion coefficients and sometimes for the specification of the electrochemical reaction type.

### ACKNOWLEDGMENT

The research was supported by the Ministry of Education and Science of the Russian Federation (contract no. 14.Z50.31.0001).

### REFERENCES

- [1] Korotcenkov G, Han S.D., Stetter J.R., Review of electrochemical hydrogen sensors, *Chem. Rev.*, 109:1402–1433, 2009.
- [2] Velasco G, Schnell J.Ph., Croset M., Thin solid state electrochemical gas sensors. *Sens. Actuators*, 2:371–384, 1982.
- [3] Dietz H., Gas-diffusion-controlled solid-electrolyte oxygen sensors, *Solid State Ionics*, 6:175–183, 1982.
- [4] Volkov A., Gorbova E., Vylkov A., Medvedev D., Demin A., Tsiakaras P., Design and applications of potentiometric sensors based on proton-conducting ceramic materials. A brief review, *Sens. Actuators B*, 244:1004–1015, 2017.
- [5] Lan R., Irvine J.T.S., Tao S., Ammonia and related chemicals as potential indirect hydrogen storage materials, *Int. J. Hydrogen Energy*, 37:1482–1494, 2012.



## SIGNIFICANTLY IMPROVING THE PERFORMANCE OF DIRECT METHANOL FUEL CELLS BY GRAPHENE OXIDE COATED MULTI-LAYER NAFION MEMBRANES

M. Hosseinpour\*, S. Holmes\*\*

\*PhD Student, School of Chemical Engineering and Analytical Science, The University of Manchester, Manchester, M13 9PL, (UK)

\*\*Reader, School of Chemical Engineering and Analytical Science, The University of Manchester, Manchester, M13 9PL, (UK)

**Abstract** - In this research the effects of coating multi-layer Nafion membranes with Graphene Oxide (GO) on the performance of a Direct Methanol Fuel Cell (DMFC) are investigated. Multi-layer membranes were prepared by hot pressing layers of Nafion NR-211, Nafion NR-212 and Nafion NR-212 together and were coated with GO by a hot spray coating technique. The results indicate that the multi-layer Membrane Electrode Assembly (MEA) delivered a peak power density of 70.36 mW/cm<sup>2</sup>, which is 34 % higher than that of the single layer MEAs with Nafion N117 and about 26 % higher than that of the MEAs with single layer Nafion N115. GO can reduce the methanol crossover in the multi-layer membranes which leads to an increase in the maximum power density by 34 % and about 43% in comparison to the MEAs with single layer Nafion N115 and MEAs with single layer Nafion N117, respectively.

**Keywords** – DMFCs, Graphene Oxide, methanol crossover, multi-layer membrane.

### I. INTRODUCTION

A significant number of investigations have been carried out during the past decades to find feasible alternative energy sources. Among new methods, fuel cells can be considered as one of the most attractive energy conversion systems. One type of fuel cells is the Direct Methanol Fuel Cells (DMFCs). The ability of using direct fuel (liquid Methanol) which is easily stored, low operating temperature and quiet operation makes them attractive for a lot of applications. However, they face some problems which act as barriers to their development and commercialization. Their membrane has some problems with methanol crossover, which is the diffusion of the methanol through the electrolyte from the anode to the cathode [1]. Methanol crossover can be reduced by changing the structure of the membrane, composite membranes which were prepared by

adding inorganic-organic and/or acidic-basic constituents can be an alternative for common membranes. Choi et al., [2] reported the synthesis of ionically conductive Nafion/GO composite membranes for DMFCs. Lin and Lu, [3] by using a vacuum filtration method prepared GO-laminated Nafion 115 as a proton exchange membrane for DMFCs. Paneri et al., [4] investigated the possibility of using the Graphene-based membranes for reducing the Methanol crossover in DMFCs by preparing a membrane via the lamination of GO nano-plates. Wu et al., [5] developed a multilayer membrane which consists of an ultra-thin reaction layer which sandwiched between two Nafion 211 membranes. They show that the DMFC which uses this composite membrane performs better than a single layer Nafion membrane. Yan et al., [6] designed a membrane which consists of two thin Nafion membranes and a monolayer of Graphene, which prepared by chemical vapour deposition (CVD) technique between them. They found that this membrane reduces Methanol crossover by 68.6% and increases the power density by 53.33%. In this research the effects of coating multi-layer Nafion membranes with GO on the performance of a DMFC is investigated.

### II. EXPERIMENTAL

Nafion membranes N115, N117, NR-211 and NR-212 (4.5 cm × 4.5 cm), Nafion solution (DUPONT D2021 NAFION (20% wt)) were obtained from Ion Power. Gas Diffusion Electrodes (GDE) PtB on SGL 29 BC and (GDE) Pt/RuB on SGL 29 BC (1.5 cm × 1.5 cm) were purchased from Fuel cell store. GO (powder 15-20 sheets, 4-10% edge oxidized) were obtained from ALDRICH Chemistry. Methanol and Ethanol were obtained from Fisher Chemical. De-ionized water was produced by using Millipore Milli-Q Academic Pure Water Purification

Copyright © 2017

system. The single layer MEAs are prepared by a hot pressing method. This procedure is divided into two steps, careful heating (which is essential based on the difference in thermal expansion of the components) and hot pressing. The heating is done at  $T=135\text{ }^{\circ}\text{C}$  for 120 seconds. Then hot pressing is done at  $\Delta P=5.5\text{ Bar}$  and  $T=135\text{ }^{\circ}\text{C}$  for 180 seconds. The hot pressing procedure is same for the multi-layer MEAs but before hot pressing the MEA, the layers of the membrane were attached to each other by using a template and applying the torque equal to  $0.7\text{ N.m}$  for 5 minutes after that the attached layers are hot pressed at  $T=135\text{ }^{\circ}\text{C}$  and  $P=5.5\text{ Bar}$  for 180 seconds. The GO coated membranes are fabricated by direct spraying of the inks into the Nafion membranes which were placed into the hot Pyrex petri dish ( $100\text{ }^{\circ}\text{C}$ ). Inks contain the calculated amounts of GO, Nafion solution (20 % wt) and ethanol. Testing the MEAs is done by using a single DMFC test setup. MEAs were tested at cell temperature of  $70\text{ }^{\circ}\text{C}$ , Methanol flow rate of  $1\text{ ml/min}$ , Methanol concentration of  $1\text{ M}$  and air flow rate of  $90\text{ ml/min}$ .

### III. RESULTS

The power density curves of the MEAs with Nafion N115, Nafion N117, Multi-layer and GO coated Multi-layer membranes are shown in figure 1. The values of the Open Circuit Voltage and the maximum power density of these MEAs are shown in Table 1.

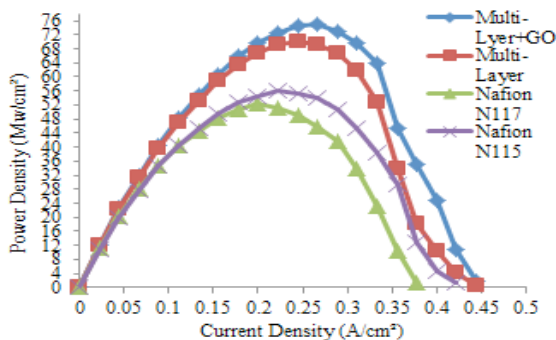


Fig. 1. Power Density Curves of MEAs

Table I O.C.V and Power Density of MEAs

Membrane	N115	N117	Multi-layer	Multi-layer + GO
O.C.V (V)	0.585	0.589	0.602	0.602
Power Density (mW/cm <sup>2</sup> )	56	52.5	70.36	75.05

The results indicate that the maximum power density of the Multi-layer membrane MEA is 34 % higher than that of the single layer membrane MEAs with Nafion N117 membrane and about 26 % higher than that of the MEAs with single layer

Nafion N115 membranes. The GO coated multi-layer membrane MEAs with Nafion NR-212, Nafion NR-212 and Nafion NR-211 were prepared. The GO is sprayed to the Nafion NR-211 layer and the coated side is placed in the anode side of the MEA. The amount of the GO is 1 % of the weight of the Nafion NR-211 membrane. According to the Table 1, the average of the O.C.V of these MEAs is bigger than the O.C.V of the Single layer membrane MEAs without GO. GO can reduce the Methanol crossover in the Multi-layer membranes which leads to an increase in the maximum power density of the Multi-layer MEAs by 34 % in comparison to the MEAs with single layer Nafion N115 membranes and about 43% in comparison to the MEAs with single layer Nafion N117 membranes.

### IV. CONCLUSION

In this research, different types of MEAs with different Nafion membranes were prepared. Among these types, multi-layer membrane MEAs with Nafion NR-211, Nafion NR-212 and Nafion NR-212 membranes show the best performance. The results show that, the performance of the DMFC is affected by the thickness of the membranes. Thinner membranes perform better as they have lower resistance. But at same thickness, the multi-layer membranes which, consists of membranes with same equivalent weight show better performance. Methanol crossover can be prevented if the membranes were coated by barrier layers directly. According to the performance of the GO coated Multi-layer membranes, it can be concluded that the GO can reduce the Methanol crossover and consequently, increase the power density of the MEAs. These membranes are much easier to fabricate than CVD graphene containing membranes.

### REFERENCES

- [1] Breeze, P, Power Generation Technologies, Elsevier, Second Edition, 2014.
- [2] Choi, B. G., Huh, Y. S., Park, Y. C., Jung, D. H., Hong, W. H., Park, H, Enhanced transport properties in polymer electrolyte composite membranes with graphene oxide sheets, Journal of Carbon, Volume 50 (15), 2012, pages. 5395–5402.
- [3] Lin, C., Lu, Y, Highly ordered graphene oxide paper laminated with a Nafion membrane for direct methanol fuel cells, Journal of Power Sources, Volume 237, 2013, Pages 187-194.
- [4] Paneri, A., Heo, Y., Ehlert, G., Cottrill, A., Sodano, H, Proton selective ionic graphene-based membrane for high concentration direct methanol fuel cells, Journal of Membrane Science, Volume 467, 2014, Pages 217-225.
- [5] Wu, Q.X, Zhao, T.S, Chen, R., AN, L, A sandwich structured membrane for direct methanol fuel cells operating with neat methanol, Journal of Applied Energy, Volume 106, 2013, Pages 301-306.
- [6] Yan, X.H., Wu, R., Xu, J.B, Luo, Z., Zhao, T.S., A monolayer graphene Nafion sandwich membrane for direct methanol fuel cells, Journal of Power Sources, Volume 311, 2016, Pages 188-194.

## EFFECT OF CO DOPANT ON HYDROGEN PROPERTIES OF BERYLLIUM INTERMETALLIC COMPOUND

J.-H. Kim\*, H. Iwakiri\*\*, M. Miyamoto\*\*\*, M. Nakamichi\*

\*Fusion Energy Research and Development Directorate, National Institutes for Quantum and Radiological Science and Technology, Japan

\*\*Faculty and Graduate School of Education, University of the Ryukyus, Japan

\*\*\*Department of Materials Science, Shimane University, Japan

**Abstract** – In the present study, synthesis of beryllium intermetallic compounds as a hydrogen storage material and the effect of Co addition on hydrogen storage capacity in Be<sub>2</sub>Zr compound are reported in terms of hydrogen desorption and hydrogen storage property.

**Index Terms** – Beryllium intermetallic compound, Be<sub>2</sub>Zr, Hydrogen capacity, Hydrogen desorption

### I. INTRODUCTION

Beryllium intermetallic compounds (beryllides) have shown a variety of applications owing to their lightness. However, few studies on syntheses and experimental verifications of the materials found because of difficulty to handling of the beryllium and its alloys hume and dust. In National Institutes for Quantum and Radiological Science and Technology, QST, beryllium handling facility was built based on regulations established by Japan government and synthesis and various experiments have been carried out as a research objective. Our group has successfully fabricated beryllides [1, 2], Be<sub>12</sub>Ti, Be<sub>17</sub>Ti<sub>2</sub>, Be<sub>12</sub>V, Be<sub>13</sub>Zr, etc. for neutron multipliers as well as Be<sub>2</sub>Ti, Be<sub>2</sub>V etc. for hydrogen storage application [3]. In this study, synthesis of beryllium intermetallic compounds as a hydrogen storage material and the effect of Co addition on hydrogen storage capacity in Be<sub>2</sub>Zr are reported in terms of hydrogen desorption and hydrogen storage property.

### II. EXPERIMENTS

In order to investigate the effect of dopant addition on hydrogen storage of Be<sub>2</sub>Zr compounds, in this study,

Be<sub>2</sub>Zr compounds doped with Co were fabricated under gas controllable glove box.

Phase identification of the samples was carried out by X-ray diffraction and electron probe micro-analysis (EPMA). For evaluating hydrogen storage capacity, we obtained the pressure-composition-temperature (PCT) curve after activation, which comprised introduction of 14 MPa H<sub>2</sub> gas at 648 K for 2 h and vacuum treatment for 3 h just before starting the measurement. The test temperatures were 423, 373, 323 K and 300 K. Additionally, hydrogen gas desorption property was investigated by gas chromatographic analysis while ramping up to 1473 K to understand hydrogen gas desorption behavior.

### III. RESULTS AND DISCUSSION

Figure.1 shows x-ray diffraction of Be<sub>2</sub>Zr, Be<sub>2</sub>Zr<sub>0.9</sub>Co<sub>0.1</sub>, and Be<sub>2</sub>Zr<sub>0.7</sub>Co<sub>0.3</sub> compounds. It depicts that almost single phase Be<sub>2</sub>Zr compound was successfully synthesized with considerably small peaks of Be<sub>5</sub>Zr despite of concerning

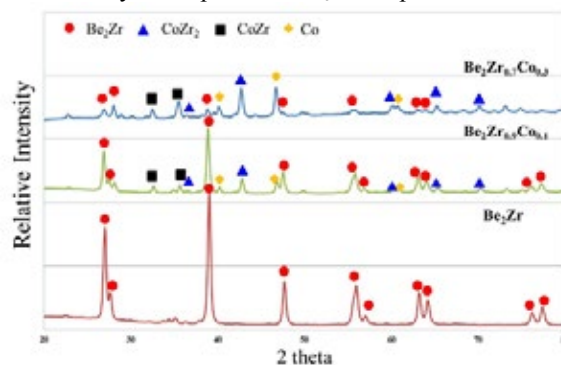


Figure.1 X-ray diffraction patterns of Be<sub>2</sub>Zr, Be<sub>2</sub>Zr<sub>0.9</sub>Co<sub>0.1</sub>, and Be<sub>2</sub>Zr<sub>0.7</sub>Co<sub>0.3</sub> compounds.

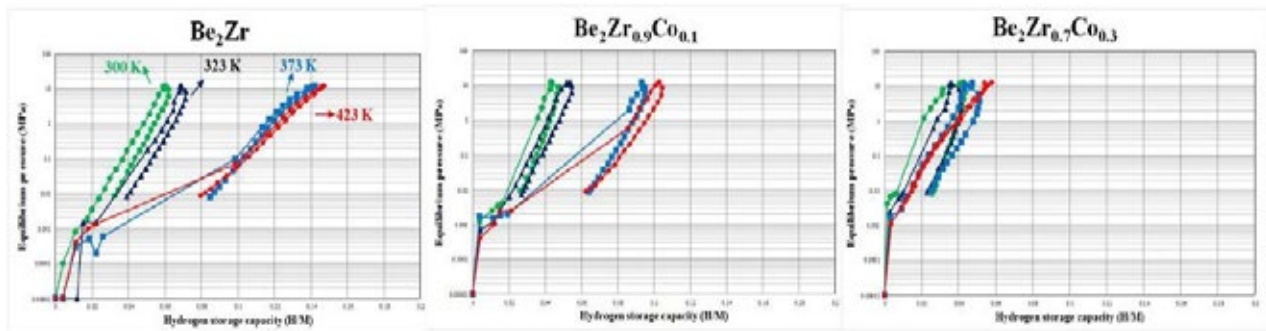


Figure.2 PCT curves of each sample at each temperature, 423, 373, 323 and 300 K.

of oxidation during the synthesis procedure. However, it was obvious that as the Co content increases, Co and some compounds, such as  $\text{CoZr}_2$  and  $\text{CoZr}$  were increases.

Figure. 2 indicates the results of PCT measurement for each sample,  $\text{Be}_2\text{Zr}$ ,  $\text{Be}_2\text{Zr}_{0.9}\text{Co}_{0.1}$ , and  $\text{Be}_2\text{Zr}_{0.7}\text{Co}_{0.3}$  compounds. The result clearly revealed that Co addition to  $\text{Be}_2\text{Zr}$  deteriorated the hydrogen storage property. Total amount of stored hydrogen was increased with increase of Co content as well as with decrease of test temperature. Currently, impurity effect, in specific, oxide layer which interrupt to absorb and desorb hydrogen, on the hydrogen capacity are undergoing.

Additionally, hydrogen desorption property of tested samples was investigated as shown in figure.3. It was clear that  $\text{Be}_2\text{Zr}$  sample indicated two peaks while  $\text{Be}_2\text{Zr}_{0.9}\text{Co}_{0.1}$  and  $\text{Be}_2\text{Zr}_{0.7}\text{Co}_{0.3}$  did three peaks, depicting that a lower temperature peak may be due to hydrogen gas desorption of either  $\text{CoZr}_2$  or  $\text{CoZr}$  compounds.

In parallel to experimental approach, the first-principles calculation of hydrogen trap site in this compound is undergoing in order to compare to empirical data.

#### IV. CONCLUSION

We successfully synthesized  $\text{Be}_2\text{Zr}$  compound under newly established gas-controllable box. The effect of Co dopant into  $\text{Be}_2\text{Zr}$  compound was investigated in the present study. It concluded that as the Co content as dopant increased, hydrogen capacity deteriorated since secondary compounds,  $\text{CoZr}$  and  $\text{CoZr}_2$ , were formed.

#### Acknowledgment

This work was supported by JSPS Grant-in-Aid for Young Scientists (B) (16K18343)

#### References

- [1] J.-H. Kim, H. Iwakiri, T. Furugen, M. Nakamichi, Fusion Eng. Des. 102 (2016) 44-49
- [2] M. Nakamichi, J.-H. Kim, Fusion Eng. Des. 98-99 (2015) 1838-1842
- [3] J.-H. Kim, H. Iwakiri, M. Nakamichi, Int. J Hydrogen Energy, 41 (2016) 8893-8899

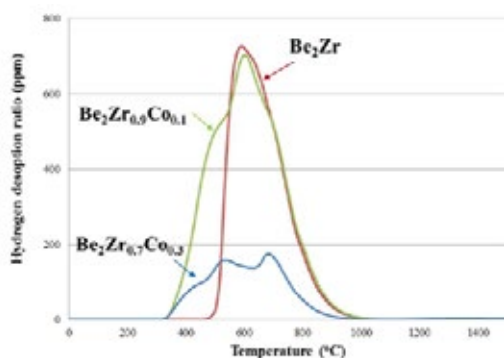


Figure.3 Hydrogen desorption ratio of samples after PCT test.

## Performance Characteristics of Open Cathode PEFC Stack

Beom Jun Kim\*, Jun-Young Kang\*\*, Jeong-Wook Yang\*\*,  
Young Gi Yoon\*

\*Hydrogen and Fuel Cell Center, Korea Institute of Energy  
Research, 20-41 Sinjaesangenoji-ro, Haseomyeon, Buan-gun,  
Jeollabuk-do, (South Korea)

\*\*Chonbuk National University, 567 Baekje-daero, deokjin-gu,  
Jeonju-si, Jeollabuk-do, (South Korea)

**Abstract** - Open cathode fuel cells make systems have simple structures, because they combine both the oxidant supply and the thermal management system by using air as the coolant. Its cathode stoichiometry ratio is above 50 times more than that of water cooling PEFC stacks. This an amount of air make very dry condition on the membrane electrode assembly, and lower the fuel cell performance. In this study, a test station for open cathode fuel cell stack was constructed and by varying operation conditions the open cathode fuel cell stack of 15 cells was tested. Impacts of the air flow rate and humidification on the water balance and fuel cell performances were tested. The anode hydrogen supply is dead-end type. Impacts of purge conditions on the stack performance were also tested.

**Index Terms** – PEFC Stack, Open Cathode, Water Management, Performance Characteristics

### I. INTRODUCTION

There are two types of polymer electrolyte fuel cell stacks, i.e. water-cooled and air-cooled. Air-cooled stacks are open cathode fuel cell stacks. Despite their relatively low voltage, and bulky volume, open cathode fuel cell stacks give many advantages in a point of view of system.

Thermal management system and air processing system are combined together in open cathode fuel cell stacks. Just a few fans do both functions. Therefore system volume and price can be significantly reduced. However, due to low heat transfer of air, the air flow rate is above 50 times of water cooled fuel cell stack. Thus, it make a very dry condition on the membrane electrode assembly of fuel cells, and limit the operation current to low range [1]. To relieve the drying problem, humidifying the supply air can be considered [2].

In this study, performance characteristics of open cathode

fuel cell stack were tested to find out the optimal operational conditions. A test bed of new design was developed.

### II. EXPERIMENTAL SETUP

The open cathode fuel cell stack is comprised of 15 cells, the active area is 200 cm<sup>2</sup>. The bipolar plates is made of metal sheet, and the stack volume is significantly reduced.



Fig. 1. Open Cathode Fuel Cell Stack

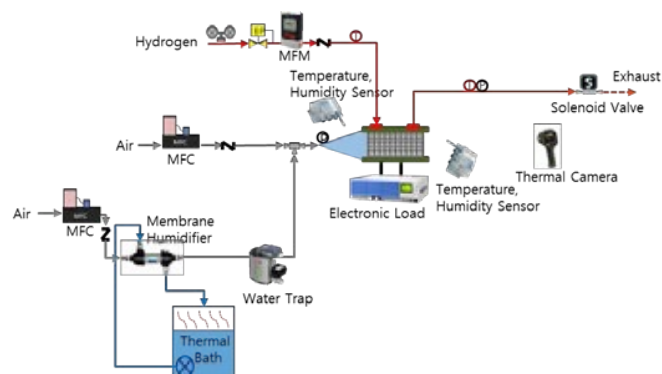


Fig. 2. Schematics of Experimental Setup



Air is supplied through the mass flow controller instead of a fan, so that the air flow rate is easily controlled. Water-to-gas membrane humidifier was adopted to humidify the supplied air. Two humidity sensors for Vaisala are used to measure the water balance.

### III. RESULTS AND DISCUSSION

Because the stoichiometry ratio of air in the open cathode fuel cell is above 100, air in the stack channel is very dry. Fig. 3 compares saturation point and water contents inside the stack along the channel direction.

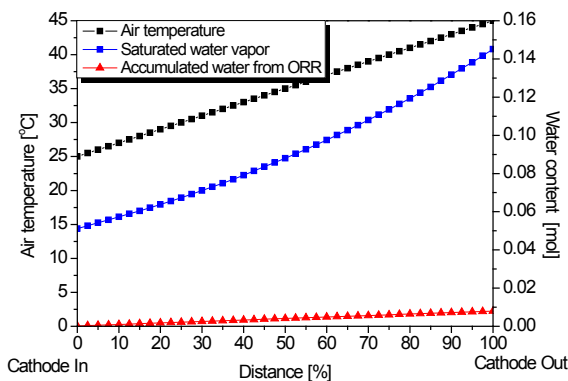


Fig. 3. Water Balance in Open Cathode Fuel Cells

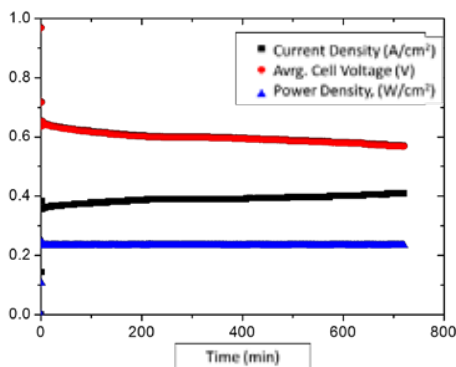


Fig. 4. Performance Curve in Continuous Operation

Air is very dry in the channel, the stack performance is decreased at continuous operation. Fig. 4 shows performance curves at continuous operation. 750 W constant power mode was used for this test. The current density is low around 0.4 A/cm², and increases as the stack performance decreases. The cell voltage is decreased at the rate of 10 mV/h.

Fig. 5 shows the temperature of air inlet and outlet. The ambient air(cathode inlet) temperature is around 20 °C. The temperature difference between cathode inlet and outlet is around 20 °C. Because of drying problem, operation

temperature should be much lower than water cooled stack. And also the air inlet temperature is equal to the ambient temperature.

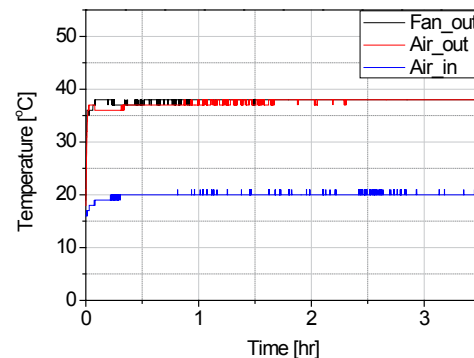


Fig. 5. Temperature Difference between Air Inlet and Outlet

### IV. CONCLUSION

To find out the performance characteristics of open cathode fuel cell stack, the new concept of test bed was constructed. Temperature difference between air inlet and outlet is 20 °C. At continuous operation, the cell voltage is decreased due to the membrane drying at the rate of 10 mV/h. Though this paper shows only the basic test results, many tests were conducted including effects of air flow rate, humidity, and purge conditions. The details will be presented at the conference.

### ACKNOWLEDGMENT

This work was supported by the New & Renewable Energy Core Technology Program of the Korea Institute of Energy Technology Evaluation and Planning (KETEP) granted financial resource from the Ministry of Trade, Industry & Energy, Republic of Korea (No. 20163010031980)

### REFERENCES

- [1] Strahl, S., Husar, A., Riera, J., Experimental study of hydrogen purge effects on performance and efficiency of an open-cathode Proton Exchange Membrane fuel cell system, Journal of Power Sources, Volume 248, 2014, pp. 474-482.
- [2] Rodatz, P., Büchi, F., Onder, C., Guzzella, L., Operational aspects of a large PEFC stack under practical conditions, Journal of Power Sources, 128(2), 2004, pp. 208-217.

(EFC17175) EFC17175

## ELECTROCHEMICAL PERFORMANCES AND POST-OPERATIONAL CHARACTERIZATION OF A SEGMENTED SOFC OPERATED UNDER LOAD FOR 15K HOURS

P. Piccardo\*, R. Spotorno\*, D. Montinaro\*\*, J.P. Ouweltjes\*\*\*, J. Laurencin\*\*\*\*, D. Vladikova\*\*\*\*\*, J.-M. Bassat\*\*\*\*\* and A. Morata\*\*\*\*\*

\*DCCI - University of Genoa, via Dodecaneso 31, 16146 Genoa, (Italy)

\*\*SOLIDPower S.p.A., Via Trento, 115/117, 38017 Mezzolombardo TN, (Italy)

\*\*\* HTceramix SA, Avenue des Sports 26, 1400 Yverdon-les-Bains, (Switzerland)

\*\*\*\* CEA - LITEN, 17 Avenue des Martyrs, 38000 Grenoble, (France)

\*\*\*\*\* ICMCB - CNRS, 87 Avenue du Dr Albert Schweitzer, 33600 Pessac, (France)

\*\*\*\*\* IEES - BAS, Acad. Georgi Bonchev Str., Block 10, 1113 Sofia, (Bulgaria)

\*\*\*\*\* IREC, Jardins de les Dones de Negre, 1, 2<sup>a</sup> pl., 08930 Sant Adrià de Besòs, Barcelona, (Spain)

**Abstract** - In the frame of the ENDURANCE FCH-JU-FP7 project (2014-2017) a segmented cell (20 segments regularly distributed from fuel inlet to fuel outlet) was operated for 15k hours in co-flow at 750°C (average temperature) in hydrogen under load.

Each segment was carefully monitored during operation by periodically acquiring the impedance spectra and constantly checking the voltage under current load.

After 15k hours of operation the test was stopped and the cell used for further investigations in order to compare the cell evolution with the segment degradation.

The overall observation in cross section of the cell has shown a good stability, however some differences were observed in the electrodes that might be related to the local operating conditions: temperature, H<sub>2</sub>/H<sub>2</sub>O ratio in the fuel stream.

The gathered results will contribute to increase the understanding the evolution of a SOFC in real operating conditions. Evidences of the effect of temperature, time and fuel pollutants were found.

**Index Terms** - Segmented cell, SOFC, Anode evolution, long lasting operation time.

### I. INTRODUCTION

To better understand the phenomena occurring in single repeating element of a stack (i.e., in large cells) under operation a special set up was designed able to host anode supported cells with on top a screen printed segmented cathode interfaced with a instrumented and segmented current collector (fig.1). The current collector acquires data from each segment separately

(i.e. T, V, i) and allows impedance measurements. Such data directly correlate the electrochemical behavior to the local operating conditions, the degradation rate, and in case of local failure to find out the source of it. The latter results useful to identify the most meaningful zone for post-experiment characterization by microscopic and spectroscopic techniques. The whole data collection is then fundamental for modeling development and refinements.

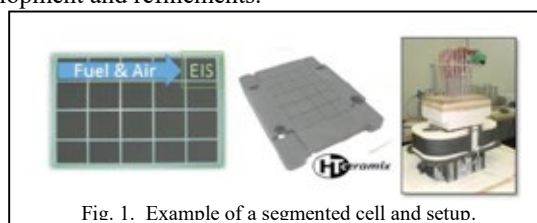


Fig. 1. Example of a segmented cell and setup.

### II. ELECTROCHEMICAL MEASUREMENTS

The sample was operated nominally at 750°C under dry hydrogen/air co-flow according to the details reported in table I.

TABLE I  
OPERATING CONDITIONS DURING THE EXPERIMENT

Type of cell	Segmented, 4 lines 5 columns, ASC, Ni/YSZ/LSCF,
Duration	15000 h
Fuel	60%/40% H <sub>2</sub> /N <sub>2</sub>
Fuel flow rate	480 Nml/min
Air flow rate	7600 Nml/min
Current load	0.5 A/cm <sup>2</sup>

Copyright © 2017

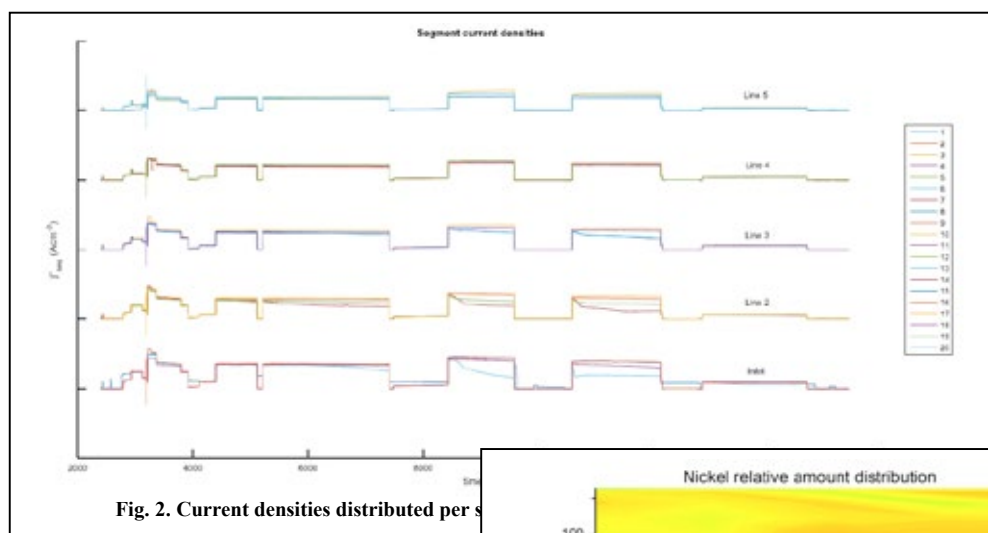


Fig. 2. Current densities distributed per s

EIS curves were acquired from each segment under specific operating conditions all along the experiment duration: 1) at various cell working point and fuel utilization under galvanostatic load (i.e. 0.2A, 0.3A, 0.4A, 0.5A, 0.6A, 0.8A, 0.9A) and normal operating conditions throughout the test (i.e. 1064h, 1544h, 2720h, 5024h, 7520h, 9750h, 12264h, 13060h, 13800h). The extrapolation of electrochemical data was interpreted according to the Gas Compositions (i.e.  $O_2 / H_2$  ratio respectively: 21%/60%; 21%/36%; 21%/26%; 17%/60%) and to the Temperatures (i.e. in the range 675°C to 780°C) directly related to the segment taken into account. No i-V curves were measured but Current densities in function of time and according to the position in the cell as shown in figure 2.

### III. POST EXPERIMENT CHARACTERIZATIONS

#### A. Scanning Electron Microscopy, Microanalysis and image analysis

Segments from a central line and covering the whole inlet to outlet distance were mounted in epoxy-resin and polished to investigate their cross sections. The anode was analysed by EDSX and image analysis on SEM-BSE pictures using the equation from [1] to establish the Ni distribution in the anode. In figure 3 the resulting Ni relative amount distribution is shown. Raman spectroscopy, SIMS and XRD were used to characterize the cathode while synchrotron nano-tomography is actually under interpretation for a whole cell 3D reconstruction.

### IV. DISCUSSION AND CONCLUSIONS

A cell in a commercial stack is confirmed to suffer temperature, current density and gases composition ranging around the average values officially declared from the inlet to the outlet. This generates a remarkable variability of working parameters causing a number of differing phenomena to appear all over the cell itself. Such position related working conditions affect the materials evolution resulting in local changes (e.g.

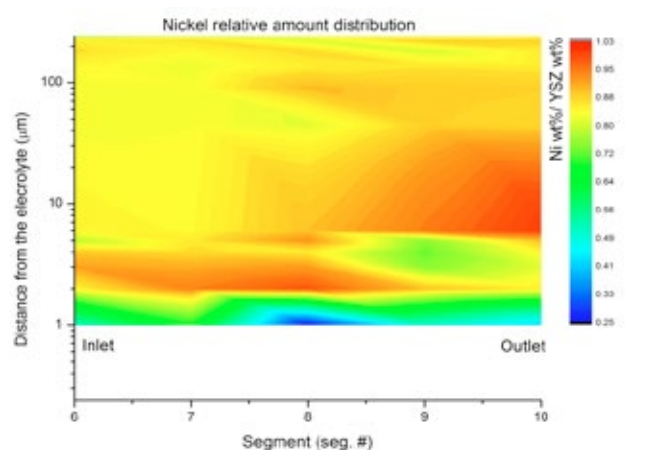


Fig. 3. Ni amount distribution in the anode according to the segment and the distance from the electrolyte

microstructural, compositional) leading to the conclusion that the overall degradation rate usually declared is the average effect of various processes occurring in the cell and the stack. As an example the tendency of Ni to migrate from the active zone in the center of the fuel path to position closer to the outlet but farther from the electrolyte/anode interface was found and investigated. Further details on degradation were found by Raman spectroscopy, SIMS and XRD applied on cells considered critical due to their electrochemical behavior. The whole activity contributed to increase the awareness on cell materials evolution in operating stacks.

### ACKNOWLEDGMENT

The research leading to these results has received funding from the European Union's Seventh Framework Program (FP7/2007-2013) Fuel Cells and Hydrogen Joint Undertaking (FCH-JU-2013-1) under grant agreement No 621207.

### REFERENCES

- [1] P. Piccardo, A. Morata, V. Bongiorno, J.P. Ouweltjes, Proc 12th European SOFC & SOE Forum, Luzern (CH) 5-8 July 2016, B1204 (2016)

## LOW COST SULFONATED MEMBRANES FOR PEM FUEL AND ELECTROLYSER CELLS BASED ON HYBRID NANOCOMPOSITE MATERIAL.

J. Bigarré\*, J. Cellier\*, P. Urchaga\*, T. Paruit\*\*\*, A. Rako\*\*\* and P. Buvat\*

\* CEA, LE RIPAUT 37260 MONTS (France)

\*\*Université de Rouen, Laboratoire "Polymère, Biopolymère, Surface", FRE 3101 CNRS, Chemistry Federation FR 3038, 76821 Mont-Saint-Aignan Cedex (France)

\*\*\* AREVA Energy Storage – Domaine du Petit Arbois – Bâtiment Jules Verne, Avenue Louis Philibert – 13547 Aix-en-Provence Cedex 4 (France)

**Abstract** – Nanocomposite hybrid membranes (NHM) were prepared based on low cost components: Poly(VinylDieneFluoride) (PVDF) as matrix and PolyStyreneSulfonic Acid (PSSA) grafted on silica nanoparticles as proton conductor. It was shown that tetrabutylammonium (TBA), used as counter ion of PolyStyreneSulfonate (PSSTBA), greatly improves the membranes microstructures, their functional properties and their fuel cell performances under  $H_2/O_2$  and  $H_2$ /Air.

**Index Terms** – Proton Exchange Membrane, Nanocomposite, Hybride, PVDF.

### I. INTRODUCTION

Large scale commercialization of PEMFC application is still hindered by the cost of components like electrodes and membrane. Then, low cost membranes for PEMFC application have been developed based on the association of low cost components (compared with perfluorated polymers): Poly(VinylDieneFluoride) (PVDF) as polymer matrix for its chemical stability and mechanical strength, PolyStyreneSulfonate (PSS) for proton conductivity and Silica nanoparticles to improve the membrane water uptake. This nanocomposite hybrid concept allows producing membranes with very attractive properties [1] but the first generation of membranes was very brittle when they were dried due to the nanoparticles aggregation and also to a bad dispersion of nanoparticle filler in PVDF.

In the present work, a new process of membrane preparation was developed to improve mechanical strength of dried membrane. It consists on exchanging the Na cation of PolyStyreneSulfonate (PSS) to Tetrabutylammonium (TBA) in order to increase the charge dispersion in solvent (DMSO) and

the compatibility with the polymer matrix (PVDF).

### II. MEMBRANES PREPARATION

The PolyStyreneSulfonate grafted silica nanoparticles ( $SiO_2$ -g-PSS) was delivered by the French company Specific Polymers (SP). The original protocol was totally described in a previous research article [1]. Since the industrial transfer, the synthesis procedure has been optimized by SP to increase the quantity produced per batch (until 200g) in order to decrease the cost and to allow an industrial production. Moreover, the new procedure increases the ion exchange capacity (from 2.3 meq/g in the previous paper [1] up to 4.6 meq/g).

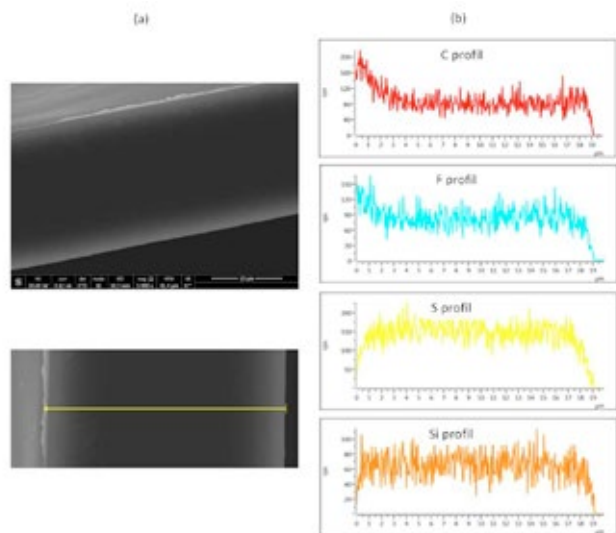
The nanoparticles filler was provided by SP in the sodium form ( $SiO_2$ -g-PSSNa). The TBA exchange step was carried out by dispersing the hybrid filler in an aqueous solution of TBAOH under stirring. Then the solution was neutralized by an HCl solution followed by 3 dialysis steps ionic residues removal (i.e.  $Na^+$ , excess TBA,  $Cl^-$ ...). A final step consisted in freeze drying the solution to obtain a fine light powder ( $SiO_2$ -g-PSSTBA). Hybrid nanoparticles were composed by 8% of  $SiO_2$ , 87% of PSSTBA and 5% of water adsorbed.

The solution was obtained by dispersing  $SiO_2$ -g-PSSTBA and PVDF into dimethyl sulfoxide (DMSO) at 60 °C under stirring. Nanocomposite Hybrid Membranes (NHM) were prepared by solution casting on plate support and solvent evaporation at 110 °C. After drying, TBA form membrane was protonated by keeping membrane in a concentrated  $H_2SO_4$  at room temperature during 4 days. Final membranes were translucent and flexible materials with thickness around 25 to 35  $\mu m$ . They contain 43.8% of nanoparticles filler in protonated form. The theoretical IEC is around 2.0 meq/g.

Copyright © 2017

### III. MEMBRANE MICROSTRUCTURE AND FUNCTIONAL PROPERTIES

SEM image of the membrane cross section in Figure 1(a) shows a dense and a homogenous material without clear evidence of phase separation. Fluorine abundance determined by EDX probing reflects the presence of the PVDF matrix while Si, and S are directly linked to the presence of the SiO<sub>2</sub>-PSSH nanoparticles. The line scans presented in Figure 7(b) clearly show homogeneous distribution of those elements through all thickness of membrane.



**Fig. 1. Cross section SEM image of a protonated SiO<sub>2</sub>-g-PSS @ P(VDF-co-HFP) membrane (a), EDX line scan through the thickness (b).**

The mean functional properties are given in Table 1 in comparison with the reference membrane NRE211. PSSA polymer allows to reach high experimental IEC (1.86 meq/g) close to the theoretical value (2.0 meq/g) and silica gives high water uptake properties (100%). Consequently, proton conductivity is very high (67 mS/cm) due to a high hydration number (40). But, in consequence, the swelling is also high (33%).

The H<sub>2</sub> crossover measured with linear voltammetry under H<sub>2</sub>/N<sub>2</sub> shows a very low value (0.3 mA/cm<sup>2</sup>) compared with NRE211 (0.8 mA/cm<sup>2</sup>).

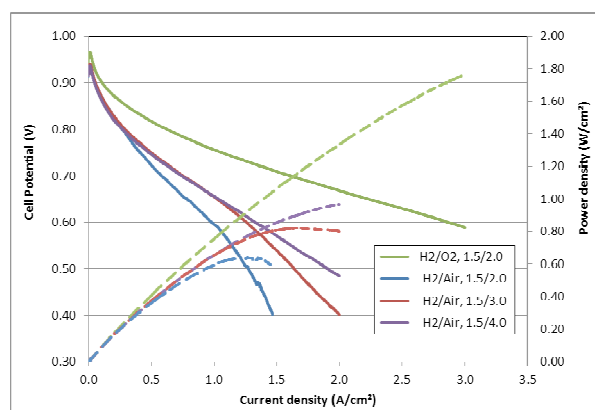
TABLE I: IN-SITU PROPERTIES OF MEMBRANE

	NRE211	NHM
Density (g/cm <sup>3</sup> )	1.95	1.40
Water Uptake (Wt%)	18	100
Swelling (z and x,y) (%)	11 8	33 35
IEC (meq/g)	0.95	1.86
Hydration number at 25°C (λ)	11	40
Proton conductivity immersed at 25°C (mS/cm)	48	67
H <sub>2</sub> crossover at 25°C (mA/cm <sup>2</sup> )	0.8	0.3

### IV. FUEL CELL PERFORMANCE

25 cm<sup>2</sup> Membrane Electrode Assemblies (MEA) were reinforced using two layers of PET acting as strengthening material for electrodes edges. The gas diffusion electrodes (GDEs) were provided by AREVA SE. The test was performed under humidified gases (H<sub>2</sub>/O<sub>2</sub> or H<sub>2</sub>/Air) at 50% Hr and 1.5 Absolute Bar. The cell temperature was 70°C. Polarization curves were plotted after 120h at 1.0 A/cm<sup>2</sup> under H<sub>2</sub>/O<sub>2</sub>.

High power density is achieved under H<sub>2</sub>/O<sub>2</sub> (1 W/cm<sup>2</sup> at 1.5 A/cm<sup>2</sup>) due to the high proton conductivity and good water uptake. Under Air condition, the performance is strongly decreased. Electrochemical Impedance Spectrometry (EIS) has shown a flooding of electrodes due to the high hydrophilic properties of nanoparticles. The increasing of air stoichiometry allows reaching 0.80 W/cm<sup>2</sup> at 1.5 A/cm<sup>2</sup> without a diffusion limitation.



**Fig. 2. Polarization curve at 70°C, 1.5 bara and 50%HR With λ<sub>H2</sub>=1.5 and λ<sub>O2</sub>=2.0, 3.0 and 4.0**

### V. CONCLUSION

Low cost membrane based on PVDF and PSSA grafted on silica nanoparticles was developed. A new process of membrane preparation, including TBA exchange step, allows the improving of the nanoparticles filler dispersion and increasing their compatibility with PVDF matrix. Membranes present better mechanical properties, proton conductivity and fuel cell performance with very low H<sub>2</sub> crossover. Then, this new nanocomposite membrane generation should also be used for PEM Electrolyser application.

### ACKNOWLEDGMENT

The authors wish to thank the French agency ADEME for its financial supports (PREMHYOME and MHYEL projects).

### REFERENCES

- [1] Niepceron F. and al., 2009, *J. Memb. Science*, 338, p. 100-110.



## NITROGEN-DOPED CARBON AEROGELS AS ELECTRODES FOR OXYGEN REDUCTION IN MICROBIAL FUEL CELLS: A GREEN APPROACH

G.P. Salvador\*, V. Margaria\*, N. Garino\*, A. Sacco\*, M. Castellino\*, V. Agostino\*\*, G. Massaglia\*, A. Chiodoni\* and M. Quaglio\*

\*Center for Sustainable Future Technologies – Istituto Italiano di Tecnologia, Corso Trento 21 – 10129 Torino, (Italy)

\*\*Applied Science and Technology Department – Politecnico di Torino, Corso Duca degli Abruzzi 24 – 10129 Torino, (Italy)

**Abstract** – In this work, we present a green approach to the synthesis of high surface area materials for the reduction of oxygen in microbial fuel cells: nitrogen-doped carbon aerogels with good conductivity and catalytic properties. Our synthesis approach is based on a water solution where different amino acids have been added to a polysaccharide (agar) to generate nitrogen sites for the catalytic reaction of oxygen reduction to water. After an electrochemical characterization, the best performing materials have been used to prepare cathodes that were tested in microbial fuel cells. After 50 days' test, the cells containing aerogels, where the doping source was glycine, showed the best results. Morphological characterizations were carried out and the obtained results could demonstrate that the nitrogen type content and the catalysis site accessibility played a key role in determining the better performance of the glycine derived samples.

**Index Terms** – Aerogels, Catalysis, Microbial Fuel Cells, Oxygen Reduction Reaction.

### I. NOMENCLATURE

MFCs: microbial fuel cells.  
ORR: oxygen reduction reaction  
RRDE: rotating rind disk electrode  
NC: nitrogen-doped carbon  
EDX: energy dispersive X-ray spectroscopy  
XPS: X-ray photoelectron spectroscopy

### II. INTRODUCTION

Fossil fuel utilization is the higher responsible for the climate changes that are happening in the World. The fossil fuel replacement with greener energy sources cannot be postponed anymore. None of the green solutions proposed till now (solar,

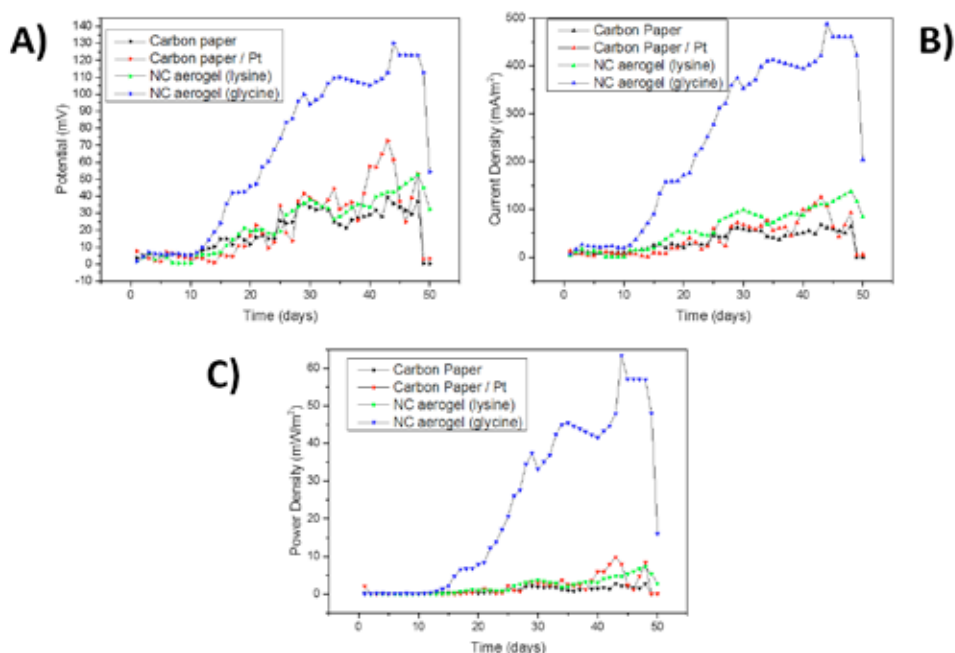
wind, water-based devices and/or technologies) can achieve this goal by itself, but all together they can give an important contribution to replace the fossil fuels. For this reason, even technologies such as MFCs that can produce small amount of energy can play a role in the solution of this important issue. Due to the low amount of energy that MFCs can produce, it is necessary to realize devices that are not much expensive, with a positive energy balance and use environmental friendly components. By using single chamber MFCs, where at the cathode the oxygen reduction reaction occurs, thanks to the presence of cathodes constituted by a conductive material with good performance in ORR, which is prepared from natural precursors by means of a green synthesis, we realized devices that comply with the features mentioned above.

### III. EXTENDED ABSTRACT PREPARATION

N-doped carbon aerogels were synthesized by means of a typical sol-gel process, starting from agar and amino acids (glycine and lysine) as C and N source, respectively. Different agar and amino acid concentrations were used. The materials were then evaluated by means of RRDE-assisted electrochemical measurements. Among all the sample prepared the best performing (one from those prepared starting from glycine and one from lysine) in terms of number of electrons, which is a good selection parameter, as reported in literature<sup>[1]</sup>, where used to prepare cathodes that were tested in MFCs for 50 days. The experiment was carried out in duplicate, by applying a load of 1000Ω and measuring the potential produced by the cells every 10 minutes. In Fig.1 are reported the potential,

current density and power density trend during the 50 days' experiment (for clarity sake only the daily averages have been reported). For comparison, MFCs where the cathodes were

constituted by carbon paper and carbon paper/Pt were also prepared.



**Fig. 1. Electrical parameters trend during the 50 days' test**

By the test results, it was clear that the cells with NC aerogels (glycine-derived) as cathode were the better performing ones. It was possible to achieve as best results: 130 mV, 487mA/m<sup>2</sup> and 63 mW/m<sup>2</sup> as potential, current density and power density values, respectively.

In order to understand the reasons because the glycine-derived NC aerogels gave better results than the lysine-derived ones, several morphological techniques were carried out.

By the comparison of the results obtained from both EDX and XPS measurements, it was possible to establish that after the thermal treatment the N amount is almost equal for all the samples. The fitting of the high resolution XPS spectra let to distinguish among the different types of N sites. This is important because different sites have different oxygen reduction performance.

Graphitic and pyrrolic N content was almost equal for all the samples (50% of the all N), while the pyridinic N (which is the better for the ORR as stated in literature<sup>[2]</sup>) percentage was higher in the glycine-derived NC aerogels (43% versus 32%). A higher amount of pyridinic N can be the reason because the glycine-derived NC aerogels gave better performance as cathodes in MFCs.

#### IV. CONCLUSION

Nitrogen-doped carbon aerogels were synthesized by means a green approach. The materials gave good electrochemical performance and were used to prepare cathodes that were tested for 50 days in MFCs. The glycine-derived NC aerogels gave the better performance, because of their higher pyridinic N content, as stated by EDX and XPS measurements.

#### ACKNOWLEDGMENT

This work was partially supported by the Office of US Naval Research Global (grant number N62909-14-1-N041)

#### REFERENCES

- [1] Zhang, J., PEM fuel cell electron catalysis and catalyst layer, Springer, 2008
- [2] Guo, D., Shibuya, R., Akiba, C., Saji, S., Kondo, T., Nakamura, J., Active sites of nitrogen-doped carbon materials for oxygen reduction reaction clarified using model catalysts, Science, Volume 351, pages 361-365, 2016

## BALANCE PROJECT - RSOC TECHNOLOGY TO INTERCONNECT POWER GRIDS AND FUEL INFRASTRUCTURE

A. Olivier Thomann\*, B. Mikko Kotisaari\* and C. Olli Himanen\*

\*VTT Technical Research Centre of Finland Ltd., Fuel Cells, Biologinkuja 5, FI-02150 Espoo, (Finland)

**Abstract** - The H2020 BALANCE project focuses on the development of reversible Solid Oxide Cells (rSOC) that are both capable of fuel cell and electrolysis operation. For that reason, rSOC technology is expected to play an important role in the integration of intermittent renewable electricity by storing the excess production and by converting the synthetic fuel back into power when it is needed. Research activities of the BALANCE project target the improvement of cell performance, finding suitable low-cost steel alloy for interconnect applications, stack design and prototyping and demonstration at system level. In addition, techno-economic analysis is being carried out to evaluate the benefits of rSOC technology in combination with synthesis step for the production of non-fossil fuels or chemicals. Lastly, BALANCE is surveying and analyzing the research effort in Europe and will publish a roadmap supporting the development and deployment of the rSOC technology. The paper here describes the different project activities and its expected outcomes.

**Index Terms** - Renewable fuel productions, Reversible Solid Oxide Fuel Cell, system demonstration

### I. INTRODUCTION

Reversible Solid Oxide Cells (rSOC) is a technology that can convert electrical power into hydrogen and convert back the hydrogen or other fuels into electrical power as illustrated conceptually in Fig 1. This allows the production of fuel from renewable electricity and act as an energy storage to balance the fluctuations of renewable electricity production. rSOC is gathering attention because of the important role it can play in integrating intermittent renewable electricity sources into the grid. However, the technology is not yet mature in terms of performance and cost for market entry. The partners of the BALANCE project are joining their efforts to develop this technology and to demonstrate its feasibility. The partners of BALANCE are VTT (FI), DTU (DK), CEA (FR), ENEA (IT), TU Delft (NL), University of Birmingham (UK), EPFL (CH) and IEn (PL). This paper presents the research activities of the BALANCE project and highlights its expected contributions.



Fig 1 rSOC integration concept.

### II. PROJECT GOALS

The goal of the BALANCE project is to advance the level of technological readiness of the rSOC technology. For this purpose, the project gathers research actors, which complimentary competences address the essential stages of the value chain of designing and manufacturing of rSOC systems. The project addresses the development of a new generation of cell, the evaluation of steel grades for interconnect application, the design and the manufacturing of rSOC stack and demonstration of rSOC systems. Moreover, techno-economic analysis of different integration scenarios of the rSOC system with downstream synthesis stage to produce non-fossil fuel or chemical will identify the most beneficial industrial environment.

In addition, the BALANCE project aims at providing guidance on the development and deployment of the rSOC technology in Europe and its integration in the strategic energy technology plan (SET plan).

### III. RESEARCH ACTIVITIES

The research activities cover the different stages of the value chain of the rSOC technologies.

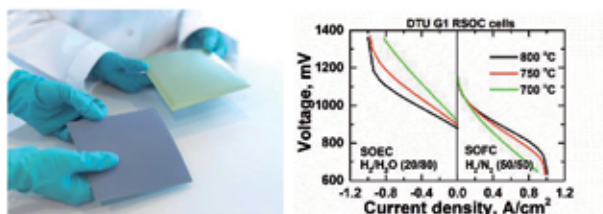
**At cell level**, alternative fuel electrode materials and nanostructured oxygen electrodes are being optimized and integrated in a new generation of cell. The aim is to allow



operation at lower temperature (700°C) with an area specific resistance of 0.2 ohm cm<sup>2</sup> in electrolysis mode.

**At metallic interconnect level**, low-cost ferritic steels with protective coating will be evaluated for operation in the atmosphere representative of electrolysis operation with high steam content on the fuel side and possibly pure oxygen on the oxygen side.

**At stack level**, stack design will be prototyped and characterized in rSOC operation. In addition, multi-kW electric stacks will be manufactured for further integration in demonstration rSOC system. The stack target is to have not less than 20% of loss of performance between cell and stack and a degradation rate of less than 2%/ 1,000 h in SOE mode. The stack prototypes will be based on the state-of-the-art cell manufactured at DTU, which performance are illustrated in Fig. 2.



**Fig 2 Picture and performance data of the cells that are used for in stack and system in the BALANCE project. Figure and picture courtesy of Ming Chen, DTU.**

**At system level**, rSOC system operation will demonstrate in 2019 the feasibility of the reversibility at system level for up to 2500 hours using stack prototyped during the project. The effect of reversibility on system complexity and lifetime will also be evaluated.

In addition, **the suitability of rSOC technology in different industrial environments is being investigated.** System modelling, exergy analysis and techno-economic analysis is being used for different rSOC plant configurations producing hydrogen or fuel via chemical conversion processes and providing grid stabilization services. The systems considered include grid connection, rSOC unit, possible hydrogen or syngas chemical conversion step and gas or fuel storage. Life cycle analysis will be conducted for deeper understanding of the process cost and environmental impacts.

Lastly, BALANCE will provide guideline for the further development and commercialization of the rSOC technology and its integration in the energy strategy of the European Union. For this, a survey is being conducted to map and analyze the level of development rSOC in Europe. Specific attention will be paid to the gaps in its development that might slow down its future development and deployment. A database

from the mapping results will be brought online and accessible outside of the consortium and the conclusion of this activity will be shared in a public advisory paper. Researcher mobility is also strongly encouraged in this project as an effective mean to exchange skills and knowledge and to achieve tight collaboration between research groups.

## CONCLUSIONS

The BALANCE project is dedicated to the development of reversible Solid Oxide Cells (rSOC) technology. Research activities covers cell microstructure improvements, low-cost steel alloy evaluation for interconnect applications, stack design and manufacturing and characterization in reversible operation and system-level demonstration. In parallel, exergy analysis and techno-economic analysis are carried out to identify the most beneficial configurations and combinations with different downstream synthesis steps. The project aims also at aligning the research efforts to fill the research gaps and provide guidance in the further development and implementation of the technology beyond the project lifetime.

## ACKNOWLEDGMENT

This project has received funding from the European Union's Horizon 2020 research and innovation programme under grant agreement No 731224.

## REFERENCES

- [1] Project website: <https://www.balance-project.org/>

## METAL OXIDE CATALYSTS FOR OER IN ALKALINE MEDIA

D. Ion-Ebrasu\*, A. Spinu-Zaulet\*, S. Enache\*, M. Dragan\*,  
D. Schitea\*, L. Patularu\*, E. Carcadea\*, M. Varlam\*, and K.  
Petrov\*\*

\*National Institute for Cyogenics and Isotopic Technologies ICSI-  
Rm. Valcea, (Romania)

\*\*2 Acad. Evgeni Budevski Institute of Electrochemistry and Energy  
Systems, Bulgarian Academy of Sciences, (Bulgaria)

**Abstract** - In this paper is presented an investigation of the  $\text{LaCoO}_3$  catalysts for Oxygen Evolution Reaction (OER) in alkaline media. The effect of various parameters such as catalyst and PTFE loading, catalyst layer thickness, and fabrication technique on the electrode performances is described. The catalytic activity towards the OER of catalysts was determined from Tafel plots obtained from galvanostatic current-voltage measurements. Electrocatalytic activity toward the ORR in 0.1 M KOH was studied with the Rotating Disk Electrode (RDE) method.

**Index Terms** – Alkaline, catalysts, electrolysis, oxides.

### I. NOMENCLATURE

OER- Oxygen Evolution Reaction.

### II. INTRODUCTION

In Polymer Electrolyte Conducting  $\text{OH}^-$  Cations Electrolysis (PEM.OH $^-$ ) the significant overpotential occurs at the anode side where the oxygen evolution reaction (OER) takes place. Improving OER kinetics would indeed favor a widespread market penetration of (PEM.OH $^-$ ) electrolyzers. Since iridium is quite expensive and, as a typical secondary metal, resource limited, many research efforts have been directed towards the development of OER catalysts with a reduced amount of Ir or based on other transition metal oxides. We report herein a study on the electrochemical properties of  $\text{LaCoO}_3$  catalyst synthesized using the solid state reaction route, and used as electrode in the form of coating on nickel foam support. The effect of various parameters such as catalyst and

PTFE loading, catalyst layer thickness, and fabrication technique on the electrode performances is studied, in comparison with commercial  $\text{IrO}_2$  catalyst. The catalytic activity towards the OER of catalysts was determined from Tafel plots obtained from galvanostatic current-voltage measurements. Electrocatalytic activity toward the ORR in 0.1 M KOH was studied with the Rotating Disk Electrode (RDE) method at room temperature.

### III. EXPERIMENTAL

The  $\text{LaCoO}_3$  (LCO) perovskite powder was synthesized using the solid state reaction route from stoichiometric amounts of  $\text{La}_2\text{O}_3$  and  $\text{Co}_3\text{O}_4$  powders as precursors. Following the dry mixing of precursors, a thermal treatment in air was applied in order to obtain the targeted single-phase material. The electrodes were prepared on a round shape Ni foam with 93% porosity and with different catalyst and PTFE loading (Table 1). Moreover, in order to improve the electrodes conductivity, silver was added in several ratios. The electrodes were prepared by a home-made developed method: the catalyst was mixed with PTFE and added on the Ni foam support that was placed in a matrix. The electrode surface is 1  $\text{cm}^2$ . The catalyst/Ni foam was pressed at 300kgf, for 1 minute, and at 300° C.

Table 1. LCO catalyst and PTFE loading		
Catalyst (mg)	PTFE (mg)	Sample name
150mg $\text{IrO}_2$	20	150 $\text{IrO}_2$ /20PTFE/ Nifoam
150 $\text{LaCoO}_3$	20	150LCO/20PTFE/

Copyright © 2017



		Nifoam
100 LaCoO <sub>3</sub>	16,6	100LCO/16.6PTFE/Nifoam
75 LaCoO <sub>3</sub>	10	75LCO/10PTFE/Nifoam

#### IV. RESULTS AND DISCUSSIONS

##### Galvanostatic measurements

To determine the effect of catalyst loading and the impact of silver mixture, the electrode voltage dependence was plotted at 50 mA. Figure 1 (a) shows the increasing of the electrode voltage as a function of the catalyst loading decreasing.

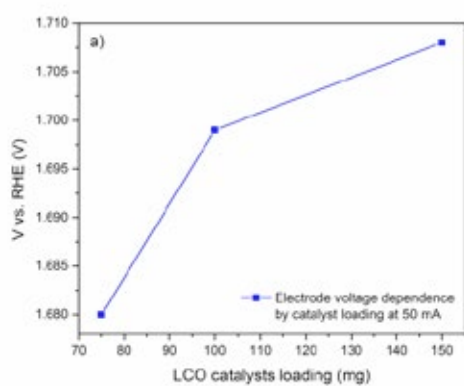


Figure 1. Electrode voltage dependence versus LCO catalysts loading calculated at 50 mA.

In Figure 2 are presented the galvanostatic current-voltage curves recorded for different LCO/PTFE loading in comparison with IrO<sub>2</sub> commercial catalyst, in domain of 0÷100 mA.

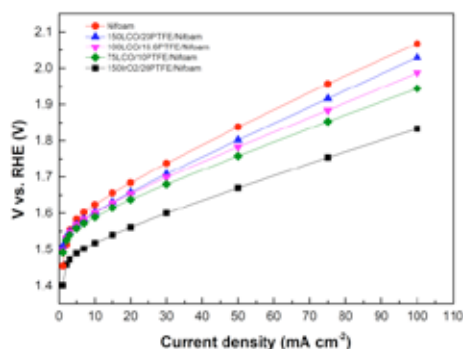


Figure 2. Galvanostatic current-voltage curves recorded for different LCO/PTFE loading in comparison with IrO<sub>2</sub> commercial catalyst, in domain of 0÷100 mA.

Figure 3 shows the Tafel plots ( $\log j$ ) versus  $V$ , and the slopes calculated from the curves presented in Figure 2. The

slopes for LCO samples are in domain of 93 mV/decade (75 mg LCO) to 133 mV/decade (150 mg LCO). It is because that the overpotential will raise slower if the current density is increasing when using this material for the catalyst in the OER. Since the overpotential is the energy loss during OER, the smaller slope indicates a better catalysis performance. The value of slope for 75LCO/10PTFE/Nifoam sample is close to the one corresponding to the commercial IrO<sub>2</sub> catalyst (87 mV/decade), which indicates that this probe can be considered to have the best electrode structure and composition for OER in alkaline media related to the perovskite catalyst presented in this work [1-2].

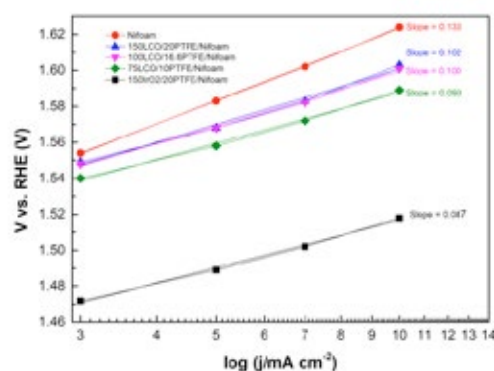


Figure 3. Tafel plots recorded for different LCO/PTFE loading in comparison with IrO<sub>2</sub> commercial catalyst, in domain of 3÷10 mA.

#### V. CONCLUSION

We have shown in this paper that LaCoO<sub>3</sub> perovskite catalyst synthesized using the solid state reaction route presents good catalytic activity and stability for OER, and confirm that the OER proceeds into four paths since this reaction involves four electron transfer

#### ACKNOWLEDGMENT

Financial Support: National Authority for Scientific Research&Innovation, RESTORE Contract 117/16.09.2016, and Romanian national R&D Program-STAR, Contract 175/20.07.2017.

#### REFERENCES

- [1] I. C. Man, Universality in Oxygen Evolution Electrocatalysis on Oxide Surfaces, Chem. Cat. Chem. Volume 3, 2011, Pages 1159 – 1165
- [3] J. Rossmeisl, Z. W. Qu, H. Zhu, G. J. Kroes, J. K. Nørskov, Electrolysis of water on oxide surfaces, J. Electroanal. Chem. Volume 607, 2007, Pages 83-89.

## OPERATIONAL STRATEGY TO ACHIEVE PREDICTABLE AND SUSTAINING POWER PERFORMANCE IN DIRECT CARBON FUEL CELLS

Hansaem Jang<sup>\*\*\*</sup>, Youngeun Park<sup>\*\*\*</sup>, and Jaeyoung  
Lee<sup>\*\*\*\*\*,†</sup>

<sup>\*</sup>Electrochemical Reaction & Technology Laboratory (ERTL),  
School of Earth Sciences and Environmental Engineering, Gwangju  
Institute of Science and Technology (GIST), Gwangju 500-712,  
(South Korea)

<sup>\*\*</sup>Chemical Energy Storage and Transformation Center, Research  
Institute for Solar and Sustainable Energies, GIST, Gwangju 500-  
712, (South Korea)

<sup>\*\*\*</sup>Ertl Center for Electrochemistry and Catalysis, GRI, GIST,  
Gwangju 500-712, (South Korea)

**Abstract** - Direct carbon fuel cells (DCFCs) have been widely believed to electrochemically oxidize solid-state carbon to produce electricity, but it is recently disclosed that gaseous molecules rather play a more crucial role in power generation. In this work, we aim at predictable and sustaining power performance in DCFCs. We control the gas composition of an anode chamber within which electrochemical oxidation reactions occur. We provide either argon or carbon dioxide gas into the chamber, by which the atmosphere of the chamber is varied. Predictable power generation is achieved when gasification caused by the intrinsic impurities of solid carbon is hindered by purge gas. Sustaining performance is observed when optimized is the loss of further oxidizable gaseous molecules that are produced by external gas supply which promotes gasification. Interestingly, when the loss is minimized, the performance exhibits a decreasing trend, not sustaining, because the intrinsic impurities of solid carbon are gradually exhausted.

**Index Terms** - Boudouard reaction, Carbon fuel cell, Direct carbon fuel cell, Solid oxide based electrode

### I. INTRODUCTION

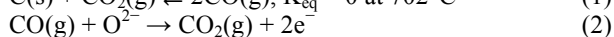
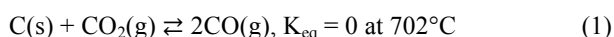
Compared with gaseous materials, the use of solid-state fuels enables facile transportation to where required. Besides, solid-state fuels are much higher in volumetric energy densities than fuels in gaseous form. Direct carbon fuel cells (DCFCs), as the name suggests, were designed to take advantage of solid carbonaceous fuel to produce electricity. When invented, DCFCs were thought to involve direct electrochemical

reactions with solid carbon [1–4]. In recent years, papers have been published claiming a new view on the role of solid carbon; that is, solid carbon acts as a precursor that undergoes gasification to produce gases which can work as fuel. [4–10].

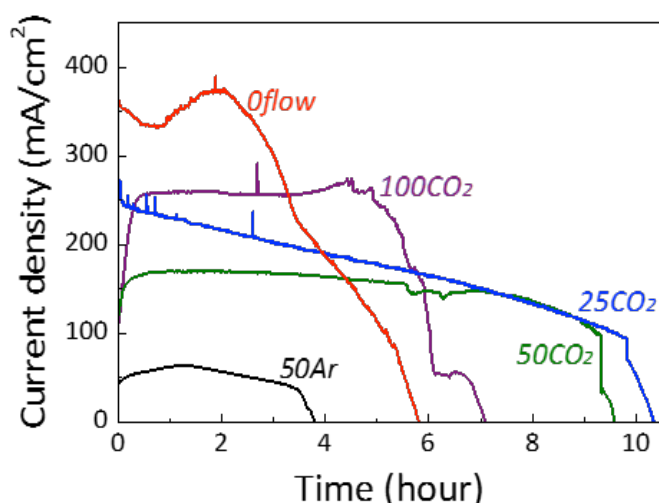
In our previous study [9], the authors have successfully demonstrated experiments proving that the new view holds true. There, a gas diffusion layer made of Al<sub>2</sub>O<sub>3</sub> wool that prevents solid fuel from reaching the anode surface was sandwiched between the anode and the solid carbon. Interestingly, the maximum power density (MPD) values with and without the Al<sub>2</sub>O<sub>3</sub> layer made no great difference, implying that gaseous molecules serve as an actual fuel. Another study conducted by Chien et al. [7] has reinforced the new view on the solid carbon. A solid oxide based cell was attached to the bottom of a cylindrical chamber with the anode side facing up, and solid carbon was placed on top of the anode surface inside the chamber. During operation of the fuel cell, they inverted the chamber so that the carbon was detached from the anode surface. They concluded “a DCFC works regardless of contact if carbon fuel is around anode.” [7]

The importance of the new view lies in the fact that gaseous molecules are practically easier to handle as a fuel in DCFCs. In this sense, we control the gas composition within an anode chamber with the help of an external gas supply by either Ar or CO<sub>2</sub>. Argon serves as a purge gas. In practical use of DCFC, it is economically less feasible to employ pure carbon source but feasible is the use of low rank coal that contains high impurities

leading to gasification. The resulting gaseous products able to be further oxidized can be electrochemically oxidized to generate electrons [11,12], and therefore the supply of Ar can interfere with this electron generating pathway. Carbon dioxide acts as a purge gas and a gasification reactant, the dual role being dependent on the flow rate as supplied. High operating temperatures in DCFC cause solid carbon to react with CO<sub>2</sub> by the reverse Boudouard reaction (Eq. (1)), producing CO that works as a major fuel source (Eq. (2)). An excessive supply of CO<sub>2</sub> into the anode chamber, however, gives rise to the release of unreacted CO molecules. Taken together, careful handling of the external gas can provide predictable and sustaining power performance by controlling the gas composition within the chamber.



## II. CONCLUSION



**Fig. 1. Long-term power performance by discharge tests at 900°C under the constant voltage of 0.6 V.**

**Note: the total charge of each test is 1489.4 mAh (0flow), 194.3 mAh (50Ar), 1756.1 mAh (25CO<sub>2</sub>), 1435.3 mAh (50CO<sub>2</sub>), and 913.3 mAh (100CO<sub>2</sub>).**

There are basically two keys to consider to achieve predictable and sustaining power performance: one is the type of gas that is provided to an anode chamber, and the other is the flow rate of that gas. The way to attain predictable performance is to provide a purge gas to minimize the effect of impurity-driven gaseous fuels. For sustaining performance, CO<sub>2</sub> supply should be balanced, the flow rate of which should be just sufficient to promote CO generation and to sweep away the impurity-driven fuels, simultaneously. In our experimental sets,

50CO<sub>2</sub> meets the both criteria because when the flow rate was lower, the gas supply was not enough to blow the impurity-driven influence away; and because when the flow rate was higher, a loss in gaseous fuel was significant. Emphasis should be placed on the fact that the optimal flow rate would vary depending on the volume and the design of an operating anode chamber. In addition, we also corroborate that it takes a finite time and an electric load to kick-start a fuel cell at a considerable gas flow rate.

## ACKNOWLEDGMENT

This work was supported by the “Climate Technology Development and Application” research project (K07723) through a grant provided by GIST in 2017.

## REFERENCES

- [1] Cao, D., Sun, Y., Wang, G., Direct carbon fuel cell: Fundamentals and recent developments, *Journal of Power Sources*, Volume 167, 2007, pp. 250–257.
- [2] Rady, A.C., Giddey, S., Badwal, S.P.S., Ladewig, B.P., Bhattacharya, S., Review of Fuels for Direct Carbon Fuel Cells, *Energy & Fuels*, Volume 26, 2012, 1471–1488.
- [3] Giddey, S., Badwal, S.P.S., Kulkarni, A., Munnings, C., A comprehensive review of direct carbon fuel cell technology, *Progress in Energy and Combustion Science*, Volume 38, 2012, pp. 360–399.
- [4] Gur, T.M., Critical Review of Carbon Conversion in “Carbon Fuel Cells”, Volume 113, pp. 6179–6206.
- [5] Tang, Y., Liu, J., Effect of anode and Boudouard reaction catalysts on the performance of direct carbon solid oxide fuel cells, *International Journal of Hydrogen Energy*, Volume 35, 2010, pp. 11188–11193.
- [6] Eom, S., Ahn, S., Rhie, Y., Kang, K., Sung, Y., Moon, C., Choi, G., Kim, D., Influence of devolatilized gases composition from raw coal fuel in the lab scale DCFC (direct carbon fuel cell) system, *Energy*, Volume 74, 2014, pp. 734–740.
- [7] Chien, A.C., Petra, M.I., Lim, C.M., Effect of Contact Mode and Flow Rate On Direct Carbon Solid Oxide Fuel Cell, *Journal of Chemical Engineering of Japan*, Volume 48, 2016, pp. 362–365.
- [8] Ong, K.M., Ghoniem, A.F., Modeling of indirect carbon fuel cell systems with steam and dry gasification, *Journal of Power Sources*, Volume 313, 2016, pp. 51–64.
- [9] Jang, H., Park, Y., Lee, J., Meticulous insight on the state of fuel in a solid oxide carbon fuel cell, *Chemical Engineering Journal*, Volume 308, 2017, pp. 974–979.
- [10] Xu, H., Chen, B., Zhang, H., Sun, Q., Yang, G., Ni, M., Modeling of direct carbon solid oxide fuel cells with H<sub>2</sub>O and CO<sub>2</sub> as gasification agents, *International Journal of Hydrogen Energy*, Volume 42, 2017, pp. 15641–15651.
- [11] Jang, H., Ocon, J.D., Lee, S., Lee, J.K., Lee, J. Direct power generation from waste coffee grounds in a biomass fuel cell, *Journal of Power Sources*, Volume 296, 2015, pp. 433–439.
- [12] Jang, H., Park, Y., Lee, J., Origin of peculiar electrochemical phenomena in direct carbon fuel cells, *Chemical Engineering Journal*, Volume 327, 2017, pp. 1163–1175.

## A COMPARATIVE STUDY OF VARIOUS IRIIDIUM ELECTROCATALYST DEPOSITION METHODS FOR OXYGEN EVOLUTION REACTION

Hansaem Jang\*\*\* and Jaeyoung Lee\*\*\*\*\*,†

\*Electrochemical Reaction & Technology Laboratory (ERTL),  
School of Earth Sciences and Environmental Engineering, Gwangju  
Institute of Science and Technology (GIST), Gwangju 500-712,  
(South Korea)

\*\*Chemical Energy Storage and Transformation Center, Research  
Institute for Solar and Sustainable Energies, GIST, Gwangju 500-  
712, (South Korea)

\*\*\*Ertl Center for Electrochemistry and Catalysis, GRI, GIST,  
Gwangju 500-712, (South Korea)

**Abstract** - Hydrogen has garnered increasing interest as future fuel because unlike other conventional fuel sources, it has less environmental impacts. In particular, when hydrogen is combusted or employed in fuel cells to produce energy, the only byproduct is water. Water electrolysis consists of hydrogen evolution reaction (HER) and oxygen evolution reaction (OER). While HER is relatively straightforward, OER is regarded as a bottleneck in water electrolysis. As an OER catalyst, iridium comes most attractive because of its high durability and low overpotential. In order to incorporate iridium electrocatalyst, three different techniques are introduced: atomic layer deposition (ALD), arc plasma deposition (APD), and anodic electro-deposition (AED).

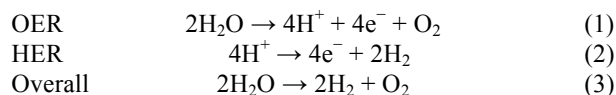
**Index Terms** – Anodic electro-deposition, arc plasma deposition, atomic layer deposition, oxygen evolution reaction

### I. NOMENCLATURE

acac	acetylacetonate
AED	Anodic Electro-Deposition
ALD	Atomic Layer Deposition
APD	Arc Plasma Deposition
CHD	cyclohexadiene
COD	cyclooctadiene
CVD	Chemical Vapor Deposition
EtCp	ethylcyclopentadienyl
MeCp	methylcyclopentadienyl
HER	Hydrogen Evolution Reaction
OER	Oxygen Evolution Reaction

### II. INTRODUCTION

Hydrogen production can be achieved in many ways. In particular, water-splitting is attractive in that it uses water as fuel without fossil fuel, and it produces only hydrogen and oxygen gases without emitting greenhouse gases [1,2]. Water splitting consists of two half reactions (eqs. 1–3, at pH = 0). When water is split, hydrogen evolution reaction (HER) occurs at cathodes generating hydrogen gas and simultaneously at anodes, oxygen evolution reaction (OER) occurs. Despite the fact that OER is the reaction producing oxygen, emphasis should be placed on OER catalysts because its overpotential is higher than that of HER. That is, OER is regarded as a bottleneck. Thus, rather than HER, designing OER catalyst is the matter of concern.



Iridium(IV) oxide shows excellent electrocatalytic activity in both alkaline and acidic water splitting. Unlike in alkaline baths, it is still challenging to introduce non-noble metal catalysts in acidic baths because of a stability issue. In fact, ruthenium(IV) oxide has higher electrocatalytic activity than  $\text{IrO}_2$  but has less stability [3–6]. In this regard, iridium(IV) oxide is considered to be the most practical catalyst in OER



except the fact that it is costly. Therefore, our primary goal of the study is to reduce the use of iridium while maintaining its catalytic behavior. In order to minimize the use of iridium, we have chosen three different deposition techniques: atomic layer deposition (ALD), arc plasma deposition (APD), and anodic electro-deposition (AED).

ALD is based on a chemical vapor deposition (CVD) technique. ALD is performed with sequential self-terminating reactions [7]. In general, the sequential reactions comprise a cycle to deposit a layer and involve the following four reactions: (i) the first reactant undergoes a self-terminating reaction; (ii) a purge gas sweeps away the non-reacted reactant as well as gaseous by-products; (iii) the second reactant undergoes a self-terminating reaction; (iv) a purge gas sweeps away the non-reacted reactant as well as gaseous by-products. The number of cycles would vary depending on a target deposition materials, that is, the third or more reactants could be introduced. A range of methods to deposit iridium-based material with ALD have been reported. Metallic iridium can be coated with the such precursors:  $\text{Ir}(\text{acac})_3$ ,  $(\text{MeCp})\text{Ir}(\text{CHD})$ ,  $(\text{EtCp})\text{Ir}(\text{COD})$ ,  $(\text{EtCp})\text{Ir}(\text{CHD})$ , and  $\text{IrF}_6$  [8].

APD evaporates a solid metal target and generates highly ionized plasma pulse. In particular, co-axial APD allows for nanoscale deposition and eventually for reducing the use of precious metal [9].

AED happens in an electrophoretic manner [10]. Unlike the two preceding techniques, it is mainly deployed to deposit  $\text{IrO}_2$  because in AED, iridium (III) is oxidized into iridium (IV) oxide. As a precursor, the followings have been reported:  $\text{IrCl}_3$ ,  $\text{IrCl}_4$ ,  $\text{K}_2\text{IrCl}_6$ ,  $\text{K}_3\text{IrCl}_6$ ,  $\text{Na}_2\text{IrCl}_6$ , and  $\text{Na}_3\text{IrCl}_6$ .

### III. EXPERIMENTAL SECTION

ALD was performed with an  $\text{Ir}(\text{acac})_3$  precursor under  $\text{O}_2$  atmosphere to deposit metallic iridium. As a purge gas, nitrogen was blown into the reactor. Optimized were the time for each step, the temperature of experiments, and the flow rate of provided gases.

APD was performed with a metallic iridium target. By varying the number of cycles, the amount of iridium precursor deposited onto a supporting material was controlled. Only a few shots of pulse resulted in an excellent electrochemical activity.

AED was performed with an  $\text{IrCl}_3$  precursor. The grounds for choosing this precursor is that it contains lower number of chloride ions as compared with the other precursors. In fact, chloride ions can affect an OER activity because it can cause chlorine evolution reaction.

### IV. CONCLUSION

In the cases of ALD and APD, it was easier to control the number of cycle and therefore the amount of iridium deposited onto a supporting material. However, in the case of AED, extra attention was paid because unlike the two other techniques, it

was performed within a solution bath and was not handled with the number of cycles but done electrochemically. The benefits of the use of each technique is as such: ALD exhibits good conformality; APD shows simplicity in operation; AED results in direct  $\text{IrO}_2$  formation. Each technique has its own advantage and therefore we suggest that combining these techniques in an optimal manner would lead us to the minimized use of iridium as well as an improved electrochemical activity.

### ACKNOWLEDGMENT

This work was supported by the Korea Institute of Energy Technology Evaluation and Planning (KETEP) and the Ministry of Trade, Industry & Energy (MOTIE) of the Republic of Korea (20162310100020).

### REFERENCES

- [1] Dunn, S., Hydrogen futures: toward a sustainable energy system, *International Journal of Hydrogen Energy*, Volume 27, 2002, pp. 235–264.
- [2] Nikolaidis, P., Poullikkas, A., A comparative overview of hydrogen production processes, *Renewable and Sustainable Energy Reviews*, Volume 67, 2017, pp. 597–611.
- [3] Trasatti, S., Electrocatalysis by oxides — Attempt at a unifying approach, *Journal of Electroanalytical Chemistry and Interfacial Electrochemistry*, Volume 111, 1980, pp. 125–131.
- [4] Man, I.C., Su, H.-Y., Calle-Vallejo, F., Hansen, H.A., Martínez, J.I., Inoglu, N.G., Kitchin, J., Jaramillo, T.F., Nørskov, J.K., Rossmeisl, J., Universality in Oxygen Evolution Electrocatalysis on Oxide Surfaces, *ChemCatChem*, Volume 3, 2011, pp. 1159–1165.
- [5] Doyle, R.L., Lyons, M.E.G., The Oxygen Evolution Reaction: Mechanistic Concepts and Catalyst Design, in: S. Giménez, J. Bisquert (Eds.) *Photoelectrochemical Solar Fuel Production: From Basic Principles to Advanced Devices*, Springer International Publishing, Cham, 2016, pp. 41–104.
- [6] Danilovic, N., Subbaraman, R., Chang, K.-C., Chang, S.H., Kang, Y.J., Snyder, J., Paulikas, A.P., Strmcnik, D., Kim, Y.-T., Myers, D., Stamenkovic, V.R., Markovic, N.M., Activity–Stability Trends for the Oxygen Evolution Reaction on Monometallic Oxides in Acidic Environments, *The Journal of Physical Chemistry Letters*, Volume 5, 2014, pp. 2474–2478.
- [7] Puurunen, R.L., Surface chemistry of atomic layer deposition: A case study for the trimethylaluminum/water process, *Journal of Applied Physics*, Volume 97, 2005, pp. 121301.
- [8] Mattinen, M., Hämäläinen, J., Gao, F., Jalkanen, P., Mizohata, K., Räisänen, J., Puurunen, R.L., Ritala, M., Leskelä, M., Nucleation and Conformality of Iridium and Iridium Oxide Thin Films Grown by Atomic Layer Deposition, *Langmuir*, Volume 32, 2016, pp. 10559–10569.
- [9] Kim, S.H., Nanocatalyst Materials Prepared by Arc Plasma Deposition, *Applied Chemistry for Engineering*, Volume 25, 2014, pp. 341–345.
- [10] Petit, M.A., Plichon, V., Anodic electrodeposition of iridium oxide films, *Journal of Electroanalytical Chemistry*, Volume 444, 1998, pp. 247–252.

## INTEGRATION OF A CALCIUM LOOPING (CaL) PROCESS WITH A MCFC: AN ENERGY ASSESSMENT

Andrea De Silvestri\*, Massimiliano Della Pietra\*\*, Stephen Mc Phail\*\*, Domenico Borello\*\*\* and Stefano Stendardo\*\*

\* Dipartimento di Ingegneria Astronautica, Elettrica ed Energetica, Sapienza Università di Roma, Via Eudossiana, 18, 00184, Roma (Italy)

\*\* ENEA, Italian National Agency for New Technologies, Energy and Sustainable Economic Development, Via Anguillarese, 301, S. Maria di Galeria, 00123, Rome (Italy)

\*\*\* Dipartimento di Ingegneria Meccanica e Aerospaziale, Sapienza Università di Roma, Via Eudossiana, 18, 00184, Roma (Italy)

**Abstract** - This study is devoted to the integration of a Calcium Looping (CaL) process with a Molten Carbonate Fuel Cell (MCFC). The CaL-based technology uses CaO based material for capturing CO<sub>2</sub>. Generally, it consists of two bubbling fluidized beds, the carbonator and the oxy-fuel calciner. We propose to run the regeneration of the sorbent by a conventional combustion in air in order to avoid the need of an ASU to produce high concentrated oxygen stream.

The aim of the work is to identify the optimal operating conditions of this hybrid system applied to a cement factory via modeling and experimental activities. Energy and economic analysis has been carried out and the results compared to the benchmark technology: a conventional Cement Plant [1].

A reduction above 90% of the equivalent CO<sub>2</sub> emissions (direct and indirect emission) can be reached.

**Index Terms** - Calcium Looping, SER Trireformer, CCS, Decarbonized Cement Industry, MCFC

### I. INTRODUCTION

The cement industry is an excellent candidate for implementing CO<sub>2</sub>-emissions mitigation strategy because it is one of the largest industrial source of CO<sub>2</sub> accounting for around 5% of global carbon dioxide emissions [1].

### II. PROCESS DESCRIPTION

A scheme of the low carbon cement making process analyzed in this work is shown in Figure 1. It is composed of a pre-calciner, a rotary kiln, the fluidized-bed carbonator (CARB1), a second reactor (CARB 2) where sorption enhanced reforming (SER) [2] and/or tri-reforming of methane (TRM) [3] occurs. In the CARB2 methane is converted to H<sub>2</sub> in order to feed the MCFC which is used as CO<sub>2</sub> concentrator [4].

In details, as reported in fig. 1, the anode side is fuelled by H<sub>2</sub>-rich stream generated by CARB2 while the CO<sub>2</sub>-diluted flue

gas leaving the pre-calciner and the kiln is properly injected into the MCFC cathode for the concentration of CO<sub>2</sub> at the anode side. The high CO<sub>2</sub>-concentrated gas leaving the anode will be sent to final disposal and or valorization processes (e.g. EOR, fuel synthesis). In the conventional cement production the CaO leaving the precalciner is sent to the rotary kiln for the production of the clinker. In this work we propose to decarbonise the gases leaving the rotary kiln and the air-fuelled precalciner by means of CARB1 and CARB2 fed by part of the CaO leaving the precalciner.

### III. EXPERIMENTAL

In order to properly verify and validate the MCFC model several tests were performed in the Hotlab (High-temperature fuel cell Operating and Testing lab) of ENEA as proposed in [5] where the experimental facility here used is also described. The tested MCFC single cell, supplied by FCES (Fuel Cell Energy Solutions GmbH), has a planar square area of 81 cm<sup>2</sup>. The anode consist of a Ni structure, the cathode is constituted by a NiO-based material and the electrolyte is composed by a mixture of lithium and potassium carbonate. Different operating parameters were changed in order to study their influence on the performance of MCFCs.

Furthermore, some experimental tests have been run by feeding the cathode with a gas emulating the composition of a decarbonised coal syngas (H<sub>2</sub>: 17%, CO: 30%, CO<sub>2</sub> 33%, H<sub>2</sub>O 19%). These values have been obtained by using the developed carbonator models fed with a raw syngas whose composition is reported in [6].

#### IV. MODELING

The proposed system has been formulated and integrated into a commercial software (Chemcad<sup>TM</sup>).



Fig. 1. Layout of the proposed low carbon cement process.

##### A. SER process

The kinetics of catalytic reforming process reviewed in [2] was here used. A semi-predictive model with two zone K-L hydrodynamics was adopted to estimate sorbent conversion for the carbonation reaction [7]. We can determine the average reaction rate assuming perfect mixing of solids and determined their average residence time in the reactor  $\tau$ , as shown in equation 1.

$$\frac{d\bar{X}}{dt} = \int_0^\infty k_r C_{CO_2} X_{max} \exp(-k_r C_{CO_2} t) \frac{1}{\tau} \exp\left(-\frac{t}{\tau}\right) dt = \frac{k_r C_{CO_2} X_{max}}{k_r C_{CO_2} \tau + 1} \quad (1)$$

It is assumed that the  $CaCO_3$  decomposes completely in the regenerator of the CaL (pre-calciner).

##### B. Molten Carbonate Fuel Cell (MCFC)

Several semi-empirical equations describing the polarization losses due to chemical as well as physical phenomena [4,5] were validated by means of experimental results collected. To study the MCFC behavior, a mathematical model in C++ environment has been formulated and implemented for simulating steady-state fuel cell. The model developed in [5] has been here adopted. In situ CO shift (WGS) reaction was also considered at the anode balance using the equilibrium constant reported in [8]. Hence, the concentration of carbon monoxide (CO) in output is well estimated by the model.

#### V. CONCLUSION

Two configurations have been extensively analysed:

- Case 1: the flue gas leaving the kiln has been sent only to the CARB1, the pre-calciner exhausted gas sent to the MCFC;
- Case 2: all the flue gases are diverted to the MCFC cathode, SER takes place in CARB2: whereas CARB1 has not been considered.

The selected processes have been designed to produce 2450 tonne/day of clinker. Preliminary results were obtained using the GIBBS model to simulate each single reactor. The fuel demand in the pre-calciner and in the kiln was estimated to be 3.30, 6.62 and 5.62 GJ/t<sub>clinker</sub> respectively for the reference cement plant, Case 1 and 2. Because of the increase of the elaborated solid sorbent flow, the consumption of primary energy increases, accordingly. Nevertheless, it is possible to recover up to 54 MWe and 192 MWth from the MCFC stacks respectively in Case 1 and 2. It is also assumed that a steam cycle with a net thermal efficiency of 33% could be integrated in order to valorise the heat waste and produce electricity by means of a captive power plant. The equivalent CO<sub>2</sub>-emission are 1.24 t<sub>CO2</sub>/t<sub>clinker</sub> for the conventional cement plant with a reduction down to 0.05 and 0.01 in Case 1 and 2, respectively. In particular, the direct CO<sub>2</sub>-emission are 1.20 (benchmark), 0.36 (Case 1) and 0.30 (Case 2) t<sub>CO2</sub>/t<sub>clinker</sub>.

While ensuring high CO<sub>2</sub> capture rate the application of this end-of-pipe option do not require structural changes to the existing cement factory and the pre-calciner is not strongly modified. However, further pre-calciners are required in order to accommodate the additional flow rate of solids.

Regarding energy penalty, the Specific Energy Consumption for equivalent CO<sub>2</sub> Avoided (SPECCA\*) index [GJ/t<sub>CO2</sub>], which measures the primary energy request to avoid CO<sub>2</sub>, was evaluated.

$$SPECCA^* = \frac{HR^* - HR_{ref}^*}{e_{ref}^* - e^*} \quad (2)$$

Where  $HR^*$  is the net primary energy demand needed by the plant to produce 1 ton of clinker, GJ/t<sub>clinker</sub>, defined as the total fuel consumption of the plant (coal in PRE-CALC and KILN, methane in CARB2) discounted by the heat needed to produce the net exported power (captive steam cycle and MCFC). The symbol  $e^*$  represents the equivalent CO<sub>2</sub> emission rate, t CO<sub>2</sub>/t<sub>clinker</sub>.

Promising SPECCA\* indexes are reached: 2.03 for Case 1 and 1.21 for Case 2, respectively.

#### REFERENCES

- [1] N.Rodríguez, R. Murillo and J. C. Abanades, CO<sub>2</sub> Capture from Cement Plants Using Oxyfired Precalcination and/or Calcium Looping, Environ. Sci. Technol. 2012, 46, Pages 2460–2466
- [2] I. Aloisi, A. Di Giuliano, A. Di Carlo, P.U. Foscolo, C. Courson, K. Gallucci, Sorption enhanced catalytic Steam Methane Reforming: Experimental data and simulations describing the behaviour of bi-functional particles, Chemical Engineering Journal, 314, 2017, Pages 570-582
- [3] R.-Y. Chein, C.-Yu Wang, C.-T. Yu, Parametric study on catalytic tri-reforming of methane for syngas production, Energy, 118, 2017, Pages 1-17
- [4] L. Duan et al., Study on a new IGCC (Integrated Gasification Combined Cycle) system with CO<sub>2</sub> capture by integrating MCFC (Molten Carbonate Fuel Cell), Energy 2015, 87, Pages 490-503
- [5] B. Bosio, N. Di Giulio, S.W. Namb, A. Moreno, An effective semi-empiric model for MCFC kinetics: Theoretical development and experimental parameters identification, Hydrogen Energy, 2014
- [6] S. Stendardo, P.U. Foscolo, M. Nobili, S. Scaccia, High quality syngas production via steam-oxygen blown bubbling fluidised bed gasifier, Energy, March 2016
- [7] D. P. Hanak, E. J. Anthony and V. Manovic, A review of developments in pilot-plant testing and modelling of calcium looping process for CO<sub>2</sub> capture from power generation systems, Energy Environ. Sci., 8, 2015, Pages 2199-2249
- [8] C.-W. Lee, M. Lee, M.-J. Lee, S.-C. Chang, S.-P. Yoon, H. C. Ham, J. Han, Effect of the flow directions on a 100 cm<sup>2</sup> MCFC single cell with internal flow channels, Hydrogen Energy, 41, 2016, Pages 18747-18760

## COMPUTATIONAL FLUID-DYNAMICS MODELLING OF BIOMASS GASIFICATION IN A FLUIDIZED BED REACTOR

F. Cipiti\*, G. Urbani\*, S. Maisano\*, G. Giacoppo, V. Chiodo\*

\* Institute CNR-ITAE, Via S. Lucia sopra Contesse n. 5, 98126 S. Lucia, Messina, (Italy)

**Abstract** - The present work concerns with Computational Fluid-dynamics modelling of biomass gasification in a fluidized bed reactor, where a dispersed phase, consisting of solid particles, is fluidized by air (fluid phase) and transported upwards through a vertical riser.

The main aims of the mathematical model were to optimize the reactor geometrical key parameters (diameter and length of bed, diameter and shape of the dispersed phase, etc.) by parametric analysis, investigating the impact of gasifier temperature and air supply in order to identify the best fluidized bed configuration. The design of the fluidized bed reactors required a comprehensive investigation in order to achieve complete information on conversion behaviour, for understanding the sources of performance limitations and identify possible means of process enhancement from the perspective of reactor configuration.

**Index Terms** - Biomass Gasification, Fluidized bed reactor, Computational fluid-dynamics, Momentum Transport Phenomena

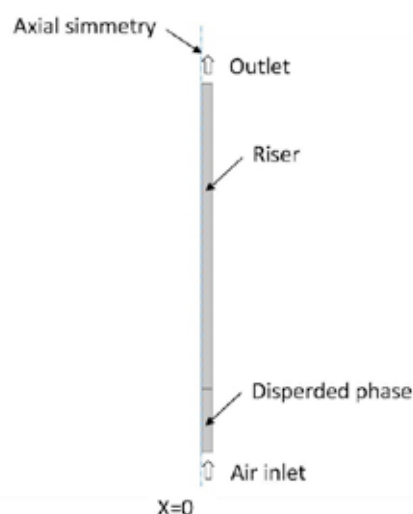
### I. INTRODUCTION

The design of a fluidized bed reactor is a key aspect for the performance and efficiency of a biomass gasifier: the reactor should be able to work under steady state, weight and volume should be minimized and the heat management system optimized for different operating conditions. Based upon the above considerations, a mathematical model, based on momentum balances, has been developed. The mathematical simulations were achieved through the description of transport phenomena by Partial Differential Equations (PDEs), numerically solved through the Finite Element Methods (FEM), using a commercial software package Comsol Multiphysics. In particular, the paper presents a two-dimensional model using a disperse method that does not explicitly track the position of the interface between the two fluids, but instead tracks the volume fraction of each phase, thus lowering the computational load. The model simulates the flow of two continuous and fully interpenetrating incompressible phases. This model requires the resolution of two sets of Navier-Stokes equations, one for each phase, in order to calculate the velocity field for each phase.

The volume fraction of the dispersed phase is tracked with an additional transport equation.

### II. MODEL DEFINITION

The main advantage of this finite-element approach is the possibility to easily adapt the model to different reactor geometry, allowing an accurate design.



**Fig. 1. Geometrical model in the mathematical simulations.**

Fig. 1 shows the geometry of the fluidized bed, and schematically describes its means of operation. The fluid phase, consisting of air is injected at the bottom of the bed. The dispersed phase, particles with a diameter of 0.5 mm are fluidized by the gas flow and transported upwards. The reactor



is rotationally symmetric, which implies that we need to model a rotational cross section of it. Table 1 summarizes the bed geometries and the properties of the phases.

TABLE I  
Fluidized bed properties

Property	Value
Particle diameter	0.5 mm
Particle density	1540 kg·m <sup>-3</sup>
Gas density (air)	1.2 kg·m <sup>-3</sup>
Gas dynamic viscosity (air)	1.8·10 <sup>-5</sup> kg·m <sup>-3</sup>
Gas inlet velocity	0.03638 m·s <sup>-1</sup>
Reactor diameter	0.027 m
Bed height	0.475 m
Initial dispersed phase column height	0.0817 m

Both phases are modeled as inter penetrating continua governed by a separate set of Navier-Stokes equations. The model includes a transport equation or the dispersed-phase volume fraction. The viscosity of the dispersed phase is defined as [1]:

$$(1) \mu_d = 0.5 \phi_d$$

where  $\phi_d$  is the dispersed-phase volume fraction.

Assume the momentum transfer to be dominated by the drag force and the drag acting on each phase is given by a drag coefficient  $\beta$  in the manner of

$$(2) F_{\text{drag},c} = -F_{\text{drag},d} = \beta u_{\text{slip}}$$

Here, the subscripts “d” and “c” indicate properties of dispersed continuous phase, respectively, and the slip velocity is defined as

$$(3) u_{\text{slip}} = u_d - u_c$$

To model the drag coefficient, the Gidaspow drag model has been used [2]:

$$(4) \beta = \frac{3\phi_c\phi_d\rho_c C_{\text{drag}}}{4d_d} |\mathbf{u}_{\text{slip}}| \phi_c^{-2.65}$$

for  $\phi_c > 0.8$ , and

$$(5) \beta = 150 \frac{\mu_c \phi_d^2}{\phi_c d_d^2} + 1.75 \frac{\phi_d \rho_c}{d_d} |\mathbf{u}_{\text{slip}}|$$

for  $\phi_c < 0.8$ .

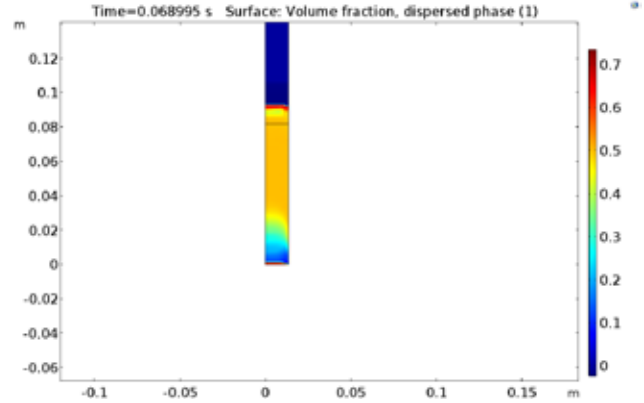
Initially all dispersed particles are positioned in a packed bed section at the bottom, of the column.

The inlet velocity is gradually ramp up as a function of time at the start of the simulation in order to avoid discontinuity with the initial velocity, using a smoothly varying rectangle function to define the packed bed column. To fluidize the bed, air is injected at the bottom: in order to assure that the initial dispersed volume fraction around the inlet matches the inlet dispersed fraction, the dispersed phase volume fraction at the inlet is set to zero. Moreover, to avoid large transient effects at the start of the simulation, the gravity is ramp up as a function of the time. In order to avoid that some particles settle towards the bottom of the reactor, a continuous phase through the inlet

has been introduced and no-slip condition has been set for the dispersed phase. In this way, the dispersed phase can settle on the bottom without conflicting with the inlet condition. For both phases, a pressure normal low condition has been used. Along the solid bed walls, a no-slip condition has been applied for the continuous phase and a slip condition for the dispersed phase.

### III. PRELIMINARY RESULTS

Fig. 2 shows a snapshot of the dispersed phase volume fraction during the start-up at the beginning of the simulation. The packed bed section is pushed upwards by the air, primarily in the center of the bed.



**Fig. 2. A snapshot of the dispersed phase volume fraction at the beginning of the simulation**

### IV. CONCLUSIONS

A simulation model based on Computational Fluid-dynamics, in order to investigate biomass gasification in a fluidized bed reactor has been successfully developed. A comprehensive sensitivity analysis is on-going.

### REFERENCES

- [1] N. Yang, W. Wang, W. Ge, and J. Li, “CFD simulation of concurrent-up gas-solid low in circulating beds with structure-depending drag coefficient”, Chemical Engineering Journal, vol. 96, pp. 71-80, 2003.
- [2] D. Gidaspow, Multiphases Flow and Fluidization, Academic Press, San Diego, 1994.

## FUEL CELLS & HYDROGEN RESEARCH IN EUROPE

L. Antoni\*, O. Jedicke\*

\* Hydrogen Europe Research, 98, rue du Trône, B-1050 Brussels,  
(Belgium)

**Abstract** - The European association of research organizations active in fuels cells and hydrogen (FCH), N.ERGHY, recently decided to change its name to Hydrogen Europe Research and to work hand in hand with Hydrogen Europe. Hydrogen Europe [1] is therefore now the common banner at European level under which three pillars - 110 industrial companies (large groups as well as SMEs), 69 research organizations, and 9 national associations – develop together and promote FCH technologies, as well as push for the right regulatory framework across EU Member States. This paper presents the active role, the main results of Hydrogen Europe Research obtained during the FCH 2 Joint Undertaking [2] and its future outlook to ensure Europe to be a major manufacturer of components and systems in the global competition, mastering security and safety of products for EU citizens in areas such as hydrogen and fuel cells.

**Index Terms** – Fuel Cells, Hydrogen, Hydrogen Europe Research, FCH Joint Undertaking

### I. INTRODUCTION

Hydrogen is a key enabler of the energy transition, as an essential vector for energy, industry, transport and residential sectors. Hydrogen is indeed the only zero-emission energy vector with electricity. Hydrogen links different energy sectors and energy T&D networks and thus increases the operational flexibility of future energy systems. EU clean power and emissions targets cannot be achieved without hydrogen as stated by 10 “Fortune 100” EU CEOs.

The FCH Joint Undertaking, as a Public Private Partnership instrument, has allowed to structure a strong ecosystem of an industry group “Hydrogen Europe” of 110 companies and a research group “Hydrogen Europe research” of 69 research centers and universities from 18 member states to deliver impactful innovations leading to European market growth, job creation, enhanced international competitiveness and benefits to society in the field of Hydrogen and Fuel Cell technologies.

### II. HYDROGEN EUROPE RESEARCH

The Association was formed and founded in 2008 by players of the European research community active in the field of fuel cells and hydrogen. It has voted on July 11, 2017 during the 20<sup>th</sup> General Assembly the change of its name from “New European Research Grouping for Fuel Cells and Hydrogen” (N.ERGHY) to “Hydrogen Europe Research” and to work hand in hand with Hydrogen Europe, its industry association counterpart. Hydrogen Europe has, in parallel during its general assembly in June, created an additional board seat for the President of Hydrogen Europe Research. This will ensure better coordination and follows a similar move from major European national and regional FCH associations who joined Hydrogen Europe last autumn, and are now also represented in Hydrogen Europe’s board.

Hydrogen Europe will therefore now be the common banner at European level under which three pillars: industry, national associations and research organizations will together develop and promote FCH technologies, as well as push for the right regulatory framework across EU Member States.

#### A. Objectives of Hydrogen Europe Research

The main objectives of Hydrogen Europe Research is:

- to promote, support and accelerate the deployment of hydrogen and fuel cell technology by aligning the European R&D community and representing it as a whole and by providing a stronghold for cooperation with industry increasing the impact of research;
- to address critical technical barriers to foster Hydrogen & Fuel Cells technologies to achieve commercialization (TRL 3-6);
- to propose clear Research and Innovation targets for the future (TRL 1-3).
- to educate, train engineers, technicians and operators and

Copyright © 2017

thus to ensure a qualified manpower the FCH .

The objectives include in particular:

a) representation and participation in the FCH Joint Undertaking.

b) scientific representation of the European FCH research community in the European Framework programme, e.g. Horizon 2020.

Hydrogen Europe Research pursues its objective inter alia by conducting the following activities in the field of FCH:

a) providing expertise and advice to stakeholders, e.g. industrial companies, the European Commission and its Member States, local and regional actors about the results and needs of European FCH research;

b) actively participating as a Partner in the creation and implementation of the FCH Joint Undertaking and in its decision process;

c) reaching a better gathering of the above-mentioned research community by promoting existing research competences, facilities and expertise and maintaining a respective knowledge base for its Members and third parties;

d) formulating joint views on existing and future needs in research infrastructures and programmes; special attention is being drawn to the interrelation and cooperation between break-through and applied research, with the support of national and European programmes;

e) issuing any other coordinated positions of the research community and representation of the interests of its Members as research organisations and the research community in general towards third parties.

#### *B. Some success stories:*

a. **Hydrogen electrolyzers allow to integrate renewable energy:** Europe is world leader in low and high temperature electrolysis which transform intermittent green electrons into a green gas. In seven years' time the max capacity increased by >100 times (150kW -> 20 MW) with serious cost reductions owing to new materials developments and increased performance and durability;

b. **Kick start of a stack manufacturing industry for automotive applications :** the "EU stack" brand and design that was created through different European research projects has led to German OEM's decision to bring the results into industrialisation aiming for 30.000 units/year, creating the first EU supply chain soon;

c. **EU leads in most advanced stationary power fuel cells:** EU masters Solid Oxide Fuel Cells (SOFC) technology with 5 top companies producing  $\mu$ CHP. R&D at EU level has led to drastic cost reduction which is backed now by new subsidies programs at national level (e.g. D, UK, FR...)

d. **Pre-normative research** provides solid information to improve and develop standards at international level (ISO, IEC), contributing to develop an adequate regulatory

framework.

#### *C. Future Outlook beyond 2020: a competitive manufacturing in Europe*

Europe can be a major manufacturer of components and systems in the global competition, mastering security and safety of products for EU citizens in areas such as hydrogen and fuel cells.

- to succeed, research technological organizations (RTOs) and universities must be first positioned at the forefront of innovation, combining technological and financial resources with the mission of safeguarding the welfare of EU citizens.

- second these R&D efforts need to be backed by the implementation of a strong industrial base to ensure a clear European value chain in the sector, and to create sustainable value add in Europe via highly-qualified jobs and great products.

- EU must fight to keep the control of the production of critical components of products within Europe starting with some pilot lines. Of particular importance are the efforts on key critical components, materials and systems which will sustain an increasing demand for them, and trigger volumes which will then lead to cost reductions.

It is therefore crucial to prepare the next generations of innovation, products and services for EU to remain in the global competition and to support and even to enhance breakthroughs and basic researches in the next decade.

### III. CONCLUSION

Hydrogen and Fuel Cells are part of the European energy transition. A strong, competitive Research and Innovation coordinated by Hydrogen Europe Research in close collaboration with European Industry is essential to foster commercialization. As progress in Research & Innovation is worldwide, all the strength of European Research & Innovation is needed and a sustainable European support is crucial to keep Europe in the top players.

### ACKNOWLEDGMENT

Hydrogen Europe Research acknowledges the European Commission for its strong and durable support to the European FCH community in particular through the FCH Joint Undertaking.

### REFERENCES

- [1] <http://www.hydrogeneurope.eu>
- [2] <http://www.fch.europa.eu>

Copyright © 2017

## NUMERICAL INVESTIGATION FOR 1KW-CLASS FT-SOFC SYSTEM TO EVALUATE THE COMPACT SIZE INTEGRATED HOTBOX DESIGN

Kashif Rashid\*\*, Sang Keun Dong\*\*

\* Department of Energy System Engineering, Korea University of  
Science and Technology (UST), Daejeon 34113 (Republic of Korea)

\*\* Thermal Energy System Laboratory, Korea Institute of Energy  
Research (KIER), Daejeon 34129 (Republic of Korea)

**Abstract** - A comprehensive CFD and experimental investigations are performed on the integrated hotbox components to determine its compactness and suitability for 1 kW-class SOFC stack system. CFD model first implemented on the standalone reformer to determine the heat energy required for desired reformat composition than in the second step, simulations using validated model has also been performed on the real-scale integrated hotbox components to ascertain the performance and effectiveness of the design. Anode and cathode off-gases are burnt in the combustor to provide the necessary energy. Numerical calculations on different heat exchanger designs are also performed separately by fixing the boundary conditions obtained from experiments. From the numerical calculations on the full-scale system, it is found that SOFC operating at a temperature of 750°C and S/C of 2.75, a combined mole fraction of H<sub>2</sub> and CO ~0.80 (methane conversion of 76%) is obtained which is comparable to the electrically-heated reformer results.

**Index Terms** – Combustor, hotbox, Solid oxide fuel cell, steam reformer

### I. INTRODUCTION

Fuel cell based energy conversion technologies have shown great promise over the conventional power generation systems due to their higher efficiencies and low pollutant emissions [1]. SOFC's have been utilized in diverse applications ranging from an auxiliary power unit (APU) to large-scale residential power plants (RPG) [2]. In the SOFC stack design, it has been of great consideration to avoid a dedicated hydrogen supply; a fuel processing system integrated into the stack is a prime objective, which can generate H<sub>2</sub>/CO rich gas by reforming natural gas (NG) and lower hydrocarbons [3]. Here we report the design and analysis of a compact 1kW-class SOFC based power generation system with higher system efficiency and very compact size. Apart from the afterburner-reformer integration, steam generation tubes and heat exchangers (for preheating of

cathode air) are also incorporated in the hotbox design to maximize the system waste heat recovery. The numerical and experimental analysis on the integrated hotbox components are performed to evaluate its compactness and suitability for 1 kW-class SOFC stack system fueled with methane.

### II. DESCRIPTION OF HOTBOX AND MODELING STRATEGY

The hotbox system for 1 kW class SOFC stack is shown in Fig.1. The present analysis was performed in two steps; firstly a CFD model is executed on a standalone reformer (shown in Fig. 2) to ascertain the heat energy requirement for the reforming process. The numerical model is then validated with experimental data (obtained on the standalone reformer placed in the furnace) at different gas hourly space velocities (GHSV). After the validation of the numerical model, simulations are performed on a real size integrated hotbox components (steam generating tube, reformer, and combustor) to ascertain the performance and effectiveness of this design. In the second part of the study, two different heat exchanger (HX) designs are considered for optimal exchange of thermal energy of the stack and the BOP components.

Several models for steam reforming have been reported in the literature, however, the intrinsic kinetics expressions presented by Xu and Froment [4] are utilized in the present modeling.

### III. RESULTS AND DISCUSSION

To validate the numerical model, simulated results were compared with the experimental data performed on a standalone steam reformer. Experiments were performed at a furnace temperature of 700°C and the effectiveness factors were used to tune the simulation results. The simulated reformed gas composition is compared with the experimental composition and their comparison is evaluated in Table I.



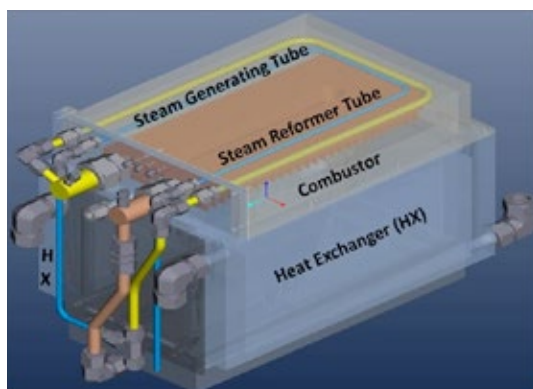


Fig. 1. Integrated Hotbox Design

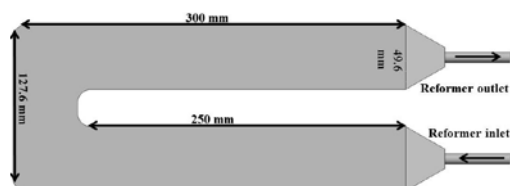


Fig. 2. Standalone Steam Reformer

TABLE I. Validation of numerical model

	Exp.		Sim.		Rel. Err.
	Mol%	LPM	Mol%	LPM	
H <sub>2</sub>	71.1	15.6	68.4	14.29	3.8
CH <sub>4</sub>	7.1	0.45	6.65	1.39	6.30
CO	10.0	2.88	10.25	2.14	2.45
CO <sub>2</sub>	11.8	1.94	12.12	2.53	2.71
CH <sub>4</sub> Conv (%)	75.4		75.9		0.74

#### A. Effect of temperature on standalone reformer

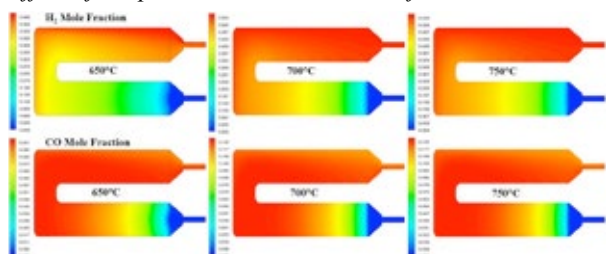


Fig. 3. Effect of GHSV on temperature

#### B. Effect of gas velocity (GHSV)

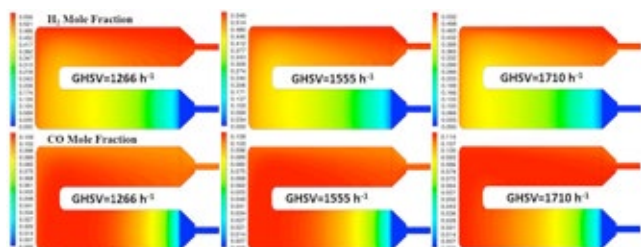


Fig. 4. Effect of GHSV on syngas concentration

#### C. Integrated burner reformer

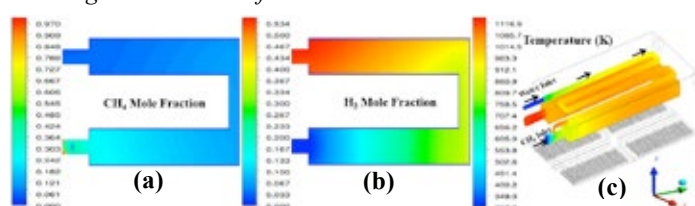


Fig. 5. (a, b) Species contour distributions in the middle plane of integrated reformer (c) Temperature distribution at the outer walls of SG and reformer

#### CONCLUSIONS

A CFD modeling was performed on the integrated hotbox components to determine its compactness and suitability for 1 kW-class SOFC stack system. The simulated results have shown that the performance of integrated reformer is comparable to those of standalone reformer tested in an electrical furnace. The methane conversion recorded in the integrated reformer system is 76.1% with syngas (H<sub>2</sub>+CO) concentration comprise of 80.81% (vol. %). The standalone reformer also exhibited similar results while operating at a temperature of 700°C i.e. methane conversion 75.4% and syngas concentration 79.89%. The results of integrated reformer combustor if evaluated with the standalone reformer show good match both in terms of reformed gas composition and methane conversion. These results reflect that the integrated hotbox system has fulfilled the energy requirements from the internal heat source and obviate any need of external energy supply.

#### ACKNOWLEDGMENT

The author gratefully appreciates the financial support of the Ministry of Trade, Industry and Energy, MOTIE (Grant No. R0002207).

#### References

- [1] S. Kang, K. Lee, S. Yu, S. M. Lee, and K. Y. Ahn, *Appl. Energy*, volume 114, 2014, pp. 114–123.
- [2] L. Venturelli, P. E. Santangelo, and P. Tartarini, *Appl. Therm. Eng.*, volume 29, 2009, pp. 3469–3475.
- [3] T. G. Ghang, S. M. Lee, K. Y. Ahn, and Y. Kim, *Int. J. Hydrogen Energy*, volume 37, 2012, pp. 3234–3241.
- [4] J. G. Xu and G. F. Froment, *Aiche J.*, volume 35, 1989, pp. 88–96.

EFC17188

## ELECTROCATALYST DERIVED FROM IRON SALT AND BENZ- AND AMINOBENZIMIDAZOLE PRECURSORS: APPLICATIONS IN MICROBIAL FUEL CELL CATHODES.

Barbara Mecheri\*, Rohan Gokhale\*\*, Carlo Santoro\*\*, Maida Aysla Costa de Oliveira\*, Alessandra D'Epifanio\*, Silvia Licoccia\*, Alexey Serov\*\*, Kateryna Artyushkova\*\*, Plamen Atanassov\*\*

\* Dept. Chemical Science and Technologies, University of Rome Tor Vergata, Via della Ricerca Scientifica, 00133, Rome, Italy.

\*\* Dept. Chemical and Biological Engineering, Center for Micro-Engineered Materials (CMEM), Advanced Materials Lab, 1001 University Blvd. SE Suite 103, MSC 04 2790, Albuquerque, NM 87131, University of New Mexico, USA.

**Abstract** – In this work, novel catalysts derived from iron and benzimidazole and aminobenzimidazole were synthesized using Sacrificial Support Method (SSM). The catalysts obtained were then tested in rotating ring disk electrode (RRDE) technique and compared with AC. Fe-based catalysts had performances much higher compared to AC and therefore are suitable for microbial fuel cell (MFC) applications. Future works will integrate the catalysts into air-breathing cathodes and test them in MFCs.

**Index Terms** – Oxygen reduction reaction (ORR), platinum group metal-free (PGM-free), neutral media electrolyte, microbial fuel cell (MFC)

### I. INTRODUCTION

Microbial fuel cell (MFC) is an interesting technology capable of degrading organic pollutants and producing useful electricity. In general, the organics are electro-oxidized into carbon dioxide, protons and electrons by electroactive bacteria. Those specific microorganisms colonize the anode electrode and are able to release the electrons from the oxidation reaction directly to the electrically conductive electrode, while protons are simultaneously released into the solution. Electrons move through the external circuit generating useful electricity. The reduction reaction occurs at the cathode in which an oxidant is reduced [1].

For several reasons such as high potential and natural availability at no additional cost, oxygen is the most used oxidant. Due to the high overpotential required for the oxygen reduction reaction (ORR) in neutral media, the addition of the catalyst is needed in order to enhance the sluggish ORR kinetics. Bacterial catalysts suffer from low kinetics and the mechanisms are still debated. Enzymatic catalysts are excellent

in neutral media but the low durability discourages the utilization for long term operations. Abiotic catalysts are then the most preferred catalysts to be adopted in MFC devices. Platinum is a rare and expensive metal, which is easily can be poisoned in polluted environment and consequently is not suitable for MFCs applications. Despite the fact that high surface area carbonaceous materials can be an alternative to substitute Pt, their performances are low. Recently we reported that platinum group metal-free (PGM-free) catalysts seem to be very promising alternatives to Pt due to their high activity in neutral media and high stability to the poisonous environment [2,3]. Those catalysts are based on the utilization of atomically dispersed transition metals coordinated with nitrogen inside of 3D carbon matrix.

In this work, two novel iron based catalysts pyrolyzed using benzimidazole and aminobenzimidazole as nitrogen rich organic precursors were synthesized and studied in rotating ring disk (RRDE) electrode in neutral media. Further studies will be developed for incorporating those catalysts in air-breathing cathodes and tested in operating MFCs.

### II. MATERIAL AND METHOD

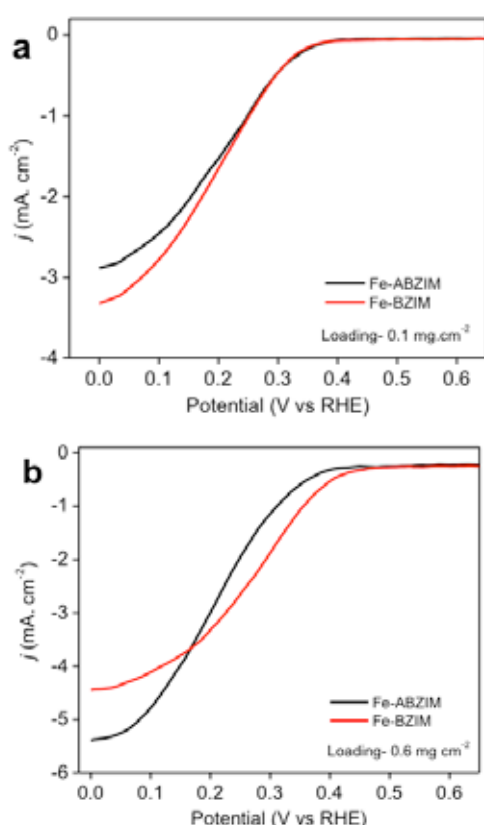
Two novel PGM-free Fe-N-C catalysts using sacrificial support method (SSM). Iron nitrate was mixed with benzimidazole and aminobenzimidazole respectively and then also with monodispersed silica used as template. The mixture was pyrolyzed at controlled temperature furnace at 900°C. The powder was inserted into a quartz tube in which inert atmosphere was present (UHP nitrogen) with a flow of 100 cm<sup>3</sup>min<sup>-1</sup>. After 45 minutes at stable temperature, the quartz

Copyright © 2017

tube was left to cool down till room temperature was reached. After this procedure, the powder was treated with HF in order to remove the silica template and create a catalyst three-dimensional structure. The powder was then washed to remove the HF and then dried. The last step consisted in grinding the catalyst using ball-milling.

Rotating ring disk electrode (RRDE) was used to study the catalyst kinetics towards ORR in neutral media. Two loadings of catalysts were applied ( $0.1$  and  $0.6 \text{ mg cm}^{-2}$ ). Activated carbon (AC) was used as control. The inks were applied on the disk and naturally dried. The electrolyte used was potassium phosphate buffer with pH of 7.5. The electrolyte was purged with oxygen before the utilization. The disk speed was 1600 rpm. Linear Sweep voltammetry (LSV) was run between 1 V and 0 V (vs RHE).

### III. RESULTS



**Fig.1** Disk current of two different loadings:  $0.1 \text{ mg cm}^{-2}$  (a) and  $0.6 \text{ mg cm}^{-2}$  (b).

LSVs shows that both Fe-ABZIM and Fe-BZIM performed better than AC since their onset potential, half wave potential and limiting current were superior compared to AC. The loading did not affect the trends despite an increase in loading brings to an increase in the half wave potential (**Fig. 1**). From those results, it can be noticed that Fe-BZIM had slightly higher

electrocatalytic activity compared to Fe-ABZIM. Fe-BZIM had an half wave potential of  $\sim 0.22 \text{ V}$  (vs RHE) and  $\sim 0.28 \text{ V}$  (vs RHE) at catalyst loading of  $0.1$  and  $0.6 \text{ mg cm}^{-2}$  respectively. In parallel, Fe-ABZIM had half wave potential of  $\sim 0.23 \text{ V}$  (vs RHE) and  $\sim 0.22 \text{ V}$  (vs RHE) at catalyst loading of  $0.1$  and  $0.6 \text{ mg cm}^{-2}$  respectively.

Peroxide production and electron transfer were also monitored (data not shown). The highest peroxide production was detected for AC while the lowest was measured for Fe-BZIM ( $\sim 4\%$ , loading  $0.6 \text{ mg cm}^{-2}$ ). It can be noticed that the peroxide produced generally decreased with the increase in catalyst loading. This might be due to the peroxide trap and further reduced within the thick catalyst layer. In parallel also the electron transfer tends to have a  $4e^-$  mechanism with the number of electrons that increases with the loading indicating a more probable  $2x2e^-$  mechanism.

Further investigations will focus on the integration of those catalysts in air-breathing cathodes and operated in microbial fuel cells. The performances will be compared with the performances of activated carbon catalyst that is by far the most utilized cathode in literature.

### IV. CONCLUSION

Oxygen reduction reaction kinetics study of Fe-based catalyst was performed in neutral media. Fe-BZIM and Fe-ABZIM performed much better compared to AC in terms of onset potential, half wave potential and limiting current. Those catalysts will be tested in microbial fuel cells once integrated in air-breathing cathodes.

### ACKNOWLEDGMENT

UNM authors would like to thank the Bill & Melinda Gates Foundation grant: “Efficient Microbial Bio-electrochemical Systems” (OPP1139954). UTV authors thank the Conselho Nacional de Desenvolvimento Científico e Tecnológico (CNPq, Brazil): grant n.200631 - 2015/2.

### REFERENCES

- [1] Santoro, C., Arbizzani, C., Erable, B., Ieropoulos, I., Microbial fuel cells: From fundamentals to applications. A review, *Journal of Power Sources*, Volume 356, 2017, pp. 225-244.
- [2] Nguyen, M.-T., Mecheri, B., Iannaci, A., D'Epifanio, A., Licoccia, S., Iron/Polyindole-based Electrocatalysts to Enhance Oxygen Reduction in Microbial Fuel Cells, *Electrochimica Acta* Volume 190, 2016, pp. 388-395
- [3] Santoro, C., Gokhale, R., Mecheri, B., D'Epifanio, A., Licoccia, S., Serov, A., Artyushkova, K., Atanassov, P., Design of Iron(II) Phthalocyanine-Derived Oxygen Reduction Electrocatalysts for High-Power-Density Microbial Fuel Cells, *ChemSusChem*, Volume 10, 2017, pp. 3243 – 3251.

# DEVELOPMENT OF PEFC POWER GENERATION SYSTEM FOR BY-PRODUCT HYDROGEN PRODUCED FROM A CAUSTIC SODA PLANT

Takahide Haneda\*

\* Tokyo Gas., Ltd, Energy System Research Institute, 1-7-7,  
Suehiro-cho, Tsurumi-ku, Yokohama, Kanagawa, (Japan)

**Abstract** – The utilization of by-product hydrogen produced from the caustic soda plant is not efficient for the plant from economic and environmental viewpoints. Therefore, we proposed a new energy system for the caustic soda plant that comprises a hydrogen-fueled PEFC and a boiler. The objective of this study is to evaluate the potential for saving energy of the energy system. The installation effect of the energy system was clarified based on the simulation with mathematical model. Moreover, we started the demonstration test for the hydrogen-fueled PEFC system with power output of 100 kW to clarify the influence of impurities in the hydrogen to the system.

**Index Terms** – PEFC, energy system, by-product hydrogen, caustic soda plant,

$h_d(t)$	kWh	Hydrogen for PEFC
$n$	Year	Payout time
$p_1$	kW	Capacity of boiler
$p_2$	kW	Capacity of PEFC

## II. INTRODUCTION

In a caustic soda plant, Sodium hydroxide (NaOH) is manufactured that also produce hydrogen by the electrolysis of brine, a salt solution. While NaOH are considered to be valuable products of this process, hydrogen is often discarded as waste stream or used for heat production, except when a neighboring chemical plant can use the hydrogen as a chemical feedstock<sup>[1]</sup>. The utilization of by-product hydrogen is not efficient for the plant from economic and environmental viewpoints. On the other hand, the power production through polymer electrolyte fuel cells (PEFC) is the most environmentally responsible way to utilize the hydrogen because it brings quite high efficiency. In the case to supply city gas to the plant instead of hydrogen for heat production and to supply hydrogen to the hydrogen fueled PEFC system (H2-PEFC), the exergy vastly can be improved and the energy consumption in the plant can be vastly reduced.

The objective of the present study was to evaluate the potential for saving energy of the energy system, which is composed of a H2-PEFC and a boiler, using by-product hydrogen produced from a caustic soda plant. The first scope of this work was to optimize the equipment capacity and the energy balance to minimize the system cost including the energy cost and amortization cost of the energy system based on mathematical model<sup>[2]</sup>. The second scope of this work was to clarify the influence of impurities in the hydrogen to the H2-PEFC with power output of 100 kW based on demonstration

## I. NOMENCLATURE

Symbol	Unit	Definition
$c_1$	\$/kWh	Specific and base cost of power grid
$c_2$	\$/kWh	Specific and base cost of natural gas
$c_3$	\$/kWh	Investment cost per capacity by PEFC
$CT$	\$/year	Total cost
$CT_1$	\$/year	Operation cost
$CT_2$	\$/year	Investment cost
$d_1(t)$	kWh	Heat demand
$d_2(t)$	kWh	Power demand
$e_1$	%	Heat generation efficiency of boiler
$e_2$	%	Heat generation efficiency of PEFC
$e_3$	%	Power generation efficiency of PEFC
$f_1(t)$	kWh	Natural gas for boiler
$f_2(t)$	kWh	Heat generated by boiler
$f_3(t)$	kWh	Heat generated by PEFC
$f_4(t)$	kWh	Heat for boiler
$f_5(t)$	kWh	Waste heat
$f_6(t)$	kWh	Power generated by PEFC
$h_1(t)$	kWh	Hydrogen generated by Electrolyzer
$h_2(t)$	kWh	Waste hydrogen
$h_3(t)$	kWh	Hydrogen for boiler



test.

### III. PEFC POWER GENERATION SYSTEM

The PEFC power generation system is composed of a H2-PEFC and a boiler. The H2-PEFC generates power and hot water from by-product hydrogen produced from the plant. The boiler generates all its steam for the plant from natural gas and the remaining by-product hydrogen produced from the plant that is not consumed by the H2-PEFC.

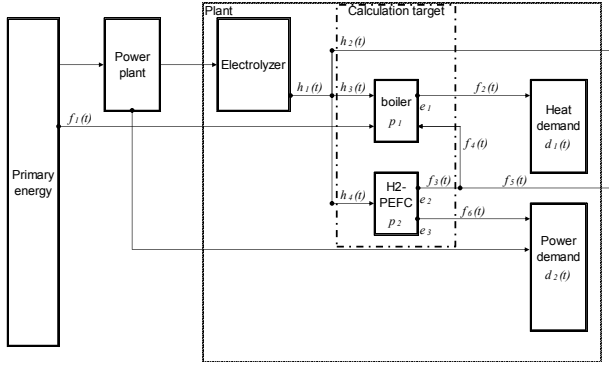


Fig.1. Configuration of PEFC power generation system

### IV. MATHEMATICAL MODEL

The capacity and the energy balance of H2-PEFC and boiler were set to satisfy Eq. (1)-(7), which means all steam was generated by the energy system from city gas and by-product hydrogen produced from the plant. Hot water generated by the H2-PEFC supplied boiler as water supply preheating and the remaining was set waste heat. Mixing rate of by-product hydrogen to city gas for boiler was set under 50%. The objective function was to minimize the system cost of the energy system including the energy cost and the amortization cost, which was defined with Eq. (8)-(10).

$$f_2(t) = e_1 \times (f_1(t) + f_4(t) + h_3(t)). \quad (1)$$

$$f_4(t) + f_5(t) = e_2 \times h_4(t). \quad (2)$$

$$f_6(t) = e_3 \times h_4(t). \quad (3)$$

$$d_1(t) = f_2(t). \quad (4)$$

$$d_2(t) \geq f_6(t). \quad (5)$$

$$h_1(t) = h_2(t) + h_3(t) + h_4(t). \quad (6)$$

$$f_1(t) \geq h_3(t). \quad (7)$$

$$CT = CT_1 + CT_2. \quad (8)$$

$$CT_1 = \Sigma (c_2 \times (f_1(t)) - (c_1 \times (f_6(t)))). \quad (9)$$

$$CT_2 = (c_3 \times p_2) / n \quad (10)$$

### V. RESULTS AND DISCUSSIONS

#### A. SIMULATION RESULT

The optimal solution for the equipment capacity and the energy balance in the PEFC power generation system was calculated on various power generation efficiencies of the H2-PEFC based on linear programming as the objective function to minimize the system cost. The system cost reduction rate as compared to the conventional system which is composed of a

boiler without the H2-PEFC at the optimization in the PEFC power generation system was shown in Fig.2. As a result, the system cost reduction compared to the conventional system have been clearly shown to be an initial cost lower than 4500 \$/kW or a power generation efficiency greater than 55%.

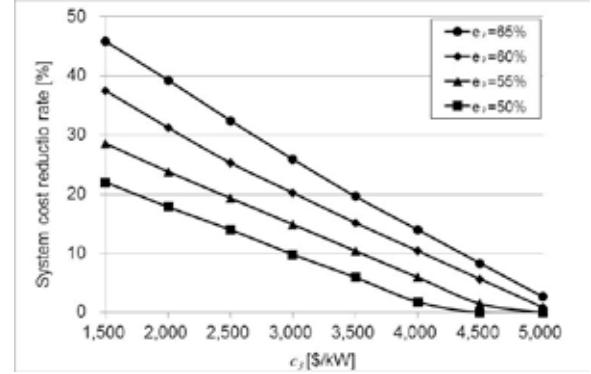


Fig.2. Correlation between the system cost ( $c_3$ ) and the initial cost on various power generation efficiencies ( $e_2$ ) of the H2-PEFC in the PEFC power generation system.

#### B. DEMONSTRATION RESULT

We started the demonstration test for the H2-PEFC with power output of 100 kW that uses by-product hydrogen. The demonstration test mainly has aimed to clarify the components, concentrations of impurities in the hydrogen and to look at the effect of impurities in the hydrogen on the H2-PEFC. As a result, we will find some technical issues and the policies for countermeasures against impurities in the hydrogen. Additionally, we will optimize the operation condition for the PEFC system to maximize the installation effect. To achieve this, we will take into consideration the partial load efficiency and change in the voltage due the influence of the impurities in hydrogen, the operation rate of the H2-PEFC.

### VI. CONCLUSION

The installation effect of the PEFC power generation system for a caustic soda plant have been clarified based on the simulation with mathematical model. Moreover, the technical issues and policies for countermeasures against impurities in the hydrogen will be found based on the demonstration test using the H2-PEFC with power output of 100 kW.

### REFERENCES

- [1] Fukuoka Masao, Utilization of hydrogen from Chlor-alkali industry in Japan, Hydrogen energy system, 28(2013), pp.16-22 [in Japanese].
- [2] Takahide Haneda, Atsushi Akisawa, Technological assessment of PEFC power generation system using by-product hydrogen produced from a caustic soda plant, International Journal of Hydrogen Energy, 42 (2017), pp. 3240-3249.



## SYN-GAS PRODUCTION BY BFB GASIFICATION: EXPERIMENTAL INVESTIGATION OF DIFFERENT FEEDSTOCKS

F. Urbani\*, S. Maisano\*, N. Mondello\*, F. Cipiti\* and V. Chiodo\*

\*Institute CNR-ITAE, via Salita S. Lucia sopra Contesse 5, 98126 – Messina (Italy)

**Abstract** - The Gasification process is considered one of the most promising and efficient techniques to hydrogen production from biomass as carbon neutral emitter. Aim of the work was to exploit the potential of residual biomass, as citrus residues (from orange fruits industries) and *Posidonia Oceanica* (Mediterranean sea plant), those are different of traditional woody biomasses. Gasification experiments were performed in a bubbling fluidized bed reactor at 1023 K, 1 bar, ER=0.3, and various steam to biomass inlet ratio ( $0.5 < S/B < 1.0$ ) in order to investigate the influence of these parameters on syngas composition and hydrogen yield. Experimental results highlighted an improvement of the gasification performances in terms of syngas and  $H_2$  production with increasing of Steam to Biomass (S/B) inlet ratio (2.1 to 2.63  $Nm^3/kg_{biomass}$  and 0.25 to 0.65  $Nm^3/kg_{biomass}$  respectively) than gasification tests performed with only air (1.91 to 2.27  $Nm^3/kg_{biomass}$  and 0.17 to 0.20  $Nm^3/kg_{biomass}$  respectively). In particular, *Posidonia Oceanica* showed the best rates both of syngas and of hydrogen yields (2.63  $Nm^3/kg_{biomass}$  and 0.65  $Nm^3/kg_{biomass}$ , respectively).

**Index Terms** - Hydrogen Production, BFB Air/Steam Gasification, *Posidonia Oceanica*, Citrus Residues.

### I. INTRODUCTION

In these recent years, the exploitation of biomasses in order to reduce the fossil-derived fuel has gained the attention of many researchers. In fact, biomass is a very important source for promoting the use of renewable energy. The main biomass conversion technologies, for biofuels production, include thermochemical conversion processes as pyrolysis and gasification [1]. Among the different gasification layouts, the Bubbling Fluidized Bed (BFB) system has resulted the best operational way to optimize the process in terms of syngas production [2]. Concerning to feedstock sources, additional environmental benefits could be achieved by using by-products, residual biomasses or wastes. Indeed, using residues could reduce the costs of feedstock supply, the amount of landfilled materials and the costs for waste management.

In this way, our investigation reports an experimental comparative study on the feasibility to convert by air-steam gasification process, different feedstocks as White-pine wood, *Posidonia Oceanica* (Mediterranean sea plant) and citrus residues (derived from orange fruits industries) in order to achieve an hydrogen-rich syngas suitable for energy production in fuel cell applications.

### II. EXPERIMENTAL

All biomasses were preventively air-dried (White-pine wood at 383 K for 6 h and *Posidonia Oceanica* and Citrus residues at 353 K for 16 h), shredded and sieved into a grain size range of  $0.4 < d < 1$  mm. Ultimate and proximate analysis were performed to determine chemical-physical characteristics of the samples (Table 1). In particular, the ultimate analysis were performed through a CHNS analyzer (Thermo Fisher Scientific, Flash EA 1112) while the thermogravimetric analysis (TGA) was adopted for the proximate analysis and to individuate the suitable operative temperature range to maximize the biomass oxidation reaction steps. TGA/DTG analysis were conducted in a temperature range from 298 K to 1173 K with a heating rate of  $10 K min^{-1}$  and under nitrogen atmosphere. Experimental were carried out in an atmospheric bench-scale fluidized bed (BFB) reactor (Height: 475 mm; Internal Diameter: 27 mm). Qualitative and quantitative analysis of the syngas was determined by a Pollution Vega micro-GC. In particular, the syngas composition was determined as the average composition of five measurements. All experiments were performed with an equivalence ratio (ER) equal to 0.3, in order to ensure the gasification and fluidization conditions, while various steam to biomass ratio (0, 0.50, 0.75 and 1.00 wt/wt) were investigated. In order to reduce the particles agglomeration and defluidization, due to the high ash content, it was decided to avoid gasification experiments at a high temperature. Hence, the reactor temperature was fixed at 1023 K.

TABLE I

		White Pine	Citrus Peel	Posidonia Oceanica
Proximate analysis (wt%)	Moisture	7.6	7.0	12.67
	V.M.	74.2	64.6	60.95
	C.F.	17.4	20.0	12.36
	Ash	0.87	9.0	14.02
Ultimate analysis (wt%) <sup>a</sup>	C	52.71	42.46	46.1
	H	5.95	6.24	6.82
	N	0.54	1.26	1.28
	S	0.2	0.13	0.3
	O <sup>b</sup>	39.53	40.85	31.41
H/C atom ratio		0.11	0.15	0.15
O/C atom ratio		0.74	0.96	0.64
HHV (MJ/kg)		19.3	17.8	18.1
LHV (MJ/kg)		18.3	16.6	17.2

a: dry basis b: by difference

### III. RESULT AND DISCUSSION

The effect of the experimental conditions on the syngas composition is shown in Figures 1a, 1b and Table II. The main syngas components ( $H_2$ ,  $CO$ ,  $CO_2$ ,  $CH_4$ ,  $N_2$ ) obtained from experimental tests, in terms of volume percentage, were reported in Table II. For all biomasses nitrogen volume percentage was reduced with the increase of steam to biomass ratio from 0.5 to 1.0 (wt/wt); the nitrogen volume percentage decreased from 60% to 42% promoting an higher syngas yield.

As expected for all samples, the carbon monoxide decreased (16.67 to 3.66 mol%), while carbon dioxide (14.47 to 20.60 mol%) and hydrogen (8.13 to 24.87 mol%) increased with S/B ratio, according to the involving of the water gas shift reaction.

TABLE II  
BIOMASSES OUTLET STREAM COMPOSITION (MOL %)

	S/B	N <sub>2</sub>	CO	CO <sub>2</sub>	CH <sub>4</sub>	H <sub>2</sub>
White-Pine	0	61.09	10.36	15.13	2.37	8.13
	0.5	60.75	6.45	17.70	1.92	12.18
	0.75	59.34	5.19	19.06	2.01	13.41
	1.0	59.22	3.66	19.98	1.87	14.27
Citrus Peel	0	52.60	12.40	18.30	3.70	10.50
	0.5	44.00	11.40	19.40	3.40	20.00
	0.75	42.40	9.90	19.60	2.70	23.80
	1.0	42.50	8.60	20.60	2.40	24.40
Posidonia Oceanica	0	55	16.67	14.47	3.04	8.49
	0.5	51.45	11.18	16.04	2.78	16.35
	0.75	49.08	6.20	18.06	2.33	22.57
	1.0	47.46	4.14	20.02	1.99	24.87

Figures 1a and 1b showed the effect of the S/B ratio on the syngas and hydrogen yields, calculated for each biomass.

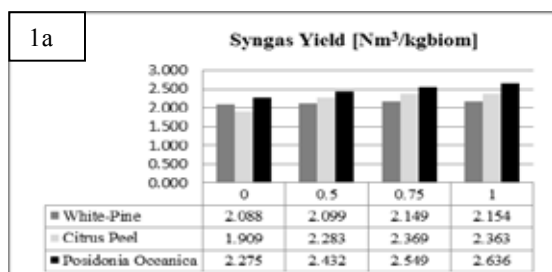


Fig. 1a - Syngas Yield

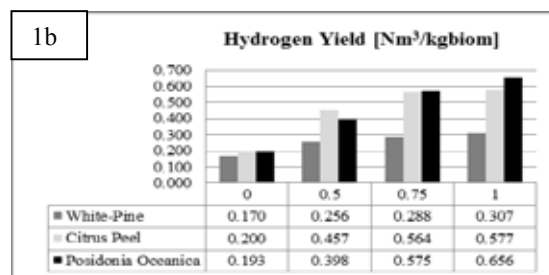


Fig. 1b - Hydrogen Yield

In air gasification conditions the syngas yield was almost the same for everything samples but this changed when the steam is added. Indeed, the effect of the introduced steam led at evident increase of the syngas yield for the Citrus peels and Posidonia Oceanica (2.28 to 2.63  $Nm^3/kg_{biomass}$ ), while it was almost constant for the White Pine (2.09 to 2.15  $Nm^3/kg_{biomass}$ ). This means that, at 1023 K for the woody sample, the heterogeneous reactions are slow [3]. This lower wood reactivity was also evidenced by the weak effect of steam on the hydrogen concentration in the produced gas (table II), with a maximum value of 14.3mol% at S/B=1.

Posidonia Oceanica showed the best rates both of syngas and of hydrogen yields (2.63  $Nm^3/kg_{biomass}$  and 0.65  $Nm^3/kg_{biomass}$ , respectively).

### IV. CONCLUSION

Air-steam gasification highlighted an improving of the gasification performances for each biomasses, in terms of syngas and hydrogen yields (2.1 to 2.6  $Nm^3/kg_{biomass}$  and 0.2 to 0.6  $Nm^3/kg_{biomass}$  respectively); Posidonia Oceanica showed the best rates both of syngas and of hydrogen yields (2.63  $Nm^3/kg_{biomass}$  and 0.65  $Nm^3/kg_{biomass}$ , respectively), resulting to be a good biomass for hydrogen production by steam gasification tests.

### REFERENCES

- [1] Chiodo V., Zafarana G., Maisano S., Freni S., Urbani F., Pyrolysis of different biomass: Direct comparison among Posidonia Oceanica, Lacustrine Alga and White-Pine, Fuel Volume 164 2016, pp. 220-227.
- [2] Wang F., Zeng X., Wang Y., Yu J., Xu G., Characterization of coal char gasification with steam in a micro-fluidized bed reaction analyzer. Fuel Processing Technology, volume 141, 2016, pp. 2-8.
- [3] Nikoo M. B., Mahinpey N., "Simulation of biomass gasification in fluidized bed reactor using ASPENPLUS", Biomass and Bioenergy Volume 32, 2008, pp. 1245-1254

## NET-TOOLS, AN E-INFRASTRUCTURE TO COMPILE AND PROVIDE E-LEARNING CONTENT TO THE FCH-COMMUNITY

O. Jedicke\*, G. Cinti\*\*, E. Slavcheva\*\*\*

\*Karlsruher Institute of Technology, Hermann-von-Helmholtz Platz  
1, 76344 Eggenstein-Leopoldshafen (Germany)

\*\*University Perugia, Piazza Dell' Università 1, 06123 Perugia  
(Italy)

\*\*\*Bulgarian Academy of Science, Institute of Electrochemistry and  
Energy Systems, Acad G Bonchev Street BL 10, 1113 Sofia  
(Bulgaria)

**Abstract** - Internet technologies, large-scale computing and digital storage resources, data search/retrieval tools, mobile devices, social media and their high uptake among different groups of people have profoundly changed the ways knowledge is created, communicated and how it can be further deployed. The digital information technology has made possible a radical transformation of the nature of science and innovation independent from scientific themes. New digital tools and also a new research cultures make it possible to perform today's education in a different way and drive research more efficiently by short communication and dissemination. However, to realize new types of education, science and research which are more harmonized, more global and collaborative and especially closer to the demands of all kind of FCH-community, a continuous development and provision of respective e-tools must get provided to support education and development on digital basis. NET-Tools project fosters exactly this aim by developing of new e-tools for e-education and e-science.

**Index Terms** – Digital Education, Digital Science, e-Tools

### I. NOMENCLATURE

FCH: Fuel Cells and Hydrogen

NET-Tools: Project funded by FCH-JU 2.0

### II. INTRODUCTION

NET-Tools project extends the scope in providing digital educational materials and new e-tools for courses and e-learning and supplying these to the European lecturer and student's community. The supply of high quality teaching and learning material is essential in building the vast human

resources needed for the further development and maintenance of FCH –technologies, infrastructures and installations expanded meanwhile to very different areas. The university type material developed within the project shall be useable for specific target groups (e.g., FCH-industry, junior researchers, regulators, first responders) but also schools since the curriculum structure is generally valid. To provide e-tools and educational materials to the respective community the integrated architecture of the NET-Tools digital platform is conceived based on detail understanding of distributed multilevel knowledge transfer processes in selected generic cases. Specific features of the platform shall consist on the development of an advanced virtual networking space with a large flexibility in integrating different types of applications able to be tailored based on the needs of the FCH community and sustainable development problems in order to make learners adaptable to changing contexts.

### III. NET-TOOLS PLATFORM

The overall concept of NET-Tools is, to realize and develop a specific e-platform as a linchpin concerning education in FCH technologies. The main target of NET-Tools is to develop and provide a European source for international collaboration and exchange of knowledge and teaching materials between providers and users arising from academia and industry. Based on open source software and components, the e-platform will be useable for free (during the course of the project at least) to everybody. Target groups are students, technicians, engineers, lectures at academic and industry side, public etc. The e-

Copyright © 2017

platform, as a linchpin for education and practicing of FCH-technologies, will also include several technical features and useable for getting viewed by all kind of communication technologies, PC, Laptop, Tablet and Mobil Phone.



**Fig.1. NET-Tools e-platform**

As mentioned, the main objective is to develop a unique European digital platform to support higher education in fuel cell and hydrogen technologies and businesses leveraging existing knowledge and enabling the development of future novel educational training to help fuel the foreseen growth of fuel cell and hydrogen markets worldwide. From this intention main objectives are consequently set as a project basis:

- Open source based e-infrastructure dedicated to FCH knowledge and science to interconnect existing knowledge
- E-infrastructure as user interfaces adapted to the different target audience, lectures, students and professionals
- Implementation of a digital laboratory workspace
- Consolidation of existing e-education and e-knowledge
- Development of novel training delivery method together with new digital practices
- Network to build collaboration and exchange of knowledge on international level

More specifically: The e-infrastructure to be developed in the course of the project will be implemented using an open source LMS (Learning Management System). It will offer best in class functionalities for e-learning and e-education, constituting a reference worldwide. The infrastructure will also be robust to future evolution and easily upgradable. NET-Tools e-infrastructure shall make the addition of valuable content easy, either by establishing connections and repositories with existing digital based knowledge or by supporting the development of various educational materials, from very interactive lessons to more static presentations.

The primary target of NET-Tools is, like any such platform, professionals. Acknowledging professionals and students have different educational needs and studying methods, NET-Tools will deliver dedicated user interfaces offering specific content, navigation possibilities, interactivity level and certification process. E-learning curricula shall be relevant and specific to learners' needs, roles and responsibilities in professional life. Skills, knowledge and information shall get provided to this end.

The implement of a digital laboratory workspace will be an additional part of NET-Tools as a unique and innovative digital instrument. The e-Laboratory includes new methods based on figurative language and representations to explain detailed physical and mathematical principles and FCH technique in its complex structure. The e-Laboratory will integrate a e-Engineering toolbox for technology and safety design of FCH-systems and infrastructures to underpin "learning by solving" education principle, and provide hydrogen industry by the state-of-the-art free access European-made tool for engineering design, as well as a e-Science toolbox for modelling and simulations of physical and mathematical phenomena underlying FCH-technologies, including CFD tools and database for e.g. technological safety.

#### IV. CONCLUSION

NET-Tools e-platform focuses on providing, expanding and disseminating already existing and new developed e-learning and teaching materials and concepts to the FCH-community supported by novel practicing tools compiled and provided by an e-laboratory.

Moreover NET-Tools like to interconnect people on international level based on common interest means, education and training. Under this light, NET-Tools has the intention to be used as some kind of repository and workspace to exchange knowledge and educational material on international level and thus to harmonize education on international level.

#### ACKNOWLEDGMENT

NET-Tools project receives funding by the Fuel Cell and Hydrogen Joint Undertaking 2.0 supported by the Framework Program HORIZON 2020 of the European Commission.

NET-Tools Consortium likes to thank each supporter of the e-platform by providing e-tools and educational materials on the respective repository.

Copyright © 2017

## A RELIABLE METHODOLOGY FOR LOW TEMPERATURE FUEL CELL STACK DESIGN

O. Barbera\* and G. Giacoppo

\*CNR - ITAE, National Research Council of Italy – Institute for  
Advanced Energies Technologies “Nicola Giordano” Via Salita  
S.Lucia sopra Contesse n.5 Messina, (Italy)

**Abstract** - In this work, a reliable methodology for low temperature fuel cell stack design is illustrated. The design methodology has been developed through an iterative approach, starting from a “primitive” fuel cell stack design, essentially based on empirical concepts. By analysing the failures, the design solutions have been conceived, validated by modelling and numerical simulation and tested. The research activity permitted the methodology to be setup, by manufacturing of several prototypes designed for different applications.

**Index Terms** – Fuel cell, Numerical simulation, PEM, Stack design.

### I. INTRODUCTION

Generating electric power using hydrogen is becoming a real hope. Hydrogen technologies could be a key factor for climate challenges overcoming and for future towns free of pollutants and noise. For this reason, research and development of hydrogen technologies are fundamental to accelerate their introduction on the market. Starting from the electrochemical process, which allow electricity production, research activity has to be addressed to the design of fuel cell, which is the device “containing” the electrochemical package. In general, a fuel cell stack is based on two kind of components: electrochemical and hardware. The electrochemical components are the “core” of a fuel cell stack based on polymer electrolyte membrane (PEM). It generates power and is placed inside a hardware that has to maintain a correct operation condition. Concerning the hardware, many authors studied the design of the components of a PEM fuel cell stack, such as bipolar plates, clamping plates, gaskets, flow – field, and so on. In this field, several issues have to be faced up: mechanical and fluid-dynamic. As example, clamping forces can induce unwanted stress and deformation of plates, compromising the mechanical

stability of the device, an uneven internal distribution of reactants and coolant can adversely affect performance; more generally, design issues can compromise durability and safety. In this work, the authors describe how, a reliable methodology for PEM fuel cell stack design has been developed and the obtained results.

### II. EXPERIMENTAL

#### A. Methodology development

The design methodology has been developed through an iterative approach, starting from a first design of a PEM fuel cell stack, essentially based on empirical concepts. By analyzing the failures, the design solutions have been conceived and validated by modeling and simulation, to attain a new and more aware design. This iterative process is characterized by a multidisciplinary approach: (i) mechanics for studying bipolar plates, current collectors and tie roads, (ii) fluid dynamic for improving the internal distribution of reactants, (iii) thermodynamics for humidity, cooling and efficiency calculations and so on.

#### B. Laboratory tests failure analysis and solutions

This activity started in 2001 with a PEM fuel cell stack of 10 cell with 100W of power. The device has been designed simply by stacking a suitable number of cells, using the same flow - field geometry of a single cell available in the laboratory. The obtained performances have been not satisfactory, indeed the stack reached the request power with a non – uniform cell voltage distribution and a high stoichiometry ratio of reactants. The failure analysis has shown that the obtained performances have been related in principal to an incorrect design for the fuel



cell stack hardware, generating internal and external leakage and an uneven distribution of clamping force (Fig.1).

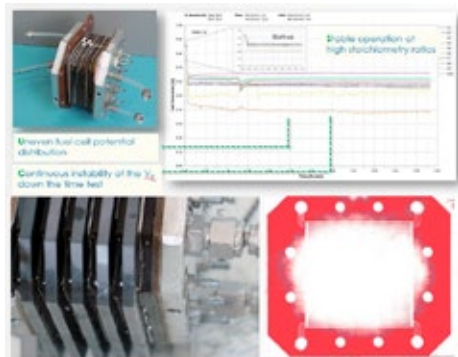


Fig. 1. The first designed stack (top, left): unstable performances (top, right), leakage (down, left); clamping pressure distribution, evaluated by pressure sensitive film (down right)

The Fig. 2 summarizes the study carried out on flow field design and on gasket influence on performance and mechanical hardware engagement.

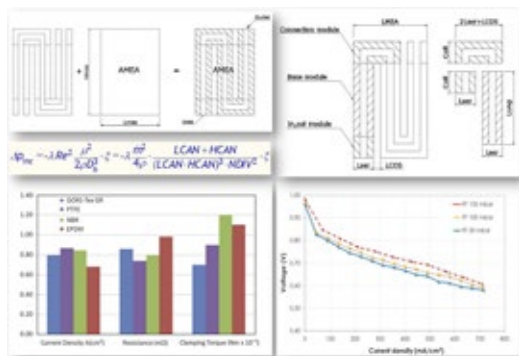


Fig. 2. Flow –field: parameterization concept (top), influence on performances of gasket material (bottom, left) and of pressure drop (bottom, right)

The flow field has been parametrised and the pressure drop expressed as a function of geometrical parameters. In this way the flow – field can be designed with the desired geometrical and fluid dynamic characteristics. Concerning the gaskets, the best compromise between clamping torque needed to avoid leakage, fuel cell stack, low ohmic resistance and obtained current density has been found. In this way the described issues have been overcome. A similar approach has been adopted for a correct design of the remaining components of the fuel cell stack (bipolar plates, current collectors, manifold size calculation and so on).

### III. RESULTS AND DISCUSSION

#### A. The methodology now

Nowadays, the methodology is reliable enough to manufacture a fuel cell stack on the basis on specific requests. Devices for different purposes and operative conditions can be

designed starting from the polarisation curve of the chosen MEA, passing by a modelling phase (if needed) and finally to the manufacture and test of the fuel cell stack (Fig. 3).

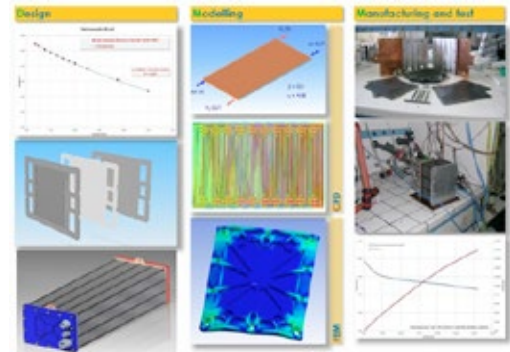


Fig. 3. Conceptual schema of the methodology design

A good agreement between the expected and real performance has been obtained, as demonstrated by numerous designed, manufactured and tested prototypes [1-5].

### IV. CONCLUSION

A reliable methodology for a correct design of low temperature fuel cell stack has been setup over 15 year of technological research activity. The combination between laboratory test and theoretical modelling of the device allowed the definition of this methodology. Now, as demonstrated by numerous prototypes, a practical tool has been setup for a continuous improvement of PEM fuel cell stack performances, in terms of power, weight, outer dimensions and costs.

### REFERENCES

- [1] Urbani F., Squadrito G., Barbera O., Giaccoppo G., Passalacqua E., Zerbiniati O., Polymer Electrolyte Fuel Cell Mini Power Unit for Portable Application, Journal of Power Sources, Volume 169, 2007, Pages 334-337.
- [2] Squadrito G., Giaccoppo G., Barbera O., Urbani F., Passalacqua E., Borello L., Musso A., Rosso I., Design and development of a 7kW polymer electrolyte membrane fuel cell stack for UPS application, International Journal of Hydrogen Energy, Volume 35, 2010 Pages 9983 – 9989.
- [3] Giaccoppo G., Barbera O., Carbone A., Gatto I., Saccà A., Pedicini R., Passalacqua E., 1.5 kWe HT-PEFC stack with composite MEA for CHP application, International Journal of Hydrogen Energy Volume 38, 2013 Pages 11619-11627.
- [4] Barbera O., Mailland F., Hovland S., Giaccoppo G., Energy and provision management study: A research activity on fuel cell design and breadboarding for lunar surface applications supported by European Space Agency, International Journal of Hydrogen Energy, Volume 39, 2014, Pages 14079 – 14096.
- [5] Barbera O., Stassi A., Sebastian D., Bonde J.L., Giaccoppo G., D'Urso C., Baglio V., Aricò A.S., Simple and functional direct methanol fuel cell stack designs for application in portable and auxiliary power units, International Journal of Hydrogen Energy, Volume 41, 2016 Pages 12320-12329.

## A COMPARISON OF METHODS FOR THE FORMATION OF CATHODIC BIOFILMS IN SINGLE-CHAMBER MICROBIAL FUEL CELLS

A. Sacco\*, G. Massaglia\*\*\*, I. Fiorello\*, V. Margaria\*, and  
M. Quaglio\*

\* Center For Sustainable Future Technologies @POLITO, Istituto Italiano  
di Tecnologia, Corso Trento 21, 10129 Torino (Italy)

\*\* Applied Science and Technology Department, Politecnico di Torino,  
Corso Duca Degli Abruzzi 24, 10129, Torino (Italy)

**Abstract** - Cathodic biofilms (CBFs) working as biocatalysts for the oxygen reduction reaction in microbial fuel cells (MFCs) have rarely been employed as the only catalyst in single-chamber devices. In this work, CBFs were grown starting from freshwater river sediment, employing two different methods: a commonly employed one, consisting in polarizing the cathodic electrode with fixed potential (0.5 V vs SHE), and an unusual one, consisting in applying a fixed resistive load (100  $\Omega$ ), without using an external potential. Both methods demonstrated to be able to form CBFs capable to product a stable current larger than 1 A/m<sup>2</sup>. These biofilms were then successfully exploited as biocatalysts at the cathodes of single-chamber MFCs. Both devices showed similar electrochemical properties, in terms of power generation (maximum power in the range 71-77 mW/m<sup>2</sup>) and of internal resistance, suggesting that the MFCs with different biocathodes can work in a similar manner.

**Index Terms** - Biocatalysts, cathodic biofilm, formation methods, single-chamber Microbial Fuel Cells.

### I. INTRODUCTION

Microbial Fuel Cells (MFCs) are bioelectrochemical devices that exploit organic matter as fuel to produce electricity [1]. The oxidation of these organic compounds is carried out by electroactive bacteria present at the anodic electrode, while at the cathode the exploited reduction reaction depends on the cell configuration. In open-air MFCs, in which cathodes are directly exposed to air or to oxygen flow, the oxygen reduction reaction (ORR) takes place [1]. Unfortunately, its kinetics is very slow, being ORR characterized by a large overpotential, therefore the use of a catalyst is mandatory. Pt is the reference material used for this purpose, even if this noble metal is obviously quite expensive [2]. In this framework, different works in the literature proposed the exploitation of biofilms grown on the

cathodic electrodes to perform ORR, in order to replace Pt-based materials [3]. These cathodic biofilms (CBFs) were employed in sedimentary and two-chamber MFCs [3], but rarely in single-chamber MFCs (SCMFCs), despite the simpler setup and fluid management. In fact, in this configuration, both electrodes share the same reactor volume, hence the formation of a non-specialized biofilm is possible also on the cathode.

In this work, the role of a CBF for SCMFCs is investigated using a freshwater river sediment as inoculum. CBFs were formed employing two methods: 1) direct polarization of the cathodic electrode with fixed potential; 2) application of a fixed resistive load, without applying external potential. In both cases, Electrochemical analysis was conducted to compare the different samples. CBFs were subsequently employed as biocatalysts in SCMFCs, and the performance of these devices were studied and compared.

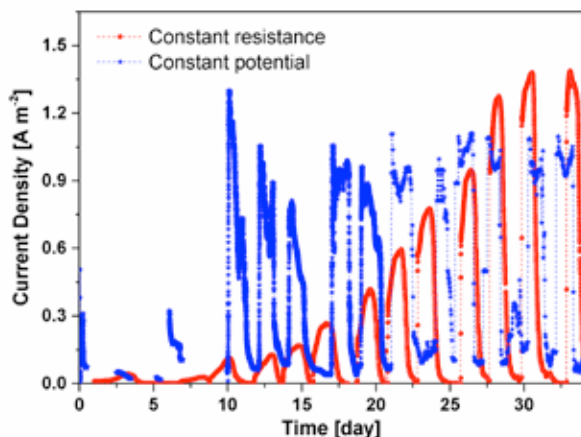
### II. EXPERIMENTAL

Square-shaped SCMFCs, fabricated through 3D printing technology, were characterized by an internal volume of 12.5 mL and electrodes area of 6.25 cm<sup>2</sup> [4]. Anodes and cathodes were constituted by carbon paper, and titanium wires were used to ensure a good electrical contact; cathode electrodes were modified employing a gas diffusion layer, to allow the oxygen flow. Pt wires were used as reference electrodes. Electrolyte was constituted by 12 mM of sodium acetate and 5.8 mM of ammonium chloride dissolved in phosphate buffer solution. Freshwater river sediment was employed as inoculum source. All experiments were conducted in duplicate. During the first part of the experiments, CBFs were formed on cathodes by applying a constant 0.5 V vs SHE potential or by employing a fixed 100  $\Omega$  resistance. After biofilm formation, cathodes were

assembled in new SCMFCs, employing anodic electrodes coming from already-working devices. A potentiostat was employed to perform linear sweep voltammetry (LSV, 0.1 mV/s scan rate), cyclic voltammetry (CV, 10 mV/s scan rate) and electrochemical impedance spectroscopy (EIS, amplitude 25 mV, frequency range  $10^{-1}$ – $10^6$  Hz) measurements.

### III. RESULTS AND DISCUSSIONS

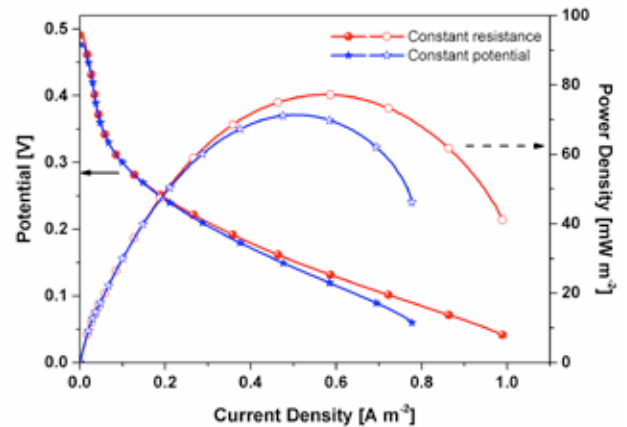
The current production associated to the two CBFs is compared in Fig. 1. As can be clearly observed, the biofilm grown through the direct polarization of the electrode (indicated as “Constant potential”) is characterized by a fast start-up period (about 10 days) and then is able to sustain a stable current density of about 1 A/m<sup>2</sup> after 25 days. On the contrary, the biofilm formed with a fixed eternal load (indicated as “Constant resistance”) exhibits a slower increase of the current; however, its final value (after 35 days) is larger with respect to other CBF. This longer start-up period could be attributed to the low value of the applied resistance (100  $\Omega$ ): this load represent an extreme condition to microorganisms, which can take a longer period to gradually adapt to this and to be able to produce large currents. On the other hand, after start-up, this biofilm is capable to efficiently sustain such high currents, with respect to other CBFs formed under “softer” conditions.



**Fig. 1. Current produced by CBFs formed through the two different methods during the start-up phase.**

After formation of the two CBFs, the electrodes were employed to fabricate SCMFCs. The performance of the two classes of cells are compared in Fig. 2. Both devices are characterized by similar open circuit potential (about 0.5 V) and maximum power density (about 75 mW/m<sup>2</sup>) values, even if “constant resistance” MFCs are characterized by slightly larger current densities in the low-potential region. This result is in agreement with the above reported analysis, i.e. CBFs accustomed to work in extremely hard conditions are then capable to sustain larger currents, as shown in Fig. 1. EIS and

CV analyses were conducted to cast light on the observed similarity of the two SCMFCs (graphs not shown). EIS demonstrated comparable values for the cathodic charge transfer resistances, related to the ORR activity. Moreover, both CBFs exhibit typical ORR peaks in their voltammograms.



**Fig. 2. Comparison of potential (left axis) and power density (right axis) dependency on current density for SCMFCs fabricated with CBFs formed through the two different methods.**

### IV. CONCLUSION

In this work the role of CBFs formed from freshwater river sediment samples by employing two different methods has been analyzed. During the start-up phase, a slower growth was observed for the biofilm formed with a fixed resistor, but with final larger produced currents with respect to CBFs acclimated with constant potential. The comparison of SCMFCs fabricated with the different biocathodes provided similar performance in terms of power generation and charge transfer resistance values, assessing that they can work in a comparable manner in SCMFC.

### REFERENCES

- [1] Logan, B., Hamelers, B., Rozendal, R., Schroder, U., Keller, J., Freguia, S., Aelterman, P., Verstraete, W., Rabaey, K., Microbial fuel cells: methodology and technology, *Environmental Science and Technology*, Volume 40, 2006, Pages 5181–5192.
- [2] Chen, Z., Higgins, D., Yu, A., Zhang, L., Zhang, J., A review on non-precious metal electrocatalysts for PEM fuel cells, *Energy & Environmental Science*, Volume 4, 2011, Pages 3167–3192.
- [3] Erable, B., Feron, D., Bergel, A., Microbial catalysis of the oxygen reduction reaction for microbial fuel cells: a review, *ChemSusChem*, Volume 5, 2012, Pages 975–987.
- [4] Garino, N., Sacco, A., Castellino, M., Muñoz-Tabares, J. A., Chiodoni, A., Agostino, V., Margaria, V., Gerosa, M., Massaglia, G., Quaglio, M., Microwave-Assisted Synthesis of Reduced Graphene Oxide/SnO<sub>2</sub> Nanocomposite for Oxygen Reduction Reaction in Microbial Fuel Cells, *ACS Applied Materials & Interfaces*, Volume 8, 2016, Pages 4633–4643.

## A MEASUREMENT METHOD OF EFFECTIVE THERMAL CONDUCTIVITY ON THE HYDROGEN STORAGE MATERIALS

Sang-Il Park, Moon-Sun Chung\*

\*Hydrogen Energy R&D Center, KIER, 71-2 Jang-dong, Yuseong-gu, Daejeon, (Republic of Korea)

### ABSTRACT

Hydrogen storage is one of the key obstacles to the commercialization as well as market acceptance of hydrogen fueled vehicle. Besides the efficiency of power system, it is an extremely challenging technology to store sufficient hydrogen on the vehicle without compromising consumer requirement such as safety, space, driving range, and fuel cost. There are three main hydrogen storage methods including compression, liquefaction and hydrogen storage materials. Among the technologies currently under development, the hydrogen storage as a highly pressurized gas is the most prominent candidate for the hydrogen powered vehicle now. The advanced automobile industries have already demonstrated the highly pressurized hydrogen system on fuel cell vehicles for past several years. The hydrogen storage materials in solid state have some advantages such as high volumetric storage capacity, little energy loss, longer storage time and highest safety. Various carbonaceous and non-carbonaceous hydrogen storage materials have been studied over the past few decades. In this presentation, we would like to introduce our new developing hydrogen storage system including a heat exchanger for FCV based on a NaAlH<sub>4</sub>. See reference [1, 2, 3].

### INTRODUCTION

To improve the adsorption/desorption performance of hydrogen storage alloys in hydrogen storage device, it is advantageous to use a hydrogen storage alloy having a highly effective thermal conductivity. Sodium aluminum hydride NaAlH<sub>4</sub> (SAH) is one type of promising hydrogen storage alloys, and used in powder or compacted pellet forms. In order to increase the volumetric storage density in the hydrogen storage device, a compacted pellet shape having a high effective density of the hydrogen storage alloy is used. The enthalpy change of SAH due to adsorption and desorption of hydrogen is approximately 40 kJ/mole of H<sub>2</sub>. The hydrogen

storage alloy should be heated and cooled rapidly to adsorb and desorb hydrogen within a short time. In this case, it is highly advantageous to increase the effective thermal conductivity of the hydrogen storage alloy.

### MEASUREMENT METHOD OF EFFECTIVE THERMAL CONDUCTIVITY

To increase the effective thermal conductivity of the hydrogen storage alloy such as SAH, a hydrogen storage alloy is mainly used in compacted pellet form, and ENG and aluminum powder, which have high thermal conductivity, are mixed. The thermal probe method is used to measure the effective thermal conductivity of SAH powder and compact.

SAH is oxidized in contact with air, and has a characteristic of ignition in contacted with water. The preparation of samples for thermal conductivity measurement takes place in a glove box in an argon atmosphere. Furthermore, because the thermal conductivity measurement is performed at high temperature and high pressure, it is advantageous to reduce the size of the sample for thermal conductivity measurement in order to reduce the risk of measurement.

In this study, to measure the effective thermal conductivity of SAH powder and compacted pellet, a small thermal probe composed of a heater tube with 0.5 mm diameter and a thermocouple tube with 0.25 mm diameter was manufactured. The effective thermal conductivity of the powder, which is raw material for SAH, was measured. In this case, various atmospheric gases were used to examine the influence of gas pressure. The compacted sample is extremely difficult to form to produce the micro-grooved moldings on which the heater tube and the thermocouple tube of this small thermal probe are installed in an argon atmosphere.

Thus, this study formed a precise groove for installing a heater tube and a heat conduction tube of a small thermal probe on a reference material with low thermal conductivity, and further installed a compacted pellet for sample thermal



conductivity of SAH is assembled on the opposite side. Under this setting, the effective thermal conductivity of the SAH sample was measured at high pressure.

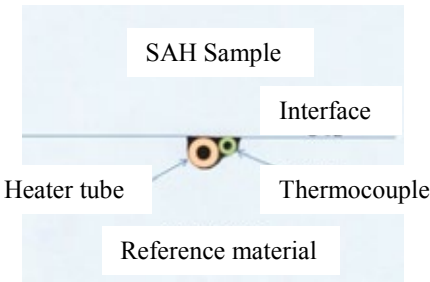


Fig. 1 A small thermal probe with a 0.5mm heater tube and 0.25mm thermocouple

The raw material of NaAlH<sub>4</sub> powder (hereinafter referred as “SAH”) was purchased from Sigma Aldrich and the effective thermal conductivity of SAH powder was measured. The samples for thermal conductivity measurement should be prepared in the globe box and it is advantageous to reduce the size of the sample for thermal conductivity measurement in order to reduce the risk of measurement.

The powder sample in the sample chamber for thermal conductivity is approximately 40 mm in diameter and approximately 60 mm in height. A 50-mm-long electric heater tube was inserted into the powder sample, and the heater tube and thermocouple tube were placed side by side and glued with each other by matching the tip of the thermocouple tube to the middle of the electric heater tube in the sample. In this case, since a separate protection tube and guide tube are not required, a thermal probe can be fabricated smaller than that of a conventional thermal probe, thereby reducing the size of a sample for thermal conductivity measurement.

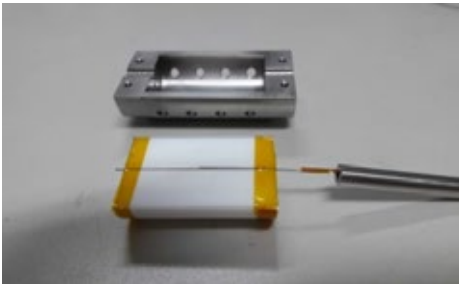


Fig. 2 A small thermal probe and sample chamber



Fig. 3 SAH pellet molding sample

The measured values of the thermal conductivities of the composites composed of the reference materials and the heat insulating materials as well as the actual values of the thermal conductivities of the respective reference materials using a correlated equation are shown in Table 1. As shown in [Table 1], a small thermal probe was installed on the insulating material, and each reference material was assembled. The error between the measured value of the thermal conductivity of the reference material and their literature value was found to be within approximately 3%.

[Table 1] The measured values of thermal conductivity for various reference materials and the actual thermal conductivity ( $W/m \cdot K$ ) of samples

Reference material	Thermal conductivity of Reference material (literature)	Measured Thermal Conductivity of composite	Calculated Thermal Conductivity of Reference material	Error (%)
Inconel	11.7	11.4	11.4	-2.56
YTZ	2.9	3.1	2.97	2.41
Quartz glass	1.36	1.51	1.346	-1.03

### SUMMARY

To measure the effective thermal conductivity of SAH powder raw material and compacted pellet, we proposed a small thermal probe method composed of a heater tube of a 0.5-mm diameter and a thermocouple tube with a 0.25-mm diameter. The measurement results for verification showed that the effective thermal conductivity for various reference materials and the actual thermal conductivity of samples are in good agreements within 3% relative errors.

### REFERENCES

[1] Y.-W. Cho, et al., “Rehydrogenation and cycle studies of LiBH<sub>4</sub>-CaH<sub>2</sub> composite”, International journal of hydrogen energy, 35 (2010) 6578-6582.

[2] Y.-S. Lee, et al., “Effect of thermal fluorination on the hydrogen storage capacity of multi-walled carbon nanotubes”, International journal of hydrogen energy, 36 (2011) 1560-1567.

[3] J. Kim, et al., “Ultrahigh Porosity in Metal-Organic Frameworks”, Science, 329 (2010) 424-428.



## IMPACT OF CATHODE POTENTIAL ON THE BIO-ELECTROCHEMICAL SYNTHESIS OF CARBOHYDRATES

A. Paniz Izadi\*, B. Jean-Marie Fontmorin\*, C. Ian Head\*\*, and D. Eileen Yu\*

\*School of Engineering, Newcastle University, (United Kingdom)

\*\*School of Natural and Environmental Sciences, Newcastle University, (United Kingdom)

**Abstract** - This study presents the effect of cathode potential on the production of carbohydrates by microorganisms in a Microbial Electrolysis Cell (MEC). Two different sources of bacteria (activated sludge from wastewater treatment plant and sediment from Tyne river (Newcastle, UK)) were collected and enriched before operating the bio-electrochemical system (BES). The influence of poised potential on bio-production of carbohydrates was investigated by applying the series of potentials at the cathode from -400 to -700 mV vs. SHE after transferring the inocula to BES.

The applied potentials were a major factor on the products of microbial electrosynthesis (MES). After applying potential of -500 mV for 14 days, 21 mg/L acetate was produced at the cells inoculated by Tyne sediment and 13 mg/L acetate at the cells by activated sludge. Applying -700 mV, methane production was mainly detected, which can be due to the enrichment of both heterotrophic and hydrogenotrophic methanogens at the enrichment step.

**Index Terms** – Microbial electrosynthesis, biocathode, CO<sub>2</sub> reduction, bio-electrochemical system

### I. INTRODUCTION

Microbial electrosynthesis (MES) is a novel technology provided the cathode-driven approach to the bio-electrochemical system (BES) using microorganisms as catalysts for wastewater treatment to remove organic matters at the anode, and carbon dioxide reduction to valuable substances at the cathode. Although many investigations have been focused on MES to have a better understanding of this technology, major limitations subsist such as the slow development of the biocatalyst at the electrode. These difficulties are referred to the ability of the bacteria to grow at the surface of the electrode, using the electrons provided from the electrode as the energy source and CO<sub>2</sub> as the carbon source. So far, successful research studies regarding CO<sub>2</sub> conversion in MES with different bio-products have been reported [1]. However, the underlying mechanisms are still

quite unclear. Therefore, investigating novel sources of bacteria and energy required for electrosynthesis (cathode potential) and their effect on the nature of bio-cathode and bio-production can lead to improvement in MES. Hence, the ultimate aim of this project is to compare the development of a low cost BES to convert CO<sub>2</sub> into valuable chemicals at different applied potentials from different sources of bacteria.

### II. MATERIALS AND METHODS

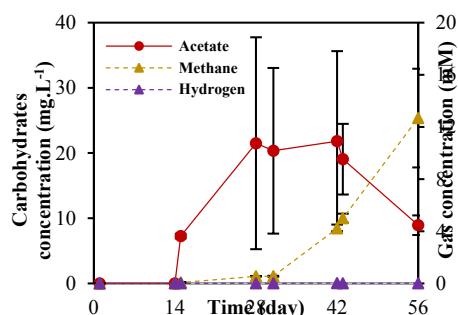
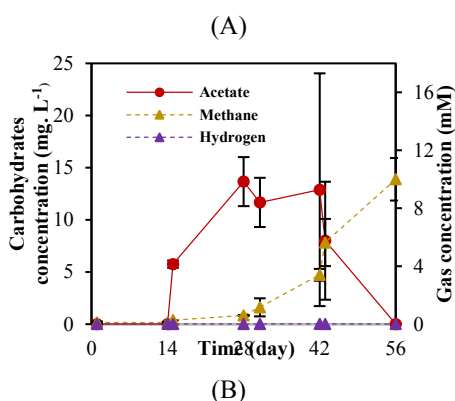
Two different bacterial sources of activated sludge (AS) and Tyne sediment (TS) were collected from the local domestic wastewater treatment plant and Tyne river (Newcastle upon Tyne, UK), respectively, and stored in the dark at 4 °C before utilization. Pre-enrichment was performed before transferring the inocula to the BES which consisted in the heterotrophic growth of inocula by glucose in the incubator in the dark at 30 °C and 125 rpm in an anaerobic basal medium as reported before [2]. 4 dual chambers BESs were constructed using two 360 ml glassy chambers with the solution volume of 310 ml. BESs were operated in duplicates for each bacteria source. Cells chambers were separated by an anion exchange membrane (Fumatech, Germany). Graphite felt with the projected surface area of 4.5 cm<sup>2</sup>, platinum mesh and Ag/AgCl electrode (BASi, USA) were used as the working (cathode), counter (anode) and reference electrodes, respectively. After heterotrophic growth of inocula on glucose with high concentration of methane inhibitor (10 mM sodium-2-bromoethane-sulfonate), the same medium used in the pre-enrichment step without glucose and 20% inoculum were transferred to BES and a potential of -400mV was applied for 30 days. Thenceforth, potentials of -400, -500, -600 and -700 mV were applied. Each potential was poised for 14 days and the performance of the cells was evaluated in terms of current consumption, bio-production of carbohydrates and gases and inorganic carbon consumption. In order to carry out the potentiostatic control of the cells and record the chronoamperometric data, cells were connected to a four-channel potentiostat (Quad Potentiostat, Whistonbrook

Technologies, UK). Gas in headspaces and liquid samples were analyzed by gas chromatograph and ion chromatograph, respectively to detect the products. Cyclic voltammetry (CV) was performed before and at the end of experiment to compare the electrochemical activity of the plain electrode and the electrode with biocatalyst. All the potential mentioned in this study is reported versus SHE.

### III. RESULTS

#### A. Effect of applied potentials on bio-products

When glucose was replaced by bicarbonate as the sole carbon source in the BES, no current and products were detected at the potential of -400 mV. However, when the potential was changed to -500 mV, the concentration of acetate increased considerably in all the cells to  $21 \pm 13.3$  mg/L and  $13 \pm 2.35$  mg/L in the cells inoculated by TS and AS, respectively (Fig. 1). Due to the fact that no hydrogen and small amount of methane (near 0.5 mM) was detected at the headspace of the reactors at -500 mV, it is assumed that bacteria could accept the electrons directly from the electrode. At a poised potential of -600 mV, cathodic current and concentration of acetate decreased and methane was detected in the headspace. This could show that the heterotrophic methanogens took over the bio-production at this stage [3]. Changing the potential to -700 mV, cells started to generate much higher cathodic current and higher concentration of methane compared to other potentials. Performing the CV from all the cells at the end of experiment, no hydrogen evolution was observed at the potential of -500 mV, confirming the hypothesis of direct electron transfer between the electrode and bacteria. Hydrogen evolution was catalyzed at the potential of -700 mV, however no hydrogen was detected in the headspace. This can suggest that apart from heterotrophic methanogens, hydrogenotrophic methanogens were responsible for the methane production at -700 mV.



**Fig. 1.** Concentration of the bio-products produced during the experiment at the BESs inoculated by A) AS and B) TS

### IV. CONCLUSION

In this study we showed how the specificity of the bio-products in MES depends on the potential applied at the electrode. Compared to the literature value of -900 mV vs. SHE, acetate was synthesized at less negative potential (-500 mV) in this study. These promising results showed that acetogens were enriched and bio-production of acetate from the acetogens could be bacteria accepting electrons from the electrode by direct electron transfer. However, the methane production particularly at the potential of -700 mV vs. SHE showed that heterotrophic growth of methanogens in the pre-enrichment step even with methane inhibitor could not cease the selection and enrichment of the methanogens over the long-term experiment. It was also observed that sources of bacteria did not affect the bio-products remarkably. However, pre-enrichment step can affect the MES performance in terms of types of products. Further investigation on improving carbohydrates production yield by overcoming the competition between the acetogens and other types of bacteria particularly methanogens through the enrichment step is ongoing.

### REFERENCES

- [1] Lovley, D.R., Powering microbes with electricity: direct electron transfer from electrodes to microbes, Environmental microbiology reports, volume 3, 2011, pp. 27-35.
- [2] Zaybak, Z., Pisciotta, J.M., Tokash, J.C., Logan, B.E., Enhanced start-up of anaerobic facultatively autotrophic biocathodes in bioelectrochemical systems, Journal of Biotechnology, volume 168, 2013, pp. 478-485.
- [3] Molenaar, S.D., Saha, P., Mol, A.R., Sleutels, T.H.J.A., ter Heijne, A., Buisman, C.J.N., Competition between Methanogens and Acetogens in Biocathodes: A Comparison between Potentiostatic and Galvanostatic Control, International Journal of Molecular Sciences, volume 18, 2017, pp. 204.

## MODELING OF RADIATIVE HEAT TRANSFER IN SOLID OXIDE FUEL CELLS

J.N. Stam\*, D.J.E.M. Roekaerts\*, and P.V. Aravind\*

\*Department of Process & Energy, Delft University of Technology,  
Leeghwaterstraat 39, 2628 CB, Delft, The Netherlands

**Abstract** – Solid oxide fuel cells (SOFCs) operate at high temperatures, leading to stringent requirements for the thin ceramic structures in these devices. Heat transfer models aimed to study the temperature distribution within SOFCs are however often simplified by ignoring radiative heat transfer (RHT). A computational model is developed to study the influence of RHT on temperature fields in SOFCs. It is shown that for internal heat transfer in a single channel SOFC, RHT can be safely ignored.

**Index Terms** – Computational Fluid Dynamics, Radiative Heat Transfer, Solid Oxide Fuel Cell.

### I. INTRODUCTION

Radiative heat transfer (RHT) becomes increasingly more important at elevated temperatures, but this mode of heat transfer is often neglected in SOFC modeling. Reasons are lack of material properties, or reducing complexity and computational time. It has been shown that RHT cannot be ignored for stack heat losses [1, 2], but there has been some debate on the role of internal RHT in SOFCs [3, 4]. Also a wide range of optical surface properties can be found, as demonstrated in Table 1.

TABLE 1:  
EMISSION CATHODE SURFACE

Emissivity $\epsilon$	Reference
1	[5]
0.9	[6]
0.8	[7]
0.7	[8]
0.55	[9]
0.35	[10]

A computational fluid dynamics (CFD) model is developed to study the influence of RHT on temperatures in SOFCs.

### II. METHODOLOGY

A 3D steady-state SOFC model is developed using Ansys Fluent. Mass, momentum, energy and charge conservation equations are solved together with the radiative transfer equation (RTE). Gas flows are laminar and ideal. The anode and cathode are modeled as porous materials.

#### A. Geometry & Mesh

A single channel of a planar cell is modelled, a schematic of the geometry is shown in Fig. 1.

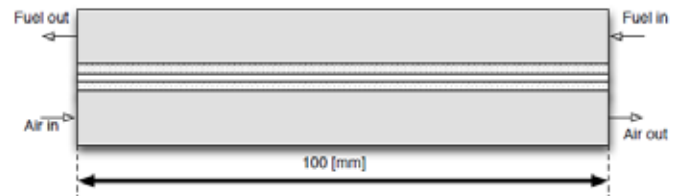


Fig. 1: Schematic representation of single cell planar SOFC

The flow channels are 2 mm wide and 1 mm high. The anode thickness is 500, cathode 50 and the electrolyte 15  $\mu\text{m}$ .

#### B. Model implementation

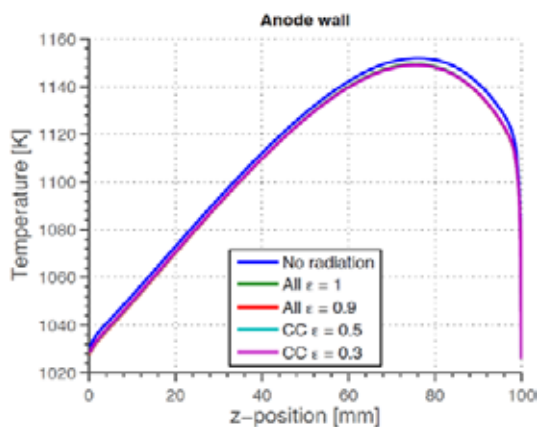
A structured mesh is developed, grid independence is achieved with 839.520 cells. The discrete ordinates method is chosen for the RTE because it spans a wide range of optical thicknesses, allows surface to surface radiation and participating media. 4 control angles per octant are used for the DO-method (after a sensitivity study), adding 32 additional transport equations per cell.

### C. Material properties & Boundary conditions

SOFC material properties are obtained from literature [11]. From an initial sensitivity study it is known that the anode and cathode can be considered to be opaque for RHT, and radiation in the electrolyte can be ignored. This is in agreement with previous studies [4, 6]. Inlet mass flows ( $H_2$  and air) and temperatures (973K) are defined, together with an average current density of 4000 A/m<sup>2</sup>. Radiative intensity at the channel boundaries (inlet and outlet) is calculated using an emissivity coefficient and an external temperature (0.9 and inlet T).

### III. RESULTS & DISCUSSION

The results in Fig. 2 show temperature profiles along the anode wall obtained with a wide range of surface properties. The first curve (blue) shows the temperature without RHT. The second curve (green) shows the results with RHT, considering all walls to be black (emissivity  $\epsilon=1$ ). The red curve shows the results with all walls considered to be grey ( $\epsilon=0.9$ ). With the anode and cathode walls kept at  $\epsilon=0.9$ , the results are obtained for current collector (CC) emissivities of  $\epsilon=0.5$  and  $\epsilon=0.3$ .



**Fig. 2: Temperature profile at anode wall of a planar single channel SOFC cell, with and without RHT**

The curves with RHT overlap, with the purple curve on top. The results show that the surface properties have a minimal influence on the results, and RHT in general has a small influence on temperatures (max 5K difference) and temperature gradients.

### IV. CONCLUSION

RHT can be neglected in the electrodes and electrolyte, which is in agreement with previous studies. The results show that RHT in the anode and cathode channel has a small influence on internal temperatures, for a wide range of different surface properties. From this can be concluded that internal RHT can be safely neglected for the case under consideration.

However, as shown in literature, RHT in and from stacks cannot always be ignored and is recommended as a topic for

further studies.

### ACKNOWLEDGMENT

This research is partially supported by the project “GasDrive: Minimizing emissions and energy losses at sea with LNG combined prime movers, underwater exhausts and nano hull materials” (project 14504) of the **Netherlands Organisation for Scientific Research (NWO)**, domain **Applied and Engineering Sciences (TTW)**.

### REFERENCES

- [1] E. Achenbach and E. Riensche, “Methane/steam reforming kinetics for solid oxide fuel cells,” *J. Power Sources*, vol. 52, no. 2, pp. 283–288, 1994.
- [2] T. Tanaka, Y. Inui, A. Urata, and T. Kanno, “Three dimensional analysis of planar solid oxide fuel cell stack considering radiation,” *Energy Convers. Manag.*, vol. 48, no. 5, pp. 1491–1498, 2007.
- [3] S. Murthy and A. G. Fedorov, “Radiation heat transfer analysis of the monolith type solid oxide fuel cell,” *J. Power Sources*, vol. 124, no. 2, pp. 453–458, 2003.
- [4] D. L. Damm and A. G. Fedorov, “Spectral Radiative Heat Transfer Analysis of the Planar SOFC,” *J. Fuel Cell Sci. Technol.*, vol. 2, no. 4, p. 258, 2005.
- [5] V. M. Janardhanan and O. Deutschmann, “Numerical study of mass and heat transport in solid-oxide fuel cells running on humidified methane,” *Chem. Eng. Sci.*, vol. 62, no. 18–20, pp. 5473–5486, Sep. 2007.
- [6] K. J. Daun, S. B. Beale, F. Liu, and G. J. Smallwood, “Radiation heat transfer in planar SOFC electrolytes,” *J. Power Sources*, vol. 157, no. 1, pp. 302–310, Jun. 2006.
- [7] C. Stiller, B. Thorud, S. Seljebo, O. Mathisen, H. Karoliussen, and O. Bolland, “Finite-volume modeling and hybrid-cycle performance of planar and tubular solid oxide fuel cells,” *J. Power Sources*, vol. 141, no. 2, pp. 227–240, 2005.
- [8] F. Calise, M. Dentice d’Accadia, and G. Restuccia, “Simulation of a tubular solid oxide fuel cell through finite volume analysis: Effects of the radiative heat transfer and exergy analysis,” *Int. J. Hydrogen Energy*, vol. 32, no. 17, pp. 4575–4590, Dec. 2007.
- [9] G. DiGiuseppe, “Surface-to-Surface Radiation Exchange Effects in a 3D SOFC Stack Unit Cell,” *J. Fuel Cell Sci. Technol.*, vol. 9, no. 6, p. 61007, Nov. 2012.
- [10] R. Suwanwarangkul, E. Croiset, M. D. Pritzker, M. W. Fowler, P. L. Douglas, and E. Entchev, “Mechanistic modelling of a cathode-supported tubular solid oxide fuel cell,” *J. Power Sources*, vol. 154, no. 1, pp. 74–85, 2006.
- [11] Z. Qu, P. V. Aravind, N. J. J. Dekker, A. H. H. Janssen, N. Woudstra, and A. H. M. Verkooijen, “Three-dimensional thermo-fluid and electrochemical modeling of anode-supported planar solid oxide fuel cell,” in *Journal of Power Sources*, 2010, vol. 195, no. 23, pp. 7787–7795.

## CURRENT DRIVEN AMMONIUM RECOVERY

P. Kuntke\*, M. Rodríguez-Arredondo\*\*\*, M. Rodrigues\*,  
T.H.J.A. Sleutels\*, A. ter Heijne\*\*, M. Saakes, H.V.M.  
Hamelers\*, and C.J.N. Buisman\*\*\*

\*Wetsus, European centre of excellence for sustainable water technology,  
P.O. Box 1113, 8900CC Leeuwarden, The Netherlands

\*\* Sub-Department of Environmental Technology, Wageningen University,  
P.O. Box 17, 6700 AA Wageningen, The Netherlands

**Abstract** – In this work we evaluated the performance of hydrogen gas recycling electrochemical systems (HRES) for the recovery of ammonium from urine. Two types of HRES were operated; a prototype and an up-scaled system. The results obtained with the prototype showed that a higher recovery could be reached at higher load ratio (i.e. current density/ammonium load) at the cost of higher energy input. The results of the up-scaled system proved that the system could be operated at higher current densities with a significant lower energy demand. The up-scaled HRES was operated at 100 A/m<sup>2</sup> removing about 600 g<sub>N</sub>/m<sup>2</sup>/d at an energy input of 6.5 kWh/kg<sub>N</sub>.

**Index Terms** – Ammonium recovery, Hydrogen recycling, Urine treatment, Wastewater treatment,

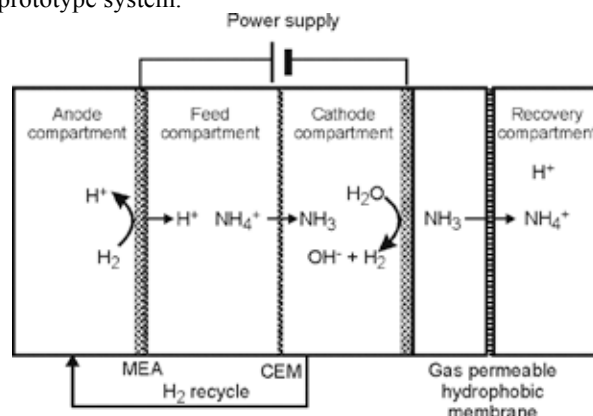
### I. INTRODUCTION

Production of ammonium based fertilizers and ammonium removal from wastewater are essential parts of the nitrogen cycle, which require large amounts of energy. Therefore, ammonium recovery from wastewater using (Bio) Electrochemical Systems ((B)ESs) has been investigated by various research groups. BESs promise to be energy efficient, while ESs promise high removal/recovery rates [1]. In this work, we investigated the use of a hydrogen gas recycling electrochemical system (HRES) for ammonium recovery which combines both energy efficiency and high removal rates. Inside this HRES, hydrogen gas produced at the cathode is oxidized at the anode, and the resulting current is used to extract ammonium from the wastewater. The HRES uses ion exchange membranes for ammonium separation and gas permeable hydrophobic membranes for ammonium recovery.

### II. MATERIALS AND METHODS

#### A. Experimental Setup and Strategy

Two types of hydrogen gas recycling electrochemical systems were used in this work. A prototype system as presented by Kuntke *et al.*, 2017 [2] and an optimized up-scaled version of the earlier prototype. The principle of the current driven ammonium recovery is explained in Fig. 1 on basis of the prototype system.



**Fig. 1.** Schematic representation of the prototype HRES used for ammonium recovery. Hydrogen gas (H<sub>2</sub>) produced at the cathode is oxidized at the anode (i.e. Membrane Electrode Assembly, MEA), the resulting current is used to separate and recover the ammonium from the wastewater using cation exchange membrane (CEM) and the gas permeable hydrophobic membrane.

The prototype was operated on source separated urine as described by Kuntke *et al.*, 2017 [2]. The modification of the up-scaled prototype included a four times larger electrode surface area and an additional anion exchange membrane for more efficient ammonium recovery. The up-scaled system was operated on synthetic urine based on previous work [3]. The



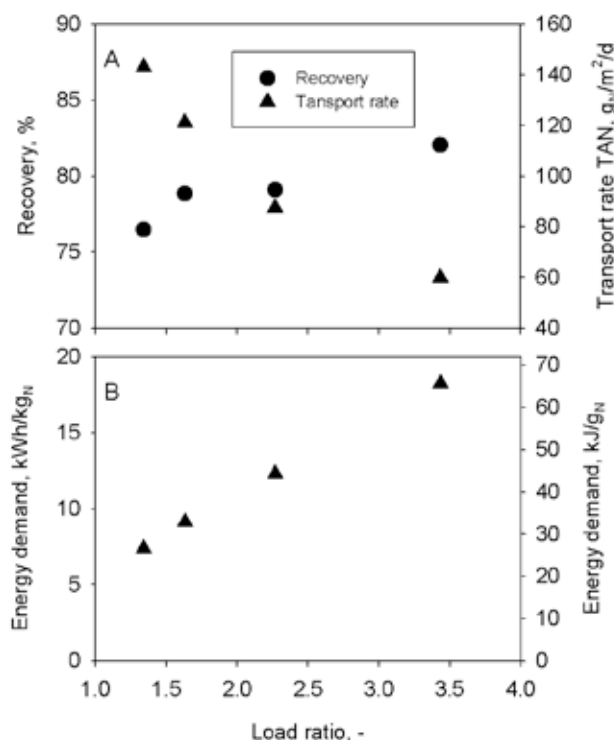
performance of these two HRESs for ammonium recovery was investigated using the load ratio concept, in which current density is matched to ammonium load [4].

### B. Calculation and Chemical Analysis

The calculations and chemical analysis were performed based on previously reported methodology [2].

## III. RESULTS AND DISCUSSION

Performance of the prototype HRES was evaluated at a current density of 20 A/m<sup>2</sup> and load ratios between 1.3 and 3.4. The results in Fig. 1 show that a higher load ratio results in a higher recovery. At the same time, the energy input increased with an increasing load ratio. These results are in agreement with earlier findings and show that a load ratio of 1.3 seems to be optimum for ammonium recovery [2,4].



**Fig. 2.** Ammonium recovery, transport rate TAN (Total Ammonium Nitrogen, including ammonium and ammonia) over the CEM (A) and energy demand (B) determined with the prototype system at a current density of 20 A/m<sup>2</sup> using different load ratio.

The up-scaled HRES was operated at current density of 20, 50, and 100 A/m<sup>2</sup> at a load ratio 1.3 to achieve high recoveries at relative low energy inputs. The Total Ammonium Nitrogen (TAN) transport rate increased more or less linearly with the increase of current density. At a current density 20 A/m<sup>2</sup> the TAN transport rate was 141±8 g<sub>N</sub>/m<sup>2</sup>/d; at 50 A/m<sup>2</sup>, 311±9 g<sub>N</sub>/m<sup>2</sup>/d and at 100 A/m<sup>2</sup>, 598±24 g<sub>N</sub>/m<sup>2</sup>/d. The ammonium recovery, however, decreased from around 74±2 % at 20 A/m<sup>2</sup> to 58±2 % at 100 A/m<sup>2</sup>. The energy demand for the up-scaled systems was found to be significantly lower than the prototype.

At a current density 20 A/m<sup>2</sup> the energy demand was 4.9±0.9 kWh/kg<sub>N</sub>; at 50 A/m<sup>2</sup>, 5.9±0.2 kWh/kg<sub>N</sub> and at 100 A/m<sup>2</sup>, 6.5±0.3 kWh/kg<sub>N</sub>. Furthermore, competing electrochemical technologies were found to be more energy demanding, while operating at lower current densities [4,5]. An analysis of the internal losses revealed that anode overpotential, ionic losses and membrane losses were significantly reduced in the up-scaled HRES compared to the smaller prototype.

## IV. CONCLUSION

These results show that energy efficient current driven ammonium recovery is possible using our hydrogen gas recycling electrochemical system. The upscaling and modifications of the HRES reduced the energy demand significantly, while the treatment capacity was increased. Therefore, the next steps of the technology development will focus on further upscaling and operation under realistic conditions with different types of wastewater.

## ACKNOWLEDGMENT

This work was performed in the cooperation framework of Wetsus, European Centre of Excellence for Sustainable Water Technology ([www.wetsus.eu](http://www.wetsus.eu)). Wetsus is co-funded by the Dutch Ministry of Economic Affairs and Ministry of Infrastructure and Environment, the European Union Regional Development Fund, the Province of Fryslân, and the Northern Netherlands Provinces. The authors like to thank the participants of the research theme “Resource Recovery” for the fruitful discussions and their financial support.

## REFERENCES

- [1] Rodríguez Arredondo, M., Kuntke, P., Jeremiasse, A. W., Sleutels, T.H.J.A., Buisman, C.J.N., ter Heijne, A., Bioelectrochemical systems for nitrogen removal and recovery from wastewater, *Environ. Sci.: Water Res. Technol.* Volume 1. 2015. Pages 22–33.
- [2] Kuntke, P., Rodríguez Arredondo, M., Widyakristi, L., ter Heijne, A., Sleutels, T.H.J.A., Hamelers, H.V.M., Buisman, C.J.N., Hydrogen Gas Recycling for Energy Efficient Ammonia Recovery in Electrochemical Systems, *Environ. Sci Technol.* Volume 51. 2017. Pages 3110–3116.
- [3] Zamora, P., Georgieva, T., Ter Heijne, A., Sleutels, T.H.J.A., Jeremiasse, A.W., Saakes, M., Buisman, C.J.N., Kuntke, P., Ammonia recovery from urine in a scaled-up Microbial Electrolysis Cell, *J. Power Sources.* Volume 356. 2017. Pages 491–499.
- [4] Rodríguez Arredondo, M., Kuntke, P., ter Heijne, A., Hamelers, H.V.M., Buisman, C.J.N., Load ratio determines the ammonia recovery and energy input of an electrochemical system, *Water Res.* Volume 111. 2017 Pages 330–337.
- [5] Desloover J., De Vrieze, J., Van De Vijver, M., Mortelmans, J., Rozendal, R., Rabaey K., Electrochemical nutrient recovery enables ammonia toxicity control and biogas desulfurization in anaerobic digestion, *Environ. Sci. Technol.* Volume 49. 2015 Pages 948–955.

## IRON-BASED CATHOLYTE EVALUATION IN MICROBIAL FUEL CELLS

MariaCatalina Vega Reyes\*, Calet Misael Garcia Marin\*, Jose Luis Zuñiga Cerroblanco\*, Sathish-Kumar Kamaraj\*y\*\*, Dante Galvez Reyes\* and Yasser Davizon Castillo\*\*.

\* Universidad Politécnica de Aguascalientes, Paseo San Gerardo No. 207. Fracc. San Gerardo. Aguascalientes, Ags. México, C.P. 20342,

\*\*Unidad Especializada en Energías Renovables – Tecnológico Nacional de México, Blvd. San Pedro 500, Parque Industrial Ferropuerto Mieleras, Torreón, Coahuila de Zaragoza, México, C.P. 27400.

**Abstract** - Herein, we present an iron-based catholyte of iron (III) chloride was evaluated in microbial fuel cells (MFCs) seeded with anion exchange membrane (AE) and gypsum based membranes. Graphite felt used as a current collector in anode and cathode. MFCs was operated in batch mode using wastewater collected from our University, served as electron donor and biocatalyst at the anodic chamber. Anion exchange membrane (AE) seeded MFCs exhibited the maximum volumetric power density ( $7.6 \text{ W} / \text{m}^3$ ). However, that would stable in a limited time, that could attribute to the crossing of chloride ion to the anodic compartment would lead to the destruction of the bacterium. Further, showed the removal of 90% COD. Gypsum based membrane MFCs showed the  $7.1 \text{ W} / \text{m}^3$  of maximum volumetric power density. Obviously, anion exchange membrane seed MFCs showed the less internal resistance than the gypsum-based membrane MFCs. These MFCs could also work as microbial disinfect cell.

**Index Terms** – microbial fuel cells, gypsum, catholyte, graphite felt.

### I. INTRODUCTION

Electricity generated from organic materials through the biological activity is one of the key issues being explored to reduce the energy consumption for the wastewater treatment process. Further development of the microbial fuel cells (MFCs) would make the wastewater treatment process into sustainable. However many factors obstacles the process of MFCs, one of the major focus is the cathodic chamber. Where the oxygen as final terminal acceptor are attractive. Though the high overpotentials and slow reaction kinetics of the oxygen reduction reaction (ORR) are one of the most limiting factors for MFCs. One of the transition metals is iron (Fe) most

abundant and cost-effective nature of this make attractive for the application of MFCs. Few reports has been reported the use of calcium hypochlorite and sodium hypochlorite as efficient catholyte and disinfection in MFCs [1]. Herein, we could added the iron (III) chloride/iron (II) chloride under the acidic condition at the cathode system, which was evaluated under the anion exchange membrane and gypsum based membrane system.

### II. MATERIALS AND METHODS

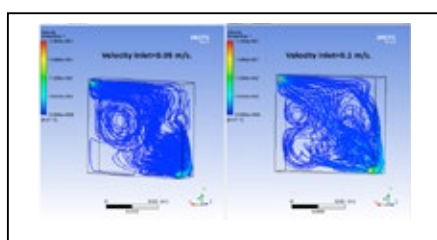
#### A. Construction of iron-based MFC, characterization, and operation

Flow-based microbial fuel cells was constructed with the aid of acrylic based material. Each compartment (anodic and cathodic) of fuel cells had the 120 mL of volume and graphite felt was used as current collector. In the anodic chamber wastewater collected from the Universidad Politecnica de Aguascalientes (UPA) served as inocula and medium to be treated. The cathodic chamber consists of iron (III) chloride/iron (II) chloride under the 0.5 M of sulfuric acid electrolyte. Both side of the fuel cells were separated from membrane of the anion exchange membrane (AE) (procured from the FuMA-Tech- Fumasep FAB-PK-130) / gypsum (Gy) based material. Evaluation of each membrane separately inside the MFCs designated as AE-MFCs and Gy-MFCs. The open circuit potential of the MFCs was monitored periodically with the aid of Fluke digital multimeter. Polarization and power curve was obtained by linear sweep voltammetry at a scan rate of 1 mV/s with two electrode configuration, where employed

cathode was working electrode and anode as a counter as well as a reference electrode. The Power density (PD,  $\text{mW/m}^2$ ,  $\text{mW/m}^3$ ) and current density (CD,  $\text{mA/m}^2$ ,  $\text{mA/m}^3$ ) were calculated on the basis of exposed surface area and volume. Electrochemical impedance spectroscopy was performed within the 100 kHz to 1 mHz at the open circuit potential. The COD and pH of the wastewater were determined according to the Standard Methods with the aid of Henna Instruments[2]

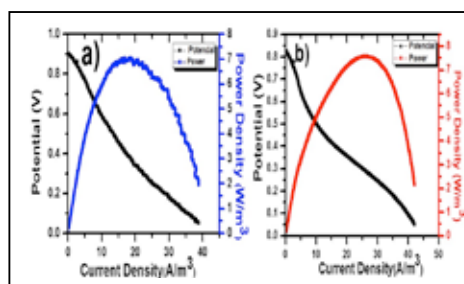
### III. RESULTS AND DISCUSSION

In the flow of anolyte and catholyte was optimized with the aid of ANSYS R16.0 tool. According to the model the solutions inlet was at the top and outlet was at the bottom. The flow rate was maintained at the 0.05 m/s and this was control by the open source Arduino system (Fig.1.).



**Fig. 1. Flow rate optimization of anodic and cathodic chamber (0.05 m/s and 0.1 m/s)**

First batch operation of open circuit potential, the stable potential was observed in the Gy-MFC and reached the maximum OCP of 1.0 V. But in the case of AE-MFC reached the Maximum Voltage of 0.8 and oscillation was observed. Further the Second Batch operation was carried with the liner sweep voltammetry and EIS studies. The maximum volumetric power was reached by the AE-MFC of  $7.6 \text{ W/m}^3$  and  $7.1 \text{ W/m}^3$  for Gy-MFC (Fig.2.). However, AE-MFCs failed to maintained



**Fig. 2. LSV characterization of a) Gy-MFC; and b) AE-MFC**

The stable potential and keep on oscillating the voltage after the 55 hrs of operation. Surprisingly Gy-MFC showed the stable power production even after 150 hrs. Promising COD removal was observed 90 % in Gy-MFC and 85% in AE-MFC. The possible reason behind the oscillation of power production in the AE-MFC could be associated with crossing of anion towards to the anolyte and further interference the process. This was also confirmed by increase of pH at the anolyte. Moreover

the period of time the microbial population was reduced /eliminated by the transfer of Chloride ion from catholyte to anolyte. Similar results was observed in Jadhav et a., 2014, also they added the possibility of trace amount of regeneration of chlorine by avoiding escape of chlorine gas in anodic chamber could change in pH, essential for better voltage in the natural ceramic basic membranes. EIS analysis exhibit the maximum resistance was observed in AE-MFC ( $549 \Omega$ ). It also showed the higher membrane resistance. This could conclude the above discussion of crossing of over of anion interference from the acidic catholyte to anolyte. In both MFCs cathodic resistance maintained equal. Further the constant phase elements (QPE) of both AE-MFC and Gy-MFC were higher. However in the Gy-MFC reveals  $400 \Omega$  of internal resistance from that showed the minimum membrane resistance (Table.1). Further experiment is needed to conclude the tolerance of the acidic catholyte in the Gy-MFCs.

**TABLE I**  
ELECTROCHEMICAL IMPEDANCE SPECTROSCOPY ANALYSIS FOR AE-MFC AND GY-MFC

Parameters	AE-MFC	Gy-MFC
$R_{an}$	287	291
$R_{sep}$	160	7
$R_{cat}$	100	100
QPE1-Q	0.89	0.9
QPE1-n	0.96	0.74
QPE2-Q	0.10	0.2
QPE2-n	0.16	0.8

### IV. CONCLUSION

Most abundant and cost-effective transition metal of Fe based catholyte was formulated under the AE-MFC and Gy-MFC system. This system could drastically reduce the COD in the wastewater as well as reduce the microbial population by the disinfection process together.

### ACKNOWLEDGMENT

KSK would like to acknowledge the funding agency of CONACYT and SEP México.

### REFERENCES

- [1] Jadhav, D. A., Ghadge, A. N., Ghangrekar, M.M., Simultaneous organic matter removal and disinfection of wastewater with enhanced power generation in microbial fuel cell, Bioresource Technology, Volume 163, 2014, Pages 328-334
- [2] Sathish-Kumar, K., Solorza-Feria, O., Tapia-Ramírez, J., Rinderknecht-Seijas, N., Poggi-Varaldo, H.M., Electrochemical and chemical enrichment methods of a sodic-saline inoculum for microbial fuel cells, International Journal of Hydrogen Energy, Volume 38(28), 2013, Pages 12600-12609.

## COMPARISON OF THE SOLID OXIDE FUEL CELL SYSTEM FOR MICRO CHP USING NATURAL GAS WITH A SYSTEM USING A MIXTURE OF NATURAL GAS AND HYDROGEN

G. Cinti\*, K. Hemmes\*\*, and G. Bidini\*

\* Università degli Studi di Perugia, Dipartimento di Ingegneria,  
Via Duranti 67, 06125 Perugia, (Italy)

\*\*TU Delft, Jaffalaan 5, 2628BX Delft, (The Netherlands)

**Abstract** - This study compares the performance of SOFC microCHP systems fueled by a fuel varying from pure hydrogen to pure methane via new mixtures of hydrogen and methane sometimes called Hythane. SOFC systems with external reforming processes were studied. The study shows that even if the stack performance increases due to a higher concentration of hydrogen in the inlet gas mixture, at a system level the natural gas based systems have a higher electric efficiency. This is because of the recovery of heat inside the system by the endothermic steam methane reforming reaction. So the blending of hydrogen into the natural gas leads to a lower electrical efficiency of the SOFC-based micro CHP system by a few point percent, but on the other hand obviously a higher useful heat production is obtained

**Index Terms** –  $\mu$ -CHP, natural gas, hydrogen, Hythane, SOFC.

### I. INTRODUCTION

One of the ways of reaching lower CO<sub>2</sub> emissions is a transition towards a hydrogen economy. In order to accelerate the transition towards a hydrogen economy the introduction of hydrogen into the natural gas grid is studied in several projects and reported in literature [1]. One of the outcomes of these studies is that a huge amount of hydrogen is needed to reach even a few percent of hydrogen in the grid and therefore conventional hydrogen production technologies from natural gas itself become a logical choice for hydrogen production. In that sense we would be less talking about mixing hydrogen into the natural gas but rather look at it as taking the carbon out. This can be done in the form of CO<sub>2</sub> (after steam reforming of natural gas) or even in the form of just carbon after thermal decomposition of the methane in the natural gas [2]. Although not everything is clear about the feasibility and desirability of introducing hydrogen into the natural gas grid, in this study we will simulate the effects of the introduction of hydrogen into the

natural gas on a micro CHP system based on the solid oxide fuel cell. The research question we would like to answer is:

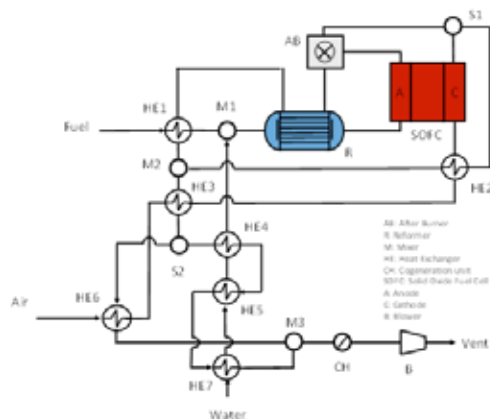
Does the efficiency of the system running with hydrogen mixed into the natural gas increase or decrease compared to the system running on pure natural gas?

### II. THEORETICAL CONSIDERATIONS.

By mixing hydrogen into the natural gas we expect the Nernst potential to increase due to the higher hydrogen partial pressure in the mixture. The higher Nernst potential or open circuit potential in general means a higher efficiency. On the other hand the reforming of natural gas is an endothermic reaction taking away a lot of the waste heat produced in the fuel cell thereby upgrading the waste heat into chemical energy again, which makes internal reforming fuel cells so very attractive from a thermodynamic point of view. On the other hand the higher Nernst potential induces a higher Nernst loss in the fuel cell because the average Nernst potential in the cell is still comparable with the situation in which less hydrogen would be introduced in the fuel yielding more or less the same averaged Nernst potential over the whole cell, making the average deviation with the higher OCV (=Nernst loss) larger. Therefore in our system simulations we must be careful to include Nernst loss in a proper way and not simply model the fuel cell with an internal resistance or just with a fixed polarization. The flow sheet program we are using is called Cycle Tempo [3]. It includes the Nernst loss in the fuel cell module in the correct way by calculating a.o. the local partial pressures of reactant and product gasses and current density as a function of the local position in the cell, as has been verified with experimental data. [4].

### III. MODEL DESCRIPTION

The scheme of the CHP system is depicted in **Figure 1**. The system integrates the SOFC stack, the external reforming operating at constant steam to carbon ratio of 2.2, and a post combustor. A complex network of seven heat exchangers allows for thermal equilibrium of the system. Heat is supplied by the stack, as high temperature off gasses and by the after burner where the unused hydrogen coming from the anode is oxidized. High temperature off gasses from the burner are supplied to the reformer, for the high temperature operation and the two gas inlet lines, included water evaporator.



**Figure 1 Scheme of the CHP unit**

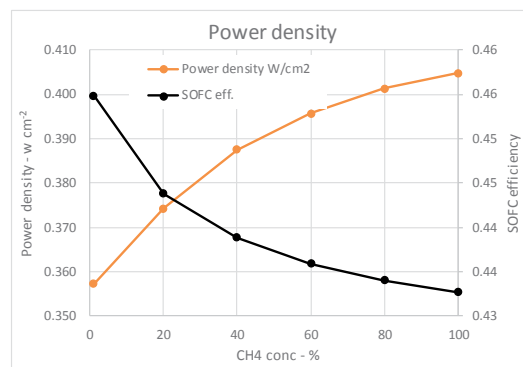
The SOFC has a total active cell area of 300 m<sup>2</sup>, an internal resistance of  $2.8 \cdot 10^{-5} \Omega \text{ m}^2$  and fuel utilization is set at 0.8. Anodic and cathodic pressure losses are 0.02 and 0.05 Bar respectively. Further design specifics are reported in **Errore**.  
L'origine riferimento non è stata trovata..

TABLE I  
DESIGN SPECIFICS OF THE SYSTEM

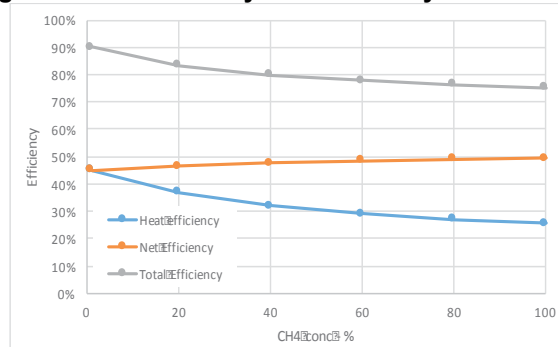
SOFC stack temperature (°C)	750
SOFC stack inlet temperature (°C)	700
SOFC stack outlet temperature (°C)	800
Reformer reaction temperature (°C)	700
Burner outlet temperature (°C)	1200
Reformer gas inlet temperature (°C)	400
Reformer gas outlet temperature (°C)	700
HE6 air outlet temperature (°C)	350
HE7 water outlet temperature (°C)	99
HE5 steam outlet temperature (°C)	101
HE4 steam outlet temperature (°C)	400
Pressure losses in Heat exchangers (bar)	0.02

### IV. RESULTS

Results of the flowsheet simulations in terms of thermal and electrical efficiency are reported in **Figure 2** and **Figure 3**. The figures show that even if SOFC efficiency increases when moving from methane to Hythane, at system level the presence of hydrogen shifts the system output from electricity to heat with an increase of total efficiency due to lower heat losses via off gasses.



**Figure 2 Power density and efficiency at SOFC level**



**Figure 3 Heat, electrical and total efficiency**

### V. CONCLUSION

The study shows how the introduction of hydrogen in natural gas pipes increases total efficiency (power + heat) of a SOFC-CHP system yet at the expense of a decrease in electric efficiency with a few point percent. It also reduces the consumption of water.

### REFERENCES

- [1] Hemmes K. Exploring new production methods for hydrogen/natural gas blends. Chapter in Enriched Methane: The First Step Towards the Hydrogen Economy (p215-234) edited by Marcello De Falco • Angelo Basile. Springer - ISSN 1865-3529 Green Energy and Technology ISBN 978-3-319-22191-5 .
- [2] Cinti G, Hemmes K. Integration of direct carbon fuel cells with concentrated solar power. Int J Hydrogen Energy 2011;**36**:10198–208.
- [3] <http://www.asimptote.nl/software/cycle-tempo/cycle-tempo-model-examples/> n.d.
- [4] Au, S. F., Woudstra, N., Hemmes, K., & Uchida, I. (2003). Verification of a simple numerical fuel cell model in a flowsheeting program by performance testing of a 110 cm(2) Molten Carbonate Fuel Cell. Energy Conversion and Management **44**, 2297-2307.



## PRELIMINARY TESTING OF THE IMPLEMENTATION PROCEDURE OF A MODEL-BASED DIAGNOSTIC ALGORITHM FOR A SOLID OXIDE FUEL CELL SYSTEM

P. Polverino\*, D. Marra\*, M. Gallo\*, M. Sorrentino\*, C. Pianese\*, M. Vidmar\*\*, A. Pohjoranta\*\*\*

\*Dept. of Industrial Engineering, University of Salerno, via Giovanni Paolo II 132, 84084 Fisciano (SA), (Italy)

\*\*INEA d.o.o., Stegne 11, SI-1000 Ljubljana, (Slovenia)

\*\*\*VTT Technical Research Centre of Finland Ltd, P.O. Box 1000, FI-02044 VTT, (Finland)

**Abstract** - The present paper describes the implementation procedure of a model-based diagnostic algorithm on a Programmable Logic Controller (PLC) directly connected to a Solid Oxide Fuel Cell (SOFC) system. The proposed work has been performed within the EU-funded project DIAMOND and focuses on an Anode Off-Gas Recycling (AOGR) SOFC system. The considered diagnostic algorithm is based on an advanced model-based approach, which uses a mathematical model to simulate the system in normal conditions and to extract residuals for fault detection and isolation. The implementation procedure entails two main steps: the first one consists in the mathematical reduction of the diagnostic algorithm, and the second one in the proper coding for PLC implementation. The authors adopted a hierarchical approach to reduce model complexity while keeping suitable accuracy for online diagnostic purposes. The correctness of the implementation procedure has been firstly verified offline and then online with the running SOFC.

**Index Terms** – *Diagnosis, PLC, Software Implementation, Solid Oxide Fuel Cell.*

### I. INTRODUCTION

In the current energetic scenario, fuel cells are becoming highly competitive with respect to internal combustion engines and batteries. Particularly, Solid Oxide Fuel Cells (SOFCs) offer a suitable solution for cogeneration applications, being capable of producing electrical and thermal energy with high efficiency and power density. Nevertheless, their performance and lifetime are highly affected by several degradation phenomena and malfunctions. Suitable diagnostic algorithms combined with dedicated control strategies can significantly improve SOFC system durability and availability.

However, the optimal development of a diagnostic algorithm may suffer from performance reduction when adapted for their implementation on commercial equipment for on-field uses.

Indeed, the authors proposed in [1] the development of a model-based diagnostic algorithm, which combined a Fault Tree Analysis (FTA) approach with a fault simulation investigation to design a Fault Signature Matrix (FSM) for an SOFC system. Afterwards, such algorithm has been characterized on a real system [2], highlighting the limitations occurring under on-board sensors reduction. In such case, the unavailability of some sensors may reduce the number of monitored variables and thus hinder univocal faults isolation. This event has been addressed to as fault clustering. To tackle this problem, the authors proposed an advanced approach by means of isolated sub-model analysis [3]. Through this methodology, the proper use of system component sub-models can increase residuals redundancy, theoretically solving the fault clustering issue. Through a real case study, the authors addressed some implementation problems when facing the online use of the algorithm.

The present work describes the implementation procedure of the diagnostic algorithm designed in [3] on a standard industrial Programmable Logic Controller (PLC) connected to an Anode Off-Gas Recycling (AOGR) SOFC system (system scheme can be found in [3]). In the next sections, the implementation procedure is firstly described, followed by the offline and online verification of proper algorithm operation.

### II. DIAGNOSTIC ALGORITHM IMPLEMENTATION ON PLC

The design of a diagnostic algorithm is usually performed offline, as done in [1] and [3]. Nevertheless, real benefits are expected within online applications. When addressing these cases, the implemented algorithm must cope with the available computational resources: it has to keep an acceptable accuracy while ensuring reasonable computational burdens.

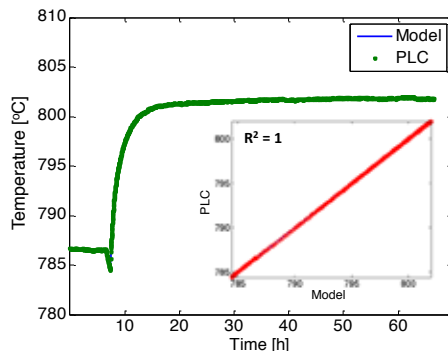
The diagnostic algorithm designed in [3] has been based on a dynamic SOFC system model developed through a lumped modelling approach [4]. This model implements mass and energy balances as well as non-linear equations for electrochemical processes. This mathematical representation is not suitable for direct PLC applications, thus requiring a proper reduction procedure.

It is worth noting that PLC devices could not handle complex nonlinear differential equations. Thus, to tackle PLC implementation, a proper finite difference approach has been chosen, to retain model accuracy and allow on-board diagnosis. Specifically, an Euler forward method has been considered for discrete time derivatives, assuming a constant time step of 60 s. Moreover, look-up tables and multi-variable regressions have been introduced instead of the non-linear electrochemical processes, while preserving acceptable physical adherence.

Once completed all system model and diagnostic equations reduction, the obtained algorithm has been properly coded for PLC operation.

### III. IMPLEMENTATION PROCEDURE VALIDATION

To verify the correct diagnostic algorithm implementation on the PLC and to detect any loss in accuracy, a first offline evaluation has been performed. The PLC algorithm outputs have been compared to those of the complete model. An example of algorithm evaluation is presented in Fig. 1 with respect to post-burner outlet temperature.



**Fig. 1. Offline PLC algorithm testing.**

The bigger plot shows the time behaviour of the outlet temperature simulated by the model (solid blue line) and by the PLC (green dots). It can be seen that the PLC algorithm perfectly reproduces the model results, as proved by the correlation plot (smaller box) and the  $R^2$  coefficient equal to 1.

### IV. DIAGNOSTIC ALGORITHM ONLINE TESTING

The diagnostic algorithm implemented on PLC has been then operated online, with the whole SOFC system running. To test the correctness of the operation, the algorithm was fed with an experimental input showing a value not corresponding to nominal state. As response, the algorithm was capable to detect the wrong system state, giving a -1 indicator as output (which

means wrong system operation, but not related to the accounted SOFC system component faults). A representation of the user interface showing the algorithm diagnostic output during the wrong system state is given in Fig. 2.



**Fig. 2. Online PLC algorithm testing.**

### V. CONCLUSION

In this work the implementation procedure of a model-based diagnostic algorithm on a PLC has been presented. The algorithm, developed following a model-based approach, aims at detecting faults at system level on an AOGR SOFC system. The implementation procedure of the algorithm on the PLC entailed two main steps: the first one consisted in the mathematical reduction of the algorithm and the second one in the proper coding for PLC. An offline evaluation of the proper algorithm implementation was accomplished, followed by an online verification of its performance.

### ACKNOWLEDGMENT

The research leading to these results has received funding from the European Union's Seventh Framework Programme (FP7/2007–2013) for the Fuel Cells and Hydrogen Joint Technology Initiative under grant agreement n° 621208 (Project - DIAMOND, Diagnosis-aided control for SOFC power systems).

### REFERENCES

- [1] Polverino, P., Pianese, C., Sorrentino, M., Marra, D., Model-based development of a fault signature matrix to improve solid oxide fuel cell systems on-site diagnosis, *Journal of Power Sources*, Volume 280, 2015, Pages 320-338.
- [2] Polverino, P., Esposito, A., Pianese, C., Ludwig, B., Iwanschitz, B., Mai, A., On-line experimental validation of a model-based diagnostic algorithm dedicated to a solid oxide fuel cell system, *Journal of Power Sources*, Volume 306, 2016, Pages 646-657.
- [3] Polverino, P., Sorrentino, M., Pianese, C., A model-based diagnostic technique to enhance faults isolability in Solid Oxide Fuel Cell systems, *Applied Energy*, 2017, In press.
- [4] Marra, D., Sorrentino, M., Pohjoranta, A., Pianese, C., Kiviahio, J., A lumped dynamic modelling approach for model-based control and diagnosis of Solid Oxide Fuel Cell system with anode off-gas recycling, *ECS Transactions*, Volume 68, 2015, Pages 3095–3106.

## M/CGO CERMET BASED ELECTRODES FOR IT-SOFC FEED WITH BIOGAS

G. Carollo\*, A. Garbujo\*, A. Bedon\*, D. Ferri\*\*, M.M. Natile\*, A. Glisenti\*

\*University of Padova/CNR-ICMATE, Department of Chemical Sciences, via Francesco Marzolo 1, Padova, Italy

\*\*Paul Scherrer Institut, Villigen PSI, 5232, Switzerland

**Abstract** – *M*-based ( $M=\text{Cu, Fe, Mo}$ ) cermets suitable for electrodes in Solid Oxide Fuel Cells (SOFCs) based on Cerium Gadolinium Oxide (CGO) electrolyte were developed and successfully tested in the intermediate temperature range. The M/CGO cermets were prepared by a self-combustion based citrate procedure and the effects of synthesis conditions were studied. Characterization of the Cu/CGO nanocomposites by XPS, XRD, SEM, EDX, TPR suggested that this procedure allows obtaining highly dispersed oxide on the cerium gadolinium oxide. Synthesis parameters affected properties and catalytic performance. The behaviour under redox conditions was studied by operando high-energy XRD

*The high stability, reversibility, catalytic activity, and electrochemical performance (EIS) make these electrodes promising for SOFCs feed with biogas.*

**Index Terms** - Biogas, Cermet, CGO, SOFC.

### I. INTRODUCTION

Ni-YSZ cermets are the most traditionally diffused anodes for Solid Oxide Fuel Cells (SOFCs) but their use in direct methane fuel cells is complicated by their capability to catalyse the formation of carbon filaments that cause the efficiency loss of the device [1]. Copper based ceria cermets demonstrated to be advantageous in replacing Ni-cermets for direct hydrocarbons SOFCs [2]. In these cermets the electrical conductivity is warranted by copper, whereas ceria is responsible for the catalytic activity in oxidation reactions. In the present contribution, we developed and optimized a new procedure for the Cu-CGO10 cermet synthesis using the citrate route in order to obtain highly dispersed oxide nanoparticles in CGO10, and investigate more metals for increase the stability of the Cu-CGO10 cermet and the electrochemical performance.

### II. EXPERIMENTAL

#### A. Synthesis

The nanocomposites M/CGO were obtained by the citrate method starting from CGO, (Sigma-Aldrich >99%, dimension 5-10nm), and M ( $M=\text{Cu/Fe/Mo}$ ). Citric acid monohydrate

(Sigma Aldrich >99%) was added to an aqueous solution of the M cations, obtained by mineralization of the metal's precursors with nitric acid, with a molar ratio of 1.9:1 with respect to the total amounts of cations. Before adding CGO powder to the solution, the pH was adjusted to reach respectively 1, 4 and 8 obtaining three different solutions from whom a different complexation and final particles' dispersion is expected. At the end of the heat treatment, the powders were grinded and calcined at 600°C for 5 h. This procedure was preferred to the traditional wet impregnation to allow the deposition of copper oxide in highly dispersed form thanks to the complexation of the citrate.

#### B. TPR

The TPR (Temperature Programmed Reduction) curves of as prepared CuO/CGO samples (Figure 1) exhibited a signal due to the  $\text{Cu(II)} \rightarrow \text{Cu(0)}$  reduction at ca. 250°C. The corresponding signal in the CuO reference was observed at 316°C. The lower reduction temperature was consistent with the extent of dispersion of CuO [3]. A weak shoulder at low temperature (180-200°C), becoming more evident as the synthesis pH increases, suggested the presence of highly dispersed nanoparticles. This important result confirmed the possibility to obtain highly dispersed particles by opportunely modifying the citrate synthesis procedure.

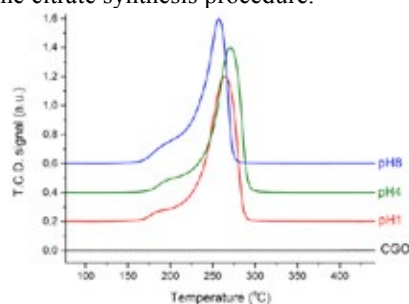


Figure 1 TPR curves of the CuO/CGO nanocomposites obtained at increasing pH from bottom to top: pH1 = red, pH4 = green, pH8 = blue. The line of CGO is reported for comparison (black line).

### C. Catalytic and electrocatalytic tests

The catalytic behaviour observed before and after the deposition of copper oxide, as an example, is reported in Figure 2.

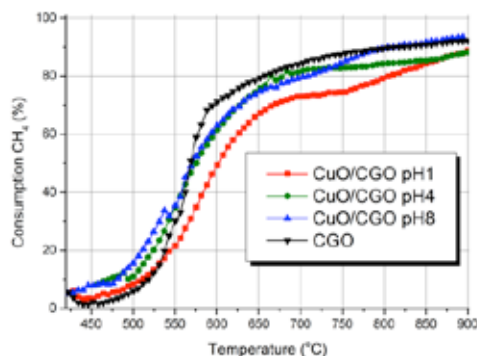


Figure 2 Catalytic activity in methane oxidation observed for the CGO before and after copper oxide deposition.

The CGO support started to be active in methane oxidation at 475°C; the  $T_{50}$  was 575°C and a conversion of more than 80% was reached at 650°C. In the temperature range more interesting for the application in SOFCs (600-800°C) the CGO showed good catalytic activity. Moreover, CGO was also selective towards the complete oxidation. The deposition of CuO did not decrease the catalytic activity significantly: the catalytic activity decreased only in the nanocomposite obtained at pH = 1 ( $T_{50}$  = 600°C; 80% conversion at 800°C).

The EIS measurements confirm that the Area Specific Resistance (ASR) significantly decreases due to presence of copper and its dispersion as a function of temperature.

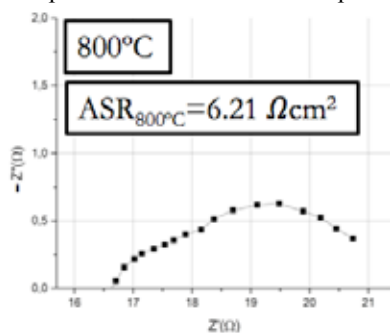


Figure 3 Nyquist Plot obtained at 800°C, CuCGO pH=8.

The Nyquist plot (Figure 3) analysis allowed to distinguish between the different contributions: at high frequencies is visible one semicircle due to the combustible's oxidising process charge transfer, and at low frequencies the contribution of diffusion process at the electrode surface [4].

Interesting results have also been obtained when considering Fe and Mo.

### D. Time-resolved XRD

The behaviour under reducing conditions was investigated in more detail by collecting time-resolved XRD patterns. Redox pulses of diluted  $H_2$  and  $O_2$  were performed at 400°C. The

phase transitions were followed at 0.5 s/pattern (Figure 4) and the products were detected with a mass spectrometer.

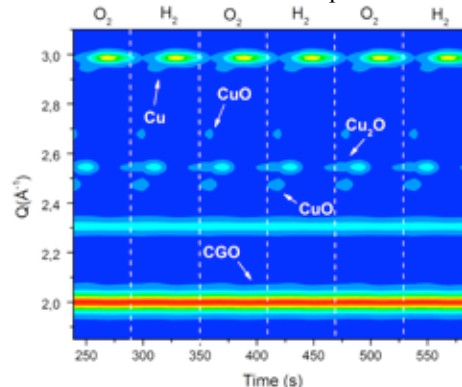


Figure 4 2D visualization of the operando XRD data acquired during repeated and consecutive pulses of 5 vol%  $H_2$ /Ar and 5 vol%  $O_2$ /Ar at 400°C.

As expected, the mass analysis revealed the formation of water as product when the sample was in reducing environment. During the redox pulsing, the copper dispersed on the CGO surface changed repeatedly and reversibly from CuO to Cu through  $Cu_2O$  in the  $H_2$  pulse and re-oxidized reversibly in the  $O_2$  pulse. The main XRD reflex of the CGO phase also exhibited a reversible change of d spacing in the reductive and oxidative pulses suggesting a reversible expansion/contraction of the CGO lattice upon oxygen exchange with the environment but without loss of the structure.

### III. CONCLUSION

In this contribution we developed a new procedure for the dispersion of metal oxides on CGO. We observed that the copper distribution can be controlled through the appropriate selection of the synthesis conditions. The highly dispersed metal enhances electron conductivity without decreasing the catalytic performance of CGO. The structural behavior observed by operando time-resolved XRD confirms the stability and reversibility of the cermet under reducing and oxidizing condition, and therefore the possibility to use this material as electrode in intermediate temperature Solid Oxide Fuel Cells.

### REFERENCES

- [1] S. Mc Intosh, R. J. Gorte; Chem. Rev. 104 (2004) 4845.
- [2] S. Park, R. J. Gorte, J.M. Vohs; Applications of heterogeneous catalysis in the direct oxidation of hydrocarbons in a solid-oxide fuel cell; Appl. Catal. A. Gen. 200 (2000) 55-61.
- [3] G. Perin, J. Fabro, M. Guioetto, Q. Xin, M.M. Natile, P. Cool, P. Canu, A. Glisenti; Cu@LaNiO3 based nanocomposites in TWC applications. App. Catal. B Environ. 209 (2017) 214 and references therein.
- [4] A. R. O. Sousa, A. J. M. Araujo, G. S. Souza, J. P. F. Grilo, F. J. A. Loureiro, D. P. Fagg, and D. A. Macedo, "Electrochemical assessment of one-step Cu-CGO cermets under hydrogen and biogas fuels," Mater. Lett., pp. 10–13, 2017.

## CARBON DIOXIDE AND PRODUCT WATER EXHAUSTS IN A SMALL DIRECT METHANOL FUEL CELL WITH DIFFERENT SIZES OF SERPENTINE CHANNELS

Kohei Nakashima\*

\*Meijo University, 1-501 Shiogamaguchi, Tempaku-ku, Nagoya, Aichi 468-8502,  
(Japan)

**Abstract** – An efficient direct methanol fuel cell (DMFC) must effectively exhaust carbon dioxide (CO<sub>2</sub>) gas bubbles and slugs from its anode channel, and product water accumulation from its cathode channel. This study utilized a transparent DMFC with different sizes of serpentine channel, and investigated the exhaust volume and behavior of CO<sub>2</sub> bubbles and slugs from the anode channel, and the exhaust volume and behavior of product water droplets and accumulation from the cathode channel, as well as cell performance. Results indicated that, compared to larger anode and cathode channels, smaller anode and cathode channels decreased the exhaust volume per CO<sub>2</sub> slug and increased cell performance.

**Index Terms** - Carbon Dioxide, Direct Methanol Fuel Cell, Flow Channel, Product Water

### I. INTRODUCTION

When a direct methanol fuel cell (DMFC) generates electricity, it produces carbon dioxide (CO<sub>2</sub>) gas bubbles at its anode. These CO<sub>2</sub> bubbles grow and eventually coalesce into gas slugs. Similarly, the cathode produces expanding water droplets. As these waste products accumulate and grow larger, they tend to block the channels, inhibiting the mass transfer of methanol and oxygen to the catalyst layers, thus decreasing cell voltage. Previous researchers used transparent DMFCs to observe the behavior of both CO<sub>2</sub> bubbles and slugs in the anode channel and product water in the cathode channel [1]. However, we have seen no full reports investigating how large the CO<sub>2</sub> slugs and product water accumulation would grow in the flow channel before exiting through the exhaust ports. This study utilized our small transparent DMFC to investigate the exhaust volume and behavior of CO<sub>2</sub> bubbles and slugs from the anode channel, and the exhaust volume and behavior of product water droplets and accumulation from the cathode channel, as well as cell power performance, as we varied flow section area of serpentine channels, as well as the flow rates of methanol-water solution and air.

### II. EXPERIMENTAL APPARATUS AND PROCEDURE

Our transparent DMFC (with an active area of 4cm<sup>2</sup>) comprised a membrane electrode assembly (MEA), gaskets, separators, gaskets with serpentine channels, and end plates. The MEA was a Nafion 112 membrane (with a thickness of 50μm) with Pt:Ru 1:1 catalysts (3mg/cm<sup>2</sup>) in the anode and only Pt (1mg/cm<sup>2</sup>) in the cathode. The gas diffusion layers were made of carbon paper (with a thickness of 0.37mm). The separator was made of carbon with a gas-impermeable treatment, and had a serpentine through-channel (with a width of 2mm, and a lateral length of 18mm). We prepared two different depths of channels. One channel had a depth of 2mm, and another had a depth of only 1.2mm to increase the supply flow velocity of methanol solution and air.

Methanol solution (3wt %) was supplied in an upward flow at rates of 0.14mL/min and 0.28mL/min, and air was supplied in a downward flow at rates of 18mL/min and 36mL/min. We set the cell temperature to 60°C, then plotted polarization curves by measuring the DMFC voltage while increasing the current density in increments of 1.25mA/cm<sup>2</sup>. When the DMFC voltage dropped below 0.4V, we used a video camera to observe CO<sub>2</sub> bubbles and slugs in the anode channel and product water droplets and accumulation in the cathode channel, as we continued to increase the current density in increments of 1.25mA/cm<sup>2</sup> every five minutes. By analyzing the observed results, we calculated the volume of CO<sub>2</sub> slugs and product water accumulation ejected from the channels through the exhaust ports.

### III. RESULTS AND CONSIDERATION

With both anode and cathode depths of 2mm, as we varied the flow rates of methanol solution and air, cell performance hardly changed, except at lower flow rates. At lower flow rates of both methanol solution and air, the cell voltage decreased at higher current densities. In all flow rates of methanol solution and air, voltage fluctuation increased at higher current



densities.

Figure 1 shows the exhaust volume of CO<sub>2</sub> slugs with both anode and cathode depths of 2mm. As the methanol solution flow rate increased the exhaust volume per CO<sub>2</sub> slug decreased, in each air flow rate. Not shown in the figure of the exhaust volume of water accumulation, when the methanol solution flow rate increased, the exhaust volume of water accumulation per unit time increased with a lower air flow rate, and decreased with a higher air flow rate. It seems that, as the methanol solution flow rate increases, CO<sub>2</sub> bubbles tend not to coalesce, and instead crossover. With this higher methanol solution flow rate and a lower air flow rate, the methanol solution by crossover may be contained in the exhaust volume of water accumulation. It is thought that crossover decreases with higher flow rates of methanol solution and air. It appears that, with a lower methanol solution flow rate and a higher air flow rate, the reaction becomes active, increasing the exhaust volume of both CO<sub>2</sub> slug and water accumulation per unit time.

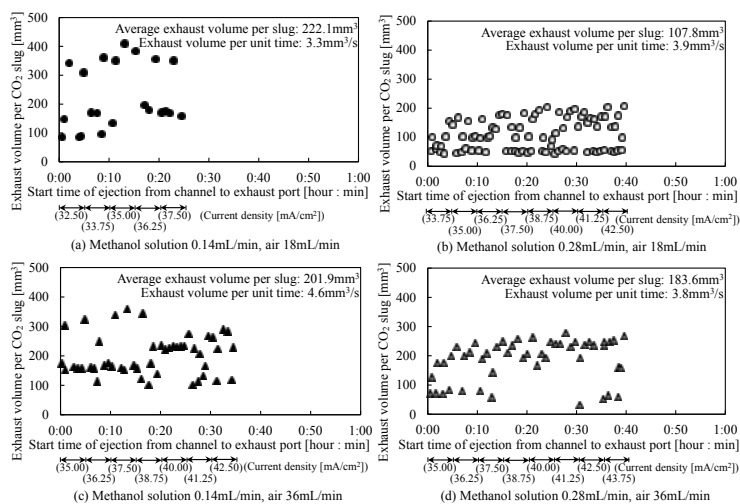


Fig. 1 Exhaust volume of CO<sub>2</sub> slugs with both anode and cathode depths of 2mm

With both anode and cathode depths of 1.2mm, in each flow rate of methanol solution and air, the cell performance hardly changed. However, compared with the deeper channel depths, here cell performance increased and voltage fluctuation decreased at higher current densities. The shallower channel depths in both anode and cathode increased the maximum power density by 5% to 12% compared with the deeper channel depths.

Figure 2 shows the exhaust volume of CO<sub>2</sub> slugs with both anode and cathode set at depths of 1.2mm. Compared with the deeper channel depths in Fig. 1, here in each flow rate of methanol solution and air, the exhaust volume per CO<sub>2</sub> slug decreased, and the exhaust volume of CO<sub>2</sub> slug per unit time increased. As the methanol solution flow rate increased, the exhaust volume per CO<sub>2</sub> slug hardly changed with a low air flow rate, but decreased with a higher air flow rate. Not shown

in a figure, when the methanol solution flow rate increased, the exhaust volume of water accumulation per unit time increased with a lower air flow rate, but did not change with a higher air flow rate. As the air flow rate increased, the exhaust volume per CO<sub>2</sub> slug increased with a lower methanol solution flow rate, and decreased with a higher methanol solution flow rate. When the air flow rate increased, in each methanol solution flow rate, the exhaust volume of water accumulation per unit time decreased. With shallower channel depths, as the methanol solution flow rate increases, crossover tends to occur, because the exhaust volume of CO<sub>2</sub> slug per unit time tends to decrease. With shallower channel depths, it seems that, as the air flow rate increases, some product water ejects from the channel by a higher air flow velocity, before the product water attaches in the channel, grows and accumulates there.

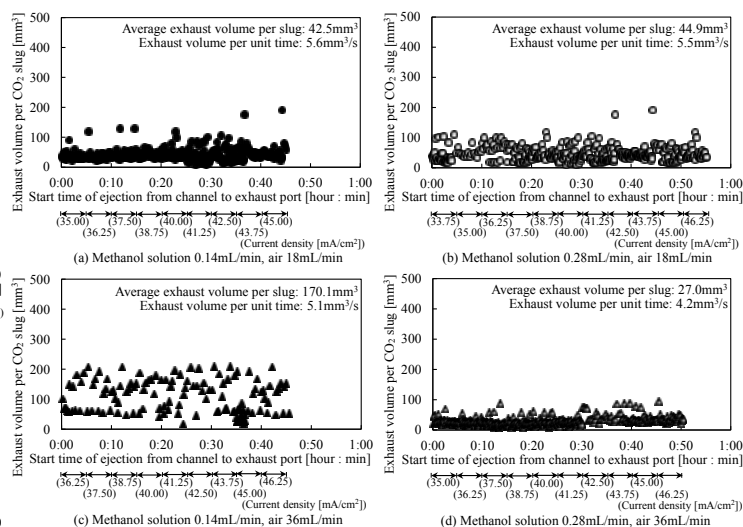


Fig.2 Exhaust volume of CO<sub>2</sub> slugs with both anode and cathode depths of 1.2mm

#### IV. CONCLUSION

Using our small transparent DMFC, we systematically examined the exhaust volume of CO<sub>2</sub> slug and water accumulation. We found that shallower channel depths in both anode and cathode decreased the exhaust volume per CO<sub>2</sub> slug, increased cell performance, and decreased voltage fluctuation at higher current densities.

#### ACKNOWLEDGEMENT

I would like to thank graduate school students Mr. Hirokazu Shimizu and Mr. Ryuta Inagaki, and undergraduate school student Mr. Daisuke Miyajima, of Meijo University at that time, for fruitful cooperation during our experimental work.

#### REFERENCES

- [1] Hsieh, S., Wu, H., Her B., A Novel Design for a Flow Field Configuration, of a Direct Methanol Fuel Cell, Journal of Power Sources, 195, 2010, pp. 3224-3230.

## AL-AIR SEMI-FUEL CELLS WITH SOLID ELECTROLYTES BASED ON CARBOHYDRATE POLYMERS

M.F. Gaele<sup>\*,\*\*</sup>, F. Migliardini<sup>\*</sup>, T.M. Di Palma<sup>\*</sup>, P. Corbo<sup>\*</sup>

<sup>\*</sup>Istituto Motori – National Research Council of Italy. Via Marconi,  
4 – Naples (Italy)

<sup>\*\*</sup>Università degli Studi di Napoli “Parthenope” Centro Direzionale  
- Isola C4 - 80143 Naples (Italy)

**Abstract** - In this paper hydrogels based on Xanthan (a bacterial polysaccharide commercially produced by secretion from the bacterium *Xanthomonas campestris* in aerobic fermentation conditions) were prepared and tested as solid alkaline (KOH) and acid (HCl) electrolytes for Al-air semi-fuel cells. Electrochemical impedance spectroscopy (EIS), potentiodynamic polarisation curves (IE) and weight loss (WL) technique were used for cell performance analysis. Results showed that high KOH and HCl concentrations (up to 8M) and xanthan/liquid solution ratios in the range 0.6–1.4 g/ml permitted the preparation of solid electrolytes stable over time, with ionic conductivities of applicative interest ( $10^{-2}$  S/cm). Discharge tests effected on Al/air cells evidenced promising values of energy delivered when gels made by 8 M solutions were used (up to about 50 mAh/cm<sup>2</sup>). The corrosion inhibiting effect of xanthan in acid media was also verified.

**Index Terms** - Al-air batteries, Gel polymer electrolytes, Xanthan.

### I. INTRODUCTION

Aluminum is a renewable energy carrier characterized by high calorific value, in particular its theoretical specific energy (about 8 kWh/kg) is comparable to that of conventional fossil fuels. Other advantages of this metal are abundance in nature and production level compatible with its large-scale integration in global energy production and storage for post-fossil fuel era. Unlike hydrogen, Al is easy and safe to transport and store [1].

The electrochemical oxidation of Al represents a high efficiency route to exploit the energy content of this metal, in particular the Al-air semi-fuel cells are the most perspective aluminum-based battery in the view of its mass utilization. The most important feature of a metal-air battery

is the coupling of a metal anode, characterized by high energy density, and an open structure catalysed cathode able to continuously draw and reduce oxygen from atmosphere [2]. This feature is responsible for the intrinsically high theoretical energy density, generally associated with this type of device.

The interest in using solid electrolytes in electrochemical devices is justified by their well-known advantages with respect to liquid ones, i.e. absence of leakage, high electrochemical stability at high voltages and excellent temperature stability, all characteristics that enhance safety issues. In this context, carbohydrate polymers have been recently proposed for numerous electrochemical applications as they can be manufactured by simple and reliable processes, and provide ion conductivities comparable to those of liquid electrolytes [3].

This paper reports performance analysis and characterization regarding the utilization of xanthan based acid and alkaline hydrogels as solid electrolytes for Al-air cells.

### II. EXPERIMENTAL

Xanthan gum (MW =  $2 \cdot 10^6$  g/mol), HCl solution (36-38 wt%), KOH solutions (45%) and pure Aluminium (99.998%, 0.5 mm thick) were used as materials for Al-air cells. Air cathodes were prepared starting from a carbon cloth (0.35 mm thick, 116 g/m<sup>2</sup>), used to sustain a Pt based catalyst. Hydrogels were prepared starting from xanthan powder and HCl or KOH solutions of different concentrations, for different solid/liquid ratios, from 0.6 to 1.4 g/ml.

Discharge tests of Al-air cells were carried out at constant

discharge current values comprised in the range 1-10 mA.

EIS and WL were used for cell performance analysis. Al corrosion evaluation was performed by WL and IE using a two electrode cell configuration versus Pt as both reference and counter electrode.

### III. RESULTS AND DISCUSSION

Table I reports ionic conductivity and anodic efficiency values for Al-air cells using selected solid electrolytes based on xanthan and KOH or HCl 1M and 8M. OCV values were comprised between 1.3 and 1.6 V for all cells. Conductivity resulted about  $10^{-2}$  S/cm as order of magnitude for all samples, before tests, and the highest values were obtained for gels based on KOH, because of the lower solid/liquid ratio that could be realized in preparation of these samples (for higher ratio not stable gels were obtained with KOH).

TABLE I  
IONIC CONDUCTIVITIES AND ANODIC EFFICIENCY OF SOLID ACID AND  
ALKALINE HYDROGELS IN AL-AIR CELLS

Electrolyte (liquid phase- xanthan/liquid ratio)	Discharge current, mA	Ionic conductivity, S/cm as prepared cell*	Ionic conductivity, S/cm, after discharge*	Anodic efficiency, %
KOH 1 M-0.6	1	$2.1 \cdot 10^{-2}$	$1.9 \cdot 10^{-2}$	44
KOH 8M-0.6	1	$8.8 \cdot 10^{-2}$	$6.8 \cdot 10^{-2}$	28
KOH 8M-0.6	10	$8.8 \cdot 10^{-2}$	$4.1 \cdot 10^{-2}$	78
HCl 1M-0.7	1	$1.8 \cdot 10^{-2}$	$0.8 \cdot 10^{-2}$	61
HCl 8M-1.4	1	$2.3 \cdot 10^{-2}$	$1.2 \cdot 10^{-2}$	76
HCl 8M-1.4	3	$2.3 \cdot 10^{-2}$	$0.5 \cdot 10^{-2}$	83

\*by EIS spectra of Al-air cells

After discharge tests conductivities hold the same order of magnitude even though a slight reduction was observed for all samples. Anodic efficiency values shown in Table I were calculated as percentage ratio between the amount of Al consumed by oxidation with current production and the total Al consumed during the discharge tests (7 h). The electrolyte based on KOH 1M and 0.6 g/ml solid/liquid ratio provided an anodic efficiency of 44%, however the related discharge test ended after only 40 minutes, when cell voltage dropped to unacceptable values (0.2 V). For alkaline 8M electrolytes the anodic efficiency increased from 28 to 78% as function of discharge current (from 1 to 10 mA). The value of 44% observed at KOH 1M was due to the short duration of the test. Anodic efficiencies higher than 60% were observed for all acid electrolytes, with a maximum of 83% for the solid/liquid ratio of 1.4 g/ml and HCl 8M at 3 mA as discharge current. The highest anodic efficiencies observed for acid solid electrolytes were correlated with a possible effect of Al corrosion inhibition of xanthan polysaccharide in acid medium. This effect was evidenced by WL, EIS and IE measurements. Gravimetric tests evidenced a minor weight loss when the solid/liquid ratio increased at parity of HCl concentration, while EIS effected after discharge tests showed a large capacitive loop at medium frequencies, correlated with the resistance of the

protective layer due to inhibiting agent. IE measurements related to gels based on HCl 5M were reported in Figure 1, and compared with data collected from 5M acid solution.

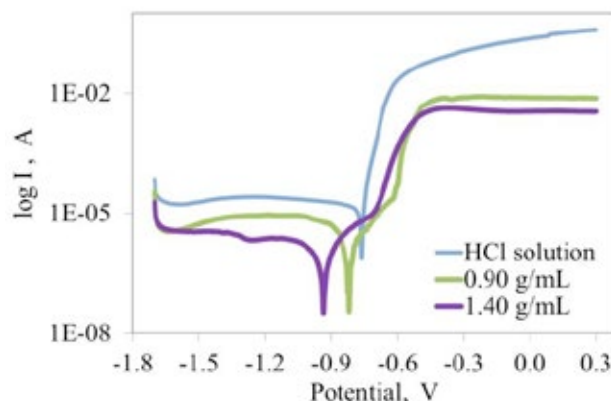


Fig. 1. Potentiodynamic polarization curves for acid solid gels based on HCl 5M at two solid/liquid ratios.

Shifts towards more negative potentials and a decrease of Tafel corrosion currents ( $j_{\text{corr}}$ ) were observed passing from liquid solution to solid electrolytes at increasing solid/liquid ratio ( $j_{\text{corr}}$  decreased from 22 to 1.5  $\mu\text{A}/\text{cm}^2$  for liquid and gel 1.4 g/ml, respectively).

### IV. CONCLUSION

A “green” and low cost polysaccharide permitted the synthesis of solid electrolytes for Al-air semi-fuel cells starting from both acid and alkaline solution at concentrations up to 8 M. The high ionic concentration together with high solid/liquid ratios in gel preparation provided ionic conductivity and cell anodic efficiency of applicative interest. The best results, obtained for acid electrolytes, were correlated with the capability of xanthan to inhibit Al corrosion in an acid medium.

### ACKNOWLEDGMENT

The authors gratefully acknowledge Dr. G. Perretta (Istituto Motori) for the support in SEM-EDS measurements, and the Italian Ministry of University and Research for financial support in “Fuel Cell Lab - Innovative systems and high efficiency technologies for poly-generation” Project.

### REFERENCES

- [1] Shkolnikov, E.I., Zhuk, A.Z., Vlaskin, M.S., Aluminum as energy carrier: Feasibility analysis and current technologies overview, Renewable and Sustainable Energy Reviews, Volume 15, 2011, pages 4611-4623.
- [2] Cheng, F., Chen, J., Metal-air batteries: from oxygen reduction electrochemistry to cathode catalysts, Chemical Society Reviews, Volume 41, 2012, pages 2172-2192.
- [3] Di Palma, T.M., Migliardini, F., Caputo, D., Corbo, P., Xanthan and k-carrageenan based alkaline hydrogels as electrolytes for Al/air batteries, Carbohydrate Polymers, Volume 157, 2017, pages 122-127.

## DEVELOPMENT OF BENDABLE PEMFC: FROM MEA TO STACK

T. Park\*, S. W. Cha\*\*, and S. J. Yoo\*\*\*

\*Department of Mechanical Engineering, Soongsil University,  
Seoul 06978 (*Republic of Korea*)

\*\*Department of Mechanical and Aerospace Engineering,  
Seoul National University, Seoul 08826 (*Republic of Korea*)

\*\*\*Fuel Cell Research Center, Korea Institute of Science and  
Technology (KIST), Seoul 02792 (*Republic of Korea*)

**Abstract** - This research is about the development of bendable polymer electrolyte membrane fuel cells (PEMFCs). Over 5 years, our research group has tried to realize flexible, thereby bendable PEMFCs by using polydimethylsiloxane (PDMS)-based and polycarbonate-based flow-field plates and coated silver nanowires percolation network on them to confer electrical conductivity. The as-fabricated bendable PEMFCs showed the maximal power density of  $117 \text{ mW/cm}^2$ , which is considered as a use power level for commercialization. However, this type of fuel cell is not durable under repeated bending. It is because by bending the bendable PEMFC is subject to strain on membrane-electrode assembly (MEA). In order to prevent such performance degradation, recently our research group is focusing on the development of bending-durable MEA and highly thin, thereby ultra-light PEMFC based on PC with suppressed strain on MEA by bending. Also we are looking for the bio-applications of bendable PEMFCs.

**Index Terms** – Bendable polymer electrolyte membrane fuel cell, bendable membrane-electrode assembly, silver nanowires percolation network, ultra-light fuel cell.

### I. INTRODUCTION

Flexible electronics and its application to wearable electronics, epidermal electronics are considered as a next-generation electronics. Recently such flexible electronics technologies show remarkable technological level and many industries are competing to develop and even commercialize flexible electronics-used applications such as bent smartphones, flexible displays, and so forth. Here, it should be noted that all the applications of the flexible electronics are all “portable devices”. It means that if somebody wants to make one electronics fully pliable, the development of flexible energy storage technologies should be accompanied together.

Current market-leading energy storage technology is

lithium-ion batteries. However, this rechargeable battery system almost confronts the thermodynamic maximum of energy storage density and the amount of lithium on earth is limited and thereby not cost-effective. Portable energy storage technology with higher energy density is required to cope with the increasing demand for future electronics.

Our research group has focused on the development of flexible and bendable polymer electrolyte membrane fuel cells (PEMFCs) to resolve this expected energy storage limitation in the future. Especially, we introduced fuel cell technology because fuel cells can have potentially higher energy density than lithium-ion batteries in the future. In addition, among various fuel cell types, we employed PEMFC because this fuel cells show currently the most matured technological level and require simple balance of plant (BOP). This research has continued over 5 years and now shows competitive performance upto commercializable scale. In this presentation, we introduce our previous research history about this bendable PEMFCs.

### II. BENDABLE PEMFCs BASED ON PDMS

The first trial for the realization of bendable PEMFC is to use polydimethylsiloxane (PDMS) as a material for flow-field plates. In this case, realizing highly flexible and stretchable current collectors is the key for successful fabrication of the bendable PEMFCs. We firstly fabricated this flow-field plates by sputtering nickel-based current collectors on PDMS [1]. However, this type of current collectors was very weak to bending and bending-induced strain. The performance was severely lowered after repeated bending. Thereby, we introduced silver nanowires current collectors on PDMS to realize high performance and more durable bendable PEMFCs

[2–7]. This approach was successful and showed maximal power density of 117 mW/cm<sup>2</sup> upto now. Interestingly, the performance of this bendable PEMFC increases with increasing bending. We hypothesized that this phenomenon is due to the generated compressive stress normal to membrane-electrode assembly (MEA) by bending. It was experimentally proven and now our understandings of this bendable PEMFCs allows us to predict the performance by various bending radius.

### III. BENDABLE AND ULTRA-LIGHT PEMFCs BASED ON PC

In the previous researches on bendable PEMFCs based on silver nanowires percolation network and PDMS revealed that still further development to achieve bending-durability and stability is needed for reliable performance of bendable PEMFCs. The most dominant performance lowering factor is, as mentioned above, the generated strain on MEAs by bending. By simulation, we concluded that if the bendable PEMFC is designed to be extremely thin, the strain will be very small and bending-induced performance degradation will be suppressed. So we introduced thermally imprinted PC and laser-machined ultra-thin metal mesh as current collectors in this bendable PEMFCs [8]. It showed peak power density of 89.2 mW/cm<sup>2</sup>, which is the highest performance per weight among bendable fuel cells in literature.

### IV. BENDING-DURABLE MEA FOR BENDABLE PEMFCs

Still the MEA remains as a significant performance-affecting factor in bendable PEMFCs of our template. Even though we could be suppressed performance degradation by designing the bendable PEMFCs very thin, radical problem is not resolved. In order to supplement normal MEA to withstand against tough bending, we adopted carbon cloth as gas diffusion layer and characterized its bending-durability and performance variation [9]. However, the characteristics of carbon cloth is not ideal compared to carbon paper. So nowadays we are developing bending-durable MEA with high-performance carbon papers. It is under active research.

### V. CONCLUSION

Our research group has lead the research of bendable PEMFCs over 5 years. Still the technological level of bendable PEMFCs is toddler level, it is highly expected that the demand for flexible power source with high energy density will arise and this research should be continued together to support flexible electronics technology in the future.

### REFERENCES

- [1] Chang I, Lee MH, Lee JH, Kim YS, Cha SW. Air-breathing flexible Polydimethylsiloxane (PDMS)-based fuel cell. *Int J Precis Eng Manuf* 2013;14:501–4.
- [2] Chang I, Park T, Lee J, Lee MH, Ko SH, Cha SW. Bendable polymer electrolyte fuel cell using highly flexible Ag nanowire percolation network current collectors. *J Mater*

*Chem A* 2013;1:8541–6.

- [3] Chang I, Park T, Lee J, Lee HB, Ji S, Lee MH, et al. Performance enhancement in bendable fuel cell using highly conductive Ag nanowires. *Int J Hydrogen Energy* 2014;39:7422–7.
- [4] Park T, Chang I, Lee J, Ko SH, Cha SW. Performance Variation of Flexible Polymer Electrolyte Fuel Cell with Ag Nanowire Current Collector under Torsion. *ECS Trans* 2014;64:927–34.
- [5] Chang I, Park T, Lee J, Lee HB, Ko SH, Cha SW. Flexible fuel cell using stiffness-controlled endplate. *Int J Hydrogen Energy* 2016;41:6013–9.
- [6] Park T, Chang I, Lee HB, Ko SH, Cha SW. Performance variation of bendable polymer electrolyte fuel cell based on Ag nanowire current collector under mixed bending and twisting load. *Int J Hydrogen Energy* 2017;42:1884–90.
- [7] Park T, Chang I, Jung JH, Lee HB, Ko SH, O'Hayre R, et al. Effect of assembly pressure on the performance of a bendable polymer electrolyte fuel cell based on a silver nanowire current collector. *Energy* 2017;134:412–9.
- [8] Park T, Kang YS, Jang S, Cha SW, Choi M, Yoo SJ. A rollable ultra-light polymer electrolyte membrane fuel cell. *NPG Asia Mater* 2017;9:e384.
- [9] Kang YS, Park T, Jang S, Choi M, Yoo SJ, Cha SW. Repetitive bending test of membrane electrode assembly for bendable polymer electrolyte membrane fuel cell. *J Ind Eng Chem* 2017;47:323–8.



## BENDING-DURABLE MEMBRANE-ELECTRODE ASSEMBLY USING PT-SPUTTERED TITANIUM MESH FOR BENDABLE PEMFCs

T. Park\*, Y. S. Kang\*\*, S. Jang\*\*\*, S. M. Kim\*\*\*\*,  
and S. J. Yoo\*\*

\*Department of Mechanical Engineering, Soongsil University, Seoul  
06978 (*Republic of Korea*)

\*\*Fuel Cell Research Center, Korea Institute of Science and  
Technology (KIST), Seoul 02792 (*Republic of Korea*)

\*\*\*Department of Mechanical and Aerospace Engineering, Seoul  
National University, Seoul 08826 (*Republic of Korea*)

\*\*\*\*Department of Mechanical Engineering, Incheon National  
University, Incheon 22012 (*Republic of Korea*)

**Abstract** – This study introduces new type of gas diffusion layer (GDL) for bendable polymer electrolyte membrane fuel cells (PEMFCs). Our research group has led the research of bendable PEMFCs over 5 years and concluded that membrane-electrode assembly (MEA) only for the use in bendable PEMFCs is required. It is because employing normal MEA in bendable PEMFCs induce severe performance fluctuation by bending and twisting. In order to suppress such variation effect, we simplified the gas diffusion layer and electro-catalytic layer by sputtering Pt onto Ti mesh. This Pt-sputtered Ti mesh was then hot-pressed to Nafion® to compose one MEA. The as-fabricated Pt-sputtered Ti mesh-based MEA has extremely low Pt loading, resulting from the use of sputter and requires very simple fabrication process, thereby highly industry-friendly. The characterization is going on and the experimental results will be presented in detail in the conference.

**Index Terms** – Bendable polymer electrolyte membrane fuel cell, gas diffusion layer, Pt sputter, Ti mesh.

### I. INTRODUCTION

Flexible electronics and wearable electronics using thereof are considered as a main future electronics due to their high flexural degree of freedom and excellent applicability to various field. It is speculated that the demand for flexible power sources with higher energy densities will increase more because newly developed electronic energy-consuming components require more energy to operate with high performance. Currently lithium-ion batteries are used as major power sources in various portable applications. However, it is noticed that

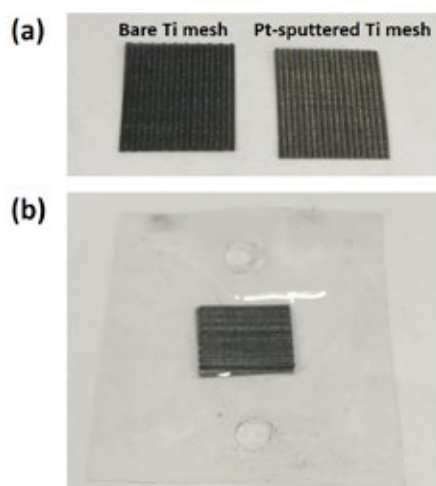
energy density of lithium-ion batteries is close to its theoretical maximum. Therefore, another flexible power source is required to satisfy the energy consumption level in the future.

Our research group thereby suggested new type of flexible power source by adopting fuel cell technology. Especially we employed polymer electrolyte membrane fuel cells (PEMFCs) because it can be operated at room temperature so requires very short start-up time, which make them attractive as a portable power source. Also PEMFCs show higher performance than other fuel cell types. However, employing normal membrane-electrode assembly (MEA) into bendable PEMFCs induces severe performance degradation by bending because an MEA is composed of brittle carbon paper-based gas diffusion layers (GDLs). Furthermore, if mesoporous layer (MPL) is included in carbon paper, performance is lowered more and more. Therefore, MEA of new type exclusively for bendable PEMFCs is highly required. In this study, we introduce such new type MEA by using Pt-sputtered Ti mesh. Because previous researches reveal that many interfaces inside the MEA are the main reason for the performance degradation [1–6], only Nafion® with two metal mesh on both sides (Anode and cathode respectively) can minimize the number of interfaces. The performance characterization of bendable PEMFC with this Pt-sputtered Ti mesh based MEA is actively under research now and going to be presented in the conference.

### II. EXPERIMENTAL DETAILS

Pt was sputtered onto Ti mesh with porosity of 73%. The

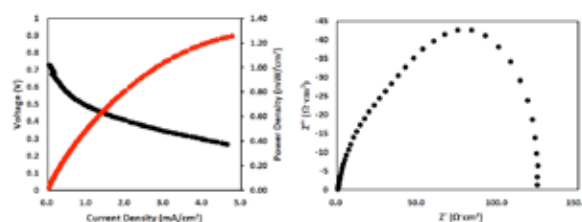
sputtering gas was argon and argon pressure, applied DC power, and target-substrate distance were 90 mtorr, 100 W, 12 cm, respectively. The resulting amount of sputtered Pt was  $<0.05 \text{ mg/cm}^2$ . The as-prepared Ti mesh was cut to make  $1 \times 1 \text{ cm}^2$  square shape to use as GDLs. Nafion<sup>®</sup> 212 was used as a polymer electrolyte membrane and sandwiched between two mesh GDLs. It was hot-pressed under 1 ton with stress-distributing supporters for 5 min. The as-fabricated MEA was assembled in unit PEMFC with flow-field size of  $1 \times 1 \text{ cm}^2$  (CNL Co., Republic of Korea) to characterize its operability in fuel cell conditions. Fully humidified hydrogen and air at room temperature were supplied with volumetric flow rates of 100 and  $150 \text{ cm}^3/\text{min}$ , respectively. Before measuring its current-voltage (I-V) characteristics, it was activated by operating it at 0.5 V vs. RHE for 30 min to stabilize the current. The I-V curves were measured by using potentiodynamic mode in Solartron 1260/1287 (Solartron Analytical Co., UK). The voltage sweep was started from open-circuit voltage (OCV) to 0.25 V, with sweep speed of 15 mV/s.



**Fig. 1. Digital camera images of (a) bare and Pt-sputtered Ti meshes and (b) hot-pressed MEA with Pt-sputtered Ti mesh.**

### III. RESULTS AND DISCUSSION

Real pictures of bare Ti mesh, Pt-sputtered Ti mesh, and MEA with this Ti mesh GDLs are shown in Fig. 1. The Pt-sputtered can easily be distinguished with naked eyes (Fig. 1(a)). In addition, the Pt-sputtered Ti meshes are attached well with Nafion<sup>®</sup> 212 membrane (Fig. 1(b)), which means electrolyte membrane is attached well with Pt and electrochemical triple-phase boundaries could be formed well. Inductively coupled plasma (ICP) analysis showed that the amount of sputtered Pt was 0.439% of total weight of Ti mesh GDL.



**Fig. 2. (Left) Current-voltage and Current-power curve of Pt-sputtered Ti mesh-used PEMFC. (Right) Electrochemical impedance spectrum corresponding to current-voltage curve at 0.5 V vs. RHE.**

However, still the performance is not comparable to normal MEA, as shown in Fig. 2. It shows  $1.20 \text{ mW/cm}^2$  which is still impractical in real applications. We speculate that such lower performance is attributed to unoptimized fabrication condition. ICP result shows that Pt is deposited on Ti mesh and the amount is enough to form triple phase boundaries. Pt, Nafion and the micro- or nano-pores for reactant gases to approach are affected sensitively to the hot-press condition and assembly pressure of the fuel cell. Electrochemical impedance corresponding to this I-V curve was also measured charge transfer resistance is too high than normal PEMFC, while ohmic resistance seems to show comparable value to that of normal PEMFC. Because this study focuses on the development of GDL for portable use, the Ti-mesh GDL was tested at room temperature. Further results are under active research and will be shown in detail later.

### IV. CONCLUSION

A new GDL for exclusive use in bendable PEMFCs is suggested. Pt was sputtered onto Ti mesh and it was hot-pressed to electrolyte membrane. Although the performance is not high, it is expected that the performance will be improved and can be used as bending-durable MEA in bendable PEMFCs.

### REFERENCES

- [1] Chang I, Park T, Lee J, Lee MH, Ko SH, Cha SW. Bendable polymer electrolyte fuel cell using highly flexible Ag nanowire percolation network current collectors. *J Mater Chem A* 2013;1:8541–6.
- [2] Chang I, Park T, Lee J, Lee HB, Ji S, Lee MH, et al. Performance enhancement in bendable fuel cell using highly conductive Ag nanowires. *Int J Hydrogen Energy* 2014;39:7422–7.
- [3] Park T, Chang I, Lee J, Ko SH, Cha SW. Performance Variation of Flexible Polymer Electrolyte Fuel Cell with Ag Nanowire Current Collector under Torsion. *ECS Trans* 2014;64:927–34.
- [4] Chang I, Park T, Lee J, Lee HB, Ko SH, Cha SW. Flexible fuel cell using stiffness-controlled endplate. *Int J Hydrogen Energy* 2016;41:6013–9.
- [5] Park T, Chang I, Lee HB, Ko SH, Cha SW. Performance variation of bendable polymer electrolyte fuel cell based on Ag nanowire current collector under mixed bending and twisting load. *Int J Hydrogen Energy* 2017;42:1884–90.
- [6] Park T, Chang I, Jung JH, Lee HB, Ko SH, O'Hayre R, et al. Effect of assembly pressure on the performance of a bendable polymer electrolyte fuel cell based on a silver nanowire current collector. *Energy* 2017;134:412–9.

## NOVEL FABRICATION AND HIGH TEMPERATURE OXIDATION OF AN ODS FERRITIC STAINLESS STEEL ALLOY INTERCONNECT FOR SOFC

A. Ajay Kumar\*, B. Ranjit Bauri\*

\*Department of Metallurgical and Materials Engineering,  
Indian Institute of Technology Madras, Chennai - 600036, (India)

**Abstract** - The oxidation behavior of interconnects is the key parameter controlling the operational integrity and service life of a SOFC stack. Moreover, the operational performance of an ODS alloy interconnect is influenced by its fabrication and/or processing route also. A novel variant of friction stir deposition process was employed to fabricate the ODS AISI 430 alloy interconnect for this study. The microstructure and high temperature oxidation behavior of the processed ODS alloy was studied. The processed ODS alloy was held at 800 °C for 100 h in ambient and 3% humid atmospheres and the resulting compositions of developed oxide layers were found to be distinct across processed zones. Iron and Mn oxides were in major proportion in the outer surface, whereas the dispersant depleted inner surface was dominated by Mn/chromium spinels. The processing of the material during the deposition seems to have a correlation with the compositional and microstructural variation of the oxidized surfaces.

**Index Terms** - High temperature oxidation, Metallic interconnects, ODS alloy, SOFC

### I. INTRODUCTION

In this era of extensive climate conscious energy requirements, Solid oxide fuel cells (SOFCs) are aspiring for their relevant contributions to clean power generation [1]. For meaningful scale up of output power, interconnects are their essential building block components. Metallic interconnects prove their preferential utility for the reasons of economics and ease of fabrication [2][3]. The inter-component matching of thermal expansion with conventional materials narrow down the choice of interconnects to ferritic stainless steels. The oxidation behavior of interconnects is the key parameter controlling the operational integrity and service life of a SOFC stack [4]. Moreover, all other operating parameters being same, the operational performance of an ODS (Oxide Dispersed

Strengthened) alloy interconnect is influenced by its fabrication and/or processing route also [5].

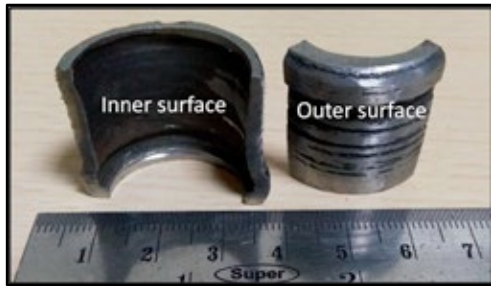
### II. EXPERIMENTAL DETAILS

In this work, ODS alloy was fabricated using a novel variant of friction deposition process. For that, holes with particular dimensions and spatial distribution were drilled in the cross-sectional surface of an AISI 430 rod and filled with 8wt% Yttria Stabilized Zirconia (8YSZ) particles. This rod sample was then rotated at high speed with heavy vertical load applied on it, which resulted into a tubular sample, as shown in Fig. 1, having 8YSZ particles dispersed over its outer surface. While the inner surface of this tubular sample was devoid of any dispersants. Square tokens of 10×10 mm were retrieved from the tubular sample and polished to mirror finish. They were then exposed to 800 °C for 100 hours in ambient and 3% humid atmospheres. The resulting oxide layers were examined using X-ray Diffraction (XRD) for phase evolutions, Scanning Electron Microscopy (SEM) for surface morphology and Energy Dispersive Spectroscopy (EDS) for elemental compositions.

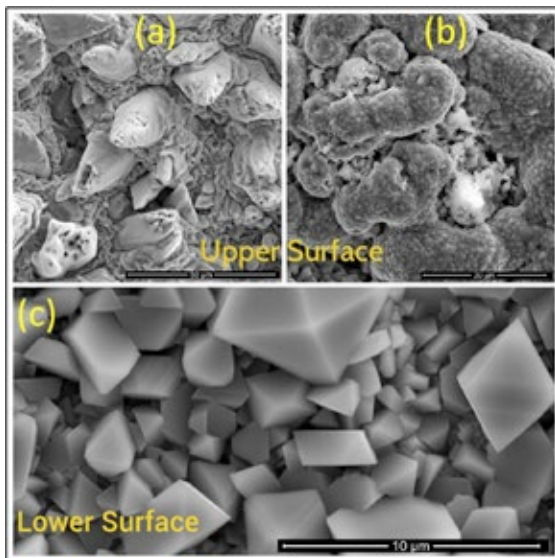
### III. RESULTS AND DISCUSSION

As shown in Fig. 2, the morphologies of oxide layers on the outer and inner surfaces of tubular product are distinct. The compositions of these surfaces are indicated in Fig. 3 by their corresponding EDS spectrum. In the presence of ambient atmosphere, Iron and Mn oxides were in major proportions in the outer surface, having dispersant particles, whereas, the inner surface, devoid of dispersant particles, was dominated by Mn/Cr spinels. Very fine sized iron oxide was present around the dispersant particles, whereas iron oxide rods and plates were in abundance in nearby regions. The effect of different atmospheres was noticeable on adhesion of oxide layers in addition to their morphology and composition. The scale of

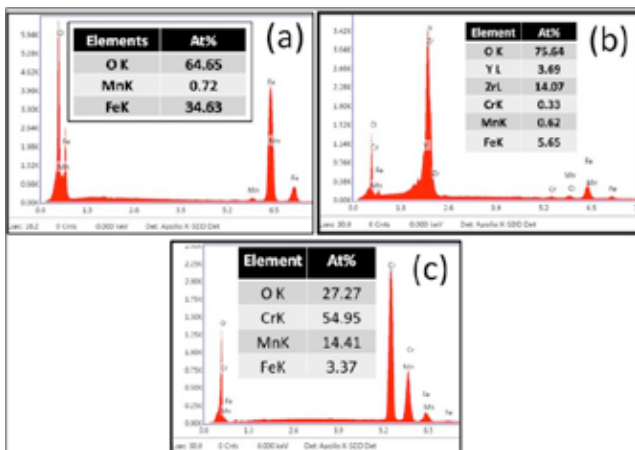
sample heated in dry air got delaminated immediately after the heating cycle.



**Fig. 1. Inner (Lower) and Outer (Upper) surfaces of tubular product**



**Fig. 2. Electron micrographs of oxides in different processing zones**



**Fig. 3. Corresponding EDS spectra of oxides in different processing zones**

#### IV. CONCLUSION

ODS alloy of ferritic stainless steel was fabricated and oxidized at 800 °C for 100 hours in different atmospheres. As expected, the processing impacted the alloy's oxidation behavior and thus distinct characteristics (morphology, composition and adhesion) of oxide scales were recorded. Iron and Mn oxides were present on the outer surface and Mn/Cr spinels were present on the inner surface.

#### REFERENCES

- [1] S. Singhal, "Solid oxide fuel cells for stationary, mobile, and military applications," *Solid State Ionics*, vol. 152–153, pp. 405–410, 2002.
- [2] J. Wu and X. Liu, "Recent Development of SOFC Metallic Interconnect," *J. Mater. Sci. Technol.*, vol. 26, no. 4, pp. 293–305, 2010.
- [3] V. V. Krishnan, "Recent developments in metal-supported solid oxide fuel cells," *Wiley Interdiscip. Rev. Energy Environ.*, 2017.
- [4] N. Shaigan, W. Qu, D. G. Ivey, and W. Chen, "A review of recent progress in coatings, surface modifications and alloy developments for solid oxide fuel cell ferritic stainless steel interconnects," *J. Power Sources*, vol. 195, no. 6, pp. 1529–1542, 2010.
- [5] W. J. Quadackers, J. Piron-Abellan, V. Shemet, and L. Singheiser, "Metallic interconnectors for solid oxide fuel cells – a review," *Mater. High Temp.*, vol. 20, no. 2, pp. 115–127, 2003.



**AN INSIGHT INTO THE CURRENT DENSITY DISTRIBUTION OF A PEM FUEL  
CELL WORKING AT DIFFERENT OPERATIVE CONDITIONS**

Giosuè Giacoppo\*, Orazio Barbera, Francesco Cipiti, Nicola  
Briguglio, Paulina Pianko-Oprych\*\* and Vincenzo Antonucci

\*CNR – ITAE National Research Council of Italy – Institute for  
Advanced Energies Technologies “Nicola Giordano”, Via Salita  
S.Lucia sopra Contesse, 5, 98126, Messina, Italy

\*\*West Pomeranian University of Technology, Szczecin, Institute of  
Chemical Engineering and Environmental Protection Processes, al.  
Piaśtów 42, 71-065 Szczecin, Poland,  
\*giacoppo@itae.cnr.it

**Abstract** - In this work, the behaviour of a single cell, operated at different cathodic flow rates and humidification both on stationary and dynamical states, was studied by a high-resolution segmented current collector. The results, allowed a better understanding of the phenomena, which occur inside a fuel cell.

The current density distribution measurement was carried out in a 50 cm<sup>2</sup> of single cell Polymer Electrolyte Fuel Cell (PEFC) equipped with a commercial Membrane Electrode Assembly (MEA). The adopted fluid distributors have double parallel serpentine, machined on both anodic and cathodic graphite plates. The single cell is equipped by a 16 x 16 segmented current collector (S++ ‘Current scan’) to collect the current flowing through each segment, during the cell operation. Experimental data was recorded using the ‘CurrentView’ software that is a part of the commercial measurement system.

The effects of operative conditions on the current density distribution of a fuel cell were examined. The high resolution, segmented current collector allowed a detailed representation of the high current density zones and how they move over the fuel cell active area. Moreover, an extensive database for future numerical studies was obtained.

**Index Terms** - - Current Density Distribution, segmented cell, Pem Fuel Cell, Operative conditions.

## I. INTRODUCTION

In a green future, fuel cells will probably become the suitable, environmental friendly technology to generate power for several applications. They, in fact, generate electricity by an electrochemical process; in particular, PEFCs use hydrogen and air as reactants in combination with a solid, proton conductor electrolyte. Due to the complexity of the phenomena that takes place inside a PEFC, scientists have focused their attention on different points, from the electrochemistry towards the fluid

dynamics to mechanics. As well as, the electrochemical components play a key role in the performance of a fuel cell, the distribution of the reactants over the electrode surfaces is fundamental for an optimal operation of the device.

To understand PEFC systems, a detailed analysis of the influence of main parameters on its performance and the development of different in situ analytical methods is fundamental. Segmented current collectors (SCC) have proven to be an excellent in situ diagnostic tool for a deep understanding of the fuel cell physics. Moreover, they were also used to study the factors influencing the unevenness of the electrochemical response of the MEA. A SCC is similar to a fuel cell ordinary current collector plate, with the exception that it is divided into smaller parts, reciprocally isolated, that can be individually interrogated for current, voltage and temperature values [1].

An important parameter of the SCC is the resolution. Indeed, the higher the number of the segments, the more the measured current is near to its local value. Consequently, a detailed description of the fuel cell operation is possible. This allows a more detailed comprehension of the physical phenomena inside a fuel cell, such as: water flooding or drying and the influence on the overall performance of the geometrical parameters of the flow – field. Moreover, this kind of device is useful for validation of numerical models based on local experimental values. [2–5].

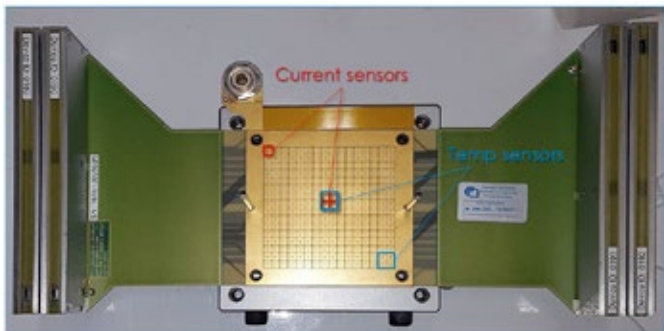
The maximum resolution used in a segmented current collector did not exceed 196 segments. In this work, tests at different operative conditions were performed with a high-resolution SCC with 256 segments. Detailed maps of current density at different operative conditions were obtained and



commented.

## II. EXPERIMENTAL

Current density distribution measurements were carried out in a 50 cm<sup>2</sup> active area single cell, with a serpentine flow field machined on anodic and cathodic graphite plates. A cell 16 x 16 segmented current collector (Fig.1) was used to measure the current flowing through each segment and the local temperature of the cell, during the operation. The 'CurrentView' software, which is a part of the commercial measurement system, was adopted to collect the current and temperature local values whereas the post processing was performed through a specific worksheet.



**Fig. 1.** Segmented current collector used in the experiments

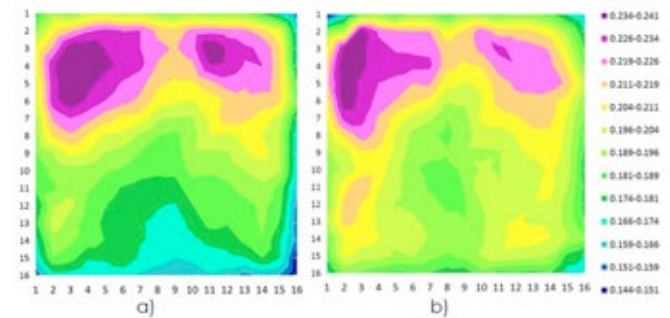
A commercial, 7 layers MEA MEP1002 from Ewii Fuel Cell® was used. The adopted MEA had the following characteristics: (i) a perfluorosulphonic acid polymeric membrane (PFSA – 850 EW) with a thickness of 20 µm, (ii) 50 wt % Pt/C 0.1 mg cm<sup>-2</sup> (anode catalyst) and 60 wt % Pt/C 0.4 mg cm<sup>-2</sup> (cathode catalyst), (iii) a Gas Diffusion Layer GDL0082 of 235 µm thickness.

To prevent gas leakage, two PTFE gaskets of 200 µm thickness were coupled with the MEA. The test station used for the experiments was the "Green Light G40".

## III. RESULTS AND DISCUSSIONS

Three sets of experiments were carried out with different humidity and stoichiometry of the inlet reactants, namely: i) high humidity ii) intermediate humidity and iii) low humidity. In the case of fully humidified reactants and high current density (Fig.2a), the maximum current is located at the gas inlet; (up right and left area) while a low current area is located in the bottom part of the cell area near the cathode exhaust. This is due to an excess of water content in the cell, which generally leads to the condensation of liquid water that limits the mass transfer to the active sites. This phenomenon is more evident at lower cathode stoichiometry, where the air flowrate is not sufficient to remove the excess water that accumulates at the cathode exit. A higher stoichiometric air value generally

mitigates this problem and allows a better distribution in the bottom part of the cell active area. A more even current distribution is reached when the cell is operated at intermediate humidity conditions (Fig. 2b). In this case, the cell is better water balanced and a flooding of channels is less probable than in the case of fully humidified reactants. In fact, as reported in fig. 2a the low current area near the cathode exit is absent and the current distributes more evenly in the middle and bottom parts of the cell. A high current area remains in the upper part of the cell, where the highest reactants concentration is present.



**Fig. 2.** Current distribution at 1A/cm<sup>2</sup>: a) fully humidified reactants b) Intermediate humidity.

## IV. CONCLUSIONS

Tests performed at different operative conditions on a 50cm<sup>2</sup> lab cells leads to the conclusion that the current distribution is highly dependent on the operative conditions. Particularly, a higher stoichiometric air value (in the range of 2-4) improves the current uniformity, in all the examined humidity conditions.

The segmented current collectors we used, showed to be a useful device to study the local distribution of the current. Extensive tests with the same device allowed the construction of a database that is useful as a reference for numerical model validation.

## REFERENCES

- [1].L. Pérez, L. Brandão, J. Sousa, A. Mendes, "Segmented polymer electrolyte membrane fuel cells - A review", *Renewable and Sustainable Energy Reviews*, 15 (2011) 169-185.
- [2] G. Bender, M. Wilson, T. Zawodzinski, "Further refinements in the segmented cell approach to diagnosing performance in polymer electrolyte fuel cells" *Journal of Power Sources*, 123 (2003) 163-171.
- [3].D. Gerteisen, N. Zamel, C. Sadeler, F. Geiger, V. Ludwig, C. Hebling, "Effect of operating conditions on current density distribution and high frequency resistance in a segmented PEM fuel cell" *International Journal of Hydrogen Energy*, 37 (2012) 7736-7744.
- [4].M. Geske, M. Heuer, G. Heideck, Z. Styczynski, "Current Density Distribution Mapping in PEM Fuel Cells as An Instrument for Operational Measurements" *Energies*, 3 (2010) 770-783.
- [5].S. Kim, M.Kim, Y.Sohn, "Segmented cell approach for studying uniformity of current distribution in polymer electrolyte fuel cell operation" *International Journal of Hydrogen Energy*, 40 (2015) 11676-11685.

## HyLIFT-EUROPE: LARGE-SCALE DEMONSTRATION OF FUEL CELL MATERIAL HANDLING VEHICLES

C. Maggi\*, A. Essam Aly\*, H. Landinger\*\*,

\*Federazione delle Associazioni Scientifiche e Tecniche (FAST), P.le Morandi 2, Milano (Italy)

\*\*Ludwig-Bölkow-Systemtechnik GmbH (LBST), Daimlerstr. 15, 85521 Ottobrunn, (Germany)

**Abstract** - HyLIFT-EUROPE is an EU-funded demonstration project that aims at deploying more than 200 fuel cell material handling vehicles (FCMHVs) and associated infrastructure at two key sites in Europe, thus demonstrating the full potential of this technology. The high volume of vehicles to be operated in the project will provide significant cost reductions allowing industries to consider the investment in fuel cell powered forklifts and warehouse trucks and laying the foundation for a supported market deployment beyond 2018.

**Index Terms** – Material handling equipment, hydrogen infrastructure, large scale demonstration, logistics solutions

### I. INTRODUCTION

The use of hydrogen FCMHVs has become a commercially mature solution in the recent years, thanks to the reduction of costs that made this technology competitive. The success of this solution has resulted in its large-scale diffusion and in a consistent growth of sales in the material handling market with about 19,000 FCMHVs operating globally in NOV 2017 [1]. The trend is much stronger in North America, where today about 18,500 FCHMV are in operation [2], located at facilities in more than 20 U.S. states [3]. Europe is also expanding the market, but cannot yet showcase any such large example of deployment.

The HyLIFT-EUROPE project addresses the topic “SP1-JTI-FCH.2011.4.1: Demonstration of fuel cell-powered Material Handling Equipment vehicles including infrastructure” in the 4<sup>th</sup> call of the European Fuel Cells & Hydrogen Joint Undertaking (FCH JU) Implementation Plan (AIP 2011). The purpose of the project is to provide the launch pad to achieve the full commercialization of the technology building the next step towards market deployment by increasing the volume beyond 200 vehicles.

### II. PROJECT CONCEPT

The aim of HyLIFT-EUROPE is to provide major companies with a fleet of FCMHVs to be used in their warehouses in order to foster future deployment through large-scale demonstrations.

In this context the project partners could convince two sites for participating in the deployment: Prelocentre, a logistics provider for fruits and vegetables and a large supermarket chain, highly appreciated because of their relevance at European level and the potential to roll out the technology at several of their sites. The advantages of choosing fuel cells to power their MHVs are multiple and combine the benefits of batteries and combustion engines. First, the systems can be used without any loss of range. Besides the electrical power, the systems generate only water and heat. Moreover, as they have no moving parts, noise and vibrations are almost zero, and in addition, the simplicity and rapidity of refuelling (less than 3 min.) lead to time savings.

The HyLIFT-EUROPE project partners cover the entire value chain and all the disciplines and technologies needed to supply hydrogen material handling solutions: vehicle manufacturers (OEM), hydrogen infrastructure provider as well as vehicle users both from large industry and small and medium enterprises. Under the coordination of Ludwig-Bölkow-Systemtechnik GmbH, are involved Still GmbH, Air Liquid Advanced Business, Prelocentre and FAST-Federazione delle Associazioni Scientifiche e Tecniche/EHA-European Hydrogen Association. The combination of these competences seems to be the best guarantee for achieving the ambitious goals of the project.

### III. OBJECTIVES

The specific goals of the project are:

- Deploy more than 200 units of fuel cell powered material handling vehicles in two relevant sites in Europe.
- Demonstrate the maturity of the hydrogen infrastructure as well as the safety of the use of hydrogen in industrial environment.
- Validate the Total Cost of Ownership (TCO) and the path towards commercial targets.
- Ensure a supported market deployment beyond 2018 by selling FCMHVs at competitive prices through original equipment manufacturers (OEM).
- Provide a best practice guide for hydrogen refuelling stations (HRS) to build, install and operate them in industrial context.
- Disseminate the project results targeting early adopters of hydrogen solutions, policy makers, industry stakeholders and the general public in order to create a network to support European industry.

The ultimate objective of the project is to achieve, through economies of scale encouraging future vehicle users to adopt the technology, a significant reduction of costs.

### IV. THE DEMONSTRATION

The HyLIFT-EUROPE project represents the next logical evolution from HyLIFT-DEMO, characterized by a large increase in production volume and related lower purchase prices.

The identification of sites to deploy large fleets of hydrogen powered vehicles should be based on individual TCO calculations, in which the cost of hydrogen supplied plays a relevant role.

The cost of hydrogen at the pump may have significant variations across Europe depending on where it is supplied and the deployment of the refuelling infrastructures highly depend on the cost of hydrogen. Consequently, it is important to identify the variables which affect the price of hydrogen delivered in order to set up a competitive business case for HRS installations.

The important parameters that influence the price of delivery are the distance from the source, the method of delivery and the quantity of each delivery.

One of the first fleets of hydrogen FCMHVs deployed in Europe within the project is being demonstrating at the Prelocentre premises, a 10,000 m<sup>2</sup> distribution center in Saint-Cyr-en-Val near Orleans, which is showing a very good operation performance so far.

### V. CONCLUSION

The HyLIFT-EUROPE project combines the efforts of

qualified partners from the logistics industry, vehicle OEMs and experienced partners in hydrogen solutions to boost large deployment of MHVs powered by hydrogen through the demonstration of the competitiveness of the solution. The demonstrations are expected to continue after the end of the project to prove the reliability of the vehicles also in the long term.

### REFERENCES

- [1] Plug Power: 2017 Third Quarter Update Letter, [http://s21.q4cdn.com/824959975/files/doc\\_financials/2017/Q3/investor-letter-third-quarter-2017.pdf](http://s21.q4cdn.com/824959975/files/doc_financials/2017/Q3/investor-letter-third-quarter-2017.pdf), download on 01 DEC 2017.
- [2] H. Landinger: Internationale Perspektiven für brennstoffzellen-betriebene Fahrzeuge in der Logistik – Update 2017, 2. VDI-Fachkonferenz „Batterie- und Ladetechnik: Energieversorgung für mobile Anwendungen in Produktion und Logistik“, 06/07 DEC 2017, Düsseldorf, Germany
- [3] U.S Department of Energy, State of the States: Fuel Cells in America, 2016.

## POTENTIAL FOR FUEL CELL-DRIVEN PASSENGER SHIPS IN NORWAY

Sepideh Jafarzadeh and Ingrid Schjølberg

Department of Marine Technology, NTNU Norwegian University of  
Science and Technology, Trondheim, Norway

**Abstract** – This paper studies the operational profile of passenger ships operating within 12 nautical miles of the Norwegian coast. The results show that these vessels mainly operate outside the optimum load range of their main engines, which increases fuel consumption and emissions. Alternative fuels and power systems are required for a substantial reduction in emissions from shipping. Hydrogen and fuel cells are among the most promising solutions from an environmental perspective. The study investigates the possibility of downsizing the main engines to operate them at an optimum point, while fuel cells and batteries take care of part and peak loads.

**Index Terms** – AIS, Fuel cells, Hydrogen, Passenger ships

### I. NOMENCLATURE

AIS: Automatic Identification system

### II. INTRODUCTION

In the period 2007–2012, shipping accounted for approximately 3% of annual global greenhouse gas emissions and approximately 15% and 13% of nitrogen oxides and sulphur oxides emissions from anthropogenic sources [1]. Various regulations are imposed on shipping to control these emissions and their adverse impacts. For instance, the North Sea is among Sulphur Emission Control Areas, where stringent limits on sulphur content of marine fuel are imposed [2].

Marine diesel engines are optimised for operation at a specific load range, which is typically 85–100% of their maximum continuous rating. At this range, fuel consumption and emissions are at their minimum. However, operational profile of vessels may include diverse operations with different power demands. During operations outside the optimum load range, fuel consumption and emissions increase. Fig. 1 illustrates the composition of propulsion systems adopted by passenger ships in Norwegian waters in 2013. Although many passenger ships use electric drives, the majority uses engines with direct/gear drives. In addition, despite having diesel-electric systems, power system of many vessels do not operate optimally [3]. For

instance, due to dynamic power demands, operators may run more diesel engine generators (gensets) than needed. This may lead to partial loading of gensets and lower energy efficiency.

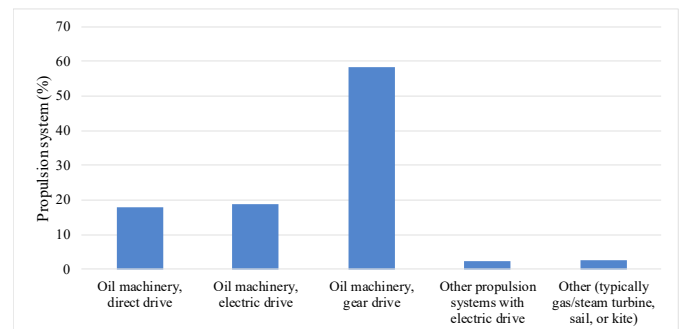


Fig. 1. Propulsion systems used by passenger ships in Norwegian waters in 2013 (based on [4]).

Diversity of operational profiles together with the increased pressure for environmentally friendly operations call for alternative fuels and power systems. One potential approach is to switch to fuels with low/zero levels of carbon and sulphur, such as hydrogen to control emission formation. Another possible approach is to use more efficient energy conversion devices, such as fuel cells. From an environmental perspective, partial or full propulsion of vessels by hydrogen and fuel cells is a promising option [5, 6].

This paper studies the operational profile of passenger ships operating within 12 nautical miles of the Norwegian coast (i.e., Norway's territorial waters). The aim is to estimate how often these passenger ships operate in the optimum load range of their engines and to investigate the possibility of downsizing the main engines to operate them at an optimum point, while fuel cells together with batteries take care of part and peak loads.

### III. MATERIALS AND METHODS

This paper uses data from the Automatic Identification

Copyright © 2017



System (AIS) to estimate operational profile of 170 passenger ships operating in Norway's territorial waters during 2016. Only vessels with engines and direct/gear drives are considered. Vessels using liquefied natural gas fuel are excluded.

#### A. Data Sources

The AIS is an automatic tracking system primarily used for collision avoidance of ships. The AIS signals provide information on ship name, ship speed over ground, and position, among others [7]. The Norwegian Coastal Administration [8] provided 12 monthly datasets during 2016. Each dataset contains processed AIS data and includes operational information on distance and time to next data point, among others. Approximately, 98% of data points have a time step below 10 minutes. IHS Markit (Sea-web) [9] provided information on vessel characteristics, such as service speed and installed power. Using this information together with empirical formulas, one can estimate operational profile of vessels.

#### B. Load estimation and Statistical Analysis

This study focuses on the propulsion power supplied by the main engines. To estimate the main engine load in each data point, equation (1) is used [7]. To illustrate the distribution of time spent by individual vessels in each load range, Tukey's boxplots are used [10].

$$\text{Load} = 0.85 \left( \frac{\text{Vessel speed}}{\text{Vessel service speed}} \right)^3 \quad (1)$$

### IV. RESULTS AND DISCUSSIONS

Fig. 2 illustrates the percentage of time the vessels spent at various load ranges. The median ship (red line) spends the majority of its time below 80% of main engine load, where the energy efficiency of engine drops. One possible approach to improve efficiency is to downsize the main engine, so that it mainly operates in the optimum load range. Fuel cells and batteries may supply the power needed outside this power range to reduce emissions. It should be noted that it is normal practice in shipping to install excess power in case of emergency. However, this study does not focus on reducing total installed power. Instead, the focus is on combining engines, fuel cells, and batteries to improve efficiency. In addition, usually propulsion is not the main power consumer of passenger ships. Instead, auxiliaries, such as hotel loads are the main consumers. This study only focuses on propulsion power due to lack of data.

### V. CONCLUSIONS

This study investigated the operational profile of passenger ships operating in Norway's territorial waters. The results show that the main engines of these vessels do not operate in their optimum load range. In order to comply with environmental regulations on shipping, various options are available. One possible solution is to downsize the engines and operate them in their optimum load range. Fuel cells and batteries can supply part and peak loads to reduce emissions.

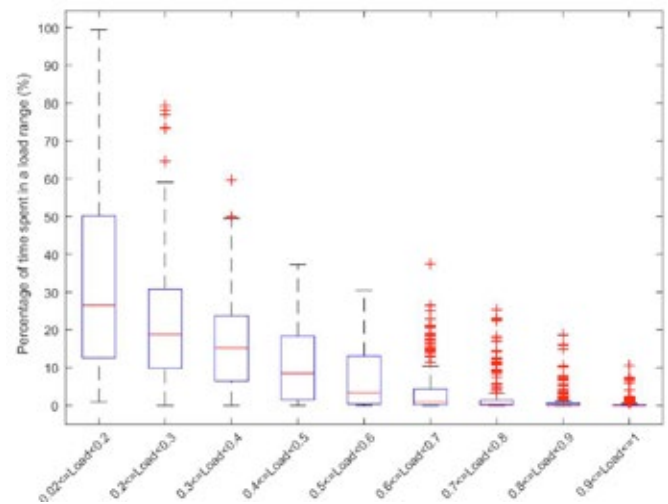


Fig. 2. Percentage of time passenger ships spent in various load ranges of their main engine while operating in Norway's territorial waters during 2016. The boxes represent the 1<sup>st</sup> and 3<sup>rd</sup> quartiles, with the median (red line). The whiskers follow Tukey's method. The pluses are outliers.

### REFERENCES

- [1] Smith, T.W.P., et al., *Third IMO GHG study*. 2014, International Maritime Organization (IMO): London, UK.
- [2] IMO. *Sulphur oxides (SOx)- Regulation 14*. 2014 [Accessed on 03.12.2014]; Available from: <http://www.imo.org/OurWork/Environment/PollutionPrevention/AirPollution/Pages/Sulphur-oxides-%28SOx%29-%E2%80%933-Regulation-14.aspx>.
- [3] Skjong, E., et al., *Approaches to economic energy management in diesel-electric marine vessels*. IEEE Transactions on Transportation Electrification, 2017. 3(1): p. 22-35.
- [4] DNV GL, *Miljøtiltak for maritim sektor- Teknisk vurdering av skip og av infrastruktur for forsyning av drivstoff til skip*. 2014, DNV GL: Høvik, Norway.
- [5] van Biert, L., et al., *A review of fuel cell systems for maritime applications*. Journal of Power Sources, 2016. 327: p. 345-364.
- [6] Jafarzadeh, S. and I. Schjøberg, *Emission reduction in shipping using hydrogen and fuel cells*. 2017. in *ASME 2017 36th International Conference on Ocean, Offshore and Arctic Engineering (OMAE2017)*. Paper No. OMAE2017-61401, pp. V010T09A011; 9 pages ISBN 978-0-7918-5778-6, Trondheim, Norway: ASME.
- [7] Goldsworthy, L. and B. Goldsworthy, *Modelling of ship engine exhaust emissions in ports and extensive coastal waters based on terrestrial AIS data – An Australian case study*. Environmental Modelling & Software, 2015. 63: p. 45-60.
- [8] The Norwegian Coastal Administration (NCA). *About the NCA*. 2017 [Accessed on 18.08.2017]; Available from: <http://www.kystverket.no/en/About-Kystverket/About-the-NCA/>.
- [9] IHS Markit. *Maritime portal*. [Accessed on 29.09.2017]; Available from: <http://maritime.ihs.com/>.
- [10] Wilkinson, L., *Geometry*, in *The Grammar of Graphics*. 2005, Springer New York: New York, NY. p. 155-178.



## ELECTRICALLY CONDUCTIVE POLYMER COMPOSITES FOR INJECTION MOLDING OF BIPOLAR PLATES

M.L. Sander<sup>1</sup>, J.T. Pritts<sup>1</sup>, B.A. Young<sup>2</sup>, A.D. Santamaria<sup>3</sup>, A.S. Hollinger<sup>1</sup>

<sup>1</sup> Department of Mechanical Engineering, Penn State Behrend, Erie, PA (USA)

<sup>2</sup> Department of Plastics Engineering Technology, Penn State Behrend, Erie, PA (USA)

<sup>3</sup> Department of Mechanical Engineering, Western New England University, Springfield, MA (USA)

**Abstract** - Electrically conductive polymer composites offer the potential for manufacturing lightweight, low-cost, fuel cell bipolar plates. In this study, carbon black and carbon fiber were added to nylon 6,6 at various weight percentages, ranging from 0 to 50%. Samples were injection-molded and then compared by measuring the electrical conductivity using a four-point probe method. Conductive filler was added to the polymer with and without a compounding process prior to injection molding. Results show that compounding the additives via a twin-screw extruder helps to disperse the filler within the polymer, but decreases conductivity due to shearing of the conductive carbon fibers. When the compounding process was removed, the conductive pathways from intact fiber bundles were maintained. Conductivities greater than 40 S/cm were achieved, nearing the U.S. Department of Energy technical target of 100 S/cm for bipolar plate electrical conductivity.

**Index Terms** – bipolar plate, carbon fiber, conductivity, nylon

### I. INTRODUCTION

Bipolar plates are one of the primary components of polymer electrolyte membrane fuel cells. These plates deliver reactants to electrodes, remove reaction byproducts, transfer heat, provide mechanical stability, and conduct electrical current. While graphite is the most commonly used material for fabrication of bipolar plates, the machining costs associated with graphite are a major drawback to mass production. In addition, graphite-based plates make the greatest contribution to the weight of the fuel cell stack. For this reason, electrically-conductive polymer composites have been explored as an alternative to the traditional metal alloys commonly used for fuel cell bipolar plates [1]. Polymer composites can reduce both the weight and cost of the bipolar plate, while still providing sufficient electrical properties.

Several factors impact the ability of a polymer composite to conduct electricity. The geometry, filler weight percent, and the physical properties of the fillers are crucial to forming an electrical pathway through the composite. In prior efforts, compression-molded, carbon fiber epoxy composites have

shown promise to achieve the electrical conductivities needed for fuel cell bipolar plates [2]. While compression molding can be used for production of high volumes, injection molding is most ideal for the levels of mass production required for full scale commercialization of fuel cells. The main objective of this study is to investigate the suitability of injection molding polymer composites with sufficient electrical conductivities.

### II. EXPERIMENTAL

#### A. Conductive Additives

In this study, carbon black (Ensaco 250G, Imerys) and carbon fiber (HT C413, Toho Tenax, 6 mm cut length) were added to nylon 6,6 (Vydyne 21SPC) at various weight percentages. Conductive filler was added to the polymer with and without a compounding process prior to injection molding. Compounding was carried out with a twin-screw extruder (Steer Engineering) to create a blend of: (i) 13.7 wt% carbon black in nylon and (ii) 40 wt% carbon fiber in nylon. These blends were mixed and injected (BOY XS) to create polymer composites with varying filler compositions. Carbon fiber was also added to nylon directly during injection (Cincinnati Milacron). In these direct injection-molded samples, carbon fiber weight percentage was varied from 0 to 50%.

#### B. Electrical Conductivity Measurements

Characterization of electrical conductivity was performed using a four-point probe method in accordance to ASTM B 193-87. A constant current was supplied (Keysight DC) to the polymer composite and the voltage drop across the sample was measured with a multimeter (Fluke 88V). Electrical conductivity,  $\sigma$ , was calculated as follows:

$$\sigma = \frac{I \cdot L}{\Delta V \cdot w \cdot t} \quad (1)$$

where  $I$  is the current,  $L$  is the distance between voltmeter probes,

$\Delta V$  is the voltage drop across the distance  $L$ ,  $w$  is the width of the sample, and  $t$  is the thickness of the sample.

### III. RESULTS AND DISCUSSION

#### A. Compounded Samples

Electrical conductivities of the compounded samples are shown in Fig. 1. Conductivity increases with carbon fiber content, and is independent of carbon black content, over the range of filler compositions tested. This result suggests that the percolation threshold for carbon black has not been reached. Prior work with carbon black in nylon shows this percolation threshold occurring around 35 wt% [3]. Conductivities of the composites can be increased moderately by sanding the surfaces of the test samples (Fig. 1). Sanding the surfaces decreases the thickness of the frozen layer, where localized nylon weight percentages are the highest. For a 2.5-mm thick sample, SEM images show that the frozen layer is approximately 0.5 mm thick. Removing a portion of this layer, decreases sample thickness and increases conductivity (Eq. 1). Compounded samples achieve a maximum electrical conductivity of 0.64 S/cm.

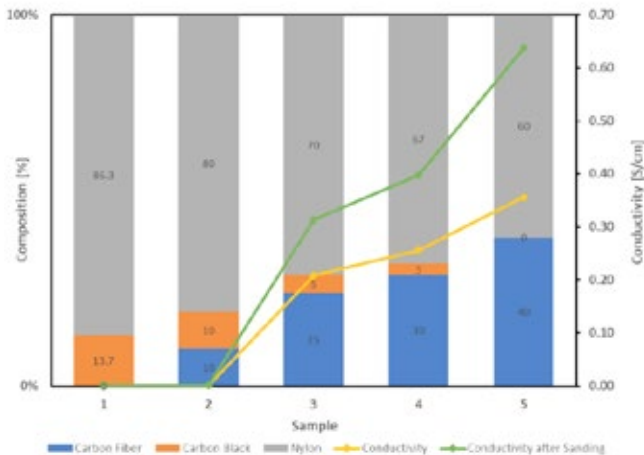


Fig. 1. Electrical conductivity of compounded samples

#### B. Direct Injection-Molded Samples

In contrast to compounded samples, carbon fibers were added to nylon during the injection process to create direct injection-molded samples. Fig. 2 shows the considerable increase in conductivity that can be achieved when directly injecting the carbon fibers. The percolation threshold for carbon fiber in nylon occurs around 20 wt% and conductivity increases considerably up to 50 wt%. As filler weight percentage increases beyond 50%, the viscosity of the polymer blend increases to levels where it is a challenge to ensure proper molding. The electrical conductivity of the 50 wt% carbon fiber sample is 43.61 S/cm. SEM images confirm that the compounding process helps to disperse the additives within the polymer, but it decreases conductivity due to the shearing of the conductive carbon fibers (Fig. 3a). SEM images show that the conductive pathways associated with intact fiber bundles can be maintained by directly injecting the carbon fibers (Fig. 3b).

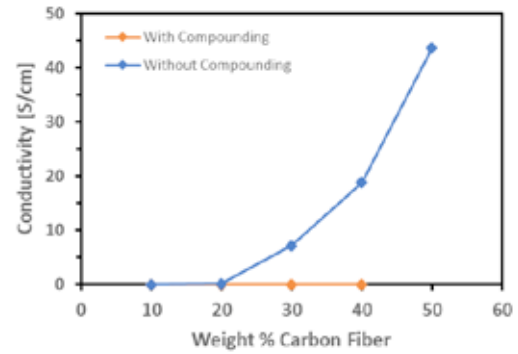


Fig. 2. Electrical conductivity of samples prepared with and without the compounding process

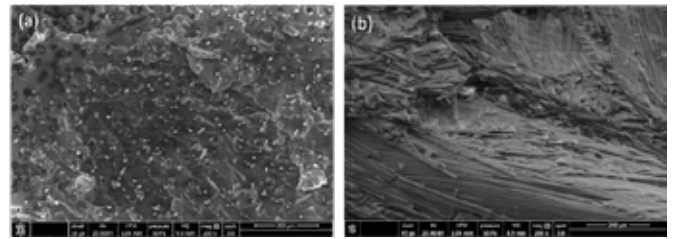


Fig. 3. SEM images of: (a) 10 wt% carbon black, 10 wt% carbon fiber (compounded), and (b) 50 wt% carbon fiber (direct injection-molded)

### IV. CONCLUSION

Polymer composites based on nylon were developed for injection molding of fuel cell bipolar plates. The highest conductivity was obtained by direct injection molding. Results show that the percolation threshold for carbon fiber in nylon occurs around 20 wt%. The addition of carbon black to direct injection-molded samples may further increase electrical conductivity due to the synergistic effects of adding multiple conductive fillers [4].

### ACKNOWLEDGMENT

The authors thank Anne Gohn and Michael Pusateri (Penn State) for assistance with this research. This work was supported by the Pennsylvania State University Research Experience for Undergraduates program.

### REFERENCES

1. Mighri F, Huneault MA and Champagne MF. (2004) Electrically conductive thermoplastic blends for injection and compression molding of bipolar plates in the fuel cell application. *Polymer Engineering & Science* 44: 1755-1765.
2. Hwang IU, Yu HN, Kim SS, et al. (2008) Bipolar plate made of carbon fiber epoxy composite for polymer electrolyte membrane fuel cells. *Journal of Power Sources* 184: 90-94.
3. Chen C-K and Kuo J-K. (2006) Nylon 6/CB polymeric conductive plastic bipolar plates for PEM fuel cells. *Journal of Applied Polymer Science* 101: 3415-3421.
4. Shen L, Wang FQ, Yang H, et al. (2011) The combined effects of carbon black and carbon fiber on the electrical properties of composites based on polyethylene or polyethylene/polypropylene blend. *Polymer Testing* 30: 442-448.

## Mn<sub>x</sub>O<sub>y</sub> DECORATED CARBON-BASED CATHODE FOR ORR CATALYSIS

A Chiodoni\*\*, L. Delmondo\*, J. A. Muñoz-Tabares\*\*, A. Sacco\*\*, N. Garino\*, G. Massaglia\*\*, M. Castellino\*\*, G. P. Salvador\*\*, C.F. Pirri\*\* and M. Quaglio\*\*

\*Center for Sustainable Future Technologies @PoliTo, Istituto Italiano di Tecnologia, C.so Trento 21, 10129 Torino (Italy).

\*\*Department of Applied Science and Technology - DISAT, Politecnico di Torino, C.so Duca degli Abruzzi 24, 10129 Torino (Italy).

**Abstract** - The need to reduce the costs of renewable energy sources such as (bio)electrochemical systems, has pushed the research towards alternative materials, especially for the oxygen reduction reaction, trying to maintain a catalytic efficiency close to that of platinum. In this work, we describe an efficient and simple method to selectively deposit manganese oxide, in particular Mn<sub>3</sub>O<sub>4</sub> in the form of nanofibres, onto conductive electrodes, starting from environmental-friendly precursors, obtaining cathodes with very good performances, comparable to those of platinum.

**Index Terms** - Carbon-based Cathode, Electrospinning, Manganese Oxide, Oxygen Reduction Reaction.

### I. INTRODUCTION

Oxygen reduction reaction (ORR) is a reaction that takes place at the cathode of many (bio)electrochemical systems, and in particular in microbial fuel cells, exploited as energy sources, bio-remediation systems or environment monitoring tools. To reduce the reaction activation energy a catalyst is needed, and usually platinum is considered the best performing one for this electrochemical reaction. However, since Pt is a rare earth and expensive element, an increasing interest has risen to test and optimize alternative electrocatalysts. In this view, transition metal oxides have emerged as a promising class of materials [1, 2], and particularly manganese oxides are considered interesting because they are cheap and can be prepared into several nanostructures. In this framework, we studied the thermal, morphological and catalytic behaviour of Mn<sub>x</sub>O<sub>y</sub> nanostructures, namely nanofibres and nanodrops, prepared through the electrospinning technique by using environmental friendly and cheap precursors, in order to select the optimal nanostructure and crystalline phase as ORR catalyst. In this

work, we show the possibility to prepare a cathode with an efficient and simple method, by reducing the electrode production costs and environmental impact, selectively depositing manganese oxide (employing, as an example, one of studied Mn<sub>x</sub>O<sub>y</sub> nanostructures, namely Mn<sub>3</sub>O<sub>4</sub> nanofibres), onto conductive electrodes (carbon paper, CP), starting from environmental-friendly precursors, with performances comparable to the more used MFC cathode, i.e. platinum supported on glassy carbon.

### II. EXPERIMENTAL

**Materials.** Mn<sub>3</sub>O<sub>4</sub> nanofibres were prepared by mixing together and stirring overnight 9 ml 5wt% of aqueous PEO solution with 3 ml of 20 wt% aqueous manganese acetate solution. Commercial carbon paper (CP) was employed as substrate during the electrospinning process. A NANON 01A electrospinning apparatus (MECC CO., LTD.) equipped with a high voltage power supply (HVU-30P100) and a syringe pump setup operating with a flow rate ranging from 0.1 ml/h up to 99.9 ml/h was used to decorate the carbon paper. During the electrospinning process, a voltage of about 12.5 kV was applied between the needle and the planar collector plate, set at a distance of 10 cm. The nanofibres were calcinated in a tubular oven (Carbolite, VST 12/300/3216) for 3 h at 480°C in air (heating rate of 2.5°C/min) in order to obtain pure Mn<sub>3</sub>O<sub>4</sub> [2].

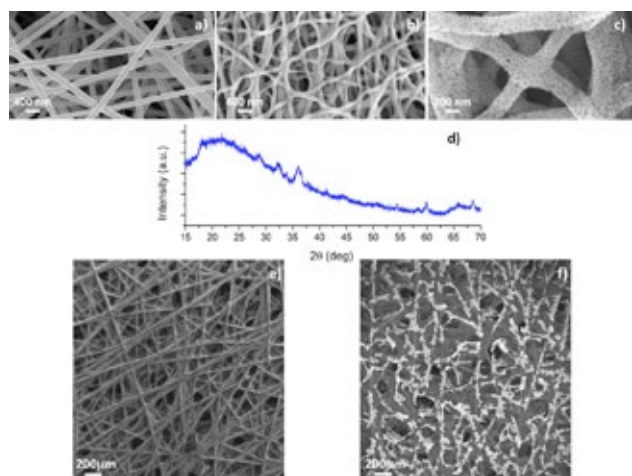
**Characterizations.** X-ray diffraction was performed in order to investigate the crystalline structure of the obtained manganese oxide, by using a PANalytical X'Pert Pro instrument. The morphology of samples was examined by means of Field Emission Scanning Electron Microscopy (FESEM, ZEISS, Supra 40). The electrochemical measurements (rotating ring

Copyright © 2017

disk electrode, RRDE measurements) were carried out through an apparatus described in [2]. Squared single chamber Microbial Fuel Cell (MFC) devices, with an open-air cathode configuration, have been used. An environmental sediment sample was selected as the inoculum source (from Ligurian sea). Commercial carbon paper has been used as anode, while  $\text{Mn}_3\text{O}_4$ -decorated carbon paper has been used as cathode. Linear Sweep Voltammetry (LSV) was performed by using a biologicVSP potentiostat with a scan rate of 0.1 mV/s on MFC containing the  $\text{Mn}_3\text{O}_4$  decorated CP, compared with the cathode based on Pt/C.

### III. RESULTS AND DISCUSSION

Structural and morphological characterizations of the catalyst, as well as a morphological characterization of the decorated CP are reported in Fig.1. In Fig.1a, a FESEM image of the as electrospun nanofibres (deposited on silicon substrate for better characterization convenience) is reported, while in Fig.1b and Fig.1c, FESEM images collected at two different magnifications, showing the nanofibres after the calcination at 480 °C, are presented. Fig.1d reports the X-ray diffraction pattern of the same sample. It is worth to note that the calcination process hasn't compromised the nano-fibred shape, and that each fibre is constituted by small nanocrystals, that X-ray diffraction reveals to be  $\text{Mn}_3\text{O}_4$  (Hausmannite, JCPDS 00-024-0734). In Fig.1e and Fig.1f, the FESEM images related to the CP as it is, and decorated with the electrospun calcinated nanofibres of  $\text{Mn}_3\text{O}_4$ , are reported, respectively.



**Fig. 1.** FESEM images of: a) as electrospun nanofibres; b) and c) two magnifications of the calcinated nanofibres; e) carbon paper; f) carbon paper decorated with  $\text{Mn}_3\text{O}_4$  nanofibres. In d), X-ray diffraction pattern of the calcinated nanofibres.

By analysing these two images, it is possible to note that the manganese oxide nanofibres are well distributed on the carbon paper, even though they are localised where the substrate is much more rough. This phenomenon could be related with the local variation of the electric field during the electrospinning process.

To study the catalytic activity of the prepared cathode, RRDE measurements were performed, comparing it to a standard Pt/C reference and the bare CP, in order to evaluate the number of electrons exchanged in the oxygen reduction reaction. In Table I, the values obtained at -0.55V are reported. As clearly evident, CP shows very low catalytic properties, as evidenced by both electron transfer number and peroxide percentage values, while quite good results were obtained for the manganese oxide-decorated electrode. Based on these results, it can be asserted that manganese oxide electrode shows performances comparable with the values related the Pt/C.

**TABLE I**  
ELECTRONS EXCHANGED AND PEROXIDE PERCENTAGE IN THE OXYGEN REDUCTION REACTION FOR DIFFERENT ELECTRODES

Material	CP	decorated CP	Pt/C
n @ -0.55V	2.4	3.65	3.94
$\text{HO}_2\text{-}\%$ @ -0.55V	78%	17.5%	3%

Linear Sweep Voltammetry (LSV) was performed on MFCs containing the decorated cathode, compared with cathode electrode based on Pt/C.

**TABLE II**  
NORMALISED POWER DENSITIES FOR THE TWO CATHODES IN MFC

Material	decorated CP	Pt/C
Current density @3mA/g	Power density 0.55 mW/g	Power density 0.7 mW/g

In table 2, the values of the normalised maximum power density obtained with the two cathodes is reported as comparison, putting in evidence the good performances of the manganese oxide-decorated cathode.

### IV. CONCLUSIONS

This study describes an efficient and simple method to selectively deposit manganese oxide onto conductive electrodes, starting from environmental-friendly precursors. The obtained results demonstrate that  $\text{Mn}_3\text{O}_4$ -based electrodes show a very good catalytic behaviour, ensuring an electron transfer number close to the ideal value of 4. MFCs with such a cathode exhibited high power density values, comparable with MFC with a cathode made of Pt/C on CP.

### REFERENCES

- [1] Zhou, Z.-Y., Tian, N., Li, J.-T., Broadwell I., Sun, S.-G., Nanomaterials of high surface energy with exceptional properties in catalysis and energy storage, Chem. Soc. Rev., volume 40, 2011, pp. 4167–4185.
- [2] Delmondo, L., Salvador, G. P., Munoz-Tabares, J. A., Sacco, A., Garino, N., Castellino, M., Gerosa, M., Massaglia, G., Chiodoni, A., Quaglio, M., Nanostructured  $\text{Mn}_x\text{O}_y$  for oxygen reduction reaction (ORR) catalysts, Appl. Surf. Sci., volume 388, 2016, pp. 631–639



## MODEL-BASED PARAMETRIC ANALYSIS OF INTERNAL CROSSOVER OCCURRING IN A SOLID OXIDE FUEL CELL

Marco Gallo, Pierpaolo Polverino, Dario Marra, Marco Sorrentino and Cesare Pianese  
Dept. of Industrial Engineering, University of Salerno, Via Giovanni Paolo II 132, 84084 Fisciano (SA), (Italy)

**Abstract** - During normal operation of a solid oxide fuel cell (SOFC), one of the most common causes of voltage drop and, thus, performance decrease is related to gases crossover (or internal leakages). Air crossover from cathode to anode or fuel crossover from anode to cathode causes an increase in temperature due to local combustion, leading to a significant local variation in fuel composition. In this paper, a simulation analysis of gas crossover occurring within an SOFC stack is performed. The model used for the investigation has been already validated by means of experimental data acquired within the framework of the EU-funded project DIAMOND. Such model has been improved implementing physical crossover equations through lumped modelling approach. The analysis aims at evaluating the effects of internal leakages on voltage, temperature and outlet composition at different leakage magnitudes. In this way, proper guidelines for the development of a suitable diagnostic strategy can be defined.

**Index Terms** – SOFC, Crossover, Leakage, Simulation Analysis.

### I. INTRODUCTION

During normal operation of Solid Oxide Fuel Cells (SOFCs), a reliable sealing of the main components is required to ensure the correct stack performance and avoid the gas leakage. To improve SOFCs lifetime, great attention is currently given to innovative materials [1] as well as proper control and diagnostic algorithms, capable of detect and isolate incipient faults and apply suitable mitigation strategies [2].

Among the most frequent faults occurring in SOFC stacks, gas crossover (or internal leakage) plays a significant role in performance reduction, due to consequent voltage degradation and temperature increase. Crossover usually takes place between anode and cathode: anodic leakage occurs when the fuel crosses the electrolyte, reaching the cathode side, whereas cathodic

leakage happens if air reaches the anode side (still by crossing the electrolyte). Crossover is usually driven by pressure and concentration gradients between cathode and anode sides, which force one reactant to cross the electrolyte and reach the other reactant side, with consequent local direct reactions [3].

Stack internal leakages have been qualitatively identified by observing changes in stack temperature [4], voltage and gas composition [5], but when approaching system diagnosis under operation, it is hard to distinguish such phenomenon from other faults (e.g., sulphur poisoning). For this reason, suitable diagnostic methodologies can be beneficial for correct fault identification, especially when considering on-board applications. However, performing experimental campaigns to investigate internal leakages is usually difficult and expensive. Therefore, numerical simulation may offer a viable solution to study the effects of crossover on both stack and system level [6].

In this work a lumped model simulating fuel crossover in an SOFC system is presented and a parametric analysis at different leakage magnitudes is performed.

### II. THE CROSSOVER MODEL

A dynamic lumped modelling approach has been adopted to simulate the electrochemistry of an SOFC stack. Energy conservation principle is applied, as shown in eq. (1), where  $K$  is the stack heat capacity,  $T$  is the stack outlet temperature,  $\dot{E}_{in}$  and  $\dot{E}_{out}$  are the inlet and outlet energy flows,  $P$  is the electrical power and  $Q$  is the heat exchanged in case of non-adiabatic conditions. More details on the approach can be found in [7].

$$K \frac{dT}{dt} = \dot{E}_{in} - \dot{E}_{out} + Q - P \quad (1)$$

Reactions occurring under internal leakage operation



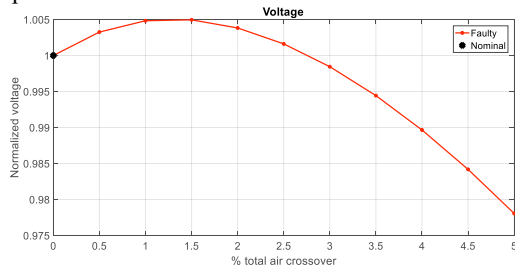
are accelerated by high operating temperatures and by the presence of catalytic active materials, causing the instantaneous formation of hotspots. Anodic leakage involves the production of carbon dioxide and steam, as described in eq. (2), whereas cathodic leakage involves the oxidation of flammable substances at anode side.



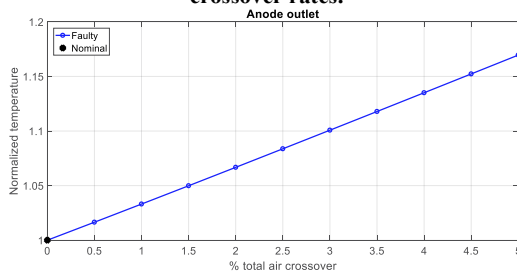
By implementing these equations in the lumped model, an air crossover throughout the electrolyte towards the anode side is simulated. The oxygen immediately reacts at the anode side with hydrogen and carbon monoxide, while the nitrogen acts as inert gas. As a result, the whole temperature arises and water is formed as by-product due to the further consumption of  $H_2$ . As main assumption, the leaked oxygen amount is considered completely depleted by hydrogen oxidation reaction, thus neglecting the other reactions of eq. (2) and then keeping unchanged the amount of the other components.

### III. PARAMETRIC ANALYSIS

The parametric analysis is performed focusing on stack voltage (Figure 1) and outlet temperature (Figure 2) under different percentage of leaked air. The trends are normalized with respect to variables nominal value, to keep the focus on the deviation from nominal conditions.



**Figure 1 - Normalized voltage behavior at different air crossover rates.**



**Figure 2 - Normalized stack outlet temperature at different air crossover rates.**

As shown in Figure 1, the voltage exhibits a parabolic behaviour due to the reaction occurring at the anode side. The generated heat causes stack temperature to increase. As presented in Figure 2, the stack outlet temperature exhibits a linear trend, due to the exothermic reactions

described in eq. (2). The non-linear trend of the voltage is due to the combined change in Nernst potential and ohmic losses. The Nernst potential shows a linear decrease with the temperature, whereas the ohmic losses, modelled through an ASR approach [7], are non-linear. As a result, the voltage initially increases due to the greater effect related to ohmic losses reduction at small crossover. Then, the decrease in Nernst potential becomes more relevant, inducing the observed voltage reduction. Concerning the temperature, the change in the electrical power is relatively small with respect to the variation in the released energy due to the crossover reaction, resulting in a linear increase.

### IV. CONCLUSIONS

The present work focuses on a simulation analysis of air crossover by means of lumped modelling approach. A parametric study of the effects of the considered fault on SOFC stack and outlet temperature has been carried-out. Variable trends have been defined with respect to different leakage amounts and can be assumed as a basis for crossover detection and isolation.

### ACKNOWLEDGMENT

The research leading to these results has received funding from the European Union's Seventh Framework Programme (FP7/2007–2013) for the Fuel Cells and Hydrogen Joint Technology Initiative under grant agreement n° 621208 (Project - DIAMOND, Diagnosis-aided control for SOFC power systems).

### REFERENCES

- [1] Nguyen, X. V., Chang, C. T., Jung, G. B., Chan, S. H., Lee, W. T., Chang, S. W., & Kao, I. C. (2016). Study of sealants for SOFC. *International Journal of Hydrogen Energy*, 41(46), 21812-21819.
- [2] Polverino, P., Pianese, C., Sorrentino, M., & Marra, D. (2015). Model-based development of a fault signature matrix to improve solid oxide fuel cell systems on-site diagnosis. *Journal of Power Sources*, 280, 320-338.
- [3] Rasmussen, J. F. B., Hendriksen, P. V., & Hagen, A. (2008). Study of Internal and External Leaks in Tests of Anode-Supported SOFCs. *Fuel Cells*, 8(6), 385-393.
- [4] Blum, L., Packbier, U., Vinke, I. C., & de Haart, L. G. J. (2013). Long-Term Testing of SOFC Stacks at Forschungszentrum Jülich. *Fuel Cells*, 13(4), 646-653.
- [5] George, R. A. (2000). Status of tubular SOFC field unit demonstrations. *Journal of Power Sources*, 86(1), 134-139.
- [6] Goll, S., Samsun, R., Peters, R. (2011). Analysis and optimization of solid oxide fuel cell-based auxiliary power units using a generic zero-dimensional fuel cell model. *J. of Power Sources*, 196, 9500-9509.
- [7] Marra, D., Sorrentino, M., Pohjoranta, A., Pianese, C., & Kiviahio, J. (2015). A lumped dynamic modelling approach for model-based control and diagnosis of solid oxide fuel cell system with anode off-gas recycling. *ECS Transactions*, 68(1), 3095-3106.

## SIMULATION OF FC SYSTEM INTEGRATED INTO CHP APPLICATION, INCLUDING ELECTROLYZER OPERATION

G. Cinti\*, G. Bidini, V. Ciotola\*\*

\*Università degli Studi di Perugia, Department of Engineering, via Duranti 93, Perugia (Italy)

\*\*SUDGEST AMBIENTE Scarl, Via Breccia a S. Erasmo 114 - 80146 Napoli, <http://www.sudgest.eu>

**Abstract** - This model allows the calculation of payback time of a Fuel Cell CHP unit once installed in an existing building. The model evaluates also the integration into the building of a renewable energy system (RES), such as PV panels or micro wind turbine, and a long-term storage realized with an electrolyzer and hydrogen storage. Based on integration and market inputs the model calculates energy flows and designs storage size. The model is implemented in an open access online tool in the frame of the NET-Tools EU project.

**Index Terms** – Cogeneration, Energy storage, Re-SOFC, Electrolyzer

### I. INTRODUCTION

This study presents a model developed in the frame of the Net-Tools European project. Net Tools aims to develop an e-infrastructure to provide digital tools and information service for educational issues and training within FCH technologies.

The tool presented in this study is a model that allows the calculation of payback time of a Fuel Cell CHP unit once installed in an existing building.

### II. METHODS

This model calculates the payback of a fuel cell system for cogeneration of heat and power (CHP) based on fuel cell technology. The unit is introduced in an existing building to optimize energy efficiencies and reduce energy price [1–3]. CHP integration is evaluated on monthly base. This means that the energy balance and the valorization of the energy in terms of consumption or supply is evaluated at the end of every month. Thermal or electric storage can be used to match the production and the consumption for smaller range of time such as days, hours, minutes and seconds. The aim of the tool is to evaluate system payback and not to optimize system design.

Required inputs:

- Building inputs: monthly electricity and heat consumption, efficiency of the existing boiler.
- CHP inputs: unit size, thermal and electrical efficiency, unit cost.
- Market inputs: electricity cost, retail price and gas cost.
- Integration strategy: utilization factor of the unit during the year.
- RES inputs: monthly RES utilization factor, RES power size and RES unit cost;
- Storage inputs: electrolyzer and fuel cell efficiency and unit cost, hydrogen storage unit cost.

General assumptions:

- The RES production and electricity consumption is balanced every month. Additional buffer for electricity balance is considered as part of the RES cost;
- The CHP unit operates in steady state with only ON/OFF operation;
- Energy values of gas and electricity are not time dependent;

Integration strategies:

- Electrolyzer and fuel cell are considered in steady state operation. Electrolyzer utilization factor is the same of RES while fuel cell operates in the remaining time of the period;
- All balances in terms of energy are realized with month as range of time;
- Extra heat produced by CHP is not valorized into the building but can be released to atmosphere with no additional cost;
- Extra production of electricity is sold to the grid at input defined retail value;

Copyright © 2017

The calculation starts from the electricity produced by RES every month, ( $RES_n$ ) and the electricity consumption of the user ( $E_{cn}$ ). Monthly balance,  $DE_{RESn}$ , is the difference between RES production and electricity consumption of the building. Hydrogen stored in the tank,  $H_2$ , is calculated starting from June. Depending from the monthly balance the storage can be increased or reduced down to zero. If there is an extra production ( $DE_{RESn} > 0$ ), electricity energy is stored with electrolyzer efficiency, if the balance is negative ( $DE_{RESn} < 0$ ) electricity can be obtained from the fuel cell, if hydrogen is available, or from the microCHP or the grid. The new electricity consumption is calculated as the new balance considering also storage and re-electrification. CHP monthly electrical production,  $E_{eCHPn}$ , is calculated as the electricity produced by the system multiplied to the operation hours of the month. Electricity balance, DE is calculated as the difference between the electricity produced by the CHP unit and electricity consumption of the building:

$$DE_n = E_{eCHPn} - E_{cn}$$

Annual  $OPEX_{CHP}$  costs (€/year) is calculated as difference between costs, electricity and gas, and income, electricity. Over production of heat is not considered as a possible income for the economic evaluations. The equation calculates electricity and gas value as cost or income depending on the relative balance.

Annual  $OPEX_{SOA}$  state of art costs (€/year) is the operational cost and is calculated as the sum of monthly electricity ( $E_c$ ) and gas costs ( $G_c$ ) of the building.  $CAPEX_{CHP}$  cost, is calculate as system size multiplied to unit cost:

$$CAPEX_{CHP} = P_{CHP} \cdot U_c$$

The  $PAYBACK_{CHP}$  (years) is the ration between  $CAPEX$  and the economies, calculated as difference between  $OPEX_{SOA}$  and  $OPEX_{CHP}$ :

$$PAYBACK_{CHP} = \frac{CAPEX_{CHP}}{OPEX_{SOA} - OPEX_{CHP}}$$

## RESULTS

The model allows to evaluate payback of the integrated SOFC CHP + electrolyzer unit. The model is now an e-tool free available online to design a convenient system. As example Figure 1 reports the energy flows of model based on the consumption of a building located in center Italy and equipped with a 2 kW photovoltaic system, 0.5 kW SOFC cogeneration unit 0.8 kW electrolyzer, 0.2 kW fuel cell and 7.3 kg of hydrogen storage.

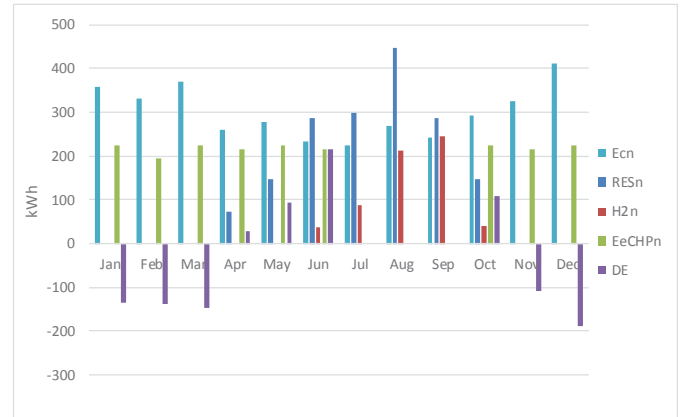


Figure 1 Results of the model example

Considering the present cost of Italian energy market and technology overview costs as reported in the MAEP [4], payback time for the system calculated is 6.7 years.

## ACKNOWLEDGMENT

The NET-TOOLS project has received funding from the European Union's Horizon 2020 research and innovation programme under Grant Agreement-736648.

This research also supported by Italian Government with the PON project "Fuel Cell Lab – Innovative systems and high efficient technologies for polygeneration – PON03PE\_00109.

## REFERENCES

1. Liso, V.; Zhao, Y.; Brandon, N. P.; Nielsen, M. P.; Kær, S. K. Analysis of the impact of heat-to-power ratio for a SOFC-based mCHP system for residential application under different climate regions in Europe. *Int. J. Hydrogen Energy* **2011**, *36*, 13715–13726, doi:10.1016/j.ijhydene.2011.07.086.
2. Naimaster, E. J.; Sleiti, A. K. Potential of SOFC CHP systems for energy-efficient commercial buildings. *Energy Build.* **2013**, *61*, 153–160, doi:10.1016/j.enbuild.2012.09.045.
3. Antonucci, V.; Brunaccini, G.; De Pascale, A.; Ferraro, M.; Melino, F.; Orlandini, V.; Sergi, F. Integration of  $\mu$ -SOFC Generator and ZEBRA Batteries for Domestic Application and Comparison with other  $\mu$ -CHP Technologies. *Energy Procedia* **2015**, *75*, 999–1004, doi:10.1016/j.egypro.2015.07.335.
4. FUEL CELLS AND HYDROGEN JOINT UNDERTAKING ( FCH2 JU ) *Multi - Annual Work Plan 2014 - 2020*; 2014;

## ENERGETIC ANALYSIS OF OXY-HYDROGEN INJECTION IN INTERNAL COMBUSTION ENGINES

F. D'Aniello, P. Polverino, I. Arsie and C. Pianese

Dept. of Industrial Engineering, University of Salerno, via Giovanni Paolo II 132, 84084 Fisciano (SA), (Italy)

**Abstract** - The use of hydrogen as additive fuel in internal combustion engines has recently drawn the attention of researchers and industrial companies. The works available in the literature analyses the use of different devices (e.g., small electrolyzers) to produce a mixture of oxygen and hydrogen to be directly injected into the engine. Benefits have been reported concerning emissions reduction and efficiency increase. Nevertheless, a proper energetic analysis focusing on the whole system (i.e., the engine coupled with the electrolyser) has not yet been addressed. The objective of this work consists in performing a thorough analysis to investigate the energy required for hydrogen production and the benefits related to hydrogen addition to conventional fuels. Particular attention is given on fuel consumption variation with hydrogen added to Diesel fuel. Moreover, the work wants to give proper guidelines to assess the real benefits of using such devices to improve fuel savings and performance.

**Index Terms** – Energetic Analysis, Fuel Saving, Hydrogen, Internal Combustion Engines.

### I. INTRODUCTION

Due to the recent increase in petroleum price and environmental issues, engine manufacturers and researchers are focusing their attention on alternative approaches to increase fuel economy and reduce engine emissions. In this context, the oxy-hydrogen mixture is recognized as a promising additive for Diesel fuel in order to comply with strict Real Driving Emissions (RDE) targets [1]. Using hydrogen as additive may significantly reduce fuel consumption and harmful emissions in conventional Diesel engines. Compared to pure Diesel fuel, hydrogen presents a higher power density and high flame speed [1]. This latter, combined with high diffusivity, can result in a faster and more complete combustion of the fuel-hydrogen mixture [2]. Hydrogen fractions ranging from 5% to 50%, at different engines loads, show reduced combustion duration and increased engine efficiency [3], [4]. Moreover, hydrogen has a wide flammability range, leading combustion to take place also with extremely lean mixtures (fuel burns completely and produces less pollutant) [2]. Finally, hydrogen exhibits relatively high self-ignition

temperature (about 858 K), which is a key factor in choosing engine compression ratios [2], [5].

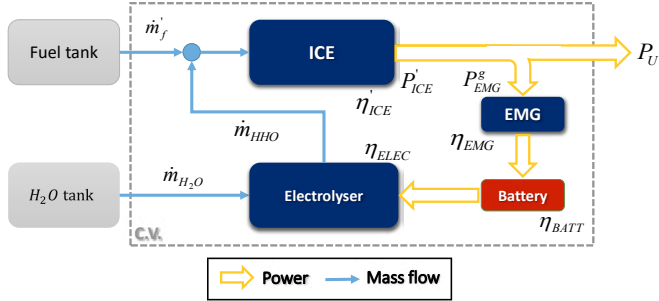
In the available literature, several works analyse the use of devices, such as small electrolyzers, to produce a proper mixture of oxygen and hydrogen (usually referred to as oxyhydrogen or HHO) to be directly injected into the engine [2], [6]. The abovementioned studies investigate the effects of HHO addition to Diesel fuel, with particular attention to engine torque variation, brake thermal efficiency, specific fuel consumption and emissions change at various operating conditions [5], [7]. It is worth remarking that engine load and speed have a significant influence on engine performance under varying load and speed [8]. Ylmaz et al. [7] highlighted the reduction in specific fuel consumption as direct consequence of increased engine performance due to hydrogen injection. Conversely, de Moraes et al. [5] did not observe significant changes in specific fuel consumption for the investigated working conditions. Nevertheless, a proper energetic analysis involving the whole system (i.e., the electric motor generator, battery and engine coupled with the electrolyser) has not yet been approached in the literature. The objective of this work consists in performing a thorough energetic analysis investigating the energy required for hydrogen production and addressing the related advantages on system efficiency and fuel consumption.

### II. ENERGETIC ANALYSIS

In this section, the energetic analysis considering costs and benefits in using hydrogen as additive into conventional engines (with embedded HHO system production) is performed. Referring to the work of Bari et al. [6], an electrolyser is here considered for HHO production. The system layout is depicted in Fig.1, where the main system components as well as mass and power flows are shown.

Regarding mass flow, the HHO mixture is produced by means of an electrolyser fed with water (taken from a tank). Concerning the power flow, the power required by the electrolyser is supplied

by a battery charged through an Electric Motor Generator (EMG) connected to the engine crankshaft. On the one hand, the fuel mass flow  $\dot{m}_f$ , engine efficiency  $\eta_{ICE}$  and power  $P_{ICE}$  refer to a conventional configuration, with no HHO addition. On the other hand, the terms  $\dot{m}'_f$ ,  $\eta'_{ICE}$  and  $P'_{ICE}$  are instead related to the same variables with HHO produced and injected into the engine.



**Fig. 1. System layout.**

An energetic balance on the control volume (C.V.) shown in Fig.1 is performed, to define the fuel consumption  $\dot{m}'_f$ :

$$P_U = \begin{cases} P_{ICE} = \eta_{ICE} \dot{m}_f H_i & \text{without HHO} \\ P'_{ICE} - P_{EMG}^g & \text{with HHO} \end{cases} \quad (1)$$

$$P'_{ICE} = \dot{m}'_f H_i \eta'_{ICE} + P_{H_2} \quad (2)$$

$$P_{EMG}^g = \frac{P_{H_2}^g}{\eta_{ELEC} \eta_{BATT} \eta_{EMG}} \quad (3)$$

$$\dot{m}'_f = \frac{P_u - P_{H_2} + P_{EMG}^g}{\eta'_{ICE} H_i} \quad (4)$$

In eq. (1),  $P_U$  is the useful power provided by the whole system,  $P_{EMG}^g$  is the gross power fed to the EMG and  $H_i$  is the fuel heating value. In eq. (2),  $P_{H_2}$  is the power generated by combustion of the HHO mass flow (coming from the electrolyser), which takes into account the engine efficiency variation due to HHO addition. In eq. (3),  $P_{H_2}^g$  is the gross chemical power available at the electrolyser outlet, whereas  $\eta_{ELEC}$ ,  $\eta_{BATT}$  and  $\eta_{EMG}$  are the electrolyser, battery and EMG efficiencies, respectively.

As reported in [6], the increase in the efficiency of a diesel engine, operating at a constant speed of 1500 rpm, with a break power of 19 kW, is about 6% (from 0.32 to 0.34) by adding 25 NL/min of HHO to the inlet air flow through a nozzle located in the intake manifold. The term  $P_{EMG}^g$  is computed by assuming ideal electrolysis reaction and considering constant electrolyser, battery and EMG efficiencies (0.77, 0.85 and 0.85, respectively). Hence, to produce 25 NL/min of HHO (which corresponds to a gross output power of 3.4 kW, based on hydrogen higher heating value) an overall power of 6.1 kW is required at EMG inlet (see eq. 3). Considering that the power  $P_{H_2}$  generated by the HHO

combustion in the engine (with 0.34 efficiency) is 1 kW, the required fuel flow, evaluated with eq. (4), is 1.6 g/s. Without HHO injection, to satisfy the same power request, a fuel rate of 1.3 g/s is needed. This means that, if the power required at EMG inlet is taken from the engine, the fuel rate increases of +23.1%. If this power is instead recovered from on board wasted energy using, for example, a thermo-electric generator, then the whole fuel consumption becomes 1.2 g/s, with a reduction of -7.7%.

### III. CONCLUSIONS

The proposed work performed an energetic analysis to investigate the energy requirements and fuel consumption of a diesel engine, with oxy-hydrogen (HHO) as fuel additive. The necessary amount of HHO was assumed being produced through an on-board electrolyser. From the achieved results, an increase in fuel consumption has been assessed if the power needed for the HHO is taken at engine outlet, whereas a reduction is instead fulfilled if the power is recovered from other sources. Although investigated in a single operating condition, the analysis and results can be easily extended to other conditions as well as engine types. As showed by the analysis, the conclusions drawn in several literature studies, if not properly contextualised, may lead to wrong results and cause an increase in fuel consumption.

### REFERENCES

- [1] Hüseyin Turan Arat, Mustafa Kaan Baltacıoglu, Mustafa Özcanlı, Kadir Aydın, Effect of using Hydroxy – CNG fuel mixtures in a non-modified diesel engine by substitution of diesel fuel, In International Journal of Hydrogen Energy, Volume 41, 2016, pp. 8354-8363.
- [2] Prashant N. Pakale, Nrendra.B.Pawar, H.G.Patil, S.U.Patel, Efficiency Improvement of SI/CI Engine by Using Blend of Oxy-Hydrogen Gas with Fuel, in International Journal of Research in Advent Technology, Volume 3, 2015.
- [3] Jinhua Wang, et al., Effect of ignition timing and hydrogen fraction on combustion and emission characteristics of natural gas direct-injection engine, in Frontiers of Energy and Power Engineering in China, Volume 2, 2008; pp.194-201.
- [4] D.B. Lata, Ashok Misra, S. Medhekar, Effect of hydrogen and LPG addition on the efficiency and emissions of a dual fuel diesel engine, In International Journal of Hydrogen Energy, Volume 37, 2012, pp. 6084-6096
- [5] André Marcelino de Moraes, Marco Aurélio Mendes Justino, Osmano Souza Valente, Sérgio de Moraes Hanriot, José Ricardo Sodré, Hydrogen impacts on performance and CO2 emissions from a diesel power generator, In International Journal of Hydrogen Energy, Volume 38, 2013, pp. 6857-6864.
- [6] S. Bari, M. Mohammad Esmail, Effect of H2/O2 addition in increasing the thermal efficiency of a diesel engine, In Fuel, Volume 89, 2010, pp. 378-383.
- [7] Ali Can Yilmaz, Erinc Uludamar, Kadir Aydın, Effect of hydroxy (HHO) gas addition on performance and exhaust emissions in compression ignition engines, In International Journal of Hydrogen Energy, Volume 35, 2010, pp. 11366-11372.
- [8] A. M. Falahat, M. A. Hamdan and J. A. Yamin, Engine performance powered by a mixture of hydrogen and oxygen fuel obtained from water electrolysis, in International Journal of Automotive Technology, Volume 15, 2014, pp. 97-101.



## DESIGN 2 SERVICE PROJECT – TOWARDS IMPROVED SERVICEABILITY AND DURABILITY OF MICRO-CHP AND SUPPLEMENTAL POWER SYSTEMS

A. Linhart, H. Bekebrok, M. Zobel, and A. Dyck  
DLR Institute of Networked Energy Systems  
Carl-von-Ossietzky-Str. 15  
26129 Oldenburg, Germany

**Abstract** – This paper gives an overview of the FCH JU project “Design 2 Service” (grant agreement no 671473) and the current project status. The project aims at improving the serviceability and durability of PEMFC and SOFC fuel cell-based micro-CHP and supplemental power systems in order to lower operational costs and thereby improve marketability of the systems. The project consortium consists of two unit manufacturers, one energy service supplier, one component supplier and two research institutes. Improvements of the serviceability are achieved by identifying typical system failures and developing countermeasures, by improving the system design towards easier maintainability and component exchange, by improving important system components with respect to life-time and minimisation of stack poisoning, and by devising concepts for intuitive manuals and troubleshooting guidelines for non-specialised installers and technicians. The system efficiencies are evaluated using specifically designed time-lapse tests. A field-trial is conducted and analysed to verify the improvements.

**Index Terms** – micro-CHP, supplemental power, fuel cells, serviceability.

### I. INTRODUCTION

Fuel cell applications have the potential to constitute important elements of modern energy supply systems. This is due to their high efficiency and smooth operation when converting the fuel – typically hydrogen, natural gas or methanol – into electricity and heat [1]. The cogeneration of electricity and heat makes them interesting for residential buildings, where the generated heat can be used for supplying domestic hot water and space heating. For this market segment, so-called micro-CHP (also  $\mu$ CHP or mCHP) systems, which can be connected to the natural gas grid serving in many countries to supply heating energy to households, have been developed in the last decades [2]. A related fuel cell-based application are supplemental or back-up power systems, which are deployed at sites that do not fully rely on the electricity

grid. Here, fuel cell system serve to supplement power when fluctuating power sources such as wind and photovoltaic power do not produce sufficient electricity, or to provide electricity in case of grid outages.

While fuel cell-based power systems pose substantial advantages over combustion engine-based technologies with respect to fuel efficiency, emissions, noise and vibrations [3], they are relatively complex technologies that in the current state of development still require considerable maintenance effort. Currently, for regular maintenance at periodic intervals as well as repairs in case of system failure, specially trained technicians and non-standardised exchange components are needed. This results in increased operational costs, which in turn reduces the competitiveness of the technology and impairs the marketability.

### II. THE D2SERVICE PROJECT

#### A. Objectives

The “Design 2 Service” project aims at improving the serviceability and durability of fuel cell-based micro-CHP and supplemental power applications. The project is funded by the Fuel Cells and Hydrogen Joint Undertaking (FCH JU) under the grant agreement no. 671473 [4]. The full name of the project is “Design of 2 technologies and applications to service”, referring to two different fuel cell technologies, PEMFC and SOFC, being employed in micro-CHP and supplemental power applications. Important aspects to be addressed by the project are system redesign to reduce the maintenance time and effort, components standardisation, costs reduction and increase of durability, and elaboration of maintenance guidelines for non-specialised service technicians.

#### B. Consortium

The consortium consists of the micro-CHP manufacturer

SOLIDpower S.p.a. (Italy) and the micro-CHP and supplemental power manufacturer Ballard Power Systems Europe A/S (Denmark), which develop and supply the systems investigated in the project. From each manufacturer, micro-CHP units are provided to either of the research institutions DLR (German Aerospace Center) Institute of Networked Energy Systems and the hydrogen and fuel cell centre ZBT GmbH (both Germany), where the systems are investigated under laboratory conditions. The energy service supplier Energy Partner s.r.l. (Italy) organises the field trial, where micro-CHP and supplemental power units will be installed at selected customer sites. The component supplier Bosal Emission Control Systems NV contributes to improving balance-of-plant components.

### C. Methodology

In the first project phase, the status quo of the service and maintenance aspects of micro-CHP and supplemental power systems was surveyed. For this, data from the field trials Callux [5], Chrisalide [6] and Danish Micro-CHP [7] was evaluated. The focus was on the analysis of frequent system failure and shutdown causes. Additionally, the maintenance procedures and the system design with regard to component exchange of the own systems were scrutinized by both manufacturers. From these analyses, possible design and service procedure improvements were identified and incorporated in the redesign of the systems. In parallel, a micro-CHP system of each manufacturer was installed and tested at DLR in a laboratory environment. In addition to installation and efficiency tests, time-lapse tests reducing the evaluation time for a full year to 30 days using realistic load profiles were performed with a test bench simulating the thermal side of a residential building energy system [8]. Observations from these tests were also integrated in the redesign of the systems. Complementing these activities, possibilities to improve selected key components were investigated by ZBT and Bosal, by identifying more durable catalyst and adsorption materials for the hydrodesulphuriser, and by minimizing the chromium evaporation of the heat exchanger of the SOFC system, respectively.

In the second project phase, the improved systems are installed in the laboratories of DLR and ZBT to test the improvements. At DLR, efficiency and time-lapse tests are performed to assess the efficiency differences to the previous system generation. To lower the specialisation requirements for installers and technicians, manual design guidelines for selected maintenance tasks that are easily understandable and avoid misunderstandings are elaborated. Furthermore, possible installation and configuration mistakes are identified and their impacts on system efficiency as well as simple diagnostic measures are investigated. At ZBT, the new hydrodesulphuriser design is tested in system operation. To verify the improvements of the systems with respect to serviceability and maintenance intervals, the redesigned systems are deployed at

selected customer sites for a field trial.

### D. Selected Project Achievements

Materials for catalyst and adsorption have been identified which extend the life-time of the hydrodesulfuration unit up to 60,000 h, eliminating the necessity of a service procedure to exchange the material during the life-time of the systems.

Favourable inverter configurations for clusters of several plants have been identified that increase the conversion efficiency and allow for partial load operation to adapt to seasonal variations of the building hot water and space heating demand.

## III. CONCLUSION

In the D2Service project, important aspects for improved serviceability and maintenance of micro-CHP and supplemental power systems based on PEMFC and SOFC technologies are addressed. The overall system design and important components are redesigned to facilitate service procedures and reduce maintenance costs. The concepts and improvements elaborated within the project are expected to significantly improve the marketability of the technology.

### ACKNOWLEDGMENT

This project has received funding from the Fuel Cells and Hydrogen 2 Joint Undertaking under grant agreement No 671473. This Joint Undertaking receives support from the European Union's Horizon 2020 research and innovation program.

### REFERENCES

- [1] Haile, S.M., Fuel cell materials and components, *Acta Mater.*, 2003, 51, 5981-6000.
- [2] Ellamla, H.R., Staffell, I., Bujlo, P., Pollet, B.G., Pasupathi, S., Current status of fuel cell based combined heat and power systems for residential sector, *J. Power Sources*, 2015, 293, 312-328.
- [3] Hawkes, A., Staffell, I., Brett, D., Brandon, N., Fuel cells for micro-combined heat and power generation, *Energy Environ. Sci.*, 2009, 2, 729-744.
- [4] Fuel Cells and Hydrogen Joint Undertaking, <http://www.fch.europa.eu/project/design-2-technologies-and-applications-service> (accessed 29.09.2017)
- [5] callux – Praxitest Brennstoffzellen fürs Eigenheim, National Organisation Hydrogen and Fuel Cell Technology, <https://www.now-gmbh.de/en/national-innovation-programme/strom-und-waerme-mit-brennstoffzellen/callux> (accessed 29.09.2017)
- [6] Crisalide Network, <http://www.retecrisalide.it/en/> (accessed 29.09.2017)
- [7] Danish Micro Combined Heat and Power - domestic energy from fuel cells, [http://www.dmkv.dk/english/index\\_en.html](http://www.dmkv.dk/english/index_en.html) (accessed 29.09.2017)
- [8] Linhart, A., Lange, M., Thomsen, T., Zobel, M., Using Reference Load and PV Profiles for Realistic Evaluations of Residential Energy Systems Including PV Systems, NEIS Conference 2016, Springer, Wiesbaden, 2017, pp 67-73.

## LANTHANUM TUNGSTATE $\text{La}_{28-x}\text{W}_{4+x}\text{O}_{54+d}\text{V}_{2-d}$ IN $\text{H}_2$ EXTRACTION MEMBRANE APPLICATIONS

M. E. Ivanova, W. Deibert, W.A. Meulenbergh, and O. Guillon  
Forschungszentrum Jülich GmbH, Institute of Energy and Climate  
Research IEK-1, Leo-Brandt-Str., 52425 Jülich (Germany)

**Abstract** - Lanthanum tungstate  $\text{La}_{28-x}\text{W}_{4+x}\text{O}_{54+d}\text{V}_{2-d}$  (LaWO) has attracted considerable attention in the recent years owing to its potential application as a membrane in  $\text{H}_2$  extraction and chemical processes involving for example  $\text{CO}_2$  utilization in a reaction with  $\text{H}_2$  to formation of biofuels or a number of other valuable chemicals. Due to its appreciable mixed conduction, which takes place by means of simultaneous bulk diffusion of protons ( $\text{H}^+$ ) and electrons ( $\text{e}^-$ ) in the crystal lattice, the material itself and the gas tight membrane made of it would act as a transport media for  $\text{H}_2$  having practically infinite  $\text{H}_2$  selectivity. The present work addresses complex interrelations of atomistic, crystallographic and (micro-)structural properties of pristine and partially substituted LaWO, its performance and manufacturing as supported 20  $\mu\text{m}$  thick gas tight membranes for  $\text{H}_2$  separation at elevated temperatures.

**Index Terms** – Ceramic membrane,  $\text{H}_2$  separation, Lanthanum tungstate  $\text{La}_{28-x}\text{W}_{4+x}\text{O}_{54+d}\text{V}_{2-d}$  (LaWO)

### I. INTRODUCTION

Hydrogen permeation ceramic membranes could be considered as an important element in reaching high energy conversion efficiency and decreasing the greenhouse gas emissions from power generation and energy-intensive industries, i.e. by capturing and utilizing  $\text{CO}_2$  or moving towards  $\text{H}_2$ -based systems by extracting pure  $\text{H}_2$  from gas mixtures. Therefore they may be of interest for integrated gasification process, and more specifically in water gas shift reactors to convert CO and steam to  $\text{CO}_2$  and  $\text{H}_2$  with subsequent extraction of  $\text{H}_2$ . Continuous removal of  $\text{H}_2$  during operation shifts the equilibrium further to the product side, which improves the hydrogen yield at elevated temperatures (600–900°C) [1]. Long term aim for industry relevant membrane application is a highly performing  $\text{H}_2$ -permeation ceramic membrane with competitive manufacturing cost and life time (> 3 years). The targeted value for the  $\text{H}_2$ -flux would be then 1-2  $\text{ml}/\text{cm}^2\cdot\text{min}$  and above. The industrial integration of

such membranes would lead to significant process intensification by (i) promoting reaction rate, (ii) maximizing product yield, (iii) saving energy and (iv) reducing final product cost thus gaining high environmental and economic impact value.

The definition of a material candidate suitable for certain membrane application addresses a number of issues as its performance, thermo-chemical/mechanical and phase stability, compatibility with other components, etc. and needs to realize an appreciable compromise between various material properties under relevant operating conditions.

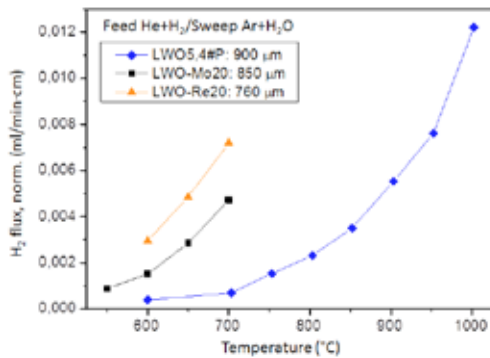
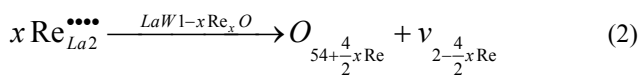
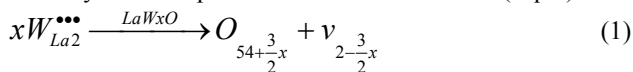
Lanthanum tungstates,  $\text{La}_{28-x}\text{W}_{4+x}\text{O}_{54+d}\text{V}_{2-d}$  (LaWO, where  $x=0.74-1.08$  and  $d=3x/2$ ), has attracted considerable attention in the recent years owing to its appreciable performance (in terms of  $\sigma_{\text{tot}}$  and  $j_{\text{H}_2}$ ) and stability both under “clean” humid ( $\text{H}_2/\text{CO}_2$ )- and Sulfur contaminated- atmospheres at elevated temperatures [2]. The present work will elucidate the fundamental understanding of the complex interrelation between structure, defect chemistry and performance of LaWO collected within the past few years (basic fund acknowledged) and the recent development steps targeting industrially relevant membrane components for  $\text{H}_2$  separation (Project ProtOMem acknowledged).

### II. LANTHANUM TUNGSTATES, $\text{La}_{28-x}\text{W}_{4+x}\text{O}_{54+d}\text{V}_{2-d}$ (LaWO)

LaWO can be nearly saturated with protons at  $T \leq 300^\circ\text{C}$  thus exhibiting predominant proton conductivity within the low temperature range, while its electronic conductivity becomes more pronounced in the high temperature range, where actually not much of the protons are left in the structure (based on thermodynamic restrictions). Therefore to enhance the ambipolar conductivity ( $\sigma_{\text{amb}}$ ) in the intermediate temperature range, partial substitution of 6-fold coordinated  $\text{W}^{6+}$  with cations similar in radius (e.g.  $\text{Mo}^{6+}$ ,  $\text{Re}^{7+}$ ) but exhibiting higher

reducibility has been aimed. The effect of substitution on the membrane performance can be clearly inferred from Fig. 1 [3].

Complex structural relations lead to convoluted chemistry and phase relation both in the pristine and substituted LaWO. Briefly, La/W ratio and the amounts of substituents (Mo or Re) play an important role into the overall defect chemistry and hydration properties of the material [4], hence affecting the final performance. W substitutes La on La2 crystallographic sites and by this it is responsible for the enhanced oxygen incorporation in the material, according to (Eq. 1). Partial substitution of W with Mo would exhibit similar behavior in terms of vacancies of oxygen, while the effect on hydration of Re substituted material would be by far more pronounced in accordance to (Eq. 2):



**Fig. 1. Temperature dependence of the  $j_{H_2}$  for pristine and substituted  $La_{28-x}W_{4+x}O_{54+d}V_{2-d}$**

### III. MANUFACTURING ASPECTS

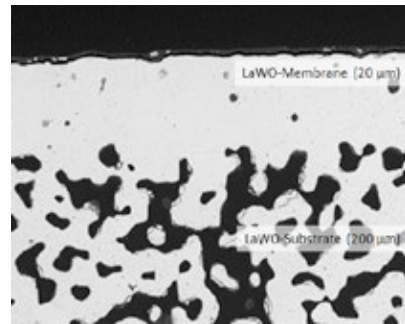
Apart from the fundamental material properties, membrane manufacturing aspects represent a significant challenge. As postulated by Wagner equation (Eq. 3),  $j_{H^+}$  depends proportionally on the temperature and the ambipolar transport of protons and electrons, and inversely proportionally on the

$$\text{membrane thickness, } L: j_{H^+} = \frac{-RT}{2F^2L} \int \sigma_{H^+} t_e d \ln p_{H_2} \quad (3)$$

Therefore decreasing the membrane thickness to several ten  $\mu\text{m}$  would be crucial for enhancing the overall membrane performance or boosting it at even lower operating temperatures. The fact that the membrane (thickness  $\approx 20\mu\text{m}$ ) is mechanically supported on a porous substrate layer (thickness  $\approx 200\text{--}500\mu\text{m}$ ) as shown in Fig. 2 makes the sintering of such asymmetric layered assemblies complex and their up-scaling to planar components of e.g.  $10 \times 10 \text{ cm}^2$  or tubular design even more challenging. The thermal and chemical compatibility play an important role for the selection of substrate material but also the production price and

reproducibility matter significantly. Therefore the sequential tape casting of ceramic layers is widely used by our group. Furthermore, the expensive LaWO substrate is replaced by a substrate made of  $\text{MgO}$ , which exhibits excellent chemical and thermal compatibility with LaWO.

In a case that tape cast and sintered stainless steel is used as a substrate, the overall manufacturing approach needs to be shifted to Plasma Spray-Physical Vapor Deposition (PS-PVD) and by this the high temperature sintering step (conventionally applied for ceramic material densification) can be dismissed. Independently on manufacturing route, He-leakage in the range of  $10^{-5} \text{ mbar}\cdot\text{l/s}$  needs to be achieved to consider the functional membrane layer as gas tight.



**Fig. 2. SEM image (polished cross section) of LaWO asymmetric membrane sintered at 1450 °C.**

### IV. CONCLUSION

This work elucidated multiple aspects of complex LaWO material behavior and manufacturing issues for its use as  $\text{H}_2$  extraction membrane.

### ACKNOWLEDGMENT

Financial support by the Helmholtz Association under the Research Programme *Energy Efficiency, Materials and Resources* and the fund from BMBF under ProtOMem Project, Grant Nr. 03SF0537A are greatly acknowledged. Our partners HZB, KIT, CSIC-UPV Spain, RWTH Aachen, MPI Stuttgart, and the division of Prof. Vaßen (FZJ/IEK-1) are appreciated for the fruitful collaboration on the LaWO thematic.

### REFERENCES

- [1] Deibert, W., Ivanova, M., et al., Ion-conducting ceramic MR for HT applications, *J. Mem. Sci.*, Vol. 543, 2017, Pages 79-97.
- [2] Seeger, J., Ivanova, M., et al., Synthesis and characterization of proton conducting  $\text{La}_{6-x}\text{WO}_{12-\delta}$ , *Inorg. Chem.*, Vol. 52, 2013, Pages 10375-10386.
- [3] Seeger, J., Development of proton conducting materials/membrane of LaWO for  $\text{H}_2$  separation, Diss., RUB, Germany, ISBN 978-3-89336-903-4.
- [4] Fantin, A., Scherb, T., et al., Relation between composition and vacant oxygen sites in the MIEC  $\text{La}_{5.4}\text{W}_{1-y}\text{M}_y\text{O}_{12-\delta}$  ( $\text{M} = \text{Mo, Re}$ ;  $0 \leq y \leq 0.2$ ) and  $\text{La}_{6-x}\text{WO}_{12-d}$  ( $0.4 \leq x \leq 0.8$ ), *Solid State Ionics*, Vol. 306, 2017, Pages 104–111.

## FCPOWERED RBS: A DEMONSTRATION PROJECT TO SUPPLY TELECOM STATIONS THROUGH FC TECHNOLOGY. DATA ANALYSIS OF REMOTE SITES AND SYSTEM OPTIMIZATION

L. Bartolucci\*, S. Cordiner\*, V. Mulone \*, G. Tomarchio\*\*

\* University of Rome Tor Vergata, via del Politecnico 1, 00133 Rome  
(Italy)

\*\* ERICSSON Italy, via Anagnina 203 00118 Rome (Italy)

**Abstract** – The previous works on the use of PEM Fuel Cell based power supply system for the operation of off-grid RBS (Radio Base Stations) sites showed a strong influence of system design parameters on the energy conversion performance. In this paper a perturbation of system design is performed through validated models to understand better the variability of performance over a full year operation.

**Index Terms** - PEM fuel cells; Alkaline electrolyzers; Radio base stations; Renewable sources; Off-grid Telecom Stations.

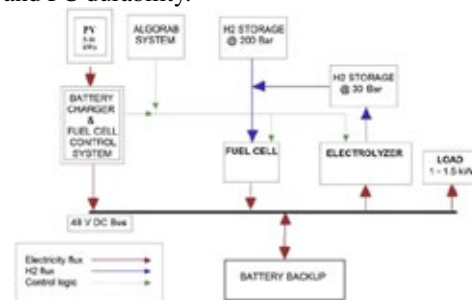
### I. INTRODUCTION

The FCpoweredRBS EU project was funded to demonstrate the potential of PEM Fuel Cells and H<sub>2</sub> electrolyzers coupled to PV modules and a BESS (Battery Energy Storage System) as a solution to supply power to off-grid Radio Base Stations (RBS) from renewable sources [1]. The project consisted of the design and realization of 13 operating telecom sites in Italy, which were tested since the beginning of 2015. Data analysis highlighted variable performances depending on the site and system design parameters. The aim of this work is to extend those considerations, studying the system performances in terms of non-dimensional indexes thus generalizing the validity of the outcomes of the project.

### II. SYSTEM DESCRIPTION

A brief description of the system layout (Figure 1) is here reported with specific regard to the site of Fiano Romano (more details and information on other sites are available in [2]). The hybrid system includes a PV module of 5 kW<sub>p</sub>, feeding a battery charger that is connected to a common 48V DC bus supplying power to the RBS load. In case of excess PV power, the energy can be stored in a battery pack or can power an electrolyzer up (that in turn fills up 30 bar H<sub>2</sub> bottles). Both batteries and electrolyzer are hooked-up in parallel to the DC bus. In case of a PV power lack, batteries or Fuel Cells (fueled by either 30 bar or

200 bar H<sub>2</sub> bottles) can supply power to the RBS load, thus ensuring its continuous operation. A rule-based control strategy has been defined [1] to maximize the renewable sources harvesting and FC durability.



**Fig. 1. FCpoweredRBS system layout [1]**

### III. NUMERICAL MODEL

A Matlab/Simulink code has been developed to represent the behavior of the HPS [3]. In this paper a perturbation of the BESS capacity and the PV peak power have been analyzed in the ranges respectively 320-960 Ah and 3.4-6.2 kW<sub>p</sub> to perform a sensitivity analysis.

In order to generalize the problem, non-dimensional parameters have been considered to analyze the performance of the system. The parameter  $I_{size}^{-1}$  [3] has been used to represent the dimensionless PV power output compared with the load request, while a  $BESS_{size}^{-1}$  dimensionless parameter can be further defined to take into account the battery capacity. The parameter is defined as:

$$BESS_{size}^{-1} = \frac{E_{BESS}}{E_{LOADDAY}^*}$$

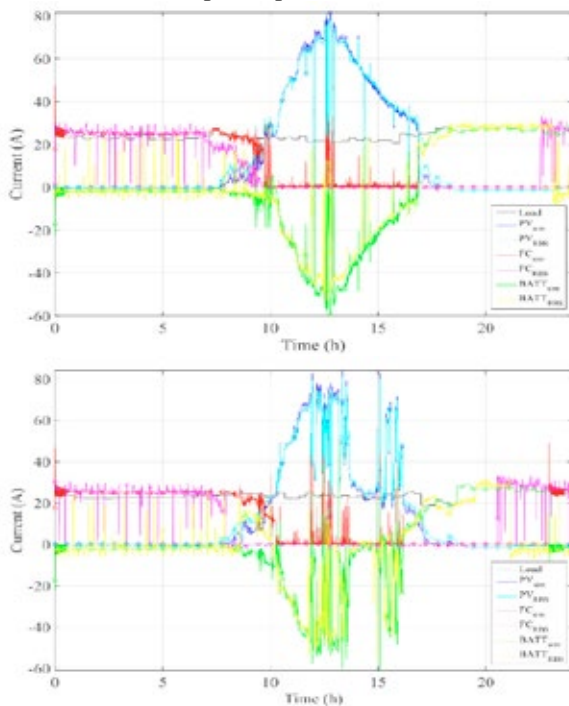
where  $E_{LOADDAY}^*$  is the mean energy consumption of the load over one day and  $E_{BESS}$  is the energy stored in the battery.



The performance parameters have been analyzed in terms of efficiency of the system  $\eta_{sys} = \frac{E_{LOAD}^*}{(E_{FES} + E_{RES}^*)}$  and ratio between the energy produced by fossil and renewables sources  $\frac{E_{FES}}{E_{RES}^*}$  as proposed in [3].

#### IV. DISCUSSION OF RESULTS

First, the numerical model has been validated against the real data collected at the Fiano Romano RBS site over the year 2015. In particular, two different representative days, respectively the best (Figure 2.A) and the worst (Figure 2.B) in September 2015 are reported in Figure 2 to show the excellent agreement between the simulated and real power profiles.



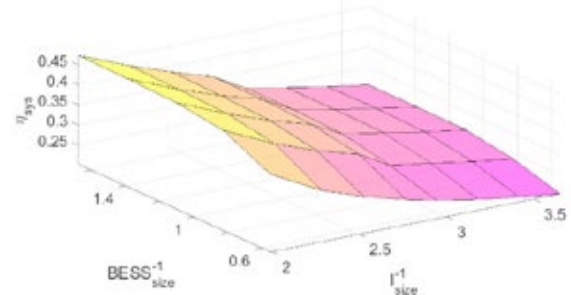
**Fig. 2. Current profile over time from different components and to the load – comparison between real and simulated data for two different cases (best day – A (top) and worst day – B (bottom)).**

The validation has also been performed over the full year confirming the excellent agreement also in terms of the total energy fluxes for the different subsystems, with small deviations within 4%.

Then the code has been used to perform a sensitivity analysis by varying sizing (design) parameters studying the behavior of the system over the full year.

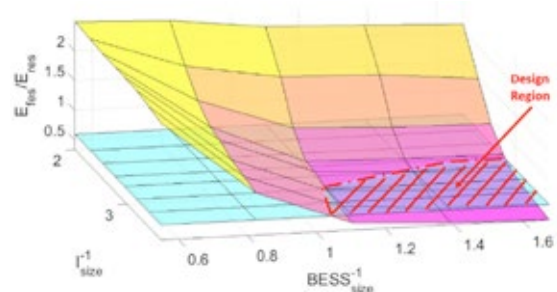
Looking at the system efficiency  $\eta_{sys}$  (Figure 3), two main effects appear worth noting: on one side the increase of the PV power output gives a reduction of the overall system efficiency due to the typically lower efficiency of the PV systems (in the range of 0.15-0.2) if compared to the PEM FC (in the range of 0.45-0.5). This means that the system is in general capable of using the extra energy produced in a quite linear fashion oversizing the PV

modules by increasing  $I_{size}^{-1}$ . This effect is also promoted by using a greater capacity BESS, as the hours of operation of the FC systems are reduced. The more evident reduction of  $\eta_{sys}$  at the lower end of  $BESS_{size}^{-1}$  depends on the other hand on the increased losses of renewable energy that is thus not shifted between the day and the night.



**Fig. 3. System efficiency as a function of design parameters.**

Figure 4 shows the effects of PV and BESS sizing on the ratio of the primary fossil energy and the renewable quota. It is worth noting that a plateau can be obtained moving towards designs characterized by larger designs, thus characterized by greater  $I_{size}^{-1}$  and  $B_{size}^{-1}$  confirming positive environmental effects, which decrease abruptly in the region characterized by smaller  $I_{size}^{-1}$  and  $B_{size}^{-1}$  couples. Therefore, once a fixed threshold for the environmental Efes/Eres index is given as a design constraint, a region of possible designs can be assigned. Within that region, the designs can be further characterized in terms of economical arguments (primarily system and operation costs), allowing for the choice of the optimal design in terms of dimensionless parameters.



**Fig. 4. Ratio between fossil and renewable sources as a function of design parameters.**

#### ACKNOWLEDGMENTS

This project is co-financed by funds from the european commission under FCH-JU, grant agreement number 278921.

#### REFERENCES

- [1] G. Bruni, S. Cordiner, V. Mulone et al., Int. J. Hydrogen Energy, 39(36):21767-21777, 2014.
- [2] S. Cordiner, V. Mulone, et al, Applied Energy, Volume 192, 2017, Pages 508-518, ISSN 0306-2619, <https://doi.org/10.1016/j.apenergy.2016.08.162>.
- [3] G. Bruni, S. Cordiner, V. Mulone, , Energy, 77:133-143, 2014.

## HIGH HYDROGEN PRODUCTION RATE ON RuS<sub>2</sub>/MoS<sub>2</sub> HYBRID NANOCATALYST DURING FLOW ELECTROLYSIS

M. Sarno\*\*\*, and E. Ponticorvo\*\*

\* Department of Industrial Engineering, University of Salerno, Via Giovanni Paolo II, 132, 84084, Fisciano (SA), (Italy)

\*\*NANO\_MATES, Research Centre for Nanomaterials and Nanotechnology at the University of Salerno, University of Salerno, Via Giovanni Paolo II, 132, 84084, Fisciano (SA), (Italy)

**Abstract** - Very small overpotential for hydrogen evolution were measured for our RuS<sub>2</sub>/MoS<sub>2</sub> hybrid nanocatalyst, prepared using a scalable approach, and consisting of RuS<sub>2</sub> nanoparticles grown directly on active MoS<sub>2</sub> nanosheets. The nanometric size of the nanoparticles, the dispersion on a electroactive and stable support, the electrical coupling between MoS<sub>2</sub> active layers and RuS<sub>2</sub> nanoparticles are the key aspects to determine the nanohybrid performance, this results in a very high hydrogen production rate, measured by means of an on-line mass spectrometry analysis.

**Index Terms** – flow electrolysis, low overpotential, on-line analysis, RuS<sub>2</sub>/MoS<sub>2</sub> nanohybrid.

### I. INTRODUCTION

Hydrogen is the cleanest energy carrier, increasingly considered as the future fuel, as well as the best alternative to fossil fuel. Water electrolysis for hydrogen production has many advantages, such as: high purity, simple process and no pollution. Industrial water electrolysis, usually carried out using a liquid alkaline electrolyte and Ni as active catalyst, is characterized by low production rates and efficiency, high energy consumption and voluminous systems. The acidic process could represent an alternative, but, due to corrosion issues, requires costly noble metals (Pt, Ir, Ru). Therefore, there is a major need to develop new active and cheap electrocatalysts for water splitting, which would offer low overpotentials for the hydrogen evolution in acidic media. Moreover, transition metal dichalcogenides have recently emerged as a promising class of materials for electrocatalysis. In this regards, MoS<sub>2</sub> nanostructures were successfully tested as catalysts for Hydrogen Evolution Reaction (HER) in acidic solution [1]. It has been forecasted an excellent electrocatalytic activity, linearly dependent by the number of edge sites, for

nano MoS<sub>2</sub> [2]. Ruthenium based materials are widely used for their exceptional electrochemical properties [3]. Different ruthenium based materials such as ruthenium complexes, metallic Ru, hydrous RuO<sub>2</sub>, amorphous RuO<sub>2</sub>, and crystalline RuO<sub>2</sub> were examined for various electrochemical applications such as electrochemical sensors, electrocatalysis, supercapacitors, and batteries [3]. However, at the best of our knowledge, nanomaterials combining the promising properties of RuS<sub>2</sub> stabilized by a MoS<sub>2</sub> nanosheets coating have been never reported for HER. It is worth noting that HER has been object of intense research activity and a lot of paper have been published, reporting in some cases fascinating results. On the other hand, this is now the time to evaluate the electrochemical properties in conditions as much as possible similar to the real cells. In this paper, we report the preparation and characterization of a new nanocatalyst, based on RuS<sub>2</sub> nanoparticles covered by MoS<sub>2</sub> nanosheets, that it is able to deliver very high exchanged current density during hydrogen production, with a small Tafel slope and overpotential. The nanocatalysts have been tested in a continuous flow system to evaluate the electrochemical properties forecasting excellent and improved electrocatalytic activity, and monitored by on-line analysis.

### II. EXPERIMENTAL SECTION

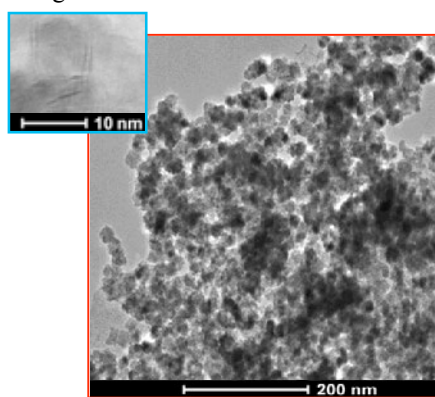
A one-step synthetic strategy [4] for the preparation of RuS<sub>2</sub>/MoS<sub>2</sub> hybrid nanocatalyst was performed by thermolysis of suitable precursors in organic solvent. To reduce the organic chains amount covering the nanoparticles, RuS<sub>2</sub>/MoS<sub>2</sub> annealed was obtained after a thermal treatment of the synthesized samples under an air flow. A wide characterization of our nanostructures, before and after the thermal treatment was

Copyright © 2017

performed. The samples were widely characterized through the combined use of different techniques: Raman spectroscopy, transmission electron microscopy (TEM), thermogravimetric analysis, x-ray diffraction (XRD) and x-ray photoelectron spectroscopy (XPS) analyses, and the HER activities were evaluated through the analysis of the Tafel plots. Long-time stability tests were also performed. HER activity was also evaluated in a continuous flow system. Additionally, hydrogen production rate was evaluated by means of an on-line mass spectrometry analysis, to confirm the results with an analytical hydrogen production valuation.

### III. RESULTS AND DISCUSSIONS

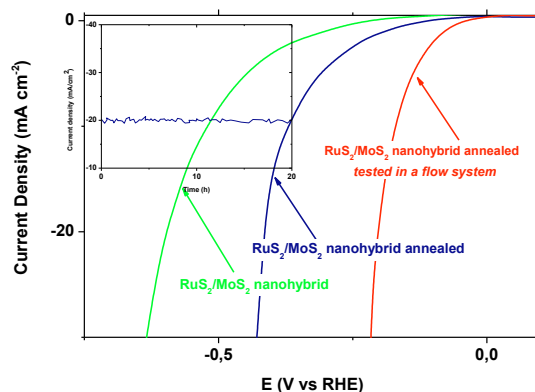
XRD and XPS analyses confirm the RuS<sub>2</sub> NPs covered by MoS<sub>2</sub> nanosheets. The TEM images (Fig.1) of RuS<sub>2</sub>/MoS<sub>2</sub> shows a lot of RuS<sub>2</sub> nanoparticles, 10-15 nm in size, covered by MoS<sub>2</sub> having a lateral size of few nanometres.



**Fig. 1. TEM images of RuS<sub>2</sub>/MoS<sub>2</sub> hybrid nanocatalyst**

We investigated the electrocatalytic HER activities of our nanomaterials deposited on a glassy carbon electrode in 0.5 M H<sub>2</sub>SO<sub>4</sub> solutions using a typical three-electrode setup and also in a continuous flow system. Polarization curves after IR-correction (i-V plot) were reported in Fig.2. RuS<sub>2</sub>/MoS<sub>2</sub> hybrid nanocatalyst annealed HER activities result excellent, they show a small overpotential for HER, beyond which the cathodic current rose rapidly under more negative potentials. Tafel slope values were calculated suggesting that HER proceed through the Volmer-Heyrovsky mechanism. Thanks to the H<sub>2</sub> and O<sub>2</sub> bubble separation on the catalyst surface, enhanced electrochemical properties were found in the same operating conditions but the continuous motion of the electrolyte. An important parameter for a HER promising material consists in its durability. The long-term stability of RuS<sub>2</sub>/MoS<sub>2</sub> hybrid nanocatalyst annealed at -0.20 V vs. RHE in 0.5 M H<sub>2</sub>SO<sub>4</sub> is shown in Fig.2 insert. At this voltage, the electrode showed a cathodic current density around 20 mA/cm<sup>2</sup> for 20 h. This nanohybrid presents an high hydrogen production rate, normalized by electrode area. The amount of hydrogen quantified (each 10 minutes) by mass spectrometer analysis

during HER matches well with the values calculated taking into account the number of charges through the electrode, indicating high hydrogen production efficiency (nearly 100%) for RuS<sub>2</sub>/MoS<sub>2</sub> hybrid nanocatalyst annealed and confirming its high electrocatalytic activity.



**Fig. 2. RuS<sub>2</sub>/MoS<sub>2</sub> hybrid nanocatalyst polarization curves at 20 mV/sec before and after the thermal treatment; in the insert, current density time dependence at -0.2 V vs. RHE in a flow system.**

### IV. CONCLUSION

A simple approach has been proposed to synthesize RuS<sub>2</sub> nanoparticles covered by MoS<sub>2</sub> nanosheets exposing large number of edge. The nanometric size of the nanoparticles, the electrical coupling between MoS<sub>2</sub> active layers and RuS<sub>2</sub> nanoparticles are the key aspects to determine the nanohybrid performance. Based on the results obtained with several electrochemical characterizations, also in a continuous flow system, emerged that the RuS<sub>2</sub>/MoS<sub>2</sub> nanohybrid is a promising electrocatalyst for hydrogen generation from water. Additionally, and this is not typically reported in the literature, hydrogen production rate was determined and theoretical efficiency of about 100% evaluated.

### REFERENCES

- [1] Sarno, M., Ponticorvo, E., Effect of the amount of nickel sulphide, molybdenum disulphide and carbon nanosupport on a Tafel slope and overpotential optimization, *Nanotechnology*, Volume 28, 2017, Pages 214003 (8pp).
- [2] Jaramillo, T.F., Jørgensen, K.P., Bonde, J., Nielsen, J.H., Horch, S., Chorkendorff, I., Identification of active edge sites for electrochemical H<sub>2</sub> evolution from MoS<sub>2</sub> nanocatalysts, *Science*, Volume 317, 2007, pp. 100-102.
- [3] Krishnamoorthy, K., Pazhamalai, P., Kim, S.J., Ruthenium sulfide nanoparticles as a new pseudocapacitive material for supercapacitor, *Electrochimica Acta*, Volume 227, 2017, pp. 85-94.
- [4] Sarno, M., Ponticorvo, E., Cirillo, C., High surface area monodispersed Fe<sub>3</sub>O<sub>4</sub> nanoparticles alone and on physical exfoliated graphite for improved supercapacitors, *Journal of Physics and Chemistry of Solids*, Volume 99, 2016, pp. 138-147.

## PtRu/MoS<sub>2</sub> NANOCOMPOSITE AS PROMISING ELECTROCATALYST IN THE METHANOL OXIDATION REACTION

M. Sarno\*\*\*, E. Ponticorvo\*\*, and C. Cirillo\*

\* *Department of Industrial Engineering*

\*\* *NANO\_MATES Research Centre,*

*University of Salerno, via Giovanni Paolo II, 132 -  
84084 Fisciano (SA), Italy*

**Abstract** – A new nanocatalyst, consisting of platinum, ruthenium and molybdenum sulphide (PtRuMoS<sub>2</sub>), was synthesized through an one-step bottom-up approach. Electrocatalytic activity toward MOR was evaluated, yielding very promising results for the use of such nanostructured material as a catalyst for an electrochemical reformer with methanol.

**Index Terms** – Electrocatalyst, Methanol Oxidation Reaction (MOR), PtRu/MoS<sub>2</sub> nanocomposite.

### I. INTRODUCTION

The use of hydrogen (H<sub>2</sub>) as an alternative energy carrier can reduce many environmental alarms related to the fossil fuels combustion [1].

However, same concerns such as: production, distribution, compression, limit the adoption of H<sub>2</sub> on a large-scale. High energy density liquid alcohols, stored and distributed through existing liquid fuel infrastructures, could be used as a bridge between gasoline and gaseous H<sub>2</sub> [2]. Methanol, in particular, is an available alcohol, which can be produced from non-renewable sources (coal, natural gas) and from renewable resources (biomass). Methanol can be used in direct methanol fuel cells (DMFCs), or converted into hydrogen by thermal or electrochemical reforming to feed powerful fuel cells (PEFCs). Although thermal reforming is a very well-established technology, it has a number of drawback, such as: weight, vibrational resistance, product purity, high operating temperatures. The methanol oxidation reaction (MOR), operating at low temperature and producing high purity H<sub>2</sub>, at much cheaper cost than water electrolysis. Moreover, Pt electrocatalysts have several serious disadvantages such as high-cost, tendency to agglomerate, and poor CO tolerance. To overcome these problems, research effort has been devoted to synthesize nanosized Pt, Pt-metal alloys and nanoparticles supported electrocatalysts [3]. Among these approaches, metals supports owing to their excellent electrocatalytic stability, CO tolerance, and physicochemical properties, has been used [4]. More importantly, high surface-area supports are beneficial for

the dispersion of Pt electrocatalysts and improved electrocatalytic activity [4]. On the other hand, MoS<sub>2</sub>, as a graphene analogue, has attracted increasing interest in sensors, catalysis, capacitors, lithium batteries and energy harvesting due to its novel nanoelectronic and optoelectronic properties [5]. Like graphene, MoS<sub>2</sub> nanosheets are also considered as a promising supporting material to stabilize metal nanoparticles, forming hierarchical nanocomposites.

Here, we report a one-step synthetic strategy for the preparation of PtRu/MoS<sub>2</sub> nanocomposite obtained by thermolysis of suitable precursors in organic solvent. Based on the obtained results, PtRu/MoS<sub>2</sub> nanocomposite acts as promising electrocatalyst for the methanol oxidation reaction.

### II. EXPERIMENTAL SECTION

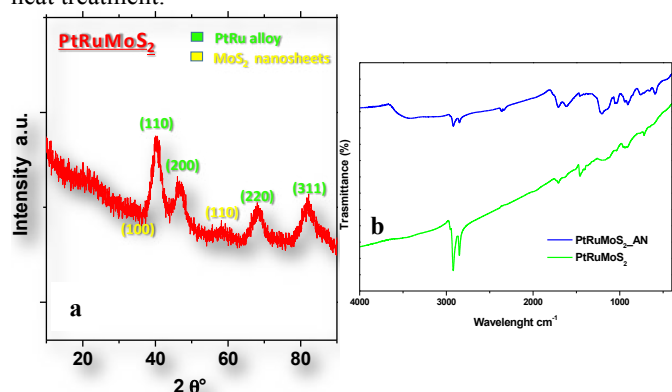
The synthesis of PtRu/MoS<sub>2</sub> nanocomposite was performed by an one-step bottom-up chemical strategy using standard airless procedures [6]. In particular, Pt(acac)<sub>2</sub> (0.1 mmol), ammonium tetrathiomolybdate ((NH<sub>4</sub>)<sub>2</sub>MoS<sub>4</sub>, 2 mmol), Ru(acac)<sub>3</sub> (0.7 mmol), 1,2-hexadecanediol (10 mmol), oleic acid (6 mmol), oleylamine (6 mmol), 1-octadecene (20 mL) were mixed and magnetically stirred under nitrogen flow. The mixture was heated to 200 °C for 120 min and, successively, further heated to reflux (285 °C) for 60 min. The obtained mixture was washed, three time, using isopropanol and hexane, in volume ratio 2:1, precipitated and separated via centrifugation. The obtained product was dissolved in hexane.

To reduce the organic chains amount, the sample was annealed in air flow at 150 °C for 8h [6], in the following PtRuMoS<sub>2</sub>\_AN. A comprehensive characterization of our nanocomposites, before and after annealing, using Raman Spectroscopy, Transmission Electron Microscopy (TEM), Thermogravimetric analysis (TG-DTG) and X-ray diffraction (XRD), Fourier Transformed Infrared spectroscopy (FT-IR) was performed. All electrochemical measurements were performed using a potentiostat Autolab 302N connected to a screen-printed electrode (SPE).



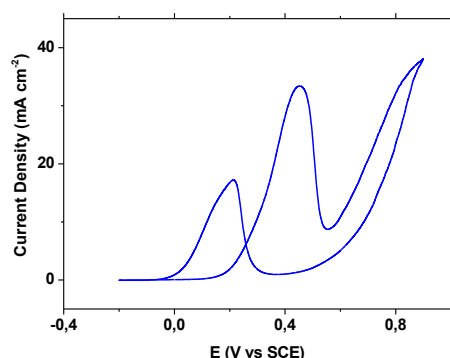
### III. RESULTS AND DISCUSSION

In Fig. 1a, the XRD profile of the synthesized PtRuMoS<sub>2</sub> is shown. The spectrum shows the reflection characteristics of the Pt fcc structure, suggesting an alloy formation based on the substitution of the Pt lattice sites [7]. It is possible, also, to assign the reflection peaks of lattices planes (100) and (110) due to MoS<sub>2</sub> [8]. In order to understand the interaction of the organic chains with the surface of the nanoparticles, FT-IR spectra were acquired. In Fig. 1b, it is possible to observe the FT-IR spectra of PtRuMoS<sub>2</sub> before (green line) and after (blue line) annealing. The PtRuMoS<sub>2</sub> sample shows, in the 1450-1649 cm<sup>-1</sup> region, the peaks associated with asymmetric  $\nu_{as}(\text{COO}^-)$  and symmetric  $\nu_s(\text{COO}^-)$  stretches, while the presence of the oleic group  $\nu(\text{C}=\text{C})$  is confirmed by the characteristic peaks of the oleic group in the 2750-3000 cm<sup>-1</sup> region [6]. The PtRuMoS<sub>2</sub> after annealing (PtRuMoS<sub>2</sub>\_AN) spectrum clearly highlights the reduction of the bands intensity due to the organic chains indicating their decrease after the heat treatment.



**Fig. 1. PtRuMoS<sub>2</sub> XRD spectrum (a), FT-IR spectra also after annealing (b).**

The catalytic activity toward the oxidation of methanol was estimated by CV tests in 0.5 M H<sub>2</sub>SO<sub>4</sub> solution containing 2 M methanol. The forward anodic peak current density (J<sub>f</sub>) for PtRuMoS<sub>2</sub>\_AN (33.4 mA cm<sup>-2</sup>) (Fig. 2) is considerably larger



**Fig. 2. Cyclic voltammogram of PtRuMoS<sub>2</sub>\_AN.** than that exhibited by commercial Pt/C electrode [9].

The tolerance of catalysts to the accumulation of

carbonaceous species is estimated by the ratio J<sub>f</sub>/J<sub>b</sub> where J<sub>b</sub> is the backward peak current densities. A J<sub>f</sub>/J<sub>b</sub> ratio increase indicates that more methanol is converted to carbon dioxide and that more poisoning species are removed from the catalysts. The J<sub>f</sub>/J<sub>b</sub> values measured for PtRuMoS<sub>2</sub>\_AN is 1.94, indicating excellent anti-poison properties.

### IV. CONCLUSION

PtRuMoS<sub>2</sub> nanocatalyst was synthesized through a one-step approach. Electrocatalytic activity toward MOR was evaluated, yielding very promising results for the use of such nanostructured material as catalyst for methanol electrochemical reforming.

### REFERENCES

- [1] Hart, D., Hydrogen – a truly sustainable transport fuel?, *Frontiers in Ecology and the Environment*, Volume 1, 2003, pp 138-145.
- [2] Lamy, C., Leger, J.M., Srinivasan, S., Direct methanol fuel cells: from a twentieth century electrochemist's dream to a twenty-first century emerging technology. In: Bockris John O'M, Conway BE, White RE, editors, *Modern aspects of electrochemistry*, New York, NY: Kluwer Academic Publishers, Volume 34, 2001, pp. 53-117.
- [3] Li, X., Faghri, A., Review and advances of direct methanol fuel cells (DMFCs) part I: design, fabrication, and testing with high concentration methanol solutions, *Journal of Power Sources*, Volume 226, 2013, pp. 223-240.
- [4] Yu, S., Liu, Q., Yang, W., Han, K., Wang, Z., Zhu, H., Graphene-CeO<sub>2</sub> hybrid support for Pt nanoparticles as potential electrocatalyst for direct methanol fuel cells, *Electrochimica Acta*, Volume 94, 2013, pp. 245-251.
- [5] Su, S., Zou, M., Zhao, H., Yuan, C., Zhang, C., Wang, L., Fan, C., Wang, L., Shape-controlled gold nanoparticles supported on MoS<sub>2</sub> nanosheets: synergistic effect of thionine and MoS<sub>2</sub> and their application for electrochemical label-free immunosensing, *Nanoscale*, Volume 7, 2015, pp. 19129-19135.
- [6] Sarno, M., Ponticorvo, E., Cirillo, C., High surface area monodispersed Fe<sub>3</sub>O<sub>4</sub> nanoparticles alone and on physical exfoliated graphite for improved supercapacitors, *Journal of Physics and Chemistry of Solids*, Volume 99, 2016, pp. 138-147.
- [7] Antolini, E., Giorgi, L., Cardellini, F., Passalacqua, E., Physical and morphological characteristics and electrochemical behaviour in PEM fuel cells of PtRu/C catalysts, *Journal of Solid State Electrochemistry*, Volume 5, 2001, pp. 131-140.
- [8] Sarno, M., Troisi, A., Supercapacitors Based on High Surface Area MoS<sub>2</sub> and MoS<sub>2</sub>-Fe<sub>3</sub>O<sub>4</sub> Nanostructures Supported on Physical Exfoliated Graphite, *Journal of Nanoscience and Nanotechnology*, Volume 17, 2017, pp. 3735-3743.
- [9] Roychowdhury, C., Matsumoto, F., Zeldovich, V.B., Warren, S.C., Mutolo, P.F., Ballesteros, M.J., Wiesner, U., Abruna, H.D., DiSalvo, F.J., Synthesis, Characterization, and Electrocatalytic Activity of PtBi and PtPb Nanoparticles Prepared by Borohydride Reduction in Methanol, *Chemistry of Materials*, Volume 18, 2006, pp. 3365-3372.



**PdPt\_GRAPHENE NANOCOMPOSITE FOR PROTON EXCHANGE MEMBRANE  
FUEL CELL**

M. Sarno\*\*\*, E. Ponticorvo\*\*, and C. Cirillo\*

\* *Department of Industrial Engineering*

\*\* *NANO\_MATES Research Centre,*

*University of Salerno, via Giovanni Paolo II, 132 -  
84084 Fisciano (SA), Italy*

**Abstract** - A promising nanocatalyst, consisting of platinum and palladium alloy NPs grown directly on the graphene surface, for ORR, was successfully synthesized through an one-step bottom-up approach. The obtained nanocatalyst showed excellent performance and the cyclic voltammetry study showed very stable performance over 1000 cycles. The activity of PdPt\_graphene nanocomposite was also investigated in a real Proton Exchange Membrane Fuel Cells showing very encouraging results.

**Index Terms** – Electrocatalysis, Energy conversion, Fuel cells, Graphene, Oxygen reduction reaction (ORR), PdPt alloy.

I. INTRODUCTION

Fuel cell reactions [1] including hydrogen oxidation reaction (HOR) and oxygen reduction reaction (ORR) have been extensively investigated for Proton Exchange Membrane Fuel Cells (PEMFCs). Highly stable and active Pt-based electrocatalysts are the best catalysts for these two reactions. The high price and low abundance of Pt have encouraged the search for alternative materials with lower cost and similar performance. Major attention has been devoted to the more cheaper Pd-based catalysts [2], since it is one of the Pt-group metals with good HOR and ORR activities [3]. In order to design new nanocatalysts a route was to disperse catalytic metal nanoparticles on conductive carbon nanomaterials (e.g. graphene, activated carbon, carbon nanotubes, reduced graphene oxide,...) [4-6]. This approach allows to avoid nanoparticles aggregation, increase stability and improve the performance of the electrocatalysts. The preparation of graphene based nanoparticles composite reduces also the graphene tendency to aggregation and restacking, enhancing exploitation of its peculiarities.

Here, we report a one-step simple synthetic strategy for the preparation of a multifunctional nanostructures made of graphene supporting PdPt alloy nanoparticles (PdPt\_graphene). Particular attention has devoted to search for a low noble metal content. They are characterized by very small (~ 1 nm) platinum and palladium alloy nanoparticles (NPs) grown directly on the graphene surface, to take advantages of the

synergistic effect of the different components. Catalyst activities, according to rotating disk electrode (RDE) evaluations, have been analyzed on the PdPt\_graphene nanocomposite. On the other hand, there is an urgent need to validate the electrocatalysts ORR performance in a real fuel cell. For this reason the activity of PdPt\_graphene nanocomposite was also investigated in a PEMFC.

II. EXPERIMENTAL SECTION

The synthesis of PdPt\_graphene nanocomposite was performed by an one-step bottom-up chemical strategy using standard airless procedures [7]. Graphene was obtained by a sonication of graphite in N-methylpyrrolidone at a concentration of 10 mg/ml for 1 h at the maximum power of ultrasound [8].

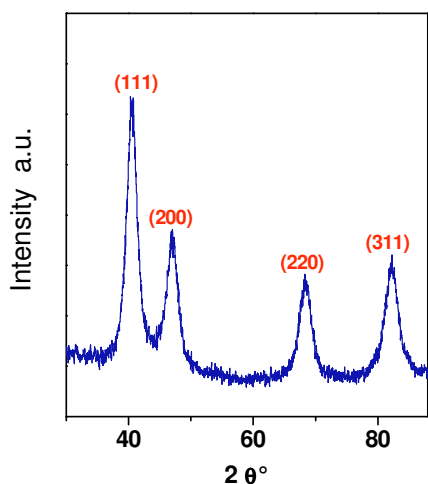
A comprehensive characterization of our nanocomposite, using Raman Spectroscopy, Transmission Electron Microscopy (TEM), Thermogravimetric analysis (TG-DTG) and X-ray diffraction (XRD), Fourier Transformed Infrared spectroscopy (FT-IR) was performed. The catalysts were tested using a conventional three electrode cell, consisting of RDE as a working electrode, a Pt wire as a counter electrode, and a saturated calomel as reference electrode (SCE). Additionally, activity of PdPt\_graphene was investigated in a fuel cell. In particular RDE experiments were carried out in 0.5 M H<sub>2</sub>SO<sub>4</sub>. To determine the activity of the catalyst, linear sweep voltammetry (LSV) was applied from 1 to 0.2 V with a scan rate of 5 mV s<sup>-1</sup> in saturated oxygen at various rpm.

In order to evaluate the performance stability/durability of the nanocomposite, cyclic voltammetry (CV) was conducted for the disk electrodes between 1 and 0.4 V with a sweep rate of 50 mVs<sup>-1</sup> for 1000 cycles. For PEMFCs tests, a membrane electrode assembly (MEA) with an active area of 25.0 cm<sup>2</sup> was fabricated. Commercial Pt/C and the PdPt\_graphene nanocomposite were used as anode and cathode catalysts, respectively. The MEA was fabricated sandwiching the membrane with the gas diffusion layers on both sides using appropriate gaskets.

Copyright © 2017

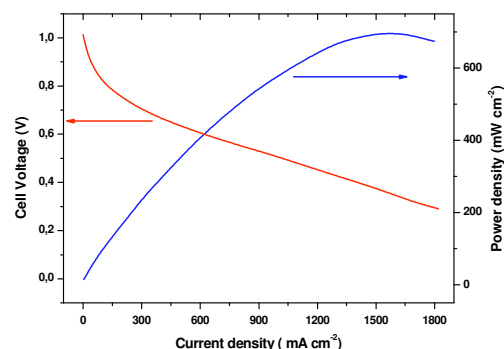
### III. RESULTS AND DISCUSSION

Fig.1 shows the diffraction pattern recorded on the reaction product, after a suitable washing, the pattern has been obtained by subtracting the typical profile of graphene. The X ray diffraction for the alloy nanocatalyst can be indexed to (111), (200), (220) and (311) diffraction peaks of the fcc structure; the peak positions of these planes are slightly different from those of the pure Pt and Pd alone. The PdPt\_graphene composition was analyzed by Energy Dispersive Spectroscopy (EDS) founding the atomic ratio Pt:Pd = 46:54.



**Fig. 1. XRD spectrum of PdPt.**

The durability of the catalyst, that is one of the major concerns in the development of an efficient cathode catalysts for fuel cells, has been investigated in a RDE test. The obtained CV curves (not shown here) compare the initial and 1000 cycles for the PdPt\_graphene cathode in O<sub>2</sub> saturated electrolyte at 800 rpm, showing no significant change in the catalytic efficiency of the catalyst toward the ORR. We found only 2.4% loss of the initial electrochemically accessible surface area (ECSA) and a slight negative shift in the half-wave potential indicating a negligible dissolution of the nanoparticles during potential cycles. Fig.2 shows the PEM fuel cell performance of the MEA with PdPt\_graphene cathode and commercial Pt/C anode catalysts using Nafion-117 membrane and H<sub>2</sub> and O<sub>2</sub> gases. Further tests will be carried out with thinner Nafion membranes. This cell gave a maximum power density of ~700 mW/cm<sup>2</sup> at a cell voltage of 0.35 V and a current density of ~1600 mA/cm<sup>2</sup>. The polarization voltage drop of the PdPt\_graphene cathode was slightly smaller than commercial Pt/C [9]. On the other hand the transport of reactant and products occurs readily from active sites thanks to the fast pathway due to the network structure of the PdPt\_graphene cathode, without mass transport limitation. Although, the technology of electrode preparation and assembly, catalyst loading efficiency, testing environment have pronounced effect on the cell performances, interesting results were obtained.



**Fig. 2. Polarization and power density plot of the PEMFC.**

### IV. CONCLUSION

Very small platinum and palladium alloy NPs grown directly on the graphene surface were synthesized by one-step simple approach. Electrocatalytic activity toward ORR was evaluated. The nanocatalyst showed excellent performance and the CV study showed very stable performance over 1000 cycles. Although there are numerous reports of new ORR catalysts only a few of these studies have investigated the performance of the catalyst in a real H<sub>2</sub>, O<sub>2</sub> fuel cell. For this reason the activity of PdPt\_graphene nanocomposite was also investigated in a PEMFC showing very encouraging results (power density peak of ~ 700 mW cm<sup>-2</sup>).

### REFERENCES

- [1] Debe, M.K., Electrocatalyst approaches and challenges for automotive fuel cells, *Nature*, Volume 486, 2012, pp. 43-51.
- [2] <<www.platinum.matthey.com/prices>>
- [3] Alia, S.M., Yan, Y., Palladium Coated Copper Nanowires as a Hydrogen Oxidation Electrocatalyst in Base, *Journal of The Electrochemical Society*, Volume 162, 2015, pp. F849-F853.
- [4] Takenaka, S., Miyamoto, H., Utsunomiya, Y., Matsune, H., Kishida, M., Catalytic Activity of Highly Durable Pt/CNT Catalysts Covered with Hydrophobic Silica Layers for the Oxygen Reduction Reaction in PEFCs, *Journal of Physical Chemistry C*, Volume 118, 2014, pp. 774-783.
- [5] Salernitano, E., Giorgi, L., Makris, T.D., Direct growth of carbon nanofibers on carbon-based substrates as integrated gas diffusion and catalyst layer for polymer electrolyte fuel cells, *International Journal of Hydrogen Energy*, Volume 39, 2014, pp. 15005-15016.
- [7] Park, J.E., Jang, Y.J., Kim, Y.J., Song, M.S., Yoon, S., Kim, D.H., Kim, S.J., Sulfur-doped graphene as a potential alternative metal-free electrocatalyst and Pt-catalyst supporting material for oxygen reduction reaction, *Physical Chemistry Chemical Physics*, Volume 16, 2014, pp. 103-109.
- [8] Guadagno, L., Sarno, M., Vietri, U., Raimondo, M., Cirillo, C., Ciambelli, P., Graphene-based structural adhesive to enhance adhesion performance, *RSC Advances*, Volume 5, 2015, pp. 27874-27886.
- [9] Yun, Y.S., Kim, D., Tak, Y., Jin, H.J., Porous graphene/carbon nanotube composite cathode for proton exchange membrane fuel cell, *Synthetic Metals*, Volume 161, 2011, pp. 2460-2465.

(EFC17228)

## INVESTIGATION OF THE SURFACE REACTIVITY OF INCONEL 625 PREPARED BY ADDITIVE MANUFACTURING

N.Ramenatte\*, L. Aranda\*, S.Mathieu\*, and M.Vilasi \*

\*Institut Jean Lamour-UMR 7198, University of Lorraine, (France)

**Abstract** - The project FAIR intends to develop a novel class of microreactor-exchanger (MR-E) based on 3D printing manufacture in order to intensify the H<sub>2</sub> synthesis process. The Ni-based superalloy Inco 625 was selected as substrate because it present appropriate high temperature mechanical and chemical properties. It can resist against Metal Dusting corrosion provided it is protected by an aluminum reach overlay. The present study allowed characterizing the physico-chemical properties of 3D printed alloys (SLM) compared to conventional melted alloys (CMA). SLM alloys have a heterogeneous microstructure, a higher sensivity to oxidation but no significant difference of Ni and Al interdiffusion compared to CMA. The parameters of the SLM and of the Aluminum deposition processes were optimized. Innovative MR-E were build and tested during a high pressure test: SML MR-E resist at more than 2400 bars without failure contrary to welded MR-E which failed at 800 bars by delamination of welded plates.

**Index Terms** - Additive manufacturing, functional coating, nickel-based superalloy, surface reactivity

### I. INTRODUCTION

The project FAIR (Additive Manufacturing for the Intensification of Reactors) aims at developing a new intensified H<sub>2</sub> synthesis process by microstructuration of metallic reactor-exchanger which would be used for Steam Methane Reforming. The device building takes advantage of the recent metallurgical progress concerning the 3D printing manufacture for creating innovative reactor-exchanger more robust and capable to withstand higher temperature and pressure during application. The success of this project will participate to the development of the "H<sub>2</sub> mobility" in France.

### II. EXTENDED ABSTRACT

The alloy Inco 625 was chosen for building the reactor-exchanger because it presents adequate mechanical properties

when classically synthesized using a melting process followed by conventional heat treatments (dissolution during 1h at 1070°C – precipitation of  $\gamma'$  during 8h at 720°C - precipitation of  $\gamma''$  during 8h at 620°C)\*. The as-obtained substrate has the following composition Ni<sub>22</sub>Cr<sub>9</sub>Mo<sub>4</sub>Nb<sub>5</sub>Fe (values are wt%) and a homogeneous  $\gamma/(\gamma'+\gamma''+\delta)$  equiaxe microstructure [1]. In oxidizing atmosphere, typically 1000°C in air, this alloy has a satisfying behavior due the formation of a superficial protective chromia scale.

#### A. Synthesis of Inco 625 via the innovative Selective Laser Melting route (SLM)

This process was conducting using the following main (non-confidential) parameters: alloy powder with a 10  $\mu$ m diameter grain size, melting under Ar atmosphere (P=1bar) and cooling at 10<sup>7</sup> K/s.

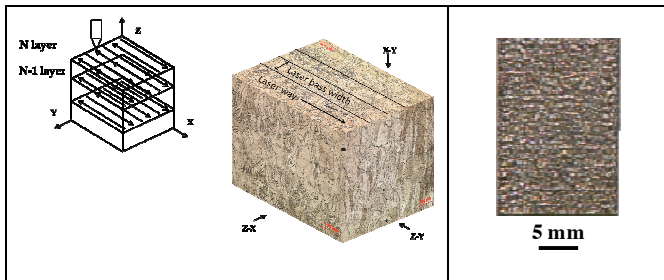
The as-obtained substrates are constituted of supersaturated  $\gamma$  grain having the nominal composition of Inco 625 and a textured microstructure showing a grain elongation parallel to the direction of growth (fig. 1).

The materials elaborated by SLM present high superficial roughness, related to the occurrence of fine spherical particles just sealed on the surface (Fig. 2).

The desired mechanical properties are then recovered by applying a heat treatment performed in the conventional conditions\*.

#### B. Oxidation behavior at 1000°C under air atmosphere

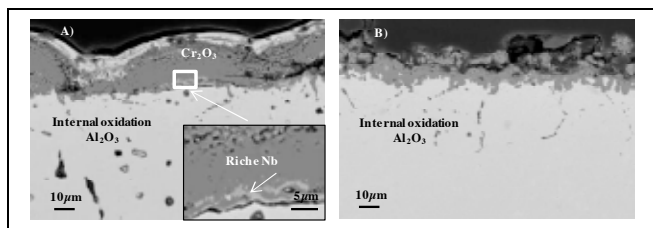
Classical isothermal thermogravimetric tests were carried out on both SLM and conventional melted alloys (CMA) during 50 hours.



**Fig. 1.** Microstructure of Inco 625 SLM with textured grain structure

**Fig. 2.** Surface morphology of the Inco 625 SLM

The mass gain of the as-printed SLM sample is high (2.2 mg/cm<sup>2</sup>) compared to CMA (1.2 mg/cm<sup>2</sup>) and the superficial Cr<sub>2</sub>O<sub>3</sub> layer is not adherent and inhomogeneous regarding its thickness (Fig. 3).



**Fig. 3.** Microstructure after oxidation heat treatment of A) SLM sample, B) CMA sample.

A primary conclusion is **the crude 3D-printed alloy has a higher sensivity to oxidation than CMA**.

Nonetheless, the behavior of both alloys is not suitable for the forecasted application, namely the SMR process. As a result, protective overlays were deposited after being optimized for the SML substrate.

### C. Coating depositions by CVD and slurry processes

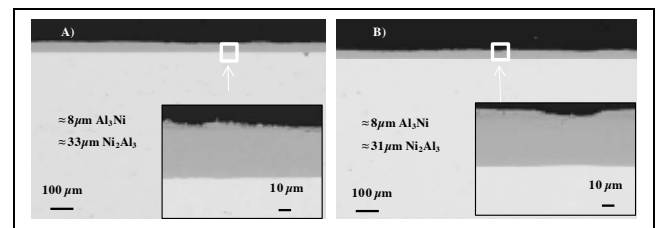
Aluminum surface enrichments were performed in order to take advantage of Alumina formation during high temperature oxidation. Two techniques were used: i) the pack-cementation as CVD technique which is well known and described in the literature [2] and ii) the slurry process [3] also widely implemented for pieces having complex geometry, such as pieces comprising internal small channels. For both techniques, the rate limiting step is the solid state diffusion of metallic elements.

The coating manufacturings were carried out on crude SLM and CMA substrates by applying a two steps heat treatment:

- the first one allows the aluminum enrichments through an annealing i) at 640°C during 4h for the pack-cementation process and ii) at 640°C and then at 700°C during respectively 4h and 1h, for the slurry process.
- The second step allows the NiAl formation by

interdiffusion of metallic species activated by a high temperature treatment at 980°C during 1h.

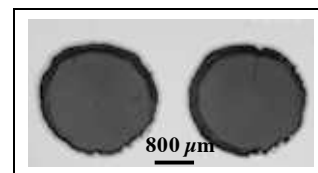
Whatever the process, after the first stage of heat treatment, the same coatings were obtained: they are 40 μm thick and are two-phased systems comprising Al<sub>3</sub>Ni and Al<sub>3</sub>Ni<sub>2</sub>. This situation is the consequence of **the similar interdiffusion coefficient of metals in SLM and CMA**. Moreover, the present experiments evidence clearly that **the rate limiting step is effectively the solid state diffusion for both synthesis techniques** (Fig. 4).



**Fig. 4.** Microstructure after the first step of the aluminum enrichments of A) SLM sample, B) CMA sample.

### III. CONCLUSION

Additive manufacturing is a new technology so that no experience feedback is available to date to address the surface reactivity issue as well as the solid state diffusion at high temperature. Then, the present results are original and their fruitful exploitation allows by now to build new reactor-exchangers withstanding very high pressure without failure (P=2400 bar) (Fig. 5).



**Fig. 5.** Micrograph of two channels of the 3D printed reactor-exchanger coated with β-NiAl.

### ACKNOWLEDGMENT

The authors are grateful to BPI France and LUE for their financial support

### REFERENCES

- [1] Wang et al., The Microstructure and Mechanical Properties of Deposited-IN718 by Selective Laser Melting, Volume 513, 2012 Pages 518-523.
- [2] Ledoux, X. (2012). (Doctoral dissertation, Université de Lorraine).
- [3] Ramenatte *et al.* «Method for depositing an anti-corrosion coating» Patent CA 2923666 A1, 2013.



## FIELD TRIAL OF SELF-STRATIFYING MEMBRANELESS MICROBIAL FUEL CELLS: INCREASED LIGHTING THROUGH SCALE-DOWN

Xavier Alexis Walter \*, Irene Merino-Jimenez \*, John Greenman\*, and Ioannis Ieropoulos \*

\* Bristol BioEnergy Centre, Bristol Robotics Laboratory, T-Block,  
Frenchay Campus, University of the West of England  
(UWE), Bristol, BS16 1QY, United Kingdom.

**Abstract** - A new type of microbial fuel cell (MFC) was recently developed: self-stratifying membraneless MFC (SSM-MFC) in which cathodes and anodes share the same electrolyte. Until now these MFCs have only been tested under controlled laboratory conditions. Hence, a field-trial was carried out at a music festival to assess its feasibility to be implemented in practice. The tested system, an autonomous self-lit urinal, consisted of a passively-fed MFC-stack of 12 modules from which the energy was harvested to power a set of 6 LED strips (lit 9h30 per day; 2.862 Wh). Under laboratory conditions, at 44h hydraulic retention time (HRT), results indicate that a cascade of 4 modules continuously produced 150mW and reduced the COD content by 88%. Once deployed in the field at the music festival, 6 cascades of 2 modules produced  $\approx 425\text{mW}$  (max.  $\approx 590\text{mW}$ ) and decreased the COD content by 48% with a HRT of 11.7h.

**Index Terms** - Membraneless microbial fuel cells, off-grid power source, sanitation, source separated waste treatments.

### I. INTRODUCTION

The main competitive advantage of the microbial fuel cell (MFC) technology is its capacity to directly generate electricity from any organic substrate. More importantly, MFCs generate electricity from organic wastes, normally considered expensive to treat. This study was carried out from an implementation perspective and is focused on the generation of energy from primarily urine. Employing urine as fuel presents several advantages, one of which being that MFCs can be fuelled directly with this abundant feedstock [1].

Implementing MFC technology in real environments presents two main challenges: affordability and power density. Self-stratifying column MFCs (SSM-MFC) have been shown to answer such a dual need [2]. Moreover, SSM-MFCs have the capacity to be scaled-up in size, up to a certain extent, without significant loss in power density [2]. However, this type of MFC has only been tested under controlled laboratory conditions [2, 3]. The aim of the present trial was to evaluate the capacity of SSC-MFC to be deployed as an electricity-generating sanitation solution in remote areas [3]. To this end, an autonomous self-lit

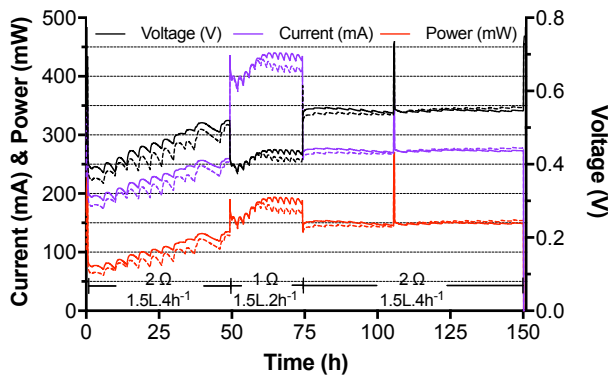
urinal was deployed at the Glastonbury 2016 Music Festival, UK's largest music festival. This implied scaling-up the size of individual MFC modules, whilst keeping the units smaller than the ones used in the PEE POWER<sup>®</sup> urinal during the Glastonbury festival in 2015 [4], adapting a passive feeding mechanism, and setting-up the appropriate energy management system to harvest the energy and power the lights. Compared to its predecessor [4], the aim was to provide twice the amount of lighting (the urinal was twice the size) with a system occupying less surface area.

### II. MATERIAL & METHODS

Due to the amount of fuel to be treated being quite high, the SSM-MFC's size was increased by a factor 2 compared to the previous lab-based study [3]. The external dimensions of a module were as follows: 400 mm (l), 300 mm (w) and 170 mm (h). A collective of 38 MFCs was inserted within a module and all connected in parallel. For a total footprint of 20.4L, the actual MFC part was only occupying 11.2L internal volume since the upper 5cm of each box served as a support for additional modules. After testing in the laboratory and in duplicate two cascades of 4 modules (19.2L displacement volume each), a stack of 12 modules was deployed in the field (57.6L displacement volume; 6 cascades of 2 modules).

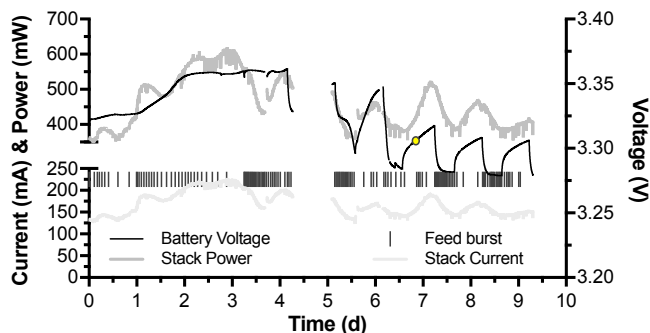
### III. RESULTS & DISCUSSION

With a feeding regime of  $1.7 \text{ L} \cdot 2\text{h}^{-1}$ , a cascade of 4 modules produced, at steady state (from 63h to 74h; Fig. 1), an average of  $181 \pm 9 \text{ mW}$  at  $425 \pm 11 \text{ mV}$  and  $425 \pm 11 \text{ mA}$ . Under lower feeding pulses ( $1.7 \text{ L} \cdot 4\text{h}^{-1}$ ), a cascade of 4 modules produced an average of  $151 \pm 2 \text{ mW}$  at  $549 \pm 4 \text{ mV}$  and  $274 \pm 2 \text{ mA}$  (from 75h to 145h; Fig. 1). With regard to the total footprint volume, these results correspond respectively to a power density of  $2.22 \text{ W} \cdot \text{m}^{-3}$  and  $1.85 \text{ W} \cdot \text{m}^{-3}$ , respectively. In terms of the displacement volume, the power densities were  $9.43 \text{ W} \cdot \text{m}^{-3}$  and  $7.86 \text{ W} \cdot \text{m}^{-3}$ , respectively.



**Fig. 1. Performance of two duplicate cascades under different feeding regimes and corresponding loads: all the MFCs within each cascade are connected in parallel**

During the 3 first days, the stack set at Glastonbury Music festival behaved as expected from the results obtained during the laboratory tests. The absolute power output gradually increased (2 days; Fig. 2) to a steady state of  $590 \pm 12$  mW at  $217 \pm 5$  mA, which was held during 28h until most of the festival attendees arrived. After adapting to a higher feeding regime, a new steady-state was reached between day 5 to day 9 (Fig. 2). The stack's average power was then of  $424 \pm 36$  mW at  $156 \pm 12$  mA.



**Fig. 2. Electrical output of the system before and during the festival: power and current output levels of the stack of 12 modules, voltage of the batteries and feeding-pulses that fed the 6 MFC cascades. The circle indicates the COD sampling point.**

At peak times of high urine volumes, the feeding regime was too high for the system, whereas during the rest of the time the feeding regimes were suboptimal. These feeding regimes correspond, for the whole system (57.6L), to a hydraulic retention time (HRT) of 2h30 min ( $\approx 559 \text{ L.d}^{-1}$ ) and  $\approx 9\text{h}$  ( $\approx 155 \text{ L.d}^{-1}$ ), respectively. These results imply that in order to accommodate higher volumes of waste, either the module size should be increased and/or the number of modules increased.

The produced power was stored in a battery bank during day time and was powering the lights (2.862W) during the night. This

duty cycle consisted of  $\approx 14\text{h}30$  charge and  $\approx 9\text{h}30$  discharge. Results indicate that a steady state seems to have been reached by day 7. However, at close inspection it seems that the charge level of the battery was slightly decreasing.

In terms of treating capacity, the COD was decreased by 48% with a HRT of 11h40 min at the time of analysis (Fig. 2). Compared to the previous trial [4], the COD removal was 92 % higher with a halved HRT. The system was treating on average  $220 \text{ L.d}^{-1}$ , slightly less than the 300 L of the previous trial (Tab. 1).

TABLE I: SUMMARY OF THE PERFORMANCES OF MFCs TREATING NEAT URINE.

Electrolyte Volume (L)	Influent COD ( $\text{mg.L}^{-1}$ )	Effluent COD ( $\text{mg.L}^{-1}$ )	HRT (h)	COD removal efficiency (%)	Volumetric power density ( $\text{W.m}^{-3}$ )	Coulombic efficiency (%)	Reference
19.2*	5586	672	44	88	9.4	5.87	This study
57.6**	6770	3540	11.7	48	7.3	2.49	This study
300**	N/A	N/A	22	25	1	N/A	[4]

\* Laboratory experiment, average of the two 4 modules cascades.

\*\* Field-trial data

#### IV. CONCLUSIONS

Overall, these results correspond to a technological improvement of 700% compared to the system employed in the previous year. Although there is room for improvement, results showed that the MFC technology is now sufficiently mature to be introduced as a carbon neutral pre-treatment system positively impacting liquid waste stream management, or as a power supply in remote areas.

#### ACKNOWLEDGMENT

The authors would like to acknowledge the Bill & Melinda Gates Foundation for funding the scientific work (grant no. OPP1149065) leading up to the festival trial. The authors would also like to thank the Glastonbury Music Festival Organisers, and Jane Healy in particular, for accommodating the PEE POWER<sup>®</sup> urinal in a well-attended area.

#### REFERENCES

- [1] Ieropoulos I, Greenman J and Melhuish C. Urine utilisation by microbial fuel cells; energy fuel for the future. *Physical Chemistry Chemical Physics* 2012;14:94-98
- [2] Walter XA, Gajda I, Forbes S, Winfield J, Greenman J and Ieropoulos I. Scaling-up of a novel, simplified MFC stack based on a self-stratifying urine column. *Biotechnology for Biofuel* 2016;9:93
- [3] Walter XA, Stinchcombe A, Greenman J and Ieropoulos I. Urine transduction to usable energy: a modular MFC approach for smartphone and remote system charging. *Applied Energy* 2017;192:575-581
- [4] Ieropoulos IA, Stinchcombe A, Gajda I, Forbes S, Merino-Jimenez I, Pasternak G, Sanchez-Herranz D and Greenman J. Pee power urinal - microbial fuel cell technology field trials in the context of sanitation. *Environmental Science-Water Research & Technology* 2016;2:336-343.

## ANALYTICAL AND EXPERIMENTAL VALIDATION OF A POLYMER ELECTROLYTE FUEL CELL COMPUTATIONAL MODEL

S. Zhang<sup>1</sup>, S.B. Beale<sup>1,2</sup>, U. Reimer<sup>1</sup>, W. Lehnert<sup>1,3,4</sup>

<sup>1</sup>Institute of Energy and Climate Research, IEK-3,  
Forschungszentrum Jülich, 52425 Jülich, Germany

<sup>2</sup>Mechanical and Materials Engineering, Queen's University,  
Kingston ON K7L 3N6, Canada

<sup>3</sup>RWTH Aachen University, Faculty of Mechanical Engineering,  
52062 Aachen, Germany

<sup>4</sup>JARA-HPC, 52425 Jülich, Germany

**Abstract** – A polymer electrolyte membrane fuel cell model was developed and applied to a number of practical designs. The model was validated by comparisons of current density and oxygen distributions with analytical solutions, and experimental polarization data. Further calculations were carried out where local current density values were compared with measured data. Excellent agreement was observed. The present model exhibited superior spatial resolution than previous numerical results.

Key words: polymer electrolyte fuel cells, validation and verification, high performance computing, current density distribution

### I. INTRODUCTION

The performance of a polymer electrolyte fuel cell (PEFC) is a function of both water and heat as well as gas composition. Both experimental and numerical studies have been conducted in the past. Experimental measurements typically provide global information: Detailed local results being much harder to come by. Computational fluid dynamics (CFD) calculations have the potential to provide local information. Previously, CFD applications were limited by computational power. This changed with the availability of massively-parallel high performance computing (HPC) facilities. Use of commercial software on HPC facilities are constrained by licensing costs, which makes the adaptation of open-source codes to fuel cell applications attractive.

A generic open-source computational code, openFuelCell, capable of reproducing every significant physico-chemical hydrodynamic process within a fuel cell, has been developed and modified by the present authors and others [1]. The code

was implemented within the OpenFOAM® platform, which enables fully-comprehensive calculations to be performed on HPC facilities.

### II. NUMERICAL APPROACH

The three-dimensional (3-D) multi-physics PEFC model considers all transport phenomena in the components of a fuel cell. These include the membrane electrode assembly, gas diffusion layers, flow channels and bipolar plates. The model is an extension of the work of Beale et al. [1] and Kvesić et al. [2]. The following salient assumptions are listed. For more information, the reader is referred to [1, 2].

- i) The flow is laminar.
- ii) The ideal law gas may be applied.
- iii) All material properties are isotropic and homogeneous.
- iv) The membrane is impermeable to gases.

The oxygen reduction reaction in the cathode catalyst layer is assumed to take place at a single interface between the electrodes and membrane. The Tafel equation was presumed to describe the activation overpotential at the cathode, and the relationship between the cell potential and current density is governed by a Kirchhoff-Ohm relation [1].

### III. RESULTS AND VALIDATION

The oxygen and current density distributions along the fuel cell were compared with solutions from a 1-D analytical model of Kulikovskiy et al. [3] as a function of cathodic stoichiometric factor. Maximum observed errors were 2.5% for oxygen

distribution and 6.7% for current density distribution. This is because the analytical model is for an idealized isothermal cell with perfect mixing and constant streamwise velocity.

Subsequently, an in-house manufactured 5-path-serpentine bi-polar plate high temperature (HT) PEFC with a nominal active area of  $17\text{cm}^2$  was used for experimental validation of the present model. Polarization curves were compared under normal operating conditions (at  $160^\circ\text{C}$  and  $101325\text{ Pa}$ , anodic/cathodic stoichiometric factors = 2/2). It can be seen from Fig. 1 that the agreement between experimental and numerical results is good, with a maximum difference of about  $40\text{mV}$  when the current density is  $0.05\text{ A/cm}^2$ .

Therefore it can be concluded that the overall performance of a HT-PEFC, in terms of cell voltage, can be reliably predicted by the present model, and that the model may be applied to other HT-PEFC designs.

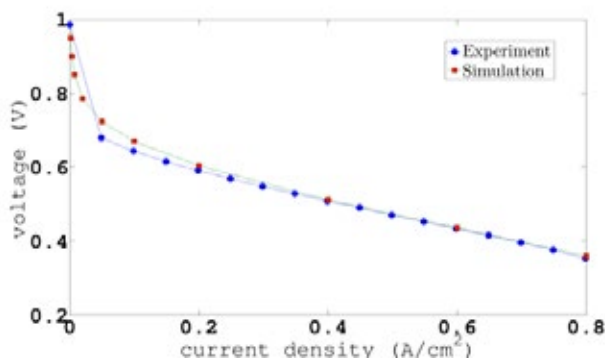


Fig. 1. Polarization curves of numerical and experimental results, stoichiometric factors (2/2).

The model was then applied to obtain performance calculations within a short (5-cell) stack. The active area of each cell is nominally  $200\text{cm}^2$ . The interior operating temperature was slightly higher than the external value ( $433\text{K}$ ). Operating pressure and stoichiometric factors were  $101325\text{ Pa}$  and 2/2, respectively.

The results from the present calculations were compared with experimental data [4] and also a previous model based on volume-averaging [2]. The polarization curves (not shown) exhibited very minor deviations between the three sets of results. Comparison of the results of the local current density distribution is critical for validation. Figure 2 shows that the current density distributions for the present and previous results are quite similar, notwithstanding the tendency for ‘smear out’ associated with the S++® segment current scan shunt employed in the experiment. The spatial resolution of the present results was much higher than the results from the experiment and previous numerical calculations.

In addition to current density, other local values, such as oxygen and water mass fraction, pressure, velocity etc. can also be displayed with a very high spatial resolution. These local

variations are important. For this reason, the present model will be most useful in future detailed design and optimization for fuel cells with complex geometry.

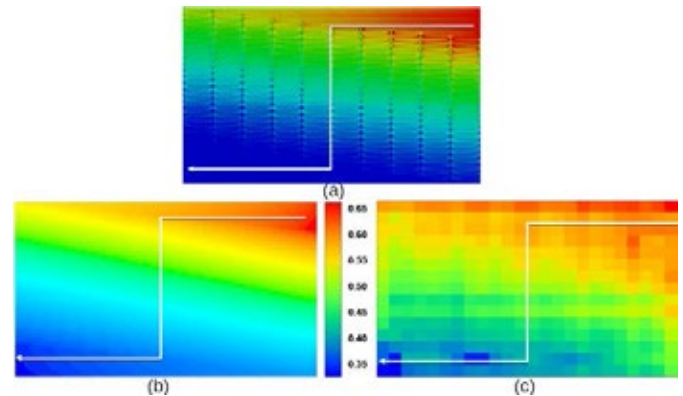


Fig. 2. Current density distributions: (a). present results, (b). Experimental result [3], (c) porous media approach based numerical result [2]; mean current density is  $0.45\text{ A/cm}^2$ .

#### IV. CONCLUSIONS

A 3-D HT-PEFC model was developed and validated. The polarization curves and current density distributions were compared with experimental and numerical results.

1. The present model is capable of reliably predicting the overall performance of a HT-PEFC, in terms of polarization curves.
2. The internal current density distribution can be predicted with a much higher spatial resolution than was previously possible.

#### ACKNOWLEDGMENT

This work is partially supported by China Scholarship Council (grant number: 201506230130). Calculations were performed on HPC hardware of the Jülich and Aachen Research Alliance(JARA), grant JARA0070. The authors are indebted to Y. Rahim for performing the current measurement experiment shown in Fig. 1.

#### REFERENCES

- [1] Beale, S.B., Choi, H.-W., Pharoah, J.G., Roth, H.K., Jasak, H., Jeon, D.H. "Open-source computational model of a solid oxide fuel cell." *Computer Physics Communications* 200 (2016): 15-26.
- [2] Kvesić, M., Reimer, U, Froning, D, Lücke, L, Lehnert, W, Stolten, D. "3D modeling of a  $200\text{ cm}^2$  HT-PEFC short stack." *International Journal of Hydrogen Energy* 37.3 (2012): 2430-2439.
- [3] Kulikovskiy, A. A., A. Kucernak, and A. A. Kornyshev. "Feeding PEM fuel cells." *Electrochimica Acta* 50.6 (2005): 1323-1333.
- [4] Lücke, L. Analyse des Betriebsverhaltens von Hochtemperatur-Polymer-elektrolyt-Brennstoffzellen. Forschungszentrum Jülich, 2013. (In German)



## A FABRICATION METHOD OF HIGH-PERFORMANCE MULTISCALE SOLID OXIDE FUEL CELL VIA ADVANCED ELECTROSPRAY DEPOSITION METHOD

Sung Soo Shin\*\*\*, Jeong Hun Kim\*\*\*, Ji-Won Son\*\*\*, Hyun Ho Shin\*, Hyoungchul Kim\*\*\*, and Mansoo Choi\*\*\*

\*Global Frontier Center for Multiscale Energy System, Department of Mechanical and Aerospace Engineering, Seoul National University, Seoul 08826, (South Korea)

\*\* Department of Mechanical and Aerospace Engineering, Seoul National University, Seoul 08826, (South Korea)

\*\*\* High-temperature Energy Materials Research Center, Korea Institute of Science and Technology, Seoul 02792, (South Korea)

**Abstract** – In this study, we developed an advanced fabrication method to fabricate uniform thin film, which is hard to get from the non-vacuum system. We optimized sol-electrospray technique via electrospray deposition (ESD) method, non-vacuum process equipment. Lanthanum Strontium Cobaltite (LSC)-Ceria thin film, which we have named nano cathode functional layer (nCFL), and LSC thin film, which we have named nano adhesion layer (nAL), were fabricated on the electrolyte substrate. With optimized thin films, we fabricated three different cells, reference cell, nAL assisted cell with LSC thin film and multiscale cathode functional layer (MCFL) assisted cell with LSC-ceria thin film. Fabricated nAL assisted cell and MCFL assisted cell resulted 1099.81mW/cm<sup>2</sup> and 1149.58mW/cm<sup>2</sup> peak power density, which is 12.67% and 17.77% higher than the reference cell's, 976.14mW/cm<sup>2</sup> at the 650°C operation temperature. From the results, it is confirmed that the thin film assisted SOFC with nAL and nCFL demonstrated improved cell performances.

**Index Terms** – Electrospray deposition, Multiscale architecturing, Sol-gel, Solid oxide fuel cell

### I. INTRODUCTION

In recent years, solid oxide fuel cell (SOFC) fabrication methods have been developed from conventional method, screen-printing, to advanced equipment, atomic layer deposition (ALD). Among the various SOFC fabrication methods, vacuum process equipment such as ALD, pulsed laser deposition (PLD), sputter resulted better cell performances than the non-vacuum process equipment such as screen-printing, aerosol deposition [1-3]. One of the most important advantages of vacuum process equipment is that it can control the cathode morphologies with nanoparticles. The cathode structure made of nanoparticles increases the reaction area, leading to cell performances improvement. However, in non-vacuum systems, it is hard to control the nanoparticles because of their

agglomeration problem. In electrospray deposition process (ESD), which is a non-vacuum process, there is a limit to the slurry process with a large particle size, and researches for sol-process have been conducted. Other studies, however, have mainly fabricated porous micro-thickness structures with a sol ESD process [4]. In this study, we fabricated a uniform thin film by the sol ESD process and applied it to the cell to compare the performance change.

### II. EXPERIMENTAL

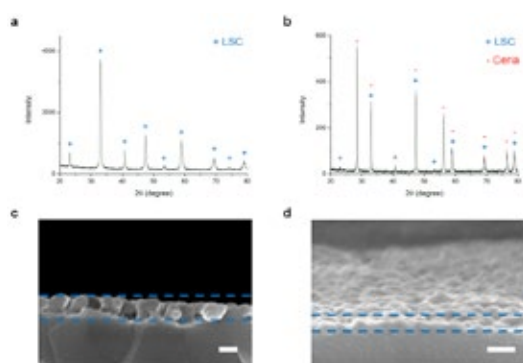
#### A. Fabrication of sprayed thin film

The ESD system consisted of a high voltage power supply (NanoNC), a pump controller (KD Scientific) and a micro-nozzle (NanoNC). We used an 8 μm diameter silica nozzle for the sol ESD experiment and a 250 μm diameter metal nozzle for the slurry ESD experiment. The applied voltage was fixed at 7 kV, and the distance between the substrate and the nozzle was fixed at 4 cm. The sintering condition of LSC sol and LSC-ceria mixed sol was 950 °C 1 hr.

We fabricated three different cells to compare the effect of thin film assisted cathode. Anode and electrolyte structure of each cell is same. Each cell's electrolyte is composed of 5 μm YSZ and 250 nm GDC. In addition, we used Ce<sub>0.9</sub>Gd<sub>0.1</sub>O<sub>1.95</sub>/La<sub>0.6</sub>Sr<sub>0.4</sub>CoO<sub>3-δ</sub> as cathode functional layer (CFL). First, the reference cell consists of anode-electrolyte-micro CFL-cathode current collecting layer (CCCL). Then we add thin film between electrolyte layer and CFL. LSC thin film, which named nano adhesion layer (nAL), was added to fabricate the second cell, nAL assisted cell. And thin film composed of LSC and ceria, which named nano cathode functional layer (nCFL) was added to fabricate the third cell, multiscale cathode functional layer (MCFL) assisted cell.

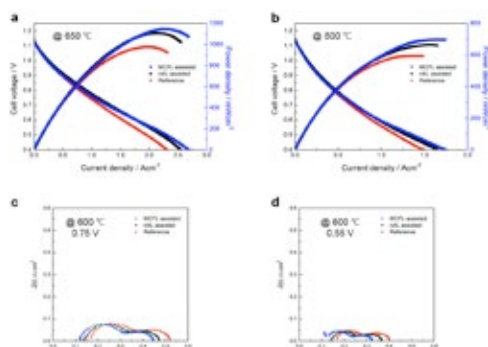
### III. RESULTS AND DISCUSSION

Figure 1a and 1b show the X-ray diffraction results for sintered LSC sol and LSC-ceria mixed sol at the condition of 950 °C 1 h. No secondary phases were seen in the LSC and LSC-ceria sol XRD patterns. The prepared sol was deposited by the ESD process and thin and uniform thin films were fabricated as shown in Figure 1c and 1d. The particle size of the LSC thin film in Figure 1c was about 100 nm, and the LSC-ceria thin film in Figure 1d was less than 20 nm. The smaller particle size of the LSC-ceria composite sol seems to be due to the different LSC and ceria particles interfere with grain growth.



**Fig. 1. X-ray diffraction patterns of (a) LSC, (b) LSC-ceria mixed sol sintered at 950 °C 1 h and cross-section SEM images of electrospayed (c) LSC thin film, (d) LSC-ceria thin film sintered at 950 °C 1 h. (scale bar is 100 nm)**

We applied optimized thin films to the interlayer between the electrolyte and the cathode to increase the transfer rate of oxygen ion. Because the transfer rate of oxygen ion between the electrolyte and the cathode is one of the most important factors, which determines the performance of SOFC[5].



**Fig. 2. The I-V-P curves at (a) 650 °C and (b) 600 °C. The EIS results at (a) 650 °C and (b) 600 °C.**

In figure 2a, fabricated nAL assisted cell and MCFL assisted cell resulted 1099.81 mW/cm<sup>2</sup> and 1149.58 mW/cm<sup>2</sup> peak power density, which is 12.67 % and 17.77 % higher than the reference cell's peak power density, 976.14 mW/cm<sup>2</sup> at the 650 °C. In figure 2c and 2d, when the nAL and MCFL are added, it

can be seen that both the ohmic resistance and the polarization resistance are reduced. This is because the added nano thin film layer increases the transfer rate of oxygen ion between the electrolyte and cathode layer. The reason MCFL assisted cell has higher performance than nAL assisted cell is that particle size, which is about 5 times smaller, seems to enlarge the reaction area of the interface between electrolyte and cathode and have influenced the transfer rate of oxygen ion. In addition, nCFL of similar composition to mCFL made better bonding of each other than the GDC-mCFL bonding of reference cell.

### IV. CONCLUSION

In summary, we optimized the fabrication of the ceramic thin film layer by an advanced fabrication method using the sol ESD process. The optimized thin and uniform LSC layer had a particle size of less than 100 nm and the LSC-ceria layer was less than 20 nm. It is confirmed that the performance is increased compared to the reference cell by applying two layers to each cell, and the composite structure using LSC-ceria thin film results higher performance.

### ACKNOWLEDGMENT

This work was supported by the Global Frontier R&D Program on Center for Multiscale Energy System funded by the National Research Foundation under the Ministry of Science, ICT & Future Planning, Republic of Korea (2012M3A6A7054855).

### REFERENCES

- [1] Marinha, D., Rossignol, C., Djurado E., Influence of electrospaying parameters on the microstructure of  $\text{La}_{0.6}\text{Sr}_{0.4}\text{Co}_{0.2}\text{Fe}_{0.8}\text{O}_{3-\delta}$  films for SOFCs, *Journal of Solid State Chemistry*, Volume 182, 2009, pp. 1742-1748.
- [2] Celikbilek, O., Jauffres, D., Siebert, E., Dessemond, L., Burriel, M., Martin, C., L., Djurado, E., Rational design of hierarchically nanostructured electrodes for solid oxide fuel cells, *Journal of Power Sources*, Volume 333, 2016, pp. 72-82.
- [3] Kim, J. H., Shin, S. S., Noh, H. S., Son, J.-W., Choi, M., Kim, H., Tailoring ceramic membrane structures of solid oxide fuel cells via polymer-assisted electrospay deposition, *Journal of Membrane Science*, Volume 544, 2017, pp. 234-242.
- [4] Hsu, C.-S., Hwang, B.-H., Xie, Y., Zhang, X., Enhancement of solid oxide fuel cell performance by  $\text{La}_{0.6}\text{Sr}_{0.4}\text{Co}_{0.2}\text{Fe}_{0.8}\text{O}_{3-\delta}$  double-layer cathode, *Journal of The Electrochemical Society*, Volume 155(12), 2008, pp. B1240-B1243.
- [5] Sharma, R., K., Burriel, M., Dessemond, L., Bassat, J., M., Djurado, E., Design of interfaces in efficient  $\text{Ln}_2\text{NiO}_{4+\delta}$  (Ln=La, Pr) cathodes for SOFC applications, *Journal of Materials Chemistry A*, Volume 4, 2016, pp. 12451-12462.

## HYDROGEN ENERGY SUPPLY SYSTEM BY USING RENEWABLE ENERGY SOURCES

Prof. Dr. T. Kono

Institute for Materials Research, Tohoku University,  
2-1-1 Katahira, Aoba-ku, Sendai 980-8577 JAPAN

**Abstract** - Hydrogen Energy Supply System consists of photovoltaic system, batteries, water electrolyzer, hydrogen storage alloy tank and water tank, and fuel cells. Electricity generated from the photovoltaic system is used to electrolyze water and produce hydrogen directory, which is stored in the hydrogen storage alloy tank and used in fuel cells that produce electricity and hot water to provide for demand.

**Index Terms** – Hydrogen Storage Alloy, Hydrogen Energy System, Pure Hydrogen Fuel Cell, Renewable Energy.

### I. INTRODUCTION

In recent years, communities on most remote islands rely on very high cost diesel power generation. This is a major problem – a very high cost and a large amount of carbon dioxide emissions. Renewable energy has been the strong solution for resolving the problems of the current dependency on fossil based fuels and hike in fuel prices in the world, but the power of renewable energies depend on the weather and will be unstable. The Hydrogen Energy Supply System is able to overcome these issues.

### II. HYDROGEN ENERGY SUPPLY SYSTEM

#### 1. Hydrogen storage alloy technology

Hydrogen storage alloys can store hydrogen as an energy source safely and easily. Therefore, hydrogen storage alloys have received much attention as a new energy conversion and storage material. The application field of hydrogen storage alloys as a new functional material covers a wide range, such as storage and transportation of hydrogen, storage and transportation of heat, conversion of heat to mechanical energy, separation and refinement of hydrogen, separation of hydrogen isotope, cells using hydrogen as an active material, catalysts in synthetics, and temperature sensors.

As described above, hydrogen storage alloys are applicable to various fields such as mechanical, physical, and chemical

fields, and mentioned as one of key materials in future industry. There are cases where metal elements which exothermically react with hydrogen, that is, which form a stable compound with hydrogen are used alone as a metal which occludes hydrogen, and cases where these metal elements alloyed with other metals are used. Figure 1 shows that hydrogen storage alloys are metallic materials that reversibly absorb and release large amounts of hydrogen from the gas phase.

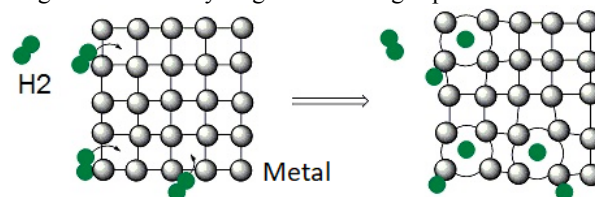


Fig. 1 Hydrogen absorption Mechanism of hydrogen storage alloy<sup>1)</sup>

#### 2. Hydrogen Energy Supply System

H<sub>2</sub>One<sup>TM</sup>, hydrogen based independent energy supply system, was launched in 2015 in Japan<sup>2)</sup>. This system combines photovoltaic system, lithium ion batteries, water electrolyzer, hydrogen tank and water tank, and fuel cells. Electricity generated from the photovoltaic system is used to electrolyze water and produce hydrogen, which is then stored in tanks and used in fuel cells that produce electricity and hot water. H<sub>2</sub>One<sup>TM</sup> designed as Resort Model has entered operation in the building of the smart hotel named Henn na Hotel, at the Huis Ten Bosch theme park in Nagasaki, Kyushu, Japan<sup>2)</sup>. This system as Resort Model is expected to be used for areas where energy infrastructure is inadequate, or where hotel operators want to minimize their environmental footprint.

Copyright © 2017

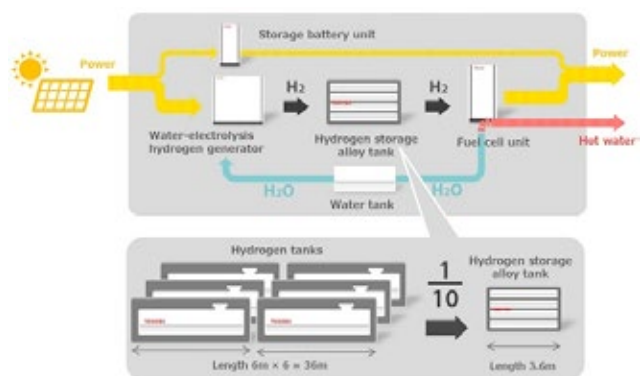


Fig. 2 System structure of hydrogen energy supply system<sup>3)</sup>

Table 1. Key system specifications of hydrogen energy supply system by using a hydrogen storage alloy<sup>2)</sup>.

Properties	Specification
Photovoltaic capacity	62 kW
Power output	54kW
Electricity storage capacity	1800kWh
Hot water supply capacity	24L/min



Fig. 3 H<sub>2</sub>One™ system in the Phase-2 building of the Henn na Hotel, at the Huis Ten Bosch theme park in Nagasaki, Kyushu<sup>2)</sup>.

This system as Resort Model is composed of a photovoltaic power generation system with lithium ion batteries for storing output power, a solid polymer electrolyte water electrolysis unit, hydrogen storage alloy tank, and pure hydrogen fuel cells. By using this system, long hours of sunshine allow photovoltaic generation to provide more than enough electricity to power the 12 rooms of Henn na Hotel's Phase 2 building during summer. This installed system will use surplus power to electrolyze pure water and produce hydrogen. The hydrogen will be stored in a tank, ready for use on demand, and in winter it will be used to power fuel cells that generate electricity and warm water.

The H<sub>2</sub>One™ as Resort Model is also equipped with the new hydrogen tank that contains the hydrogen storage alloy supporting much improved high-density storage. This new tank is less than one-tenth of the size of the conventional model it replaces, and suitable for use even in small spaces in Figure 2. The hydrogen will be stored in the system's integrated tank, ready for use on demand, and in winter powers fuel cells that generate electricity and warm water. The system designed as Resort Model has enough capacity to supply this smart hotel with electricity throughout the year.

By making full use of renewable energy and hydrogen-powered fuel cells, the system designed as Resort Model offers CO<sub>2</sub>-free solution that can produce all the energy needed by hotels and other resort facilities. In this configuration, it delivers a real CO<sub>2</sub>-free solution for hotels and other resort facilities environmentally.

EMS (Energy Management System) is the key technology that is designed for optimal production and storage of hydrogen based on electricity supply and demand forecasts. The long hours of summer sunshine of Kyushu, the third largest and southernmost of Japan's main islands, allow the photovoltaic energy system to generate enough renewable energy to meet all the requirements of the 12 rooms in the hotel, and additional power to electrolyze water and produce hydrogen.

#### References

- [1]<http://www.sigmaaldrich.com/materialsscience/alternative-energy-materials/hydrogen-storage-alloys.html>
- [2][http://www.toshiba.co.jp/about/press/2016\\_03/pr1402.htm](http://www.toshiba.co.jp/about/press/2016_03/pr1402.htm).
- [3][http://www.toshiba.co.jp/about/press/2015\\_10/pr0701.htm](http://www.toshiba.co.jp/about/press/2015_10/pr0701.htm)
- [4] <https://www.toshiba-newenergy.com/en/reference/>
- [5]<http://www.toshiba.co.jp/product/fc/english/whatsnew/info/20150406.htm>



## Role of Strain and Ligand Effect in H<sub>2</sub> Formation from HCOOH Decomposition on Bimetallic Pd/M (M=Late Transition FCC Metals) Alloys

Jinwon Cho<sup>1</sup>, Sangheon Lee<sup>1,3</sup>, Sung Pil Yoon<sup>1</sup>, Jonghee Han<sup>1,2</sup>, Suk Woo Nam<sup>1,2</sup>, Kwan-Young Lee<sup>2,\*</sup>, and Hyung Chul Ham<sup>1,\*</sup>

<sup>1</sup>Fuel Cell Research Center, Korea Institute of Science and Technology (KIST), Hwarangno 14-gil 5, Seongbuk-gu, Seoul 136-791, Republic of Korea

<sup>2</sup>Green School (Graduate School of Energy and Environment), Korea University, 145, Anam-ro, Seongbuk-gu, Seoul, 136-701, Republic of Korea

<sup>3</sup>Department of Chemical Engineering and Materials Science, Ewha Womans University, 52 Ewhayeodae-gil, Seodaemun-gu, Seoul, 03760, Republic of Korea

**Abstract** - In this study, we have elucidated the role of heteronuclear interactions in determining the selective H<sub>2</sub> formation from HCOOH decomposition on bimetallic Pd<sub>shell</sub>/M<sub>core</sub> (M = Rh, Pt, Ir, Cu, Au, Ag) catalysts. We found that HCOOH decomposition strongly depends on the variation of surface charge polarization (ligand effect) and lattice distance (strain effect), which are caused by the heteronuclear interactions between surface Pd and core M atoms. That is, the surface lattice contraction leads to the downshift of d band centers in comparison to the pure Pd case, while the electronic charge increase in surface Pd atoms results in the depletion of the density of states for d<sub>z<sup>2</sup></sub>, d<sub>yz</sub>, and d<sub>xz</sub> orbitals. Our study highlights the importance of properly tailoring lattice and charge state of the surface by tuning heteronuclear interactions in bimetallic Pd<sub>shell</sub>/M<sub>core</sub> catalysts for enhancing the catalysis of HCOOH decomposition toward H<sub>2</sub> production, and other chemical reactions.

**Index Terms** - Formic acid, Hydrogen, Catalyst, Density Functional Theory

### I. INTRODUCTION.

Formic acid (HCOOH) is a nontoxic liquid at room temperature, and during the last few years there has been a revitalization of effort in developing economically viable HCOOH-based *in situ* H<sub>2</sub> production systems.[2] In the presence of a suitable catalyst, HCOOH decomposes

primarily into H<sub>2</sub> and CO<sub>2</sub> and secondarily into H<sub>2</sub>O and CO.[2,3] Considering the notorious CO-poisoning effect of platinum-based fuel cell electrodes, Pd-based catalysis are widely used in HCOOH decomposition because of its high productivity to H<sub>2</sub>, however, the selectivity is still to be improved.[1,2] To solve such issue, the bimetallic alloy Metal-Pd core-shell (Pd/M) catalyst has been proposed to improve both the productivity and selectivity of Pd toward H<sub>2</sub> production from HCOOH decomposition, where M is Rh, Pt, Ir, Cu, Pd, Au, and Ag.

### II. RESULTS AND DISCUSSION

In our previous study, we initially modeled the gas-phase reaction on the (111) surfaces of Pd/Ag structure as a starting point to understand catalytic decomposition of HCOOH and thickness effect of Pd shell [8]. When the Pd shell is the thinnest, enhanced reaction rate toward H<sub>2</sub> production from HCOOH decomposition was observed and with this results we performed the formic acid decomposition over the Pd monolayer based Pd/M (M = FCC transition metals such as Pt, Ir, Pd, Au, Ag, Cu, Rh) catalysts to find the most economical use of rather expensive noble metal and to further understand a role of alloying effect such as strain and ligand effect towards hydrogen production rate and selectivity simultaneously.

To begin, we calculated the overall activation energy of dehydrogenation pathway for Pd/M and the barrier of Pd/Cu is the lowest (E<sub>a</sub> = 0.78eV) whereas for Pd/Pt is the highest (E<sub>a</sub> = 0.94eV)

while the energy barrier of dehydration pathway is the highest for Pd/Cu ( $E_a = 2.02\text{eV}$ ) and the lowest for Pd/Pt ( $E_a = 0.99\text{eV}$ ). Considering CO contamination is detrimental to the Pd surface, the ideal condition for catalyst is to have low dehydrogenation activation energy barrier and high dehydration activation energy barrier as possible. Accordingly, we also calculated barrier difference ( $\Delta E_a$ ) between dehydrogenation pathway and dehydration pathway which is related to the selectivity in formic acid decomposition, and the selectivity of Pd/Cu core-shell structure ( $\Delta E_a = 1.26\text{eV}$ ) is revealed to be enhancing the selectivity to  $\text{H}_2$  production, while for Pd/Pt ( $\Delta E_a = 0.05\text{eV}$ ) the opposite is true. At this point, we asked ourselves for what reasons Cu and Ag shows better  $\text{H}_2$  productivity whereas Pt has worse selectivity than Pure Pd.

The answer to the question is the strong understanding of structure and underlying mechanism in the bimetallic core-shell alloy catalyst is essential for determining the catalytic performance. Particularly, the interatomic mixing between the surface and subsurface layer and the mismatch of lattice parameter between the two atoms is one of the most important factors that can significantly affect the surface reactivity of alloy catalysts. As in Figure 1, there is a considerable variation in the binding energy of  $\text{HCOO}$  and  $\text{HCO}+\text{OH}$  which are known as the key intermediate in dehydrogenation and dehydration pathway respectively. Such strain effect is due to the downshift of d-band center and as reported in the previous studies, downshift of d-band center leads to decrease in the binding energy. This tendency also hints that the Pd surface strain should be compressive as possible in order to achieve the maximum  $\text{H}_2$  selectivity from  $\text{HCOOH}$  decomposition.

On the other hand, the amount of calculated ligand contribution is directly proportional to the amount of charges on the surface, which is transferred from the subsurface M, more the charge transfers, and more the ligand contribution on the surface. This relationship also suggests that the ligand contribution on the surface is determined by the transferred charges to the surface since the gained charges mixes with the charges of Pd on the surface. Such charge transfer behavior is confirmed in density of states in Figure 2. As there are more charge accumulation on Pd surfaces  $d_{yz}$  orbital, which is responsible for the adsorption of  $\text{HCOO}$ , the density near the fermi energy is empty. In other words, the interaction between  $\text{HCOO}$  and the surface is weakened, and so that the dissociation of H from  $\text{HCOO}$  becomes easier. In order for maximum  $\text{H}_2$  selectivity from  $\text{HCOOH}$ , compressive strain and charge gained surface is required.

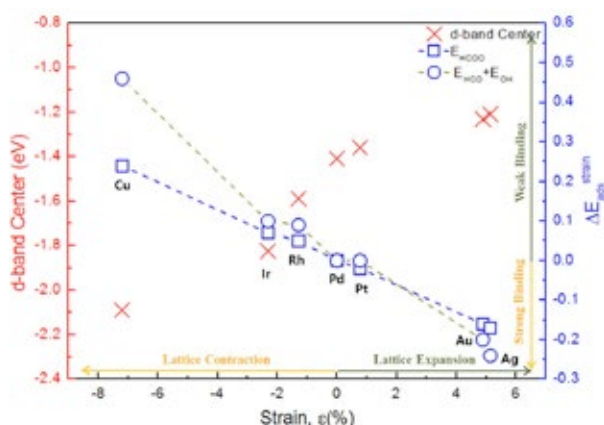


Figure 1. Effect of lattice parameter on d-band center and the change in binding energy of  $\text{HCOO}$  and  $\text{HCO}+\text{OH}$  with respect to Pd.

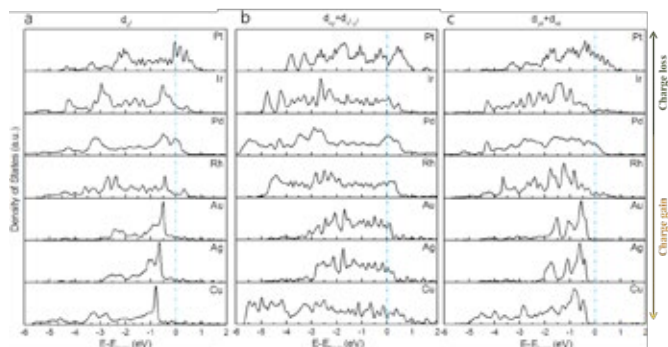


Figure 2. Projected local density of states of Pd/M surfaces. a)  $d_{yz}$  b)  $d_{xy} + d_{x^2+y^2}$ , and c)  $d_{yz} + d_{xz}$ .

### III. CONCLUSION

In this study, the DFT calculations have been performed to understand the role of Pd shell thickness, strain effect and ligand effect in the bimetallic Pd/M catalysts in the decomposition of  $\text{HCOOH}$ . For such purposes, we separated strain and ligand effect. Here, the interatomic mixing between the surface and subsurface layer, the ligand effect, is responsible for dehydrogenation since excessive charge on the Pd surface reduces energy barriers, such as Pd/Cu, Pd/Ag, and Pd/Rh, and the mismatch of lattice parameter between the two different atoms, the strain effect, is key to dehydration since it ultimately raises CO production energy barriers. Our theoretical calculation offers the fundamental mechanism of  $\text{HCOOH}$  decomposition on Pd/M catalysts and also provides physical and chemical intuition for the next generation bimetallic catalyst.

### IV. REFERENCES

- (1) (a) Ojeda, M.; Iglesia, Angew. Chem. 2009, 48 (26), 4800–3. (b) Haan, J. L.; Masel, R. I. Electrochim. Acta 2009, 54 (16), 4073–4078.
- (2) Tedsree, K.; Li, T.; Jones, S.; Chan, C. W.; Yu, K. M.; Bagot, P. A.; Marquis, E. A.; Smith, G. D.; Tsang, S. C. Nat. Nanotechnol. 2011, 6 (5), 302–7.
- (3) Kresse, G.; Furthmüller, J. Vienna University of Technology: Vienna, Austria, 2001.
- (4) Blochl, P. E. Phys. Rev. B 1994, 50 (24), 17953–17979
- (5) Blochl, P. E.; Jepsen, O.; Andersen, O. K. Phys. Rev. B 1994, 49 (23), 16223–16233
- (6) Henkelman, G.; Uberuaga, B. P.; Jonsson, H. J. Chem. Phys. 2000, 113, 9901.
- (7) Hammer, B.; Hansen, L. B.; Nørskov, J. K. Phys. Rev. B 1999, 59 (11), 7413–7421.
- (8) Cho, J.; Lee, S.; Han, J.; Yoon, S. P.; Nam, S. W.; Choi, S. H.; Lee, K.-Y.; Ham, H. C. J. Phys. Chem. C 2014, 118 (39), 22553–22560.
- (9) Cho, J.; Lee, S.; Han, J.; Yoon, S. P.; Nam, S. W.; Choi, S. H.; Ahn, S. A.; Lee, K. -Y.; Ham, H. C. J. Nanosci. Nanotechnol. 2015, 15 (10), 8233–8237.
- (10) Lee, S.-Y.; Jung, N.; Cho, J.; Park, H. -Y.; Ryu, J.; Jang, I.; Kim, H.-J.; Cho, E.; Park, Y.-H.; Ham, H. C.; Jang, J. H.; Yoo, S. J. ACS Catal. 2014, 4 (8), 2402–2408.
- (11) Mavrikakis, M.; Hammer, B.; Nørskov, J. Phys. Rev. Lett. 1998, 81.
- (12) Maark, T. A.; Peterson, A. A. J. Phys. Chem. C 2014, 118 (8), 4275–4281.
- (13) Ham, H. C.; Manogaran, D.; Lee, K. H.; Kwon, K.; Jin, S. A.; You, D. J.; Pak, C.; Hwang, G. S. J. Chem. Phys. 2013, 139 (20).

## PERFORMANCE ASSESSMENT OF AN AMMONIA-FUELED SOFC SYSTEM FOR COGENERATION OF ELECTRICITY, HEAT AND HYDROGEN

A. Perna<sup>\*</sup>, M. Minutillo<sup>\*\*</sup>, E. Jannelli<sup>\*\*</sup>, V. Cigolotti<sup>\*\*\*</sup>, S. W. Nam<sup>\*\*\*\*</sup>, J. Han<sup>\*\*\*\*</sup>

<sup>\*</sup>Department of Civil and Mechanical Engineering, University of Cassino and Southern Lazio, Cassino (Italy)

<sup>\*\*</sup>Department of Engineering, University of Naples "Parthenope", Naples (Italy)

<sup>\*\*\*</sup>ENEA - Italian National Agency for New Technologies, Energy and Sustainable Economic Development, Rome (Italy)

<sup>\*\*\*\*</sup>Fuel Cell Research Center, Korea Institute of Science and Technology KIST, Seoul (South Korea)

**Abstract** - In this paper a small-scale tri-generation system (~20 kW<sub>el</sub>), in which ammonia is used as a fuel for a SOFC system to produce hydrogen for refueling up to 20~30 fuel cell vehicles per day (100 kg/day) as well as electricity and heat for local use, is proposed. Thermo-chemical and electrochemical models have been developed by using experimental data, carried out at the KIST, on a single SOFC-O, with the objective to define the optimal plant configuration that allows to minimize the SOFC stack size. The experimental tests have been performed by varying the anode gas composition, the fuel utilization factor and the operating temperature.

**Index Terms** – Ammonia, SOFC, hydrogen, tri-generation

### I. INTRODUCTION

Ammonia (NH<sub>3</sub>) is a promising hydrogen carrier thanks to its high hydrogen density, low production cost, and ease in liquefaction and transport. The NH<sub>3</sub> decomposition into nitrogen and hydrogen is a mildly endothermic process that occurs at temperatures close to the operating conditions of solid oxide fuel cells (SOFCs). Therefore, the use of NH<sub>3</sub> as fuel in a SOFC system for cogeneration of heat, electricity and hydrogen could be beneficial in terms of energy management and of simplified generation systems development.

In this paper a small-scale tri-generation system, in which ammonia is used as a fuel for a SOFC system to produce hydrogen for refueling up to 20~30 fuel cell vehicles per day (100 kg/day) as well as electricity and heat for local use, is proposed. Two plant configurations have been evaluated and compared. The analysis has been carried out by using thermo-chemical and electrochemical models; in particular the SOFC model, previously developed by the authors for natural gas and reformat feeding [1,2], has been applied for predicting the

SOFC performance by using NH<sub>3</sub> as fuel. The model has been calibrated and validated by means of experimental data obtained on a single solid oxide cell at the Korea Institute of Science and Technology (KIST).

### II. PLANT CONFIGURATIONS

In this study two plant configurations for the tri-generation of electricity, heat and hydrogen have been proposed, as shown in Figures 1 and 2.

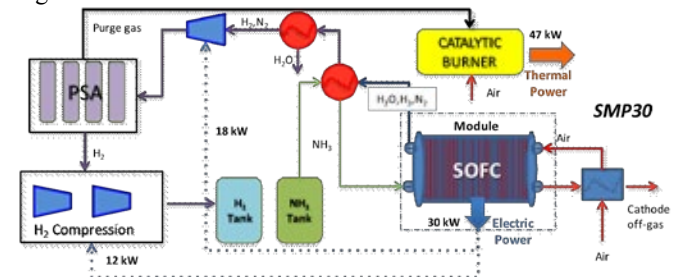


Fig. 1 SPM30- Plant lay-out

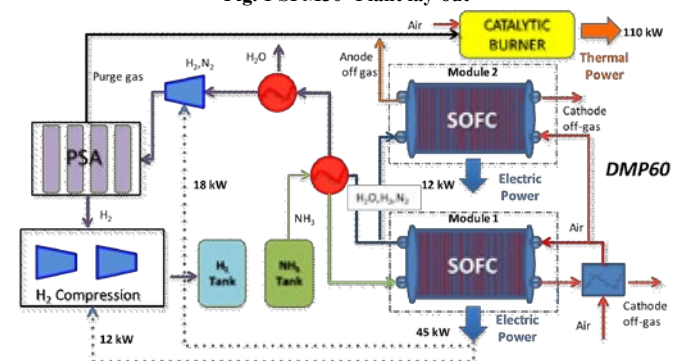


Fig. 2 DPM60- Plant lay-out

Copyright © 2017

In the first configuration (Single Power Module, SPM30), the plant has been sized in order to guarantee 100 kg/day of hydrogen by minimizing the SOFC size (i.e. the capital costs). In the second one (Double Power Module, DPM60), the plant has been sized for providing in addition to hydrogen, heat and electricity.

### III. RESULTS AND DISCUSSION

#### A. Experimental tests on SOFC-NH<sub>3</sub> single cell

In order to define the optimal plant configuration that allows to minimize the SOFC stack size, thermo-chemical and electrochemical models have been developed by using experimental data on a single SOFC (the active electrode area was 16 cm<sup>2</sup>), manufactured, installed and tested at the KIST. Details of cell characteristics and fabrication procedure are described in previous works [3,4]. The tests were carried out by varying the cell temperature, the anode gas composition and fuel utilization factor, whereas the air flow rate at the cathode was kept constant. Results showed that, for cell temperatures greater than 650°C, the NH<sub>3</sub> decomposition is close to 100%, as depicted in fig. 3, where the comparison between the polarization curves for H<sub>2</sub> 75%-N<sub>2</sub> 25% and 100% NH<sub>3</sub> are reported.

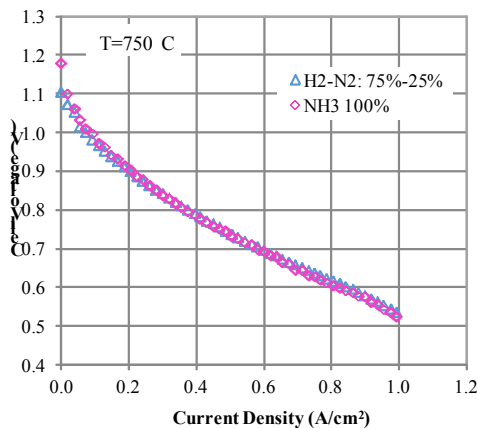


Fig. 3. Polarization curves comparison for dilute hydrogen and ammonia feeding

#### B. Plant's Performance Assessment

The plant's performances have been compared in terms of electricity (E), heat production (Q), hydrogen production ( $\Phi_{H_2}$ ) and trigeneration efficiency, that is calculated as:

$$\eta_{tr} = \frac{E + Q + \Phi_{H_2}}{\Phi_{NH_3}} \quad (1)$$

where  $\Phi_{NH_3}$  is the chemical power of the ammonia feeding the plant (LHV is 22.5 MJ/kg). Table 1 lists the main operating data and performances of the proposed SMP30 and DMP60.

### IV. CONCLUSION

From the results reported in table 1 it is worth noting that the proposed configurations are characterized by the same performances in terms of trigeneration efficiencies even if net

electric power is generated in DMP60 configuration, but the size is quite different. Thus, the choice of the optimal plant configuration depends on economic evaluations based on capital costs and on revenues from produced heat and electricity.

TABLE I. PLANTS PERFORMANCES

Plant Configuration	SPM30	DPM60
<b>Power System</b>	Module	Module 1/Module 2
Stacks number	3	15/4
Cell numbers x stack	50	32
Active area (cm <sup>2</sup> )	550	256
U <sub>F</sub>	0.208	0.208
Average Cell Voltage (V)/Current Density (A/cm <sup>2</sup> )	0.73/0.50	0.73/0.50
NH <sub>3</sub> flow rate (g/s)	11.7	17.6
Anode off gas flow rate (g/s) and composition (% mol)	15.2 (59.5 H <sub>2</sub> ; 25 N <sub>2</sub> ; 15.5 H <sub>2</sub> O)	22.8 (59.5 H <sub>2</sub> ; 25 N <sub>2</sub> ; 15.5 H <sub>2</sub> O)/5.5 (47 H <sub>2</sub> ; 25 N <sub>2</sub> ; 28 H <sub>2</sub> O)
Anode off gas to PSA (%)	100	66.7
Stream flow rate (g/s) to CB and LHV (MJ/kg)	10.1; 5.86	15.4; 8.80
Heat recovery efficiency from CB exhausts (%)	80	80
Stack Power (kW)	10	3
Module Power (kW)	30	45/12
<b>PSA Unit</b>		
Operating p/T (bar/°C)	20/40	20/40
Feeding stream (d.b.g/s)	11.3	11.3
H <sub>2</sub> separation efficiency (%)	70	70
Intercooled Compressor Consumption (polytropic efficiency 60%) (kW)	18	18
<b>H<sub>2</sub> Storage</b>		
Storage pressure (bar)	820	820
Intercooled Compressor Consumption (polytropic efficiency 60%) (kW)	12	12
H <sub>2</sub> stored (g/s)	1.16	1.16
<b>System Performances</b>		
Net electric power	-	27
Thermal power (kW)	47	110
H <sub>2</sub> chemical power (kW)	139	139
NH <sub>3</sub> chemical power (kW)	264	396
Trigeneration efficiency (%)	70.4	69.8

### REFERENCES

- [1] M. Minutillo, A. Perna, E. Jannelli, SOFC and MCFC system level modeling for hybrid plants performance prediction, on Int. J. of Hydrogen Energy, 39 (2014) 21688-99.
- [2] A. Perna, M. Minutillo, E. Jannelli, V. Cigolotti, S.W. Nam, P.Y. Sung. Performance assessment of a hybrid SOFC/MGT cogeneration power plant fed by syngas from a biomass down-draft gasifier. Applied Energy 2017; <https://doi.org/10.1016/j.apenergy.2017.08.077>
- [3] S.-i. Lee, J. Kim, J.-W. Son, J.-H. Lee, B.-K. Kim, H.-J. Je, H.-W. Lee, H. Song, K.J. Yoon, Journal of Power Sources, 250 (2014) 15-20.
- [4] [2] K.J. Yoon, S.-i. Lee, H. An, J. Kim, J.-W. Son, J.-H. Lee, H.-J. Je, H.-W. Lee, B.-K. Kim, International Journal of Hydrogen Energy, 39 (2014) 3868-3878.



## FUEL CELLS AND RELEVANT ENERGY SYSTEMS UNDER DEVELOPMENT AT HYSA SYSTEMS CENTER OF COMPETENCE, UWC, SOUTH AFRICA

S. Pasupathi, C. Sita, and V. Linkov

HySA Systems, SAIAMC, University of the Western Cape, Bellville  
7530, South Africa

**Abstract** - HySA Systems Competence Centre is part of a long-term (15-year) Hydrogen and Fuel Cell Technologies (HFCT) Research, Development, and Innovation (RDI) strategy, which officially was launched in September 2008 by the Department of Science and Technology (DST) in South Africa. HySA Systems Competence Centre is a system integration and technology validation competence centre focused on research, development and innovation in the field of hydrogen and fuel cell technologies. The centre is based at the South African Institute for Advanced Materials Chemistry at the University of the Western Cape.

The main objective with HySA Systems is to (i) develop Hydrogen and Fuel Cell systems, prototypes and products, (ii) perform technology validation and system integration and (iii) focus on system oriented material research in two key HySA-programmes: (1) Combined Heat and Power (CHP) and (2) Hydrogen Fuelled Vehicles (HFV). HySA Systems is also responsible for the development, prototyping, testing and commissioning of the following key technologies: Membrane Electrode Assemblies (MEAs) for High Temperature (HT) ( $\geq 120^\circ\text{C}$ ) Proton Exchange Membrane (PEM) fuel cells and metal hydrides for hydrogen storage and compression. One of the principal objectives for HySA Systems is to establish long-term collaborations with industrial partners, including technology development, engineering and manufacturing companies in South Africa and the rest of the world involved in Hydrogen and Fuel Cell Technologies.

HySA Systems has developed several prototype fuel cell systems, including a 1kW<sub>e</sub> fuel cell combined heat and power (FC-CHP) system, a 2.5 kW backup power system, a 3 tonne fuel cell forklift containing hybrid metal hydride hydrogen storage, to name a few. Currently HySA Systems is busy integrating a 3.2 kW FC system for installation in a rural school. The results from the prototype systems will be presented and discussed.

**Index Terms** – Fuel Cells, Prototype demonstration. System integration, Technology validation.

### I. INTRODUCTION

HySA Systems is one of three National Competence Centres which makes up HySA (Hydrogen South Africa). Initiated by the Department of Science and Technology (DST) and approved by the Cabinet in May 2007, HySA is a long-term (15-year) programme within their Research, Development, and Innovation (RDI) strategy, officially launched in September 2008. This National Flagship Programme is aimed at developing South African intellectual property, knowledge, human resources, products, components and processes to support the South African participation in the nascent but rapidly developing international platforms in Hydrogen and Fuel Cell Technologies. The programme strives towards a knowledge-driven economy meaning that innovation will form the basis of South Africa's economy; this includes an aggressive capacity-development programme's approach. HySA also focusses on (i) the "Use and Displacement of Strategic Minerals", (ii) ways of harnessing South Africa's mineral endowments to promote both the hydrogen economy and renewable energy use, and (iii) seeking the most cost-effective and sustainable ways of incorporating PGM-based components in hydrogen fuel cell and other technologies, in turns resulting in commercialisation ventures and a viable industry around mineral beneficiation.

HySA Systems has integrated, validated and demonstrated various fuel cell powered systems [1]. This presentation will discuss the results from some of these prototypes.

### II. RESULTS AND DISCUSSION

#### A. 1kW<sub>e</sub> CHP System

The CHP system consist of three modules: Power Management & Energy Storage Module (PM&ESM), Reformer

& Fuel Cell Module (R&FCM) and Thermal Energy Storage Module (TESM). The system can be supplied with methane, natural gas or city gas and FLOX®-Compact Steam Reformer C1-HT is used to convert hydrocarbons into hydrogen rich gas. The start-up time is about 1 hour and during this time reformer and fuel cell is preheated to the operating temperature, 840°C and 140°C, respectively. During start-up PM&ESM supplies electrical energy to the system components. 50-cell, 1 kWel HT-PEMFC stack (HTPEM is identified as one of the most suitable technology for CHP application) is integrated within the system construction to generate electrical energy. Non-linear stack voltage is regulated with the aid of DC/DC converter and DC/AC inverter is used to supply AC voltage for the user. The system is designed for standalone operation mode. The heat from stack cooling system is used to heat the water stored in TESH. Two additional heat exchangers are installed to recuperate waste heat from burner and fuel cell stack cathode outlet to increase overall system efficiency. SIEMENS programmable logic controller (PLC) and Weintek human machine interface (HMI) touch panel with data logging functionality is used for system control, communication and data storage.

Figure 1 presents values of temperatures measured at different locations within the system as well as HT-PEMFC stack voltage and current values. As it can be seen the system is ready for operation after about 1 hour of preheating. During this time the reformer is preheated to about 840°C and the fuel cell stack to 140°C prior to supply of the anode with the reformat gas. During the operation the stack temperature is maintained at the level of 160°C and the average single cell voltage stays within safe limit of about 0.6 V measured at stack current density fluctuating between 0.31 A/cm<sup>2</sup> and 0.36 A/cm<sup>2</sup>. TESH nominal operating temperature of 55°C is reached only 5 hours after the fuel cell stack start-up.



**Fig. 1. Selected parameters recorded during FC-CHP system operation**

## B. Fuel Cell 3 Tonne Forklift

HySA Systems has developed a new hydrogen storage system for electric forklifts based on the combination of metal hydride (MH) and compressed hydrogen gas (CGH<sub>2</sub>) hydrogen storage. The system uses original engineering solution of “distributed hybrid” (both metal hydride and CGH<sub>2</sub> hydrogen storage and allows to keep the same hydrogen storage capacity as purely CGH<sub>2</sub> storage tank but at two times lower refuelling pressure. Advanced design of the MH tank allows to achieve good H<sub>2</sub> charge / discharge dynamic performance: more than 95% of the usable H<sub>2</sub> capacity can be reached in 15 minutes of the refuelling at P=185 bar and ambient temperature (83% during 6 minute-long refuelling at the same conditions).

The system was integrated in a commercial 3-tonne electric forklift (STILL) equipped with a commercial fuel cell power module (Plug Power). In addition, a prototype refuelling station (dispensing pressure up to 185 bar) with the integrated MH hydrogen compressor (both MH and CGH<sub>2</sub>) has been developed. Since October 2015, both forklift and refuelling station are under uninterrupted operation at the site of industrial customer, Impala Platinum Limited (South Africa).

## III. CONCLUSION

HySA Systems has delivered successfully and has advanced extremely well against their Business Plans since 2008. The Centre:

- has established some manufacturing facilities/capabilities for HFC components and systems in South Africa
- has demonstrated several prototypes
- has been partnering with key international HFC and local industries to ‘leap-frog’ the technologies for both domestic and automotive applications
- has been disseminating their findings/work in High Impact Factor Journals & National/International Conferences
- has generated Intellectual Property in key HFC technologies
- is working very closely with the HFCT markets and has a competitive edge in some technologies

## ACKNOWLEDGMENT

The authors would like to thank the Department of Science and Technology in South Africa (DST) for financial support under the Hydrogen and Fuel Cell Technologies RDI Programme (HySA).

## REFERENCES

- [1] B G. Pollet, S Pasupathi, G Swart, K Mouton, M Lototskyy, M Williams, P Bujlo, S Ji, B J Bladergroen, V Linkov. Hydrogen South Africa (HySA) Systems Competence Centre: Mission, objectives, technological achievements and breakthroughs. Int. J. Hyd. Energy. 39, 2014, 3577-3596

Copyright © 2017

## EVALUATION OF CO POISONING OF A HT-PEM FUEL CELL BY DISTRIBUTION OF RELAXATION TIMES ANALYSIS

F. Zhou\*, S. K. Kær\*

\*Department of Energy Technology, Aalborg University,  
Pontoppidanstræde 111, Aalborg (Denmark)

**Abstract** – In this work, the distribution of relaxation times (DRT) is used as an alternative method to analyze the impedance spectrum of a HT-PEM fuel cell under different CO poisoning conditions. The results show that there are 3 or 4 peaks in the DRT spectrum in the low (P1), intermediate (P2) and high frequency range (P3 and P4), which can be attributed to mass transfer, cathode charge transfer and anode charge transfer, respectively. P3 and P4 are sensitive to the CO concentration in the H<sub>2</sub>, while operating temperature can influence P2, P3 and P4. This work demonstrates that the DRT analysis is a useful method in analyzing the impedance spectrum of the HT-PEM, especially under CO poisoning conditions.

**Index Terms** – HT-PEM fuel cell; EIS; CO; DRT.

### I. INTRODUCTION

Although higher operating temperature brings better CO tolerance to the HT-PEM fuel cell than its low temperature counterpart, high CO concentration can still influence its cell performance. Electrochemical impedance spectroscopy (EIS) is a commonly used diagnostic tool for the HT-PEM fuel cell. Normally, the impedance spectra of the fuel cell are interpreted with an equivalent circuit (EC) model. However, the EC model approach has some weaknesses. Firstly, the physical meanings of the electric elements in the EC are ambiguous. Furthermore, it is difficult to distinguish different polarization resistances of the fuel cell with different frequency features from the impedance spectrum. Physical based modeling is another method to analyze the impedance data of a HT-PEM fuel cell [1]. In this work, the distribution of relaxation times (DRT) is used as an alternative method for analyzing the impedance spectra of a HT-PEM fuel cell under different CO poisoning conditions in this work.

### II. EXPERIMENTAL

#### A. Experiments

A single HT-PEM fuel cell based on phosphoric acid doped PBI membrane with an active area of 50 cm<sup>2</sup> was adopted in

this work. For all experiments, the compressed air was fed to the cathode with stoichiometry of 4, while pure H<sub>2</sub> or CO contaminated H<sub>2</sub> was fed to the anode with stoichiometry of 2. The current load of the fuel cell was kept at 10 A. The impedance spectrum of the fuel cell was measured and recorded by a Gamry Reference 3000 potentiostat under galvanostatic mode. The frequency of superimposed AC ranged from 10k Hz to 0.1 Hz, and the amplitude was 5% of the current load (0.5 A). In the first set of experiments, the operating temperature was kept at 150 °C while the CO concentration increased from 0% to 1%, 2% and 3%. Then the CO concentration was kept at 3%, the operating temperature was increased from 150 °C to 160 °C and 170 °C.

#### B. DRT analysis

The DRT analysis is based on the fact that every impedance spectrum which obeys the Kramers-Kronig relations can be represented by an infinite numbers of R//C elements [2]. After validated by the Kramer-Kronig relations, the impedance spectrum can be fitted to a model which is composed of quasi-infinite R//C-elements in series. The complex impedance  $Z(\omega)$  is written as:

$$Z(\omega) = R_o + \int_0^{\infty} \frac{\gamma(\tau)}{1 + i\omega\tau} d\tau \quad (1)$$

In Eq. (1)  $R_o$  is the ohmic resistance, while  $\gamma(\tau)$  is the distribution function of relaxation times. The area of the peak equals the polarization resistance of the corresponding loss mechanism. Then the distribution function is discretized to a limited number of time constants.

In this work, a freely available MATLAB GUI, named DRTtools which is based on Tikhonov regularization, was used to calculate the DRTs from the obtained impedance spectra [3]. The regularization parameter was set at 10<sup>-6</sup>, which is a compromise between the oscillation of the calculation residuals and the quality of the DRT profile.

Copyright © 2017

### III. RESULTS AND DISCUSSION

All the obtained impedance spectra were evaluated by Kramer-Kronig relations before they were analyzed by DRTs. The residuals for both imaginary part and real part were less than 0.5%, which proved the good quality of the impedance spectra.

The DRTs of the impedance spectra of the fuel cell under different CO concentrations with the operating temperature of 150 °C are shown in Fig. 1. For fuel cell operated with pure H<sub>2</sub>, there are 3 peaks in the DRT spectrum. While for fuel cell operated with CO poisoning, the DRT spectra show 4 main peaks in the whole frequency range (P1 around 10 Hz, P2 around 10<sup>2</sup> Hz, P3 and P4 around 10<sup>3</sup> Hz). CO in the anode side of fuel cell can strongly bond with the platinum catalyst, covering the surface of catalyst particles and therefore impeding the hydrogen oxidation reaction. Higher CO concentration results in higher CO coverage on the catalyst surface and higher anode charge transfer. From Fig. 1 it can be seen that with CO poisoning there is one more peak around the frequency of 10<sup>3</sup> Hz compared with the spectrum without CO, and the area of P3 increase with the increase in CO concentration. In addition, the anode charge transfer have higher frequency feature compared with cathode charge transfer and mass transfer because of the faster HOR kinetics than the ORR kinetics. Therefore, it is reasonable to deduce that P3 and P4 are related with anode charge transfer resistance. When the operating temperature is stable, the change in the area under the peak P3 reflects the CO concentration level in the H<sub>2</sub>. P1 and P2 remains almost unchanged with the increase in the CO concentration, indicating that the CO poisoning does not influence the mass transfer and ORR in the cathode.

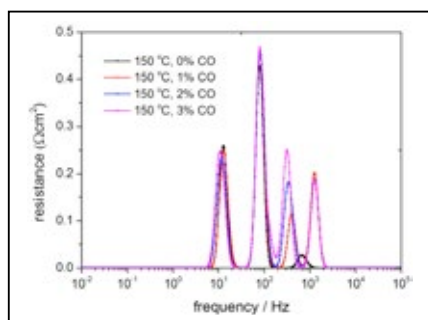


Fig. 1. DRTs calculated from the impedance spectra of the HT-PEM fuel cell operated under different CO concentrations in the H<sub>2</sub> with the operating temperature of 150 °C

In Fig. 2 the DRT spectra of the impedance spectra of the fuel cell under the same CO concentration and different operating temperature conditions are illustrated. With the CO concentration of 3%vol, the increase in the operating temperature brings lower area under the peaks P2, P3 and P4. Higher operating temperature can improve the electrode reaction kinetics for both anode and cathode. Since P3 and P4 are related with the anode charge transfer resistance, the peak

P2 should be related with the cathode charge transfer resistance. P1 is not affected by the CO poisoning and operating temperature, thus it should be related with the mass transfer resistance. Therefore, the mass transfer resistance and the charge transfer resistances in the anode and cathode can be separated in the DRT spectrum.

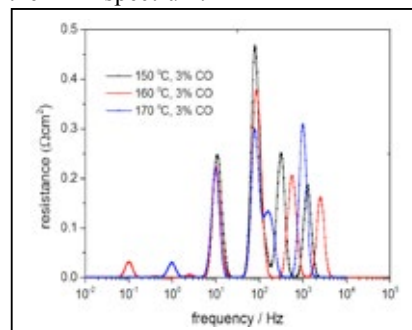


Fig. 2. DRTs calculated from the impedance spectra of the HT-PEM fuel cell under different operating temperatures with 3% of CO in the H<sub>2</sub>

### IV. CONCLUSION

There are 3 or 4 peaks in the DRTs of the impedance spectrum of the HT-PEM fuel cell. P1 in the low frequency range is related with the mass transfer. P2 in the intermediate frequency range is related with cathode charge transfer. While anode charge transfer is responsible for the P3 and P4 which are sensitive to the CO concentration in the H<sub>2</sub>. Operating temperature can affect P2, P3 and P4. The results from this work demonstrate that the DRT is a suitable method for analyzing the impedance spectra and a good diagnostic tool for the HT-PEM fuel cell, especially under CO poisoning conditions.

### ACKNOWLEDGMENT

The authors appreciate the financial support from EUDP project ADDpower (grant number 64014-0525).

### REFERENCES

- [1] Baricci A, Zago M, Casalegno A. A Quasi 2D Model of a High Temperature Polymer Fuel Cell for the Interpretation of Impedance Spectra. *Fuel Cells* 2014;926–37. doi:10.1002/fuce.201300147.
- [2] Voigts M, Kru A, Schichlein H, Mu AC. Deconvolution of electrochemical impedance spectra for the identification of electrode reaction mechanisms in solid oxide fuel cells q. *J Appl Electrochem* 2002;32:875–82.
- [3] Hei T, Saccoccio M, Chen C, Ciucci F. Influence of the Discretization Methods on the Distribution of Relaxation Times Deconvolution: Implementing Radial Basis Functions with DRTtools. *Electrochim Acta* 2015;184:483–99. doi:10.1016/j.electacta.2015.09.097.



(Put paper number here) EFC17242

## DEVELOPMENT OF HIGH PERFORMANCE PROTON-CONDUCTING ELECTROCHEMICAL CELL FOR INTERMEDIATE TEMPERATURE APPLICATION

T. Yamaguchi\*, H. Shimada\*, Y. Fujishiro\*, K. Yamauchi\*\*,  
Y. Mikami\*\*, N. Taniguchi\*\*, T. Kuroha\*\* and Y. Tsuji\*\*

\*Inorganic Functional Materials Research Institute, National  
Institute of Advanced Industrial Science and Technology, 2266-98  
Anagahora, Moriyama-ku Nagoya 463-8560, (Japan)

\*\*Advanced Research Division, Panasonic Corporation, 3-1-1  
Yagumo-naka-machi, Moriguchi 570-8501, (Japan)

**Abstract** - SOFCs have attracted much attention as a highly efficient and low-pollution power generation system. The introduction of a proton conductor as the electrolyte material is expected to improve the fuel cell performance, since the  $H_2$  concentration at the anode side is kept constant regardless of the fuel utilization, and the activation energy of the charge carrier,  $H^+$ , is small. As a result, the power generation performance can be improved over a wide range of the operating temperature.

Among several proton-conducting materials with Perovskite crystal structure were reported to exhibit high conductivity below 750 °C and high chemical stability even under  $CO_2$  and  $H_2O$  atmospheres.  $Ba(Zr_{0.8}Yb_{0.2})O_{3-\delta}$  was selected as an electrolyte material, and Ni-  $Ba(Zr_{0.8}Yb_{0.2})O_{3-\delta}$  cermet and  $(La,Sr)CoO_3$ - $Ba(Zr_{0.8}Yb_{0.2})O_{3-\delta}$  composite were selected as a fuel and an air electrodes materials, respectively. The cell showed open circuit voltages over 1.0 V and worked as a SOFC within the whole temperature range.

**Index Terms** - Solid oxide fuel cell, Proton-conducting electrolyte, Perovskite material, Anode supported cell

### I. INTRODUCTION

Several proton-conducting materials with superior proton conductivity, such as doped  $BaCeO_3$ ,  $SrCeO_3$ ,  $BaZrO_3$ , and  $SrZrO_3$  [1, 2], have been considered as candidate SOFC electrolyte materials. Among these proton-conducting materials, a barium zirconate ( $BaZrO_3$ ) was reported to exhibit high conductivity below 750 °C and high chemical stability even under  $CO_2$  and  $H_2O$  atmospheres [3, 4]. Despite the significant efforts and the potential of wide range of applications, these proton-conducting materials still require improved sinterability to achieve performance by reducing the grain boundary resistance. There have been some attempts to improve the

sinterability of  $BaZrO_3$  by adding a few mole percent of transition metal oxides as sintering aids [5,6]. NiO is one of the particularly successful additives because NiO diffuses into the electrolyte layer during co-sintering of an electrolyte and the conventional NiO-containing anode [7-9].

In this work,  $Ba(Zr_{0.8}Yb_{0.2})O_{3-\delta}$  (BZYb) was selected as a proton conducting material for fuel cell applications. In this study, an anode-supported coin-type cell with a dense BZYb electrolyte layer on the porous anode support was fabricated via co-sintering technique at around 1500 °C. The effect of anode porosity on the cell performance was investigated in the point of view of gas diffusion polarization.

### II. EXPERIMENTAL PROCEDURE

#### A. Cell Fabrication

The anode with 60wt% NiO-40wt% BZYb composition and the BZYb electrolyte were prepared by tape-casting method using slurries ball-milled for 48 hours in an organic solvent. The electrolyte and anode tapes were heat-pressed, then the laminated tape was cut into 30mm-diameter coin shape. We prepared two types of the anode slurries, with/without carbon pore former.

The coin-shaped laminates were sintered in air at around 1500°C for 2 hours, followed by a formation of a 70wt%  $(La,Sr)CoO_3$  (LSC)-30wt% BZYb composite cathode on the BZYb electrolyte surface using screen-printing and heating at 950°C for 1 hour.

The finally fabricated sample was the anode-supported coin-type cell with the anode and cathode diameter of 25mm and 8mm, respectively, and the total thickness of 0.5mm.

Copyright © 2017

### B. Coin Cell Performance Measurement

Current density-voltage (I-V) measurements were carried out for the anode-supported coin cell at 600 °C using 3 vol.% humidified H<sub>2</sub>/N<sub>2</sub> as fuel at a feed rate of 100 mL/min and 3 vol.% humidified air as oxidant at a feed rate of 200 mL/min. Before the electro-chemical measurements, a gold paste was painted on the top surface of both anode and cathode to reduce the current collection loss.

### III. RESULTS AND DISCUSSION

The anode open porosities with and without pore former after reduction in the H<sub>2</sub> atmosphere at 700 °C were 24.0 vol.% and 33.8 vol.%, respectively.

The coin cell was measured using a dual chamber testing method [10]. Figure 1(a) and (b) show the OCV and I-V performances of the cell without pore former, respectively, at 600 °C. The OCV was stable above 0.95 V under the 50 vol.% H<sub>2</sub>-50 vol.% N<sub>2</sub> mixed fuel supply, however the OCV fell down gradually below 0.1 V under the 25 vol.% diluted H<sub>2</sub> fuel supply.

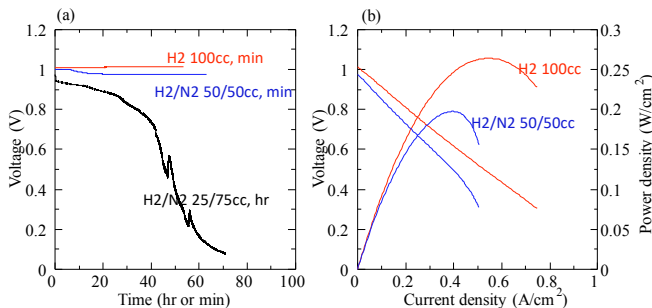


Fig.1 Electrochemical performance of the coin cell without pore former, (a) OCV and (b) I-V curve, at 600 °C

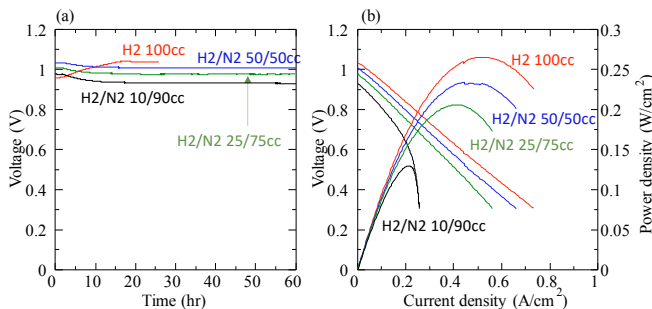


Fig.2 Electrochemical performance of the coin cell with pore former, (a) OCV and (b) I-V curve, at 600 °C

Figure 2(a) and (b) show the OCV and I-V performances of the cell with pore former, respectively, at 600 °C. Unlike Fig.1, the OCV was stable above 0.90 V even under the 10 vol.% H<sub>2</sub>-90 vol.% N<sub>2</sub> mixed fuel supply. The concentration polarization in Fig. 2(b) appeared under the 10 vol.% diluted H<sub>2</sub> fuel, while the polarization in Fig. 1(b) appeared even under the 50 vol.% diluted H<sub>2</sub> fuel.

The protonic transport number of BaZrO<sub>3</sub>-based electrolyte is known to be lower than 1.0, therefore in the case of insufficient anode open porosity, the OCV should decrease below the theoretical OCV due to the internal current leakage by hole conduction at the BZYb electrolyte layer. We successfully defined that the cell performance at lower H<sub>2</sub> concentration condition was improved by controlling the anode open porosity, while the two cells showed almost the same I-V property at higher H<sub>2</sub> concentration condition.

### IV. CONCLUSION

In this study, the NiO-BZYb anode open porosity had a clear criterion for H<sub>2</sub> gas diffusion at around 30 vol.%, just which was a percolation porous structure. The cell with pore former can work as proton conducting fuel cell under a wide H<sub>2</sub> concentration condition.

### ACKNOWLEDGMENT

This research is partially supported by the New Energy and Industrial Technology Development Organization (NEDO).

### REFERENCES

- [1] K. Katahira, Y. Kihchi, T. Shimura, H. Iwahara, Protonic conduction in Zr-substituted BaCeO<sub>3</sub>, volume 138, 2000, pp. 9-98.
- [2] H. Shimada, T. Yamaguchi, H. Sumi, K. Nomura, Y. Yamaguchi, Y. Fujishiro, Improved transport property of proton-conducting solid oxide fuel cell with multi-layered electrolyte structure, volume 364, 2017, pp. 458-464.
- [3] Y. Oyama, A. Kojima, X. Li, R. B. Cervera, K. Tanaka, S. Yamaguchi, Phase relation in the BaO-ZrO<sub>2</sub>-YO<sub>1.5</sub> system: Presence of separate BaZrO<sub>3</sub> phases and complexity in phase formation, Solid State Ionics, Volume 197, 2011, pp. 1-12.
- [4] K. Bae, D. Y. Jang, H. J. Choi, D. Kim, J. Hong, B. Kim, J. Lee, J. Son, J. H. Shim, Demonstrating the potential of yttrium-doped barium zirconate electrolyte for high -performance fuel cells, Nature Communications, Volume 8, 2017, pp. 14553.
- [5] T. Shimura, H. Tanaka, H. Matsumoto, T. Yogo, Influence of the transition-metal doping on conductivity of a BaCeO<sub>3</sub>-based protonic conductor, Solid State Ionics, volume 176, 2005, pp. 2945-2950.
- [6] S. Ricote, N. Bonanos, Enhanced sintering and conductivity study of cobalt or nickel doped solid solution of barium cerate and zirconate, volume 181, 2010, pp. 694-700.
- [7] T. Yamaguchi, H. Shimada, U. Honda, H. Kishimoto, T. Ishiyama, K. Hamamoto, H. Sumi, T. Suzuki, Y. Fujishiro, Development of anode-supported electrochemical cell based on proton-conductive Ba(Ce,Zr)O<sub>3</sub> electrolyte, volume 288, 2016, pp. 347-350.
- [8] E. Kim, Y. Yamazaki, S. M. Haile, H. I. Yoo, Effect of NiO sintering-aid on hydration kinetics and defect-chemical parameters of BaZr<sub>0.8</sub>Y<sub>0.2</sub>O<sub>3-δ</sub>, volume 275, 2015, pp. 23-28.
- [9] J. Tong, D. Clark, M. Hoban, R. O'Hayre, Cost-effective solid-state reactive sintering method for high conductivity proton conducting yttrium-doped barium zirconium ceramics, volume 181, 2010, pp. 496-503.
- [10] M. Liu, J. Gao, D. Dong, X. Liu, G. Meng, Comparative study on the performance of tubular and button cells with YSZ membrane fabricated by a refined particle suspension coating technique, volume 35, 2010, pp. 10489-10494.

## CONCENTRATION GRADIENT OF REACTANTS IN FUEL CELLS EXTENDING FROM REACTION SITES INWARD THE INLET PERIPHERY

Özgür Aydın\*, H. Nakajima\*, and T. Kitahara\*

\*Department of Mechanical Engineering, Faculty of Engineering,  
Kyushu University, 744 Motooka, Nishi-ku, Fukuoka, 819-0395  
(Japan)

**Abstract** –In regard of the mass transport limitation in fuel cells, although the major attention is put on the flow fields in the active area of cells, modules, or stacks, assuming effective transport of species to the active field, we herein present the onset of mass transport limitation already from the inlet periphery, i.e., extension of concentration gradient of hydrogen from reaction sites inward the inlet piping at high rates of fuel utilization in a microtubular Solid Oxide Fuel Cell (SOFC). We disclose the computational error arising from the extended concentration gradient in estimating the concentration of the involving species; to eliminate it, we propose a practical method.

**Index Terms** - Mass Transport Limitation, Concentration Gradient, Inlet Periphery, Modeling Fuel Cells

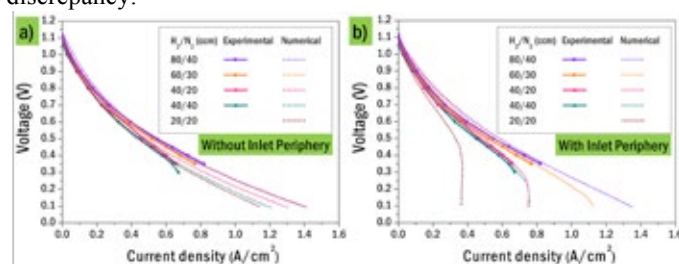
### I. INTRODUCTION

Fuel cells are open systems with continuous inflow of reactants and outflow of surplus reactants along with the reaction products. Transport of both reactants and products to/from reactions sites is crucial in terms of the electrochemical energy conversion performance. At high reactant utilization rates, in fact, mass transport can be the performance-limiting process, giving rise to significant variations of current and related properties (temperature, etc.) in the active part; the variations lead to both performance and structure degradations [1]. To overcome mass transport limitations, reactants can be supplied at sufficiently high rates by proper flow fields (external/internal manifolds, channels, etc.), for design of which numerical modeling is indispensable [2,3]. With an exclusive focus on the inlet periphery, we devoted this study to improving reliability of the numerical studies in terms of modeling mass transport leaning upon longitudinal current measurements in microtubular SOFCs [4].

### II. METHODOLOGY

For investigating mass transport limitation, we conducted

spatially resolved current measurements by applying segmentation method on anode-supported microtubular SOFCs under diverse inflow conditions [4]. The reactant species were dry hydrogen and oxygen being both mixed with nitrogen in anode and cathode, respectively. For simulating the experimental findings, we built a two-dimensional axisymmetric model of the microtubular SOFC in COMSOL Multiphysics [4]. Upon validating the model by conventional current/voltage (I/V) curves under low fuel utilization conditions ( $H_2/N_2=80/40$  ccm), we investigated the electrochemical performance of the cell under higher fuel utilization conditions (Fig. 1). By comparing the numerical and experimental data for the identical conditions, and numerically investigating the properties associated with the flow field, e.g., fluid velocity and hydrogen concentration, we clarified the cause of the discrepancy among the experimental and numerical data, and then we explored ways to reduce the discrepancy.

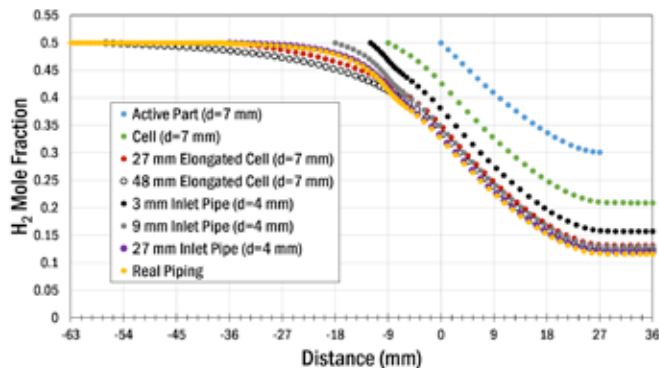


**Fig. 1. In situ acquired conventional I/V curves of the microtubular SOFC with the numerical counterparts computed with/out the inlet periphery for the inlet flow rates shown on the graphs.**

### III. RESULTS AND DISCUSSION

When we built the model solely on the **active part** of the cell [4], neglecting the inlet periphery (passive part, opening,

and piping), as Fig. 1 (a) clearly illustrates, mass transport limitation was not captured at all. Upon investigating the concentration of hydrogen along the inlet periphery as well as along the cell based on Fig. 2, we understand that in reality (Real Piping) mass transport limitation was commencing already from the inlet piping around -36 mm due to the limited convective mass transport associated with the small fluid velocity. As a result, concentration of hydrogen begins to diverge from ca. -36 mm until the reactions sites, making the hydrogen concentration in the cell much lower than that is computed without the inlet periphery (Active Part). We can thus deduce that without considering the inlet periphery the mass transport limitation in the cell was underestimated (Fig. 1(a)) due to the “over-defined” hydrogen concentration at the inlet boundary of the active part. After incorporating the inlet periphery into the model, we were able to simulate the experimental data accurately as in Fig. 1(b).



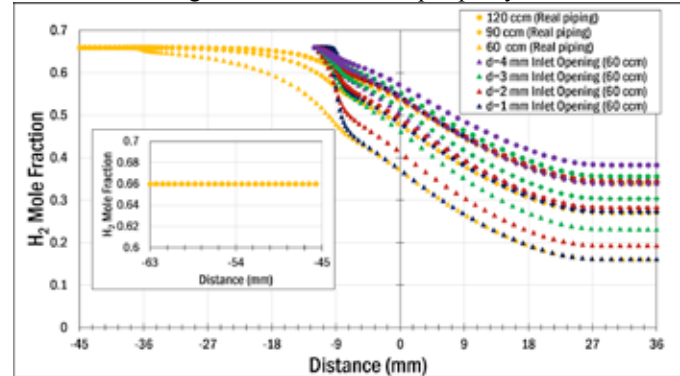
**Fig. 2. Distribution of the hydrogen mole fraction at the centerline of the system from inlet to outlet boundary with respect to the type of the inlet piping at 0.4 V and 80 ccm (298 K) where  $x_{H_2} = 0.5$ .**

Being associated with the velocity of the fuel stream, as Fig. 2 depicts, the extension of the concentration gradient grows with the diameter of the inlet pipe, provided that the inlet opening and the inlet pipe have the identical dimension. Fig. 3 discloses however that the crucial part in the inlet periphery is the inlet opening determining the flow field before the active part of the cell. It further reveals that the hypothetical boost of the convective mass transport by a relatively thin pipe ( $d=1$  mm) can prevent extension of the concentration gradient of hydrogen inward the inlet piping, and hence it can enable accurate computation of the flow field in the active part of the cell.

#### IV. CONCLUSION

We concluded that at high reactant utilization rates mass transport limitation might commence already from the inlet periphery, where the inlet opening plays the critical role. Flow field in the inlet periphery is hence crucial for accurately

defining the inflow conditions at the inlet boundary of numerical models of fuel cells. To accurately compute the mass transport limitation by a numerical model in a channel, cell, or stack of fuel cell, we draw the conclusion that one should either incorporate the inlet periphery, or s/he should design an inlet opening at sufficiently small diameter (Fig. 3) to hypothetically enhance convective mass transport for preventing development of concentration gradient into the inlet periphery.



**Fig. 3. Concentration profiles of hydrogen at the centerline of the system from inlet to outlet boundary with respect to the diameter of the inlet opening at 0.4 V for various inlet flow rates ( $x_{H_2} = 0.66$ ).**

#### ACKNOWLEDGMENT

The first author gratefully acknowledges JSPS (Japanese Society for the Promotion of Science) for “Postdoctoral Fellowship for Overseas Researchers”. The expenses for this conference were covered by the JSPS grant (Grant-in Aid for Young Scientists) No:17F17069.

#### REFERENCES

- [1] D.J.L. Brett, A.R. Kucernak, P. Aguiar, S.C. Atkins, N.P. Brandon, R. Clague, L. Cohen, G. Hinds, C. Kalyvas, G.C. O’er, B. Ladewig, R. Maher, A. Marquis, P. Shearing, N. Vasileiadis, V. Vesovic, What happens inside a fuel cell? Developing an experimental functional map of fuel cell performance, *ChemPhysChem*, Volume 11, 2010, Pages 2714–2731.
- [2] J. Wang, Theory and practice of flow field designs for fuel cell scale-up: A critical review, *Applied Energy*, Volume 157, 2015, Pages 640-663.
- [3] D. Chen, Q. Zeng, S. Su, W. Bi, Z. Ren, Geometric optimization of a 10-cell modular planar solid oxide fuel cell stack manifold, *Applied Energy*, Volume 112, 2013, Pages 1100-1107.
- [4] Ö. Aydın, H. Nakajima, T. Kitahara, Reliability of the numerical SOFC models for estimating the spatial current and temperature variations, *Int. J. Hydrogen Energy*, Volume 41, 2016, Pages 15311-15324.



## ASSESSMENT OF A METHODOLOGY FOR THE CONTROL OF METHANOL CONCENTRATION IN A DIRECT METHANOL FUEL CELL

D. Borello\*, A. Calabriso, F. Rispoli

DIMA Sapienza – Università di Roma, Via Eudossiana 18, Italy

**Abstract** - One of the main issue of DMFC systems is the complexity of the management of anode molar concentration. Since high concentration determines high fuel cross over rate, while low concentration results in high concentration losses, the methanol percentage in the fuel solution is the most important parameter to be constantly monitored and controlled. In this paper, a control algorithm to keep constant the methanol concentration in the anode circuit was implemented and tested. The test was performed on a DMFC short stack made of 5 MEAs with surface area  $25 \text{ cm}^2$  each, load catalysts of  $4 \text{ mg cm}^{-2}$  with only Pt at the cathode and a bimetallic Ru/Pt catalyst at the anode. The control was tested at different temperature conditions (60, 65 and  $70^\circ\text{C}$ ), at cathode-anode overpressure of  $\pm 30 \text{ mbar}$  and evaluating the percentage displacement from the molar concentration set point.

**Index Terms** – Direct Methanol Fuel Cell, Fuel Crossover.

### I. INTRODUCTION

Commercial systems control the molar concentration by methanol sensors. Even if the cost of the methanol sensor on commercial prototype can increase up to 15 % the cost of the whole system, new sensors based on new technologies are going to reduce sensor costs [1]. However, sensor-less systems [2] could reduce costs and maintenance issues, even if their algorithms can hardly take into account the rate of degradation of the DMFC, which performances could change depending on its operating conditions (temperature, number of startup, quality of the fuel and water) [3]. On the contrary, the strong advantages of sensor-based algorithms are 1) reliability, 2) easy management and 3) unnecessary preliminary characterization of the stack crossover and catalyst degradation.

### II. EXPERIMENT SET UP

Fuel reintegration, during fuel cell operation, depends on the generated current and crossover losses. The dedicated test bench, in this study, is equipped with a refractometer, which detect the methanol concentration continuously, a current

sensor, to take into account the methanol consumption, pressure transducers and thermocouples to monitor pressure and temperature of the system. An analogical signal switches the pump on, when fresh fuel is needed computing the time and the pump flow rate at each reintegration. Furthermore, a sensor level located on the mixing tank switches the Water Dosing Pump on when the fuel level in the mixing tank drops. Such pump, in real applications would be replaced by a condenser, which recovers generated and cross over water from cathode channels. A scheme of the assembled test bench is shown in Fig. 1.

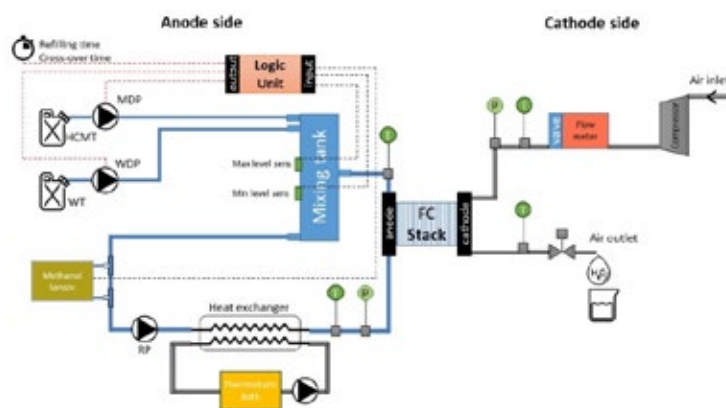


Fig. 1 – Test bench set up

The stack is a 5 DMFCs assembly, with  $240 \text{ cm}^2$  of total surface, made with Nafion membrane and Pt-Ru catalysts at the anode and Pt catalysts at the cathode. The control of methanol concentration in the anode side, represented with the Logic Unit box, was implemented with a PID control developed within a Labview code.

### III. RESULTS

#### A. Crossover measurement

Since high concentration determines high fuel cross over rate, while low concentration results in high concentration losses, the methanol percentage in the fuel solution is the most important parameter to be constantly monitored and controlled. In order to set a range of appropriate flow rate for fresh fuel delivered by the Methanol Dosing Pump (MDP), a preliminary experiment performed the measurement of the fuel lost from the anode through membrane permeation at zero current. In order to consider a variable range of working conditions, the temperature was limited in a range of  $60\div 70\text{ }^{\circ}\text{C}$  and the anode overpressure set at 30 mbar as it is shown in Fig. 2.

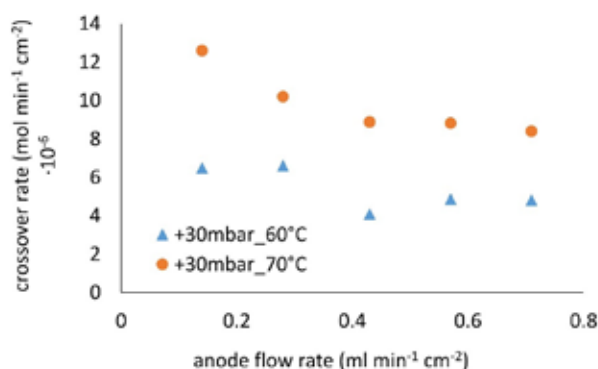


Fig. 2 – Crossover rate with anode overpressure

Sometimes, it could be convenient reducing the anode overpressure in order to reduce the osmotic crossover rate. In Fig. 3, a cathode overpressure of 30 mbar was set by a valve located downstream the cathode.

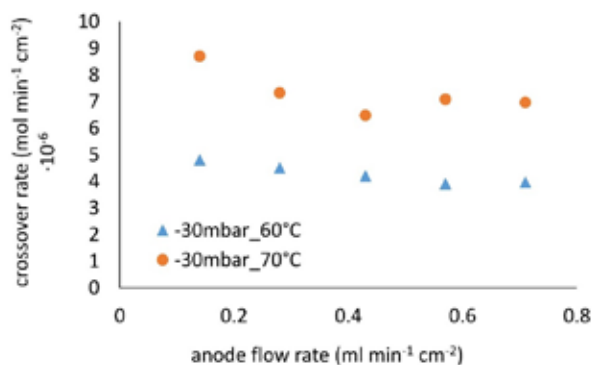


Fig. 3 – Crossover rate with cathode overpressure

The results showed a decrease in crossover rate of about a 20%. These preliminary tests were useful to set the nominal crossover around a mean flow rate of  $7\text{ mL min}^{-1}\text{ cm}^{-2}$  and to determine the mean flow rate of dosing pumps.

#### B. Test of control algorithm

The proportional and integrative coefficients were set in order to keep the methanol concentration constant around an

optimal value of 0.8 M, which keeps the diffusive crossover losses low [4]. As it can be seen from Fig. 4, after the methanol concentration reaches the set point value (at 190'), the methanol consumed by a current generation of  $100\text{ mA cm}^{-2}$  and by the membrane permeation is replaced with a small fresh fuel quantity continually delivered by the MDP in the mixing tank.

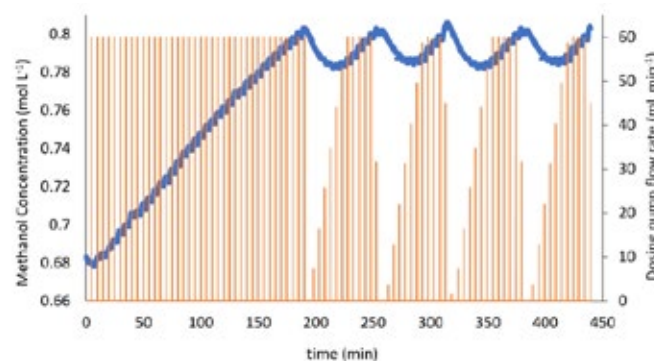


Fig. 4 – Methanol concentration (blue) and fresh methanol flow (red) at the anode inlet

When the measured concentration drops down the pump delivers an increasing quantity of fresh methanol until the set point value is reached again. The control allows to keep constant the methanol concentration for long time within a percentage range of 1.2 %.

### IV. CONCLUSION

A control algorithm to regulate the methanol concentration in the anode side of a DMFC system has a primary importance for system engineering. The PID control implemented in this work keeps the molar concentration constant in a range of 1.2 % around the set point value. A preliminary crossover test was performed in order to characterize the stack losses and to define the operating range of water and methanol dosing pumps.

### REFERENCES

- [1] E. Akbari, Z. Buntat, A. Nikoukar, A. Kheirandish, M. Khaledian e A. Afroozeh, «Sensor application in Direct Methanol Fuel Cells (DMFCs),» *Renewable and Sustainable Energy Reviews*, vol. 60, pp. 1125-1139, 2016.
- [2] M. G. An, A. Mehmood e H. Y. Ha, «A sensor-less methanol concentration control system based on feedback from the stack temperature,» *Applied Energy*, vol. 131, pp. 257-266, 2014.
- [3] K. S. Shen, C. C. Wan, Y. Y. Wang, T. L. Yu e Y. J. Chiu, «An algorithm for sensor less fuel control of direct methanol fuel cells,» *Journal of Power Sources*, vol. 195, pp. 4785-4795, 2010.
- [4] A. Calabriso, S. Santori, L. Del Zotto, L. Cedola e F. Rispoli, «Performance investigation of passive direct

## HYDROGEN PRODUCTION FROM GLYCEROL STEAM REFORMING: A THERMODYNAMIC AND EXPERIMENTAL INVESTIGATION OVER HYDROXYAPATITE CATALYSTS

R. Z. Domingues<sup>1</sup>, A. Lima da Silva<sup>1</sup>, T. Matencio<sup>1</sup>, S. N. da Silva<sup>2</sup>, and D. B. Mendes<sup>1</sup>.

<sup>1</sup>Federal University of Minas Gerais (UFMG), Materials and Fuel Cell Laboratory (LAMPAC), Av. Pres. Antônio Carlos, 6627 – 31270-901 – Belo Horizonte, MG (Brazil)

<sup>2</sup>Federal Center for Technological Education of Minas Gerais (CEFET/MG), Av. Amazonas, 5253 – 30421-169 – Belo Horizonte, MG, (Brazil)

**Abstract** - In the present work, hydrogen production through glycerol steam reforming has been investigated both theoretically and experimentally. Glycerol conversion into H<sub>2</sub> and CO is evaluated over Ni-supported hydroxyapatite catalyst, in the temperature range of 573-873K, for H<sub>2</sub>O/glycerol molar ratio of 6:1. Then, thermodynamic analysis based on Gibbs energy minimization approach is carried out to evaluate the performance of synthesized catalyst. The catalytic activity is very low in temperature range of 573-673K; however, its activity is greatly improved at 773 and 873K, resulting in H<sub>2</sub> concentrations of 51 and 68%, respectively, comparing well with thermodynamic results (50 and 63%). In absence of catalyst, H<sub>2</sub> concentration is of only 9 and 38% at 773 and 873K, respectively. The suitable catalytic activity at relatively low temperatures (773-873K) shows that Ni-supported hydroxyapatite could be a potential candidate for application in reformers of Combined Heat and Power units based on Solid Oxide Fuel Cells (SOFC-CHP).

**Index Terms** – Catalysis; Glycerol; Hydrogen Production; Hydroxyapatite.

### I. INTRODUCTION

Fuels from renewable sources, such as biodiesel and ethanol, are already well established in several markets, but there are others such as bio-kerosene, green diesel and hydrogen that have enormous potential for technological application. Nowadays, approximately 48% of all hydrogen produced comes from steam reforming methane, 30% from naphtha reform and 18% from coal gasification, nonrenewable source substrates. However, other sources for hydrogen generation have been considered to reduce the use of fossil materials, such

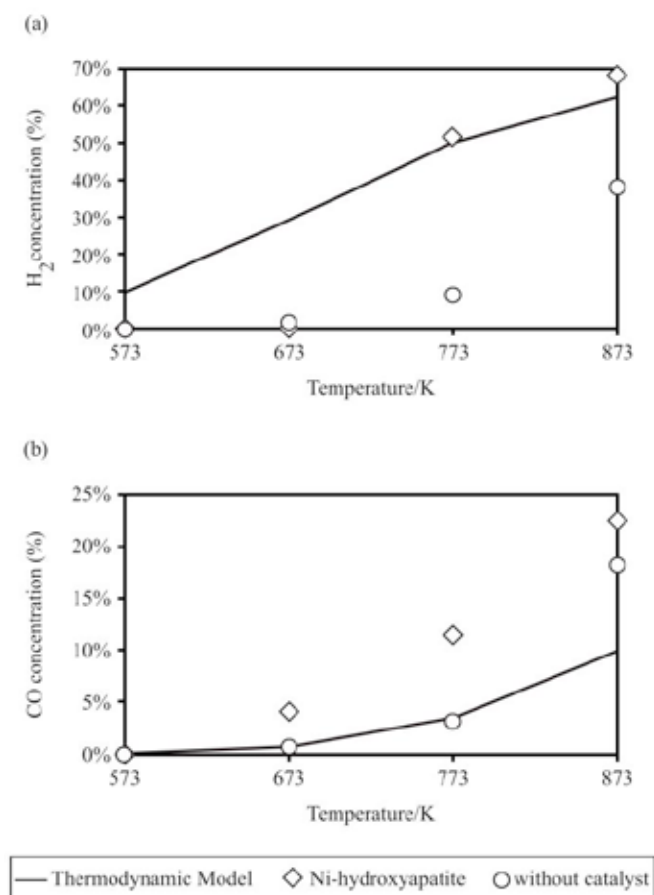
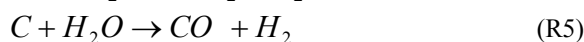
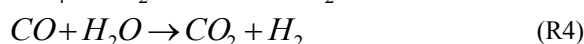
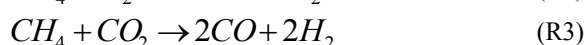
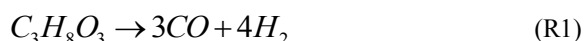
as sodium borohydride (NaBH<sub>4</sub>), as well as steam reforming of ethanol and glycerol [1]. Among these options, catalytic reform presents a great potential, since the industry already uses this process extensively, not requiring major changes in production and distribution facilities. The present work evaluates the hydrogen production from glycerol steam reforming using both thermodynamic simulation and experimental investigation, over Ni-hydroxyapatite catalysts.

### II. METHODOLOGY

The synthesis of the catalyst/support is carried out using the neutralization method; Ni-doped hydroxyapatite samples were prepared adding NiO in phosphoric acid before neutralization [2]. The nickel content as well the grain size of the formed catalysts were chosen to provide homogeneous products. Samples used in this work have 3 % mole of Ni and grain sizes of 100 microns. X-ray diffraction (DRX) confirmed the crystallinity of hydroxyapatite formed. The Ca/P ratio of 1.67 remains after Ni introduction. The reform system consists of a peristaltic pump that feeds one side of a stainless-steel tube through a needle, and the glycerol: water mixture is driven by an inert gas. The opposite side of this tube is connected to a gas chromatograph (GC). Experimental essays for glycerol steam reforming were conducted at H<sub>2</sub>O/C<sub>3</sub>H<sub>8</sub>O<sub>3</sub>=6:1, in temperature range of 573-873K. The measured concentrations (expressed in dry basis, inert free) of H<sub>2</sub>, CO, CO<sub>2</sub> and CH<sub>4</sub> are compared with thermodynamic results.

### III. RESULTS

**Figure 1** shows experimental data ( $H_2$  and CO concentrations) along with thermodynamic results for glycerol steam reforming. Thermodynamic analysis shows that, in temperature range of 573-873K, glycerol is entirely converted into  $H_2$ , CO,  $CO_2$  and  $CH_4$ . As one can see from theoretical curves,  $H_2$  and CO concentrations increase with increasing temperature. This behavior is attributed to endothermic reactions of glycerol decomposition (R1), methane steam reforming (R2) and methane dry reforming (R3). While  $CO_2$  production is maximized at low temperatures, CO is greatly increased at higher temperatures, which is supported by the exothermic water-gas shift reaction (R4).



**Fig.1** Concentration (mole%, dry basis, inert free) of (a)  $H_2$  and (b) CO.

Thermodynamic curves are useful for evaluating the performance of synthesized catalysts. **Fig. 1(a)** shows that in absence of catalyst,  $H_2$  concentration is much lower than that predicted by thermodynamics, and high temperatures would be required to enhance glycerol pyrolysis. However, in the presence of Ni-hydroxyapatite catalyst,  $H_2$  concentration is greatly enhanced at 773 and 873K, reaching values very close to those predicted by thermodynamics. At lower temperatures, the catalytic activity was very low. **Fig.1(b)** shows that experimental CO concentration is much greater than theoretical one, specially at 873K. This behavior can be attributed to experimental approach adopted in this study. The samples were continuously heated from 573 to 873K in the same reactor; in this way, the cumulated carbon over Ni catalyst could be continuously gasified during experiments through reaction (R5), leading to  $H_2$  and CO concentrations greater than thermodynamic values. In this sense, our research group is currently working in new tests to overcome this issue. At 873K, the composition achieved with Ni-hydroxyapatite catalyst was 68%  $H_2$ , 23% CO, 13%  $CO_2$  and 4%  $CH_4$ ; under the same conditions, thermodynamic composition is 62%  $H_2$ , 10% CO, 24%  $CO_2$  and 4%  $CH_4$ .

### IV. CONCLUSION

Preliminary evaluation of Ni-hydroxyapatite catalyst for glycerol steam reforming was carried out. The catalyst exhibits high activity at relatively low temperatures, 773-873K, which makes it a potential candidate for reformers in SOFC-CHP applications.  $H_2$  concentration was close to thermodynamic predictions, of 50-68%, in temperature range of 773-873K.

### ACKNOWLEDGMENT

CAPES, CNPq, FAPEMIG, UFMG, CEFET/MG.

### REFERENCES

- [1] EBSHISH, A. *et al.* The Activity of Ni-Based Catalysts on Steam Reforming of Glycerol for Hydrogen Production. *International Journal of Integrated Engineering*, v. 3, n. 1, p. 5–8, 2011.
- [2] STANIĆ, V. *et al.* Synthesis, characterization and antimicrobial activity of copper and zinc-doped hydroxyapatite nanopowders. *Applied Surface Science*, v. 256, n. 20, p. 6083–6089, 2010.



## INTERFACE DIFFUSION IN $\text{Gd}_{0.1}\text{Ce}_{0.9}\text{O}_{1.95}$ THIN BUFFER LAYERS SPUTTER DEPOSITED ON CRYSTALLINE SUBSTRATES FOR SOLID OXIDE CELLS APPLICATIONS

N.Coppola\*, G.Carapella\*\*, L.Maritato\*, C.Sacco\*, C.Pianese\*\*\*

\* Dipartimento di Ingegneria Industriale-DIIN, Università di Salerno and CNR-SPIN, Fisciano (SA), (Italy)

\*\*Dipartimento di Fisica-DF, Università di Salerno and CNR-SPIN, Fisciano (SA), (Italy)

\*\*\*Dipartimento di Ingegneria Industriale-DIIN, Università di Salerno, Fisciano (SA), (Italy)

**Abstract-** GDC thin buffer layers have been grown on different crystalline substrates by RF Sputtering techniques. The diffusion phenomena at the GDC/substrate crystalline interfaces have been analyzed in view of future applications for PVD deposited Solid Oxide Cells (SOC).

**Index Terms** – Solid Oxide Cells, Sputtering, Crystalline substrate, Interface diffusion phenomena.

### I. INTRODUCTION

Solid Oxide Cells (SOC) are among the most efficient devices for energy conversion, acknowledged for their great efficiency, low emissions, the possibility to operate with a great variety of fuels, in case of Solid Oxide Fuel Cells (SOFC) [1], and great performances in fuel's regeneration in case of Solid Oxide Electrolyser Cells (SOEC) [2]. Large scale production and use of SOC aims at the reduction of process costs and the improvement of their durability. Presently, working temperatures of commercial SOC, generally using Y-stabilized Zr (YSZ) as electrolyte, range from 800°C to 1000°C, determining quite fast performance degradation of the materials composing the cell, mainly at the interfaces. The use of Physical Vapour Deposition (PVD) techniques for the production of SOC is very promising to this respect, allowing both reduced electrolyte thickness (below 1  $\mu\text{m}$ ) and lower working temperatures [3]. Moreover, recent results [4] have shown that the presence of a thin Gadolinium Doped Ceria (GDC) buffer layer at the cathode/electrolyte interface is able to limit inter-diffusion processes and to increase the final performances of the device. PVD RF Sputtering techniques are widely used in several large scale industrial applications and have been recently proposed for innovative SOC production processes [5]. We deposit thin GDC buffer layers by RF Sputtering technique on different crystalline substrates ( $\text{Al}_2\text{O}_3$ ,

$\text{MgO}$ ,  $\text{SiO}_2$  and YSZ) to study, at different annealing maximum temperatures, the surface morphology, the growth of spurious phases and the inter-diffusion phenomena in the presence of different clean GDC/substrate interfaces. The obtained results are very promising for future developments in the PVD production of thin GDC buffer layers on YSZ commercial electrolytes.

### II. EXPERIMENTAL

#### A. Research Methods

GDC buffer layers are deposited by RF Sputtering technique by two different processes: 1) a reactive RF Sputtering process starting from a metallic target [6] (Ce-Gd 90-10 at% ), and 2) a standard RF Sputtering process using an oxide target ( $\text{CeO}_2\text{-Gd}_2\text{O}_3$  90-10%). In particular, when using the metallic target beside the process gas, which is Ar, we also add oxygen in the deposition chamber to obtain desired oxide. Typical deposition parameters are: 400 W applied to a 6 inch diameter target for both processes; Ar partial pressure of 2.0-4.5 mTorr and  $\text{O}_2$  partial pressure of 0.5 mTorr for the reactive RF Sputtering and Ar pressure of 4.5 mTorr for the standard process.

Low angle X-Ray Reflectivity (XRR) and high angle X-Ray Diffraction (XRD) measurements are performed using a diffractometer in Bragg-Brentano geometry. The analysis of XRR allows the measure of the GDC buffer layer thickness, while XRD analysis gives information on the crystal phases present in the sample.

We investigate and study the sample surface morphology by Atomic Force Microscopy (AFM), the local stoichiometric composition by Energy Dispersive Spectroscopy and the

GDC/substrate interface diffusion by transverse Scanning Electron Microscopy.

## B. Results

Firstly we have compared the two RF Sputtering processes in terms of the GDC deposition rates and the as-grown stoichiometry of the produced layers. The varied parameters were the applied power and the gas pressure. In Fig.1 we show XRR spectra and the related deposition rates typically obtained by the two processes. The two final rates, evaluated as in [7], are very close. This is probably due to the oxidation of the metallic target after a certain number of subsequent depositions. Nevertheless, process 2) causes a greater overheating of the target and this can limit its use in industrial scale applications or may lead to a longer process.

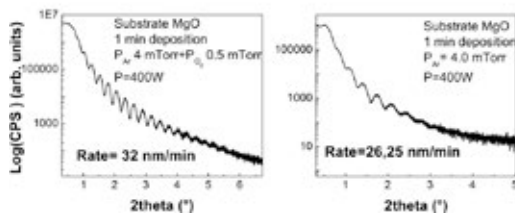


Fig. 1. XRR spectra, related deposition rates and deposition parameters for: a sample grown with process 1) and with process 2).

XRD measurements on the as-grown samples do not show the presence of any significant spurious crystal phase with the GDC peaks located at lower angles than those expected for the bulk material ( $2\theta_{111}=28.53$ ) [8]. A post deposition annealing treatment in atmosphere for two hours with increasing annealing temperatures  $T_a$ , see Fig. 2, results in (111) reflection peaks closer to the bulk values as the temperature increases. For  $T_a > 700^\circ\text{C}$ , we have obtained the expected bulk peak value with the related bulk c-axis value of  $c_{111}=5.41\text{\AA}$ , thus confirming the achievement of the optimal oxidation and stoichiometry on our sputtered samples.

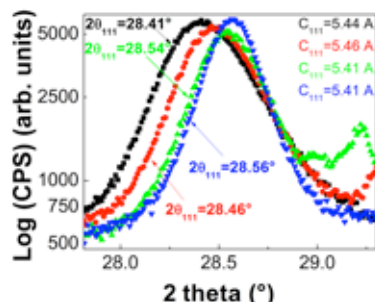


Fig. 2. (111) diffraction peaks position as a function of the annealing temperature  $T_a$  for a sample grown by process 2) on  $\text{SiO}_2$  substrate. Black  $T_a=600^\circ\text{C}$ , red  $T_a=700^\circ\text{C}$ , green  $T_a=800^\circ\text{C}$ , blue  $T_a=900^\circ\text{C}$

In Fig.3 we show an AFM surface image of the sample deposited using process 2) on  $\text{SiO}_2$  and annealed at  $900^\circ\text{C}$ . The 300 nm thick film shows a good surface roughness, as low as  $S_q=1.7\text{ nm}$  on a micron squared. As can be appreciated, the layer is nano-crystalline and rather dense, a quite desirable

property for using GDC thin film as diffusion barrier. Similar measurements are in progress on GDC buffer layers deposited on YSZ crystalline substrates annealed at different  $T_a$  values. Also for these samples, the presence of interface spurious phases and the GDC/substrate inter-diffusion is investigated by XRD and transversal Scanning Electron Microscopy.

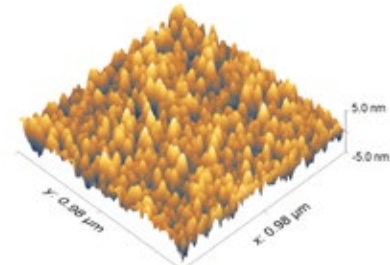


Fig. 3 AFM scan of sample grown with process 2) on  $\text{SiO}_2$  substrate (thickness=300nm) after annealing treatment at  $900^\circ\text{C}$ .

## III. CONCLUSION

GDC thin buffer layers have been grown on different crystalline substrates by RF Sputtering techniques. The obtained results give important insights in the study of the inter-diffusion phenomena at a clean GDC/substrate interface. In particular, the performed analysis at the GDC/YSZ crystalline interface will represent the first step for the evaluation of the final performances of PVD deposited GDC barrier layers in real SOC using porous YSZ as electrolyte and will open the way to innovative applications of PVD techniques for SOC large scale production.

## REFERENCES

- [1] Ravi Chandran, P., Arjunan, T. V., A review of materials used for Solid Oxide Fuel Cells, International Journal of ChemTech research, Vol. 7, No.01, pp 488-497, 2014-2015
- [2] Hauch, A., Jensen S. H., Ebbesen S. D., Mogensen M., Durability of Solid Oxide electrolysis cells for hydrogen production, Risoe reports. 1608: 327-338, 2009
- [3] Kerman, K., Lai, B., Ramanathan, S., Free standing oxide alloy electrolytes for low temperature thin film solid oxide fuel cells, Journal of Power Sources, 202, pp 120-125, 2012
- [4] Huang, H. Nakamura, M., Su, P., Fasching, R., Saito, Y., Prinz, F. B., High-Performance ultrathin Solid Oxide Fuel Cells for Low-temperature operation, Journal of the Electrochemical Society, 154(1), B20-B24, 2007
- [5] Beckel, D., Bieberle-Hütter, A., Harvey A., Infortuna, A., Muecke, U.P., Prestat, M., Rupp, J.M.L., Gauckler, L.J., Thin films for micro solid oxide fuel cells, Journal of Power Sources, 173(1), 325-345, 2007
- [6] Maritato, L., Falco, C.M., Deposition Techniques for high  $T_c$  films, Modern Physics Letters B, vol. 04, Issue 10, 639, 1990
- [7] Fewster P.F., X-Ray analysis of thin films and multilayers, Reports on progress in Physics, vol 59, pp. 1339-1407, 1996
- [8] Cheng, J., Zha, S., Huang, J., Liu, X., Meng, Y., Sintering behavior and electrical conductivity of  $\text{Ce}_{0.9}\text{Gd}_{0.1}\text{O}_{1.95}$  powder prepared by the casting process, Materials Chemistry and Physics 78, pp. 791-795, 2003

<sup>1</sup> In terms of Miller Index

## QUALITY ASSURANCE IN SOFC MANUFACTURING – THE qSOFC PROJECT

Stephen J. McPhail<sup>a</sup>, Anton Litke<sup>b</sup>, Roderik Höppener<sup>b</sup>,  
Markus Rautanen<sup>c</sup>, Sergii Pylypko<sup>d</sup>, Enn Öunpuu<sup>d</sup>, Simon  
Hailer<sup>e</sup>, Matti Noponen<sup>f</sup>, Robert Berger<sup>g</sup>, Sven Aheimer<sup>h</sup>

<sup>a</sup> ENEA, Via Anguillarese 301, Rome (Italy)

<sup>b</sup> Haiku Tech, Spoorweglaan 16, Maastricht (Netherlands)

<sup>c</sup> VTT, Biologinkuja 5, Espoo (Finland)

<sup>d</sup> Elcogen AS, Valukoja 23, Tallinn (Estonia)

<sup>e</sup> ElringKlinger, Max-Eythstraße 2, Dettingen (Germany)

<sup>f</sup> Elcogen Oy, Niittyvillankuja 4, Vantaa (Finland)

<sup>g</sup> Sandvik AB, Asgatan 1, Sandviken (Sweden)

<sup>h</sup> MüKo Mascinenbau, Heinkelstrasse 46, Weinstadt (Germany)

**Abstract** – In the qSOFC project, funded by the FCH 2 JU, improvements are being realized in the manufacturing processes across the entire SOFC stack supply chain. In this article, the first results of a non-destructive 3D visual inspection system are presented, that should allow fault detection in line with the fabrication process, which allows to increase the quality assurance of produced cells, reduce scrap rates and processing times.

**Index Terms** – SOFC, manufacturing, quality assurance.

### I. INTRODUCTION AND AIM OF THE QSOFC PROJECT

The qSOFC project combines leading European companies and research centres in the stack manufacturing value-chain with two companies specialized in production automation and quality assurance to optimize the current stack manufacturing processes for mass production. Currently the state-of-the-art SOFC system capital expenditure (capex) is 7000-8000 €/kW of which the stack is the single most expensive component. This project focuses on SOFC stack cost reduction and quality improvement by replacing manual labour in all key parts of the stack manufacturing process with automated manufacturing and quality control.

During the qSOFC project, key steps in cell and interconnect manufacturing and quality assurance will be optimized to enable mass-manufacturing. This will include development and validation of high-speed cell-manufacturing process, automated 3D machine vision inspection method to detect defects in cell manufacturing and automated leak-tightness detection of laser-welded/brazed interconnect-assemblies.

The project is based on the products of its industrial partners in stack-manufacturing value-chain (ElringKlinger, Elcogen AS, Elcogen Oy, Sandvik) and motivated by their interest to further ready their products into the mass manufacturing market. Two companies specialized in production automation and quality control (Müko, HaikuTech) provide their expertise to the project. The two research centres (VTT, ENEA) support these companies with their scientific background and validate the produced cells, interconnects and stacks.

### II. 3D VISION INSPECTION SYSTEM FOR CELL QUALITY ASSURANCE

Elcogen AS and HaikuTech tasks in qSOFC are the development of a high-speed cell-manufacturing process with an in-line automated 3D vision inspection to detect cell defects down to 10 micron pinhole size. The defects to be detected range in size from 10 micrometre holes to large cracks. The in-line inspection has to be carried out within seconds at high magnification, thus requiring challenging optics and data analysis rates.

The illumination was optimized to see surface and sub-surface 3D features in the ceramic plates. The 3D craters, cracks and pinholes present can be perceived by humans, but are very difficult to detect by conventional image analysis algorithms, leading to either under detection of faults or a large number of false-positives. To address these issues, HaikuTech is exploring Neural Networks for machine vision analysis. The recent quantum leap in availability of low cost computational power enables a fast progress of Deep Learning. Akin to human vision,

Neural Networks can learn to recognise features present in images with better than 99% reliability. This is especially interesting for detection of surface and sub-surface 3D defects in SOFC cells. Intelligent object recognition and classification can also be used for smart quality control and product grading based on the size, type, and location of surface defects with negative impact on the cell's performance. At the same time surface features with little to no adverse effect can be ignored by the system reducing the number of false positive detections.

Early results obtained with Deep Learning for detection and categorization of 3D surface defects (Figure 1) look very promising. Currently, HaikuTech works on further optimization of image analysis algorithms and development of an automated Intelligent Optical Analysis System prototype.

### III. CONCLUSION: OPTIMIZATION OF THE ENTIRE SOFC STACK MANUFACTURING CHAIN

In line with the innovations brought about by Elcogen AS and HaikuTech on in-line automated 3D vision inspection, ENEA will validate achieved improvements in Elcogen AS cell manufacturing processes through focused, in-depth electrochemical characterization of the successive cell batches being produced. But other SOFC stack manufacturing processes are also being addressed in qSOFC.

ElringKlinger will develop automated interconnect manufacturing processes with MüKo Maschinenbau and quality control based on their vast experience in fuel cell stack-building and stack design, but also in mass-manufacturing of automotive steel parts. In addition, a specific failure modes and effects analysis for SOFC interconnects will be performed by ElringKlinger. Sandvik Materials AB will supply optimized pre-coated steel for the manufacturing of reliable and cost-effective interconnects. Together with Elcogen Oy, prescribing the interconnect design, quality assurance methods for the complete interconnect-assemblies will be implemented, including processes for fast leak tightness and planarity measurements.

Elcogen Oy and VTT will collaborate on optimizing stack assembly and reducing factory through-time by speeding up the stack conditioning process. The assembled stacks will be adequately characterized and quality checked for the validation of the integrated manufacturing improvements. These should lead to stack costs of 1000 €/kW and create a further cost reduction potential down to 500 €/kW at mass production (2000 MW/year).

### ACKNOWLEDGMENT

This project is supported by the European Commission through the Fuel Cells and Hydrogen Joint Undertaking (FCH 2 JU) under Grant agreement 735160.

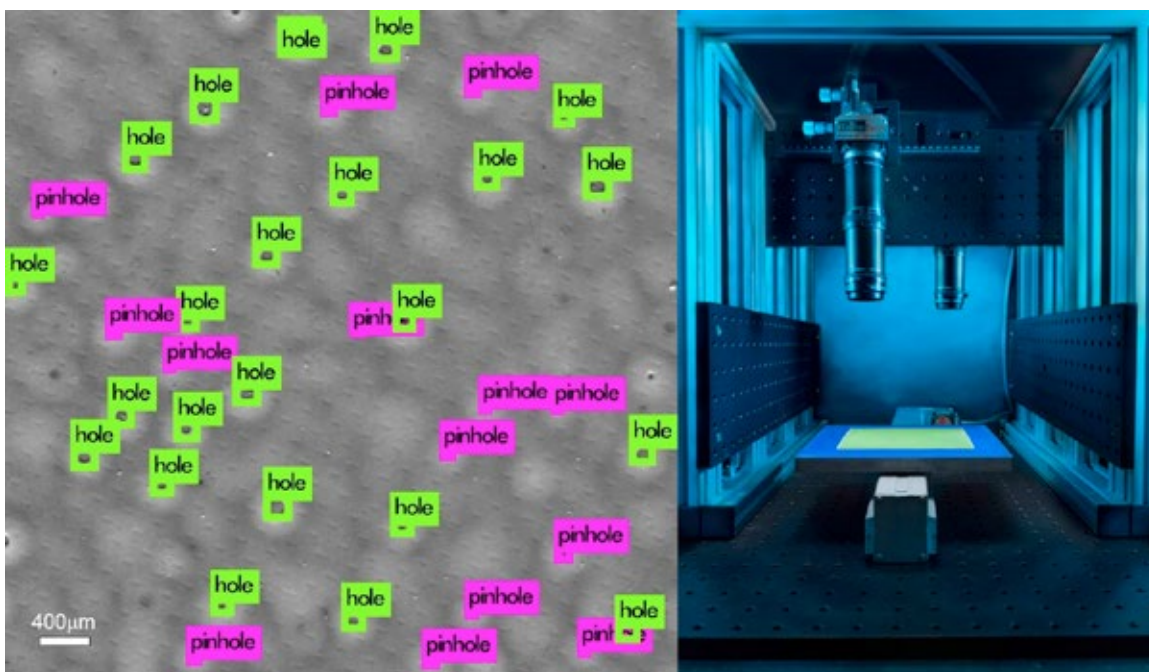


Fig. 1. Results of analysis of a high resolution image with detected large holes and pinholes (10-30 μm) in the ceramic layer (left). The setup developed automatic acquisition and analysis of high resolution images of green and fired ceramic samples (right).



## INFLUENCE OF THE GEOMETRY AND NATURE OF SUBSTRATE IN BIOFILM FORMING THERMOTOGA NEAPOLITANA CULTURES

G. Squadrito<sup>a</sup>, A. Fontana<sup>b</sup>, G d'Ippolito<sup>b</sup>, A. Sardo, P. Cristiani<sup>c</sup>

<sup>a</sup>Institute of Advanced Technologies for Energy (ITAE), National Research Council (CNR), Messina Italy

<sup>b</sup>Institute of Biomolecular Chemistry (ICB), National Research Council (CNR), Pozzuoli (Na) Italy

<sup>c</sup>RSE – Ricerca sul Sistema Energetico S.p.A., via Rubattino, 54, 20100 Milano, Italy

**Abstract** – The capability of hyperthermophilic and strict anaerobic *Thermotoga neapolitana* to adhere on different materials was investigated in this work. Different geometries of conductive and not conductive substrates are tested, including: porous alluminosilicate (unconductive), carbon cloth (conductive) carbon felt (conductive) and other substrates. The materials were tested in bioreactors of 250 mL, operated for 14 days at temperature of 80°C with a culture media of *T. neapolitana* containing 5 g/L glucose. A specimen of the tested substrates were immersed on the bottom of the bioreactors, one in each bioreactors. The results demonstrated the *T. neapolitana* aptitude to attach on conductive graphite as well as on porous alluminosilicate. Time differences in the biofilm evolution were detected, main depending of the material.

**Index Terms** – *Thermotoga neapolitana*, biofilm, carbon cloth, graphite felt.

### I. INTRODUCTION

*Thermotoga neapolitana* (DSM 4359, ATCC 49049) is a rod-shaped, gram-negative, non-sporulating bacterium, that more than the other thermotogales is able to accumulate biohydrogen and produce lactic acid from waste organic matter, in a selective environment (>80°C). These performances make the bacterium suitable for biotechnology applications of energy interest [1-4]. Nevertheless, the possible active role of Thermotogales in bioelectrochemical systems was rarely investigated [5,7].

A first approach to the electroactivity of bacteria led to the study of a possible interaction of individual cells with conductive materials and, most consistently, to the formation of a settled colony that can electrochemically interact with the substrate, in a biofilm network. The tendency of individual cells floating in solution to attach on a solid substrate forming a biofilm depends on the type of surface to adhere as well

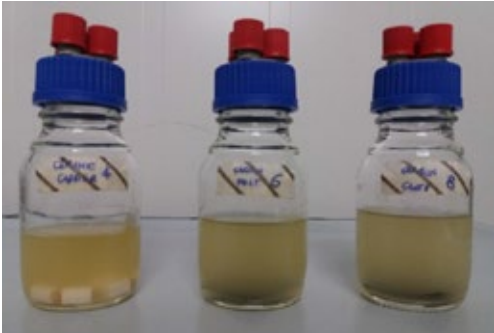
chemical physical stresses. In the specific cases of thermotogales, a close hyperthermophilic bacterium (*Thermotoga maritima*) was found by Pisz et al. [7] to attach glass walls, nylon meshes and polycarbonate filters on maltose-based media at 80°C. Most notably in this work, *T. maritima* biofilm-bound cells exhibited increased transcription of genes involved in iron and sulfur transport, as well as in biosynthesis of NAD, and isoprenoid side chains of quinones. Redox mediators are involved in these chains and this suggest the possibility of using biofilm forming Thermotogales strains for bioelectrochemical applications.

In the case of *T. neapolitana*, individual cells were immobilized on stable cationic hydrogel bearing amine groups [8], but there are no report about the rationale screening of conductive materials for bacteria attachment and biofilm formation. In this work, the same broth of *Thermotoga neapolitana* were exposed to different conductive and not conductive solid substrates, including graphite textures (carbon cloth and carbon felt), aluminosilicate (3D porous ceramic), conductive carbon paint (coating), stainless steel (mesh). The relevance of geometry and the nature of the solid substrate to improve or inhibit the cell attachment has been studied. The aim of the research is to exploit this kind of bacteria in microbial fuel cells and other bioelectrochemical systems.

### II. MATERIALS AND METHODS

*T. neapolitana* was grown anaerobically in the *Tn* medium supplemented with 5g/L glucose, and sparged with CO<sub>2</sub> to ensure capnophilic conditions [2]. Cells were cultured in fed-batch modality in bioreactors of 250 ml with a working volume of 150 ml and maintained at 80°C in static conditions. Each tested materials was inserted on the bottom of a bioreactors (Fig. 1) and exposed for 1 and 2 weeks to the

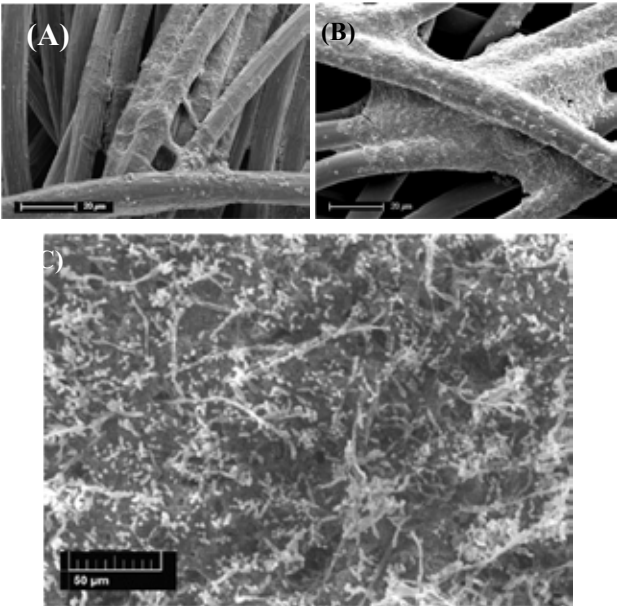
medium, then collected, dried, golden and analyzed with Scanning Electron Microscope (SEM), Figure 2.



**Fig. 1: Cultures of *Thermotoga neapolitana* in bioreactors with ceramic carrier (left), Carbon Felt (middle) and Carbon Cloth (right).**

III. RESULTS

All the tested materials didn't show any interference with cell growth (Fig. 1) and all them were colonized by bacteria in time. The porosity of the ceramic material were firstly colonized and bacteria colonies enriched on the surface for the first week, creating a permanent biofilm attachment. SEM images (Fig. 2C) revealed massive colonization and cells appeared connected in the biofilm forming a multi-layer assemblage.



**Fig. 2. SEM image of *T. neapolitana* biofilm on carbon felt (a), carbon cloth (b) and ceramic carrier (c) after 14 days of cultivation**

Also in the case of carbon cloth (Fig. 2A), the interaction

between bacteria and support seems to indicate a good feeling to the attachment for individual cells. It can be hypothesized that component of *T. neapolitana* toga includes exopolysaccharides useful for cell attachment to the tested surfaces. Carbon felt and stainless steel was colonized slower, probably because the smoother surface than the other materials. An indicative susceptibility of materials to be colonized is summarized in the table 1.

TABLE I  
BIOFILM ATTACHMENT ON DIFFERENT MATERIALS

Support / Time	6days	12 days
Aluminosilicate	Diffused	Uniform and dense
Carbon cloth	Locally dense	Localized and dense
Carbon felt	Limited	Locally Dense
Stainless Steel	Limited	Localized

IV. CONCLUSION

All the tested materials are partially or massively colonized by *T. neapolitana* biofilm, depending of the exposition time, the architecture and porosity of the tested material. It seems that surface roughness and materials porosity enhance the growth and distribution of bacteria population. These results indicate the possibility to study and plan a direct interaction of *T. neapolitana* with conductive surface and, consequently, with the electrodes used in bioelectrochemical systems, such as microbial fuel cells.

ACKNOWLEDGMENT

This work was financed by the Italian Ministry of University and Research (MIUR) and by the Research Fund for the Italian Electrical System in compliance with the Decree of March, 19th 2009. GdI and AF were grateful to Lucio Caso for technical assistance. GS like to thanks Dr. Lidia Pino for its friendly support to the research.

REFERENCES

[1] d'Ippolito G, Dipasquale L, Vella FM, Romano I, Gambacorta A, Cutignano A, Fontana A. Int J Hydrogen Energy 2010;35:2290–5. doi:10.1016/j.ijhydene.2009.12.044.

[2] Dipasquale L, d'Ippolito G, Fontana A Int J Hydrogen Energy 2014, 39, 10: 4857-4862,

[3] d'Ippolito G, Dipasquale L, Fontana A. ChemSusChem. 2014 Sep;7(9):2678-83

[4] Pradhan N, Dipasquale L, d'Ippolito G, Panico A, Lens PN, Esposito G, Fontana A. Int J Mol Sci. 2015 4;16(6):12578-600

[5] S. Hirano & N. Matsumoto, Biosci Biotechnol Biochem. 2017 Aug;81(8):1619-1626

[6] Van Eerten-Jansen, M., Ter Heijne AA, Grootscholten T.,Steinbusch K, Sleutels T, Hamelers, H and Buisman C. Sustainable Chemistry & Engineering 1(8) 2013:1069-1069

[7] Pysz MA, Conners SB, Montero CI, Shockley KR, Johnson MR, Ward DE, Kelly RM. Appl Environ Microbiol. 2004 Oct;70(10):6098-112.

[8] Basile MA, Carfagna C, Cerruti P, Gomez d'Ayala G, Fontana A, Gambacorta A, Malinconico M, Dipasquale I. 2012 RSC Adv., 2, 3611-3614

## PRESSURIZED REVERSIBLE OPERATION OF A 30-CELL SOLID OXIDE CELL STACK USING CARBONACEOUS GASSES

S. H. Jensen\*, H. Langnickel\*, N. Hintzen\*, M. Chen\*, X.

Sun\*, A. Hauch\*, G. Butera\*\*, L. R. Clausen\*\*

\*DTU Energy, Frederiksborgvej 399, 4000 Roskilde

\*\*DTU Mechanical Engineering, Akademivej, B. 358, 2700 Lyngby  
Technical University of Denmark

**Abstract** - Recent theoretical studies show that reversible electrochemical conversion of  $H_2O$  and  $CO_2$  to  $CH_4$  inside novel pressurized solid oxide cells (SOCs) combined with subsurface storage of the produced gasses can facilitate seasonal electricity storage with a round-trip efficiency 70-80% and a storage cost below 3 €/kWh. Here we show test results from a 30-cell SOC stack operated with carbonaceous gasses at 18.7 bar at 700 °C in both electrolysis and fuel cell mode. The GC data from the electrolysis test results show 18% methane in the dry outlet gas, i.e. substantial methane formation inside the SOC stack. Further we observed degradation rates comparable to that of ambient pressure operation with  $H_2/H_2O$  gas mixtures.

**Index Terms** - Pressure, Methane, Efficiency, Storage

### I. INTRODUCTION

As intermittent wind and solar power displace fossil fuels, the need increases for seasonal storage and production of transportation fuels. Power-to-gas (and fuels) is interesting although the conversion efficiency is normally rather low for hydrogen production. Internal methanation in SOCs have been proposed to increase conversion and storage efficiency [1] and coupling with pressurized subsurface gas storage could provide cost efficient large-scale electricity storage [2].

Catalytic  $CH_4$  formation (and internal reforming) kinetics on a SOC fuel electrode have previously been studied at single-cell level at open circuit voltage (OCV) and ambient pressure [3] and recently at electrolysis conditions at pressures up to 10 bar [4]. It was found that reaction kinetics only to a limited degree influences the outlet gas composition.

Here we present the test results from electrolysis and fuel cell test of a 30-cell SOFCMAN stack at 18.7 bar on carbonaceous gasses.

### II. EXPERIMENTAL

A 30-cell SOFCMAN 301 stack with 63 cm<sup>2</sup> active electrode area per cell [5,6] was operated in a dedicated pressure test setup [7]. First the stack was heated to 750 °C followed by reduction of the NiO in the fuel electrodes. Subsequently the temperature was reduced to 700 °C. The remaining stack test is divided in five parts. Gas compositions for each part is specified in Table I.

Part 1: The pressure was increased in four steps from 1 to 18.7 bar. i-V curves and impedance spectra were recorded at each step.

Part 2: An equilibrium fuel gas mixture (neglecting higher hydrocarbons than  $CH_4$ ) was fed to the stack. The gas composition was measured using an Agilent micro GC 490. Inlet gas composition, as well as the stack outlet composition at OCV, at -0.1 A/cm<sup>2</sup> and at -0.2 A/cm<sup>2</sup> was measured.

TABLE I  
FUEL GAS FLOW RATE IN NORMAL LITERS PER HOUR DURING TEST

Test Part	Fuel side					Air side	
	H <sub>2</sub>	H <sub>2</sub> O	CO	CO <sub>2</sub>	CH <sub>4</sub>	O <sub>2</sub>	N <sub>2</sub>
1	200	200	0	0	0	126	474
2	31.5	140	6.2	36.8	1.3	126	474
3	31.5	140	6.2	36.8	1.3	40	1800
4	64.2	40.9	5.9	6.1	42.1	170	1800
5	64.2	40.9	5.9	6.1	42.1	170	1800

Part 3: Subsequently the stack was operated at -0.1 A/cm<sup>2</sup> for about 100 hours. The oxygen concentration at the air side was reduced to minimize oxygen leaking from the air side to the fuel side.

Part 4: Next the stack was operated with an equilibrium gas having a lower O-content. The gas composition was measured using the GC. Inlet gas composition, and the stack outlet gas

composition was measured at OCV, 0.1 A/cm<sup>2</sup> and 0.2 A/cm<sup>2</sup>.

Part 5: After part 4, the stack was operated at 0.1 A/cm<sup>2</sup> for about 12 hours.

### III. RESULTS

In part 2 the GC measurements revealed ~20 vol% N<sub>2</sub> in the stack fuel outlet gas. The N<sub>2</sub> entered the fuel gas from the air electrodes via seal and/or electrolyte leaks. The air leak partially oxidized the fuel. Correcting for the N<sub>2</sub> content in the fuel gas and adjusting for the associated fuel gas oxidation (by shifting the measured gas concentrations to the right on the x-axis in Fig. 1) it is observed that the outlet gas almost reach the equilibrium composition before it exits the stack. Importantly the outlet gas contained 18 vol% CH<sub>4</sub>. Arguably a part of the measured deviation from equilibrium concentration could also be related to kinetic limitation of the methane formation [3,4].

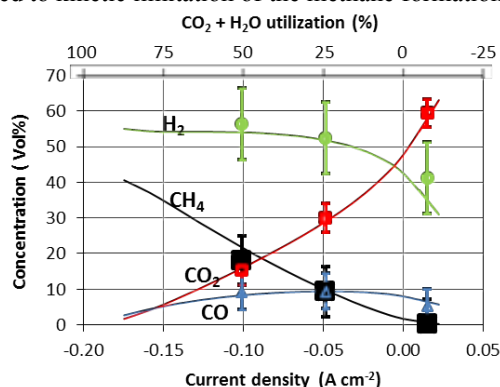


Fig. 1. Gas composition as function of electrolysis current density corrected for internal stack leak. Lines represents theoretical concentration, points measured values. Uncertainty bars reflect the GC measurement uncertainty.

In part 3, the stack voltage was measured as function of time (Fig. 2). During the test the stack was exposed to a pressure cycle which didn't affect OCV and equilibrated stack voltage at -0.1 A/cm<sup>2</sup>. The stack voltage as function of time gradually increased at a rate of 14% per 1000 hours (green line in the figure). This is comparable to a degradation rate of ~12% per 1000 hours at -0.15 A/cm<sup>2</sup> at 800 °C in a H<sub>2</sub>/H<sub>2</sub>O mixture to the fuel electrode of a similar 30-cell stack [5]. At the end of test part 3, a decreasing steam supply resulted in a decreasing stack voltage. This could indicate an increased methane production.

During part 4, the stack exhibited a degradation rate of 3.2% per 1000 hours (not shown). This can be compared to a degradation rate of 2.3% per 1000 hours for a 5-cell SOFCMAN stack operated at ambient pressure with H<sub>2</sub> and air at 0.4 A/cm<sup>2</sup>[6]. The GC measurements in part 5 confirmed decreasing CH<sub>4</sub> and increasing CO<sub>2</sub> concentration with increasing FC current density.

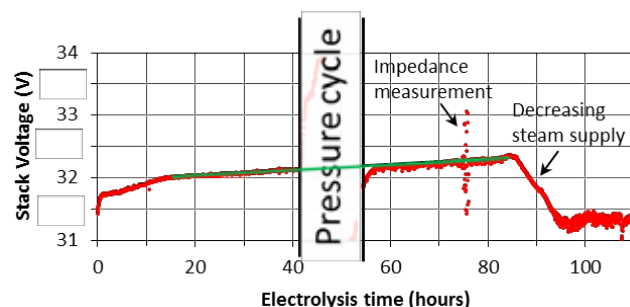


Fig. 2. Stack voltage during electrolysis operation at -0.1 A cm<sup>2</sup> operated with the gas flow rates specified in test part 3, Table I. At the end, the steam supply gradually decreased to 84 NLH.

### IV. CONCLUSION

Internal methane formation inside an SOFCMAN 30-cell was demonstrated. Such operation mode can substantially increase power-to-gas conversion efficiency. The stack was operated with an inlet equilibrium gas composition with less than 1 vol% CH<sub>4</sub>. When the current density was increased to -0.2 A/cm<sup>2</sup>, the CH<sub>4</sub> concentration at the outlet increased to 18 vol%. The stack was subsequently operated in SOFC mode with a methane rich inlet gas. Degradation rates in both modes seem comparable with ambient pressure degradation rates.

### ACKNOWLEDGMENT

The authors acknowledge financial funding from the Energy Technology Development and Demonstration Program (EUDP) via project no. 64015-0523 "Maturing SOEC".

### REFERENCES

- [1] D. M. Bierschenk, J. R. Wilson, S. A. Barnett, High efficiency electrical energy storage using a methane-oxygen solid oxide cell, *Energy Environ. Sci.*, **4** 944 (2011)
- [2] S.H. Jensen, C. Graves, M. Mogensen, C. Wendel, R. Braun, G. Hughes, Z. Gao, S.A. Barnett, Large-scale electricity storage utilizing reversible solid oxide cells combined with underground storage of CO<sub>2</sub> and CH<sub>4</sub>, *Energy Environ. Sci.*, **8** 2471 (2015)
- [3] H. Timmermann, W. Sawady, R. Reimert, E. Ivers-Tiffée, Kinetics of (reversible) internal reforming of methane in solid oxide fuel cells under stationary and APU conditions, *J. Power Sources* **195** 214 (2010)
- [4] L. Bernadet, J. Laurencin, G. Roux, D. Montinaro, F. Mauvy, M. Reytier, Effects of Pressure on High Temperature Steam and Carbon Dioxide Co-electrolysis, *Electrochimica Acta. Accepted manuscript*, <http://dx.doi.org/10.1016/j.electacta.2017.09.037>
- [5] Y. Zheng, Q. Li, W. Guan, C. Xu, W. Wu, W. Wang, Investigation of 30-cell solid oxide electrolyzer stack modules for hydrogen production, *Ceramics International*, **40** 5801 (2014)
- [6] L. Jin, W. Guan, X. Ma, H. Zhai, W. Wang, Quantitative contribution of resistance sources of components to stack performance for planar solid oxide fuel cells, *J. Power Sources*, **253** 305 (2014)
- [7] S. H. Jensen, C. Graves, M. Chen, J. B. Hansen, X. Sun, Characterization of a Planar Solid Oxide Cell Stack Operated at Elevated Pressure, *J. Electrochem. Soc.*, **163** F1596 (2016)



## FIELD TESTING OF FLOATING MICROBIAL FUEL CELLS FOR ENERGY HARVESTING IN AERATED WATER AND WASTEWATERS

P. Cristiani\*, F. Pizza\*\*, I. Gajda\*\*\*, J. Greenman\*\*\*, P. Bonelli\*\*\*\*, I. Ieropoulos\*\*\*

\* RSE – Ricerca sul Sistema Energetico S.p.A., via Rubattino, 54, 20100 Milano, (Italy)

\*\* Milano Depur SpA, WWTP of Milano-Nosedo, via San Dionigi 90, 20139 Milano, (Italy)

\*\*\* Bristol BioEnergy Centre, Bristol Robotics Laboratory, University West England, Bristol, UK,

\*\*\*\* CISE 2007, Milano, (Italy)

**Abstract** - In the present work several prototypes of floating MFCs have been tested in fresh, clean water and in anoxic wastewater. The performance of floating MFCs suitably designed for aerobic and anaerobic water environments were studied in long-term experiments. Several designs of flat and tubular MFCs were tested, using low-cost materials, such as plastic lunch boxes, polystyrene or wood to keep the systems afloat. Untreated carbon cloth was used for electrodes, insulated by felt or clay. Flat MFCs generated up to 15 mW/m<sup>2</sup> of power, depending on nutrient availability in the water, whereas the cylindrical MFCs generated up to 8 mW/m<sup>2</sup>. The experiments were carried out in Milano (Italy) at the wastewater plant Milano-Nosedo and in the pool of the city garden “Orto Botanico Città Studi”. A new, simple low-energy remote system (LORA) for MFC data transmission over distances of >500m, was successfully used.

**Index Terms** – Microbial fuel cells, Floating MFCs, wastewaters, low-energy remote data transmission.

### I. INTRODUCTION

Microbial Fuel Cells (MFCs) are a promising technology with the dual benefit of harvesting energy from and sensing within aquatic environments. Several prototypes of sediment MFCs have been previously tested<sup>1</sup> and floating systems<sup>2</sup> have more recently been reported investigated as well, with promising results. The challenge is now to scale up laboratory MFC designs for self-powering sensors of water quality and implement these in real environments where electricity sources may not be available. In the present work, the performance of floating MFCs suitably designed for aerobic and anaerobic water environments were studied in long-term experiments. Several designs of flat and tubular cells were tested, using low-cost materials, such as plastic lunch boxes, polystyrene or wood to keep the system afloat. Untreated carbon cloth (flat

MFCs) and untreated carbon veil (ceramic MFC) was used for both the anode and cathode electrodes. A new generation of low-energy remote system (LORA) was integrated in an electronic circuit for harvesting the generated power from MFCs and using that to transmit signals over long distances. The experiments were carried out in Milano (Italy) at the wastewater plant Milano-Nosedo and in the pool of the city garden “Orto Botanico Città Studi”.

### II. MATERIALS AND METHODS

#### A. Flat MFCs in anoxic wastewater

Flat MFCs of different geometries<sup>3</sup> (10 x 10 cm<sup>2</sup> the smallest and 50 X 40 the largest, Fig. 1) were immersed in the denitrification (anoxic) pool of the wastewater plant Milano-Nosedo. The cathode and anode were both made of carbon cloth free of any chemical catalyst (cod. SCCT-8, SAATI, Legnano, Italy). The anode of the MFCs was immersed in the wastewater and an identical cathode was floating on the top, facing the air.

#### B. Tubular ceramic MFCs in anoxic wastewater

A total of 16 terracotta tubular MFCs (L=7 cm, d=1.5 cm each) with anodes made from carbon fibre veil and cathodes made of activated carbon were inserted into a polystyrene material, cut to the shape of a small boat, as a second system for testing in the same wastewater environment, located next to the flat MFCs (Fig. 1).

#### C. Floating MFCs in aerated fresh waters

For the experiments in fresh/clean water, flat MFCs were set up with the cathode made from carbon cloth, placed at the bottom of the box, directly submerged into water. The anode, made of the same carbon cloth, was buried in the bottom of the box, insulated from the cathode with a polypropylene felt and a

layer (1 cm) of clay. Over the anode another layer of clay and a thick layer of soil was placed, enriched with local vegetation and grass. Anode and cathode were suitably connected with a power management system able to supply an LED light, a buzzer or to harvest energy for the remote data transmission system.



**Fig 1. Floating plate microbial fuel cells in the anoxic tank of wastewater plant Milano-Nosedo. Inset: boat-shaped floating system with 16 terracotta MFCs.**

### III. RESULTS AND DISCUSSION

#### A. MFCs in anoxic wastewater

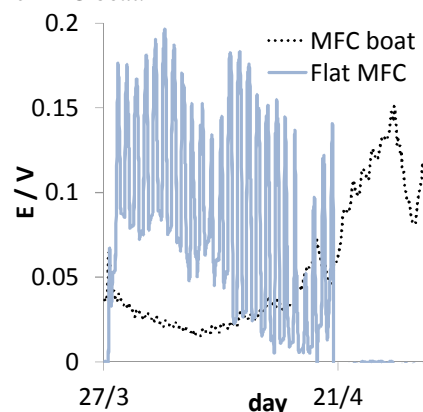
The flat MFCs tested in anoxic wastewaters were quickly and covered by photosynthetic organisms and the power was initially positively affected by light (oscillation in Fig. 2). As time progressed, spontaneous vegetation of grass, herbs and shrubs grew on the cathode of these MFCs (top surface, exposed to air), demonstrating a wetland phenomenon, whose root system gently covered the electrode without damaging it or preventing oxygen to permeate through. After the growth of vegetation, the MFC voltage was no longer affected by light, but mainly by nutrients availability. This kind of flat MFCs were able to supply power in the range of 15 - 7 mW/m<sup>2</sup>, depending of the cell size<sup>3</sup>.

The boat MFC, which is still running to this day after two years of continuous operation, has been generating power in the range of 0.04 - 0.25mW of power, measured across a 100Ω load (20 - 160mV; 0.2 - 1.6mA; Figure 2). The data shown in Figure 2 represent only a part of the whole data set for the 2-year period, but clearly demonstrate the viability of the MFC system as both an energy harvester and a sensor in a real environment, for prolonged periods.

#### B. MFCs in fresh/clean water

These MFCs became a “floating garden” with time, fluctuating on the surface of the water body, as previously described<sup>2</sup>. All the tested MFCs achieved continuous power

during the year, although the productivity was strongly affected by the season and weather, more than the MFCs floating in wastewater, mostly due to a more pronounced temperature oscillation. Nevertheless, LEDs and buzzers were continuously powered by this type of MFC, although the frequency of the signal varied as a function of the produced power. A new, simple low-energy remote system (LORA) for MFC data transmission over distances of >500 m, was also successfully tested. The work in progress now aims to fully power the LORA transmission system with a power management interface system connected to the three parallel floating MFCs and also the MFC boat.



**Fig. 2. Initial voltage trends across 100 Ω of a flat MFC (size 25 x 25 cm) and the MFC boat.**

### IV. CONCLUSIONS

All the tested MFC designs achieved continuous power, with greater stability in wastewater than in aerated waters, and the data were logged continuously. A new, simple low-energy remote system (LORA) has been successfully tested, showing great promise for a cost effective way of data transmission that could be implemented in remotely monitoring and controlling water quality based on MFCs.

### ACKNOWLEDGMENT

This work was financed by the Research Fund for the Italian Electrical System in compliance with the Decree of March, 19<sup>th</sup> 2009. The work done for the boat MFC made in the Bristol BioEnergy Centre, has been funded by the Bill & Melinda Gates Foundation (grant no. OPP1094890) and the EPSRC, UK (grant no. EP/L002132/1).

### REFERENCES

- [1] C.E. Reimers, L.M. Tender, S. Fertig, W. Wang. Environ. Sci. Technol. 35, 2001, 192e195A.
- [2] Schievano, A. Colombo, M. Grattieri, S.P. Trasatti, A. Liberale, P. Tremolada, C. Pino, P. Cristiani. Journal of Power Source, V. 340, 2017, 80–88.
- [3] E. Martinucci, F. Pizza, E. Guerrini, A. Colombo, S.P.M. Trasatti, A. Lazzarini Barnabei, A. Liberale, P. Cristiani. Int. J. of Hydr. Energy 40 (42) 9 (2015), 14683–14689.

## OPERATION OF REAL LANDFILL GAS FUELED SOLID OXIDE FUEL CELL (SOFC) USING INTERNAL DRY REFORMING

H. Langnickel\*, A. Hagen\*

\*DTU Energy, Technical University of Denmark,  
Frederiksborgvej 399, 4000 Roskilde, (Denmark)

**Abstract** – Biomass is one renewable energy source, which is independent from solar radiation and wind effect. Solid oxide fuel cells (SOFC's) are able to convert landfill gas derived from landfill directly into electricity and heat with a high efficiency. In the present work a planar 16cm<sup>2</sup> SOFC cell was operated with a real landfill gas from one of the largest Danish waste dump sites and additional carbon dioxide reforming agent at 750°C, both with gas cleaning through an active carbon filter and without. The tests showed an electric efficiency up to ~60%. It was found that the active carbon filter was necessary to prevent poisoning and thereby to decrease the degradation rate.

**Index Terms** – Landfill gas, Solid oxide fuel cell, Efficiency, Dry reforming, Poisoning

### I. INTRODUCTION

For an electricity production based on 100% renewable energy sources options are needed which are independent of the fluctuating solar radiation and wind profiles. Considering biomass as renewable resource one option could be landfill gas derived from landfill. Landfill gas consists of carbon dioxide, methane and impurities as for example sulfur containing compounds. Most landfill gasses are unattractive for low efficient combustion engines due to their low heating values. Solid oxide fuel cells (SOFC's) could be a more efficient alternative to convert carbon containing fuels, like landfill gas, into electricity and the side product heat.

As pointed out in thermodynamic studies (e.g. Sasaki et al [1]) a reforming agent is needed to prevent carbon formation during the direct conversion of carbon containing fuels into electricity and heat in a SOFC. Beside the well-known reforming agent steam also carbon dioxide (dry reforming) can be used. The advantage is that landfill gas already contains a certain amount of the needed carbon dioxide. Furthermore, the

dry reforming path in the SOFC was found to be less sensitive to sulfur contaminants in the biogas [2] and thus the demands for gas cleaning and system complexity might be less compared to steam reforming.

In the presented work a SOFC cell was operated with a real landfill gas from one of the largest Danish waste dump sites and additional carbon dioxide reforming agent at 750°C. This study evaluates the effect in terms of the SOFC power density output and electric efficiency.

### II. EXPERIMENTAL

An anode supported planar Ni-YSZ/YSZ/LSCF:LSM with a CGO barrier layer was used. The SOFC cell had an active area of 16cm<sup>2</sup> and was operated at 750°C in an alumina test house equipped with gas supplies, current collectors and voltage probes. A detailed description can be found in reference [3]. Before entering the test house, the landfill gas was mixed with the reforming agent carbon dioxide and could pass or by pass an active carbon filter at room temperature. The landfill gas composition is shown in table 1.

TABLE I  
APPROXIMATELY FUEL COMPOSITION

Component	Landfill gas				CO <sub>2</sub> RA*
	CH <sub>4</sub>	CO <sub>2</sub>	O <sub>2</sub>	N <sub>2</sub>	
Amount	23 vol%	15 vol%	1 vol%	28 vol%	33 vol%

\*RA: Reforming agent

During this study two testes were carried out at a current density of 0.5A/cm<sup>2</sup> and a fuel utilization of ~63%. The cathode side was supplied with air during all tests. For test 1 the fuel was passed through the filter whereas for test 2 the filter was bypassed for 46 hours as illustrated in table 2. Before and after each test iv-curves were recorded under the same conditions.

Copyright © 2017

TABLE 2  
TEST PROCEDURE IN TERMS OF THE ACTIVE CARBON FILTER FOR TEST 1 AND 2.

Test	Filter on	Filter off	Filter on	Total time
1	130 hr			130 hr
2	2 hr	46 hr	202 hr	250 hr

### III. RESULTS

The power density and the electric efficiency of test 1, passing the fuel through the active carbon filter, and test 2, by passing the filter, for 46 hours are shown in figure 1. The results of test one show a stable power density of approximately 0.4 W/cm<sup>2</sup> (black line) which corresponds to an efficiency of around 61% (green line). The degradation rate of the power output was calculated assuming linear behavior and was 1.1%/1000h. The power density of test 2 (blue line) starts at the same value as in test 1. After 2 hours (filter bypassed) the power density starts to decrease slowly and after approximately 20 hours more rapidly. After 48 hours of operating the SOFC, the power density had dropped by 0.04 W/cm<sup>2</sup> which corresponds to an efficiency loss of ~9% and a degradation rate of 239%/1000 h. After passing the fuel through the cleaning filter again, the power density still decreased for the next approximately 20 hours to a minimum of 0.34 W/cm<sup>2</sup>, followed by a period of recovery to a power density of 0.36 W/cm<sup>2</sup>. After 250 hours, the loss of power output was 0.04 W/cm<sup>2</sup> in respect to the initial power density of 0.4 W/cm<sup>2</sup>. This corresponds to an electric efficiency drop of around ~5%.

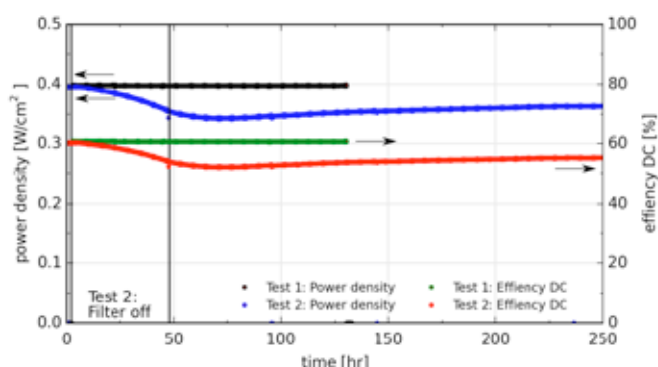


Figure 1: Power density and electric efficiency over time for test 1 and 2. For test1 the fuel was passed through the carbon filter were as for test2 the filter was bypassed in the initial 46 h [4].

Considering the area specific resistance (ASR) of the cells from the iv-curve recorded before and after test 1 one can conclude that the ASR had not changed. It was around 0.45 Ωcm<sup>2</sup> (see figure 2). The ASR recorded before test 2 is similar to the initial ASR value of test 1. However, after test 2 the ASR reached a value of 0.56 Ωcm<sup>2</sup>, which corresponds to an increase of 24% in relation to the value before test 2. The constant ASR in test 1 and increase in test 2 correlate well with the power density drop and the efficiency drop as shown in figure 1.

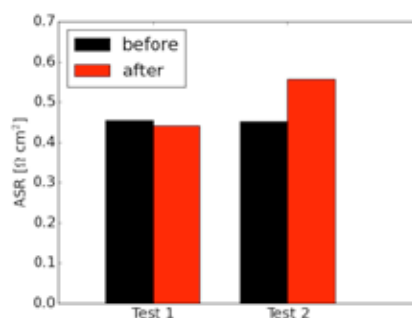


Figure 2: Comparison of the area specific resistance (ASR) of the iv-curves before and after test 1 and 2.

### IV. CONCLUSION

In the current work, the operation of state of the art solid oxide fuel cell fueled with real landfill gas plus carbon dioxide using internal dry reforming was investigated. Gas cleaning using an active carbon filter was necessary to maintain a stable power output. While bypassing the cleaning filter resulted in significant degradation rates of 239%/1000 h, a stable operation with a small degradation rate of 1.1%/1000 h was achieved when cleaning the landfill gas.

### V. ACKNOWLEDGMENT

The authors are very grateful to Ulrik Lønkjær and Rasmus Olsen from Odense Renovation for providing real biogas from the landfill unit in Odense Renovation. We also thank Nils Hintzen, Ole Hansen and Henrik Henriksen from DTU Energy for collecting the biogas and technical assistance.

### VI. REFERENCES

- [1] SASAKI, K. & TERAOKA, Y.: Equilibria in fuel cell gases - I. Equilibrium compositions and reforming conditions. In: Journal of the Electrochemical Society 150 (2003), Nr. 7, S. A878-A884
- [2] JOHNSON, G. B.; HJALMARSSON, P.; NORRMAN, K.; OZKAN, U. S. & HAGEN, A.: Biogas Catalytic Reforming Studies on Nickel-Based Solid Oxide Fuel Cell Anodes. In: Fuel Cells, April 2016, Vol.16(2), pp.219-234 16 (2016), Nr. 2, S. 219
- [3] BOARO, M. & SALVATORE, A. A.: Advances in medium and high temperature solid oxide fuel cell technology: Springer. 574, 2016
- [4] GRAVES, C.: RAVDAV data analysis software, version 0.9.7, 2012.



# Design and testing of a monopolar configuration direct methanol fuel cell stack for portable applications

D'Urso<sup>a\*</sup>, A. Stassi<sup>a</sup>, V. Baglio<sup>a</sup>, O. Barbera<sup>a</sup>, G. Giacoppo<sup>a</sup>,  
M. Sgroi<sup>b</sup>, M. Shuster<sup>b</sup>, A.S. Aricò<sup>a</sup>

<sup>a</sup> CNR-ITAE, National Research Council of Italy, Institute for Advanced Energy Technologies, Via Salita S. Lucia sopra contesse, 598126 Messina, Italy

<sup>b</sup> Centro Ricerche FIAT, Strada Torino 50, Orbassano (TO), Italy

<sup>c</sup> FUMATECH BWT GmbH, Carl-Benz-Strasse 4, Bietigheim-Bissingen D-74321, Germany

**Abstract** – In this work, a simple and functional stack design was developed for direct methanol fuel cells (DMFCs) with the aim of reducing capital costs. A simplified planar ministack, with a reduced number of components, was designed for portable applications. This planar design facilitated the manufacturing of a compact passive mode operation ministack. The ministack provided an output power of 1.30 W under air-breathing mode operation, at room pressure and temperature without any auxiliary. The device consisted of 10 cells, two circuit boards were used to clamp and support MEAs and to electrically connect the electrodes. The ministack, for the passive mode operation, achieved a normalized power density of  $30 \text{ mW cm}^{-2}$  with 5 M methanol feed. The tests were carried out using membrane-electrode assemblies (MEAs) with different membranes as electrolytes. These results favorably compare with the best performance reported in the literature for passive-mode DMFC mini-stacks based on Nafion 115 membrane. Passive DMFCs can potentially result in high reliability, low cost, high fuel utilization and high energy density (using a concentrated methanol solution), which are in favour of portable equipment in future electronic devices.

**Index Terms** – Direct Methanol Fuel Cells, Electrochemistry, Portable application, Stack Design.

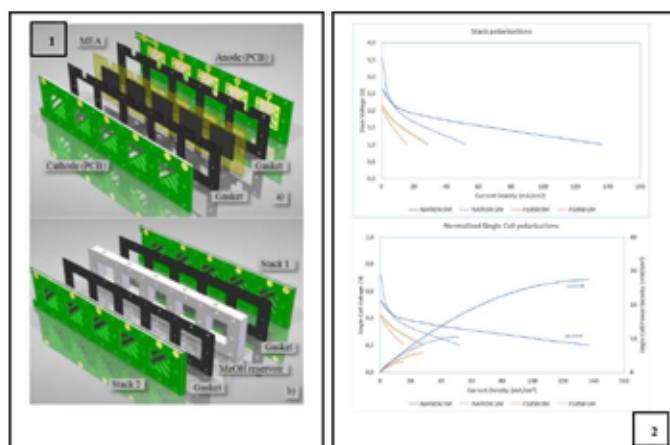
## I. INTRODUCTION

DMFCs have received worldwide attention because of several intrinsic advantages, such as simplicity of operation, high theoretical energy density, easy recharging. Compared their counterpart, proton exchange membrane (PEM) fuel cells, DMFCs are simpler in construction and do not need high-pressure hydrogen gas storage delivery or processing. Additional simplification in DMFCs includes air-breathing operation for low power application [1]. However, the sluggish electro-oxidation kinetics and high crossover rate of methanol are the main factors that hinder the commercialization of DMFCs. During the past few decades, developments in electro – active materials and PEM technology design promoted the application of DMFCs in small portable power devices. To generate an appropriately sized DMFC stack, a suitable number of unit cells should be designed, and the operating conditions optimized to enhance the power density of the DMFC system. DMFC stacks are classified into two types, based on the configuration of electrodes, membranes, and bipolar plates [2]. The first type is a monopolar stack, which is assembled by placing electrodes of the same polarity on the same side of the membrane and then electrically connecting the anodes and cathodes in series. Despite the easy supply of reactants, the monopolar stack could be affected by a high internal resistance because the electric current flows along conductive strips. The second type of stack is a bipolar design, which consists of a

number of repeating units of membrane electrode assembly (MEA) and bipolar plate. The bipolar plate separates each MEA and provides an electrical connection in series between the adjacent cells in the stack. It also supplies reactants to each cell through flow channels formed on both sides of the plates. The bipolar stack has lower internal resistance and, thus, is more adequate for larger stacks than the monopolar design, which is more suitable for portable applications [3]. Advances in the development of portable fuel cells should have a great impact on the use and development of modern electronic devices. Passive DMFC can potentially result in high reliability, low cost, high fuel utilization and high energy density (using a concentrated methanol solution), which are in favor of portable equipment in future electronic devices.

## II. EXPERIMENTAL

A direct methanol fuel cell mini-stack for portable applications was designed with two strings composed of 5 cells connected in series, whereas, the two strings were connected in parallel, the single cell area was  $4.85 \text{ cm}^2$  and the operating conditions were ambient pressure and temperature. For portable applications, the device has to be as simple as possible, thus, it should be operated without recirculation pump or fan to feed methanol and air, respectively, assembled with a limited number of parts, light and easy to recharge.



**Fig.1. 1.** Assembling concept of a string (a) and of the two strings with the reservoir (b); **2.** Polarization curves of different MEA with two methanol concentrations

To meet these requirements, the architecture of the 10-cell stack was conceived as planar, and modular, each pair of current collector and clamping plates unified on a single component, the reactants provision in passive mode (spontaneous diffusion, natural convection). The stack was composed of two sets of MEAs consisting of 5 cells each, arranged in a planar configuration. Each MEA was prepared allocating the 5 active electrodes on both sides of a single membrane. The MEAs were prepared by hot-pressing at  $130^\circ\text{C}$  for 3 min and  $20 \text{ kgcm}^{-2}$ . The electrodes consisted of carbon paper backings, diffusion and

catalytic layers. An unsupported PtRu catalyst was employed at the anode; whereas, an unsupported Pt catalyst was utilized for cathode fabrication. The MEAs were prepared by using new FUMATECH proton exchange membranes, characterized by very low methanol crossover and good performance, as the electrolyte, and compared to a benchmark Nafion® 115 membrane in terms of performance and methanol cross-over.

Two printed circuit boards (PCB) were chosen to clamp and support an MEA and to electrically connect the five electrodes by thin gold strips. In correspondence of each active area, for air and methanol feeding, five windows were machined on the boards (Fig. 1). Polarization curves for the ministack were obtained using a Potentiostat-Galvanostat AUTOLAB PGSTAT302. The monopolar stack was connected to an AUTOLAB electrochemical apparatus, and then the methanol reservoir was filled with  $30 \text{ cm}^3$  of 1 M or 5 M methanol solution with the cathode side exposed to the ambient atmosphere. By imposing a discharging current density, ranging from 0 to  $200 \text{ mAcm}^{-2}$  with

a step of  $10 \text{ mAcm}^{-2}$ , the corresponding stack potential was recorded. Chrono-potentiometric discharge curves for the DMFC ministack were also registered.

## III. CONCLUSION

The fuel cell ministack achieved a maximum power of 1.2 W at 1.2 A, operating under passive mode, room temperature, air-breathing, natural convection, with 5 M methanol. The approach was to use a minimum number of components for stack assembling, to provide concrete perspectives to reduce capital costs and operating expenditures. A compact design for monopolar configuration operating at low temperature under passive mode was demonstrated. This configuration was elected as a proof-of-concept for portable applications. It provided a normalized power density of about  $30 \text{ mWcm}^{-2}$  under passive mode.

## ACKNOWLEDGMENT

The research leading to these results has received funding from the European Community's Seventh Framework Programme (FP7/201-2014) for the Fuel Cells and Hydrogen Joint Technology Initiative under grant agreement DURAMET n° 278054.

## REFERENCES

- [1] Liu H, Zhang J, editors. Electrocatalysis of direct methanol fuel cells. Weinheim, Germany: Wiley-VCH Verlag GmbH & Co. KGaA; 2009.
- [2] Dillon R, Srinivasan S, Aricò AS, Antonucci V. International activities in DMFC R&D: status of technologies and potential applications. J Power Sources 2004;127:1120-26.
- [3] Baglio V, Stassi A, Matera FV, Di Blasi A, Antonucci V, Aricò AS. Optimization of properties and operating parameters of a passive DMFC mini-stack at ambient temperature. J Power Sources 2008;180:797-802.

## DEVELOPMENT OF ADVANCED CATHODES FOR IT-SOFC

L. Navarrete\*, C. Solis\*\*, M. Balaguer\*\*\*, V.B. Vert\*\*\*, M. Fabuel\*\*\* and J.M. Serra\*\*

\*Instituto de Tecnología Química (UPV-CSIC)  
Avda Los Naranjos, S/N, 46022 Valencia (Spain)

\*\* Technical University of Munich. Research Neutron Source Heinz  
Maier-Leibnitz (FRM II). 85748 Garching (Germany).

\*\*\* Instituto de Tecnología Química (Universitat Politècnica de  
València – Consejo Superior de Investigaciones Científicas), 46022  
Valencia (Spain)

*Fuel cells have grown interest in the market during the last years due to their high efficiency and multifuel capacity. For instance, Solid Oxide Fuel Cells (SOFCs) can achieve efficiencies around 80 % when the heat generated in the cell is used by a cogeneration system. However, the SOFC's performance is limited by the cathode efficiency. In order to overcome that problem, alternative strategies have been used in the present work to improve the cathode performance of a pure electronic conductor material and a mixed electronic and ionic conductor compound.*

**Index Terms** – Cathodes, composite, infiltration, nanocatalyst.

### I. INTRODUCTION

$\text{La}_{1-x}\text{Sr}_x\text{MnO}_{3-\delta}$  (LSM), a widely cathode material employed for SOFCs, has been used as starting material. LSM combines high electronic conductivity with remarkable catalytic properties. Besides, LSM is compatible with most electrolyte materials, at low temperature the lack of ionic conductivity limits its application as SOFC cathode. Thus, different approaches can be followed in order to improve the cell performance of LSM-based cathodes fuel cells. The first strategy is the addition of an ionic conductor phase. For instance, the addition of the ceria phase would allow the ionic transport increasing the triple phase (TPB) length in the electrode. Additionally, the infiltration of a nanocatalyst into the composite electrode (LSM-ceria) would further improve the electrode performance [1].

In addition, the properties of a state-of-the-art material with a mixed ionic-electronic conductor material have been tailored.  $\text{La}_2\text{NiO}_{4+\delta}$  belongs to the Ruddlesden-Popper series, where a rock-salt layer and a perovskite layer are interspersed in the structure. In order to improve the oxygen reduction reaction activity of that compound, Pr and Co have been introduced in La and Ni sites, respectively. All materials synthesized exhibit

a single phase structure and the electrochemical characterization of the cathode materials has been performed by measuring the DC total electrical conductivity and the polarization resistance.

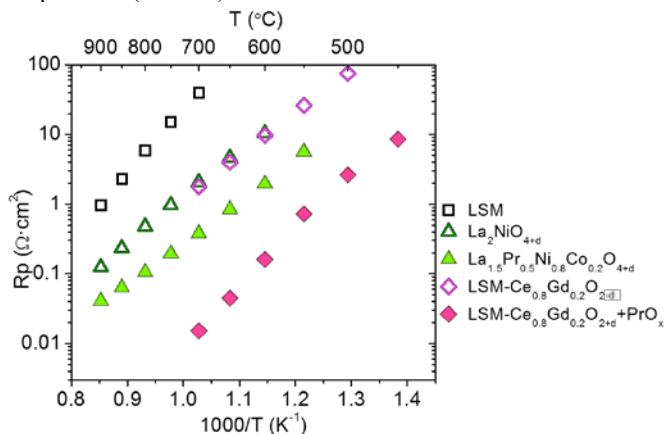
### II. EXTENDED ABSTRACT

Composites made of LSM and lanthanide doped ceria ( $\text{Ce}_{1-y}\text{Ln}_y\text{O}_{2-\delta}$  Ln Pr, Er, Gd and Tb) have been tested by means of the Electrochemical Impedance Spectroscopy (EIS) in symmetrical cell. The influence of the addition of different nanocatalysts oxides, as praseodymium, cobalt, zirconium, cerium and samarium was studied.

The performance of the LSM state-of-the-art was improved by introducing an ionic phase ( $\text{Ce}_{1-y}\text{Ln}_y\text{O}_{2-\delta}$ ) [2]. Due to the presence of that second phase with ionic conductivity and the enlargement of the Triple Phase Boundary along the electrode, the processes at low and medium frequencies could be enhanced, as was confirmed by Electrochemical Impedance Spectroscopy measurements. This robust LSM- $\text{Ce}_{0.8}\text{Gd}_{0.2}\text{O}_{2-\delta}$  composite was used as backbone electrode for the infiltration of different catalysts. Different precursors were infiltrated in the backbone and after firing, oxides of Sm, Zr, Ce, Ba, Co and Pr were dispersed as nanoparticles [3]. Catalysts candidates were screened using symmetric cells supported on  $\text{Ce}_{0.8}\text{Gd}_{0.2}\text{O}_{2-\delta}$  electrolyte. Different electrocatalytic behavior was observed depending on the oxide infiltrated. Sm, Zr, Ce and Pr oxide catalysts improved the electrode performance by promoting the surface processes and reducing the resistance at medium frequency. In contrast, Co and Ba catalyst worsen the cell performance increasing the resistance at medium frequencies. By the introduction of Pr oxide nanocatalyst in the reference



backbone (LSM-Ce<sub>0.8</sub>Gd<sub>0.2</sub>O<sub>2-δ</sub>), the polarization resistance was reduced 40 times, obtaining 0.016 Ω·cm<sup>2</sup> at 700 °C (Figure 1). Scanning Electron Microscopy was employed to study the microstructure of the different electrodes tested and the morphology and dimension of the nanoparticles infiltrated. All infiltrated oxides showed a sphere-like shape, except the Pr oxide with a needle-like shape. Furthermore, the particle size of the different oxides was kept below 40 nm due to the firing temperature (700 °C).



**Fig. 1.** Polarization resistance ( $R_p$ ) in air of the different cathodes as function of temperature.

The stability of the different activated cathodes in operation conditions was systematically studied at two different temperatures (700 °C and 600 °C). Firstly, a slight increase in the polarization resistance with time until was obtained for all infiltrated compounds, reaching a constant value afterwards. However, Zr catalyst showed a particular case, since the polarization resistance decreased with time until achieve a constant value.

Finally, the best infiltrated composite (LSM-Ce<sub>0.8</sub>Gd<sub>0.2</sub>O<sub>2-δ</sub>+PrO<sub>x</sub>) was tested in a fully assembled Ni-YSZ supported cell. The cell tested in a fuel cell mode achieved a 5-fold power density improvement respect to the sample without the nanocatalysts infiltration.

The unit cell parameters and bond distances for the as-synthesized Ruddlesden-Popper materials were obtained by Rietveld refinement technique. The substitution of Pr in the La site and Co in the Ni site induced the reduction of c cell parameter length, even though the orthorhombic Fmmm structure was maintained. Additionally, Ni/Co-O bond distance was reduced and the electronic conductivity was improved. The enlargement of La/Pr-O bond and the higher hyperstoichiometry (obtained by iodometric titration) showed for the doped compounds led to a higher ionic conductivity. On the other hand, all materials studied showed a p-type conductivity and the total conductivity behavior was dependent on the dopant. For instance, a non-metallic-like behavior was obtained for the materials which Co was introduced in the structure, whereas the cobalt-free compounds maintained the metal-like behavior of the parent La<sub>2</sub>NiO<sub>4+δ</sub>.

These structural changes and the electrocatalytic properties of the cations selected as dopants, played an important role in the enhancement of the low frequency processes, that are usually ascribed to the oxygen reduction reaction. All these properties combined were responsible of the polarization resistance reduction of La<sub>2</sub>NiO<sub>4+δ</sub> (Figure 1). The best cathode performance was obtained with La<sub>1.5</sub>Pr<sub>0.5</sub>Ni<sub>0.8</sub>Co<sub>0.2</sub>O<sub>4+δ</sub>, which presents similar recorded values than the well-studied Nd<sub>2</sub>NiO<sub>4+δ</sub> SOFC cathode.

### III. CONCLUSION

The different strategies carried out in the present work could improve the performance of the pristine cathodes, reducing the polarization resistance even more than two orders of magnitude.

### ACKNOWLEDGMENT

This work was financially supported by Spanish Government; ENE2011-24761 and SEV-2012-0267. Electron Microscopy Service of the UPV is also acknowledged and anode supported cells were kindly supplied by Forschungszentrum Julich.

### REFERENCES

- [1] E. Perry, S. A. Barnett. (La,Sr)MnO<sub>3</sub>-(Ce,Gd)O<sub>2-x</sub> composite cathodes for solid oxide fuel cells, Solid State Ionics, Volume 143, 2001, Pages 265-273.
- [2] L. Navarrete, M. Balaguer, V.B. Vert, J.M. Serra, Tailoring electrocatalytic properties of Solid Oxide Fuel Cell composite cathodes based on (La<sub>0.8</sub>Sr<sub>0.2</sub>)<sub>0.95</sub>MnO<sub>3+d</sub>. Fuel Cells. Volume 17, 2017. Pages 100-107.
- [3] L.Navarrete, C. Solis, J.M. Serra. Boosting the oxygen reduction reaction mechanisms in IT-SOFC cathodes by catalytic functionalization. Volume 3, 2017, Pages 16440-16444.



## PERFORMANCE AND DEGRADATION PHENOMENA OF A PLANAR IT-SOFC UNDER CRITICAL OPERATING CONDITIONS

D.M. Silva-Mosqueda\*, D. Pumiglia\*\*, F. Elizalde-Blancas\*, S.J. McPhail\*\*, F. Santoni\*\*, and C. Boigues-Muñoz\*\*

\*University of Guanajuato, Lascurain de Retana No. 5, Guanajuato, Guanajuato 36000 (Mexico)

\*\*ENEA CR Casaccia, Via Anguillarese 301, Rome 00123 (Italy)

**Abstract** – To simulate realistic operating conditions and analyze their effect on the performance of planar intermediate temperature solid oxide fuel cell (IT-SOFC) systems, a large-area (11x11 cm<sup>2</sup>) anode-supported single cell was tested for ~500h, at 650°C and 245 mA/cm<sup>2</sup>, corresponding to 43% of fuel utilization (FU), running on pre-reformate natural gas. In order to correlate the evolution of the anode reactions with temperature, and contributions from specific processes or components to the voltage drop and total resistance as a function of time, localized gas analyses and temperature measurements throughout the anode surface using a particular spot-sampling set-up, as well as I-V curves and EIS measurements, were frequently carried out. During its operation, the cell sequentially experienced several events to which thermo-cycling and intrinsic degradation have been correlated. Experimental results revealed that cathode degradation was the dominant contribution to the performance deterioration, where the formation of some insulating phases is suspected.

**Index Terms** – Cathode degradation, large-area IT-SOFC, pre-reformate natural gas, water accumulation.

### I. INTRODUCTION

Understanding the reactions and mechanisms that influence the performance, durability/long term stability, and degradation behavior of SOFCs under realistic operating conditions are still issues of major concern for the development of SOFC technology [1-3].

However, durability and performance determination of SOFCs under such conditions is complicated by the costly work and the extended time needed. In this context, it is possible to gain information by testing the cells under multiple severe operating conditions associated with their real operation. Since a strong interaction of the degradation mechanisms can be observed under such conditions, thermo-cycling and/or intrinsic chemical degradation can arise. However, each of those degradation mechanisms may become dominant under certain conditions [3]. Hence, in order to find out about the degradation origins, it is helpful

to look at the influence of the operating parameters.

Thus, the present study has been focused on the correlation of the cell operation and experienced problems with its performance and degradation phenomena.

### II. EXPERIMENTAL SET-UP AND TESTING PROCEDURE

A planar IT-SOFC with an active area of 11x11cm<sup>2</sup> provided by Elcogen AS was tested. This kind of cells are based on a 403±11 µm thick supporting and active NiO-YSZ cermet anode, a 3-6 µm thick YSZ electrolyte, and a 12±5 µm thick LSC cathode with a GDC barrier.

The novel and particular multisampling set-up used for the present study is described in detail elsewhere [4].

On the other hand, the followed testing procedure was 1) heating the cell from room temperature to 700°C at a rate of 0.5°C/min using pure N<sub>2</sub> in the anode and compressed air in the cathode, 2) the NiO in the anode and support layer was reduced using 10% H<sub>2</sub> in N<sub>2</sub>, 3) the cell was cooled to 650°C and characterized in OCV under the simulated pre-reformate natural gas composition feeding the anode (31/23/12/4/30%, H<sub>2</sub>/CO<sub>2</sub>/CH<sub>4</sub>/CO/H<sub>2</sub>O at a flow rate of 582 Nml/min) and compressed air supplied to the cathode (2240 Nml/min), 4) during the operation, constant current mode at 245 mA/cm<sup>2</sup> corresponding to 43% of FU, the cell was at the beginning (0h) and regularly characterized (every 100-150h), obtaining I-V curves, performing gas analyses under load, EIS in OCV, and temperature measurements in both, OCV and under load. Besides, after the test a SEM/EDS post-mortem analysis was carried out.

### III. RESULTS AND DISCUSSION

During the ~500h of cell operation, several events were experienced, their impact on the performance is shown in Fig. 1. Extremely high water concentration in the downstream region under discharge condition was generated as a result of the cell large-area, the high water content in the fuel and the involved electrochemical and internal reforming reactions. Hence, water accumulation at

the anode outlet was present, which also may be owed to the testing system configuration. Consequently, backflow, a momentary fuel stagnation and partial fuel depletion in the downstream region, as gas analyses also suggest, have taken place. Additionally, some sudden blackouts also have occurred. All the aforementioned events may be the cause of thermal stresses, and the subsequent cracks formation and cathode gas humidification that could have taken place through the cracks and owed to the aforesaid water accumulation. The presence of water at the cathode is not, from a fundamental point of view, expected to have an influence on SOFC performance. However, studies have shown that humidity can have a negative effect, resulting in a severe voltage drop [2].

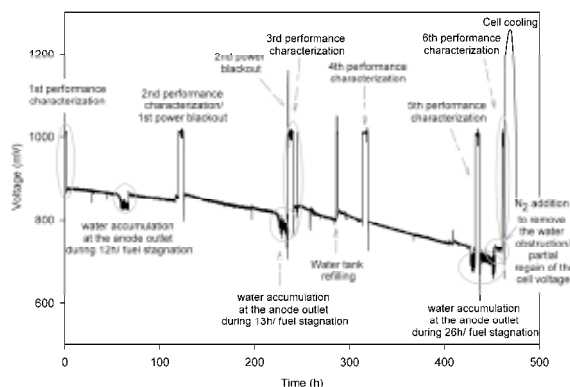


Fig. 1. Cell voltage variation with some representative events during cell operation at 245 mA/cm<sup>2</sup> (FU 43%) and 650°C.

From the obtained polarization curves it was also confirmed that the I-V characteristics of the cell were significantly degraded as a function of time. Besides, based on EIS analysis, the cell degradation has been reflected in a simultaneous increase of the internal but predominantly in the polarization resistance, which is mainly ascribed to process-related microstructural changes on the cathode [2, 3]. Furthermore, initial and final comparison of Bode plots confirm that the change in the imaginary part spans a large frequency region (~1 to 350 Hz) with the largest increase around a frequency of 35 Hz, which to a great extent coincides with the frequency range affected by oxygen partial pressure, i.e., the frequency range where cathode processes dominate [5, 6]. In addition, the region assigned to anode processes changed slightly, as polarization curves also suggested, resulting in an increase in the activation and concentration resistances [1]. However this latter was affected to a smaller extent suggesting that cathode degradation was the main contribution to the performance deterioration.

It was very tempting to interpret the fast performance degradation in the sense of a traditional poisoning effect in the cathode with a blocking of active sites. Nevertheless, as no change was observed in the OCV and a very small amount of chromium was detected by EDS analysis, which is within the error range [1], such possibility was discarded. Additionally, the SEM analysis of the anode and cathode showed that there was no visible nickel agglomeration in the anode nor delamination in any electrode, suggesting a more complex nature of the main degradation mechanism. However, the relative low anode degradation can easily be

explained by the cracks, visible to the naked eye, suggesting a thermomechanical mechanism that may arose from thermo-cycling, i.e., thermal stresses, owed to the experienced blackouts and/or the high partial pressure of water because of the backflow phenomenon at the outlet region, where the cracks and rusty zones were observed. The fact that OCV remained constant despite the cracks could be explained by the region in which the cracks were formed, since they were located in the corners of the cell at the outlet region, their contribution seemed not to be enough as to have a notable effect on the global OCV.

Since SEM/EDS analysis in the cathode showed no evidence of any particular degradation phenomenon, thus, on the basis of the experimental results along with an extensive literature review, it is suspected on the cathode/electrolyte interface interactions as the most probable cause of cathode degradation mechanism, since cathode humidification is known to make specific elements more mobile or catalyze certain processes, acting as a barrier to the ion conduction [2, 3, 7-9]. Additionally, such degradation mechanism is reported to become more evident when testing in air at the cathode side instead of pure oxygen, being strongly dependent on the oxygen partial pressure as well [8], and perfectly correlating with the EIS findings. However, as direct identification of such phases requires more advanced techniques than just SEM/EDS [2, 8], a more appropriate analysis is suggested.

#### IV. CONCLUSIONS

Although a clear assessment of the degradation mechanisms could not be given from post-mortem analysis, on the basis of all the experimental results along with an extensive literature review, a supported description of the reasons behind the resulted increase in the overall cell resistance, performance degradation and durability has been given. Thus, from this experimental investigation it has been suspected on the formation of isolating phases as the main contribution and degradation effect that arose from critical events of the real mode operation of large-area SOFCs, greatly increasing the overall cell resistance, and causing low cell performance and durability.

#### REFERENCES

- [1] Lim, H.-T., Hwang, S. C., Jung, M. G., Park, H. W., Park, M. Y., Lee, S.-S., Jung, Y.-G, Fuel cells, Vol. 13, 2013, 712-719.
- [2] Nielsen, J., Hagen, A., Liu, Y. L., Solid State Ionics, Vol. 181, 2010, 517-524.
- [3] Yokokawa, H., Tu, H., Iwanschitz, B., Mai, A., J. Power Sources, Vol. 182, 2008, 400-412.
- [4] Santoni, F., Silva, D. M., Pumiglia, D., Viceconti, E., Conti, B., Boigues, C., Bosio, B., Ulgiati, S., McPhail, S. J., J. Power Sources, Vol. 370, 2017, 36-44.
- [5] Hjelm, J., Søgaard, M., Wandel, M., Menon, M., Mogensen, M., Hagen, A., ECS Trans., Vol. 7, 2007, 1261-1270.
- [6] Kromp, A., Weber, A., & Ivers-Tiffée, E., ECS Trans., Vol. 57, 2013, 3063-3075.
- [7] Lee, T. H., Park, K.-Y., Kim, J.-T., Seo, Y., Kim, K. B., Song, S.-J., Park, B., Park, J.-Y., J. Power Sources, Vol. 276, 2015, 120-132.
- [8] Hagen, A., Liu, Y.-L., Barfod, R., Hendriksen, P.-V., ECS Trans., Vol. 7, 2007, 301-309.
- [9] Tao, Y., Shao, J., Wang, W. G., Wang, J., Fuel Cells, Vol. 9, 2009, 679-683.

## REVERSE OPERATION OF A SINGLE MOLTEN CARBONATE FUEL CELL: NUMERICAL AND EXPERIMENTAL COMPARISON

Juan Pedro Pérez-Trujillo\*, Francisco Elizalde-Blancas\* and Massimiliano Della Pietra\*\*

\*Department of Mechanical Engineering, DICIS, University of Guanajuato, 36885, Salamanca, (Mexico)

\*\*ENEA R. C. Casaccia, DTE-PCU-SPCT, Via Anguillarese 301, 00123, Rome, (Italy)

**Abstract** – This work summarizes the performance of a single Molten Carbonate Fuel Cell when operated in reverse mode. The experimental results were compared with a 0-D electrochemical model to evaluate the performance when the gas composition entering the fuel electrode and oxygen electrode, flow rates of fuel and oxygen electrodes and the operating cell temperature was varied. During the first 100 hours of test, experimental and numerical data showed a good agreement increasing discrepancies when an evident degradation occurred. The fast degradation is mainly associated to the combination of three main phenomena: electrolyte evaporation, NiO cathode dissolution, gas composition. These phenomena are increased by a high content of carbon dioxide in the oxygen electrode as was previously reported in the literature. More tests are required in order to get a better understanding of the phenomena associated with the degradation in this operating mode.

**Index Terms** – Electrolysis, Numerical modeling, Reverse Mode Operation, Single Molten Carbonate Fuel Cell.

### I. INTRODUCTION

Our planet is suffering important alterations caused by the great increase in the greenhouse gas (GHG) emissions produced by the excessive use of fuels to maintain our actual lifestyle. Carbon dioxide (CO<sub>2</sub>) represents about 95% of the energy-related emissions, also represents around 80% of the global anthropogenic GHG emissions [1]. Facing this problem, some approaches for limiting climate change include: enhance energy efficiency, use of renewable energies, decrease deforestation, reduce industrial and agricultural emissions and compensate the continuous emissions by reducing the CO<sub>2</sub> in the atmosphere by the development and implementation of carbon dioxide removal technologies [2].

Fuel cells play an important role because they can be integrated in a Power-to-Gas (PtG) system to convert surplus electricity coming from a renewable sources (e.g. wind) into gaseous energy carriers, mainly hydrogen and

methane that can be transformed back into electricity. The surplus electricity is converted into hydrogen using electrolysis, and the electricity demanded can be produced again using fuel cells [3]. Molten Carbonate Fuel Cells (MCFCs) are high temperature fuel cells that can be used in PtG processes. Nevertheless, Molten Carbonate Electrolysis Cells (MCECs) unlike Solid Oxide Electrolysis Cells (SOECs) have not been studied widely, and these studies are limited only to lab scale experiments to understand the performance during electrolysis mode using button cells [4-6]. Besides, MCFCs can also be used to separate and re-use CO<sub>2</sub> when these work in cell mode [7], this fact results interesting because they can be coupled to PtG technologies and help decreasing the GHG emissions.

### II. DEVELOPMENT

In order to assess the performance of a single MCFC working in reverse mode, an experimental campaign was carried out varying some operational parameters, which include: the gas composition entering the fuel and oxygen electrode, the fuel/oxygen electrodes flow rate (EFR) and cell operating temperature. A reference condition for MCEC operation was defined as 25/25/25/25% corresponding to H<sub>2</sub>O/CO<sub>2</sub>/H<sub>2</sub>/N<sub>2</sub> molar composition in fuel electrode and 25/25/50% corresponding to CO<sub>2</sub>/O<sub>2</sub>/N<sub>2</sub> composition in oxygen electrode. The tested gas compositions were 25/30/40/50% for H<sub>2</sub>O, 25/30/40/50% for CO<sub>2</sub> and 25/15/5% for H<sub>2</sub> in fuel electrode; in the case of oxygen electrode the following compositions were tested, 25/20/15/10/5% for O<sub>2</sub> and 25/20/15/10/5% for CO<sub>2</sub>. The tested temperatures were 650/630/610/590/570°C using the reference composition. A change of one variable was tested at a time, while the others were maintained constant with the exception of nitrogen composition that was used to balance the mixture.

### III. RESULTS

All of the cases listed above were tested in cell and electrolysis mode. The single cell was run during ~700h, only in cell mode, with the aim of getting stabilized conditions and to study the cell performance under typical conditions in order to compare with six actual electrochemical models, which were evaluated at 100mA/cm<sup>2</sup>. The minimum error between the numerical and experimental voltage was 11.6%. In order to get a better correlation, the model with the lowest error was chosen [8] and the coefficients related to the concentration and polarization were recalculated, decreasing the error until 0.3%. The recalculated coefficients were higher indicating that concentration polarization is greater in this configuration.

The cell was also operated in reverse mode; it was found that electrolysis mode shows a lower polarization resistance, which can be good to explore new applications of this kind of fuel cells. Regarding flow rate variations, it was found that increasing the EFR ratio improves the performance of the cell. Related with composition variations, in the fuel electrode was found that hydrogen quantities close to zero diminish the performance of the cell; in the case of oxygen electrode a low percentage of oxygen or a big amount of carbon dioxide causes a low performance as [9] had found, moreover it can accelerate electrolyte evaporation and nickel dissolution. The error between the numerical and experimental performance is small at the first 100 hours of operation, increasing when the tests progress, which could be explained by a degradation of the components. However, in all the cases the trend of performance compared with the parameters tested is maintained, indicating that the model is useful to evaluate the performance of the cell working in reverse mode as is indicated in Fig. 1 which presents the performance of the cell in reverse mode in terms of water effect.

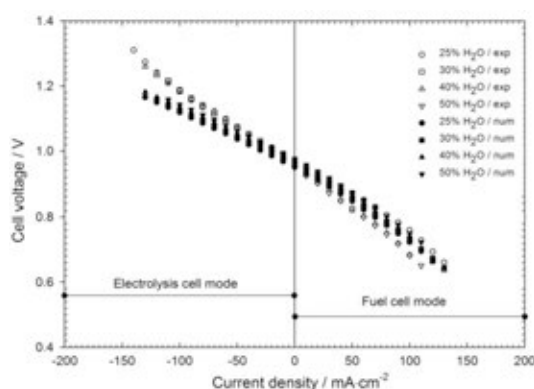


Fig. 1. H<sub>2</sub>O concentration effect supplied to the fuel electrode during MCFC reverse operation.

Fig 2 summarizes the evolution of the internal resistance during the experimental campaign divided in three zones 1) cell mode, 2) reverse mode and 3) electrolyte refilling performed to diminish the internal resistance. The first zone related to cell mode, from 350h to ~700h, does not have significant changes in the internal resistance. Contrary for the second zone where reverse mode was tested, from

~700h to ~1000h, which presents a significant rise in the internal resistance about  $4.2 \times 10^{-5} \Omega/h$ . This degradation is mainly related to an atmosphere in the oxygen electrode rich in CO<sub>2</sub> causing electrolyte loss and Ni dissolution.

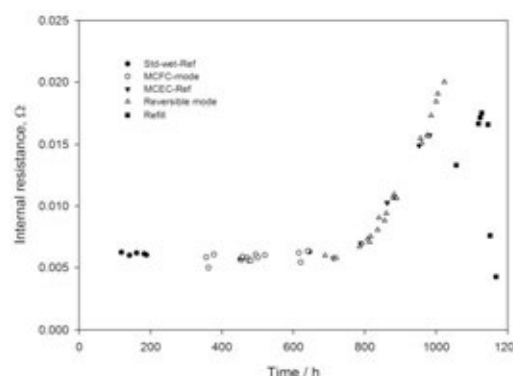


Fig. 2. Internal resistance during all the operation of the cell.

The third zone, from ~1 000h to ~1 200h, presents the electrolyte refilling, which was added during the operation of the cell using the cell reference composition, 70/18/12% of H<sub>2</sub>/CO<sub>2</sub>/H<sub>2</sub>O in the fuel electrode and 6/12/82% of CO<sub>2</sub>/O<sub>2</sub>/N<sub>2</sub> in the oxygen electrode at 650°C. It can be observed that in this zone the addition of electrolyte helps to decrease the internal resistance, however this technique should be improved in order to avoid high corrosion on the components.

### IV. CONCLUSIONS

A single MCFC was operated in reverse mode showing that in electrolysis mode a lower polarization resistance is present. Moreover a numerical comparison was performed showing a good relationship between the tested parameters and its influence on the performance. Nevertheless, it was found that a high partial pressure of carbon dioxide in the flow entering the oxygen electrode, is the main cause of deterioration of the cell, related to the electrolyte evaporation and Ni dissolution. In general the results show that MCECs can be used as an alternative technology to produce hydrogen, however more experiments should be performed to understand deeply the occurring phenomena.

### REFERENCES

- [1] R. Quadrelli, S. Peterson, Energy policy, vol. 35, 2007, pp. 5938-5952.
- [2] C. B. Field, K. J. Mach, Science, vol. 356, 2017, pp. 706-707.
- [3] M. Beaudin, H. Zareipour, A. Schellenbergglabe, W. Rosehart, Energy for Sust. Develop., vol. 14, 2010, pp. 302-314
- [4] L. Hu, I. Rexed, G. Lindbergh, C. Lagergren, Int. Journal of Hydrogen Energy, vol. 39, pp. 12323-12329.
- [5] L. Hu, G. Lindbergh, C. Lagergren, Journal of The Electrochemical Society, vol. 162, 2015, pp. F1020-F1028.
- [6] L. Hu, G. Lindbergh, C. Lagergren, Faraday Discussions, vol. 182, 2015, pp. 493-509.
- [7] J.-H. Wee, Renewable and Sustainable Energy Reviews, vol. 32, 2014, pp. 178-191.
- [8] E. Arato, E. Audasso, L. Barelli, B. Bosio, G. Discepoli, Journal of Power Sources, vol. 330, pp. 18-27, 10 2016.
- [9] H. Morita, M. Kawase, Y. Mugikura, K. Asano, Journal of Power Sources, vol. 195, pp. 6988-6996, 2010.



## SABATIER BASED POWER-TO-GAS SYSTEM: DESIGN AND THERMOECONOMIC ANALYSIS

C. Toro\*, E. Sciubba\*

\* Department of Mechanical and Aerospace Engineering, University of Roma "Sapienza", Italy

**Abstract** – Object of this paper is the modelling, process design and simulation of a CO<sub>2</sub> methanation plant based on the Sabatier reaction. Through methanation, H<sub>2</sub> is converted into CH<sub>4</sub> which can be then stored in the existing natural gas network. When the methane thus produced is burned, the CO<sub>2</sub> absorbed in the process returns to the environment, in a global sense realizing a quasi- zero-emissions cycle. A thermoeconomic analysis is presented to evaluate the exergetic performance of the proposed system and the final cost of products and to compare it with other current carbon capture and energy storage technologies considering the effect of the main plant parameters.

**Index Terms** - Methanation, CCS, system simulation, thermo-economics.

### I. INTRODUCTION

Numerous different carbon capture techniques have been explored through the years to develop an alternative solution to geological sequestration, which is still facing several technical and economic challenges. Among many, the most promising and well-established method is the hydrogenation of carbon dioxide, i.e. the reaction of carbon dioxide with hydrogen in presence of a catalyst. A useful product of this combination is methane (CH<sub>4</sub>): through the well-known Sabatier reaction or methanation, captured exhaust CO<sub>2</sub> can be transformed and chemically recycled in a very valuable and easy-to-use fuel. Methanation is also a promising process for electric energy storage. Surplus renewable electricity can feed an electrolyser to split water (H<sub>2</sub>O) into oxygen (O<sub>2</sub>) and hydrogen (H<sub>2</sub>). Through methanation, H<sub>2</sub> is converted into CH<sub>4</sub>, which is more suitable to be stored, burned or sent into natural gas pipelines.

In this study the captured CO<sub>2</sub> is chemically converted and stored into an easy-to-use fuel (SNG): surplus renewable electricity feeds an electrolyser to split water (H<sub>2</sub>O) into oxygen. The thermodynamic models of these components have

been developed and implemented into the library of an in-house modular object-oriented process simulator, CAMEL-Pro™ [1]; thus, the preliminary layout of the proposed methanation plant has been designed and simulated, then, by means of this simulator, the exergetic performance and the thermoeconomic assessment of the plant have been analyzed.

### II. SIMULATION OF THE INTEGRATED CO<sub>2</sub> CHEMICAL SEQUESTRATION PLANT

The schematic diagram of the proposed power to gas plant is reported in Fig 1. The main input of the system are the CO<sub>2</sub> mass flow rate (0,145 kg/s) and the electrical power consumption (4,15 MW).

For the complete reaction of the CO<sub>2</sub>, the stoichiometry of the reaction requires 0,01 kg/s of H<sub>2</sub>, produced by a fed water electrolyser, operating at 381 K and 202,6 kPa. The electrical consumption of the water electrolyser is 43,4 kWh/kg<sub>H<sub>2</sub></sub>, which is reflected in an electrolysis efficiency of 90,8%. The electrolyser absorbs therefore 19,3 kWh per kg of CH<sub>4</sub> produced, with a chemical efficiency of 64,53% calculated considering the LHV of CH<sub>4</sub>. Moreover 3,48 kg of O<sub>2</sub> per kg of CH<sub>4</sub> are available as a by-product of the process. Oxygen is produced consuming 5,47 kWh/kg<sub>O<sub>2</sub></sub>. The products of the Sabatier Reactor are 0,06 kg/s of CH<sub>4</sub> and 0,11 kg/s of steam, both exiting from the reactor at 573,15 K and 194 kPa. About 0,42 kg of CH<sub>4</sub> are produced per each kg of CO<sub>2</sub> captured, resulting from a Sabatier reaction CO<sub>2</sub> conversion yield of 93.48%; therefore, considering the LHV of CH<sub>4</sub>, from the sequestration process 18,47 MJ/kg<sub>CO<sub>2</sub></sub> are recovered. The mass composition of the produced syngas is CH<sub>4</sub> (81,5%), CO<sub>2</sub> (15,5%) and H<sub>2</sub> (2,86%), with these values the product is suitable to be injected into the natural gas network and its LHV is 44,2 MJ/kg. The thermal power produced by the Sabatier reaction is recovered: a water evaporative cooler is adopted and the additional steam generated contributes to the

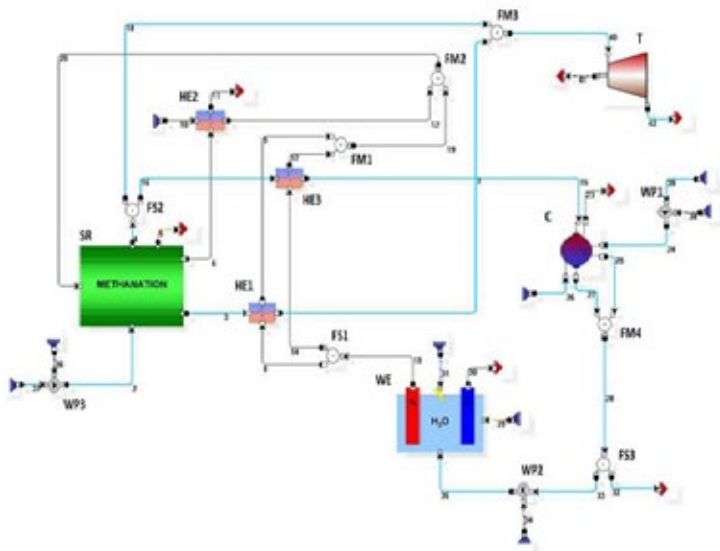
Copyright © 2017

exchange heating network. The cooling steam is split and used to heat up the remaining share of hydrogen mass flow up to the design conditions. With this system configuration it has been calculated that it is possible to cover the 100% of the heating demand.

### III. THERMO-ECONOMIC ANALYSIS RESULTS

The evaluation is performed with the following assumption for the inlet parameters: CO<sub>2</sub> sequestration cost equal to 25€/t<sub>CO2</sub> and the CO<sub>2</sub> emission trades to 9€/t<sub>CO2</sub> [2]; the cost of electricity equal to 20€/MWh (nearly half of the market price[3]) and  $\tau=7008$  h.

Fig. 1. Flowsheet of the CO<sub>2</sub> methanation system



In Table I the obtained products costs are reported.

CH <sub>4</sub> cost [€/smc]	0.47
O <sub>2</sub> cost [€/smc]	0.003
Electricity cost [€/MWh]	50.44

The effect of the electricity cost, the CO<sub>2</sub> emission trades, the CO<sub>2</sub> sequestration costs and the working hours of the plant on products cost have been evaluated.

The simulation were performed considering three load periods: the peak load (30% of the yearly hours), the lower load (45%) and the base load period (80%). The cost of CH<sub>4</sub> is higher for the shortest period of plant operation at full load, due to a minor amortization of the plant capital investment. As it possible to see the plant results economically convenient only if working for the base load. The second parameter which effect of the system is the cost of CO<sub>2</sub>. This dependence is composed by two different aspects: one is connected to the emission trades and the other one to the sequestration costs. For this analysis the system is considered working for 7008 h per year (base load) and there will be compared the effect of the

emission trades assuming different and relatively low costs of electricity (0 €/MWh, 5 €/MWh, 10 €/MWh and 15 €/MWh). The dependence from the CO<sub>2</sub> emission trades is slight compared to the dependence on the electricity cost.

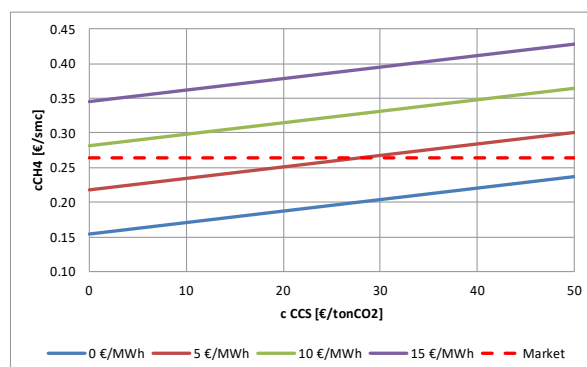


Fig. 2. CH<sub>4</sub> cost variation with with electricity cost

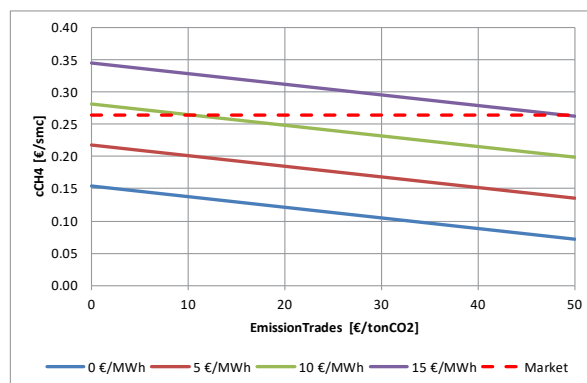


Fig. 2. CH<sub>4</sub> cost variation with emission trades

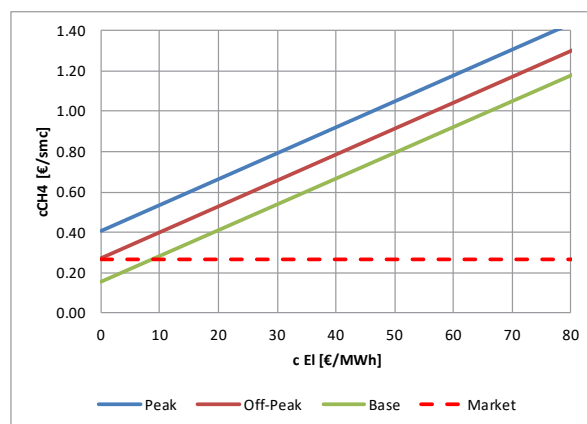


Fig. 2. CH<sub>4</sub> cost variation with load periods

## REFERENCES

- [1] Romano SL, Sciubba E, Toro C. Design and Thermoeconomic Evaluation of a Waste Plant With an Integrated CO<sub>2</sub> Chemical Sequestration System for CH<sub>4</sub> Production. 2014;V06BT7A056.
- [2] G, Simbolotti et al., IEA Energy Technology Essentials, CO<sub>2</sub> Capture & storage, OEC/IEA 2006.
- [3] <http://www.mercatoelettrico.org/it/>

**EFC17265**

**RELIABILITY OF NiO-GDC/GDC/LSCF-GDC MANUFACTURED BY TAPE  
CASTING AND REACTIVE MAGNETRON SPUTTERING PROCESSES FOR THEIR  
APPLICATION IN SOLID OXIDE FUEL CELLS.**

C.I. Hernandez Londoño\*, L. Combemale\*\*, and A. Billard\*

\*Femto-ST, 4FEMTO-ST (UMR CNRS 6174), Energy Department, Univ. Bourgogne Franche-Comté, UTBM, Rue Thierry Mieg, F90010 Belfort Cedex, (France)

\*\*ICB Dijon, 2ICB- Département I.R.M. Université de Bourgogne-CNRS UMR 6303, (France)  
carlos.hernandezlondono@utbm.fr

**Abstract** - Reactive magnetron sputtering deposition technique was used for formation of gadolinium doped ceria oxide (GDC) thin films 1-10µm.. In order to optimize the deposition of GDC to obtain high electrochemical performance of the cells, the influence of film thickness was studied. The GDC10 thin films were deposited on porous NiO-GDC (nickel oxide-Gadolinium stabilized ceria), the pre-sintered anode green tape were coated with a GDC electrolyte film by reactive magnetron sputtering using PEM (Plasma Emission Monitoring). An Alcatel SCM650 sputtering chamber was used for synthesizing the dense GDC layers. A Ce-Gd metallic target (90-10% at) was powered by a pinnacle + pulsed current generator from Advanced Energy. The structural, microstructural and morphological features of the half-cells were deposited and after different annealing treatments. The obtained half-cell, 28 mm of diameter, anode supported solid oxide fuel cell, the porous Ni-GDC10 composite anodes have been elaborated by tape casting method. The chosen ceramic powders in suspension were prepared with the mass ratio of 65:35 for NiO to GDC10. The cathode, which is made of (LSCF-GDC10) was screen printed onto electrolyte film and sintered to form a complete SOFC. Finally, the microstructural morphological /porosity/surface features of the cell were analyzed by Scanning Electron Microscopy (SEM) and X-ray diffraction (XRD). Pycnometry and porosimetry techniques were primarily used to determine pore size and pore volume by equation Washburn and Ideal gas law-method.

**Index Terms** – SOFC, PEM, Tape Casting

## I. INTRODUCTION

It was recognized that a massive use of solid oxide fuel cells goes through a reduction of the operating temperature around 500-600 °C in order to limit the cost of materials and the reactivity between the components of the fuel cell core and thus increase their service life. The planar and circular support anode configuration ( $\varnothing = 28$  mm) was chosen. Indeed, this type of stack has a mechanical stability, one of the main difficulties related to the shaping of the cell is the adhesion between the different layers. The samples of this work are constituted by the tape casting of the anode and the electrolyte by physical vapor deposition (Physical Vapor Deposition) and finally the cathode by screen printing.

## II. EXPERIMENTAL

### A. Synthesis and Preparation

The chosen anode material was NiO (Sigma-Aldrich). It was used with GDC10 (Neyco-Vacuum & Materials) electrolyte to make a composite cermet and Cathode with LSCF (Neyco-Vacuum & Materials). This

cermet structure will be employed to give high fuel conversion efficiency and create as large TPB (Triple phase boundary) as possible to enhance performance. The chosen ceramic powders in suspensions was prepared with mass ratio of 65:35 for NiO to GDC10 Fig 1. We report our finding on fabrication that was prepared with mass ratio of 35:65 GDC10 to LSCF cathodes with graded microstructures fabricated by screen printing Fig. 2. The effect of the amount of pore formers on the performance of the graded cathode was determined. The chosen ceramic powders in suspensions was prepared with mass ratio of 65:35 for NiO to GDC10. This gives the best optimal performance and after reduce the amount of 40% volume of Ni remains in the cermet. The pore formers are not active materials as it burn out during sintering step. In first attempt, graphite was used as pore former. Different percentage of pore former was tried and results were discussed and then other pore former carbon black was tested. Slurry or suspension preparation; Once all the ceramic powders, solvents (Ethyl Methyl Ketone (MEK)), dispersants (Triethanol amine), binders, plasticizers (BBP- Benzol Butyl phthalate and PEG-Poly Ethylene glycol), pore formers (graphite) are selected; these are taken in grinding jar. The zirconia balls of diameter 10mm were used along with the ingredients to grind or mill them. Slurry preparation was generally done in two steps to ensure homogeneous suspension. One-step ceramic powders, dispersants, solvents are added in and made to disperse well; pore formers are also added in the first step of the preparation of electrode slurry. In the second step binders, plasticizers are added and milled. This is made to mill well for 24 hours (Turbular-System Schatz Willy a Bachofeng (Ball Milling)). So now, the suspension is ready to use. The viscosity of the suspensions is already custom made according to the amount of powders and solvents used. Casting of suspension was done usually on glass plate sheet made of polyethylene glycol. This will help to peel the tape easily after drying. The thickness of layer to be casted will depend on the electrode suspension. There is certain minimum thickness of blade to be maintained during casting for an anode support AFL (Anode Functional Layer) + AS (Anode Substrate) with Elcometer 4330. This range is from 300 to 400µm. Sintering is the heating step done to a tape. The synthesis of the cathode requires the installation of a stainless steel mask (AISI 304L) from Goodfellow (thickness of 100 microns). The operating conditions used must make it possible to reach a thickness of 60 µm after sintering. Scanning electron microscope observations are used to define the thickness after thermal cycling (1100 °C) for different chemical formulations LSCF48 + C (Graphite). The electrolyte was deposited on the unreduced anode by a

Copyright © 2017

thin layer deposition technique (PVD). Reactive Magnetron Sputtering (RMS) technique was suitable to deposit thin and dense layer electrolyte in An Alcatel SCM650. Gadolinine ceramics (GDC10) was made from a metal target of Ce-Gd in a reactive atmosphere. Reactive condition allows better process control and higher deposition rates compared to the use of a ceramic target. It turned out that the series of anodes were usable as a substrate; to deposit electrolyte by magnetron sputtering. The choice of temperature is crucial to obtain porous electrodes while maintaining the best possible dense electrolyte. Our preliminary progress in building a planar anode supported based on GDC electrolyte fabrication of a 28mm bilayer structure.

TABLE I THE POROSITY OF ANODE.

	Mercury Intrusion Porosimetry - Auto Pore IV	Pyno Accuracy 1340 MICROMERITICS
Density	6.51 g/cm <sup>3</sup>	6.51 g/cm <sup>3</sup>
Porosity	48.80%	-
Pore Diameter (μm)		348 to 0.003 μm

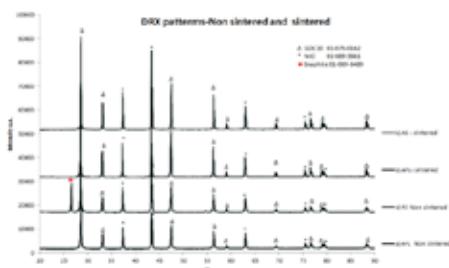


Fig. 1. Structure analysis of tape casting slurries used for anode support and anode functional layer

### III. RESULTS AND DISCUSSION

The morphological and structural characterizations of deposited GDC films, and composite ceramic substrates at various stages were studied using SEM (JEOL JSM-78000F) and XRD (Bruker D8 Advances) with Cu-Kα radiation source, respectively. Fig 2. In order to distinguish the different phases in the composite samples. The porosities of the sintered Ni/GDC10 layers were determined using either Hg porosimetry (Porosimetry - Auto Pore IV) or a standard test method based ideal gas law-method on by measuring the mass of that could be absorbed into the NiO/GDC10 layer. Thus, Fig.2. a disk-shaped anode substrate, having a diameter of about 2.8 cm, a thickness of 0.30 mm or 0.4 mm, and a porosity of about 48.8%, was then produced Table I.

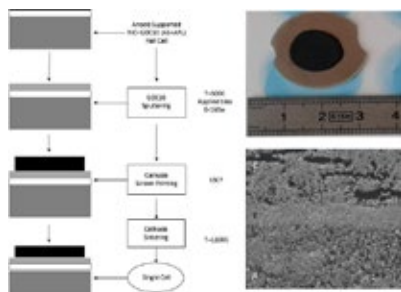


Fig. 2. Flow chart of the experimental procedure followed for fuel cell preparation of 28 mm. On the left side schematic drawing displays the fuel cell configuration. SEM micrograph of cross-section of a single cell.

### IV. CONCLUSION

The potential use of half-cell NiO-GDC/GDC10 prepared in this study reveals that the GDC film on anode-grade ceramic has thickness of 6-8 μm with relative density of 95% by pyno Acuracy 1340 and, Mercury Intrusion Porosimetry that used primarily to determine pore size and pore volume information with graded porous cathodes were fabricated via a low-cost multilayer screen printing technique. Based on interfacial resistance characterization, three-layer LSCF cathode with 5wt%. A homogenous anode microstructure was maintained the XRD patterns before sintering anode layer with C impurity phases and the temperature at the end of removal of the organic products (binder + plasticizer) is between 280 and 1100 ° C. These steps each result in an exothermic carbon peak on the thermal deviation curve at 644 ° 28 mm planar bilayer structure with GDC electrolyte film supported on NiO-GDC10 anode substrate were successfully fabricated using Magnetron Sputtering from a Gd-10 at% Ce alloy target in reactive oxygen then were made to undergo a post-treatment at 800°C for 2h. The GDC electrolyte film was almost fully dense, crack surface, and 6 μm in thickness. NiO-GDC anode substrates were almost successfully fabricated by based tapes casting method. The influence of applied bias in the properties of magnetron sputtered gadolinia-doped ceria diffusion barrier layers was studied. The applied bias had a clear effect on the microstructure and growth rate of the interlayer. Increasing bias power, in the 0-120w range, progressively inhibited the columnar structure and favored a more continuous and denser microstructure.

### ACKNOWLEDGMENT

The authors thank Université Bourgogne-Franche-Comte. Ecole Doctorale: SPIMSciences Physiques pour l'ingénieur et Microtechniques. Unité Recherche : FEMTO-S UMR6174, Univ. de Bourgogne Franche-Comté, UTBM, 90010 Belfort.

### REFERENCES

- [1] Performance of Ni/ScSZ cermet anode modified by coating with Gd<sub>0.2</sub>Ce<sub>0.8</sub>O<sub>2</sub> for an SOFC running on methane fuel Bo Huang\*, X.F. Ye, S.R. Wang, H.W. Nie, J. Shi, Q. Hu, J.Q. Qian, X.F. Sun, T.L. Wen Shanghai Institute of Ceramics, Chinese Academy of Sciences (SICCAS), 1295 Dingxi Road, Shanghai 200050
- [2] Synthesis and characterization of 10%Gd doped ceria (GDC) deposited on NiO-GDC anode-grade-ceramic substrate as half-cell for IT-SOFC M.G. Chourashiya a,\*, L.D. Jadhav b a Department of Physics, Shivaji University, Kolhapur 416 004, India b Department of Physics, Rajaram College, Kolhapur 416 004, India.
- [3] Fabrication and characterization of Ni-SSZ gradient anodes/SSZ electrolyte for anode-supported SOFCs by tape casting and co-sintering technique Chao Jin a, Yachun Mao c, Naiqing Zhang b,c,\*, Kening Sun b,c,\* a Department of Chemistry, Harbin Institute of Technology.
- [4] Manufacturing and Characterization of Single cell Intermediate-Temperature Solid Oxide Fuel Cells for APU in transportation application. Visweshwar Sivasankaran. Dijon France. 2ICB- Département I.R.M. Université de Bourgogne-CNRS
- [5] [5.] F. Perry, A. Billard, C. Frantz, Surface Coatings Technology 94-95 681 (1997).
- [6] . E. Charsley et al., American Laboratory, January, 1990
- [7] Properties of bias-assisted sputtered gadolinia-doped ceria interlayers for solidoxide fuel cells F.C. Fonseca, S. Uhlenbrucka,\*, R. Nedélécia, H.P. Buchkremer a Forschungszentrum Jülich GmbH, D-52425 Jülich, Germany b Instituto de Pesquisas Energéticas e Nucleares, 05508-000 São Paulo, Brazil
- [8] Gadolinia-doped ceria films deposited by RF reactive magnetron sputtering Yu-Lin Kuo a,□, Chiapng Lee b, Yong-Siou Chen b, Hsuang Liang b a Department of Mechanical Engineering, National Taiwan University of Science and Technology, Taipei 10672.
- [9] Graded porous solid oxide fuel cells fabricated by multilayer tape casting and co-firing progress Lifang Nie a,\*, Quan Sun a, Ze Liu b, Mingfei Liu b a School of Materials Science and Engineering, Tianjin Polytechnic University, Tianjin, China b School of Materials Science and Engineering, Georgia Institute of Technology, Atlanta, GA, USA





## INFLUENCE OF TAR AND HCL ON SOFC ANODES IN INTEGRATED BIOMASS GASIFIER SOLID OXIDE FUEL CELL SYSTEMS

A. Cavalli\*, M. Kunze\*\*, and P. V. Aravind\*

\*Process & Energy Department, 3me Faculty, Delft University of Technology, Leeghwaterstraat 39, 2628 CA, Delft, (The Netherlands)

\*\*Institute of Energy and Process Systems Engineering, Technical University Braunschweig, Franz-Liszt-Straße 35, D-38106, Braunschweig, (Germany)

**Abstract** - Integrated Biomass Gasifier Solid Oxide Fuel Cell Systems represent an alternative to fossil fuel based power plants. Hot gas cleaning and direct internal tar reforming are fundamental to achieve high efficiency and decrease system complexity. In this paper, we mainly present the results of short-term experiments on the cross-influence of HCl and tar on Ni-GDC SOFC. The cell was fed with humidified hydrogen and an increasing concentration of toluene (2.5, 4.2 and 8.5 g/Nm<sup>3</sup>) and HCl (8, 42 and 82 ppmv). Successively, 8.5 g/Nm<sup>3</sup> of toluene and an increasing concentration of HCl were fed to the cell. We used Current-Voltage curves and outlet gas composition to evaluate the contaminants effects. The cell seems not to be affected by the tested concentration of HCl and toluene but HCl decreases the concentration of CO<sub>2</sub> and CO. The results suggest the feasibility of tar internal reforming and the importance of studying contaminants cross-influence.

**Index Terms** – Biomass Gasifier, HCl, SOFC, Tar

### I. INTRODUCTION

Integrated biomass gasifier SOFC systems have received considerable attention for sustainable micro-CHP generation. Tar direct internal reforming represent a relevant option to decrease system complexity and further increase the efficiency thus easing the market penetration of these systems. Nonetheless, tar might cause performance losses due to carbon deposition and thermal stress. Despite internal tar reforming has been investigated with thermodynamic equilibrium calculations (e.g., [1] and [2]), and with experiments using both humidified hydrogen (e.g., [3] and [4]) and syngas (e.g., [5], [6] and [7]), there is not yet general agreement on the fate of this contaminant in the anode chamber. Furthermore, the cross influence with other biosyngas contaminants such as HCl has not been studied yet in detail, but preliminary tests have been

performed in TU Delft [8]. In this paper, we mainly present the results of short-term experiments on the cross-influence of HCl and tar on Ni-GDC SOFC.

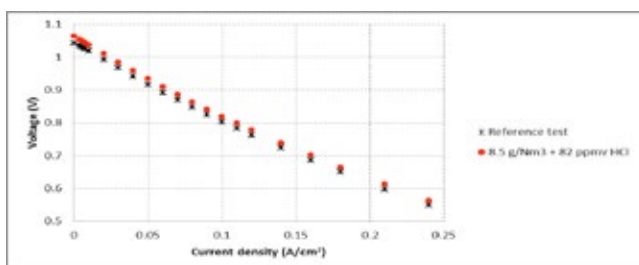
### II. METHODOLOGY

To determine the cross-influence of tar and HCl we used an electrolyte supported Ni-GDC/YSZ/YSZ-LSM cell (H.C. Starck, Germany). After having reduced the cell at 950 °C, we fed the cell with an increasing concentration of HCl first and afterward of toluene (2.5, 4.2 and 8.5 g/Nm<sup>3</sup> corresponding to 611, 1022 and 2059 ppmv) carried by a mixture of 40%vol H<sub>2</sub>, 4.2%vol H<sub>2</sub>O and balance N<sub>2</sub>. The cell was then exposed to 8.5 g/Nm<sup>3</sup> of toluene and an increasing amount of HCl (8, 42 and 82 ppmv). The exposure time to each concentration was 30 minutes for HCl, and 60 minutes for toluene and combined HCl + toluene. The cell was operated at 750 °C under a mild current of 80 mA/cm<sup>2</sup>. The anode flow rate was maintained at 1400 NmL/min while the cathode one at 1800 NmL/min air. The desired concentrations of toluene were obtained by bubbling part of the dry nitrogen flow in anhydrous toluene 99.8% (Sigma Aldrich, USA). The remaining part of N<sub>2</sub> and the H<sub>2</sub> were passed in a humidifier to reach the desired concentration of steam. HCl was added using a gas bottle containing 300 ppmv of the contaminant in H<sub>2</sub> (Linde, Germany). Initially, thermodynamic equilibrium calculations were performed using the software FactSage version 5.4.1 (Thermfact/CRCT, Montreal, Canada and GTT-Technologies, Aachen, Germany) to assure the cell was operated outside the possible carbon formation region of the ternary diagram. The cell performances were evaluated by means of i-V curve recorded using an external load PLZ603W (Kikusui Electronics Corp., Japan) and a DC power supply SM120-25D (Delta Elektronika B.V.,

The Netherlands). The extent of reforming was evaluated by monitoring the outlet gas composition using a microGC Agilent 490 with a CP-Molsieve 5Å capillary for measuring CO, H<sub>2</sub>, N<sub>2</sub> and CH<sub>4</sub> and a PoraPlot U capillary for measuring CO<sub>2</sub> (Agilent, USA). The outlet gas composition was monitored during the whole duration of the test. The total anode outlet flow rate was back-calculated from the inlet N<sub>2</sub> flow rate and the N<sub>2</sub> outlet concentration.

### III. RESULTS

The cell performance seems not to be aggravated by the tested concentration of HCl and toluene separately. The presence of toluene increases the cell voltage indicating the occurrence of reforming. There was no observable negative effect on current and power production when the two contaminants were jointly fed to the cell, as visible in Fig. 1. Indeed, the voltage results higher due to toluene reforming.



**Fig. 1. Cell performances with 40%vol H<sub>2</sub>, 4.2%vol H<sub>2</sub>O and balance N<sub>2</sub> (Reference test) and after 60 minutes exposure to 8.5 g/Nm<sup>3</sup> toluene + 82 ppmv HCl**

It appears toluene is converted into H<sub>2</sub>, CO and CO<sub>2</sub>. A very small amount of CH<sub>4</sub> (less than 0.05%vol) is also detected at the cell outlet. When HCl is fed together with toluene, the amounts of CO<sub>2</sub> and CO decrease indicating an effect of hydrogen chloride on tar reforming, even at low concentrations. The outlet flow rates are presented in Table 1. Quantification of toluene extent of reforming is suggested as part of future work.

**TABLE I**  
MOLAR FLOW RATES (MOL/MIN) OF CO AND CO<sub>2</sub> WHEN 8.5 G/NM<sup>3</sup> TOLUENE ARE FED TO THE CELL WITH INCREASING CONCENTRATION OF HCL

[HCl]	0 ppmv	8 ppmv	42ppmv	82 ppmv
CO (mol/min)	4.89E-04	4.41E-04	4.41E-04	3.84E-04
CO <sub>2</sub> (mol/min)	8.63E-05	7.88E-05	7.77E-05	7.11E-05

### IV. CONCLUSION

Toluene is reformed inside the anode chamber. Concentrations up to 8.5 g/Nm<sup>3</sup> do not aggravate the cell performances on the short term. However, the feasibility of direct internal tar reforming has to be confirmed by long term tests using biosyngas as tar gas carrier. Hydrogen chloride does not affect the cell performance but it hinders toluene reforming. Therefore, contaminants cross-influence is fundamental to

assure safe and efficient operation of Integrated Biomass Gasifier SOFC systems.

### ACKNOWLEDGMENT

This research is partially supported by the project “FlexiFuel-SOFC”. The project has received funding from the European Union’s Horizon 2020 research and innovation programme under grant agreement No. 641229. The authors acknowledge the preliminary work done in the internship of Y.H. Liu, supervised by Dr. M. Liu and Dr. P. V. Aravind.

### REFERENCES

- [1] D. Singh, E. Hernández-Pacheco, P.N. Hutton, N. Patel, M.D. Mann, Carbon deposition in an SOFC fueled by tar-laden biomass gas: A thermodynamic analysis, *J. Power Sources*. 142 (2005) 194–199. doi:10.1016/j.jpowsour.2004.10.024.
- [2] J. Mermelstein, M. Millan, N. Brandon, The impact of steam and current density on carbon formation from biomass gasification tar on Ni/YSZ, and Ni/CGO solid oxide fuel cell anodes, *J. Power Sources*. 195 (2010) 1657–1666. doi:10.1016/j.jpowsour.2009.09.046.
- [3] P. V. Aravind, J.P. Ouweltjes, N. Woudstra, G. Rietveld, Impact of Biomass-Derived Contaminants on SOFCs with Ni/Gadolinia-Doped Ceria Anodes, *Electrochem. Solid-State Lett.* 11 (2008) B24. doi:10.1149/1.2820452.
- [4] J. Mermelstein, N. Brandon, M. Millan, Impact of steam on the interaction between biomass gasification tars and nickel-based solid oxide fuel cell anode materials, *Energy and Fuels*. 23 (2009) 5042–5048. doi:10.1021/ef900426g.
- [5] D. Pumiglia, S. Vaccaro, A. Masi, S.J. McPhail, M. Falconieri, S. Gagliardi, L. Della Seta, M. Carlini, Aggravated test of Intermediate temperature solid oxide fuel cells fed with tar-contaminated syngas, *J. Power Sources*. 340 (2017) 150–159. doi:10.1016/j.jpowsour.2016.11.065.
- [6] A. Baldinelli, G. Cinti, U. Desideri, F. Fantozzi, Biomass integrated gasifier-fuel cells: Experimental investigation on wood syngas tars impact on NiYSZ-anode Solid Oxide Fuel Cells, *Energy Convers. Manag.* 128 (2016) 361–370. doi:10.1016/j.enconman.2016.09.048.
- [7] M. Liu, A. van der Kleij, A.H.M. Verkooijen, P. V. Aravind, An experimental study of the interaction between tar and SOFCs with Ni/GDC anodes, *Appl. Energy*. 108 (2013) 149–157. doi:10.1016/j.apenergy.2013.03.020.
- [8] Y.H. Liu, The impact of tar and HCl on SOFC performance for gasifier-SOFC system development, 2014.

## MULTISCALE MULTIPHASE SIMULATIONS AT THE GAS CHANNEL/GAS DIFFUSION LAYER INTERFACE INSIDE POLYMER ELECTROLYTE FUEL CELLS

M. Andersson\*\*\*, J. Yu\*\*, S. Beale \*\*\*\*\*, D. Froning \*\*  
and W. Lehnert \*\*\*\*\*

\* Lund University, Energy Sciences, 22100 Lund (Sweden)

\*\* Forschungszentrum Jülich, IEK-3, 52425 Jülich (Germany)

\*\*\* Queen's University, Mechanical and Materials Engineering,  
Kingston ON K7L 3N6 (Canada)

\*\*\*\* RWTH Aachen University, Modelling in Electrochemical  
Process Engineering, 52056 Aachen (Germany)

\*\*\*\*\* JARA-HPC, 52425 Jülich (Germany)

**Abstract** - A computational fluid dynamic model describing a straight channel, relevant for water removal inside a PEFC, is developed. A volume of fluid (VOF) approach is used to investigate the two-phase interface resolved flow behavior inside the gas channel including the gas diffusion layer (GDL) surface. The size and contact angle of the liquid inlet at the interface are calculated with the lattice Boltzmann approach. From our study, it is clear that the impact on the two-phase flow pattern for different hydrophobic/hydrophilic characteristics, i.e., contact angles, at the walls and at the GDL surface is significant, compared to a situation where the walls and the interface are neither hydrophobic nor hydrophilic, i.e., 90° contact angle at the walls and also at the GDL surface. A location at the side of the channel gives corner flow with a convex surface shape, while a location of the GDL surface liquid inlet in the middle of the gas channel gives droplet formation, having hydrophilic walls and a hydrophobic GDL surface.

**Index Terms** – PEFC, volume of fluid, gas channel, gas diffusion layer

### I. INTRODUCTION

With the increased concern about energy security, global warming, and air pollution, the prospect of using polymer electrolyte fuel cells (PEFCs) in forthcoming renewable and sustainable energy systems has reached significant momentum. A typical PEFC flow field consists of a series of mini/microchannels. The continuous removal of liquid water from the cathode channels is a critical issue, as rather large water droplets forming in the channels can cause flooding, i.e.,

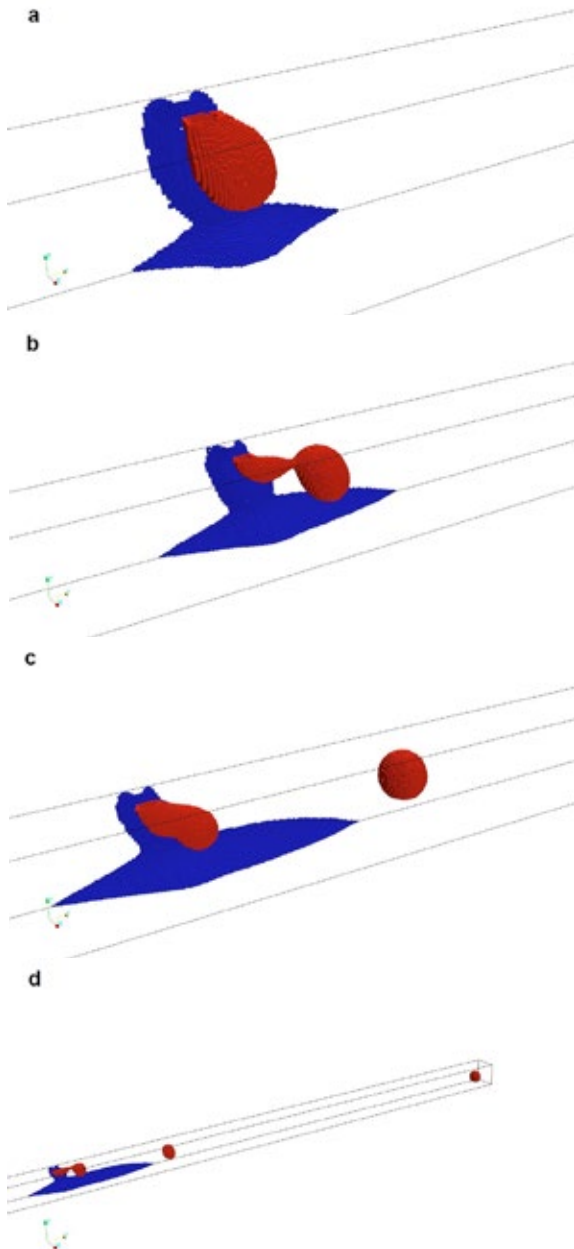
blocking the transport of gaseous oxygen to the active sites. This phenomenon gives not only an uneven current distribution, substantial loss of performance, but also, unstable operation and increased degradation rates [1]. Water generated by the electrochemical reactions often condenses into liquid form, potentially flooding the GC (gas channel), the GDL, the micro porous layer (MPL) and the catalyst layer. Insight into the fundamental processes of liquid water transport and evolution is still not complete, preventing further FC development [1,4].

Computational fluid dynamics (CFD) models make it possible to reduce the number of experiments needed for cell design and development [1-3]. The aim of this work is to obtain an increased understanding of the impact of the size of the liquid inlet at the GDL surface, for gas channels relevant for PEFCs. CFD calculations, in OpenFOAM with the VOF approach are used to be able to resolve the liquid/gas interface. The VOF model is an interface-resolving method and has become a widespread methodology for solving two-phase flow phenomena inside PEFCs. The volume fraction of liquid water at the computational cell volume schemes, with the VOF approach used to track the interface between the phases [1,5].

A model describing one straight channel with one gas inlet, one liquid inlet (at the GDL surface) and one two-phase outlet is developed. The operating parameters belong to the laminar flow regime. Notice that a developing flow region covers the entire channel. The values for viscosities, densities, and surface

tension correspond to a temperature of 60°C. The uniqueness of this work includes a calculation of contact angles at the GDL interface as well as the size of the liquid inlet, by the authors, with lattice Boltzmann calculations (3D nineteen-velocity (D3Q19) pseudopotential multiphase multicomponent isothermal LBM).

## II. RESULTS



**Fig. 1.** A side [blue] and a middle [red] location for the liquid inlet (time 0.005 (a), 0.01 (b), 0.015 (c) and 0.03 s (d)).

The location of the liquid inlet at the side of the channel is compared to a location in the middle of the channel. It is clear that a location in the middle of the channel results in droplet formation (**b**, **c** and **d**). A location close to the wall results in convex surfaced corner flow (**a**, **b**, **c** and **d**). Note that, the water stays in the channel for a significantly increased period (**d**) when the liquid inlet is located close to the wall. The water does not attach to the GDL surface for neither of the cases, besides for positions close to the liquid inlet (**a**, **b**, **c** and **d**).

## III. CONCLUSION

A CFD model describing a straight channel, relevant for water removal inside a PEFC, is developed. A VOF approach is used to investigate the interface resolved two-phase flow behavior inside the gas channel including the GDL surface.

A location of the GDL surface liquid inlet in the middle of the gas channel gives droplet formation, while a location at the side of the channel gives corner flow with a convex surface shape (having hydrophilic walls and a hydrophobic GDL interface).

## ACKNOWLEDGMENT

Financial support for this work comes from the European Commission and the Swedish government via VINNOVA (2015-01485). The RWTH Aachen University Compute Cluster (project jara0070) is used for the parallelized computer simulations.

## REFERENCES

- [1] M. Andersson, S. Beale, M. Espinoza, Z. Wu, W. Lehnert, A Review of Cell-Scale Multiphase Flow Modelling, including Water Management, in *Polymer Electrolyte Fuel Cells*, Applied Energy, 180, 2016, pp. 757–778.
- [2] M. Andersson, H. Nakajima, T. Kitahara, A. Shimizu, T. Koshiyama, H. Paradis, J. Yuan, B. Sundén, Comparison of humidified hydrogen and partly pre-reformed natural gas as fuel for solid oxide fuel cells applying computational fluid dynamics, *International Journal of Heat and Mass Transfer*, 77, 2014, pp. 1008-1022.
- [3] M. Andersson, J. Yuan, B. Sundén, SOFC Cell Design Optimization Using the Finite Element Method Based CFD Approach, *Fuel Cells*, 14, 2014, pp. 177-188.
- [4] E.C. Kumbur, M.M. Mench, *Fuel Cells - Proton Exchange Membrane Fuel Cells | Water Management*, in: J. Garche (Ed.) *Encyclopedia of Electrochemical Power Sources*, Elsevier, Amsterdam, 2009, pp. 828-847.
- [5] C.W. Hirt, B.D. Nichols, Volume of Fluid (VOF) Method for the Dynamics of Free Boundaries, *Journal of Computational Physics*, 39, 1981, pp. 201-225.



## REDOX POLYMERS FACILITATE ELECTROCHEMICAL COMMUNICATION BETWEEN BACTERIAL CELLS AND ELECTRODES

L. Gorton<sup>1\*</sup>, G. Pankratova\*, and L. Hederstedt\*\*

<sup>\*</sup>Department of Biochemistry and Structural Biology, P.O.Box 124,  
SE-221 00 Lund, (Sweden)

<sup>\*\*</sup>Department of Biology, Sölvegatan 35, SE-22362 Lund, (Sweden)

**Abstract** – One way to facilitate electrochemical communication between bacterial cells and electrodes is the use of artificial redox mediators. There are, however, a number of drawbacks when they are used in their freely diffusing monomeric form. In contrast when bound to flexible polymeric backbones they not only serve as mediators but also as an immobilization matrix forming a 3D hydrogel on the electrode surface allowing substrates and products to freely diffuse in and out of the 3D network.

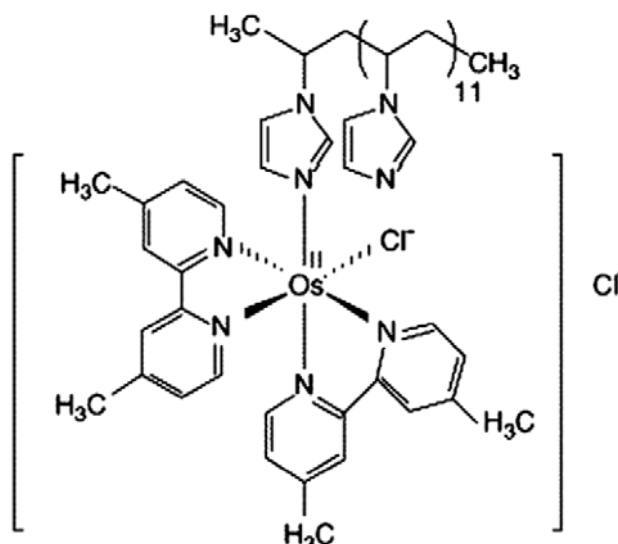
**Index Terms** – osmium redox polymer, Gram negative bacteria, Gram positive bacteria, thylakoid membrane, cyanobacter

### I. INTRODUCTION

Electrochemical communication between viable bacterial cells and electrodes could found the basis for small scale energy production, bioremediation of waste water, and (bio)electrosynthesis in microbial electrochemical systems if an efficient electrochemical communication can be established between the cells and the electrode. Only few bacterial strains have a natural built in electron transfer (ET) pathway allowing an extracellular ET (EET) connecting the cytosol through the periplasmic and outer membrane with the extracellular environment [1-4]. Examples of such bacteria are Gram negative *Geobacter* ssp. and *Shewanella* ssp.. They both have cytochromes located in the outer membrane and they may also form conductive pili or nanowires facilitating ET.

However, already in 2004 we could show that efficient EET could be mediated through “wiring” Gram negative *Gluconobacter oxydans* cells with high molecular weight osmium redox polymers (ORPs) onto both carbon and gold electrodes [5,6]. Figure 1 shows an ORP that was used as an effective redox polymer for “wiring” various bacterial cells [6]. As the ORP is highly cationic (irrespective of the pH) it will form strong electrostatic binding with enzymes and also whole

bacterial cells, most of which are negatively charged in the neutral pH range. This electrostatically formed complex will precipitate onto the surface of an electrode and form a 3D-structure, a hydrogel, within which substrates and products freely diffuse to/from the bacterial cells. The ORP thus serves additionally as an immobilization matrix for the cells. Thus even planktonic cells can be trapped and bound onto an electrode surface even though they are not naturally forming a biofilm on electrode surfaces.



**Figure 1. Chemical structure of the osmium redox polymer [poly(1-vinylimidazole)<sub>12</sub>-[Os-(4,4'-dimethyl-2,2'-dipyridyl)<sub>2</sub>Cl<sub>2</sub>]<sup>2+/+</sup>].**

Later we showed that additionally Gram positive bacteria such as *Bacillus subtilis* [7] and *Enterococcus faecalis* [8]

could be wired with such ORP. Recently additionally both ferrocene and quinone based redox polymers have also been successfully used to “wire” both Gram negative and positive bacteria as well as intact chloroplasts [4].

Recently photosynthetic cyanobacteria have been at focus as suitable organisms that can be used in biophotovoltaic cells [8]. When such bacteria are immobilized onto especially carbon based electrodes and illuminated, a photocurrent is usually observed. However, when also using an ORP, the photocurrent is dramatically much higher [9].

## II. CONCLUSION

For the future success in microbial fuel cell work it is essential to find ways on how to optimize the cell-electrode ET communication to reach high current values and the long term viability of the cells on the electrode surface. Here we have shown that the use of a flexible redox polymer can largely help increase the ET kinetics. However, any osmium based redox polymer system will never found the basis for any real practical applications of microbial fuel cells because of high costs and toxicity of osmium. Therefore in the future it is very essential to find alternative synthetic routes that will come up with well functioning redox polymers based on more environmentally friendly chemistry. Other ways to improve the ET communication has also been to engineer the electrode surface both to facilitate the growth of the cells on the electrode surface as well as to increase the electrode surface area e.g., by introducing conductive nanoparticles or to engineer the microbial cell to facilitate the ET between the cells and the electrode [1-4].

## ACKNOWLEDGMENT

The authors thank the European Commission (project “Bioenergy” FP7-PEOPLE-2013-ITN-607793) and the Swedish Research Council (project 2014-5908) for financial support.

## REFERENCES

- [1] Patil, S. A., Hägerhäll, C., Gorton, L. Electron transfer mechanisms between microorganisms and electrodes in bioelectrochemical systems, *Bioanalytical Reviews*, Volume 4, 2012 Pages, 159-192.
- [2] White, G.F., Edwards, M.J., Gomez-Perez, L., Richardson, D.J., Butt, J.N., Clarke, T.A. Mechanisms of bacterial extracellular electron exchange, in: *Advances in Microbial Physiology*, Elsevier, Volume 68, Pages 87-138.
- [3] Kumar, A., Hsu, L. H.-H., Kavanagh, P., Barrière, F., Lens, P. N. L., Lapinonnière, L., Lienhard, J.H., Schröder, U., Jiang, X., Leech, D. The ins and outs of microorganism–electrode electron transfer reactions, *Nature Reviews Chemistry*, Volume 1, 2017, Article number 0024.
- [4] Pankratova G., Gorton, L., Electrochemical communication between living cells and conductive surfaces. *Current Opinion in Electrochemistry*, in press, doi.org/10.1016/j.coelec.2017.09.013
- [5] Vostiar, I., Ferapontova, E. E., Gorton, L. Electrical “wiring” of viable *Gluconobacter oxydans* cells with a flexible osmium-redox polyelectrolyte, *Electrochemistry Communications*, Volume 6, 2004, Pages 621-626.
- [6] Hasan, K., Patil, S. A., Leech, D., Gorton, L. Electrochemical communication between microbial cells and electrodes via osmium redox systems, *Biochemical Society Transactions*, Volume 40, 2012, Pages 1330-1335.
- [7] Coman, V., Gustavsson, T., Finkelsteinas, A., von Wachenfeldt, C., Hägerhäll, C., Gorton, L. Electrical wiring of live, metabolically enhanced *Bacillus subtilis* cells with flexible osmium redox-polymers, *Journal of the American Chemical Society*, Volume 131, 2009, Pages 16171-16176.
- [8] McCormick, A. J., Bombelli, P., Bradley, R. W., Thorne, R., Wenzel, T., Howe, C. J., *Biophotovoltaics: oxygenic photosynthetic organisms in the world of bioelectrochemical systems. Energy and Environmental Science*, Volume 8, 2015, Pages 1092-1109.
- [9] Hasan, K., Grippo, V., Sperling, E., Packer, M. A., Leech, D., Gorton, L. Comparison of photocurrent generation by cyanobacteria and algae to harness sunlight, *ChemElectroChem*, Volume 4, 2017, Pages 412–417.

## NOVEL BIOINSPIRED PROTON EXCHANGE POLYSULFONE MEMBRANE CONTAINING GRAMICIDIN.

K. Szalata\*, J. Ma\*, and T. Gumi\*

\*Universitat Rovira i Virgili, Av. Paisos Catalans 26, 43007  
Tarragona, (Spain)

**Abstract** - In this work we present a new composite polysulfone membrane containing gramicidin immobilized with the use of magnetic ferrite nanoparticles. We evaluated two protein attachment methods: physical and chemical immobilization. Then, membranes were characterized in terms of morphology using ESEM, water interaction using CA, and transport properties by means of ion diffusion transport and current-voltage measurements. Results demonstrate that both modification methods enhances transport efficiency of polysulfone membranes. As well, successful gramicidin immobilization resulted in improvement of membrane selectivity, making it an attractive material to be used in fuel cell application.

**Index Terms** – composite membranes, gramicidin, ion transport, polysulfone.

### I. INTRODUCTION

Proton-exchange membrane fuel cells (PEMFCs) are promising technology for clean and efficient power source in the twenty-first century. Potential successful exchange membrane need to be characterized by high proton conductivity and selectivity, good chemical/thermal stability, good mechanical properties and low cost [1-2]. One of the approaches is creation of bioinspired materials, composed of biological and non-biological component, what connects the advantages of artificial polymeric films with biofunctionality of proteins, usually in terms of ion transport velocity and selectivity. Nevertheless biomolecule immobilization tends to be challenging due to often incompatibilities with polymer or lose of protein's biological activity [3-5].

Polysulfone (Psf) is known from its outstanding chemical, thermal and mechanical stability, while gramicidin is membrane ion channel characterized by fast and selective transport of monopositively charged ions. Purpose of this work was to design a material combining robustness of polysulfone with bioactivity of gramicidin (gA). Physical immobilization is

considered to be a good strategy of protein immobilization, without affecting their biofunctionality. Nevertheless, chemical attachment is stronger and prevent protein detachment.

In this study we evaluated two immobilization methods: physical immobilization, consisting of surfactant/gramicidin micelles formation and their immobilization on polysulfone membrane, containing magnetite nanoparticles (MNP); and chemical immobilization via glutaraldehyde coupling, which have been previously reported as a good method of biomolecules covalent immobilization to the artificial materials.

### II. MEMBRANES PREPARATION

Polymeric solutions were prepared by dissolving 15 wt% of Psf pellets in dimethylformamide. Then, 25wt% of MNP was added to the solution and the mixture was sonicated for 10 minutes. Membrane films were prepared using a casting knife with thickness of 200  $\mu\text{m}$  and films were left overnight to evaporate the solvent. Physical immobilization of protein was performed by immersing the membranes in phosphate buffer saline (PBS) solution. Next, Triton X100 (TRX) and gA were added. Surfactant concentration was above 0.29 mM. Protein concentration was 0.4 mg protein/mg of MNP. Samples were stirred during 72h at room temperature. Chemical immobilization was performed by immersing the membranes in phosphate buffer saline solution, containing >0.29 mM of TRX and 0.4mg of gramicidin/mg of MNP. Next, glutaraldehyde was added to the solution, to the final concentration of 500 mM. The membranes were stirred during 72h at room temperature. Afterwards, membranes were treated with sodium borohydride solution prepared in the basic (pH=10) carbonate-bicarbonate buffer. Then washed firstly with 2 M NaCl in phosphate buffer saline and then with 1% (v/v) TRX in phosphate buffer saline.

### III. RESULTS

#### A. Static contact angle

Copyright © 2017

The results of statistical evaluation of contact angle results are presented in the Table 1.

TABLE I  
STATISTICAL ANALYSIS RESULTS OF CONTACT ANGLE MEASUREMENTS

Membrane	p-value for CA measurements
MNP-NH <sub>2</sub> /TritonX100/gA	<0.0001
MNP-NH <sub>2</sub> /glutaraldehyde/gA	<0.0001

\*For statistical analysis the following hypothesis have been made: the CA of the non-modified MNP membranes is more than 5 degrees different from the CA of modified membranes. The p-values below 0.05 correspond to the samples which are in agreement with this assumption.

We can observe, that both immobilization methods significantly influence hydrophobic properties of polysulfone membrane.

### B. ESEM

All the investigated membranes present sponge-like morphology (Fig. 1), which is not affected by any of the immobilization treatments.

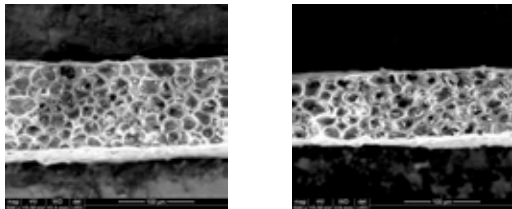


Fig. 1. The cross-section of membranes: a) Plain Psf with MNP, b) Psf with MNP, containing covalently immobilized gA.

### C. Ion diffusion experiment

As it is presented on the Fig 2, both immobilization methods enhances ion permeability.

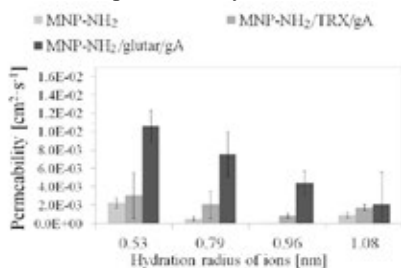


Fig 2. Permeability values in respect to the hydration radius of ions K<sup>+</sup>, Na<sup>+</sup>, Ca<sup>2+</sup> and Mg<sup>2+</sup> respectively.

Nevertheless, it is clearly visible that membrane with chemically immobilized gA, in the case of the diffusion of all the tested ions, presents the best performance.

### D. Current-voltage measurements

CV experiments results are presented on the Fig 3.

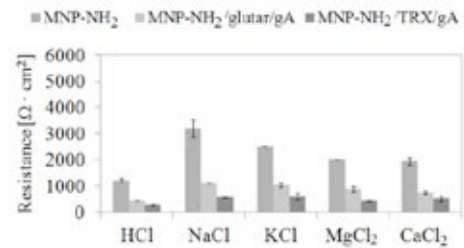


Fig 3. Ohmic resistance of the membranes with immobilized gramicidin.

We can observe, that both immobilization methods significantly decrease membrane resistance value, increasing ion conductance. However, similar like in the case of ion diffusion, the best performance is presented by the membrane with covalently attached protein.

## IV. CONCLUSION

Ion channel Gramicidin was immobilized on polysulfone membranes by two methods: physical and chemical one. Results show that both immobilization methods significantly change hydrophobic nature of polysulfone, but do not affect its morphology. Ion transport properties of the membranes are enhanced: both permeability and conductance increase is observed, especially in the case of the membrane with chemically immobilized gramicidin. This result reveals potential of this novel material in fuel cells application, because it combines resistance of the polymeric material with functionality of biomolecule.

## REFERENCES

- [1] Peighambardoust, S.J., Rowshanzamir, S., Amjadi M., Review of the proton exchange membranes for fuel cell applications, International Journal of Hydrogen Energy, Volume 35, 2010, Pages 9349-9384.
- [2] Devrim, Y., Erkan, S., Baç N., Eroğlu, I., Preparation and characterization of sulfonated polysulfone/titanium dioxide composite membranes for proton exchange membrane fuel cells, International Journal of Hydrogen Energy, Volume 34, 2009, Pages 3467-3475.
- [3] Jochems P., Satyawali Y., Diels L., et al., Enzyme immobilization on/in polymeric membranes: status, challenges and perspectives in biocatalytic membrane reactors (BMRs), Green Chemistry, Volume 13, Pages : 1609-1623, 2011.
- [4] Cao L., Immobilised enzymes: science or art?, Current Opinion in Chemical Biology, Volume 9, Pages : 217-226, 2005.
- [5] Gauthier M.A., Klok H.A., Peptide/protein-polymer conjugates: synthetic strategies and design concepts, Chemical Communications Volume 23, Pages : 2591-2611, 2008.



## ENHANCEMENT OF THE PERFORMANCE OF OXYGEN REDUCTION REACTION: THE CHARACTERISTIC ROLE OF Fe-N COORDINATIONS

Yi Wang<sup>a\*</sup>, Yongqi Hua<sup>b1</sup>, Mi Yi<sup>a1</sup>, Kun Wang<sup>b</sup>, Shuqin Song<sup>b\*</sup>,  
Angeliki Brouzgou<sup>c</sup>, Panagiotis Tsiakaras<sup>c,d,e\*</sup>

<sup>a</sup>The Key Lab of Low-carbon Chemistry & Energy Conservation of Guangdong Province, School of Chemical Engineering and Technology, Sun Yat-sen University, Zhuhai 519082, China.

<sup>b</sup>School of Materials Science and Engineering, Sun Yat-sen University, Guangzhou 510275, China.

<sup>c</sup>Laboratory of Electrochemical Devices based on Solid Oxide Proton Electrolytes, Institute of High Temperature Electrochemistry, Yekaterinburg 620990, Russia.

<sup>d</sup>Laboratory of materials and devices for electrochemical power industry, Ural Federal University, 19 Mira Str., Yekaterinburg 620002, Russia

<sup>e</sup>Department of Mechanical Engineering, School of Engineering, University of Thessaly, Pedion Areos, 383 34, Greece.

**Abstract** - Here we developed a robust and universal non precious metal catalyst, Fe<sub>3</sub>O<sub>4</sub> nanoparticles (particle size: ~50 nm) embedded in 3D cross-linking hierarchically porous N-doped carbon (noted as Fe<sub>3</sub>O<sub>4</sub>@HPNC), as a good ORR performance catalyst in both basic and acidic media. More importantly, in this hybrid there exists no Fe<sub>3</sub>C phase, which makes it easier to identify the prominent group contributing to the enhanced ORR performance. Taking into account that the enhancing factor of the ORR half-wave potential at Fe<sub>3</sub>O<sub>4</sub>-300@HPNC with respect to that at HPNC in acidic media (36.6%) is much higher than that in basic media (7.6%), it could be deduced that the role of the Fe-N coordinations for ORR in acidic media is more dominating than that in basic media. Optimized Fe<sub>3</sub>O<sub>4</sub>-300@HPNC exhibits comparable ORR activity in acidic, or even better in basic media, good stability and MeOH tolerance compared with the commercial Pt/C.

**Index terms:** Oxygen reduction reaction, Fe-N Coordination, Pyridinic N, Basic and acidic media.

### I. INTRODUCTION

Oxygen reduction reaction (ORR) is considered as a vital electrochemical process for low temperature operating electrochemical cells, unfortunately with sluggish kinetics and high over-potential values, especially in acidic media. Although Pt and Pt-based alloys have been well recognized as the best ORR catalysts, their instability, high cost and limited world reserves of Pt impedes their large-scale applications [1, 2]. Great efforts have been devoted for developing new highly efficient, durable and inexpensive alternatives to Pt-based ORR catalysts. Among them, Fe-N<sub>x</sub>-C materials, well-known *non-precious metal catalysts* (NPMCs), have been extensively investigated due to their outstanding ORR performance [3]. Generally, Fe-N<sub>x</sub>-C catalysts were synthesized

through the direct pyrolysis of precursors containing Fe, N, and C. However, even though Fe<sub>3</sub>C, pyridinic N, and Fe-N coordinations were widely recognized as active sites for catalyzing the ORR, it is still not clear the dominating functional group responsible for the enhancement of ORR performance, especially in acidic media.

Herein, we report a versatile *non-precious metal catalyst* (NPMCs), Fe<sub>3</sub>O<sub>4</sub> nanoparticles embedded in 3D cross-linking hierarchically porous N-doped carbon (denoted as Fe<sub>3</sub>O<sub>4</sub>@HPNC), synthesized by a modified classical gas-gel preparation method. In this process, (NH<sub>4</sub>)<sub>2</sub>CO<sub>3</sub> was adopted as the polymerization catalyst, N precursor, and pore-forming agent, considering that (NH<sub>4</sub>)<sub>2</sub>CO<sub>3</sub> can be easily decomposed into NH<sub>3</sub> and CO<sub>2</sub> during the pyrolysis process. Fortunately and interestingly, Fe<sub>3</sub>C phase did not exist in the as-prepared Fe<sub>3</sub>O<sub>4</sub>@HPNC hybrid, providing the guarantee of accurately investigation on the role of the Fe-N coordinations in enhancing ORR performance in both acidic and basic media.

### II. MATERIALS PREPARATION AND CHARACTERIZATION

Firstly, 1.50 mL ammonia (32 wt %) was added into the mixture solution of deionized water (40.0 mL) and ethanol (28.0 mL) with vigorous stirring. Then 300 mg resorcinol, 0.42 mL formaldehyde, 1.0000 g (NH<sub>4</sub>)<sub>2</sub>CO<sub>3</sub> and different volumes of iron chloride (0.1 mol L<sup>-1</sup> FeCl<sub>3</sub>) were added into the above mixture, followed by stirring at 30°C for 24 h. After that, the mixture was sealed in a Teflon-lined stainless-steel autoclave. The autoclave was heated to 100°C and maintained at this temperature for 24 h. The obtained brown product was centrifuged at 8,000 rpm for 3 min with washing by deionized water and ethanol, followed by desiccation at 50°C in air. Finally, the as-prepared materials were pyrolyzed at 910°C for 3

<sup>1</sup> Yi Mi contributed the same as. Yongqi Hua.

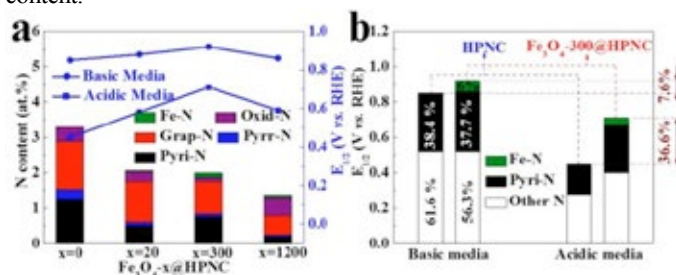
\*Corresponding authors: wangyi76@mail.sysu.edu.cn (Y. Wang); stsssq@mail.sysu.edu.cn (S. Song); tsiak@uth.gr (P. Tsiakaras),

h under flowing  $N_2$  atmosphere with a heating rate of  $5^\circ C\ min^{-1}$ . According to the adopted volume of  $FeCl_3$  aqueous solution (0, 20, 300, and 1200  $\mu L$ ), the samples were denoted as HPNC,  $Fe_3O_4$ -20@HPNC,  $Fe_3O_4$ -300@HPNC, and  $Fe_3O_4$ -1200@HPNC, respectively.

The as prepared materials were: **I**) physicochemically characterized by a) wide-angle X-ray powder diffraction, b) Transmission electron microscopy, c) energy dispersive spectrometer, d) high-resolution TEM, e) scanning transmission electron microscopy. f) X-ray photoelectron spectroscopy, g) BET; and **II**) electrochemically characterized by the aid of a rotating disk electrode and linear sweeping voltammetry.

## II. RESULTS AND DISCUSSION

In order to clarify the contributing effect of the active sites on enhanced ORR performance, based on the obtained results reported the correlations between the content of N configurations and the half wave potential ( $E_{1/2}$ ) for ORR at HPNC,  $Fe_3O_4$ -20@HPNC,  $Fe_3O_4$ -300@HPNC and  $Fe_3O_4$ -1200@HPNC in both basic and acidic media are summarized and plotted in **Fig. 1a**. Obviously, after the Fe precursor is introduced, the ORR performance is improved in some extent, especially in acidic media. Moreover,  $Fe_3O_4$ -300@HPNC possesses the best ORR performance in both basic and acidic media, which may be caused by the largest Fe-N content.



**Figure 1.** Correlation between the atomic percentage of five N configurations in the total N content and the ORR half-wave potential ( $E_{1/2}$ ) in basic and acidic media (a); Correlation between the enhancement factor of  $E_{1/2}$  and two active sites (pyridinic N and Fe-N) in basic and acidic media.

The results indicate that the improved ORR performance of  $Fe-N_x$ -C materials is related with not only the total N content but also the particular N configurations. Furthermore, considering that pyridinic N and Fe-N are the two recognized active sites for ORR in  $Fe-N_x$ -C materials, the corresponding dependence of the relative-change of  $E_{1/2}$  value of ORR in basic and acidic media on the atomic percentage of pyridinic N and Fe-N in the total N content for HPNC and  $Fe_3O_4$ -300@HPNC catalysts is further summarized (**Fig. 1b**) based on the XPS and linear sweeping voltammetry results. It can be distinguished that in the basic media, the  $E_{1/2}$  of ORR at  $Fe_3O_4$ -300@HPNC is increased by 7.6 % with respect to that at HPNC. Comparatively, in the acidic media, the corresponding increment becomes much more significant, with an enhancement factor of 36.6%. By comparing the components of the HPNC and  $Fe_3O_4$ -300@HPNC samples, it can be found that they have almost similar proportion of pyridinic N for HPNC (38.4 at. %) and for  $Fe_3O_4$ -

300@HPNC (37.7 at. %), while it is obvious the absence Fe-N coordinations in HPNC but presence of Fe-N coordinations in  $Fe_3O_4$ -300@HPNC. Based on the above analysis, one can easily infer that the role of Fe-N coordinations for the improved ORR performance in acidic media is more dominating than that in basic media.

## III. CONCLUSIONS

In summary, we have developed a novel non precious metal carbon ORR electrocatalyst,  $Fe_3O_4$  nanoparticles embedded in 3D cross-linking hierarchically porous N-doped carbon by a modified gas-gel-preparation method. It possesses almost the highest ORR activity among all reported NPMCs in basic media and even higher ORR performance in acidic media compared with the recently reported various NPMCs. It has been clarified that the role of Fe-N coordinations for improving ORR performance in acidic media is more dominating than that in basic media, which have almost not been reported yet; both Fe-N and pyridinic N improve ORR performance in basic media, while in acidic media Fe-N plays a more dominant role than the pyridinic N. This greatly provides a theoretical support for developing efficient and long-term durability non-precious metal catalyst, especially in acidic media. In addition, the optimized  $Fe_3O_4$ -300@HPNC exhibits comparable ORR activity in acidic media, or even better in basic media, superior stability and methanol tolerance compared with commercial Pt/C.

## ACKNOWLEDGMENT

The work was financially supported by the National Natural Science Foundation of China (21575299, 21576300). Prof. Song is grateful to the Tip-top Scientific and Technical Innovative Youth Talents of Guangdong special support program (No. 2016TQ03N322) for financial support. Prof. Tsiakaras is grateful to the Ministry of Education and Science of Russian Federation (Mega-Grant, no. 14.Z50.31.0001) for funding part of electrochemical tests.

Dr A. Brouzgou is grateful to the Hellenic State Scholarship Foundation (IKY) for the financing support with the Post-doctoral program NSRF (2014-2020).

## REFERENCES

- [1]. T. Jiang, L. Yan, Y. Meng, M. Xiao, Z. Wu, P. Tsiakaras, S. Song, Glucose electrooxidation in alkaline medium: performance enhancement of PdAu/C synthesized by  $NH_3$  modified pulse microwave assisted polyol method, Appl. Catal. B: Environ. 162 (2015) 275-281.
- [2]. H. Li, S. Ma, Q. Fu, X. Liu, L. Wu, S. Yu, Scalable bromide-triggered synthesis of Pd@Pt core-shell ultrathin nanowires with enhanced electrocatalytic performance toward oxygen reduction reaction, J. Am. Chem. Soc. 137 (2015) 7862-7868.
- [3]. K. Wang, Y. Wang, Y. Tong, Z. Pan, S. Song, A robust versatile hybrid electrocatalyst for the oxygen reduction reaction, ACS Appl. Mater. Interf. 8 (2016) 29356-29364.

## H<sub>2</sub>-PEMFC PERFORMANCE ON CARBON SUPPORTED ULTRA-LOW Pt (Pd<sub>x</sub>Pt<sub>y</sub>) ELECTROCATALYSTS

A. Brouzgou<sup>1</sup>, Y. Wang<sup>2</sup>, S. Song<sup>3</sup>, S. Cavallaro<sup>4</sup>, S. Freni<sup>5</sup> and P. Tsiakaras<sup>1,6,7\*</sup>

<sup>1</sup>Department of Mechanical Engineering, School of Engineering, University of Thessaly,  
Pedion Areos, 383 34, Greece.

<sup>2</sup>The Key Lab of Low-carbon Chemistry & Energy Conservation of Guangdong Province,  
School of Chemical Engineering and Technology, Sun Yat-sen University, Zhuhai 519082, China.

<sup>3</sup>School of Materials Science and Engineering, Sun Yat-sen University, Guangzhou 510275, China.

<sup>4</sup>Department of Industrial Engineering and Materials Engineering, University of Messina,  
Salita Sperone, 31 P.O. Box 29, 98166 S. Agata, Messina, Italy.

<sup>5</sup>Institute of Advanced Energy Technologies (ITAE) of the Italian, National Research Council  
(CNR) Via Salita S. Lucia sopra Contesse 5, 98126 Messina, Italy.

<sup>6</sup>Laboratory of Electrochemical Devices based on Solid Oxide Proton Electrolytes,  
Institute of High Temperature Electrochemistry, Yekaterinburg 620990, Russia.

<sup>7</sup>Laboratory of Materials and Devices for Electrochemical Power Industry,  
Ural Federal University, 19 Mira Str., Yekaterinburg 620002, Russia.

\*E-mails: tsiak@mie.uth.gr (P. Tsiakaras); brouzgou@gmail.com (A. Brouzgou); wangyi76@mail.sysu.edu.cn (Y. Wang)

**Abstract** - Very low Pt-containing electrocatalysts, Pd<sub>97</sub>Pt<sub>3</sub>/XC-72, Pd<sub>98</sub>Pt<sub>2</sub>/XC-72, Pd<sub>99</sub>Pt<sub>1</sub>/XC-72 and pure Pd/C are prepared and examined for the hydrogen oxidation reaction (HOR) in 0.5M H<sub>2</sub>SO<sub>4</sub> at room temperature. The electrocatalysts are prepared via a modified pulse-microwave assisted polyol method and they are physicochemically characterized with techniques of X-ray diffraction (XRD), transmission electron microscopy (TEM) and combined Scanning electron microscope - energy dispersive spectroscopy - electron backscatter diffraction (SEM-EDS-EBSD). According to the obtained results, all the as-prepared PdPt bimetallic electrocatalysts exhibit higher electrocatalytic activity towards HOR than pure Pd. Among the investigated electrocatalysts Pd<sub>98</sub>Pt<sub>2</sub>/C exhibited the highest electrocatalytic activity and for this reason is examined as anode electrode in a single hydrogen proton exchange membrane fuel cell.

**Keywords:** low-Pt electrocatalyst, palladium-platinum, hydrogen oxidation reaction, oxygen reduction reaction

### I. INTRODUCTION

Great attention has been paid the last decades to the proton exchange membrane fuel cells (PEMFCs) fueled by H<sub>2</sub>. Platinum (Pt) is the most commonly used and active electrocatalyst for both oxygen reduction and hydrogen oxidation reaction. However, due to the rareness and the expensiveness of Pt, it is necessary to develop low-Pt or non-Pt catalysts [1-3]. Reducing cost and improving durability are two of the most significant challenges for

intensifying the commercialization of H<sub>2</sub>-PEMFCs. The present investigation has been focused on Pd-based electrocatalysts with very low Pt loading for the hydrogen oxidation reaction in a H<sub>2</sub>-PEMFC.

### II. EXPERIMENTAL

Vulcan XC-72R (Cabot Corporation) carbon powder was used as the support material. PdCl<sub>2</sub> and H<sub>2</sub>PtCl<sub>6</sub>•6H<sub>2</sub>O were the corresponding metal precursors. All aqueous solutions were prepared by ultrapure water (18.2 MΩ cm Millipore-MilliQ) during catalyst preparation. Ethanol (>99% purity) (Sigma Aldrich) and Nafion® (5 wt.%, Dupont Company) were used for catalyst ink preparation.

**Catalysts preparation:** Pd<sub>x</sub>Pt<sub>y</sub> (x:y=97:3, 98:2 and 99:1) with different Pd/Pt molar ratios supported on Vulcan-XC72 carbon (the metal loading was kept at 20 wt.% for all the catalysts) were prepared by a modified pulse-microwave assisted polyol synthesis procedure [4].

**Membrane electrode assembly fabrication:** A Toray carbon paper (Toray TGP-H-060, Toray Industries Inc.) was used as the anode and cathode backing layer. Carbon black ink containing Vulcan XC-72R carbon black and polytetrafluoroethylene (PTFE, Aldrich) was painted onto the backing layer to form a microporous layer. To fabricate the anode catalyst layer, the Pd<sub>x</sub>Pt<sub>y</sub>/C catalyst and Nafion® solution were ultrasonically suspended in water and then brushed onto the microporous layer at 70 °C. The anode and cathode (2.5cm × 2.5cm) were placed onto each side of a

Nafion NRE-212 membrane (Aldrich) and hot-pressed at 135 °C and 1 MPa for 3 min to form the MEA.

**Physicochemical characterization:** The structure of the as-prepared catalysts was identified via the X-Ray diffraction (XRD) and transition electron microscopy (TEM) techniques. The distribution of the catalysts on the membrane electrode assembly (MEA) was investigated with the scanning electron microscopy-energy dispersive X-ray spectrometry-electron backscatter diffraction (SEM-EDS-EBSD) method.

**Electrochemical measurements:** the RDE technique is used for the investigation of hydrogen oxidation reaction over the as-prepared electrocatalysts. The membrane electrode assembly was investigated with fuel cell I-V measurements.

### III. RESULTS & DISCUSSION

#### A. Physicochemical characterization

From the XRD results the diffraction peaks of  $\text{Pd}_x\text{Pt}_y/\text{XC-72}$  catalysts at about  $40^\circ$ ,  $46^\circ$ ,  $68^\circ$  and  $81^\circ$  are attributed to the (1 1 1), (2 0 0), (2 2 0) and (3 1 1) planes of the face center cubic (fcc) structure of the PdPt alloys. Moreover, according TEM results the smallest nanoparticles and the most homogeneously distributed ones are observed for the  $\text{Pd}_{98}\text{Pt}_2/\text{C}$ ,  $\sim 5.0\text{nm}$ . Then the  $\text{Pd}_{97}\text{Pt}_3/\text{C}$  follows with  $\sim 5.5\text{nm}$  nanoparticles size and finally the  $\text{Pd}_{99}\text{Pt}_1/\text{C}$  with  $\sim 6.0\text{nm}$  nanoparticles size and inhomogeneous distribution. SEM-EDS-EBSD results for the  $\text{Pd}_{98}\text{Pt}_2/\text{XC-72}$ , shows that carbon, palladium and platinum are homogeneously distributed on the membrane.

#### B. Electrochemical characterization

The electrochemical activity of the electrocatalysts was investigated in a hydrogen saturated 0.5M  $\text{H}_2\text{SO}_4$  aquatic solution. The results from the kinetic analysis (after iR-corrected values) according to Tafel-Heyrovsky-Volmer equation are depicted in Fig. 1.

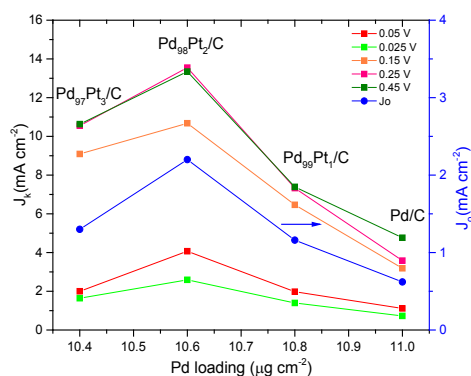


Fig. 1 Dependence of exchange current density ( $J_0$ ) and kinetic current density ( $J_k$ ) on Pd loading, according to RDE measurements in 0.5M  $\text{H}_2\text{SO}_4$ .

In all potential values, a volcano behavior is obtained. The addition of a little Pt to pure Pd electrocatalyst significantly

enhances the activity of Pd. As it is observed  $\text{Pd}_{98}\text{Pt}_2/\text{XC-72}$ .

#### C. Single fuel cell operation

The power density and polarization curves for single  $\text{H}_2\text{-O}_2$  PEMFC at different temperatures from 30°C to 80°C are respectively shown in Fig. 2. It is observed that from 30°C to 80 °C, the power density increases, from  $206\text{mW cm}^{-2}$  (or  $0.32\text{ mW } \mu\text{g}^{-1}\text{Pt}$ ), to  $313\text{ mW cm}^{-2}$  ( $0.48\text{ mW } \mu\text{g}^{-1}\text{Pt}$ ).

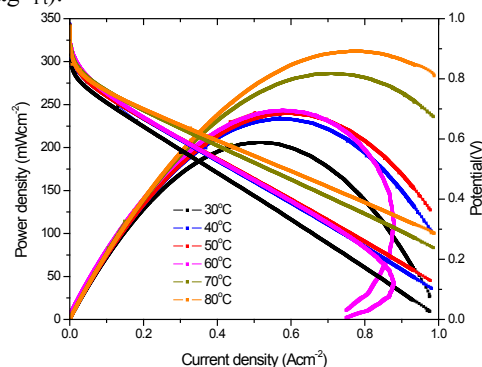


Fig. 2  $\text{H}_2$ -PEMFC operation with  $\text{Pd}_{98}\text{Pt}_2$  (20wt%)/XC-82 (anode) and  $\text{Pt}$  (40wt%)/XC-72 (cathode),  $T=30\text{-}80^\circ\text{C}$ ,  $P=1\text{ atm}$ .

### IV. CONCLUSION

According to the experimental results and the kinetic analysis, the addition of a little amount of Pt to pure Pd electrocatalyst enhances electrocatalytic activity towards HOR and ORR. More precisely, the exchange current density for HOR was calculated to have the following order:  $\text{Pd}_{98}\text{Pt}_2/\text{XC-72}$  ( $2.2\text{ mA cm}^{-2}$ ) >  $\text{Pd}_{97}\text{Pt}_3/\text{XC-72}$  ( $1.3\text{ mA cm}^{-2}$ ) >  $\text{Pd}_{99}\text{Pt}_1/\text{XC-72}$  ( $1.16\text{ mA cm}^{-2}$ ) >  $\text{Pd}/\text{XC-72}$  ( $0.62\text{ mA cm}^{-2}$ ), presenting a volcano-type dependence on Pd loading. Among the examined electrocatalysts  $\text{Pd}_{98}\text{Pt}_2/\text{C}$  and  $\text{Pd}_{97}\text{Pt}_3/\text{C}$  exhibited better activity for HOR at room temperature. Testing the first one in a single  $\text{H}_2$ -PEMFC for various fuel cell temperature values the power density was measured ca  $300\text{ mW cm}^{-2}$  at  $80^\circ\text{C}$ .

### ACKNOWLEDGMENT

Prof. Tsiakaras is grateful to Ministry of Education and Science of the Russian Federation (Mega-Grant, contract no. 14.Z50.31.0001) for support. Dr A. Brouzgou is grateful to the Hellenic State Scholarship Foundation (IKY) for financing the Post-doctoral program NSRF (2014-2020).

### REFERENCES

- [1] A. Brouzgou, S.Q. Song, P. Tsiakaras, Applied Catalysis B: Environmental, 127 (2012) 371-388.
- [2] M. Tavakkoli, N. Holmberg, R. Kronberg, H. Jiang, J. Sainio, E.I. Kauppinen, T. Kallio and K. Laasonen, ACS Catal 7, 2017, 3121-3130.
- [3] I. Ledezmayanez, W.D.Z. Wallace, P. Sebastián Pascual, V. Climent, J.M. Feliu and M.T.M. Koper, Nat. Energy 2, 2017, 17031.
- [4] S. Song, Y. Wang, P.K. Shen, Journal of Power Sources, 170 (2007) 46-49.



## ALUMINUM DOPING EFFECT ON HYDROLYSIS REACTION OF POROUS AMORPHOUS SILICA FOR HYDROGEN SEPARATION MEMBRANES

Jayoung Yoon, Ji Won Yu, and Sangheon Lee  
Department of Chemical Engineering and Materials  
Science, Ewha Womans University, 52, Ewhayeodae-gil,  
Seodaemun-gu, Seoul 03760, Republic of Korea

**Abstract** - Silica membranes exhibit poor hydrothermal stability in moist atmospheres, which is the major problem for their application in hydrogen separation processes. In this work, we examine how the hydrothermal stability of amorphous silica ( $a\text{-SiO}_2$ ) pore surfaces is affected by aluminum doping by employing first-principles calculations combined with a multiscale approach. We find that the incorporation of aluminum atoms into the  $a\text{-SiO}_2$  surface network indeed leads to the strengthening of the hydrothermal stability of the  $a\text{-SiO}_2$  pore surfaces. Thermodynamics of the surface hydrolysis reaction proves to play a key role in stabilizing  $a\text{-SiO}_2$  pore surfaces, while the influence of kinetics is negligible.

**Index Terms** - Hydrogen, Separation, Membrane, Density-functional theory

### I. INTRODUCTION

Hydrogen as a high-quality and clean energy carrier has attracted renewed and ever-increasing attention around the world in recent years, mainly due to developments in fuel cells and environmental pressures including climate change issues. One of the roadblocks to success of the hydrogen economy is the hydrogen production. Hydrogen ( $\text{H}_2$ ) is currently produced mainly from fossil fuels by steam reforming. However, this process also produces carbon monoxide (CO) as a by-product at concentrations typically in the order of 1%. The small amount of CO must be removed to prevent poisoning of the fuel cell electrodes, particularly the platinum-based anode catalysts of polymer electrolyte membrane fuel cells. Removing CO in a  $\text{H}_2$ -rich stream is a critical yet challenging issue. Although thin palladium films offer infinite  $\text{H}_2$  selectivity, palladium-based membranes have critical issues of high cost and poor thermomechanical stability.<sup>1</sup>

Amorphous silica ( $a\text{-SiO}_2$ ) typically has micropores of 0.5-2 nm in diameter with a narrow pore size distribution, which

allows selective permeation of  $\text{H}_2$  from complex gas mixtures in methane steam reforming processes. Despite of the many advantages,  $a\text{-SiO}_2$  membranes exhibit poor hydrothermal stability in moist atmospheres, which is the major problem for their application in  $\text{H}_2$  production processes.<sup>2</sup> One possible solution for improving the hydrothermal stability of the  $a\text{-SiO}_2$  membranes is doping of transition metals, such as aluminum, titanium, cobalt, and nickel. However, little is known about the fundamental causes of such stabilization of the doped  $a\text{-SiO}_2$ .

In this work, we examine how the hydrothermal stability of  $a\text{-SiO}_2$  pore surfaces is affected by aluminum (Al) atoms incorporated into the silica matrix by employing first-principles based computational methods. To this end, we calculate free energy changes and kinetic energy barriers associated with incorporation of  $\text{H}_2\text{O}$  into model  $a\text{-SiO}_2$  pore surfaces with and without an incorporated Al atom. Comparison of the calculated energy values enables us to elucidate the fundamental mechanism of how the Al doping leads to modification of the hydrothermal stability of  $a\text{-SiO}_2$  pore surfaces.

### II. CALCULATION METHODS

We view that the poor hydrothermal stability of  $a\text{-SiO}_2$  pore surfaces is attributed to the repeated surface reactions of (i) hydrolysis of  $\text{-Si-O-Si-}$  bonding networks and formation of mobile  $\text{-SiOH}$  (silanol) groups, (ii) diffusion of the mobile  $\text{-SiOH}$  groups, and (iii) subsequent condensation of redistributed  $\text{-SiOH}$  groups.<sup>3</sup> We take the resistivity of this ring-opening hydrolysis reaction as a descriptor to evaluate the hydrothermal stability of the given  $a\text{-SiO}_2$  pore surface structures.

Figure 1 exhibits the model structures that we employed. First, we obtain a model  $\text{SiO}_2$  nanoparticle ( $\text{SiO}_2\text{-nc}$ ) structure with 24 Si and 48 O atoms by performing continuous random network based Metropolis Monte Carlo (CRN-MMC) simulations based on a valence force field (VFF). As shown in Fig. 1A, the resulting  $\text{SiO}_2\text{-nc}$  (referred to as model-A, hereafter) takes a sphere-like shape and contains 7 two-membered  $\text{-Si-O-}$

Si-rings. The highly strained two-membered -Si-O-Si- rings are likely to be open by forming silanol (-SiOH) groups as a result of the hydrolysis reaction with H<sub>2</sub>O. With this regard, we introduce 3 H<sub>2</sub>O molecules into model-A and perform density-functional theory (DFT) calculations to obtain SiO<sub>2</sub>-nc with 6 -SiOH groups, as shown in Fig. 1B (referred to as model-B, hereafter). In model-B, we substitute a Si atom within a selected -SiOH group with a pair of Al and H, resulting in an Al-doped SiO<sub>2</sub>-nc with 6 -SiOH groups (referred to as model-D, hereafter), as shown in Fig. 1D. Model-C and model-E result from the additional hydrolysis reactions of the Si-O-Si bridge bonding between the two -SiOH groups in model-B and model-D, respectively. These two additional hydrolysis reactions (B→C and D→E) becomes the descriptor reactions to evaluate the hydrothermal stability of the *a*-SiO<sub>2</sub> pore surface structures without Al (B→C) and with Al (D→E), respectively. For the two descriptor reactions, we calculate free energy changes ( $\Delta G$ ) and kinetic energy barriers ( $E_a$ ) by using density-functional theory calculations.

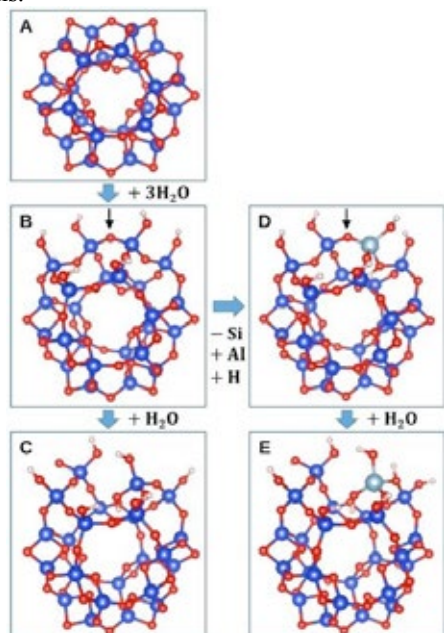


Fig. 1. Model structures that we employed. Blue, red, white, and light blue balls represent Si, O, H, and Al atoms, respectively.

### III. RESULTS AND DISCUSSION

Figure 2 displays the calculated reaction energy barriers ( $\Delta E$ ) as well as free energy changes ( $\Delta G^\circ$ ) calculated at the standard condition for the two descriptor reactions (B→C without Al and D→E with Al). For the reaction energy barriers, we find little difference between the two descriptor reactions, while both reactions yield about 1.6 eV. For the free energy changes between the initial and final states, we find significant differences between the two descriptor reactions. While both reactions are endothermic, the reaction D→E ( $\Delta G^\circ = 0.96$  eV) exhibit much greater free energy changes the reaction B→C

( $\Delta G^\circ = 0.38$  eV). The difference (0.58 eV) in the calculated free energy changes between the two reaction steps indicates that there is much more significant resistivity in dissociating the Si-O-Al bridge bond than the Si-O-Si bridge bond due the relatively strong Al-O interaction.

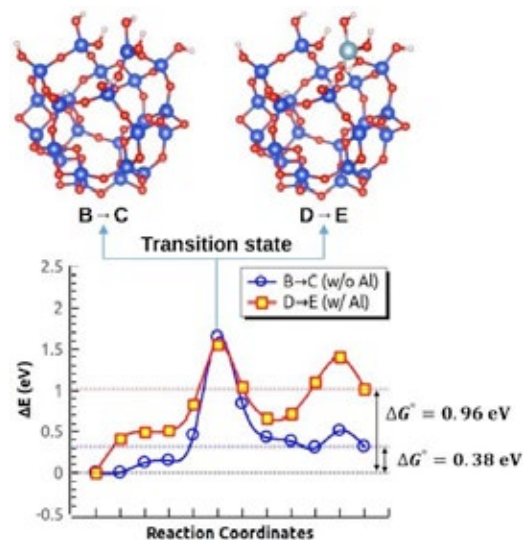


Fig. 2. Calculated reaction energy barriers ( $\Delta E$ ) as well as free energy changes ( $\Delta G^\circ$ ) at the standard condition for the two descriptor reactions (B→C without Al and D→E with Al). Two inset configurations represent transition state configurations for the respective reactions.

### IV. CONCLUSION

These calculation results suggest that the incorporation of Al into the surface SiO<sub>2</sub> network indeed leads to the strengthening of the hydrothermal stability of the *a*-SiO<sub>2</sub> pore surfaces. Thermodynamics rather than kinetics proves to play a key role in stabilizing *a*-SiO<sub>2</sub> pore surfaces, which is particularly relevant for membranes operating at high temperature conditions.

### ACKNOWLEDGMENT

This work was also financially supported by the Basic Science Research Program through the National Research Foundation (NRF) of Korea funded by the Ministry of Education (NRF-2013R1A6A3A04059268).

### REFERENCES

- [1] Yun, S., Oyama, S.T., Correlation in palladium membranes for hydrogen separation: A review, *Journal of Membrane Sciences*, Volume 375, 2011, pp. 28-45.
- [2] Battersby, S., Smart, S., Ladewig, B., Liu, S., Duke, M.C., Rudolph, V., Diniz da Costa, J.C., Hydrothermal stability of cobalt silica membranes in a water gas shift membrane reactor, *Separation and Purification Technology*, Volume 66, 2009, pp. 299-305.
- [3] Duke, M.C., Diniz da Costa, J.C., Do, D.D., Gray, P.G., Lu, G.Q., Hydrothermally robust molecular sieve silica for wet gas separation, *Advanced Functional Materials*, Volume 16, 2006, pp. 1215-1220.

## HYDROCARBON REMOVAL EFFICIENCY IN BIOELECTROCHEMICAL SYSTEMS INOCULATED WITH *CUPRIAVIDUS METALLIDURANS* CH34

A. Espinoza\*, M. Daglio\*, G. Beretta\*, S. Zordan\*, M. Seeger\*\* and A. Franzetti\*

\* University Milano-Bicocca, Piazza Della Scienza 1, Milan, (Italy)

\*\* Technical University Federico Santa María, Avenida España 1680, Valparaíso, (Chile)

**Abstract** - Bioelectrochemical remediation is an effective strategy in environments where the absence of suitable electron acceptors limits classic bioremediation, and in which bioelectrochemical systems are used for the removal of pollutants from environmental matrices. The aim of this work was to study the current production and toluene removal by *Cupriavidus metallidurans* CH34. This exoelectrogenic hydrocarbonoclastic strain was studied in three different bioelectrochemical set ups: Microbial Fuel Cells (MFCs), Microbial Electrolysis Cells (MECs) and MECs supplemented with Neutral Red (NR) as mediator. The application of an overpotential in the MEC increased toluene removal, current density and coulombic efficiency. However, the application of Neutral Red did not show any significant improvement.

**Index Terms** - Toluene, biodegradation, bioelectrochemical systems, exoelectrogenic, *Cupriavidus metallidurans* CH34

### I. INTRODUCTION

Oil spills are frequent events during routine operations such as exploration, production, refining, transportation and storage [1]. The discharge of these compounds into the environment is the principal cause of water and soil contamination [2]. Conventional strategies to bioremediate environments polluted by recalcitrant organic compounds often relies on the stimulation of the microbial population (biostimulation) by the addition of soluble electron acceptors (e.g., oxygen). Bioelectrochemical systems are a novel technology for the decontamination of environmental matrices in which the electrode can serve as alternative electron acceptor for the anaerobic respiration and as support for microbial growth. Morris and Jin (2008) used a BES to couple hydrocarbons removal with electric power production [3]. Since then, BESs have been used to study the electrochemical-driven biodegradation of hydrocarbons in water soil and sediments [2]. BTEX have been used as model hydrocarbons and their degradation in BESs has been observed both with pure cultures and communities [2,4]. BES have been used with different configurations. If artificial electron shuttles

are introduced, specific strains may improve current production in BESs [5]. *Cupriavidus metallidurans* CH34 is a model metal-resistant strain whose capacity to degrade toluene anaerobically and whose exoelectrogenic capacity have recently been described. The aim of this study was to determine whether different BES set-ups had an influence on toluene removal, current production and coulombic efficiency by strain CH34.

### II. MATERIALS AND METHODS

#### A. Strain and carbon source

After an abiotic start up period MFCs and MECs supplemented with toluene (0.65 mM) as sole carbon source and 3-amino-7-dimethylamino-2-methyl phenazine (Neutral Red, NR) (100 mM) if required were inoculated to a final OD<sub>600</sub> value of 0.1 with pure *Cupriavidus metallidurans* CH34 culture.

#### B. BESs operation

Dual-chamber custom-made three-neck glass reactors separated by a cation exchange membrane (Ultrax CMI-7000S, Membranes International Inc., USA) with 320 mL total volume were used for all bioelectrochemical experiments. Graphite rods of 8 cm<sup>2</sup> (geometric area) were used as anodes and graphite rods of 11 cm<sup>2</sup> as cathodes. No catalyst was used on the cathode. The system was autoclaved at 121 °C for 30 min, filled with sterile M9 minimal medium and flushed for 30 min with sterile-filtered N<sub>2</sub> to eliminate dissolved oxygen. According to the experiment, BESs were operated as an MFC or a two-electrodes MEC (with connection to a self-made power supply, by applying 800 mV of external voltage). Current production was measured with a data logger (Grant-Logger Type 2010). Periodical sampling was performed in order to measure toluene concentration by GC-FID. An abiotic control was set and operated in all the experiments.

#### C. Effect of the addition of Neutral Red as electron carrier

To elucidate if the addition of an electron carrier enhances current production and the efficiency of the toluene removal

process NR was used as electron transporter. Strain CH34 was grown in a MEC with toluene as sole carbon source, supplemented with NR (100 mM) by applying 800 mV between the anode and the cathode.

### III. RESULTS

Current density in the inoculated MFC ranged between 0.05 and 0.24 mA/m<sup>2</sup>, while in the abiotic control no current was detected. In the inoculated MFC toluene decreased from 61 ppm to 37 ppm (39% toluene removal) within 17 days (Fig.1B), corresponding to a degradation rate of 1 mg/L·d (Fig.1A). CE calculated after the respike until the end of the experiment was 1% (Fig.1C).

When an external voltage of 800 mV was applied between the anode and the cathode to stimulate microbial metabolism in the MEC, current densities in the inoculated reactor increased up to 47 mA/m<sup>2</sup>, while in the abiotic control current densities reached a steady state of about 10 mA/m<sup>2</sup> after 8 days. In the biotic reactor, a decrease of toluene concentration was observed after every respike. Strain CH34 was able to degrade up to 87% toluene within 18 days (Fig.1B), removing up to 3 mg/L·d (Fig.1A). CE from days 0 to 11 were not determined due to toluene adsorption processes on the abiotic reactor that could affect the CE calculation. Coulombic efficiencies of the toluene mineralization process increased during incubation from 11% up to 77% in the last batch cycle (Fig.1C). Toluene concentration in the abiotic reactor remained stable between 50 and 60 ppm during 110 days. These results suggest that strain CH34 may perform extracellular electron transfer to a solid anode, that the rate of electrons transferred to the electrode increases by applying an external voltage and that toluene is efficiently removed in a BES by *Cupriavidus metallidurans* CH34.

To determine if the application of an external electron carrier has an influence on current production, NR was supplemented in a MEC with toluene as sole carbon source. Maximum toluene removal (82%) was achieved during the fifth batch cycle (Fig.1B), corresponding to 2 mg/L·d (Fig.1A). Current density peaks reached 54 mA/m<sup>2</sup> during the second and third batch cycle, and diminished during the last two cycles (up to 50 mA/m<sup>2</sup>). Current outputs obtained in the BES amended with NR are similar to those reported in the reactor without electron carrier, demonstrating that NR had no impact in current production. In the abiotic reactor, current density maintained stable at 10 mA/m<sup>2</sup> during the whole experiment, as previously reported for abiotic MEC. CE reached a maximum value of 66% during batch cycle 3 (Fig.1C), but decreased during the last two periods. By comparing the rate and the percentage of toluene removal (Fig.1A and 1B) in the three configurations, we observed that the application of an overpotential improved the removal of the pollutant. However, no significant difference is observed when NR was added. CEs were greatly improved from the MFC to the MEC configuration (Fig.1C), probably because due to the migration of O<sub>2</sub> that acted as a competitor with the anode, from the cathodic chamber in the MFC. A significant difference between CEs in the MEC with and without NR was observed.

NR might have acted as electron-acceptor competitor with the anode. Moreover, the decrease of the efficiency of the process might be attributed to a toxic effect of NR, that in high concentrations, has been reported to inhibit cell growth, especially for gram positive microorganisms [6].

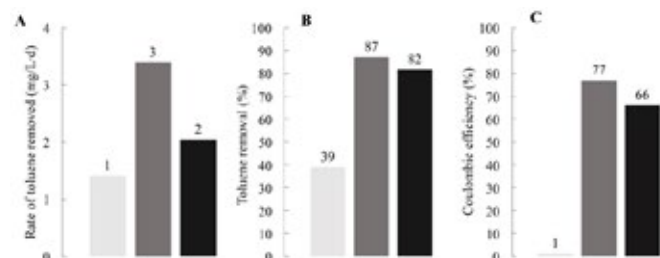


Fig. 1. Efficiency of the systems in terms of (A) rate of toluene removed, (B) percentage of toluene removed, (C) coulombic efficiency in MFC (light gray bar), MEC (gray bar) and MEC supplemented with NR (black bar).

### IV. CONCLUSION

In this study, toluene removal coupled with current generation by *C. metallidurans* CH34 was observed in MFC and improved in MEC. The addition of NR did not show a significant influence on the performance of toluene removal, indicating that it is not involved in the mechanism of electron exchange with the anode, or is in competition with it.

### ACKNOWLEDGMENT

AE gratefully acknowledge CONICYT and the DGIIP of UTFSM for PhD fellowships. MS acknowledges support from Fondo Nacional de Desarrollo Científico y Tecnológico (FONDECYT 1110992 and 1151174) and Universidad Técnica Federico Santa María grants. MD, GB and AF are supported by Fondazione Cariplo in the framework of the project BEvERAGE-BioElectrochemical Remediation of Groundwater plumes (2015-0195).

### REFERENCES

- [1] Fuentes, S., Méndez, V., Aguila, P., Seeger, M., Bioremediation of petroleum hydrocarbons: catabolic genes, microbial communities, and applications, Appl. Microbiol. Biotechnol., Volume 98, 2014, Pages 4781–4794.
- [2] Daghighi, M., Aulenta, F., Vaiopoulou, E., Franzetti, A., Arends, J., Sherry, A., Suárez-Suárez, A., Head, I.M., Bestetti, G., Rabaey, K., Electrobioremediation of oil spills, Water Res., Volume 114, 2017, Pages 351–370.
- [3] Morris, J., and Jin, S., Feasibility of using microbial fuel cell technology for bioremediation of hydrocarbons in groundwater, J. Environ. Sci. Health., Volume 43, 2008, Pages 18–23.
- [4] Daghighi, M., Espinoza, A., Leoni, B., Bioelectrochemical BTEX removal at different voltages: assessment of the degradation and characterization of the microbial communities, J Hazard Mater Volume 341, 2018, Pages 120–127.
- [5] Chang, I.S., et al., Electrochemically active bacteria (EAB) and mediator-less microbial fuel cells, Volume 16, 2006, 163–177.
- [6] Lin, C., Wu, H., Chiu, Y., and Tsai, S., Effects of different mediators on electricity generation and microbial structure of a toluene powered microbial fuel cell, Fuel, Volume 125, 2013, Pages 30–35.



## ASSESSMENT OF SOLID PHASE-MFC'S BEHAVIOUR AND PERFORMANCE BY USING DIFFERENT INOCULA

F. Flagiello\*, R. A. Nastro\*, G. Falcucci\*\*, L. Comunale \*\*\*, M. Minutillo\*

\* Department of Engineering, University of Naples Parthenope, Naples (Italy)

\*\* Department of Enterprise Engineering "Mario Lucertini", University of Rome Tor Vergata, Rome (Italy)

\*\*\* C.E.A. Spa (Consorzio Energie Alternative), km 17.700 Località Sanganiello - Caivano (NA)– (Italy), <https://www.cea.na.it>

**Abstract** –Microbial Fuel Cells (MFCs) have the potential to play an important role in developing sustainable waste recycling systems. However, the application of MFCs to the treatment and valorization of solid organic residues shows different issues, mainly linked to the high internal resistance and to the acidogenic metabolism, prevailing in the endogenous microflora. This last feature is an essential factor as it is at the basis of pH drop, which affects the cell electrochemistry and represents a crucial issue in the choice of cell materials, electrodes first.

In this work, we report the results of a survey aimed at assessing the performance of MFCs fed with a slurry composed by vegetable residues and PBS, with and without the addition of *Pseudomonas aeruginosa* ATCC 15692. *P.aeruginosa* is an exo-electrogenic bacterium responsible for vegetable residues spoilage and, for this reason, it can be a potential candidate microorganism for the performance improvement of MFCs applied to solid organic waste treatment.

**Index Terms** - Microbial Fuel Cell, *Pseudomonas aeruginosa*, Acidogenic microflora, Solid Organic Residues

### I. INTRODUCTION

Scientific interest towards Microbial Fuel Cells (MFCs) has grown in recent years thanks to the ability of MFCs to convert chemical energy in organic matter to electric power and the potential application of MFCs to both solid and liquid waste treatment is being widely explored [1], [2], [3]. The research about microbial consortia and inocula, electrodes layout and materials, boosts the progress of this energy technology [4]. *Pseudomonas aeruginosa* is a gram negative, aerobic microorganism, environmental ubiquitous and involved in food spoilage. *P.aeruginosa*, among electroactive bacteria proved to

improve MFCs efficiency by the production of phenazines, which act as a shuttle for the electrons transfer to the anode [4]. We found, in a previous research, a positive interaction among an environmental *P.aeruginosa* strain and fermentative bacteria belonging to *Lactobacillus* and *Bacillus* genera at the graphite cathode of a single-chamber, air-cathode MFC fed with the Organic Fraction of Municipal Solid Waste [3]. In this work we investigated the efficiency of single chamber, air-cathode and membranless MFCs fed with a slurry containing vegetable residues using *P. aeruginosa* ATCC 15692 as sole microorganism and the endogenous microflora, occurring in vegetable residues. MFCs had a cubic shape with a carbon fiber brush anode and a cathode composed by a nickel mesh current collector, an activated carbon layer, and a porous PTFE (Polytetrafluoroethylene) diffusion layer [1]. The organic substrate was a composed by PBS/mixed vegetables slurry (3:1 ratio). Performances were investigated in terms of Power Density (PD) and Current Density (CD). Our results showed an improvement of MFC performance in presence of *P.aeruginosa* ATCC 15692, which opportunely added to vegetable residues, can improve the MFC electric outputs.

### II. MATERIALS AND METHODS

A *Pseudomonas aeruginosa* ATCC 15692 strain was purchased from DSMZ strains collection and opportunely cultured in sterilized Tryptic Soy Broth (TSB) (Oxoid®). After 24h of incubation at 30°C, 10 µl of suspension was streak-plated on Tryptic Soy Agar (TSA). After 24h, bacteria colonies, were used to prepare 5 ml of a 1 OD<sub>600nm</sub> microbial suspension

Copyright © 2017

which was added to a slurry composed by homogenized vegetables, autoclaved at 120°C (1 atm) and added with PBS and glucose (0.5% final concentration). Final *P.aeruginosa* concentration in MFC feedstock was of 10<sup>4</sup> CFU/ml.

A second feedstock composed by not sterilized and homogenized vegetable residues and PBS was prepared with a 1:3 solid/liquid ratio. The endogenous microflora was analysed as reported in [3]. Glucose was added as well (0.5% final concentration) and pH adjusted to 7 and checked everyday. A cathode material composed by nickel mesh as current collector, an activated carbon layer, and a porous PTFE (Polytetrafluoroethylene) diffusion layer was purchased from VITO (Mol, Belgium). The PTFE cathode had a circular shape (3.5 cm radius; 7 cm<sup>2</sup> projected active surface). A carbon fiber brush (Mill-Rose Ltd.) was used as anode. Cuboid MFCs (in duplicate) were filled with 30 ml of slurry. Two test cases were conducted: 1) MFC that uses vegetable residues as substrate and has endogenous microflora (N-MFC\_end); 2) MFC that uses sterilized vegetable residues as substrate and has *P.aeruginosa* (N-MFC\_P). The operating data of the MFC reactors (Figure 1) were measured by a data acquisition system, based on the Arduino board MEGA 2560. The MFCs were monitored for 15 days.



Figure 1: Cuboid\_MFC with PTFE cathode.

The software for data acquisition was ad-hoc developed in our Lab with LabVIEW Interface for Arduino, (LIFA) package. Experiments were carried out every 48 hours using resistors from 100 Ω to 1 MΩ: voltage (V) was measured, while power (P) and current (C) were calculated. The measurement cycle consisted of two main steps: *Open Circuit Voltage* (OCV) for 24h and *Maximum Power Tracking*. An acquisition loop for the measure of the OCV, Pmax and polarization curve was implemented.

### III. RESULTS

Figure 2 shows the trend of power and voltage versus current for test cases N-MFC\_end and N-MFC\_P. These data were referred to the cathode surface (m<sup>2</sup>) and amount of solid residues (kg).

N-MFC\_P showed highest cell performances in terms of both maximum power and maximum current confirming the ability of *P.aeruginosa* ATCC 15692 to convert the organic matter from vegetable residues into electricity. The microbial microflora naturally occurring is mainly composed by *Lactobacillus*, *Bacillus*, *Clostridium* strains. This endogenous

microflora shows a worse behavior with respect to the electric power production[1,5]. The different metabolisms of in MFCs were confirmed by the pH drops (with values of 4.6±0.2) in N-MFC\_end, but not observed when *P.aeruginosa* was present.

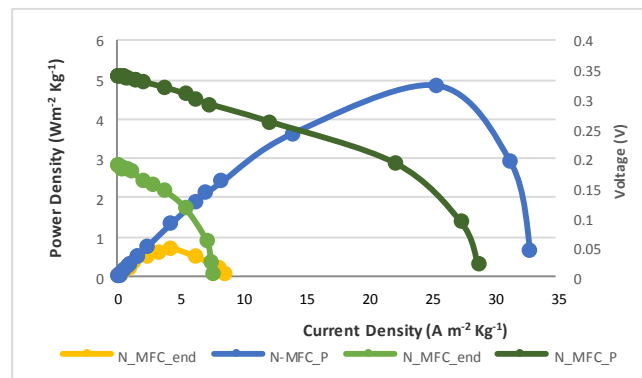


Figure 2 : Polarization and power curves at after 7 days. N-MFC\_end: MFC with endogenous microflora; N-MFC\_P: MFC with *P.aeruginosa* ATCC 15692

### CONCLUSIONS

The abundance of fermentative bacteria in vegetable residues can limit the performances of MFC application to solid waste treatment and valorization. Our results suggest that an improvement of the MFC performances could be achieved by enriching the biomass with an attenuated *Pseudomonas aeruginosa* strain. Nevertheless, further studies aimed to a direct utilization of phenazines instead of the whole microorganism (a potentially pathogenic bacteria) or other non pathogenic, phenazines producers *Pseudomonas* strains will be carried out.

### ACKNOWLEDGEMENT

This research was funded by the Italian Government, with the PON project “Smart Generation - Sustainable Systems and Technologies for the energy generation – PON03PE\_00157”

### REFERENCES

- [1] Nastro, R.A., Jannelli, N., Minutillo, M., Guida, M., Trifuoggi, M., Andreassi, L., Facci, A.L., Krastev, V.K. and Falcucci, G., Performance evaluation of Microbial Fuel Cells fed by solid organic waste: parametric comparison between three generations. ,2017, Energy Procedia, Volume 105, Pages 1102-1108.
- [2] Pandey P, Shinde V, Deopurkar R, Kale S, Patil S, Pant D. Recent advances in the use of different substrates in microbial fuel cells toward wastewater treatment and simultaneous energy recovery. Appl Energy 2016;168:706–23.
- [3] Jannelli N., Nastro R.A., Cigolotti V., Minutillo M., Falcucci G.(2017). Low pH, high salinity: too much for Microbial Fuel Cells? Applied Energy 192, 543-550.
- [4] Qiao Y. J., Qiao Y., Long Z., Xiao-Shuai W., Jian-Hua L., Biofilm promoted current generation of *Pseudomonas aeruginosa* microbial fuel cell via improving the interfacial redox reaction of phenazines. Bioelectrochemistry, 2017, Page 117.

## MOLTEN CARBONATE STEAM ELECTROLYSIS POWERED WITH CONCENTRATING SOLAR ENERGY: A FIRST EVALUATION OF THE POTENTIAL OF A NEW PROCESS FOR RENEWABLE HYDROGEN PRODUCTION

L. Turchetti\*, A. Tiberi\*\*, D. Mazzei, R. Liberatore\*, S.  
Frangini\*, C. Felici\* and M.C. Annesini\*\*

\*ENEA - Italian National Agency for New Technologies, Energy  
and Sustainable Economic Development. Via Anguillarese, 301-  
00123 Roma (Italy)

\*\*Dipartimento di Ingegneria Chimica Materiali Ambiente,  
Sapienza Università di Roma, Via Eudossiana, 18 - 00184  
Roma (Italy)

**Abstract** - A first flowsheet of a novel Molten Carbonate Steam Electrolysis process is developed and a strategy for its integration with a parabolic trough CSP plant using molten salts as heat transfer fluid proposed. The aim is to carry out a first assessment of the potential of the process and provide some guidelines for the future development of this technology.

**Index Terms** – Molten Carbonate, Process analysis, Solar energy, Steam electrolysis.

### I. INTRODUCTION

High-temperature steam electrolysis (HTSE) is gaining an increasing interest as hydrogen production process, especially in conjunction with the use of renewable energy sources. Compared to low-temperature water electrolysis, HTSE is potentially more exergetically efficient, because it can be operated with lower cell potentials and takes a non-negligible share of its energy input as heat. This also makes the integration of HTSE with concentrating solar power (CSP) plants, which may feed the process with both renewable power and heat, particularly interesting.

The current research on HTSE is mostly focused on the use of solid oxide electrolyzers operating above 700°C. Such systems have a relatively high technological maturity and their potential integration with CSP plants was already investigated [1]. More recently, molten carbonate steam electrolysis (MCSE) was proposed as an alternative HTSE process operating at temperatures around 500°C [2]. Such lower temperature may offer advantages for equipment materials and allows to take advantage of thermal storage solutions

commercially available for CSP plants, even if the operating potential is increased.

In this paper, a first flowsheet of the whole MCSE process is developed and a strategy for its integration with a parabolic trough CSP plant using molten salts as heat transfer fluid proposed. The aim is to carry out a first assessment of the potential of the process and provide some guidelines for the future development of this technology, whose maturity is currently rather low.

### II. MOLTEN CARBONATE STEAM ELECTROLYSIS

The MCSE reactor is schematized in Fig. 1. Steam and carbon dioxide are fed to the cathodic space ( $\text{CO}_2/\text{H}_2\text{O}$  molar ratio,  $s_{\text{CO}_2}=1$ ). However,  $\text{CO}_2$  is not produced or consumed in the electrolyser, but only split in the outlet gases. Downstream of the electrolyzer, water is condensed from the cathodic gas and each outlet stream is sent to a separate amine absorption column to remove  $\text{CO}_2$ , which is recycled to the electrolyser feed. A single column is used to regenerate the rich amine stream coming from both absorption columns.

MCSE was assumed to be carried out at 500°C, pressure slightly above 1 atm and close to thermoneutral conditions (1.28 V at 500°C); steam conversion was conservatively set to 60%. A flowsheet of the whole process was developed with the software AspenPlus®, used to simulate the operation and calculate the energy requirement of the plant. The production of 4000 kg/d of hydrogen at 20 bar with a purity of 99.996% on a molar basis was considered in the simulations.

### III. INTEGRATION WITH CSP PLANT

The integration of the proposed MCSE flowsheet with a 50 MW parabolic trough plant using molten salts as heat transfer fluid was considered. The CPS plant has a solar field (SF) of the same type as the Archimede plant in Priolo Gargallo (Italy) and Akesai Solar Thermal Power Plant (China, under development) [3], which provides heat to a superheated steam cycle; furthermore, the plant is equipped with a two-tank molten salt thermal energy storage (TES) system. The CSP plant is oversized compared to the power requirement of the MCSE plant, so that significant grid export is also envisaged. The heat requirement of the MCSE plant is fulfilled with service steam (saturated, 130°C) produced with molten salts from the cold tank (CT, Fig. 2) through an intermediate thermal oil circuit.

The H<sub>2</sub> production plant is assumed to work continuously. When the solar plant is not operating or the cold tank temperature is too low (<280°C), electricity is drawn from the grid and heat produced with a methane burner.

The plant was assumed to be located in Ben Guerir (Morocco), with a SF size of about 454,500 m<sup>2</sup> and 10 h nominal TES capacity.

### IV. RESULTS

Hydrogen production by the proposed flowsheet requires about 12.5 MW, 51% of which as low-temperature heat and 49% as power. Heat is required for steam production (18%) and amine regeneration (82%). Power is used for electrolysis (93%) and pumps and compressors (7%).

One year operation of the solar plant was simulated with a 0.5 h timestep, accounting for changes in Direct Normal Irradiance (DNI) and local atmospheric conditions. The results obtained for some key performance indicators are summarized in Tab. 1. Where applicable, the performance of the CSP plant alone is compared with the integrated CSP-MCSE plant.

### V. CONCLUSIONS

The approach proposed for the integration with the MCSE plant requires virtually no change to the CSP plant configuration, leads to a better exploitation of the SF (+1.5% solar energy collected) and reduces the thermal losses (-9.6 %); however, a minor reduction of the total power production is observed (-3.1%). Nearly 50% renewable H<sub>2</sub> production can be achieved even with continuous operation of the MCSE plant.

The results are encouraging and even better performance figures can be expected if the SF and TES size are optimized for the integration with the MCSE plant and higher steam conversion rates can be attained. Integrated MCSE-CSP plants appear as a new interesting option for the production of renewable hydrogen.

Collected solar energy	GWh	545.5	553.8
Dumped solar energy	GWh	11.1	6.5
Thermal losses	GWh	50.6	45.8
Energy from methane combustion	GWh	3.8	31.4
Power production	GWh	202.0	195.8
Power to grid	GWh	202.0	171.3
Overall efficiency	%	18.8	20.2
Renewable energy in H <sub>2</sub>	%	N/A	48.3

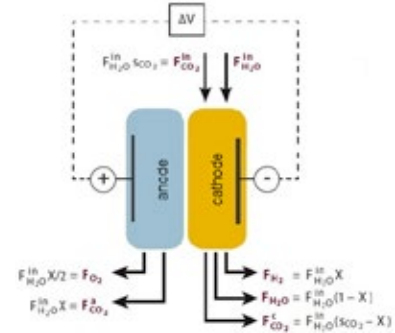


Fig. 1. Schematics of the MCSE reactor (electrolyzer)

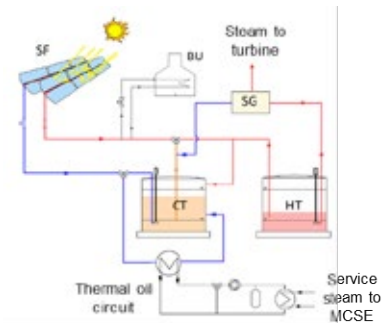


Fig. 2. Strategy proposed for the integration of the CSP and MCSE plants.

### ACKNOWLEDGMENT

This research was supported by the European Commission through the Seventh Framework Programme (FP7), project STAGE-STE, Grant agreement no: 609837.

### REFERENCES

- [1] A. Houaijia et al. (1999). International Journal of Energy Research, 39 (2015), pp. 1120-1130.
- [2] S. Frangini et al., ECS Transactions, 61 (2014), pp. 13-25.
- [3] A. Maccari et al., AIP conference Proceedings, (2016), pp. 1734

TABLE I

KEY PERFORMANCE INDICATORS OF THE CSP AND CSP-MCSE PLANTS (1 YEAR OPERATION)

Indicator	Units	CSP	CSP-MCSE
-----------	-------	-----	----------



## BIOELECTROCHEMICAL SYSTEM FOR REMOVING HEXAVALENT CHROMIUM FROM WATERS

G. Beretta\*, D. Calloni\*, A. Mastorgio\*, E. Sezenna\*, and S. Saponaro\*

\* Politecnico di Milano DICA Environmental section, Piazza  
Leonardo da Vinci 32, Milano 20133, (Italy)

**Abstract** - BES include a set of technologies that exploit the ability of certain microorganisms to use electrodes as the electrons acceptors/donors and to catalyze redox reactions in order to promote a flow of electrons. In the present study, we have assessed the possibility to remove Cr(VI) in a biocathodic chamber of a dual-chamber (2C) Microbial Electrolysis Cell (MEC) with cathode as the sole electron donor.

The cathode was first put into the anodic compartment of a 2C-Microbial Fuel Cell (MFC) inoculated with sludge from an anaerobic digester. After the acclimation period, the electrode was transferred into the cathodic chamber to work at -300 mV (vs. Standard Hydrogen Electrode - SHE) as the biocathode in a Cr(VI)-reducing MEC with 2000 µg Cr(VI)/L. The acclimation phase in the 2C-MFC allowed to shorten the time for the electroactive-biofilm growth, and to increase the efficiency of the Cr(VI)-reducing MEC. The bioelectrochemical system ensured higher removal efficiency than the pure chemical process.

**Index Terms** – Biocathode, Bioelectrochemical system, Hexavalent chromium reduction.

### I. INTRODUCTION

Groundwater is the environmental matrix most frequently affected by anthropogenic hexavalent chromium contamination. Due to its cancerogenicity, Cr(VI) has to be removed, hopefully using environmental-friendly and economically sustainable remediation technologies (e.g. Bioremediation techniques). The aim of bioremediation is to enhance the removal and transformation of pollutants by microorganisms through the addition of: nutrients and/or final electron acceptors (biostimulation), selected bacterial strains or consortia that are able to degrade contaminants (bioaugmentation), or chemicals that increase the contaminant bioavailability.

To overcome the limits of currently applied bioremediation technologies (substances to be injected, production of side metabolites, etc.), an alternative strategy is the use of BioElectrochemical Systems (BES) to stimulate bioreduction of Cr(VI), without affecting the natural groundwater conditions.

BES are biological reactors where an electrode (anode) works as the final electron acceptor for the oxidation of organic compounds; then electrons pass through the circuit and reach the cathode, which acts as the electron donor for the reduction of metals and/or chlorinated compounds. In BES for the removal of metals, cathode is used as an electron donor to reduce metallic ions present as oxidized species. Tandukar and colleagues (2009) observed for the first time biological chromium reduction at the cathode of a Microbial Fuel Cell (MFC) [1]. Huang and colleagues tested a MEC (Microbial Electrolysis Cell) with the biocathode polarized at -300 mV (vs. Standard Hydrogen Electrode - SHE), which was able to efficiently reduce Cr(VI) [2]. Unlike previous works, the aim of this study was to evaluate the possibility to remove Cr(VI) in a biocathodic chamber of a dual-chamber (2C) MEC with cathode as the sole electron donor.

### II. MATERIALS AND METHODS

#### A. Biocathode production

A dual-chamber H-shaped reactor, made of 2 pirex-glass bottles separated by Cation Exchange Membrane (CEM), with 1100 mL total volume was used in this study. Graphite cylinders (length: 6 cm, diameter: 1 cm, geometric area: 18.85 cm<sup>2</sup>) locked on stainless steel wires were used as the electrodes. The cathodic chamber was filled with sterile M9 minimal medium (autoclaved twice at 120 °C for 30 min). The anodic chamber was also filled with sludge from an anaerobic digester (20% final volume) and glucose (2 g L<sup>-1</sup>) to provide sufficient carbon substrate for bacterial growth. Then the anodic chamber was flushed for 15 min with sterile-filtered N<sub>2</sub> to establish anaerobic conditions. During 50 days of anode acclimation, glucose concentration has been periodically replaced when the voltage has dropped below 0.01 V. For the whole test, the voltage across an external resistance (1000 Ω) was

continuously recorded using a Picolog 1012 logging system. At the end of the period, this bioelectroactive anode was used as the biocathode in a Cr(VI)-reducing MEC [3].

#### B. Cr(VI)-reducing MEC set up and operation

The Cr(VI)-reducing MEC set up was the same as for the 2C-MFC used for the biocathode production. The cathodic solution was composed of M9 minimal medium,  $\text{KHCO}_3$  ( $1 \text{ g L}^{-1}$ ) as the sole carbon source, and hexavalent chromium ( $2000 \mu\text{g L}^{-1}$ ). The anodic chamber, instead, was the same as for the cathodic chamber of the 2C-MFC, with the addition of  $\text{KHCO}_3$  ( $1 \text{ g L}^{-1}$ ) to balance charges between the two compartments. At the biocathode a potential of  $-500 \text{ mV}$  against Ag/AgCl reference electrode (i.e.,  $-300 \text{ mV}$  vs. SHE) was imposed [4]. The Cr(VI)-reducing MEC was operated for two cycles of 9 days each, 20 days one from the other. Hexavalent chromium dissolved concentration was analyzed at the beginning, during the experiment, and at the end of each cycle by spectrophotometric method. During the entire duration of two cycles, the current intensity was monitored by a potentiostat connected to a personal computer. Alongside tests of removal, an abiotic control and an open circuit were also operated in parallel, in order to assess the electrochemical removal component from the biological one.

### III. RESULTS

#### A. Current trends in the MFC

Current density in the MFC ranged between  $0.53$  and  $38.2 \text{ mA m}^{-2}$ . A relationship between substrate availability and current production was observed, as rapid increase in the circulating current was recorded after glucose addition, carried out when the current density has dropped below  $1 \text{ mA m}^{-2}$ .

#### B. Current trends in the MEC and the abiotic control

Current density in Cr(VI)-reducing MEC ranged between  $20$  and  $60 \text{ mA m}^{-2}$  in the first cycle, and increased up to  $70 \text{ mA m}^{-2}$  in the second cycle. In the abiotic control, the current density was below  $10 \text{ mA m}^{-2}$ .

#### C. Reduction of Cr(VI) in the MEC

A decrease in Cr(VI) concentration was observed at the end of the tests (Fig.1). In the Cr(VI)-reducing MEC and in the open circuit system, an increase in Cr(VI) removal efficiency was observed during the second cycle compared to the first cycle. This increased Cr(VI) removal efficiency was ascribed to the selection of a bacterial community containing electro-active and Cr(VI) reducing/resistant bacteria. However, the MEC system ensured higher removal efficiency (65%) than the pure chemical process (49%).

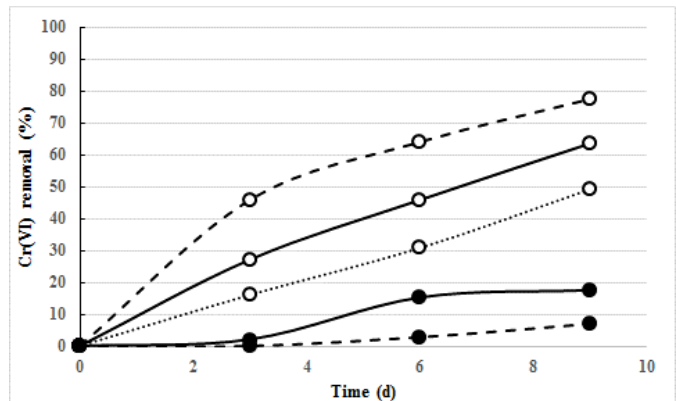


Fig. 1 Cr(VI) removal efficiency: open circuit system (broken line), Cr(VI)-reducing MEC (solid line), and abiotic control (pointed line). First cycle (black dots), second cycle (white dots).

### IV. CONCLUSION

The acclimation phase in the MFC allowed to shorten the time for the electroactive biofilm to deposit on the electrode, and to increase the efficiency of the Cr(VI)-reducing MEC. The bioelectroactive film was essential for generating current; higher current values were measured in the Cr(VI)-reducing MEC than in the abiotic control.

Although BESs require further laboratory testing and scale up, the use of bioelectrochemical systems for removing hexavalent chromium is a new, sustainable and promising approach to remove this and other contaminants from polluted aquifers.

### ACKNOWLEDGMENT

This work has been supported by Fondazione Cariplo in the framework of the project BEVerAGE - BioElectrochemical Remediation of Groundwater plumes (2015-0195).

### REFERENCES

- [1] M. Tandukar, S. J. Huber, T. Onodera, S. G. Pavlostathis, and E. Engineering, "Biological Chromium ( VI ) Reduction in the Cathode of a Microbial Fuel Cell," *Environ. Sci. Technol.*, vol. 43, no. 21, pp. 8159–8165, 2009.
- [2] H. Wang and Z. J. Ren, "Bioelectrochemical metal recovery from wastewater: A review," *Water Res.*, vol. 66, pp. 219–232, 2014.
- [3] X. Wu, X. Zhu, T. Song, L. Zhang, H. Jia, and P. Wei, "Effect of acclimatization on hexavalent chromium reduction in a biocathode microbial fuel cell," *Bioresour. Technology*, vol. 180, pp. 185–191, 2015.
- [4] L. Huang, X. Chai, G. Chen, and B. E. Logan, "Effect of set potential on hexavalent chromium reduction and electricity generation from biocathode microbial fuel cells," *Environ. Sci. Technol.*, vol. 45, no. 11, pp. 5025–5031, 2011.

## SAFE OPERATING RANGE, DYNAMIC ANALYSIS, AND TUNING OF THE TEMPERATURE AND REACTANT UTILIZATION CONTROL FOR SOLID OXIDE CELLS

G.Botta \*, M. Romeo \*/\*\*, A. Fernandez \*, and P. V. Aravind\*

\*Delft University of Technology, Leeghwaterstraat 39, 2628 CB Delft, The Netherlands.

\*\*Politecnico di Milano, Piazza Leonardo da Vinci 32, 20133 Milano, Italy.

**Abstract** - Solid Oxide Cells systems (SOCs) are increasingly being considered as an electrical energy storage method and therefore as a means to boost the penetration of Renewable Energy and to improve the grid flexibility by power-to-gas electrochemical conversion. However, temperature and reactant utilization control become crucial if the systems are to be used in dynamic operation with intermittent electrical power sources. In the present work, two 1D models of SOC stacks are built and used to study the dynamic behaviour of such stacks, and to select and tune the best control systems. After having compared with literature the accuracy of the models, safe operating ranges are determined to respect the thermal constraints of the stack. The dynamic analysis points out that inputs ( $\dot{m}_{fuel}$ ,  $\dot{m}_{air}$ ) and outputs ( $U$ ,  $\Delta T_{max}$ ) are strongly decoupled; therefore, proportional-integral control strategy has a good potential to prevent dangerous operating conditions in dynamic operation. Finally, the controllers are tuned and their transfer functions are reported.

**Index Terms** – Dynamic Analysis, Renewable Energy, Solid Oxide Cells, Temperature and Reactant Utilization Control.

### I. INTRODUCTION

Efficient Electrical Energy Storage (EES) with power-to-gas solutions could play a substantial role in decarbonising the electricity sector, integrating different energy grids and infrastructures, and increasing the penetration of renewable energy resources. Among the EES, SOC systems are of considerable interest. In fact, they can balance the dynamic and decentralized nature of renewable sources and back up the grid because they can store electricity by producing a synthetic fuel in the electrolysis mode and generate electricity by electrochemically oxidising fuel in the fuel cell mode.

When SOC systems are used in dynamic operation (i.e., when balancing the power production and consumption curves) temperature control strategy become fundamental to prevent deleterious stack thermo-mechanical stress and thermal

excursion in time. Also, an adequate reactant utilization control strategy is important to avoid that the utilisation rate increases dramatically thus irreversibly damaging the stack. In addition, the temperature control strategy could assist in maintaining a constant operating condition (i.e., endothermic, exothermic or thermoneutral) of the stack and consequently simplify the system design.

This work focuses on the dynamic analysis of SOC systems and investigates the potential of controlling the temperature variation and the fuel utilization of the stack through the change in the air and fuel flow rate.

### II. METHOD AND IMPLEMENTATION

#### A. Model Description

Based on a SOFC template available in *Modelon* library, the SOEC is coded in *Modelica* environment. This includes connectors for mass flow, heat transfer and electrical current. A temperature state is introduced and energy balance is defined. The cells are electrically and thermally connected in series to model a substack, while the complete stack is created assembling in parallel several substacks. Maximum temperature difference along the cell, and heat exchange with the environment are defined at stack level, while reactant utilization ( $U$ ) and inlet air to steam molar ratio ( $\gamma$ ) are defined at substack level.

#### B. Safe Operating Range of SOFC and SOEC, and Operating Conditions

Initially, the physical and geometrical stack characteristics are defined and fixed. The stacks are fed with a constant flow of  $H_2O/H_2$  mixture, the maximum utilization factor is set to 75% for avoiding structural damages to the stack. The air flow entering the stack is also constant but three different cases are analyzed:  $\gamma$  equal to 8, 12, 16 and 0.8, 1.6, 2.4 are evaluated for

both SOFC and SOEC, respectively. These values are chosen considering a trade-off between sufficient electrical energy and H<sub>2</sub> productions in the two working modes, without incurring in serious additional energy costs.

The stack operates at ambient pressure and the inlet mixtures are set at 750 C° in both electrodes channels. The stacks undergo a current density ramp (1000-10000 and 1000-15000 A/m<sup>2</sup> for SOFC and SOEC, respectively). Coherently to what reported in [1], all the current densities values for which the  $\Delta T_{\max}$  is lower than 10 K/cm are selected as safe operating range. For each value of  $\gamma$ , a maximum current is determined. Nominal current is set at ~75% of maximum current for SOEC and ~60% for SOFC, while for both the minimum current corresponds to ~50% of the maximum current, accordingly to [2] and [3].

### C. Dynamic Analysis and Control Tuning

Dynamic analysis is performed for all values of  $\gamma$  while the control study focuses only on one value of  $\gamma$  for SOFC and one for SOEC. The matrix of the transfer functions between inputs ( $\dot{m}_{fuel}$ ,  $\dot{m}_{air}$ ) and outputs (U,  $\Delta T_{\max}$ ) is derived and analyzed:

$$G(s) = \begin{bmatrix} \frac{\Delta U(s)}{\delta \dot{m}_{fuel}(s)} & \frac{\Delta U(s)}{\delta \dot{m}_{air}(s)} \\ \frac{\Delta(\Delta T_{\max})(s)}{\delta \dot{m}_{fuel}(s)} & \frac{\Delta(\Delta T_{\max})(s)}{\delta \dot{m}_{air}(s)} \end{bmatrix} = \begin{bmatrix} G_{11}(s) & G_{12}(s) \\ G_{21}(s) & G_{22}(s) \end{bmatrix} \quad (1)$$

The control strategy to ensure the running of the stack within the operating safe range and at 75% utilization rate, is designed on the base of the analysis of transients in order to have the highest achievable reliability. The controller transfer function is studied and tuned to guarantee the stability of the stack.

## III. RESULTS

The models developed are first compared with the results from [4] and [5] and similar trend are observed. The maximum safe operating current and its relative nominal and minimum value are reported for SOEC and SOFC in TABLE I.

TABLE I  
MAXIMUM, NOMINAL, MINIMUM CURRENT DENSITY FOR SOCs

SOEC	$\gamma=1.6$
Maximum Current Density [A/m <sup>2</sup> ]	13963
Nominal Current Density [A/m <sup>2</sup> ]	10500
Minimum Current Density [A/m <sup>2</sup> ]	6700
SOFC	$\gamma=12$
Maximum Current Density [A/m <sup>2</sup> ]	6735
Nominal Current Density [A/m <sup>2</sup> ]	4050
Minimum Current Density [A/m <sup>2</sup> ]	3250

The dynamic analysis shows that in SOEC, the increase of air mass flow rate strongly influences the  $\Delta T_{\max}$ , while in SOFC this aspect is less pronounced due to the strong exothermic behavior close to cell inlet. Nonetheless, an increase of  $\gamma$  will result in a mitigation of the thermal gradients along the flow direction. The relative gain array matrix of our multi-input and multi-output system resulted strongly decoupled both in SOFC and SOEC. As a consequence, two separated control loops can be adopted. A proportional-integral (PI) control strategy is

chosen since phase anticipation via derivative action in our case is not required. To solve the control system the crossover frequencies  $\omega_c$  are assumed 0.1 rad/s for utilization rate and 0.01 rad/s for temperature gradient, and the phase margin is set 80°. The parameters for control tuning (i.e., the proportional gain  $K_p$  and the integral time  $T_i$ ) are obtained and shown in TABLE II.

TABLE II  
CONTROLLERS PARAMETERS FOR SOCs

SOEC	$K_p$ [-]	$T_i$ [s]
U	$-7.858 \cdot 10^{-7}$	0.001
$\Delta T_{\max}$	$-1.63 \cdot 10^{-3}$	335.8
SOFC	$K_p$ [-]	$T_i$ [s]
U	$-3.163 \cdot 10^{-7}$	0.001
$\Delta T_{\max}$	$-4.28 \cdot 10^{-2}$	232.4

The transfer function of the control loop is resulted as:

$$L(s) \sim \frac{1}{1 + \frac{s}{\omega_c}} \quad (2)$$

and the time to reach the equilibrium defined as:

$$T_{eq} = \frac{5}{\omega_c} \quad (3)$$

Both SOFC and SOEC stacks take up to ~50 seconds for U to become stable while  $\Delta T_{\max}$  reached equilibrium over a greater time, ~500 seconds.

## IV. CONCLUSION

Two 1D dynamic models of SOCs are built and compared with literature. After having evaluated the safe stack operating ranges, the models are employed to study the dynamic behaviour of such stacks and the prospect for stack temperature and utilization rate control through variation of air and fuel flow rates. The stacks appeared as stable and controllable with two PI controllers, without need of more aggressive or expensive control strategies. This study is a first step in the dynamic analysis of a reversible stack switching between SOFC and SOEC mode.

## REFERENCES

- [1] H. Severson and M. Assadi. Analysis of residual and operational thermal stresses in a planar SOFC. Journal of Fuel Cell Science and Technology, 10, 2013, 061001.
- [2] S.D. Ebbensen, R. Knibbe, and M. Mogensen. Co-electrolysis of steam and carbon dioxide in solid oxide cells. Journal of The Electrochemical Society, 159, 2012, 482-489.
- [3] C.H. Wendel, P. Kazempoor, and R.J. Braun. Novel electrical energy storage system based on reversible solid oxide cells: System design and operating conditions. Journal of Power Sources, 276, 2015, 133-144.
- [4] D.F. Cheddle and N.D.H. Munroe. A dynamic 1D model of a solid oxide fuel cell for real time simulation. Journal of Power Sources, 171, 2007, 634-643.
- [5] J. Udagawa, C.S. Adjiman, and N.P. Brandon. Hydrogen production through steam electrolysis: Model-based dynamic behaviour of a cathode-supported intermediate temperature solid oxide electrolysis cell. Journal of Power Sources, 180, 2008, 46-55.



## AUTORE (AUTOMOTIVE DERIVATIVE ENERGY SYSTEM): 2 YEARS IN

G J. Kelsall\*, S. Ubertini\*\*

\*GE Gas Power Systems, Newbold Rd, Rugby, CV21 2NH (UK)

\*\*Dept. of Economics, Engineering, Society and Business  
Organization, University of Tuscia, 01100 Viterbo, (Italy)

**Abstract** – AutoRE is a multi- partner project funded under the FCH-JU FCH-02.5-2014 call, aimed at demonstrating an automotive derivative fuel cell integrated with a natural gas reformer to make the required high purity hydrogen. The system prototype, to be demonstrated at GE's Rugby site in the UK, has a targeted electrical efficiency of 38-40%, with parallel component developments, such as hydrogen separation membranes, undertaken to increase the efficiency of a subsequent commercial system to >45%. The market for the product will be 50-100kWe applications in industrial and commercial buildings in combined heat and power (CHP) mode. At this scale, the fuel cell based CHP system has potential cost of electricity and emissions advantage over competing technologies. The project is now in its third year, with the build of the prototype system significantly underway. This paper gives the status of the project as reported at the mid-term meeting.

**Index Terms** – PEM fuel cell, natural gas reformer, CHP, 50kWe demonstration

### I. INTRODUCTION

#### A. Project Objective

The aim of the AutoRE project is to create the foundations to commercialise an automotive derivative fuel cell system in the 50-100 kWe range, for combined heat and power (CHP) in commercial and industrial buildings. More specifically the objectives are to:

- develop system components allowing reduced costs, increased durability and efficiency
- build/validate a 50 kWe PEM prototype CHP system

The respective roles of the project partners to achieve these objectives are shown in Table I.

Table I. Role of AutoRE partners

Partner name	Role
Alstom UK	<ul style="list-style-type: none"> <li>• Project Management</li> <li>• 50 kW system set-up, testing and validation</li> <li>• Performance modelling</li> </ul>
GE Switzerland	<ul style="list-style-type: none"> <li>• Dissemination</li> <li>• RAMS modelling</li> <li>• 3D printing HEX/reformer prototype manufacturing</li> <li>• Reformer manufacturing and commissioning</li> </ul>
Helbio	<ul style="list-style-type: none"> <li>• Control system</li> <li>• System integration support</li> <li>• Testing of PEM short stacks on reformat</li> </ul>
Daimler /NuCellSys	<ul style="list-style-type: none"> <li>• Manufacturing and commissioning of fuel cell automotive system and two short stacks.</li> <li>• Support in control system integration, diagnostic on FC system support.</li> </ul>
Uni Split	<ul style="list-style-type: none"> <li>• Diagnostic</li> <li>• New concepts for cogeneration</li> </ul>
Unitus	<ul style="list-style-type: none"> <li>• Performance modelling of test rig, final system</li> <li>• Modelling of integration of fuel cell system in a building environment</li> </ul>
SINTEF	<ul style="list-style-type: none"> <li>• Membrane development and testing, diagnostic modelling</li> </ul>

### II. RESULTS ACHIEVED TO DATE

#### A. 50 kWe Prototype System

The fuel cell CHP prototype facility is shown schematically in Figure 2.

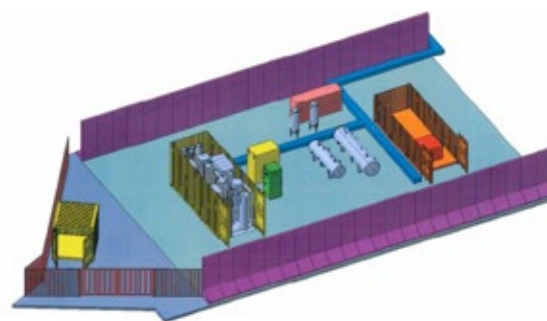


Fig 2: 3D Model of Prototype Test Facility Layout

The Fuel Cell Container including the automotive derivative PEM fuel cell supplied by NuCellSys has been installed. The

H<sub>2</sub> production unit is in the final stages of commissioning with delivery to the prototype test site in Rugby UK scheduled for Jan 2018. This latter item has been held up significantly, most recently due to a corrosion issue within the reformer causing unacceptably high pressure drop, but this has now been rectified by using corrosion resistant FeCrAlloy material.

### B. Component Development and Testing

Lab-scale testing of enhancements to the prototype system, to reduce its cost of electricity/foot-print and increase its performance are underway. Testing of selective membranes (to replace the Pressure Swing Absorber (PSA) unit to produce high purity H<sub>2</sub>) with increased system efficiency has been carried out (Figure 3). Compared to the baseline configuration, cooling and dehydration of the reformed natural gas feed before the H<sub>2</sub> purification step are not required. Innovative heat exchanger design concepts using selective laser melting have been prepared to reduce the size of heat exchangers within the H<sub>2</sub> production unit and improve their efficiencies. The final lab-scale testing carried out is that of short stack PEM fuel cell units at different operating conditions. Increasing the proportion of CO<sub>2</sub> reduced the performance of the fuel cell, although this performance was fully recovered when pure hydrogen fuel was re-introduced. The decline in performance was attributed to CO poisoning, where CO is formed following the reverse water gas shift reaction.

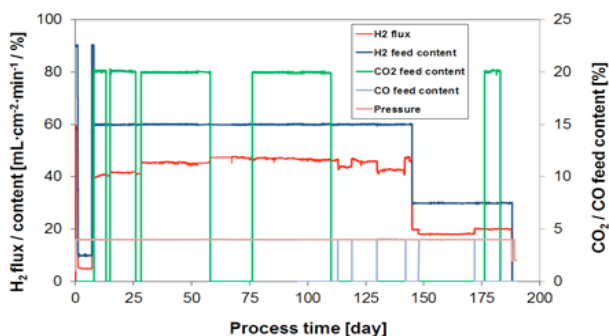


Fig 3: Hydrogen Membrane Testing Results

### C. System Modelling

Extensive modelling of the fuel cell based CHP system has been carried out, both for the baseline configuration (Figure 4) and including future design improvements such as replacement of the PSA with a selective membrane based system. The outcome of the modelling at this stage is that whilst increasing the nominal power of the fuel cell section of the CHP plant has a certain positive impact on plant performance, its adoption should be subject to careful economic evaluation. On the other hand, thermal integration of the reformer improves the plant performance without drawbacks and should be adopted. Selective membranes should be integrated in the water gas shift

reactor of the H<sub>2</sub> production unit (and not used as a standalone component) and allows significant efficiency improvements if the H<sub>2</sub> pressure can be reduced.

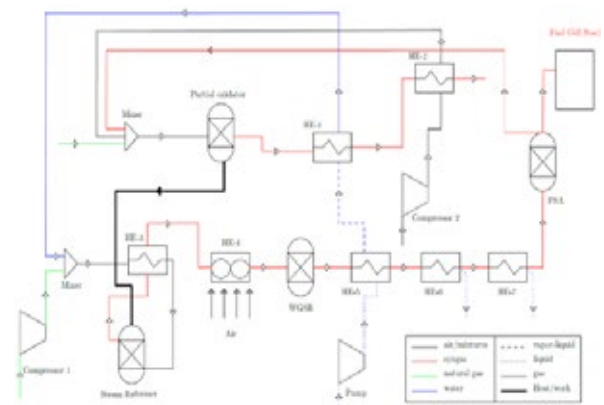


Fig 4: Schematic of the CHP plan concept: energy system

Additional modelling is underway to look at aspects of the plants reliability, availability and maintainability, and to look at fuel cell degradation. This latter modelling activity has leveraged on the results of a previous project (SAPPHIRE) which also targeted a CHP fuel cell system.

## III. CONCLUSION

The AutoRE project remains on track to deliver the project objectives. Key results from the project are due in the final year, particularly the 3000h prototype tests.

## ACKNOWLEDGMENT

This project has received funding from the Fuel Cells and Hydrogen Joint Undertaking under grant agreement No 671396. This Joint Undertaking receives support from the European Union's Horizon 2020 research and innovation programme and UK, Germany, Greece, Croatia, Italy, Switzerland, Norway. Swiss partners are funded by the State Secretariat for Education, Research & Innovation of the Swiss Confederation.

## REFERENCES

- [1] Facci G., Loreti G., Peters T., Ubertini S., Numerical modeling of an automotive derivative PEM fuel cell CHP system with selective membranes. EFC 2017, Naples, 2017
- [2] Facci G., Ubertini S., Analysis of the performances of a fuel cell CHP system under different energy demand and climate scenarios. EFC 2017, Naples, 017.
- [3] Peters T.A. et al., Palladium membranes - from innovation to industrial application, Presentation at CLIMIT SUMMIT, Oslo, Norway, 2017.

Copyright © 2017

## SANDVIK SURFACE TECHNOLOGY. COMMERCIALIZING FUEL CELL TECHNOLOGY: SOFC INTERCONNECTS

C. Bernuy-Lopez\*, R. Berger\* and J. Westlinder\*

\* SMT R&D, AB Sandvik Materials Technology, 81181 Sandviken,  
Sweden

**Abstract** – Sandvik Surface Technology is a production unit within Sandvik Materials Technology (SMT). SMT belongs to the Sandvik group and is a world-leading manufacturer of advanced stainless steels and special alloys for the most demanding industries. Sandvik Surface Technology offers a portfolio of cost effective coated steel strip for electronics applications, interconnects for and bipolar plates for Polymer Electrolyte Fuel Cells. Manufactured in the large-scale production facility, the coated steel strip is ready for stamping, offering the customer the possibility for significant cost savings compared to conventional batch coating processes. Regarding Solid Oxide Fuel Cells (SOFC), Sandvik Sanergy™ HT 441 is a 441-type stainless steel coated by physical methods with Ce and Co. The Ce-Co coating reduces the chromium evaporation by up to one order of magnitude, increasing the long time efficiency of the fuel cell. In addition, the material has excellent surface conductivity compared to uncoated stainless steel.

**Index Terms** – Coating, Interconnect, Steel, SOFC

### I. INTRODUCTION

Sandvik Surface Technology produces nanocoatings for SOFC stainless steel interconnects. The roll-to-roll coating lines for mass production provides an outstanding opportunity for the cost effective industrial mass production of interconnects. The pre-coated solution reduces some of the handling that comes with batch coating of individual plates. Figure 1 shows a schematic of the coating line developed in Sandviken (Sweden).

Coils of any steel grade according to customer specifications with a width smaller than 800 mm and a thickness between 0.07 and 0.8 mm are introduced in the coating line. Prior coming to the coating line the coils are cleaned by a wet chemical de-greasing process, followed by surface inspection. This process is followed by an in-line plasma cleaning/etching. In the next process the metal layers are deposited on the coil by Sandvik's continuous PVD coating process. Later, the coated

coils are automatic X-ray inspected in order to assure the thickness and quality of the coating. Finally, the coils are going through testing, slitting and packaging processes ready to deliver to the customer according to the specifications.

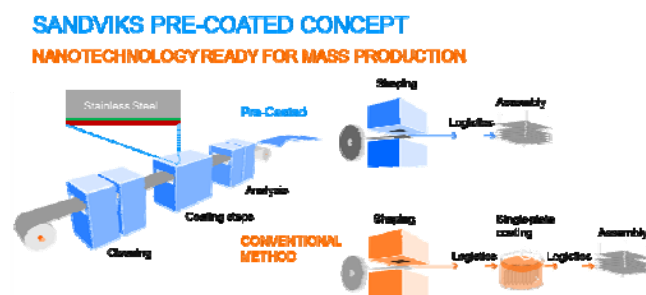


Fig. 1. Schematics of the roll to roll coating line developed for Sandvik Surface Technology and the cost-effective advantage of our pre-coated solution versus the conventional batch method.

### II. SANDVIK SANERGY™ 441 CE/CO COATED

The ASTM 441 steel grade, double coated with Cerium and Cobalt, have been shown to be excellent material to work as SOFC interconnects (1-3). The material have shown to form a protective spinel layer with a  $(\text{Co},\text{Mn})_3\text{O}_4$  composition by diffusion of Mn from the steel over time. This spinel phase is well known to improve the properties of the interconnect material due to the higher electronic conductivity that the  $(\text{Cr},\text{Mn})_3\text{O}_4$  spinel that is formed in the uncoated materials. In addition, this  $(\text{Co},\text{Mn})_3\text{O}_4$  spinel has the capability to reduce in more than one order of magnitude Cr vaporization which otherwise lead to cathode poisoning and therefore, dramatic loss of performance in the SOFC stack.

The addition of Ce has the result of reducing the growth of the  $\text{Cr}_2\text{O}_3$  scale layer that is typically formed as the inner part of

the growing scale. Recent studies (3) have shown that the increased growth of the  $\text{Cr}_2\text{O}_3$  layer is the major contributor to the loss of performance in the SOFC stack due to the large difference in thickness between this passive layer formation ( $>10\text{ }\mu\text{m}$  after 10000 h) versus the protective  $(\text{Co,Mn})_3\text{O}_4$  spinel layer (less than  $2\text{ }\mu\text{m}$ ).

The pre-coated coil developed by Sandvik has excellent self-healing properties as well. Fig. 2 shows SEM images on samples after 10 % biaxially strained. After only a few hours, closure of cracks is detected. The crack heal is made by oxidation of the metallic coating over time. In addition, no increase in Cr-evaporation have been recorded due to the presence of cracks.

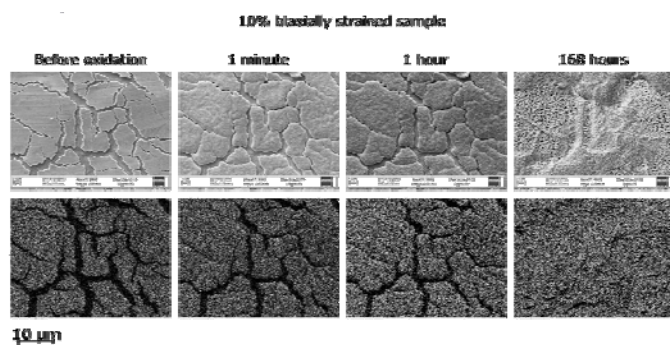


Fig. 2. SEM samples of a pre-coated coil after 10 % biaxial strained and oxidation at  $800\text{ }^{\circ}\text{C}$  over time.

Finally, the Ce/Co coated 441 steel grade shows excellent surface conductivity as shown in Figure 2. After more than 35000 h of exposure the material shows ASR values below  $50\text{ m}\Omega\text{ cm}^2$  and a degradation rate of less than  $1\text{ m}\Omega\text{ cm}^2$  per 1000 h. These are values within the specifications required for the SOFC stack manufacturers.

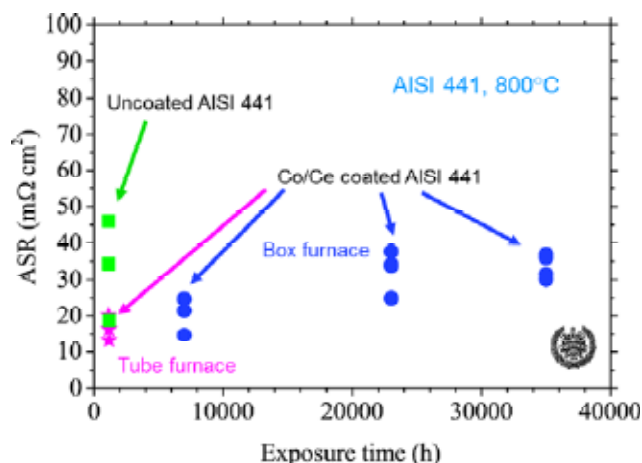


Fig. 3. Area Specific Resistance (ASR) versus exposure time of a Ce/Co coated 441-steel grade interconnect at  $800\text{ }^{\circ}\text{C}$

### III. SUMMARY

Sandvik Surface Technology develops nanocoating for SOFC interconnect. The material is produced in a roll to roll coating line for mass production that provides an excellent opportunity to reduce cost and make fuel cell technology a more competitive technology. Sandvik Sanergy<sup>TM</sup> HT is the product made by Sandvik to work as a SOFC interconnect. This product can be tailored regarding steel grade and metal coating according to customer specifications. A 441-steel grade coated with Ce and Co have shown to be a very efficient SOFC interconnect with thin  $\text{Cr}_2\text{O}_3$  scale formation, excellent self-healing properties as well as low surface resistances ( $<1\text{ m}\Omega\text{ cm}^2$ ) after more than 35000 h.

### ACKNOWLEDGMENT

The authors gratefully acknowledge the High Temperature Corrosion (HTC) Center of Chalmers University in Gothenburg (Sweden) for the ASR measurements.

### REFERENCES

- [1] J. Froitzheim, S. Canovic, M. Nikumaa, R. Sachitanand, L.G. Johansson and J. E. Svensson. Long term study of Cr evaporation and high temperature corrosion behaviour of Co coated ferritic steel for solid oxide fuel cell interconnects Journal of Power Sources, Volume 220, 2012 pp 217-227.
- [2] J.G. Grolig, J. Froitzheim, J.E. Svensson. Coated stainless steel 441 as interconnect material for solid oxide fuel cells: Evolution of electrical properties. Journal of Power Sources, Volume 248, 2015, pp 321-327
- [3] H. Falk-Windisch, J. Claquesin, M. Sattari, J.-E. Svensson, J. Froitzheim. Co- and Ce/Co-coated ferritic stainless steel as interconnect material for Intermediate Temperature Solid Oxide Fuel Cells. Journal of Power Sources, Volume 343, 2017, pp 1-10.



## **CHALLENGES AND SOLUTIONS IN THE R2R MANUFACTURING OF THE FUEL CELL MEMBRANE ELECTRODE ASSEMBLY**

Dr. Nico Meyer<sup>1</sup>, Thomas Kolbusch<sup>1</sup>, Dr. Klaus Crone<sup>1</sup>, Dr. Martin Busch<sup>1</sup>

<sup>1</sup> Coatema Coating Machinery GmbH, Dormagen, Germany.

Uniform interface layers of electrode membranes and gas diffusion layers are the most critical part in fuel cell technology for efficient and reliable operation. Yet, mass production remains challenging and competing technologies have emerged during the recent years. Especially the low-cost high-throughput production requires quality improvements for a constant output of uniform electrodes and membranes. During the recent years intense research and development has been directed on the enhancement and safe implementation of critical production steps.

We provide at first an overview on the roll-to-roll impregnation, coating, membrane washing, drying and lamination process of membranes and electrodes. Subsequently, an insight into the practical realization of the manufacturing is presented. Latest updates in coating and drying technology and exemplary results are discussed. A deeper look is taken into precision coating and uniform catalyst impregnation by knife coating, continuous and interrupted slot die coating, patterned coating by screen printing, membrane washing and technologies for uniform drying and selective lamination for reliable fuel cell manufacturing. Practical experiences and specific issues are addressed in order to share lessons learned and implemented solutions.

*Index Terms: R2R-Equipment, Upscaling, Pilot-Lines, One-Stop-Shop Solution,*

### ACKNOWLEDGMENT

Parts of the results presented by Coatema received funding from the European Union's Framework Programme 7, the **Horizon 2020** research and innovation programme and the European **RegiOnal** Collaboration on **Key** Enabling Technologies programme:

- EELICON-Project (GA 604204)
- Pi-SCALE-Project (GA 688093)
- iCOAT-Project (ROCKET-I-007).



## NUMERICAL MODELING OF SOLID OXIDE FUEL CELLS: AN OVERVIEW

N. Massarotti, D. Sainas, L. Vanoli

Dipartimento di Ingegneria, Università degli Studi di Napoli  
"Parthenope", Centro Direzionale, Isola C4, 80143 Napoli, (Italy)

**Abstract** - This work presents an overview of some of the available studies on macroscopic numerical modeling of Solid Oxide Fuel Cells (SOFCs). Several mathematical models have been developed, both at cell and stack level, to solve transport equations and electrochemical processes within this kind of fuel cells. Tubular and planar configurations have been studied and the importance of developing and employing detailed numerical models, validated against experimental data, to effectively study these systems has been recognized in the available literature.

**Index Terms** – Modeling, SOFC, Macroscopic, Overview.

### I. INTRODUCTION

The increase of energy consumption and the higher prices of fossil fuels have motivated the scientific and technological community to pay more attention on alternative energy conversion systems. Small-scale power generation plants, such as fuel cells, are recognized as a promising environmental friendly alternative to traditional systems. One of the reasons is that this technology is able to provide both heat and power, working in cogenerative arrangement.

Fuel cells based energy conversion systems offer the possibility to directly convert the chemical energy of a fuel into electric energy, with heat and water as byproduct, avoiding intermediate thermal energy conversions, resulting in a more efficient energy conversion process.

The two main types of fuel cells studied in the literature are the Proton Exchange Membrane Fuel Cell (PEMFC) [1, 2], that is a low temperature operating device, and the Solid Oxide Fuel Cell (SOFC) [3], that operates at intermediate or high temperature. Among the different types of fuel cells, the high temperature ones are of great interest since they offer several advantages such as: the possibility of high temperature thermal cogeneration, the ability to use inexpensive catalytic materials, and the capability to be directly fed by other fuels (natural gas, biogas, etc.) rather than pure hydrogen.

This work presents an overview of the macroscopic numerical modeling approaches, employed in the literature to simulate the operation of SOFCs, both at cell and stack level.

### II. NUMERICAL MODELS OF SOLID OXIDE FUEL CELLS

An early numerical macro-model was developed by Vayenas and Debenedetti [4], who considered the high temperature fuel cell as a chemical reactor, analyzing the steady-state behavior of a single cell as a solid-state electrocatalytic reactor. Then, they introduced a 2D mixing cell model for the simulation of the distribution of species, temperature, and current density [5].

Other relevant works were successfully reviewed by Kakaç et al. [6], who concluded that more research effort is needed to develop cogeneration systems based on SOFCs fed with fuels which need internal reforming. Moreover, the lack of experimental data for validation purposes and the need of a deeper insight on the temperature management of these systems are relevant considerations highlighted in their work.

Then, Calise et al. [7] developed a finite volume model of a tubular internal reforming SOFC stack, taking into account different sub-systems and including also the thermal radiation effects within the heat transfer model, improving the models previously developed.

Another comprehensive review work was carried out by Hajimolana et al. [8], who analyzed the mathematical modeling of SOFCs for both tubular and planar configurations, considering polarization losses, mass, momentum and energy conservation, diffusion through porous media and electrochemical phenomena in the positive-electrolyte-negative electrode region and shift/reforming reactions. They confirmed the relevance of information regarding temperature management and experiments, and also concluded that more research effort is needed to analyze the effects of momentum balance inside porous electrodes on SOFC performance.

Then, Arpino et al. [9, 10] developed a zero-dimensional model for the simulation of a SOFC based micro-cogenerative power system for residential use, further proving the importance of taking into account both experimental data with measurement uncertainties and a proper thermal management of the stack, in order to estimate the system performance. In particular, it was

observed that the metrological performance of the flow rate meters has a significant influence on the evaluation of key parameters, such as fuel utilization factor and module efficiency [9]. Moreover, the model allowed finding out the actual operating conditions in which an emergency system shut-down is avoided [10], as shown in Fig. 1. These conditions are strongly related to the temperature management of the SOFC based system, and can be obtained for some combinations of fuel utilization factor and stack power.

As concerns further numerical modeling of SOFCs at single cell level, Mauro et al. [11] developed a model based on a single domain approach to study fuel and oxidant channels, anode, cathode and electrolyte as a whole, by properly taking into account the coupled phenomena occurring in these domains. They also analyzed the influence of the operating temperature on the fuel cell overall performance [12].

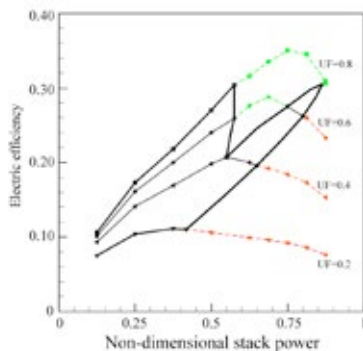


Fig. 1 Operating conditions of a SOFC based stack: allowed points (black), points out of the operating range due to low temperature (green) and high temperature (red).

Steilen et al. [13] analyzed, by means of an overall system model, a SOFC based plant, further proving the importance of taking into account the heat transfer within the components of the stack. In particular, they integrated a set of sub-models in order to predict the heat losses within the plant and to find out the actual operating range that allows avoiding undesired conditions. Operating limitations were found for the SOFC, due to thermal management issues, in order to exclude operating points that could damage the system.

Recently, Nishida et al. [14] carried out an interesting experimental-numerical work on a SOFC stack. They developed a 3D computational fluid dynamic model for the whole stack and compared the numerical predictions, in terms of voltage and temperature distributions, with the data acquired experimentally for tests within a furnace. They provided an experimental validation of their model, taking into account electrochemical reactions, heat and mass transport phenomena for the actual SOFC stack. The model predicts slightly larger temperature values with respect to experimental results, and this could be due to the estimation of heat losses, further proving the importance of properly taking into account the heat transfer

inside these systems.

### III. CONCLUSIONS

Some of the macroscopic numerical models available in the literature for the simulation of SOFC based systems have been reviewed in the present work. From this analysis, it is evident that the thermal management of SOFCs plays a crucial role on the performance of the stack, and of the hybrid systems based on this kind of fuel cell. The heat transfer mechanisms and the heat losses should be properly taken into account, in order to avoid operating conditions that could damage these systems.

### REFERENCES

- [1] Brandon, N., Thompsett, D., Fuel cells compendium, 2005.
- [2] Hoogers, G., Fuel cell technology handbook, 2003.
- [3] Singhal, S.C., Kendall, K., High-temperature solid oxide fuel cells: fundamentals, design and applications, Kidlington, 2003.
- [4] Vayenas, C.G., Debenedetti, P.G., Steady-state analysis of high temperature fuel cells. Chemical Engineering Science, Volume 38, 1983, pp. 1817-29.
- [5] Vayenas, C.G., Debenedetti, P.G., Yentekakis, I., Hegedus, L.L., Cross-flow solid-state electrochemical reactors: a steady-state analysis. Industrial & Engineering Chemistry Research Fundamentals, Volume 24, 1985, pp. 316-24.
- [6] Kakaç, S., Pramuanjaroenkij, A., Zhou, X.Y., A review of numerical modeling of solid oxide fuel cells, International Journal of Hydrogen Energy, Volume 32, 2007, pp. 761-786.
- [7] Calise, F., Ferruzzi, G., Vanoli, L., Parametric exergy analysis of a tubular Solid Oxide Fuel Cell (SOFC) stack through finite-volume model, Applied Energy, Volume 86, 2009, 2401-2410.
- [8] Hajimolana, S.A., Hussain, M.A., Wan Daud, W.M.A., Soroush, M., Shamiri, A., Mathematical modeling of solid oxide fuel cells: A review, Renewable and Sustainable Energy Reviews, Volume 15, 2011, pp. 1893-1917.
- [9] Arpino, F., Massarotti, N., Mauro, A., Vanoli, L., Metrological Analysis of the Measurement System for a Micro-Cogenerative SOFC Module, International Journal of Hydrogen Energy, Volume 36, 2011, pp.10228-10234.
- [10] Arpino, F., Dell'Isola, M., Maugeri, D., Massarotti, N., Mauro, A., A new model for the analysis of operating conditions of micro cogenerative SOFC units, International Journal of Hydrogen Energy, Volume 38, 2013, pp. 336-344.
- [11] Mauro, A., Arpino, F., Massarotti, N., Nithiarasu, P., A novel single domain approach for numerical modelling Solid Oxide Fuel Cells, International Journal of Numerical Methods for Heat & Fluid Flow, Volume 20, 2010, pp. 587-612.
- [12] Mauro, A., Arpino, F., Massarotti, N., Three-dimensional simulation of heat and mass transport phenomena in planar SOFCs, International Journal of Hydrogen Energy, Volume 36, 2011, pp. 10288-10301.
- [13] Steilen, M., Saletti, C., Heddrich, M.P., Friedrich, K.A., Analysis of the influence of heat transfer on the stationary operation and performance of a solid oxide fuel cell/gas turbine hybrid power plant, Applied Energy, Volume 211, 2018, pp. 479-491.
- [14] Nishida, R.T., Beale, S.B., Pharoah, J.G., de Haart, L.G.J., Blum, L., Three-dimensional computational fluid dynamics modelling and experimental validation of the Jülich Mark-F solid oxide fuel cell stack, Journal of Power Sources, Volume 373, 2018, 203-210.



# PROCEEDINGS

OF THE 7<sup>TH</sup> EUROPEAN FUEL CELL  
PIERO LUNGHI CONFERENCE

# CONTENTS



**European Fuel Cell**

Conference & Exhibition

---

**12-15** december 2017 / **NAPLES**



<b>AB. COD.</b>	<b>AUTHOR</b>	<b>PAGE</b>
EFC17001	Milewski Jarek	17
EFC17004	Donazzi Alessandro	19
EFC17005	Pilinski Nadine	21
EFC17006	Okpu Onne Ambrose	23
EFC17007	Obata Oluwatosin	25
EFC17008	Vladikova Daria	27
EFC17009	Spedicato Luigi	29
EFC17010	Li Shian	31
EFC17011	Di Lorenzo Mirella	33
EFC17013	Rolf Hempelmann	35
EFC17015	Ota Kenichiro	37
EFC17017	Jung Aeri	39
EFC17018	Conti Bruno	41
EFC17019	Gr_ger Fabian	43
EFC17020	Dohkoh Tatsuki	45
EFC17021	Hansen John B_gild	47
EFC17022	Scott Janet	49
EFC17023	Kamaraj Sathish-kumar	51
EFC17024	Kamaraj Sathish-kumar	53
EFC17027	Ubertini Stefano	55
EFC17028	Ubertini Stefano	57
EFC17029	Facci Andrea Luigi	59
EFC17030	Martino Marco	61
EFC17031	Poehere Chong	63
EFC17032	Paritosh Kumar Mohanta	65
EFC17033	Busby Yan	67
EFC17034	Iordache Ioan	69
EFC17035	Wang Jiatang	71
EFC17037	Motyliniski Konrad	73
EFC17038	Argumosa Maria Pilar	75
EFC17039	Ruocco Concetta	77
EFC17040	Messaggi Mirko	79
EFC17041	Tucci Matteo	81
EFC17042	Ritzberger Daniel	83
EFC17043	K_ Peter	85
EFC17045	Arico' Antonino Salvatore	87
EFC17046	Emma Roubaud	89
EFC17047	Santamaria Anthony	91
EFC17048	Tanaka Yohei	93
EFC17052	Vita Antonio	95

<b>AB. COD.</b>	<b>AUTHOR</b>	<b>PAGE</b>
EFC17053	Sisani Elena	97
EFC17054	Baldinelli Arianna	99
EFC17055	Felix P. Lohmann	101
EFC17056	Leites Keno	103
EFC17057	Maximilian Wagner	105
EFC17058	Baricci Andrea	107
EFC17059	Higgins Scott	109
EFC17061	Siegwart Muriel	111
EFC17062	Rabissi Claudio	113
EFC17064	Di Marcoberardino Gioele	115
EFC17065	Cuneo Alessandra	117
EFC17066	Massaglia Giulia	119
EFC17069	Guandalini Giulio	121
EFC17070	Guandalini Giulio	123
EFC17072	Villarini Mauro	125
EFC17073	Grimler Henrik	127
EFC17074	Bettermann Hans	129
EFC17075	Minutillo Mariagiovanna	131
EFC17076	Garbujo Alberto	133
EFC17077	Lamberti Thomas	135
EFC17078	Kupecki Jakub	137
EFC17079	Kupecki Jakub	139
EFC17080	Quaglio Marzia	141
EFC17081	_zoğul Buğ_e	143
EFC17082	Karaeyvaz Mukaddes Candan	145
EFC17084	Italiano Cristina	147
EFC17086	Taccani Rodolfo	149
EFC17087	Colbertaldo Paolo	151
EFC17088	Lamberti Thomas	153
EFC17090	Ihringer Raphael	155
EFC17091	Acevedo Gomez Yasna	157
EFC17092	Pezzini Paolo	159
EFC17093	Tucker David	161
EFC17094	Bisello Andrea	163
EFC17095	Oryshchyn Danylo	165
EFC17097	Shadle Lawrence	167
EFC17098	Eriksson Bj_rn	169
EFC17100	Kim Dong Kyu	171
EFC17101	Barelli Linda	173
EFC17103	Taccani Rodolfo	175



<b>AB. COD.</b>	<b>AUTHOR</b>	<b>PAGE</b>
EFC17104	Papurello Davide	177
EFC17105	Spinelli Maurizio	179
EFC17106	Holtappels Peter	181
EFC17107	Kang Sanggyu	183
EFC17108	Montaner Rios Gema	185
EFC17109	Kang Sanggyu	187
EFC17110	Marzorati Stefania	189
EFC17111	Colombo Alessandra	191
EFC17112	Goglio Andrea	193
EFC17113	Falcucci Giacomo	195
EFC17115	Iulianelli Adolfo	197
EFC17117	Loipersb_ck J_rgen	199
EFC17118	Joris Proost	201
EFC17119	Merino Jimenez Irene	203
EFC17120	Thomann Olivier	205
EFC17121	Papurello Davide	207
EFC17122	Papurello Davide	209
EFC17123	Tsiakaras Panagiotis	211
EFC17124	Petrillo Antonella	213
EFC17126	Mehmeti Andi	215
EFC17128	Lee Seungbok	217
EFC17129	Forcina Antonio	219
EFC17130	Perna Alessandra	221
EFC17131	Graziadio Marco	223
EFC17132	Hodnik Nejc	225
EFC17133	Lubrano Lavadera Antonio	227
EFC17134	Hwang Sang Soon	229
EFC17135	Pivac Ivan	231
EFC17137	Bharti Abha	233
EFC17139	Hack Jennifer	235
EFC17140	Mora Joy Marie	237
EFC17141	Divinagracia Maricor	239
EFC17142	Guarnieri Massimo	241
EFC17143	Vanhoof Liesbet	243
EFC17144	Guarnieri Massimo	245
EFC17145	Mansilla Christine	247
EFC17146	Jeon Dong Hyup	249
EFC17147	Rosa Anna Nastro	251
EFC17148	Gandiglio Marta	253
EFC17150	Audasso Emilio	255



<b>AB. COD.</b>	<b>AUTHOR</b>	<b>PAGE</b>
EFC17151	De Campo Marco	257
EFC17152	Ploner Alexandra	259
EFC17153	Audasso Emilio	261
EFC17154	Unsal Secil	263
EFC17156	Lidasan Jun Jeffri	265
EFC17157	Krummrein Thomas	267
EFC17158	Lin Zijing	269
EFC17159	Lin Zijing	271
EFC17162	Rao Marco	273
EFC17163	Ortenero Joseph	275
EFC17165	Bonde Jacob Lindner	277
EFC17166	Theodosiou Pavlina	279
EFC17168	Molala Benny	281
EFC17169	Ucar Nihat Ozer	283
EFC17170	Erable Benjamin	285
EFC17171	Tsiakaras Panagiotis	287
EFC17172	Hosseinpour Milad	289
EFC17173	Kim Jae-hwan	291
EFC17174	Kim Beom-jun	293
EFC17175	Piccardo Paolo	295
EFC17176	Janick Bigarr_	297
EFC17177	Salvador Gian Paolo	299
EFC17178	Thomann Olivier	301
EFC17180	Ion-Ebrasu Daniela	303
EFC17181	Jang Hansaem	305
EFC17182	Jang Hansaem	307
EFC17183	De Silvestri Andrea	309
EFC17185	Cipiti' Francesco	311
EFC17186	Antoni Laurent	313
EFC17187	Rashid Kashif	315
EFC17188	Mecheri Barbara	317
EFC17189	Haneda Takahide	319
EFC17190	Urbani Francesco	321
EFC17191	Jedicke Olaf	323
EFC17193	Barbera Orazio	325
EFC17195	Sacco Adriano	327
EFC17197	Chung Moon-sun	329
EFC17198	Izadi Paniz	331
EFC17199	Stam Jelle	333
EFC17200	Kuntke Philipp	335

<b>AB. COD.</b>	<b>AUTHOR</b>	<b>PAGE</b>
EFC17201	Kamaraj Sathish-kumar	337
EFC17202	Cinti Giovanni	339
EFC17203	Marra Dario	341
EFC17204	Carollo Giovanni	343
EFC17205	Nakashima Kohei	345
EFC17206	Gaele Maria Felicia	347
EFC17207	Park Taehyun	349
EFC17208	Park Taehyun	351
EFC17209	Kumar Ajay	353
EFC17210	Giacoppo Giosue	355
EFC17212	Aly Ahmed	357
EFC17213	Jafarzadeh Sepideh	359
EFC17214	Hollinger Adam	361
EFC17215	Chiodoni Angelica	363
EFC17216	Polverino Pierpaolo	365
EFC17217	Cinti Giovanni	367
EFC17218	Polverino Pierpaolo	369
EFC17219	Linhart Andreas	371
EFC17220	Ivanova Mariya E.	373
EFC17221	Mulone Vincenzo	375
EFC17222	Ponticorvo Eleonora	377
EFC17223	Cirillo Claudia	379
EFC17224	Ponticorvo Eleonora	381
EFC17229	Michel Vilasi	383
EFC17230	Dushina Anastasia	385
EFC17232	Walter Xavier Alexis	387
EFC17235	Zhang Shidong	389
EFC17236	Shin Sung Soo	391
EFC17237	Kono Tatsuoki	393
EFC17238	Cho Jinwon	395
EFC17239	Cigolotti Viviana	397
EFC17240	Linkov Vladimir	399
EFC17241	Fan Zhou	401
EFC17242	Yamaguchi Toshiaki	403
EFC17244	Aydin _zg_r	405
EFC17245	Calabriso Andrea	407
EFC17247	Domingues Rosana	409
EFC17249	Coppola Nunzia	411
EFC17250	Mcphail Stephen	413
EFC17251	Squadrito Gaetano	415



<b>AB. COD.</b>	<b>AUTHOR</b>	<b>PAGE</b>
EFC17255	Jensen S_ren H_jgaard	417
EFC17256	Cristiani Perangela	419
EFC17257	Langnickel Hendrik	421
EFC17258	D'urso Claudia	423
EFC17260	Navarrete Laura	425
EFC17261	Silva Mosqueda Dulce Maria	427
EFC17262	Perez Trujillo Juan Pedro	429
EFC17263	Toro Claudia	431
EFC17265	Hernandez Londono Carlos Ignacio	433
EFC17266	Cavalli Alessandro	435
EFC17267	Andersson Martin	437
EFC17268	Gorton Lo	439
EFC17269	Ma Jie	441
EFC17270	Tsiakaras Panagiotis	443
EFC17271	Tsiakaras Panagiotis	445
EFC17274	Yoon Jayoung	447
EFC17276	Espinoza Tofalos Anna	449
EFC17277	Flagiello Fabio	451
EFC17279	Turchetti Luca	453
EFC17280	Beretta Gabriele	455
EFC17281	Botta Giulia	457
EFC17283	Ubertini Stefano	459
EFC17284	Bernuy-Lopez Carlos	461
EFC17285	Meyer Nico	463
EFC17286	Sainas Domenico	465







# European Fuel Cell

Conference & Exhibition

---

**12-15 december 2017 / NAPLES**

## TOPICS

Materials Science  
Modeling  
Testing and Characterizations  
System Design  
Hydrogen, Fuels and decarbonizing society  
Hydrogen and Fuel Cell applications  
Microbial Fuel Cell  
Marketing and Policy pathways to full commercialization of Fuel Cells and Hydrogen technologies  
Cross-cutting Issues  
New ideas and crazy ideas in Fuel Cells and Hydrogen technologies

## TOPICS DEDICATED TO SPECIAL SESSIONS

Fuel cell Modelling and Validation  
Dissemination of European project on Fuel Cells and Hydrogen Technologies  
LEAP03 - Low Emission Advanced Power cycles: pressurised fuel cell system

PRESENTED AT

**European Fuel Cell 2017 | Piero Lunghi Conference & Exhibition**

DECEMBER 12-15, 2017 | NAPLES, ITALY

ORGANIZED BY

**ENEA**

**University of Perugia**

**University of Naples "Parthenope"**

**Atena**

ORGANIZED BY

Angelo Moreno, Conference Chairman, ENEA  
Viviana Cigolotti, Technical Program Manager, ENEA





[europeanfuelcell.it](http://europeanfuelcell.it)

